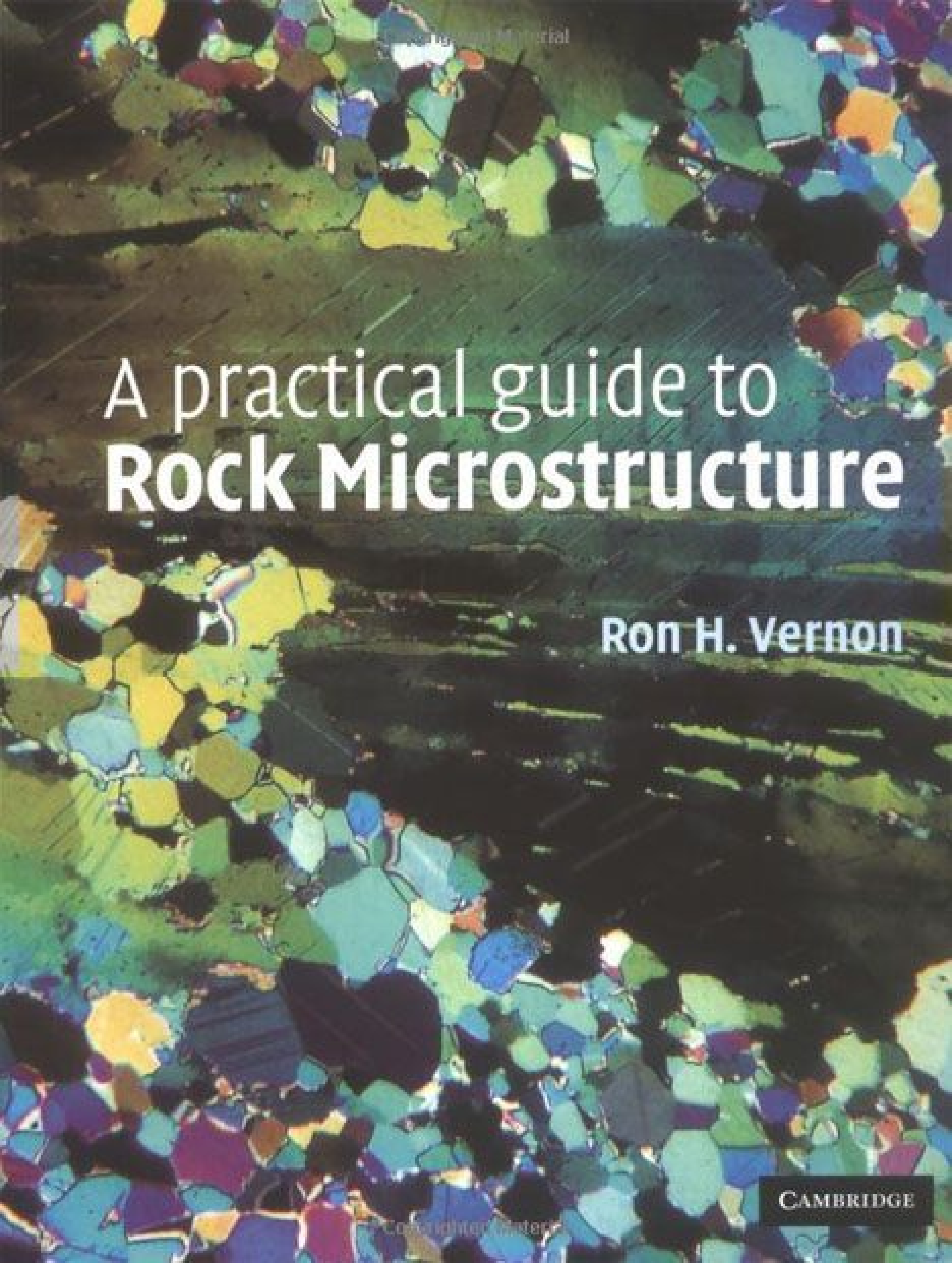

A practical guide to Rock Microstructure

Ron H. Vernon

CAMBRIDGE

A Practical Guide to Rock Microstructure

Ron H. Vernon
Department of Earth and Planetary Sciences,
Macquarie University, Sydney

CAMBRIDGE
UNIVERSITY PRESS

CAMBRIDGE UNIVERSITY PRESS
Cambridge, New York, Melbourne, Madrid, Cape Town, Singapore, São Paulo, Delhi

Cambridge University Press
The Edinburgh Building, Cambridge CB2 8RU, UK

Published in the United States of America by Cambridge University Press, New York

www.cambridge.org
Information on this title: www.cambridge.org/9780521891332

First published 2004
Reprinted 2008

Printed in the United Kingdom at the University Press, Cambridge

A catalogue record for this publication is available from the British Library

Library of Congress Cataloguing in Publication data
Vernon, R. H. (Ronald Holden)
A practical guide to rock microstructure / Ron H. Vernon.
p. cm.
Includes bibliographical references and index.
ISBN 0 521 81443 X – ISBN 0 521 89133 7 (paperback)
1. Rocks – Analysis. 2. Metamorphism (Geology) I. Title: Rock microstructure. II. Title.
QE434.V37 2004
552′.06 – dc22 2003069081

ISBN 978-0-521-81443-0 hardback
ISBN 978-0-521-89133-2 paperback

Preface

Learning about rocks can give much pleasure to anyone interested in Earth and its development. I hope that readers of this book will share my enthusiasm for examining rocks with the microscope. I planned the book to be an introductory review of the main processes responsible for the microstructures of Earth rocks. However, I soon realized that if I did that, the book would be a collection of half-truths, with little scientific value. Though many rock microstructures are understood fairly well, the interpretation of many others involves considerable controversy, and new ideas are being published all the time. So, I have felt compelled to mention problems of interpretation and to present alternative views, where appropriate. Thus, the book has evolved into (1) a basic explanation of the main processes, (2) an introduction to more complex issues of interpretation and especially to the relevant literature, and (3) an outline of modern approaches and techniques, in order to emphasize the ongoing, dynamic nature of the study of rock microstructure. Because complicated problems cannot be discussed in detail in a book of this kind, I have tried to provide a sufficient number of references to enable the reader to delve more deeply.

I assume that the reader has a basic knowledge of geology, rock types and microscopic mineral identification. Thus, the book is aimed mainly at senior geoscience undergraduates and above. Emphasis is placed on higher-temperature processes, i.e. those that occur under igneous and metamorphic conditions, although the book begins with a brief discussion of sedimentary microstructures, as background for some of the metamorphic microstructures. The mineral abbreviations used follow those suggested by Kretz (1983), as extended by Bucher & Frey (1994), and are listed at the start of the book. There is an extensive glossary of microstructural terms at the end of the book.

I also hope that materials scientists may also gain some benefit and interest from the microstructures discussed and illustrated, because rocks are the 'materials' of Planet Earth, in the sense of 'materials science': the branch of science that links all solid materials, such as metals, ceramics, glass, organic polymers and, of course, rocks.

I took all the photographs, except where otherwise acknowledged. I am also responsible for most of the line drawings, with the assistance of Dean Oliver

(Figs. 5.11, 5.37) and Daleth Foster (Fig. 5.93). I thank David Durney, Dick Flood, Scott Johnson and Scott Paterson for critically reading parts of the typescript, Judy Davis for assistance with computer techniques, Geoff Clarke for access to specimens at the University of Sydney, Ross Both, John Fitz Gerald and Neil Mancktelow for providing images, and John Lusk, John Ridley, David Durney and Pat Conaghan for providing specimens of opaque minerals, deformed rocks/veins and sedimentary rocks at Macquarie University. People who kindly provided other samples or thin sections are acknowledged in the figure captions.

Contents

Chapter 1
Background

1.1 Introduction

I wrote this book to help you to interpret what you see when you look at thin and polished sections of rocks with the microscope. I say 'help', rather than 'teach', because I don't want to give the impression that every microstructure you see can be easily and unambiguously interpreted in terms of processes that produced the rock. Many can, but in many other instances, conventional interpretations are ambiguous or poorly understood. So I intend the book to be only a guide, and I present alternative ideas where appropriate. A healthy scepticism should be maintained when interpreting rock microstructures yourself and also when reading the interpretations of others.

1.2 History of the examination of rocks with the microscope

Rocks in natural outcrops, in samples knocked off these outcrops and in drill cores, are beautiful and instructive. We can see different minerals, and identify many of them with the aid of a hand lens. We can also see some of the more obvious structures in the rocks. However, cutting a slice (section) though a rock with a diamond-impregnated circular saw and polishing the sawn surface shows us the various minerals alongside each other, rather than piled confusingly all around each other. This reveals the structure even more clearly, as can be seen in the polished facing slabs on many buildings and bench tops.

But we always want to see more. So, when D. Brewster in 1817 and William Nicol about 1830 showed how to make a slice of crystalline material thin enough to transmit light (0.03 mm is the standard thickness), stuck to a glass microscope slide (Shand, 1950, p. 6; Loewinson-Lessing, 1954), it wasn't surprising that a curious person, such as Henry Sorby, should start looking at these *thin sections* of rocks (Sorby, 1851, 1853, 1856, 1858, 1870, 1877, 1879, 1880, 1908). Sorby learnt the technique of making thin sections from W. C. Williamson in 1848 (Judd, 1908; Folk, 1965) and made the first rock thin section in 1849 (Judd, 1908). He was the first to look seriously at rock sections with the microscope, beginning with a study of chert, a siliceous sedimentary rock that was a very appropriate choice for microscopic investigation, in view of its very fine grain-size. He described and suggested a mechanical origin for slaty cleavage (Sorby, 1853, 1856), noticed many of the basic features of igneous and metamorphic rocks, made many important observations on sedimentary rocks, including carbonate rocks (Sorby, 1851, 1879), investigated pressure-solution (using fossil crinoids), described meteorites, and published the first papers on the examination of polished sections of metals with the microscope (Sorby, 1864, 1887). So not only is he the founder of petrography (the description of rocks), but the founder of metallography as well (Smith, 1960). He also investigated fluid inclusions in minerals, heating crystals to watch the gas bubbles disappear, in order to get an estimate of the temperature of crystallization of the mineral (Sorby, 1858; Folk, 1965).

Sorby was followed soon after by many others, as discussed by Johannsen (1939) and Loewinson-Lessing (1954). Among them were Dawson (1859), Zirkel (1863, 1866, 1876), Vogelsang (1867), Fouqué& Michel-Lévy (1879), Allport (1874), Rosenbusch (1873, 1877) and Teall (1885, 1886). Since those days, the light microscope has become the main tool for identifying minerals and examining their microstructures, although it has been augmented by many modern techniques (Section 1.6).

1.3 How relevant is the microscope today?

Many petrologists concentrate on the mineralogical and chemical aspects of rocks, without spending much time looking at rocks with the microscope. In fact, in these days of marvellous techniques for the chemical and isotopic analysis of minerals, some people may feel that simply looking at and measuring the shapes and arrangements of crystals in rocks with the microscope is a little out of date. However, carrying out detailed chemical and isotopic analyses of minerals when you don't understand the relationships of these minerals to other minerals in the rock makes little sense. It's a waste of expensive resources, at very least.

On the other hand, many structural geologists look at the physical or structural aspects of minerals and rocks, especially from the viewpoint of deformation processes and preferred orientations of grains, without being concerned about the chemical aspects of these processes. Both approaches are valuable, of course, but their interrelationships can be particularly illuminating. Fortunately, many researchers are attempting to integrate the chemical and physical approaches, and the study of rocks with the microscope provides a link between them. In fact, the detailed study of processes in rocks at the microscopic scale is now a major area of research, especially among younger people, in many universities and other research institutions. Moreover, new observational techniques are being developed and used, as discussed in Section 1.6.

Research microscopes commonly have both transmitted and reflected light facilities. An excellent example of the simultaneous use of transmitted and reflected light microscopy is the study of Columbia River basalts by Long & Wood (1986), in which reflected and transmitted light photographs are arranged side by side, clearly revealing the dendritic shapes of the opaque Fe–Ti oxide minerals and their relationships to the transparent and translucent silicate minerals. Some leading books and review articles on minerals in reflected light, with emphasis on microstructures, are those of Bastin (1950), Edwards (1947, 1952), Cameron (1961), Ramdohr (1969), Stanton (1972), Craig & Vaughan (1994) and Craig (1990a,b).

1.4 Mineral identification

Learning to identify minerals takes time and practice, and is outside the scope of this book. Close teaching in a laboratory situation is the best way to learn about the optical properties of minerals, using textbooks specifically written for the purpose (e.g. Fleischer *et al.*, 1984; Shelley, 1985a; Nesse, 1991; Gribble & Hall, 1992; Deer *et al.*, 1992). Ideally, this should go hand-in-hand with learning about microstructures.

1.5 The concept of a section

Thin and polished sections are two-dimensional sections through three-dimensional objects, and this must always be kept in mind, as explained in some detail by Hibbard (1995). Mineral grains can have unexpectedly complex three-dimensional shapes (see, for example, Rigsby, 1968; Byron *et al.*, 1994, 1995, 1996). Two or even three orthogonal sections may be necessary to reveal the structure of structurally anisotropic rocks, and some recent detailed microstructural studies have used: (1) *serial sectioning* (see, for example, Byron *et al.,* 1994, 1995, 1996; Johnson & Moore, 1996), coupled with *image analysis* by computer, to construct a three-dimensional image of the microstructure, and (2) *computed X-ray tomography* (Section 1.6), to reveal the three-dimensional distribution of large crystals (porphyroblasts) in metamorphic rocks (Carlson & Denison, 1992; Denison & Carlson, 1997), plagioclase chains in basalts (Philpotts *et al.*, 1999), and former melted rock (leucosome) in migmatites (Brown *et al.*, 2002).

1.6 Newer techniques

This book deals mainly with microstructures visible in the optical (light) microscope, in standard thin or polished sections, with the use of polarized light. However, some newer techniques are very useful for revealing features not apparent or less clearly shown in polarized light, as outlined below. Several examples of photographs taken with these techniques will be presented in the book. The new techniques underline the fact that the study of rock microstructure is a dynamic, progressive field of research.

(1) **Cathodoluminescence** (CL) is a technique that can reveal internal microstructures of grains of some minerals, for example, compositional zoning, overgrowths, microcracking and replacement veining in quartz, calcite, dolomite, magnesite, zircon, plagioclase, K-feldspar, diamond, fluorite, sphalerite, kyanite, pyrope garnet, corundum, cassiterite, anhydrite and apatite (Sippel & Glover, 1965; Smith & Stenstrom, 1965; Zinkerngel, 1978; Matter & Ramseyer, 1985; Owen & Carozzi, 1986; Sprunt, 1978, 1981; Sprunt & Nur, 1979; Field, 1979; Reeder & Prosky, 1986; Padovani *et al*., 1982; Hanchar & Miller, 1993; Marshall, 1988; Ramseyer *et al*., 1988; Morrison & Valley, 1988; Mora & Valley, 1991; Yardley & Lloyd, 1989; Hopson & Ramseyer, 1990; Barker & Kopp, 1991; Shimamoto *et al*., 1991; Williams *et al*., 1996; Mora & Ramseyer, 1992; D'Lemos *et al*., 1997; Watt *et al.,* 1997, 2002; Hayward, 1998; Müller *et al*., 2000; Pagel *et al*., 2000; Janousek *et al*., 2000; Ahn & Cho, 2000; Götze, 2000; Rubatto & Gebauer, 2000; Penniston-Dorland, 2001; Rubatto *et al*., 2001; Hermann *et al*., 2001; Barbarand & Pagel, 2001; Peppard *et al*., 2001; Rusk & Reed, 2002; Viljoen, 2002; Rougvie & Sorensen, 2002). CL is especially useful for revealing microstructural details in minerals that are colourless in the light microscope, for example calcite, quartz and feldspar. For example, quartz, untwinned K-feldspar and untwinned plagioclase may be distinguished by their CL colours in fine-grained aggregates, and CL can assist in provenance and diagenetic studies in sedimentary rocks. The technique is not suitable for iron-rich minerals. Some applications of CL are discussed in Sections 3.11.7, 3.11.9 and 5.9.3.

It can be used with the light microscope (producing true CL colours with a spatial resolution of 1–2 μm), or the scanning electron microscope (producing grey-scale variations with a spatial resolution of less than 1 μm), and may be combined with CL spectroscopy to enable spectral spot analysis of revealed features. CL is combined with X-ray tomography to reveal the internal structure of diamonds (see, for example, Field, 1979).

CL is caused by defect structures in the crystal lattice, such as impurity atoms (transition metals, rare earth elements, lead, titanium, actinides), vacancies and dislocations produced during formation and/or deformation of the mineral, which therefore reflect conditions of crystallization, deformation and alteration. The technique involves coating a polished thin section with carbon and bombarding it with electrons in a vacuum. This bombardment produces light from substitutional atoms in an excited state.

(2) **Laser-interference microscopy** is a relatively new optical technique that detects small differences in refractive index, and so can reveal, in great detail, subtle compositional differences (on which refractive index depends), for example in zoned plagioclase (Chao, 1976; Pearce, 1984a,b; Pearce *et al*., 1987a,b).

(3) **Scanning electron microscopy** (see, for example, Lloyd, 1987) is capable of revealing sharp microstructural details in shades of grey, although arbitrary colours may also be assigned to form a false-colour image. It involves

backscattered and forescattered imaging in the scanning electron microscope (SEM). This is particularly useful for (a) revealing the detailed microstructure of small grains and fine-grained aggregates and intergrowths (see, for example, Vernon & Pooley, 1981; Wirth & Voll, 1987; Cashman, 1988; Simpson & Wintsch, 1989; Swanson *et al.*, 1989; Johnson & Carlson, 1990; van der Voo *et al.*, 1993; Brodie, 1995; Lloyd & Prior, 1999; Drüppel *et al.*, 2001; Blundy & Cashman, 2001; Rickers *et al.*, 2001; de Haas *et al.*, 2002; Schieber, 2002), (b) identifying very fine-grained minerals (see, for example, Prior *et al.*, 1999), (c) revealing fine-scale compositional zoning in minerals (see, for example, Yardley *et al.*, 1991; Müller *et al.*, 2000; Piccoli *et al.*, 2000; Kuritani, 2001; Alexandrov, 2001; Rubatto *et al.*, 2001; Hermann *et al.*, 2001; Ginibre *et al.*, 2002a,b; Lentz, 2002), (d) measuring orientation differences between grains and subgrains as small as 1 μm across (Prior *et al.*, 1996, 1999; Lloyd *et al.*, 1997; Trimby *et al.*, 1998; Wheeler *et al.*, 2001; Bestmann & Prior, 2003), and (e) revealing domains of different orientation in optically isotropic minerals, such as garnet (Spiess *et al.*, 2001; Prior *et al.*, 2000, 2002) and pyrite (Boyle *et al.*, 1998).

(4) **Transmission electron microscopy** (TEM) assists in the interpretation of some microstructures that can be optically ambiguous, such as some recovery features in deformed quartz (Section 5.4) and fine exsolution lamellae (Section 4.11). The principles and some applications have been reviewed by Champness (1977), Putnis & McConnell (1980), McLaren (1991) and Putnis (1992). TEM resolves very small objects, such as very fine to submicroscopic intergrowths, exsolution features, inclusions and twins and can reveal the arrangement of defects (including dislocations, discussed in Section 5.3.2) in the atomic structure of individual grains of both optically transparent and opaque minerals (see, for example, McLaren *et al.*, 1967; McLaren, 1974, 1991; McLaren & Retchford, 1969; Phakey *et al.*, 1972; Green & Radcliffe, 1972; McLaren & Hobbs, 1972; Champness & Lorimer, 1976; Champness, 1977; McLaren & Etheridge, 1976; Zeuch & Green, 1984; Doukhan *et al.*, 1985; Allen *et al.*, 1987; Cox, 1987a; Couderc & Hennig-Michaeli, 1989; Hennig-Michaeli & Couderc, 1989; Green, 1992; Ando *et al.*, 1993; Doukhan *et al.*, 1994; Vogelé*et al.*, 1998).

(5) **X-ray tomography** (in full: high-resolution computed X-ray tomography) is a more recent development in the study of rock microstructure (see, for example, Mees *et al.*, 2003). This technique maps the variation of X-ray attenuation within solid objects, the attenuation varying with each mineral present. A source of X-rays and a set of detectors revolve around the rock sample, producing images in layers or cross-sections. The series of two-dimensional images can be computed into a three-dimensional representation of the grains and aggregates in the rock (see below), which gives a clearer picture of spatial relationships and crystal size distributions (see, for example, Carlson & Denison, 1992; Carlson *et al.*, 1995, 1999; Denison *et al.*, 1997; Brown *et al.*, 1999; Philpotts *et al.*, 1999).

(6) **Computer-aided construction of three-dimensional images** is a technique whereby serial two-dimensional optical or X-ray tomographic images can be scanned and imported into suitable computer graphics programs to provide three-dimensional constructions (Johnson & Moore, 1993, 1996; Carlson *et al.*, 1995, 1999; Pugliese & Petford, 2001; Castro *et al.*, 2003). This approach is used in confocal laser scanning microscopy (CLSM), which enables objects (such as inclusions in minerals) to be viewed in focus through a thickness of sample in a single image (Petford & Miller, 1992; Petford *et al.*, 1995; Sheppard & Shotton, 1997; Bozhilov *et al.*, 2003), as described in Section 4.4.5. Readily available computer software can also be used to animate images, producing a more complete visualization of features such as grain shapes, grain distributions and vein networks (see, for example, Johnson & Moore, 1996; Carlson *et al.*, 1999; Pugliese & Petford 2001).

(7) **X-ray compositional mapping** produces maps of compositional zoning in crystals (see Sections 3.11, 4.12). Such maps are produced by multiple stage-scan chemical analyses made with wavelength-dispersive spectrometers on an electron microprobe, different colours being assigned to different concentrations of the analysed element. Examples are shown in Section 4.12. The technique can also be used for more clearly revealing mineral or compositional domains in fine-grained aggregates (see, for example, Lang & Gilotti, 2001; Williams *et al.*, 2001; Clarke *et al.*, 2001; Daczko *et al.*, 2002a,b). Raw X-ray intensity maps may be converted to maps of oxide mass percent by appropriate matrix corrections (Clarke *et al.*, 2001).

1.7 Quantitative approaches

Although most work on rock microstructures is qualitative, involving description and interpretation, quantitative methods are also used. For example, grain measurement is important in the classification and interpretation of clastic sedimentary rocks in terms of transport and depositional environments (Section 2.2.3). Grainsize is also used in the classification of igneous rocks, though less precisely, and crystal size distributions (CSD) are being increasingly investigated in igneous and metamorphic rocks (Sections 3.4, 4.3.1). Various statistical techniques are used to determine spatial distribution patterns (SDP) of grains and crystals in rocks (see, for example, Flinn, 1969; Kretz, 1966b, 1969; Jerram *et al.*, 1996; Denison & Carlson, 1997; Daniel & Spear, 1999; Jerram & Cheadle, 2000). Numerical modelling has been used to convert two-dimensional measurements of grain shapes and sizes in thin section to three-dimensional grain shapes and true crystal size distributions (Higgins, 1994, 2000; Peterson, 1996). Moreover, computer software is readily available to do this and to make animated images, as mentioned in the previous section. Interfacial angles have been measured in many metamorphic rocks, sulphide rocks and igneous cumulates, as indicators of mutual solid-state growth of minerals (Section 4.2). In addition, the orientations of inclusion trails in porphyroblasts have been used as indicators of tectonic processes (Section 5.10). Numerical simulation of the development of metamorphic and deformation microstructures is also well under way (Jessell, 1988a,b; Jessell *et al.*, 2001).

1.8 Some terms

Although no hard and fast rule exists, it is probably best to use *crystal* for a volume of crystalline mineral with well-formed, planar faces (called crystal faces or facets), and *grain* for any other volume of crystalline mineral. For me, the shapes, arrangements and orientation of the minerals constitute a rock's *fabric*. At the microscope scale, the fabric (*microfabric*) consists of the grain shapes and arrangement (the *microstructure*) and the spatial orientation of the minerals (the *preferred orientation*). However, many people equate 'fabric' with 'preferred orientation', as recommended by the IUGS Subcommission on the Systematics of Metamorphic Rocks (Brodie *et al.*, 2002).

It would be good to make materials scientists more interested in rocks, as they are the great class of natural solid materials. Therefore, because 'texture' means 'preferred orientation' to most materials scientists and an increasing number of structural geologists, it would be best not to use it instead of 'microstructure' as many petrologists do. However, although 'microstructure' is gaining in popular usage, 'texture' is common, and no ambiguity is caused among petrologists by using it. Actually, 'microstructure' appears to have priority, because the first publications on the microscopic examination of rocks referred to 'microscopical structure' or 'microscopic structure' (see, for example, Sorby, 1851, 1858; Dawson, 1859; Allport, 1874). Moreover, the IUGS Subcommission on the Systematics of Metamorphic Rocks has recommended that the term 'texture' be replaced by 'microstructure', which is defined as 'structure on the thin section or smaller scale' (Brodie *et al.*, 2002). The term 'microtexture', which unfortunately is starting to enter the literature, is a tautology, because 'texture' refers to the microscopic scale.

Of course, every gradation in scale exists between the microscopic and macroscopic (outcrop) scales, and so I have not been able to confine the discussion to the microscopic, although this is by far the main scale discussed.

1.9 Traditional rock groupings

Many rock-forming processes apply to more than one of the traditional igneous, sedimentary and metamorphic rock groups. For instance, similar basic principles governing the nucleation and growth of crystals apply to all rocks, and grain growth in the solid state occurs not only in metamorphic rocks (in which it is a universal process), but also in the late stages of formation of some rocks conventionally regarded as igneous. In addition, growth of new minerals in the solid state (*neocrystallization*) occurs not only in metamorphic rocks, but also in the late-stage alteration (*deuteric alteration*) of igneous rocks, and in the low-temperature alteration (*diagenesis* or *burial metamorphism*) of rocks that many people would consider to be still sedimentary. Moreover, metamorphic rocks begin to melt at high temperatures, producing rocks with both igneous and metamorphic features. In addition, radiating crystal aggregates (spherulites) commonly grow in glass, which, though technically solid, is liquid-like with regard to its atomic structure. Furthermore, exsolution, which is a solid-state process, occurs in both igneous and metamorphic minerals. As if that isn't enough, fragmental material thrown out of explosive volcanoes produces rocks that are technically sedimentary, but consist entirely of igneous material, and may also show evidence of solid-state flow of glass. The result of this cross-linking of processes is that, though this book adheres roughly to the traditional sedimentary–igneous–metamorphic subdivision, processes discussed under one of these headings may also be relevant to another of these groups. These instances are cross-referenced.

1.10 Importance of evidence

Science relies on *evidence*. An assertion made without evidence isn't worth very much. Yet I often read statements such as: 'the microstructural (textural) evidence indicates . . .' This implies that the writers are asserting that their interpretations are so obviously right that they don't have to go to the bother of describing what they saw and evaluating the evidence.

Of course, recognizing evidence takes practice. As noted by Chalmers (1999):

> It is necessary to learn how to see expertly through a telescope or microscope, and the unstructured array of bright and dark patches that the beginner observes is different from the detailed specimen or scene that the skilled viewer can discern.

Whenever you make interpretations based on microscopic examination of rocks, you should: (1) *describe* clearly what you see and (2) *evaluate* the possible interpretations. If one or more interpretations are valid, you should not arbitrarily favour one of them, unless other evidence (e.g. field or chemical evidence) clearly points in that direction. This is the 'method of multiple working hypotheses' advocated by Chamberlain (1890). In many instances, the microstructural evidence may not be at all clear, in which case you shouldn't use it to support a hypothesis. Maybe you will have to suggest equally valid alternative interpretations and leave it at that.

The paramount importance of evidence in making scientific inferences is emphasized in the following quotation.

> On so important a question, the evidence must be airtight. The more we want it to be true, the more careful we have to be. No witness's say-so is good enough.

> People make mistakes. People play practical jokes. People stretch the truth for money or attention or fame. People occasionally misunderstand what they're seeing. People even sometimes see things that aren't there.

Carl Sagan (1996) was referring to UFOs, but at least some of these statements could refer to petrologists interpreting rock microstructures. People do make mistakes and even see things that aren't there, and though practical jokes may be uncommon in such a serious pursuit as petrology(!), people certainly do occasionally misunderstand what they're seeing. We all do, in fact. Most important, we often want something to be true so much that we may be tempted to gloss over the evidence, whereas we should be doubly careful, in order to save ourselves falling into the trap of a woefully wrong interpretation, no matter how attractive it may seem.

It doesn't matter how many times an assertion is repeated or how loudly it is trumpeted in conversation, in the scientific literature, in textbooks or even on the Internet, it is only as good as the evidence for it. Another point to remember is that an interpretation presented by a great authority on the subject, though worthy of respect perhaps, is also only as good as the evidence for it. Such 'arguments by authority' can subdue interpretations based on careful accumulation of evidence (Vernon, 1996b).

Too often we see examples of interpretations based on inadequate evidence used to support a preferred model. Even some well-accepted interpretations may be wrong. A good example is the common belief that an 'order of crystallization' in igneous rocks can be inferred by looking at the microstructure. Generally this is impossible, as explained in Section 3.6. If the microstructure cannot give you the evidence, please don't try to extract it anyway!

In fact, the more I examine and read about rock microstructures, the more cautious I become about interpreting them, and that will be a constant theme in this book. As mentioned below (Section 1.11), recent work on the direct microscopic observation of developing microstructures in organic compounds used as mineral analogues has revealed many unexpected processes, and has shown that similar microstructures may have very different histories. They remind us of the necessity for caution in the interpretation of natural rocks.

So I will try to give explanations that are sufficiently general to be regarded by most people as 'reasonable' on the available information, and that students can infer largely from the optical microstructure. Where alternatives need to be discussed, the relevant publications will be mentioned. Moreover, where pitfalls exist, they will be pointed out, and it must be re-emphasized that the book is only the most general of guides. It indicates what to look for and how to start (not stop) thinking about what is observed. Finally, it is as well to keep in mind the wise words of John Spong (*Sydney Morning Herald*, June 9, 2001): 'Explanations are always compromised by the levels of knowledge available to the explainer.' That applies to me just as much as to any other explainer!

1.11 Kinds of evidence used

What evidence is useful in interpreting rock structures? Imagine you had never seen a rock section, either a thin section or a slab cut through a hand sample. How could you begin to interpret the crystal shapes and arrangements you see? You must have some guides. These are *field relationships* and *experimental evidence* on rocks and minerals, assisted by some general inferences from experiments on other materials, such as metals, ceramics, organic polymers and synthetic ice. For example, when Sorby first looked at thin sections of slates with the microscope, he would have already known that slates are formed by strong deformation and that the deformation is in some way responsible for their characteristic strong foliation (slaty cleavage). Furthermore, once Sorby had observed and described the features shown by the microstructure of the slate, others were in a position to recognize similar cleavages in thin sections of rocks from other areas. In this way, general guides to the interpretation of rock microstructures have been established.

If we can observe rocks forming, as with sedimentary and volcanic rocks, we are on firm ground for making inferences about how the microstructures were formed. We are on much shakier ground when it comes to intrusive igneous and metamorphic rocks. However, we can learn much from careful interpretation of field relationships, although strong differences of interpretation are common. In addition, experiments on the cooling of melted rocks and the melting of solid rocks are valuable guides to the interpretation of rocks involving melts, and many recent experimental advances have been made in the interpretation of igneous microstructures (see, for example, Lofgren, 1971b, 1973, 1974, 1976, 1980; Lofgren *et al.*, 1974; Fenn, 1974, 1977, 1986; Donaldson, 1976, 1977, 1979; Swanson, 1977; Swanson & Fenn, 1986; London, 1992). However, we should keep in mind possible problems caused by the short duration of experiments.

Experimentally determined stability fields of mineral assemblages in different bulk chemical compositions reveal the conditions of pressure, temperature and fluid composition that occur during metamorphism. However, it is not as easy to conduct successful experiments on the development of microstructures in metamorphic rocks, because of the high temperatures and pressures involved in the experiments and the generally small size of the samples used.

Many important experiments on mineral and rock deformation have been carried out (Chapter 5), but again we can only observe the finished product, not the stages along the way. Fortunately, experiments on ice deformation have helped our understanding of progressive microstructure development during deformation (see, for example, Wilson, 1984, 1986; Wilson *et al.*, 1986). Moreover, a new experimental technique based on transparent and translucent organic compounds that behave somewhat similarly to minerals has been developed, and is being applied with great effect to the interpretation of microstructures, especially deformation features (see, for example, Means, 1977, 1981, 1983, 1989; Means & Jessell, 1986; Means & Park, 1994; Means & Ree, 1988; Park & Means, 1996;

Urai, 1983a,b, 1987; Urai & Humphreys, 1981; Urai *et al.*, 1980, 1986; Ree, 1991; Ree & Park, 1997). Because these compounds deform, melt and crystallize rapidly at room temperatures, the processes can be observed and photographed in progress in the microscope ('see-through' experiments). Of course, we must keep in mind that these materials are generally not minerals, but they have provided some startling insights into possible grain-scale processes that may occur in natural rocks.

In the absence of reliable experimental evidence, it is necessary to fall back on 'common-sense' interpretations, based on accumulated experience of the type outlined previously. This applies especially to metamorphic rocks. Unfortunately, common sense isn't so common, and what makes perfectly good sense to one person may make no sense at all to somebody else. The most important thing is to be as honest and logical as possible, and to evaluate (and if necessary retain as possibilities) every interpretation that can reasonably explain the observations. If the end result is the unsatisfying conclusion that you cannot make an unambiguous interpretation on the available evidence, leave it at that. No harm will be done. On the contrary, many a doubtful interpretation, presented as being reliable, has been accepted at face value and used in later work, thereby misleading subsequent researchers.

1.12 Complexity

A rock's microstructure is the product of a complicated sequence of events and processes. So is a rock's chemical analysis. Both may tell us something about the rock's history, but neither can fully reveal all the historical complexities. This is a problem that petrologists have to accept. We do our best with the evidence available, without taking it too far, and we must acknowledge that our interpretations are often incomplete.

Another point to add to the complexity is that superficially similar microstructures may be formed in different ways, as with exsolution and epitactic (epitaxial) replacement producing similar intergrowths (see, for example, Craig, 1990). For example, hematite lamellae in magnetite, usually inferred to be of replacement origin, may be due to exsolution in some rocks (Edwards, 1949). Another complication is the optical similarity between subgrains formed by recovery and similar features formed by fracture, as discussed in Section 5.4. Other complexities of rock microstructure will become apparent in the following chapters.

Chapter 2
Microstructures of sedimentary rocks

2.1 Introduction

Although this book is mainly concerned with igneous, metamorphic and deformation processes, in this chapter I briefly review the main sedimentary microstructures, partly because they need to be understood in order to interpret residual sedimentary microstructures in some metamorphic rocks.

The basic sedimentary microstructures are relatively straightforward, but variations (reflecting variable sedimentary environments) can be very complex, and many complicated classification schemes to deal with this complexity have been suggested. Classification schemes, microstructural details and discussions of sedimentary environments can be found in many excellent books (e.g. Pettijohn, 1949; Williams *et al*., 1954; Carozzi, 1960; Milner, 1962; Folk, 1968; Selley, 1970; Blatt *et al*., 1972; Bathurst, 1975; Friedman & Sanders, 1978; Adams *et al*., 1984, Greensmith, 1989; Boggs, 1992; McPhie *et al*., 1993; McLane, 1995).

Sediments are loose, unconsolidated fragments, and sedimentary rocks are the consolidated or lithified equivalents. *Residual (pedogenic)* sediments are essentially *in situ* deposits of the products of rock weathering, for example weathering crusts, soils and regoliths. *Epiclastic* (*terrigenous*) sediments are accumulations of solid fragments formed by erosion of existing rocks. *Pyroclastic* sediments are deposits of fragmented igneous material (e.g. volcanic glass and crystal fragments) ejected from volcanoes in explosive eruptions directly onto Earth's surface. *Bioclastic* sediments are accumulations of organic skeleton or shell fossils that have been at least slightly transported. *Chemical* sediments are precipitated directly from aqueous solution or by replacement of existing sediment. *Polygenetic* sediments consist of mixtures of the foregoing types, and are named according to the dominant kind of sediment present (e.g. fossiliferous limestone, tuffaceous sandstone). Moreover, epiclastic rocks commonly contain chemical components in the form of a *cement* (Section 2.2.5).

2.2 Epiclastic ('terrigenous') sedimentary rocks

2.2.1 Detrital (clastic, fragmental) minerals

Quartz and the clay minerals constitute up to about 70–80% of the epiclastic sedimentary rocks, with less abundant feldspar, mica and carbonate. The clay minerals belong to a group of very fine-grained, water-rich, complex aluminosilicates with various other elements, especially potassium, magnesium and iron. Generally they are too fine-grained to be identified with the optical microscope, and so other techniques (especially X-ray diffraction) are used for their accurate determination. Other chemically and physically resistant minerals, such as zircon, tourmaline, ilmenite, magnetite, monazite, rutile, topaz and garnet, are also commonly present in very small quantities: generally no more than 1%, except in local 'black sand' concentrations.

The detrital (clastic, fragmental) minerals in epiclastic sediments depend on (1) their presence in the source rocks, (2) their resistance to mechanical abrasion, and (3) their chemical stability in the surface environment. Common fragmental minerals are those that are most stable in Earth's atmosphere, especially quartz and the clay minerals. Quartz is the most common mineral that is stable in Earth's atmosphere, and is released from rocks undergoing weathering as individual grains or fragments. In contrast, clay minerals are formed by the chemical breakdown of minerals that are not as stable in the atmosphere, especially feldspars and the ferromagnesian minerals (pyroxene, olivine, biotite and amphibole). However, these less stable minerals can occur as fragments in sediment that has been transported relatively short distances and/or deposited rapidly.

2.2.2 Fragment size and sorting

Transport at normal conditions in water tends to sort the fragments (detritus) into different sizes, namely: pebbles (>2 mm in diameter), sand ($2-\frac{1}{16}$ mm in diameter), silt ($\frac{1}{16}-\frac{1}{256}$ mm in diameter) and clay ($<\frac{1}{256}$ mm in diameter). Prolonged washing of sediment, for example in waves in relatively shallow water (involving traction currents), leads to a well-sorted sedimentary rock with a relatively even grainsize (Figs. 2.1, 2.2), whereas if the sediment is deposited rapidly (for example, in turbidity currents produced by submarine slumps on continental slopes), the fragments tend to have very different sizes (said to be poorly sorted or unsorted), as shown in Figs. 2.3–2.7.

Generally, well-sorted sedimentary rocks tend to have rounded fragments (Section 2.2.4) and *vice versa* (Figs. 2.1, 2.5), but not necessarily (Figs. 2.2–2.4). Sedimentary rocks composed mainly of pebbles, sand and clay are called conglomerates or rudites (Figs. 2.7, 2.8), sandstones or arenites (Figs. 2.1–2.6) and shales, claystones, mudstones or pelites (Fig. 2.9), respectively.

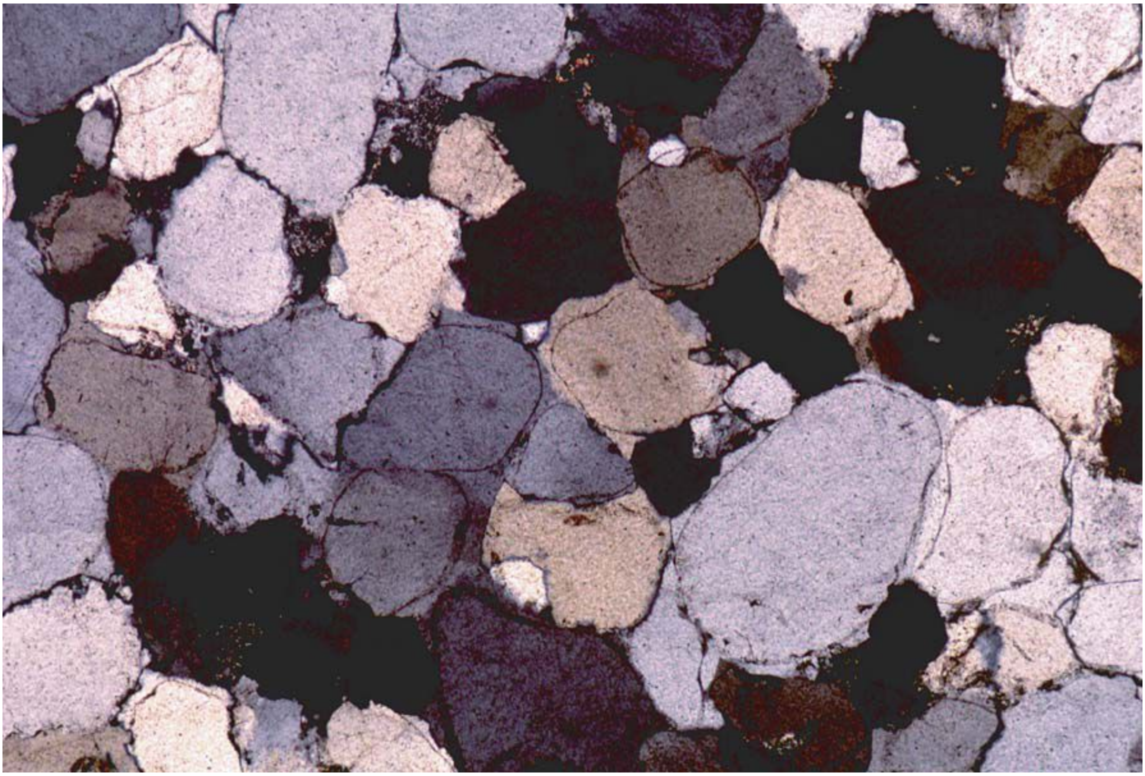

Fig. 2.1: Orthoquartzite, consisting of well-sorted, rounded clastic quartz grains (outlined by minute, dusty-looking inclusions) with secondary overgrowths (forming a quartz cement) in optical continuity with the clasts. The resulting new grains (clasts plus their overgrowths) form a roughly polygonal aggregate (compare with Fig. 2.13). Some of the grain contacts are irregular to sutured (stylolitic surfaces; Section 5.9.2), owing to 'pressure-solution' in response to local stress increases as the grains were pressed together, during either compaction or weak tectonic activity (Chapter 5). Crossed polars; base of photo 2.8 mm.

Poorly sorted sediments commonly contain a *matrix*, which is finer-grained material of detrital origin that partly or completely fills spaces (interstices) between the larger clastic grains that form the framework of the rock. For example, poorly sorted sandstones may have a clay and/or silt matrix, and poorly sorted conglomerates may have a sand matrix. Clay minerals in the matrix tend to bind the larger clasts, especially after being neocrystallized (Section 2.2.7) during burial, and so help produce a consolidated rock. In many volcanic sandstones (often called 'greywackes'), what appears to be a primary clay matrix may actually be an aggregate of clay minerals and/or chlorite that replace volcanic glass fragments and are squashed between the quartz, feldspar and rock fragments (Figs. 2.5, 2.6).

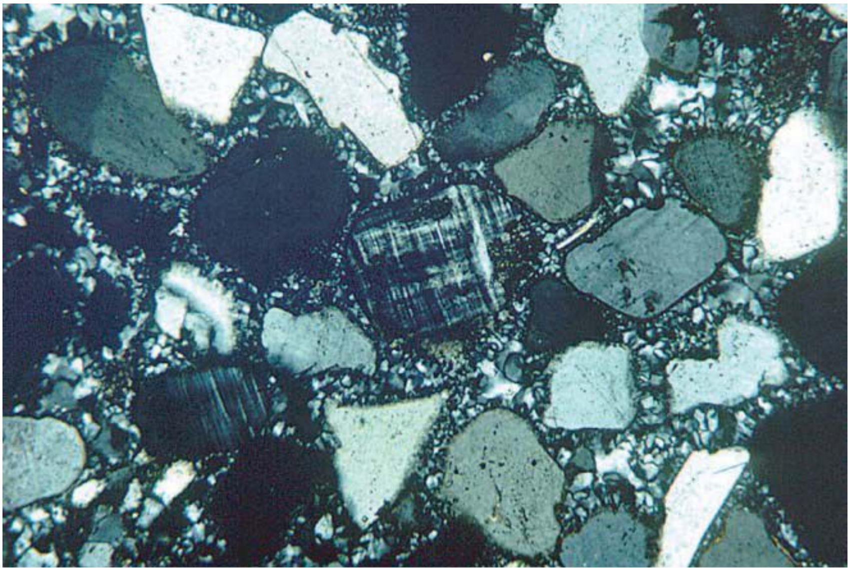

Fig. 2.2: Relatively well-sorted sandstone consisting of fragments of quartz and feldspar (mainly microcline, showing tartan twinning; Section 4.8) that are mainly well rounded, though some are sub-rounded to angular. The fragments have been cemented by fine-grained aggregates of quartz precipitated from hydrous solutions percolating between the clasts; the quartz cement grains nucleated on the clasts, forming 'micro-vughs'. From Vernon (2000b, fig. 103). Crossed polars; base of photo 1.3 mm.

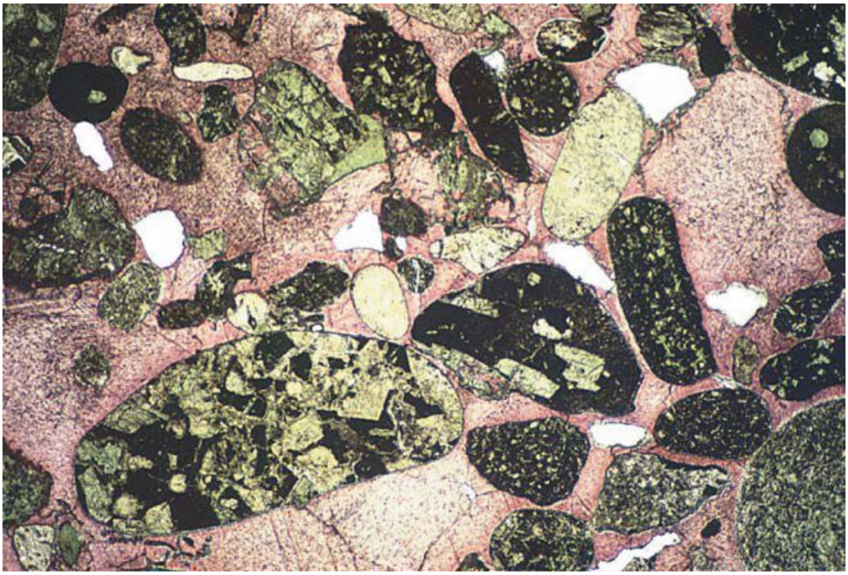

Fig. 2.3: Moderately poorly sorted volcanic sandstone composed of clasts of volcanic rock fragments with igneous microstructures, including phenocrysts (Chapter 3). The feldspar of the rock fragments has been replaced by fine-grained, green chlorite. The clasts have been cemented by calcite in grains that are much larger than the clasts ('*lustre mottling*' structure). The calcite (which is normally colourless in thin section) has been stained with an organic dye (alizarin red S), to distinguish it from other carbonate minerals. From Vernon (2000b, fig. 104). Plane-polarized light; base of photo 4.4 mm.

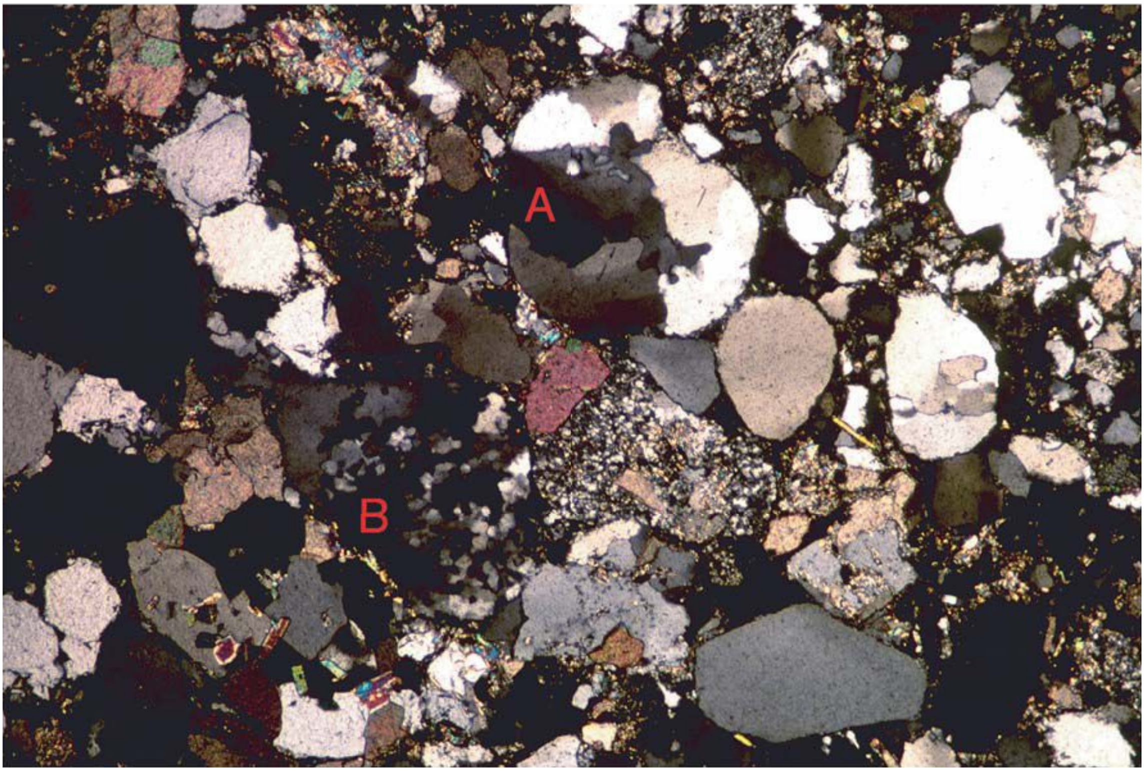

Fig. 2.4: Poorly sorted sandstone, consisting mainly of angular to rounded quartz fragments, with some altered feldspar, carbonate and fine-grained rock fragments, all cemented by opaque iron oxide. Some of the quartz clasts show evidence of recovery (A) and/or recrystallization (B), as discussed in Section 5.4, owing to deformation in the source area; such microstructures assist in determining the source (provenance) of the sediment. Crossed polars; base of photo 4 mm.

Turbidity currents (turbid flows) that transport and dump unsorted material commonly briefly interrupt slow deep-water (pelagic) deposition of clay-size fragments. The rapidly moving currents commonly disrupt the underlying mudstone beds and incorporate fragments of them (rip-up clasts), as shown in Fig. 2.10.

2.2.3 Fragment shapes

The general shapes of clastic grains depend largely on shapes inherited from the parent rock, modified by abrasion during transport. Abrasion of fragments wears away their sharp corners, eventually producing rounded sand grains and pebbles. Grains are said to be *angular, subangular, subrounded, rounded* or *well-rounded*, depending on their degree of rounding (Fig. 2.11). Softer mineral and rock fragments become rounded much more quickly than harder ones, quartz being so

A

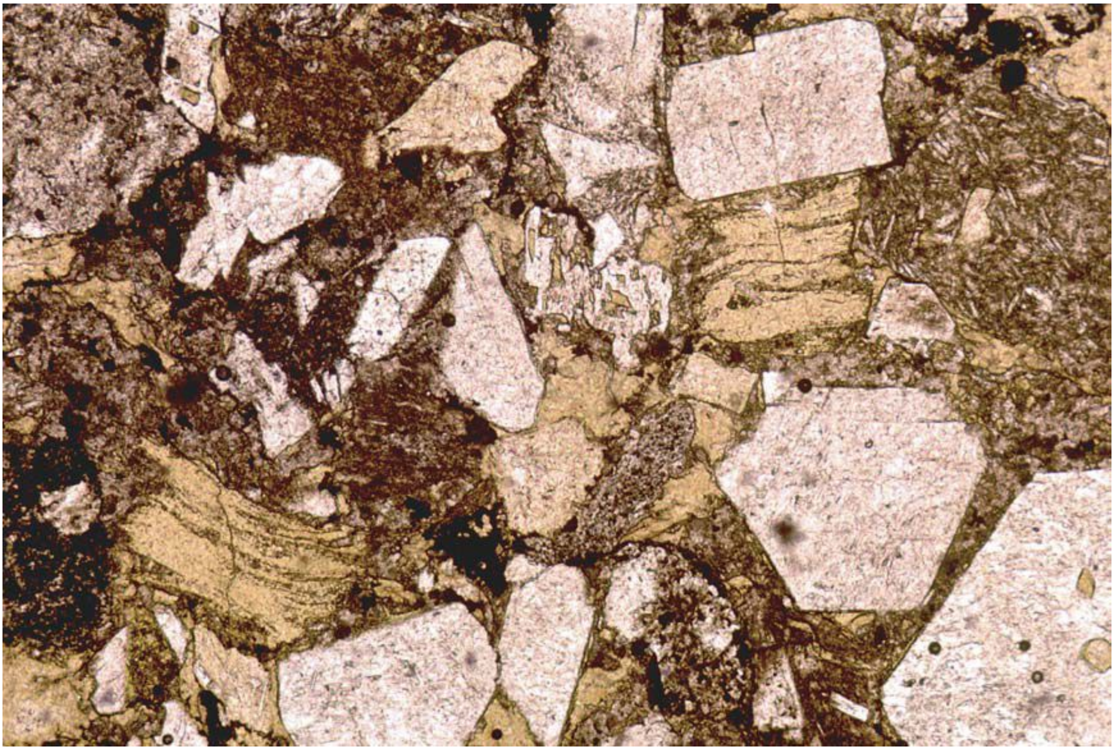

Fig. 2.5: (A) Poorly sorted volcanic sandstone ('greywacke') consisting of angular fragments of quartz and plagioclase (some with remnants of crystal faces) and volcanic rock fragments, some with feldspar laths aligned in a magmatic flow structure (right), as discussed in Section 3.9, with a fine-grained chlorite-rich matrix (pale yellowish green). The presence of former glassy volcanic rock fragments with residual flow lines, in which the glass has been replaced by similar chlorite, suggests that the chlorite in the matrix may also have replaced volcanic glass fragments, after which it was squeezed between the clasts by compaction. Plane-polarized light; base of photo 2.8 mm. (B) Same field of view. The almost isotropic nature of the matrix is due to the abundance of very fine-grained chlorite, with a low birefringence, and not unaltered volcanic glass. Crossed polars; base of photo 2.8 mm.

hard that it resists rounding in all sedimentary environments except high-agitation areas, such as beaches and wind dunes. Fragments that are not transported very far tend to have angular shapes (Fig. 2.10), whereas fragments transported over long distances and/or rubbed together in energetic water environments (such as waves) tend to have more rounded shapes (Figs 2.1, 2.7, 2.8).

Elongate grains (said to have a *low sphericity*) may be well rounded, and equant grains (*high sphericity*) may be angular. Roundness may also be inherited from grains in parent rocks, for example older sedimentary rocks with rounded quartz grains.

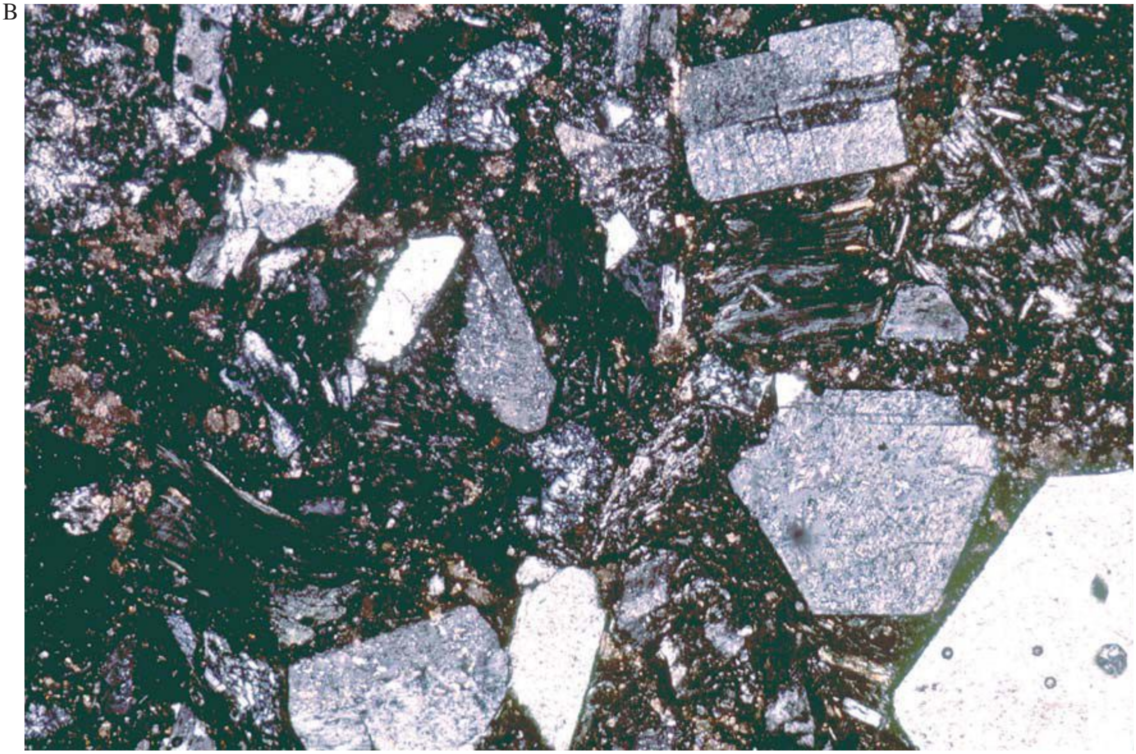

Fig. 2.5: (*cont.*)

2.2.4 Maturity

Epiclastic sediments may be classified on the basis of 'textural maturity'. *Immature* sediments have at least 5% matrix, with poorly sorted, angular grains; *submature* sediments have less than 5% matrix, with poorly to moderately sorted, angular grains; *mature* sediments have less than 5% matrix, with well-sorted, angular grains, and *supermature* sediments have no matrix, with well-sorted, rounded grains.

Catastrophic conditions, such as floods, coastal cyclones and mass-flows, are very unfavourable for sorting. For example, in mountainous areas, where the rain runoff and hence the erosion rate are very high, rock fragments of various sizes may accumulate with sand and soil in the lower regions as alluvial fans. Similarly, mass-flows in submarine canyons at the edge of a continental shelf dump poorly sorted material in turbidite fans. In addition, transport of sediment by ice in alpine glaciers does not involve much sorting or abrasion, so that fragments deposited in glacial moraines tend to be poorly sorted and angular.

Fig. 2.6: Clast of formerly glassy volcanic rock with embayed phenocrysts of quartz and smaller phenocrysts of altered feldspar, the glass having been replaced by very fine-grained chlorite (green). Embayments are common in volcanic phenocrysts, and so are relatively good indicators of volcanic source rocks. A few of the quartz clasts in this rock also show embayments, suggesting former volcanic phenocrysts (Section 3.13). Plane-polarized light; base of photo 5.2 mm.

2.2.5 Cement

Loose sediment is deposited in beds in subsiding areas of Earth's crust. As the sediment becomes buried, it is compacted, and groundwater begins to circulate through the spaces between the particles. Chemical compounds dissolved in this water may be precipitated as new minerals (*cement*) in spaces between the fragments, forming a solid sedimentary rock by cementing the clasts together (Figs. 2.1–2.4, 2.7, 2.8, 2.12).

The most common cement minerals are silica minerals (quartz, chalcedony, opal), carbonates (calcite, aragonite, dolomite, siderite), hematite, 'limonite' (hydrated iron oxides), chlorite and clay minerals (especially kaolinite). Cement should be contrasted with matrix (Section 2.2.2). Clay from outside the site of deposition and either deposited at the same time as the larger fragments (during

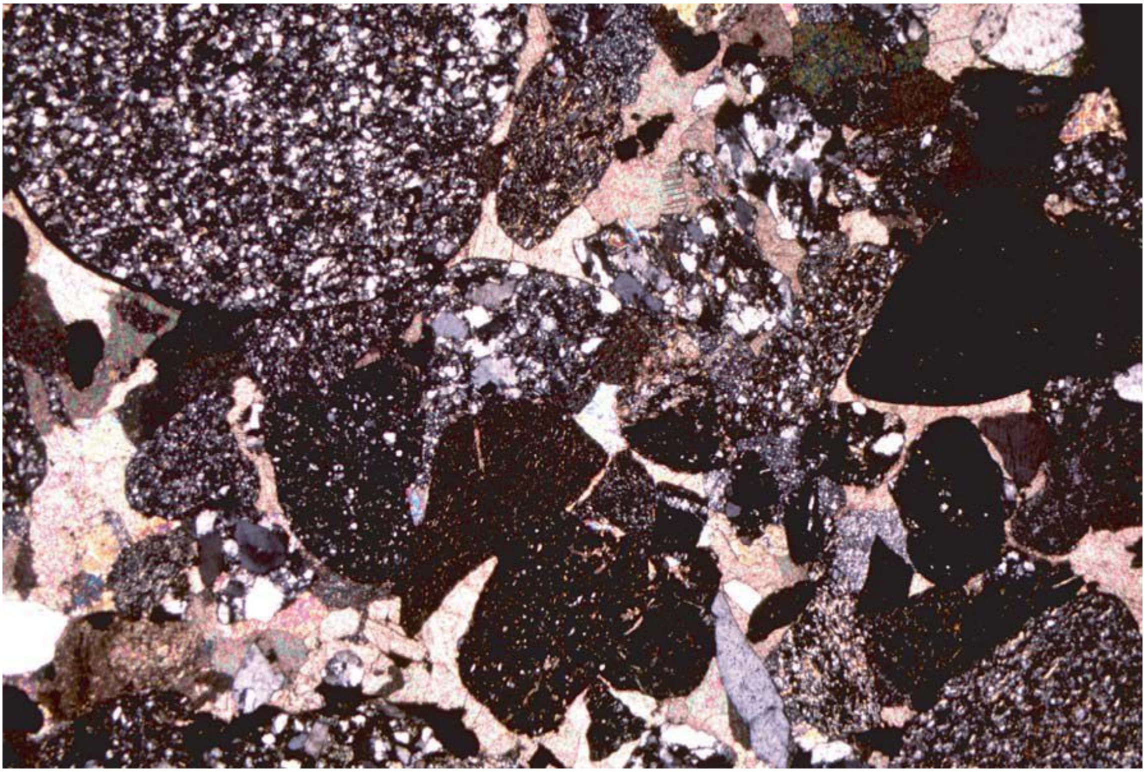

Fig. 2.7: Poorly sorted volcaniclastic conglomerate (sandy conglomerate) composed mainly of rounded clasts of volcanic rocks, cemented by very large grains of calcite (compare with Fig. 2.13). Crossed polars; base of photo 5.2 mm.

rapid deposition) or mixed with sand by bioturbation (churning by burrowing animals) forms a matrix between the larger clasts. This is called *allogenic* clay, in contrast to *authigenic* clay minerals, which are either precipitated chemically as a cement or formed by replacement of chemically unstable minerals, such as feldspar. Cement and matrix can coexist in coarser-grained, poorly sorted rocks consisting of larger clasts and finer-grained matrix, with cement-filled spaces between the larger fragments in the matrix.

In some rocks the cement grains are at random (Fig. 2.7), whereas in others they are arranged perpendicular to the clast surfaces, forming a kind of miniature vugh ('micro-vugh') structure (Section 5.9.3), as shown in Figs. 2.2 and 2.8. In other rocks, cement minerals (e.g., calcite) may occur locally as radiating aggregates (Fig. 2.12). Some cement minerals, especially quartz, nucleate in the same crystallographic orientation as clasts of the same mineral (epitactic nucleation; Section 4.3.1), forming *overgrowths*, the process being known as secondary enlargement (Figs. 2.1, 2.13). The overgrowth continues until the

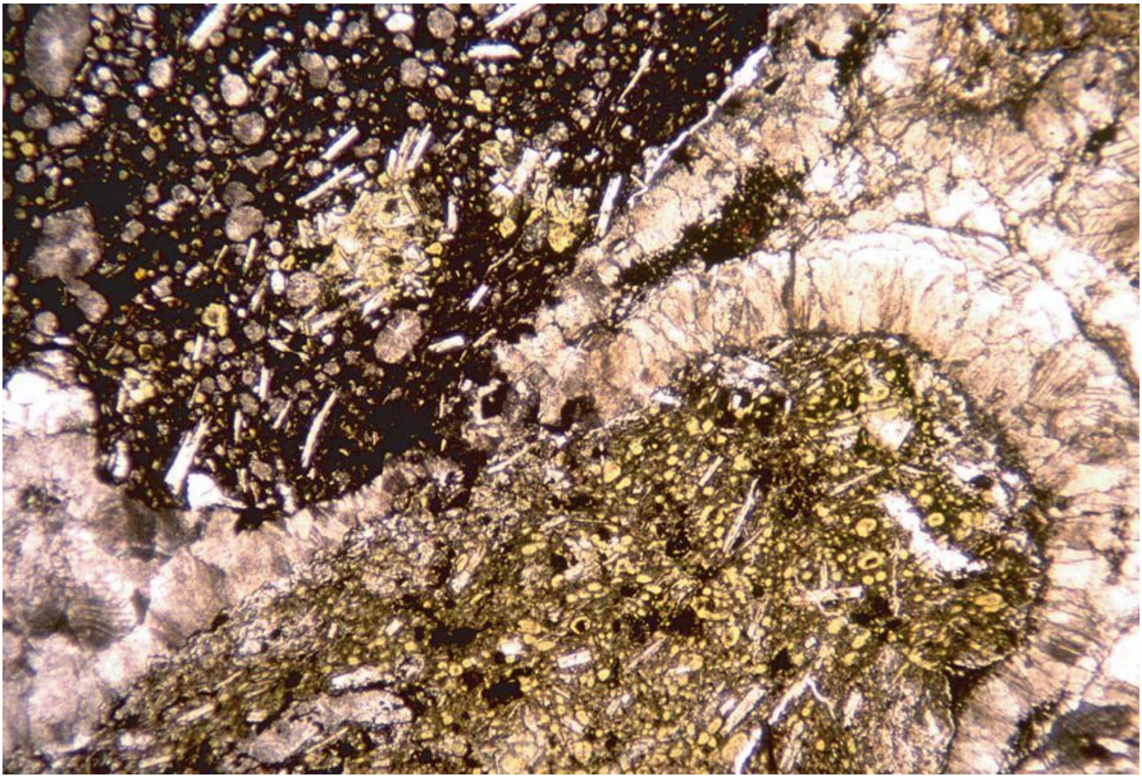

Fig. 2.8: Volcaniclastic conglomerate composed mainly of rounded clasts of amygdaloidal volcanic rocks, cemented by calcite grains that nucleated on the clasts and grew inwards towards the centres of the cavities between the clasts, forming a vugh-like microstructure. Plane-polarized light; base of photo 11 mm.

pores are filled, forming a mosaic of cement grains or ‘overgrowth cement’, the resulting new grains (fragments plus their overgrowths) tending to have polygonal shapes (Figs. 2.1, 2.13). The shapes of the original detrital grains are commonly outlined by minute inclusions (e.g. clay flakes or iron oxide particles). Quartz sandstones cemented in this way are called *orthoquartzites*, which should be distinguished from *metaquartzites*, which are formed by recrystallization of quartz sandstone under metamorphic conditions (Section 4.2), and which do not show overgrowths.

If the nucleation rate is low, the cement grains may be few but very large, each one cementing many clasts (Figs. 2.3, 2.7, 2.13). Common examples are calcite and gypsum in well-sorted quartz sandstones, but the situation may also occur in volcanic sandstones and conglomerates (Fig. 2.7). Commonly the cement crystals are large enough to show up in freshly broken hand specimens as shiny cleavage surfaces (‘lustre mottling’).

Fig. 2.9: Shale from the Wianamatta Group, Sydney area, New South Wales, Australia, showing flakes of clay minerals and/or mica aligned parallel to the bedding. Plane-polarized light; base of photo 2.8 mm.

2.2.6 Source of sediment (provenance)

Pebbles in conglomerates and sand grains in sandstones may indicate what types of original rock were broken down to form the sediment. For example, the clasts in the sandstones of Figs. 2.3 and 2.12 and the conglomerates of Figs. 2.7 and 2.8 are mainly fragments of volcanic rocks, indicating that volcanoes were eroded to produce the fragments. Conglomerates are especially useful for determining provenance, because coarse-grained rocks, such as granites and high-grade metamorphic rocks, can be preserved as pebbles.

Sandstones containing fragments of quartz and feldspar imply coarse-grained quartzofeldspathic source rocks, such as granite or felsic gneiss, because weathering and abrasion can only make original grains smaller. Microcline (Fig. 2.2) suggests deformed granitic parent rocks (Sections 5.7.6, 5.7.9). Some microstructures of quartz clasts are distinctive enough to suggest broad parent rock-types. For example, embayed quartz grains (Section 3.13) indicate volcanic parent rocks (Fig. 2.6), which are best preserved in pyroclastic and

Fig. 2.10: Two dark mudstone chips (rip-up clasts) in a poorly sorted volcaniclastic sandstone with predominantly angular fragments and an altered clay (possibly former fragmental glass) matrix from the Abercrombie River, central western New South Wales, Australia. The incompletely consolidated nature of the mudstone clasts when they were incorporated in the sediment is indicated by their indentations by the other clasts. Plane-polarized light; base of photo 5.2 mm.

Fig. 2.11: Diagrams showing the main grain shape variations in clastic sedimentary rocks.

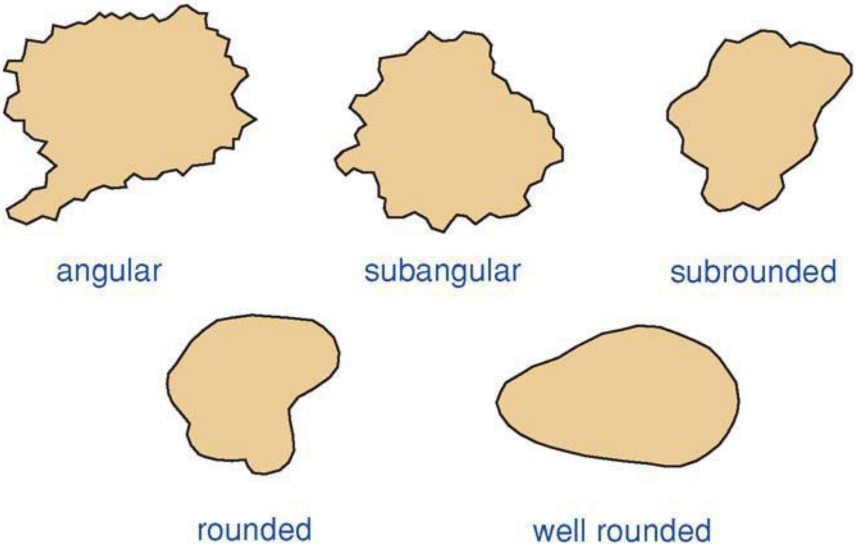

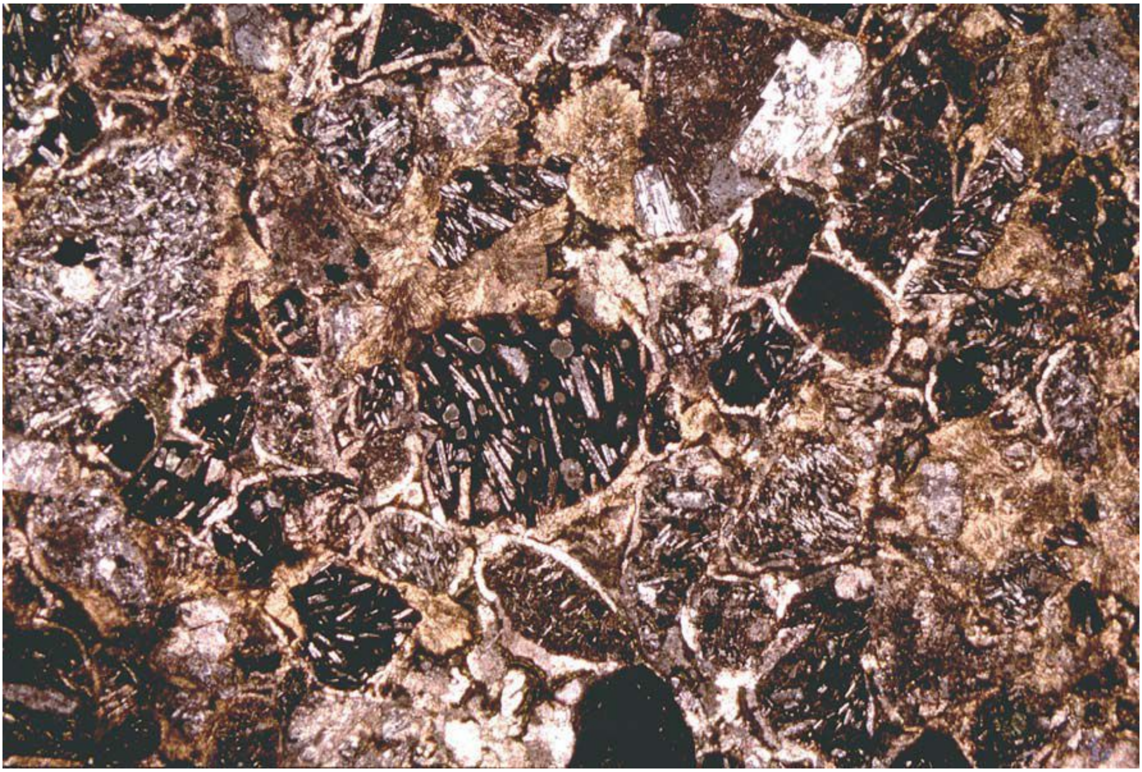

Fig. 2.12: Volcanic sandstone from the Illawarra area, south of Sydney, New South Wales, Australia, consisting of volcanic rock fragments (many of which show alignment of feldspar laths, reflecting flow of lava; Section 3.9) cemented by calcite, which locally occurs in radiating aggregates. Crossed polars; base of photo 5.2 mm.

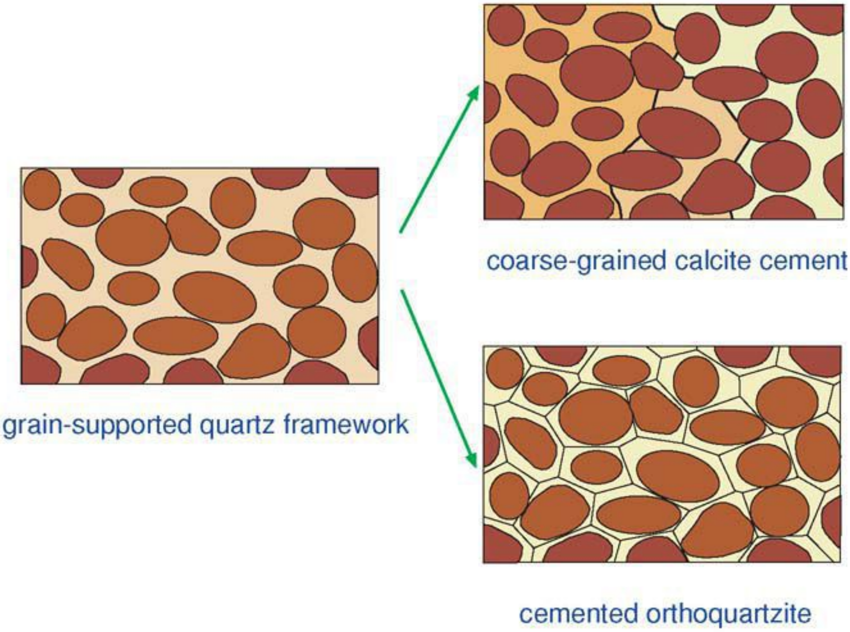

Fig. 2.13: Diagrams showing cementing overgrowths (secondary enlargement) on detrital grains, as with quartz in quartz sandstones (compare with Fig. 2.1) and cement formed by very large grains of calcite ('poikilitic microstructure', 'lustre-mottling').

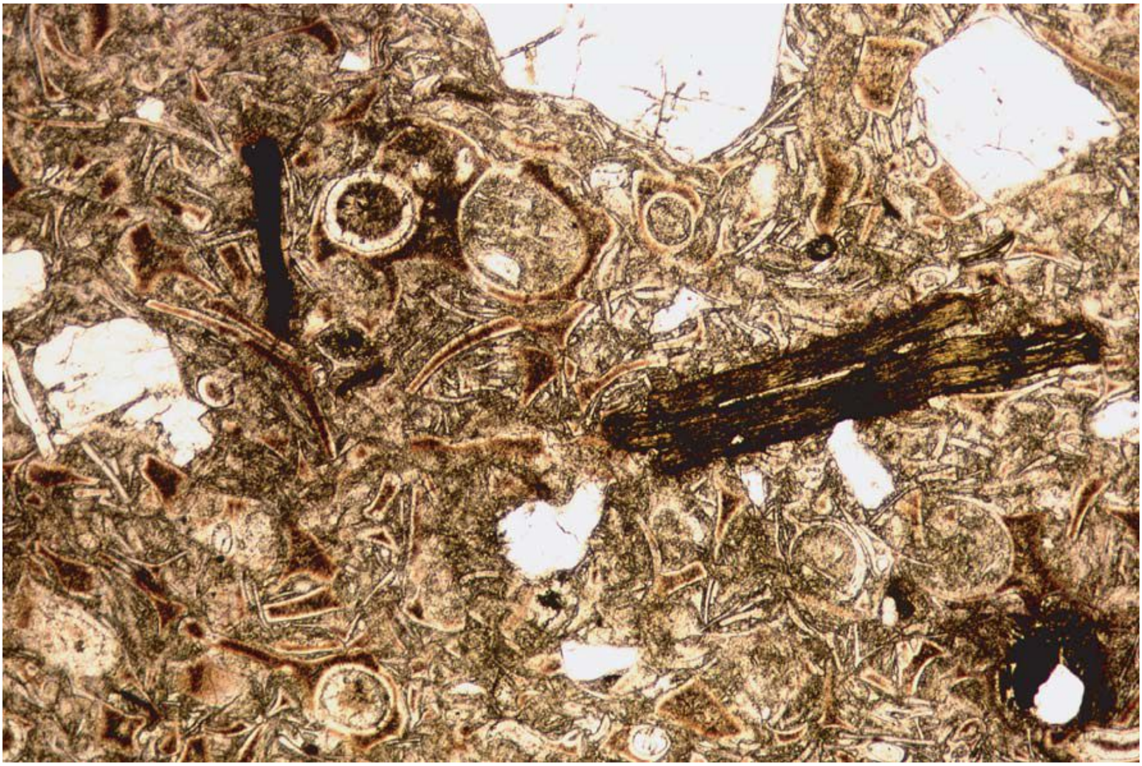

Fig. 2.14: Carboniferous ash-fall tuff from the Hunter Valley, New South Wales, Australia, composed mainly of glass and phenocryst fragments (quartz, feldspar and deformed biotite) ejected in an explosive eruption. The fragments (glass shards) were formed by fragmentation of pumice (Fig. 3.95), the curved edges, sharp corners and Y-shapes reflecting former vesicles in the pumice. A few small pumice fragments with one or two gas bubble holes are present. The glass has been replaced by hematite (reddish brown) and zeolite (colourless). Plane-polarized light; base of photo 4.4 mm.

volcaniclastic sediments, and strongly deformed quartz with the microstructural features described in Sections 5.3 and 5.4 (such as subgrains and recrystallization) indicates a regional metamorphic terrane (Fig. 2.4). Clasts made up of parallel, elongate quartz grains may have been derived from quartz veins in a regional metamorphic source region (Section 5.9.3).

Because weathering tends to break down minerals that are less stable in Earth's atmosphere, many sediments contain only a few of the minerals present in the source rocks. However, some of the minor minerals in the source rocks are relatively resistant to erosion and transport, and are deposited as dispersed grains or concentrated layers of 'heavy minerals', which may be general indicators of parent rock-types. For example, garnet and staurolite indicate metamorphic source

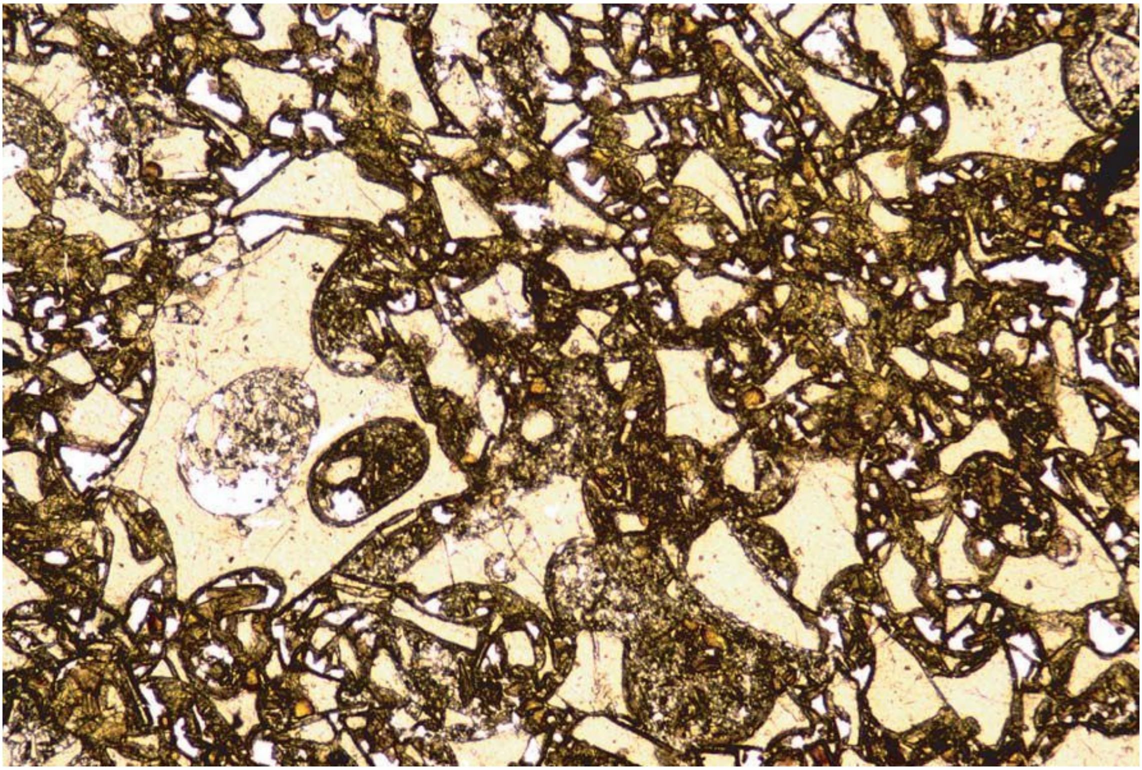

Fig. 2.15: Mafic tuff from Iceland, consisting of curved angular fragments (shards) of basalt glass that has been altered to submicroscopic chloritic aggregates. The larger clasts have gas bubble holes that have become filled or partly filled with small fragments. The sizes and shapes of the bubble holes in the large clasts have evidently controlled the shapes of the larger shards. Plane-polarized light; base of photo 4 mm.

rocks, chromite indicates ultramafic source rocks, and tourmaline and topaz are consistent with granitic or metamorphic source rocks.

2.2.7 Diagenetic changes

Minerals formed after deposition of the detrital (allogenic) materials are said to be authigenic. Some authigenic minerals (e.g. cement minerals) are deposited from aqueous solution, but many are formed from low-temperature reactions involving detrital material, the process bring called *diagenesis*. For example, volcanic glass clasts (Section 2.2) may alter ('neocrystallize') to clay minerals, chlorite or zeolites (Figs. 2.3, 2.5, 2.6), and detrital clay minerals may dehydrate and alter to chlorite and/or white mica. These reactions are very common in the matrix of sandstones. Another example of a post-depositional change

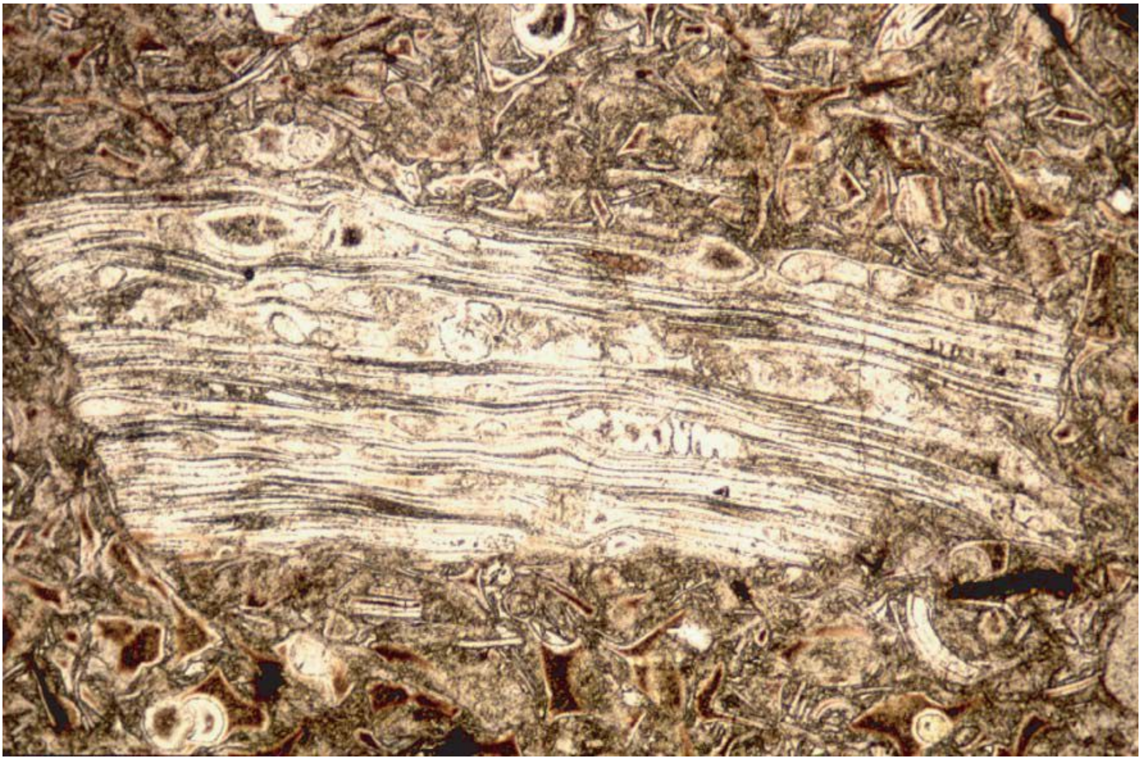

Fig. 2.16: Carboniferous ash-fall tuff from the Hunter Valley, New South Wales, Australia, similar to that shown in Fig. 2.14, but showing a large clast of highly vesicular glass with flow structure (Section 3.9). From Vernon (2000b, fig. 86). Plane-polarized light; base of photo 4.4 mm.

is the replacement of fragmental volcanic glass by opaline silica or silica gel, which are eventually replaced by very fine-grained quartz, forming a variety of *chert*.

Some diagenetic changes occur in sediments even before they are buried, for example recrystallization of aragonite to calcite and the alteration of some clay minerals to minerals such as glauconite, illite and chlorite. However, many diagenetic changes occur after burial, at considerable depths in the sedimentary succession, so that diagenesis grades into low-grade metamorphism (burial metamorphism). For example, zeolites replaced glass and detrital minerals in volcaniclastic sediments buried to depths of up to 15 km in Southland, New Zealand (Coombs, 1954; Turner, 1981). Identical minerals were formed at much shallower depth in volcaniclastic sediments in the Kiama area, south of Sydney, Australia, owing to geothermal heat in a subvolcanic region (Raam, 1968). These mineralogical changes are generally classified as belonging to the zeolite facies of regional metamorphism (Chapter 4).

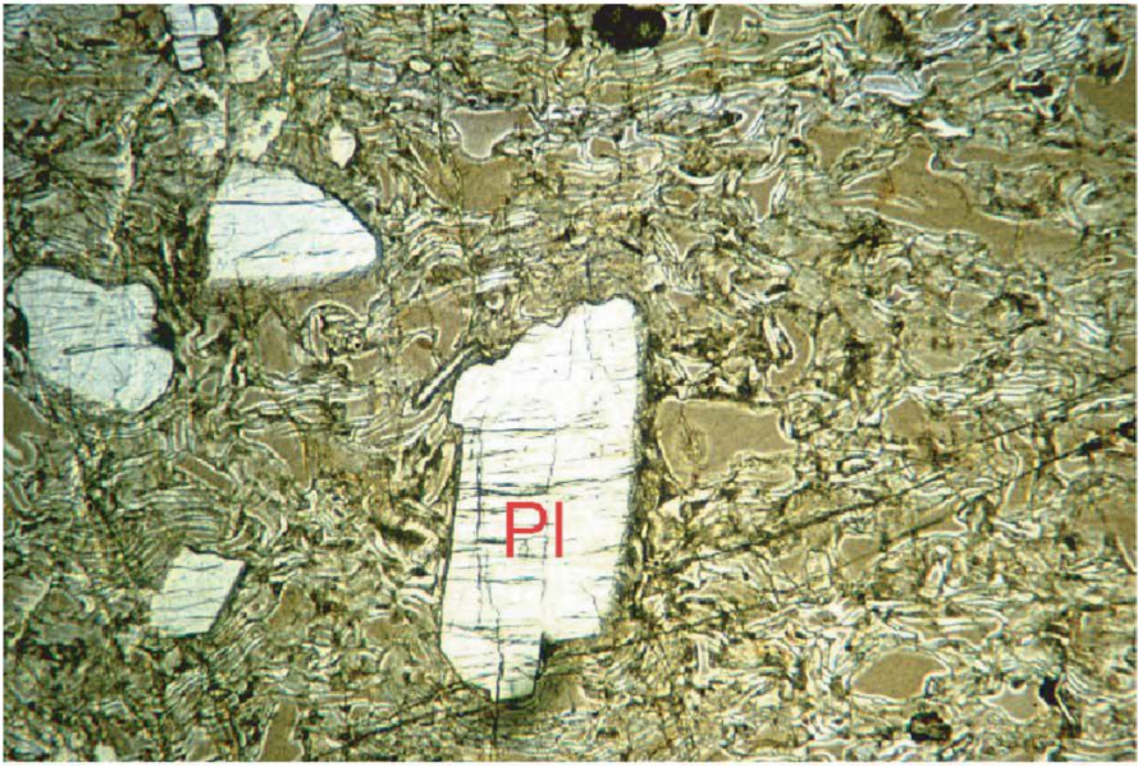

Fig. 2.17: Welded ash-flow tuff (ignimbrite) from Barraba, New South Wales, Australia, consisting of fragments of plagioclase (Pl) phenocrysts and abundant glass shards with rounded corners, owing to welding during cooling. From Vernon (2000b, fig. 92). Plane-polarized light; base of photo 3.5 mm.

Other possible products of diagenesis are pyrite framboids, which are rounded, porous, raspberry-shaped (hence the name) structures that occur in organic-rich sedimentary rocks of Precambrian to Recent age (see, for example, Chen, 1978). They commonly range from 1 to 20 μm in diameter. Many of these framboids in sedimentary rocks have been inferred to be of early diagenetic origin (see, for example, Love & Amstutz, 1966); this interpretation is supported by the observation of pyrite framboids in recent sediment at the water–sediment interface, under reducing conditions (Park, 1969). Some have suggested that they are fossils, whereas others have favoured biogenic deposition. Close relationships in some rocks between framboidal and colloform (colloid-like) pyrite suggest chemical precipitation (Chen, 1978), and both structures have been produced by inorganic laboratory synthesis (Berner, 1969). SEM and TEM investigations reveal that many pyrite aggregates in sedimentary rocks contain structures indicative of microbial remains, including some aggregates superficially similar to, though different in detail from, typical pyrite framboids (Schieber, 2002).

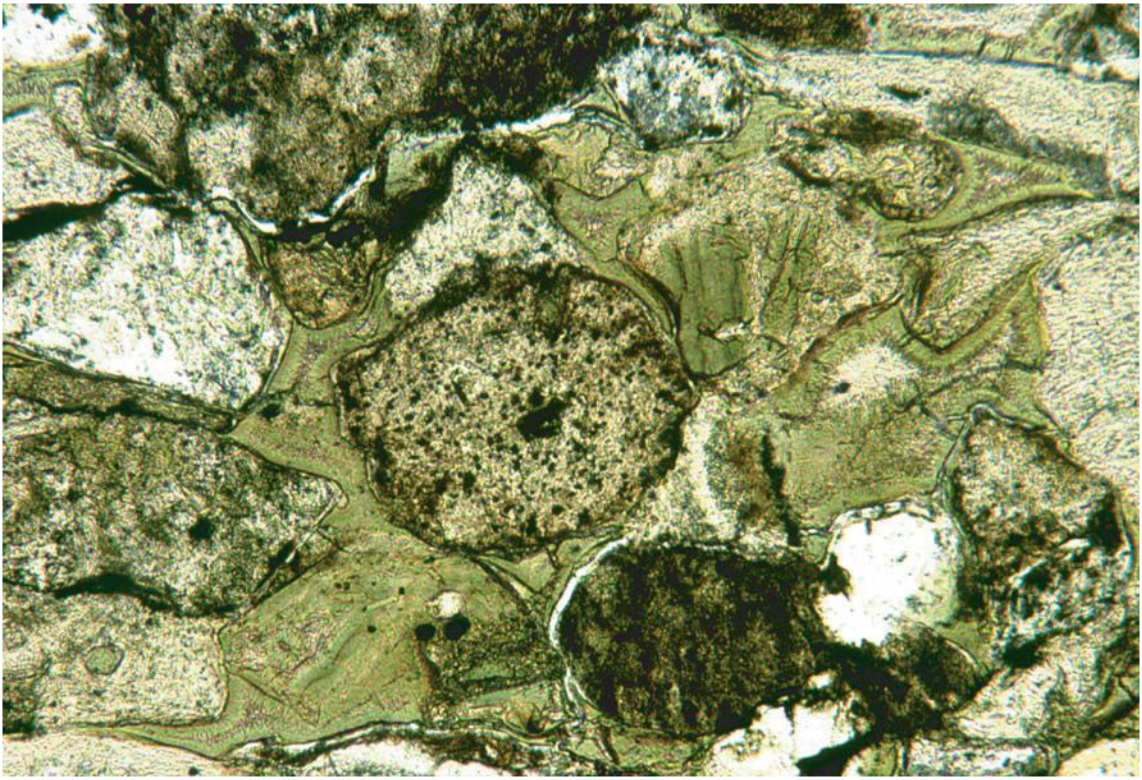

Fig. 2.18: Crystallization of chlorite as fibrous aggregates from the edges towards the centres of glass shards (axiolitic microstructure) in a tuff from Minchinbury, west of Sydney, New South Wales, Australia. Plane-polarized light; base of photo 1.3 mm.

2.3 Pyroclastic sedimentary rocks

Pyroclastic sediment is entirely of local volcanic provenance, and is deposited during explosive volcanic eruptions of predominantly felsic magma (Fig. 2.14), although intermediate and mafic magma may also produce pyroclastic rocks (Fig. 2.15). During these explosive eruptions, the lava solidifies and shatters into fragments, which may be scattered over large areas. The main reason for the explosive eruptions is that felsic magma is relatively rich in water (up to 10%). As the magma rises, cools and precipitates minerals (most of which don't contain water), the concentration of water in the melt increases, and begins to form bubbles of gas (superheated steam). The gas builds up pressure inside the magma trapped just below volcanoes, until the covering rocks fracture. The release of pressure allows the steam to escape suddenly.

During an explosive eruption, the escaping gas boils off, leaving the shapes of many small bubbles in the viscous lava, which cools and solidifies very rapidly, to form a glass froth called *pumice* (Fig. 3.95). The bubble holes may remain

A

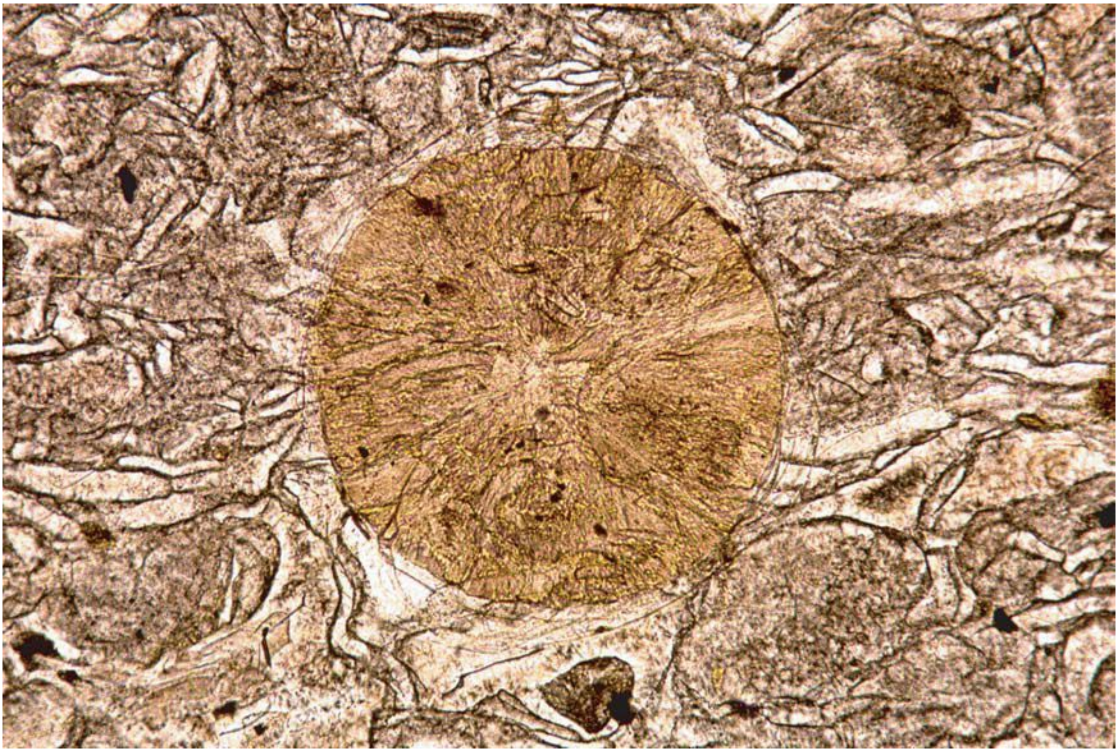

Fig. 2.19: (A) Spherulite (composed largely of fibres of alkali feldspar) that has replaced glass, preserving the shapes of the distorted shards, in an ignimbrite from the Hunter Valley, New South Wales, Australia. Presumably the spherulite fibres were able to grow at the same rate in all directions because all the fragments are of the same glass composition. The outlines of the shards are preserved probably because of minute inclusions or alteration products at their edges that were not needed by the growing feldspar fibres. Plane-polarized light; base of photo 1.5 mm. (B) Same field of view in crossed polars, showing the optical isotropism of the glass, as well as an extinction cross (Section 3.5.5) in the spherulite, caused by the optical extinction of feldspar fibres (each with one of its principal optical vibration directions parallel or nearly parallel to its length) that are approximately parallel to the vibration directions of the polarizer and analyser.

empty, but when hot watery solutions percolate along small cracks in the pumice for thousands or even millions of years, the holes may become filled with minerals precipitated from the solutions (Fig. 2.14). Filled vesicles are called amygdales or amygdules (Section 3.14.2).

During the eruption, the gas continues to escape so fast that it breaks the pumice into large lumps and small, sharp glass pieces or shards (Fig. 2.14). Crystals in the pumice that had crystallized from the magma when it was trapped below the surface and cooling slowly are also fragmented (Fig. 2.14). The high

B

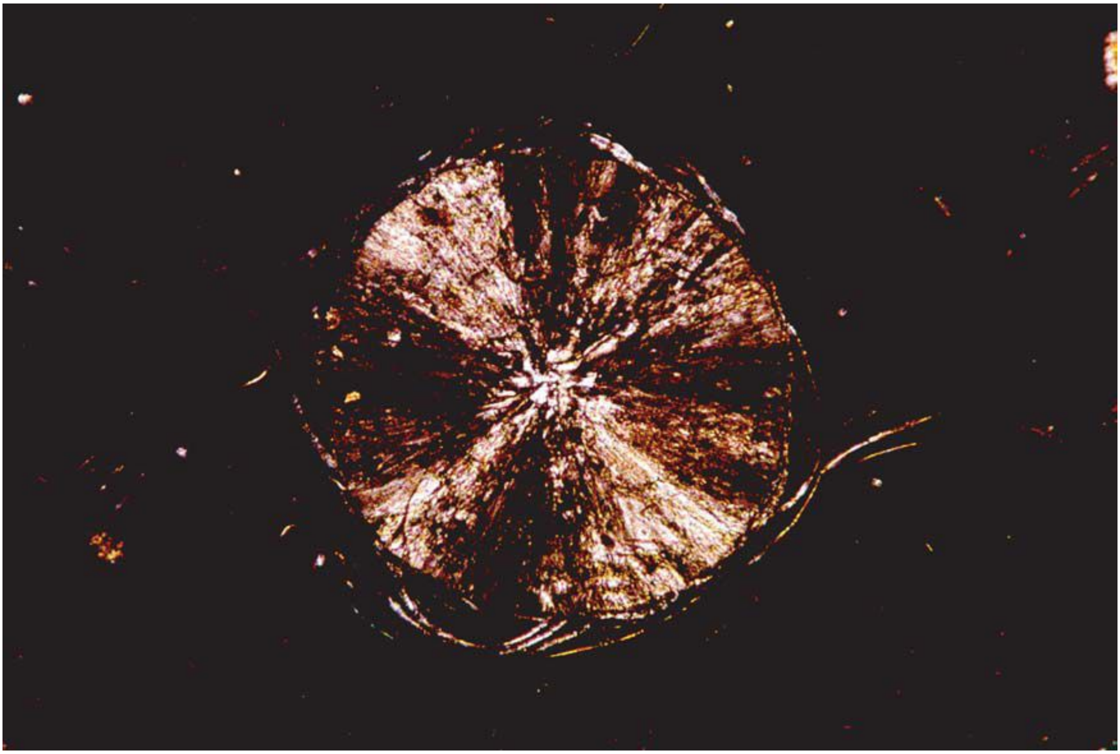

Fig. 2.19: (*cont.*)

gas pressure forces the mixture of glass fragments, pumice fragments, crystal fragments and gas high into the atmosphere. The glass and crystal fragments are mainly of sand size (Section 2.2.2), and are called volcanic ash. The falling ash, together with larger pumice fragments, forms a fragmental deposit called *ash-fall tuff*, in which the sharp-cornered, curved shapes of glass fragments can be seen with the microscope (Fig. 2.14). Some of the curved edges of these fragments may be the typical curved (conchoidal) fractures that glass produces when it breaks, but most of the Y-shaped curved surfaces probably represent glass walls at the junction of bubbles in the original pumice (see, for example, Ross & Smith, 1961), as suggested by Figs. 2.14 and 2.15. Ash-fall tuffs may show all stages from relatively large pumice or highly vesicular glass fragments, some of which have been stretched during the eruption (Fig. 2.16), through small chips in which only one or two bubble shapes are present, to individual shards (Fig. 2.14).

The high gas pressure may also blow out the side of the volcano, forcing the very hot mixture of glass fragments, pumice fragments, crystal fragments and gas to rush down the slopes at speeds of over 100 km h^{-1}. This is a fragmental flow, not a lava flow, and is called an *ash flow*. When the flow slows down, it deposits the ash as a thick deposit (ash-flow tuff, ignimbrite).

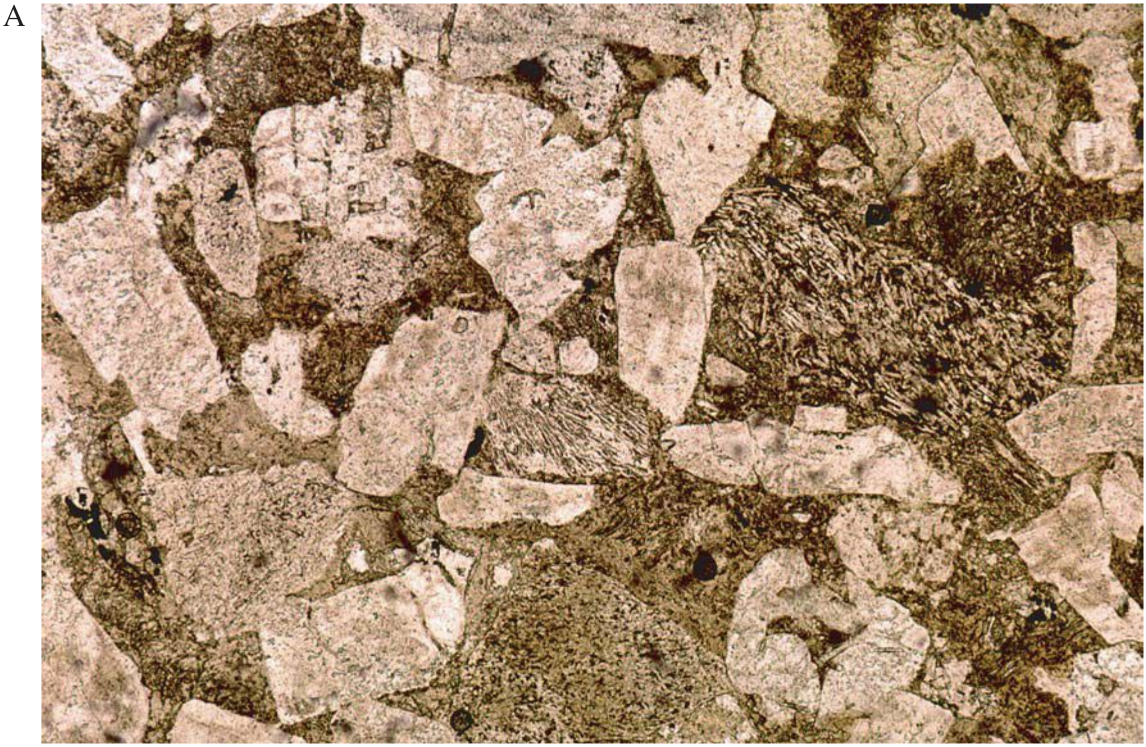

Fig. 2.20: (A) Volcanic sandstone (probably a reworked tuff) consisting of abundant clasts of former feldspar phenocrysts, many of which are euhedral, together with volcanic rock fragments and a chlorite-rich matrix showing shapes suggestive of former glass fragments. Plane-polarized light; base of photo 2.8 mm. (B) Same field of view in crossed polars, showing the almost optically isotropic matrix, which is due probably to the very fine-grained chlorite, not glass, although it may have been mainly glass originally.

Many ash flows are so hot when they come to rest that the still soft glass and pumice fragments become compressed and squashed together (Fig. 2.17). The flattened pumice fragments acquire distinctive lenticular shapes and are called fiamme, which is the Italian word for flames (the singular being fiamma). If the glass and pumice fragments become fused together by the heat and pressure, the rock is appropriately called a welded tuff. The formerly sharp glass fragments become rounded and squashed in the welding process (Fig. 2.17). Extreme flattening and slight flow may almost obscure the original clastic structure (Ross & Smith, 1961).

The glass and pumice fragments tend to crystallize (devitrify) with time, the glass being replaced by fine-grained crystal aggregates. Acicular (needle-like) crystals commonly grow perpendicular to the walls of the glass shards (a variety of axiolitic structure), as shown for a more mafic tuff in Fig. 2.18, and spherulites

Fig. 2.20: (*cont.*)

(Section 3.5.5) may also grow, preserving the shapes of the glass fragments (Fig. 2.19).

After initial accumulation, some reworking and redeposition of the pyroclastic material may occur, but provided this is not enough to change the shapes of the original particles (especially glass shards) or mix it with other sediment, the resulting sediment can still be called 'pyroclastic'. Otherwise, the sediment becomes epiclastic, and the more general term 'volcaniclastic' is appropriate. The rock shown in Fig. 2.20 may well be a reworked tuff, as it is clast-rich, but has residual glass shapes in the chlorite matrix.

2.4 Organic and bioclastic sedimentary rocks

Rocks composed mainly of calcite ($CaCO_3$) are called *limestones*. The calcite can be deposited directly from seawater to form *pelagic limestone* (Fig. 2.21), but usually is deposited in the shells of marine animals. In many skeletons and shells, the $CaCO_3$ is precipitated as aragonite (the orthorhombic polymorph), but it is less stable than calcite (the trigonal polymorph), to which it eventually changes, and so it is not found in old limestones. Fossil-rich limestones (Fig. 2.22) may be

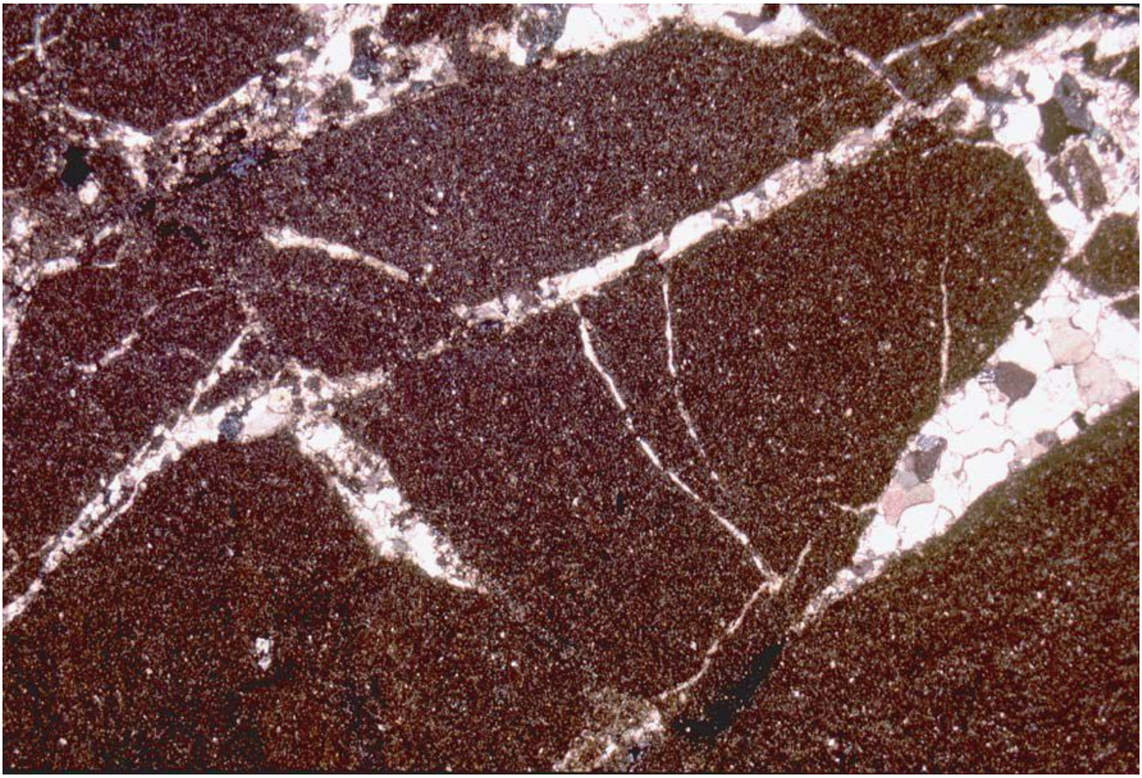

Fig. 2.21: Extremely fine-grained pelagic limestone (carbonate deposited directly from seawater) with later calcite veins. Crossed polars; base of photo 5.2 mm.

autochthonous, the skeletons remaining in the position of life and death without transport (e.g. in coral or algal reefs), or *allochthonous* (e.g. fragments eroded from reefs). In allochthonous limestones (*bioclastic limestones, calcarenites*), the skeletons or shells may be complete or broken into fragments (Fig. 2.22). Later the shells and fragments are cemented together, generally with more calcite. Fossiliferous limestones are named after the predominant fossil present, e.g. ‘crinoidal limestone’, ‘coral limestone’, or ‘algal limestone’. Microstructural details of shells can be seen clearly in thin section, the calcite or aragonite crystals generally being fibrous and aligned perpendicular or approximately parallel to the walls of the shells. Cavities in shells are commonly filled with relatively coarse-grained mosaics of authigenic calcite.

Calcareous rocks composed of dolomite, $CaMg(CO_3)_2$, are called *dolomites* or *dolostones*, and rocks with both calcite and dolomite are called *dolomitic limestones* or *calc-dolomites*. Generally some ankerite, $CaFe(CO_3)_2$, component is present in the dolomite. Dolomite can be distinguished from calcite in thin section by staining techniques. Because dolomite is not precipitated by organisms, most dolomite is probably formed by the replacement of calcite (‘dolomitization’).

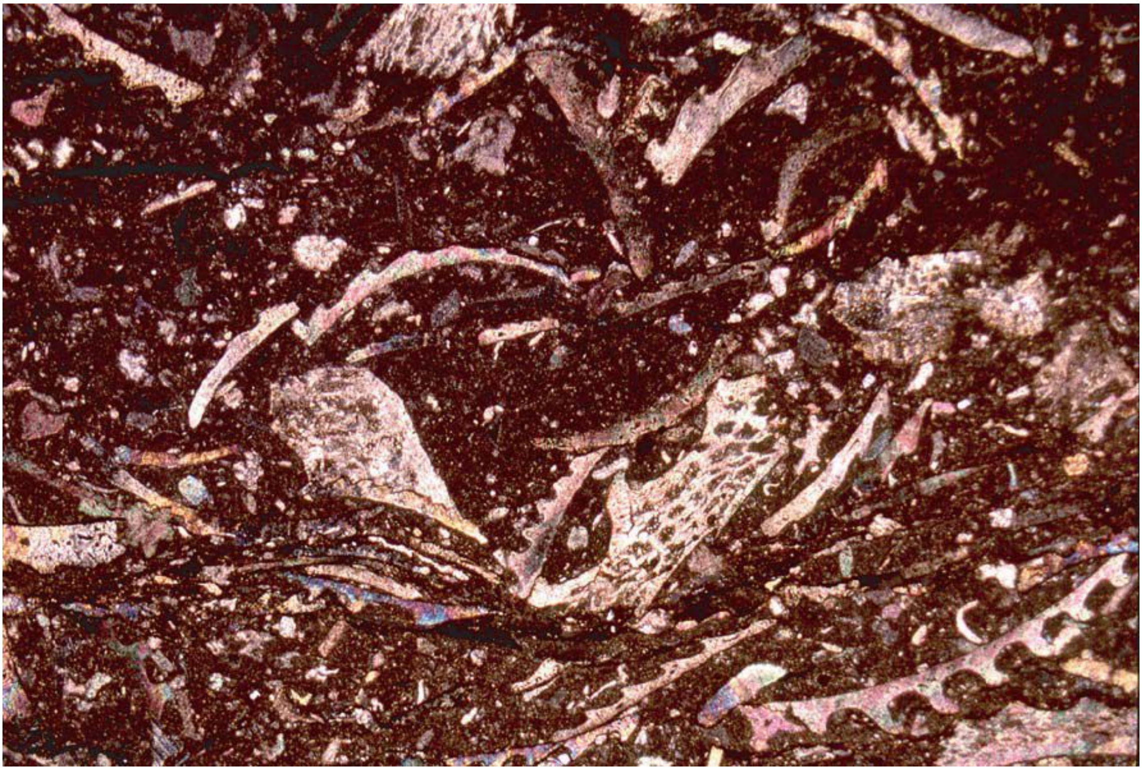

Fig. 2.22: Fossil limestone consisting mainly of fragments of mollusc shells in very fine-grained calcite mud. Crossed polars; base of photo 5.2 mm.

Some dolomite may be precipitated in highly saline lake and sea waters (e.g. in evaporite successions; Section 2.5), although replacement of earlier deposited calcite or aragonite is commonly a possible alternative interpretation. Much evidence of the replacement of calcite fossils by dolomite has been described, but dolomite filling cavities and veins is probably primary. Many dolomites consist mainly of polygonal aggregates or mosaics, without much microstructural evidence of their original nature.

Detrital minerals may also be mixed with the carbonate (Fig. 2.23), especially quartz and clay minerals, but also non-carbonate fossils, such as radiolarians, sponge spicules and diatoms, and pyroclastic fragments (Section 2.3). Limestones with high proportions of detrital material are called ‘impure limestones’, and at least 50% carbonate must be present for the term ‘limestone’ to apply. Non-carbonate authigenic minerals in limestones include quartz, chalcedony, gypsum, anhydrite, glauconite and pyrite. Very clay-rich carbonate rocks are called *marls*. Many limestones are very fine-grained, and form as chemically precipitated lime mud (Fig. 2.21), commonly mixed with introduced clay and silt.

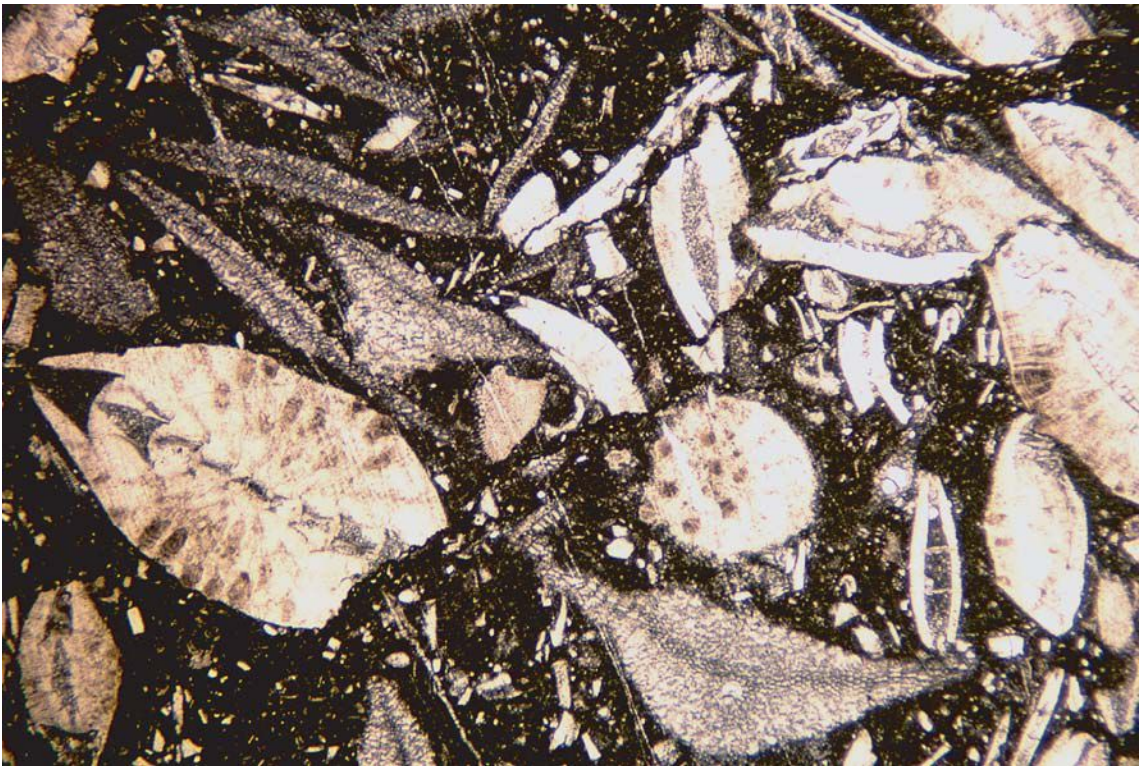

Fig. 2.23: Impure limestone (marl) from the Eocene of the Southern Pyrenees, Spain, consisting of fossil skeletons (mainly nummulites) in a clay–silt matrix. Many skeletons are truncated by dark seams (stylolites) formed by pressure-solution (Section 5.9.2). Sample by courtesy of David Durney. Plane-polarized light; base of photo 11 mm.

Impure (quartz and clay-bearing) limestones (Fig. 2.23) and dolomites produce spectacular metamorphic mineral assemblages when heated (Chapter 4).

Although limestones and dolomites consist mainly of authigenic carbonate, they have very variable and complex microstructures, owing to other contributing processes, such as fragmentation and detrital deposition of skeletons, addition of external detrital material, diagenetic recrystallization and organic accretion (e.g. the formation of ooids; Section 2.5).

2.5 Chemical sedimentary rocks

Chemical sediments are either (1) deposited directly from supersaturated aqueous solution, owing to chemical reactions or evaporation (e.g. in a land-locked lake), forming *evaporites*, such as halite-rock ('rock-salt') and gypsum-rock, or (2) formed by replacement of pre-existing sedimentary material (e.g. some cherts).

Fig. 2.24: Oolitic limestone, Lake Keepit area, north-western New South Wales, Australia. The limestone consists mainly of fossil shell and crinoid (sea-lily) fragments that probably accumulated in a lagoon near a coral reef being eroded by wave action. The dark rims of the ooids were formed by very fine-grained algal mud sticking to them as they were gently washed about in the lagoon. The shapes of the ooids are determined by the shapes of the original clasts. The fragments and ooids are cemented by calcite. From Vernon (2000b, fig. 111). Plane-polarized light; base of photo 1.8 cm.

Material formed in these ways is said to be *orthochemical*, but if it is moved and reorganized into new shapes by chemical, physical or biological processes within the depositional basin, it is said to be *allochemical*. Examples of allochemical sediment include *ooids* (ooliths), which are spherical accretions of chemically precipitated aggregates, and *faecal pellets*, which are rounded particles of carbonate mud produced by sediment-ingesting animals.

Limestones rich in ooid*s* are called *oolitic limestones* or *calcareous oolites* (Fig. 2.24). The ooids are spherical or ellipsoidal, and consist of calcite or aragonite deposited and accreted by chemical precipitation and/or physical plastering of carbonate mud in layers around nuclei, such as fossil fragments or sand clasts. Many ooids have shapes determined by the shapes of their nuclei (Fig. 2.24). They

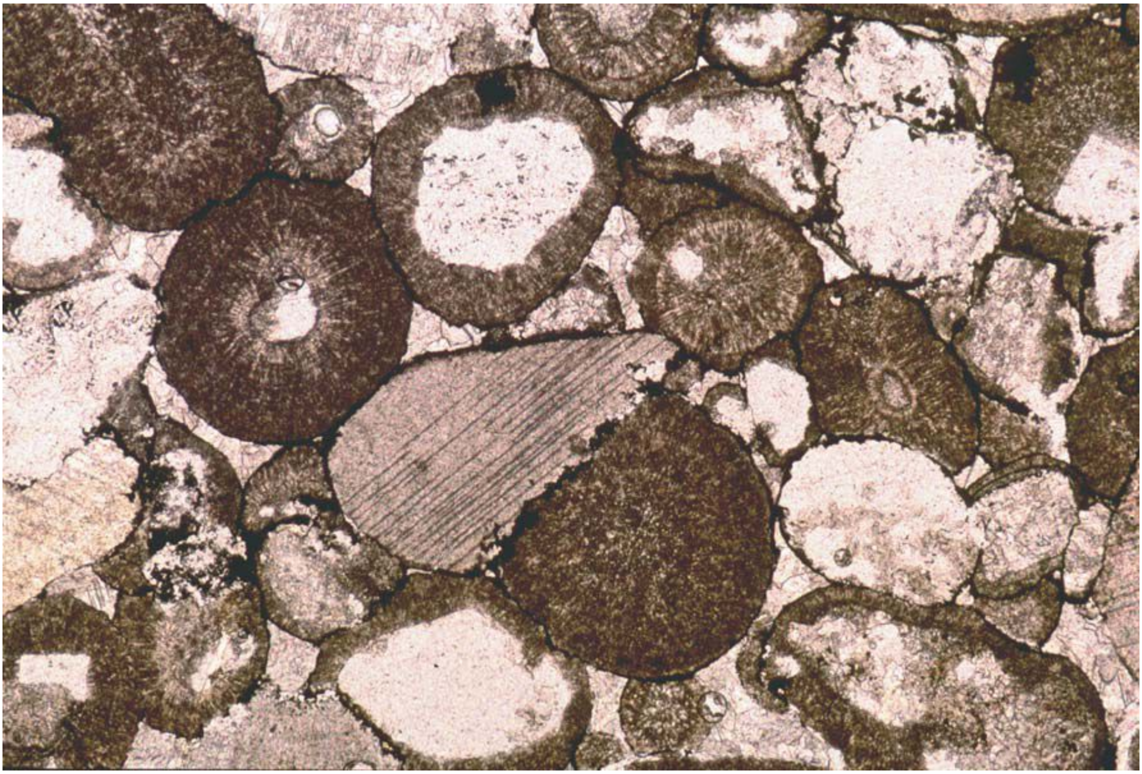

Fig. 2.25: Oolitic limestone, in which many of the ooids have a radial structure, cemented by calcite. Some calcite clasts are also present. Most of the ooids and the clasts meet along irregular solution surfaces, and some have been markedly truncated by stylolitic solution seams (Section 5.9.2). Plane-polarized light; base of photo 2.8 mm.

are generally well sorted. Some show radial microstructures (Fig. 2.25), which may result from recrystallization of ooids with concentric layering (Williams *et al*., 1954, p. 344; Boggs, 1992, pp. 428–29). Chlorite may also occur as ooids (Fig. 2.26).

In contrast to the separate particles of clastic rocks, chemical precipitates typically form aggregates of interlocking grains and crystals (Fig. 2.27). Crystals precipitating from a supersaturated solution commonly settle to the bottom of a sea or lake, where they continue to grow until they impinge, forming laminated microstructures or mosaics of grains. Mosaics may also be formed when fine-grained, chemically precipitated calcite or aragonite is replaced by coarser-grained dolomite (Section 2.4), although rhombic crystals of dolomite in a calcite matrix may result when the replacement is incomplete. Mosaics are commonly formed when anhydrite ($CaSO_4$) is replaced by gypsum ($CaSO_4.2H_2O$), although pseudomorphs of gypsum after anhydrite may also be present. Replacement may

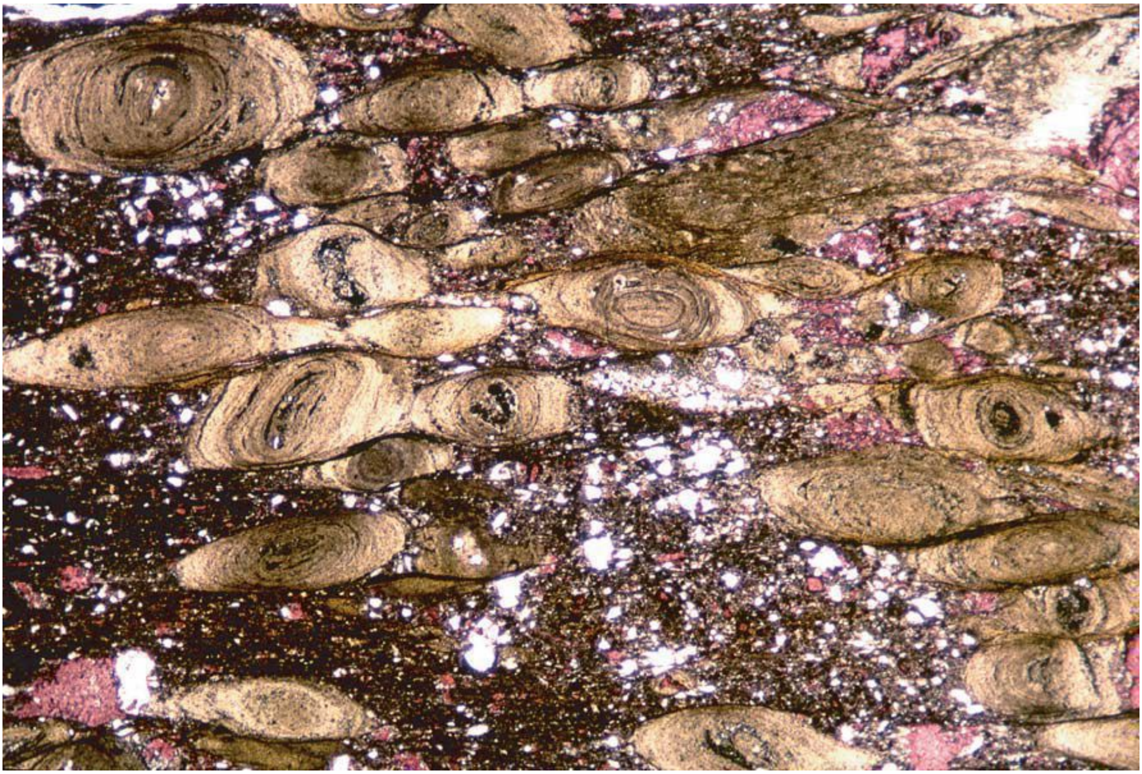

Fig. 2.26: Chlorite ooids in a calcareous shale from the Swiss Alps. The ooids have been distorted and elongated by deformation, and many have had their shapes truncated by solution seams (Section 5.9.2). The rock has been stained to reveal calcite (pink dye). Sample by courtesy of David Durney. Plane-polarized light; base of photo 4 mm.

also produce interpenetrating, radiating and even spherulitic aggregates of elongate crystals (Carozzi, 1960), as shown in Fig. 2.27.

The most common minerals in chemical sediments are carbonates, mainly calcite and dolomite (70–85%), quartz (10–15%), and mineral 'salts' (mainly gypsum, anhydrite, halite and sylvite). Gypsum in evaporites may be formed by replacement of anhydrite and *vice versa*. Many other mineralogical and microstructural diagenetic changes are typical of buried evaporites saturated with concentrated brine, because of the solubility and reactivity of the minerals involved. Some anhydrite and gypsum rocks may contain introduced sand, silt, clay and carbonate minerals.

Chemical processes can also contribute to residual (pedogenic) sediments, by precipitation of clay minerals, silica minerals, iron oxide minerals and carbonate minerals in small spherical accretions (*nodules*, *pisoliths*). Resulting rocks include pisolitic bauxite (composed of hydrated aluminium oxide minerals, as

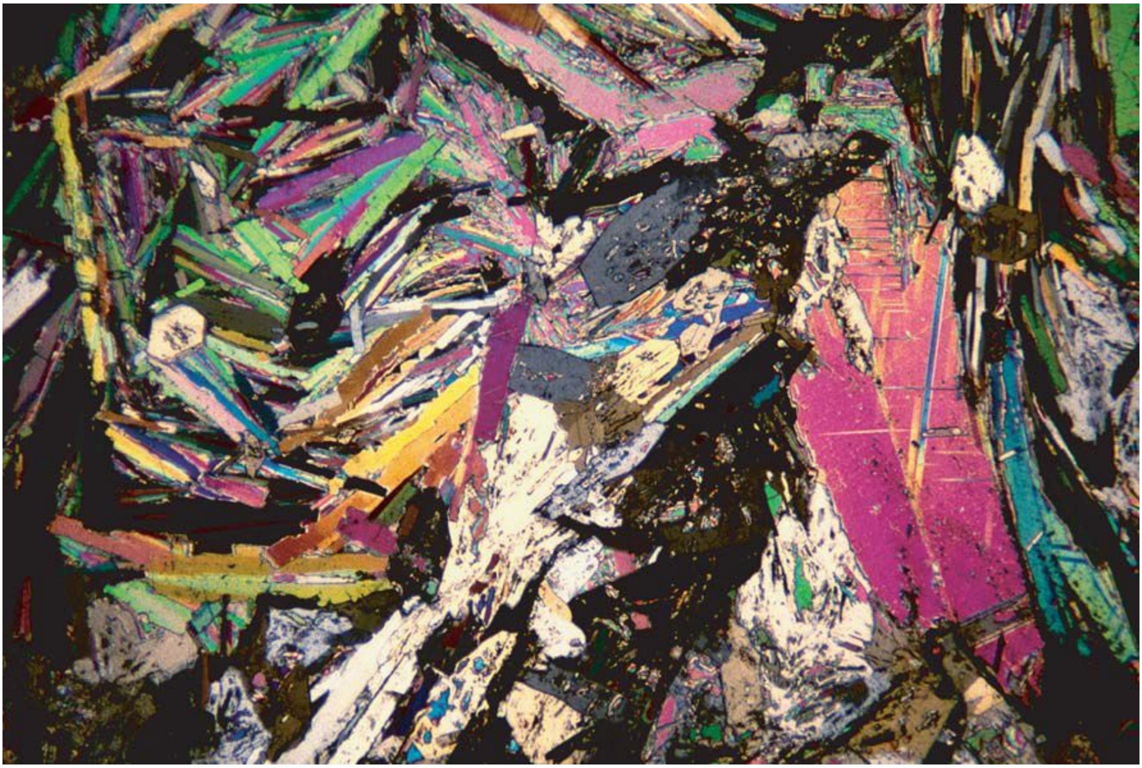

Fig. 2.27: Anhydrite, formed by displacive and replacive growth in clay–carbonate mud and calcareous rudite, Munta-1 exploration oil well, Tanana Formation, Ungoolya Group, Officer Basin, South Australia (Akouri *et al.*, 2000). Specimen by courtesy of Pat Conaghan. Crossed polars; base of photo 11 mm.

well as iron oxide and hydrated iron oxide minerals) and pisolitic caliche (carbonate minerals). The process involves fluctuating groundwater levels, leading to concentration and precipitation of dissolved chemical components by surface evaporation.

Other essentially chemically deposited sedimentary rocks are siliceous (cherts), ferruginous (ironstones) and phosphatic (phosphorites), with a wide variety of microstructures (including nodular, oolitic and finely granular) complicated by mixing with various other types of sedimentary material, as discussed by Pettijohn (1949) and Williams *et al.* (1954), among others.

Chapter 3

Microstructures of igneous rocks

3.1 Introduction

This chapter is concerned with the shapes of crystals and aggregates formed when melted rocks and glass crystallize, solid rocks melt, and melts boil. These processes are broadly grouped together as ‘magmatic (igneous) processes’.

As discussed in introductory geology courses, partial melting of solid rock to form *magma* occurs in Earth’s mantle, producing mainly *mafic* (basaltic, silica-poor) magma, and also in the deeper parts of Earth’s crust, producing mainly *felsic* (granitic, silica-rich) magma. Magma may reach the surface as volcanic rocks or solidify in the crust as intrusive rocks. Magma bodies may encounter other magma bodies and mix or mingle with them. Microstructures may preserve evidence of these and other processes, such as magmatic flow and conditions of crystallization, and in this chapter I present this evidence and discuss its reliability.

When a liquid becomes *supersaturated* with a dissolved chemical component (i.e. the dissolved component reaches a concentration at which the liquid can hold no more of the component in solution), a new phase theoretically is produced. A phase is a chemically and physically homogeneous part of a *system* (e.g. a body of magma) that is bound by an interface with other phases (e.g. the melt phase and other crystal phases in a magma). Generally, the new phase is a crystalline solid (which in rocks we call a mineral), and the phase change is called *crystallization* or *freezing*. However, if a magma becomes supersaturated with water or another volatile component, the new phase is a gas, and the phase change is called *boiling* or *vesiculation* (Section 3.14). Although even slight supersaturation should theoretically produce a phase change, this is generally delayed until a higher degree of supersaturation occurs, as discussed in Section 3.3.1.

Magmas freeze (solidify by crystallization) as they cool, because the solubility of chemical components in the melt decreases at lower temperatures. Because natural silicate melts are complex solutions, various chemical components saturate the melt at different temperatures, so that some minerals crystallize earlier than others. This leads to an *order of crystallization*, which is determined by melting experiments on the magma composition concerned, but which generally cannot be determined by inspection with the microscope (Section 3.6). Magmas may also crystallize in response to sudden loss of water (Sections 3.4.4, 3.4.7) or changes in pressure.

The complexity of magmas and their individual histories — potentially involving changes in temperature, pressure and water content, as well as mixing with other magmas (Section 3.10.3) and contamination with foreign crystals (Section 3.10.2) — implies that most of the following explanations are only broadly applicable. Each body of magma requires individual, detailed investigation to work out its crystallization history.

3.2 Structure of silicate melts and glasses

The atomic structure of silicate melts determines several major features of igneous rocks, namely: (1) the rate of flow of magma, (2) the explosiveness of volcanic eruptions, (3) the rate of crystallization (and hence the grainsize), and (4) the extent to which glass is formed during rapid cooling (Section 3.5.6). Therefore, at least a basic idea of melt structure helps to understand many magmatic processes.

Theoretical and X-ray diffraction studies have indicated that the atoms in silicate melts (the liquid parts of natural magmas) are bound together in extensive networks (polymerized) to varying degrees, depending on the composition of the melt (see, for example, Hess, 1980, 1995; Mysen, 1988, 1999, 1980a,b, 1981a,b). This polymerization applies especially to O–Si and O–Al bonding. Silicate melts consist essentially of linkages of Si^{4+} and Al^{3+} ions with four O^{2-} ions. In view of the large amount of SiO_2 in most igneous rocks, the degree of polymerization depends largely on the O : Si ratio of the melt. Melts with higher O : Si ratios (as in mafic or basaltic magmas) tend to consist mainly of separate $[SiO_4]^{4-}$ groups (tetrahedra), without much polymerization, although X–ray evidence of isolated silicate chains has been obtained for melts of pyroxene composition. Such relatively silica-poor melts tend to be relatively fluid, as evidenced by extensive basalt lava flows, and gas escapes relatively easily from them, as evidenced by the relatively weakly explosive nature of basalt volcanic eruptions.

However, melts with lower O : Si ratios (as in felsic or granitic magmas) have more Si–O bonding, so that more continuous silicate networks are formed, increasing the viscosity (stiffness) of the melt. The result is that felsic magmas, being viscous, flow for relatively short distances or plug the vent of the volcano. Moreover, because gas escapes much less readily from viscous magmas, felsic volcanic eruptions are commonly very explosive, producing fragmental (pyroclastic) rocks (Section 2.3).

Melts of pure SiO_2 composition (i.e. with the lowest O : Si ratios of all) are strongly polymerized and show diffuse X-ray peaks similar to the main peaks of cristobalite, a high-temperature polymorph of SiO_2 (Hicks, 1967). Although the degree of linking of their $[SiO_4]^{4-}$ tetrahedra is very high, the arrangement of the tetrahedra is not as regular as in crystalline silica. When a pure silica melt changes to a glass by very rapid cooling (Section 3.5.6), very little rearrangement of the Si–O network is required (Brückner, 1983).

3.2.1 Effect of melt structure on crystallization

Poorly polymerized (Si-poor) melts crystallize more readily than polymerized (Si-rich) melts (see, for example, Kirkpatrick, 1983). In fact, experimental quenching of liquids of ultramafic composition, without the formation of at least some small crystals, is very difficult or impossible. Melts of basalt composition can be cooled quickly without crystallizing, as evidenced by natural occurrences of basaltic glass (*tachylite* or *tachylyte*). However, this is much less common than natural glass (Section 3.5.6) of SiO_2-rich composition (*obsidian*), and industrial glasses generally are SiO_2-rich.

Although glasses have the rigidity of solids, they have atom arrangements more like those of liquids. In this sense, they are supercooled (undercooled) liquids, having a high degree of polymerization, which accounts for their rigidity. The polymerized structure of Si-rich melts enables them to pass relatively easily from a liquid to a glassy state on rapid cooling, despite the fact that the crystalline state has a lower free energy than glass at low temperatures. In fact, glass is metastable, with respect to crystals of equivalent composition. Because of this, glass tends to change into the lower-energy crystalline state with time. However, this involves breaking strong Si–O and Al–O bonds, and can take place only if some other factor permits the necessary energy barriers to be surmounted. Possible factors include reheating of the glass (e.g. following burial of volcanic glass) and water, which tends to break strong Si–O bonds and which can be added to volcanic glass along cracks, after burial, especially in pyroclastic rocks (Section 2.3).

3.2.2 Effect of volatiles on viscosity and crystallization of magmas

Volatile components in the melt, especially water and fluorine, cause disruption of O–Si bonds and a reduction in polymerization. This is because ions such as $(OH)^-$ and F^- substitute for O^{2-} ions. Whereas each O^{2-} ion links to two Si^{4+} ions, $(OH)^-$ or F^- ions can link to only one. Thus, $(OH)^-$ and F^- ions break polymerized Si–O groups. This decreases the viscosity of the melt, because the remaining Si–O groupings become independent and so can move more easily. Therefore, volatile components, especially water (present as hydroxyl ions) can have a large effect on the viscosity and flow of silicate magmas. For example, although water dissolved in a felsic melt reduces the viscosity and so helps the magma to move through the crust, once the water escapes as gas (steam), owing to reduction in pressure at or near Earth's surface, the melt becomes very viscous, with the result that felsic lava flows with great difficulty. In fact, the rapid escape as steam of the relatively large amounts of water in felsic magmas contributes strongly to the explosive nature of most felsic volcanic eruptions.

Volatiles also decrease the rate of formation of crystals. Because the O–Si networks are disrupted, the atoms and atomic groupings can less easily coalesce to form crystal nuclei (Section 3.3.1). This applies especially to felsic melts, which are richer in water than mafic melts. The effect is particularly pronounced in felsic melts with unusually abundant water and other volatile components (e.g. F, B, Li), which commonly crystallize as rocks with very large grainsizes, called *pegmatites* (Section 3.4.6).

3.3 Crystallization (freezing) of magma: nucleation and growth

3.3.1 Nucleation

Crystallization of liquids does not take place by the co-operative action of all atoms present. Instead, local thermal, compositional or deformational fluctuations enable small aggregations of atoms of the new crystal to occur with a minimum expenditure of energy. These aggregates are called *nuclei*, which probably consist of 10 to 1000 atoms (Lasaga, 1998). So far, we cannot observe nuclei forming, and so the nucleation step in the crystallization of natural liquids is poorly understood.

Because most liquids have no long-range order of their atoms, and crystals do, the change from liquid to solid is generally a discontinuous process. The relatively sudden change of atomic structure at the liquid–solid interface produces a definite boundary with a specific *interfacial energy* (γ) per unit area. This energy is due to the fact that atoms at the surface of the crystal are not as well bound to the lattice (the array of linked atoms in the crystal) as those in the interior, and so have a higher energy.

Crystallization of liquids (e.g. melts) can occur only if a decrease in the total free energy of the system (G_t) results. At temperatures below the equilibrium freezing temperature, the crystal has a lower chemical free energy per volume (G_v) than the liquid. However, the formation of a nucleus (i.e. a *volume* of new crystal), which decreases the chemical free energy of the volume of the system converted from liquid to crystal (G_v), is accompanied by the formation of an *area* of interface, which increases the interfacial free energy (γ). Therefore, the free energy change (ΔG_t) involved in nucleation is:

$$\Delta G_t = -(4/3)\pi r^3 \Delta G_v + 4\pi r^2 \Delta\gamma,$$

where ΔG_v is the difference in free energy between the solid and the liquid (the volume free energy) and r is the radius of the embryonic nucleus (assumed to be spherical). Spontaneous nucleation can occur only if ΔG_t is negative. As shown in Fig. 3.1, a nucleus of less than a critical radius (r^*) is unstable and can dissolve, because its area is too large relative to its volume, and so $4\pi r^2 \Delta\gamma$ is

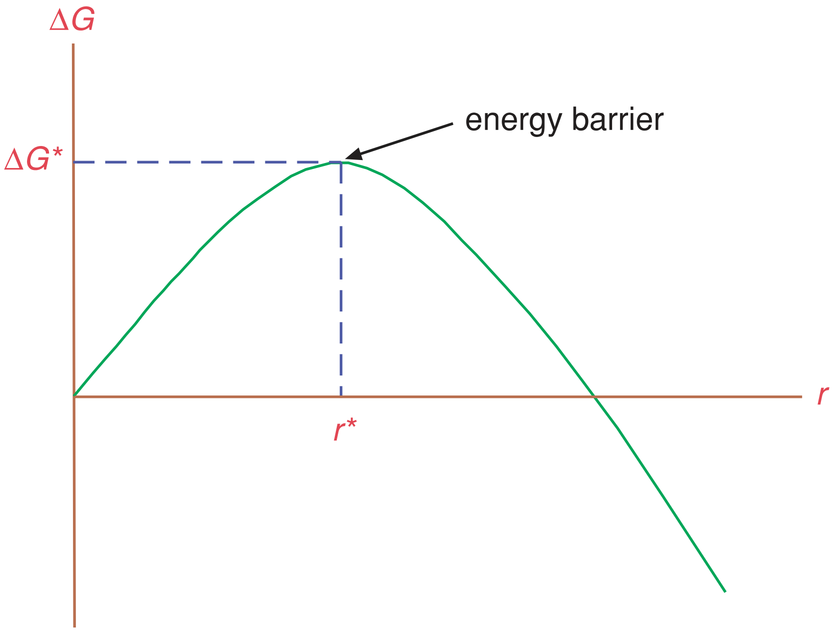

Fig. 3.1: Free energy of nucleation (ΔG) plotted against radius of nuclei (r). Stable nuclei must have radii greater than the critical radius (r^*), having surmounted the energy barrier (ΔG^*).

larger than $(4/3)\pi r^3 \Delta G_V$. Nuclei of radius larger than r^* are stable, and can grow into crystals. These nuclei have been called 'critical clusters' (see, for example, Walton, 1965). Smaller atomic clusters tend to dissolve in the melt.

The *energy barrier* to nucleation (Fig. 3.1) means that a certain amount of *undercooling* or *supercooling* (depression of temperature below the equilibrium freezing temperature) must occur before crystallization can take place (Fig. 3.2). In fact, all changes that involve a nucleation step (including solid-state metamorphic reactions, discussed in Chapter 4) involve some *overstepping* of reaction boundaries (e.g. with regard to temperature and/or pressure).

Nucleation is *homogeneous* if it occurs as a result of random thermal fluctuations in the liquid and *heterogeneous* if assisted by solid material, on which the new crystal can nucleate much more easily. The amount of undercooling required for heterogeneous nucleation is much less than for homogeneous nucleation. The solid material (which could be minute crystals, phenocrysts, foreign rock fragments, or the walls of a vein or magma chamber) forms a crystalline 'substrate', as shown in Fig. 3.3, which also shows the interfacial energies involved. A certain proportion of the area of the nucleus is a nucleus–substrate interface (γ_{NS}), the remainder being a nucleus–liquid interface (γ_{NL}), as in homogeneous nucleation. Heterogeneous nucleation is favoured because γ_{NS} is typically much less than γ_{NL} (especially where relatively good atomic registry occurs across the

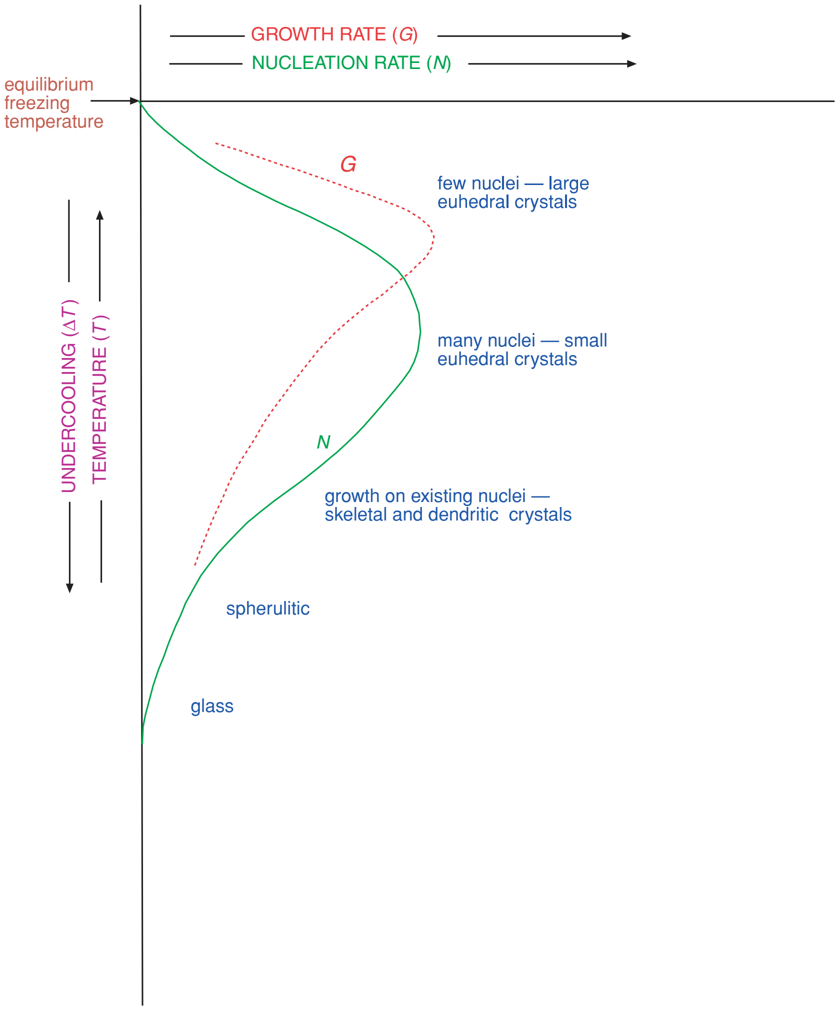

Fig. 3.2: Typical curves for variation of nucleation rate (*N*) and growth rate (*G*) with increasing undercooling (ΔT), showing the general grainsizes and shapes produced at each stage.

nucleus–substrate interface), so that the value of $4\pi r^2 \Delta\gamma$ in the above equation is reduced.

Although the even, apparently random distribution of phenocrysts in many volcanic rocks suggests homogeneous nucleation (see, for example, Cashman, 1988, p. 204), submicroscopic crystalline particles, such as xenocrysts (foreign crystals) or restite (unmelted minerals or minerals formed in the melting reaction that produced the magma) may be dispersed through the magma, and so may act as nucleating agents. Unfortunately, this possibility cannot be easily tested, as the nucleation stage cannot readily be observed. Some have suggested that

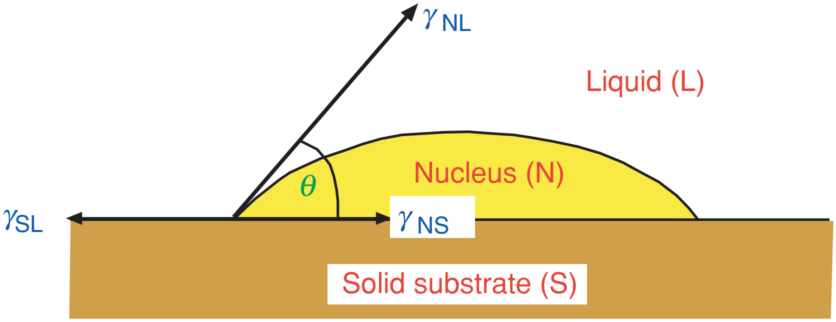

Fig. 3.3: Idealized non-spherical nucleus on a solid substrate in heterogeneous nucleation, showing the relevant interfacial energies (γ) acting at a point, so that $\gamma_{SL} = \gamma_{NS} + \gamma_{NL}\cos\theta$.

heterogeneous nucleation is the rule in magmas (see, for example, Berkebile & Dowty, 1982; Lofgren, 1983). For example, Campbell (1978) indicated that homogeneous nucleation is restricted to conditions of strong supercooling (several hundreds of degrees), whereas heterogeneous nucleation requires only a few degrees of supercooling.

A good example of heterogeneous nucleation is shown by glassy basalts of Hawaiian lava lakes, in which progressive stages of crystallization are preserved by rapid cooling (Kirkpatrick, 1975, 1981). The increase in size and number of crystals as crystallization proceeds indicates simultaneous nucleation and growth, and the clustering of crystals is consistent with heterogeneous nucleation. A glassy basalt with similar clustering is shown in Fig. 3.4.

Nucleation rates depend on many factors, such as the viscosity of the magma (which in turn depends on the composition and water content of the magma), temperature, oxygen activity and degree of undercooling (Lofgren, 1980, p. 543). Experiments have suggested that olivine and oxide minerals tend to nucleate in mafic magmas more readily than pyroxene, which nucleates much more readily than feldspar and quartz (Lofgren, 1980, p. 544). The common clustering of plagioclase in basalts (Kirkpatrick, 1975, 1981; Philpotts *et al.*, 1998, 1999) is consistent with the tendency of plagioclase to nucleate less readily than clinopyroxene in experiments (Kirkpatrick, 1975).

Twinning (Section 3.12) can probably assist nucleation. For example, the almost ubiquitous presence of simple twinning in magmatic K-feldspar (Vernon, 1986a, 1999a) in both the phenocrysts and groundmass crystals of trachytes (Fig. 3.5) implies twinned nuclei, because both twin individuals in each crystal are very similar or identical in size, and so must have been initiated at the same time. The abundance of simple twinning in K-feldspar in igneous rocks may be due to a general difficulty in forming viable nuclei of K-feldspar in magmas, which is suggested by the experiments of Fenn (1977), especially for hydrous melts. Twinning may assist attachment of atoms to the nuclei because

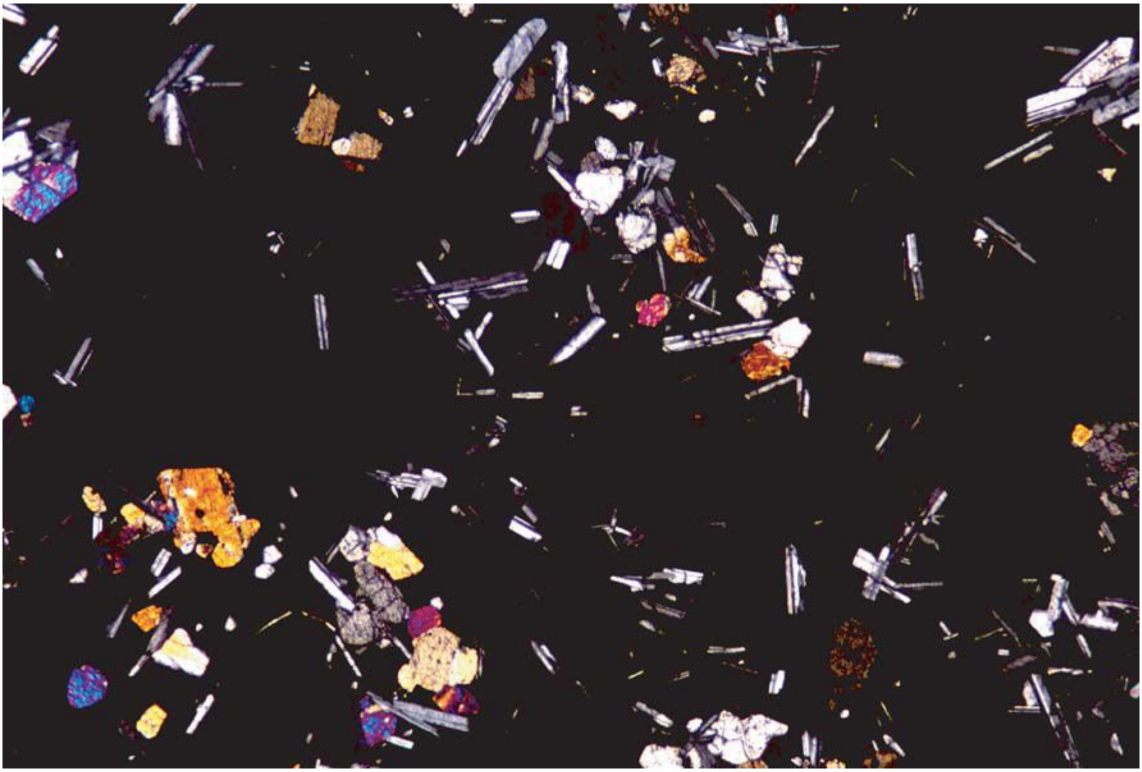

Fig. 3.4: Clusters of plagioclase and plagioclase–olivine crystals in glass in a rapidly cooled basalt from Iceland. The clustering is consistent with heterogeneous nucleation. Crossed polars; base of photo 4 mm.

of the re-entrant at the twin interface or because of concentrations of dislocations along the twin plane (Baronnet, 1984). Twinned feldspar crystals have been observed experimentally to grow faster than untwinned crystals (Dowty, 1980b, p. 434). Twinning in metamorphic K-feldspar (Chapter 4) is rare or absent, probably because nucleation in metamorphic rocks can occur on existing crystalline material. If so, nucleation of K-feldspar in melts may be largely homogeneous, although this is impossible to verify at present. In contrast, untwinned K-feldspar may precipitate from melt produced by partial melting of metasedimentary rocks during high-temperature metamorphism (Chapter 4), because it nucleates on existing K-feldspar, forming euhedral overgrowths (Vernon, 1999a; Vernon & Johnson, 2000).

Nucleation in multicomponent systems, such as magmas, is more complicated than in simple systems (Toramaru, 1991), because as crystals of a particular mineral grow they affect the composition of the remaining liquid (depleting it of some chemical components) and consequently the formation of later nuclei. Because the composition of the liquid varies with the number of nucleated crystals, the

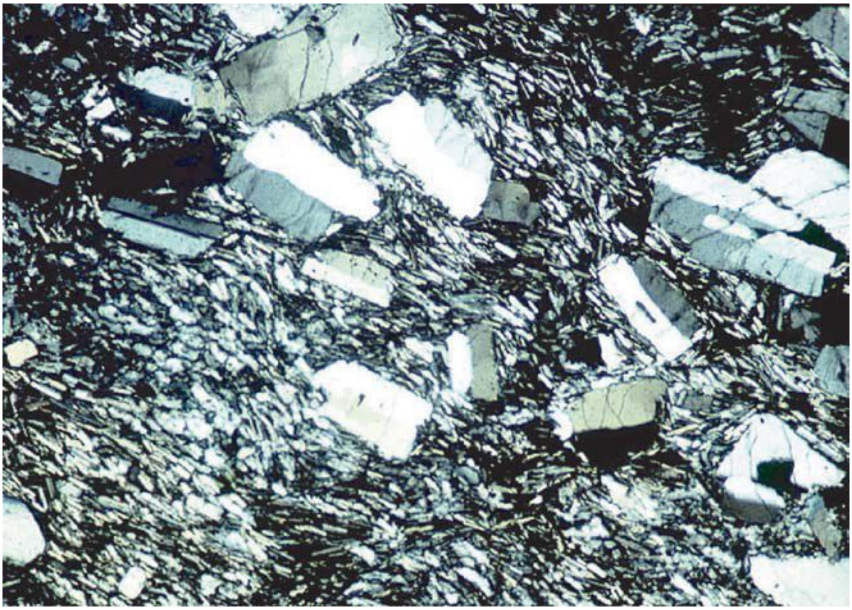

Fig. 3.5: Trachyte with flow alignment of euhedral phenocrysts and groundmass crystals of K-feldspar with simple twinning. Crossed polars: base of photo 4.4 mm. From Vernon (2000b, fig. 16).

effective undercooling changes as crystal growth proceeds, even at the nucleation stage and even at constant temperature. Therefore, subsequent nucleation stages may depend not only on cooling, but also on the growth process of crystals nucleated earlier. This coupling of nucleation and growth processes determines the duration of nucleation and the peak nucleation rate, and so determines the total number of crystals (Toramaru, 1991). Toramaru (1991) found that diffusivity (ease of diffusion of chemical components) is the most important among the various factors that can affect nucleation in multicomponent systems. Because the diffusivity is determined by the chemical composition and temperature of the magma, Toramaru (1991) inferred that hot magmas with high diffusivity should nucleate fewer crystals of a particular mineral than would be nucleated in a cooler magma with low diffusivity.

Although it is usual to think of each crystal in magmas growing from a single nucleus, Hall *et al*. (1986) have described compositionally complex pyroxene grains in dolerites that appear to have developed from several nuclei of different composition.

3.3.2 Growth

After nuclei of the new mineral have been produced, a process called *ageing* ('Ostwald ripening') may occur, whereby no new nuclei are formed and larger nuclei grow at the expense of smaller nuclei, over a much longer time than it takes for nucleation to occur (see, for example, Ostwald, 1901; Lovett *et al.*, 1978). Homogeneously distributed nuclei are potentially unstable, because if a few dissolve, nearby nuclei grow, which induces diffusion towards the instability, promoting further crystal growth there (Lovett *et al.*, 1978; Tikare & Cauley, 1998). The surviving pieces of crystalline material grow into observable crystals. The process occurs in the crystallization of synthetic materials. Therefore, it may be applicable to rocks (see, for example, Baronnet, 1982), for example, in the early stages of the crystallization of magma.

Ostwald ripening reflects the greater solubility of very small crystalline particles compared with that of larger ones (Buckley, 1961; Voorhees, 1992), in response to the tendency to reduce the total interfacial free energy of all the particles of that phase (Baronnet, 1984, p. 224). Because the surface energies of particles are not large enough to drive diffusion over large distances, surface energy is an important driving force for dissolution in the liquid when crystals are very small, in the micrometre or smaller size range (Jackson, 1967; Martin & Doherty, 1976; Baronnet, 1982; Lasaga, 1998, p. 514; Cabane *et al.*, 2001). When crystals grow large enough to be observed in the light microscope, they are much more stable than submicroscopic particles (Martin & Doherty, 1976, pp. 174–6). Boistelle & Astier (1988) noted that 'Ostwald ripening' is generally very fast for particles of radius less than 1 μm, fast for particles around 1 μm, and very slow for particles around 100 μm. However, organic crystals of radius up to 1.5 mm have been developed by 'Ostwald ripening' in experiments of two months' duration (Ng *et al.*, 1996). Suppression of nucleation near larger grains may also occur, according to Berger & Roselle (2001), though this is not usually referred to as Ostwald ripening.

Ostwald ripening produces a population of *viable* nuclei that can grow into crystals. The relative crystal size distribution produced may be preserved during subsequent crystal growth (Eberl *et al.*, 2002). Thus, some crystal size distributions (e.g. distributions skewed towards larger grainsizes) suggest that Ostwald ripening may have occurred (see, for example, Miyazaki, 1991; Kile *et al.*, 2000; Zieg & Marsh, 2002, p. 99) to produce the viable nuclei. However, typical crystal size distributions in igneous rocks (Section 3.4.2) are interpreted as reflecting simple nucleation and growth (see, for example, Zieg & Marsh, 2000).

Crystals grow by advancement of the interface into the liquid. The resulting shapes (Section 3.5) depend not only on the atomic structure of the mineral concerned, but also on external factors, such as (1) the flow of latent heat of crystallization away from the growing crystal surface, (2) the rate at which nutrient chemical components can diffuse through the liquid to the advancing interface, (3) the rate at which unwanted chemical components can diffuse, or be convected, away from the advancing interface, and (4) reactions at the crystal–melt interface. Factor (1) is generally unimportant for magmas, because heat flow is several orders of magnitude faster than diffusion in silicate melts. Therefore, thermal gradients are much smaller than compositional gradients around crystals (Kirkpatrick, 1981, p. 349). The following two general 'end-member' situations apply to growing crystals in magmas, although both may operate in intermediate situations (Kirkpatrick, 1981, p. 350).

(1) The growth rate (G) is controlled by the attachment of atoms at the crystal–melt interface when diffusion in the melt is much faster than the uptake and rejection of components at the interface, so that the interface composition remains constant, with the composition of the bulk liquid. This applies especially at a small degree of undercooling (ΔT), where G is relatively small and the rate of diffusion (D) is large, owing to the relatively high temperature (Fig. 3.2).

(2) G is controlled by D in the melt when the rate of uptake or rejection of components is much faster than diffusion in the melt. This applies especially at large ΔT (Fig. 3.2), where G is larger and D is smaller (owing to the lower temperature).

3.4 Grainsize in igneous rocks

3.4.1 Effect of undercooling

As stated previously, some undercooling (supercooling) must occur before nuclei can grow into crystals. The undercooling (ΔT) is defined as the difference between the liquidus temperature, T_L (the temperature at which the mineral concerned would crystallize from the melt at equilibrium conditions) and the actual temperature ($\Delta T = T_L - T$). The general situation with regard to undercooling (ΔT) is illustrated in Fig. 3.2, which shows typical curves determined experimentally for some silicate minerals, such as nepheline (Fig. 3.6). The nucleation rate (N) and the growth rate (G) both rise with increasing degrees of undercooling to maxima, but G increases at a smaller ΔT than N. Both N and G decline with further undercooling, because lower temperatures reduce the rates of diffusion of chemical components in the increasingly viscous melt. This reduces the rates of aggregation of atoms to form new nuclei (affecting N) and inhibits addition of atoms to the growing crystal (affecting G). However, G remains higher than N at lower ΔT, so that $N:G$ decreases.

Crystallization of liquids with many chemical components (i.e. liquid solutions), such as magmas, is more complicated than for simple melts (see, for example, Cashman, 1990). This is mainly because minerals have compositions different from that of the bulk melt, and so crystallization continually changes the liquid composition. This lowers T_L, thus altering the effective ΔT at the temperature concerned, as well as N and G. For example, a mineral has a lower G in multicomponent systems than in a pure melt of its own composition (Cashman, 1990, p. 268). The effect of diffusion rates of different components on the shape of crystals is discussed in Section 3.5.

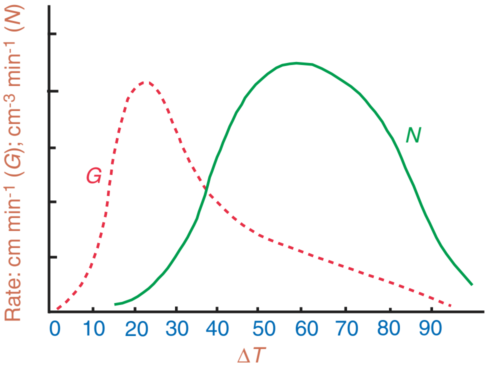

Fig. 3.6: Plot of nucleation rate (*N*) and growth rate (*G*) versus degree of undercooling (Δ*T*) for nepheline, determined experimentally by H. G. F. Winkler, as reported and slightly modified by Shaw (1965).

3.4.2 Grainsize in volcanic igneous rocks

Grainsize in liquid crystallization is generally thought of as being controlled by the ratio of the nucleation rate (*N*) to the growth rate (*G*), as shown in Fig. 3.2 (Brophy *et al.*, 1964; Shaw, 1965), although possible complications can be caused by solution of some nuclei and growth of others ('Ostwald ripening'), as discussed in Sections 3.3.2 and 3.4.3. At low degrees of undercooling, when both *N* and *G* and especially *N* : *G* are low, large, well-formed (*polyhedral, euhedral, idiomorphic*) crystals develop (Figs. 3.5, 3.7–3.9). At larger Δ*T*, both *N* and *G* rise, but *G* tends to decline before *N*, and a situation of high *N* : *G* is reached; at this stage, many small euhedral crystals develop in the groundmasses of many volcanic rocks. These are called crystallites (Figs. 3.24, 3.62) if very small, microlites (Figs. 3.5, 3.7) if larger. At even higher Δ*T*, both *N* and *G* become very small, so that no new nuclei form; consequently growth is forced to occur only on existing crystals (Sections 3.5.3, 3.5.5). At extreme degrees of undercooling, crystallization fails to occur, and *volcanic glass* is formed (Section 3.5.6).

The sizes of crystals and grains in rocks reflect the average growth rate and the time the crystals grow or reside in the magma (Marsh, 1988a). As nucleation occurs during crystallization, a range of grainsizes is produced in the resulting rock if it is quenched, which is the situation for volcanic rocks (Marsh, 1988a). *Crystal size distributions* (CSDs) have been obtained, by plotting numbers of crystals against size, by Marsh (1988a,b), Cashman & Marsh (1988), Cashman (1988, 1990) and others. They found that plotting the population density, ln(*n*), where *n* is the number of crystals of size *L* per unit volume, against *L* (crystal length in millimetres or centimetres) commonly gives a straight line with a negative slope for minerals in volcanic rocks (Fig. 3.10). For example, this applies to

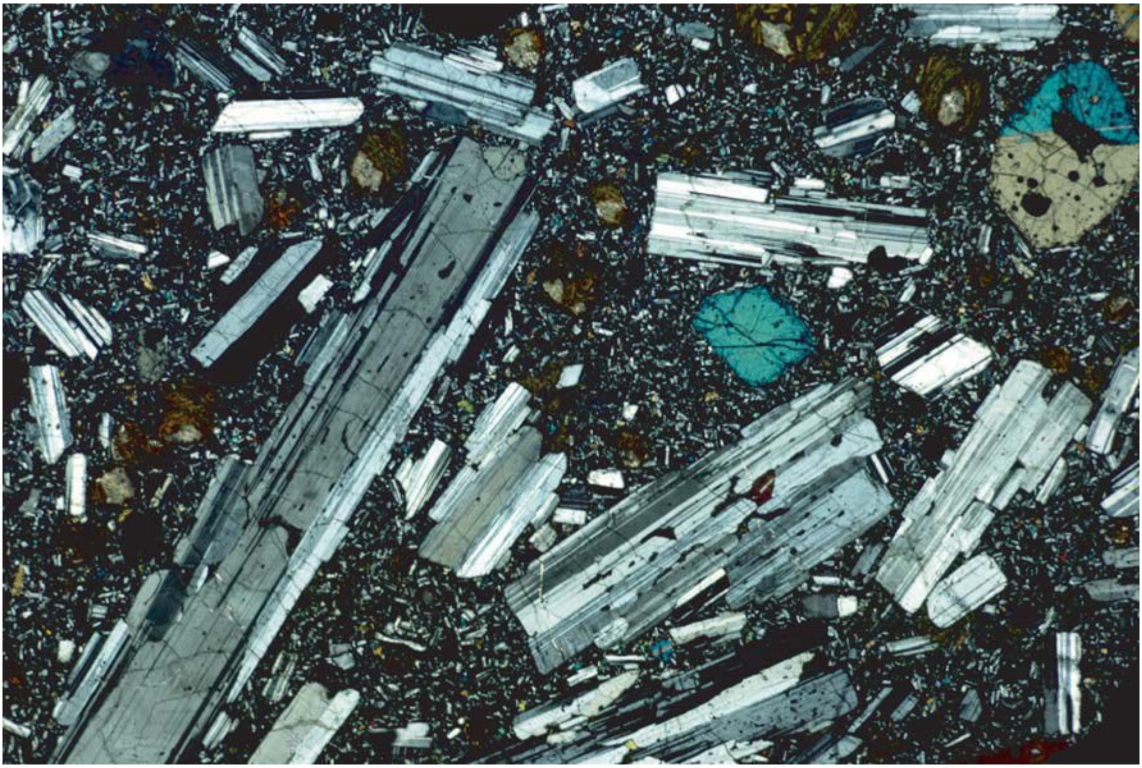

Fig. 3.7: Andesitic basalt with euhedral phenocrysts of plagioclase (grey interference colours, multiple twinning) and pyroxene (higher-order interference colours) set in a glassy groundmass with plagioclase microlites. Crossed polars; base of photo 1.8 cm.

plagioclase from many volcanic rocks (Marsh, 1988a; Cashman & Marsh, 1988). Moreover, despite the apparent bimodal distribution suggested by the presence of phenocrysts and groundmass, porphyritic volcanic rocks show smooth log-linear CSD trends (Marsh, 1988a), which are consistent with uniform cooling rates.

The CSD theoretically enables growth rate, nucleation rate and nucleation concentration to be determined quantitatively for each mineral. The intercept of the line at zero grainsize is inferred to be the nucleation concentration (n_0), and the slope is taken to be a measure of the product of growth rate (G) and growth time (τ). For example, Marsh (1988a) and Cashman & Marsh (1988) inferred growth rates of about 10^{-10} cm s^{-1} from CSDs of basalts from drill cores from the lava lakes of Kilauea Volcano, Hawaii, for which τ is known. Shallow slopes are inferred to reflect slow cooling, so that samples collected from different places in an intrusion or from suites of related volcanic rocks may show a range (‘fan’) of CSD slopes (see, for example, Zieg & Marsh, 2002, fig. 9).

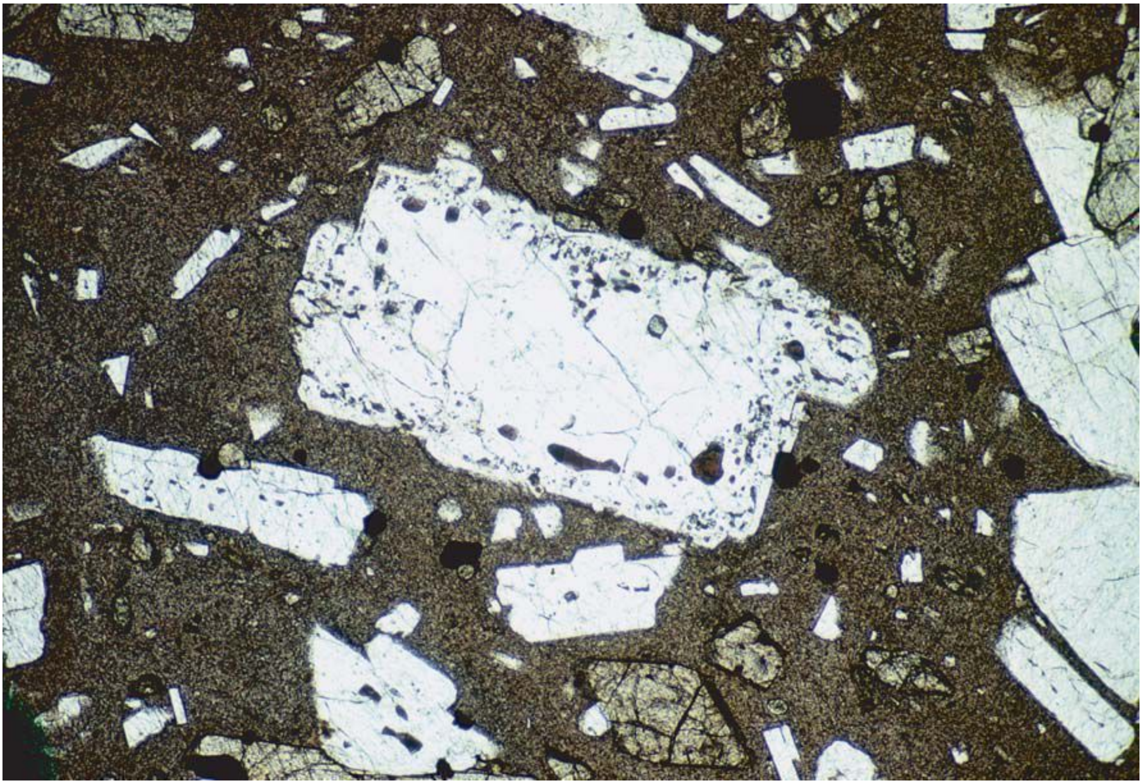

Fig. 3.8: Euhedral crystals of plagioclase (colourless), clinopyroxene (pale green) and magnetite (opaque) in a glassy andesite from the Hunter Valley, New South Wales, Australia. Glass and clinopyroxene inclusions are abundant in some of the outer concentric zones of the plagioclase (Section 3.11). Plane-polarized light; base of photo 4.4 mm.

The usual linear CSD may theoretically be modified by magmatic processes, such as crystal accumulation and loss (e.g. by gravity settling or floating of crystals in the magma), as shown in Fig. 3.11. Mixing of magmas may also cause variations in the CSD if the magmas involved have different CSDs. Physical addition of grains of metamorphic or plutonic igneous rocks (e.g. from partly melted xenoliths, partly melted source rocks, or physically disintegrated other rocks from the source area) should produce CSDs with a ‘hump’ in the middle, because most metamorphic and plutonic igneous rocks have few small crystals and a distinct mean grainsize, as discussed in Section 4.3.1.

Variations in grainsize through an individual dyke, sill, lava flow sequence or pluton are generally relatively small (2–3 orders of magnitude), except for chilled margins, suggesting that the crystallization process and/or rate does not vary very much (Cashman, 1990, p. 282). Studies of crystal size in dykes, as

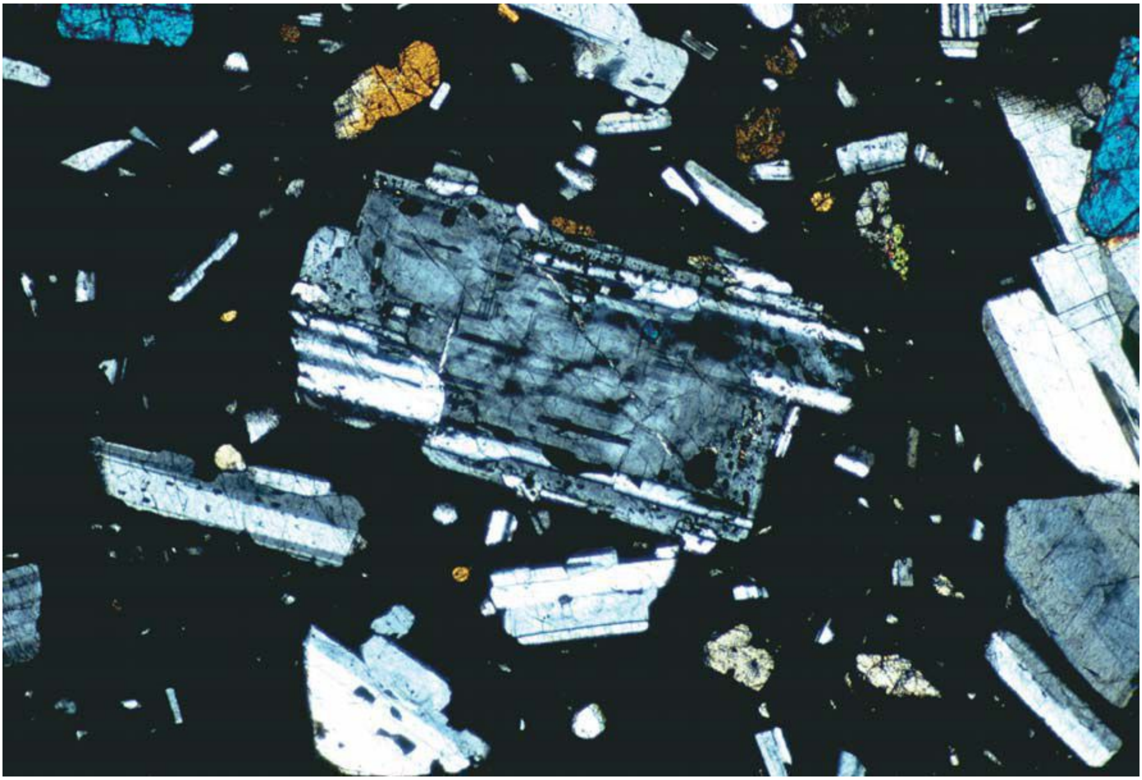

Fig. 3.9: Same field of view as for Fig. 3.8, but in crossed polars, so that the minerals show interference colours (plagioclase with grey interference colours and multiple twinning; clinopyroxene with grey to higher-order interference colours) and the glass is black (optically isotropic). Note the optical difference between the opaque mineral (magnetite), which is black in both plane-polarized and crossed polarized light, and the glass, which is black only in crossed polars. Crossed polars; base of photo 4.4 mm.

related to inferred growth rates, have been summarized by Cashman (1990, pp. 283–5).

Suggesting that ln(n) versus L plots suffer from inherited correlation, Pan (2001) challenged the validity of currently used CSD plots, erroneously according to Schaeben *et al*. (2002), Marsh & Higgins (2002) and Higgins (2002), but correctly according to Pan (2002a,b,c). Another objection was raised by Eberl *et al*. (2002), on the basis that the current interpretation of CSDs assumes that crystal growth rates at a particular time are identical for all crystals and therefore independent of crystal size, whereas growth rates that generally increase with crystal size provide a better explanation of observed CSDs for most crystallizing systems.

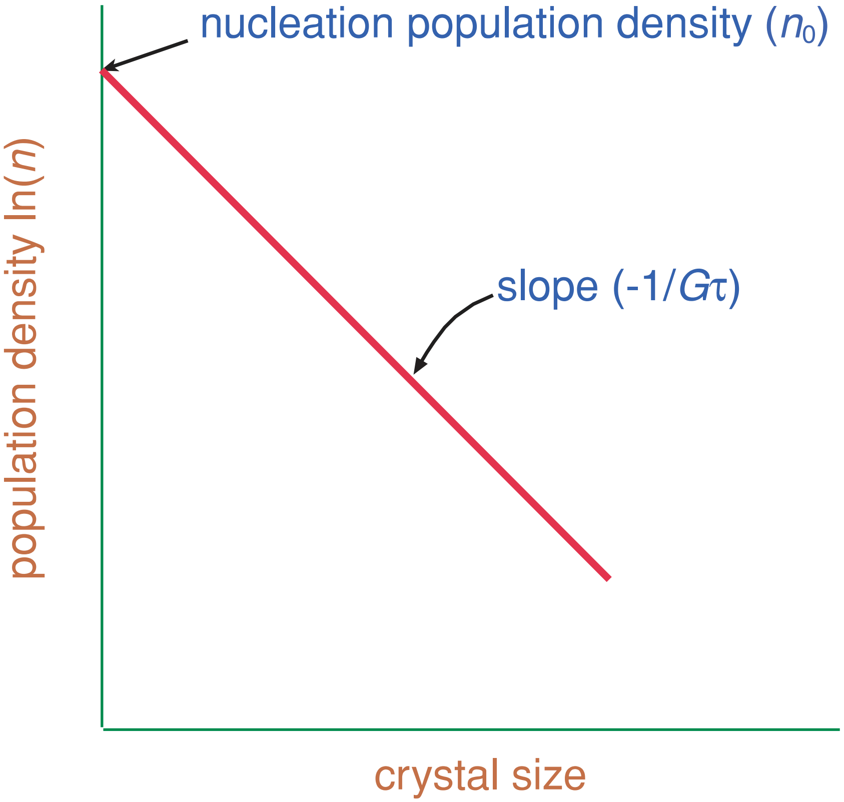

Fig. 3.10: Crystal size distribution (CSD) plot for a typical volcanic rock. Plotting the population density, ln (n), where n is the number of crystals of size L per volume (i.e. number per cm^4), against L (in mm or cm) commonly gives a straight line with a negative slope for minerals in volcanic rocks. After Marsh (1988a, fig. 4A).

3.4.3 Grainsize in plutonic igneous rocks

The relatively small size range of each mineral in coarse-grained ('plutonic') igneous rocks needs explanation, in view of the range of sizes observed in volcanic rocks. Even if the magma is held at the same small degree of undercooling for most of its cooling history, the last remaining magma would be expected to nucleate new crystals, so that some small crystals should always be present. One explanation is that the latest small crystal particles or nuclei are resorbed, and their material is added to the larger crystals (see, for example, Marsh, 1988a, p. 290) by Ostwald ripening (Section 3.3.2).

Evidence for the process has been observed in experiments on felsic and mafic magmatic systems (Jurewicz & Watson, 1985; Park & Hanson, 1999). Thus, in igneous rocks and the molten parts of migmatites (Section 4.16), Ostwald

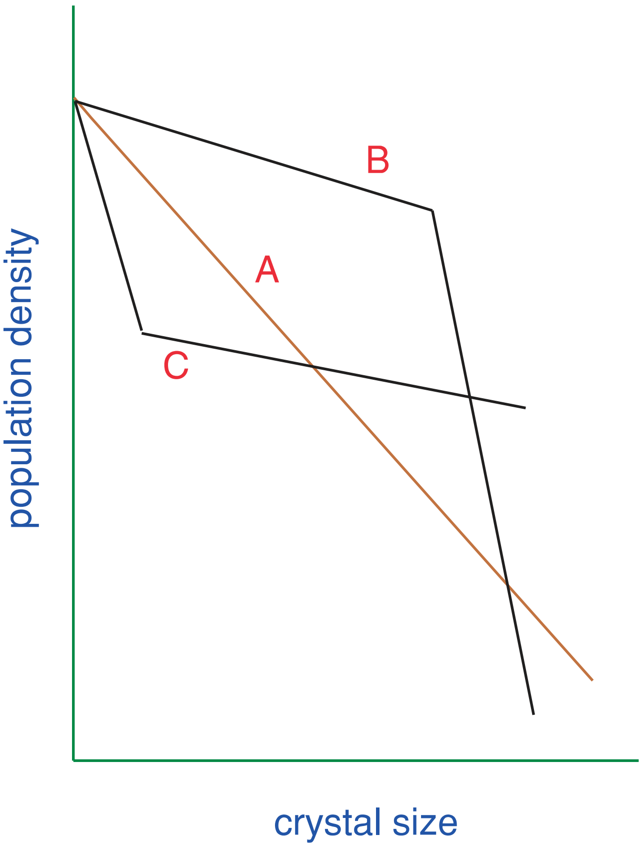

Fig. 3.11: Diagram showing how the linear crystal size distribution (CSD) plot of Fig. 3.10 (reflecting normal nucleation and growth) may be modified by other processes in magmas. The original CSD (plot A) develops a concave downwards deflection if large crystals settle out of the magma (plot B, reflecting an increased proportion of smaller crystals left behind in the magma). In contrast, it develops a concave upwards deflection by either addition of crystals or destruction and removal of nuclei or the smallest crystals, even during a constant nucleation rate (plot C, reflecting an increased proportion of larger crystals accumulated in the magma). After Marsh (1988a, fig. 7b).

ripening, as well as normal nucleation and growth, theoretically may influence the CSD (Higgins, 1998; Berger & Roselle, 2001), although it does not necessarily occur (Berger & Roselle, 2001). Moreover, in migmatites the process is probably masked by other processes, such as solution of crystals during melting reactions and later precipitation (Cabane *et al.*, 2001).

The experimental result of Cabane *et al.* (2001), namely that quartz cannot coarsen by Ostwald ripening at reasonable times if the initial grainsize is about 1 mm or more, indicates that coarsening of quartz is restricted to the late nucleation stages. This result is supported by experience with synthetic systems, including metals (Jackson, 1967; Martin & Doherty, 1976). Therefore, although Ostwald ripening may occur for the smallest crystals throughout the cooling history of plutonic igneous rocks, as suggested by Means & Park (1994), it is unlikely to occur to all grains. Many nuclei or small crystals may be dissolved in the later stages of nucleation events (Cabane *et al.*, 2001), implying that the conventional view of the control of grainsize by $N : G$ may be oversimplified. Nevertheless, the grainsize of granites is likely to be due to events at the nucleation and early growth stages, rather than to late grain coarsening. Thus, grainsize in non-deformed igneous rocks appears to be controlled by the nucleation rate of *viable* nuclei (i.e. those that do not redissolve) and the growth rate.

Another potential explanation of the small grainsize range in plutonic igneous rocks (Lofgren, 1980) is the probable presence of pre-existing, small (even submicroscopic) crystalline nuclei (e.g. restite, consisting of incompletely melted grains of the source rock or minerals produced in the melting reaction), which could promote the formation of all nuclei (heterogeneous nucleation) at about the same time. This should apply also to equivalent lavas and shallow intrusive rocks, but if so, it evidently doesn't control the CSD. Therefore, dissolution of nuclei or very small crystals (Cabane *et al.*, 2001) may be a more likely explanation.

Another factor operating against solid-state grain coarsening in granites is the relatively low temperature of final crystallization (the *solidus* temperature) of granite magmas and the consequently relatively short cooling period, especially where granites intrude cool rocks. Little convincing evidence has been presented for appreciable solid-state grainsize or grain shape changes in non-deformed granites (Section 4.6.2), although intragranular processes, such as exsolution in alkali feldspar (Section 4.9.1), are common.

On the other hand, hot magmas, such as gabbros and ultramafic cumulates, have long cooling periods, even after they have completely solidified (*subsolidus* cooling period), during which changes in the shapes and sizes of grains may occur (see, for example, Voll, 1960; Weedon, 1965; Vernon, 1970; Hulbert & von Gruenewaldt, 1985; Reynolds, 1985; Mathison, 1987; Hunter, 1987, 1996), as discussed in Section 4.6.1. The process is driven by a tendency to reduce the total interfacial energy of the aggregate (Section 4.2), so that lower-energy grain shapes and larger grainsizes are produced by diffusion of chemical components from high-energy to lower-energy sites, in residual melt (while present) and/or along solid grain boundaries.

3.4.4 Porphyritic igneous rocks

Porphyritic igneous rocks consist of larger crystals (phenocrysts) in a distinctly finer-grained aggregate (groundmass), as shown in Figs. 3.5 and 3.7–3.9. This is regardless of the absolute grainsize, although volcanic and shallow intrusive rocks are much more commonly porphyritic than deeper, coarser-grained intrusive rocks.

Traditionally, porphyritic structure in volcanic and high-level intrusive rocks has been interpreted as resulting from slow crystallization at depth to form the phenocrysts, followed by rapid cooling (due to extrusion onto Earth's surface or intrusion into colder rocks) to form the groundmass. However, porphyritic structure can also form in a single, uninterrupted cooling event, which has been confirmed many times experimentally (Swanson, 1977; Lofgren, 1980). Lofgren (1980, p. 530) inferred that for porphyritic structure to develop with a steady cooling rate, the first precipitating ('liquidus') mineral must crystallize alone for a certain time. For example, if pyroxene begins to crystallize in a basalt magma and plagioclase nucleation is delayed, the melt may become so strongly supersaturated with plagioclase that when it does precipitate it forms many small crystals (Fig. 3.2). This, in turn, supersaturates the liquid in pyroxene, which continues to crystallize, not as phenocrysts, but as small crystals in the groundmass. The result is a groundmass of small plagioclase and pyroxene crystals surrounding the earlier-formed pyroxene phenocrysts.

However, this does not explain phenocrysts of alkali feldspar in a groundmass of the same mineral in some trachytes (Fig. 3.5). A two-stage cooling process may apply, but a single cooling event is also possible. For example, Fig. 3.2 shows that the growth rate reaches a peak and then declines rapidly as ΔT increases, so that a steady increase in ΔT should induce a relatively rapid change from large to smaller crystals. This effect is assisted by the rapid increase in nucleation rate as the growth rate declines (Fig. 3.2).

Porphyritic structure could also be produced by rapid loss of water dissolved in the melt component of a magma crystallizing slowly at depth; this would raise the equilibrium freezing temperature ('liquidus') of the melt, and so effectively increase ΔT. This is because water-bearing melts typically have lower freezing temperatures than equivalent dry melts.

Porphyritic structure in deep intrusive rocks (for example, megacrysts of K-feldspar in granites) is very unlikely to be due to two-stage cooling, because these rocks crystallize slowly and at relatively uniform rates in large magma bodies (plutons). It is probably due to different nucleation rates for different minerals, as discussed in Sections 3.4.3 and 3.4.5.

3.4.5 Very large crystals in igneous rocks

A common example of porphyritic structure in intrusive rocks is the occurrence of very large euhedral crystals (megacrysts), up to about 20 cm long, of K-feldspar in some granites (Vernon, 1986a), as shown in Figs. 3.12 and 3.13. The simplest explanation of their large size is that these megacrysts develop at conditions of unusually low $N : G$, presumably at low degrees of undercooling (Fig. 3.2), as suggested by Swanson (1977). The experiments of Fenn (1977) show markedly reduced nucleation rates for alkali feldspar in hydrous felsic melts. The reason for the unusually low $N : G$ in megacrystic granite magmas is unknown, as

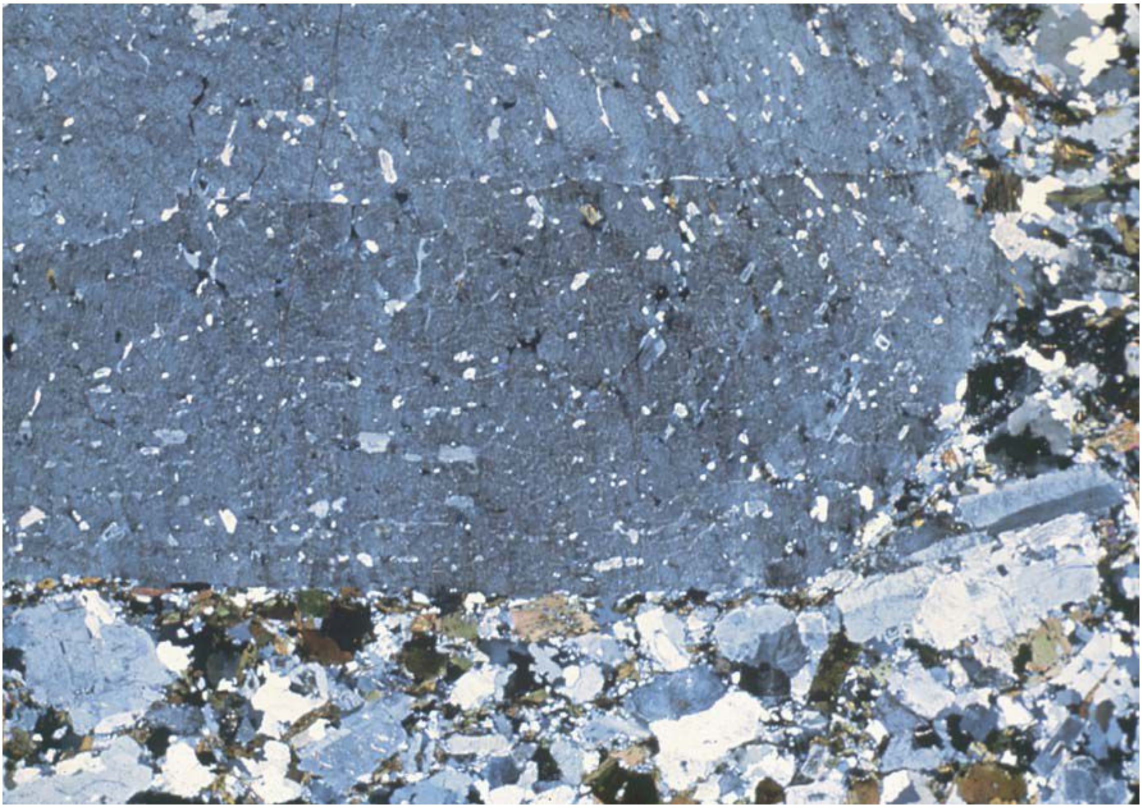

Fig. 3.12: Part of a large euhedral phenocryst (megacryst) of K-feldspar with concentrically arranged inclusions of plagioclase, in the Wuluuman Granite, Wellington, New South Wales, Australia. Parallel to the lines of inclusions are faint darker and lighter bands that represent oscillatory concentric zoning (Section 3.11.5). Crossed polars; base of photo 22 mm. Photo by W. F. D'Arcy.

controlling factors for nucleation cannot be observed in action, but the low nucleation rate could be connected with local abundance of water, which would tend to break Si–O and Al–O bonds in potential nuclei. The nucleation difficulty does not appear to be connected with the major-element chemical composition of the magma, as megacrystic granites may be compositionally identical to adjacent non-megacrystic granites (Bateman & Chappell, 1979).

As mentioned previously, problems of nucleation of K-feldspar in magmas are exemplified by the commonly observed abundance of simple twinning in igneous K-feldspar (Eggleton, 1979), compared with its rarity to absence in strictly metamorphic K-feldspar, that is, K-feldspar that has grown in the solid state, not in a liquid (Vernon, 1999a). For example, K-feldspar crystals occurring both as phenocrysts and in the groundmass of trachytes invariably have simple

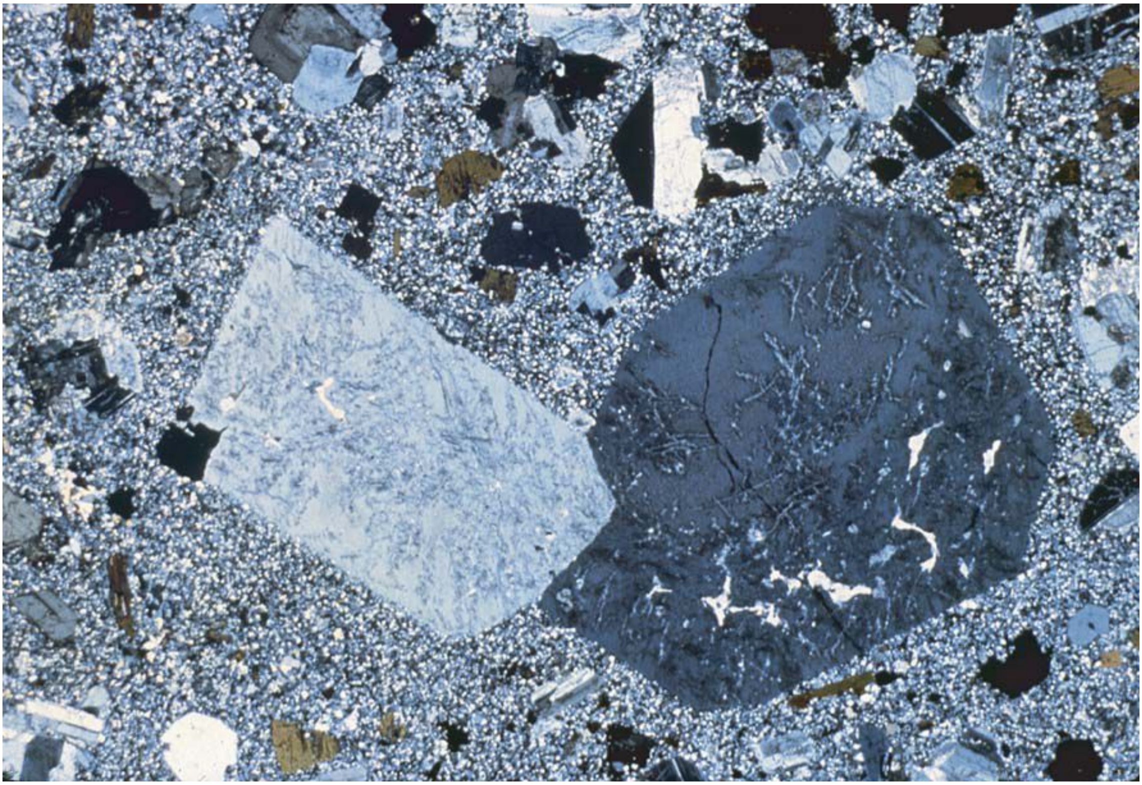

Fig. 3.13: Large euhedral phenocrysts (megacrysts) of K-feldspar in porphyritic microgranite, margin of the Yetholme pluton, east of Bathurst, New South Wales, Australia. Crossed polars; base of photo 19 mm. Photo by W. F. D'Arcy.

twinning (Fig. 3.5), which is also common in K-feldspar megacrysts in granite (Vernon, 1986a).

Higgins (1999) suggested that megacrysts of K-feldspar in a granodiorite were formed by coarsening (textural coarsening, ageing, or Ostwald ripening) of smaller, earlier-formed crystals, rather than resulting from low $N : G$ ratios during their crystallization. However, Berger & Roselle (2001) found that the CSD of K-feldspar megacrysts in migmatite leucosomes (Section 4.16) reflects the interplay between nucleation and growth rates at the initial stage of crystallization, not grain coarsening, and Cabane *et al.* (2001) found that coarsening is inappropriate for quartz grains larger than 1 mm in granitic melts. Extrapolating from their experimental results, Cabane *et al.* (2001) found that grainsizes produced by Ostwald ripening of quartz after a million years (1 Ma) would range from 12 to 70 μm, depending on the water content of the liquid. This suggests that K-feldspar megacrysts up to 25 mm long are unlikely to be due to Ostwald ripening, as inferred by Higgins (1999).

Higgins (1999) suggested that concentrations of K-feldspar megacrysts in granites are also due to Ostwald ripening, which he inferred to have removed existing crystals (presumably in the millimetre size range) and so expose channels for K-rich melt to precipitate and so concentrate megacrysts *in situ*. However, abundant evidence indicates that the K-feldspar megacrysts in granites commonly move as large independent crystals and concentrate mechanically, rather than being the result of crystallization *in situ*. Of course, this does not preclude Ostwald ripening at the nucleation and very early growth (submicroscopic) stages, establishing the number of viable nuclei, as discussed in Section 3.4.3. Evidence of movement of megacrysts includes: (1) their accumulation, either as (a) abundant, megacryst-rich layers in granites (Vernon, 1986a; Wiebe, 1994, 1996; Healy *et al.*, 2000; McMurry, 2001; Wiebe *et al.*, 2002) or (b) flow-sorted layers (schlieren) in granites (commonly with graded-bedding and cross-bedding), together with mafic minerals, xenoliths (Section 3.10.2) and microgranitoid enclaves (Section 3.10.3), as described by Gilbert (1906), Cloos (1936), Phillips (1968, p. 180), Wilshire (1969, p. 244), Wahrhaftig (1979), Barrière (1981), Vernon (1986a, pp. 7–8), Abbott (1989), Reid *et al.* (1993), Tobisch *et al.* (1997), Clarke & Clarke (1998) and Weinberg *et al.* (2001); (2) their common alignment in flow structures, as reviewed by Vernon (1986a, pp. 5–7); (3) imbrication (tiling) of megacrysts without internal deformation, reflecting their mechanical alignment during magmatic flow (Paterson *et al.*, 2004); (4) their occurrence in tubular diapiric bodies (Reid *et al.*, 1993; Weinberg *et al.*, 2001; Paterson *et al.*, 2004); (5) concentrations of megacrysts apparently formed by being pushed ahead of large moving objects, such as falling xenoliths (Paterson *et al.*, 2004); and (6) their physical incorporation in more mafic magma during magma mixing (Section 3.10.3) — commonly before the resulting hybrid magma is incorporated as enclaves by magma mingling (Vernon, 1983, 1986a, 1990a, 1991a) — which implies the existence of megacrysts at a relatively early stage of the history of the enclosing magma. Furthermore, the following difficult-to-answer questions are posed by the 'Ostwald ripening' hypothesis of Higgins (1999). (1) Why weren't megacryst-free areas adjacent to megacryst concentrations similarly affected by the postulated 'Ostwald ripening'? (2) Why do some mafic schlieren contain megacrysts, whereas immediately adjacent schlieren have none?

As reviewed by Vernon (1986a, p. 10), higher Ba concentrations generally occur in the cores of K-feldspar megacrysts, the rims having low Ba contents (normal Ba zoning; Section 3.11.8), similar to those of groundmass K-feldspar grains. In contrast, zoning patterns expected to be produced by coarsening of existing crystals should show reverse zoning, at least for part of their growth history, because early-formed small crystals that are dissolved should add progressively more Ba to the growing larger crystals. This is the explanation offered by Higgins (1998) for reverse zoning in the plagioclase of an anorthosite, which he inferred to have grown by precipitation consequent on the solution of smaller Ca-rich plagioclase grains.

K-feldspar megacryst concentrations may consist almost entirely of K-feldspar (Vernon, 1986a; Weinberg *et al.*, 2001; Paterson *et al.*, 2004). The inference of Higgins (1999) that they are formed from continually replenished magma in flow channels fails to explain why the inferred percolating melt failed to precipitate quartz, plagioclase and biotite (with which it should have been saturated), along with the K-feldspar. Moreover, as noted by Gilbert (1906, p. 322) and Wilshire (1969, p. 244), the concentrated K-feldspar megacrysts typically do not interpenetrate (even where in contact), but generally remain separate in the concentrating process, whereas simultaneous growth of K-feldspar crystals *in situ* might be expected to produce moulding of one megacryst around another. In addition, local zoning truncations occur where one megacryst appears to have impinged on another in K-feldspar aggregates (Paterson *et al.*, 2004), owing probably to contact melting (Section 5.11.3).

The experimental result of Cabane *et al.* (2001), namely that quartz cannot coarsen at reasonable times if the initial grainsize is about 1 mm or more, indicates that the size of quartz grains in granites is probably due to events at the nucleation and early growth stages, rather than to coarsening of existing crystals. However, Ostwald ripening may occur in the later stages of nucleation events, removing many nuclei (Cabane *et al.*, 2001), as discussed in Sections 3.3.2 and 3.4.3.

3.4.6 Pegmatites

The largest crystals occur in *pegmatites* (Palache, 1923; Frondel, 1935; Jahns, 1953; Rickwood, 1981). Some are extremely large: so large, in fact, that a quarry is reputed to have been opened up in a single feldspar crystal (Lindgren, 1933; Rickwood, 1981). Examples of the largest recorded silicate crystals (with approximate size and mass) are beryl (18 metres long, 379 tonnes), spodumene (13–14 m long, 28–66 t), microcline (49 m long, 16 000 t), perthite (11 m long, 230 t), orthoclase (10 m long, 102 t) and muscovite (5 m × 3 m, 77 t), as recorded by Rickwood (1981). Obviously most pegmatite fabrics are outside the range of the microscope, but they reflect the kinds of controlling processes discussed in this chapter, and so are relevant to the discussion.

Most large bodies of felsic magma at depth cool slowly to produce coarse-grained granites with restricted grainsize, and most small bodies of felsic magma at high crustal levels cool rapidly to produce much finer-grained microgranites and aplites. Yet most pegmatite bodies are relatively small (generally less than 50 m long) and most cool at relatively high levels in the crust, so that cooling rate cannot be the main factor in controlling their grainsize. The very coarse grainsize of most pegmatites — larger than about 3 cm (Clarke, 1992) — reflects a very low $N : G$ (Section 3.1), which appears to be related mainly to an abundance of water in the melt. For example, Fenn (1974) found experimentally that the nucleation of alkali feldspar is greatly delayed in water-saturated melts. In fact, the giant crystals mentioned above result from the lowest $N : G$ ratios in Earth's crust.

The difficulty of nucleation in hydrous melts is generally ascribed to the ability of water to hydrolyse and therefore break O–Si and O–Al bonds, so inhibiting the formation of viable nuclei, as discussed in Section 3.2.1. However, experimental data on aluminosilicate glasses suggest that the hydroxyl associates mainly with K and Al, so that nucleation of feldspars is inhibited to a greater degree than that of quartz (London, 1992). The addition of B or P also decreases nucleation rates (London, 1992).

The experiments of Fenn (1974) show that although nucleation rates for alkali feldspar are much lower in water-rich granitic melts than in water-undersaturated melts, once nucleation occurs, growth is relatively rapid. The experiments of Swanson (1977) also revealed rapid growth rates for feldspar and quartz. In fact, growth rates of feldspar and quartz in silicate melts determined experimentally could produce crystals as large as those observed in typical pegmatites in just a few years (London, 1992) or much less in small pegmatite bodies. For example, thermal modelling of mineral growth rates has suggested that crystallization in the centre of pegmatite dykes emplaced into rocks at 150 °C at 5 km depth can be complete in *c*. 9 years for a dyke 25 m thick and as little as *c*. 5 days for a dyke 1 m thick (Webber *et al*., 1999). However, these are minimum cooling times, based on an assumption that crystallization begins at the time of emplacement, whereas nucleation could be delayed.

The change from a granite grainsize to a pegmatite grainsize is usually explained by a felsic magma becoming oversaturated in water, implying that water vapour and silicate melt are involved in the formation of pegmatites (see, for example, Jahns & Burnham, 1969; Jahns, 1982). However, experiments have shown that the presence of water vapour in felsic melts actually reduces crystal growth rates, relative to vapour-free melts (Swanson, 1977; Fenn, 1977). Moreover, petrological and fluid-inclusion studies suggest that pegmatite magmas do not become water-saturated until almost solid (London, 1992, p. 535). In addition, large, abrupt grainsize changes have been produced experimentally in water-undersaturated melts, suggesting that the large grainsize of pegmatites is not related to water saturation (London *et al*., 1989; London, 1992, 1996). However, the occurrence of miarolitic cavities (Section 3.14.6) in the core zones of some pegmatites confirms that water may be released in the late stages of crystallization (Webber *et al*., 1999, p. 709). Moreover, Veksler *et al*. (2002) have presented evidence for the coexistence of three immiscible fluids in pegmatite bodies, and have suggested that the pronounced mineralogical variation of pegmatites may be due to gravitational separation of low-viscosity, volatile-rich pegmatitic fluids. London (1999) suggested that accumulation of volatile-rich melt expelled ahead of a front of crystallization could produce sharp compositional and structural zones in pegmatites, as well as volatile-rich miarolitic zones at or near the centre of pegmatite bodies.

An alternative suggestion is that the large grainsize of pegmatites may be due to injection of hydrous granitic magma into much cooler rocks, which effectively quenches the magma (London, 1992), thus undercooling it, lowering $N : G$ and delaying nucleation. The water and other volatile components of the magma reduce N to a minimum, while promoting high G. This can explain the grainsize of pegmatites intruded into cool rocks, but many pegmatites occur in relatively high-temperature regional metamorphic terranes. For these pegmatites, delaying of nucleation (caused by difficulty of nucleation in the hydrous volatile-rich melt) for a long enough part of the cooling period could force crystallization in the remaining part of the cooling period to be rapid. This could also apply to high-level pegmatites if the overall cooling rate were relatively slow after the initial quench.

Thus, the unusually large crystals in pegmatites result from exceptionally low N and exceptionally high G in the hydrous magma. This is an example of crystallization at strongly supersaturated conditions (Sections 3.5.1, 3.5.4) in a plutonic environment, showing that large grainsizes may be produced — even during rapid crystallization — if $N : G$ is exceptionally low. The reason it doesn't generally occur in such environments is probably mainly that larger bodies of granitic magma do not undergo much undercooling, and that their water and volatile contents are more normal, promoting a larger $N : G$. Another process contributing to the very large grainsize could be solution of small crystal particles and nuclei, and the concomitant growth of large crystal particles, in the nucleation and early growth stage, by the process of Ostwald ripening (Higgins, 1998).

Because of the long delay in nucleation, crystals are forced to nucleate heterogeneously on the walls of the magma chamber (e.g. dyke walls) and grow inwards, producing the spectacular 'comb structure' (Section 3.5.4) shown in some pegmatite bodies. Strong supersaturation can also explain the dendritic grain shapes shown by many pegmatites (Section 3.5.3). The numerical modelling of Baker & Freda (1999) has reproduced the dendritic grain shapes and highly variable mineral distributions of pegmatites, on the basis of local variations in growth and diffusion rates.

The relative rarity of pegmatitic rocks of mafic composition is probably due to the lower degree of polymerization and consequently higher N of mafic melts (Section 3.2). However, coarse-grained segregations of plagioclase, clinopyroxene and Fe–Ti oxide minerals occur in the upper parts of some dolerite sills and even very fine-grained basalt flows (see, for example, Puffer & Horter, 1993, and references therein). Puffer & Horter (1993) attributed the segregations to the crystallization of residual melt carried up through the hot interiors of flows or sills by vapour bubbles. Any small crystals or crystal nuclei would be dissolved as the melt passed through the hot interior of the magma body, greatly reducing N and hence $N : G$. Diffusion of chemical components in the water-enriched melt would assist the rapid growth (Puffer & Horter, 1993). In contrast, the adjacent,

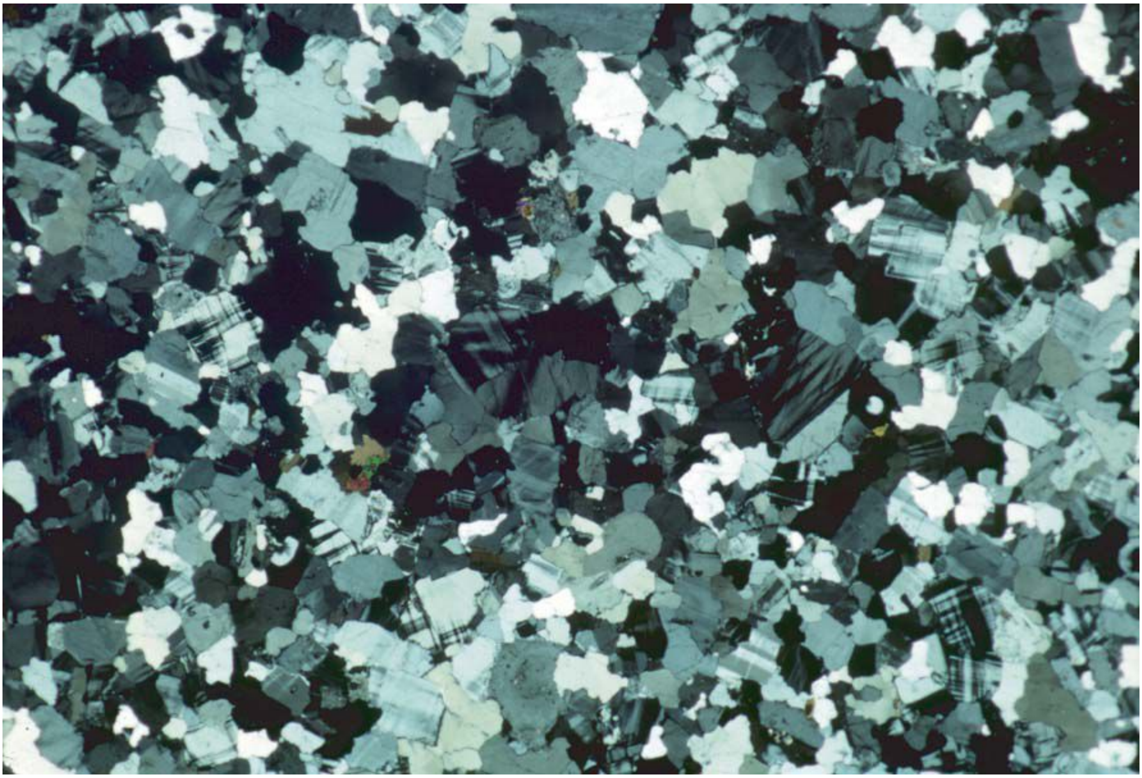

Fig. 3.14: Aplite, consisting of relatively fine-grained, equigranular quartz, K-feldspar (with prominent microcline twinning), and minor plagioclase, Tioga Pass, Sierra Nevada, California, USA. Indented grain boundaries are common in aplites, and probably reflect mutual interference of minerals crystallizing together at the solidus. The indentations may be due to: (1) all these minerals having relatively isotropic crystal structures, such that no low-energy planar interfaces are formed, or (2) formation of local segments of relatively low-energy interfaces (Section 4.2.4). Crossed polars; base of photo 5.5 mm.

water-poor magma crystallized as a much finer-grained rock, owing to a much larger $N : G$.

3.4.7 Aplites

The common occurrence of fine-grained *aplites* (Fig. 3.14) adjacent to compositionally similar pegmatites suggests that both rock types can crystallize simultaneously at the same temperature. The aplites may result from rapid loss of water and/or other volatile components, consequent on pressure release ('pressure quenching'), as suggested by Jahns & Tuttle (1962). This would increase the proportion of O–Si and O–Al bonding in the melt and hence increase the formation of feldspar and quartz nuclei, resulting in larger *N* : *G*. A sudden drop in pressure (Webber *et al.*, 1999) or extraction of boron from the melt by crystallization of tourmaline (Rockhold *et al.*, 1987) can also produce conditions favourable for the development of aplite. Presumably these factors also account for the fine grainsize of the groundmass in microgranite dykes formed by rapid cooling at high crustal levels. In contrast, pegmatites retain water and/or other volatile components, inhibiting nucleation and promoting rapid growth on scarce nuclei (smaller *N* : *G*).

3.5 Grain shapes in igneous rocks

3.5.1 Introduction

The most general factor controlling the shapes ('habits') of crystals growing in liquids is the *degree of supersaturation*, which is the difference between the actual concentration of a chemical component in the liquid and the concentration at equilibrium (i.e. when the magma is just saturated with the component) at a specified temperature and pressure. Supersaturation is a useful general term that embraces the effects of undercooling (Fig. 3.2), as well as changes in pressure and in the concentration of components in the liquid. For example, the larger the ratio of growth rate of the crystal (*G*) to the diffusion rates (*D*) of 'nutrient' (chemical components required by the growing crystal) and 'impurity' (chemical components not wanted by the growing crystal) in the melt, the larger the degree of supersaturation (Keith & Padden, 1963; Tiller, 1964; Knight, 1967). In effect, concentration gradients are set up in the liquid immediately surrounding the growing crystal, which consequently is forced to grow in a melt of locally changed composition, which in turn forces it to change its growth habit (Section 3.5.3). Thus, grain shape is controlled by the ratio *D* : *G*, where *D* is the diffusion rate of a rate-controlling chemical component (i.e. a chemical component governing the growth of the crystal) in the liquid, and *G* is the crystal growth rate, as used previously.

Euhedral (idiomorphic, automorphic, polyhedral) crystals (Section 3.5.2) grow at small to moderate degrees of supersaturation (Fig. 3.2), where *G* is small and *D* is large (interface-attachment-controlled *G*; Section 3.3.2). In contrast, skeletal and dendritic crystals (Section 3.5.3) and spherulites (Section 3.5.5) grow at greater degrees of supersaturation (see, for example, Donaldson, 1974), where *G* is large and *D* is small (diffusion-controlled *G*; Section 3.3.2). To avoid a stage of polyhedral crystal growth altogether, a high enough degree of supersaturation must be induced fast enough to avoid nucleation under conditions of low supersaturation, as in the eruption of crystal-free lava.

Dendritic crystals typically grow relatively rapidly (in response to high *G*), for example, in quenched experimental melts (see, for example, Lofgren, 1980), chilled lavas (see, for example, Bryan, 1972) and meteorites, as shown in

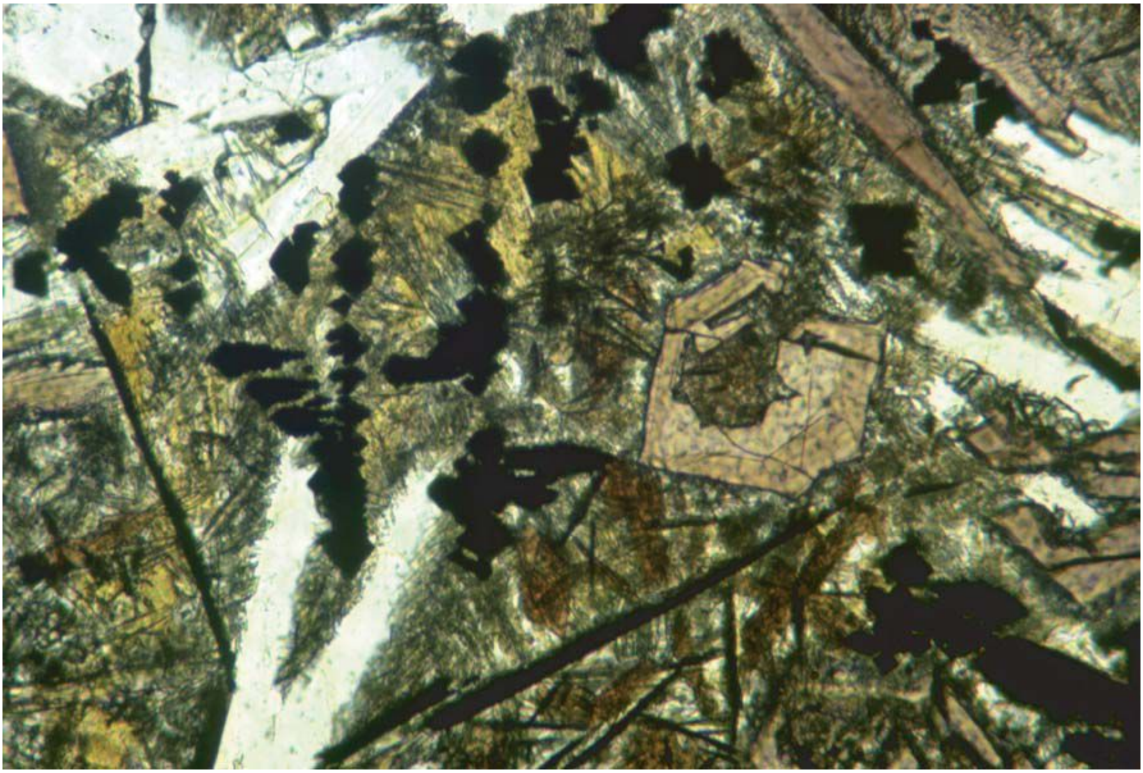

Fig. 3.15: Dendritic crystals of titanomagnetite (opaque), skeletal crystals of clinopyroxene (purple-brown titanaugite) and acicular (needle-like) microlites of pyroxene, titanomagnetite and apatite in basalt, Bowral, New South Wales, Australia. Plane-polarized light; base of photo 0.8 mm.

Figs. 3.15–3.24. However, dendritic habits may also occur in intrusive, coarse-grained, mafic–ultramafic rocks (see, for example, Donaldson, 1974) and granites (see, for example, Moore, & Lockwood, 1973; Vernon, 1985), which are generally in large intrusions that cool much more slowly, indicating that $D : G$, not G alone, is the controlling factor in dendritic growth. Dendritic growth habits may also occur in granitic pegmatites, which are generally in small intrusions that have been inferred to cool much more rapidly, despite their very coarse grainsize (London, 1992), although delayed nucleation is an alternative explanation, as discussed in Section 3.4.6.

3.5.2 Euhedral (idiomorphic, polyhedral) crystals: growth mechanisms

For large bodies of magma crystallizing slowly at depth, the degree of undercooling is small, and the process controlling the growth rate is the reaction at the

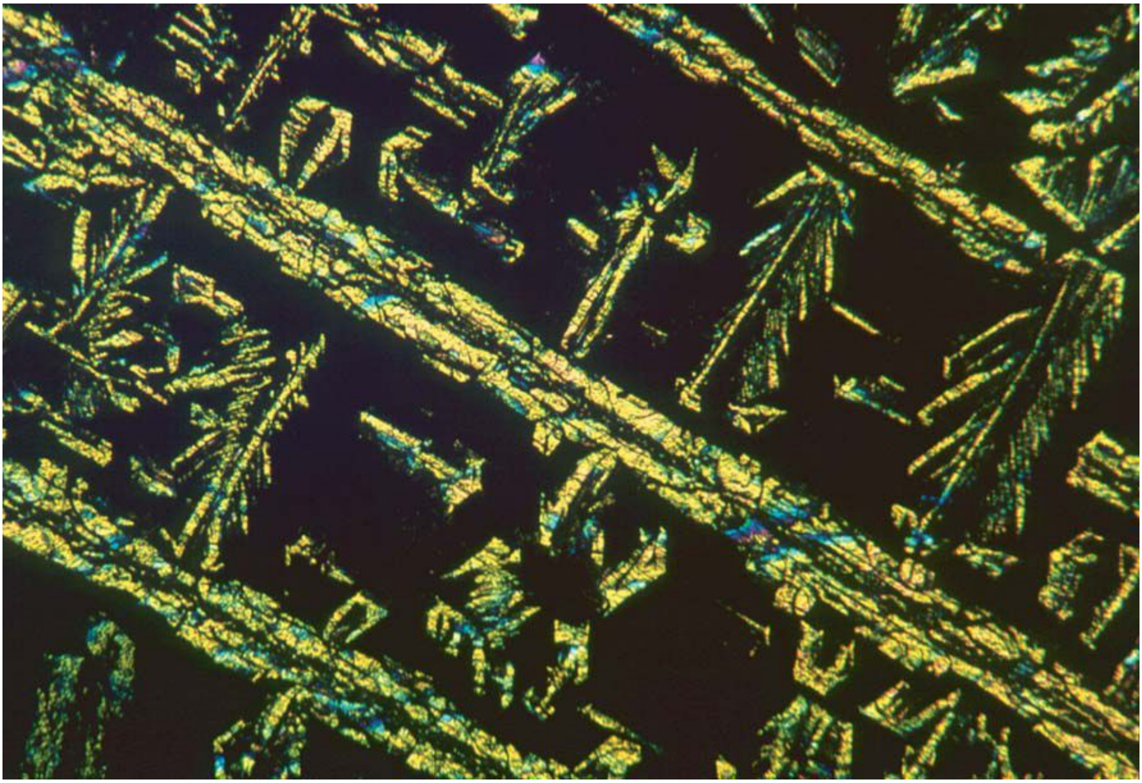

Fig. 3.16: Furnace slag with highly dendritic crystals of olivine that are similar to dendritic olivine in komatiites, chilled basalts and chondrules in chondritic meteorites. Crossed polars; base of photo 3.5 mm.

interface between the crystal and the liquid (Kirkpatrick, 1975, 1981). That is, diffusion of chemical components in the melt is too fast to control the growth rate.

The shape of a volume of a phase in equilibrium with another phase is governed by the tendency to minimize the total interfacial free energy between them, which is a function of the interfacial free energy (γ) and the area of the interface concerned. If both phases were isotropic with regard to their atomic organization, the equilibrium shape would be a sphere, because this reduces the interfacial area to a minimum. However, because of the anisotropic atomic structure of most solid compounds, solid–vapour, solid–liquid, and solid–solid interfacial energies (Sections 3.2 and 4.2) are also generally anisotropic. Therefore, many crystals growing freely in fluids develop planar rational faces (crystallographic planes with simple Miller indices), which are at least indirectly determined by the crystal's atomic structure (see, for example, Buerger, 1947; Fullman, 1957; Hartman, 1958, 1973, 1978, 1982; Hartman & Perdok, 1955; Jackson *et al.*, 1967; Hartman & Bennema, 1980).

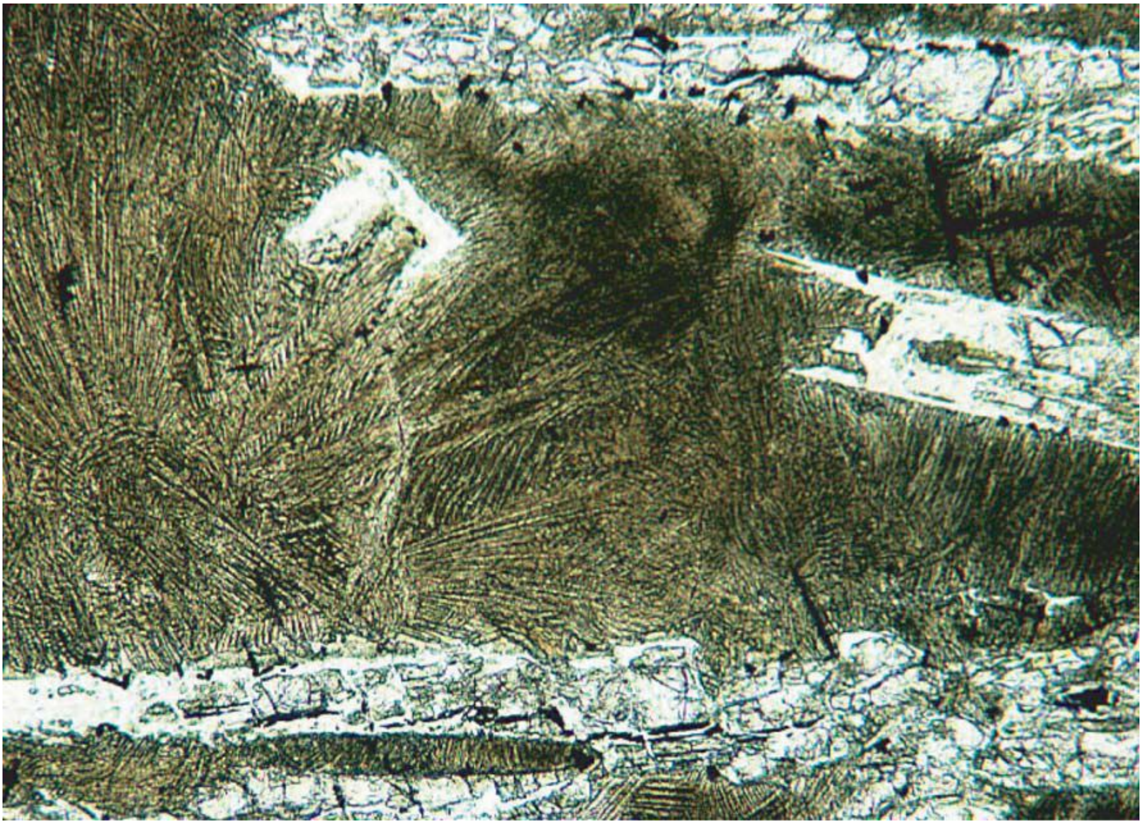

Fig. 3.17: Skeletal phenocrysts of olivine (partly pseudomorphed by low-temperature serpentine) in a groundmass of fern-like, radiating, dendritic crystals of pyroxene, in an Archaean ultramafic volcanic rock (komatiite) from Western Australia. The olivine phenocryst at right has spikes developed from its corners. This and the fern-like pyroxene microstructures were formed in response to the rapid cooling of the lava. From Vernon (2000b, fig. 64). Plane-polarized light; base of photo 3.5 mm.

For a given degree of undercooling, the crystal adopts a shape that allows the highest rate of growth (Tiller, 1964). At small degrees of undercooling, the growth rate is low (Fig. 3.2), so that the crystal–liquid interface moves slowly relative to the removal of unwanted components. Under these conditions, a planar interface can develop.

The equilibrium form (equilibrium shape) of most mineral crystals is bounded by planes (faces) of lowest interfacial free energy. Theoretical equilibrium forms may vary from symmetrical polyhedra to smoothly curved shapes, and some forms have both planar and curved portions (Hartman, 1973). For example, spherical grains of carbonate in carbonatites have been interpreted as phenocrysts with primary shapes, as produced experimentally (see, for example, Gittins, 1973,

Fig. 3.18: Skeletal phenocrysts of olivine (mainly pseudomorphed by low-temperature serpentine) aligned by magmatic flow, in a groundmass of spiky, fern-like, dendritic crystals of pyroxene, in an Archaean ultramafic volcanic rock (komatiite) from Western Australia. From Vernon (2000b, fig. 65). Plane-polarized light; base of photo 3.5 mm.

p. 226). However, silicate minerals typically develop planar crystal faces when growing freely in silicate magmas (Figs. 3.5–3.9). This is because their faces are parallel to particularly densely packed planes of atoms, which should be flat, according to the theoretical analysis of Jackson (1958). Crystal faces are *surfaces of least bonding* (Dowty, 1976a), which implies that strong bonds occur parallel to the faces, but relatively weak bonding occurs across them.

The actual shapes (growth forms) of crystals in a liquid may differ from the theoretical equilibrium forms. For example, the equilibrium form of fluorite is the octahedron, but the growth form is generally the cube. Departure from the equilibrium form may occur because of non-equilibrium (kinetic) factors, such as the adsorption of impurity atoms onto the interface, altering its energy (Kretz, 1966a; Jackson, 1967; Hartman, 1973). The adsorbed impurity atoms change the rates at which atoms or atom groups can join or leave the growing crystal, and so may change the crystal shape (Jackson, 1967).

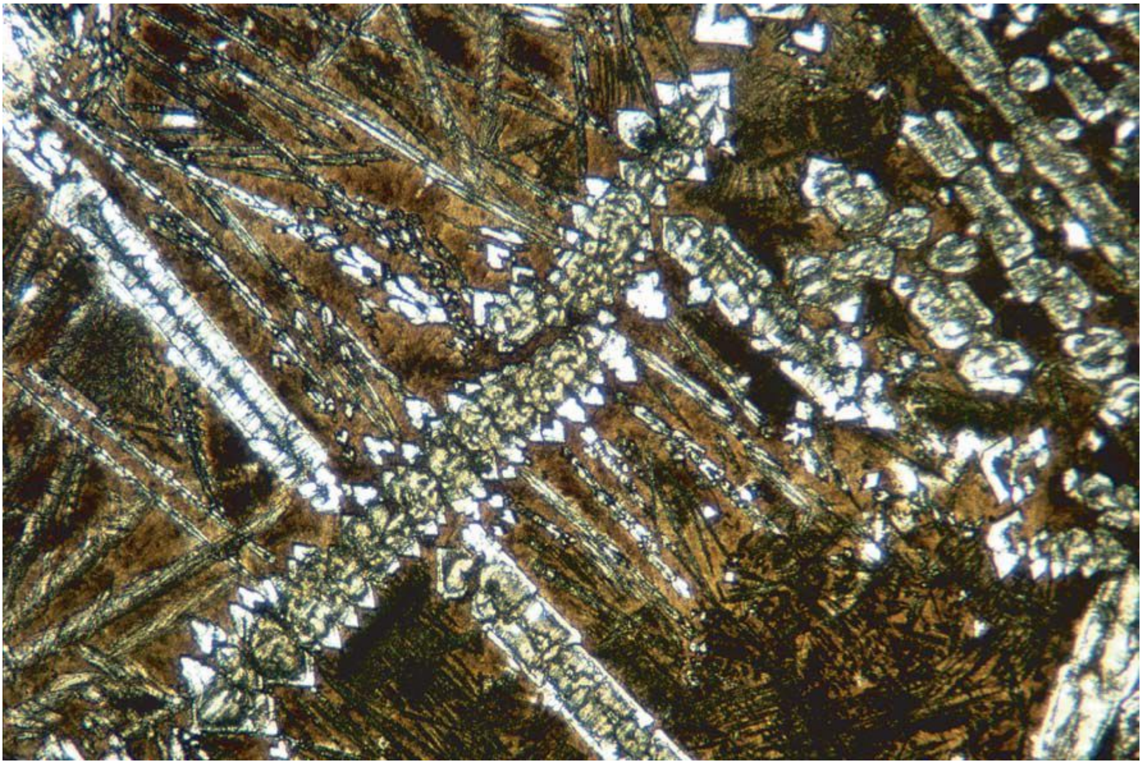

Fig. 3.19: Dendritic phenocrysts of olivine in a glassy groundmass, in a komatiite from Western Australia. Plane-polarized light; base of photo 4 mm.

Free growth of crystals in silicate magmas and hydrous solutions (as in cavities and veins; Section 5.9.3) generally results in polyhedral growth forms, but crystal faces may not develop where crystal growth is impeded by other crystals (Section 3.5.9).

The rate of advance of a crystal boundary depends on the details of the interface structure, involving factors such as direction and strength of atomic bonding, which control the ease of attachment of atoms and atom groups (Jackson *et al.*, 1967). During growth of a euhedral crystal, higher-energy faces tend to grow faster than lower-energy faces, so that they are eventually removed, leaving a crystal bounded by slower-growing, lower-energy faces, which are the most stable under the prevailing conditions (Fig. 3.25A). This is because higher-energy faces are *stepped* and so have more attachment sites for atoms or atom groups (Fig. 3.25B). In contrast, advance of *planar* crystallographic interfaces is generally much slower, at comparable degrees of undercooling, because growth has to occur by the lateral propagation of growth steps across the interface, the steps permitting more secure attachment of atoms (Southin & Chadwick, 1969; Lewis, 1974), as shown in Fig. 3.26. Thus, the growth form of a crystal is actually

Fig. 3.20: Long, delicate spikes that grew on a plagioclase phenocryst during rapid cooling. Later spherulitic growth occurred in the groundmass. From Vernon (2000b, fig. 80). Plane-polarized light; base of photo 4.4 mm.

controlled by the rate at which atoms can attach to different faces, as emphasized by Dowty (1976a), although this is indirectly related to the crystal structure. The overall result is that low-energy faces determine the crystal shape (habit).

Originally, steps were thought to originate by repeated nucleation of new surface layers, which is a requirement of the simple model of addition of atoms to a surface, because completion of a layer would leave no step for the growth of a new layer. However, the theoretical prediction of the rate at which a crystal should grow by this mechanism at low supersaturation was smaller than the observed rate by a factor of 10^{1000}, which may take the record for the greatest ever discrepancy between theory and experiment (Fullman, 1955, p. 2). This result necessitated the discovery of a mechanism involving continuous creation of new layers at persistent surface defects, but no suitable mechanism was available until Franck's (1949) suggestion that a *screw dislocation* emerging at the surface of a growing crystal could provide a permanent step (Fullman, 1955; Southin & Chadwick, 1969), as explained below.

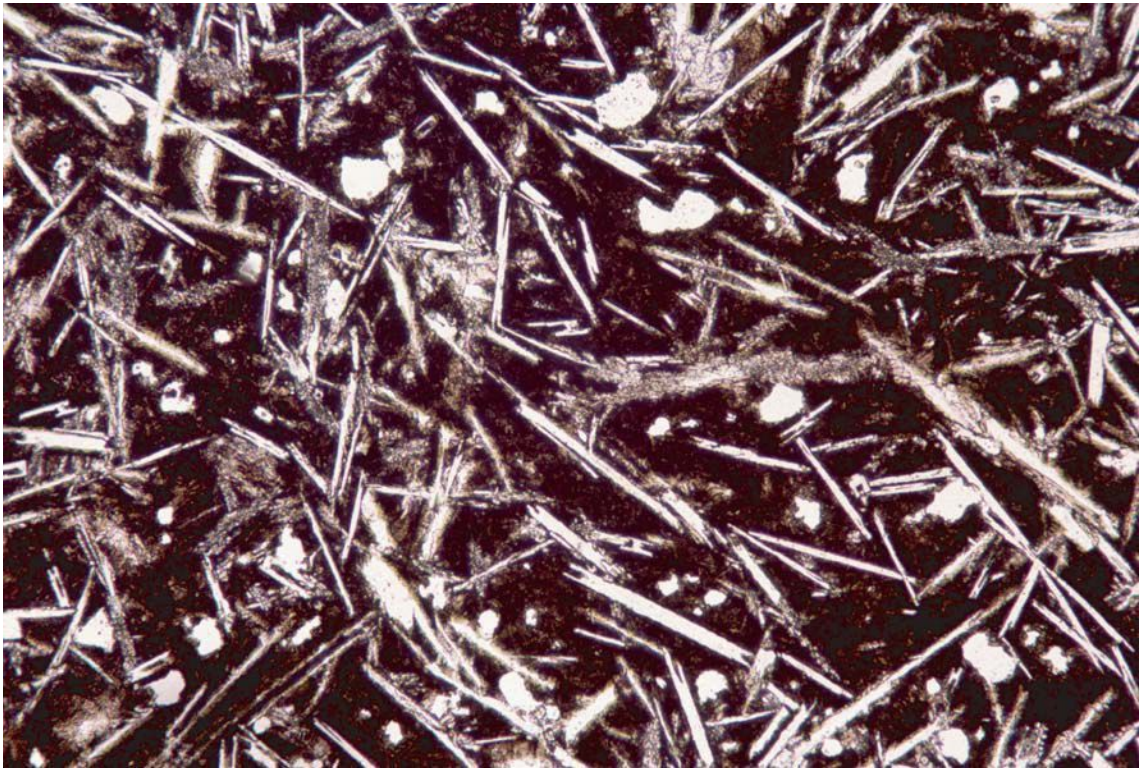

Fig. 3.21: Spiky plagioclase crystals ('swallow-tail' microlites) and dendritic olivine phenocrysts (higher relief) in basalt from Iceland. Plane-polarized light; base of photo 0.7 mm.

Dislocations (line defects) are invariably present in crystalline materials. They may be formed during crystal growth and especially during deformation (Section 5.3). A relatively clear picture of a simple dislocation is shown in Fig. 3.27. Dislocations are of two 'end-member' types, namely edge dislocations and screw dislocations, in-between varieties being known as general dislocations (Fig. 3.28). If screw dislocations intersect the surface of a crystal, they produce spiral ramps (Fig. 3.29), as observed on the surfaces of some synthetic crystals. Similar stepped, spiral growth patterns have also been observed on the surfaces of many natural crystals (graphite, sphalerite, pyrite, quartz, hematite, corundum, fluorite, calcite, barite, topaz, muscovite, biotite, phlogopite, garnet, beryl and clay minerals) that have grown in open spaces from hydrothermal solution or vapour (Seager, 1953; Sunagawa, 1964, 1974, 1977, 1981, 1984, 1987; Baronnet, 1972, 1975; Sunagawa & Koshino, 1975; Sunagawa *et al.*, 1974).

These observations have been made on solid–fluid interfaces. Unfortunately, the solid–solid interfaces of crystals in rocks generally cannot be observed in this

Next Page

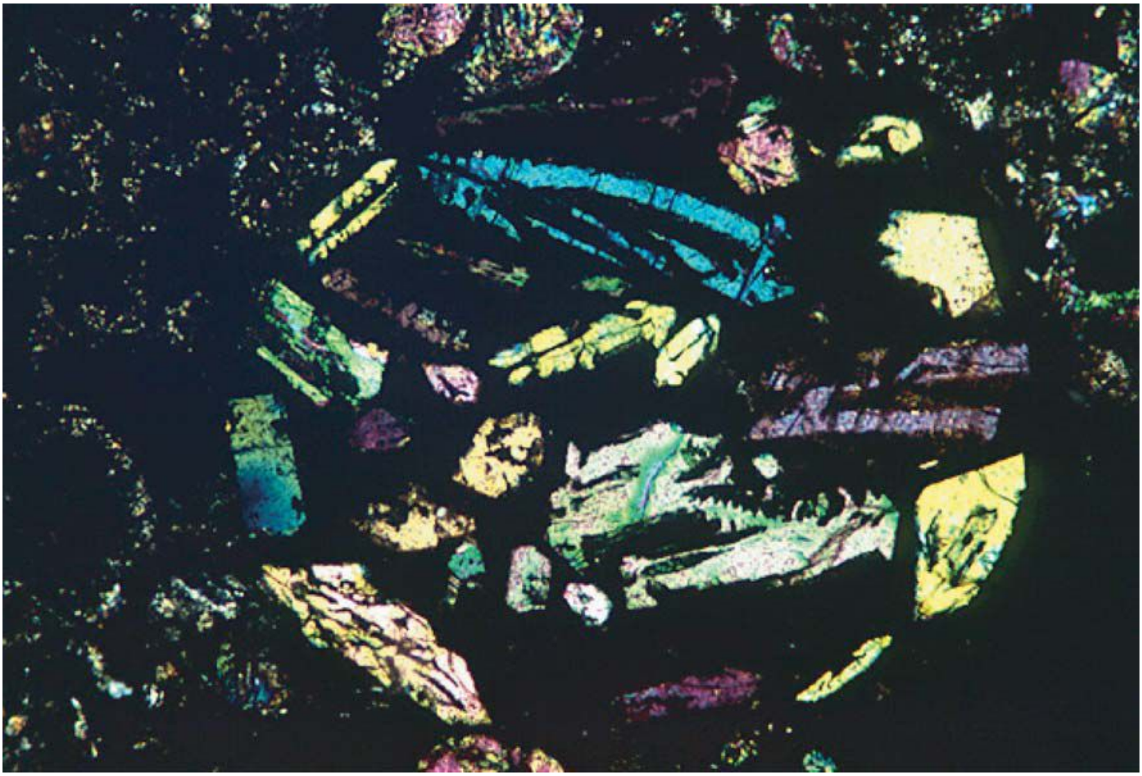

Fig. 3.22: Skeletal olivine phenocrysts in a glassy chondrule in a chondritic meteorite found east of Tillibigeal, New South Wales, Australia. The spherical chondrule was formed by the very rapid cooling of a melt droplet in the solar nebula. From Vernon (2000b, fig. 170). Plane-polarized light; base of photo 1.75 mm.

way, owing to the difficulty of breaking grains perfectly along the original interface between them. However, Pearce (2001) described garnet phenocrysts with well-preserved crystal faces separated from a trachytic tuff, which he examined with Nomarski differential interference contrast in reflected light. This technique revealed spiral growth pyramids with steps less than 0.5 μm high, suggesting growth involving screw dislocations. The steps are too small to see in a transmitted light microscope, in which they resemble the oscillatory zoning (Sections 3.11.5, 4.12.1) that is also present. However, the compositional zones are about five times thicker than the steps, suggesting that two processes may act concurrently during growth, namely (1) surface growth controlled by screw dislocations on the scale of about 150 unit cells, and (2) crystal–liquid interactions producing broader chemical oscillations at a slower rate. In addition, possible growth steps and even spirals have been found on the interfaces of some grains physically separated from metamorphic rocks (Section 4.4.2).

Previous Page

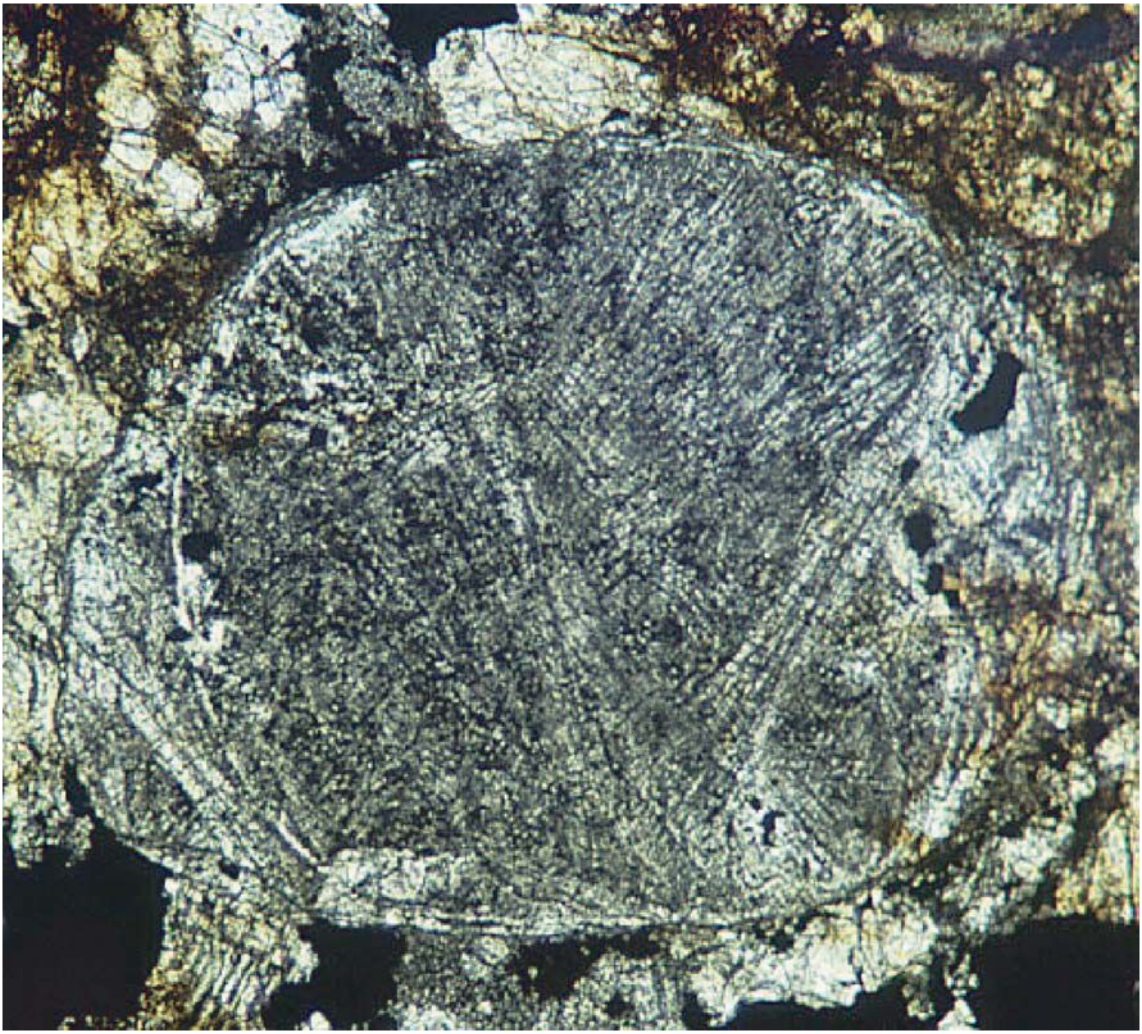

Fig. 3.23: Spiky pyroxene crystals in a chondrule in a chondritic meteorite (chondrite) from Wanaaring, New South Wales, Australia. From Vernon (2000b, fig. 171). Plane-polarized light; base of photo 1.2 mm.

Euhedral crystals of the same mineral may be elongate in some igneous rocks and more equant in others. The following explanation has been suggested by Higgins (1994). The faster-growing faces tend to deplete the adjacent liquid in nutrient components more than slower-growing faces. In stagnant liquid, this tends to slow the advance rate of these faces, with the result that the crystal tends to be relatively equant. However, if new liquid is brought into contact with the crystal (e.g. by flow in the magma), the faster-growing faces can continue to grow, and so the crystal becomes more elongate.

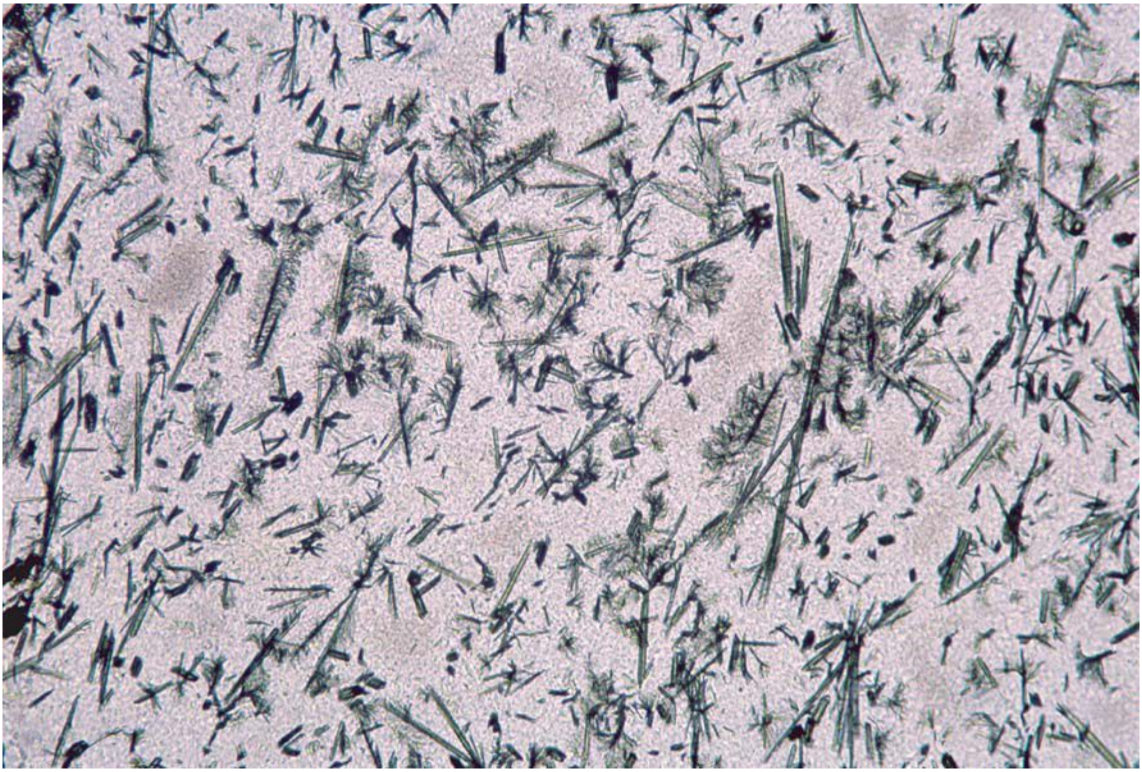

Fig. 3.24: Acicular, spiky and fern-like crystallites and microlites in felsic volcanic glass (obsidian), formed as a result of rapid cooling on Earth's surface. Plane-polarized light; base of photo 4 mm.

3.5.3 Skeletal and dendritic crystals in volcanic rocks

Skeletal crystals are incomplete polyhedral single crystals with internal cavities that are commonly crystallographically controlled (Figs. 3.15, 3.17, 3.18, 3.22). In skeletal crystals in igneous rocks, the cavities are filled with glass (Section 3.5.6) or crystalline groundmass material. *Dendritic crystals* (dendrites) are also single crystals (not aggregates), but have branch-like growth forms (Tiller, 1964; Shumskii, 1964; Doherty, 1975), as shown in Figs. 3.15, 3.16 and 3.19. Spikes and dendrites may form overgrowths on polyhedral crystals (see, for example, Bryan, 1972, p. 5814), as shown in Figs. 3.17, 3.20 and 3.21.

The relatively large interfacial free energies caused by the large interfacial areas of spiky (needle-like, acicular), skeletal and dendritic crystals should be unfavourable for stable growth. Under small degrees of supersaturation, polyhedral crystals with minimum interfacial free energies form instead, as discussed above. However, if the degree of supersaturation is large, skeletal and dendritic crystals are forced to develop by *constitutional (compositional) supersaturation*.

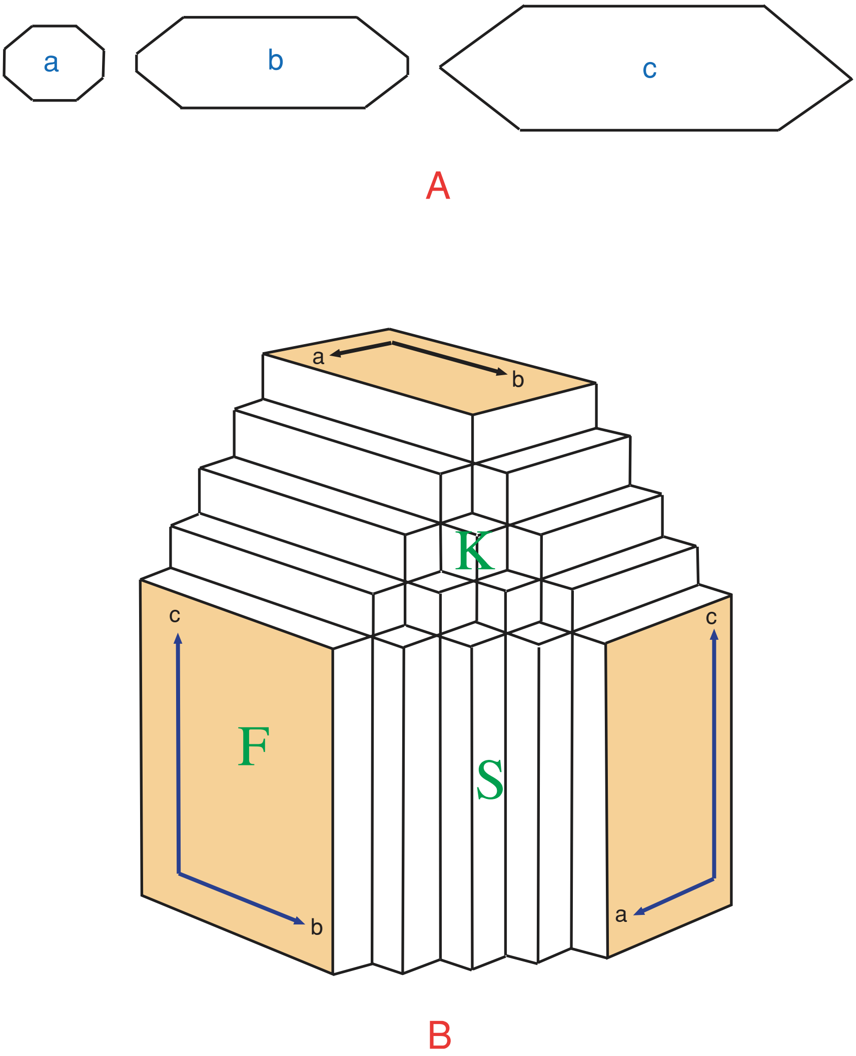

Fig. 3.25: (A) Sketches illustrating the progressive removal (from a to c) of more rapidly growing crystal faces, so that the final polyhedral crystal is bounded only by the slowest-growing faces. (B) Sketch showing contrast between high-energy, stepped faces and low-energy, smooth crystal faces. More secure attachment sites occur on the stepped faces, and so they grow fastest, eventually to be eliminated in favour of the slower-growing low-energy faces. Chains of strongly-bonded atoms are represented by a, b and c. The three flat, low-energy faces (F) have two such chains, and so have more strong bonds parallel to their surfaces. The two singly stepped faces (S) have only one such chain and the doubly stepped ('kinked') face (K) has none. Attachment of new atoms is most secure and hence most likely at the kinked face, less so at the singly stepped face, and even less so at the flat face. After Hartman (1973).

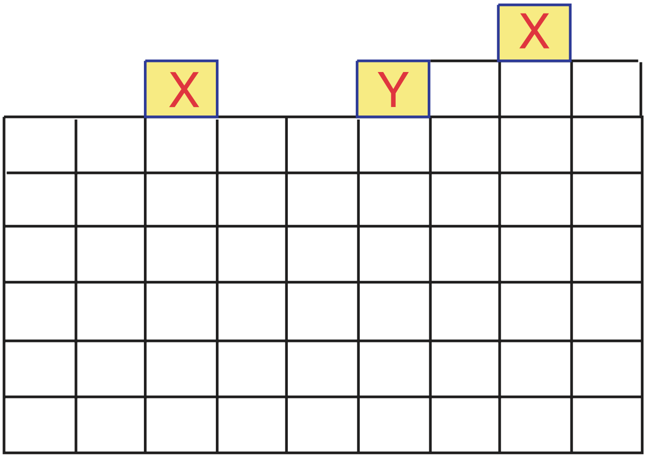

Fig. 3.26: Sketch contrasting the increased attachment of an 'atom' at site Y (on the edge of a step on the surface of a crystal growing in a fluid) compared with the decreased attachment of an isolated atom ('two-dimensional nucleus') on the crystal surface (sites X).

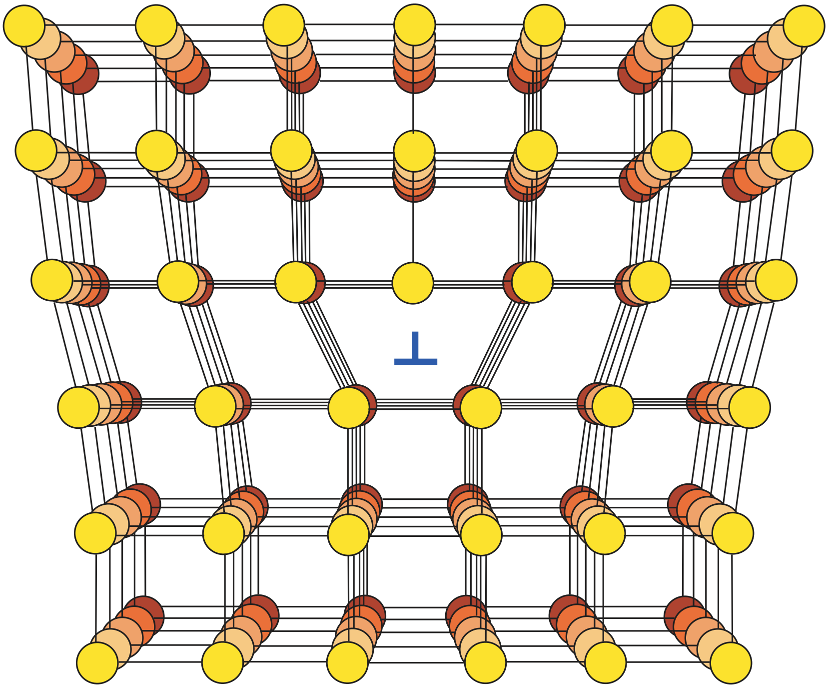

Fig. 3.27: Diagram of part of a simplified cubic crystal, showing an extra half-plane of atoms and the consequent point of emergence of a dislocation (line defect) represented by the inverted T symbol; i.e. the dislocation is a line pointing away from you. This is an *edge* dislocation (see Fig. 3.28). Based on a diagram in Guy (1959, p. 110).

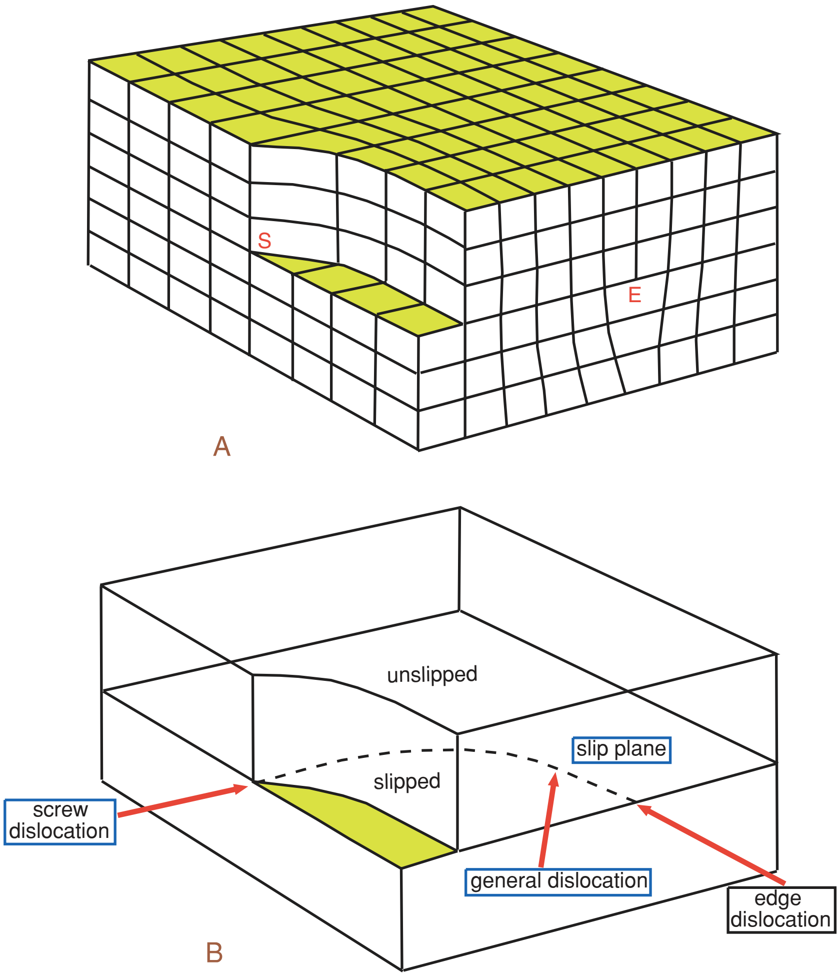

Fig. 3.28: (A) Diagram of dislocations inside a portion of an idealized cubic crystal, showing an *edge dislocation* (E) and a *screw dislocation* (S), with a *general dislocation* between. (B) Diagram helping to visualize the situation in (A). The dislocation is a line (line defect) separating portions of crystal that have been displaced (slipped) by movement of the dislocation from portions that have not been displaced (unslipped). The terms 'slip' and 'slip plane' are especially applicable to dislocations formed and moved by deformation (Section 5.3).

In a polycomponent system (such as a silicate melt), if low-temperature components not wanted by the growing crystal cannot diffuse away into the liquid fast enough, they become concentrated in a narrow zone adjacent to the interface (Fig. 3.30), especially if their diffusion rates (*D*) in the liquid are very low at the temperature concerned. The concentrated 'impurity' components effectively lower the equilibrium freezing temperature ('liquidus'), which reduces the degree of supersaturation for the crystallizing mineral at the interface (Fig. 3.30). In most minerals, the crystal has a higher concentration of the

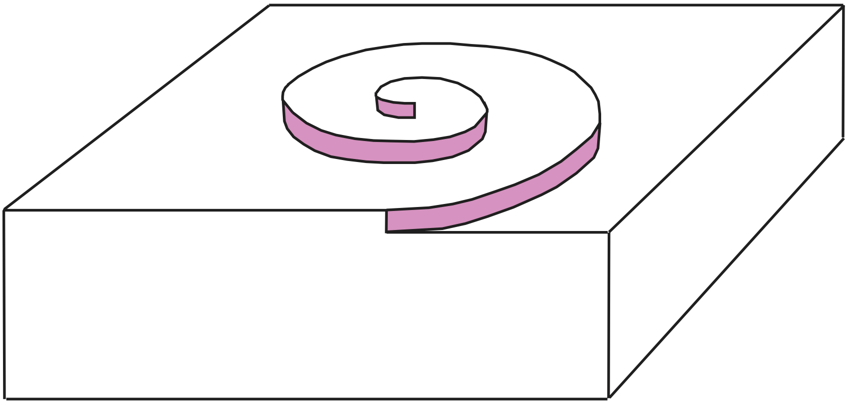

Fig. 3.29: A screw dislocation outcropping on the surface of a crystal can provide a permanent step for the addition of atoms (Fullman, 1955, p. 4). A screw dislocation can be imagined as resulting from a cut through the crystal, followed by slipping of the two sides over one another. The resulting step is anchored at the end of the cut, which causes the step to pivot around the anchor as atoms are added at the step.

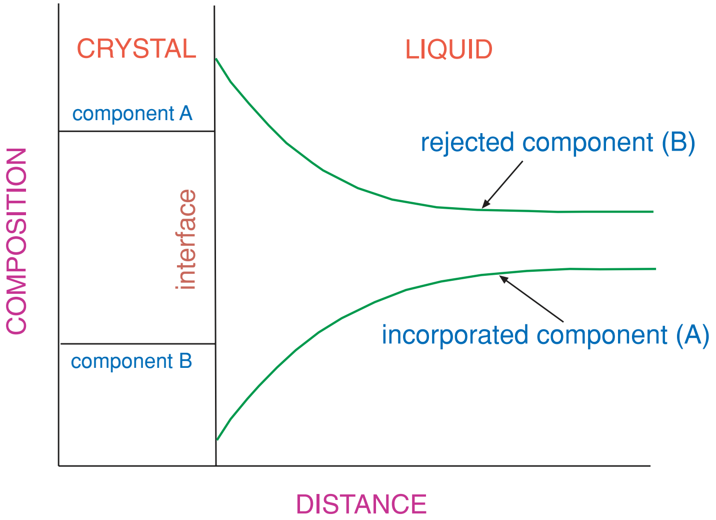

Fig. 3.30: Composition gradients in melt adjacent to a growing crystal when diffusion is not fast enough to eliminate gradients; after Kirkpatrick (1981, fig. 34), with permission of the Mineralogical Society of America.

higher-temperature melting components, e.g. the anorthite component for plagioclase (Fig. 3.31A), so that the expelled lower-temperature melting component (albite for plagioclase) concentrates at the interface, thereby reducing the liquidus temperature to the smallest value of any composition in the surrounding liquid (Fig. 3.31B). In addition, the liquid right at the interface has the highest temperature of any of the surrounding melt, owing to release of latent heat of

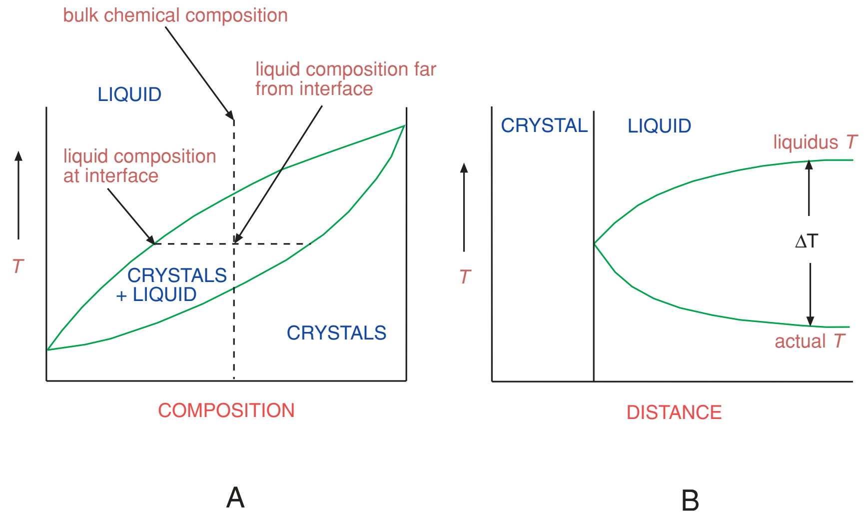

Fig. 3.31: (A) Compositions involved in diffusion-controlled growth of crystals of a mineral that is a solid solution of two chemical components (e.g. plagioclase). After Kirkpatrick (1981, fig. 37), with permission of the Mineralogical Society of America. (B) Undercooling distribution in the melt adjacent to a growing crystal that is rejecting impurity components. After Kirkpatrick (1981, fig. 38), with permission of the Mineralogical Society of America.

crystallization by the growing crystal, although this diffuses away much faster than impurity components and so has a much smaller effect. The accumulation of ‘impurity’ components around the crystal means that the supersaturation of the melt increases with increasing distance from the interface until it reaches a steady value (Fig. 3.30). Further crystal growth is only possible in liquid further away from the interface, where liquid of normal composition is available (Fig. 3.30).

Planar interfaces are unstable under these conditions of strong constitutional supersaturation, and change into a collection of projections or spikes. The reason is that if part of the interface advances ahead of the rest, it encounters liquid that is poorer in ‘impurity’ components and richer in ‘nutrient’ components, and so it can continue to grow (Fig. 3.32A). Moreover, because of its large interface area, it can lose impurity components more easily. However, owing to the tendency for heat and impurity components to accumulate around the spikes themselves, secondary spikes may be forced to develop on the primary spikes, for crystallization to continue (Fig. 3.32B). These lead to a dendritic habit.

The projections may originate at small protuberances on a formerly planar interface or at corners of former polyhedral crystals, which grow preferentially because of lower impurity concentrations at those points (Fig. 3.32). These lower concentrations are due to the larger ratio of melt volume to crystal surface area at the corners, so that expelled components can diffuse away from the interface

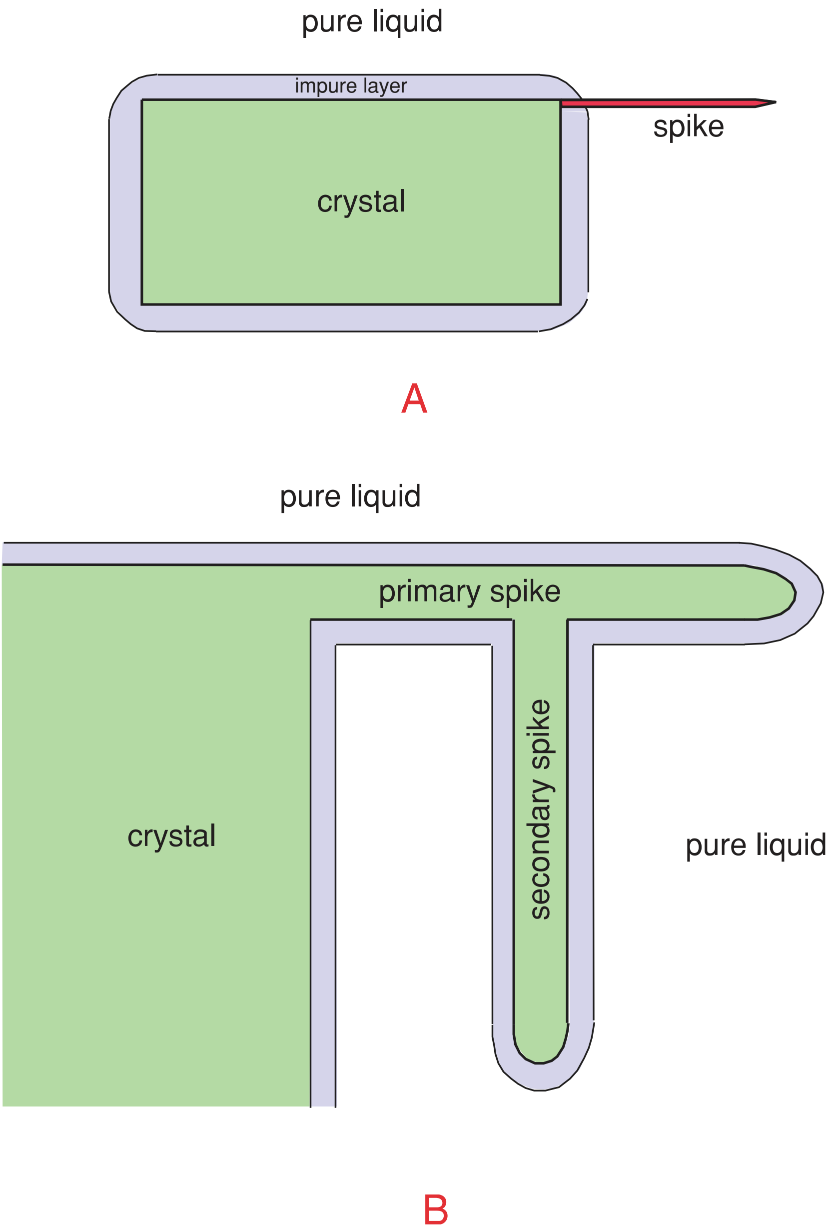

Fig. 3.32: (A) Sketch of spike projecting from crystal corner, through layer of liquid rich in impurity components into pure liquid, initiating dendritic growth habit. (B) Sketch showing development of secondary spike on primary spike, in response to accumulation of impurity components around the primary spike.

faster at corners than from the centres of crystal faces (Kirkpatrick, 1981, p. 366). Growth of spikes from corners is especially common, leading to ‘swallow-tail’ shapes (Figs. 3.17, 3.21), spiky fringes (Fig. 3.20) or extended series of small crystals that grow from the tip of another in a direction bound symmetrically by the slowest-growing faces. Not only the branch directions, but also the spike boundaries are crystallographically controlled (Figs. 3.15–3.21). Note that, although parts of dendrites may appear to be isolated in thin section (Figs. 3.15, 3.16, 3.19, 3.22), they are connected in three dimensions, as witnessed by their identical crystallographic orientation (e.g. same interference colour and simultaneous extinction).

Skeletal, dendritic and spiky crystals of plagioclase (Fig. 3.20), olivine (Figs. 3.16, 3.17, 3.19, 3.21), pyroxene (Fig. 3.15) and magnetite (Fig. 3.15) occur in quenched volcanic rocks (see, for example, Drever & Johnston, 1957, 1972; Gibb, 1974; Gélinas & Brooks, 1974; Haggerty, 1976; Long & Wood, 1986; Bloomer & Hawkins, 1987; Stimac *et al.*, 1990; van der Voo *et al.*, 1993), including submarine basalts (Bryan, 1972), lunar basalts (Dowty *et al.*, 1974; Donaldson *et al.*, 1976) and Archaean magnesian basalts or komatiites (see, for example, Viljoen & Viljoen, 1969; Nesbitt, 1971; Pyke *et al.*, 1973; Dickey, 1973; Fleet, 1975a,b; Fleet & MacRae, 1975; Arndt *et al.*, 1977; Arndt & Nisbet, 1982; Arndt, 1986). For example, Gélinas & Brooks (1974) described excellent examples of dendritic plagioclase (acicular, hollow, swallow-tail forms, rosettes, and some with very acicular extremities), clinopyroxene (plumose, radiating to sheaf-like) and olivine (hollow, skeletal, skeletal chains and lantern-like) in some Archaean tholeiitic basalts. Skeletal chromite may also occur in komatiites (Barnes, 1998).

Skeletal and dendritic crystals of olivine and/or pyroxene also occur in quenched artificial melts in experiments and slags (Fig. 3.16; Müller *et al.*, 1988; Lofgren & Russell, 1986; Faure *et al.*, 2003b), in glassy chondrules in chondritic meteorites (Figs. 3.22, 3.23), and in shock-melted rocks in meteorite impacts and fault zones (Carstens, 1975; Maddock, 1983; Magloughlin & Spray, 1992; Camacho *et al.*, 1995), as discussed in Section 5.7.10. Therefore, it appears that olivine, pyroxene and plagioclase in most volcanic and synthetic melts are dendritic because of rapid cooling (quenching). The relationship between growth habits and crystal structure has been discussed for olivine by Bezzi & Picasdo (1971), Fleet (1975a), Hart (1978a,b) and Faure *et al.* (2003a) and for clinopyroxene by Fleet (1975b).

Experiments by Lofgren (1974, 1980), Donaldson (1976, 1979) and others have duplicated natural dendritic shapes of olivine, pyroxene and plagioclase. For example, Lofgren (1974) and Corrigan (1982) found that the shapes of plagioclase crystals grown experimentally from the melt vary considerably with degree of undercooling (ΔT). They range from tabular at small ΔT (about 50 degrees) to skeletal (ΔT about 100 degrees), dendritic (ΔT about 200 degrees), and spherulitic (ΔT about 400 degrees).

Dendritic crystals can also grow in felsic lavas (Fig. 3.20). For example, Vogel *et al.* (1987) and Swanson *et al.* (1989) described dendritic overgrowths on crystals of plagioclase, hornblende and biotite in rhyolite, and Ross (1962) described microlites of pyroxene, amphibole, biotite, sanidine and magnetite in unaltered felsic glasses. The pyroxene microlites are of two types: (1) parallel slender prisms, aligned during magmatic flow, and (2) random varieties, occurring as loops, spirals and helices, complexly twisted spidery groups, or beadlike strings of minute segments. These complex shapes would have been disrupted by magma movement and, moreover, some have grown in pumice fragments that collapsed after emplacement. Therefore, Ross (1962) inferred that type (1) microlites grew before emplacement and type (2) microlites grew in glass after emplacement. Swanson *et al.* (1989) described rod- and chain-like microlites of plagioclase and clinopyroxene in obsidian, which they attributed to degassing of rhyolite lava, which caused an increase in ΔT, prior to eruption. Acicular and curved microlites and crystallites (too small to show birefringence) in rhyolite glass are shown in Fig. 3.24.

Dendritic crystals of quartz have been grown experimentally at relatively strong undercooling (Swanson & Fenn, 1986; Fenn, 1986; MacLellan & Trembath, 1991). The dendrite arms grow parallel to the *a* and *c* crystal axes, with smaller branches from the main arms. The experiments indicate that undercooling more than 55 degrees in less than 24 hours is necessary to form the dendrites, which is probably why quartz phenocrysts in felsic volcanic and shallow intrusive rocks are generally not dendritic. However, dendritic quartz has been observed in some shallow-level granites (Shannon *et al.*, 1982), which suggests rapid undercooling of more than 55 degrees, on the basis of the experimental evidence. In addition, some quartz phenocrysts with strongly indented shapes that have been interpreted as being due to magmatic resorption may be caused by dendritic crystallization (Section 3.13).

3.5.4 Dendritic crystals, comb layering and orbicular structure in intrusive rocks

Elongate and dendritic crystals in intrusive rocks (from ultramafic rocks to granites, including pegmatites) appear to have been formed at conditions of strong supersaturation (see, for example, Petersen, 1985). This has been confirmed experimentally by Lofgren & Donaldson (1975) and Donaldson (1977). For example, large, dendritic and radiating plagioclase crystals occur in some slowly cooled, intrusive ultramafic rocks (Berg, 1980; Peterson, 1985). In addition, large dendritic crystals of olivine occur in both Archaean ultramafic volcanic rocks (‘*spinifex structure*’) and some intrusive layered cumulates (‘*harrisitic structure*’), as shown in Fig. 3.19 (Drever & Johnston, 1957; Viljoen & Viljoen, 1969; Nesbitt, 1971; Bezzi & Picardo, 1971; Pyke *et al.*, 1973; Donaldson, 1974; Fleet & MacRae, 1975; Arndt *et al.*, 1977; Berg, 1980; Echeverría 1980; Arndt & Nisbet, 1982). The crystals form aggregates of parallel plates, random plates, skeletal crystals, and branching dendritic crystals (Donaldson, 1974, p. 1722). Other examples are elongate crystals and branching crystal aggregates oriented perpendicular to a wall of a magma chamber or an internal rock–magma interface (see, for example, Drever & Johnson, 1957, 1972; Wager & Brown, 1968; Moore & Lockwood, 1973; Donaldson, 1974; Lofgren & Donaldson, 1975; Petersen, 1985), as shown in Fig. 3.33. The structure is often called *comb layering*, and is a type of unidirectional solidification structure, involving heterogeneous nucleation. The crystals may also be aligned perpendicular to the surface of an enclave or megacryst in the magma, forming *orbicular structure*, the origin of which has

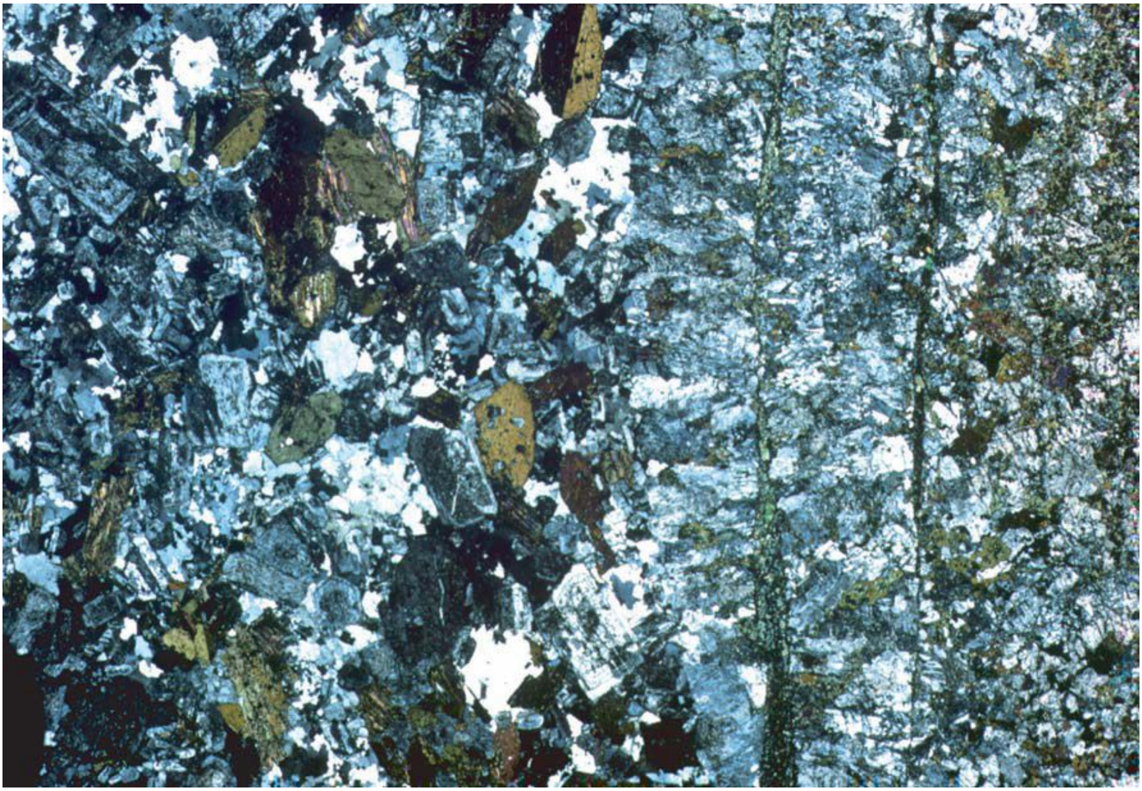

Fig. 3.33: Comb layering in the fringe between a microgranitoid enclave (right) and the host granodiorite (left), Ravenswood Granodiorite, north Queensland, Australia. Three comb layers are shown (the right-hand one being very narrow in parts), each characterized by elongate plagioclase crystals aligned perpendicular to the layering. Crossed polars; base of photo 25 mm.

been discussed by Moore & Lockwood (1973) and Vernon (1985), as outlined below.

Because these structures may occur in large bodies of intrusive rock, the strong supersaturation required to form dendritic crystals is unlikely to be due consistently to rapid cooling of the magma body. The similarity of skeletal and dendritic olivine in rocks to olivine formed by rapid cooling in slags (Fig. 3.16), chondrules in chondritic meteorites (Figs. 3.22, 3.23) and experiments strongly suggests that it grew relatively rapidly, even at the slow cooling rates that probably were involved in the crystallization of layered mafic–ultramafic intrusive complexes. This can be explained (see also Section 3.5.3) by delayed nucleation, which contributes to the strong supersaturation necessary for rapid growth. If nucleation is delayed long enough, the crystallization may occupy a relatively small part of the total cooling time for these rocks. Therefore, although dendritic habits imply rapid growth rates, the process causing this effective supersaturation or undercooling (ΔT) can be independent of cooling rate.

For example, experiments by Donaldson (1976) suggest that skeletal and dendritic olivine grow at much slower cooling rates in olivine-rich and other fluid melts, although the ΔT is unaffected by the olivine content. Therefore, the dendritic olivine in Archaean olivine-rich lavas (komatiites) need not imply unusually rapid cooling rates. Moreover, many volcanic rocks are composed largely of small polyhedral crystals without dendritic features, despite rapid cooling (Fig. 3.5). As discussed in Section 3.5.1, the controlling factor is a low $D : G$.

Transitions from euhedral to dendritic quartz occur in some high-level intrusive felsic rocks, indicating increasing undercooling during crystallization (Swanson & Fenn, 1986). The undercooling may be due to periodic loss of water vapour, which also produced interstitial aplite (Section 3.4.7). The experiments of MacLellan & Trembath (1991) show that the shapes of quartz crystals and quartz–feldspar aggregates vary with ΔT and time. Therefore, a granitic melt cooling at a constant rate may crystallize two or more quartz shapes at different stages in the cooling history. This may account for numerous observations of sequential changes in quartz morphology in granitic rocks, and removes the need for explanations involving sudden changes in temperature, pressure or water activity in the melt. For example, the occurrence of quartz in some aplites as phenocrysts, groundmass grains and granophyric intergrowths overgrown by larger quartz grains in the groundmass is similar to the sequence produced in a rapid cooling experiment (MacLellan & Trembath, 1991).

Dendritic quartz, as well as skeletal feldspar and white mica, have also been observed in pegmatites (Jahns, 1955; Swanson & Fenn, 1986). In these rocks the dendritic growth habit does not appear to be related to the presence or absence of water vapour, as the pegmatites contain no aplite or miarolitic cavities (Sections 3.4.7, 3.14.5), and experiments indicate that it is not related to the order of mineral crystallization or pressure variation. Instead, it appears to be due solely to undercooling (supersaturation). The cause of the undercooling in pegmatites (Section 3.4.6) could conceivably be a rapid cooling rate for small intrusions, but may also be delayed nucleation caused by local composition gradients (constitutional undercooling) and high water and/or boron contents of the melt.

Delayed nucleation caused by a change in water content was invoked by Vernon (1985) to explain orbicular structure in granites. The water lowers the liquidus temperature (as determined experimentally), dissolving potential nuclei and so delaying nucleation at the temperature concerned. Eventual crystallization is forced to occur rapidly (forming elongate crystals) on existing solid crystals, such as the walls of the intrusion (producing comb layering) and solid enclaves (producing the orbs that characterize orbicular granites, diorites and gabbros). An alternative possibility is the chilling (supercooling) of one magma by another at lower temperature, as with the chilling of magma globules to form microgranitoid enclaves, many of which have dendritic microstructures (see, for example,

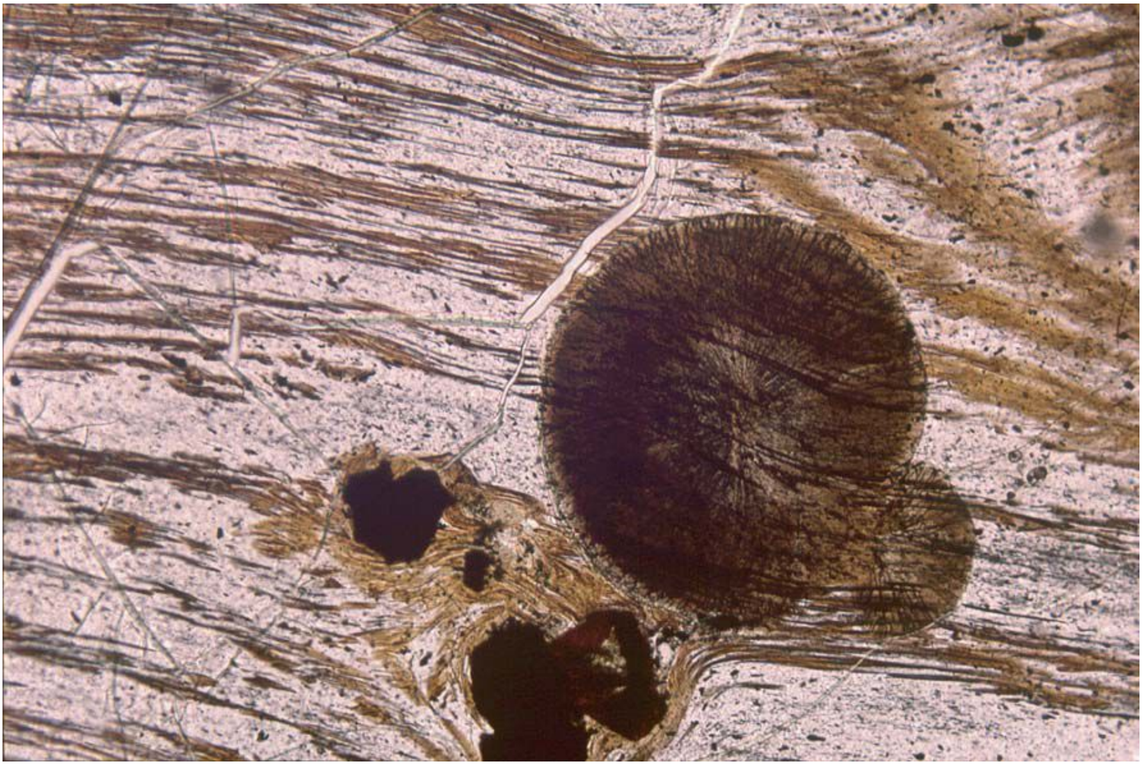

Fig. 3.34: Spherulite in glassy, flow-banded rhyolite, Ngongataha Quarry, Rotorua, New Zealand. The flow lines pass through the spherulite without deflection, indicating that the spherulite grew after the development of the flow lines, in either solid glass or a very viscous melt. Folds in the banding (deflected by opaque phenocrysts) formed during flow of the lava (Section 3.9). Plane-polarized light; base of photo 0.8 mm.

Vernon, 1983, 1984, 1990a, 1991a), as discussed in Section 3.10.3. This process was also suggested by Berg (1980) to explain coarse-grained dendritic and radiating plagioclase by supercooling of an ultramafic magma as it intruded a more basaltic magma.

3.5.5 Spherulitic aggregates

Spherulitic aggregates (spherulites) are radiating arrays of fibrous (needle-like, acicular) crystals that are common in glassy felsic volcanic rocks (Figs. 2.18, 2.19, 3.34–3.40). Early descriptions of spherulites are by Cross (1891) and Iddings (1891), and an excellent summary account of spherulites is that of Harker (1909).

Each fibre has the same crystallographic axis parallel to its length, and each has an orientation slightly different from that of its neighbours. Thus, in contrast

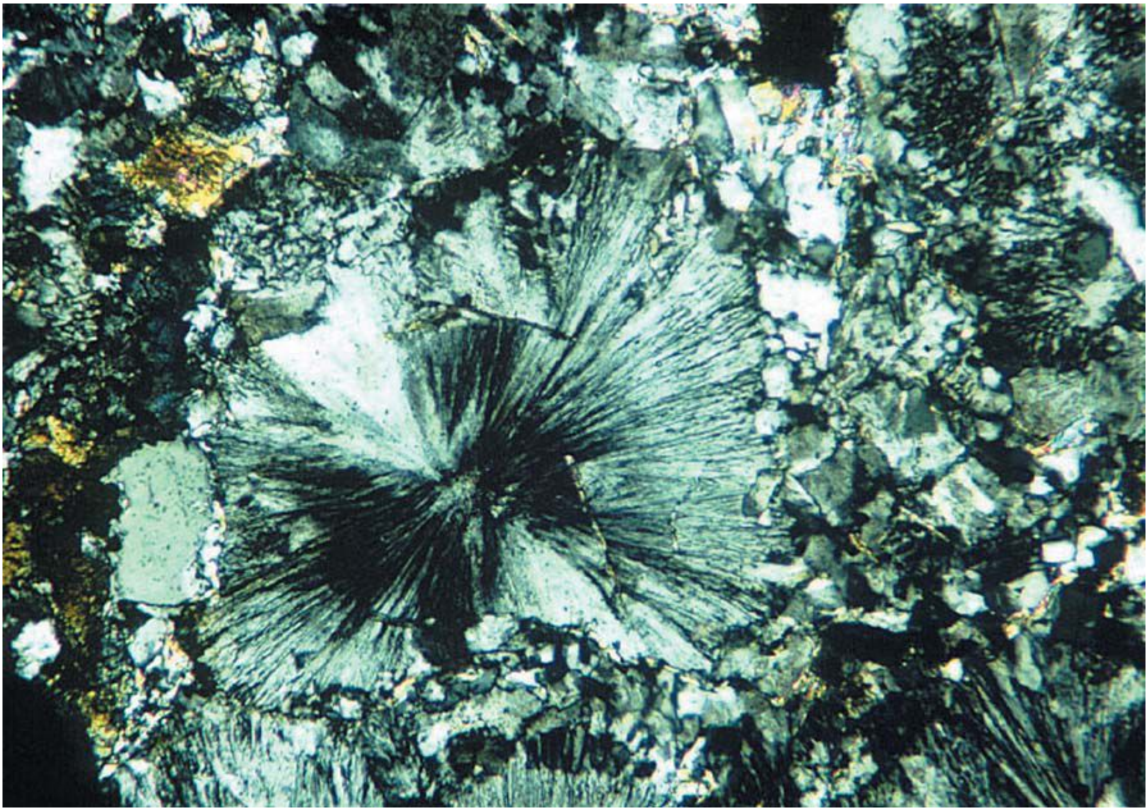

Fig. 3.35: Formerly glassy rock that has been completely replaced by spherulites and some granular quartz–feldspar aggregates, Bathurst area, New South Wales, Australia. The spherulites consist mainly of alkali feldspar, with some quartz. Micrographic intergrowths of quartz and alkali feldspar occur mainly at the edges of the spherulites. From Vernon (2000b, fig. 82). Crossed polars; base of photo 1.3 mm.

to dendrites, spherulites are aggregates of separate crystals, rather than branched single crystals. Concentric banding, resembling Liesegang rings, is a feature of many spherulites (Fig. 3.38). The banding is probably due to rhythmic supersaturation in minor chemical components of the melt or glass, either (1) adjacent to the spherulite as it grew or (2) by 'self-organizing' diffusion after growth of the spherulite.

A dark 'extinction cross' is common in spherulites observed in crossed polars (Fig. 2.19B), because many fibres (each with one of the principal optical vibration directions parallel to its length) are parallel or approximately parallel to the vibration directions of the polarizer and analyser, no matter what the orientation of the spherulite.

In many felsic volcanic rocks, flow lines pass undisturbed through spherulites (Figs. 3.34, 3.38), indicating that the spherulites grew after development of the

Fig. 3.36: Spherulite that appears to have grown on plagioclase phenocrysts, in a glassy rhyolite, Ngongataha Quarry, Rotorua, New Zealand. Plane-polarized light; base of photo 2.8 mm.

flow lines, probably in solid glass ('devitrification'). This is also indicated by shard-shapes passing uninterrupted into spherulites in ignimbrites (Fig. 2.19) and by fibrous aggregates pseudomorphing glass shards (Fig. 2.18), as described by Ross & Smith (1961). Strictly speaking, crystallization of spherulites in glass is a solid-state transformation, but glass is so like a melt in terms of its atomic structure (Section 3.5.6) that its discussion here is appropriate.

However, evidence of slight deformation of flow structures around some spherulites has been observed (Ewart, 1971, p. 426), indicating that spherulites may grow in viscous silicate melts. This is confirmed by Fig. 3.39, which shows a fragmented spherulite, with evidence of flow of magma between the fragments; flow lines pass through parts of this and adjacent spherulites, indicating that they grew after much of the flow of the lava, but before final consolidation of the very viscous melt as glass. Spherulitic crystallization in melts is also suggested by experiments on the crystallization of plagioclase (Lofgren, 1974), the microstructures of certain lunar and terrestrial basaltic rocks (Lofgren, 1971a;

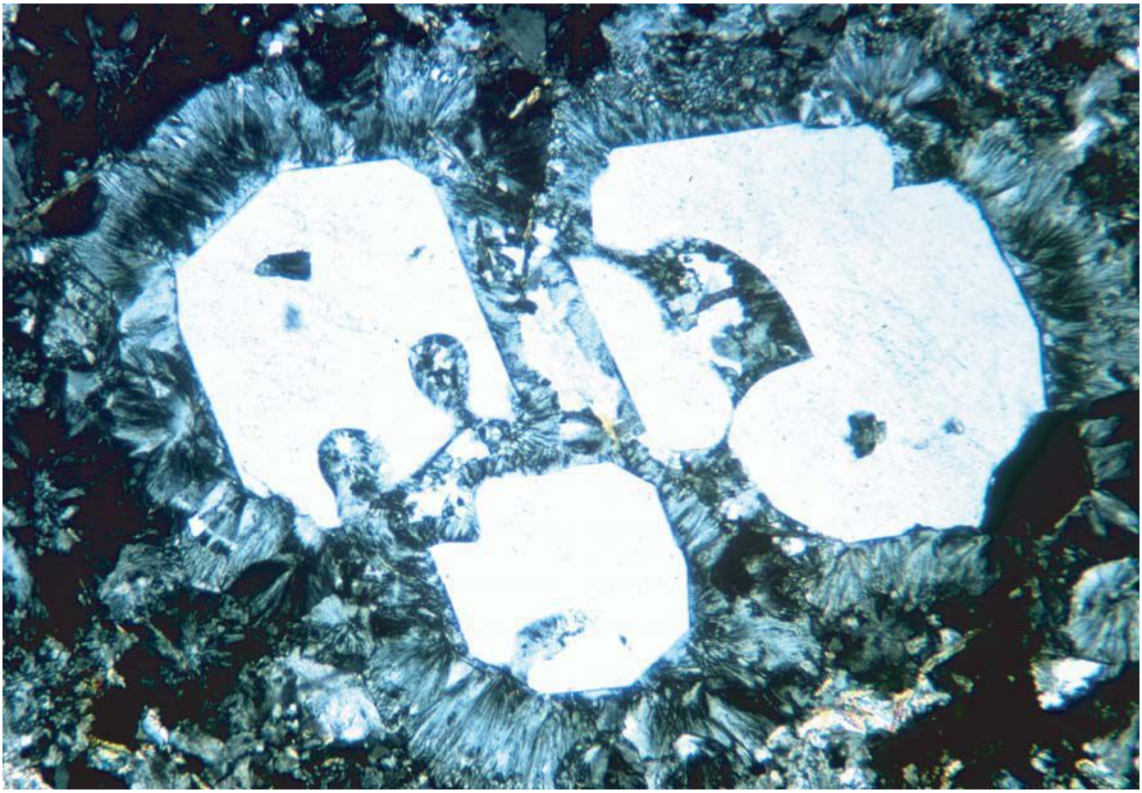

Fig. 3.37: Fringes of fibrous, spherulitic feldspar and quartz that have grown on euhedral, embayed quartz phenocrysts. Crossed polars; base of photo 3.5 mm.

Drever & Johnston, 1972), and experiments on the growth of alkali feldspar in melts (Fenn, 1977).

Spherulitic aggregates typically nucleate on existing crystalline material (Figs. 3.36, 3.37), although small crystalline nuclei are easily missed by the section plane, and so may not be seen in thin section. Once a radial growth habit is established, growth continues uniformly in all directions, as suggested for natural spherulites by Popoff in 1902 (Harker, 1909). This is probably because the crystals grow in a homogeneous material, such as a liquid or glass. If growing spherulites impinge on one another, polyhedral boundaries between them are formed, as shown experimentally by Fenn (1977, fig. 10c).

Omnidirectional growth of fibres from a single point-nucleus (a small crystal or crystal fragment) produces a spherical aggregate or spherulite (Figs. 3.34, 3.36, 3.38). Incomplete radiation results in fan, bow-tie (sheaf-like), and plumose aggregates (Lofgren, 1971a). Axiolitic spherulites (Fig. 3.40) result from fibres radiating or projecting out from a line or plane, probably owing to water penetrating along a crack and promoting crystallization of the adjacent glass or viscous

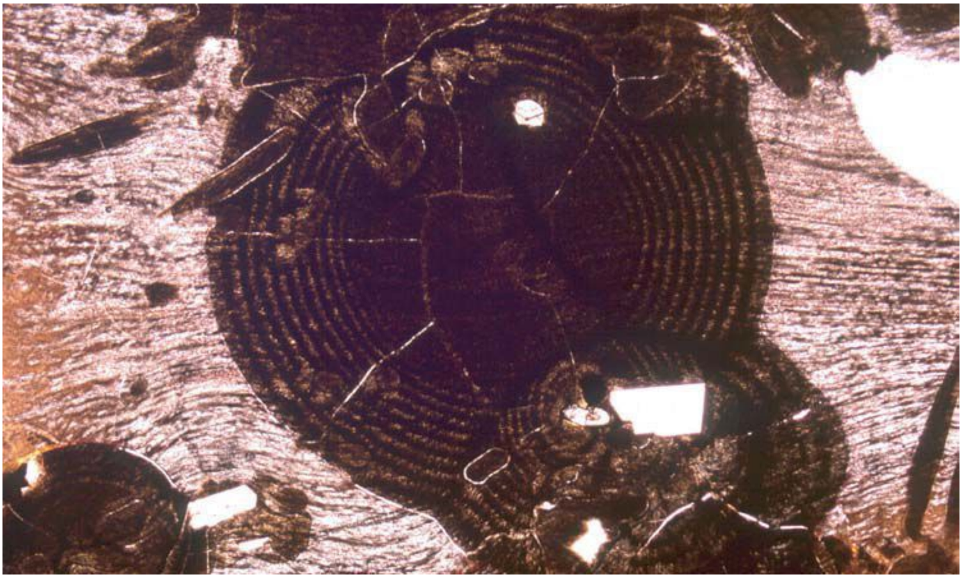

Fig. 3.38: Spherulite in glassy, flow-banded rhyolite, Ngongataha Quarry, Rotorua, New Zealand. The spherulite shows concentric banding resembling Liesegang rings. The banding probably is due to rhythmic supersaturation in minor chemical components of the melt or glass, either (1) adjacent to the growing spherulite or (2) by 'self-organizing' diffusion after growth of the spherulite. Plane-polarized light; base of photo 5.2 mm.

melt. Axiolitic aggregates also form by crystallization of glass shards, from the edges inwards, in tuffs (Fig. 2.18). Spherulites may also nucleate on and radiate out from phenocrysts, forming partly spherical shapes if the phenocrysts are small (Fig. 3.36) and fan-like aggregates and even continuous fringes if the phenocrysts are larger (Fig. 3.37). Small spherulites may nucleate on the surfaces of larger ones (Ewart, 1971) and repeated nucleation may occur during the growth of a spherulitic aggregate (Lofgren, 1971b, fig. 1).

Spherulites form under conditions of very strong supersaturation (Fig. 3.2). The reason for the development of spherulites, rather than dendrites, is that the diffusion rate (D) is even lower than for dendritic growth, as expected for glasses and viscous silicate melts (Fig. 3.2). In spherulitic growth, an extremely narrow 'impurity' layer of thickness $\delta = D/G$ (commonly less than 10^{-4} cm wide) develops around the very slowly growing crystal (Fig. 3.41). The result is that minute projections on the nucleus grow into new crystals and, furthermore, that very small projections on the fibres themselves can develop into new fibres.

From theoretical considerations, Keith & Padden (1963) estimated that the diameter of the fibres is about equal to δ. In explanation, Keith & Padden (1963, p. 2417) considered a small projection of height y' on a flat crystal surface adjacent to an 'impurity'-rich layer of melt of thickness δ (Fig. 3.41). 'Impurity'

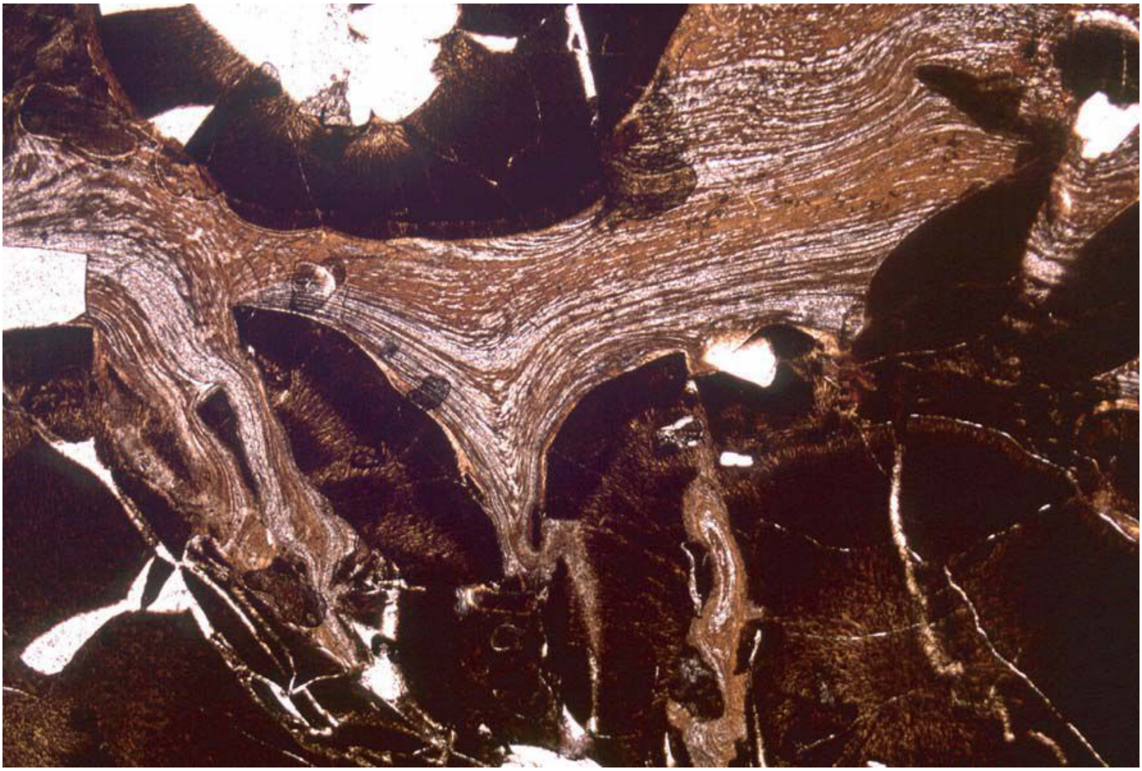

Fig. 3.39: Spherulite in glassy, flow-banded rhyolite, Ngongataha Quarry, Rotorua, New Zealand. The spherulite has been broken during flow of the viscous lava, and melt has flowed between the spherulite fragments. However, some flow lines pass through parts of this and nearby spherulites without deflection, indicating that the spherulite grew after most of the flow of the lava, but before its final consolidation as a glass. That is, the spherulite grew in a very viscous melt. Plane-polarized light; base of photo 5.2 mm.

components diffuse away from the projection in the direction ρ, hindering the formation of neighbouring projections within a 'circle of influence', owing to the lowering of the crystallization temperature of the liquid (or glass) within this circle. The radius of this circle depends on the competition between D and G during the time interval (dt) when the interface as a whole advances for a distance y'. Thus the radius of the circle must be related in some way to δ. Keith & Padden (1963) inferred that if the projection (y') is larger than δ it breaks up into smaller projections, and if it is much smaller than δ it is swallowed up by other projections of more suitable size. Therefore, projections persist and grow only if they are about the same size as δ (Fig. 3.41). Within these constraints, the greater the degree of supersaturation, the smaller the spacing between the fibres; a decrease in fibre spacing from the centre to the edge of a plagioclase

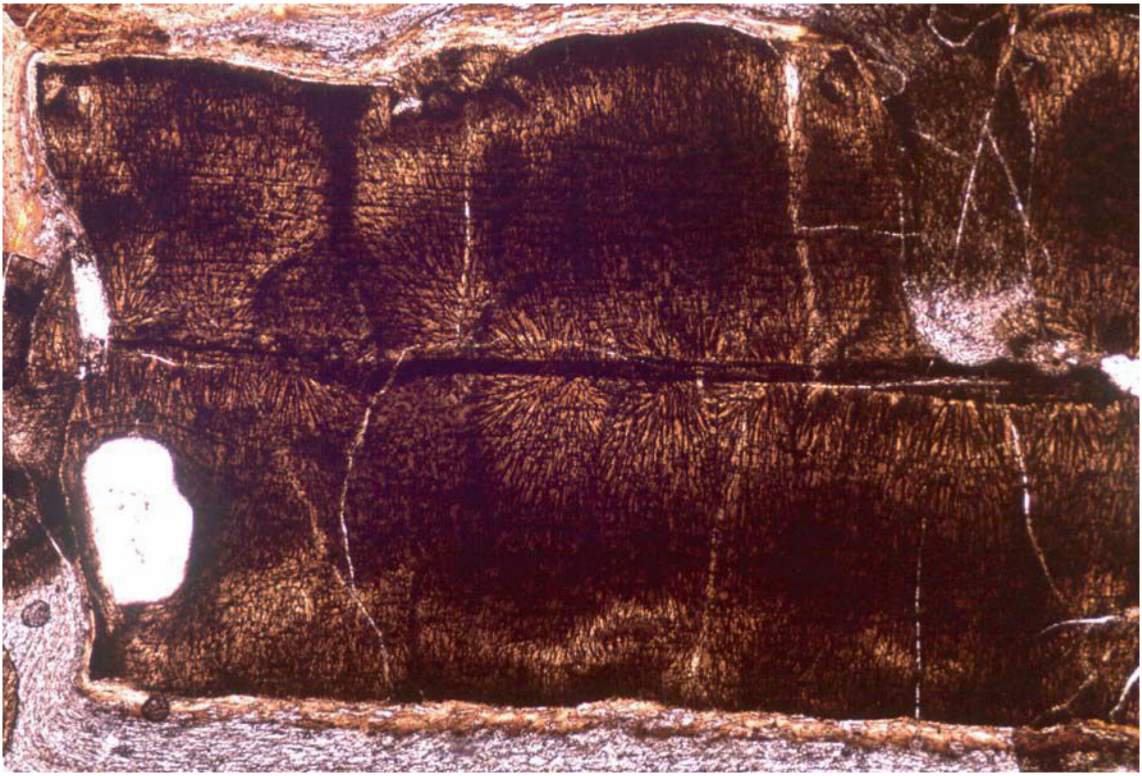

Fig. 3.40: Spherulitic aggregates projecting and radiating outwards from a crack (a type of axiolitic structure), probably owing to fluid passing along the crack and assisting crystallization, Ngongataha Quarry, Rotorua, New Zealand. The aggregate has been broken apart (left of photo) and magma has flowed into the gap, indicating that the spherulitic crystallization occurred after cracking of the magma, but before final solidification of the melt to a glass, i.e. the spherulitic aggregate grew in a very viscous melt. Plane-polarized light; base of photo 2.8 mm.

spherulite has been observed in the SEM (Kirkpatrick, 1981, fig. 59). Because the projections are very minute, δ must also be very small for them to persist and produce fibres. In dendritic growth, δ is probably too large, so that potential projections are incorporated by larger, crystallographically oriented projections.

Experimental work on the formation of spherulites in organic melts (Keith & Padden, 1963) and silicate systems (Lofgren 1971a,b, 1974) has confirmed that spherulitic growth is favoured by very small values of $D : G$, even smaller than for dendritic growth. Low nucleation rates, which are typical of high degrees of supersaturation (Fig. 3.2) are essential for both dendritic and spherulitic growth, forcing growth to occur on existing crystals.

Typically the whole of the spherulite consists of radiating fibres, which implies that each fibre has repeated low-angle fibres (non-crystallographic branching)

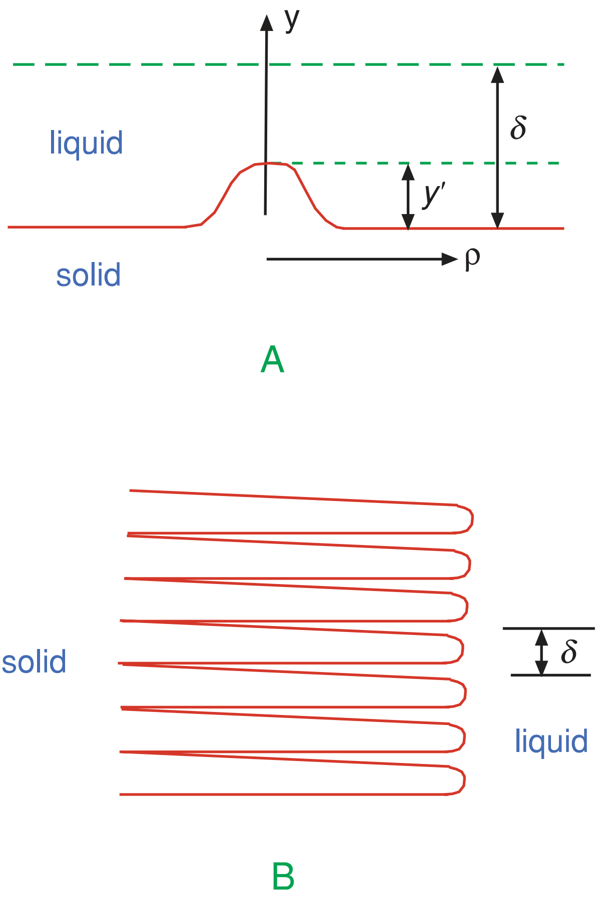

Fig. 3.41: (A) Projection on a solid–liquid interface, showing the growth direction of a projection (y), the height of the projection (y'), the width of the impurity layer (δ), and direction of diffusion of impurity parallel to the surface (ρ). After Keith & Padden (1963, p. 2417). (B) Diagrammatic development of fibrous projections from a cellular solid–liquid interface, the interfibre distance depending on the thickness of the impurity layer (δ). After Keith & Padden (1963, p. 2417).

branching from it, although open spherulites also exist, especially in the early stages of spherulite development (Lofgren, 1971b; Fenn, 1977) or at relatively low degrees of supersaturation (Fenn, 1977, p. 146). Low-angle branching is necessary to fill space, because growth of fibres outwards from a small nucleus soon covers the whole surface of the nucleus, inhibiting further nucleation there and so requiring new nuclei to form on the fibres themselves.

Many spherulites are two-mineral aggregates, formed by initial spherulitic growth of one mineral and later crystallization of a second mineral from the liquid or glass between the fibres. Common examples in rhyolitic or ignimbritic rocks are spherulites of K-feldspar fibres with interstitial quartz or the metastable high-temperature SiO_2 polymorphs, tridymite or cristobalite. If the spherulite grows when the glass is relatively hot, it grows as the higher-temperature polymorphs of $KAlSi_3O_8$ (sanidine) and SiO_2 (tridymite or cristobalite), as observed in young welded tuffs (Ross & Smith, 1961). The quartz observed in older spherulites is probably due to recrystallization of the original high-temperature SiO_2 polymorphs, which are less stable than quartz at lower temperatures.

Some spherulites consist of micrographic intergrowths (Section 3.8) of quartz and alkali feldspar, especially at their margins (Fig. 3.35), suggesting simultaneous growth of the two minerals. The quartz may be *micropoikilitic*, in that each quartz grain may enclose many feldspar fibres (Lofgren, 1971b, p. 117), forming what has been called 'snowflake' microstructure (Anderson, 1969; Lofgren, 1971a); presumably this microstructure is formed where the nucleation rate for quartz is lower than that for feldspar. A range of spherulitic microstructures in ignimbrites was illustrated by Ross & Smith (1961).

Spherulitic aggregates ('*varioles*') in some Earth and lunar basalts consist of plagioclase and clinopyroxene (see, for example, Hatch *et al.*, 1949, fig. 118; Lofgren, 1971a, 1974) or plagioclase with interfibrillar clinopyroxene (see, for example, Harker, 1909, fig. 91; Tyrrell, 1929, fig. 40C). Fig. 3.17 shows dendritic clinopyroxene in an ultramafic lava, with a strong tendency towards a radiating habit. Spherulites consisting of plagioclase fibres and interfibrillar K-feldspar and biotite in a pyroxene-andesite have been described by Kesler & Wieblen (1968). Radiating aggregates of fibrous pyroxene may also occur in meteorite chondrules (Section 3.5.7) and pseudotachylites (Section 3.5.8).

3.5.6 Glass

If the degree of undercooling is extreme (Fig. 3.2), as when lava is rapidly quenched in air or water, crystallization may fail to occur, and *volcanic glass* results (Figs. 3.7–3.9, 3.34, 3.36, 3.38, 3.39). Silica-rich melts form glass more readily than mafic melts, because of the higher degree of polymerization of $[SiO_4]^{4-}$ tetrahedra in silica glass (Section 3.2).

As discussed in Section 3.1, glass has the rigidity of a solid, but the atomic arrangement more akin to that of a silicate melt, characterized by short-range order, as opposed to the long-range order of atomic arrangements in crystalline materials. This makes glass optically isotropic (Fig. 3.9). Because this less ordered arrangement of atoms represents a higher-energy situation than a compositionally equivalent crystalline material, glass is metastable and tends to crystallize ('devitrify') with time, especially in the presence of water, forming spherulitic or axiolitic aggregates (Section 3.5.5). Therefore, most volcanic glasses are geologically young (Cainozoic), although much older glasses can persist in tectonically stable regions (e.g. Carboniferous glasses in the Hunter Valley of New South Wales, Australia), and glass has persisted on the Moon for billions of years,

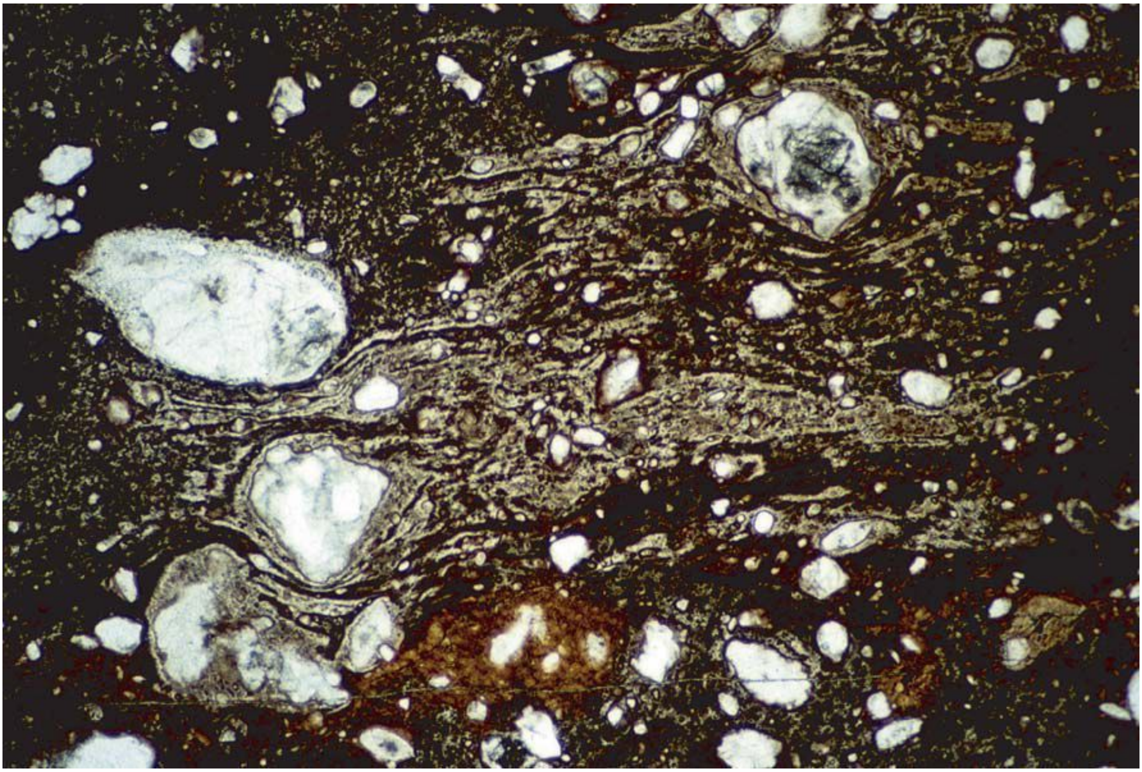

Fig. 3.42: Glass with stretched gas bubbles (vesicles) and flow banding in pseudotachylite, eastern Musgrave Ranges, central Australia. Plane-polarized light; base of photo 4 mm.

owing to the lack of water and tectonic activity. These occurrences indicate that the catalytic action of water or hydroxyl ions may be necessary for spherulites to grow in glass, especially in the absence of later heating.

3.5.7 Dendrites, spherulites and glass in meteorites

Many stony meteorites, known as chondrites, contain round globules (‘chondrules’) containing dendritic crystals, the shapes of which suggest that the globules were once droplets of melted rock (Figs. 3.22, 3.23). Skeletal crystals of olivine have shapes similar to those produced in slags and volcanic rocks (Section 3.5.3) and radiating, fibrous needles of pyroxene resemble variolitic (spherulitic) aggregates in some basalts (Section 3.5.5). The melt droplets may originally have been dustballs that were melted by flash-heating events in the solar nebula, before accretion of the globules into asteroids. The causes of the heating are unknown, but may be shock waves.

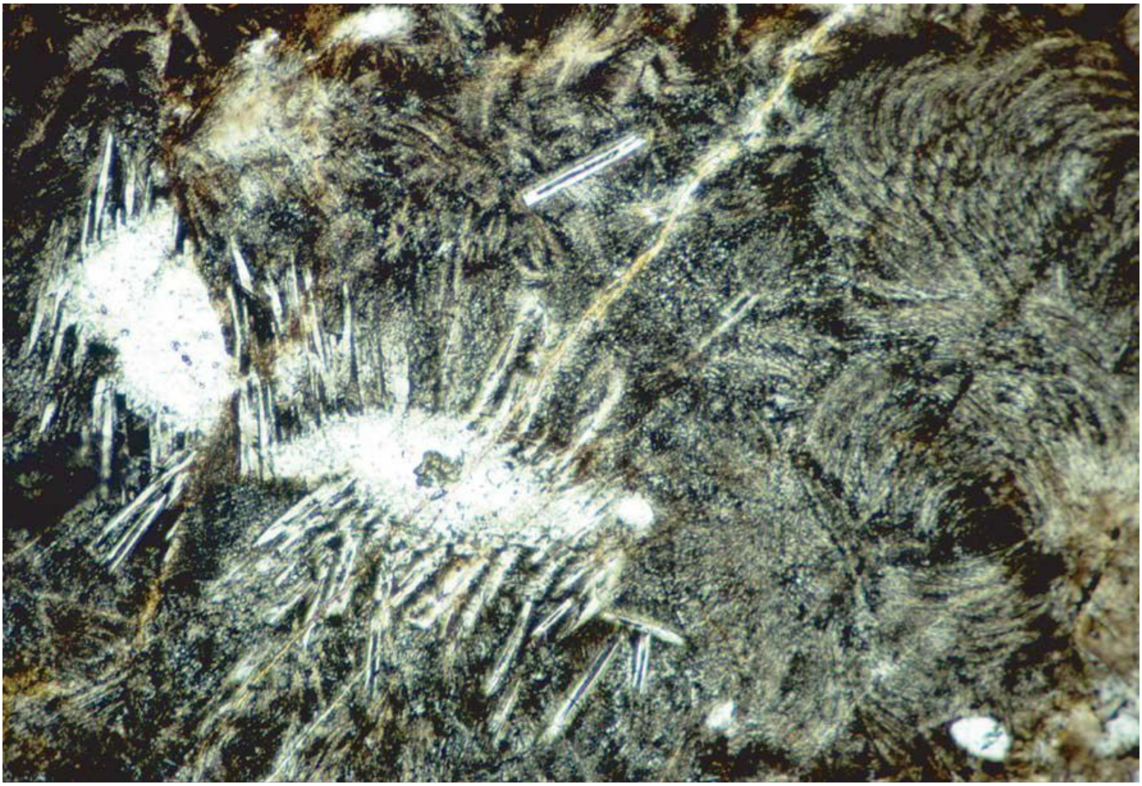

Fig. 3.43: Spiky outgrowths on plagioclase fragments (colourless) and radiating, fern-like, dendritic aggregates of clinopyroxene (pigeonite) in pseudotachylite, eastern Musgrave Ranges, central Australia. Plane-polarized light; base of photo 0.7 mm.

3.5.8 Dendrites, spherulites and glass in pseudotachylites

Pseudotachylites are fragmental, glassy-looking rocks formed by either (1) rapid frictional heating in faults or (2) rapid heating in meteorite impacts, as discussed in Section 5.7.10. The extremely rapid cooling can form glass and/or spectacular skeletal, dendritic and spherulitic microstructures. Examples include glass with stretched gas bubbles (Fig. 3.42), dendritic overgrowths of plagioclase on fragments of plagioclase (Fig. 3.43), tendril-like branches of pigeonite (a metastable, high-temperature, Ca-poor clinopyroxene) on fragments of orthopyroxene, fern-like 'forests' of feathery pigeonite dendrites (Fig. 3.43), and spherulitic aggregates in altered glass (Fig. 3.44), as described by Camacho *et al.* (1995). All these crystals and aggregates have the dendritic to fibrous habits characteristic of high degrees of supersaturation (Sections 3.5.3, 3.5.5).

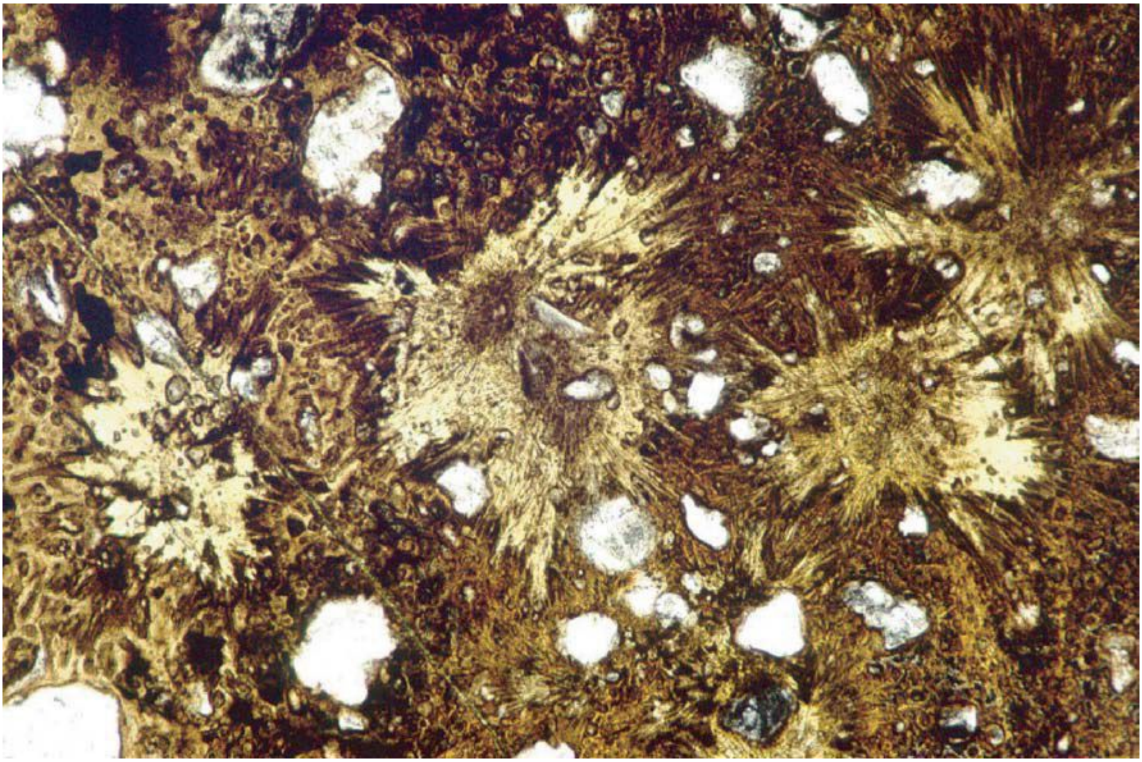

Fig. 3.44: Spherulitic aggregates that grew in glass with abundant gas bubbles (vesicles) and some unmelted fragments of quartz and cloudy feldspar in pseudotachylite, eastern Musgrave Ranges, central Australia. From Vernon (2000b, fig. 102). Plane-polarized light; base of photo 4.4 mm.

3.5.9 Microstructures of coarse-grained igneous rocks

Some of the structures of coarse-grained igneous rocks, such as comb layering and orbicular structure, have already been mentioned, including the large grainsize of pegmatites. However, the foregoing discussion applies only as long as crystals can grow freely in liquid. After grains impinge on one another, their final shapes depend on (1) the crystal shapes present on impingement and (2) the extent to which further microstructural changes occur under the influence of solid–solid interfacial energies (Chapter 4). As noted long ago by Sorby (1877), the irregular outlines of quartz grains in many granites are ‘due to the mutual interface of the individual imperfectly grown crystals, which could not develop their true crystalline planes of any considerable extent’. Because all the minerals in a granite (apart from those that have previously reacted with the liquid) crystallize right to the solidus (the temperature at which the rock becomes completely solid), all minerals must impinge on each other in the final stages of crystallization. The shapes of the final grain boundaries are determined by the relative interfacial energies of the minerals concerned (Section 4.2). Minerals characterized by low-energy crystal faces, such as biotite and hornblende, may retain their crystal faces after impingement, but quartz, plagioclase and K-feldspar commonly develop irrational, high-energy boundaries. For example, although plagioclase is commonly euhedral in volcanic rocks (Figs. 3.7–3.9) and some plutonic rocks, the commonly reported euhedral shape of plagioclase in granites generally applies only to the internal growth zoning (which preserves a history of development of faces as the crystal grew in liquid, unhampered by other growing crystals), not the outer edges of the grains (which reflect the last stages of the crystal's growth, in competition with the other minerals also growing near the solidus), as shown in Fig. 3.45.

Other aspects of the microstructures of coarse-grained igneous rocks, especially the problem of 'order of crystallization' and the effects of largely solid-state changes in grain shape and size during slow cooling, are discussed in Sections 3.6, 3.7 and 4.6.

3.6 Order of crystallization in igneous rocks

3.6.1 General problems

Many petrologists have asserted that a sequence of crystallizing minerals can be inferred by inspection of microstructures, using the following two main criteria: (1) euhedral minerals are older than anhedral minerals, and (2) inclusions are older than the host grain. However, both criteria are commonly misleading, as discussed below.

Because igneous rocks crystallize from compositionally complex magmas over a temperature range, different minerals begin to precipitate at different temperatures, as determined experimentally. However, once they have begun to grow, all the minerals crystallize together for the rest of the cooling range of the magma — right to the solidus in fact — unless eliminated by a reaction with the melt, such as the reaction of olivine and melt to produce orthopyroxene, or of orthopyroxene and melt to produce biotite. Such reactions can be inferred if they are incomplete, so that the product mineral forms a reaction rim around the reactant mineral. Unless this kind of reaction relationship is clearly visible, microstructural evidence cannot be used to determine the order of beginning of crystallization in a magmatic rock (Flood & Vernon, 1988).

Yet many published crystallization histories infer not only the commencement of crystallization for all the minerals, but also the cessation of crystallization of some of them. However, if no reaction relationship exists, the concept of cessation of crystallization, except at the solidus, is meaningless. For example, common minerals in granitic magmas (namely quartz, K-feldspar, plagioclase, biotite and

Fig. 3.45: Tonalite, San José pluton, Baja California, Mexico, showing oscillatory concentric zoning in plagioclase (Section 3.11.5). Most of the plagioclase grains are actually anhedral, despite the euhedral growth zoning produced when the crystal was growing freely in a liquid. Irregularities in the boundaries of plagioclase against other minerals are due to fortuitous impingement and mutual interference of these minerals as they crystallized from interstitial melt. Some solid-state adjustment during cooling may have contributed to the irregularities, in an attempt to minimize local interfacial energies (Section 4.2), but the evidence is not clear. Crossed polars; base of photo 4 mm.

hornblende) all crystallize together to the solidus. Simultaneous crystallization is confirmed by the commonly irregular interpenetrating edges of grains of quartz and feldspar in granitoid rocks (Fig. 3.45). Hornblende and biotite show irregular margins less commonly, presumably owing to the lower energy of their crystal faces (Section 4.2), which consequently tend to persist, even where these minerals are growing in competition with neighbouring grains; thus, their crystal faces cannot be used in inferring an order of crystallization.

In the gabbro (‘orthocumulate’) shown in Fig. 3.46, pyroxene is interstitial to plagioclase, and so may appear to have crystallized between existing plagioclase crystals. However, this microstructural relationship may be simply the result of a higher $N:G$ ratio of the plagioclase, compared with the pyroxene (see, for

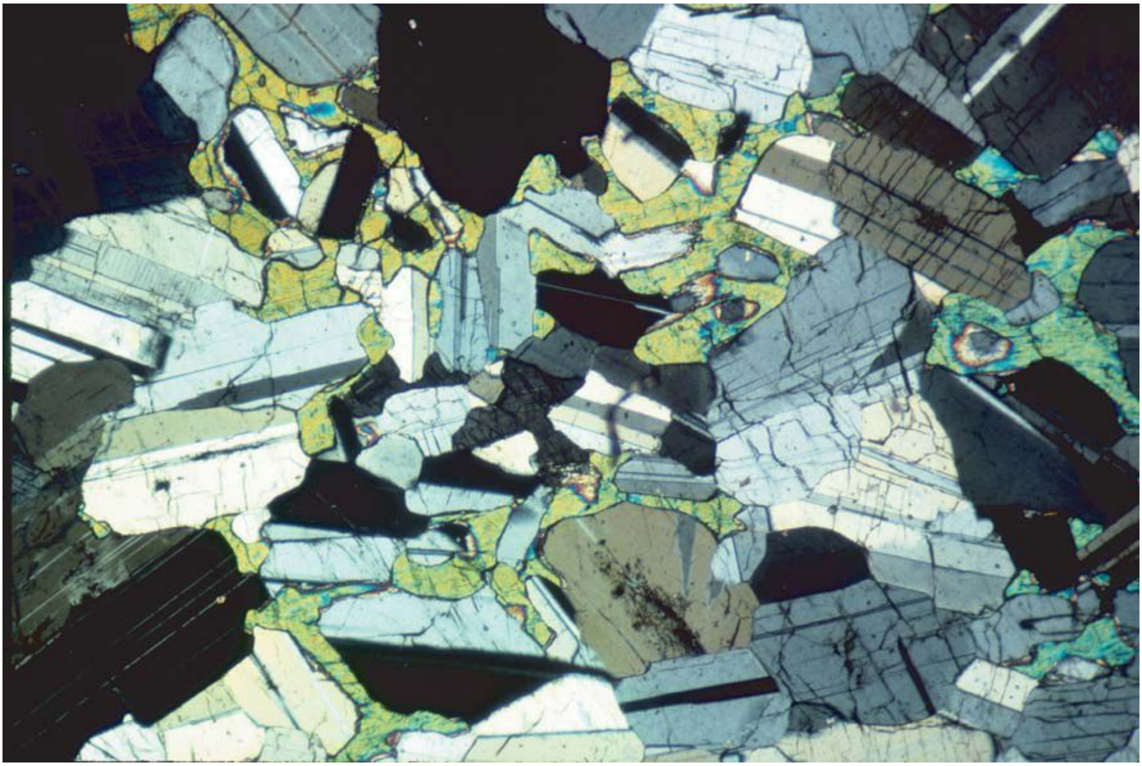

Fig. 3.46: Gabbro from the Bushveld mafic–ultramafic igneous complex, South Africa, showing moderately aligned, elongate grains of twinned plagioclase (grey, first-order interference colours), with clinopyroxene (bright green, second-order interference colours) containing inclusions of plagioclase (ophitic intergrowth). The inclusions of plagioclase are smaller than the plagioclase outside the clinopyroxene, reflecting the shorter growth period of the included plagioclase. However, the rounded corners of the plagioclase inclusions, together with the clinopyroxene versus plagioclase/plagioclase dihedral angles (Section 4.2.4) indicate that solid-state adjustment of grain boundaries occurred during slow cooling. A growth origin of the plagioclase twins (Section 3.12) is indicated by the simple twins, as well as the steps in the multiple twins (e.g. the grain just above and to the left of centre). Crossed polars; base of photo 4.4 mm.

example, Vernon, 1977a; Flood & Vernon, 1988). In some orthocumulates, the pyroxene grains are very large, owing to an exceptionally low $N : G$, and are called ‘oikocrysts’. Moreover, the commonly smaller size of plagioclase inclusions in the central parts of the large pyroxene grains, becoming larger towards their edges (see, for example, Mathison, 1987), implies mutual crystallization of the plagioclase and pyroxene through most of their growth history (McBirney & Hunter, 1995, p. 116). In fact, the common inference that interstitial minerals begin to crystallize later than other minerals has led to incorrect interpretations

Previous Page

of the microstructures of some cumulates, as discussed in Sections 3.6, 3.7 and 4.6.1.

Thus, the sizes and shapes of crystals and grains in slowly cooled igneous rocks are much more a reflection of variations in $N:G$ and interfacial free energies, respectively, than they are reflections of an order of crystallization. This applies also to metamorphic rocks (Section 4.3.5).

The conclusion is that, although the order in which the magma becomes saturated in various minerals during cooling can be determined by experiments (e.g. those of Clemens & Wall, 1981), microstructural evidence is inadequate for this purpose, except for reaction relationships (Flood & Vernon, 1988). This applies even to porphyritic rocks. Although the phenocrysts are generally inferred to have grown before the groundmass minerals, the order in which the phenocrysts first appear cannot be determined microstructurally, either because they are not in contact or, even where they are, for reasons already mentioned.

Moreover, even in megacrystic granodiorites, we cannot be sure that the large K-feldspar phenocrysts grew before the groundmass minerals, because experiments indicate that the magma generally becomes saturated in other minerals, such as hornblende, biotite and plagioclase, first. Therefore, the K-feldspar must have grown larger than the other minerals because of its much lower $N:G$ ratio in the magma concerned (Sections 3.4.3, 3.4.5), not because it began to crystallize earlier than the other minerals. It may be thought that, if the K-feldspar is a relatively late-nucleating mineral, the amount of melt remaining would be insufficient for large polyhedral crystals to develop. However, experiments have shown that in typical felsic magmas, about 60–70% of the magma is still melt when K-feldspar nucleates (Clemens & Wall, 1981; Winkler & Schultes, 1982), and this provides enough room for the K-feldspar megacrysts to develop (Vernon, 1986a).

3.6.2 Problem of inclusions

Microstructural features often used to infer orders of commencement of crystallization are inclusions and partial inclusions. Assumptions commonly made are that (1) inclusions begin to crystallize earlier than their host mineral, and (2) a mineral begins to crystallize later than a mineral on which it is 'moulded' (partly surrounds). However, the only logical inference than can be made from igneous (or metamorphic; Section 4.3.5) microstructures of this kind is that an included or partly surrounded mineral finished growing before the host or the surrounding mineral, but only for that particular grain of the host mineral. Elsewhere in the same rock, the included mineral may still be growing.

Even where one mineral is consistently enclosed or partly enclosed in another, nothing can be inferred about the relative beginning of crystallization of each mineral. The two minerals may have nucleated at exactly the same time, but one grew faster and outlasted the growth of the other (see, for example, Vernon,

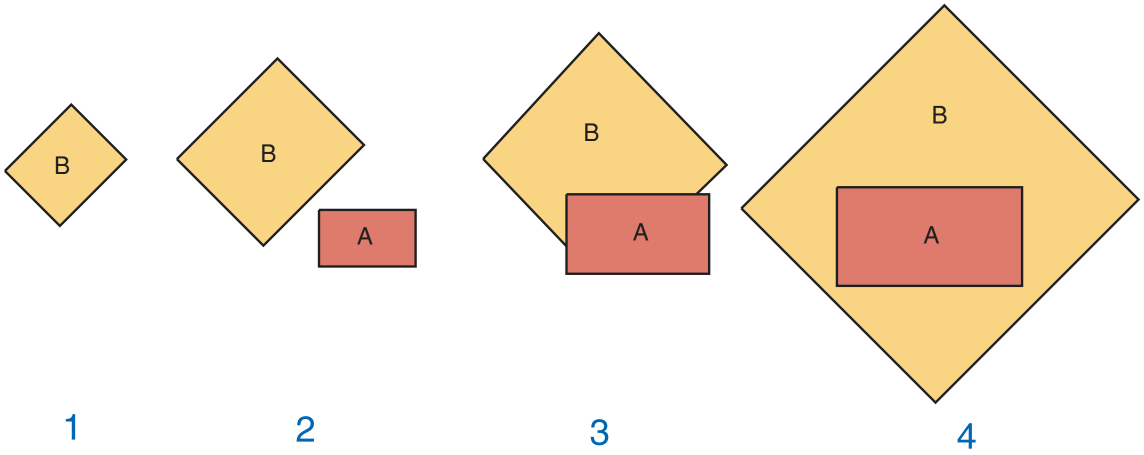

Fig. 3.47: Sketch showing that the order of nucleation of two minerals, one included in the other, cannot be determined by inspection of the microstructure. In this example, the eventual host mineral (B) nucleates before the eventual included mineral (A). This situation applies to both igneous and metamorphic rocks.

1977a). In fact, the host mineral may have nucleated before the included mineral (Fig. 3.47). It's just a question of different $N : G$ ratios for the two minerals involved (Section 3.3).

A clear example is ophitic structure (a variety of poikilitic microstructure) in dolerite (Fig. 3.48) or gabbro (Fig. 3.49), in which elongate grains of plagioclase are enclosed in much larger grains of clinopyroxene. Both these minerals crystallize together at a eutectic for most of the cooling history, as determined experimentally. Because the plagioclase is included or partly included in the pyroxene, it may be tempting to infer that the plagioclase nucleates before the pyroxene, but experiments indicate that both minerals grow at the same time. Therefore, we cannot infer from the microstructure which mineral nucleates first. We cannot even infer that all the plagioclase finished crystallizing before the pyroxene, because we know they both crystallize together right to the solidus. In other words, although the plagioclase may have finished crystallizing before the pyroxene in one place, this cannot apply everywhere in the rock. Ophitic microstructure is the result of more abundant nucleation of plagioclase and less abundant nucleation of pyroxene (Wager, 1961). In this context, nucleation refers to the production of viable nuclei, taking into account the possibility of Ostwald ripening at the immediate post-nucleation stage. Occurrences of either the plagioclase or the pyroxene as phenocrysts, as well as in intergrowths with the other mineral, implies that the phenocryst mineral grew before the intergrowths, which could be due to (1) its presence in excess of eutectic proportions, or (2) delayed nucleation of the other mineral (see, for example, Lofgren, 1980). The same

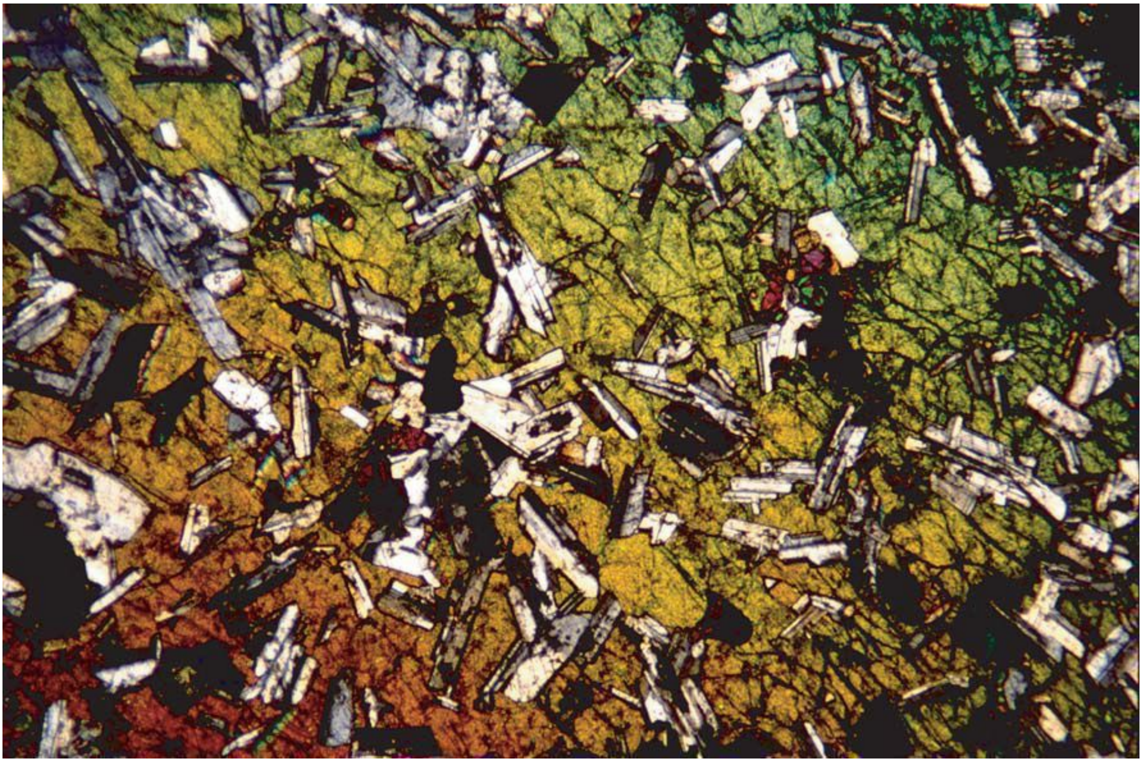

Fig. 3.48: Many small crystals of plagioclase (twinned, with grey, first-order interference colours) enclosed in part of a single large grain of clinopyroxene (green to red, second-order interference colours), in an ophitic intergrowth in a dolerite. Experiments indicate that both minerals grew simultaneously, the plagioclase having a much lower *N* : *G* than the clinopyroxene. Crossed polars; base of photo 11 mm.

principles apply to the interpretation of poikilitic microstructure between other minerals.

Hawkes (1967) showed that changes in the order of mineral nucleation can vary with small amounts of undercooling in a mafic layered intrusion. A striking experimental confirmation of the importance of nucleation rates in determining microstructural relationships is the work of Lofgren (1983), who showed that by altering the concentration of nuclei (1–5 μm feldspar crystals), the microstructures of basaltic rocks could be made to vary from ophitic (small plagioclase crystals fully enclosed in large pyroxene grains) to subophitic and intersertal (small pyroxene grains between plagioclase crystals) within a few millimetres of each other. This is a clear demonstration of the futility of attempting to infer an order of beginning of crystallization from microstructural observations, in the absence of reaction relationships.

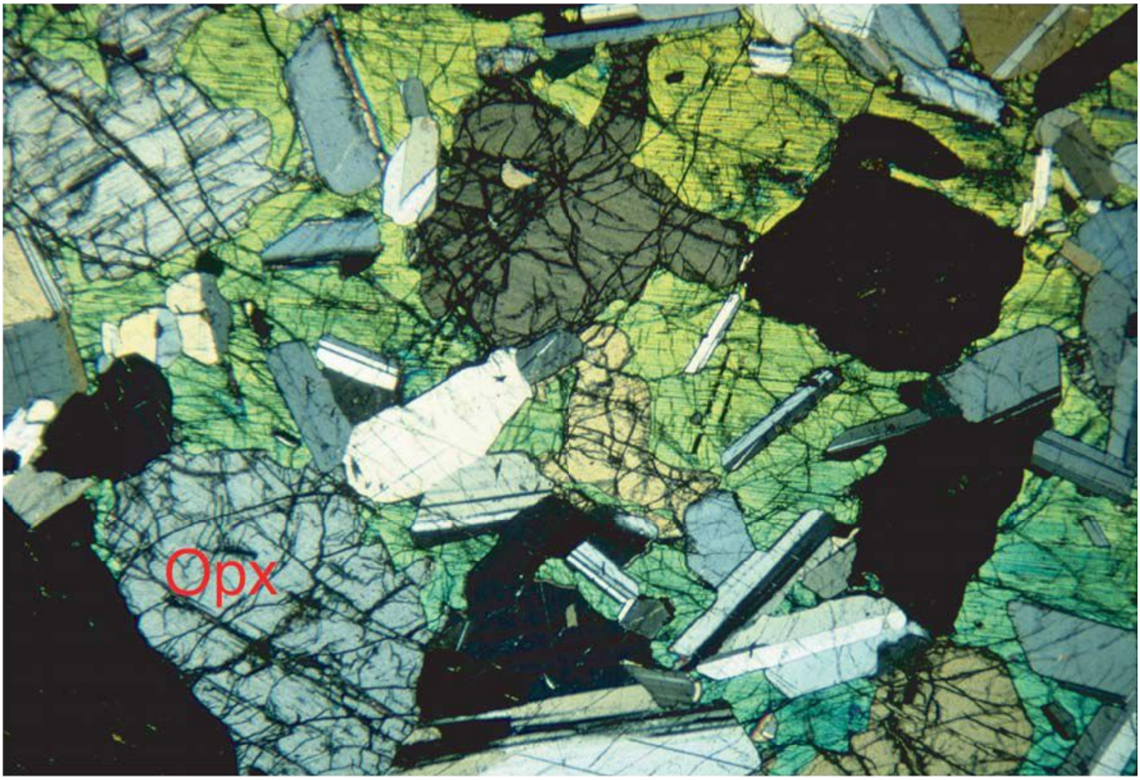

Fig. 3.49: Large grain of clinopyroxene (bright second-order interference colours) with inclusions of elongate plagioclase grains, forming an ophitic microstructure. Also present are inclusions of orthopyroxene (Opx). Crossed polars; base of photo 12 mm.

3.6.3 Problem of apatite needles

A particular problem is the common inference that small, euhedral crystals (e.g. needles of apatite) necessarily crystallize early. However, because of their small size, they may crystallize in interstitial melt at any stage during the cooling history (see, for example, Evans & Hanson, 1993). They are invariably engulfed by larger grains of other minerals, even those that begin to grow *before* the apatite crystals concerned. Therefore, the apatite could have formed at any time, which cannot be determined from microstructural observation.

Alternatively, the occurrence of minor minerals may reflect the small concentrations of some of their components in the magma (e.g. of phosphorus for apatite). For example, because P is relatively insoluble in felsic melts (Watson & Capobianco, 1981), apatite may precipitate around crystals of other minerals that reject P as they grow. Thus, the *local* order of crystallization of minor minerals can vary from the overall order.

3.7 Distribution of minerals in igneous rocks

3.7.1 Random distributions: interfacial energy considerations

The few studies that have been carried out indicate that in most granitic rocks (Rogers & Bogy, 1958) and metamorphic rocks (Kretz, 1966b, 1973; Flinn, 1969), the distribution of grains of different minerals tends to be random or nearly so, which may be interpreted as implying a tendency for minerals to remain separate, rather than to aggregate. Random dispersions imply that interfacial energy induces little or no tendency to change this situation during slow cooling. Random distributions could reflect a general tendency for intermineral boundaries to have lower free energies than boundaries between grains of the same mineral (Section 4.2.4), except for specific low-energy interfaces caused by connections of identical crystal faces, as in synneusis (Section 3.7.2). However, they may be more related to diffusion restrictions on the nucleation of nearby grains of the same mineral, once a grain of that mineral nucleates and starts to grow. Although random or apparently random distributions of minerals are common in igneous rocks, clustering tendencies and single-mineral aggregates have been described, as discussed in the next section.

3.7.2 Single-mineral concentrates in igneous rocks

In a study of grain contacts in some volcanic rocks, Vance & Gilbreath (1967) found a tendency for like minerals to cluster, and others have observed single-mineral clusters, especially of plagioclase in basalts (Philpotts *et al.*, 1999), plagioclase in granites (Vance, 1969) and olivine in basalts (Schwindinger & Anderson, 1989). Jerram & Cheadle (2000) also illustrated clusters of olivine phenocrysts in komatiite (olivine-rich basalt), and used statistical cluster analysis to reveal clustering tendencies in rocks. In this section, some examples of clustering and single-mineral aggregates in igneous rocks are outlined, and possible mechanisms are discussed.

(1) Chain microstructure

Chain microstructure (Sampson, 1932; Bastin, 1950; Campbell, 1978) refers to open aggregates of chromite, pyroxene or plagioclase (see, for example, Sampson, 1932, p. 130; Philpotts *et al.*, 1998, 1999). They could be formed by (i) self-nucleation (Campbell, 1978) or (ii) adhesion of fortuitous impinging crystals of the same mineral, essentially involving ‘pressure-solution’ at the points of contact (Bastin, 1950, p. 7; Park & Means, 1996). Chains of plagioclase plus pyroxene (Philpotts & Dickson, 2002) indicate that a similar process can involve more than one mineral. Plagioclase clusters or networks in a basalt are shown in Fig. 3.50.

Self-nucleation, which is common in chemical systems (Campbell, 1978), may apply to aggregates of small crystals in volcanic rocks (Fig. 3.50), for

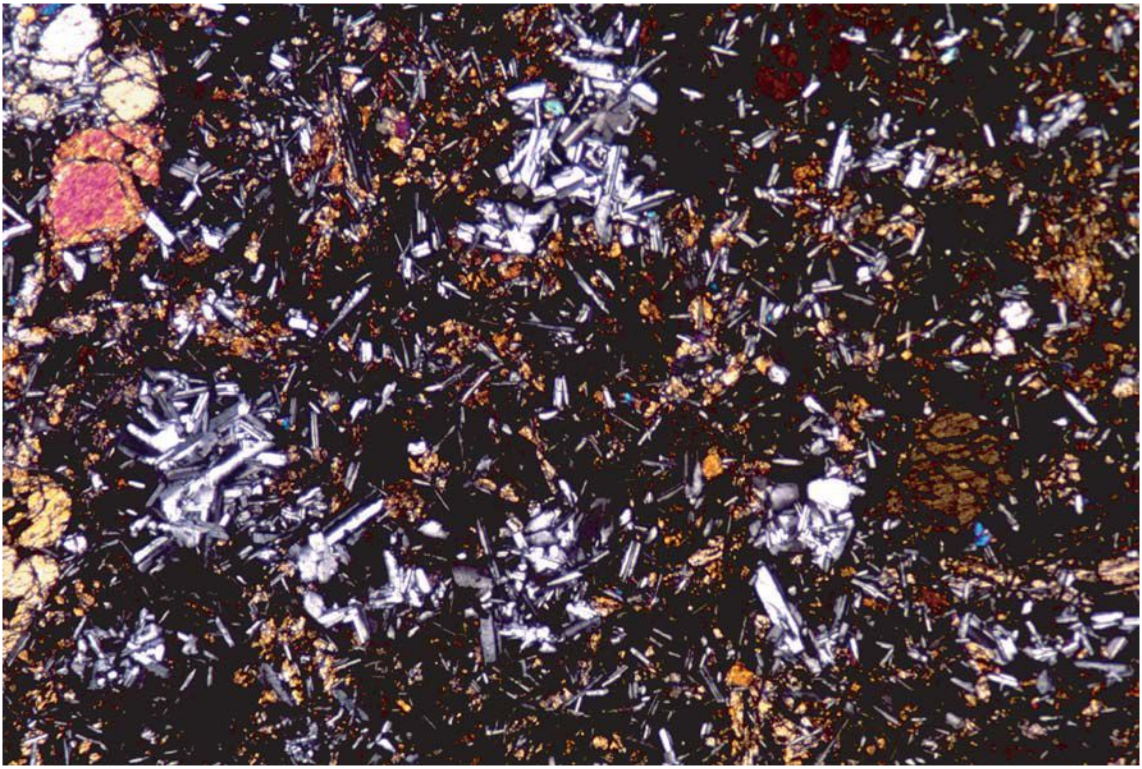

Fig. 3.50: Clusters of plagioclase crystals in a basalt from Iceland. Also present are scattered phenocrysts of olivine, aggregates of clinopyroxene and interstitial glass (isotropic). Crossed polars; base of photo 4 mm.

example aggregates of plagioclase in glassy basalts in the Makaoputi and Alae lava lakes, Kilauea Volcano, Hawaii, as illustrated by Kirkpatrick (1977, 1981). However, clusters involving plagioclase, pyroxene and olivine are equally common (Kirkpatrick, 1977, fig. 5), as shown in Fig. 3.4. Campbell (1987) stated that self-nucleation is due to a lower 'wetting angle' between the nucleus and substrate, implying a surface free-energy effect. This suggestion would be stronger if it could be shown that low-energy surfaces separate the crystals, whereas the crystals in most chains appear to be variably oriented (see, for example, Kirkpatrick, 1977, fig. 5; Philpotts *et al.*, 1999). Therefore, the situation appears to be different from synneusis (see below), which produces crystals separated by low-energy crystallographic planes. Moreover, dihedral angle measurements indicate that contacts between grains of the same mineral should have lower free energies than contacts between grains of different minerals (Section 4.2.4). Perhaps it is more of a chemical control at the atomic level, namely easier nucleation on chemically identical material.

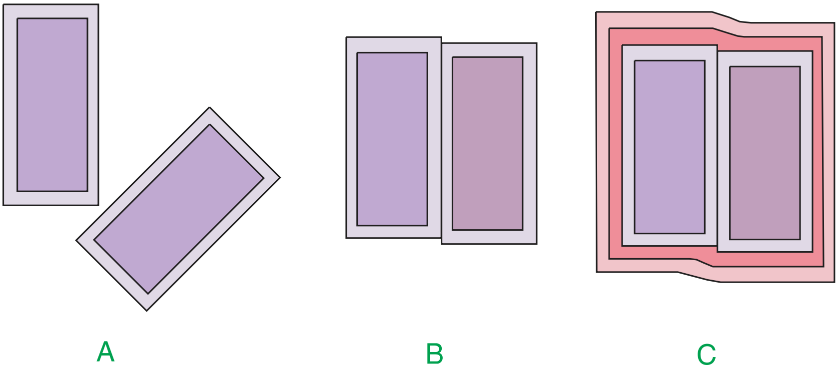

Fig. 3.51: Diagrammatic representation of stages in the development of synneusis aggregates of zoned phenocrysts. Two initially isolated crystals (A) drift together and unite (B), after which post-synneusis overgrowth occurs (C). Note the complete zoning in individual crystals formed prior to synneusis, and the zoning around the whole aggregate formed after synneusis. Based on Vance (1969, p. 9).

An alternative interpretation of chains is that fortuitously impinging crystals adhere because of the formation of a small area of lower-energy grain boundary that replaces very high-energy points of collision, and so reduces the total interfacial free energy. Single-mineral aggregates would be strongly favoured if that mineral were the only one precipitating from the magma at that stage of crystallization. Normal concentric zoning patterns in plagioclase crystals in chains described by Philpotts *et al.* (1999) indicate that the crystals had a brief period of independent crystallization before linking together.

(2) Synneusis

'Synneusis is the process of drifting together and mutual attachment of crystals suspended in a melt' (Vance, 1969, p. 7). Fortuitous physical accumulation of crystals in specific low-energy orientations by synneusis (Vogt, 1921, p. 321; Vance & Gilbreath, 1967; Vance, 1969), followed by adhesion, can form a type of 'glomeroporphyritic aggregate' (Fig. 3.51). The process has been observed in slags (Vogt, 1921). The reason for the adhesion is probably the low free energy of specific faces on which the minerals collide and attach, for example (010) twin interfaces in plagioclase. Therefore, although the final aggregate is controlled by interfacial free energy, the initial aggregation is not. The magma must be fluid enough to enable movement of the crystals.

Vance (1969) suggested that synneusis occurs in the earlier stages of consolidation and is related to turbulence. In plagioclase aggregates, early-formed zoning patterns don't go around all the crystals, but later zones do (Fig. 3.51). The centre of concentric zoning in each individual crystal is offset from the mutual boundary. Dowty (1980a) suggested that random sections through a zoned

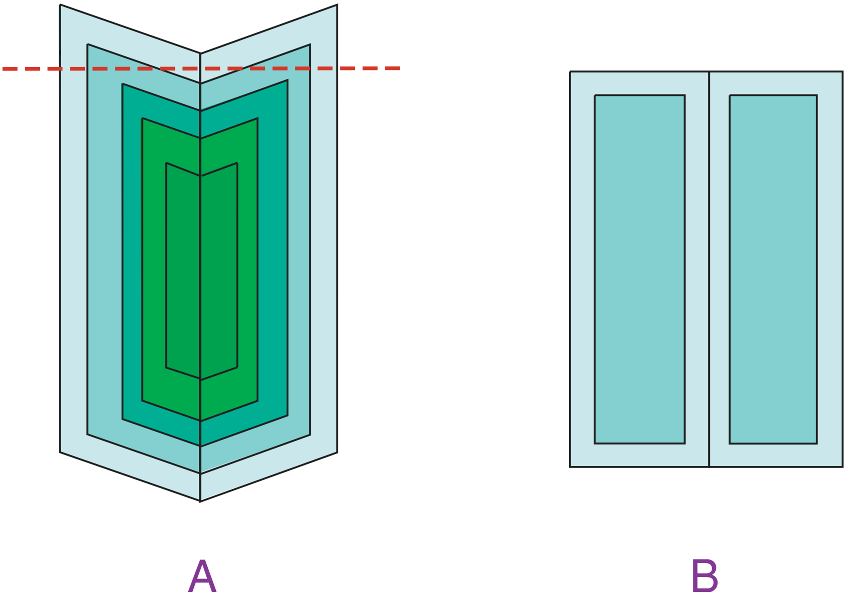

Fig. 3.52: Sketch showing how a section (B, cut along the dashed line in A) cut through a zoned crystal with a simple growth twin can show offsets of the centre of concentric zoning in each individual crystal identical to those expected from zoned crystals joined by synneusis; after Dowty (1980a).

crystal with a simple growth twin could show identical offsets (Fig. 3.52). However, he also suggested that because clusters are formed by crystal–crystal contact in laboratory experiments, at least occasional occurrences of synneusis in nature are to be expected (Dowty, 1980a, p. 83). He recommended serial sectioning and microprobe analysis to determine carefully whether separate true zoning centres are present.

Another probable example of synneusis is the attachment of small plagioclase (less commonly biotite) crystals to the faces of K-feldspar megacrysts growing in a granitic magma, producing a concentrically zoned (crystallographically controlled) pattern of inclusions in the megacryst (see, for example, Hibbard, 1965), as shown in Figs. 3.12 and 3.53. An alternative explanation is that the plagioclase or biotite nucleated epitactically on the K-feldspar (Dowty, 1980a; Bard, 1986, p. 51). However, epitactic nucleation of plagioclase on K-feldspar faces would produce asymmetrically zoned plagioclase inclusions, with no zoning on the innermost face and zoning on the others, whereas concentric zoning typically completely surrounds the observed plagioclase inclusions (Fig. 3.53).

Synneusis of olivine in an olivine-rich volcanic rock from Hawaii has been inferred by Schwindinger & Anderson (1989). Most of the crystals in aggregates have their *a* crystallographic axes parallel and their *c* axes either parallel or perpendicular. If synneusis did occur, the magma must have been very fluid, as

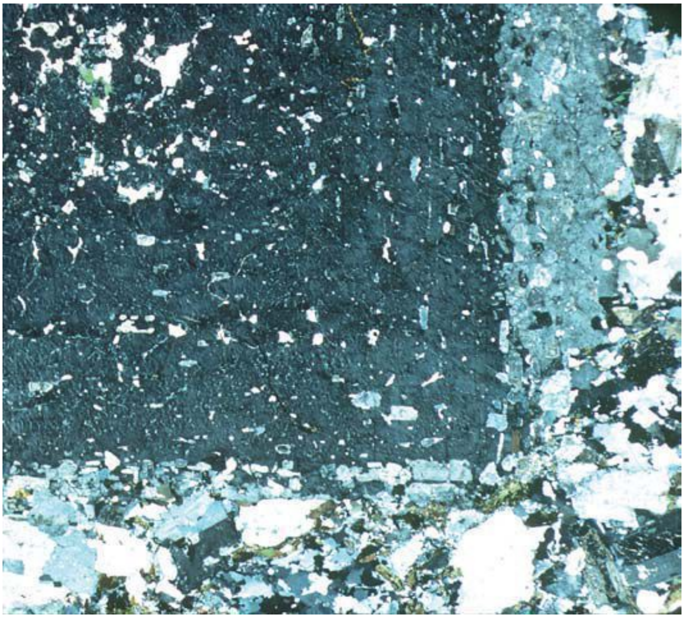

Fig. 3.53: Corner of a K-feldspar megacryst, Wuuluman Granite, Wellington, New South Wales, Australia, showing plagioclase inclusions arranged and aligned in concentric zones, as well as concentrations of plagioclase crystals similarly aligned against the faces of the megacryst. The plagioclase crystals may have adhered to the K-feldspar by synneusis (Section 3.7.2) or heterogeneous nucleation (Section 3.3.1). Photo by W. F. D'Arcy. Crossed polars; base of photo 10 mm.

very small crystals were involved. Schwindinger & Anderson (1989) suggested that the minimum aggregation time could be of the order of minutes! Synneusis has also been inferred for chromite crystals in some ultramafic rocks (see, for example, Vogt, 1921; Bastin, 1950, plate 2, fig. 3).

Hogan (1993) described glomeroporphyritic aggregates of plagioclase, within which the grains are random and meet along irregular boundaries. He inferred that the crystals were dissolving (owing to changes in temperature, pressure or water activity in the melt), in order to explain the irregular, embayed grain shapes, and suggested that as the irregularly shaped grains came close together, the trapped melt became supersaturated with the dissolving crystals and so crystallized, joining the grains together.

(3) Single-mineral adcumulates

The word cumulate was applied originally to magmatic basic or ultrabasic rocks in which precipitated crystals were inferred to have grown to a relatively large size before physical accumulation by either floating or sinking. If these crystals were inferred to continue to grow by precipitation from the interstitial liquid (which was inferred to require diffusive exchange of components with the main magma) and so fill space, the resulting rock was called an adcumulate (see, for example, Wager, 1963; Wager *et al.*, 1960). If the accumulated (cumulus) crystals were inferred to have stopped growing, and new minerals crystallized from the interstitial liquid, the resulting rock was called an *orthocumulate* (Fig. 3.46).

These terms and the inferences behind them are based on over-simple interpretations of the rocks' microstructures. For example, orthocumulate structure (Fig. 3.46) is typically formed by simultaneous crystallization of the main and the interstitial mineral (Section 3.6.1). Similarly, the polygonal grain shapes of adcumulates (Section 4.6.1) may be explained better by the mutual growing together of accumulated crystals, in response to reduction of interfacial free energy during slow cooling (Voll, 1960; Weedon, 1965; Vernon, 1970; Campbell, 1978; Hulbert & von Gruenewaldt, 1985; Reynolds, 1985; Hunter 1987, 1996), rather than growth by exchange of components with overlying liquid. The mechanism is discussed in Section 4.6.1, as it is largely a solid-state process, driven by interfacial energy, as discussed in Section 4.2.

On the other hand, the initial development of single-mineral aggregates in adcumulates (Section 4.6.1) in layered mafic–ultramafic igneous complexes is essentially a primary magmatic process, such as *size-density sorting* (see, for example, Irvine, 1974) or *rhythmic supersaturation* (see, for example, Lofgren & Donaldson, 1975; Campbell, 1978, 1987; McBirney & Noyes, 1979). The possibility that self-nucleation is responsible for single-mineral adcumulates has been put forward by Campbell (1978). However, growth from a liquid supersaturated in the nucleated mineral, but not in the other potential mineral or minerals (owing to rhythmic supersaturation, for example) could have the same result. In other words, if only one mineral can precipitate in the prevailing compositional environment, it would be forced to self-nucleate under conditions of heterogeneous nucleation. Thus, rhythmic supersaturation can produce alternating single-mineral aggregates, owing to compositional restrictions at a growing crystal or crystal aggregate interface, unrelated to grain-boundary free energy.

Other more complex processes may also contribute to the development of these rocks. For example, Walker *et al.* (1988) have shown experimentally that differential solubility along a temperature gradient can cause redistribution and concentration of olivine in the cooler parts of a crystal–liquid aggregate, forming adcumulate-like olivine aggregates. However, whether such gradients are likely in large bodies of mafic magma is debatable.

Therefore, crystallization *in situ* appears to have made a major contribution to the formation of ultramafic cumulates in layered complexes, even if crystal settling was also involved (see, for example, Campbell, 1978). In fact, the word 'cumulate' has evolved to mean an igneous rock with a composition that does not correspond to that of a magma (see, for example, McBirney & Hunter, 1995), without the necessary implication of crystal settling or floating. Many cumulates may form by physical accumulation of crystals; if not, some other process must lead to the accumulation.

(4) Spherulites

Most spherulites grow as single-mineral aggregates, at least in the earlier stages of their development (Section 3.5.5). They are characterized by repeated nucleation of new fibres on existing fibres. This form of 'self-nucleation' is probably due to the fact that only one mineral is precipitating at the time, under conditions of forced heterogeneous nucleation.

(5) Comb layering and orbicular structures

Delayed nucleation, in conjunction with rhythmic supersaturation, can force clustering to occur. An extreme situation is the formation of comb layering (Fig. 3.33) and orbicular structures. Strongly delayed nucleation causes heterogeneous nucleation, and rhythmic supersaturation induces crystallization of one mineral and then another in the compositionally layered shells (see, for example, Moore & Lockwood, 1973; Vernon, 1985).

(6) Flow sorting

Physical segregation of layers rich in mafic minerals (mafic schlieren) in granitic magma (Moore & Lockwood, 1973; Barrière, 1981; Vernon, 1986a; Berry & Flint, 1988; Clarke, 1992; Pitcher, 1993; Reid *et al.*, 1993; Tobisch *et al.*, 1997; Weinberg *et al.*, 2001), caused by sorting during magmatic flow (Section 3.9), can also lead to single-mineral aggregates. Sorting may occur during shearing, owing to variation in properties such as the size, shape and density of crystals, grains or aggregates. Accumulations of K-feldspar megacrysts in granite may also form in this way (Gilbert, 1906; Vernon, 1986a), as discussed in Section 3.4.5. Milord & Sawyer (2003) described biotite schlieren in granitic magma (diatexite) in a migmatite terrane (Section 4.16.1), the sorting being accomplished initially by segregation of small biotite grains from large plagioclase grains (forming biotite-rich schlieren and forcing flow to be concentrated in these layers, thereby increasing the biotite alignment) and eventually by the squeezing out of melt from between the biotite grains to concentrate them.

(7) Partial melting residuals

Concentrations of the same mineral may also occur if a solid rock is partly melted, producing melt and solid crystals. These crystals may be left behind as the melt moves away from the source rock. This occurs in the formation of basalt magma by melting of peridotite in Earth's mantle (see, for example, McBirney & Hunter, 1995, p. 115), producing olivine-rich concentrates, as shown by some ultramafic xenoliths in basalts, and also can account for non-magmatic compositions of leucosomes in some migmatites (Section 4.16).

3.8 Mineral intergrowths in igneous rocks

Under some conditions, minerals form regular intergrowths in igneous rocks. Common examples are *graphic intergrowths* of quartz and alkali feldspar in

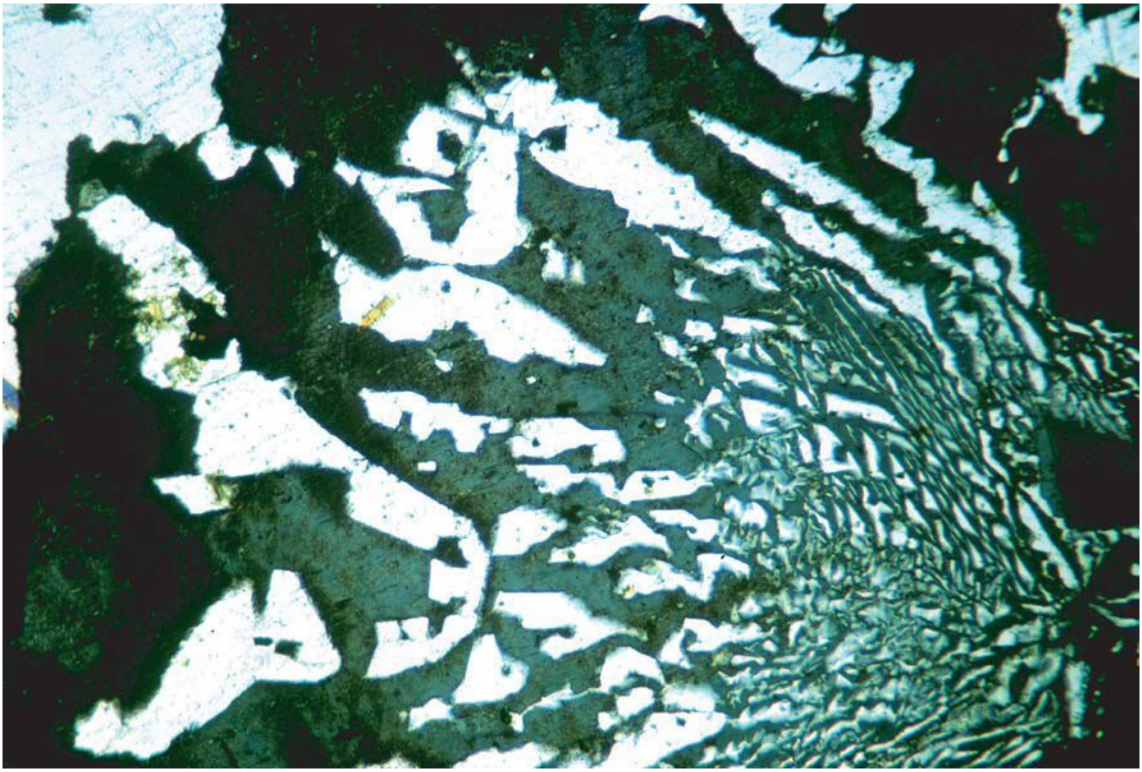

Fig. 3.54: Graphic (granophyric) intergrowth of quartz and K-feldspar (at or near extinction) in a granite. Note that all the quartz portions have the same crystallographic orientation, and only one orientation of K-feldspar is also present. This indicates that both minerals are parts of large single grains, implying a low nucleation rate for each. Crossed polars; base of photo 3.5 mm.

granites and pegmatites (Fig. 3.54), in high-level felsic intrusions (Fig. 3.55) and in the interstices of some mafic rocks (Fig. 3.56). Graphic intergrowths have also been found in lunar granites (Warren *et al.*, 1983). Plagioclase–clinopyroxene intergrowths in dolerites (Fig. 3.56) have similar microstructures, but are less common. Many other minerals also have been observed in graphic intergrowths (Harker, 1909, p. 271). Detailed descriptions and discussions of the origin of graphic intergrowths in feldspars are given by Smith (1974, pp. 593–608).

Graphic intergrowths are so called because many of them resemble ancient forms of writing. According to Barker (1970), the term ‘granophyric’ implies a graphic intergrowth of quartz and either K-feldspar or Na-rich feldspar, rather than a quartz and alkali feldspar solid solution, although Lentz & Fowler (1992) regarded the term as the ‘irregular, finer-grained counterpart’ of the graphic intergrowth, and Best (2003, p. 699) equated it with ‘micrographic’. I will use ‘granophyric’ in a general way for micrographic intergrowths of quartz and alkali feldspar.

Fig. 3.55: Fine-grained micrographic (granophyric) intergrowth of quartz and alkali feldspar in the groundmass of a felsic dyke, eastern Musgrave Ranges, central Australia. Skeletal phenocrysts of plagioclase are also present. Sample by courtesy of Alfredo Camacho. Crossed polars; base of photo 1.75 mm.

The quartz : alkali feldspar ratio and chemical composition of some granophyric intergrowths approximate the composition of the 'ternary minimum' (cotectic) in the system Or–Ab–Qtz (Vogt, 1921; Dunham, 1965; Barker, 1970; Hughes, 1971). This is the temperature at which the melt is saturated with both quartz and alkali feldspar at a particular water pressure, so that the two minerals crystallize together. For example, the proportion of quartz at the ternary minimum at 650 °C and water saturation is 28 molecular percent. However, the compositions of other granophyric intergrowths show some departures from this ideal composition. For example, the reported quartz content varies from 25 to 29% by volume, although the proportion is constant for each rock examined, suggesting a recurrent process (Lentz & Fowler, 1992). This led Smith (1974, p. 607) to suggest that kinetic factors may be more important than cotectic composition. The experiments of Fenn (1986), though consistent with cotectic crystallization, also suggest that this condition may not be necessary for the formation of granophyric intergrowths. He suggested that the intergrowth forms by simultaneous crystallization driven by the rates of growth and diffusion in the melt adjacent to the intergrowth. This interpretation is supported by Lentz & Fowler (1992), who inferred that slow diffusion of Al to a growing feldspar interface causes Si to increase, saturating the local melt in quartz. This depletes the adjacent melt

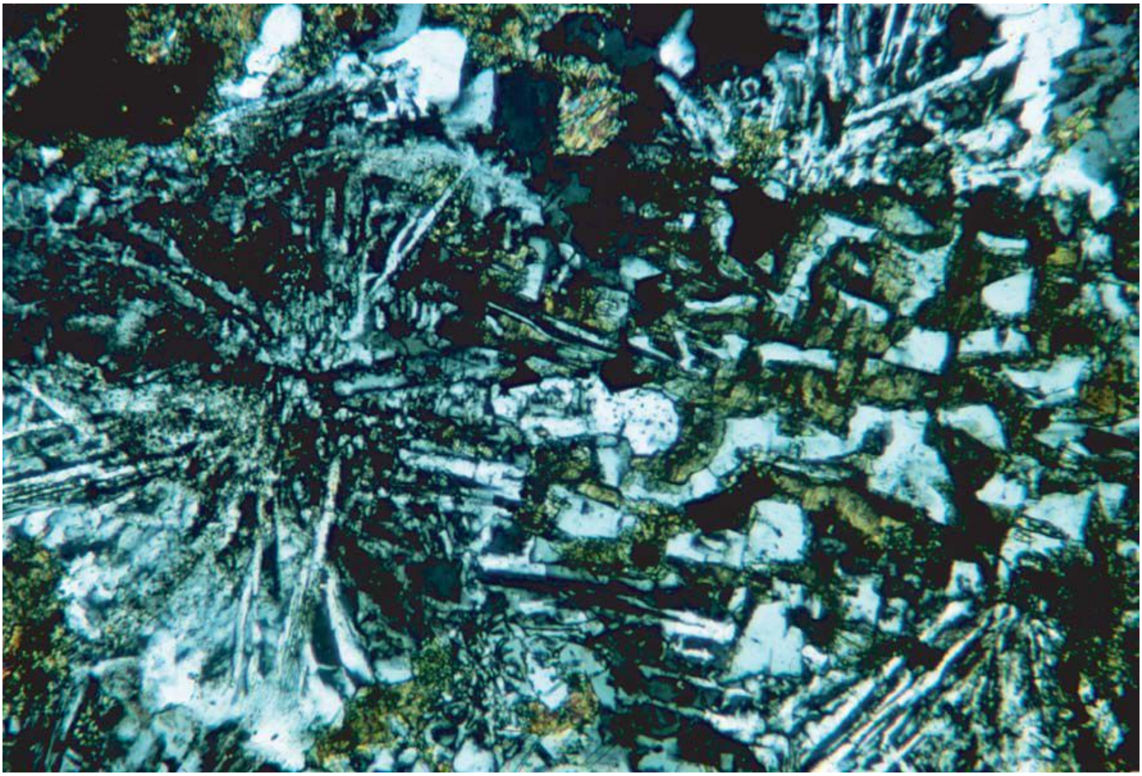

Fig. 3.56: Coarser-grained micrographic intergrowth of plagioclase and clinopyroxene (right) and finer-grained micrographic intergrowths of quartz and alkali feldspar (left, top right and bottom right) in a dolerite from Launceston, Tasmania, Australia. Crossed polars; base of photo 1.3 mm.

in Si, causing feldspar saturation, and hence rhythmic precipitation of both minerals results. Thus, although the magma as a whole is saturated with respect to both quartz and alkali feldspar, and so both minerals crystallize simultaneously in terms of the history of the overall magma, local growth–diffusion relationships cause their growth to alternate on the scale of the intergrowth.

In graphic and similar intergrowths, both minerals grow as single crystals (see, for example, Smith, 1974), forming rods or lamellae with shapes at least approximately controlled by crystal structure (Fig. 3.54). For example, Carstens (1983) described quartz rods oriented perpendicular to crystal growth faces of alkali feldspar, the intergrowths being arranged in sectors and the quartz maintaining a constant orientation in all sectors. Lentz & Fowler (1992) found that the quartz in graphic intergrowths occurs as angular rods with an irregular inner surface and a planar outer interface against the alkali feldspar. Along with Vadilo (1971, reported by Smith, 1974, p. 607) and Smith (1974, p. 607), they interpreted these observations as implying epitactic nucleation of quartz on corners and edges of irregular surfaces of alkali feldspar. Presumably the dendritic habit of the alkali feldspar is due to growth at conditions of strong supersaturation; London (1999) found experimentally that undercooling of felsic melts by as little as 75 degrees can cause the development of graphic quartz–feldspar intergrowths.

Experimentally produced granophyric intergrowths also consist of two single crystals (Fenn, 1986, pp. 326–7). The quartz in many of the intergrowths resembles dendritic crystals. Evidently nucleation rates for both minerals are relatively low at the prevailing temperature or water content of the magma, so that once a nucleus of each mineral forms, growth of the same crystal continues, instead of the formation of new nuclei.

Some granites have euhedral phenocrysts of quartz, with interstitial micrographic intergrowths of quartz and alkali feldspar. This observation is consistent with the experiments of Swanson & Fenn (1986), which showed that euhedral crystals of quartz grow at small degrees of undercooling (ΔT less than 55 degrees) and that skeletal quartz occurs with greater amounts of supercooling. The supercooling could be induced by reduction in temperature as the magma moves to higher crustal levels, or by loss of water. Nucleation of granophyric intergrowths on quartz phenocrysts typically results in optical continuity of the quartz of the phenocryst and the quartz in the adjacent intergrowth (Hughes, 1972). Rare plagioclase phenocrysts may also act as a nucleating substrate, resulting in optical continuity of the phenocryst rim and the alkali feldspar in the intergrowth (Hughes, 1972).

Experiments by Swanson (1977), Lofgren (1976), Freda & Baker (2000) and Baker & Freda (2001) have shown that quartz and alkali feldspar may nucleate and grow together as radiating (spherulitic) graphic intergrowths in a supercooled melt (Fig. 3.57). Commonly the quartz poikilitically encloses the feldspar, forming 'snowflake' microstructure (Anderson, 1969). This structure has also been produced by experimental crystallization of glass (Lofgren 1971b), and is common in felsic lava flows and ignimbrites, which suggests that some snowflake microstructure may form by glass devitrification, rather than direct crystallization from a melt.

3.9 Magmatic flow

Many extrusive and intrusive igneous rocks show evidence of *magmatic flow* (Figs. 3.5, 3.58–3.63). Clear microstructural evidence of magmatic flow is common in volcanic rocks, in which flow can be observed in progress. Flow lines appear most clearly in glassy rocks (Fig. 3.58); they are commonly contorted and folded during the flow (Figs. 3.60–3.62) and may be delineated by concentrations of crystallites or microlites (Fig. 3.62). However, although magmatic flow microstructures are generally less obvious in coarse-grained intrusive rocks, they may be spectacular. For example, the plagioclase crystals in some gabbros and cumulates have a strong preferred orientation (see, for example, Higgins,

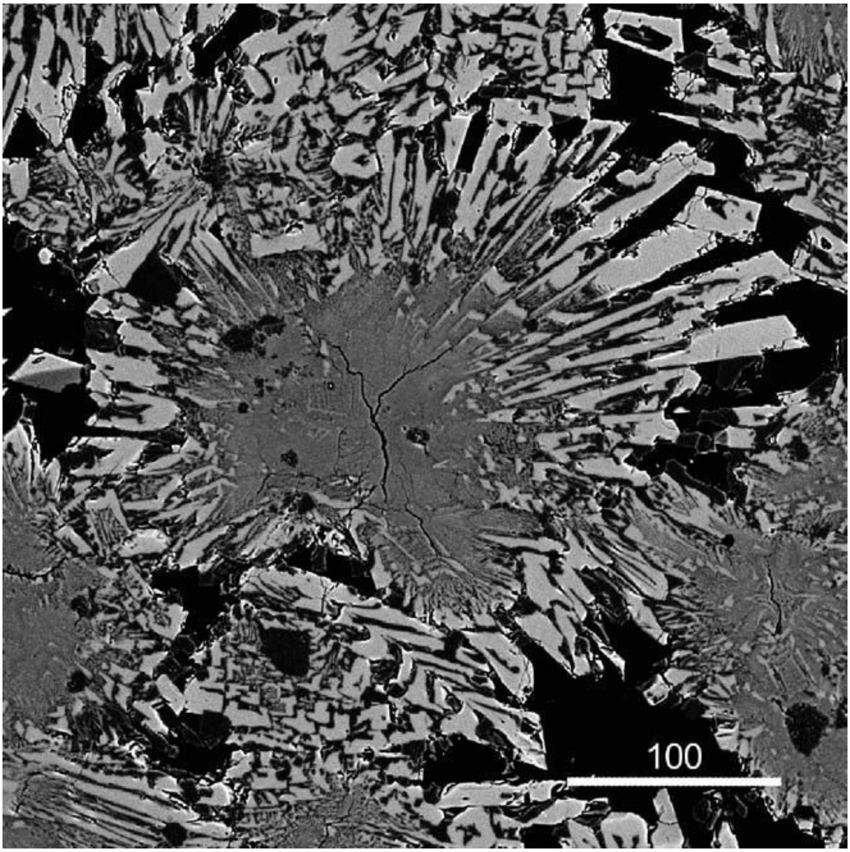

Fig. 3.57: SEM image of a radiating graphic (granophyric) aggregate of quartz and alkali feldspar grown experimentally from a supercooled melt (Freda & Baker, 2000; Baker & Freda, 2001). Image kindly provided by Don Baker. The scale represents 100 μm.

1994), as shown in Fig. 3.63. This is probably mainly caused by flow currents in the magma and/or rotation during compaction. In some cumulates, aligned plagioclase crystals are draped around olivine oikocrysts with random plagioclase inclusions, suggesting progressive alignment by compaction (McBirney & Hunter, 1995, p. 119) or by increasing flow later in the history of the magma.

Magmatic flow involves change of shape of magma, with sufficient melt for the crystals to rotate passively into alignment without them deforming internally (S. R. Paterson *et al.*, 1989; Vernon, 2000a). The microstructural evidence for magmatic flow has been reviewed by Vernon (2000a). Relevant features include: (1) parallel or subparallel alignment of elongate euhedral crystals (see, for example, Benn & Allard, 1989; Vernon, 2000a; Spanner & Kruhl, 2002), commonly feldspar, hornblende or olivine, that are not internally (plastically) deformed (Figs. 3.5, 3.59, 3.63), implying rotation of the crystals in a relatively

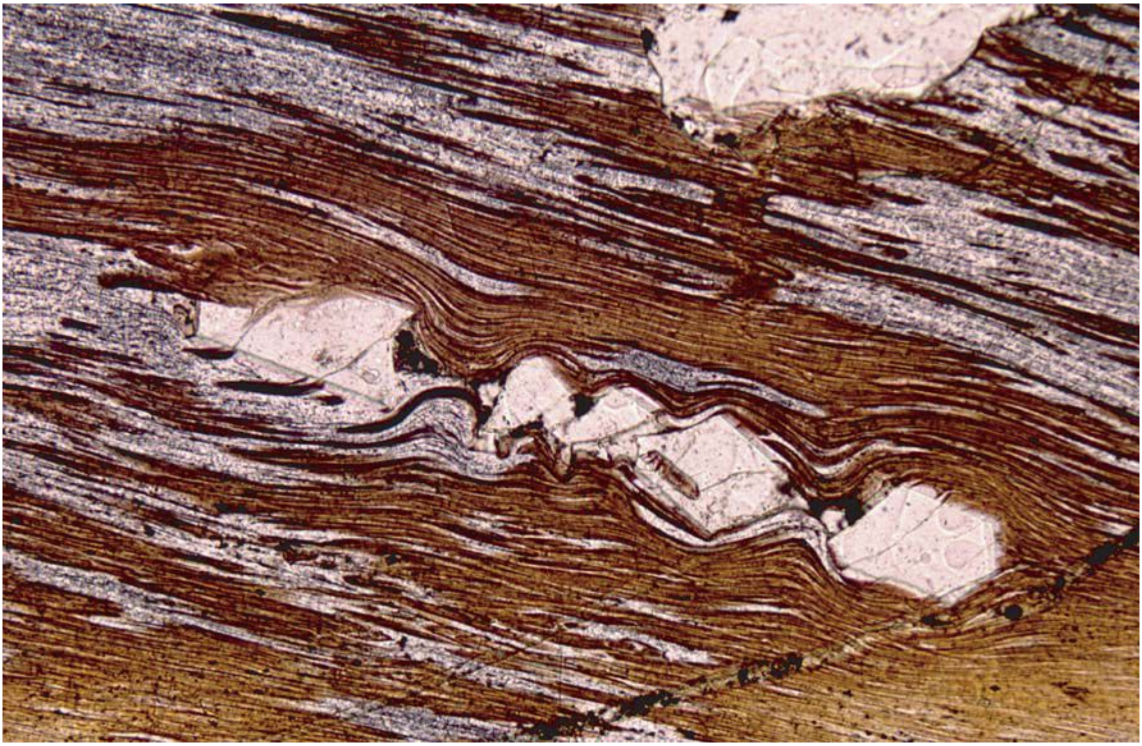

Fig. 3.58: Flow layering in glassy rhyolite, Ngongataha Quarry, Rotorua, New Zealand. The layering is deflected around fragments of feldspar phenocrysts that have been broken, probably during the final stages of magmatic flow, when the lava became very viscous. The fragments have been rotated, producing imbrication (tiling). Plane-polarized light; base of photo 1.5 mm.

weak medium, such as melt; (2) imbrication (tiling) of elongate euhedral crystals that are not internally deformed (Fig. 3.64) or of fragments of phenocrysts that have undergone boudinage (Fig. 3.58), as described by den Tex (1969), Blumenfeld (1983), Shelley (1985b), Blumenfeld & Bouchez (1988), Philpotts & Asher (1994) and Spanner & Kruhl (2002); (3) insufficient solid-state strain (Chapter 5) in regions between aligned or imbricated crystals to accommodate crystal rotation; (4) elongation of microgranitoid enclaves (Section 3.10.3) without plastic deformation (Chapter 5) of the minerals, as discussed by many people, including Gilbert (1906), Pabst (1928), Vernon, (1983, 1984, 1996b), Vernon *et al.* (1988), S. R. Paterson *et al.* (1989) and Tobisch *et al.* (1997); (5) magmatic flow foliations and elongate microgranitoid enclaves deflected around phenocrysts or xenoliths (Section 3.10.2), as described by Pabst (1928) and Hurlbut (1935); (6) layers (schlieren) of crystals of mainly mafic minerals formed by sorting during magmatic flow, in the absence of plastic deformation of the minerals involved; (7) contorted and folded flow lines (commonly caused by concentrations

Fig. 3.59: Alignment of elongate plagioclase crystals in a basalt, in response to flow of the lava. Crossed polars; base of photo 1.8 cm.

of minute crystals and/or devitrification products) in glassy volcanic rocks (Figs. 3.60–3.62); and (8) elongation of gas bubbles (Section 3.14), as shown in Fig. 3.62, which may occur parallel to the axial surfaces of folds in a magmatic flow foliation (Vernon, 1987c). In addition, Philpotts & Asher (1994) used granophyric segregations at the corners of plagioclase phenocrysts as flow-direction indicators.

Magmatic flow can occur only if crystals can slip past each other, owing to lubrication by melt. The required proportion of melt varies from relatively small (perhaps around 10%) for magmas containing mostly crystals of the same mineral, such as gabbroic anorthosite (Nicolas, 1992) to perhaps as much as 20–40% for magmas with many minerals of different shapes and sizes, such as granite (see, for example, Vernon & Paterson, 1993, p. 21; Byron *et al.*, 1996; Paterson *et al.*, 1998; Vernon, 2000a).

Magmatic flow can be distinguished microstructurally from solid-state flow (Section 5.11.2), as discussed in detail by Vernon (2000a). However, if a granite magma cools during regional deformation, it goes through a transition between magmatic flow and solid-state flow (see, for example, S. R. Paterson *et al.*, 1989; Tribe & D'Lemos, 1996; Miller & Paterson, 1994; Vernon, 2000a). This is

Fig. 3.60: Magmatic flow layering in glassy rhyolite from Glass Mountain, Medicine Lake Volcano, northeastern California, USA. The deflection of the layering around the dark solid objects (heavily altered crystal fragments or possibly altered glass globules of a composition different from that of the groundmass), indicates that they were rotated during flow of the lava. The flow lines have been tightly folded against the large fragment during its rotation, indicating the sense of rotation, which is opposite to that shown in Fig. 3.61. From Vernon (2000b, fig. 75). Plane-polarized light; base of photo 1.75 mm.

because the crystal : melt ratio increases as magma crystallizes, so that the magma changes from a crystal suspension to a crystal framework with an interconnected network of melt-filled pores, to restricted pore networks, and eventually to isolated pores just above the solidus. Deformation during this transition has been called ‘submagmatic flow’ (S. R. Paterson *et al.*, 1989), which, though perhaps not an ideal term, at least implies that magmatic flow is no longer possible. It has also been called ‘grain-supported flow’, to distinguish it from ‘suspension flow’ (magmatic flow), but this term does not effectively distinguish it from completely solid-state flow. Microstructural evidence for submagmatic flow is discussed in Section 5.11.3.

An alternative explanation of at least some flow banding in felsic volcanic rocks has been presented by Tuffen *et al.* (2003). They suggested that rising rhyolitic magma may be repeatedly fractured and healed at shallow crustal

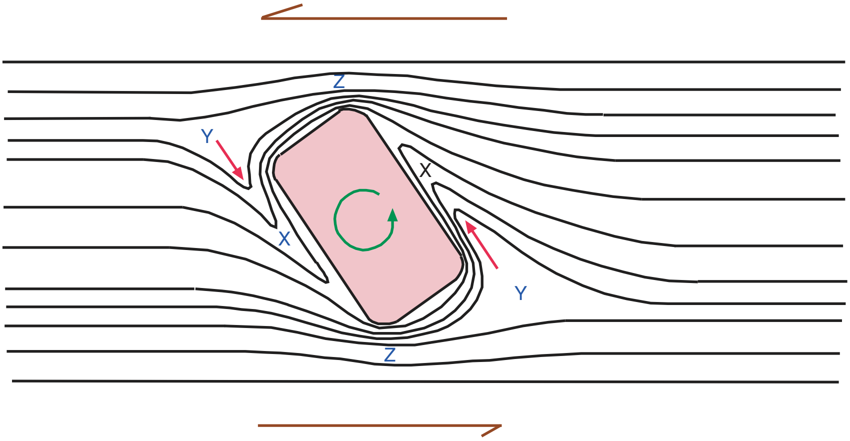

Fig. 3.61: Sketch showing microstructural features ideally developed around a rotating phenocryst in a relatively homogeneous groundmass flowing by simple shear (Vernon, 1987c). Compression of the flow layers occurs at X, expansion occurs at Y, and deflection around the phenocryst occurs at Z. The small arrows show the direction of closure of the microfolds and the sense of rotation of the phenocryst. The overall sense of shear is indicated by the large top and bottom arrows.

levels, as indicated by anastomosing fragmental ('tuffisite') veins formed by shear fracture of viscous magma in the transition to glass. Thorough welding of the fragments during subsequent deformation would allow repeated fracturing of the same magma body. The similarity between the deformed tuffisite veins and layers of different colour and microlite concentration in glassy volcanic rocks (Figs. 3.34, 3.58, 3.60) led Tuffen *et al.* (2003) to suggest that flow banding in felsic volcanic rocks may be due to this welding of fragmental material deposited in former short-lived fractures.

3.10 Enclaves in igneous rocks

3.10.1 General comments

Enclaves are mineral aggregates that do not crystallize *in situ* from the magma in which they occur. The main examples are: (1) fragments of rock (*xenoliths*) or individual grains (*xenocrysts*) that are broken off the walls of the magma chamber and incorporated into the ascending magma, the process being known as 'magmatic stoping'; (2) *microgranitoid enclaves* (igneous enclaves, 'mafic enclaves'), which are globules of other magma bodies mingled with the enclosing ('host') magma; (3) concentrations of fine-grained, early-precipitating aggregates that have been broken up and incorporated into the same or a later magma body; and (4) refractory residual grains and aggregates, which may be carried in the magma from the source area, but may be difficult to detect (owing to reaction

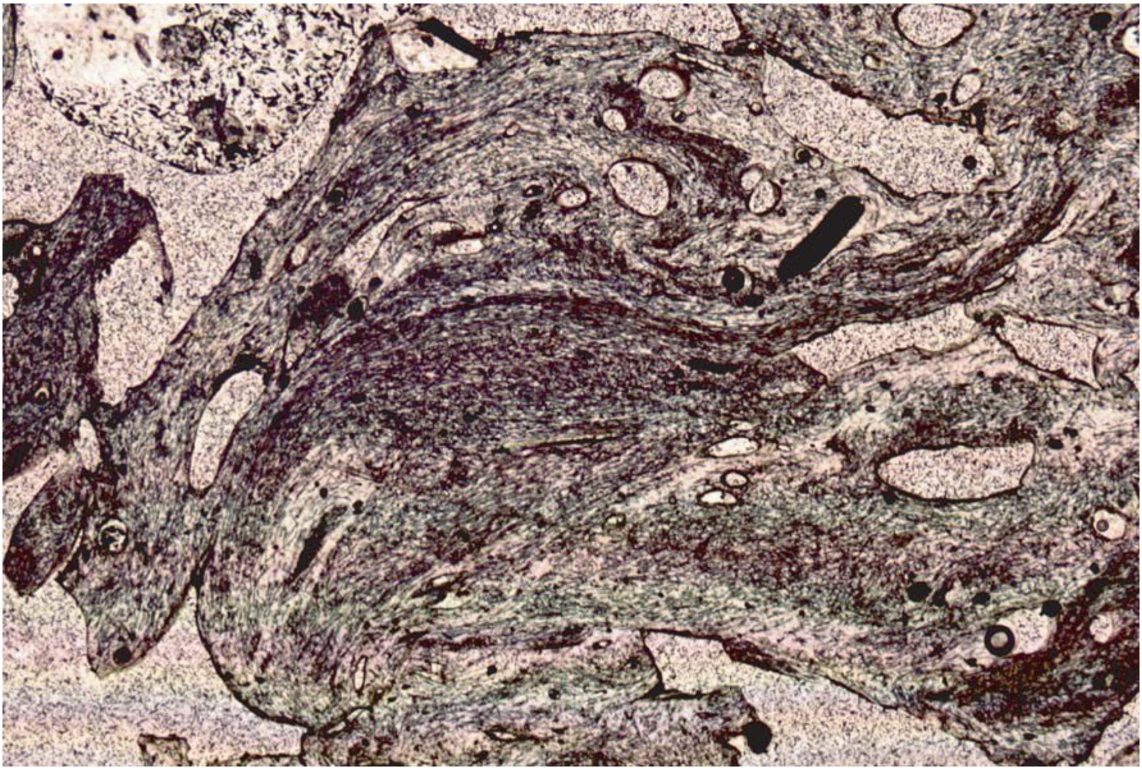

Fig. 3.62: Glassy rhyolite, Oregon, USA, showing folded magmatic flow layering. The layering is delineated by feldspar microlites. Also present are vesicles (gas bubbles), as discussed in Section 3.14.2, several of which have been stretched and folded parallel to the flow layering. Plane-polarized light; base of photo 1.5 mm.

with the host magma and re-equilibration to lower temperatures and pressures during ascent); the amount present in any one rock is often a matter of considerable controversy. The two most common types of enclave are xenoliths and microgranitoid enclaves.

3.10.2 Xenoliths and xenocrysts

Most xenoliths and xenocrysts have angular or irregular shapes, although xenocrysts may become rounded if they partly melt in the host magma. In submarine basalts, olivine grains inferred to be xenocrysts are anhedral, and may show fracturing and optical evidence of plastic deformation, in contrast to the polyhedral and skeletal shapes of typical phenocrysts in these rocks (Bryan, 1972, p. 5814). If xenocrysts or xenoliths are unstable in the magma, they show reaction rims or partly melted rims and/or interiors (Fig. 3.65).

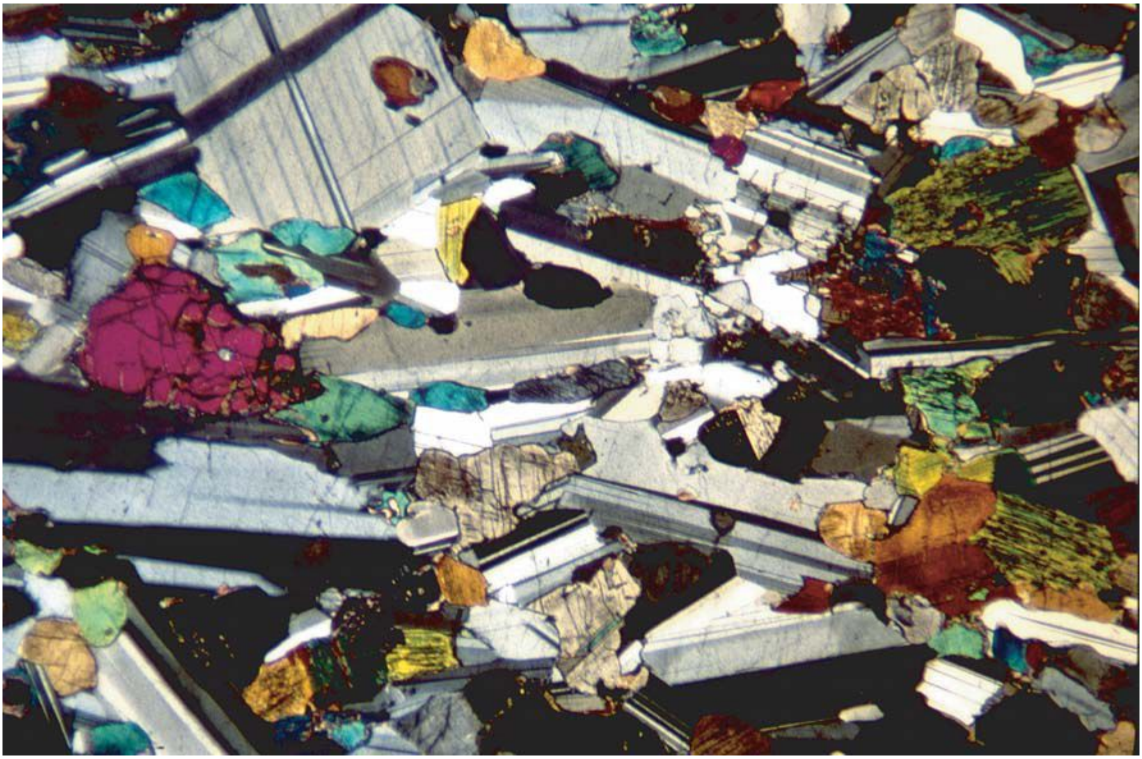

Fig. 3.63: Gabbro, consisting of plagioclase (elongate grains with grey first-order interference colours and multiple twinning), clinopyroxene and olivine. The plagioclase grains are preferentially aligned in a magmatic flow foliation, but the individual grains do not show evidence of internal plastic deformation, apart from minor deformation twinning (Chapter 5). Crossed polars; base of photo 4.4 mm.

Some xenoliths are enclosed by microgranitoid enclaves (Section 3.10.3), forming a variety of 'double enclave', owing to incorporation of a rock fragment in a magma that subsequently becomes mingled with the present host granite. Other xenoliths or xenocrysts are surrounded by spectacular, compositionally layered rims of elongate crystals, in a variety of comb layering, forming orbs dispersed through the host granite ('orbicular granite') as discussed in Section 3.5.4.

3.10.3 Microgranitoid enclaves (magma mixing and mingling)

Microgranitoid enclaves (igneous enclaves, 'mafic enclaves') are very common in granitoid rocks (Phillips, 1880; Harker & Marr, 1891; Harker, 1904, 1909; Pabst, 1928; Blake *et al*., 1965; Wiebe, 1968, 1973, 1974, 1994, 1996; Didier,

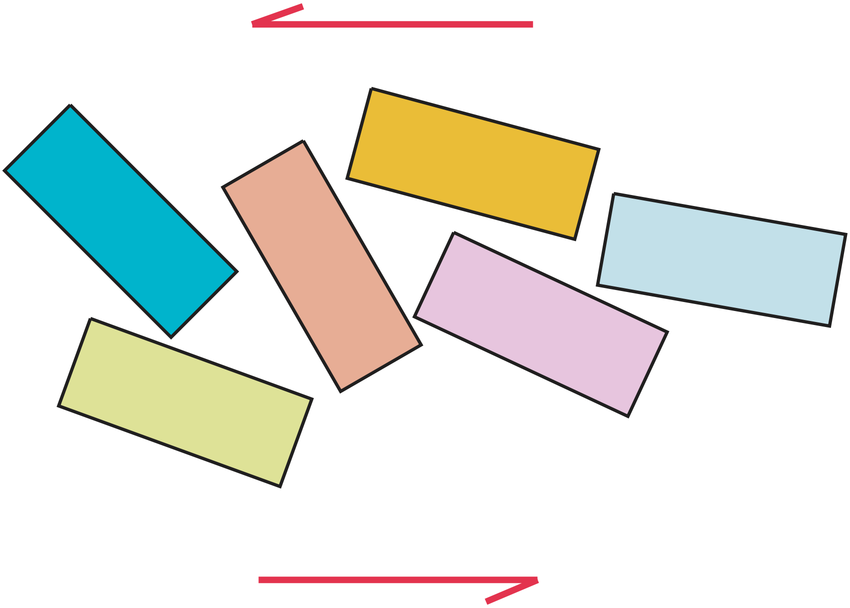

Fig. 3.64: Sketch showing imbrication (tiling) of crystals formed during magmatic flow.

1973; Fershtater & Borodina, 1977; Blake, 1981; Hibbard, 1981; Reid *et al.*, 1983; Vernon, 1983, 1984, 1986a, 1990a, 1991a, 1996b; Vernon *et al.*, 1988; Didier & Barbarin, 1991). They are generally felsic to intermediate in composition (rarely mafic), are rounded, scalloped or lenticular in shape, and are finer-grained and typically more mafic than the host granite. They have igneous microstructures, commonly with euhedral phenocrysts, oscillatory zoning in plagioclase (Section 3.11.5), and mineral alignment reflecting magmatic flow (Figs. 3.66–3.74). Some show chilled margins against the host granite. These features indicate that the enclaves were originally magma globules that flowed and quenched to finer-grained solid enclaves in the host magma (Walker & Skelhorn, 1966; Blake 1981; Reid *et al.*, 1983; Vernon, 1983, 1984).

Microgranitoid enclaves also occur in compositionally equivalent volcanic rocks (Wilcox, 1944; Bacon & Metz, 1984; Stimac *et al.*, 1990; Vernon, 1990a, 1991a), where the presence of a commonly partly glassy groundmass confirms that the enclaves were magma globules in the parent granitic magma (Vernon, 1983, 1991a), as shown in Figs. 3.70–3.72 and 3.74.

Some early workers recognized the igneous nature of these enclaves (see, for example, Phillips, 1880; Harker & Marr, 1891; Pabst, 1928), but from around 1920 to 1980, most petrologists favoured a solid-state (xenolith) origin, even inferring that reaction of a solid rock with the host magma somehow produced ‘igneous-looking rocks’ (see, for example, Nockolds, 1933; Grout, 1937; Fenner,

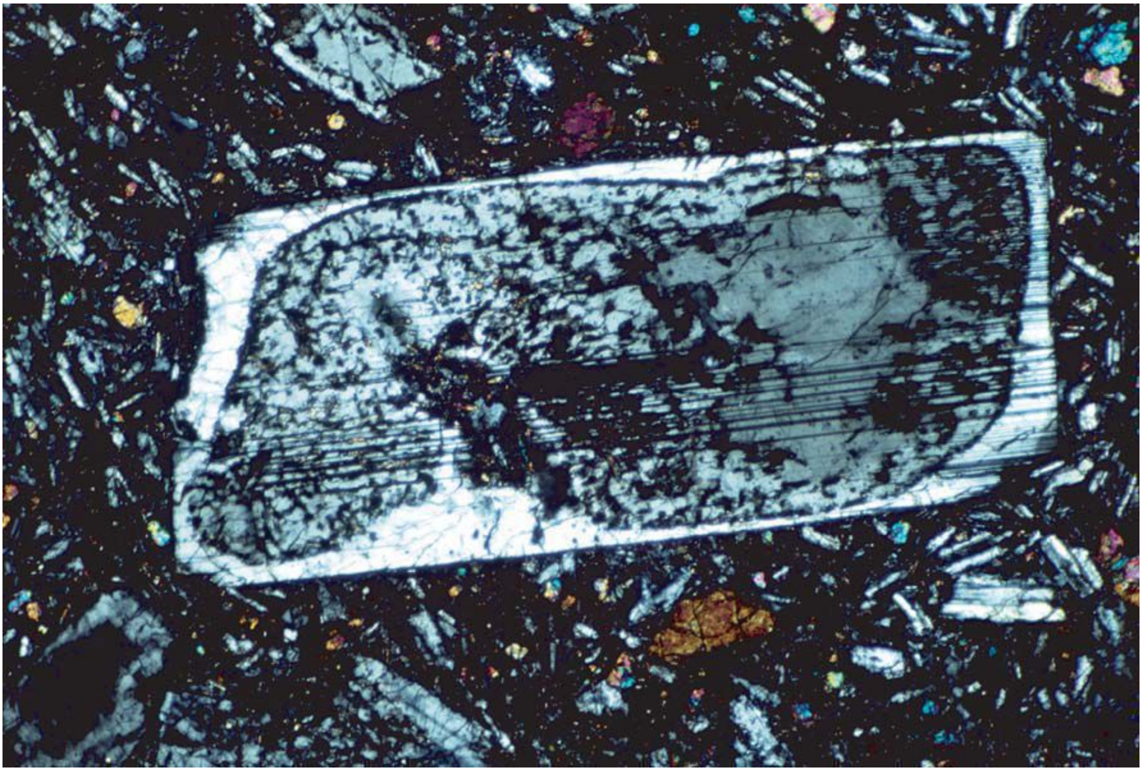

Fig. 3.65: Plagioclase phenocryst showing evidence of rounding and internal corrosion by dissolution in the magma, followed by deposition of new plagioclase as a rim, in basalt from Mount Tomah, New South Wales, Australia. Crossed polars; base of photo 4.4 mm.

1938, 1944). However, recent work has produced overwhelming evidence of a magmatic origin, although much remains to be done on the origin of the magma globules and especially on details and location of mixing processes. The history of changing ideas on microgranitoid enclaves and magma mingling/mixing has been reviewed by Vernon (1996b) and Wilcox (1999).

Microgranitoid enclaves commonly show evidence that they were formed by *magma mixing* ('hybridism') before they were incorporated into the host granitic magma (*magma mingling*). Magma mingling involves the interpenetration of two or more magmas without pervasive mixing of their melt components, whereas magma mixing involves homogenization of the melts and either the conversion of any pre-existing crystals to minerals stable in the hybrid (mixed) melt or their armouring by stable minerals (Vernon, 1983, p. 90).

Observations on and discussion of the processes of magma mixing and magma mingling have been published by many people, especially for volcanic and shallow

Next Page

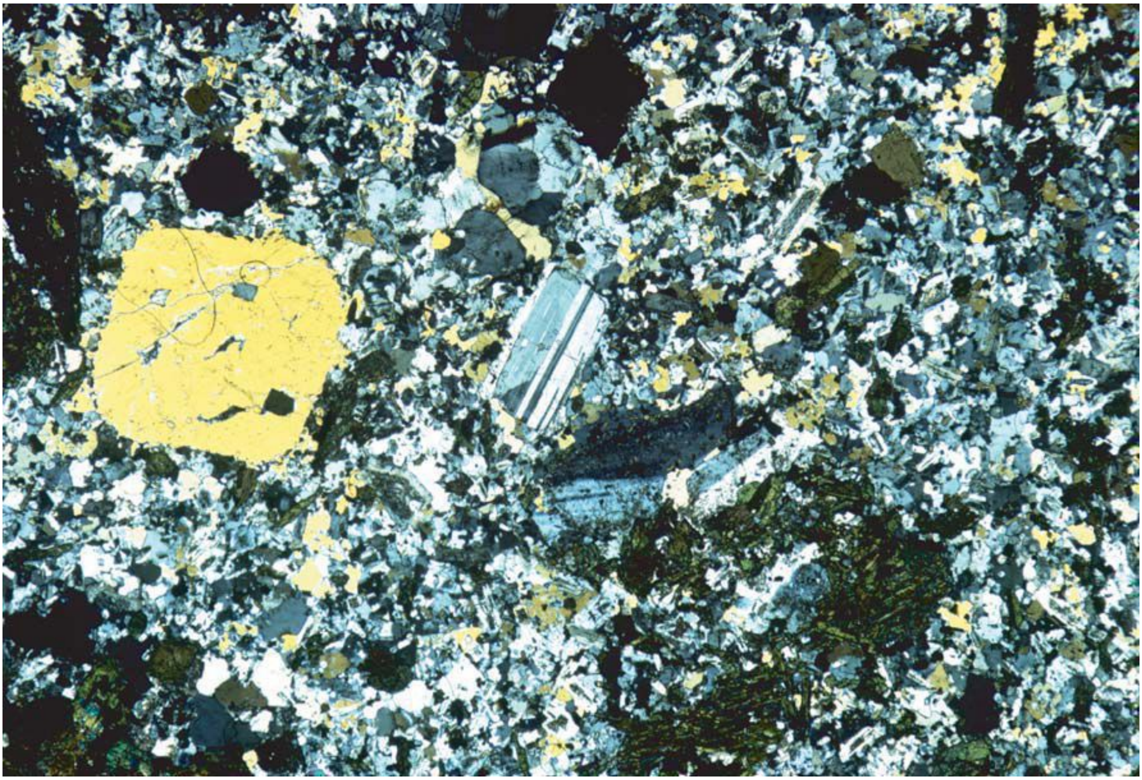

Fig. 3.66: Microgranitoid enclave with euhedral phenocrysts of quartz and plagioclase, New England Batholith, New South Wales, Australia. Crossed polars; base of photo 8.4 mm.

intrusive rocks (see, for example, Harker, 1904, 1909; Wilcox, 1944; King, 1964; Blake *et al*., 1965; Wager *et al*., 1965; Thompson, 1969; Wiebe, 1973, 1974; Gamble, 1979; McSween *et al*., 1979; Taylor *et al*., 1980; Vernon *et al*., 1988). Some mixing may occur locally in the host granite before the enclaves solidify (see, for example, Frost & Mahood, 1987; Vernon, 1990a; Wiebe, 1994, 1996; Collins & Wiebe, 1998), but the local proportion of mafic to felsic magma needs to be high enough to keep the more mafic magma fluid enough for mixing to occur. Generally, the enclaves are too small and isolated for mixing to take place *in situ*, except perhaps in the very margins of some enclaves, so that most mixing occurs elsewhere, presumably in magma bodies that break up on encountering the main magma body to form enclaves that become dispersed in the host magma. The following microstructures in microgranitoid enclaves indicate magma mixing (Vernon, 1983, 1986a, 1990a, 1991a).

(1) *Quartz xenocrysts* may be incorporated in the more mafic magma from the more felsic magma. The xenocrysts are unstable in the more mafic magma and

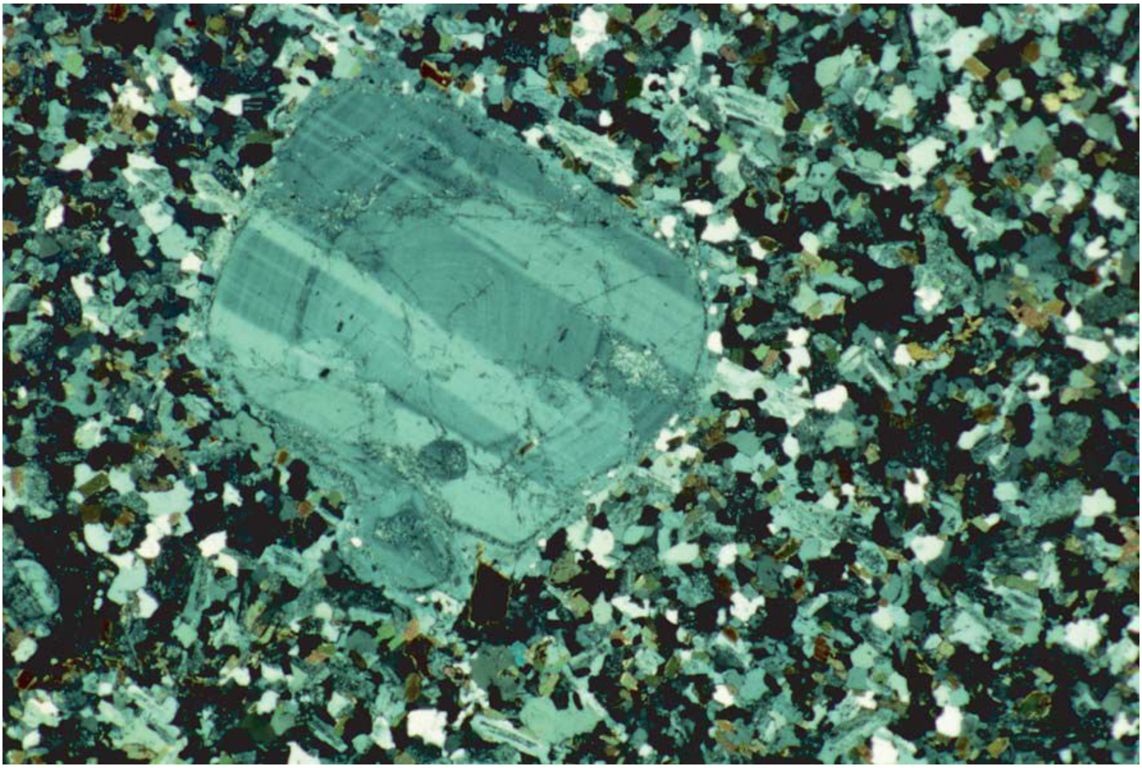

Fig. 3.67: Microgranitoid enclave containing euhedral phenocryst of plagioclase with oscillatory zoning and laths of elongate plagioclase crystals in the groundmass, Shap Granite, northwest England. Crossed polars; base of photo 4 mm.

so start to dissolve. For example, glass rims on corroded quartz xenocrysts are preserved in some microgranitoid enclaves in volcanic rocks (Vernon, 1990a, 1991a), as shown in Fig. 3.74. The latent heat of crystallization required to dissolve the quartz is taken from the immediately adjacent magma, and this effectively undercools the magma locally. This promotes fine-grained crystallization of minerals in which the magma is currently saturated. The result is quartz xenocrysts with hornblende-rich mantles in metaluminous granites and volcanic rocks (Fig. 3.73) and quartz xenocrysts with orthopyroxene-rich mantles in peraluminous granites and volcanic rocks (Fig. 3.74), as discussed by Vernon (1983, 1990a, 1991a). These mantled quartz xenocrysts are usually called 'ocelli', but this term is also applied to some felsic segregations inferred to represent immiscible liquids (see, for example, Philpotts, 1976) and so the term should be used with caution or avoided. 'Mantled quartz xenocrysts' may be a better term.

(2) *K-feldspar megacrysts* in microgranitoid enclaves are out of place in relatively mafic magmas, and so are of xenocrystic origin, having been incorporated

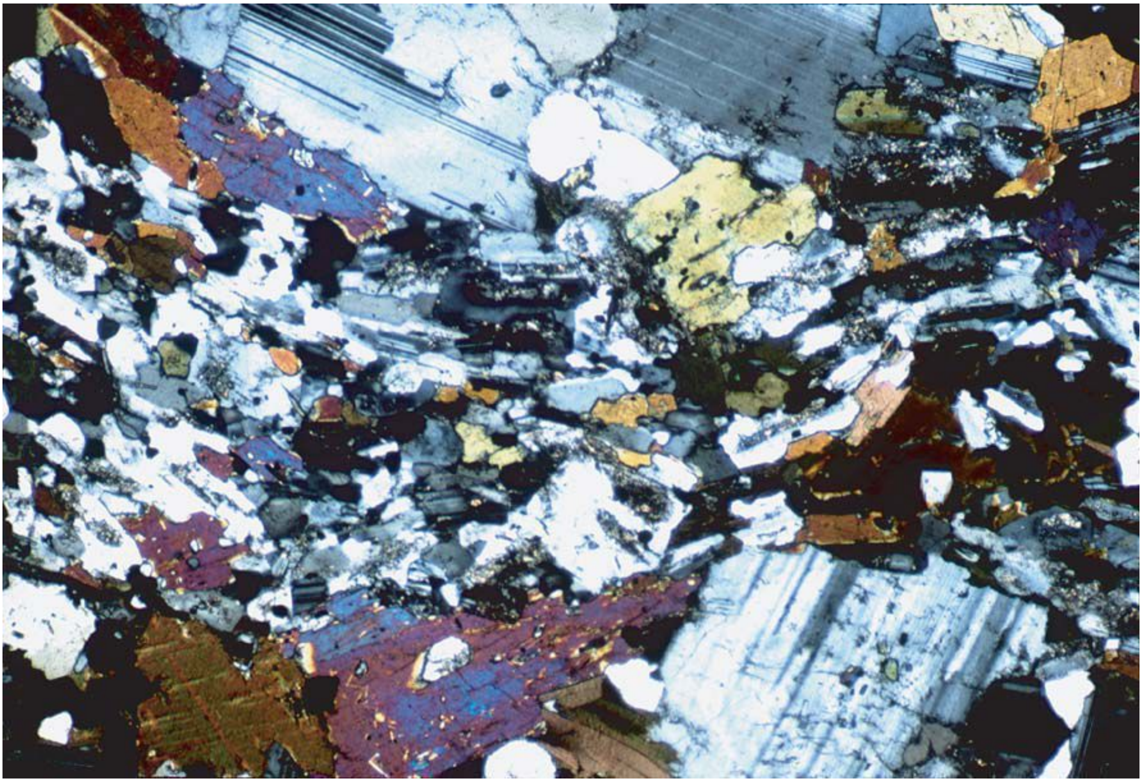

Fig. 3.68: Small microgranitoid enclave that has been stretched during magmatic flow in tonalite, Tarandore Point, Tuross Heads, New South Wales, Australia. The alignment of the plagioclase and biotite grains, coupled with the absence of internal plastic deformation, indicates that the enclave flowed as a magma (Section 3.9). The biotite shows shades of brown, owing to its strong absorption colour masking the high-order interference colours. Crossed polars; base of photo 4.4 mm.

from the more felsic magma (see, for example, Harker & Marr, 1891; Harker, 1909; King, 1964; Wilcox, 1944; Hibbard, 1981; Reid *et al.*, 1983; Vernon, 1983, 1986a, 1990a, 1991a; Cox *et al.*, 1996). They show typical features of K-feldspar phenocrysts in granites, namely oscillatory zoning (Section 3.11.5), simple twinning and zonally arranged, euhedral plagioclase inclusions (Vernon, 1983, 1986a, 1990a, 1991a; Cox *et al.*, 1996). In fact, they are commonly identical to K-feldspar megacrysts in the adjacent granite (see, for example, Vernon, 1990a), suggesting that the mixing involved the actual host magma, either at the present site of the enclave (Vernon, 1990a) or elsewhere. Many K-feldspar xenocrysts are partly dissolved and rounded, owing to their instability in the hybrid magma, and many are rimmed with plagioclase, with which the more mafic magma is saturated, forming a variety of 'rapakivi structure' (Phillips, 1880; Harker & Marr, 1891;

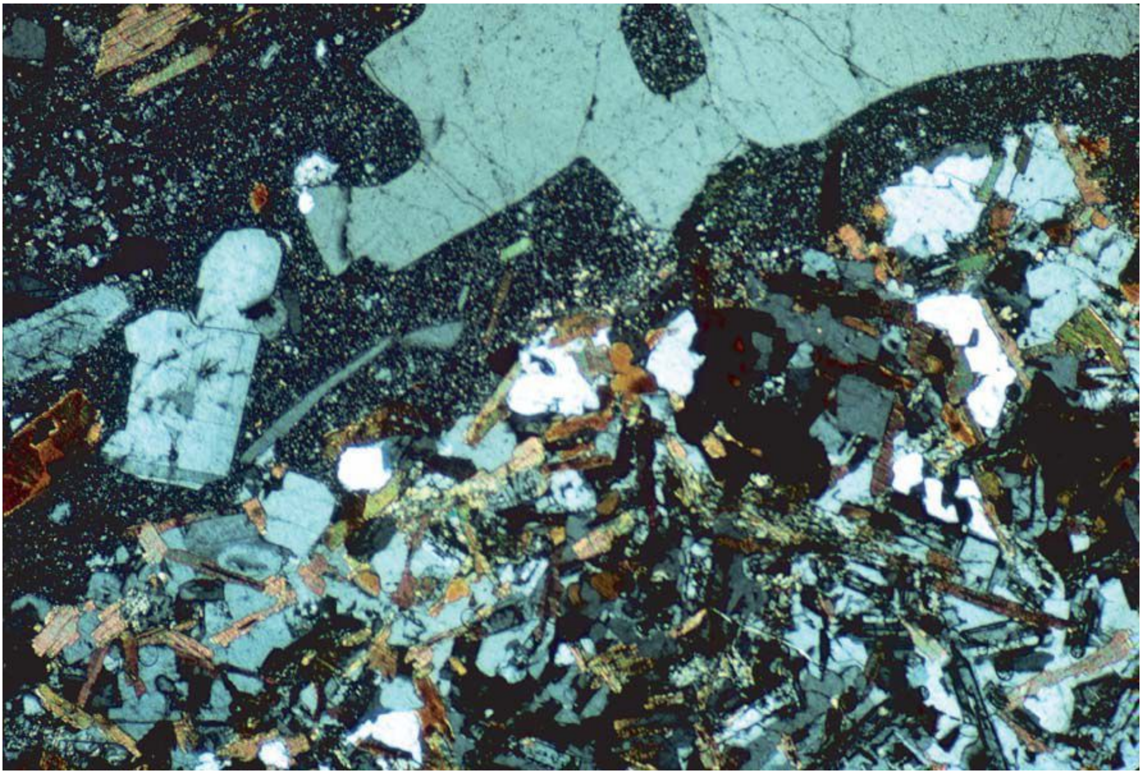

Fig. 3.69: Microgranitoid enclave (bottom right half of photo) in ignimbrite (Section 2.3), Violet Town Volcanics, Victoria, Australia. The enclave has an igneous microstructure, with elongate grains of plagioclase and biotite (shades of brown), with interstitial quartz. The host rock (top left half of photo) shows a large, embayed phenocryst of quartz (Section 3.13). Crossed polars; base of photo 4.4 mm.

Hibbard, 1981), as shown in Fig. 3.75. Megacrysts may project out from the enclave into the host granite, commonly with a thin ‘skin’ of enclave material partly draped around them, indicating that the megacrysts were in the enclave magma and were left projecting out of the enclave during the magma mingling process (Vernon, 1986a, p. 50). Resorbed K-feldspar xenocrysts also occur in magmatic enclaves in rhyolite (Bacon & Metz, 1984) and trachyte (Cantagrel *et al*., 1984).

Overgrowths of K-feldspar on the mechanically incorporated megacryst may be produced by precipitation from the hybrid magma (Vernon, 1990a). An example described by Vernon (1990a, figs. 6a, 6b) has the usual rectangular plagioclase inclusions in the main part of the megacryst (these having grown in the felsic magma before mixing with the more mafic magma) and random inclusions of the same minerals as those in the adjacent enclave at the margins of the megacryst

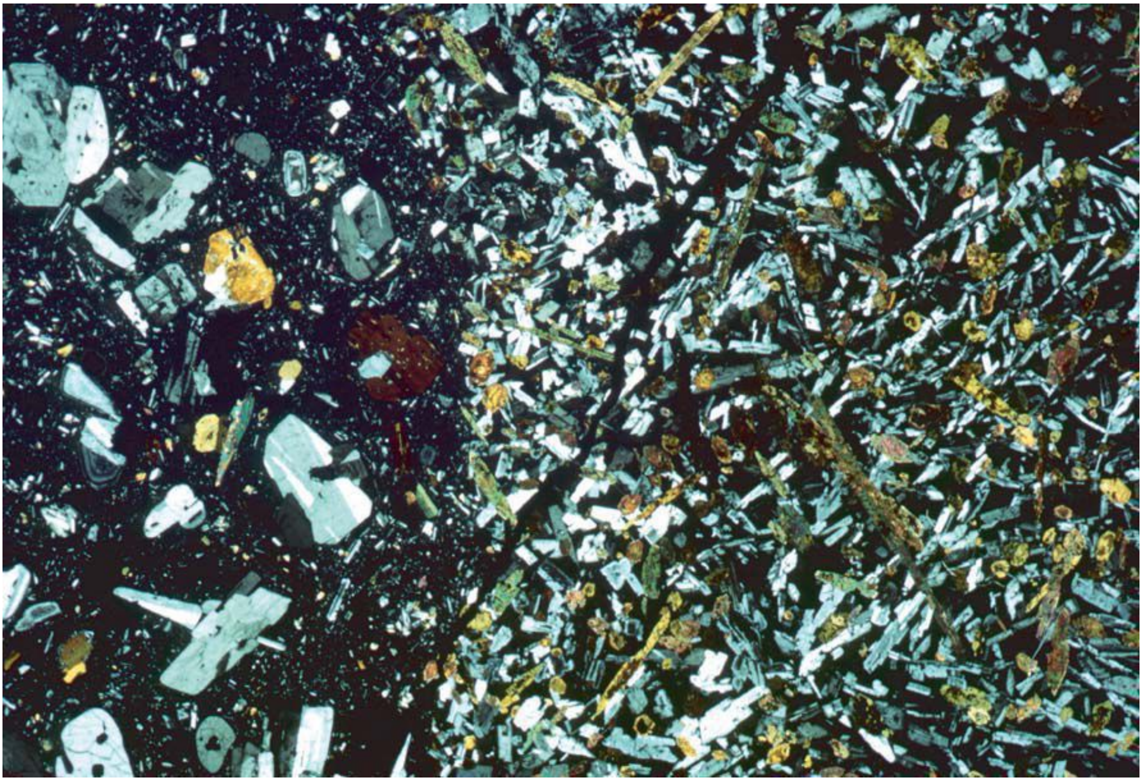

Fig. 3.70: Microgranitoid enclave, consisting of elongate laths of plagioclase and biotite in glass (right half of photo) in glassy andesite (left half of photo). The presence of glass confirms that the microgranitoid enclave was a magma globule. Crossed polars; base of photo 16 mm.

(these having been incorporated by the overgrowth). Moreover, the enclave minerals against the megacryst are aligned, showing that the enclave magma flowed after the overgrowth was formed, which is good evidence that the enclave was a magma globule.

(3) *Corrosion, overgrowths and sharp zoning discontinuities (compositional spikes)* are common features of plagioclase in microgranitoid enclaves and in the host granite. For example, King (1964) described oligoclase with calcic overgrowths in hybrid enclaves in the British Tertiary province, and Hibbard (1981) described corroded grains of plagioclase (from the more felsic magma) with dendritic overgrowths of more calcic plagioclase (precipitated from the hybrid melt), the dendritic habit resulting from the strong undercooling and compositional change of the melt caused by the magma mixing.

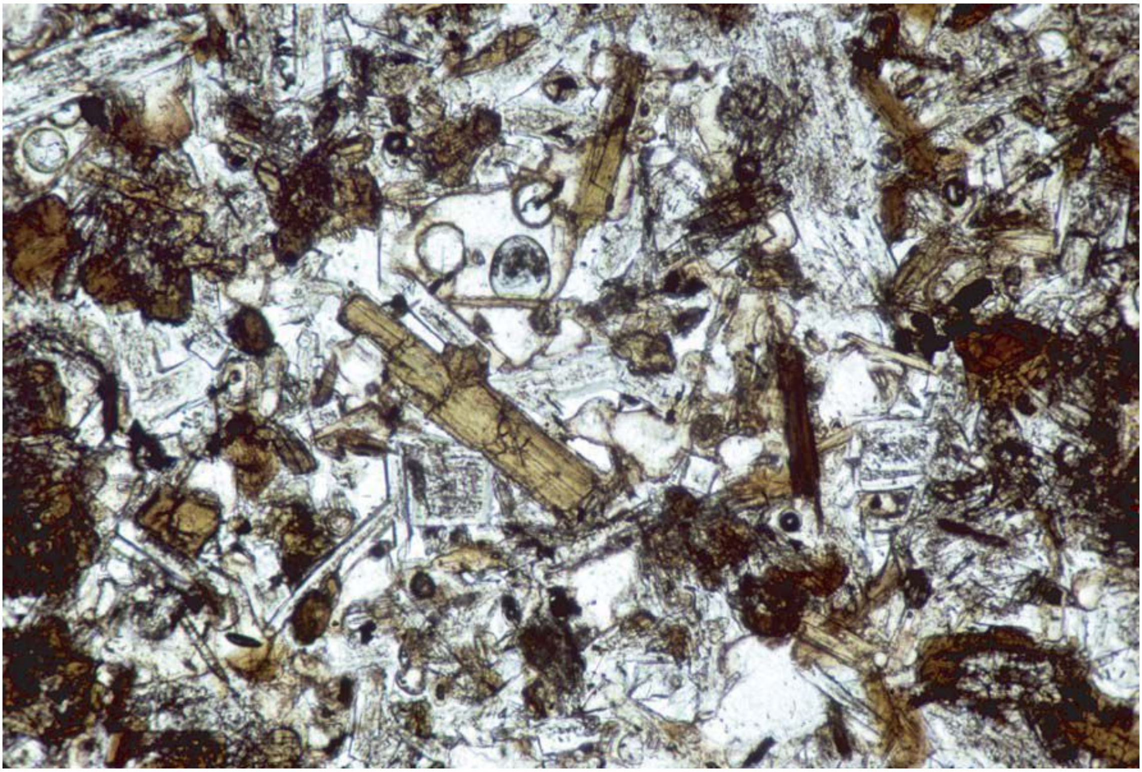

Fig. 3.71: Glassy microgranitoid enclave in aluminous volcanic rock (dacite), Hoyazo, Spain. The enclave consists of plagioclase (colourless, but extensively replaced by clay minerals, giving it a cloudy appearance), biotite (shades of brown), orthopyroxene (high relief), apatite (very long needles) and interstitial glass with vesicles (gas bubbles). The glass confirms that the microgranitoid enclave was a magma globule. Plane-polarized light; base of photo 1.75 mm.

Wiebe (1968) observed plagioclase phenocrysts in microgranitoid enclaves with corroded cores of bytownite or labradorite that have sodic plagioclase rims where the phenocrysts are in contact with the enclosing peraluminous quartz monzonite. Identical plagioclase phenocrysts occur in the quartz monzonite, the inference being that calcic plagioclase grains were extracted from the more mafic melt during magma mixing, and partly melted in the felsic magma (in which they were unstable), after which the more sodic plagioclase (with which the felsic magma was saturated) precipitated on the corroded cores. In addition, a calcic zone (‘spike’) is constantly present in the plagioclase of the quartz monzonite; this zone truncates earlier zones, and is due to ‘a period of partial resorption when the more sodic phenocrysts initially came into contact with hotter, more mafic magma’ (Wiebe, 1968, p. 697).

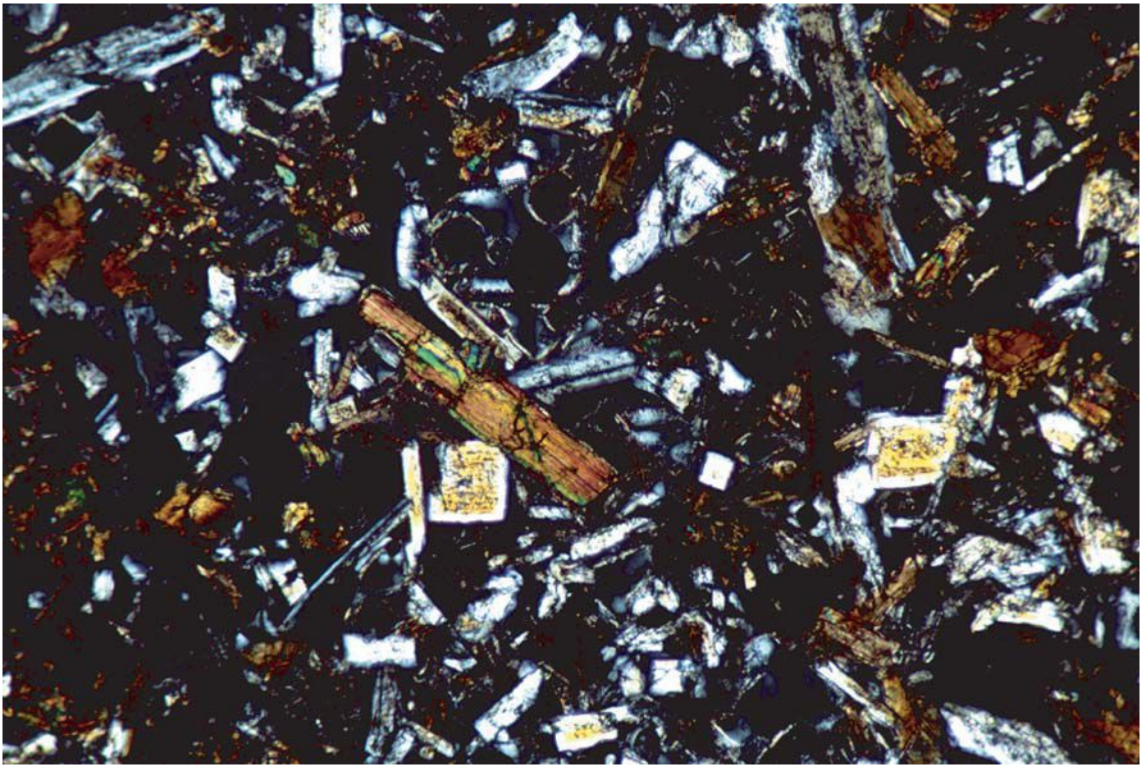

Fig. 3.72: Same field as shown in Fig. 3.71, but in crossed polars, to show the glass (isotropic). Crossed polars; base of photo 1.75 mm.

3.11 Compositional zoning in igneous minerals

3.11.1 General comments

Minerals belonging to a solid-solution series (e.g. plagioclase) react continuously with the surrounding liquid as it cools. The attainment of equilibrium between a complete growing crystal and the melt during cooling should produce a compositionally uniform crystal. However, diffusion and ion exchange in many minerals is commonly too slow for the whole growing crystal to adjust its composition to changing conditions (e.g. falling temperature), so that only the rims can equilibrate with the liquid. The result is *compositional zoning* (Figs. 3.45, 3.76, 3.77).

The most common form of compositional zoning is *concentric zoning*, in which the zones are parallel to the advancing crystal faces (Figs. 3.45, 3.76, 3.77), which distinguishes it from other forms of zoning, such as *patchy zoning* (Section 3.11.6) and *sector zoning* (Section 3.11.11). Concentric zoning patterns reflect the growth history of the crystal (Fig. 3.77), as discussed in Section 3.11.10.

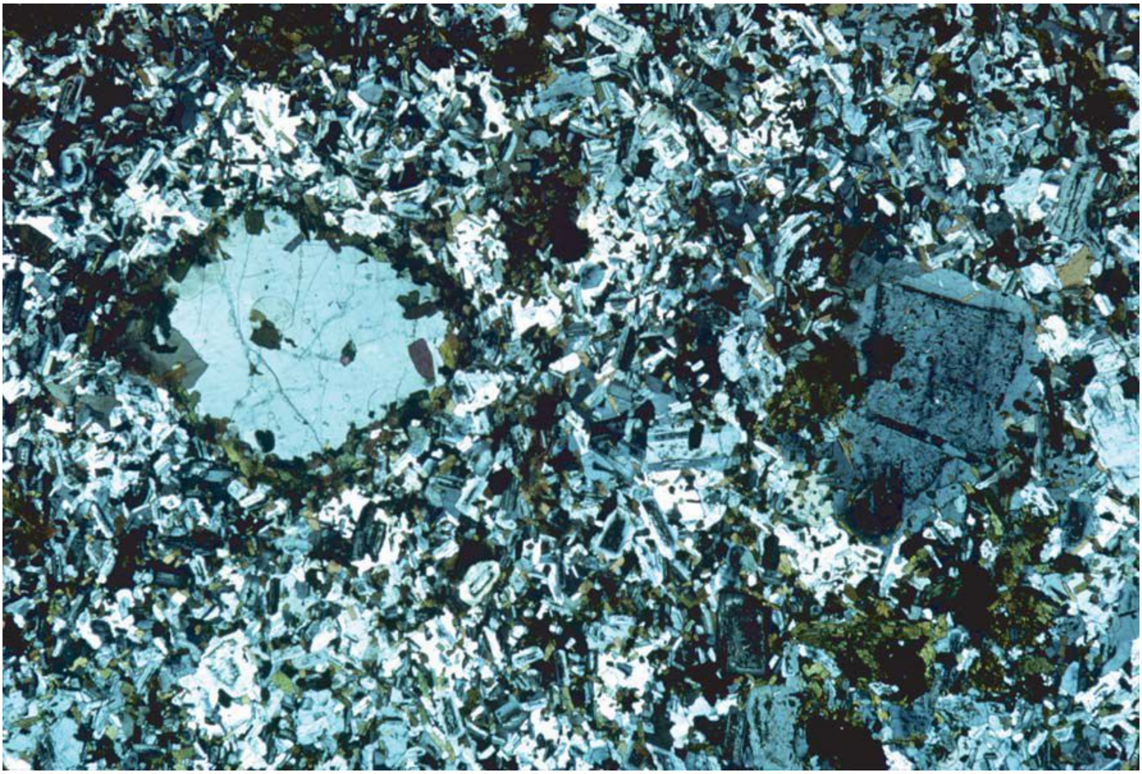

Fig. 3.73: Microgranitoid enclave containing mantled xenocryst ('ocellus') of quartz (left), phenocryst of plagioclase (right) and groundmass with elongate laths of plagioclase and interstitial quartz. The mantle on the quartz xenocryst consists of hornblende. Crossed polars; base of photo 8.4 mm.

A good example of a mineral that commonly shows concentric compositional zoning in igneous rocks is plagioclase, in which the compositional variation depends on substitution of Ca+Al for Na+Si. This substitution involves the breaking of strong O–Al and O–Si bonds, which probably explains why chemical equilibrium is rarely achieved through the whole crystal. Quartz in some granites and rhyolites also shows concentric zoning (Section 3.11.7), as does K-feldspar in some granites (Section 3.11.8).

Inclusions commonly follow the patterns outlined by concentric zoning (Figs. 3.12, 3.75), owing to either nucleation or physical accumulation ('synneusis'; Section 3.7.2) of other crystals on faces of the growing crystal. Concentric zoning in plagioclase may be marked by zones rich in small rounded mineral and/or glass inclusions (Fig. 3.8), which may represent (1) marked changes in conditions during growth, such as a change from slow regular growth to more rapid 'cellular' or semidendritic growth (Section 3.5.3), or (2) resorption of selected zones as a result of instability brought about by major movement of the crystal in

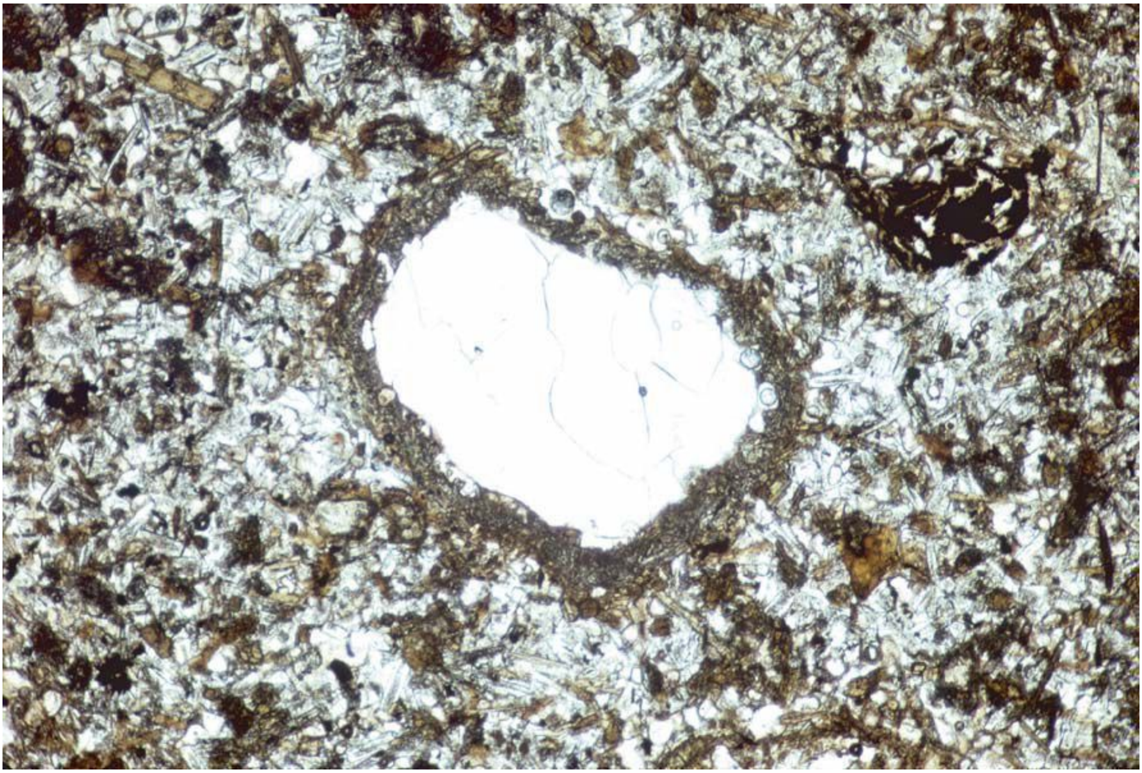

Fig. 3.74: Glassy microgranitoid enclave in dacite, Hoyazo, Spain. The enclave contains a mantled xenocryst ('ocellus') of quartz in a fine-grained groundmass consisting of elongate grains of plagioclase (colourless), biotite (shades of brown) and orthopyroxene (high relief), with interstitial glass (colourless). The mantle on the quartz xenocryst consists of orthopyroxene. Crossed polars; base of photo 4.4 mm.

the magma, followed by partial crystallization of the trapped melt. Nakamura & Shimakita (1998) produced similar glass inclusions by partly melting plagioclase crystals.

Concentrations of inclusions in concentric zones in muscovite have been described by Roycroft (1991), among them sillimanite needles aligned parallel to muscovite crystal faces, indicating that the sillimanite precipitated from the enclosing peraluminous granitic magma; if so, sillimanite inclusions are not necessarily indicators that the muscovite is of metamorphic or xenocrystic origin.

Recently developed microscopic techniques for observing plagioclase zoning, namely (1) backscattered electron imaging, (2) Nomarski contrast interferometry (based on the examination of preferentially etched compositional zones in polished section in reflected light), and (3) laser-interference (depending on refractive index variations, which reflect compositional differences) reveal very detailed zoning patterns (Anderson, 1983; Pearce, 1984a,b; Pearce *et al.*, 1987a,b;

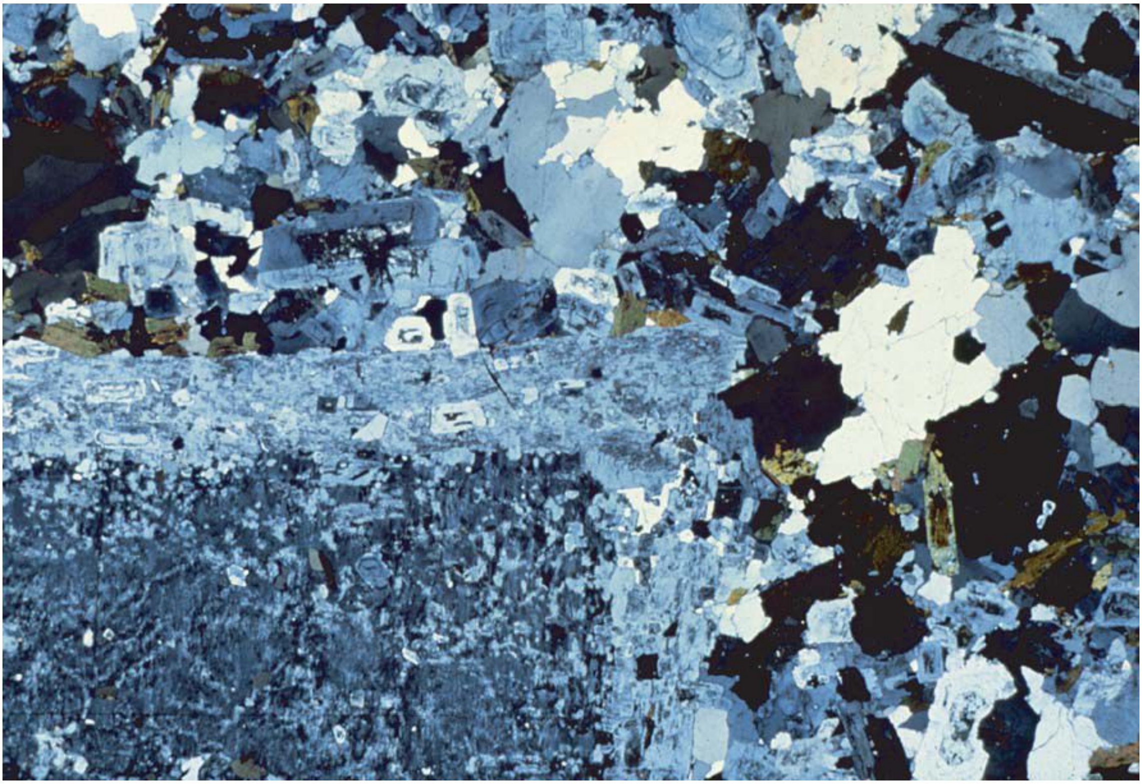

Fig. 3.75: Corner of a K-feldspar megacryst with concentrically arranged plagioclase inclusions and a plagioclase-rich rim (*rapakivi structure*), Wuluuman Granite, Wellington, New South Wales, Australia. The plagioclase crystals in the overgrowth are aligned parallel to the faces of the K-feldspar megacryst, and probably crystallized in response to a change in the chemical composition of the magma caused by mixing of more mafic magma with the granite magma. Photo by W. F. D'Arcy. Crossed polars; base of photo 9 mm.

Nixon & Pearce, 1987; Pearce & Kolisnik, 1990; Stimac *et al.*, 1990; Ginibre *et al.*, 2002a,b).

3.11.2 Normal concentric zoning in plagioclase

Plagioclase cores commonly reflect crystallization at relatively high temperatures, so that they are relatively rich in Ca and Al, and successive outer zones are progressively richer in Na and Si, in response to falling temperature, as determined by well-known experiments on plagioclase crystallization. This is called *normal discontinuous zoning* (Lofgren, 1974), and has been produced in all feldspars grown experimentally over a cooling temperature interval (Lofgren, 1980).

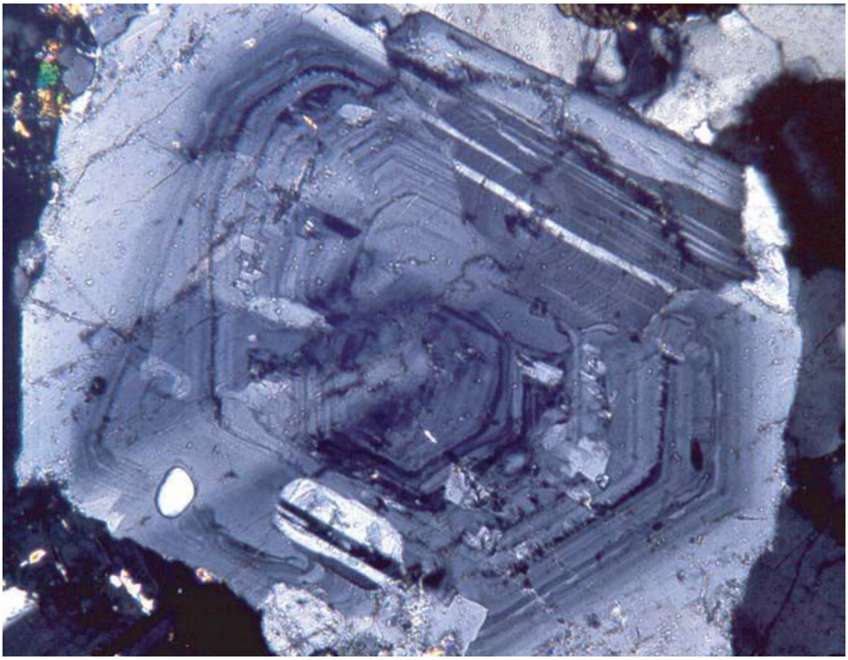

Fig. 3.76: Plagioclase with well-developed oscillatory zoning. Crossed polars; base of photo 1.5 mm.

Continuous zoning within individual discontinuous zones also has been observed in natural and experimentally crystallized plagioclase (Lofgren, 1974).

3.11.3 Reverse zoning in plagioclase

Reverse discontinuous zoning also occurs in igneous rocks, but is uncommon. However, it has been produced experimentally as a result of variation in growth rates. If this applies in magmas as well, a rapidly induced ΔT (for example, caused by a volcanic eruption, rapid movement of magma in a chamber or conduit, rapid release of volatiles in a water-saturated magma, or magma mixing) could produce reverse zoning in plagioclase.

3.11.4 Major versus minor zoning discontinuities

Zoned plagioclase crystals commonly have zones with a composition very different from that of the preceding zones (Fig. 3.77). If such zones occur throughout a magma body, they are likely to be due to external factors (see, for example, Sibley *et al.*, 1976; Wiebe, 1968), such as magma mixing (Section 3.10.3) or increase and release of water pressure. However, narrow zones caused by small rhythmic compositional fluctuations are more likely to be due to very local

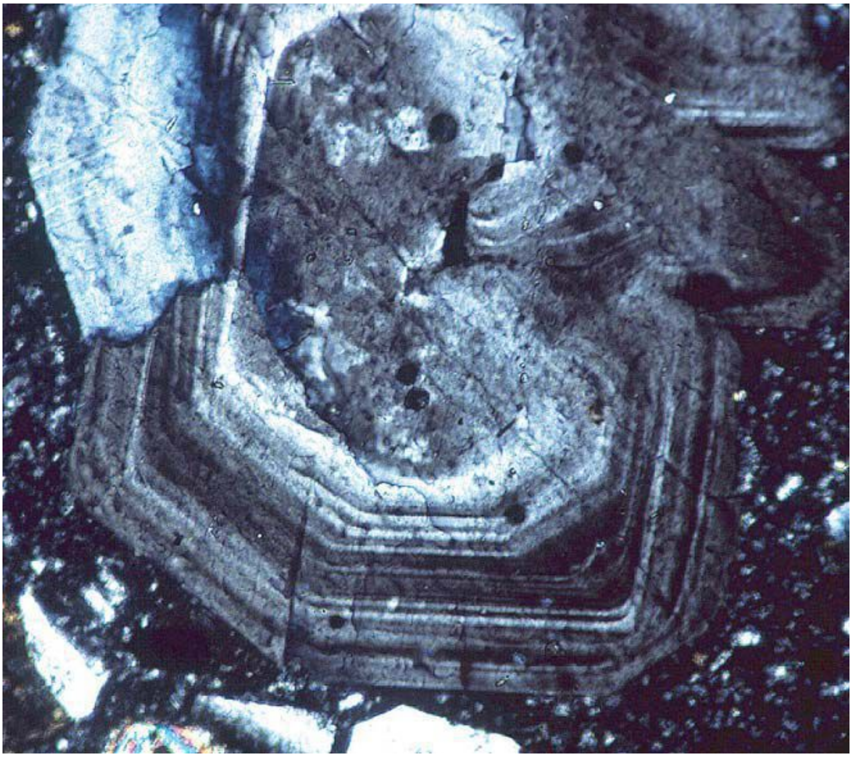

Fig. 3.77: Plagioclase phenocryst showing a marked discontinuity between a core with patchy zoning (Section 3.11.6) and a rim with oscillatory zoning (Section 3.11.5) in an andesite from Fiji. The zoning in the bottom right part of the phenocryst shows the progressive loss and re-establishment of a crystal face during the growth of the crystal. Crossed polars; base of photo 1.75 mm.

diffusion–growth relationships at the growing crystal interface (see, for example, Sibley *et al*., 1976), as discussed in the next section.

3.11.5 Oscillatory zoning

Oscillatory zoning involves repeated small composition changes that occur during growth of a crystal, and is particularly common in plagioclase (Figs. 3.76, 3.77), though it also occurs in other minerals, as discussed below. It has been produced experimentally at constant temperature, indicating that it is caused by local compositional variations in the melt immediately surrounding the growing crystal, rather than by temperature variations.

Oscillatory zoning in plagioclase, involving alternating calcic and sodic zones with small compositional differences, has been explained by diffusion-controlled, recurrent supersaturation of the melt in anorthite and then albite components adjacent to the growing crystal (see, for example, Harloff, 1927; Vance, 1962;

Bottinga *et al.*, 1966; Sibley *et al.*, 1976; Haase *et al.*, 1980; Allègre *et al.*, 1981). Buildup of unwanted components in the melt adjacent to the growing crystal occurs because the growth rate is too fast relative to the rate of diffusion of chemical components in the melt. It occurs in stagnant (non-convecting) melt, and is a local effect at the advancing crystal interface, being independent of physical and chemical changes in the magma as a whole.

Normal oscillatory zoning and *reverse oscillatory zoning* in plagioclase have also been described, the overall normal or reverse zoning trends being complicated by minor oscillations in composition. Plagioclase with oscillatory zoning superimposed on normal zoning has been produced experimentally (Lofgren, 1980).

Oscillatory zoning may also occur in other minerals in igneous rocks, such as clinopyroxene (Wass, 1973; Downes, 1974; Eriksson, 1985; Clark *et al.*, 1986; O'Brien *et al.*, 1988), alkali feldspar (Fig. 3.12; Section 3.11.8), quartz (Section 3.11.7), olivine (Clark *et al.*, 1986), muscovite (Roycroft, 1989, 1991) and melanite garnet (Pearce, 2001), hornblende and tourmaline. For example, it is common in titanium-rich clinopyroxene (see, for example, Wass, 1973; Downes, 1974), and has been produced experimentally in this mineral (Usselman & Lofgren, 1975, 1976). The composition oscillates between augite and subcalcic augite, probably in response to local diffusion limitations, as with plagioclase (Lofgren, 1980, p. 522). Oscillatory zoning due to variable substitution of Fe for Mg has been observed in dolomite in sedimentary rocks, and is most clearly revealed by cathodoluminescence (Reeder & Prosky, 1986).

3.11.6 Patchy zoning in plagioclase

In many igneous rocks (especially calc-alkaline, plagioclase-rich volcanic and plutonic rocks), the plagioclase shows *patchy zoning* (Vance, 1965), which consists of irregular corroded cores, the corroded portions having been filled and surrounded in crystallographic continuity by more sodic plagioclase (Fig. 3.77). Several stages of patchy zoning may be present. This microstructure has been interpreted (Vance, 1965) as being due to initial crystallization of relatively calcic plagioclase in a water-undersaturated magma at depth, followed by a decrease in confining pressure, causing resorption, owing to the fact that the melting point decreases with falling pressure in most water-deficient systems. The resorption appears to be followed by new crystallization of more sodic plagioclase that is stable under the lower-pressure conditions (Vance, 1965), as rims on the cores and as fillings of cavities in the cores, forming pseudo-inclusions of sodic in more calcic plagioclase. Small inclusions (e.g. of pyroxene) that commonly occur in the patches of more sodic plagioclase may have crystallized from melt trapped in the corroded cores (Vance, 1962). Patchy zoning in plagioclase has also been attributed to magma mixing (Section 3.10.3).

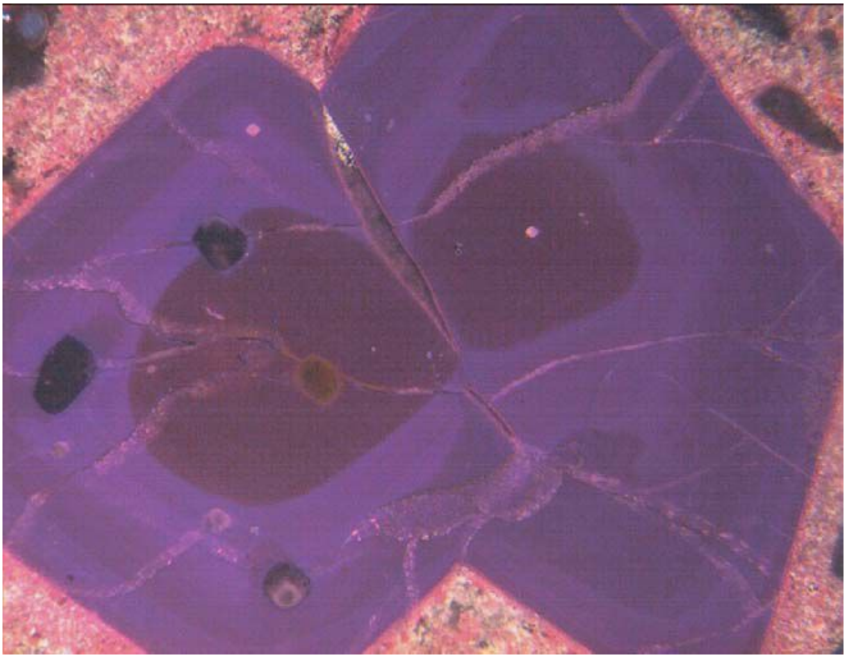

Fig. 3.78: Concentric zoning in quartz phenocrysts in the Weinheim Rhyolite, Odenwald, Germany, revealed by cathodoluminescence (CL). The cores of the crystals are rounded, suggesting resorption, and growth impediments around inclusions (black) are also visible, as are healed cracks marked by fluid inclusions (pink dots). The rims of the crystals are characterized by discontinuous (stepped) zoning, three steps being evident. Fine-scale oscillatory zoning occurs within each step zone, but this is less easily seen in optical CL images than in SEM-CL images, as shown in Fig. 3.79. Photo by Axel Müller. Base of photo 1 mm.

3.11.7 Zoning in quartz

Complex concentric zoning (both discontinuous and oscillatory) occurs in quartz phenocrysts in some granites (D'Lemos *et al.*, 1997; Müller *et al.*, 2000, 2002a,b) and felsic volcanic rocks (Laemmlein, 1930; Schneider, 1993; Watt *et al.*, 1997; Müller *et al.*, 2000; Peppard *et al.*, 2001), as shown in Figs. 3.78 and 3.79. Although zoning in quartz is rarely visible optically, it is revealed as colour variations by cathodoluminescence (CL) microscopy (Fig. 3.78). Details of fine zoning patterns are well shown in SEM-CL photos (Fig. 3.79). CL can reveal different quartz generations, growth structures (especially zoning), resorption features and alteration patterns.

The CL of quartz is due to defects associated with trace elements, such as H, Al, Ti and Fe (Ramseyer *et al.*, 1988; Müller *et al.*, 2000). The red to brown colours are associated with enrichment in water and Al, whereas the blue to violet colours are associated with enrichment in Ti (Müller *et al.*, 2000). High-resolution black

Fig. 3.79: SEM-CL image of a quartz phenocryst from the Spitzkopje Granite in Namibia. It shows discontinuous (stepped) zoning, with subordinate oscillatory zoning, and evidence of two major resorption events. The two thin bright zones (stepped zones) show 'wavy zoning', which is of unclear origin. It may be due to a very high growth rate, resulting in irregular growth, or to diffusion processes in the crystal near the boundary layer (Axel Müller, pers. comm.). Photo by Axel Müller. Base of photo 800 μm.

and white images of zoning in quartz are obtained by using a scanning electron microscope with a CL detector, dark areas corresponding to red or brown, and light areas corresponding to blue or violet in the optical CL images (Müller *et al.*, 2000).

3.11.8 Zoning in K-feldspar

Normal zoning of barium is common in K-feldspar megacrysts in granites (Kerrick, 1969, p. 842; Higgins & Kawachi, 1977, p. 277; Vaniman, 1978; Mehnert & Büsch, 1981; Brigham, 1984). The cores are richer in Ba and the rims are relatively poor in Ba, similar to Ba concentrations of K-feldspar grains in the groundmass. This zoning has been produced in experiments (Long & Luth, 1986).

Oscillatory zoning can be well developed in K-feldspar megacrysts in porphyritic granites (see, for example, Vaniman, 1978; Mehnert & Büsch, 1981; Brigham, 1984; Long & Luth, 1986), as reviewed by Vernon (1986a, pp. 11–12). The oscillations may involve Na/K variation, but commonly involve variation in barium content (Ba/K). The zoning is generally visible optically in crossed polarized light, at least faintly (Figs. 3.12, 5.52), but can be enhanced by chemical staining (Brigham, 1984). Oscillatory zoning is one of the most important of the many pieces of evidence for the igneous origin of K-feldspar megacrysts in granites, as reviewed by Vernon (1986a), and in augen gneisses (Section 5.7.9).

3.11.9 Concentric zoning in zircon

Concentric zoning is common in zircon that crystallizes in magma, and may be preserved during subsequent metamorphism. SEM-CL images of zircon (Figs. 3.80, 3.81) are commonly used to reveal details of the zoning, as well as corrosion events, which assist in making interpretations of the growth history and age of zircon in rocks, especially by using ion microprobe (SHRIMP) dating (see, for example, Vavra, 1990; Williams *et al.*, 1996; White & Clarke, 1999; Rubatto & Gebauer, 2000; Rubatto *et al.*, 2001; Hermann *et al.*, 2001; Daczko *et al.*, 2002a,b). CL in zircon depends on many factors, such as the concentration of trace elements (e.g. Dy, Hf, Y and U) and the degree of lattice deterioration from radioactive decay (see, for example, Koschek, 1993; Hoffman & Long, 1984; Hanchar & Miller, 1983; McLaren *et al.*, 1994; Williams *et al.*, 1996). Low CL response commonly correlates with high U content (Williams *et al.*, 1996; White & Clarke, 1999).

3.11.10 Concentric zoning as an indicator of growth history in magmas

Comparison of concentric zoning can reveal constancy or change in the habit of a crystal as it grew (Fig. 3.77). For example, Sempels (1978) carried out a detailed study of zoned plagioclase crystals from volcanic and intrusive granitic igneous rocks, and found that, although some show evidence of a change in habit (with a tendency for the fastest-growing faces to be removed), most show constant habit during growth, implying a constant ratio of growth rates of the various faces involved.

Sharply defined concentric zones ('stepped zones') have been produced in relatively large (3–4 mm long) crystals of plagioclase grown from the melt under experimental conditions by Lofgren (1974). Rapid drops in temperature during crystallization produce concentric zones of progressively more albitic composition from the core outwards (normal oscillatory zoning). The discontinuous zones produced experimentally are either homogeneous or have internal continuous reverse zoning formed under constant temperature and pressure, owing to a complex interplay between (1) the effective distribution coefficient relating the partitioning of elements between crystals and liquid, (2) the growth rate, (3) the amount of supercooling, (4) the composition of the melt, and (5) the water content of the system (Lofgren, 1974). In natural plagioclase, sharp compositional

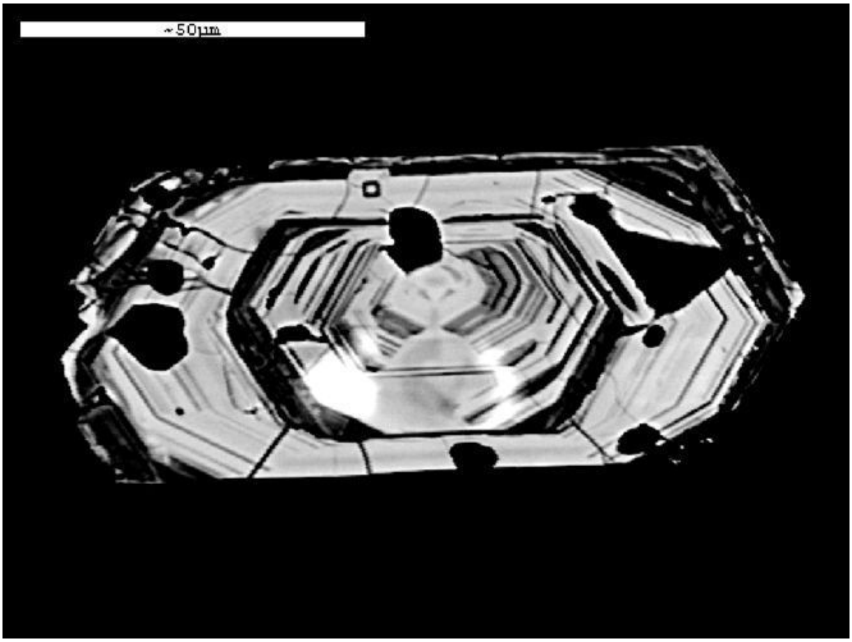

Fig. 3.80: SEM-CL image of a polished thin section of a crystal of zircon from the Congi Creek intrusion of the zoned Walcha Road pluton, New England area, New South Wales, Australia, showing well-developed concentric compositional zoning. The etching is probably due to destruction of the zircon by radioactive bombardment in high-uranium zones. Image by Carol Lawson, provided by courtesy of Stirling Shaw and Dick Flood. Scale bar *c.* 50 µm.

zoning discontinuities could be due to sudden changes in temperature, pressure and/or magma composition (Pringle *et al.*, 1974; Bottinga *et al.*, 1966; Allègre *et al.*, 1981; Shore & Fowler, 1996). For example, complex zoning heterogeneities (such as truncated zoning) revealed by SEM-CL in quartz in some granites have been attributed to magma mixing by D'Lemos *et al.* (1997).

Several people have attempted to work out a crystallization history of plagioclase ('plagioclase stratigraphy') by detailed examination of concentric zoning patterns in phenocrysts in volcanic rocks (see, for example, Kuo & Kirkpatrick, 1982; Anderson, 1984; Pearce *et al.*, 1987a,b; Nixon & Pearce, 1987; Stamatelopoulou-Seymour *et al.*, 1990; Ginibre *et al.*, 2002b). Although correlation of zoning profiles between neighbouring crystals is often unsuccessful, major resorption zones (e.g. due to eruption) or compositional breaks (e.g. due to magma mixing) may be identified in most phenocrysts of an individual volcanic rock.

Sharp zoning discontinuities also occur in quartz in some phenocrysts in granites and rhyolites, as revealed by CL (Müller *et al.*, 2000), as shown in Figs. 3.78 and 3.79. Discontinuities have also been observed in concentric

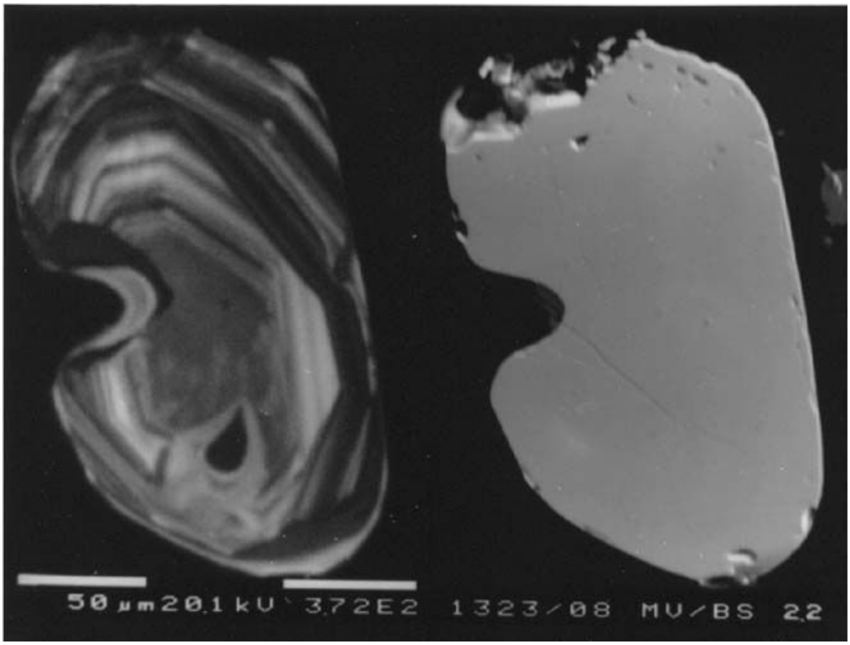

Fig. 3.81: SEM-CL image (left) and backscattered electron image (right) of a polished thin section of a crystal of zircon from the western Musgrave Block, Western Australia. The CL image shows concentric zoning cut by an embayment caused by local solution of the zircon. The overgrowth in the embayment also shows concentric zoning. Photo by Richard White. Scale bar 50 µm.

barium zoning in K-feldspar, related to magma mixing events (Section 3.10.3) that result from intrusion of more mafic magma into a granitic magma (Cox *et al.*, 1996).

Discontinuous zoning has been described in titanite in granite (B. A. Paterson *et al.*, 1989). Complex zoning discontinuities have also been observed in magmatic muscovite (Roycroft, 1989, 1991), clinopyroxene (O'Brien *et al.*, 1988; Clark *et al.*, 1986) and olivine (Clark *et al.*, 1986).

3.11.11 Sector zoning

Sector ('hour-glass') zoning is common, especially in clinopyroxene in basalts (Hollister & Gancarz, 1971; Wass, 1973; Nakamura, 1973; Leung, 1974; Downes, 1974), as shown in Figs. 3.82 and 3.83. It has also been produced experimentally in clinopyroxene (Lofgren *et al.*, 1974). Each pair of opposite sectors has identical optical and chemical properties, distinctly different from those of the other pair of sectors. These compositional differences give rise to different colour intensity or birefringence. In titanaugite, $\{100\}$ sectors are richer in Ti, Al and Fe^{3+} and

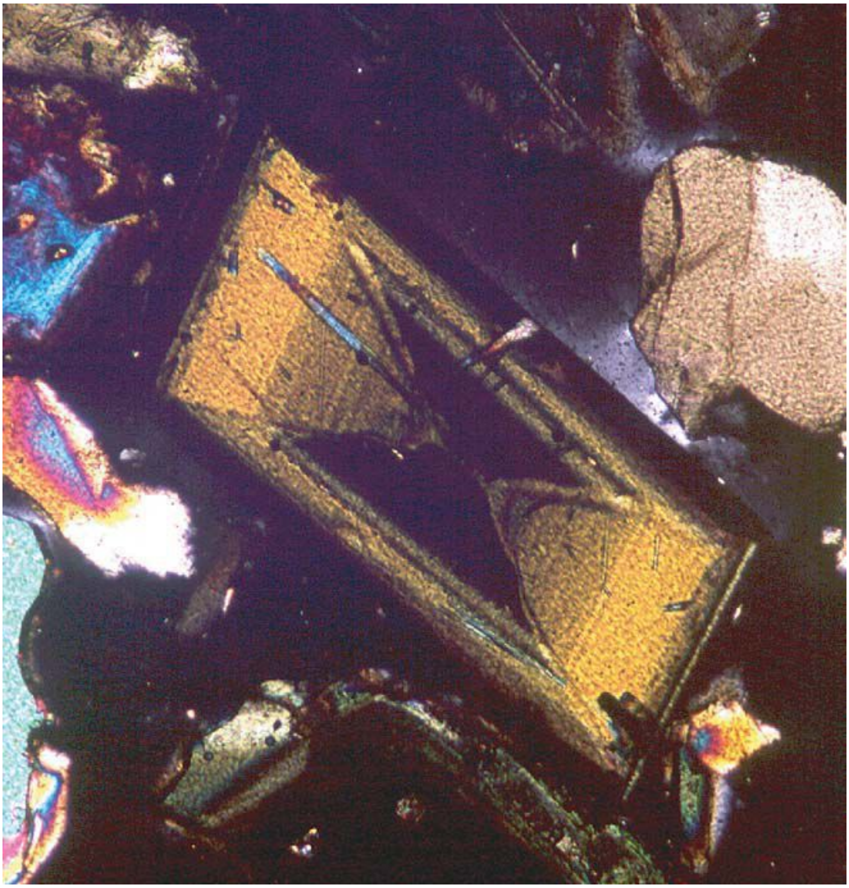

Fig. 3.82: Sector ('hour-glass') zoning and concentric zoning in a clinopyroxene crystal from an ash fall near Mount Vesuvius, Italy. Crossed polars; base of photo 1 mm. Sample by courtesy of Pat Conaghan.

darker in colour. The general three-dimensional shape of sectors is illustrated in Fig. 3.84.

Sector zoning is formed by different faces growing with slightly different chemical compositions (Hollister, 1970; Nakamura, 1973; Dowty, 1976b; Shimizu, 1981; Reeder & Paquette, 1989; Watson & Liang, 1995), leaving behind pyramid-shaped sectors extending out from the centre of the crystal as it grows. Wass (1973) found that either the dark or the light sectors may be contiguous, indicating that either may nucleate and grow initially. Normal and oscillatory concentric zones persist across the sectors (Fig. 3.82), and because concentric zones define time boundaries during the growth of the crystal, both pairs of sectors must grow simultaneously, even though either pair may nucleate first. Simultaneous growth of sectors with slightly different compositions indicates metastable (disequilibrium) growth (see, for example, Reeder & Prosky, 1986).

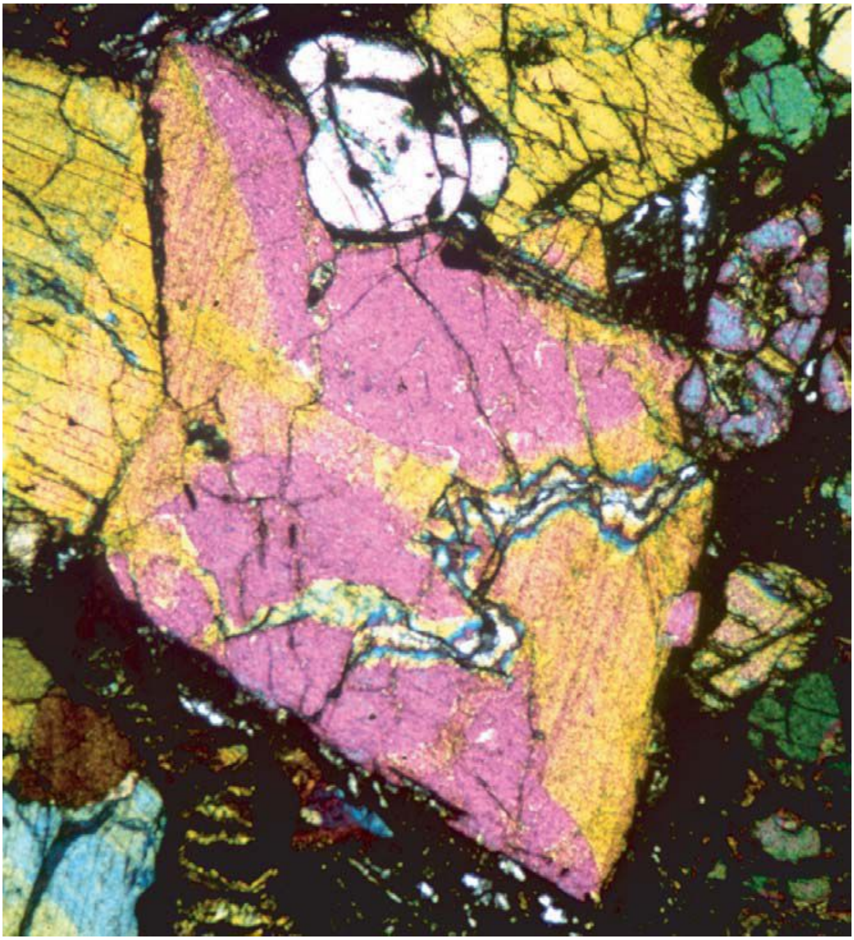

Fig. 3.83: Sector zoning in a clinopyroxene phenocryst in olivine basalt. Crossed polars; base of photo 4 mm.

The reason for compositional differences in the different zones of sector-zoned minerals is complex, and has been discussed in detail by Dowty (1976b). The general situation is that certain growing faces expose different proportions of bonds, which consequently attract different cations, especially during non-equilibrium (e.g. relatively rapid) growth, but also during slow growth, if the diffusion rate for the specific incorporated component in the crystal (e.g. Zr in zircon) is low (Watson & Liang, 1995), as discussed below.

Titanaugite with sector zoning is especially common in relatively rapidly cooled rocks (Fig. 3.82). For example, it occurs in dendritic ('swallow-tail') crystals of titanaugite in chilled basalt. Under these conditions, involving a relatively high D/G, disequilibrium between the sectors and the liquid occurs (see, for example, Wass, 1973). However, sector zoning may also develop in slowly

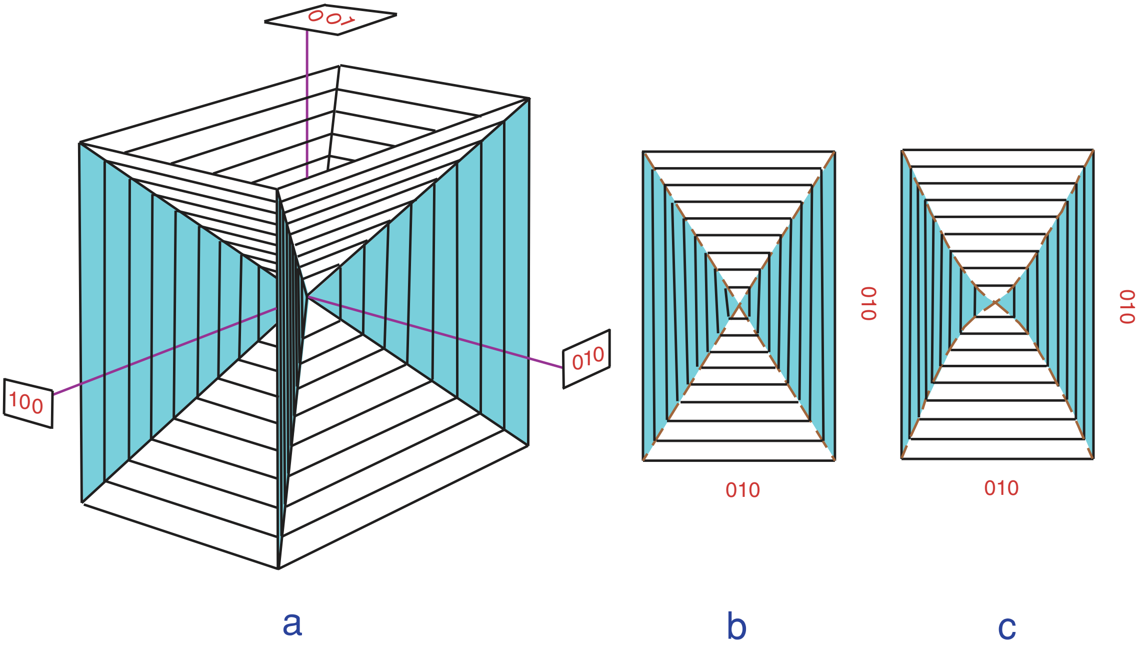

Fig. 3.84: Sector zoning, caused by growth with slightly different compositions on crystallographically different faces (a). If the growth rates of adjoining faces are constant, the sector boundary is straight (b), but if they vary, the boundary is curved (c). After Philpotts (1990, fig. 12-12).

growing crystals (Watson & Liang, 1995), provided that the ratio of the crystal growth rate to the rate of lattice diffusion in the near-surface layer of the growing crystal is large enough to prevent the crystal from equilibrating with the adjacent liquid.

Sector zoning may also occur in plagioclase that has grown rapidly in basalt lava chilled in seawater (Bryan, 1972); the zoned plagioclase has {010} sectors with more Ca than {001} sectors. Sector zoning has also been produced experimentally in plagioclase (Lofgren, 1973) and alkali feldspar (Long, 1978). Sector zoning in K-feldspar megacrysts in granites develops during slow growth, and is commonly associated with variations in concentrations of inclusions in the different sectors (see, for example, Vaniman, 1978; Brigham, 1984).

Sector zoning has also been described in igneous zircon and titanite (Hoffman & Long, 1984; Paterson & Stephens, 1992; B. A. Paterson *et al.*, 1989; Hanchar & Miller, 1993; Vavra, 1990; Watson & Liang, 1995), igneous muscovite, the sectors being delineated by concentrations of inclusions (Roycroft, 1991), igneous phlogopite (Wagner *et al.*, 1987), and calcite and dolomite in sedimentary rocks (Reeder & Prosky, 1986; Reeder & Paquette, 1989). Sector zoning in metamorphic minerals is discussed in Section 4.12.2.

3.12 Growth twinning in crystals in igneous rocks

During growth of a polyhedral crystal in a liquid, atoms or atomic groups may be added to the surface in the same orientation as the pre-existing crystal (Section 3.3.2). Alternatively, they may start a growth layer in another specific orientation, such that a *growth twin* is formed. Although a new internal boundary (*twin interface*) is formed inside the crystal, it can be tolerated if the resulting increase in interfacial free energy is relatively small, as occurs when atomic structures are in a *twin relationship* to each other. Although the twins have the same chemical composition, they are misoriented with respect to each other, in such a way that a lattice row and plane are common to both, and that the crystal lattices are rotated and/or reflected across the twin interface by angles that are specific to the mineral concerned.

The twin interface is often called the '*composition plane*' by mineralogists, but this may be confusing, as no composition change is involved, just an orientation change. Also, what is technically called the '*twin plane*' is the plane across which the two lattices are related geometrically. It may be the same as the twin interface, as in albite-law twinning in plagioclase, but the two need not coincide, as in carlsbad-law twinning in K-feldspar.

The new twin may continue to grow by addition of atoms in the same orientation, but after a time another atomic group may be attached in a different twin orientation, producing a new lamella on another law, or reverting to a lamella with the orientation of the original crystal. Thus, *multiple* (lamellar) *twinning* may occur during growth of crystals in liquids (Figs. 3.4, 3.7, 3.9, 3.45, 3.46, 3.59, 3.63, 3.67, 3.68, 3.76). The process is favoured by relatively rapid growth (Buerger, 1945), probably because of the increased chances of attachment of atom groups in twin orientation.

If the twinning process occurs only once, a *simple twin* is formed (Figs. 3.5, 3.46, 3.85). Because the individuals of a simple twin are typically of approximately equal size (Fig. 3.85), they must have grown for the same time. Therefore, simple twins probably initiate at the nucleation stage (see, for example, Dowty 1980b, p. 76). Combinations of simple and multiple twins may occur also (Figs. 3.85, 3.86). Simple growth twins are particularly common in K-feldspar, for example in trachytes, in which phenocryst and groundmass K-feldspar crystals are invariably twinned (Fig. 3.5), and in granites, in which megacrysts (large phenocrysts) also show a high incidence of simple twinning (Vernon, 1986a, 1999a). Simple and multiple growth twins are common in plagioclase (Figs. 3.85, 3.86), hornblende and pyroxene. Twins are also common in quartz and sheet silicates, but are not visible in normal thin sections, because all the orientations show parallel extinction.

Multiple (not simple) twins can also be formed during deformation of crystals (Section 5.3.3), and these are called 'mechanical', 'secondary' or *deformation twins*. Growth twins can be distinguished microstructurally from deformation

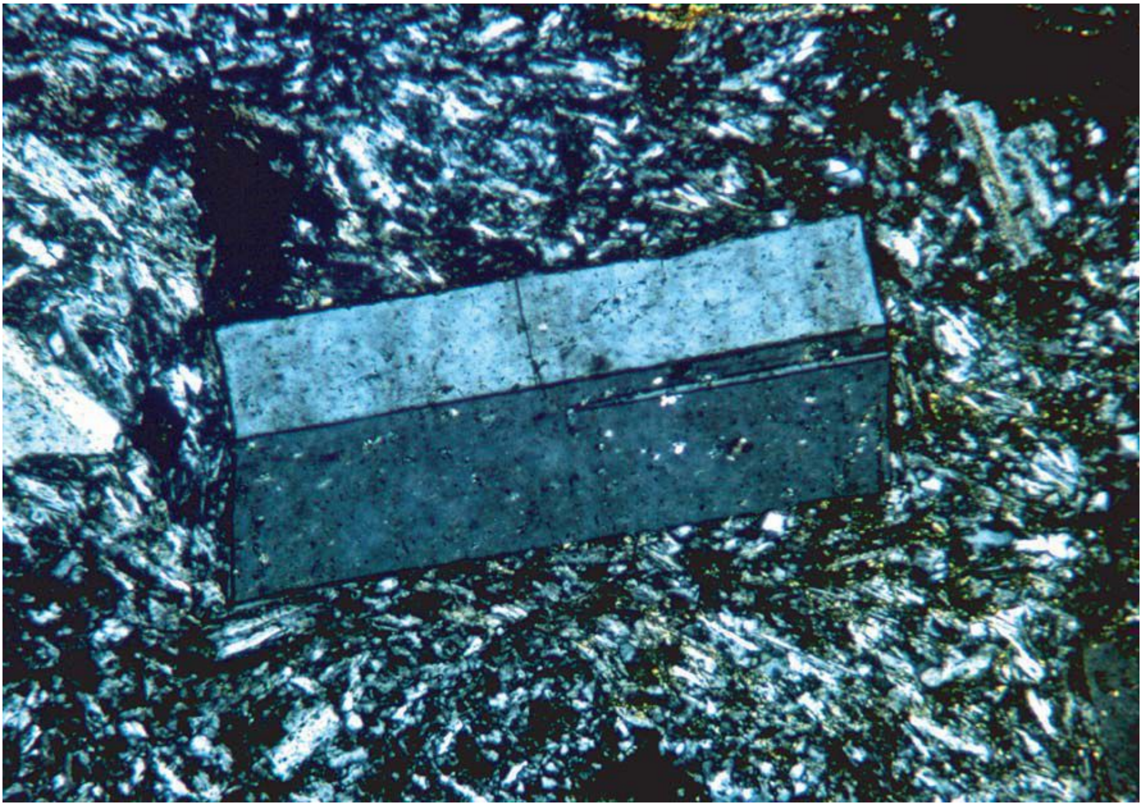

Fig. 3.85: Simple twin in a phenocryst of plagioclase, showing the re-entrant angle formed where the twin interface intersects the crystal boundary. At first sight, this may appear to be a simply twinned K-feldspar crystal, but the small lamellar twin indicates that it is plagioclase. The simple twin is of growth origin, and the tapering shape of the lamellar twin suggests an origin by deformation. Crossed polars; base of photo 1.3 mm.

twins on the scale of the light microscope, by the features listed in Table 3.1. (Vance, 1961; Seifert, 1964; Vernon, 1965), as shown in Fig. 3.87. *Growth twins* (1) may be simple or lamellar, (2) have planar interfaces, (3) may have abrupt steps in the interface, and (4) may have abrupt (planar) terminations (Fig. 3.88). In compositionally zoned crystals grown in magma, the zones are deflected at their intersection with growth twins, as described by Vance (1961), and re-entrant angles occur where growth twins intersect crystal faces (Fig. 3.85). *Deformation twins* are lenticular and their concentration may be related to local intensity of deformation (Fig. 3.89). They are particularly common in plagioclase and calcite (Figs. 3.89, 3.90). They may taper to a termination against (Fig. 3.91) or be deflected where they cross earlier-formed deformation twins (Fig. 3.90). Growth and deformation twins may occur in the same plagioclase grain, owing to

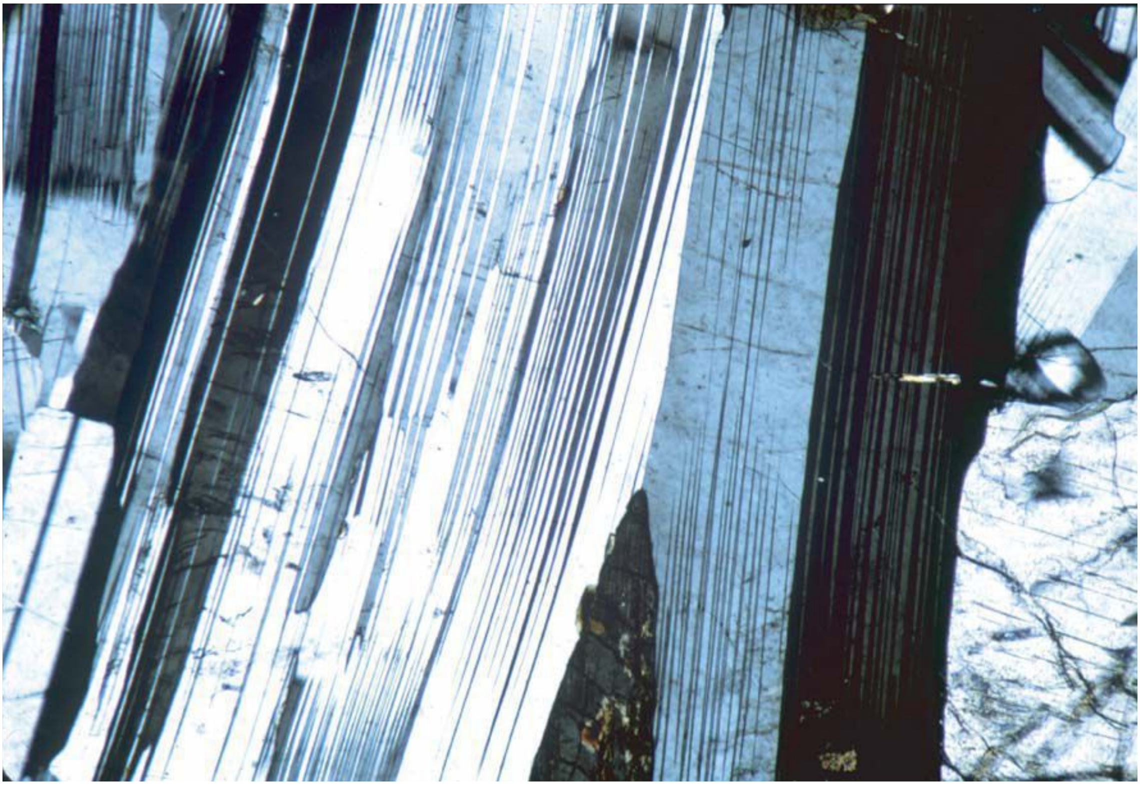

Fig. 3.86: Simple and multiple twinning in plagioclase. Crossed polars; base of photo 1.5 mm.

solid-state deformation after the growth twins had been formed during crystallization (Fig. 3.88).

Sector twinning ('cyclic' or 'concentric' twinning) commonly occurs in cordierite that precipitates from a melt (see, for example, Deer *et al.*, 1992). This is also common in metamorphic cordierite (Section 4.7).

3.13 Embayments

Phenocrysts, especially quartz and olivine, in some volcanic and high-level intrusive rocks show rounded embayments (Figs. 3.37, 3.69, 3.81, 3.92, 3.93), which may appear as complete 'inclusions' where intersected perpendicular to their direction of elongation by the section-plane. Commonly these are interpreted as the result of *magmatic corrosion* (resorption, dissolution), resulting from a change of conditions that cause a previously stable crystal to become unstable with respect to the liquid and so to begin dissolving, for example in response to a change in pressure or a change in chemical composition of the melt caused by mixing of magmas (Section 3.10.3). This interpretation is favoured where (1) the

Table 3.1. *Microstructural features of growth and deformation twins*

Growth twins (Fig. 3.87A)	**Deformation twins** (Fig. 3.87B)
Twinning is simple (Fig. 3.85) or multiple (lamellar), as shown in Fig. 3.88	Twinning is multiple (Figs. 3.89–3.91)
Twin lamellae are uniform in width or stepped; i.e. the interface is planar or abruptly stepped (Fig. 3.88)	Lamellae may be uniform in width across a grain, or more common, change width gradually; i.e. the interface is smoothly curved (Figs. 3.89–3.91)
Changes in width are independent of other lamellae and unrelated to later bending of the grain (Fig. 3.88)	Changes in width commonly occur in unison with, and in the same direction as, other deformation twin lamellae; commonly in conjunction with bending of the grain (Fig. 3.89)
Lamellae cross whole grains or terminate abruptly (i.e. with planar terminations) within grains (Fig. 3.88), independently of later bending or fractures; twins terminate abruptly against other growth twins (Fig. 3.88)	Lamellae cross whole grains or terminate by tapering to a point within grains; terminations are commonly related to bending (Fig. 3.89); twins may also terminate at fractures (where terminations may be planar against fracture planes) or against twins formed earlier (where terminations generally are tapered and may induce strain in the earlier lamella, as shown in Fig. 3.91), or are deflected where they cross earlier twin lamellae (Fig. 3.90). Twins may also taper may where they impinge on grain boundaries

corners of the crystal are rounded (but see below), (2) compositional zoning is truncated by the embayments, and (3) the embayments can be related to fractures in the crystal, since solution would tend to begin at fractures where atoms are more loosely bonded than in a crystal without such defects. The interpretation is also favoured where new minerals are deposited on the surface of the embayed crystal, as products of the reaction with the melt (Fig. 3.65); in this instance, the embayed crystal may be foreign to the magma (Section 3.10.3) or may be a phenocryst that has reacted in response to changing conditions.

Although embayments are typically rounded, some relatively planar, crystallographically controlled embayments may be present (Müller *et al.*, 2000), as shown in Fig. 3.94. Laemmlein (1930), Foster (1960), Donaldson & Henderson (1988), Lowenstern (1995) and Swanson & Fenn (1986) have suggested that embayments in quartz may be growth features (i.e., the embayments are partial inclusions). Dendritic shapes in quartz have been produced in experiments, and have also been observed in some rocks (Swanson & Fenn, 1986; Fenn, 1986), as discussed in Section 3.5.3. Thus, in some instances an interpretation involving incorporation of liquid groundmass by the growing crystal may

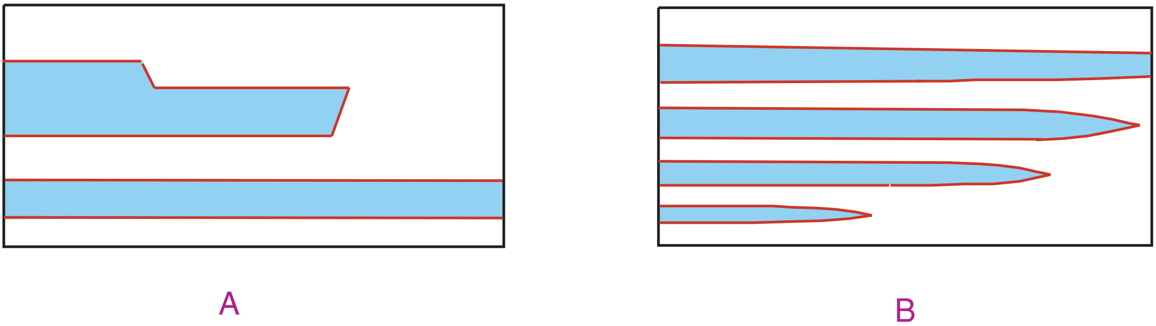

Fig. 3.87: Sketch showing the ideal differences between lamellar growth twins (A) and deformation twins (B).

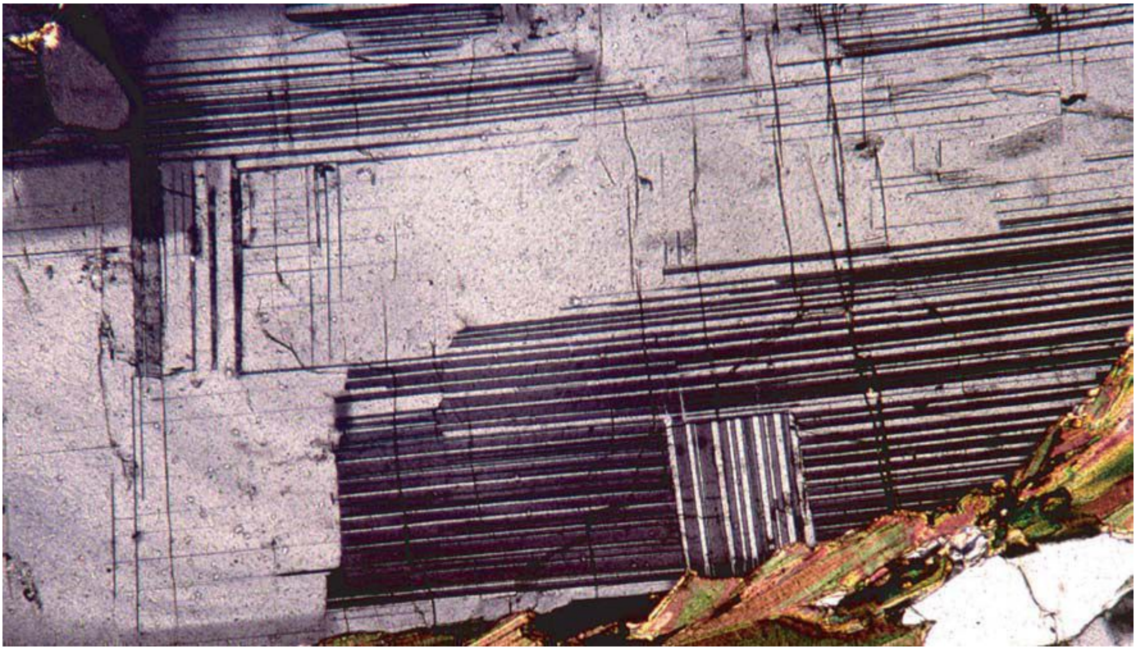

Fig. 3.88: Lamellar growth twins in plagioclase, characterized by abrupt terminations, San José pluton, Baja California, Mexico. Some lamellar deformation twins, characterized by lenticular terminations, are visible in the top half of the photo. Crossed polars; base of photo 1.5 mm.

be valid. This applies especially to phenocrysts with repeated indentations that appear to be crystallographically controlled (Fig. 3.94), suggesting skeletal crystal growth.

Dendritic growth seems to be the only possible explanation of concentric zoning that is deflected (convoluted) around glass embayments in phenocrysts

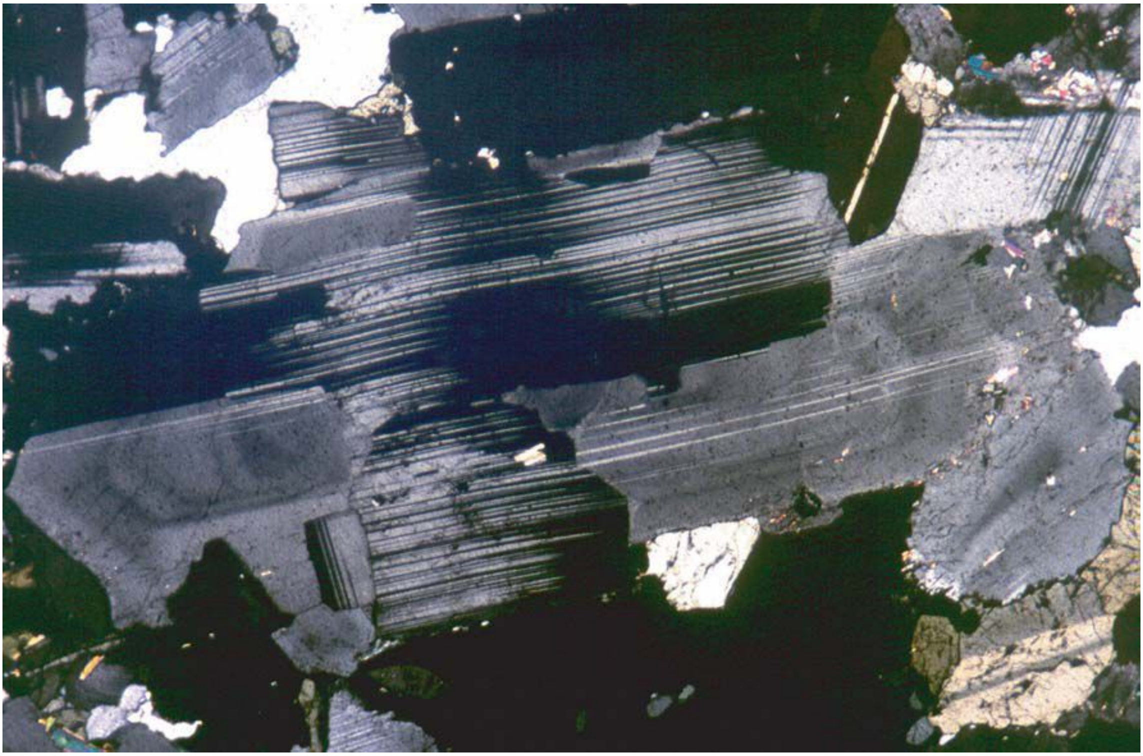

Fig. 3.89: Lenticular deformation twins in plagioclase, their concentration varying with local strain variation inside the grain. Crossed polars: base of photo 1.5 mm.

of plagioclase (Blackerby, 1968) and quartz (Müller *et al.*, 2000). Moreover, hollow crystals, melt inclusions and pseudo-resorption shapes have been produced experimentally in crystallizing plagioclase by growth without resorption (Lofgren, 1974). In these instances, the crystal cannot eliminate the melt inclusions because, as the crystal grows into them, the residual melt (which is isolated from the liquid surrounding the crystal) becomes so enriched in albite component that crystallization of the plagioclase with which the melt is saturated at that temperature is impeded.

Thus, the problem of distinguishing between possible *corrosion embayments* and *inclusion embayments* should always be kept in mind (Blackerby, 1968). Local rounded embayments and phenocryst corners are most likely to be due to corrosion, whereas more branch-like, repeated, crystallographically controlled embayments are most likely to be due to dendritic growth. However, in many instances, it may be impossible to be sure of the correct interpretation.

As if to further complicate the picture, Donaldson (1985), reviewing experimental results on a variety of minerals, concluded that, although dissolution in magmas generally produces rounded shapes, it can produce crystal faces

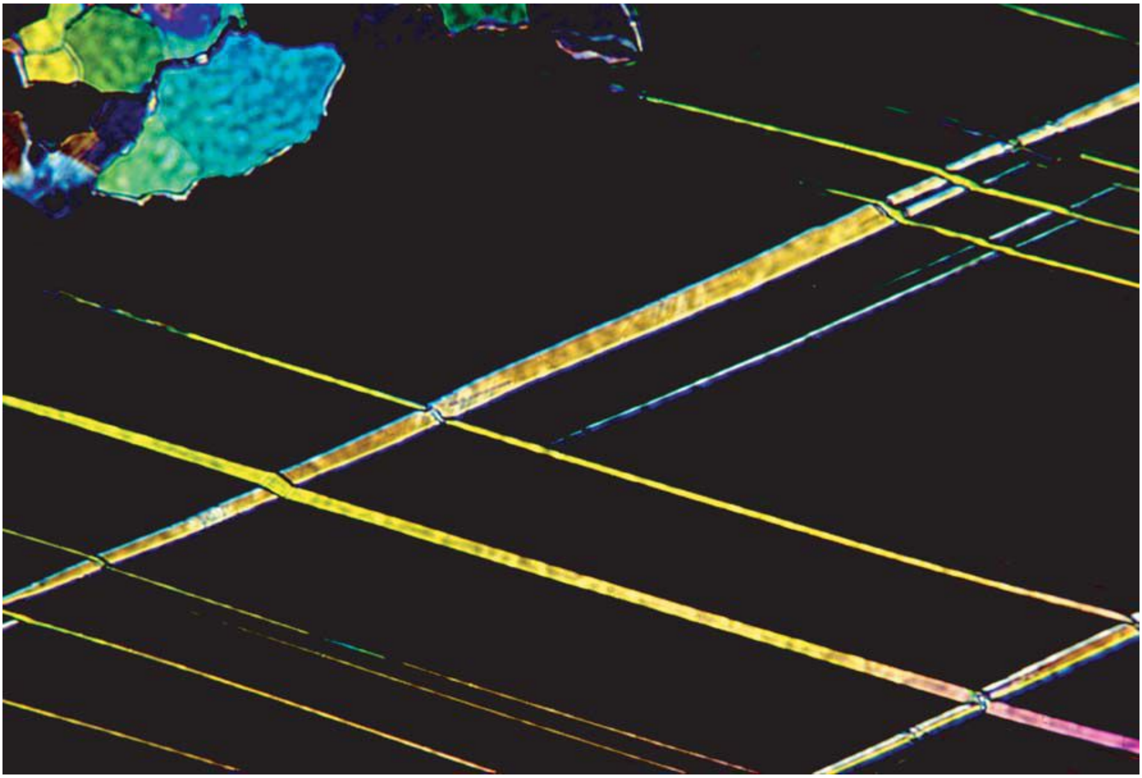

Fig. 3.90: Lenticular deformation twins in calcite, Tungkillo, Mount Lofty Ranges, South Australia. Note deflections where earlier twins are intersected. The section is ultrathin (about 0.005 mm thick), to show the microstructural features more clearly. Crossed polars; base of photo 0.5 mm.

in special conditions, namely where diffusion of dissolved components in the melt is very rapid, so that the rate of the solution process is controlled by release of components at the crystal interface. This process may apply to very fluid magmas, such as picrites, komatiites, basalts at high pressure, and pegmatites.

Furthermore, Nakamura & Shimakita (1998) partly melted plagioclase crystals in a melt saturated in more calcic plagioclase, and produced reaction zones developing from the edges inwards. These zones consisted of newly crystallized, more calcic plagioclase and melt channels (forming glass after quenching the experiments), the resulting glass inclusions having shapes similar to those of common glass inclusions in plagioclase in volcanic rocks (Fig. 3.8), which are usually attributed to incorporation during growth of the plagioclase. This emphasizes the care needed in distinguishing between former melt inclusions formed during growth from those formed by partial melting.

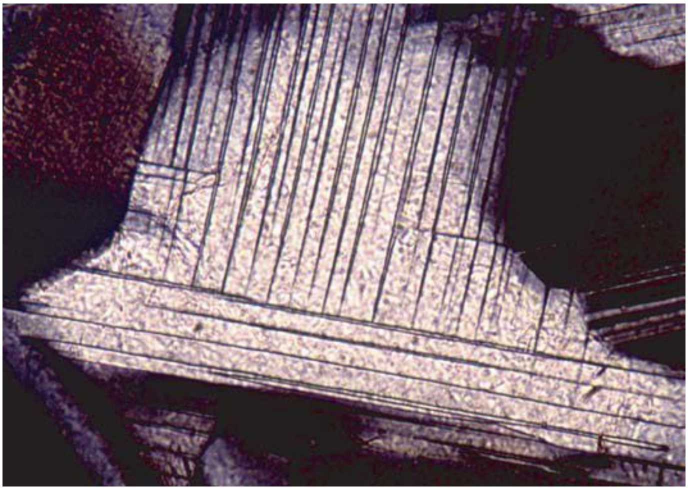

Fig. 3.91: Albite-law and pericline-law deformation twins in plagioclase, San José tonalite, Baja California, Mexico. The twins taper to points where they meet earlier twins. Crossed polars; base of photo 0.4 mm.

3.14 Microstructures formed by boiling (vesiculation) of magma

3.14.1 Nucleation of gas bubbles

Exsolution of gas from a magma occurs when the melt becomes supersaturated with a volatile component, especially water, in response to (1) crystallization of non-volatile minerals (which increases the volatile content of the residual melt) and/or (2) a decrease in pressure. This process is a phase change (Section 3.1), and so a nucleation step is involved, involving the formation of an interface between the gas and liquid phases. Nucleation may be either homogeneous or heterogeneous, but experimental evidence indicates that heterogeneous nucleation of bubbles on crystals is more likely (Hurwitz & Navon, 1994). An example of heterogeneous nucleation is shown by bubbles aligned perpendicular to the surface of the plagioclase crystal shown in Fig. 3.95. The bubbles have stretched in an attempt to escape into the melt, but the melt quenched to a glass before they could leave the crystal surface.

3.14.2 Vesicles

The shapes of former gas bubbles in igneous rocks are called *vesicles*. Bubble shapes can be preserved if the magma becomes viscous enough to preserve them before they collapse as the gas escapes (Figs. 3.62, 3.95, 3.96). Many vesicles are spherical, which minimizes the area of the interface between the gas and the melt, thereby minimizing the interfacial free energy (γ). However, others are

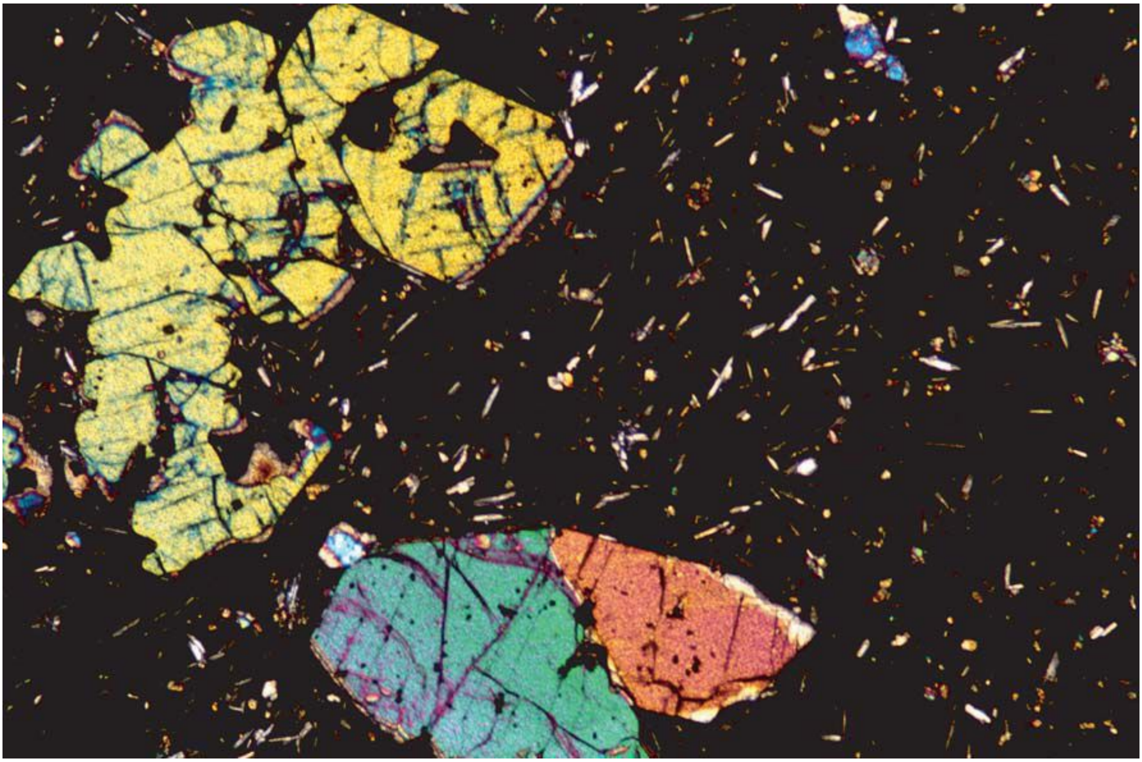

Fig. 3.92: Embayed olivine phenocryst in glassy basalt from Iceland. Crossed polars; base of photo 2 mm.

ellipsoidal, owing to flow of the magma (Section 3.9), as shown in Figs. 3.62 and 3.96. Elongate vesicles may be aligned in the axial surfaces of magmatic flow folds in glassy rhyolite (*obsidian*), as described by Vernon (1987c). These vesicles are compressed and stretched as the folds tighten, and their shapes are preserved as the lava rapidly solidifies to form the glass, its flow lines outlining the fold. The traces of gas bubbles that stream upwards from the base of basalt flows may be preserved as *pipe vesicles*, the curvature of which reflects the flow direction of the lava. Bubbles formed when the magma has many crystals may have irregular and angular shapes. A detailed discussion of microstructural aspects of vesiculation is given by Cashman & Mangan (1994). Three-dimensional distributions of vesicles have been produced by computed high-resolution X-ray tomography (Carlson *et al.*, 1999).

Aqueous solutions circulating through cracks may dissolve chemical components from buried sequences of volcanic rocks and deposit secondary minerals in vesicles, forming *amygdales (amygdules)*. Minerals such as chlorite, quartz, calcite, zeolites and prehnite are common in amygdales (Fig. 3.97). Typically these minerals nucleate on the vesicle walls and grow inwards until they either

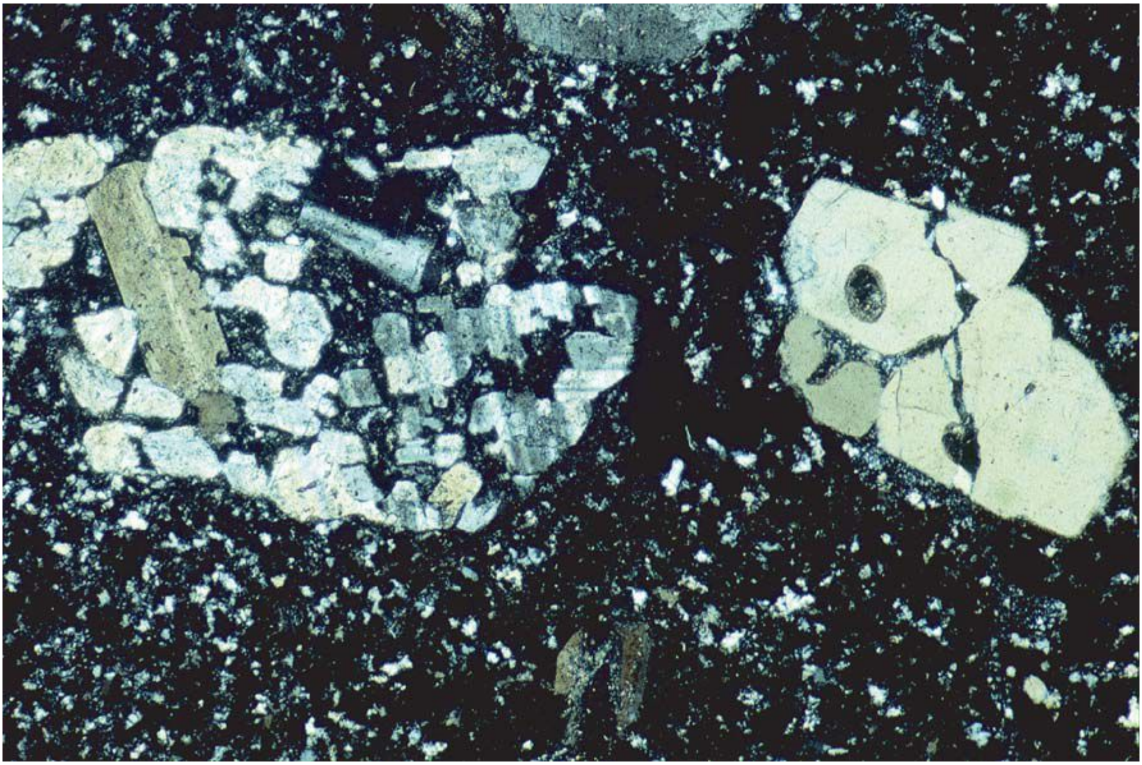

Fig. 3.93: Embayed plagioclase (left) and quartz (right) phenocrysts in dacite. Crossed polars; base of photo 4 mm.

interfere, and so lose their crystal faces, or stop growing, preserving their crystal face terminations (Fig. 3.98). Later influx of solutions of different composition may deposit different minerals in any remaining space (Fig. 3.98). Less commonly, radiating (spherulite-like) aggregates are produced.

3.14.3 Scoria and pumice

The fluidity of mafic magma allows the relatively small amount of gas in this kind of magma to escape readily on reduction of pressure. Mafic volcanic rocks with abundant vesicles are said to be *scoriaceous*. Felsic magmas are commonly richer in water, so that reduction of pressure during a volcanic eruption rapidly releases copious amounts of gas. Effectively, the lava boils, and the remaining liquid cools so fast that it forms glass (Section 3.5.6). The result is a 'glass froth' called *pumice*, which is so light it can float on water. The vesicles may be equant (Fig. 3.95) or show evidence of stretching during flow of the lava (Fig. 3.96). The reason that so many small bubbles are formed appears to be that the bubble

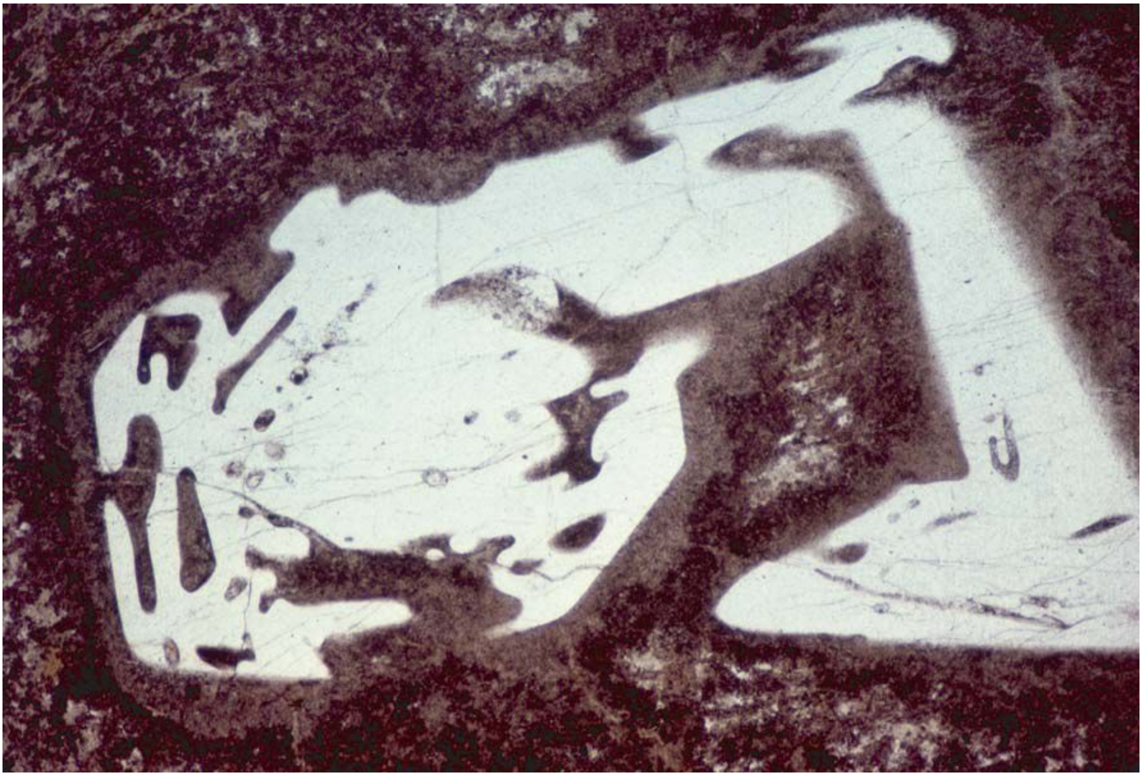

Fig. 3.94: Quartz phenocryst with intricate, crystallographically controlled embayments suggesting dendritic crystallization, as an alternative to magmatic corrosion. Plane-polarized light; base of photo 4.4 mm.

nucleation rate is very rapid, as shown experimentally (Williams & McBirney, 1979), whereas the diffusion rate of water in silicic melts is very slow.

The change from liquid to gas produces an increase in volume, so that the magma expands as vesiculation occurs. This can exert enough pressure to fracture overlying rocks and so produce explosive eruptions. Another probable contributor to the buildup of pressure is the formation of pumice, because loss of relatively large amounts of water makes the melt so viscous that the bubbles can no longer expand. The pressure inside the bubbles increases as water slowly diffuses into them, and if the gas pressure in the bubbles exceeds the strength of the viscous melt, they tend to explode. The explosive eruption shreds the vesicular lava and ejects it from the volcano as blocks and small fragments of pumice, together with fragmented phenocrysts and released gas. The very hot mass of crystal fragments, pumice fragments and gas is hurled into the atmosphere and can cover large areas, forming *ash-fall tuff* and *ash-flow tuff* (*ignimbrite*). The resulting tuffs are fragmental sedimentary rocks composed of igneous materials, as discussed in Section 2.3.

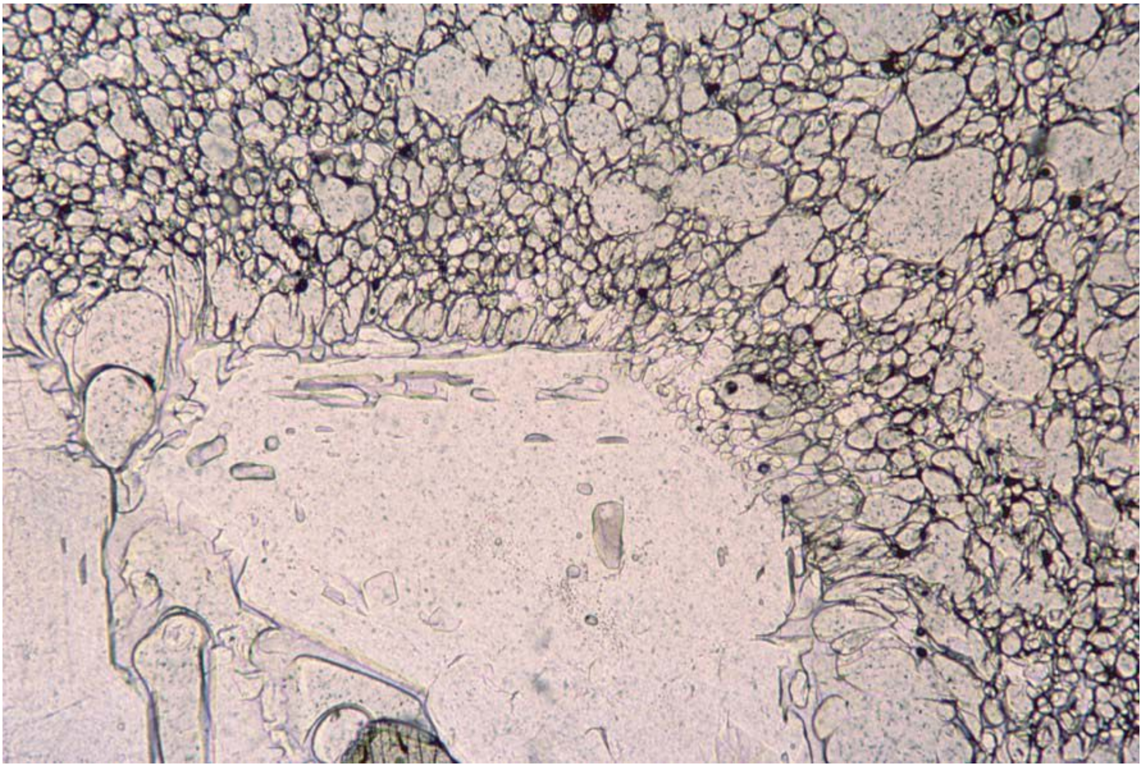

Fig. 3.95: Pumice (felsic glass froth), showing evidence of nucleation of bubbles on a plagioclase phenocryst, the elongation of the bubbles reflecting their attempts to escape into the liquid as it was quenched to solid glass. Plane-polarized light; base of photo 1.5 mm.

3.14.4 Segregation vesicles in submarine basalt

Vesicles partly filled with residual melt segregated from the surrounding magma have been described from submarine basalts, subaerial basalts and dolerite dykes (Smith, 1967; Anderson *et al*., 1984; Sanders, 1986; Caroff *et al*., 2000). These *segregation vesicles* (Fig. 3.99) are distinct from amygdales or vughs, which are filled with hydrothermal minerals after the magma crystallizes. However, in segregation vesicles that are only partly filled by melt, the remaining space may be filled much later by secondary minerals, as in normal amygdales (Fig. 3.99).

The igneous material in the segregation vesicles is typically richer in K, Ti and P than the surrounding rock, which is consistent with residual melt that migrated into the vesicles (Anderson *et al*., 1984). Segregation vesicles form when the pressure of the melt exceeds the pressure of the vapour inside the vesicle. Various processes have been suggested, and the literature has been reviewed by Caroff *et al*. (2000). For example, Smith (1967) inferred that when vesicular basalt magma is subjected to a larger pressure (for example, when it flows into deeper

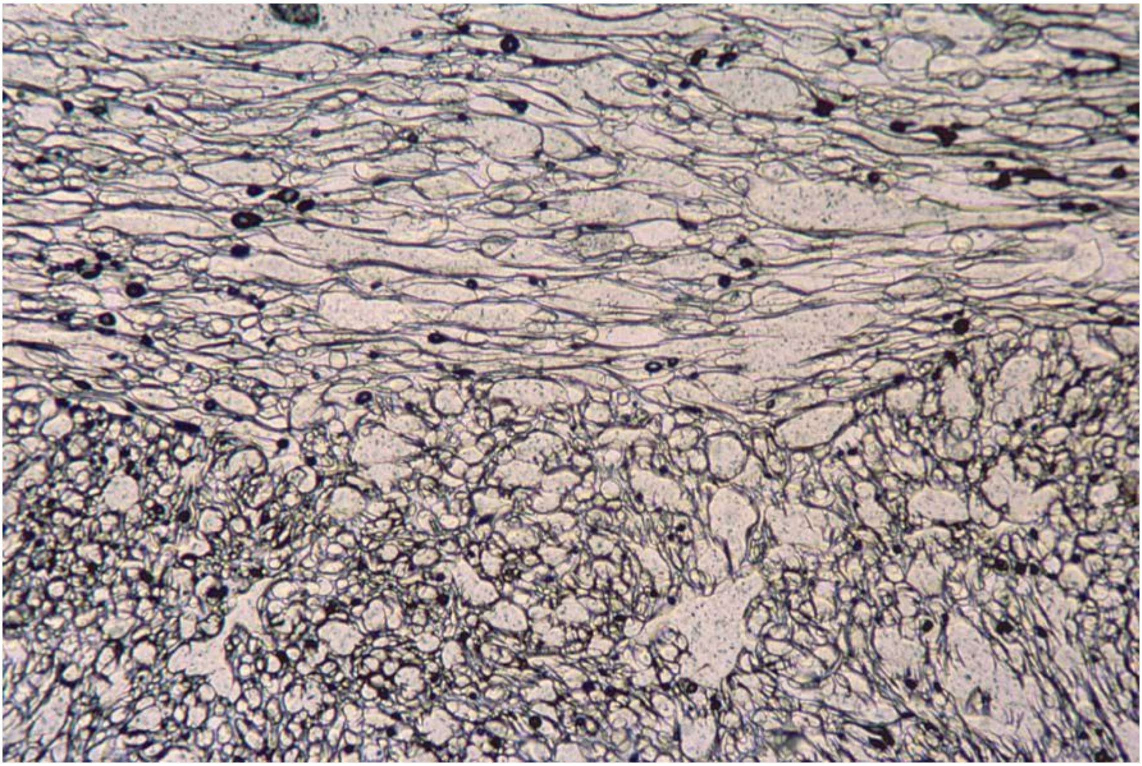

Fig. 3.96: Pumice, showing local stretching of bubble shapes caused by flow of the lava before quenching on Earth's surface. From Vernon (2000b, fig. 85). Plane-polarized light; base of photo 1.5 mm.

water), residual melt may be forced into the vesicles (Fig. 3.100). However, a more general explanation is needed, at least for segregation vesicles in terrestrial basalts and dolerite dykes. Anderson *et al*. (1984) and Sanders (1986) suggested that 'gas filter-pressing' is the most realistic mechanism. The process involves initial vesiculation in a magma that remains vapour-saturated. As crystallization continues and the volume of vapour-saturated melt declines, new bubbles nucleate, forcing the melt to migrate through the crystal network into the vesicles by increasing the pressure in the melt relative to the pressure in the vesicles. Their wide variety implies that a number of mechanisms are required for the origin of segregation vesicles (Caroff *et al*., 2000).

3.14.5 Miarolitic cavities

Miarolitic cavities ('miaroles') are approximately spherical to irregularly shaped bodies partly filled with crystals of magmatic minerals, such as feldspar, quartz and mica, many also containing a wide variety of other minerals, such as beryl,

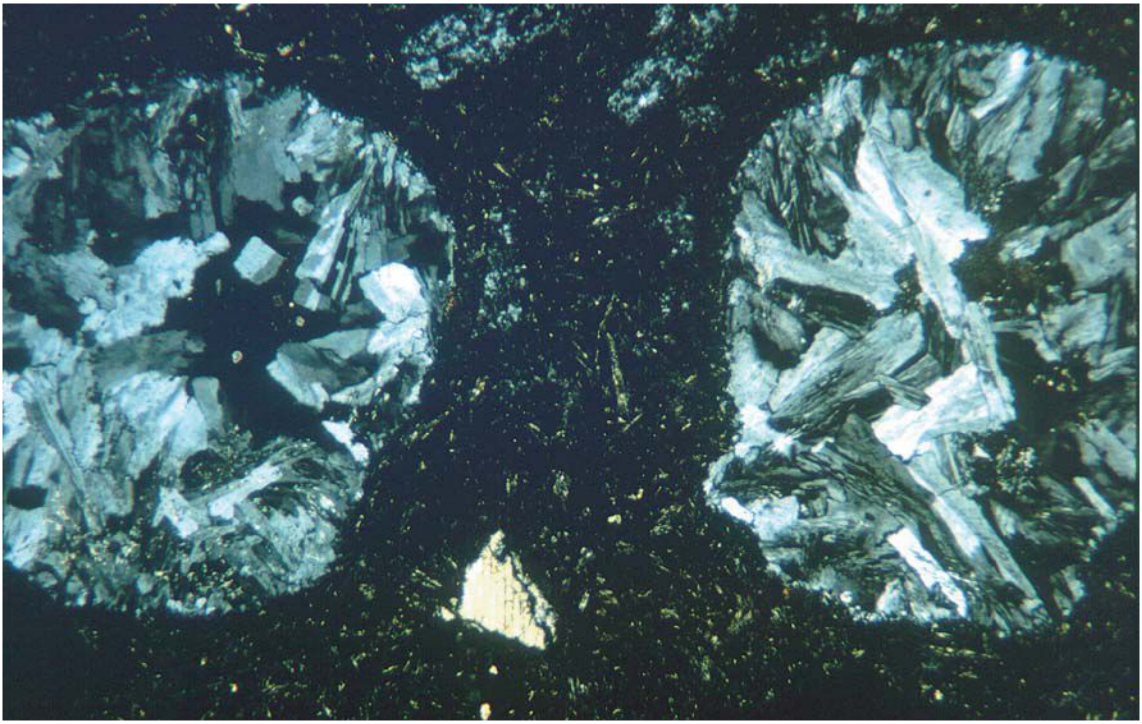

Fig. 3.97: Amygdales filled with sodic plagioclase in altered basalt, Sofala, New South Wales, Australia. Crossed polars; base of photo 3.5 mm.

topaz, tourmaline, fluorite and epidote (Fig. 3.101). These crystals nucleate on the walls of the host granite and project into either an empty cavity or an aggregate of low-temperature minerals (such as quartz, calcite or chlorite) that precipitated later in the cavity from hydrothermal solutions (Candela, 1997). Miarolitic cavities occur in some leucocratic, silica-rich, felsic, relatively fine-grained intrusive rocks that crystallize at high crustal levels (less than 3 kbar and probably 0.5–1 kbar). These rocks commonly contain granophyric quartz–alkali feldspar intergrowths, which probably grow at conditions of strong supersaturation (Section 3.8). However, Ridley (2002) found elongate miarolitic pipes and gashes in a granite inferred to have crystallized at 4–6 kbar.

Miaroles have been inferred to form from vapour released from granitic magma (Candela, 1997). Vapour (supercritical fluid) bubbles form as locally water-saturated magma rises and crystallizes in response to decompression, which causes the vapour to escape. This decreases the concentration of water in the melt, which raises its liquidus temperature and effectively undercools the melt. The result is a relatively fine-grained granite with granophyric intergrowths. At the same time, crystals grow in the cavities, by precipitation from the vapour phase. Candela & Blevin (1995) described miarolitic cavities, with a high degree

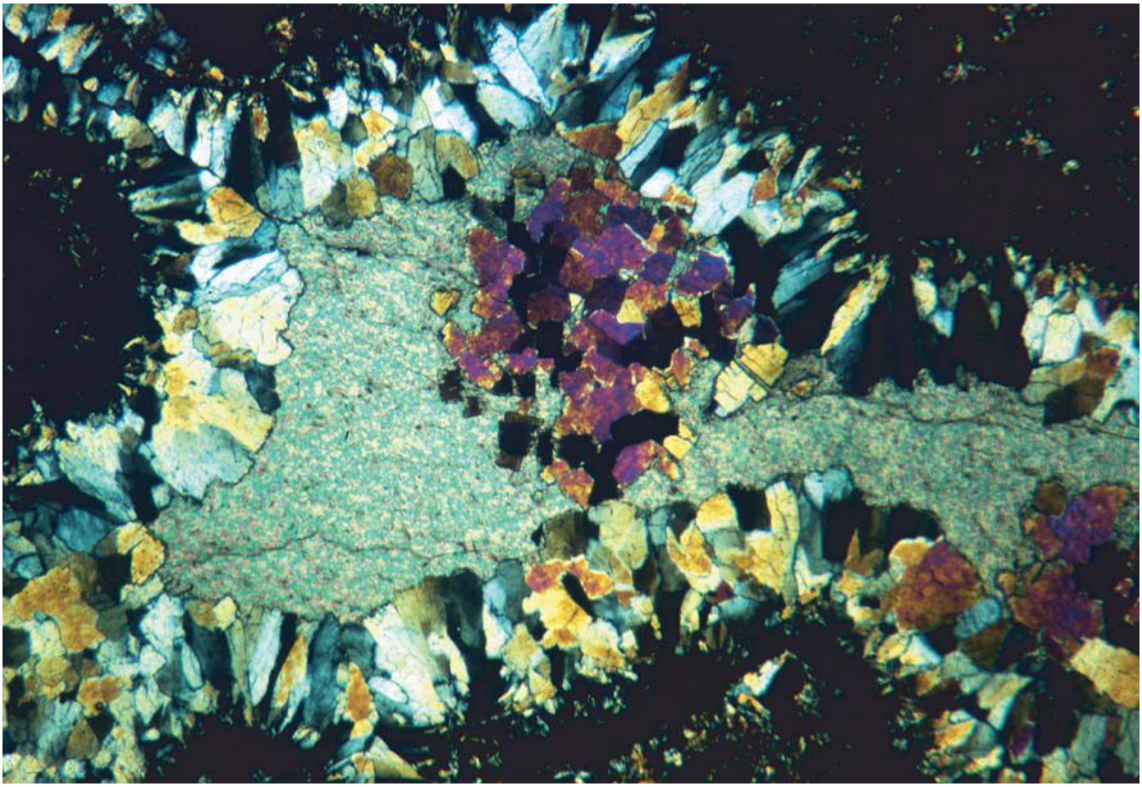

Fig. 3.98: Amygdale with rim of columnar prehnite (low to upper first-order interference colours, depending on orientation) projecting into the cavity with crystal terminations, the remainder of the space having been filled by a single grain of calcite (very high interference colours) in altered dolerite, near Cessnock, New South Wales, Australia. This 'crustification' structure is common in many veins and other cavity fillings (Section 5.9.3). Crossed polars; base of photo 3.5 mm.

of connectivity, enclosed in aplite, which they called 'interconnected miarolitic texture'. They inferred that the cavities were formed by transport of a magmatic volatile phase, presumably trapped by the rapidly crystallizing aplite.

Although most miaroles tend to be roughly spherical, those that form in response to late-stage release of volatiles have irregular shapes, controlled by spaces available between crystals of minerals already crystallized from the magma (see, for example, McMillan, 1986). In addition, late-released vapour tends to be pervasively dispersed through the remaining vapour-saturated melt, attacking and replacing primary minerals by minerals precipitating from the vapour in the miaroles (McMillan, 1986). Moreover, if the fluid accumulates in opening fractures, elongate miarolitic cavities may be produced (Fig. 3.102) (Ridley, 2002). If quartz-saturated fluid bubbles concentrate in fractures beneath the roof of a magma body, comb-layered prismatic quartz crystals may be deposited, the

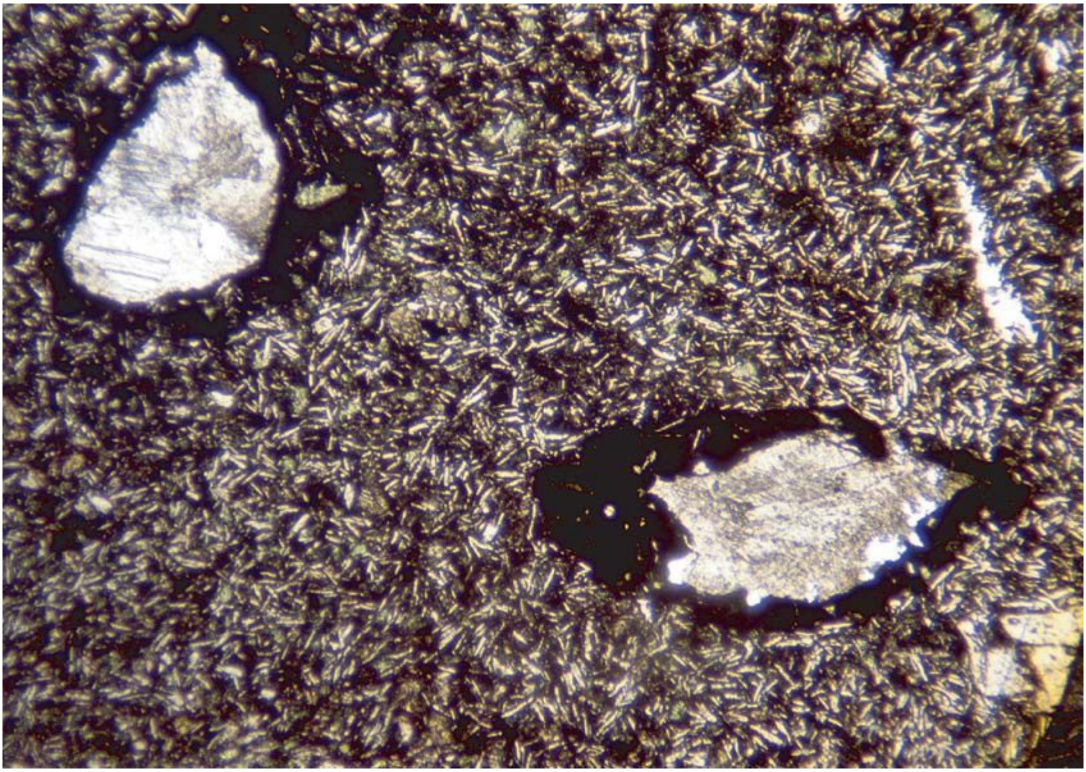

Fig. 3.99: Segregation vesicles in basalt from central-western New South Wales, Australia. The dark rims of the vesicles have been inferred by Smith (1967) to represent residual melt (cooled to glass, now altered) that leaked into the gas bubbles from the surrounding magma (Fig. 3.100). The rock has been subjected to low-grade burial metamorphism (Chapter 4), and so contains secondary minerals, such as chlorite (green) and calcite that filled the space remaining after the melt leaked into the vesicles. Plane-polarized light; base of photo 11 mm.

crystals showing concentric growth zoning caused by concentrations of minute fluid inclusions and high concentrations of trace elements, such as Na, K, Ca, Mn, Ti, Fe, Ge and Rb (Lowenstern & Sinclair, 1996). These concentrations contrast with typically low values for magmatic quartz, confirming the hydrothermal origin (Lowenstern & Sinclair, 1996).

3.15 Liquid unmixing in magma

Spherical globules of contrasting composition in igneous rocks — for example, felsic silicate and sulphide globules in mafic and ultramafic rocks — have been interpreted as being due to segregation of liquids (*liquid immiscibility*) during cooling (see, for example, McLean, 1969; Skinner & Peck, 1969; Roedder &

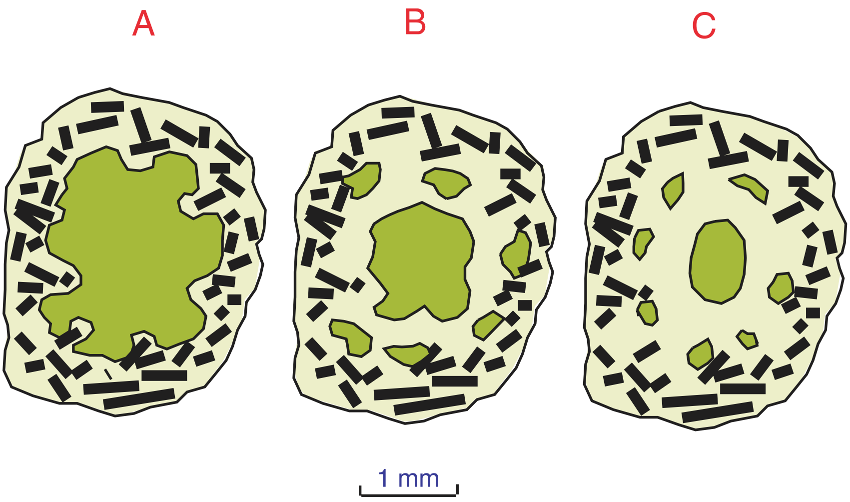

Fig. 3.100: The progressive formation of segregation vesicles in submarine basalt (Fig. 3.99), according to the hypothesis of Smith (1967). The pale yellow areas represent glass, and so represent influx of magma into the vesicle from the surrounding basalt. Unfilled areas are shown in green, and crystals are represented by black rectangles.

Weiblen, 1970; Shima & Naldrett, 1975; Philpotts, 1971, 1976, 1977, 1979, 1982, 1990; Roedder, 1979b; Czamanske & Moore, 1977; Ulff-Möller, 1985). The two liquids are inferred to have been in chemical equilibrium at the time the segregation occurred.

Good evidence of immiscibility of silicate liquids has been found in the residual glasses of many lunar rocks (Roedder & Weiblen, 1970) and some Earth basalts (Roedder & Weiblen, 1971; De, 1974). Iron-rich immiscible globules in silica-rich glass have been produced experimentally in a tholeiitic basalt (Philpotts & Doyle, 1980), and felsic globules have been produced by experimental cooling of some melted alkaline mafic and ultramafic rocks with felsic globules ('ocelli') by Philpotts (1971) and Ferguson & Currie (1971), as reviewed by Philpotts (1976).

Microstructural criteria for immiscibility have been suggested by Philpotts (1977, p. 141), on the basis of experimentally produced microstructures, namely uniform globule size and an absence of sharp cusp-like boundaries where droplets coalesce. However, the interpretation of globular structures in crystallized igneous rocks can be difficult (Philpotts, 1977). The following criteria have been proposed to support an immiscibility origin for fully crystallized globules (Foley, 1984). (1) Mafic minerals appear to have nucleated inside the globule, rather than on the boundaries, indicating that the globule was fully occupied by melt, as opposed to growth from the edges inwards for filled cavities.

Fig. 3.101: Radiating aggregates of K-feldspar, some graphically intergrown with quartz, projecting into a miarolitic cavity, the centre of which is filled with coarser-grained quartz. Crossed polars; base of photo 4 mm.

(2) Cores of mafic minerals in the globule are of similar composition to those in the surrounding rock, but rim compositions follow different trends, in response to the different bulk chemical compositions of the two melts. Natural immiscible silicate liquids preserved as glasses (Philpotts, 1982; Kuo *et al.*, 1986) confirm that the process of liquid immiscibility occurs in basaltic magmas.

Small spherical sulphide bodies, inferred to be formed by liquid immiscibility, have been described in basalts from lava lakes, pillow margins and mid-ocean ridges (see, for example, Desborough *et al.*, 1968; Skinner & Peck, 1969; Pedersen, 1979; Czamanske & Moore, 1977). They are composed of Fe–Ni–Cu sulphide minerals with variable amounts of magnetite. In comparison, immiscible sulphide blebs in lunar basalts and chondritic meteorites have no magnetite and have other Ni–Fe compounds (Pedersen, 1979, p. 397). The bodies contain bleb-like grains of minerals and have been interpreted as eutectic quench microstructures, by comparison with experiments on the Ni-poor part of the Fe–Ni–S system (Pedersen, 1979). Sulphide 'droplets' also occur in the minerals of peridotite xenoliths and clinopyroxene xenocrysts (megacrysts) extracted from

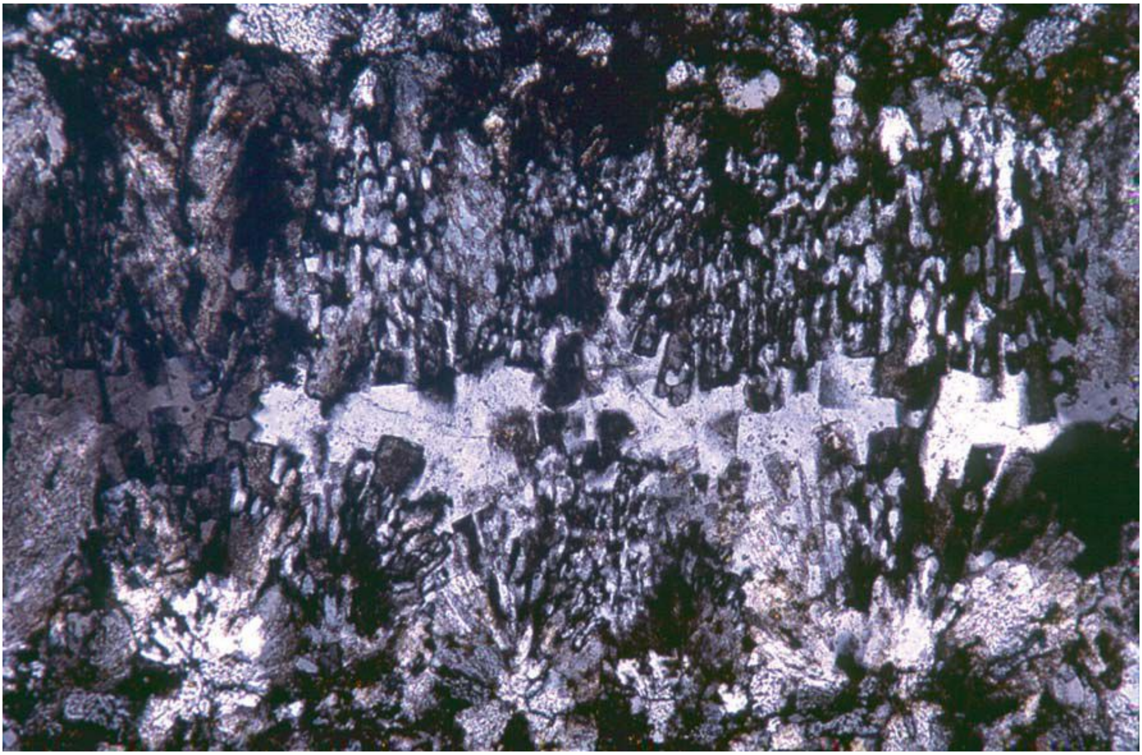

Fig. 3.102: Elongate type of miarolitic cavity in microgranite. Aggregates (some radiating) of crystals of K-feldspar graphically intergrown with quartz project into the cavity, the centre of which is filled by coarser-grained quartz. Crossed polars; base of photo 1.5 mm.

the mantle and brought up in basalts and kimberlites, the sulphides being either Fe–Ni sulphides or pyrrhotite–chalcopyrite aggregates (Andersen *et al*., 1987). The inclusions in the pyroxene megacrysts have been interpreted as trapped droplets of immiscible sulphide melt that nucleated on the surface of crystals growing in basaltic magma in the mantle (Andersen *et al*., 1987).

Chapter 4

Microstructures of metamorphic rocks

4.1 Introduction

Once you have seen what the microstructures of sedimentary and igneous rocks look like, you are in a good position to appreciate what happens to them when they are heated (Chapter 4) and deformed (Chapter 5) in Earth's crust. These processes can greatly alter the microstructure, producing no less beautiful, but very different grain and crystal shapes. Moreover, during heating, new minerals are produced.

This chapter is concerned with microstructures formed in the solid state, mainly as a result of metamorphism, but also discusses exsolution, which, though a solid-state process and so appropriate to this chapter in that sense, also occurs during the slow cooling of minerals in igneous rocks.

The microstructure of a metamorphic rock is the end-product of a complex history that may involve sequences of complicated chemical reactions, and commonly also repeated deformation events. Although microscopic evidence is used to infer the metamorphic or deformation history, we should be careful not to try to extract too much information from it, and should remain aware of complexity and possible alternative interpretations.

4.1.1 Evidence for metamorphism

How do we know that rocks remain solid during metamorphism in Earth's crust? The evidence consists of residual sedimentary and igneous structures (Section 4.15), such as phenocrysts and amygdales (filled gas bubbles; Section 3.14.2) in metavolcanic rocks, fragmental grain shapes in metasandstones, distorted pebbles in metaconglomerates, and, less commonly, fossils replaced by metamorphic minerals. However, although the rocks remain solid, a great deal of evidence indicates that small amounts of water- or CO_2-rich fluid are involved in many metamorphic reactions. One of the main reasons for the presence of fluid is that most chemical reactions that occur during progressive heating of rocks (*prograde metamorphism*) release fluid, especially water (in *dehydration* reactions) or CO_2 (in *decarbonation* reactions).

As metamorphism becomes more intense, the preservation of original structures becomes less likely, owing to the appearance of new grain shapes and arrangements (Section 4.2). Moreover, at the highest metamorphic temperatures, rocks begin to melt, which introduces new microstructural complications (Section 4.16). The reasons we can be sure that these strongly modified rocks were once sedimentary or igneous rocks are that: (1) in many areas (especially contact metamorphic aureoles around igneous intrusions), gradations from unmetamorphosed, through weakly metamorphosed, to strongly metamorphosed rocks can be seen; and (2) the chemical compositions of the strongly metamorphosed rocks are broadly similar to those of typical igneous and sedimentary rocks.

Another line of evidence is provided by experiments, in which mixtures of various chemical composition are heated to varying degrees and quenched, after which the resulting minerals are identified. In this way, natural mineral assemblages can be compared with those produced experimentally, so that the temperatures and pressures at which the natural minerals crystallize can be inferred.

4.1.2 Metamorphic reactions

Metamorphic reactions occur in response to changes in temperature, pressure or chemical environment (e.g. composition of fluids) in rocks that remain solid, despite small amounts of fluid, except where melting occurs at the highest metamorphic temperatures (Section 4.16). Metamorphic reactions are typically complex, involving many or all minerals in the rock, and commonly involving dissolved chemical components in fluid as well (see, for example, Carmichael, 1969). A fluid is important for transporting chemical components to and from reaction sites, which is a much faster process than diffusion of components through crystals (see, for example, Ferry, 2001; Putnis, 2002).

Metamorphic reactions may be pseudomorphous (see, for example, Guidotti & Johnson, 2002) or involve the formation of symplectic coronas (Section 4.10), so that plausible chemical reactions may be inferred. However, growth of new minerals commonly occurs at various sites (see, for example, Carmichael, 1969), often with reactants and products not in contact, making it difficult to infer metamorphic reactions involved in a change from one mineral assemblage (*paragenesis*) to another.

Reactions involve nucleation and growth, as in igneous rocks (Section 3.3). Nucleation in metamorphism is invariably heterogeneous, because of existing crystals, in which the new minerals nucleate and grow. Barriers to nucleation apply to metamorphic rocks, as to igneous rocks, except that (1) similarity in atomic structure can assist one mineral to nucleate inside another (Section 4.2.1) and so lower the energy barrier, and (2) *strain energy* may make an additional contribution to raising the energy barrier, because of possible volume differences between the old mineral and the new mineral nucleating in it, or may reduce the energy barrier by providing deformed material (Section 5.3) that could assist nucleation. As in igneous rocks, *overstepping* of the equilibrium reaction temperature and/or pressure is the rule. This applies especially to solid–solid reactions. For example, the barrier for nucleation of sillimanite in andalusite is so high that andalusite commonly persists metastably into the sillimanite pressure–temperature (*P*–*T*) stability field (see, for example, Vernon, 1987a).

Metamorphic reactions tend to approach equilibrium at higher grades in prograde metamorphism, owing to increased diffusion rates at high temperatures. Evidence of incomplete reaction and disequilibrium is more typical of retrograde metamorphism, owing to reducing temperatures and/or restricted supply of volatile components, as explained in the next section. Incomplete and metastable reactions are also common in contact metamorphism (see, for example, Hollister, 1969; Loomis, 1976), for which the duration of heating may be too short for reactions to go to completion.

4.1.3 Metamorphic history

As rocks heat and cool, their minerals and structures progressively change, and so the main aim of studying the microstructures of metamorphic rocks is to try to infer the history of these changes. During prograde metamorphism, newer minerals and microstructures progressively destroy older ones, eventually leaving little or no evidence of them, except in less metamorphosed rocks (low-grade metamorphism). In such situations, the best or even the only way to infer the complete prograde metamorphic history is to examine a sequence of rocks of increasing metamorphic grade, rather than examining just the high-grade rocks themselves.

On the other hand, cooling rocks preserve much more evidence of their post-‘metamorphic peak’ history. Cooling causes lower-grade minerals to replace the high-grade ones produced during prograde metamorphism (*retrograde* reactions), the process being called *retrograde metamorphism*. In effect, the prograde reactions are reversed as the rock cools. Evidence of retrograde reactions is commonly preserved because: (1) cooling reduces the rates of diffusion (movement) of atoms, and so slows down the rates of reactions, which consequently are commonly incomplete, so that both the unstable high-grade minerals and the more stable lower-grade minerals occur together; and (2) most retrograde reactions require the addition of the same kinds of fluids that were driven out of the rocks during prograde reactions; because access of these fluids can be difficult in solid rocks, the resulting retrograde reactions are typically very patchy in their development (Vernon & Ransom, 1971; Vernon, 1976). In fact, the most complete development of retrograde reactions is in local zones of strong deformation, in which fluids can gain ready access (Vernon & Ransom, 1971; Vernon, 1976; White & Clarke, 1997), as discussed in Sections 4.13.2 and 5.6.5.

4.1.4 Polymetamorphism

Many parts of Earth's crust show evidence of several metamorphic/deformation events. Microstructural evidence of *polymetamorphism* includes: (1) a set of compatible minerals (*mineral assemblage* or *paragenesis*) partly replaced by another, and (2) a mineral assemblage inferred to have grown during the development of a specific deformation event (Section 5.10), followed by another assemblage developed during a subsequent deformation event. Microstructural evidence can indicate the relative timing of events, but absolute timing of these events must rely on geochronological measurements (Section 5.10.3). Sensitive high-resolution ion microprobe (SHRIMP) analysis, laser isotopic techniques and electron microprobe analysis of monazite (Section 5.10.3) enable the dating of individual grains and parts of grains, so that details of the history can be revealed.

The evaluation of evidence for the metamorphic and deformation history (*tectonometamorphic* history) of complex metamorphic rocks (Section 5.10.3) is an exciting aspect of modern metamorphic and structural petrology. Needless to say, the microstructural interpretations must be made with the greatest of care, because much depends on them (Vernon, 1996b). Mistakes and unjustified inferences are easy to make, and can lead to wrong tectonometamorphic interpretations.

4.2 Processes controlling grain shapes in metamorphic rocks

Some grain boundaries in metamorphic rocks are crystal faces (low-energy boundaries) parallel to densely packed planes in the crystal lattice of one of the minerals in contact (Section 3.5.2). Twin boundaries (Sections 3.12, 4.7) are also of relatively low energy, but the interfacial (grain-boundary) energy progressively increases as the angle of misorientation of grain boundaries increases (Fig. 4.1). Most grain boundaries in metamorphic rocks are apparently random (high-energy boundaries), and generally are curved in the optical microscope. However, a few boundaries with special orientation relationships between grains have slightly lower energy (coincidence boundaries), and can lead to departures from smooth grain-boundary curvatures, as discussed in Section 4.2.2. Fig. 4.1 refers only to the angle of misorientation between boundaries in two dimensions, and does not take into account the orientation of the boundary itself. Therefore, the situation in actual grain boundaries is more complicated.

4.2.1 Energy considerations

When an unstable aggregate of minerals is replaced by a more stable aggregate during metamorphism, the first step is nucleation of new (lower energy or more stable) minerals. This involves (a) assembly of the required atoms by diffusion

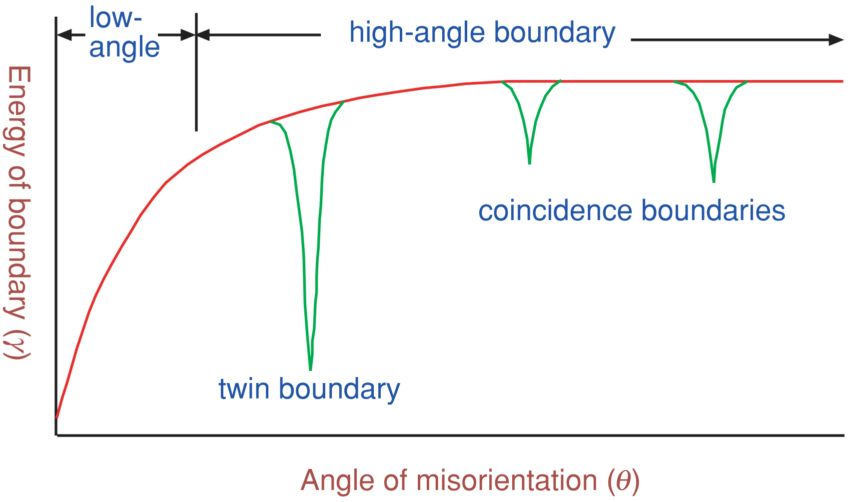

Fig. 4.1: Diagrammatic plot of interfacial energy (γ) versus angle of misorientation (θ) across a hypothetical grain boundary, showing the general trend of the curve, with an average high-energy 'plateau' value for high-angle interfaces, and low-energy 'cusps' (green lines) representing *coincidence boundaries*, which correspond to a degree of atomic registry across the boundary. Coincidence boundaries may account for minor deflections of otherwise smoothly curved interfaces in solid-state aggregates (Section 4.2.1). The lowest-energy cusp is for a *twin boundary*, which is a special type (*coherent interface*) of coincidence boundary (Sections 3.12 and 4.7).

inside the old minerals, (b) probable change of the atomic arrangement into one or more unstable intermediate structures ('activated complexes') and (c) formation of a nucleus of a new stable or metastable mineral. At this stage, in theory, smaller nuclei or crystal particles may be dissolved and larger ones may grow into viable nuclei, the process being known as 'Ostwald ripening' (Section 3.3.2), although whether this process can account for grainsizes of metamorphic minerals is open to question at this stage (Section 4.3.1). The formation of viable nuclei is followed by their *growth* to form crystals or grains, which involves (a) diffusion of the required chemical components through the old minerals and through any fluid between them, (b) transfer of these components across the boundary into the new mineral and (c) concomitant diffusion of unwanted components from the reaction site.

The water produced in dehydration reactions (such as $KAl_3Si_3O_{10}(OH)_2 + SiO_2 = KAlSi_3O_8 + Al_2SiO_5 + H_2O$) or carbon dioxide produced in decarbonation reactions (such as $CaCO_3 + SiO_2 = CaSiO_3 + CO_2$) must be continually removed from the reaction site for the reaction to continue. Presumably this is achieved by diffusion to local pockets of fluid that migrate through the rock (see, for example, Etheridge *et al.*, 1983, 1984) in response to: (1) fluid pressure that exceeds the local minimum compressive stress (σ_3) plus the local tensile strength of the rock, and so opens up local fractures, especially along grain boundaries (Etheridge *et al.*, 1983, 1984), and/or (2) deformation, which opens transient local spaces, owing to strength differences between minerals.

The grains of new minerals initially grow as products of metamorphic reactions, in an attempt to minimize the chemical free energy of the system. Some metamorphic reactions are *pseudomorphous*, in that the new mineral or aggregate of minerals replaces an existing mineral grain or crystal, preserving its shape, as where garnet is pseudomorphed by chlorite or andalusite is pseudomorphed by sillimanite (Section 4.13).

Nucleation may be *epitactic* ('epitaxial'), which means that the atomic structure of the new mineral is closely related to the atomic structure of a pre-existing mineral. An example is andalusite replaced by sillimanite (Fig. 4.2), such that microscopically the *c*-axes of both coincide, and the *a*- and *b*-axes are exchanged (Vernon, 1987a), as shown in Fig. 4.3. However, TEM investigation has shown

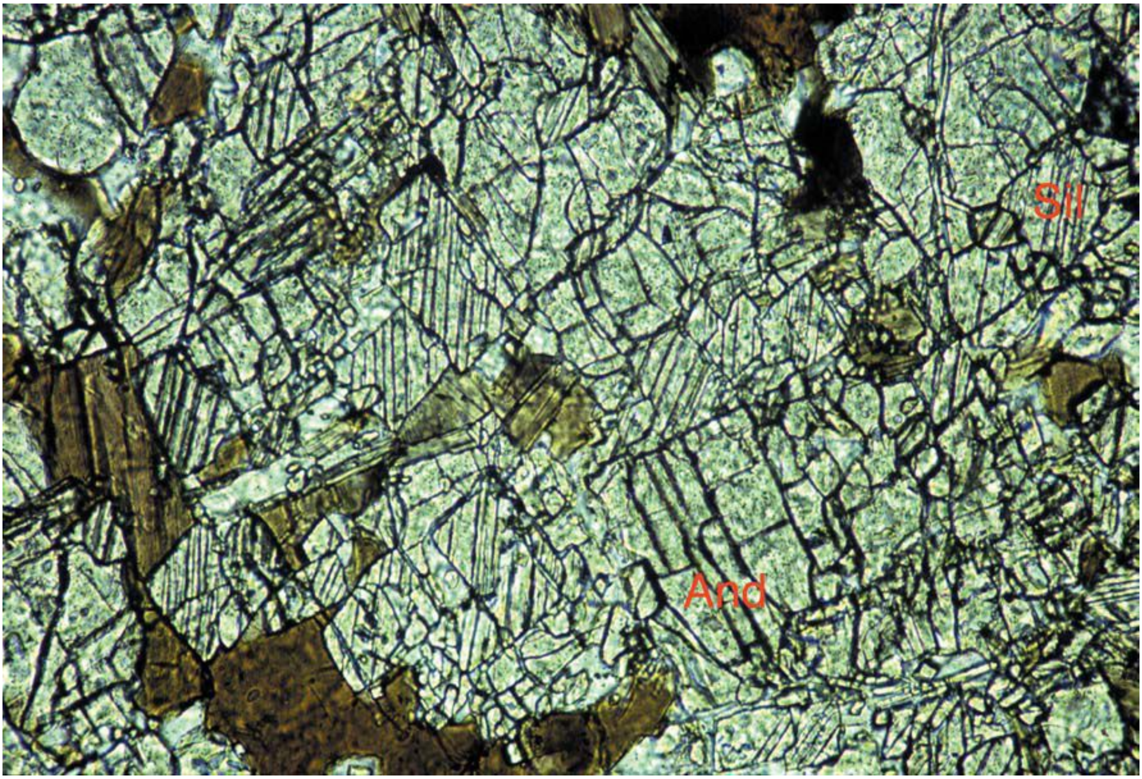

Fig. 4.2: Sillimanite (diamond-shaped crystals with a single cleavage) that has epitactically ('epitaxially') replaced andalusite (orthogonal cleavages) in a high-grade metapelite from Mount Stafford, central Australia. Compare with Fig. 4.3. Plane-polarized light; base of photo 0.7 mm.

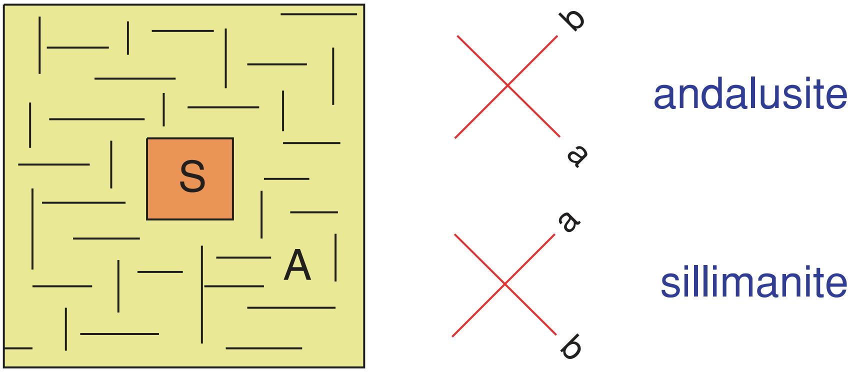

Fig. 4.3: Approximate epitactic relationship of andalusite (A) replaced by sillimanite (S), such that the *c*-axes of both coincide and the *a*- and *b*-axes are exchanged (Vernon, 1987a). Compare with Fig. 4.2.

that the optical coincidences are only approximate, because the andalusite and sillimanite lattices are misoriented by a rotation of approximately 2.5° around the andalusite *a*-axis (sillimanite *b*-axis), which brings into coincidence planes with the smallest misfit between the two lattices, namely andalusite $\{032\}$ and sillimanite $\{302\}$ (Cesare *et al.*, 2002a).

As noted previously, most metamorphic reactions are more complicated, not obviously pseudomorphous, and involve several minerals. In either situation, nucleation in the solid-state is assumed to be invariably heterogeneous, though details of the nucleation processes are obviously obscure.

Once the grains of stable minerals have impinged on one another, and the whole volume is filled with the new minerals, the chemical free energy of the system is reduced to a minimum. Various replacement microstructures may or may not be present, but subsequent grain-boundary adjustment processes may remove them. At this stage, interfacial free energy (γ) takes over, causing the grainsizes and grain shapes (but not the minerals) to change still further, to minimize the total interfacial free energy of the system (grain growth). The interfacial free energy is due to atoms at grain boundaries being not well accommodated in either grain, and so being in positions of higher potential (free) energy than they would be if they were in regular atomic arrays inside grains. Although the interfacial free energy is much smaller than the chemical free energy, it nevertheless controls the final shapes of the grains.

If the rock stays hot enough for long enough (e.g. at high grades of metamorphism), the grain boundaries continue to move, in an attempt to reduce γ to a minimum. The usual explanation is that this involves either: (1) reducing the interface *area* to a minimum, which reduces the total proportion of atoms in high-energy sites (namely in grain boundaries, as opposed to those in lower energy sites in the more regular, internal parts of grains) or (2) the production of *low-energy crystal faces* ('idioblastic crystals'). Process (1) occurs mainly in minerals that have 'relatively isotropic' crystal structures (though not completely structurally isotropic and not necessarily optically isotropic, of course), such as quartz, feldspar, calcite, scapolite, olivine, chromite, magnetite, galena, pyrite and ice, whereas process (2) occurs in minerals with strongly anisotropic structures, such as the sheet silicates (e.g. mica, chlorite), hematite, molybdenite, graphite and sillimanite. However, some minerals (e.g. garnet, staurolite and andalusite) develop crystal faces in many rocks, but not in others, indicating that crystal structure is not the only factor controlling the development of crystal faces in metamorphic rocks.

Process (1) is generally inferred to form random boundaries of roughly uniformly high energy (Fig. 4.1). However, the atomic structures of these boundaries are not well understood. Generally high-energy (high-angle, random) boundaries are thought of as arrays of densely packed lattice defects that are necessitated by the misorientation of neighbouring lattices and their random intersection with the boundary between them. These boundaries commonly appear to be smoothly curved in the optical microscope, and may also be smoothly curved in SEM images of grains extracted intact from metamorphic rocks (Kretz, 1994, fig. 5.41). However, some show sharp bends (steps, facets), as observed for some grain boundaries in zinc by Bishop & Chalmers (1971). For example, quartz grain boundaries in some high-grade metamorphic rocks have roughly rectangular steps or 'sutures'. These facets suggest the existence of selected (lower-energy) relationships between the orientation of the boundary and the crystal structure (such as the lower-energy cusps in the curve of Fig. 4.1), and so may reflect attempts to minimize the interfacial free energy at the local scale by forming relatively low-energy interfaces (Kruhl, 2001; Kruhl & Peternell, 2001, 2002). McLaren (1986) has presented evidence that specific grain-boundary misorientations in quartz may be of lower energy, owing to twin relationships.

Moreover, examination of optically curved boundaries at very high magnification in a high-resolution TEM, so that individual rows of atoms are imaged (Wolf & Merkle, 1992), commonly reveals short straight segments (too short to be seen optically) with high degrees of atomic registry between adjacent grains. Therefore, what appears optically to be the result of an attempt to simply reduce interfacial area may also involve an attempt to form relatively low-energy, crystallographically controlled grain-boundary segments (Kruhl, 2001). This appears to be especially applicable to movement of grain boundaries in the presence of a fluid (Sections 4.4, 5.4.2). Nevertheless, grain boundaries in many aggregates grown in the solid state appear to be smoothly curved at the optical scale, and the basic processes controlling such aggregates are described in the next section.

The discussion applies only to random grains that have grown to a high degree of microstructural stability without the effect of imposed differential stress ('static grain growth'). At low grades of metamorphism and where the duration of metamorphism is relatively short, these ideal shapes may not be achieved.

Furthermore, growth during deformation (Chapter 5) can give rise to grain boundary irregularities, elongate shapes and strong preferred orientations, although the interfacial angles may still tend towards low-energy configurations.

Although grain growth tends to produce new metamorphic microstructures, numerical simulations of the process suggest that grains that survive the coarsening contain a single core of material unaffected by the 'sweeping' of the moving grain boundaries, and so may preserve some information about the original rock (Jessell *et al.*, 2003).

Solid-state grain growth probably should not be referred to as 'Ostwald ripening' (see, for example, Shelley, 1993; Best, 2003), even though both processes cause grain coarsening, because the two processes can be distinguished (Martin & Doherty, 1976, p. 234; Tikare & Cawley, 1998). Grain growth is a solid-state process involving migration of grain boundaries at the microscopic scale or greater, including growth in the same mineral, whereas 'Ostwald ripening' typically refers to coarsening of very small crystal particles dispersed in a liquid or solid of a different composition. It involves solution of the smaller particles and their reprecipitation on larger ones, under conditions at which surface energy differences can drive diffusion over the very small distances involved (see, for example, Tikare & Cawley, 1998), as discussed in Section 3.3.2.

4.2.2 Low-energy grain shapes of 'structurally isotropic' minerals

A general idea of typical grain shapes resulting from process (1) (above) can be obtained from the examination of foams, such as soapy water–air froths and especially beer–air froths, as seen in the necks of beer bottles after the beer has been poured (Vernon, 1976). Similar grain or cell configurations are shown by sections of annealed metals and sintered ceramics (Harker & Parker, 1945; Smith, 1948, 1953, 1964; McLean, 1957; Chalmers, 1959; Kingery, 1960; Brophy *et al.*, 1964), organic cellular aggregates (Smith, 1954), and minerals with structures that are relatively uniform in three dimensions, such as quartz, feldspar, calcite, fluorite, scapolite, olivine, galena, pyrite, pyrrhotite, sphalerite, chromite, magnetite and ice (Buerger & Washken, 1947; MacGregor, 1950; von Steinemann, 1958; Bathurst, 1958; Voll, 1960; Shumškii, 1964; Stantoǹ, 1964; Kretz, 1966a; Vernon, 1968, 1976; Ostwald & Lusk, 1978; McClay, 1982a,b; Lusk & Ostwald, 1983; Frater, 1985; Rosière *et al.*, 2001) as shown in Figs. 4.4–4.9.

In foam-like aggregates seen in two dimensions, three grains or cells meet at a point ('triple-junction') and the interfacial angles closely approximate 120°, these being the two-dimensional geometrical results of an attempt to fill space and reduce the interface area to a minimum (see, for example, Harker & Parker, 1945; McLean, 1957). Because thin and polished sections are two-dimensional slices through three-dimensional grain aggregates, the interfacial angles seen are *apparent* angles. For opaque minerals (Fig. 4.8), it is necessary to measure

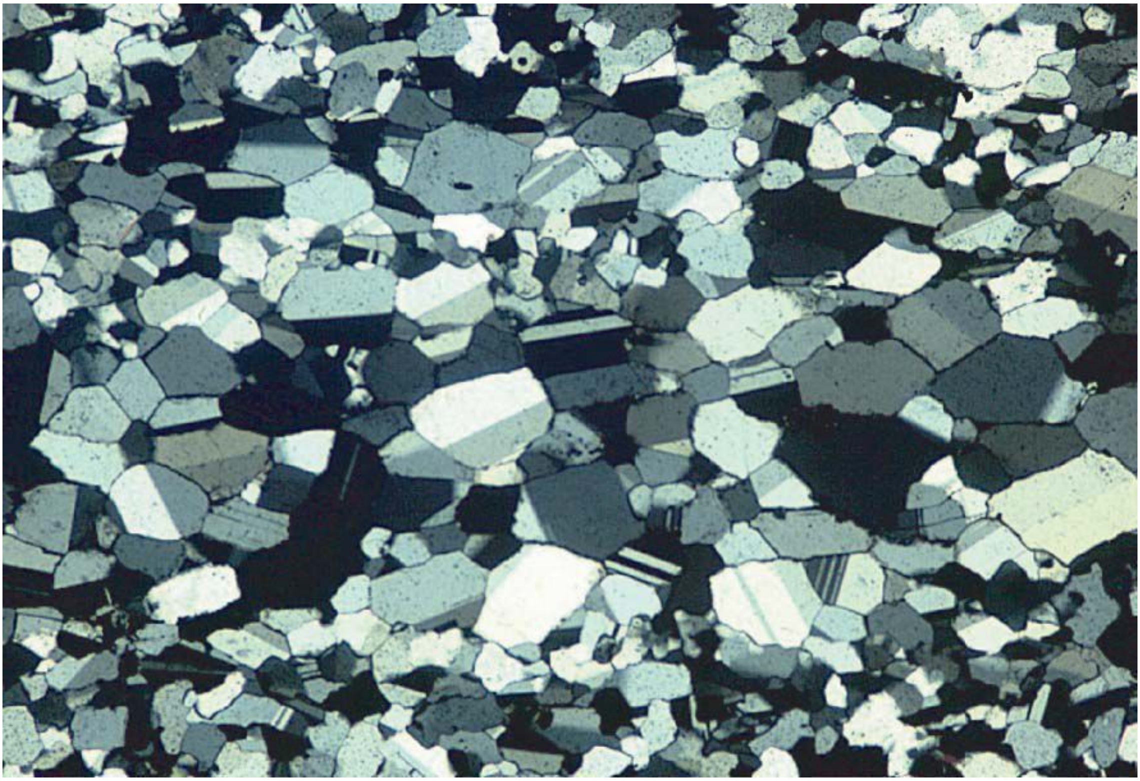

Fig. 4.4: Polygonal aggregate of albite, Broken Hill, New South Wales, Australia. Growth twins (Section 4.7), both simple and multiple, are abundant. From Vernon (2000b, fig. 122). Crossed polars; base of photo 4.4 mm.

apparent angles in a polished section on the normal microscope stage and then make a statistical correction to obtain true angles (see, for example, Harker & Parker, 1945; Riegger & van Vlack, 1960; Holcombe, 1977; Jurewicz & Jurewicz, 1986; Rosenberg & Riller, 2000). This technique also applies to interfacial angle measurements made on photomicrographs of, for example, backscattered SEM images or TEM images, unless care is taken to orient the interfaces (see, for example, Hiraga *et al*., 2002). However, the fact that thin sections of non-opaque minerals have a definite thickness (typically 0.03 mm) means that grain boundaries can be sharpened in appearance when rotated to the vertical on a universal stage. This makes them appear as sharp, thin lines, rather than blurred, thicker lines, so that their orientation can be measured accurately (Kretz, 1966a; Vernon, 1968, 1970). Either the stage can be adjusted so that the three interfaces are vertical and the angles between them measured directly, or the orientations of interfaces can be plotted on an equal-area stereonet and the angles determined graphically. Both methods allow accurate determination of true interfacial angles, without the need for apparent angle distribution curves. Therefore, the use of statistically

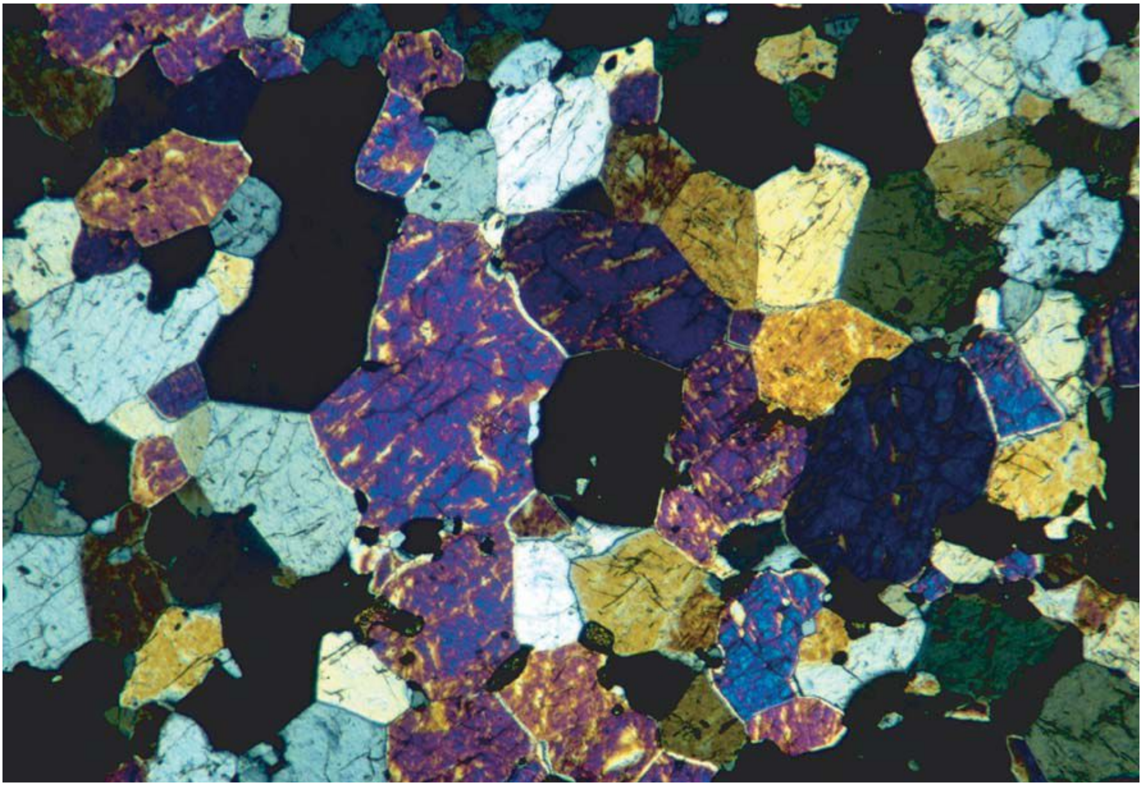

Fig. 4.5: Polygonal aggregate of scapolite, Mount Lofty Ranges, South Australia. Crossed polars; base of photo 1.3 mm.

corrected flat-stage measurements (see, for example, Hunter, 1987; Elliott *et al.*, 1997) is unnecessary, as pointed out by Vernon (1997). Once true angles have been obtained with a universal stage, dispersion of these angles about the mean of 120° (see below) can then be interpreted (e.g. as an effect of anisotropy of crystal structure or of departure from equilibrium), without unnecessary statistical complications (Vernon, 1997).

In two dimensions, five-sided grains or cells are the most common. As foams grow, large bubbles or cells with many sides grow bigger, at the expense of grains with few sides, which get smaller, eventually becoming three-sided (in two dimensions), before disappearing and so being replaced by a new triple junction. This process is shown in Fig. 4.10, which illustrates a progressive sequence of photographs of changing shapes during grain growth in an organic compound observed with the microscope.

In three dimensions, four grains or cells meet at a point, the ideal interfacial angle being the internal angle subtended by lines from the corners of a tetrahedron, namely 109°28′. The three-dimensional polyhedron that fills space and best fits

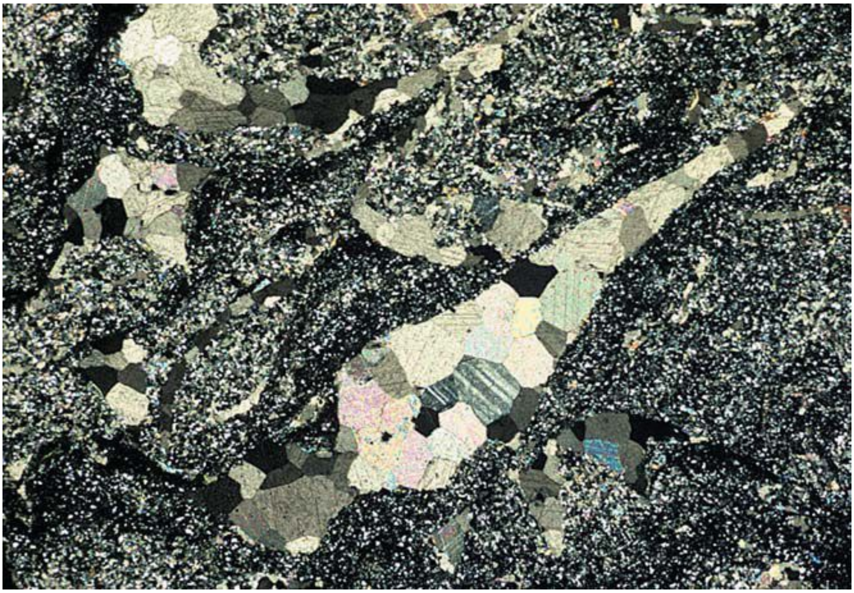

Fig. 4.6: Polygonal aggregates of calcite (extremely high-order interference colours) that have replaced fossil shells in a contact metamorphic rock (hornfels) from Hartley, west of Sydney, New South Wales, Australia. From Vernon (2000b, fig. 119). Crossed polars; base of photo 1.8 cm.

observations of grain aggregates is the β-tetrakaidekahedron (Williams, 1968). The actual three-dimensional shapes of grains in polygonal aggregates have been well illustrated by Rostoker & Dvorak (1965, p. 7) in material broken out of a Ti alloy cast.

The grain boundaries move towards their centres of curvature, and in this way the grainsize increases (Fig. 4.10). The process slows down as interface curvatures decrease. In foams, all boundaries eventually disappear, but in crystalline materials many boundaries remain. Grain growth can also be retarded by small dispersed mineral grains (Smith, 1953; Voll, 1960; Krabbendam *et al.*, 2003). For example, layers containing many small mica grains have much finer-grained quartz than mica-free layers in metasedimentary rocks (Figs. 4.11, 4.29B).

Foams and organic cellular aggregates are isotropic, so that 120° angles in two dimensions are attained. However, all crystalline materials (even cubic ones) are anisotropic with regard to their detailed atomic structures (and hence many of their physical, though not necessarily their optical, properties). This means that the interfacial free energy is also anisotropic, which implies that some apparently random grain boundaries have slightly smaller free energies than others, in contrast to the situation in foams, in which all interfaces have equally high energies. In metals, it has been found that most boundaries can be regarded statistically as high-energy boundaries. The same is probably approximately true

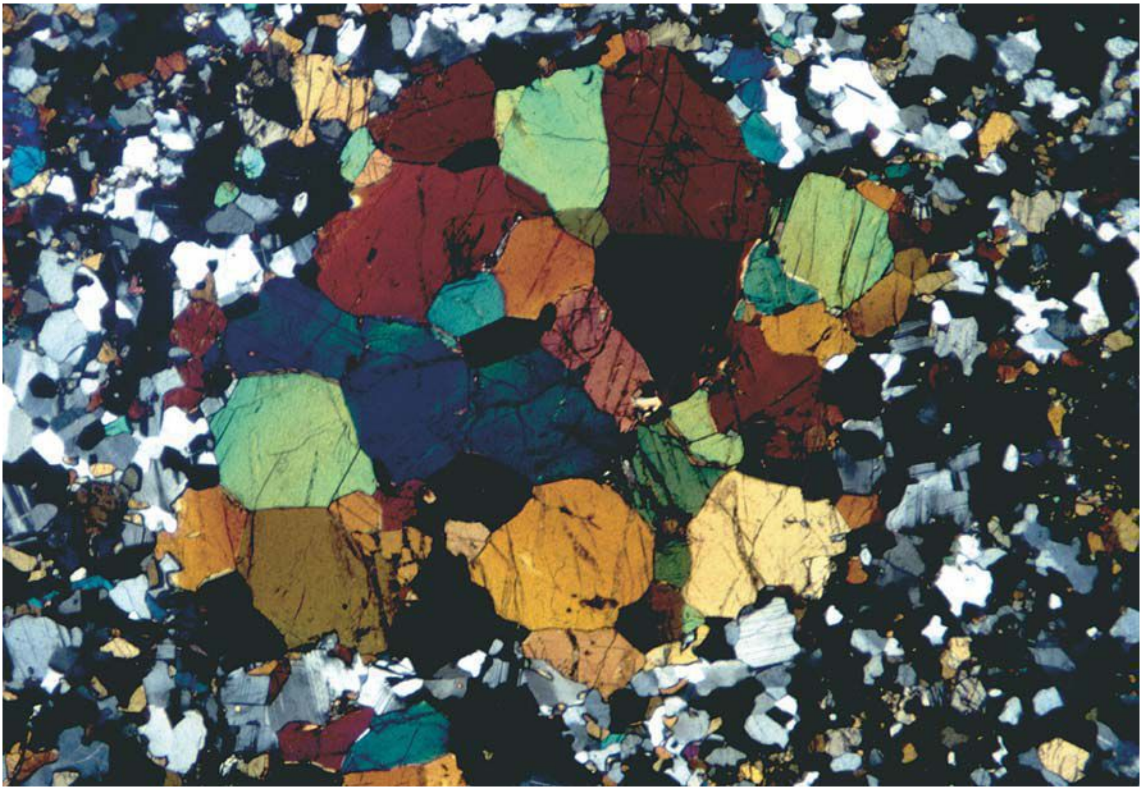

Fig. 4.7: Polygonal aggregate of hornblende that has replaced a former phenocryst (probably pyroxene) in a metagabbro from the Adirondack Mountains, New York, USA. Crossed polars; base of photo 11 mm.

of most minerals, except for those that are strongly anisotropic (Section 4.2.3). The effects of structural anisotropy are to (1) increase the spread of interfacial angles about the mean of 120° (Smith, 1948; Kretz, 1966a; Vernon, 1968), as shown for orthoclase in a high-grade metamorphic rock in Fig. 4.12, and (2) cause microscopic and submicroscopic deflections in apparently random grain boundaries, as mentioned in the previous section. Nevertheless, the aggregate is polygonal (*granoblastic*) and foam-like in appearance. Polygonal aggregates of this type have been produced experimentally in ice, quartz, calcite, fluorite, olivine, anhydrite and sulphides (Buerger & Washken, 1947; von Steinemann, 1958; Stanton, 1964).

In somewhat more anisotropic minerals observed in the microscope, a few interfaces may be partly parallel to planes of specific low-energy crystal forms, such as {110} of hornblende or pyroxene, the rest being curved (Vernon, 1968, 1976). This may be a more obvious effect of the ability of apparently random interfaces to develop local lower-energy segments.

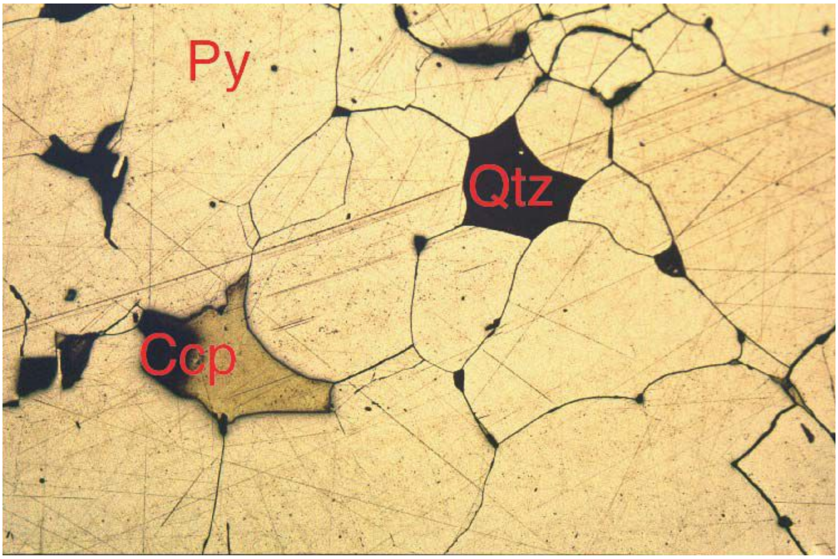

Fig. 4.8: Polygonal aggregate of pyrite (Py), Mount Morgan, Queensland, Australia. Also present are chalcopyrite (Ccp) and quartz (Qtz), showing dihedral angles against the pyrite (Section 4.2.4). Plane-polarized reflected light; base of photo 0.8 mm.

4.2.3 Low-energy grain shapes in structurally anisotropic minerals

In more structurally anisotropic minerals (such as mica and sillimanite), low-energy forms (e.g. {001} in mica and {110} in sillimanite) dominate the microstructure. Aggregates of mica provide common examples in metamorphic rocks. The mica aggregates may be random ('decussate'), as shown in Fig. 4.13, or aligned, as shown in Fig. 4.14. These examples illustrate the marked contrast between polygonal aggregates (Figs. 4.4–4.9) and aggregates dominated by crystal faces. The microstructure of aggregates of structurally anisotropic minerals appears to be the result of mutual *impingement*, rather than mutual *adjustment* of interfaces (Vernon, 1976), so that local dominance of low-energy faces of one grain or the other depends on accidents of nucleation and impingement.

The predominance of crystal faces implies their greater stability, relative to random boundaries, in minerals of this type. Considerations of relative interfacial energies in structurally isotropic minerals (Fig. 4.15A) imply that planar boundaries (involving interfacial angles of 180°) should have infinitely *large* interfacial energies. However, the influence of structural anisotropy in mica and sillimanite is so strong that this situation does not apply (Smith, 1953; Kretz, 1966a). In effect, the extent and strength of atomic bonding parallel to a particular atomic plane, such as {001} in mica, compared with the bonding in other planes, causes the formation of a crystal face that is so stable (i.e. it has such a *small* interfacial

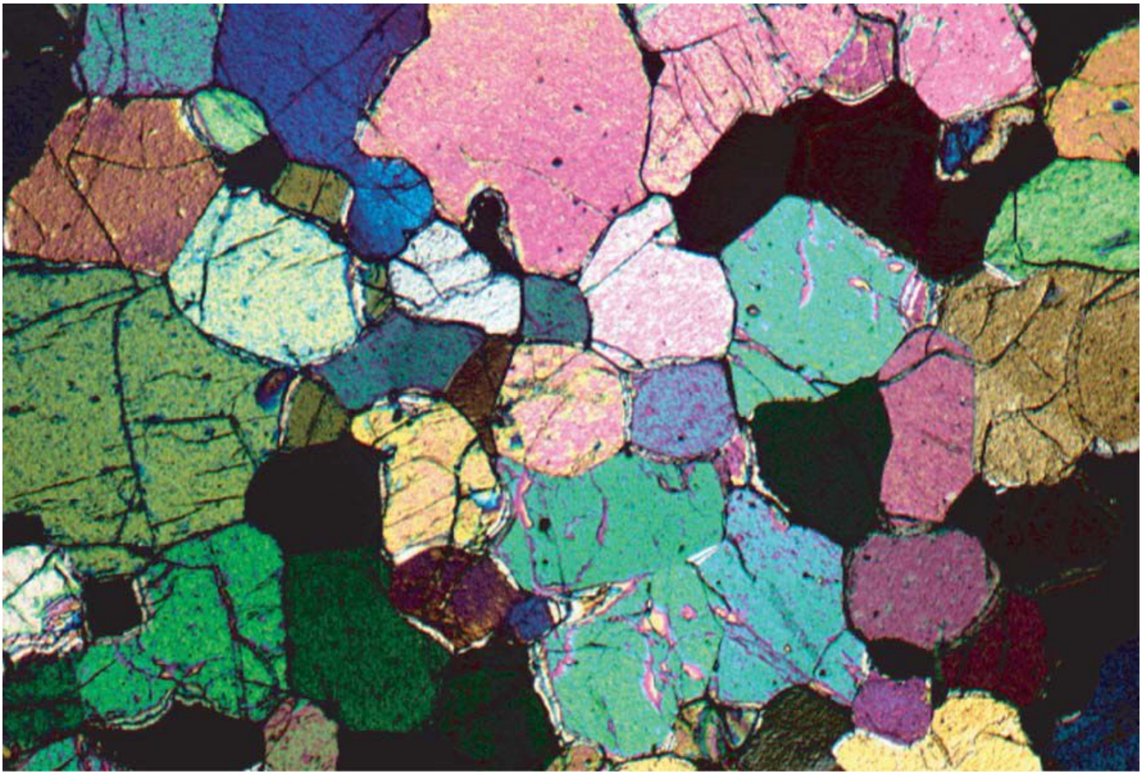

Fig. 4.9: Polygonal aggregate of olivine in a peridotite from Earth's outer mantle, brought up as a xenolith in basalt, Hawaii. From Vernon (2000b, fig. 123). Crossed polars; base of photo 4.4 mm.

energy) that no other boundary can affect it (Fig. 4.16), as discussed by Spry (1969, p. 46). To change these very low-energy interfaces into curved boundaries would require a very large increase in the energy of the system. Even a slight change towards a curvature of the {001} face would markedly increase its energy, and so is not favoured (Vernon, 1999a). In other words, the energy of the boundary reduces abruptly when it is exactly parallel to {001} from relatively high values in all other orientations.

In crystal-face (rational) boundaries of this type, the atomic bonding is strongest parallel to the crystal face and weakest oblique to the face (see, for example, Etheridge *et al.*, 1983; Vernon, 1999a). This may have consequences for the presence of fluid in producing crystal faces in metamorphic minerals, as discussed in Section 4.4.

As mentioned previously, crystal faces are common for many minerals in metamorphic rocks as well as mica and sillimanite, for example, andalusite (Fig. 4.17), chloritoid (Fig. 4.18), garnet (Fig. 4.19) and staurolite (Fig. 4.20).

A B C D

E F G H

Fig. 4.10: Static grain growth in octaochloropropane (OCP) observed with the microscope, shown as a progressive sequence of photos. Grain boundaries migrate in the directions of their centres of curvature, and several grains become progressively smaller and disappear as the average grain size increases. Although the experiment is at room temperature, this is 70% of the absolute melting temperature of OCP, which means that diffusion rates are high enough to promote rapid grain boundary migration. From the CD *Microstructures* by Y. Park, J.-H. Ree and W. D. Means, State University of New York at Albany, 1995.

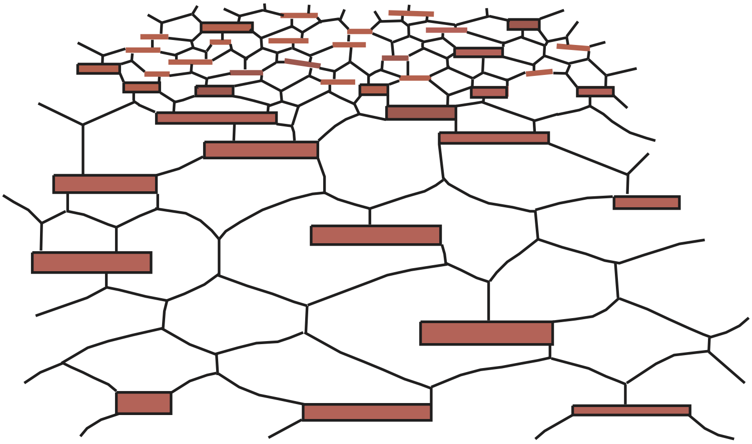

Fig. 4.11: Sketch of a two-dimensional aggregate of a layered quartz–mica rock. Growth of quartz has been retarded in the mica-rich layer by the presence of numerous small mica flakes, to which many of the quartz–quartz boundaries have become attached. The quartz–quartz interfaces meet mica {001}–quartz interfaces at approximately 90° or are joined to the edges of the mica flakes.

However, these minerals do not invariably form crystal faces, as can be seen by comparing the staurolite shown in Fig. 4.20 with that shown in Fig. 4.21. This problem is discussed in Section 4.4.

4.2.4 Polymineral aggregates of structurally isotropic minerals

The same energy considerations apply to two-mineral and polymineral aggregates, except that the angle formed where a grain of one mineral (α) meets two grains of another mineral (β) varies with the minerals involved (Fig. 4.22). This

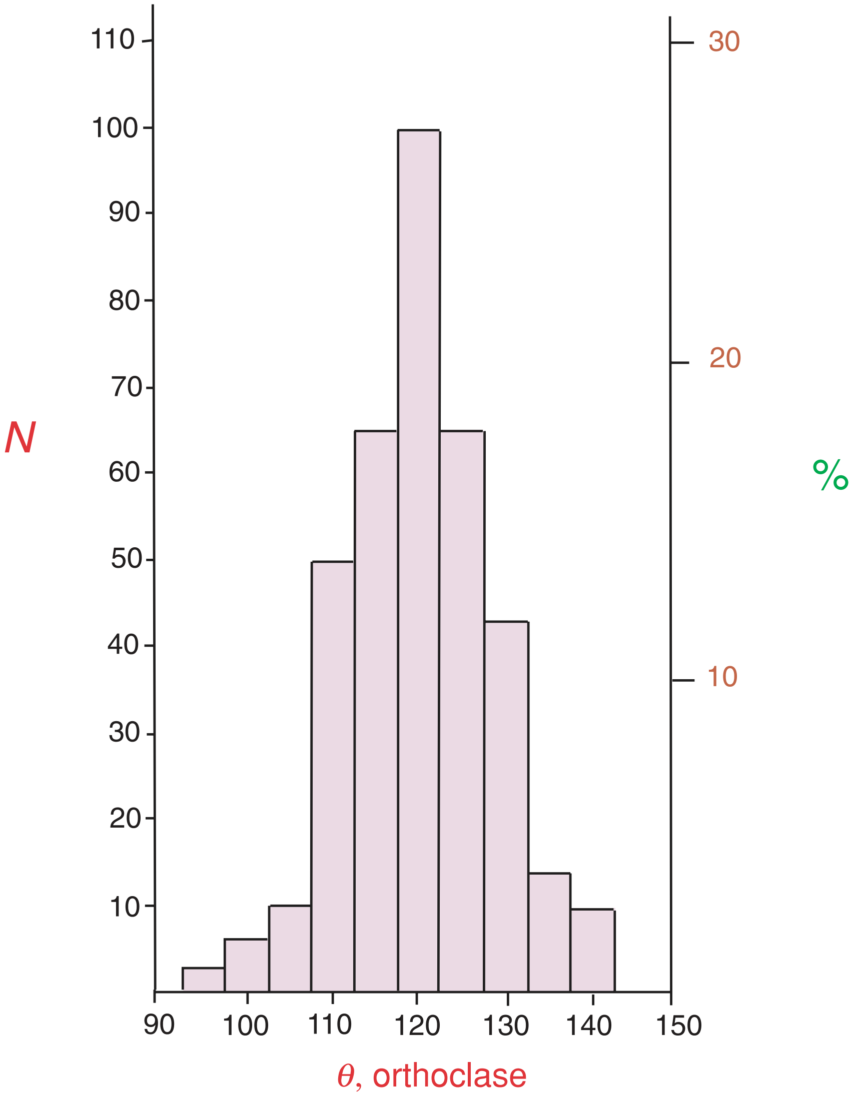

Fig. 4.12: Distribution of true interfacial angles (366 measurements made with a universal stage) in a polygonal aggregate of orthoclase in a high-grade metamorphic rock from Broken Hill, Australia. Although the mean is 120°, with a standard deviation of 7.7°, the spread of angles is from 94° to 142°, with a normal distribution about the mean. After Vernon (1968).

angle is known as the *dihedral angle* (θ) and is generally designated 'θ α vs. β/β' (e.g. θ quartz vs. orthoclase/orthoclase). If the energy (γ) of the grain boundary (β/β) is less than that of the interphase boundaries (α/β), the angle (θ α vs. β/β) is greater than 120°, and vice versa (Fig. 4.15B). The relation between θ and γ

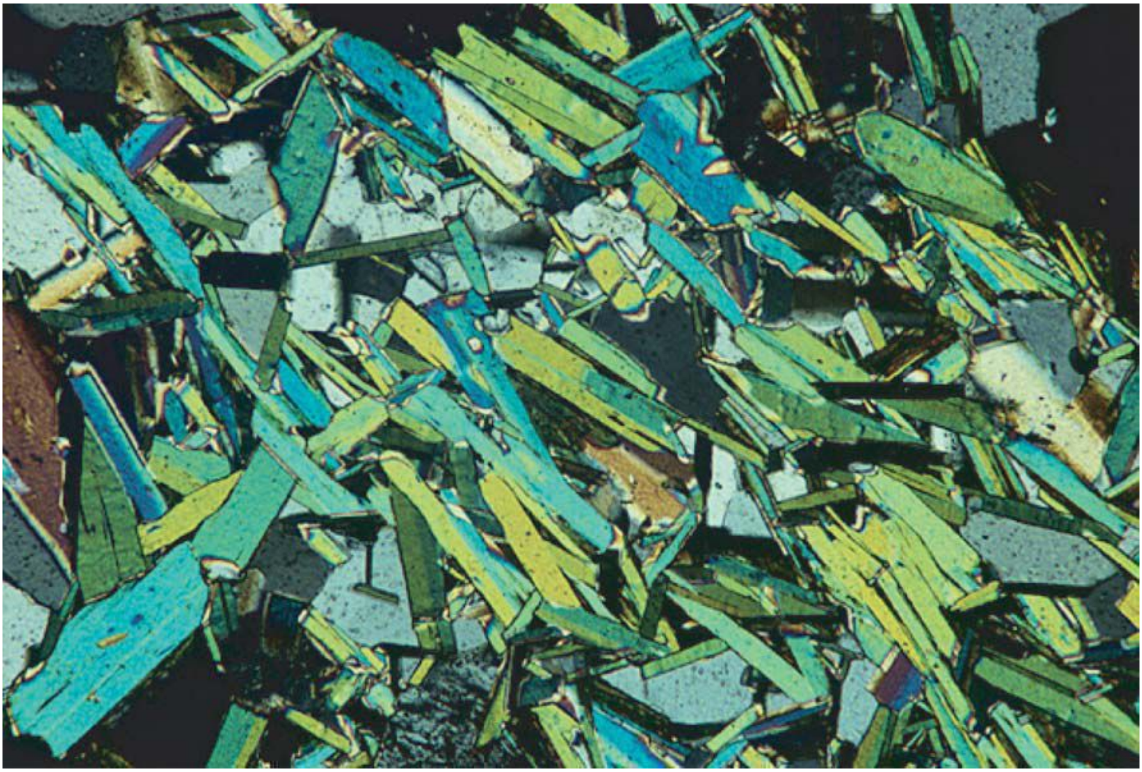

Fig. 4.13: Random ('decussate') aggregate of muscovite dominated by low-energy $\{001\}$ crystal faces, Stirling Vale, Broken Hill, New South Wales, Australia. From Vernon (2000b, fig. 125). Crossed polars; base of photo 1.75 mm.

(Smith, 1948, 1953) is:

$$\theta = 2\cos^{-1}\frac{\gamma_{\beta\beta}}{2\gamma_{\alpha\beta}}.$$

In effect, as large an area of the lower-energy boundary as possible replaces the higher-energy boundary. Surprisingly, θ is commonly less than 120°, which implies that boundaries between grains of the same mineral tend to have higher interfacial free energies than boundaries between grains of different minerals. This has been verified by measurements on many different minerals and metals (Smith, 1948, 1964; Stanton, 1964; Vernon, 1968, 1970). Dihedral angles for silicate minerals in most metamorphic rocks vary from about 95° to 145° (Vernon, 1968), most commonly being 105° to 135°. Dihedral angles in sulphide mineral aggregates vary from 102° to 134° (Stanton, 1964). Despite the spread of angles, all these aggregates are essentially polygonal in appearance (Figs. 4.23, 4.24), although some variable angles may be evident (Fig. 4.25).

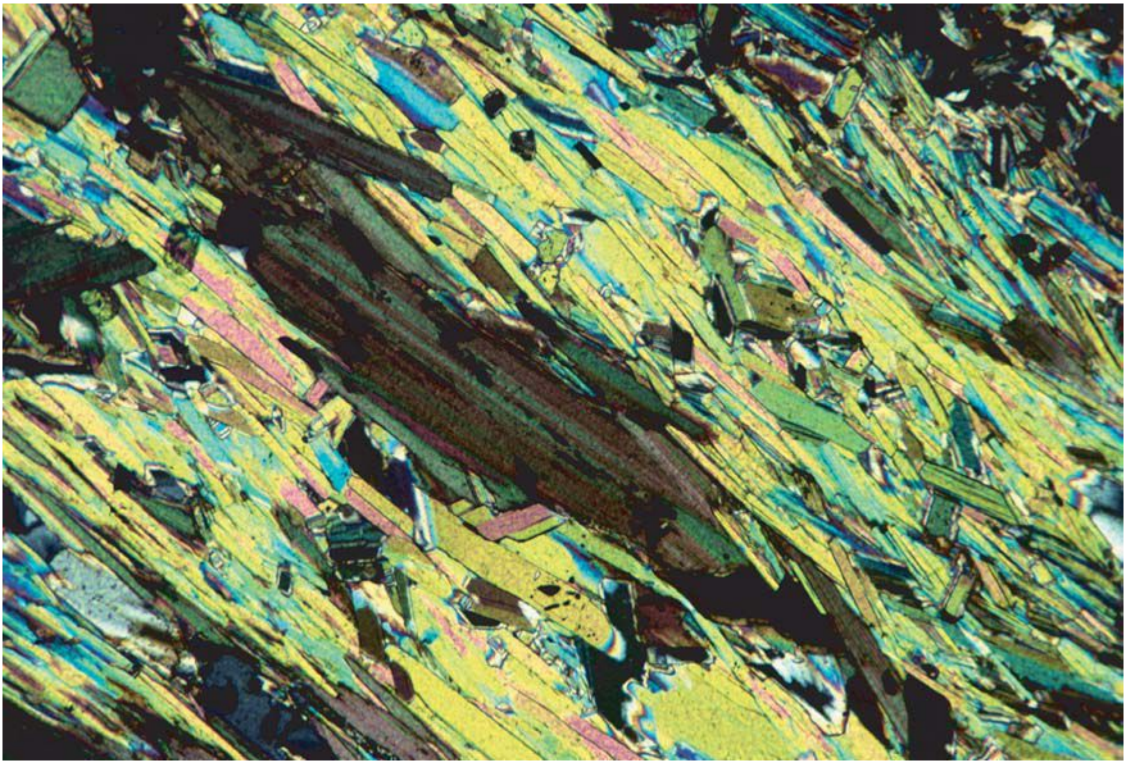

Fig. 4.14: Strongly aligned aggregate of muscovite and biotite, dominated by low-energy {001} crystal faces, Stirling Vale, Broken Hill, New South Wales, Australia. The brown absorption colour of the biotite dominates the high-order interference colours. Crossed polars; base of photo 1.75 mm.

Much smaller angles occur when melt is present (see, for example, Smith, 1953; Jurewicz & Watson, 1985), markedly changing the appearance of the aggregates, as discussed in Section 4.16.

4.2.5 Polymineral aggregates of structurally anisotropic minerals

In polymineral aggregates of structurally anisotropic minerals, such as biotite, muscovite and sillimanite, low-energy faces (rational-impingement interfaces) dominate, as discussed previously for single-mineral aggregates. Examples are biotite–sillimanite (Fig. 4.26) and biotite–muscovite (Fig. 4.14) aggregates.

4.2.6 Aggregates of both 'isotropic' and anisotropic minerals

In polymineral aggregates with both structurally isotropic and structurally anisotropic minerals, low-energy faces of the anisotropic minerals dominate the

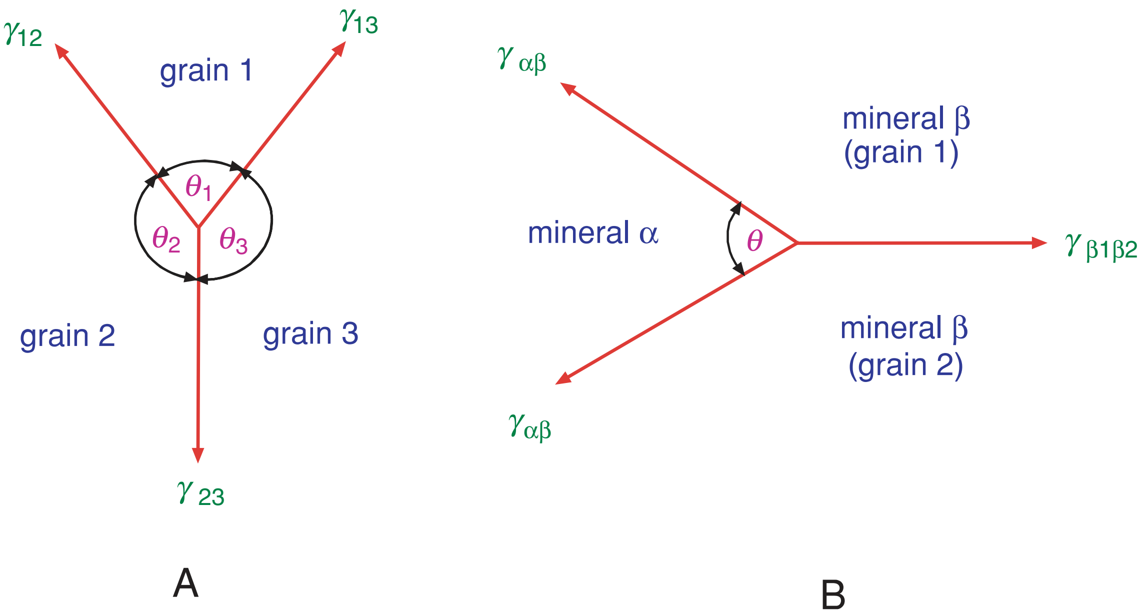

Fig. 4.15: Two-dimensional interfacial energy relationships at a triple junction for (A) a single-mineral aggregate and (B) a two-mineral aggregate, assuming perfectly isotropic materials. In (A) the interfacial free energies (γ) balance each other at equilibrium, producing interfacial angles of 120°. In (B), the dihedral angle (θ α vs. β/β) depends on the relative values of the grain boundary energy ($\gamma_{\beta\beta}$) versus the intermineral boundary energy ($\gamma_{\alpha\beta}$). If $\gamma_{\alpha\beta}$ is smaller than $\gamma_{\beta\beta}$, the area of the β/β boundary is reduced, producing a smaller dihedral angle.

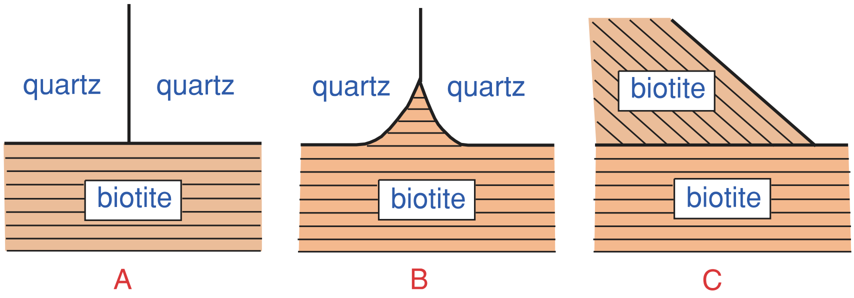

Fig. 4.16: (A) Typical *impingement* triple junction between two random grains of quartz and a crystal of biotite with {001} planes (shown diagrammatically as parallel lines) perpendicular to the plane of the drawing. (B) Hypothetical *adjustment* triple junction with a mica versus quartz/quartz dihedral angle of less than 180°.
(C) Impingement of one biotite grain on the {001} plane of another, the {001} planes of both being shown as parallel lines. After Vernon (1999a, fig. 11), with permission of the *Canadian Mineralogist*.

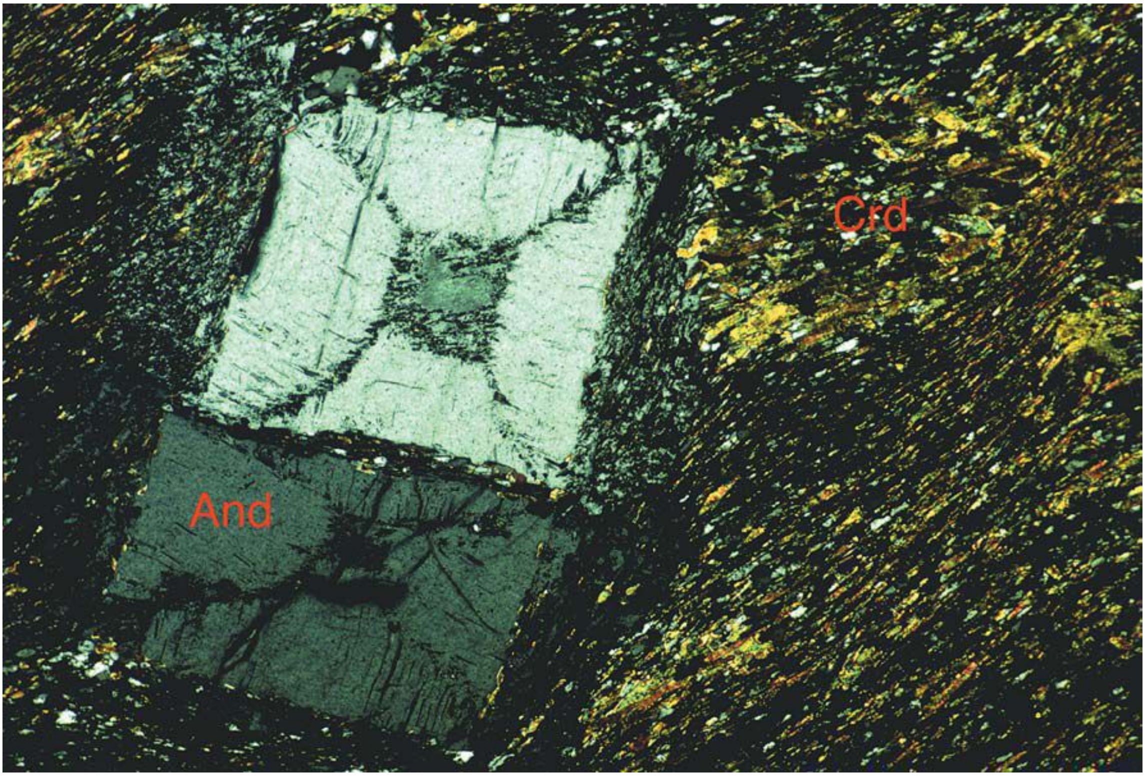

Fig. 4.17: Two idioblastic porphyroblasts of andalusite (And) with typical cruciform patterns of graphite-rich inclusions in a schist from the Foothills terrane, central Sierra Nevada, California, USA. Andalusite with this inclusion pattern is commonly called 'chiastolite'. Also shown is a xenoblastic porphyroblast of cordierite (Crd) that has been pseudomorphed by a biotite-rich aggregate, owing to a later metamorphic reaction. Crossed polars; base of photo 4.4 mm.

microstructure, such as {001} planes in mica and {110} planes in sillimanite (Figs. 4.11, 4.27–4.29). A common association in metamorphic rocks is quartz–mica or quartz–feldspar–mica. The {001} planes of the mica crystals are so stable that they remain unaffected by quartz–quartz or quartz–feldspar interfaces. In other words, biotite–quartz interfaces show no tendency to be drawn into dihedral angles (Figs. 4.11, 4.16). The result is that quartz–quartz and quartz–feldspar boundaries meet mica {001} faces at 90°, in order to minimize their area, or become attached to the ends of mica grains (Voll, 1960, 1961; Vernon, 1976, 1999a), as shown in Figs. 4.11, 4.16 and 4.27–4.29. Curved quartz–quartz and quartz–feldspar boundaries can move across the mica {001} surfaces, but when they reach an edge they become immobilized ('pinned'). This can result in elongate quartz and feldspar grain shapes in rocks with a strong alignment of mica grains (Fig. 4.29B), as noted long ago by Sorby (1877). This pinning effect

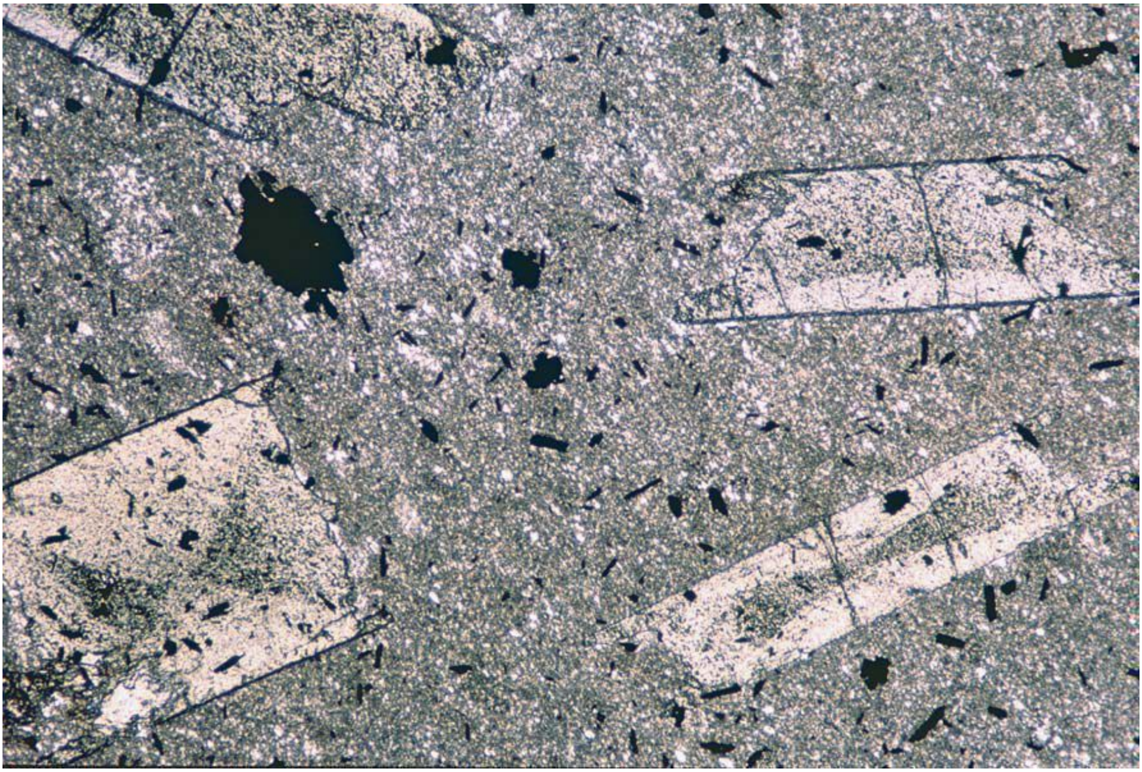

Fig. 4.18: Porphyroblasts of chloritoid, with crystal faces and sector zoning (Section 4.12.2) marked by concentrations of small opaque and quartz inclusions, in a metashale from the Grenville Province, Ontario, Canada. The faces at the bases of the sectors are irregular, owing to arrested partial inclusion of matrix quartz grains, whereas the faces parallel to the length of the porphyroblasts are much smoother. Plane-polarized light; base of photo 4 mm.

can also inhibit grain growth, with the result, for example, that layers of quartz with abundant small grains of mica are finer-grained than adjacent layers with fewer mica grains (Fig. 4.29B). In contrast, interfaces between quartz and biotite oblique to {001} form rounded adjustment boundaries (Vernon, 1999a, fig. 12), as shown in Fig. 4.30A, because of a lack of strong crystal anisotropy in the biotite {001} plane.

4.2.7 Low-energy shapes of inclusions

The shapes of included minerals (Section 4.3.2) are sensitive indicators of structural anisotropy, because the interface between an inclusion and its host is a true grain boundary. The inclusion typically belongs to the same mineral assemblage as the host mineral, and so the two are chemically compatible. Nevertheless, the interfacial energy of the inclusion–host boundary tends to a minimum, as

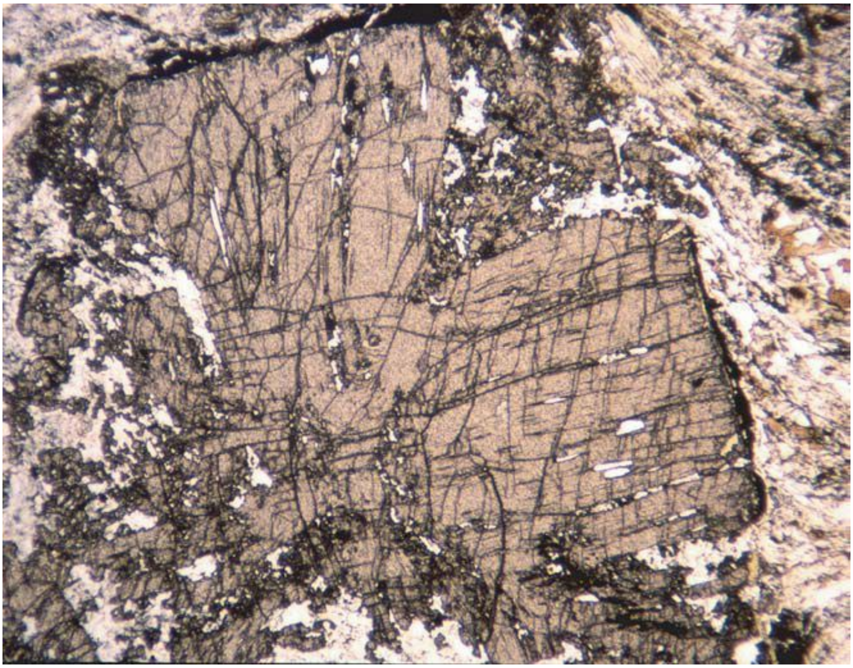

Fig. 4.19: Porphyroblast of garnet from the Chiwaukum Schist, Cascades, Washington, USA, showing opaque graphite 'bars', inclusion-rich re-entrants (producing a roughly dendritic habit) and tubular ('type-2') quartz inclusions (Section 4.3.3). Plane-polarized light; base of photo 9 mm.

it does in the surrounding aggregates of independent grains. If both inclusion and host are structurally isotropic, the resulting shape is a sphere, which has the minimum surface area per unit volume, and if both minerals are not too structurally anisotropic, spherical or elliptical shapes are approached (Fig. 4.30). Even where the inclusions are elongate and aligned (forming 'inclusion trails'; Section 4.3.2), they tend towards rounded shapes (Fig. 4.30B). Common examples are quartz inclusions in feldspar or cordierite, individual inclusions tending to be spherical, and aggregate inclusions showing dihedral angles where quartz–feldspar or quartz–cordierite interfaces meet quartz–quartz interfaces (Fig. 4.30).

However, if one mineral is relatively structurally isotropic and the other strongly anisotropic, planar low-energy boundaries appear, these effectively lowering the grain boundary free energy (Fig. 4.30). Even so, corners of the inclusions, which are sites of high atomic misfit (and hence high interfacial free energy), tend to be rounded (Fig. 4.30). Sections approximately parallel to the plane of strong structural anisotropy (e.g. sections that do not show the {001} cleavage of mica) tend to be rounded (Fig. 4.30), as all interfaces in such sections have approximately equal energies.

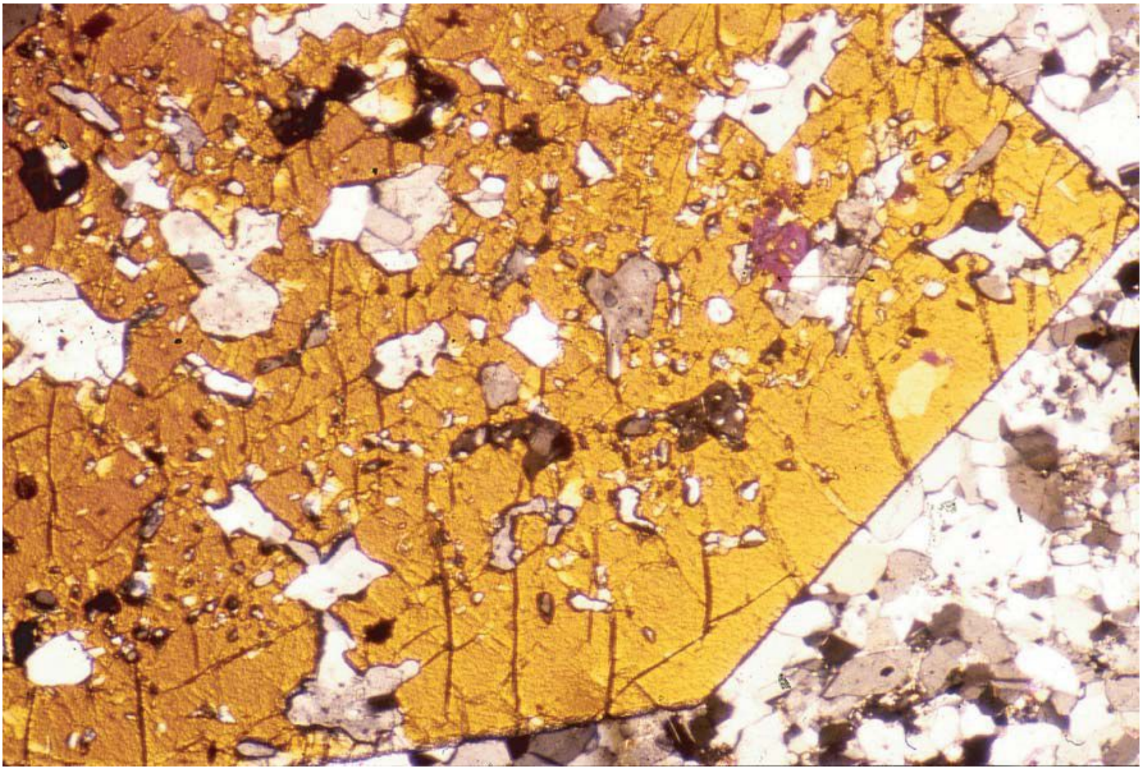

Fig. 4.20: Idioblastic porphyroblast of staurolite in a quartz-rich schist from Stirling Vale, Broken Hill, New South Wales, Australia. Although the porphyroblast has straight crystal faces against quartz in the matrix, the quartz inclusion shapes are irregular to rounded. Plane-polarized light; base of photo 3 mm.

Moreover, as with grains in aggregates, inclusion shapes can be modified by the presence of other minerals. For example, although quartz inclusions in K-feldspar normally approach spherical shapes, they can be partly planar or irregular if attached to small grains of strongly anisotropic minerals, such as sillimanite (Vernon & Flood, 1977).

4.2.8 Temperature dependence of dihedral angles

The discussion of grain shapes and dihedral angles in the foregoing sections assumes a close approach to equilibrium, which is probably reasonable, as the values reported are mainly from high-temperature metamorphic rocks, in which high temperatures are maintained for long periods. However, experimental evidence indicates that dihedral angles in two-mineral aggregates typically decrease with increasing temperature, so that minimum-energy angles and grainsizes may not be attained in lower-grade rocks. For example, Stanton & Gorman (1968)

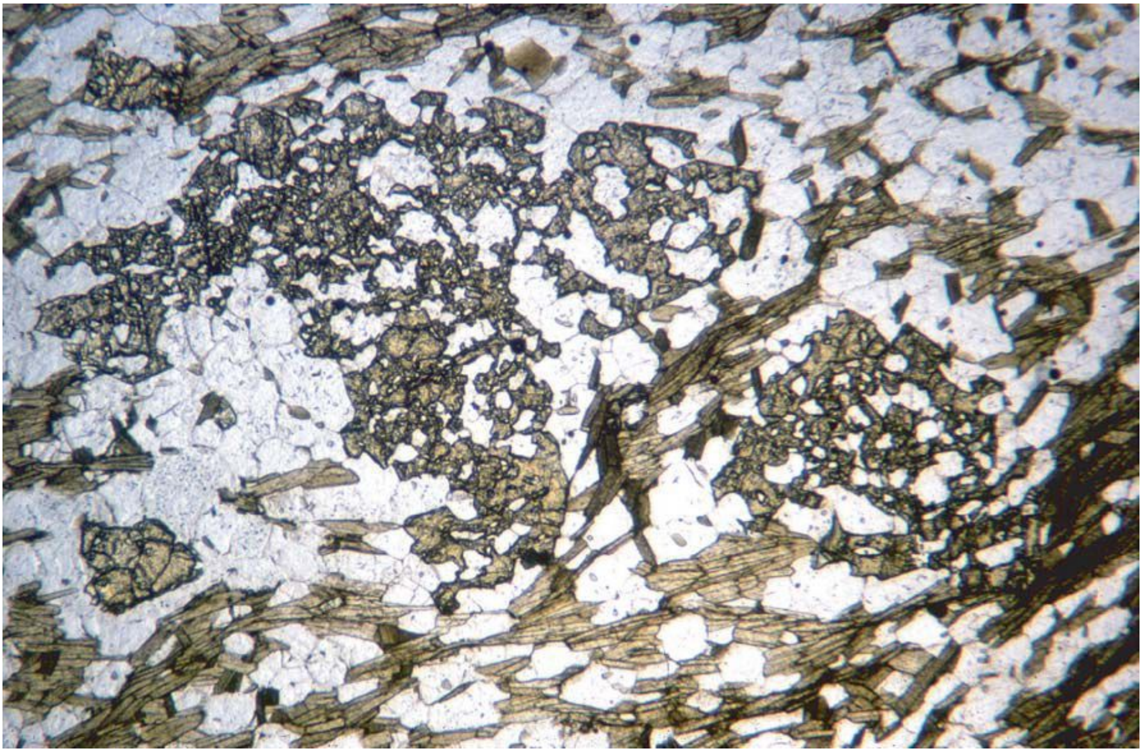

Fig. 4.21: Porphyroblast of staurolite with irregular xenoblastic shape (compare with Fig. 4.20) in a quartz–biotite matrix in a schist from the Mount Lofty Ranges, South Australia. Plane-polarized light; base of photo 3.5 mm.

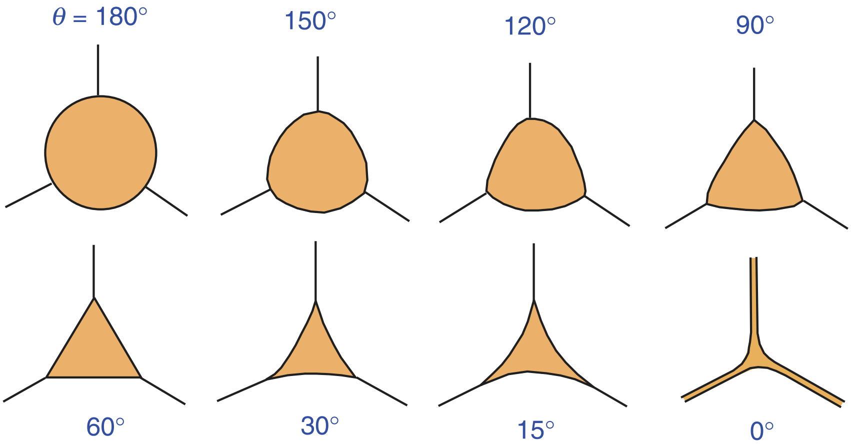

Fig. 4.22: Sketches showing the two-dimensional variation in the distribution of a minor mineral (stippled) at a triple junction between three grains of a major mineral, with variation in the dihedral angle.

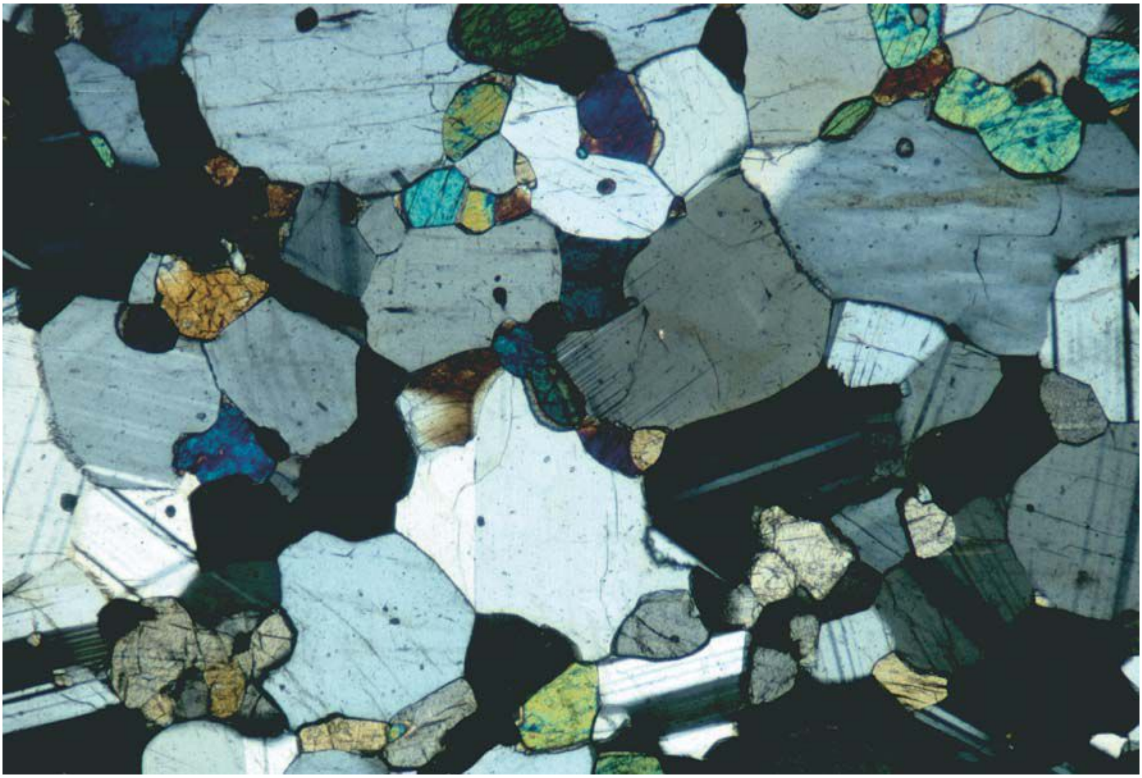

Fig. 4.23: Polygonal aggregate of plagioclase, orthopyroxene and clinopyroxene in a gabbro metamorphosed at granulite facies conditions. Most interfaces are smoothly curved at the optical scale. Crossed polars; base of photo 4 mm.

found experimentally that θ galena vs. sphalerite/sphalerite decreases between 300 and 1000 °C, and Lusk *et al.* (2002) showed experimentally that θ galena vs. sphalerite/sphalerite, θ sphalerite vs. galena/galena, and θ pyrrhotite vs. sphalerite/sphalerite all decrease between 280 and 980 °C. In addition, the experiments of S. Ikeda *et al.* (2002) showed that θ melt vs. olivine/olivine also decreases with increasing temperature (Section 4.6.1). On the other hand, experiments conducted by Holness *et al.* (1991) indicated that θ forsterite vs. calcite/calcite increased from 110° at 600 °C to 165° at 750 °C.

4.3 Grainsize and porphyroblasts

During grain growth in solid aggregates of the same mineral, a few grains may grow abnormally large, the process being called 'exaggerated grain growth' or 'secondary recrystallization' in materials science (see, for example, Kingery, 1960). However, in the early stages of metamorphism, minerals initially grow in

Previous Page

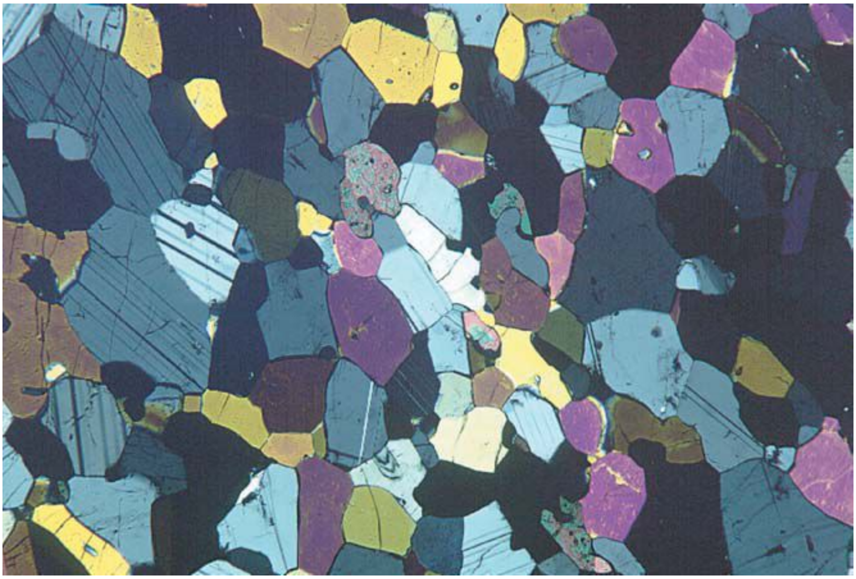

Fig. 4.24: Polygonal aggregate of plagioclase (first-order grey interference colours) and epidote (first- to second-order interference colours), Mount Painter, South Australia. From Vernon (2000b, fig. 121). Photo by Graham Teale. Crossed polars; base of photo 4 mm.

aggregates of different minerals, as isolated products of the chemical reactions. Thus, metamorphism involves nucleation and growth of new minerals, as in igneous rocks, before grain growth can occur.

4.3.1 Nucleation and growth of porphyroblasts

As with igneous rocks, the size of isolated crystals in metamorphic rocks depends on the ratio of nucleation rate (N) to growth rate (G). If abundant viable nuclei are able to form, many grains are produced, whereas if nucleation is difficult, few grains grow and well separated, large grains (*porphyroblasts*) are formed. The nucleation rate depends strongly on temperature, as well as on minerals available to act as nucleating agents. For example, nucleation may be assisted by crystallographic ('coaxial' or 'epitactic') relationships between new and old grains (see, for example, Bosworth, 1910; Chinner, 1961; Spry, 1969; Brearley, 1987; Vernon, 1987a; Worden *et al.*, 1991; Putnis, 1992), as illustrated in Figs. 4.2 and 4.3.

In theory, the number of viable nuclei may be controlled not only by the initial number produced, but also by a tendency of smaller ones to dissolve and larger ones to grow ('Ostwald ripening') while the crystal particles are at the submicroscopic scale, as discussed in Section 3.3.1. However, Carlson (2000,

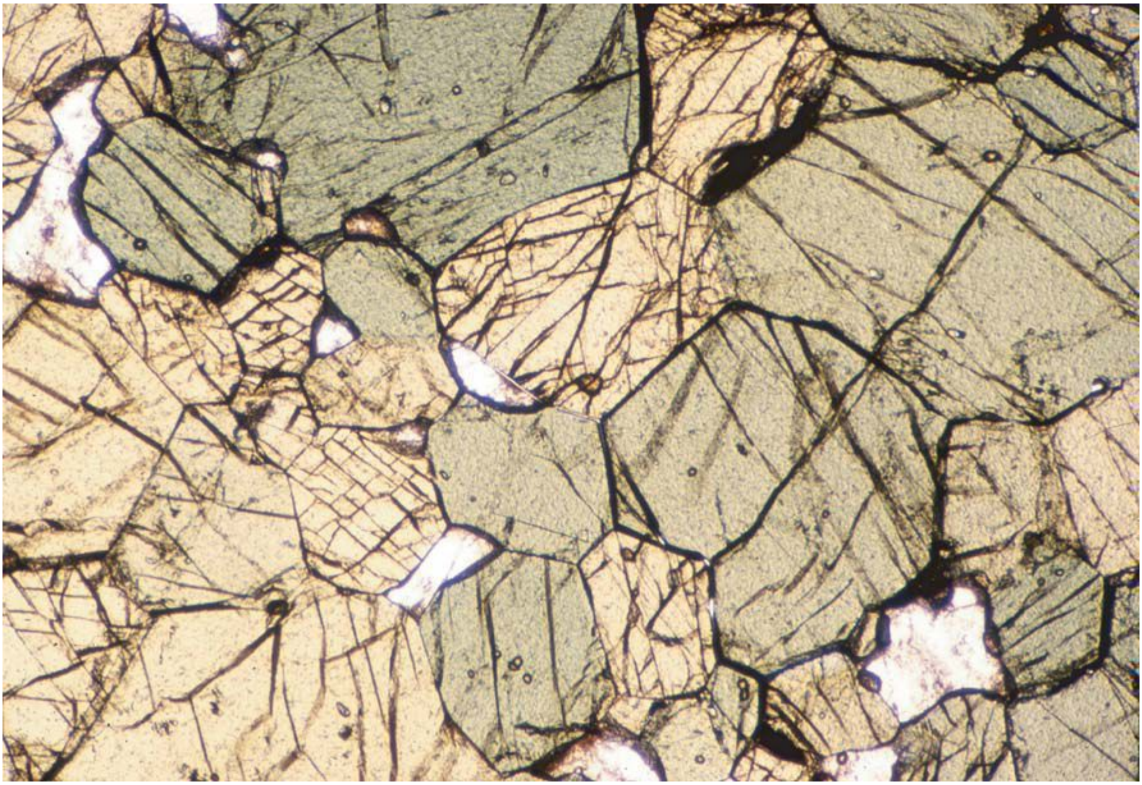

Fig. 4.25: Polygonal aggregate of clinopyroxene (shades of green) and plagioclase (colourless), showing relatively small θ plagioclase vs. clinopyroxene/clinopyroxene. Plane-polarized light; base of photo 4.4 mm.

p. 1031) has argued that nucleation and growth, not Ostwald ripening, are likely to control porphyroblast sizes, owing to their larger driving force (see below). The driving forces (chemical potential differences and corresponding concentration differences), and hence the resulting reaction rates, are many orders of magnitude larger for nucleation and growth than for Ostwald ripening (Carlson, 2000).

Porphyroblasts are large crystals or grains dispersed through a distinctly finer-grained matrix in a metamorphic rock (Figs. 4.17–4.21). Superficially they resemble phenocrysts in a finer-grained groundmass in igneous rocks. However, porphyroblasts generally grow at the same time as the minerals in the surrounding matrix, as products of the same prograde metamorphic reaction. No time difference is implied by a grainsize difference. This has been explained in detail by Vernon (1977a).

Porphyroblasts develop especially in metapelites (metamorphosed shales). During the progressive metamorphism of shale to slate, phyllite, schist and gneiss,

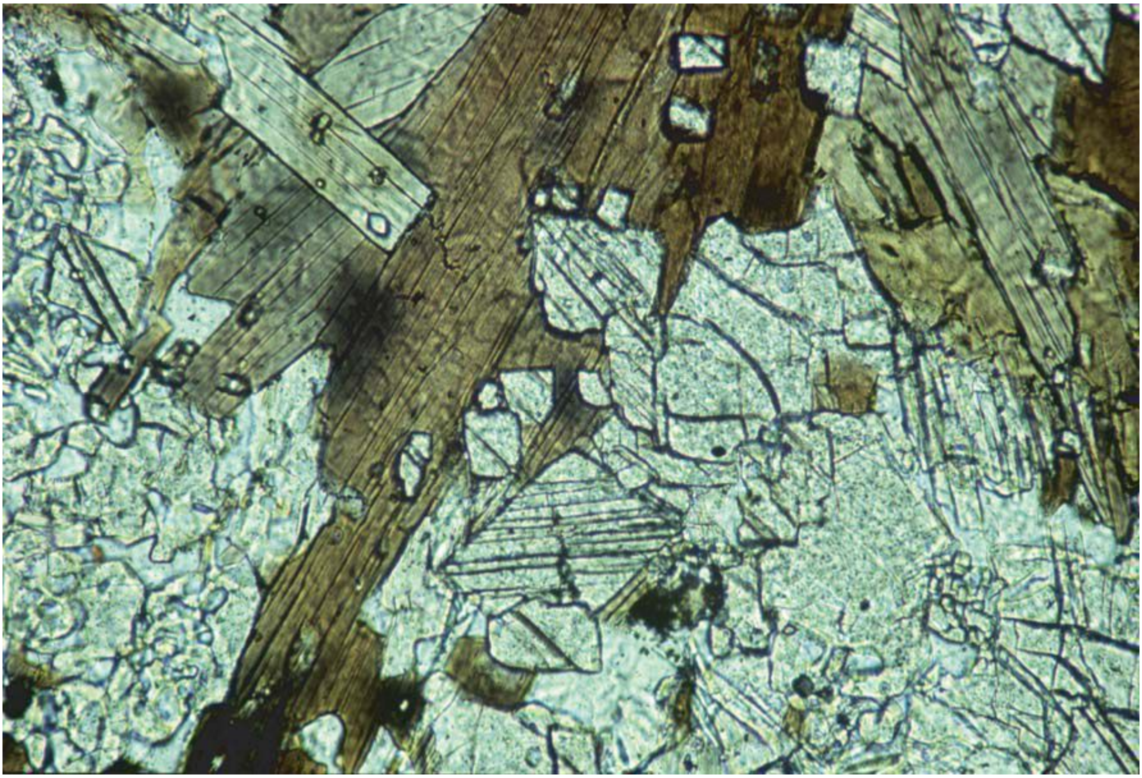

Fig. 4.26: Aggregate of biotite (brown) and sillimanite (colourless) in a high-grade metamorphic rock from Mount Stafford, central Australia, both minerals showing a strong tendency to preserve low-energy crystal faces. Plane-polarized light; base of photo 0.7 mm.

many nuclei are available for quartz and mica, which consequently form a relatively fine-grained matrix (high $N:G$). However, when minerals such as cordierite, andalusite, garnet and staurolite are produced by prograde reactions, few or no suitable minerals to act as nuclei are present, with the result that only a few nuclei can form, and therefore these minerals typically grow as porphyroblasts (Figs. 4.17–4.21).

At the same time as the porphyroblasts grow, mica and quartz in the matrix continue to grow, but remain as much smaller grains, owing to an abundance of suitable nuclei. Even at the highest metamorphic grades, readily nucleated minerals such as quartz, biotite and sillimanite may remain relatively fine-grained, commonly occurring as inclusions in, or as folia anastomosing around, large grains of the other minerals, such as garnet, cordierite and K-feldspar (Fig. 4.31). One of the reasons for the fine grainsize of sillimanite may be that it appears to nucleate easily in mica (Chinner, 1961; Vernon, 1979, 1987a).

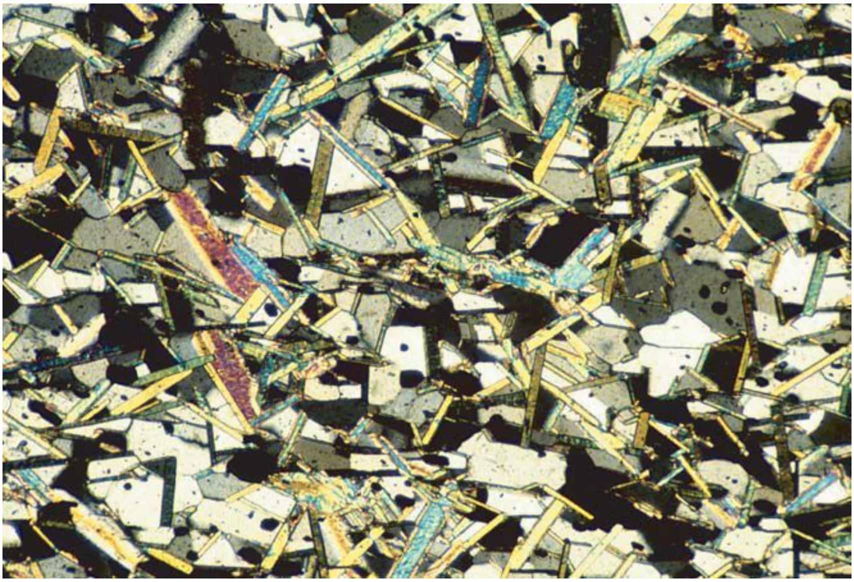

Fig. 4.27: Aggregate of quartz (first-order grey interference colours) and muscovite (higher-order interference colours) in a high-grade (amphibolite facies) metamorphic rock from the Grenville Province, Ontario, Canada. The microstructure is dominated by {001} crystal faces of the muscovite, the quartz grains being 'interstitial'. However, this does not mean that the quartz grew after the muscovite, as both minerals grew simultaneously as part of the same paragenesis. Crossed polars; base of photo 2 mm.

Both fine-grained and coarse-grained minerals can belong to the same compatible mineral assemblage (Vernon, 1996a). Unfortunately, some have made the unjustified assumption that the minerals in finer-grained folia form later than the porphyroblasts around which the folia anastomose (Fig. 4.31), whereas commonly they grow simultaneously in the folia because of their ability to nucleate readily and survive under conditions of strong deformation. This is simply an example of *deformation partitioning*, as emphasized by Bell & Rubenach (1983) and discussed in Section 5.7.

The common preservation in porphyroblasts of inclusion trails (Section 5.10.1) outlining pre-existing microstructures (Fig. 4.30B), such as microfolds and bedding, indicates that porphyroblasts replace an equal volume of old matrix minerals. This is also implied by uncommon porphyroblasts that preserve the shapes of former matrix mica grains, as discussed in relation to prefoliation porphyroblasts in Section 5.10.7. Of course, this does not mean that the entire metamorphic reaction is restricted to the volume now occupied by the porphyroblast, as chemical components are exchanged with other grains that are dissolving and growing throughout the rock. In addition, Vernon & Flood (1979), Lister *et al.* (1986), Miyake (1993) and Barker (2002) have shown that parts of porphyroblasts may

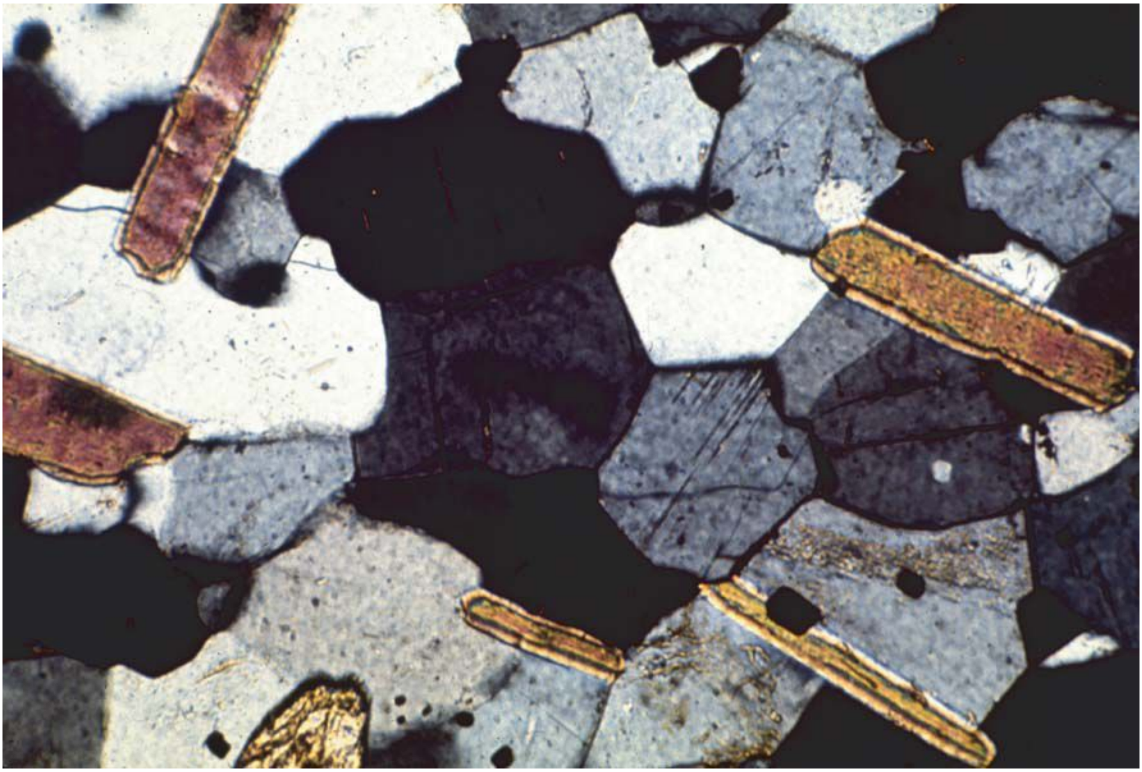

Fig. 4.28: Aggregate of quartz, feldspar (with cleavage) and biotite in a high-grade (amphibolite facies) metamorphic rock from the Grenville Province, Ontario, Canada. Although the quartz and feldspar form polygonal aggregates, interfaces between these minerals meet biotite {001} planes at right angles or attach to the ends of the biotite grains. Crossed polars: base of photo 1 mm.

grow by the filling of cracks opening during deformation at relatively low metamorphic grades ('crack–fill porphyroblastesis'). The growth of matrix minerals may or may not involve equal-volume replacement of old minerals, depending on local mass transfer and mineral density changes. This may apply also to porphyroblasts without inclusion trails.

As mentioned previously, new minerals require nucleation, and this involves some 'overstepping' of the temperature and/or pressure of the reaction boundary. If the overstepping is large enough, owing to nucleation difficulties (Rubie, 1988), a metastable reaction may occur (see, for example, Hollister, 1969; Vernon, 1976; Rubie, 1988; Waters & Lovegrove, 2002). In addition, some minerals may survive into a pressure–temperature stability field in which they are unstable. This is known as *metastable persistence*. For example, metastable persistence of andalusite into the stability field of sillimanite is common in the prograde metamorphism of metapelitic rocks (Vernon, 1987a). Another example has been

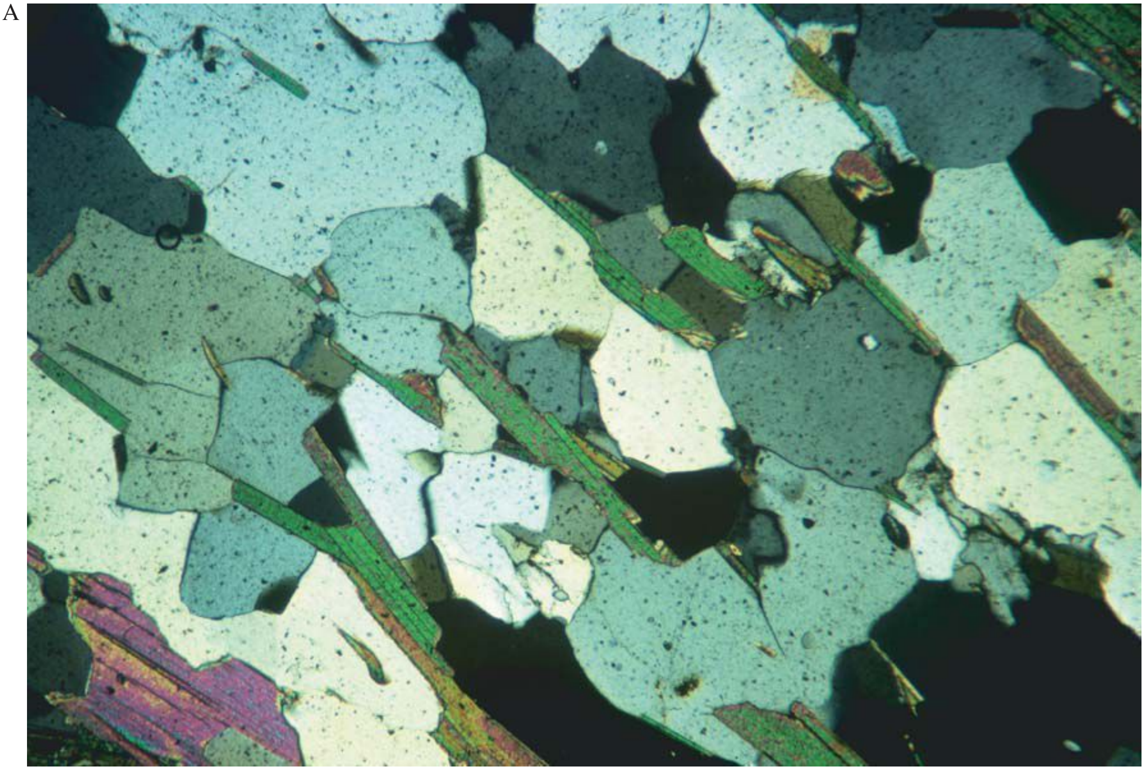

Fig. 4.29: (A) Aggregate of quartz and aligned mica (muscovite and biotite) in a high-grade (amphibolite facies) metamorphic rock from Mount Isa, Queensland, Australia. Owing to the dominance of the mica {001} planes, some of the quartz grains tend to be elongate parallel to the foliation caused by the mica grains. Crossed polars; base of photo 3.5 mm. (B) Quartz–quartz grain boundaries meeting quartz–(001) muscovite boundaries at right angles, or 'pinned' to the ends of the muscovite grains, leading to elongated, rectangular shapes of some of the quartz grains, as well as to a markedly smaller grainsize in the mica-rich layer. Simplon area, Lepontine Alps. Photo by Neil Mancktelow. Crossed polars; base of photo 9 mm.

described by Waters & Lovegrove (2002), who noted that the sequence of porphyroblast development inferred from microstructures in contact metamorphic rocks beneath the Bushveld Complex, South Africa, shows considerable overlap of the growth periods of porphyroblasts of staurolite, cordierite, biotite and andalusite, and the metastable persistence over a similar interval of the inferred reactant mineral, chloritoid. The inferred order of appearance and disappearance of the porphyroblastic minerals is different from the order predicted from calculated equilibrium phase relationships (Waters & Lovegrove, 2002), showing the potential importance of kinetic factors, such as nucleation rates, in determining the actual metamorphic history.

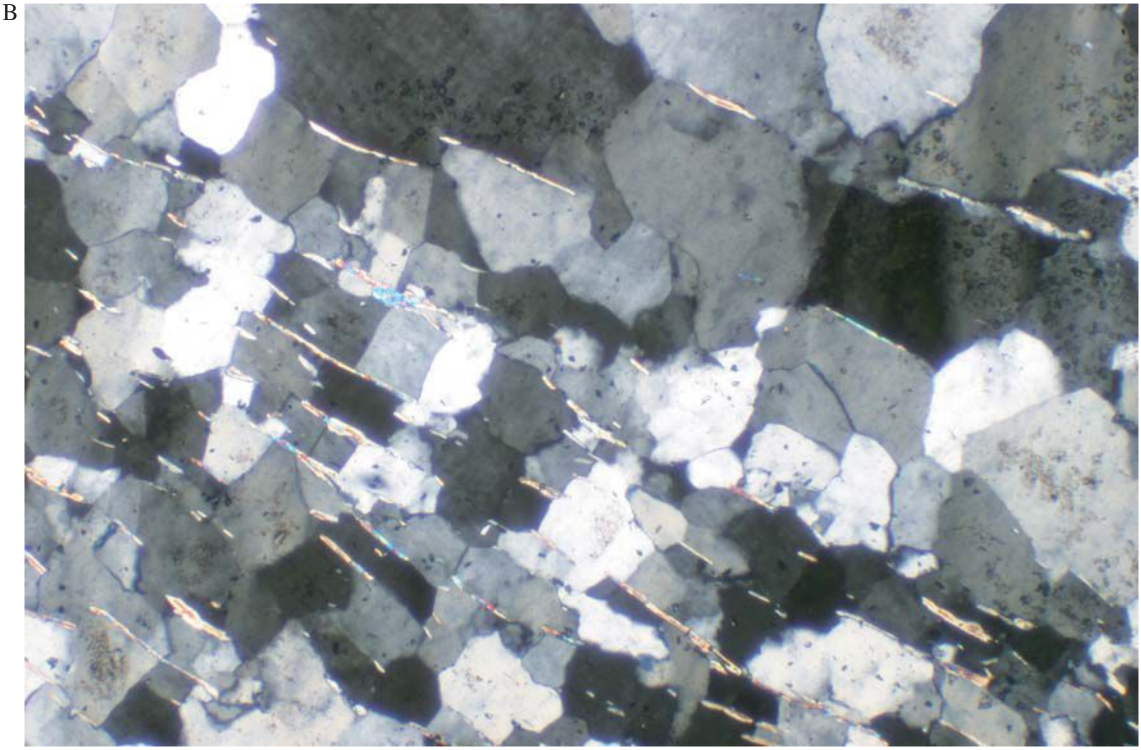

Fig. 4.29: (*cont.*)

As summarized by Daniel & Spear (1999), the processes involved in the nucleation and growth of metamorphic minerals are: (1) after some overstepping of the reaction pressure–temperature boundary, the reactant mineral locally breaks down (presumably dissolving in a small amount of fluid in most instances); (2) the new mineral nucleates; (3) nutrient chemical components are transported to the nucleus and waste components are transported away; and (4) the nutrient components are incorporated into the growing mineral at the interface with the matrix. Denison & Carlson (1997) found that three-dimensional spatial distributions, crystal size distributions (CSD) and compositional zoning patterns indicate that the nucleation and growth rates of garnet porphyroblasts are controlled by rates of transport of chemical components though intergranular fluid. This has been confirmed by Hirsch *et al.* (2000) in an evaluation of spatial correlation functions. Presumably transport-controlled nucleation and growth mechanisms also govern growth of most other porphyroblasts.

This should not be taken to imply that a fluid covers all grain boundaries in metamorphic rocks, as this would tend to weaken the rock by reducing the effective normal stress across the boundaries. However, a relatively connected network of fluid-filled pores may be established and maintained by local fluid

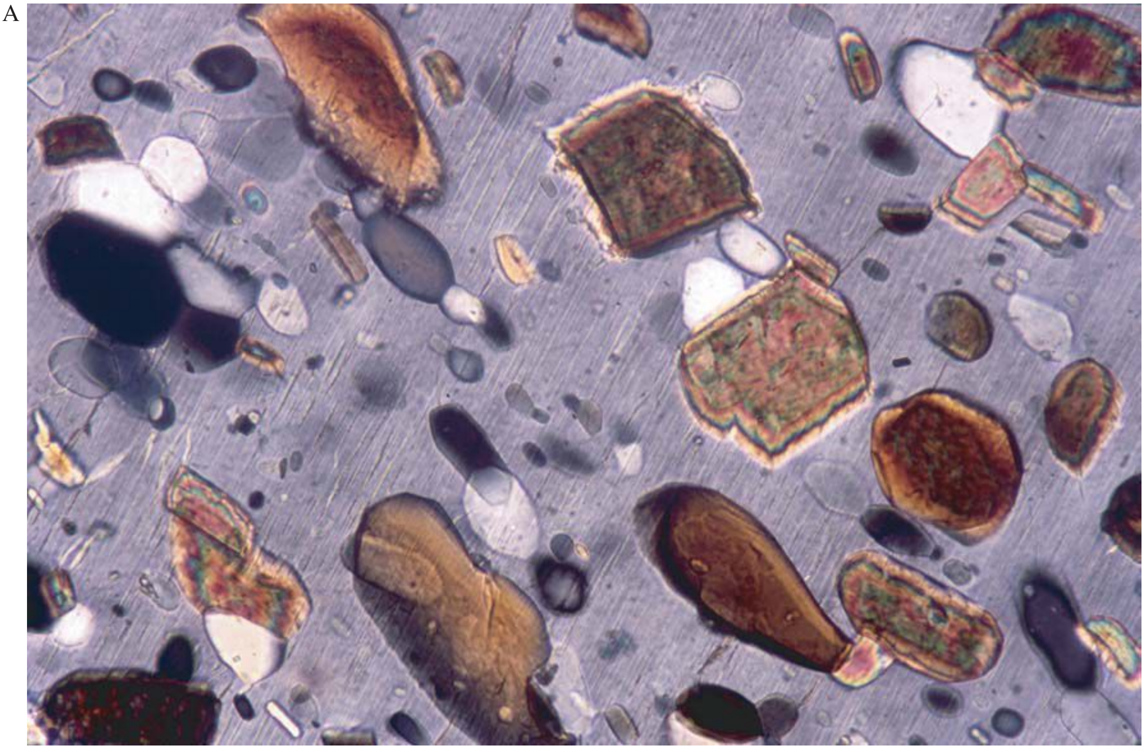

Fig. 4.30: (A) Inclusions of quartz and biotite (brown) in K-feldspar, Cooma Complex, south-eastern New South Wales, Australia. The quartz inclusions are rounded, and quartz–feldspar interfaces show dihedral angles where they meet quartz–quartz interfaces. Sections of biotite inclusions with cleavage show {001} crystal faces (commonly with rounded corners), whereas sections of biotite inclusions without cleavage are rounded. Also shown are thin, continuous, regular exsolution lamellae of albite (Section 4.9). Crossed polars; base of photo 0.7 mm. (B) Elongate, aligned inclusions of microcline, forming *inclusion trails* ('internal foliation') in andalusite, Mount Stafford area, central Australia. The inclusions have rounded shapes. Crossed polars; base of photo 1.5 mm.

pockets, especially during deformation, as openings are made in response to different deformation rates of adjacent grains of unlike orientation and unlike minerals, as well as by forced opening of local fractures by fluid released by metamorphic devolatilization reactions.

Compared with CSDs for volcanic igneous rocks (Section 3.4), CSDs for metamorphic rocks (apart from porphyroblasts) generally show a more restricted range of grainsizes. For relatively even-grained aggregates, including typical matrices of porphyroblastic rocks, this distribution is due to grain growth (Section 4.2), which tends to eliminate smaller grains and produce relatively uniform grainsizes, resulting in normal (gaussian, bell-shaped) CSD curves (Covey-Crump &

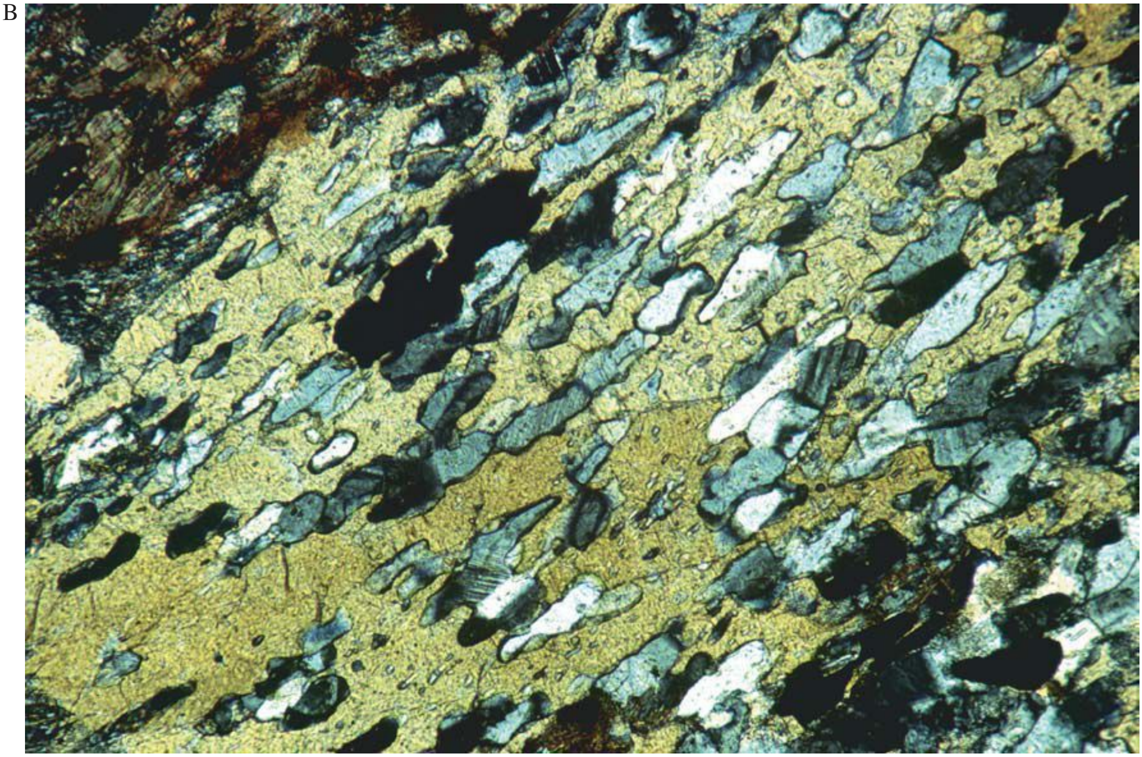

Fig. 4.30: (*cont.*)

Rutter, 1989; Buntebarth & Voll, 1991; Miyake, 1998; Nam *et al.*, 1999). The grain growth process has been referred to by some people as 'Ostwald ripening' (Sections 3.3.2, 3.4.3). However, the intergranular diffusion rate of Al is too slow to permit 'Ostwald ripening' to control the sizes of crystals larger than a fraction of a micrometre (Carlson, 1999, 2000). An example of inferred mineral growth by Ostwald ripening in the appropriate micrometre size range is the hydrothermal growth of monazite crystals achieved experimentally by Ayers *et al.* (1999). As noted in Section 3.4.2, the statistical validity of the current CSD approach has been challenged and is under discussion.

CSD curves for garnet porphyroblasts studied by Jones & Galwey (1964) are similar to those of volcanic rocks (Section 3.4.2) and appear to reflect nucleation and growth processes. CSD curves for garnet and magnetite porphyroblasts in some schists (Cashman & Ferry, 1988) are partly curved and bell-shaped, in response to a deficiency of smaller sizes, compared with CSDs of volcanic rocks (Fig. 4.32). However, the CSDs are straighter lines for larger grainsizes (Fig. 4.32). Cashman & Ferry (1988) interpreted these curves as resulting from grain growth (reducing the number of smaller grains and accounting for the curved

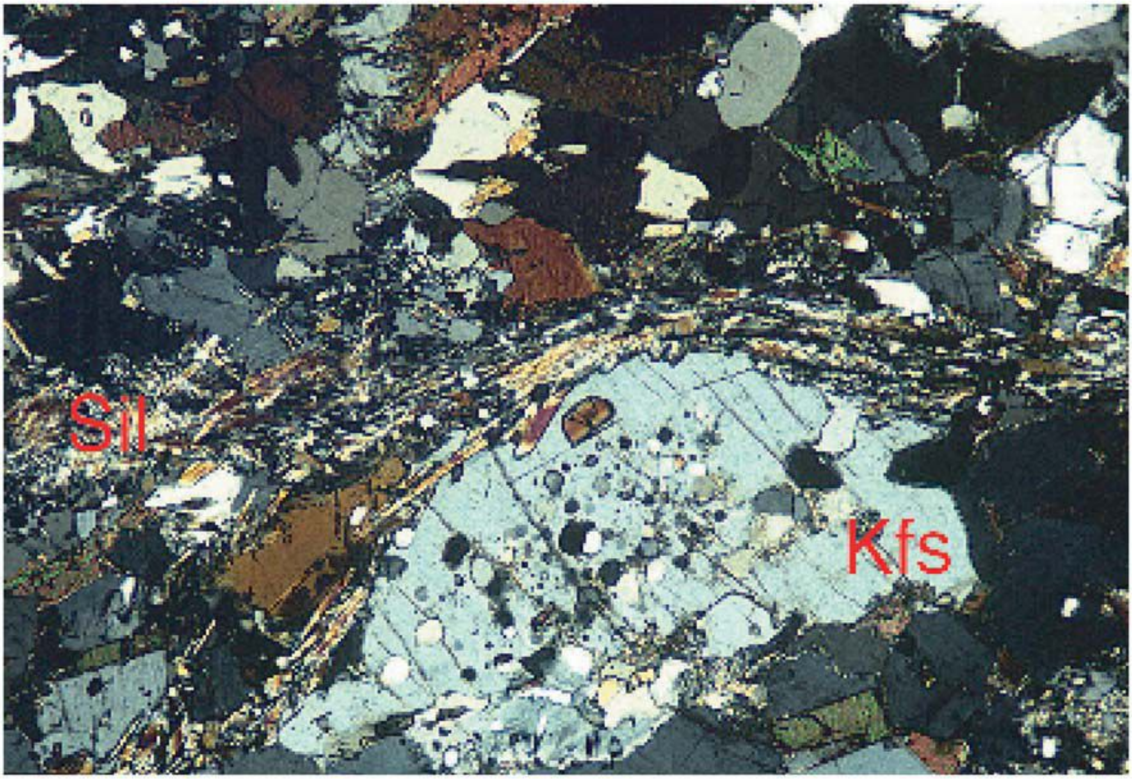

Fig. 4.31: Folium of fibrous and prismatic sillimanite anastomosing around a porphyroblast of K-feldspar with rounded inclusions of quartz, in a metapelitic gneiss from Broken Hill, New South Wales, Australia. Minerals in the folium and the porphyroblast may belong to the same mineral assemblage (Sections 4.3.4, 4.13.4). From Vernon (2000b, fig. 155). Crossed polars: base of photo 4.4 mm.

part of the CSD curve) following normal nucleation and growth (accounting for the straight part). Despite the inferred addition of material from former small grains onto the larger grains, their overall size distribution was inferred to be relatively unaffected. Therefore, Cashman & Ferry (1988) concluded that the larger porphyroblasts are reliable indicators of nucleation and growth processes, but that smaller grain sizes are not, as they have been reduced in size. However, Carlson (1999, 2000) stated that, although grain coarsening is typical for single-mineral and many polymineral aggregates (Section 4.2), it is unlikely to apply to separated porphyroblasts (in agreement with Jones & Galwey, 1964); this is because the process is too slow to affect the CSD, and the mechanisms involved are quite different, involving solution, transport in fluid and reprecipitation. The diffusional transport would have to occur along grain boundaries from small crystals to large ones, over distances of the order of the mean separation between porphyroblasts.

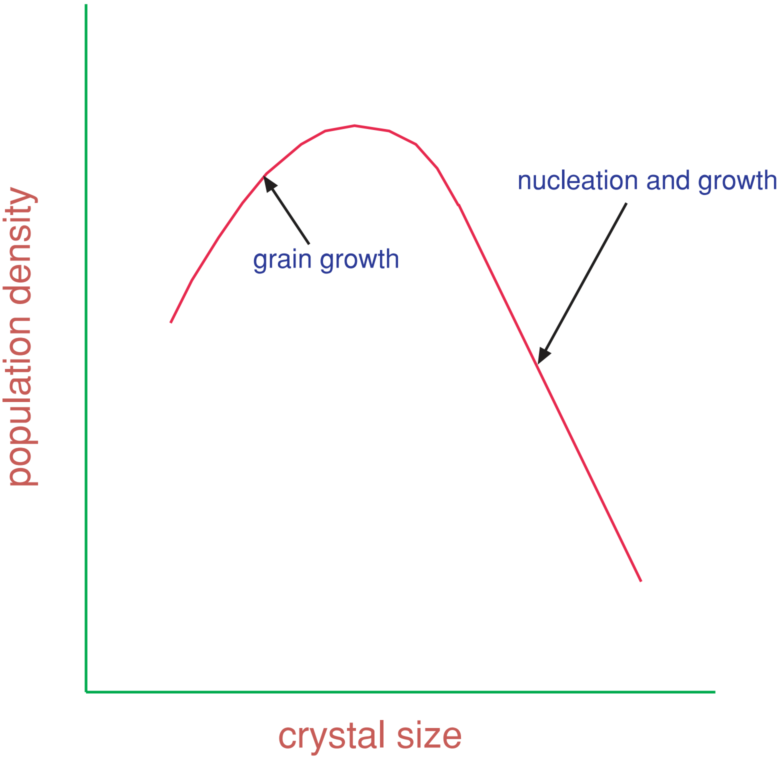

Fig. 4.32: Typical CSD plot for porphyroblasts in metamorphic rocks, based on Cashman & Ferry (1988), showing a curved portion, which they infer reflects grain growth (reduction in the proportion of small grains), and a straight portion reflecting nucleation and growth.

Because the growth of porphyroblasts is controlled by diffusion rates in the matrix, existing porphyroblasts deplete the local supply of nutrient components, and so suppress nucleation in the nearby matrix. This leads to spatial ordering of crystal centres. As this process continues, depleted zones around adjacent porphyroblasts impinge, with the result that these porphyroblasts tend to be smaller than more isolated crystals that nucleate at the same time (Hirsch *et al*., 2000).

Another aspect of the problem was discussed by Ridley (1985), who emphasized that in metamorphic reactions absorbing large amounts of heat (strongly endothermic reactions) the local temperature can fall in response to nucleation of a mineral produced in the reaction. This can suppress further nucleation of that mineral, so that growth continues on existing nuclei, resulting in a normal CSD with a grainsize maximum and relatively few small crystals. In reactions involving small amounts of heat absorption, the suppression of nucleation is less, and small grains tend to predominate.

The observed general increase in average grainsize with increasing metamorphic grade is the result of nucleation and growth occurring over a range of temperatures (Carlson, 1999). Nucleation rates increase with the amount of overstepping of the reaction temperature boundary, and diffusion rates increase with increasing temperature. At higher metamorphic temperatures, diffusion rates dominate nucleation rates, so that rapid growth occurs on few nuclei, whereas at lower metamorphic temperatures, nucleation rates dominate diffusion rates, so that slower growth occurs on more nuclei (Carlson, 1999).

Porphyroblasts are generally thought of as growing from single, separated nuclei, as they are mostly single crystals, well separated from other porphyroblasts. Spear & Daniel (1998) explained complex compositional variations inside some garnet porphyroblasts as being due to coalescence of close, distinct nuclei, but later electron backscatter diffraction and orientation contrast imaging has shown that the garnet porphyroblasts concerned are crystallographically continuous, so that conventional nucleation applies (Spear & Daniel, 2001; Hirsch *et al.*, 2003). Mn-rich areas in the porphyroblasts were evidently incorporated into the garnet structure from Mn-rich precursor minerals, forming 'overprint zoning' (Hirsch *et al.*, 2003). However, Spiess *et al.* (2001) and Dobbs *et al.* (2003) described a rare example of composite garnet porphyroblasts that appear to have grown from many clustered nuclei. Fig. 4.33 shows garnet crystals that grew from separate, close nuclei and have impinged on and become moulded around each other; no time difference in nucleation is implied by this microstructure.

Various models for factors controlling the growth of garnet in metamorphic rocks have been proposed, which apply under different circumstances. For example, Kretz (1966b, 1973) inferred that the spatial distribution of garnet grains in a schist from Yellowknife, Canada, is random, and that the sizes of the garnet grains are unrelated to the distance to their nearest neighbour grains. This, together with the nature of compositional zoning in crystals of different sizes, indicates that the rate of increase of surface area is approximately constant, which implies that the reaction rate increases with time, possibly as a result of temperature increase with prograde metamorphism. New garnet crystals nucleate constantly during the period of garnet production, and the crystal distribution indicates that N increases and then decreases, locally pulsating and so producing a bimodal or trimodal size distribution. However, the garnet of another schist in the same area suggests that $N : G$ and the reaction rate may vary considerably from place to place, even where the overall temperature distribution is the same (Kretz, 1973). The variation may be due to the different reactant compositions or minerals, strain variations and differences in the ability of water to escape during metamorphism.

Daniel & Spear (1999) found a weak to strong clustering of garnet porphyroblasts in a schist from Connecticut, USA, the clustering possibly reflecting minor bulk compositional variations. They found only a very weak correlation between crystal size and nearest-neighbour distance, broadly in agreement with the result

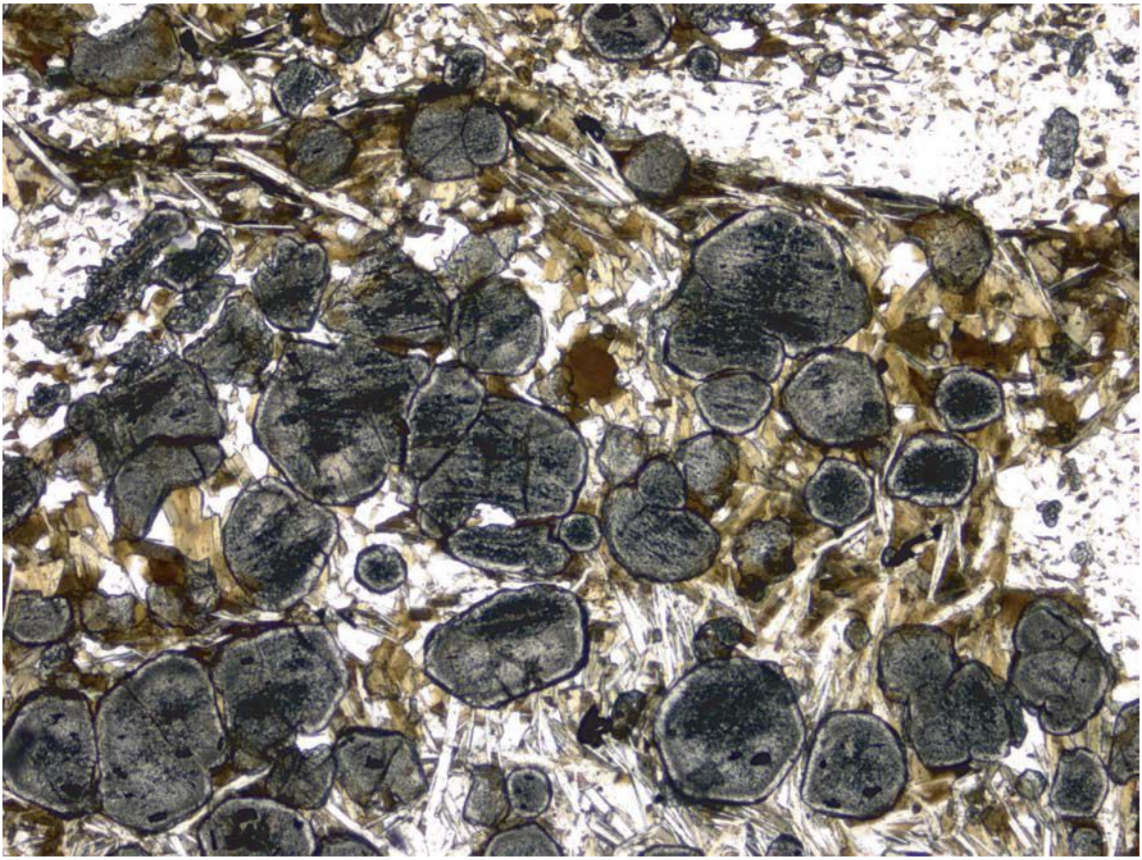

Fig. 4.33: Garnet crystals that have impinged on and moulded around each other, having grown from separate nuclei. No time difference between grains is necessarily implied by the moulding. Specimen by courtesy of Charles Guidotti. Plane-polarized light; base of photo 3 mm.

of Kretz (1966b). They also used radius – growth rate plots, calculated from electron microprobe composition maps of the garnet crystals, to show that garnet crystals of different sizes grew at similar rates, and they inferred progressive nucleation with prograde metamorphism.

Kretz (1973, 1974) suggested that garnet maintains equilibrium with the *P–T* conditions during growth, its composition changing as reactants are used up as the reaction proceeds (Carlson, 1989, 1991; Carlson & Denison, 1992; Carlson *et al*., 1995; Denison & Carlson, 1997; Foster, 1999). If the distances over which diffusion is effective are relatively large, all garnet porphyroblasts are similarly affected. However, in some situations, the diffusion distances are relatively short, so that the changing garnet compositions (1) reflect reaction progress in local zones around each porphyroblast (Chernoff & Carlson, 1997, 1999), (2) reflect components inherited from the distribution of precursor minerals (Daniel &

Spear, 1998; Hirsch *et al.*, 2003); and/or (3) are controlled by localized exchange reactions (O'Brien, 1999). Carlson (2002) suggested that local disequilibrium with respect to some chemical components, not others ('partial disequilibrium'), is common in prograde metamorphism. Moreover, a garnet composition may be modified (for example, during cooling) by diffusion of chemical components (obtained by local reaction with adjacent minerals) around its edges, especially close to fast diffusion pathways, such as fractures or grain boundaries (Matthews *et al.*, 1992; Erambert & Austrheim, 1993).

Some have suggested that porphyroblasts can physically push aside the surrounding matrix as they grow, rather than replacing it. This problem is discussed in Section 5.10.11, in relation to the relative timing of mineral growth and deformation. The process is doubtful, although pressure exerted by a growing crystal conceivably could cause solution of adjacent grains and hence promote further growth of the porphyroblast (Fletcher & Merino, 2001), as suggested for the fracturing of adjacent quartz by growing calcite crystals in sedimentary rocks (Buczynski & Chafetz, 1987; Maliva & Siever, 1988; Dewers & Ortoleva, 1990).

Ferry (2001) related 'force of crystallization' to the development of porphyroblasts, suggesting that the negative volume change of hydration and carbonation reactions typical of retrograde metamorphism (Sections 4.4.1, 4.13.5) causes a low 'force of crystallization' and so promotes pseudomorphism by making space for new minerals in the confines of the old mineral. In contrast, he inferred that the positive volume change of dehydration–decarbonation reactions typical of prograde metamorphism favours growth of new minerals outside the confines of the old mineral grain. However, pseudomorphs formed by prograde metamorphic reactions have been described (see, for example, Guidotti & Johnson, 2002). Moreover, the main controlling factor in pseudomorphism is conservation of volume of the solid minerals involved in the replacements, rather than the volume change of the total reaction (Putnis, 2002, p. 692).

A common observation is that, in graphitic schists, the growth of porphyroblasts of andalusite (generally chiastolite) and garnet in fine-grained layers rich in white mica and graphite may result in the accumulation of these minerals (especially graphite) as bars or arcs (domes) adjacent to crystal faces (Harker, 1932, fig. 7; Spry, 1969, plate XIIIc; Ferguson *et al.*, 1980; Ward, 1984a,b; Rubenach & Bell, 1988; Rice & Mitchell, 1991; Rice, 1993; Vernon *et al.* 1993b), as shown in Fig. 4.19. The growth of the porphyroblast by replacement of the matrix appears to involve solution of most components and passive concentration of the inert graphite ahead of the advancing crystal face, space for the graphite presumably being made by solution of matrix minerals (see, for example, Yardley, 1974). The symmetrical shapes of the arcs or domes suggest that the graphitic concentrations are formed independently of deformation. For example, the chiastolite porphyroblast with graphitic domes and bars illustrated by Spry (1969, plate XIIIc) grew after formation of the matrix foliation, which passes continuously into the porphyroblast as inclusion trails (Section 5.10.1).

Some porphyroblasts may be relics that survive later reactions, both in prograde and especially retrograde metamorphism (Sections 4.1, 4.13), and in mylonite zones (Section 5.7.6). Therefore, care must be taken when inferring whether or not porphyroblasts belong to a mineral assemblage that grew at a particular time or at a particular set of metamorphic conditions (Vernon, 1996a).

4.3.2 Inclusions in porphyroblasts

Owing to their relatively low $N : G$ ratios, porphyroblasts overtake and enclose smaller grains (*inclusions*) of matrix minerals (Figs. 4.17–4.21, 4.30 and 4.31). Some inclusions may be relics inherited from lower grades of metamorphism (see below), but generally most belong to the same metamorphic assemblage as the porphyroblast. That is, the inclusions are generally either products of, or excess reactants in, the prograde reaction that produced the porphyroblast. Therefore, many or most of them grow at the same time as (but at a much slower rate than) the porphyroblast that engulfs them. Consequently, the inclusions do not react chemically with the porphyroblast, but tend to change their shapes to minimize the interfacial free energy of their boundaries with the porphyroblast (Section 4.2.7). This mutual grain-boundary adjustment confirms that the two minerals were chemically compatible under the prevailing metamorphic conditions. The use of inclusion trails in porphyroblasts to relate mineral assemblages to deformation events is discussed in Section 5.10.

Inclusions of minerals inherited from a previous assemblage may be either stable or metastable relics (e.g. quartz or graphite) or minerals from an unstable earlier assemblage (absent from the matrix) trapped in the porphyroblast and hence isolated from further reaction with matrix minerals. Such inclusions have been used to unravel the metamorphic history (Krogh, 1982; St Onge, 1987).

Putnis (2002) suggested that inclusions in porphyroblasts are minerals that crystallize in holes left from the pseudomorphous replacement of a pre-existing mineral grain by the porphyroblast. However, (1) no previous porphyroblast is generally present, (2) partial inclusions (projecting outside the porphyroblast) would have to represent former holes that somehow extended outside the original grain, when they are supposed to be the result of a pseudomorphous reaction, and (3) elongate holes would have to develop parallel to existing inclusion trails in order to allow the formation of inclusion trails in the new porphyroblast. The process is unlikely for most porphyroblasts.

4.3.3 Crystallographic (zonal) arrangement of inclusions

Sector inclusion patterns — called ‘textural sector zoning’ by Rice (1993) — are characterized by regular variations in the distribution of inclusions (Harker, 1932: Rast, 1965; Spry, 1969; Shelley, 1993; Andersen, 1984; Burton, 1986; Rice &

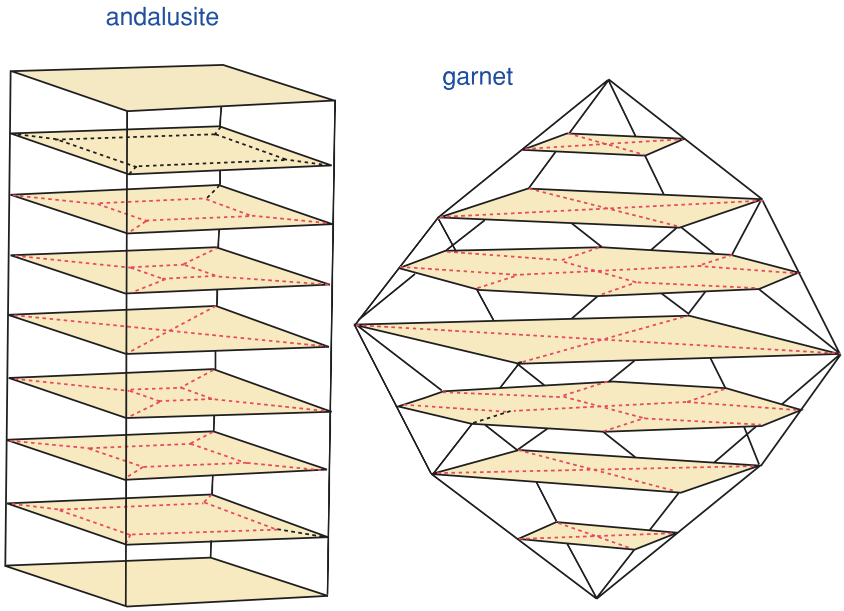

Fig. 4.34: Sector patterns of inclusions in series of sections through porphyroblasts of an orthorhombic mineral (staurolite or andalusite) and garnet. After Harker (1932, figs. 8B and 8C).

Mitchell, 1991; Rice, 1993; Hiroi *et al.*, 1998), as shown in Figs. 4.17, 4.18 and 4.34. As mentioned for igneous minerals in Section 3.11.11, a sector-zoned crystal consists of a set of 'growth pyramids', the apices of which join at the centre, the bases constituting the crystal faces (Fig. 3.84). The sector boundaries seen in thin section are the intersections between adjacent growth pyramids, and differently oriented sections though the crystal have very different sector patterns (Fig. 4.34). Within each pyramid, growth occurs in discrete units ('lineages') that are slightly misoriented with respect to each other, but approximately perpendicular to the growing crystal faces (Petreus, 1978). Sector inclusion patterns are prominent in chiastolite (a variety of andalusite with sector-zoned inclusion patterns, as shown in Fig. 4.17), garnet and, less commonly, staurolite and chloritoid (Fig. 4.18) in graphitic schists (Harker, 1932).

The inclusions are of two types (Rice, 1993). 'Type 1 inclusions' are incorporated from the matrix during growth of the porphyroblast, and so may preserve the geometry of pre-existing matrix microstructures (e.g. foliations); they are concentrated along the pyramid boundaries and are commonly fine-grained graphite (Fig. 4.17). 'Type 2 inclusions' (really intergrowths) are rod-shaped, single grains of quartz, from a few micrometres to 0.1 mm in diameter, that grow at the same time as, and in the growth direction of, the host crystal (Burton, 1986; Rice, 1993), as shown in Fig. 4.19. Similar Type 2 rods composed of a range of minerals, including quartz, rutile, graphite and pyrrhotite, have been described by Hiroi *et al.* (1998).

Possible mechanisms for forming the Type 1 inclusion patterns have been discussed by Frondel (1934), Spry (1969), Shelley (1993), Rice & Mitchell (1991) and Burton (1986). Frondel (1934) and Shelley (1993) suggested that the growing porphyroblast selectively adsorbs certain minerals (notably graphite) onto specific sites, especially edges and corners, which inhibits growth at these sites, causing re-entrants and concentrating inclusions in the characteristic 'Maltese cross' pattern (Figs. 4.17, 4.34). Passively concentrated graphite (Yardley, 1974) could also be concentrated in the re-entrants.

In some sector inclusion patterns, one pair of sectors contains more inclusions than the other. This difference may be due to faster growth rates of the faces concerned, inhibiting elimination of partly included grains. For example, the chloritoid porphyroblasts shown in Fig. 4.18 have many more quartz and opaque inclusions in two opposite sectors.

4.3.4 Recognition of a metamorphic paragenesis

One of the main aims when examining a metamorphic rock with the microscope is to correctly identify all the minerals belonging to the same metamorphic assemblage (paragenesis), namely the minerals that grew simultaneously and therefore at the same metamorphic conditions. Microstructural evidence (Vernon, 1976, 1977a) of minerals that grew together in apparent chemical compatibility (strictly speaking, chemical equilibrium can never be proved) include: (1) crystal faces or smoothly curved adjustment boundaries between the minerals concerned (Section 4.2); (2) adjustment boundaries between a mineral occurring as inclusions and the host mineral (Section 4.2.7); (3) lack of evidence of replacement (partial pseudomorphism) of one mineral by the other; (4) symplectic intergrowth of the minerals concerned (Section 4.10), referring to the minerals in the intergrowth only, not the mineral with which the intergrowth is in contact; (5) exsolution lamellae of one mineral in another, implying chemical compatibility at the time of exsolution; and (6) lack of evidence of chemical zoning at contacts of the minerals involved, which may or may not be visible optically, and which may require chemical analysis for verification. Absence of these criteria does not exclude the possibility of chemical compatibility, but their presence helps to infer a paragenesis with more confidence.

As pointed out by Vernon (1996a), care is needed with questionable criteria that are often taken to infer lack of compatibility of minerals and assemblages, especially the inferences that: (1) minerals occurring as inclusions are necessarily older than the host mineral; and (2) minerals occurring in folia that wrap around porphyroblasts are necessarily younger than the porphyroblast. These problems are discussed in Sections 4.3.5 and 5.10.

4.3.5 'Order of crystallization' in metamorphic rocks

An order of crystallization of minerals in metamorphic rocks cannot be inferred from the microstructure, unless (1) reactions are indicated by partial replacement (Sections 4.1.2, 4.13.3), or (2) mineral growth can be reliably related to a sequence of foliation development (Section 5.10.2). As with igneous rocks (Section 3.6), microstructures such as inclusions and partial inclusions are inadequate for inferring the relative order of beginning or cessation of crystallization of the two minerals concerned (Vernon & Powell, 1976; Vernon, 1977a, 1996a; Vernon & Flood, 1977; Flood & Vernon, 1988), as shown in Fig. 3.47, unless the included minerals occur only in the cores of larger grains and not at all in the matrix. Moreover, the concept of an 'order of crystallization' is irrelevant for minerals belonging to the same metamorphic paragenesis, which form simultaneously as products of the same reaction. Of course, grains of minerals that do not take part in the reaction (e.g. graphite or zircon) remain. So too do reactant minerals present in excess of the amounts required to form the new mineral assemblage, but these are usually recrystallized, to become part of the microstructure of the new assemblage.

Minerals should not generally be considered in isolation when attempting to infer sequences of mineral growth in metamorphic rocks. All observations must be consistent with parageneses inferred from microstructural and mineralogical evidence.

4.4 Effect of fluids on crystal faces in metamorphic rocks

4.4.1 General aspects

Most prograde metamorphic reactions release volatile components from the breakdown of lower-grade minerals as fluid (e.g. water in dehydration reactions and carbon dioxide in decarbonation reactions), which must be removed from the reaction site for the reaction to proceed. Moreover, retrograde reactions generally require the addition of water and/or carbon dioxide. In fact, for any metamorphic reaction to proceed, nutrient chemical components must be transported to the growing grain and waste components transported away. It is generally assumed that the transport occurs by diffusion through an intergranular fluid, which could occur as an at least locally connected phase along grain edges. Its local distribution probably fluctuates as transient spaces along grain boundaries open and close, depending on (1) devolatilization reactions (which can release rapid accumulations of fluid, forcing open transient spaces along grain boundaries by 'hydrofracturing') and (2) deformation (which can also open and close pores, and which is almost universal in regional metamorphism). These two processes can also lead to mobility of the fluid (fluid advection), which produces even more rapid transfer of chemical components.

Although fluid moves through rocks during metamorphism (see, for example, Etheridge *et al.*, 1983, 1984), this does not mean that a continuous fluid film is present along all grain boundaries, as such a film would weaken the rock to an unrealistic extent. However, local interfaces may have fluid films (Section 4.4.2), and transient, mobile 'bubbles' of water may occupy grain boundaries as they move through the rock.

Veins, solution seams and stylolites in metamorphic rocks result from fluid movement, as discussed in Section 5.9. At high grades, partial melting also produces fluid in metamorphic rocks, as discussed in Section 4.16. Therefore, in view of the abundant evidence of fluid activity in metamorphism, the question arises as to whether the microstructures of metamorphic rocks can be affected by the presence of fluid, as discussed in the next section.

4.4.2 Effect of fluid in controlling crystal faces in solid-state aggregates

In Section 4.2.3, the development of low-energy interfaces was discussed in terms of anisotropy of interfacial free energy in purely solid aggregates. However, metamorphic fluids may conceivably play a part in the formation of crystal faces (Vernon, 1999a), as discussed in the following sections.

In igneous rocks, the shapes of crystals are controlled by $D : G$ (Section 3.5), as may also be true of crystals in metamorphic rocks, at least as far as elongate habits are concerned (Section 4.5). However, crystal growth in melts and other liquids is dominated by the development of low-energy crystal faces, regardless of the details of the shape. In metamorphic rocks, crystal faces are common in some minerals (e.g. mica, sillimanite, staurolite, garnet, graphite and hornblende), but not others (e.g. cordierite, quartz, feldspar), although considerable variation can occur between shapes adopted by the same mineral in different rocks (Figs. 4.20, 4.21), suggesting that the factors governing grain shape may be complex.

Kingery (1960, p. 367), Coble & Burke (1963) and Budworth (1970) described idioblastic crystals of spinel or Al_2O_3 dispersed through a polygonal aggregate of the same compound, formed as a result of heating (sintering) a powder. Although the matrix grains develop polygonal shapes, in order to minimize interfacial free energy, the large crystals develop faces that are quite straight, except where deflected around partial inclusions. Kingery (1960, p. 367) suggested that the development of the idioblastic crystals depends on the accumulation of a separate impurity phase along the crystal boundary. A similar explanation, suggested by Kooy (Budworth, 1970), is that a small amount of liquid (formed from impurities in the original mixture) is present, so that the large crystals virtually grow in a liquid and consequently develop their characteristic growth habit. This suggestion has also been made by Sunagawa (1974), Sunagawa *et al.* (1974), Tomura *et al.* (1979) and Rakovan & Jaszczak (2002) to explain idioblastic crystals in metamorphic rocks. In support of this idea, Sunagawa *et al.* (1974) observed growth spirals on the surfaces of kaolinite, white mica and chlorite grains that have grown from hydrothermal solutions, and Tomura *et al.* (1979) observed steps on the surfaces of mica grains mechanically separated from low- to medium-grade metamorphic rocks (chlorite to garnet zones), implying growth and/or dissolution in a fluid (Section 3.5.2). In addition, Kretz (1973, p. 16) reported growth steps on crystal faces of garnet grains physically separated from a schist, which is also consistent with growth in contact with a fluid. Kretz (1994, fig. 5.39) also showed an illustration of growth steps on a crystal of phlogopite extracted from a marble. Rakovan & Jaszczak (2002) observed growth spirals, with steps up to 4 μm high, on crystals of graphite from marble, which they studied by the new techniques of differential interference contrast (DIC) microscopy and atomic force microscopy (AFM). Crystallographically controlled growth steps have also been observed on natural diamond crystals (see, for example, Orlov, 1973). Unfortunately, mechanical separation of grains without damaging grain boundary steps is difficult or impossible for most rocks.

This interpretation involving fluid is relevant to the problem of why some minerals (e.g. staurolite) develop crystal faces in many metamorphic rocks (Figs. 4.20, 4.35), but not all (Fig. 4.21). A spectacular problem is presented by stibnite, a sulphide mineral with a strongly anisotropic crystal structure that normally forms very elongate crystals, as displayed in beautiful museum specimens. However, when it is deformed, it recrystallizes (Section 5.4.2) to form polygonal aggregates (Edwards, 1947), rather than the crystal faces that typically develop in structurally anisotropic minerals; for example, mica typically forms recrystallized aggregates of elongate crystals (Figs. 4.13, 4.14). Evidently the development of crystal faces requires something more than just an anisotropic crystal structure. The answer may be that stibnite is *dry* when it recrystallizes, whereas mica accumulates enough fluid on its crystal faces to permit them to grow. Is the presence of fluid necessary for the development of crystal faces in metamorphic rocks?

If porphyroblasts grow in dry, completely solid aggregates, they should have *adjustment* boundaries, with concave-outwards cusps along the boundary (Fig. 4.36). This curvature is due to the fact that the porphyroblast has many more sides than its neighbours and so grows at their expense (Section 4.2.1), as in exaggerated (secondary) grain growth or the development of 'runaway' grains in metals and ceramics (see, for example, Kingery, 1960, p. 363). In other words, interfacial angles should develop where the porphyroblast boundary meets other boundaries. How, then, are perfectly planar crystal faces formed in metamorphic rocks?

Vernon (1999a) suggested that as a slowly advancing boundary of a growing idioblastic porphyroblast (Figs. 4.20, 4.35) encounters matrix quartz grains (forming partial inclusions and eventual inclusions) and mica grains (which it consumes to make more staurolite), water on the quartz grain boundaries and water released from the breakdown of mica diffuses to the porphyroblast boundary, where it accumulates as a thin fluid layer and so promotes the development of a crystal face. Diffusion of water into the film as quartz inclusions are

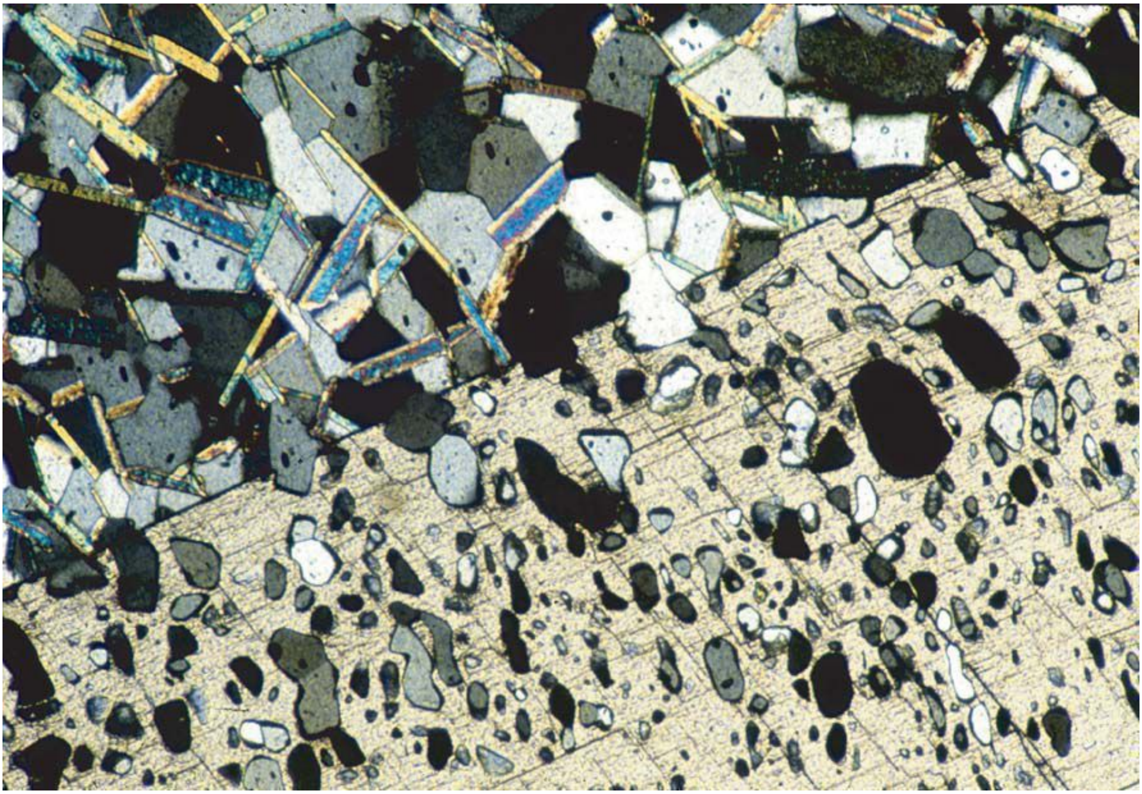

Fig. 4.35: Staurolite porphyroblast in a quartz–muscovite–staurolite schist, showing planar, rational, low-energy faces of muscovite against quartz in the matrix, and also a perfectly straight low-energy crystal face of staurolite against quartz grains in the matrix. In contrast, quartz grains included and partly included in the staurolite have curved, high-energy quartz–staurolite boundaries. Crossed polars; base of photo 2 mm.

incorporated into the growing porphyroblast dehydrates the boundaries between the developing quartz inclusions and their host staurolite. In other words, although both are quartz–staurolite interfaces, the boundary of staurolite against quartz inclusions is dry, whereas the boundary of staurolite against matrix quartz grains is wet (Vernon, 1999a). The result is that the inclusions develop rounded shapes, as are typical of quartz inclusions that have adjusted their shapes in the solid state in the absence of fluid. In contrast, the quartz–staurolite interface at the edge of the porphyroblast effectively evolves in a fluid and so develops a crystal face, as is typical of growth in liquids (Chapter 3). Which came first: the fluid or the planar interface? I suggest that the growing staurolite would begin to accumulate fluid at a very early stage, and so should start to grow crystal faces as a result. Bouillier & Nicolas (1975) and Drury & van Roermund (1989) suggested that well-formed olivine crystals formed by dynamic recrystallization (Section 5.4.2)

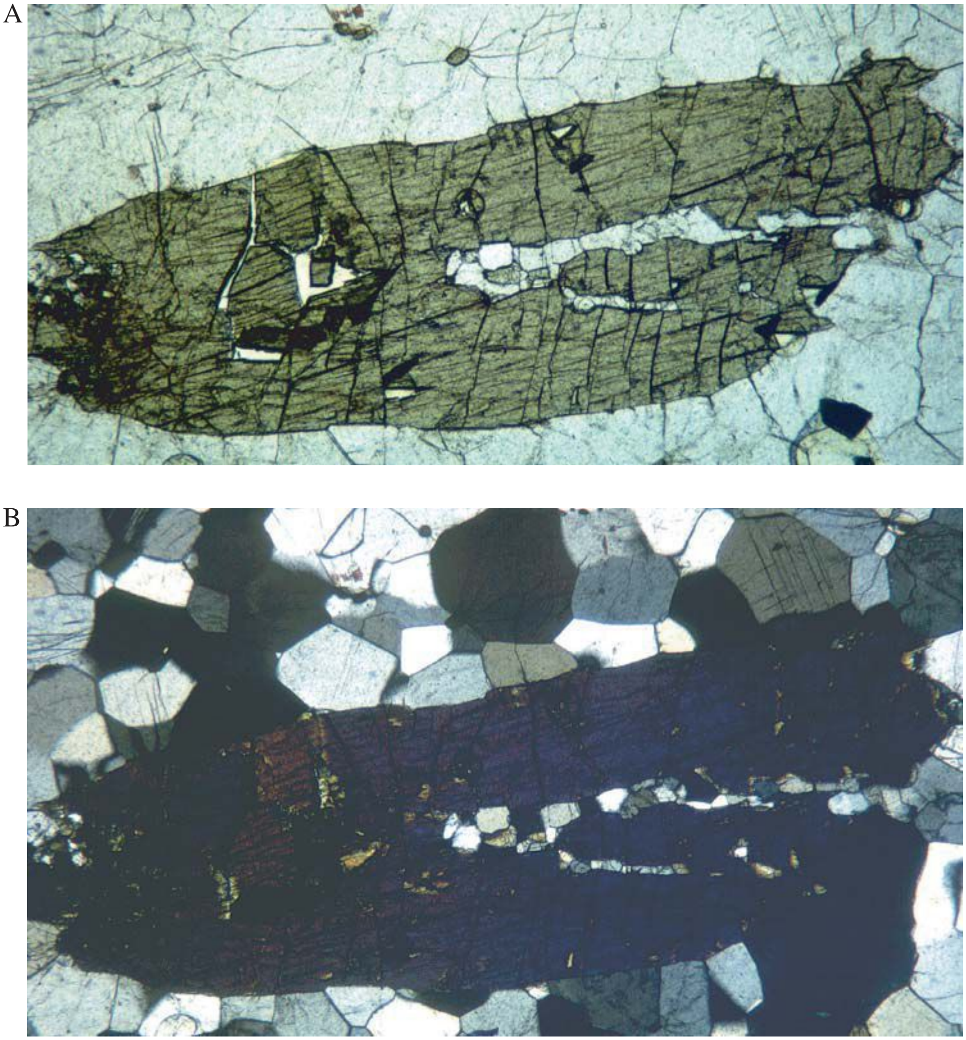

Fig. 4.36: Hornblende porphyroblast with adjustment boundaries concave outwards, showing dihedral angles where plagioclase–plagioclase and plagioclase–quartz boundaries meet hornblende–quartz and hornblende–plagioclase boundaries at triple junctions. Similar adjustments have also occurred at the edges of the quartz–plagioclase aggregate enclosed by the hornblende. The grain boundary adjustments occurred during high-temperature, dry metamorphism at granulite facies conditions. Mud Rock Tank, Arunta Block, central Australia. (A) Plane-polarized light; from Vernon (1999a, fig. 14), with permission of the *Canadian Mineralogist*. (B) Crossed polars; base of photos 4.8 mm.

in mantle peridotites are due to growth in the presence of a fluid film along the boundary. Furthermore, experiments on salt rocks (Urai, 1983b; Urai *et al.*, 1986) have shown that well-formed crystals may grow by fluid-assisted grain-boundary migration recrystallization (Section 5.4.2).

4.4.3 Some problems

A relevant question is: why didn't the staurolite porphyroblast shown in Fig. 4.21 develop crystal faces? On the foregoing hypothesis, the answer would be that the boundary of the porphyroblast did not accumulate fluid, for some reason. Perhaps removal of the water was more efficient, possibly owing to deformation of the matrix, but this explanation is speculative.

A similar problem is that hornblende develops crystal faces in some rocks and adjustment boundaries in others. The hornblende adjustment boundaries shown in Fig. 4.36 developed in dry, granulite facies conditions (apart from hydroxyl in the structure of the hornblende), which is consistent with the foregoing explanation. However, if crystal faces on hornblende in other rocks are due to growth in a fluid film, the reason for the accumulation of the fluid is unknown.

A problem is also presented by minerals such as cordierite, olivine, quartz and feldspar, which almost never develop crystal faces in metamorphic rocks. Yet these minerals develop crystal faces when they grow in a magma, including cordierite (see, for example, Deer *et al.*, 1992, plate 1A). Considering a cordierite porphyroblast in a matrix of quartz, the free energy of quartz–cordierite boundaries is so similar to that of quartz–quartz boundaries that triple junctions are formed wherever quartz–quartz boundaries intersect quartz–cordierite boundaries, leading to an irregular interface for the cordierite porphyroblast as a whole. Similarly, all boundaries involving quartz and feldspar have little difference in interfacial energy. However, this applies only to dry aggregates, and the euhedral shapes of magmatic cordierite, quartz and feldspar suggest that porphyroblasts of these minerals should also develop crystal faces if a fluid were present along their boundaries. So, the problem is: why are the interfaces of porphyroblasts of cordierite and feldspar invariably so dry in metamorphic rocks? The answer could be that these interfaces do not provide enough unsatisfied chemical bonds to accumulate a water film (see next section).

4.4.4 Model for low-energy (crystal) faces in metamorphic rocks

A simple explanation of the abundance of low-energy mica {001} interfaces in metamorphic rocks at all grades is that the proportion of bonds directed oblique to {001} and available for linking to unsaturated bonds from a neighbouring grain is very small. In contrast, the crystal structure of quartz, for example (Bragg, 1937), is such that many bonds would be available from quartz, regardless of the crystallographic orientation of the interface. The result would be a high proportion of unsaturated bonds at a quartz–{001} mica interface. The same argument would apply to the impingement of a mica grain with {001} oblique to the {001} plane of another mica grain (Fig. 4.16C). The unsaturated bonds could be satisfied by the adsorption of impurities, especially hydroxyl, possibly leading to the development of a water-rich film along the low-energy interface (Etheridge *et al.*, 1983; Vernon, 1999a, p. 519). In effect, the interface would grow and advance in a fluid, on this interpretation. The observed curved, high-energy adjustment boundaries between quartz–feldspar and biotite oblique to {001} presumably are dry because abundant bonds are available from the biotite in that orientation, as well as from the quartz and feldspar (Vernon, 1999a, p. 519).

4.4.5 Fluid inclusions

Small fluid-rich inclusions are common in minerals and meteorites (Roedder & Coombs, 1967; Poty *et al.*, 1974; Weisbrod *et al.*, 1976; Hollister & Crawford, 1981; Roedder, 1972, 1979a,c, 1984; Touret, 1977; Barker, 1990). They are especially common in veins, which crystallize from fluid (Section 5.9.3). The detailed study of fluid inclusions trapped in minerals as they grow (primary inclusions) or formed in them after growth (secondary inclusions) is too specialized for this book. However, they represent an important aspect of rock microstructure, and so the main features will be mentioned.

As emphasized by Roedder (1984), fluid inclusions are generally the only direct evidence of fluids existing at the time of a rock's formation. For example, primary inclusions may give an idea of the composition and temperature of fluids present when the mineral formed (see, for example, Roedder, 1972, 1979a, 1984; Hollister & Crawford, 1981; Fyfe *et al.*, 1978).

At small magnifications, fluid inclusions optically resemble dust, scattered randomly or in aligned trails (Fig. 4.37A). Most are less than 0.03 mm across. The shapes and internal structures of larger inclusions can be studied optically, but the smallest fluid inclusions (down to 0.02 μm across) are best seen in the transmission electron microscope (see, for example, Green & Radcliffe, 1972). An important technique that reveals the detailed three-dimensional shapes and arrangements of fluid and mineral inclusions is confocal laser scanning microscopy (CLSM), as described by Petford & Miller (1992), Petford *et al.* (1995), Sheppard & Shotton (1997) and Bozhilov *et al.* (2003). The method involves reflection of a focussed laser beam from a polished section surface and its focussing onto a photodetector after passing through a confocal aperture ('pinhole'), which produces a high-definition image free of stray light. The focussed point is then scanned across the surface to produce a two-dimensional image, which is stored in a computer imaging system. The depth of the focal plane is then progressively changed and the procedure repeated until a series of optical sections is obtained. These sections are combined to make a three-dimensional image that is in focus at all scanned levels.

Fluid inclusions are examined on a heating and cooling microscope stage, which measures the temperatures of phase changes in individual inclusions (*microthermometry*). Compositions and densities of inclusions can be determined from this information and used to help interpret the history of the mineral. Composite liquid inclusions may contain a gas bubble and one or more crystals

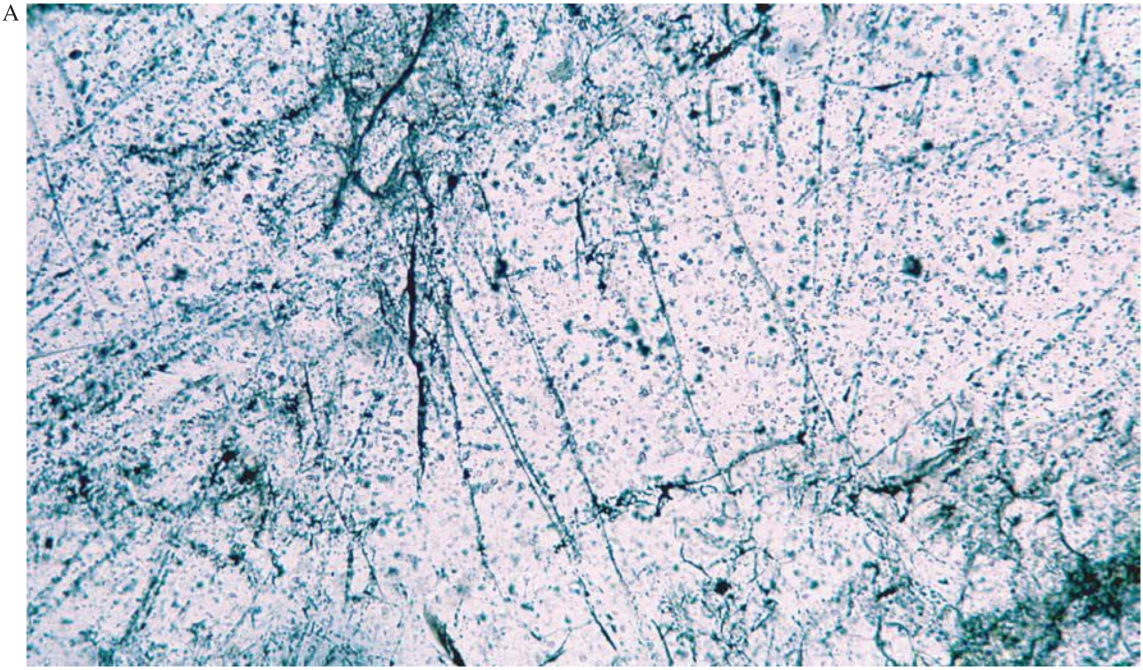

Fig. 4.37: (A) Abundant fluid inclusions in vein quartz (Fig. 5.71) from Murunna Point, south coast of New South Wales, Australia. Many appear as 'dusty' swarms, but others are in linear arrays along fractures; these are more obviously secondary inclusions formed by penetration of fluid along the cracks. Plane-polarized light; base of photo 1.5 mm. (B) Magnified view of part of the vein illustrated in (A) to show that many of the trails are lines of secondary fluids isolated by crystallization of the quartz during the 'healing' of the fractures, presumably to minimize the quartz–fluid interfacial energy. Sample by courtesy of David Durney. Plane-polarized light; base of photo 0.3 mm.

formed as the liquid cooled from high temperatures and pressures ('daughter crystals'). Heating the host mineral homogenizes the inclusion, the temperature of the homogenization giving an indication of the temperature of formation of the mineral, provided a correction can be made for the inferred pressure.

Primary fluid inclusions range from *liquid inclusions*, through *gaseous inclusions* to *melt inclusions* (Section 3.11.1). Primary inclusions typically occur in crystals that grow in veins and other cavities (Section 5.9.3). For example, vein quartz is commonly rich in liquid inclusions (see, for example, Poty *et al.*, 1974), as shown in Fig. 4.37. Primary melt inclusions may be trapped in crystals growing in magmas or in crystals produced in incongruent melting reactions in high-temperature metamorphic rocks (Section 4.16) (Cesare & Maineri, 1999; Cesare *et al.*, 2003). The compositions of melt inclusions depend on the melting reaction; for example, rhyolitic melt inclusions result from partial melting of metapelite (Cesare *et al.*, 2003), whereas mafic melt results from partial melting of peridotite

B

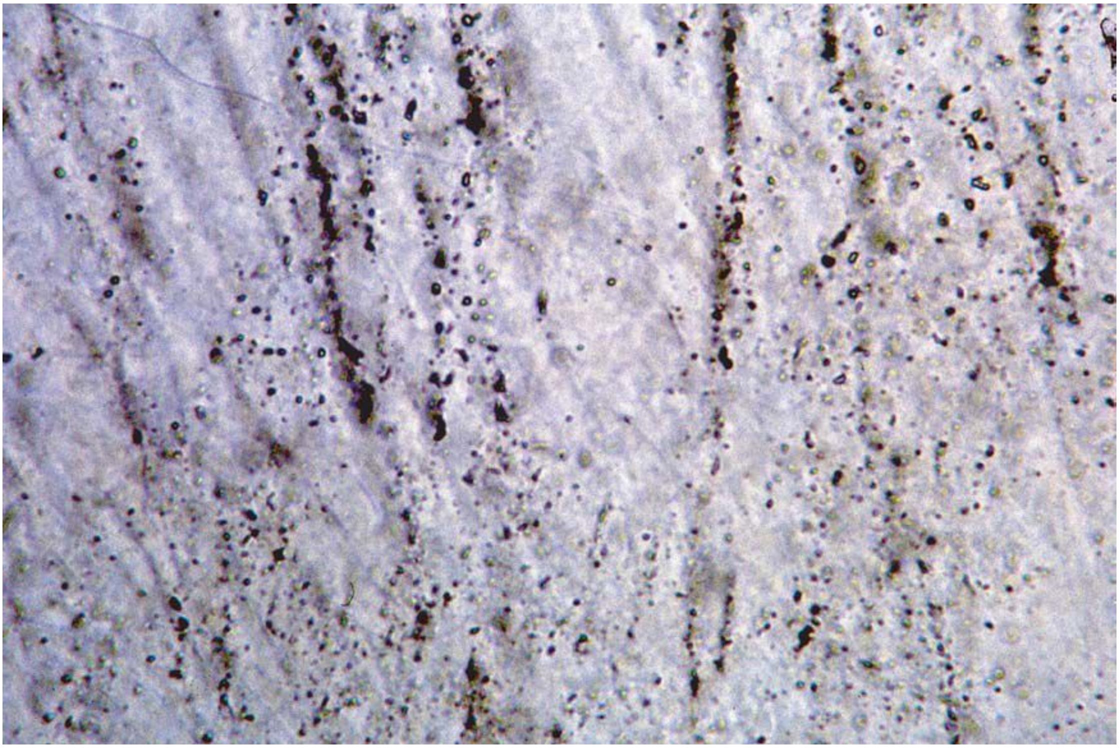

Fig. 4.37: (*cont.*)

in Earth's mantle (see, for example, Walker *et al.*, 2003). Melt inclusions consist mainly of glass in rapidly cooled rocks or crystallization products in more slowly cooled rocks. Glass inclusions commonly have 'shrinkage bubbles', which are immobile, in contrast to gas bubbles in liquid fluid inclusions.

Primary inclusions, both liquid and melt, commonly occur in arrays parallel to crystal faces (see, for example, Heinrich & Gottschalk, 1995) and the resultant concentric zoning may preserve evidence of fluid history during growth of the crystal. They commonly have planar boundaries (with rounded corners), reflecting the crystal structure of the host mineral (see, for example, Fitz Gerald & Stünitz, 1993a; Heinrich & Gottschalk, 1995), as expected from solid interfaces developed in contact with fluid (Section 4.4.2). These shapes are often called 'negative crystal' shapes. Primary inclusions in metamorphic minerals may react with their host mineral and reflect the progress of metamorphic reactions (Heinrich & Gottschalk, 1995).

Most fluid inclusions are *secondary inclusions*, which are formed when fluid enters minerals along fractures (Fig. 4.37A) and subsequent mineral growth traps the fluid as strings of isolated inclusions ('healed fractures'), as shown in Fig. 4.37B. Conversion ('necking down') of elongate fluid inclusions to separate, more rounded inclusions, or even 'negative crystal' shapes, occurs after entrapment in order to reduce the interfacial free energy. Secondary inclusions that occur in lines transecting grain boundaries are especially good indicators of growth in former fractures. Changing the microscope focus can reveal arrays of secondary fluid inclusions arranged in dipping planes. Unfortunately, most fluid inclusions in metamorphic rocks are secondary, because prograde metamorphism tends to destroy primary inclusions. Thus, the inclusions mainly reflect conditions during the uplift history of the rock (see, for example, Hollister, 1969; Barker, 1990).

Metamorphic minerals commonly contain small (less than 0.02 mm across) fluid inclusions rich in water, with varying amounts of CO_2 and ions such as K^+, Ca^{2+}, Na^+, Cl^-, CO_3^{2-} and SO_4^{2-}. Water-poor, high-grade metamorphic rocks may either have no fluid inclusions or contain carbon dioxide-rich inclusions.

Many rocks from the deeper parts of Earth's mantle are free of fluid inclusions, but large numbers of bubbles of carbon dioxide are common in the olivine and pyroxene of ultramafic xenoliths in basaltic rocks, which are believed to have been extracted from depths of 60–200 km in Earth's mantle (Roedder, 1965). Some of these bubbles are spherical, others capsule-shaped (Green & Radcliffe, 1972). The latter have partly planar boundaries ('negative crystal' shapes), reflecting anisotropy of surface energy of the host crystal (Miller & Chadwick, 1969).

4.5 Elongate and dendritic crystals in metamorphic rocks

Some minerals, such as sillimanite, stilpnomelane, tremolite–actinolite and wollastonite, nearly always form elongate crystals in metamorphic rocks (Fig. 4.38). This is despite the relatively large interfacial area of these crystals and aggregates, compared with the more equant grains typical of most metamorphic rocks. Presumably the large area is partly compensated for by the relatively low energy of the faces of these crystals. Dendritic and skeletal shapes (Figs. 4.19, 4.39) may also occur, especially in andalusite, staurolite and garnet in graphitic metasedimentary rocks. Dendritic and radiating aggregates of fine-grained graphite in high-grade marble, occuring mainly as overgrowths on idioblastic graphite crystals, appear to represent disequilibrium growth during a metamorphic event after the main metamorphism (Weis, 1980).

Many elongate grains in metamorphic rocks are in radiating aggregates (Fig. 4.38), which imply growth of many crystals on a single nucleus, indicating a low nucleation rate. The explanations given for dendritic and spherulitic growth in igneous rocks (Sections 3.5.3 and 3.5.5) may apply in a general way to similar crystals and aggregates in metamorphic rocks (Rast, 1965). In other words, a low nucleation rate (N), coupled with a low ratio of diffusion rate to growth rate ($D : G$), would favour dendritic and radiating growth. For example, if a mineral is being produced at a certain rate in a metamorphic reaction, its G in a particular matrix may be too fast for 'impurity' components to diffuse from, and for

Fig. 4.38: Aggregates of columnar crystals of wollastonite that have replaced fossil shells (Fig. 4.6), preserving the curved outlines of the shells, in a contact metamorphic rock (hornfels) from Hartley, west of Sydney, New South Wales, Australia. The wollastonite is the product of a reaction between the calcite of the shells and quartz in the matrix. From Vernon (2000b, fig. 120). Crossed polars; base of photo 1.8 cm.

‘nutrient’ components to diffuse to, the boundary at a sufficiently rapid rate to permit a uniformly advancing interface. If so, projections into ‘less polluted’ matrix may be necessary to keep the crystal growing fast enough for the reaction to proceed.

Dendritic crystals are less common in metamorphic than in igneous rocks. However, relatively common examples are dendritic andalusite and garnet, which are characteristic of some graphitic schists (Figs. 4.19, 4.39B). A possible explanation is that the graphite (which is not involved in the metamorphic reactions) accumulates against the advancing interfaces of the porphyroblast and retards its growth. Therefore, the porphyroblast is forced to send out arms into matrix areas that contain more nutrient and fewer waste components. Commonly the graphite builds up as passive accumulations against the advancing interfaces (Fig. 4.19), as discussed in Section 4.3.1.

Next Page

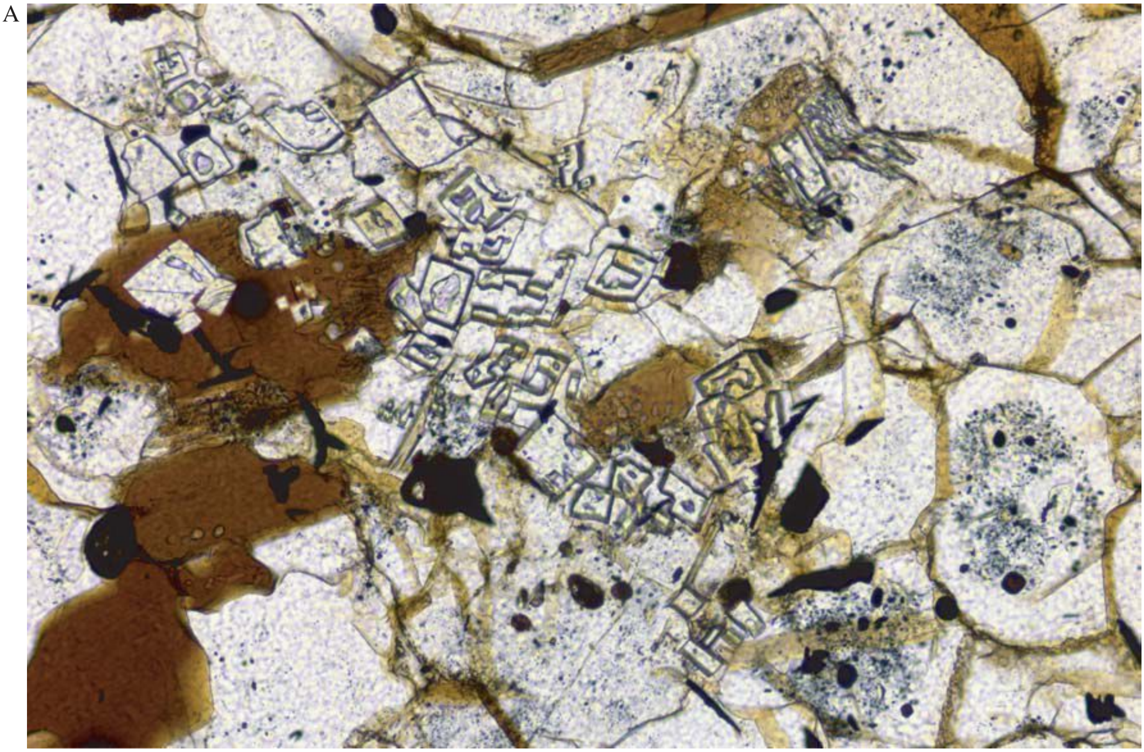

Fig. 4.39: (A) Hollow crystals of sillimanite in a cordierite–biotite–sillimanite granofels near the Sierra de Castillio pluton, Baja California, México. Sample by courtesy of Erwin Melis. Plane-polarized light; base of photo 0.6 mm. (B) Dendritic porphyroblast of andalusite in a graphitic schist, Appleton Ridge, Maine, USA. Sample by courtesy of Charles Guidotti and Scott Johnson. Crossed polars; base of photo 3 mm.

Rarely, a mineral that normally forms polygonal aggregates in metamorphic rocks locally develops an elongate habit. An example is elongate olivine of metamorphic origin (Evans & Trommsdorf, 1974), which contrasts strongly with the usually polygonal olivine of metamorphic rocks (Fig. 4.9), including mantle rocks (Section 5.12). This elongate metamorphic olivine is distinguishable from dendritic olivine in magnesian volcanic rocks (Figs. 3.17–3.19). Not only is the chemical composition different (low Ni and Ca), but the habit of the metamorphic olivine is simpler, the crystals being either needle-like or bladed, but not skeletal or feathery. They occur as criss-cross, radiating and parallel aggregates, and may overgrow microfolds of layering. Evans & Trommsdorf (1974, p. 132) suggested that the elongate habit is connected with the presence of talc and abundant pore fluid. Perhaps the fluid allowed crystal faces to initiate (Section 4.4), in contrast to the situation in dry rocks, such as peridotites, in which polygonal olivine normally occurs.

Previous Page

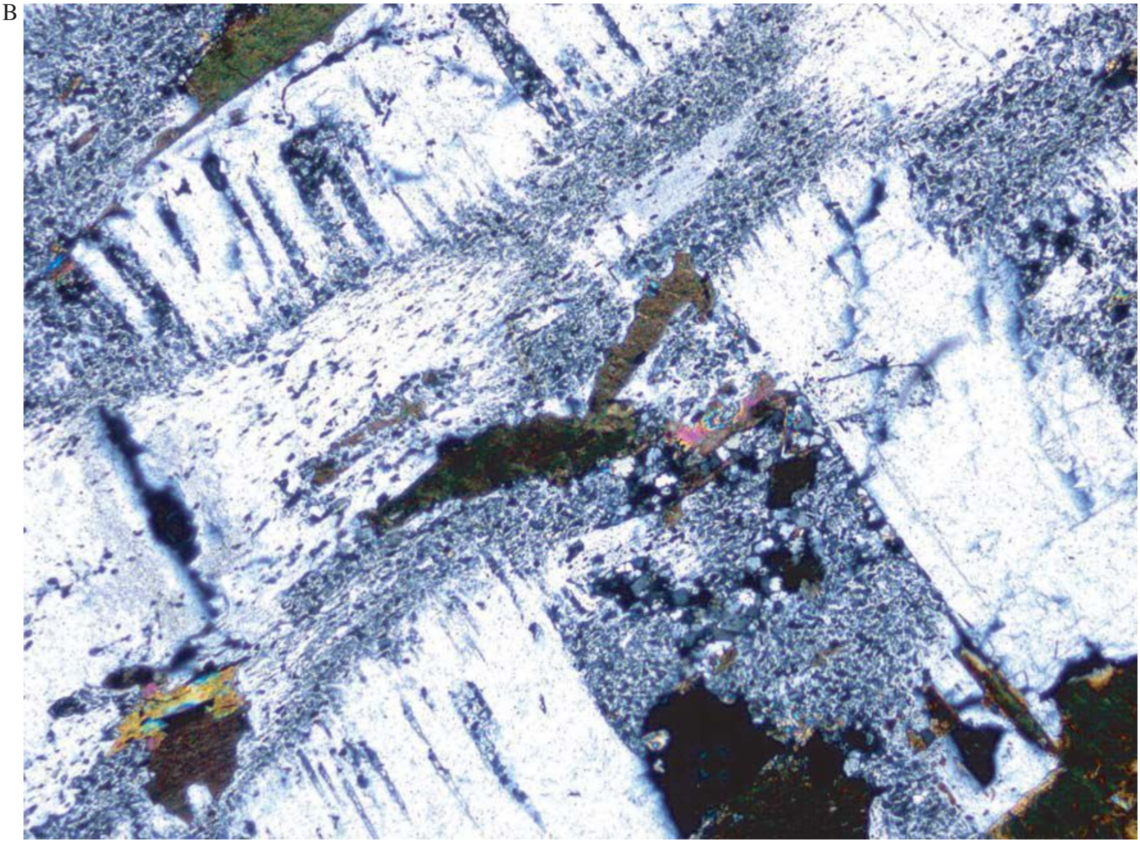

Fig. 4.39: (*cont.*)

Conversely, a mineral that usually occurs with an elongate habit rarely develops polygonal aggregates in some rocks. For example, wollastonite may develop polygonal aggregates in granulite facies rocks, in which the absence of water inhibits the initiation of crystal faces and forces polygonal growth to occur instead.

4.6 Solid-state effects in slowly cooled igneous rocks

The foregoing discussion of solid-state microstructures has mainly used crustal metamorphic rocks as examples, including silicate, sulphide and oxide rocks. However, the principles apply equally well to rocks that are much closer to their melting temperatures (see, for example, Vernon, 2000b), such as glacial ice and mantle peridotites, in which polygonal aggregates are also typical (Figs. 4.9, 4.43). In fact, they apply to any crystalline aggregate that remains hot long enough for interfaces to adjust to minimize their interfacial free energy. Therefore, the microstructures of slowly cooled igneous rocks are worth examining for possible evidence of solid-state (*subsolidus*) grain-boundary adjustment, as mentioned previously (Section 3.5.9).

4.6.1 Mafic–ultramafic compositions

The final crystallization (*solidus*) temperatures of mafic igneous rocks are so high (around 850 °C) that slow cooling after crystallization, through an interval of several hundred degrees, may provide sufficient heat long enough for solid-state grain-boundary adjustment to occur after initial crystal impingement. During this slow cooling from high temperatures, lower-energy grain shapes and larger grain-sizes may be produced, owing to a tendency to reduce the total interfacial energy of the aggregate. The process occurs by diffusion of chemical components from high-energy to lower-energy sites, in residual melt (while present) and/or along solid grain boundaries.

Many cumulates in layered mafic–ultramafic complexes have predominantly polygonal grain shapes (Figs. 4.40 and 4.41) and rounded inclusions (Fig. 4.42). These shapes appear to be due to solid-state interface adjustment (Voll, 1960; Weedon, 1965; Vernon, 1970; Hulbert & von Gruenewaldt, 1985; Reynolds, 1985). Some sections of these 'adcumulates' show grain shapes that are so polygonal that they could be mistaken for high-grade metamorphic rocks (Figs. 4.40, 4.41A). However, other sections may reveal residual elongate shapes inherited from the stage of magmatic crystallization (Fig. 4.41B). In two-mineral aggregates, dihedral angles provide evidence of solid-state grain-boundary adjustment (Fig. 3.46).

In layered cumulates, the earlier stages of this grain-boundary adjustment presumably occur in the presence of some interstitial melt. Solution occurs at some sites and the dissolved components are transferred in the liquid, to be reprecipitated on other sites. The process has been related to 'liquid-phase sintering' (Jurewicz & Watson, 1985; Hulbert & von Gruenewaldt, 1985; Reynolds, 1985). Sintering is an industrial process in ceramics and metals that involves the growing together of powders to form solid aggregates. It also occurs in the conversion of snow to firm and solid ice in glacial ice sheets (Fig. 4.43). The process involves minimization of the total interfacial free energy by increasing the area of solid–solid interfaces, which have lower interfacial free energy (γ) than solid–fluid interfaces (Kingery, 1960, p. 370; Coble & Burke, 1963). Once the crystals come into contact, a solid–solid grain boundary is formed between them: either a fortuitously low-energy interface, if the crystals come to rest on crystal faces of both crystals, or a higher-energy interface for random collisions. As γ crystal–crystal is lower than γ crystal–melt, the tendency is to increase the area of crystal–crystal boundaries — by diffusion and especially solution–precipitation (see, for example, Cooper & Kohlstedt, 1984) — and so expel melt from the crystal aggregate. A polygonal aggregate results if all the melt is locally expelled, after which further adjustment of grain boundaries may occur in the solid

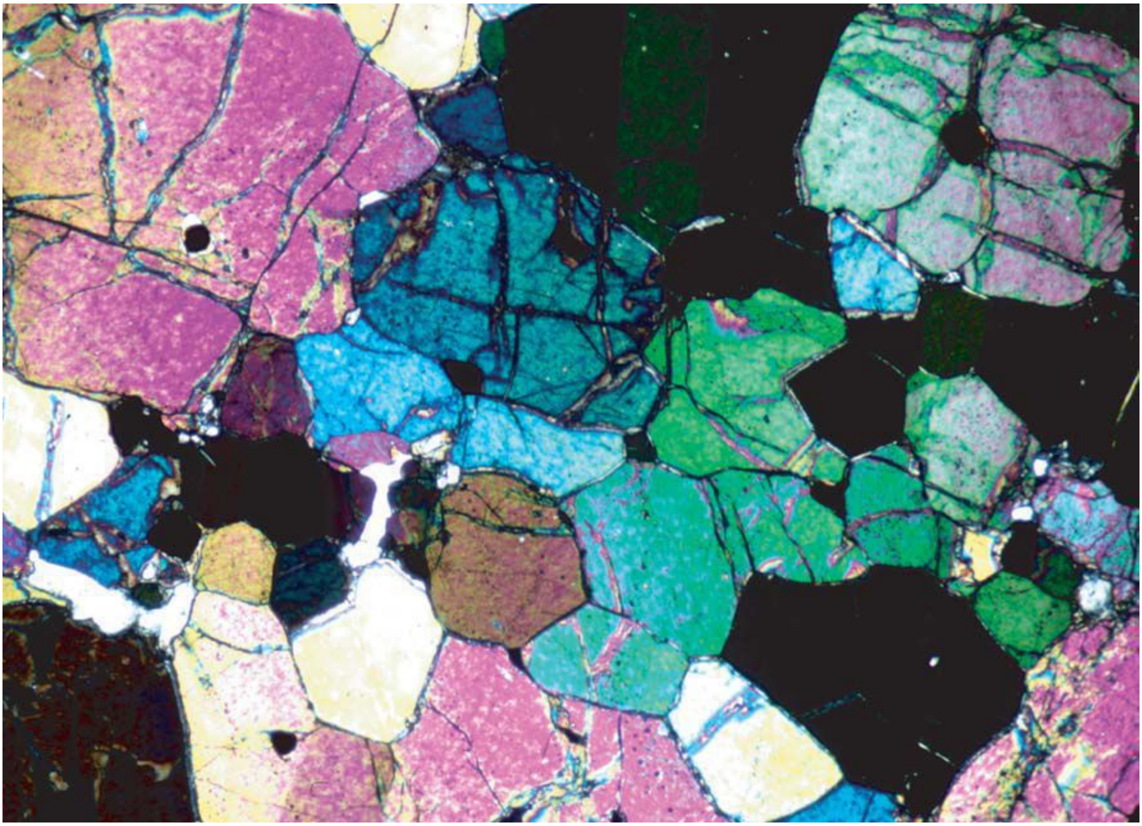

Fig. 4.40: Polygonal aggregate of olivine in an ultramafic igneous cumulate (dunite), Rhum igneous complex, Scotland. Crossed polars; base of photo 4.4 mm.

state, as discussed in Section 4.2.2. Because this can occur only by solid-state diffusion along grain boundaries and through grains, it is a slower process (Hunter, 1987).

Experiments by S. Ikeda *et al.* (2002) have shown that θ melt vs. olivine/olivine decreases with increasing temperature. Because this dihedral angle increases as olivine-rich magma cools, the result is a greater tendency for crystal clustering (increasing the area of olivine–olivine contacts), which assists the segregation of melt from crystals.

The rounded corners of inclusions in both adcumulates and orthocumulates (Figs. 3.46, 4.42; Hunter, 1987, figs. 10–15) may be due to subsolidus grain-boundary adjustment (Vernon, 1970), rather than to rounding in the melt as suggested by Hunter (1987). Such rounded corners are typical of solid-state adjustment (Section 4.2.7), as in high-grade metamorphic rocks (see, for example, Kretz, 1966a; Vernon, 1968, 1970), but not of crystals freely suspended in magma (Section 3.5.2).

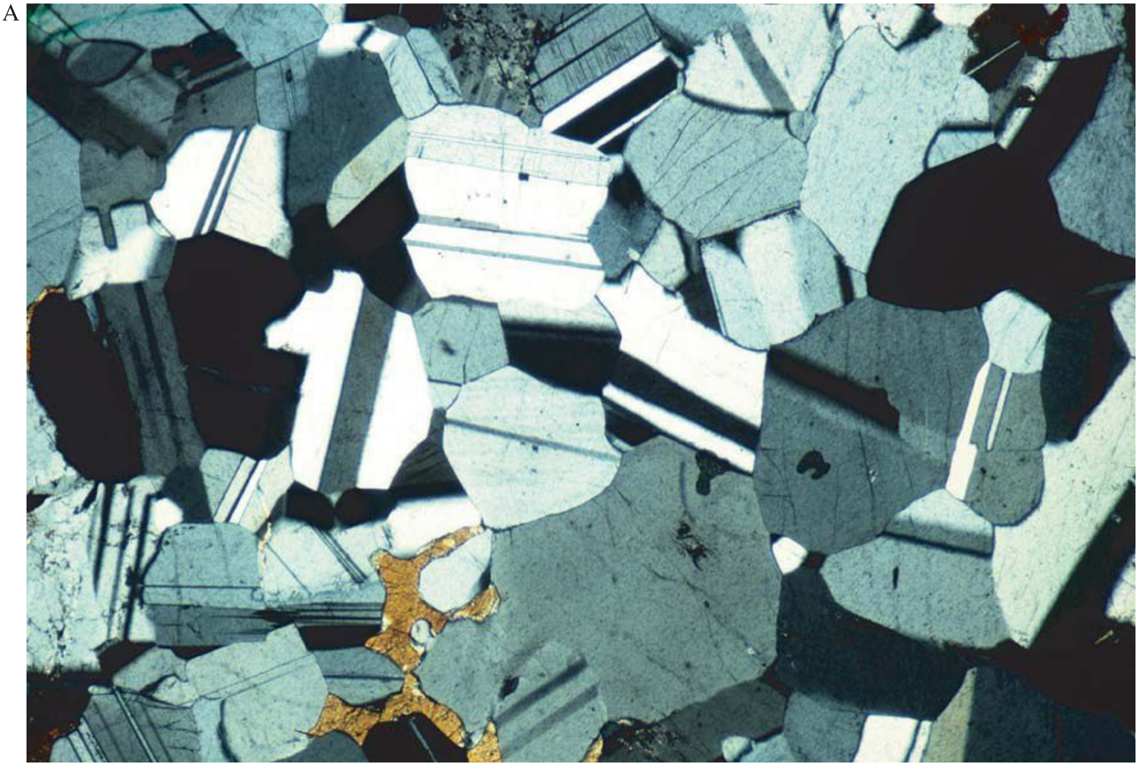

Fig. 4.41: (A) Polygonal aggregate of calcic plagioclase in an anorthosite cumulate from the Bushveld Complex, South Africa. Crossed polars; base of photo 4.4 mm. (B) Polygonal aggregate of calcic plagioclase, in a section perpendicular to that shown in (A). Despite the solid-state grain-boundary adjustment, elongate grain shapes inherited from crystals precipitated from the melt and aligned by magmatic flow (e.g. as a result of compression) have been preserved. Crossed polars; base of photo 4.4 mm.

4.6.2 Felsic compositions

If gabbros and related rocks can undergo some solid-state interface adjustment during slow cooling, the question arises as to whether granites also can, at least to a small extent, despite their lower solidus temperatures. However, the polygonal grain shapes that are characteristic of feldspar in metamorphic rocks and adcumulates are generally absent from granites, suggesting that intergranular solid-state changes are minimal. As discussed in Section 3.5.9, the reason that granites appear to show little tendency for their grain boundaries to change after impingement is probably that their subsolidus cooling interval is too short and the temperatures too low.

Although many granites show elongate plagioclase grains with oscillatory concentric zoning that typically reflects euhedral growth of crystals in a liquid

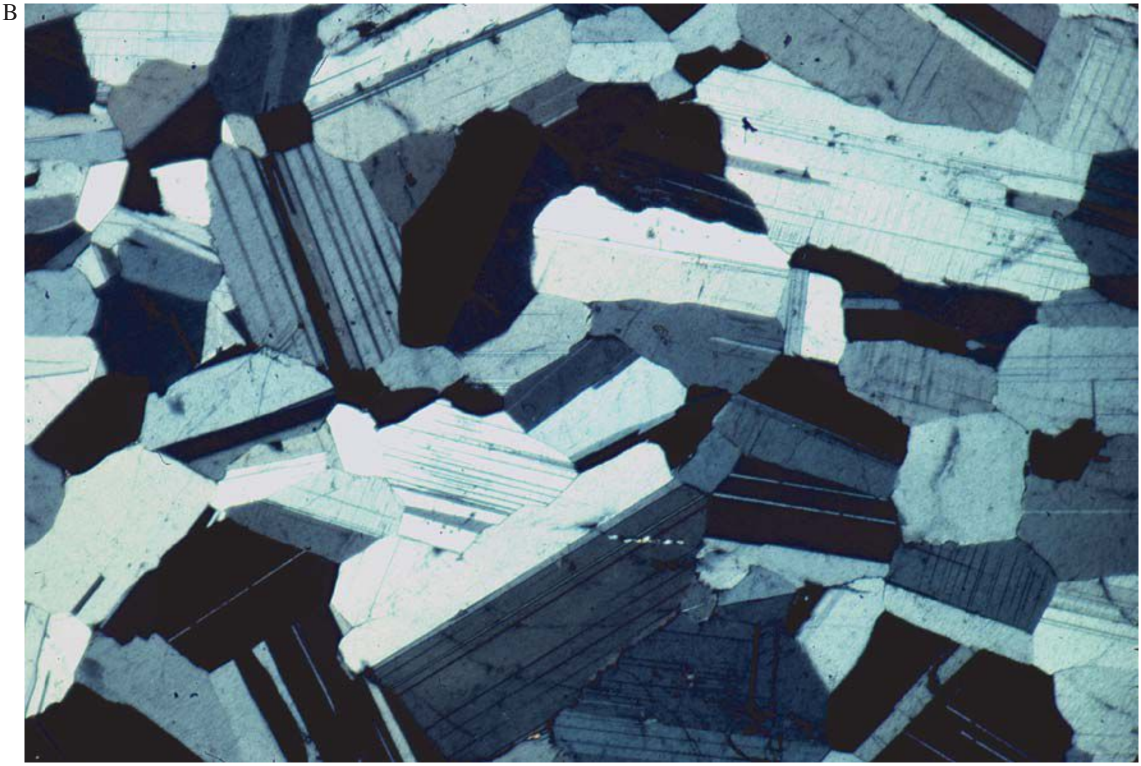

Fig. 4.41: (*cont.*)

(Section 3.5.2), the margins of these grains are rarely crystal faces (Fig. 3.45) unless the plagioclase occurs as inclusions (Figs. 3.12, 3.75). However, this need not be due to solid-state grain-boundary adjustment, because the plagioclase grows in competition with quartz, K-feldspar and biotite (± hornblende) right to the solidus (Section 3.6). As all interfaces between grains of quartz and feldspar have about the same interfacial free energies, no crystal faces are likely to form where they meet one another, with the result that irregular grain boundaries are common in granites (Fig. 3.45), even where no solid-state adjustment has occurred.

4.7 Growth twinning in metamorphic minerals

Solid-state growth twins are common in some minerals, especially plagioclase (Fig. 4.44A; Vernon, 1965), pyroxene, hornblende, sphalerite (Stanton, 1964, 1972; Stanton & Gorman Wiley, 1971; McClay, 1982c), chloritoid, and less commonly chalcopyrite (Stanton, 1972). Twinning is also common in quartz, but cannot be seen in normal thin sections because the *c*-axes are identically oriented

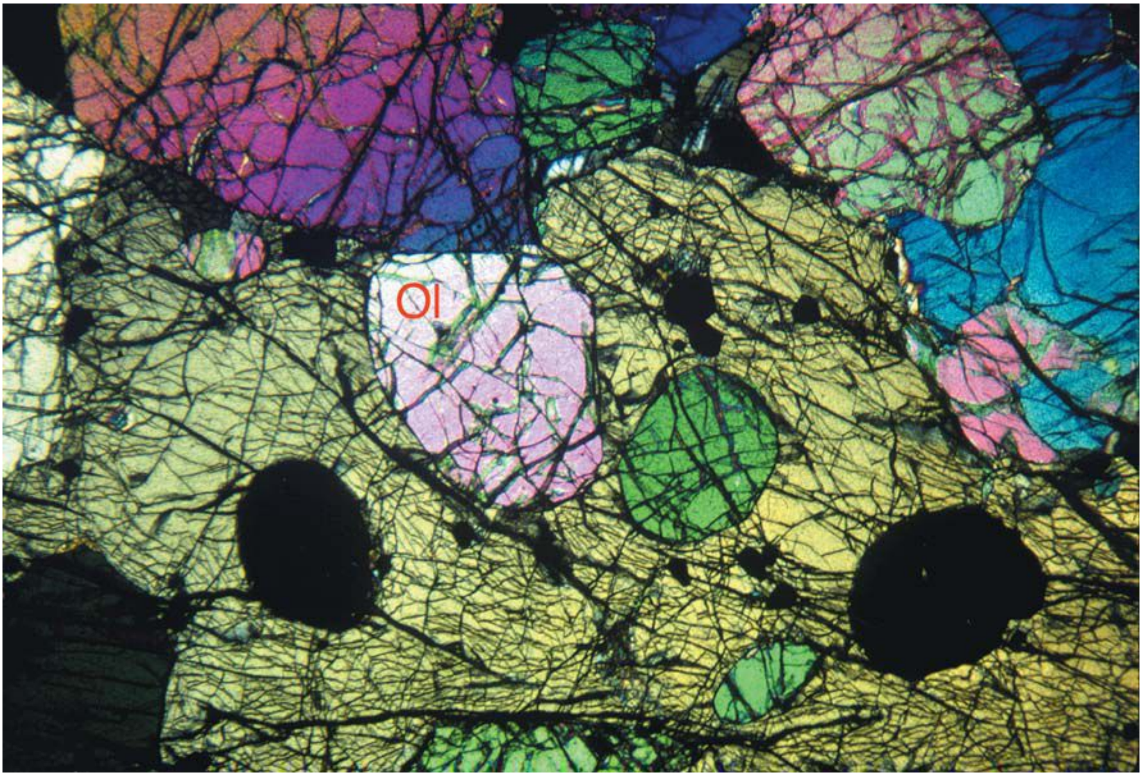

Fig. 4.42: Large grain ('oikocryst') of orthopyroxene (first-order interference colours) with rounded inclusions of olivine (Ol) in an ultramafic igneous cumulate (harzburgite) from the Stillwater Complex, Montana, USA. Crossed polars; base of photo 1.7 mm.

in both twin individuals. Twinning also occurs in sheet silicate minerals but, although the *c*-axis is reflected across the twin plane, an optical vibration plane is parallel to the twin plane (the cleavage plane), and so both individuals are optically identical.

As with igneous minerals, growth twins in solid-state aggregates (Fig. 4.44A) may be simple or multiple, and their interfaces are either straight or abruptly stepped (Vernon, 1965), in contrast to deformation twins, which are smoothly curved (at least on the light microscope scale) and lenticular (Section 3.12).

Fortuitous encounters during grain growth can produce twin boundaries, which are relatively stable because twin interfaces have much lower interfacial free energy (γ) than random grain boundaries. One way in which this can be achieved is shown in Fig. 4.44B. Because growth twins in metamorphic plagioclase depend on fortuitous encounters, (1) they are less common than in igneous plagioclase, (2) fewer twin interfaces occur per grain, and (3) grains showing

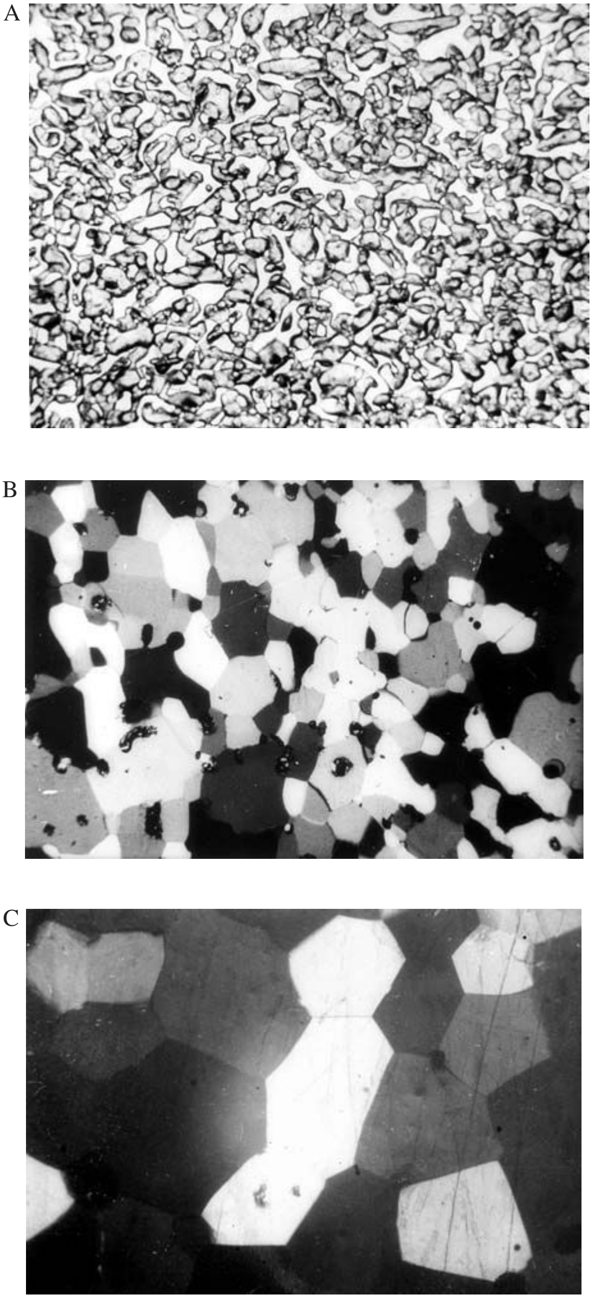

Fig. 4.43: Progressive stages in the conversion of snow to solid ice in the Antarctic ice sheet. (A) Firn, consisting of connected ice globules that have partly grown ('sintered') together to reduce the interfacial free energy. (B) Deeper, more completely sintered ice, showing polygonal grain shapes and air bubbles (very high relief). (C) Coarse-grained, polygonal ice without air bubbles. Photos by Jon Stephenson. (A) Plane-polarized light; (B, C) crossed polars; base of photos *c.* 2 mm.

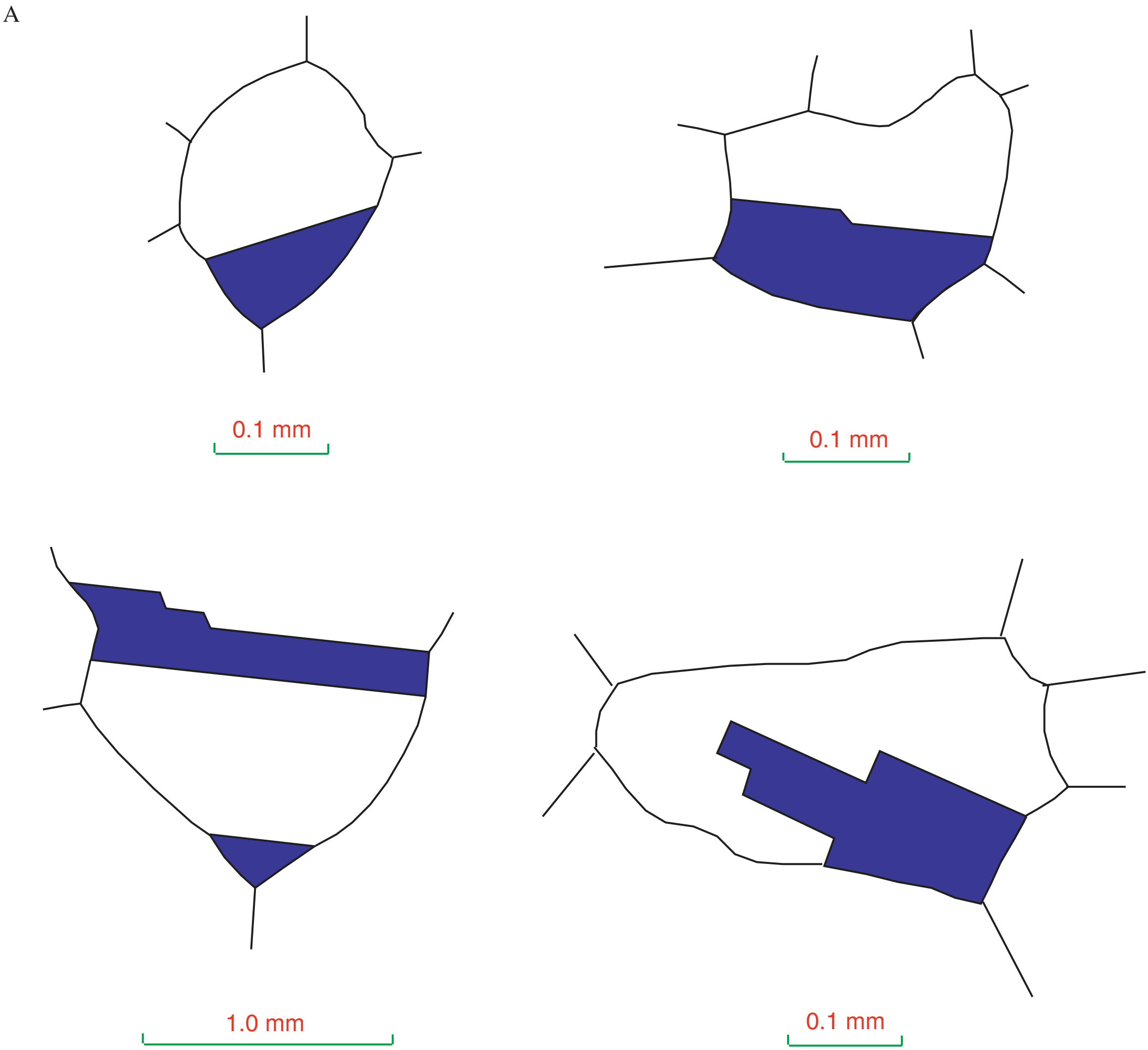

Fig. 4.44: (A) Sketches of growth twins in plagioclase in granulite facies metabasic rocks from Broken Hill, Australia (based on Vernon, 1968). The twins are simple and multiple, with straight or abruptly stepped interfaces. (B) Sketch showing development of growth twins during solid-state grain growth. Growth begins with random (statistically high-energy) boundaries (AB, AC, BC) moving in the direction of their centres of curvature, but as growth proceeds, a twin boundary is produced. The formation of the new orientation A′ leads to the formation of new, lower-energy ('coincidence') boundaries A′B and A′C. The production of the twin is favoured if the total free energy (γ) of these new coincidence boundaries, plus the new twin boundary (with very low γ), plus the original unaffected high-energy boundary (BC) is less than the total γ of the original three high-energy boundaries.

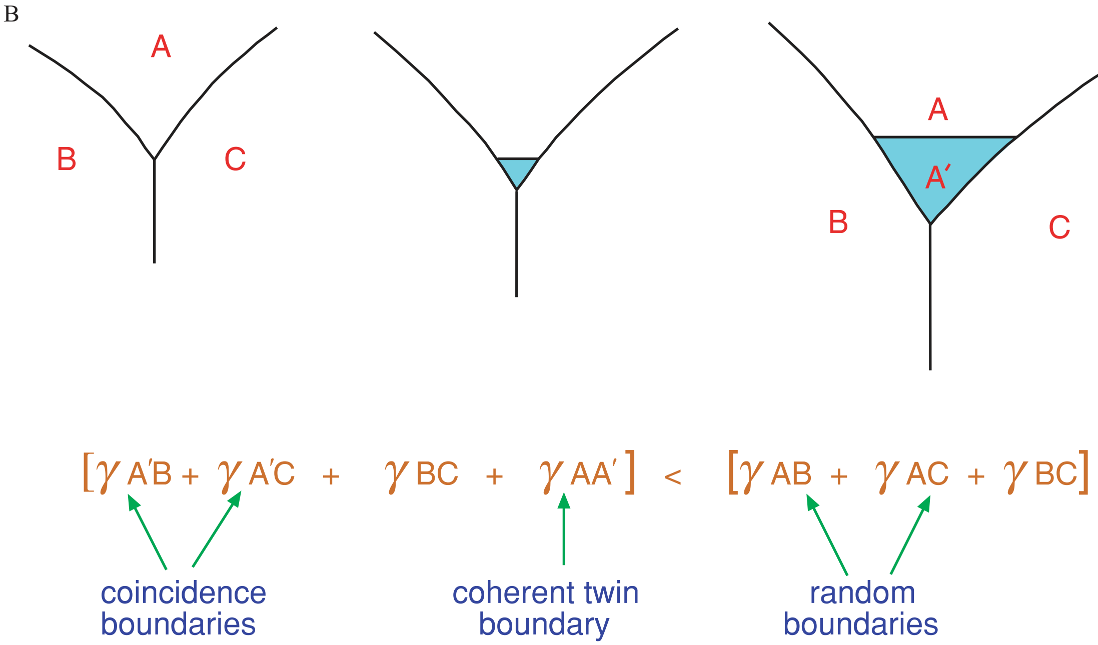

Fig. 4.44: (*cont.*)

simple twinning, without multiple twins, are more common than in igneous plagioclase. These features are all shown by the plagioclase twins in Fig. 4.44A.

Cordierite commonly has three sets of multiple twins oriented at 60° or 120° to each other (Deer *et al*., 1992), as shown in Fig. 4.45. They can be distinguished from multiple twins in plagioclase (which has similar relief and birefringence) on the basis of these angles (plagioclase twins intersect at nearly 90°), provided the section is oriented perpendicular to the twin interfaces; oblique sections show diffuse twin boundaries and smaller angles. Abruptly stepped and terminated twins (Figs. 4.45, 4.46) suggest a growth origin, their arrangement apparently being related to the pseudohexagonal symmetry of cordierite. Multiple twins may show abruptly stepped and lenticular interfaces in the same cordierite crystal, suggesting solid-state deformation after the growth twins had been formed during crystallization (Fig. 4.45).

Cordierite also commonly has *sector twinning* (‘cyclic twinning’), as shown in Fig. 4.46. This involves only changes in orientation, not in chemical composition, and so should not be confused with sector zoning (Sections 3.11.11, 4.12.2). The crystallographic relationships of sector and multiple twinning in cordierite are illustrated by Deer *et al*. (1992, fig. 46). Sector twinning may be of growth origin, and also appears to be connected with the pseudohexagonal symmetry of cordierite.

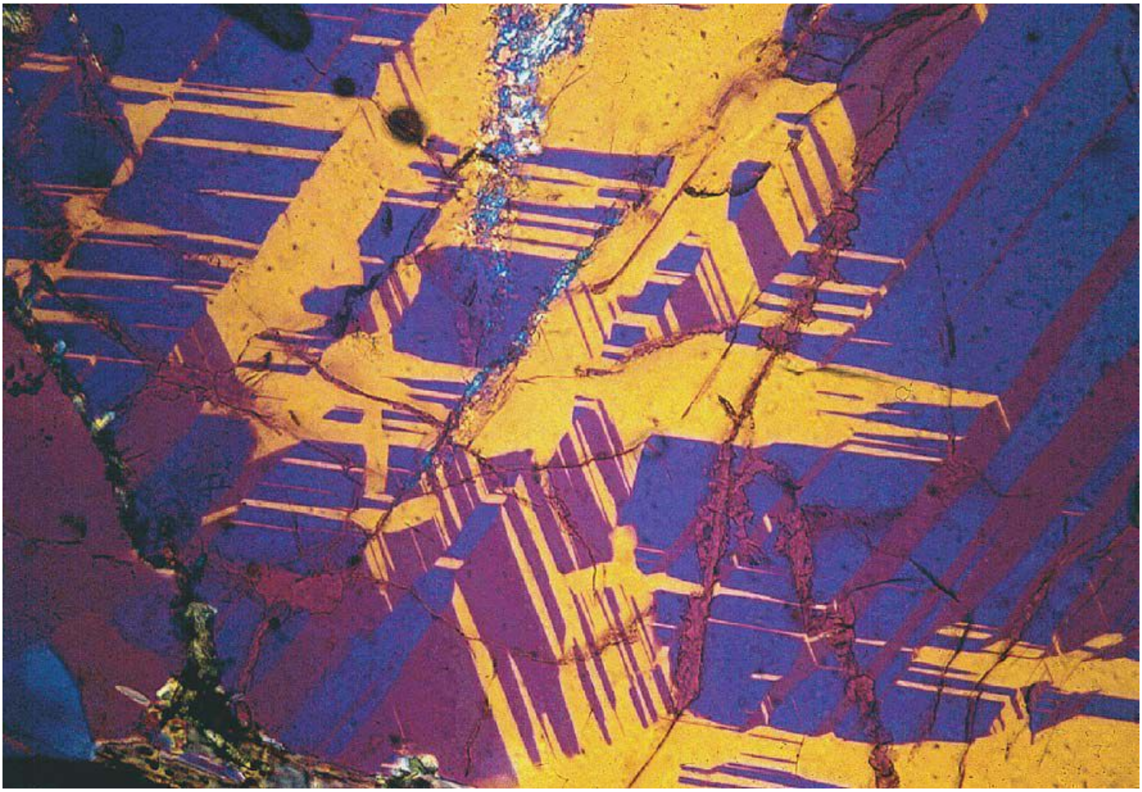

Fig. 4.45: Multiple twins in three orientations (each showing a different interference colour in response to a quarter-wave plate used in the photograph) in cordierite from a high-grade metamorphic rock from the Arunta Inlier, central Australia. Some of the twins are abruptly stepped, suggesting a growth origin, whereas others are lenticular, suggesting later solid-state deformation. Crossed polars; base of photo 1.5 mm.

4.8 Transformation twinning

Transformation twinning occurs in the solid state, as a mineral changes from a higher to a lower symmetry. For example, orthoclase (monoclinic) transforms to microcline (triclinic) with slow cooling through about 500 K. The change in the angle between the *b* and *c* crystallographic axes from 90° in orthoclase to an oblique angle in microcline leads to two possible orientations that are in albite-law twin relationship and two others in pericline-law twin relationship (Section 5.3.3), as shown in Fig. 4.47. Complex, almost orthogonal sets of randomly distributed albite and pericline twins are characteristic of microcline (Figs. 4.48–4.50). This transformation twinning may be too fine to see clearly with the microscope, but tectonic strain and/or hydrothermal alteration cause it to coarsen into the clear tartan (cross-hatched) pattern that is diagnostic of microcline (Eggleton, 1979;

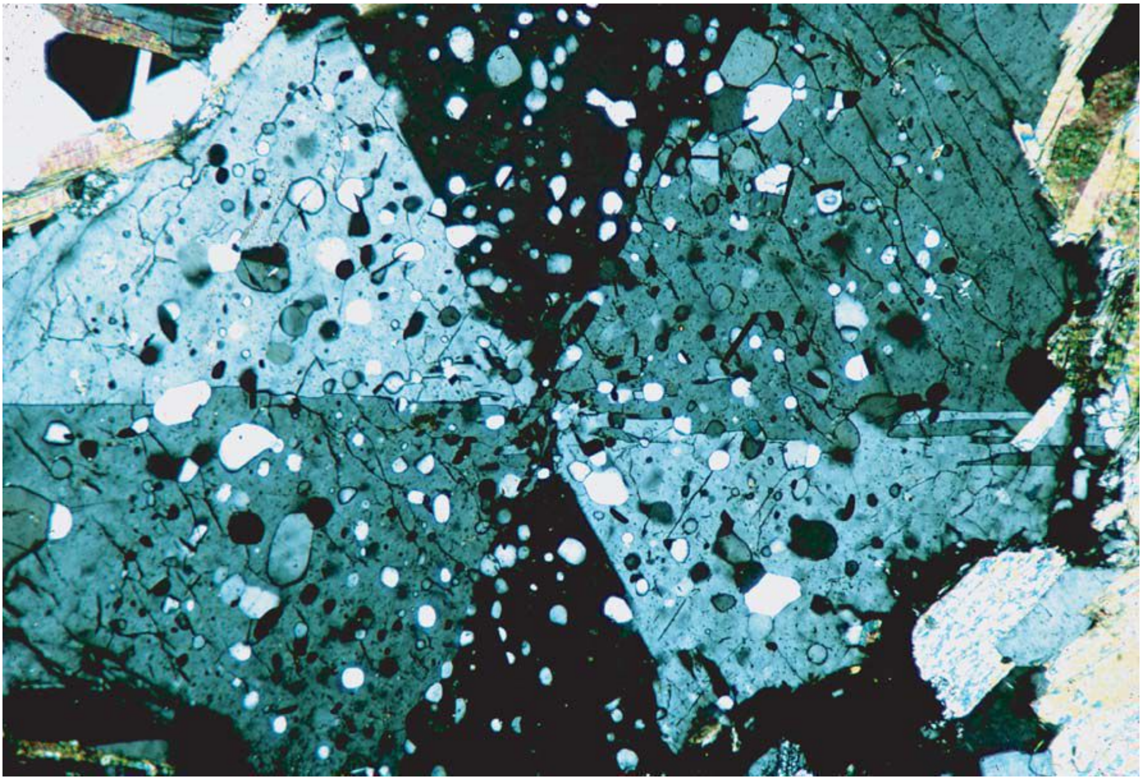

Fig. 4.46: Sector twinning in cordierite with abundant rounded inclusions of quartz. Opposite sectors have the same crystallographic orientation, as shown by the interference colours; two are at extinction. The bottom right sector also shows some abruptly terminated and stepped growth twins. Crossed polars; base of photo 2 mm.

Eggleton & Buseck, 1980; Brown & Parsons, 1989; Bell & Johnson, 1989b). Fitz Gerald & McLaren (1982) found that microcline twinning did not occur in the absence of stress in their experiments. In fact, optically visible microcline twinning is characteristic of K-feldspar that has been deformed in the solid state (Sections 5.7.6, 5.7.9). For example, Fig. 4.49 shows subgrains in quartz and patchy microcline twinning, both microstructures being typical of the solid-state deformation of granitic rocks. Microcline twinning can also be caused by lattice strain adjacent to thick exsolved lamellae of albite (Fig. 4.50). Waldron *et al.* (1993) suggested that the orthoclase–microcline transformation may require local interaction with fluid.

Dauphiné twins in quartz, which are formed as a result of strain associated with the transformation from the high-temperature to the low-temperature polymorph (see, for example, Putnis & McConnell, 1980, p. 92), are revealed by chemical etching of polished surfaces or by scanning electron microscopy in orientation contrast mode (see, for example, Trepmann & Stöckhert, 2003).

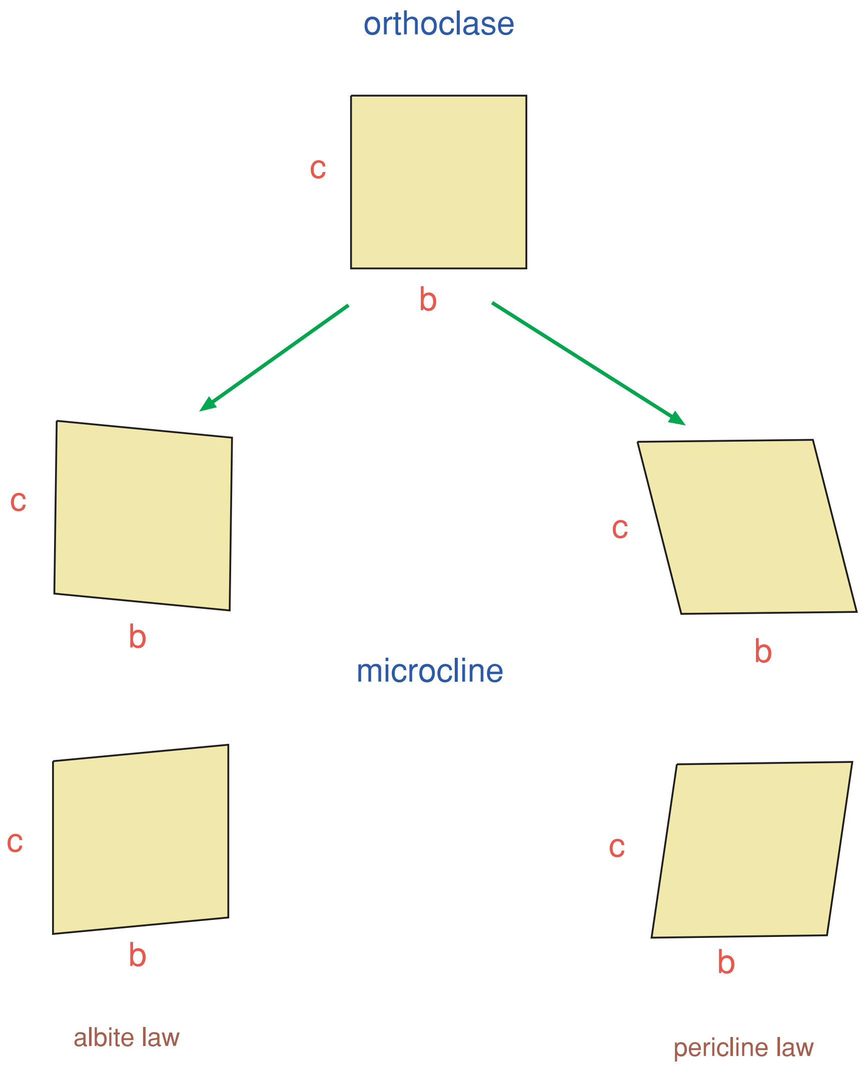

Fig. 4.47: Sketch showing a *b*–*c* section of orthoclase, with the four possible orientations (in albite and pericline twin relationship) caused by the solid-state change to the lower-symmetry, triclinic microcline. Based on Putnis & McConnell (1980).

4.9 Exsolution

Exsolution (unmixing) occurs when a homogeneous solid solution (i.e. a single mineral) becomes unstable and breaks down into two minerals. It may occur in igneous as well as metamorphic minerals, but is discussed here because it is a solid-state process. Exsolution generally occurs with decreasing temperature, because at higher temperatures the larger vibrations of the atoms enable the

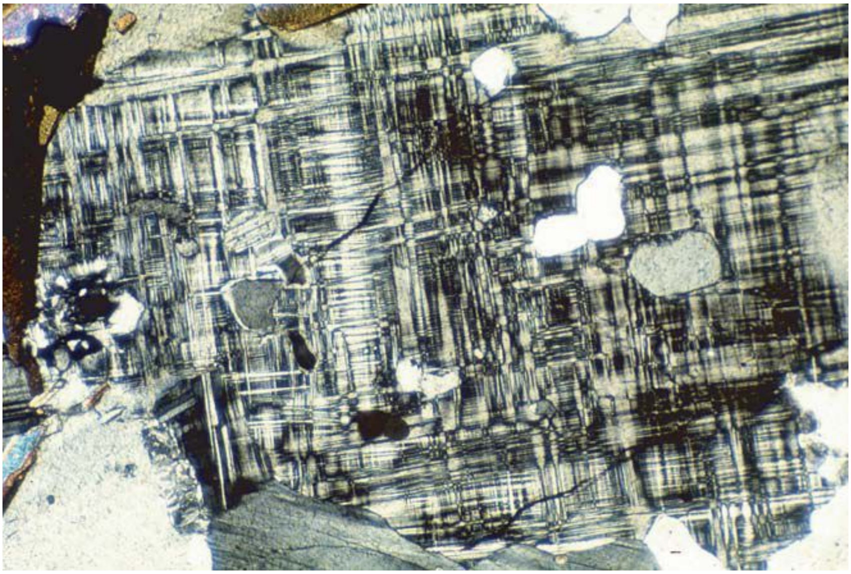

Fig. 4.48: Well-developed tartan twinning in microcline in a metamorphosed granitic rock from Sweden. The microcline has rounded quartz inclusions. Crossed polars; base of photo 2 mm.

substitution of 'foreign' atoms in the crystal structure. As the temperature drops, the 'foreign' atoms are forced out of the homogeneous structure, because the vibrational energy of atoms is lowered and so the cation sites become smaller. The ejected atoms are accommodated in grains of a new mineral that nucleates inside the original homogeneous grain. Thus, exsolution is an intragranular solid-state process involving diffusion of atoms through the solid crystal structure. Exsolution is common in silicate minerals (especially feldspar, amphibole and pyroxene), as well as in sulphide and oxide minerals (Figs. 4.30, 4.50–4.55). Mechanisms of exsolution have been reviewed by Yund & McCallister (1970), Champness & Lorimer (1976) and Putnis & McConnell (1980).

The intergrown minerals typically have related atomic structures, with the result that one of the minerals generally occurs as lamellae in crystallographic relationship with the other ('host') mineral (see, for example, Schwartz, 1931; Edwards, 1947, 1952; Deer *et al.*, 1992; Putnis & McConnell, 1980). This produces minimum-energy interfaces between the two exsolved minerals.

The nature of the interface is determined by the crystal structures of the two minerals (Fig. 4.52). If they are similar, the lattice matching across the boundary is good, resulting in a low-energy *coherent* interface, in which the only distortions are elastic (no broken bonds). Less perfect fits result in higher-energy *semi-coherent* and *incoherent* interfaces, containing dislocations. For example, interfaces between albite and K-feldspar are incoherent; so, although thin albite

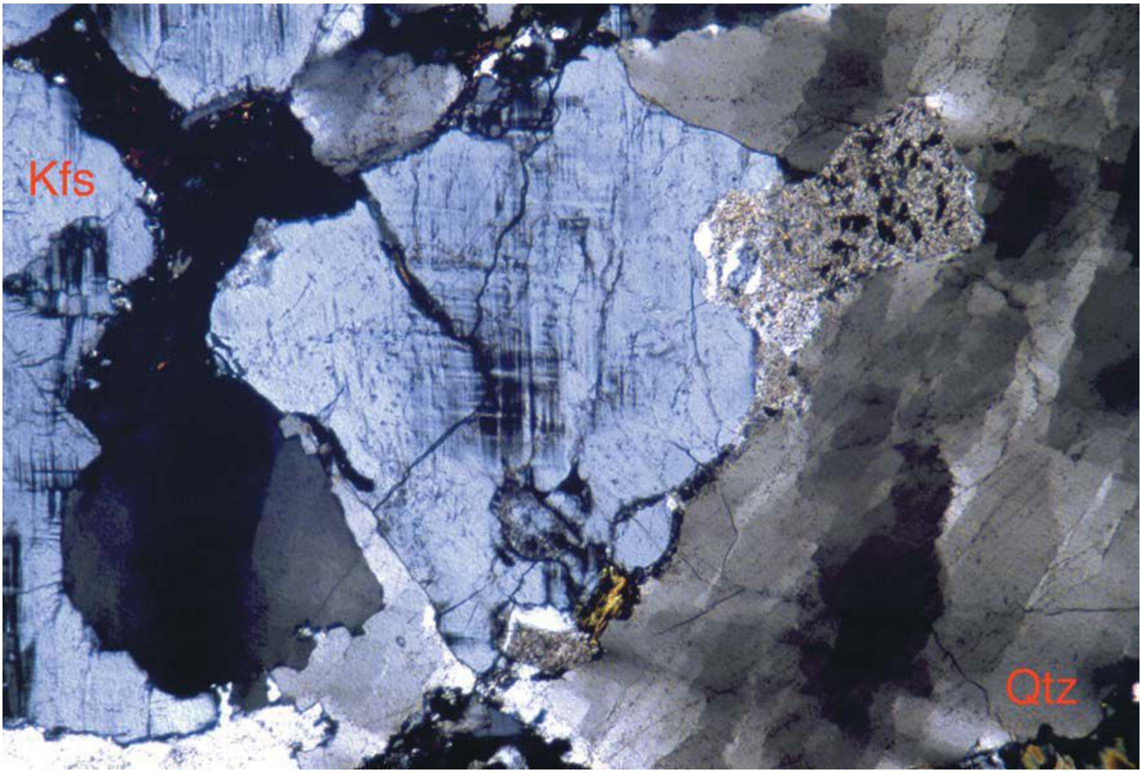

Fig. 4.49: Patchy tartan twinning in microcline (Kfs) in a deformed granite from the Bega Batholith, south-eastern New South Wales, Australia. Also shown are blocky subgrains in quartz (Qtz), discussed in Section 5.4.1. Both the microcline twinning and the quartz subgrains are due to solid-state deformation (Chapter 5). Crossed polars; base of photo 4 mm.

lamellae in K-feldspar are relatively regular (Figs. 4.30, 4.54), thicker lamellae tend to be lenticular and irregular (Figs. 4.50, 4.51).

4.9.1 Exsolution in silicate minerals

Good examples of exsolution in silicate minerals are seen in the pyroxene and feldspar groups. Most natural alkali feldspars are mixtures of exsolved K-rich and Na-rich feldspars, although a complete solid solution between sanidine and albite occurs at high ('hypersolvus') temperatures (see, for example, J. Smith, 1974, 1983; Yund, 1983; Deer *et al.*, 1992). Below a particular temperature (the 'solvus' temperature) for a particular composition of alkali feldspar, the homogeneous solid solution breaks down (unmixes, exsolves) into two minerals (K-rich and Na-rich feldspar), which generally occur as lamellar intergrowths, owing to

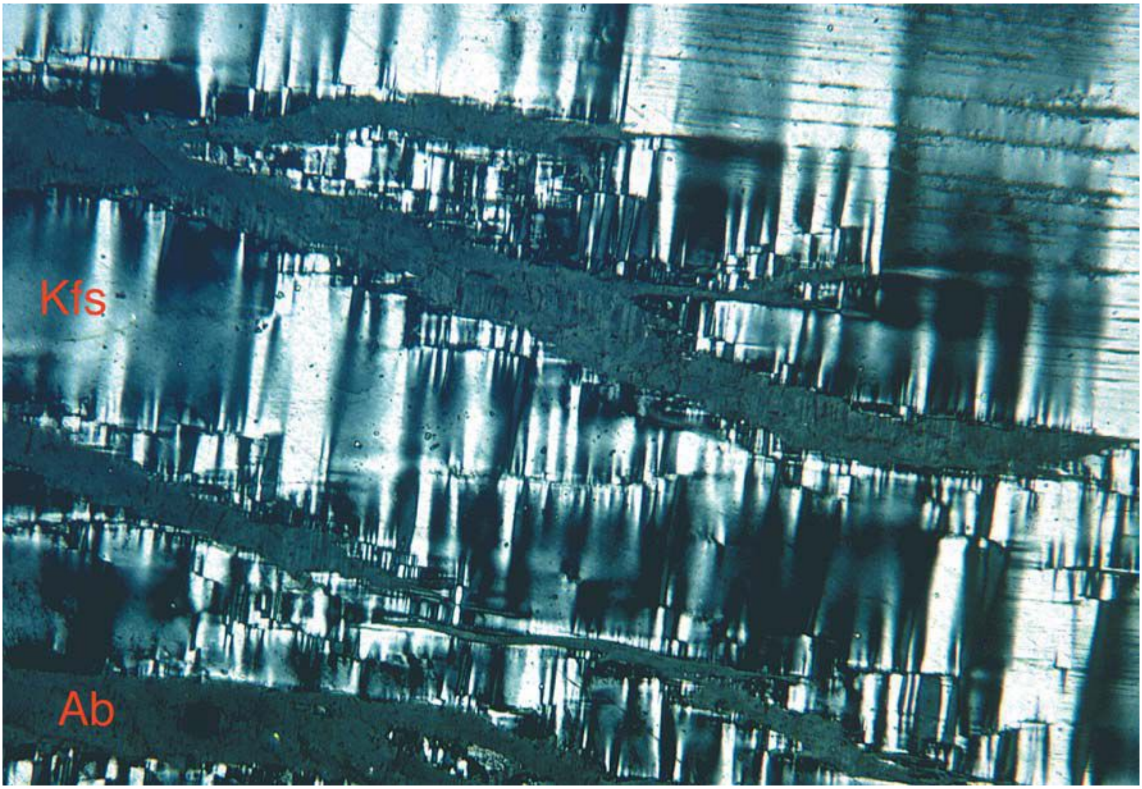

Fig. 4.50: Microcline perthite in a coarse-grained granitic rock from Japan. The exsolved albite (Ab) lamellae anastomose and are of variable width. The microcline twinning is most intense adjacent to the albite lamellae, which probably reflects lattice strain caused by differences in the crystal structures of the two minerals. Crossed polars; base of photo 1.3 mm.

some degree of structural similarity of the two minerals (Figs. 4.30, 4.50, 4.51, 4.54). The intergrowth is called *perthite*. The most common perthitic intergrowth seen with the microscope (*microperthite*) consists of incoherent exsolution lamellae of albite in a K-feldspar host (orthoclase or microcline). The lamellae are commonly lenticular and may bifurcate, as shown in Figs. 4.50 and 4.51. Although commonly they are relatively uniformly distributed through the host grain (Fig. 4.30), they may be irregular and patchy (Fig. 4.51). Extremely lenticular albite lamellae occur in the aptly named ‘flame perthite’ (Fig. 4.54), for which a replacement, rather than an exsolution, origin has been suggested (Sections 5.6.6, 5.7.9). Alkali feldspar in volcanic rocks may have exsolution lamellae that are too fine to see optically, requiring X-ray diffraction or TEM for identification (*cryptoperthite*).

Plagioclase also forms a solid solution of albite and anorthite at high temperatures, but most natural plagioclase consists of exsolution intergrowths of various

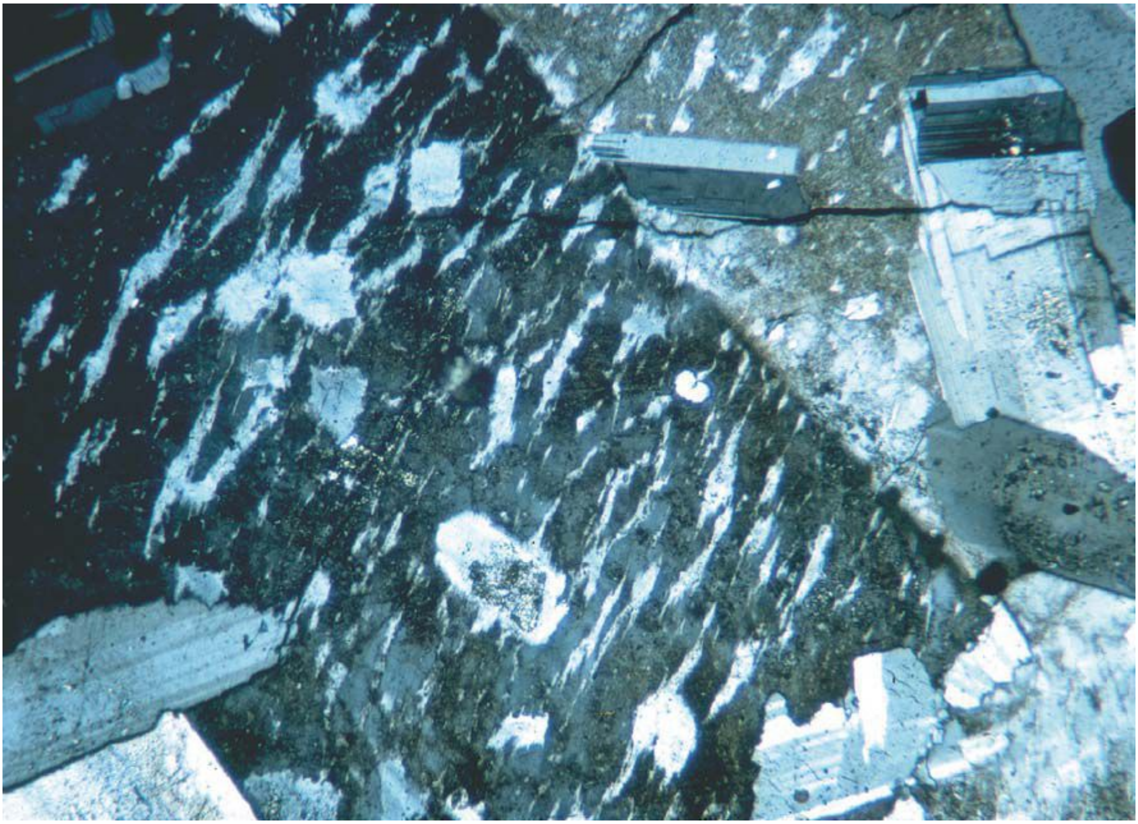

Fig. 4.51: Patchy, lenticular exsolution lamellae of albite in K-feldspar in a granite. The K-feldspar shows a simple twin and contains several euhedral inclusions of plagioclase. Some of the plagioclase inclusions have developed irregular shapes, as a result of precipitation of albite on them during the exsolution process. Crossed polars; base of photo 3.5 mm.

plagioclase compositions and structures. Although these intergrowths are generally too fine to detect optically, they are revealed by TEM (Fig. 4.55). For example, optically homogeneous plagioclase between An_{02} and An_{16} is actually an exsolution intergrowth (*peristerite*) consisting of submicroscopic lamellae of An_0 and An_{25} (J. Smith, 1983; Deer *et al*., 1992).

4.9.2 Exsolution in metals, sulphides and oxides

Exsolution is common in metals, and in sulphide and oxide minerals (Fig. 4.53). The relationship of exsolution to atomic structure has been discussed by Edwards (1947, 1952), Bastin (1950) and Stanton (1972), who listed some 50 exsolution mineral pairs, and a compendium has also been published by Ramdohr (1969). Experiments relevant to exsolution microstructures in Cu–Fe sulphide minerals

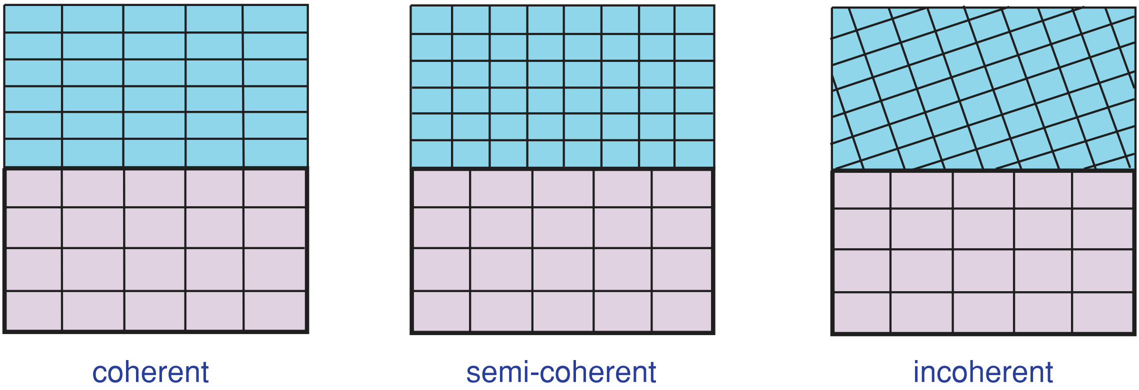

Fig. 4.52: Sketches to illustrate coherent, semi-coherent and incoherent interfaces between two minerals. Based on Putnis & McConnell (1980).

have been discussed by Brett (1964) and Brett & Kullerud (1967), and exsolution in terrestrial oxide minerals has been discussed in detail by Haggerty (1976).

Exsolution microstructures in opaque minerals can be observed in plane-polarized reflected light if the two minerals are sufficiently different in colour (Fig. 4.53) and in crossed polars if the two minerals are sufficiently different in bireflection colours. Chemical etching may reveal or enhance the appearance of twin lamellae in some instances (Edwards, 1947, figs. 91, 92, 98).

Many intergrowths develop from relatively few nuclei and grow as strongly oriented lamellar intergrowths, the atomic structure of both minerals being closely related (Stanton, 1972), as shown in Fig. 4.53. Examples include nickel-rich exsolution lamellae in an iron-rich host (*Widmanstätten structure*) in iron meteorites, as well as exsolution intergrowths of chalcopyrite–cubanite (Fig. 4.53) (Bastin, 1950, plate 2, fig. 5; Stanton, 1972), chalcopyrite–bornite (Bastin, 1950, plate 3, fig. 1; Durazzo & Taylor, 1982), chalcocite–bornite (Edwards, 1947, fig. 77), magnetite–ilmenite (Bastin, 1950, plate 2, fig. 4; Edwards, 1947; Haggerty, 1976), and ilmenite–hematite (Bastin, 1950, plate 2, fig. 6; Edwards, 1947; Haggerty, 1976; Craig & Vaughan, 1994).

Care should be taken to distinguish exsolution lamellae from possible lamellae formed by replacement along specific crystallographic planes. A good example is the common replacement (oxidation) of magnetite by hematite ('martitization'). In less common exsolution intergrowths of these minerals, the hematite lamellae are evenly distributed through the magnetite and are of uniform thickness, whereas in replacement intergrowths the lamellae tend to concentrate at the magnetite grain boundaries (commonly forming an irregular rim) and along fractures, owing to the progressive replacement of the magnetite from the grain edges towards the centre (Edwards, 1949). Of course, both kinds of intergrowth may form (at different times) in the same grain, which increases the difficulty of interpretation.

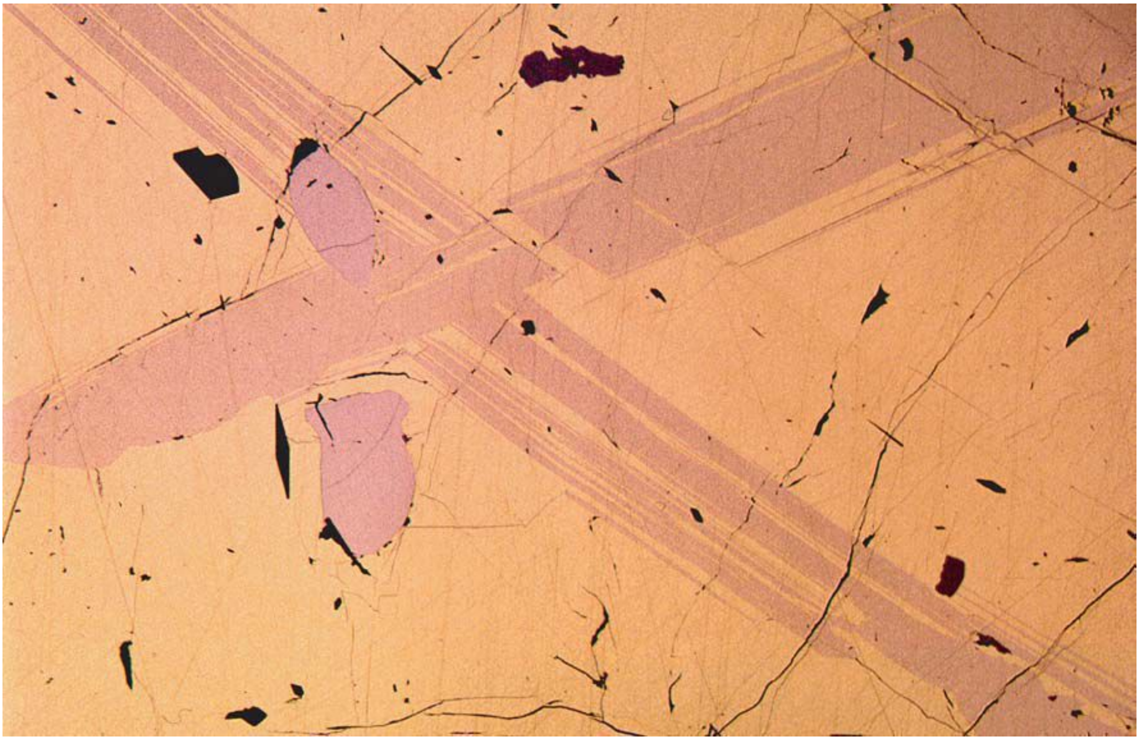

Fig. 4.53: Exsolved lamellae of cubanite in chalcopyrite from Broken Hill, New South Wales, Australia. Polished section in plane-polarized reflected light; base of photo 1.5 mm.

In some examples, the exsolved mineral tends to form separate nuclei, and may grow into oriented lenses and apparently unoriented blebs, even where a close lattice relationship exists between the host and exsolved minerals, as with sphalerite–chalcopyrite and pentlandite–pyrrhotite (Stanton, 1972). Rods and isolated blebs of chalcopyrite in sphalerite may also occur. Traditionally these have been regarded as being of exsolution origin (see, for example, Schwartz, 1931; Borchert, 1934; Edwards, 1947). However, Wiggins & Craig (1980), Hutchison & Scott (1981) and Sugaki *et al*. (1987) have suggested that the solubility of chalcopyrite components in sphalerite is too small to account for the observed amounts of chalcopyrite by exsolution. An origin by replacement has been suggested instead (see, for example, Barton & Bethke, 1987; Eldridge *et al*., 1988). A similar argument concerns the occurrence of sphalerite 'stars' (skeletal crystals) in chalcopyrite. For example, Marignac (1989) found that Zn is present in excess of the amounts predicted experimentally for the inferred temperature of formation of the natural intergrowth. However, Sugaki *et al*. (1987) found that exsolution is consistent with the Zn content of some chalcopyrite with sphalerite 'stars' in some Japanese ore deposits. Evidently, the situation is complicated, and each example may require individual interpretation.

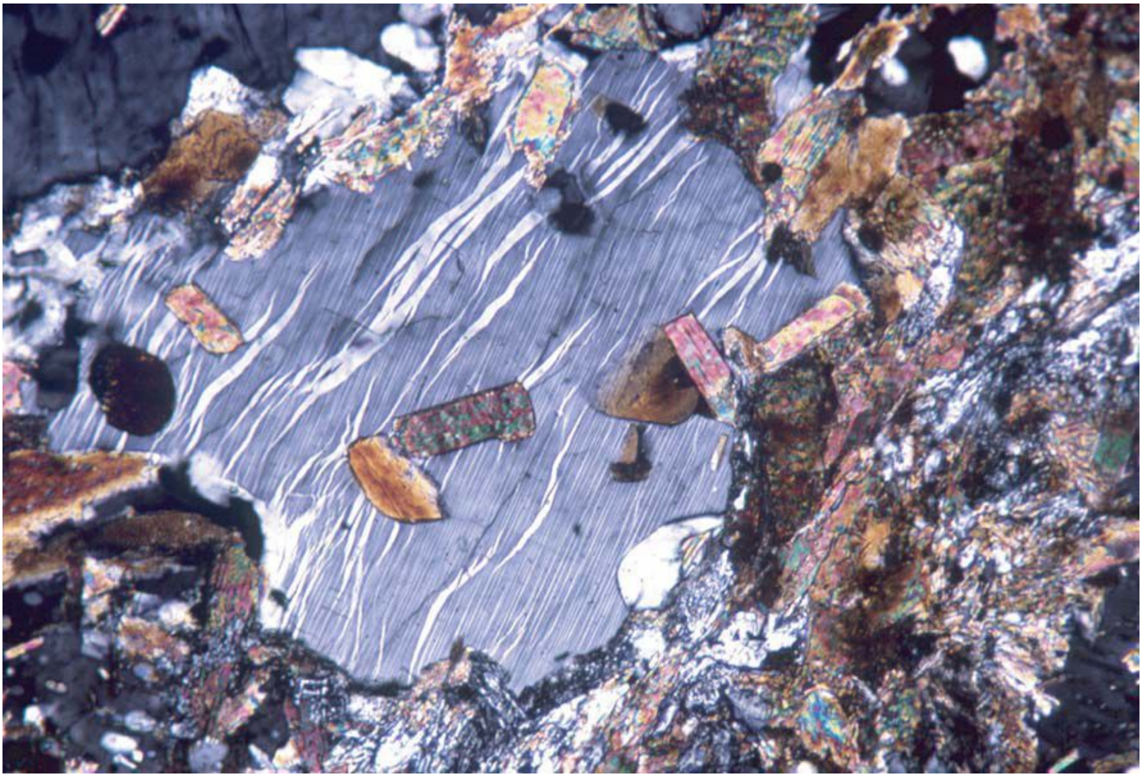

Fig. 4.54: Tapering, wavy, flame-like lamellae of albite in 'flame perthite', in an amphibolite-facies metapelitic rock from the Cooma Complex, south-eastern New South Wales, Australia. The concentration of the albite lamellae varies considerably through the host K-feldspar grain. Flame perthite has been inferred to be the result of replacement of K-feldspar by albite in high-strain sites during deformation (Sections 5.6.6, 5.7.9). Also present are thin, continuous lamellae of albite produced earlier by unmixing of a homogeneous alkali feldspar during cooling from peak metamorphic temperatures. Crossed polars; base of photo 1.7 mm.

4.10 Symplectic intergrowths

4.10.1 Definition and identification

Symplectic intergrowths ('symplectites') are vermicular (worm-like) intergrowths of minerals that grow simultaneously in a solid-state reaction (Figs. 4.56–4.62). The most common example is *myrmekite* (Figs. 4.56, 4.57), a symplectic intergrowth of quartz and sodic plagioclase (Section 4.10.4), but many other silicate and oxide minerals (Section 4.11.5), as well as sulphide minerals (Section 4.10.6), occur in symplectites. In addition, symplectites have been observed in martian basaltic meteorites (Aramovich *et al.*, 2002).

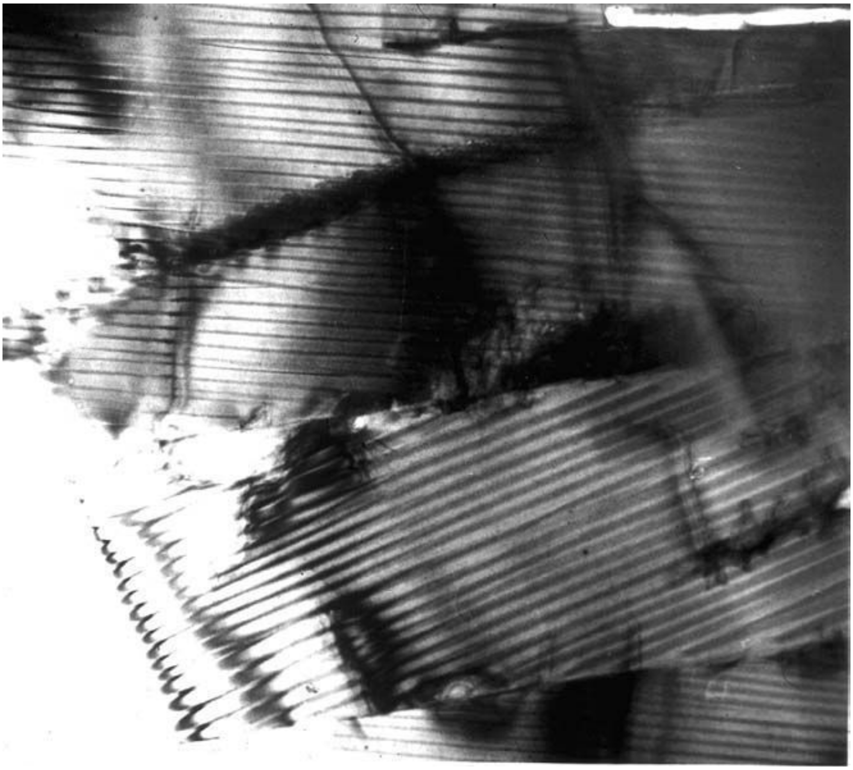

Fig. 4.55: Peristerite exsolution intergrowth in oligoclase from Mount Isa, Queensland, Australia, as seen in the TEM. The orientation of the exsolution lamellae changes across albite-law twin boundaries. Photo by courtesy of Alec McLaren and John Fitz Gerald. Base of photo 3 μm.

Although most symplectites are formed in solid-state metamorphic reactions, fluids may be involved in the transport of chemical components. Moreover, symplectites may develop in the presence of small amounts of residual magma in cooling igneous rocks, such as olivine–plagioclase symplectites in some gabbros (de Haas *et al.*, 2002).

The minerals in many symplectites can be identified in the light microscope. Minerals in fine-grained symplectites are best observed in polished sections, whether in transmitted or reflected light, because reflected light images are generally sharper (see, for example, Drüppel *et al.*, 2001). SEM images (Fig. 4.59) reveal the most detail, and also enable chemical analysis of each mineral to be carried out (see, for example, Vernon & Pooley, 1981; Brodie, 1995; Wirth & Voll, 1987; Carswell *et al.*, 1989; Thost *et al.*, 1991, fig. 8; Harlov & Wirth, 2000; Rickers *et al.*, 2001; Aramovich *et al.*, 2002). Colour X-ray composition maps (Fig. 4.60) are being increasingly used in work on symplectites (see, for example, Aramovich *et al.*, 2002). Cathodoluminescence has also been used

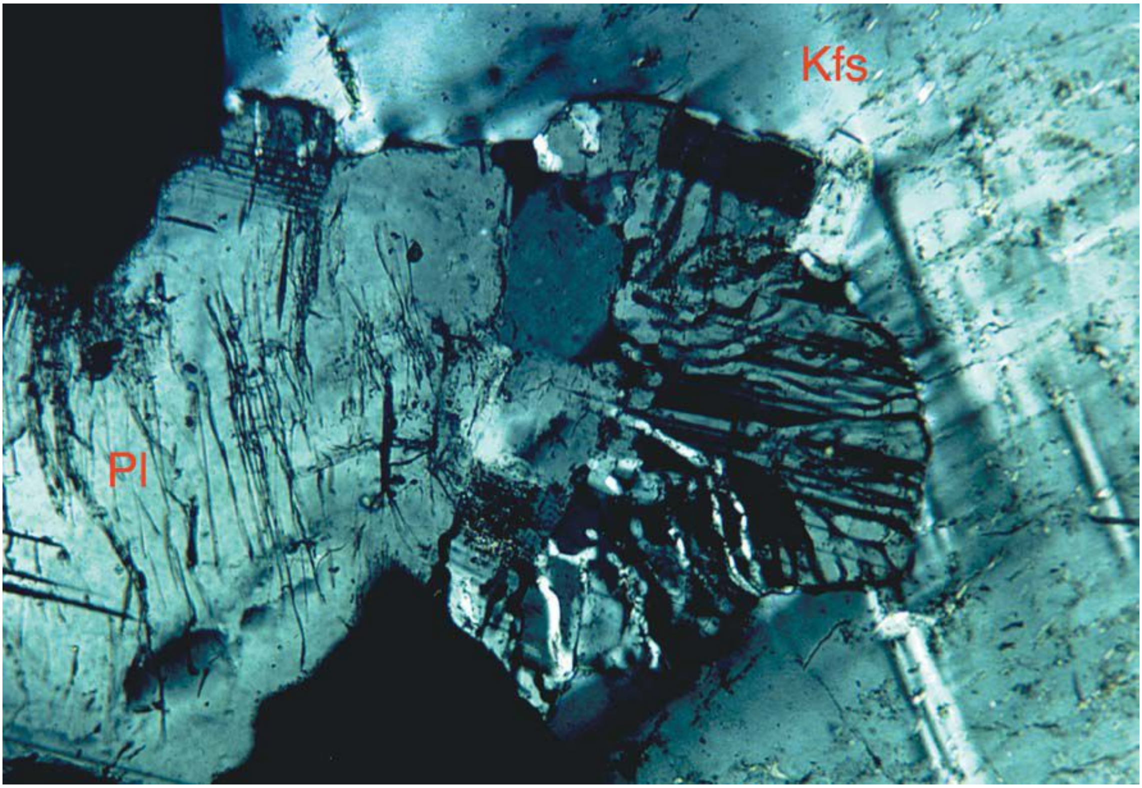

Fig. 4.56: Myrmekite (symplectic intergrowth of quartz and sodic plagioclase) replacing microcline (Kfs) in a deformed granite. The lamellar twins in the primary (magmatic) plagioclase (Pl) are parallel to those in the plagioclase of the myrmekite 'colony', indicating that the myrmekitic plagioclase nucleated on the magmatic plagioclase. Crossed polars; base of photo 1.3 mm.

for the examination of myrmekite (Hopson & Ramseyer, 1990; Garcia *et al.*, 1996).

4.10.2 Importance of symplectites in metamorphism

Experiments on minerals and synthetic materials, such as steel, have shown that the minerals in symplectic intergrowths grow simultaneously. Therefore, symplectites help in inferring the solid products of metamorphic reactions. Moreover, symplectite-forming reactions commonly are incomplete, probably owing to the fact that the symplectite grows inside a crystalline grain, in which diffusion rates are relatively slow. The symplectite commonly occurs as lobes projecting into, or as a rim (*corona*) around, the grain being replaced. As a result, both the reactant mineral and the solid products are generally observable. This enables realistic chemical equations to be written, although the reactions involved may be complex

Fig. 4.57: Myrmekite 'colonies' replacing a porphyroclast of microcline (with tartan twinning) around its edges in a felsic mylonite (Section 5.7.6) from near Lago Maggiore, northern Italy. From Vernon (2000a, *Journal of Electronic Geosciences*, vol. 5, p. 7, fig. 15), with permission of Springer-Verlag. Crossed polars; base of photo 4.4 mm.

and may involve components in solution from outside the symplectite. Therefore, symplectic intergrowths can be very useful in working out a rock's metamorphic history. If the *P–T* stability fields of the mineral assemblages in the intergrowths are known from experimental studies and/or thermochemical calculations, symplectites can also be useful for inferring tectonothermal histories of metamorphic terranes.

Symplectites grow in low-strain localities, as evidenced by the random arrangement of delicate shapes, which could not survive in high-strain environments (Hanmer, 1982). In fact, they become distorted and recrystallized into granular aggregates when deformed (Vernon *et al.*, 1983). However, they may develop during deformation, forming as oriented intergrowths in low-strain sites (Brodie, 1995) or as 'colonies' inside porphyroclasts (Simpson & Wintsch, 1989), and strain may contribute indirectly to their formation (Vernon, 1991b), as discussed in Section 5.6.6.

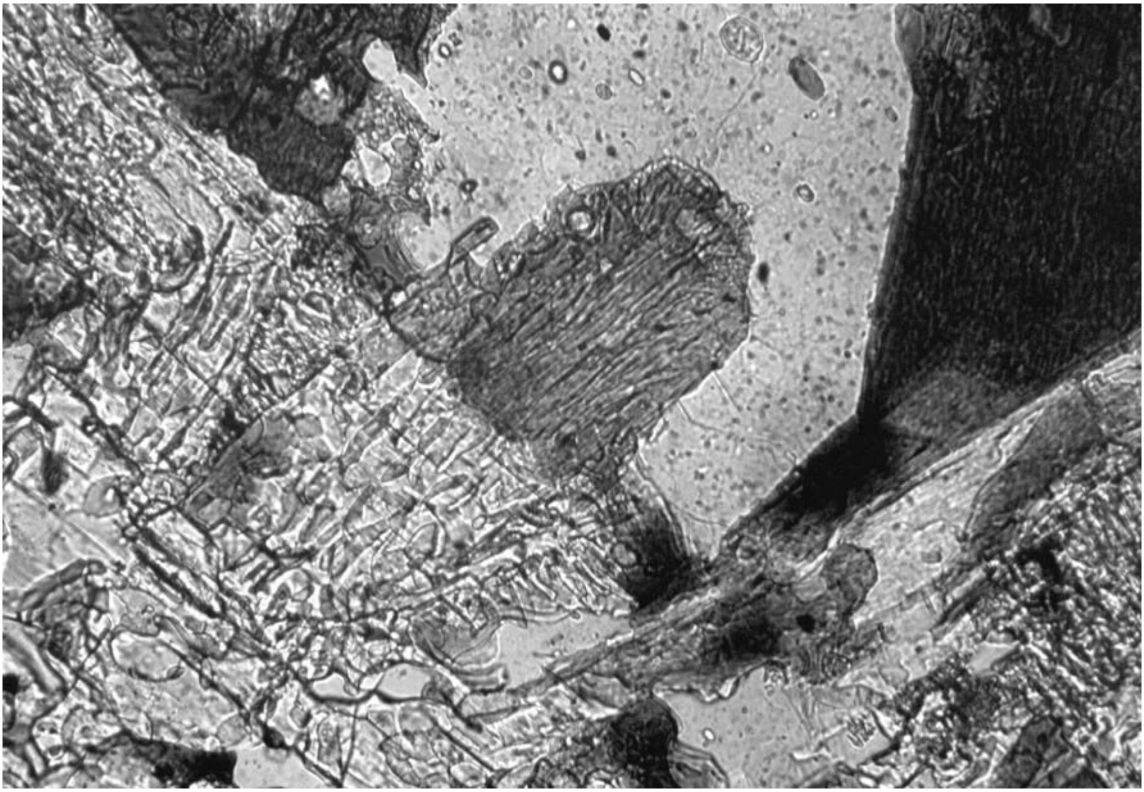

Fig. 4.58: Symplectic intergrowths of quartz–andalusite (bottom left) and quartz–biotite (centre) that formed as a result of the reaction: cordierite + K-feldspar = quartz + andalusite + biotite, in an amphibolite facies rock from the Cooma Complex, south-eastern Australia. The quartz rods run continuously from the andalusite into the biotite (as shown in Fig. 4.59). A 'colony' of quartz–biotite symplectite has partly replaced cordierite (with yellow pleochroic haloes around minute inclusions of radioactive minerals). Plane-polarized light; base of photo 0.75 mm.

4.10.3 Nucleation and growth of symplectites

Symplectites nucleate at existing grain boundaries, which are sites of high atomic disorder that permit diffusion of components to the new minerals (Smith, 1953). The grain on which the intergrowth grows typically acts as the nucleus for the more abundant of the two minerals, e.g. plagioclase in myrmekite (Section 4.10.4), which retains the same orientation as that grain (Fig. 4.56).

Once a viable nucleus of each mineral is formed, the minerals grow together as rods or lamellae. The boundaries between the rods or lamellae are rarely planar, and so probably have dislocations along them, which can cause them to change shape if heated and/or deformed (Section 4.11.3). Movement of the

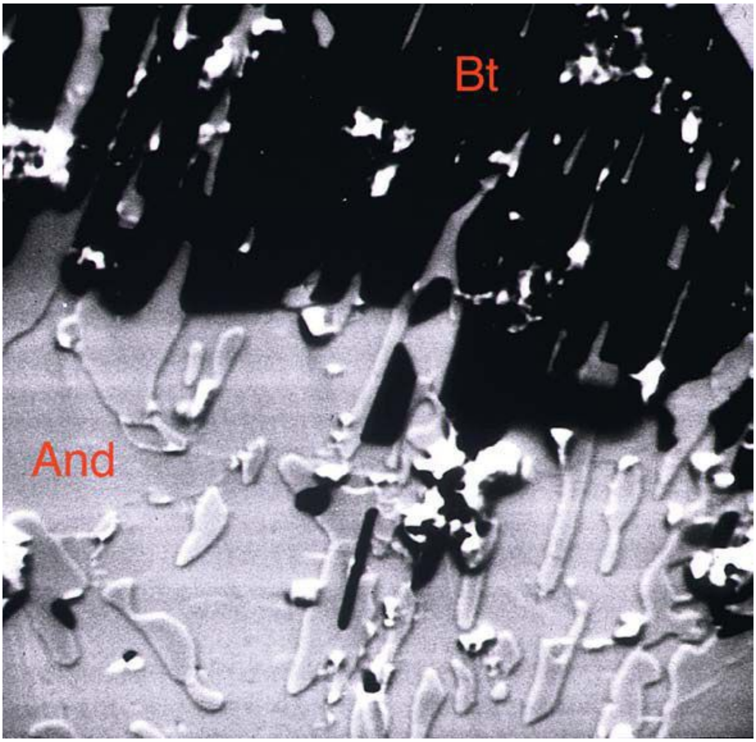

Fig. 4.59: Symplectic intergrowths of quartz–andalusite (And) and quartz–biotite (Bt), similar to those shown in Fig. 4.58, as observed in the SEM. Some of the quartz rods pass continuously from the andalusite into the biotite. Amphibolite facies rock from the Cooma Complex, south-eastern Australia. Base of image 0.1 mm. Reprinted from Vernon & Pooley (1981, fig. 1B, p. 76), with permission of Elsevier.

boundary of the intergrowth into the grain being replaced transforms it into the new intergrowth, although the chemical reaction involved may not be simple and may involve components brought into and taken out of the host grain, presumably along the advancing symplectite interface (see, for example, Mongkoltip & Ashworth, 1983).

The reasons that an intergrowth (involving the formation of a relatively large grain-boundary area) forms, rather than separate grains, are probably that (1) nucleation rates are very low, at least for one of the minerals involved, and (2) diffusion rates are low, relative to growth rates, so that elongate, somewhat dendritic grain shapes tend to be more favourable than equant grain shapes (Sections 3.5.3, 4.5). The vermicular shape presumably results from the inability of either mineral to impose a crystal form against the other (see, for example, Kretz, 1966a; Vernon, 1968), coupled with growth outwards from a single nucleus.

Factors controlling the spacing of lamellae or rods in all symplectic intergrowths presumably are basically the same, regardless of the minerals involved.

Previous Page

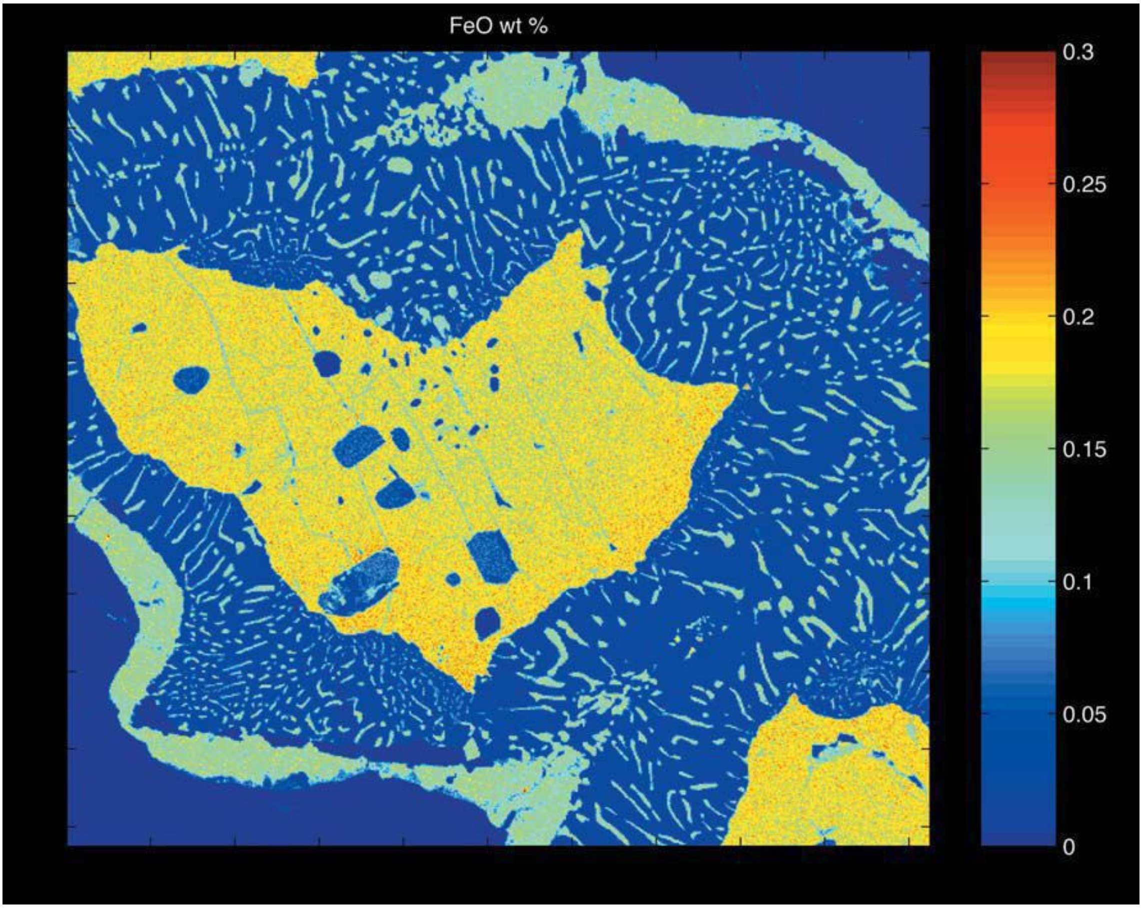

Fig. 4.60: X-ray composition map (Section 1.6), matrix-corrected, showing the distribution of FeO (wt %) in a symplectic intergrowth of cordierite (blue) and orthopyroxene (light blue-green) replacing garnet (yellow) in a granulite facies rock from the Rauer Islands, east Antarctica. An outer orthopyroxene rim (corona) occurs between the intergrowth and quartz. High Fe contents have been assigned 'warm' colours and low Fe contents have been assigned 'cool' colours. The reaction is inferred to have occurred in response to decompression from about 10 kbar to 4 kbar at about 750 °C. Image by Geoff Clarke. Base of image 0.5 mm.

The main controlling factor is the *diffusion rate*, in both eutectic (melt crystallization) and eutectoid (solid-state) transformations (see, for example, Chalmers, 1959, p. 415). A well-studied synthetic example is the eutectoid transformation in steel of austenite (gamma iron) to a lamellar symplectic intergrowth ('pearlite'), consisting of 'cementite' (iron carbide) and alpha iron (Chalmers, 1959; Brophy *et al*., 1964; van Vlack, 1964; Rostoker & Dvorak, 1965; Reed-Hill, 1973). Thick lamellae in pearlite develop at relatively high transformation

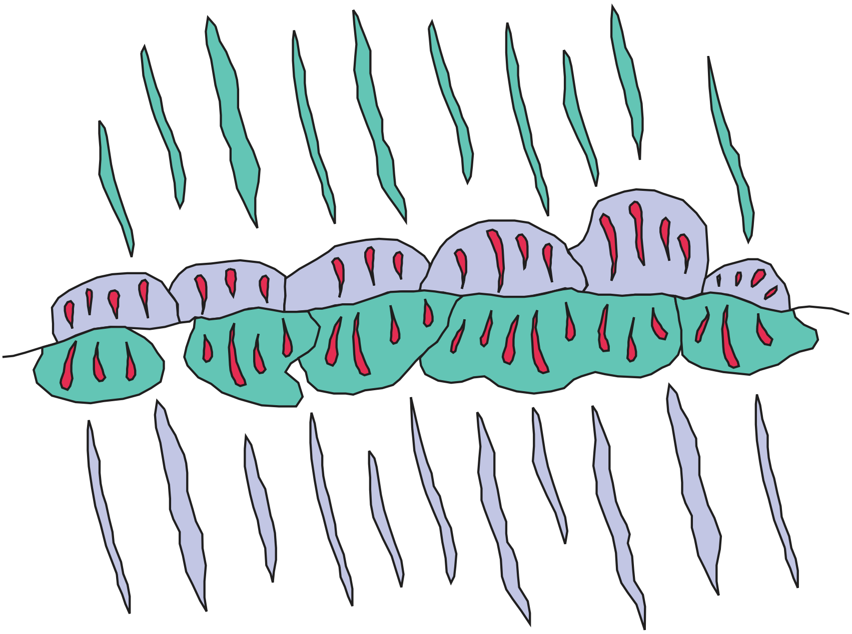

Fig. 4.61: Sketch showing 'swapped rims' of myrmekite replacing perthitic K-feldspar. The orientation of the plagioclase in the rims is the same as that of the exsolved albite in the opposite microperthite grain, suggesting that the rim plagioclase nucleated on the exsolved albite and grew into the adjacent grain. Swapped rims are commonly albite (Voll, 1960, fig. 7), but may be myrmekitic (Vernon, 1991b, fig. 1), as shown here.

temperatures, whereas fine-grained intergrowths, even beyond optical resolution, develop at lower temperatures (Brophy *et al.*, 1964, p. 125), owing to the effect of temperature on diffusion rates.

As a certain volume of one phase grows, it expels components needed by the other phase, so that the two phases grow simultaneously, without the formation of new nuclei, and steady-state lateral diffusion gradients are established. If the concentration of unwanted components increases too much adjacent to one of the phases, development of the other phase is stimulated, so that the interlamellar spacing is small. As this situation develops with slow diffusion rates, it follows that more rapid diffusion promotes coarse-grained symplectites. Although the interlamellar spacing of symplectites correlates mainly with temperature in steel, fluid activity could conceivably also contribute in rocks. Wider lamellar spacing with increasing temperature has been inferred for myrmekite by Wirth & Voll (1987).

Diffusion occurs parallel to the interface between the intergrowth and the grain being replaced. Probable diffusion paths have been illustrated for steel by Chalmers (1959, fig. 8.51) and for natural symplectites, including myrmekite, by Mongkoltip & Ashworth (1983). Mongkoltip & Ashworth (1983) noted that

Fig. 4.62: Myrmekite and muscovite formed along a fracture during deformation of weakly perthitic K-feldspar, Cooma Complex, south-eastern Australia. Crossed polars; base of photo 1.9 mm.

(1) for a two-mineral symplectic intergrowth to develop, at least two chemical components must have restricted diffusion ranges; and (2) the half-spacing of lamellae in symplectic intergrowths is the diffusion range of the slowest-diffusing component. The restricted components for myrmekite (Section 4.10.4) presumably are Si and Al, as suggested for some other symplectites by Waters (2001). Restricted diffusion, resulting in local equilibrium, is typical of symplectic reactions, as emphasized by detailed chemical studies of the minerals involved (see, for example, Grant, 1988; Carswell *et al.*, 1989).

4.10.4 Myrmekite

The most common symplectite in rocks is *myrmekite*, a vermicular intergrowth of quartz and sodic plagioclase (generally oligoclase), as shown in Figs. 4.56 and 4.57. A great deal has been written about the origin of myrmekite, and various hypotheses have been reviewed by Phillips (1974, 1980) and Simpson & Wintsch (1989). Myrmekite typically occurs as lobes projecting into K-feldspar from adjacent grains of plagioclase. In general, myrmekite is attributed to solid-state replacement of K-feldspar accompanying deformation. This inference is based partly on an analogy with evidence provided by symplectites in metals, and partly on the commonly observed crystallographic continuity of the symplectic plagioclase with primary plagioclase (see point 3, below). The following are typical features of myrmekite.

(1) Myrmekitic intergrowths are very common in deformed granitoid rocks, such as augen gneisses and felsic mylonites (see, for example, Binns, 1966; Phillips *et al.*, 1972; Vernon *et al.*, 1983; Simpson, 1985; Simpson & Wintsch, 1989; Tsurumi *et al.*, 2003), suggesting that the development of myrmekite is connected with deformation (Vernon *et al.*, 1983; Simpson & Wintsch, 1989; Vernon, 1991b; Tsurumi *et al.*, 2003), as discussed in Section 5.7.6. It is also common in less obviously deformed granites, although the K-feldspar typically shows optically visible microcline twinning, which has been inferred to indicate solid-state deformation (Eggleton & Buseck, 1980; Fitz Gerald & McLaren, 1982; Bell & Johnson, 1989b), as discussed in Section 5.7.6, as well as evidence of recovery and/or recrystallization of quartz. These features are consistent with deformation contributing to the formation of myrmekite.

(2) Myrmekite also occurs in metapelitic gneisses (see, for example, Vernon 1978b, 1979; Nold, 1984; Vernon *et al.*, 1990), where it replaces K-feldspar during late deformation.

(3) Most commonly, myrmekite occurs as lobes or colonies projecting into K-feldspar (typically microcline) from the margins. The myrmekite replaces K-feldspar, the plagioclase component typically nucleating on adjacent primary plagioclase grains, so that the plagioclase of the myrmekite has the same crystallographic orientation as that of the primary plagioclase (see, for example, Hubbard, 1966, p. 770), as indicated by twins parallel in both (Fig. 4.56). Rare observations of optical continuity between the quartz of the intergrowth and primary quartz (Stel & Breedveld, 1989) suggest that some myrmekite initiates by heterogeneous nucleation on primary quartz.

(4) Sodic plagioclase may also grow as globular rims on perthitic alkali feldspar interfaces; it appears to nucleate on albite lamellae in perthite, retaining the crystallographic orientation of the lamellae, with the result that rims of sodic plagioclase (which may or may not be myrmekitic) on each side of an original boundary between two perthite grains take the orientation of the albite lamellae of the *opposite* parent grain, forming '*swapped rims*' (Voll, 1960; Hubbard, 1966, p. 770; Vernon, 1999b), as sketched in Fig. 4.61.

(5) The proportion of quartz in the intergrowth increases progressively with increasing anorthite content of the plagioclase (Phillips & Ransom, 1968), probably because the more calcic the plagioclase, the less Si it contains.

(6) The chemical reactions responsible for myrmekite appear to be complicated. They require Na and Ca to be brought to the reaction site and K to be removed (Becke, 1908). This probably involves breakdown of other minerals in

the rock (Vernon *et al*., 1983; Simpson, 1985; Simpson & Wintsch, 1989) in a series of related ('cyclic') reactions (Section 5.6.6). For example, Ca and Na released from plagioclase reacting to form muscovite could be transferred (presumably in a fluid) to myrmekite replacing K-feldspar, from which K could be transferred to the muscovite growing in plagioclase (Simpson & Wintsch, 1989).

(7) Some myrmekite develops with muscovite (Fig. 4.62) by hydrous replacement of K-feldspar (Ashworth, 1972), for example during retrograde metamorphism (Phillips *et al*., 1972) and the deformation of granite (Vernon *et al*., 1983). Myrmekite of this type may occur along fractures in the K-feldspar, indicating that access of fluid is required (Vernon *et al*., 1983).

(8) The complex diffusion of components necessary for the aggregate to grow (Mongkoltip & Ashworth, 1983) may necessitate the presence of fluid along the boundary between myrmekite and K-feldspar, the access of such a fluid being favoured by a reduction of approximately 10 % in volume accompanying the replacement of K-feldspar by myrmekite (Simpson & Wintsch, 1989, p. 271). This film of fluid could explain the planar boundaries (possible crystal faces) of some myrmekite colonies, and is a preferable explanation to growth in a magma (Hibbard, 1979). Of course, this magmatic interpretation is inapplicable for the much more common myrmekite lobes projecting into K-feldspar, or for swapped-rim structure. Moreover, as pointed out by Simpson & Wintsch (1989), the presence of melt is out of the question for granitoids undergoing subsolidus deformation millions of years after they have crystallized. For example, myrmekite was formed in felsic rocks in retrograde zones following peak granulite facies metamorphism at Broken Hill, Australia (Phillips *et al*., 1972). Myrmekite was also formed in felsic gneisses and mylonites produced in shear zones in the Anmatjira Range, central Australia (Collins & Teyssier, 1989), 1400 Ma after the formation of the parent granitoids, the temperatures during the mylonitic deformation being too low to permit remelting.

(9) In mylonites, myrmekite grows into relatively weakly or non-deformed K-feldspar, while being deformed and recrystallized at the rear of the growing lobes (Vernon *et al*., 1983; Vernon, 1991b). This suggests that strain energy does not contribute to the advance of the growth interface of the myrmekite colony, although it appears to accompany the formation of the myrmekite, and may well contribute to access of fluids responsible for transporting the necessary chemical components for the myrmekite-forming reaction (Vernon, 1991b). The inference of Cesare *et al*. (2002b) that myrmekite may grow in the absence of deformation is based on its occurrence in contact metamorphic rocks. However, absence of deformation in contact metamorphism cannot be assumed (Vernon & Powell, 1976). Therefore, minor deformation may have contributed to the transfer of chemical components, especially as fine-grained aggregates resembling those formed by the recrystallization of myrmekite during deformation (Vernon *et al*., 1983) locally occur adjacent to the myrmekite colonies (Cesare *et al*., 2002b, p. 207).

(10) Myrmekite grows at 450–500 °C, according to Tribe & D'Lemos (1996) and between 500 and 670 °C, according to Wirth & Voll (1987). This inference is based on temperatures indicated by other minerals in the same rocks as the myrmekite.

4.10.5 Symplectites in other silicate and oxide minerals

Many different symplectic intergrowths have been reported in rocks. A few examples, illustrating the wide range of minerals involved, are: intergrowths of andalusite–quartz and biotite–quartz replacing cordierite (Vernon, 1978b; Vernon & Pooley, 1981); K-feldspar–biotite, oligoclase–biotite, oligoclase–muscovite, and oligoclase–andalusite (Vernon & Pooley, 1981); Al silicate-quartz, Al silicate – aluminous anthophyllite, Al silicate – aluminous orthopyroxene (Vernon & Pooley, 1981); sapphirine–plagioclase (Carswell *et al.*, 1989); spinel–hornblende (Mason, 1967; Ward, 1984a); spinel–orthopyroxene (Harley *et al.*, 1990); pyroxene–ilmenite (Dawson & Reid, 1970); orthopyroxene – opaque oxide (van Lamoen, 1979; Barton & van Gaans, 1988); pyroxene–plagioclase (Boland & van Roermund, 1983; Thost *et al.*, 1991); orthopyroxene–cordierite (Droop & Bucher-Nurminen, 1984; Harley *et al.*, 1990); cordierite–orthopyroxene–garnet (Schreyer & Abraham, 1978); sapphirine–cordierite (Droop & Bucher-Nurminen, 1984; Harley *et al.*, 1990); sapphirine–orthopyroxene (Harley *et al.*, 1990; Harley & Fitzsimans, 1991; Rickers *et al.*, 2001); cordierite–quartz (Lonker, 1988), plagioclase–orthopyroxene–spinel (Brodie, 1995), hornblende–clinozoisite (Daczko *et al.*, 2002a), clinopyroxene–kyanite (Daczko *et al.*, 2002a), biotite–quartz (Waters, 2001) and clinozoisite–quartz–kyanite–plagioclase (Daczko *et al.*, 2002a).

Many symplectites are formed during a change of pressure, either a pressure increase (see, for example, Griffin, 1971) or, more commonly, a pressure decrease. For example, jadeite-rich pyroxene formed at high pressure in eclogites is commonly replaced by a symplectic intergrowth of lower-pressure minerals. Another example, which well illustrates reaction complexity and local equilibrium, is sapphirine–plagioclase symplectite replacing kyanite, as a result of a complex reaction involving loss of grossular component from original garnet and jadeite component from original clinopyroxene (Carswell *et al.*, 1989). The inferred reaction is: garnet$_1$ + clinopyroxene$_1$ + kyanite = garnet$_2$ + clinopyroxene$_2$ + sapphirine + plagioclase. The reaction can be balanced using the actual compositions of the minerals involved. Later symplectic orthopyroxene–spinel–plagioclase, occurring along garnet–clinopyroxene boundaries, was produced by the reaction: pyrope component of garnet + Ca-Tschermaks and jadeite components of clinopyroxene = orthopyroxene + spinel + plagioclase (An_{80}). Both reactions were restricted to small rock volumes, presumably owing to reduced diffusion rates at the essentially fluid-absent conditions. Therefore, on a wider scale (such as that of a hand specimen) the rock would have been in chemical disequilibrium (Carswell *et al.*, 1989, p. 462).

4.10.6 Symplectites in sulphide minerals

Symplectic intergrowths of sulphide minerals are common, and some have been reproduced experimentally. Many examples have been listed by Stanton (1972, p. 266). Following the terminology used for metals, these symplectites are commonly referred to as 'eutectoid' intergrowths, because they mostly grow in the solid state. This distinguishes them from eutectic intergrowths formed by solidification of molten sulphides. The formation of some of these intergrowths involves closed-system segregation within a parent grain, whereas other intergrowths require components from an external source (Stanton, 1972, p. 267).

4.11 Modification of deformation twins, exsolution lamellae and other intergrowths

As already discussed (Section 4.2), normal grain boundaries (*intergranular* interfaces) are modified by heating. The question arises as to whether other interfaces, such as those in symplectites, and even interfaces within grains, such as twin boundaries and exsolution lamellae (*intragranular* interfaces) can be modified by later heating. Owing to evident crystallographic control on the orientation of all these boundaries, at least to a general extent, the expectation is that they should be of lower energy and therefore more resistant to modification than normal high-energy grain boundaries. However, perfect atomic matching across these interfaces is uncommon (Sections 4.9, 4.10, 5.3.3; Table 3.1) and so they must have some interfacial energy, which could promote boundary movement. Furthermore, deformation can produce local strain variations along and across these various interfaces, which can lead to variable boundary movement during later heating (Section 5.4.2). Because heating and deformation generally operate together, their effects will be combined in this discussion.

4.11.1 Modification of twins

Growth twins (Sections 3.12, 4.7), with planar interfaces precisely parallel to low-energy planes, may survive later heating and deformation very well, for example, simple twins in K-feldspar in strongly deformed mylonites (Section 5.7.6). However, deformation twins (Sections 3.12, 5.3.3; Table 3.1) have curved interfaces on the optical microscope scale (Figs. 3.89–3.91), owing to dislocations or more evenly distributed elastic strain along them. Therefore, these interfaces have higher energy than growth-twin boundaries. Consequently, heating and/or deformation may promote movement of these interfaces, in an attempt to produce lower-area, and hence lower-energy, configurations. The boundaries bulge, and

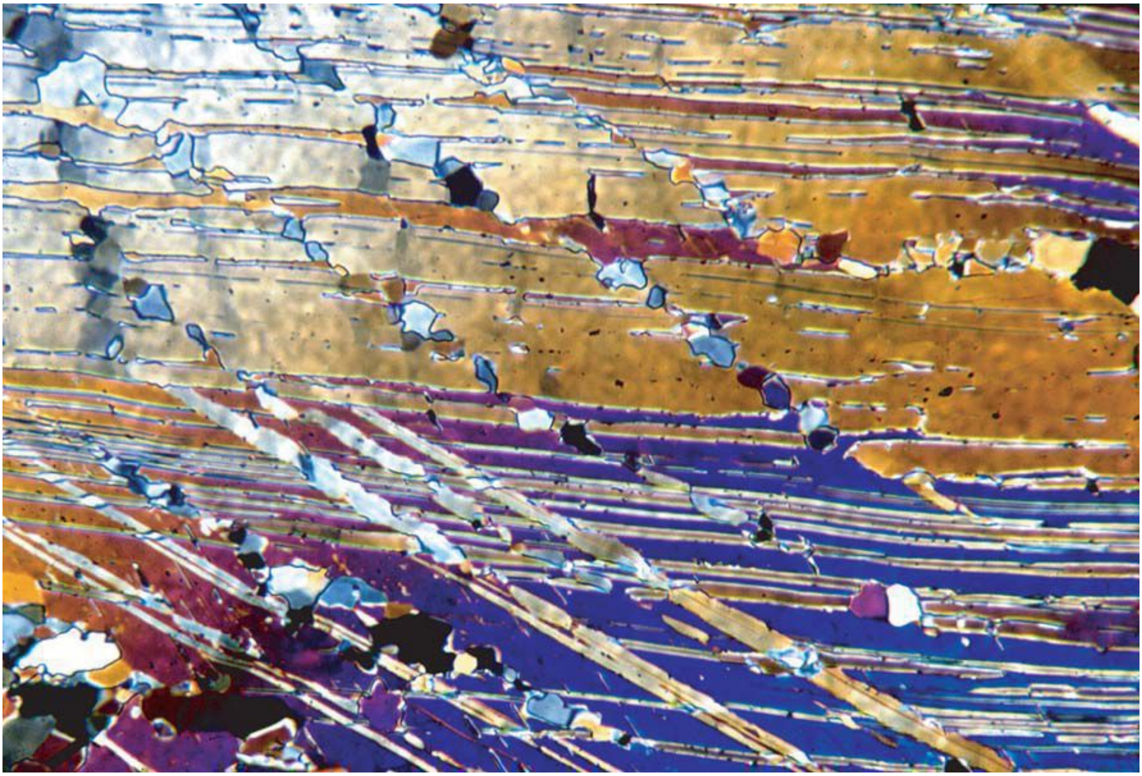

Fig. 4.63: Migrated twin boundaries in calcite in deformed marble from the Mount Lofty Ranges, South Australia. Some twin interfaces have been unaffected, others have migrated slightly, and still others have migrated so much that recrystallization has occurred, forming isolated grains or strings of new grains marking the positions of former twin lamellae. The calcite has been ground much thinner than usual, namely to about 0.005 mm thickness (as indicated by the first-order interference colours), which has removed the usual interference fringes at the bevelled edges of grains, twins and grinding pits (caused by the strong birefringence of calcite at 0.03 mm thickness), and so has revealed twin and grain boundaries as single dark lines. Crossed polars; base of photo 0.5 mm.

the twins may break up into lines of isolated grains; eventually they may be obliterated in favour of a single crystal orientation or an aggregate of recrystallized grains. The effects are well shown by calcite and plagioclase (Voll, 1960). An example is the calcite shown in Fig. 4.63 (Vernon, 1981).

4.11.2 Modification of exsolution lamellae

Similar considerations apply to exsolution lamellae (Section 4.9). As pointed out by Smith (1953), nuclei of exsolved minerals tend to select orientations that form

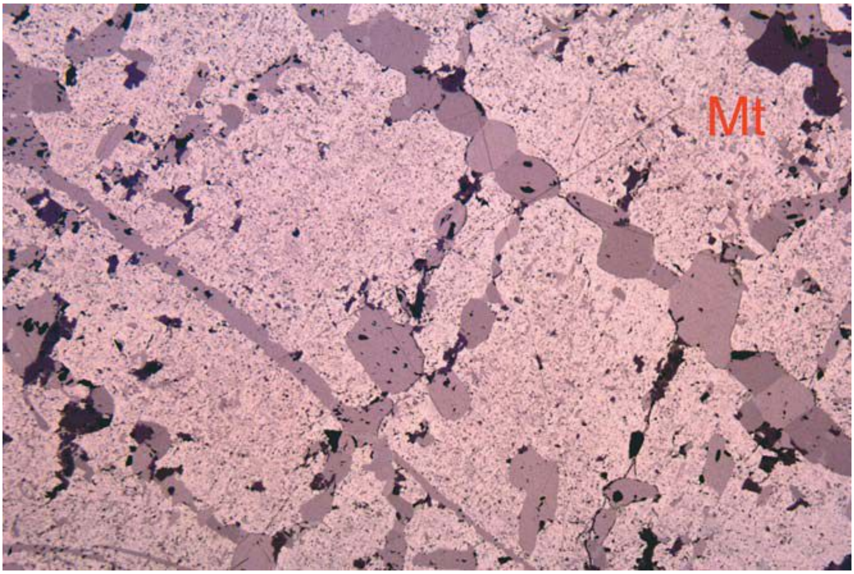

Fig. 4.64: Migration of boundaries between exsolved lamellae of ilmenite and host magnetite (Mt). Although some twins remain unaffected, most have extensively migrated, leading to the formation of lines of new (recrystallized) grains. Polished section, reflected light, crossed polars; base of photo 1.5 mm.

interfaces of low energy. If the interfaces are planar and precisely in low-energy orientations, the exsolution lamellae may be resistant to shape change during later heating. However, many exsolution lamellae, though evidently approximately controlled by crystal structure, are relatively irregular, as in most microperthite (Section 4.9.1). This increases their interfacial free energy, so that heating can cause the interfaces to locally move, producing elongate, rounded grains of the exsolved mineral and/or linear aggregates of new grains (with dihedral angles indicative of solid-state grain-boundary migration) delineating the position of the original lamellae (Fig. 4.64). A similar effect may be produced by deformation of the lamellae prior to heating (Smith, 1953). Moreover, if recrystallization (Section 5.4.2) of the host grain also occurs, a polygonal aggregate of both minerals may be produced. A good example is orthopyroxene with exsolved clinopyroxene converted by high-temperature deformation into a polygonal aggregate of both minerals (Section 5.4.2).

4.11.3 Modification of intergrowths

Many graphic or symplectic intergrowths undergo coarsening, in response to later heating, especially in deformed rocks. The driving force is a tendency to reduce the total interfacial free energy by reducing the total grain-boundary area (Section 4.2.2). The process involves diffusion of the chemical components from the small to the larger particles in the solid state, driven by a reduction in interfacial free energy, and is common in the coarsening of lamellar and rod-like intergrowths in metals (see, for example, Martin & Doherty, 1976). The coarsening of very fine-grained intergrowths has been referred to as 'Ostwald ripening' (Cahn, 1970, p. 506), which involves solution of the smallest grains (typically submicroscopic) and reprecipitation on the larger ones. However, many of the natural intergrowths are too coarse-grained for this process, and so are probably modified by solid-state grain-boundary migration driven by locally high interfacial energy.

Granophyric intergrowths in igneous rocks (Section 3.8) may be modified by heating. Typically, reduction in the interfacial area of the quartz–feldspar intergrowth leads to the development of ellipsoidal to spherical grains of quartz in the alkali feldspar (Fig. 4.65A). It may be impossible to distinguish between normal rounded inclusions of quartz in metamorphic K-feldspar (Fig. 4.30) and a completely modified graphic intergrowth, unless intermediate stages are present (Fig. 4.65A). If not, a modified intergrowth interpretation is reasonable if it can be shown that the original rock was granitic.

An important feature of symplectic intergrowths (Section 4.10) is that they tend to be well preserved in low-strain parts of deformed rocks, and so may retain evidence of metamorphic reactions, even in relatively high-strain zones of a metamorphic terrane. However, heating and/or deformation (Chapter 5) can alter their shapes or remove them. This is because their boundaries, though apparently subject to some crystallographic control, commonly are irregular (Figs. 4.56–4.59). Therefore, heating induces movement of the interfaces, in an attempt to reduce their interfacial area. Initially this produces rounded shapes replacing formed lamellae or rods (Fig. 4.65B) and eventually forms a polygonal aggregate of new grains with dihedral angles indicative of solid-state grain-boundary migration (Fig. 4.65C,D). Vestiges of the original rods or lamellae are often preserved, at least locally (Fig. 4.65C). A similar process occurs where myrmekite is converted to fine-grained polygonal aggregates in deformed granites (see, for example, Vernon *et al.*, 1983). An analogous process is the conversion of lamellar (symplectic) aggregates of 'pearlite' in steel to globular ('spheroidized') aggregates by prolonged heating (see, for example, van Vlack, 1964, p. 306).

4.12 Compositional zoning in metamorphic minerals

Before the advent of the electron probe microanalyser, much compositional zoning in metamorphic minerals, especially in optically isotropic minerals such as garnet, went unnoticed. However, the electron probe microanalyser produces accurate chemical analyses of very small areas, so that compositional zoning profiles across individual grains can be obtained. These days, compositional zoning in metamorphic minerals is determined routinely.

A recent development of electron microprobe analysis is the production of colour-enhanced X-ray element-intensity maps showing two-dimensional

A

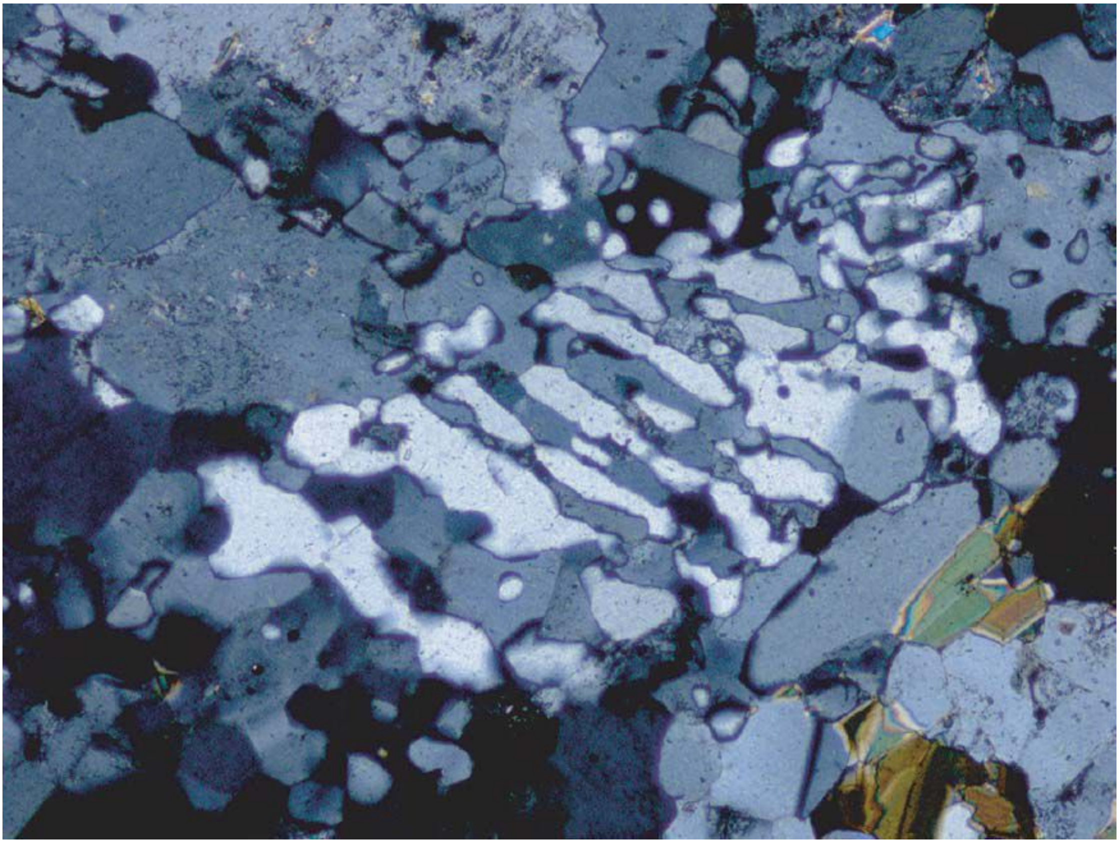

Fig. 4.65: (A) Granophyric intergrowth (graphic intergrowth of quartz and K-feldspar) modified to form bulged, irregular lamellae and relatively rounded grains. (B) Myrmekite intergrowth modified to form relatively rounded quartz grains. (C) Myrmekite almost completely recrystallized to form a polygonal aggregate. Samples A, B, and C are from Baja California, México, by courtesy of Erwin Melis. Crossed polars; base of photos 1.2 mm. (D) Modified symplectic intergrowth of plagioclase and pyroxene in a metagabbro from the Finero Complex, southern Alps, Italy. Evidence of migration of the original vermicular grain boundaries to form more independent grains is indicated by the strong tendency to form dihedral angles indicative of solid-state grain-boundary adjustment. Polygonal new grains and elongate relics of the original lamellae are present. Sample by courtesy of Jörn Kruhl. Crossed polars; base of photo 1 mm.

compositional variations within whole grains (see, for example, Pattison & Bégin, 1994; Schumacher *et al.*, 1999; Spiess *et al.*, 2001; Stallard & Hickey, 2002) and between different layers of reaction coronas (see, for example, Lang & Gilotti, 2001). Arbitrary false colours may be assigned to different concentrations of the analysed element (Figs. 4.66, 4.67). This technique is particularly useful for garnet, revealing information not determinable by optical means, and has assisted

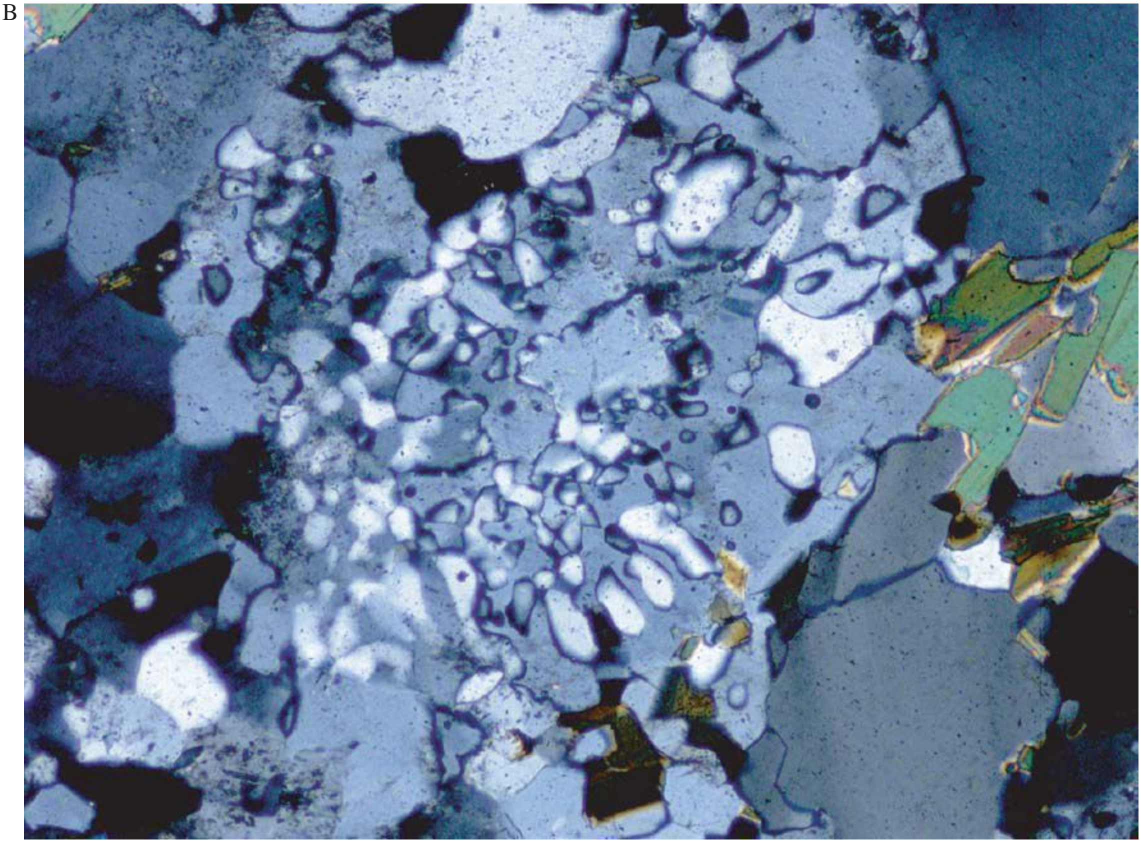

Fig. 4.65: (*cont.*)

in the detailed interpretation of metamorphic histories and reactions. Serial two-dimensional X-ray composition maps may be converted to three-dimensional compositional zoning images (Daniel & Spear, 1998).

Compositional zoning is commonly produced during growth, owing to preferential concentration of certain chemical components in the growing mineral, but may also be produced by exchange of chemical components between the outer parts of a mineral and the matrix as metamorphic conditions change after growth of the mineral, for example during cooling from high temperature (see, for example, Pattison & Bégin, 1994). Such exchange may involve all grains of the minerals concerned at high temperatures and/or where intergranular fluid (assisting diffusion of chemical components) is present, but may be very local at lower temperatures and/or where intergranular fluid is absent.

Zoning may also be produced by overgrowths on cores (commonly corroded) that are either detrital or the products of an earlier metamorphic event. For example, Rumble & Finnerty (1974), Tracy (1982), Karabinos (1984) and Ganne *et al.* (2003) have interpreted discontinuous zoning in garnet porphyroblasts as

C

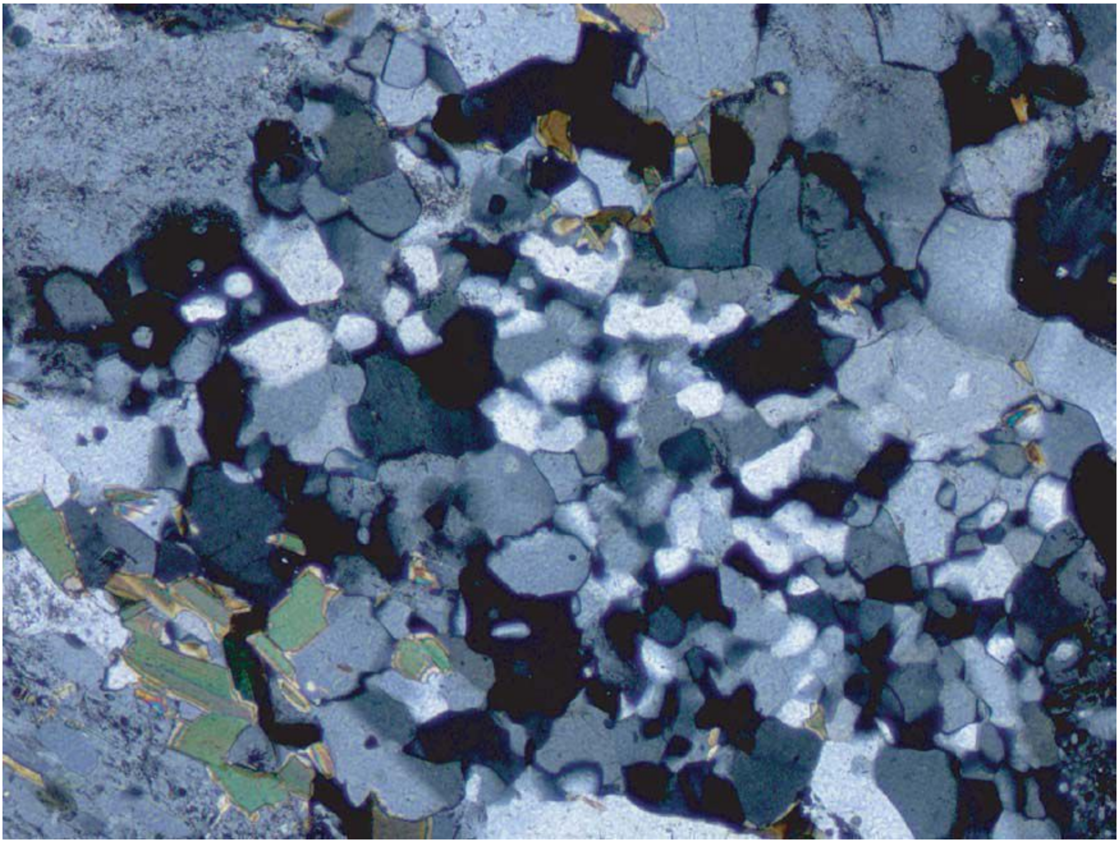

Fig. 4.65: *(cont.)*

indicating polymetamorphism, and Kaneko *et al*. (2003) described and illustrated (cathodoluminescence (CL) and backscattered electron (BSE) images) SHRIMP-dated zones in zircon crystals, revealing a multistage growth history involving an inner detrital core, overgrown by two metamorphic domains, the outer one resulting from metamorphism at ultrahigh pressure (27–32 kbar), as evidenced by minute inclusions of the high-pressure silica polymorph, coesite. On the other hand, Thompson *et al*. (1977) showed that discontinuous garnet zoning may be due to multiple reactions in a single metamorphic event in some rocks.

4.12.1 Concentric compositional zoning

Concentric compositional zoning in metamorphic minerals commonly reflects progressive growth of idioblastic crystals as the availability of chemical components changes in response to metamorphic reactions. For example, detailed

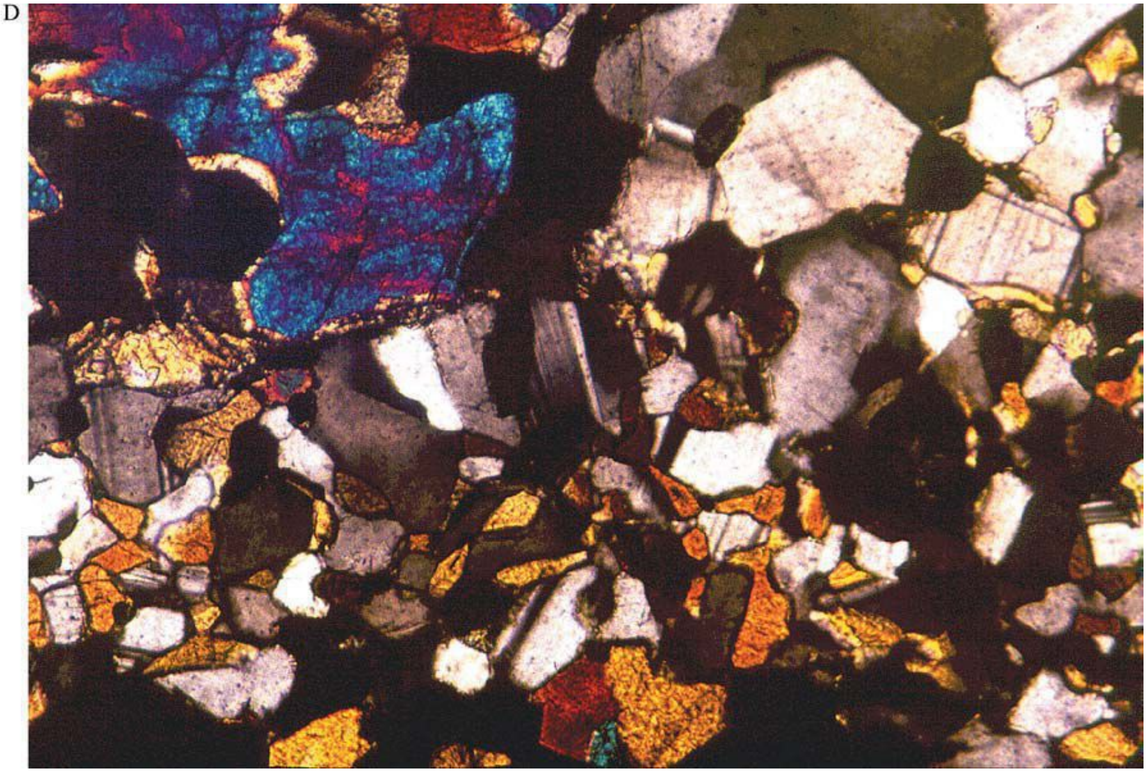

Fig. 4.65: (*cont.*)

investigations and numerical modelling have shown that concentric compositional zoning in garnet porphyroblasts is related to metamorphic reactions involving other minerals in the rock (Thompson *et al.*, 1977; Loomis & Nimick, 1982; Tracy, 1982; Lanzirotti, 1995; Loomis, 1986; Spear *et al.*, 1991; Vance & Holland, 1993; Pyle & Spear, 1999; Yang & Rivers, 2002). Zoning may also be marked by variation in the concentration of inclusions (Powell & Vernon, 1979; Lanzirotti, 1995; Passchier & Trouw, 1996, fig. 7.43; Yang & Rivers, 2002).

In general, concentric compositional zoning in metamorphic minerals is less complex than in igneous rocks, and is commonly of a simple ‘core-and-margin’ type or patchy (Fig. 4.68). A common ‘core-and-margin’ type in garnet shows high Mn in the core and lower Mn towards the rim (‘bell-shaped’ zoning profile), owing to the strong tendency for garnet to absorb Mn, leading to Mn depletion in the surrounding matrix. Such zoning is generally inferred to be developed during growth of the garnet.

Patchy zoning is probably due mainly to dissolution and overgrowth in response to changing metamorphic and deformation conditions, as are irregularities in broadly concentric zones (Fig. 4.66A).

Fig. 4.66: (A) Colour-enhanced X-ray composition map (Section 1.6) showing the distribution of Mg in a concentrically zoned garnet porphyroblast in a felsic gneiss from the Himalayas. Irregularities in the zoning patterns are probably due to resorption, owing to successive metamorphic reactions involving other minerals in the rock. High Mg contents have been assigned 'warm' colours and low Ca contents have been assigned 'cool' colours. Bar scale at bottom left. (B) Colour-enhanced X-ray composition map, showing the distribution of yttrium in the same garnet porphyroblast shown in (A). The roughly concentric zoning is oscillatory, showing 'spikes' (narrow zones) of relatively high Y content, formed in response to a reaction producing rutile from titanite (containing Y) in the matrix. High Y contents are shown in 'warm' colours. Images by Norm Pearson.

Oscillatory zoning is uncommon or only poorly developed in metamorphic minerals, except for grandite (grossular–andradite) garnet, in which it is commonly clearly revealed (see, for example, Deer *et al*., 1992; Rice, 1993), as shown in Fig. 4.69. It is an anomalous birefringence effect with a complex origin, and appears to be due to partial ordering of Al^{3+} and Fe^{3+} in the grandite structure, as well as strain due to mismatch between the structures of the

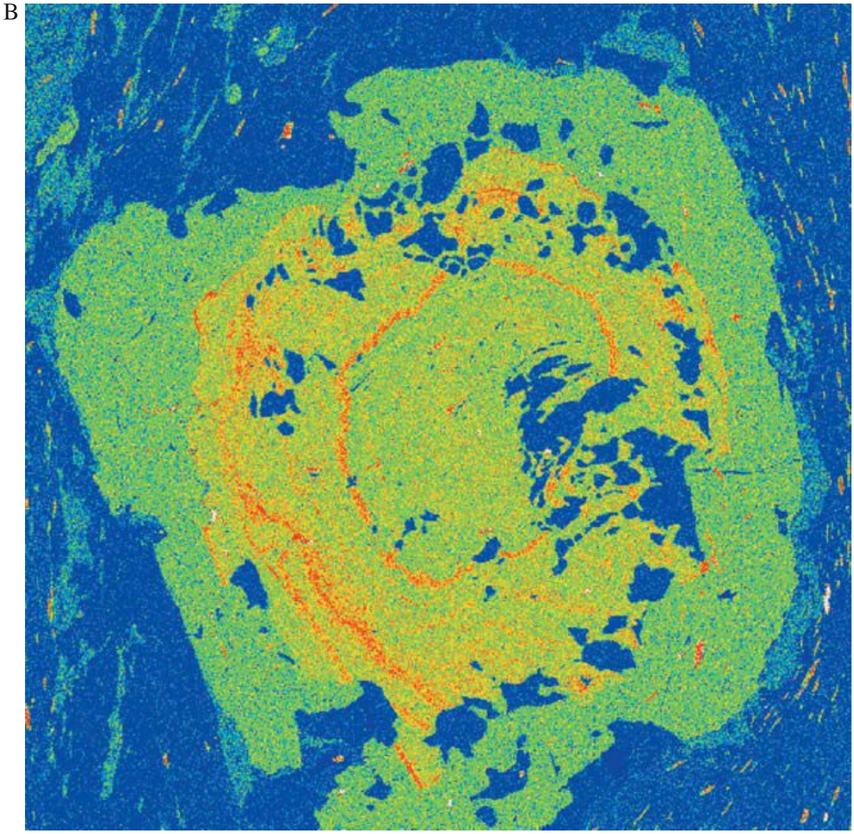

Fig. 4.66: (*cont.*)

different garnet compositions (Lessing & Standish, 1973; Schutkenberg *et al.*, 2001). In places, zoned grandite crystals in iron-rich calcsilicate rocks (skarns) occur as vein-like aggregates filling or projecting into cavities (*vughs*), suggesting growth in a fluid. Moreover, even where the zoned garnet occurs in apparently random aggregates with other minerals, the former crystal shapes indicated by the concentric zoning suggest growth in at least a small amount of fluid (Section 4.4). For example, the shapes of the zoned grains in Fig. 4.69 are consistent with growth in a vugh (Section 5.9.3). This also could apply to the epidote and allanite with spectacular oscillatory rare-earth element zoning in high-pressure carbonate rocks described by Boundy *et al.* (2002), and the Fe-rich mica with oscillatory Mg–Ti zoning in skarn described by Kwak (1981).

In fact, oscillatory zoning in metamorphic minerals is generally attributed to open-system growth conditions involving changes in fluid composition

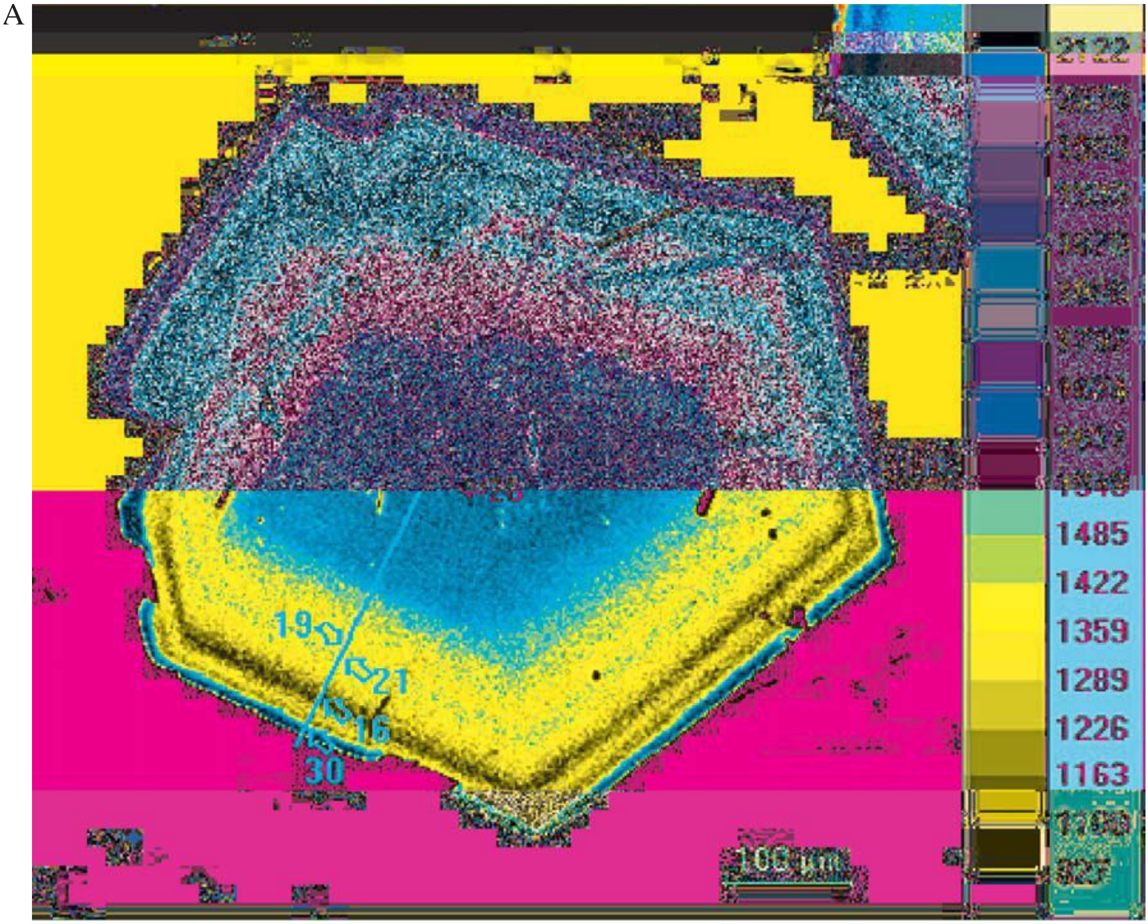

Fig. 4.67: (A) Colour-enhanced X-ray composition map (see Section 1.6) showing oscillatory concentric zoning caused by variations in the proportions of spessartine and almandine components in a garnet porphyroblast from the western Erzgebirge, Germany. The oscillatory zoning is superimposed on normal concentric zoning from Mn-rich in the core to less Mn towards the margin, except for a very narrow Mn-rich rim. Warmer colours represent larger concentrations of Mn, and cooler colours represent smaller concentrations of Mn. The numbers refer to molar proportions of spessartine component. The molar proportions of Mn in ilmenite inclusions are also shown. (B) Colour-enhanced X-ray composition map showing oscillatory zoning caused by variations in the proportions of grossular and almandine components in the outer parts of a garnet porphyroblast from the western Erzgebirge, Germany. The oscillatory zoning is superimposed on normal concentric zoning from Ca-rich in the core to less Ca towards the margin. The core is irregular, suggesting a period of corrosion. Warmer colours represent larger concentrations of Ca, and cooler colours represent smaller concentrations of Ca. The numbers refer to molar proportions of grossular component. Both images are from Schumacher *et al*. (1999, fig. 4a), with permission of the *Canadian Mineralogist*. Images kindly supplied by Renate Schumacher.

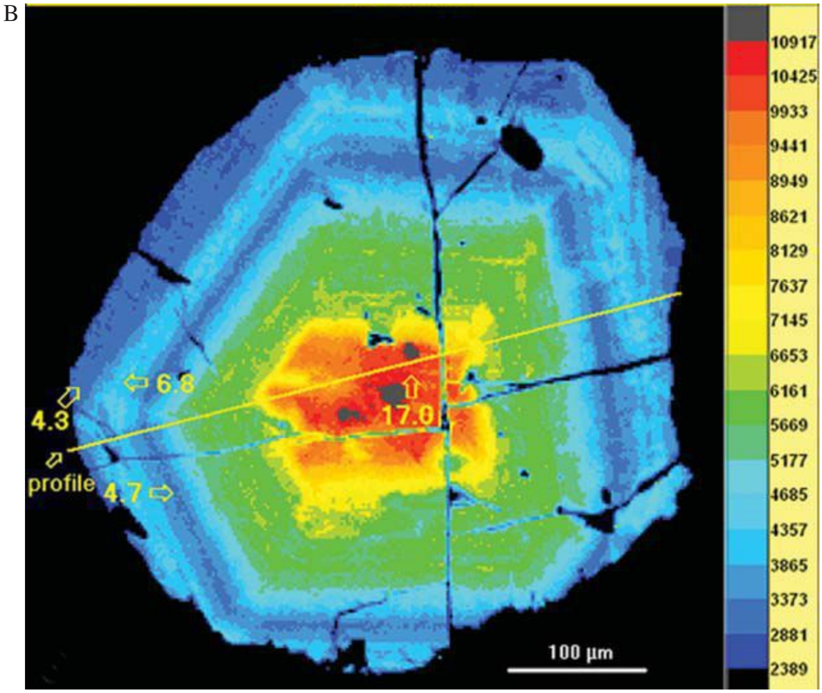

Fig. 4.67: (*cont.*)

(Jamtveit, 1991; Jamtveit & Andersen, 1992; Jamtveit *et al.*, 1993; Clechenko & Valley, 2003). For example, oscillatory zoning in prehnite and clinopyroxene precipitated from hydrothermal fluids in cavities has been observed by Yardley *et al.* (1991).

However, oscillatory zoning has also been reported for major elements in garnet in metapelites (Schumacher *et al.*, 1999; Stallard & Hickey, 2002). For example, Schumacher *et al.* (1999) illustrated concentric oscillatory almandine–spessartine and grossularite–almandine zoning in garnet that appears to have grown as normal porphyroblasts in phyllites and mica schists (Fig. 4.67). In addition, Yang & Rivers (2002) illustrated oscillatory Mn and Y zoning in garnet porphyroblasts in calcareous metapelites and metapelites. Oscillatory zones in metapelitic garnet are generally not as sharp, narrow or numerous as those in oscillatory zoning attributed to growth in a fluid, although a few relatively sharp zones ('spikes' or 'annuli') rich in Y have been observed in some garnet porphyroblasts (Lanzirotti, 1995; Pyle & Spear, 1999; Yang & Rivers, 2002), and generally correlate with the abundances of Y-bearing minor minerals (such as xenotime and apatite) in the matrix. The Y-rich zones shown in Fig. 4.66B have been inferred to reflect conversion of titanite (containing Y) to rutile in the matrix (Norman J. Pearson, personal communication).

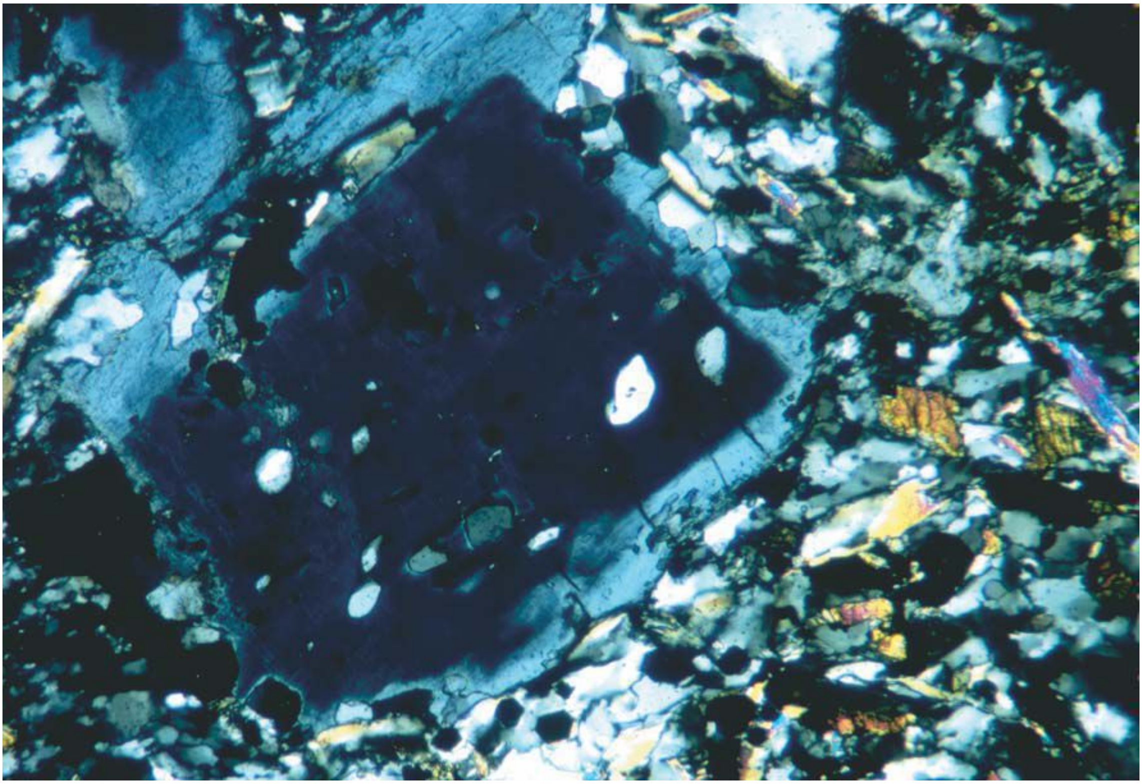

Fig. 4.68: Simple core-and-margin zoning in Na-amphibole in a metabasic rock from Japan. Crossed polars; base of photo 3.5 mm.

The oscillatory Y zoning in garnet observed by Lanzirotti (1995) occurs in garnet porphyroblasts showing normal core-and-margin zoning ('bell-shaped' composition profiles) for Mn and Fe. The recognition of the Y zoning adds more detailed information about chemical reactions that occur during prograde metamorphism. Lanzirotti (1995) suggested that the Y zoning could be due to (1) breakdown of Y-bearing minerals, (2) changes in garnet growth rate, and/or (3) breakdown and reprecipitation of garnet as reactions involving garnet change.

Schumacher *et al*. (1999) attributed the oscillations they observed to local variations in the rate of decompression of the rocks. However, as discussed in Section 4.4, fluid may be involved in the development of crystal faces in porphyroblasts, which raises the possibility that changes in local fluid composition (related to reactions involving other minerals in the rock) may contribute to oscillatory zoning, even for garnet in metapelites.

Fine concentric oscillatory zoning generally provides a good way of distinguishing between igneous and metamorphic feldspar. For example, complex oscillatory Ba/K zoning in K-feldspar appears to be a good indicator of

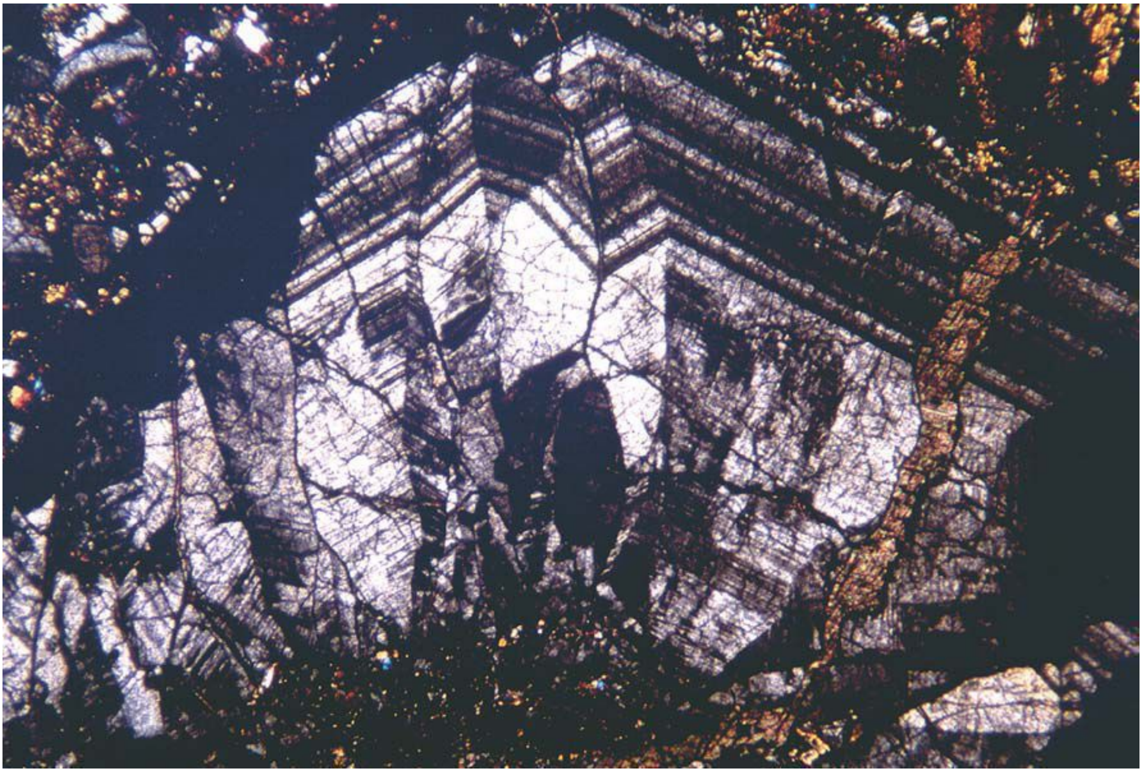

Fig. 4.69: Sharp oscillatory zoning in grandite (grossular–andradite) garnet from an iron-rich calcsilicate hornfels (skarn). The shapes of the zoned grains are consistent with growth in a vugh (Section 5.9.3). Crossed polars; base of photo 11 mm.

precipitation from a melt, because it is common in K-feldspar phenocrysts in granites, whereas it does not occur in K-feldspar in metapelites (Vernon, 1986a, 1999a). Similarly, complex oscillatory Na–Si/Ca–Al zoning in plagioclase is also diagnostic of a magmatic origin, except perhaps for uncommon examples that appear to have crystallized from hydrous solution in cavities in metamorphic rocks (Vernon, 1976, p. 91). Most zoning in metamorphic plagioclase is relatively simple or patchy, and reverse zoning (with rims more calcic than cores) is more common in metamorphic than in igneous rocks. This is especially so if the zoning is formed during increasing temperature, because calcic plagioclase tends to become progressively more stable at higher temperatures. Compositional zoning may be clearly revealed for intermediate to calcic plagioclase by cathodoluminescence (Ahn & Cho, 2000). This is especially useful for fine-grained aggregates, in which plagioclase and quartz may be otherwise very difficult to distinguish optically.

Concentric and patchy compositional zoning may also occur in other metamorphic minerals, such as epidote, allanite, corundum, tourmaline, mica (see, for example, Kwak, 1981), hornblende (Fig. 4.68), zircon and garnet, as well as in many sulphide and metallic oxide minerals, such as cassiterite, rutile, ilmenite, chromite, pyrite, galena, stibnite and cobaltite (Edwards, 1947), sphalerite (Barton, 1970), arsenopyrite (Lentz, 2002) and bravoite (Craig & Vaughan, 1994). In opaque minerals, the zoning can be observed in plane-polarized reflected light if the zones are sufficiently different in colour, and zoning may be revealed more clearly by backscattered SEM imaging (Lentz, 2002) or chemical etching (Craig & Vaughan, 1994).

4.12.2 Sector zoning in metamorphic minerals

Compositional sector zoning has been observed in many minerals, including silicates, carbonates, phosphates, sulphates, sulphides, oxides, fluorides and halides (Rice, 1993; Reeder & Prosky, 1986). It is common in metamorphic staurolite (Hollister, 1970; Ward, 1984a,b), but also occurs in andalusite (Rice & Mitchell, 1991; Rice, 1993), epidote (Dowty, 1976b), kyanite (Hollister, 1970), chloritoid (Fig. 4.18) (Spry, 1969, plate XIIId) and iron-rich biotite (Kwak, 1981).

In sector compositional zoning, which commonly occurs with zonal concentrations of inclusions (Section 4.3.3), faces of different crystal forms have different compositions (Kouchi *et al.*, 1983). The colour variation in sector-zoned staurolite is due to variation in Ti. In andalusite it appears to be due to variation in Fe (presumably Fe^{3+} substituting for Al^{3+}) and Ti, and in epidote it appears to be due to variation in Fe^{3+} (Dowty, 1976b; Ward, 1984b). Sector zoning in staurolite has been discussed in detail by Hollister (1970), Dowty (1976b) and Ward (1984b).

4.13 Criteria for inferring metamorphic reactions

Microstructural evidence may be useful for inferring metamorphic reactions, but care needs to be taken, especially for the more complex reactions. In general, the approach is to infer minerals that appear to have replaced other minerals, analysing the minerals with the electron probe microanalyser, and then writing balanced chemical equations on the basis of the volumes and chemical compositions of the minerals and volatile components (such as water) inferred to have been involved.

4.13.1 Prograde reactions

A few prograde reactions involve pseudomorphism of one mineral by another or by an aggregate of minerals of the same composition, suggesting a possible reaction. However, many prograde metamorphic reactions are less easy to infer, even where pseudomorphism is involved, because components external to the pseudomorph are commonly also involved (see, for example, Vernon & Pooley, 1981; Likhanov & Reverdatto, 2002; Guidotti & Johnson, 2002). Carmichael

(1969) explained how a net change from one mineral to another can be the result of several linked subreactions or partial reactions, involving diffusion of chemical components in fluid from one local reaction site to another, the partial reactions combining to form an overall 'cyclic' reaction. Cyclic ionic reaction patterns were inferred by Yardley (1977b, fig. 2) to account for pseudomorphs of sillimanite after garnet, the development of which involved movement of aluminium from staurolite and mica in the matrix to the well-separated garnet porphyroblasts. Studies by Foster (1977, 1981, 1986, 1999) and Likhanov & Reverdatto (2002) have revealed the complexity of typical prograde reactions, showing that net reactions occurring in volumes as small as 1 cm^3 may be the result of several even more local reactions. *Local equilibrium* is also indicated by the growth in cordierite of biotite grains with Ti contents that vary with distance from the nearest Ti source, such as ilmenite (Waters & Charnley, 2002). Careful microstructural interpretation, chemical analysis and numerical calculation are necessary to unravel the intricacies of most prograde reactions.

4.13.2 Incomplete reactions

Incomplete metamorphic reactions enable recognition of both solid reactants and solid products, which assist in the writing of realistic metamorphic reaction equations. This situation is most likely to be encountered in retrograde metamorphic rocks. In conjunction with available experimental and theoretical calculations on mineral stability, and taking all necessary precautions (Vernon, 1996a; Johnson *et al*., 2003), the inferred reactions help to work out the metamorphic history of a rock, i.e. the way in which *P* and *T* change with time (the *P–T–t* path of the rock). Unfortunately, enough care in inferring reactions is not always taken, and this can lead to misleading interpretations of the metamorphic history of a region.

4.13.3 Reliable microstructural criteria for inferring metamorphic reactions

Partial pseudomorphism (constant-volume replacement) is the most reliable criterion of a reaction (Vernon, 1996a), because the replaced mineral and the solid products can be observed (see, for example, Guidotti & Johnson, 2002). The replacement minerals may project inwards from fractures (Fig. 4.70) or from grain boundaries (Fig. 4.71), but may begin internally (Fig. 4.72). Radiating aggregates of the new mineral inside porphyroblasts of the old mineral (Fig. 4.72) are relatively reliable indicators of a reaction.

Even where replacement is complete, original grain shapes may be preserved (Fig. 4.73), as revealed by (1) crystal shapes of former phenocrysts, (2) preservation of inclusions with boundaries that show evidence of solid-state microstructural adjustment with the former host mineral, now completely replaced by finer-grained aggregates that could not have equilibrated microstructurally with the

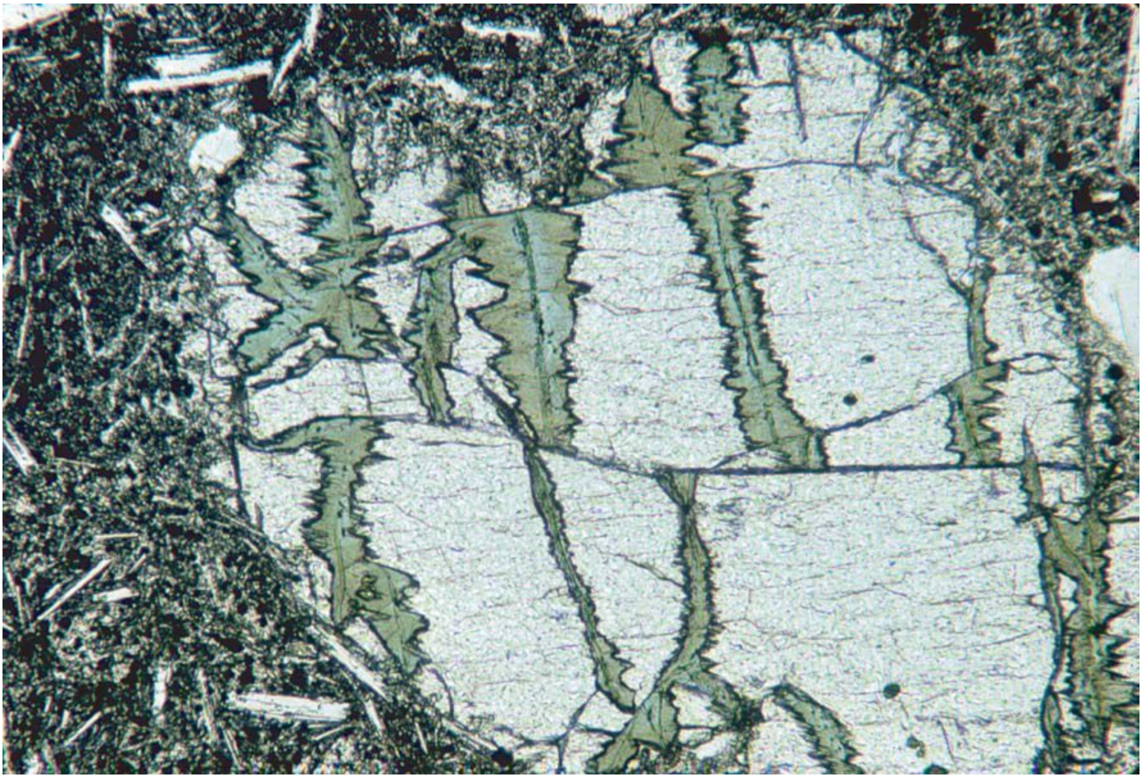

Fig. 4.70: Olivine partly replaced by chlorite along fractures in altered basalt from Mount Wilson, New South Wales, Australia. Plane-polarized light; base of photo 1.3 mm.

much larger inclusions, (3) shapes of former polygonal grains now completely occupied by much finer-grained aggregates, which could not have produced such coarser-grained polygonal shapes by interface adjustment, because their individual grains are far too small (Fig. 4.73), and (4) crystallographically controlled ('epitactic', 'coaxial') replacement of one mineral by another, such as andalusite by sillimanite (see, for example, Bosworth, 1910; Vernon, 1987a), as shown in Fig. 4.2, and biotite by sillimanite (Chinner, 1961).

Examples of pseudomorphous reactions are (1) aggregates of kyanite replacing andalusite (Ward, 1984c; Brown, 1996, fig. 7), shown in Fig. 4.72, (2) epidote + margarite + quartz + plagioclase replacing lawsonite (Selverstone, 1993; Droop, 1985), and (3) aggregates of kyanite and staurolite replacing andalusite (Evans & Berti, 1986), all of which have been used to infer a pressure increase. Pseudomorphs of muscovite replacing staurolite and of biotite + sillimanite replacing garnet have been described by Guidotti & Johnson (2002). Another common example is the serpentinization of olivine in hydrated peridotites (Fig. 4.73).

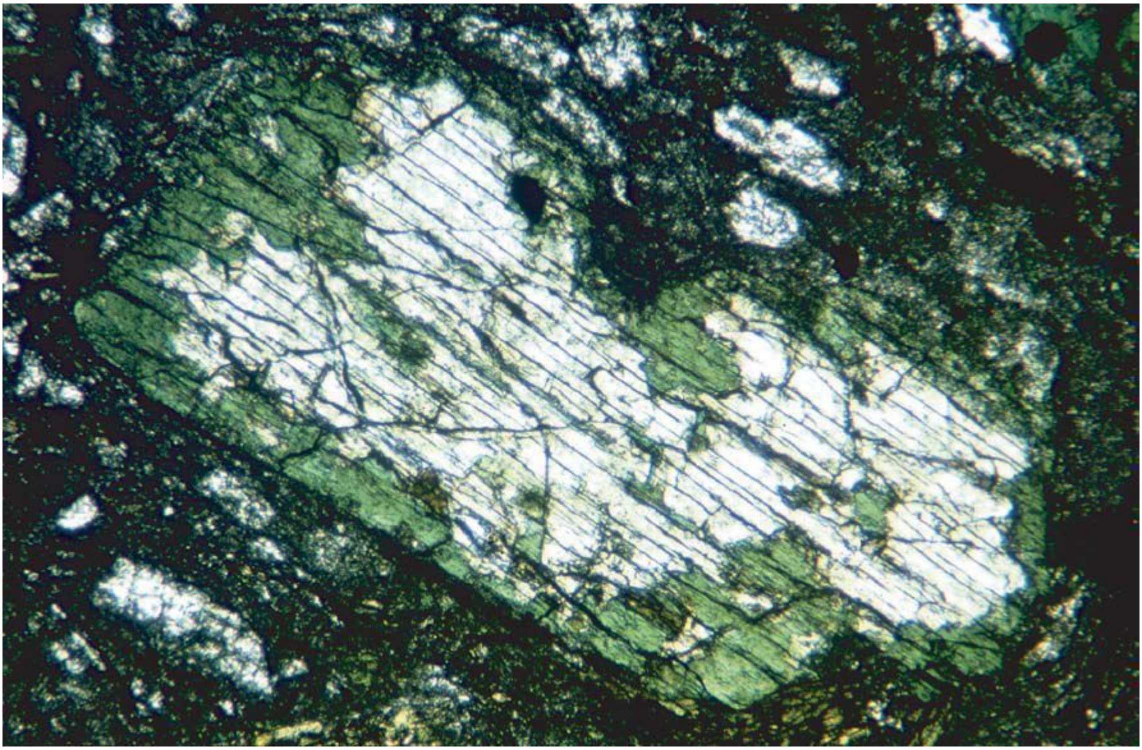

Fig. 4.71: Clinopyroxene partly replaced by green hornblende around its margins in a metabasic rock from Wellington, New South Wales, Australia. Plane-polarized light; base of photo 3.5 mm.

Fig. 4.38 shows aggregates of wollastonite that have replaced aggregates of calcite (Fig. 4.6), preserving the curved shapes of shells in which the calcite originally grew.

Although pseudomorphs are especially common in retrograde metamorphic rocks (see, for example, Ferry, 2001), they may also occur in prograde situations, especially if the deformation is weak (e.g., Guidotti & Johnson, 2002).

High-pressure minerals occuring as inclusions in garnet and zircon that have been pseudomorphed by lower-pressure minerals formed during exhumation have been described (see, for example, Song *et al.*, 2003, fig. 4), namely quartz pseudomorphing coesite, calcite pseudomorphing aragonite, and K-feldspar + quartz pseudomorphing what was probably an ultrahigh-pressure aggregate of K-cymrite + coesite (Song *et al.*, 2003, p. 633).

Coronas, many of which are symplectic (Section 4.10), provide excellent examples of incomplete solid-state reactions, and many examples have been described. Some corona symplectites form partial to complete pseudomorphs of an earlier mineral, whereas others replace two minerals as they react along their

Next Page

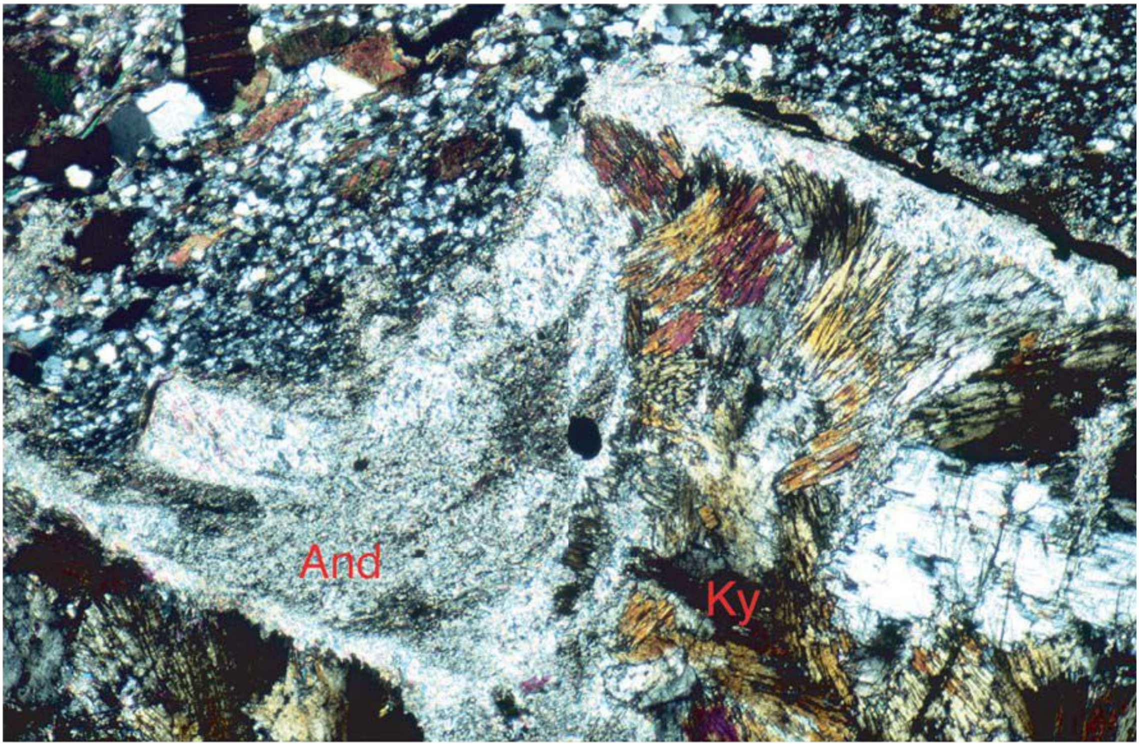

Fig. 4.72: Andalusite (And) porphyroblast partly replaced by radiating aggregates of kyanite (Ky) in a schist from Fiordland, New Zealand. Sample by courtesy of Chris Ward. Crossed polars; base of photo 4.4 mm.

grain boundaries. Corona structures are preserved best in volumes of rock that have not been strongly deformed, and so may provide information about reactions in adjacent rocks in which deformation has removed the evidence of incomplete reactions.

Although coronas are potentially useful for inferring metamorphic reactions, care should be taken in their interpretation, for the following reasons. Many, if not most, symplectic coronas reflect disequilibrium and consequent breakdown of pre-existing minerals separated by the coronas, incompleteness of the reaction being due to the armouring by the coronas and by slower reaction rates with lowering of temperature. However, some reflect changes in the volumes of minerals as P–T conditions change within the stability field of a single mineral assemblage; i.e. all the minerals remain in equilibrium (White *et al.*, 2002). Factors such as strain, nucleation and growth rates, and changing volumes of equilibrium, may control the proportions of minerals produced in the intergrowths (White *et al.*, 2002). In addition, some coronas involve kinetically controlled reactions that have not reached equilibrium (see, for example, Tracy & McLellan, 1985).

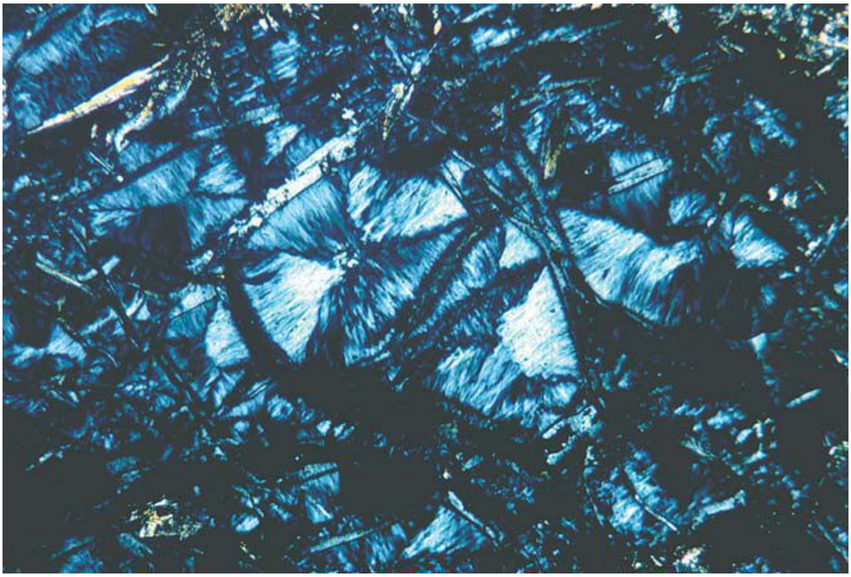

Fig. 4.73: Serpentinized peridotite from the Archaean of Western Australia. Despite the complete pseudomorphism, the shapes of the original polygonal grains of olivine have been preserved. Crossed polars; base of photo 1.3 mm.

Some coronas are multiple and complex. Their microstructures are controlled by: (1) the chemical reaction(s) involved; (2) the rate(s) of the reaction(s); (3) the relative rates of intergranular and intragranular diffusion of the chemical components involved in the reaction(s); (4) whether or not components are added or removed from outside the volume occupied by the obvious reactants; and (5) the temperature and pressure and their variation during growth of the corona (White & Clarke, 1997). For example, complex multiple coronas may develop from an apparently simple reaction between two minerals, owing to relative rates of diffusion of migrating chemical elements (Grant, 1988; Johnson & Carlson, 1990). Moreover, in multiple coronas, the layers may not all grow at the same time, because changes in temperature and pressure can cause reaction between two early layers to form a younger intermediate layer (Griffin, 1972; Indares, 1993).

4.13.4 Unreliable criteria for inferring metamorphic reactions

Microstructures that generally do *not* indicate metamorphic reactions (Vernon, 1996a) include the following.

(1) Inclusions and partial inclusions ('moulding' relationships) are unreliable, because included and host minerals can nucleate simultaneously or in either order (Vernon, 1977a), as shown for inclusion relationships in igneous rocks in

Fig. 3.47, which apply equally well here. If an included mineral is absent from the matrix everywhere (i.e. on the scale of a large thin section) it may be a remnant of an older assemblage, and so the inference of a reaction may be justified (see, for example, Thompson *et al.*, 1977; Krogh, 1982; St Onge, 1987).

(2) The 'wrapping' of porphyroblasts by minerals in folia is often used as an indication that the foliated assemblage is younger than the mineral around which it is deflected. A good example is illustrated in Fig. 4.31, which shows folia rich in biotite and sillimanite wrapping around pods rich in cordierite or garnet. The temptation may be to infer a reaction between cordierite and garnet to produce biotite and sillimanite, but this is unjustified (Vernon, 1996a), because the relationship commonly results from simultaneous growth of all the minerals, the difference in occurrence being simply due to deformation partitioning (Section 5.7). Biotite and sillimanite can grow and survive in zones of strong deformation, forming folia that are squashed against and consequently anastomose around the much stronger pods rich in cordierite and garnet growing at the same time (Fig. 4.31). If the biotite and sillimanite also occur as inclusions in contact (without reaction between them) inside the cordierite and garnet porphyroblasts, this would confirm that all four minerals are part of the same compatible assemblage (paragenesis) and that no reaction between them should be inferred (Vernon, 1996a). Of course, if the mineral in the resistant pods is strongly deformed, recrystallized or partly replaced by new minerals that are compatible with a lower-temperature assemblage in the matrix, as in many retrograde schists (Sections 4.13.5, 4.13.6) and mylonitic rocks (Section 5.7.6), the inference of a reaction may well be justified.

4.13.5 Retrograde metamorphic reactions

Preservation of microstructural evidence of reactions is most pronounced in retrograde metamorphism. This is partly because falling temperature tends to slow down reaction rates, and also because retrograde reactions generally require addition of water or carbon dioxide, which have to be returned to a rock that was devolatilized during prograde metamorphism. The same situation applies to the low-grade metamorphism of igneous rocks, which requires the addition of water, in order to form hydrous amphibole, epidote and chlorite from anhydrous pyroxene, olivine and plagioclase.

For this reason, retrograde metamorphism is commonly incomplete and patchy. However, in deformation zones (e.g. mylonitic or retrograde schist zones), the deformation opens up transient spaces. These low-pressure sites suck in fluid, and so promote retrograde reactions. Consequently, the reactions tend to go to completion in these zones, in contrast to typically incomplete reactions in the adjacent, less deformed rocks (Vernon & Ransom, 1971; Corbett & Phillips, 1981; White & Clarke, 1997).

4.13.6 'Effective reactive system'

A common assumption is that metamorphism is essentially isochemical, apart from loss of water and/or carbon dioxide, except for clear examples of major chemical change (*metasomatism*). However, this is difficult to prove for metasedimentary rocks, because of sampling problems across a metamorphic terrane. For example, how can we be sure of always sampling the same sedimentary bed or unit, and even if we are, can we assume that its chemical composition originally was constant along its length? Some people have argued for isochemical prograde metamorphism (see, for example, Shaw, 1956; Butler, 1965; Atherton, 1977; Yardley, 1977a; Moss *et al*., 1995, 1996; Cardenas *et al*., 1996; Roser & Nathan, 1997), whereas others have argued for bulk chemical changes during prograde metamorphism of metasedimentary rocks (see, for example, Ague, 1991, 1994, 1997; Haack *et al*., 1984).

Microstructural and chemical evidence shows that, even if the metamorphism is isochemical overall, the 'effective reactive system' (i.e. the mineral assemblage actually involved in a metamorphic reaction) can change as metamorphism progresses. This can be due to the following causes.

(1) Cation leaching

Local leaching of cations by acid solutions (*hydrogen metasomatism*), for example along grain boundaries or in narrow deformation zones, can change the chemical composition of the local reacting system. This can permit the formation of minerals that would not otherwise have formed, such as Al-rich minerals (e.g. andalusite, sillimanite and cordierite) in rocks of felsic igneous composition (Gresens, 1971; Vernon *et al*., 1987; McLelland *et al*., 2002a,b), as shown in Fig. 5.60. Another example is the development of late fibrous sillimanite replacing all minerals, from their grain boundaries inwards, in metapelitic rocks at Cooma, SE Australia (Vernon, 1979). A similar effect occurs in the hydrothermal alteration of felsic rocks, including geothermal alteration of volcanic and tuffaceous rocks, and during advanced 'argillic alteration' of volcanic or high-level intrusive rocks in the 'porphyry copper' environment (see, for example, Espenshade & Potter, 1960; Hemley & Jones, 1964; Gustafson & Hunt, 1975; Lowder & Dow, 1978; Valiant *et al*., 1983). The inference of a hydrothermal origin for veinlets of andalusite and sillimanite in altered rhyolite suggests a continuum between hydrothermal alteration and regional metamorphism (see, for example, Vernon, 1976, pp. 17, 18). If rocks hydrothermally metasomatized at low temperatures (forming aluminous clay minerals or pyrophyllite) are later metamorphosed, high-grade aluminous minerals may be formed.

The anastomosing folia of sillimanite (Fig. 4.31) that are so common in high-grade regional metapelitic rocks (see, for example, Harker, 1932, fig. 106; Vernon, 1987a,b) require explanation. How are the Al-rich folia segregated from the other minerals? Alternative explanations are that (1) the sillimanite replaces an earlier-formed Al_2SiO_5 polymorph, such as andalusite, and is then deformed into folia, or (2) local base-cation leaching occurs in zones of high strain and high fluid flow, leaving residual concentrations of sillimanite (Fig. 5.60).

(2) Porphyroblasts

Once formed, porphyroblasts may fail to react, or react only at their margins during progressive metamorphism, owing to slow diffusion rates inside many minerals and to the resistance of large grains to deformation, which would otherwise assist reactions to occur in their interiors by creating and moving crystal defects and by promoting recrystallization (Chapter 5). Therefore, the part of the chemical system that is inside the porphyroblast is isolated from the reactive system, and so only the matrix and reacting edges of the porphyroblasts constitute the reactive system from that stage onwards. Thus, the bulk chemical composition of the 'effective reactive system' can change during progressive metamorphism. For example, if Mn preferentially enters garnet porphyroblasts and these do not react during subsequent heating, the 'effective reactive system' would be poorer in Mn than the original reactive system. An example of the progressive removal of chemical components trapped in garnet cores from the 'effective reactive system' has been described for eclogite facies rocks in New Caledonia by Marmo *et al.* (2002).

This situation is even more pronounced during retrograde metamorphism, where falling temperatures and restricted availability of fluid may localize reactions. Residual prograde porphyroblasts may again be isolated, except at their margins, so that the effective reactive volume is limited. In the absence of deformation, retrograde minerals may replace matrix minerals, leaving porphyroblasts as relics, commonly with partial replacement along fractures and along grain boundaries. In contrast, grain deformation and recrystallization or neocrystallization are much more pervasive in high-strain, mylonitic zones ('shear zones'), and therefore assist retrograde reactions to proceed towards completion. For example, in granulite facies rocks at Broken Hill, Australia, generally only part of the rock undergoes retrograde reactions outside shear zones, whereas the whole rock tends to be involved in reactions inside shear zones; however, even there some high-grade porphyroblasts may remain, such as garnet with sillimanite inclusions (Vernon & Ransom, 1971). Another example occurs in the western Musgrave Ranges, Western Australia, where White & Clarke (1997) observed that mafic rocks outside shear zones are partly converted to eclogite facies minerals, with the development of corona structures, whereas in shear zones complete transformation to finely neocrystallized hydrous aggregates has taken place.

Residual porphyroblasts may even provide completely separate chemical environments for retrograde reactions. For example, Clarke *et al.* (1995) found that during retrograde metamorphism the chemical reaction and consequent mineral assemblage developed inside large porphyroblasts of andalusite differed markedly from those in the surrounding matrix, so much so that corundum grew inside the andalusite, despite the abundance of quartz in the matrix; these two minerals would have reacted with each other under the prevailing metamorphic conditions had they come into contact. This is an example of the effective localization and separation of two reactive systems, which is most likely to occur during the cooling conditions of retrograde metamorphism.

(3) Zoned minerals

The growth of chemically zoned minerals may also affect the effective reactive system. Stüwe (1997) explained that, during cooling, progressively larger proportions of zoned minerals are removed from the effective reacting system, thereby changing its composition, because of the changing chemical composition of the zones. However, the extent of the effect depends on the grainsize of the zoned mineral. Because the sequence of reactions depends on bulk chemical composition, two rocks of identical composition, but of different grainsize, may undergo different reaction sequences.

(4) Development of foliations

Medium- and high-grade regional metapelitic rocks generally have differentiated crenulation cleavages (Section 5.8.3), the formation of which involves extensive to complete recrystallization and neocrystallization of all the matrix minerals (see, for example, Hobbs *et al.*, 1976; Marlow & Etheridge, 1977; Bell & Rubenach, 1983; Williams, 1990). These foliations are characterized by alternations of quartz-rich and mica- (and/or sillimanite-) rich folia. Selective loss of the more soluble chemical components (especially of quartz) from the micaceous and/or sillimanite-rich folia and even from the whole rock, may occur, at least on the hand-specimen scale (see, for example, Williams, 1972; Marlow & Etheridge, 1977), although some have suggested that no bulk chemical change is involved. The problem has been reviewed by Vernon (1998) and is discussed in Section 5.9.4.

The relevant point here is that, if selective loss of soluble components is involved in the production of a foliation, the remaining rock would have a different (generally more aluminous) composition than before the development of the foliation concerned, even though all of the remaining rock may participate in further metamorphic reactions. Therefore, metamorphism of foliated metapelitic rocks would be strictly isochemical only for restricted periods between the formation of one foliation and the next, and could not be considered to be isochemical for a whole prograde metamorphic event.

4.14 Distribution of minerals in metamorphic rocks

Minerals appear to be distributed at random in many metamorphic rocks. This may be expected intuitively, as nucleation and growth of one mineral would tend to deplete the immediately surrounding volume in nutrient components and enrich it in waste components, which should inhibit nearby nucleation of the same mineral. Moreover, the separation of different minerals in metamorphic rocks is expected from the observation that interfacial energies of boundaries between grains of the same minerals tend to be higher than those of boundaries between grains of different minerals (Section 4.2.4). However, other factors may complicate this situation.

Detailed studies of three-dimensional distributions of grains and grain compositions in metamorphic rocks are few. Flinn (1969) found that boundaries between grains of the same mineral tend to be slightly less common than boundaries between grains of different minerals. Kretz (1966b, 1973) found that the spatial distribution of garnet grains in a schist from Yellowknife, Canada, is random, but Daniel & Spear (1999) found a weak to strong clustering of garnet porphyroblasts in a schist from Connecticut, USA, the clustering possibly reflecting minor bulk compositional variations. Kretz (1969) inferred a random distribution of minerals in a high-grade (granulite facies) metamorphic rock from Québec, Canada, but Jerram & Cheadle (2000), using statistical cluster analysis, found a tendency for titanite grains to cluster (though generally not touch each other) in this rock. This is probably due to the grain network of the more abundant minerals (pyroxene and scapolite) forcing the titanite grains to develop a non-random distribution, but it could be due to the original distribution of chemical components used to make the titanite dictating the nucleation pattern (Jerram & Cheadle, 2000).

Although minerals tend to be separate in most metamorphic rocks, local single-mineral aggregates occur in some rocks. The following are some of the processes that can lead to the formation of single-mineral aggregates in metamorphic rocks. They all involve the formation of domains in which only one mineral can be present, either because they involve isochemical changes within a formerly large grain or because metasomatism reduces the number of minerals to one (Korzhinskii, 1950, 1959).

(1) The replacement (recrystallization) of a former large grain by an aggregate of the same mineral in response to deformation (Section 5.4.2) produces single-mineral aggregates (Voll, 1960; Spry, 1969; Stanton, 1964, 1972; Vernon, 1975, 1976; Hobbs *et al.*, 1976; McClay & Atkinson, 1977; McClay, 1982a,b,c). Examples include recrystallized polygonal calcite, olivine and plagioclase, oxide minerals and sulphide minerals. Other common examples are 'decussate' aggregates of biotite (see, for example, Kretz, 1966a; Vernon, 1968, 1977b), especially in deformed granites (Vernon *et al.*, 1983). Similarly, the recrystallization of originally large grains during strong deformation in mylonites (Section 5.7.6) commonly produces polygonal single-mineral aggregates in a compositional foliation (Vernon, 1974).

(2) Variation in stress and/or strain can produce compositional layering due to deformation (Cobbold, 1977). The alternative suggestion of Yardley (1989,

p. 170) that compositional layering is formed in metamorphic rocks because of a preference for single-mineral aggregates based on interfacial free energies is less likely, for reasons given previously (Section 4.2.4). Experiments have shown that physical separation of strong and weak minerals during deformation can lead to the formation of a compositional ('differentiated') layering, e.g. the separation of rigid mica from weak, ductile salt (Means & Williams, 1974) and rigid mica from weak, ductile ice (Wilson, 1984). This purely physical process could develop single-mineral aggregates.

(3) Single-mineral aggregates also may be formed where other minerals have been dissolved and removed from high-strain zones (limb-zones) of a crenulation-foliation, producing mica (Williams, 1972, 1990) or sillimanite (Vernon, 1987a) domains, as discussed in more detail in Sections 5.8 and 5.9. This is a type of local metasomatic reaction (see (6) below), for which considerable amounts of evidence have been accumulated (see, for example, Vernon, 1998).

(4) Pseudomorphous polymorphic transformations, such as sillimanite or kyanite replacing andalusite (Figs. 4.2, 4.72), produce single-mineral aggregates, (see, for example, Bosworth, 1910; Vernon, 1987b).

(5) Some other pseudomorphous reactions may also produce single-mineral aggregates; for example, white mica replacing staurolite (Guidotti & Johnson, 2002). These are metasomatic reactions (see (6) below) on the scale of the pseudomorph.

(6) Metasomatism tends to reduce the number of minerals (see, for example, Korzhinskii, 1950, 1959), and so may lead to the formation of single-mineral aggregates.

(7) Fortuitous bulk-rock compositions may also lead to single-mineral aggregates, for example in the metamorphism of beds or clasts of pure quartz sandstone or limestone (Fig. 4.6).

4.15 Residual microstructures in metamorphic rocks

Many residual structures are best seen at the outcrop scale, but microstructural relics can also be seen in some metamorphic rocks, despite the tendency for metamorphism to adjust grain boundaries and so change original grain shapes. Microstructural relics occur especially at low metamorphic grades, but also occur in some high-grade rocks in relatively low-strain zones, even adjacent to rocks that have undergone strong multiple deformation (see, for example, Williams, 1991, fig. 11). They are useful for helping to determine parent rock-types, which is not only important for working out the complete metamorphic history of an area, but also for the search for potentially economic mineral resources in metamorphic terranes.

Metapelitic and calcsilicate precursor rocks are generally readily identified on the basis of bulk chemical composition and abundance of aluminous or calcareous minerals, respectively. However, quartzofeldspathic metasediments (epiclastic and pyroclastic) and meta-igneous rocks (plutonic and volcanic) commonly do not have sufficiently distinctive minerals or bulk compositions, and so mesoscopic and microstructural evidence is the most reliable for determining their general nature.

4.15.1 Residual sedimentary microstructures

In general, sedimentary microstructures are not well preserved in metamorphic rocks, although mesoscopic structures commonly are. Clastic quartz grains may be preserved in incompletely recrystallized metasandstones and metasiltstones at low metamorphic grades (Fig. 4.74). Thin bedding also is commonly preserved, and can be seen most clearly where it is oblique to the foliation (Fig. 5.53). Fossil remnants replaced by recrystallized calcite (Fig. 4.6) or higher-grade metamorphic minerals, such as wollastonite (Fig. 4.38), may also be preserved, especially in low-strain regional metamorphic rocks and contact metamorphic rocks.

4.15.2 Residual igneous microstructures

Igneous microstructures have a better chance of preservation, as foliations generally don't develop as readily in igneous rocks. Even where deformation and recrystallization–neocrystallization have removed much of the primary igneous microstructure, many magmatic features can be at least partly preserved. This may occur even at granulite facies conditions, especially in zones of relatively low strain accumulation. For example, euhedral megacrysts of K-feldspar (with the simple twinning, zonally arranged plagioclase inclusions and oscillatory zoning characteristic of K-feldspar megacrysts in granites) may be preserved in augen gneisses and mylonites (Sections 5.7.6, 5.7.9), though generally showing some evidence of deformation in the form of microcline twinning and/or marginal recrystallization (Vernon, 1986a, 1990b; Vernon & Williams, 1988; Vassallo & Vernon, 2000).

Though viewed as relatively unimportant minerals in many metamorphic reactions, quartz and feldspar are the most useful minerals for determining igneous parent rocks (Vernon, 1999a), in the following way.

Residual crystal faces and embayments in quartz indicate a volcanic or subvolcanic precursor (Vernon, 1986b; Williams & Burr, 1994), as shown in Fig. 4.75. This is an especially useful criterion, as chemical distinction between plutonic and volcanic felsic rocks may be impossible. Quartz phenocrysts may be preserved even in strongly deformed rocks of the amphibolite facies (Fig. 4.75), because large single crystals tend to be much stronger than fine-grained aggregates in a former groundmass, especially if the groundmass minerals are involved in metamorphic reactions that liberate water pervasively at the grain scale. Water may assist deformation by permitting grains to slide past one another, as well as

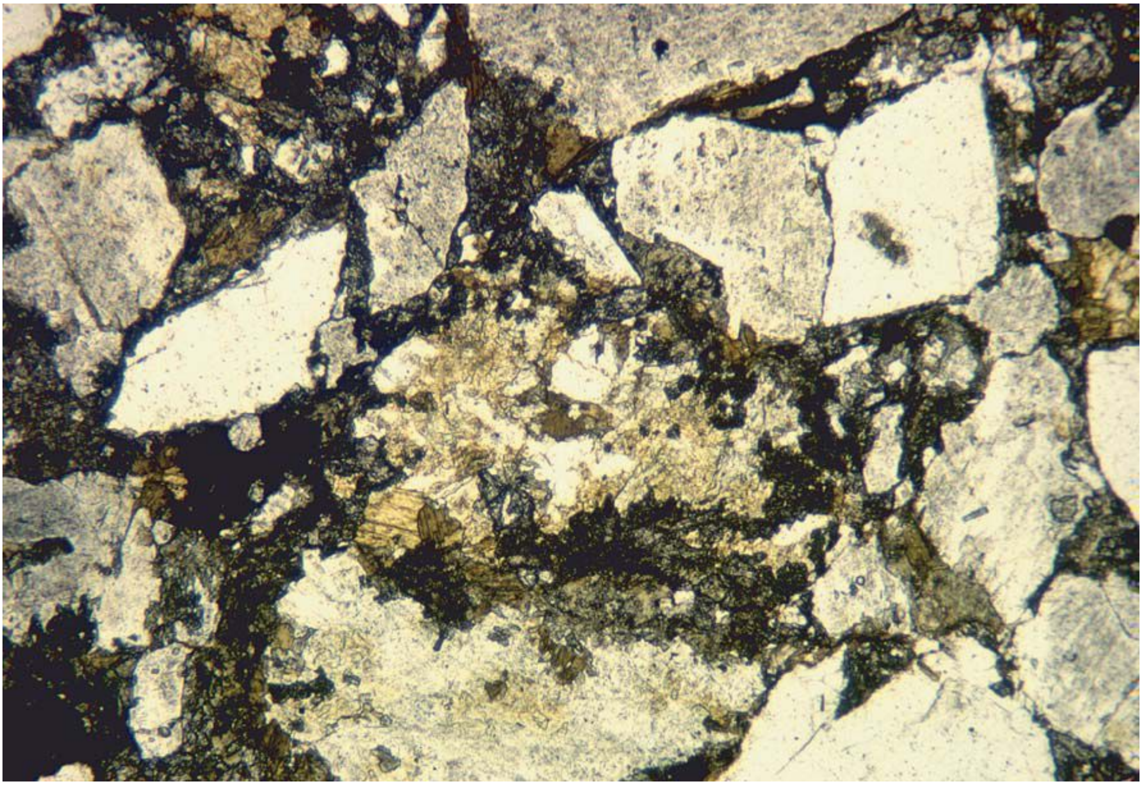

Fig. 4.74: Volcaniclastic sandstone that has undergone low-grade (greenschist facies) regional metamorphism, Hill End Trough, New South Wales, Australia. Abundant fine-grained metamorphic epidote (high relief), titanite (very high relief) and biotite (brown) have grown in the former matrix and in some of the clasts, but the overall detrital microstructure (characterized by angular fragments) has been preserved. Detrital K-feldspar is indicated by light yellow staining with sodium cobaltinitrite. Plane-polarized light; base of photo 4.8 mm.

weakening some minerals internally (Section 5.3), and reactions promote breakdown of old minerals and growth of new ones, thereby assisting realignment of the microstructure.

Crystal faces in feldspar are potentially good indicators of an igneous precursor. For example, some metavolcanic rocks preserve euhedral plagioclase phenocrysts, some with concentric zoning (Fig. 4.76). In others, the general shapes of feldspar phenocrysts and even elongate groundmass crystals are preserved, despite neocrystallization (Walker *et al.*, 1960, fig. 1A), as shown in Fig. 4.77.

In some metavolcanic rocks, both quartz and feldspar phenocrysts may be preserved, but commonly the feldspar is altered to fine-grained mica-rich aggregates, especially at lower metamorphic grades. These aggregates deform

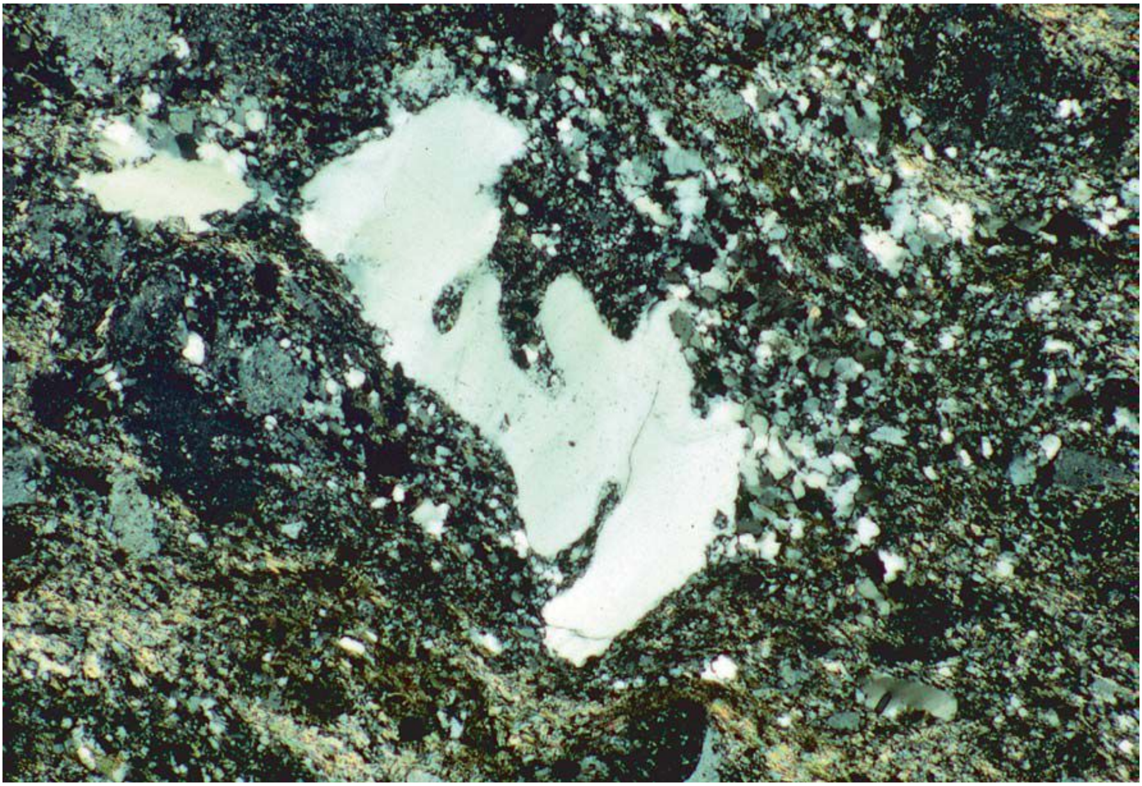

Fig. 4.75: Embayed quartz phenocryst preserved in a metarhyolite metamorphosed at amphibolite facies conditions, Picuris Range, New Mexico, USA (Vernon, 1999a, fig. 3), with permission of the *Canadian Mineralogist*. Crossed polars; base of photo 4 mm.

relatively easily, and so become part of the fine-grained matrix flowing around the quartz phenocrysts. The result is a schist with residual quartz phenocrysts ('quartz-eye rock'), which can be useful when searching for volcanic-hosted mineral resources. The absence of feldspar phenocrysts has led some to suggest that these rocks are not metavolcanic, but that the quartz 'eyes' are formed by silica metasomatism. However, the microstructural evidence is strongly in favour of a volcanic origin (Vernon, 1986b; Williams & Burr, 1994).

Crystal faces are not very common in coarse-grained, intrusive igneous rocks. Although internal zoning reflects euhedral crystal growth and may give the impression of overall euhedral crystal shape, the actual grain boundaries are commonly anhedral, owing either to mutual impingement during the crystallization of granitic magma or to grain-boundary adjustment of minerals that crystallize simultaneously near the solidus (Section 3.5.9). Nevertheless, elongate shapes of plagioclase grains (with twins parallel to the elongation) may be preserved in strongly recrystallized metagabbros and metadolerites, even in

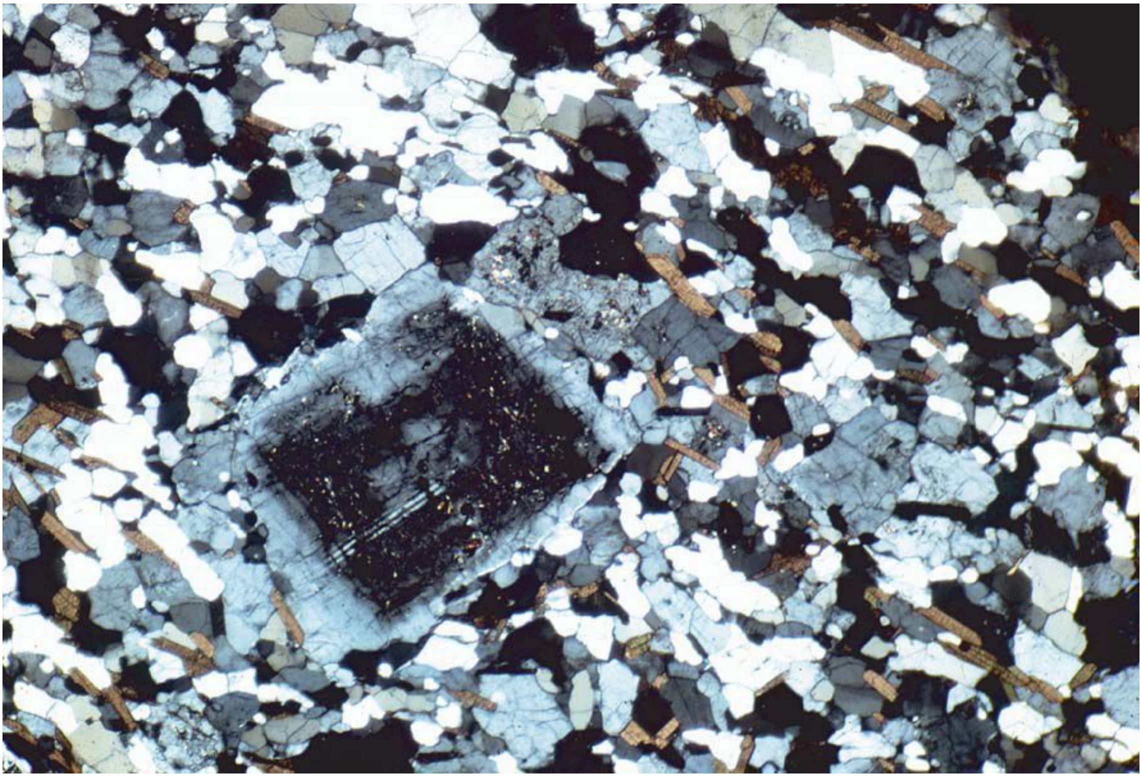

Fig. 4.76: Residual euhedral plagioclase phenocryst with concentric zoning in an amphibolite facies metavolcanic schist from the Mount Lofty Ranges, South Australia. Crossed polars; base of photo 4.4 mm.

high-grade metamorphic rocks (Figs. 4.78, 4.79), as illustrated by Philpotts (1966, plate 1A) and Glassley & Sørensen (1980, fig. 4a). For example, Fig. 4.78 shows a gabbro metamorphosed at high metamorphic grade, which retains residual elongate shapes of igneous plagioclase, despite extensive recrystallization. On the other hand, many thoroughly recrystallized mafic rocks show few or no elongate plagioclase relics (Fig. 4.79). Moreover, some gabbros undergo solid-state adjustment of their grain boundaries during slow cooling, without external heating or deformation (Section 4.6.1).

Other useful criteria of an igneous parent rock using feldspar are simple twinning in K-feldspar (Vernon, 1986a), oscillatory zoning in K-feldspar and plagioclase (Vernon, 1976, 1986a; Mehnert & Büsch, 1981) and concentric zoning truncated by metamorphic grain boundaries (Vernon *et al.*, 1987; Vernon, 1999a). Truncated zoning implies grain boundary movement in the solid state, removing pre-existing igneous zoning, whereas metamorphic zoning typically follows the boundaries of the metamorphic grains. Aligned, elongate crystals of feldspar

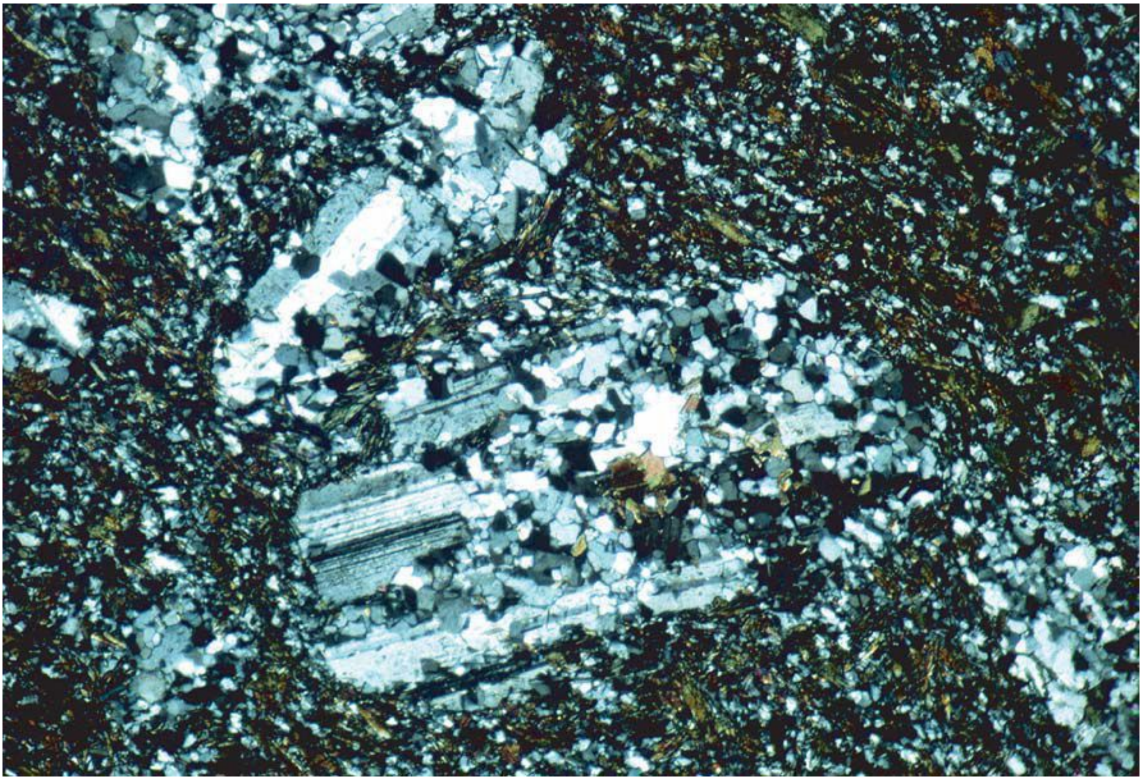

Fig. 4.77: Partly and completely recrystallized plagioclase phenocrysts in a metabasalt from the Snowy Mountains, south-eastern New South Wales, Australia. Crossed polars; base of photo 4.4 mm.

indicate an igneous precursor that has undergone magmatic flow (S. R. Paterson *et al.*, 1989; Vernon, 2000a), as discussed in Section 3.9.

Plagioclase and quartz inclusions can be useful for distinguishing residual phenocrysts from porphyroblasts of K-feldspar. K-feldspar phenocrysts (megacrysts) are characterized by crystallographically (zonally) oriented inclusions, especially of euhedral plagioclase (Vernon, 1986a), as shown in Figs. 3.12 and 3.75, whereas K-feldspar porphyroblasts are characterized by approximately spherical plagioclase (and quartz) inclusions (Section 4.2.7) at random (Figs. 4.30A, 4.31) or aligned in inclusion trails (commonly with biotite) that mimic an overgrown foliation (Vernon, 1999a).

4.16 Microstructures formed by melting of solid rocks

Melting occurs in four main situations in Earth, namely in: (1) the mantle asthenosphere, producing basaltic magma; (2) the lower crust, producing granitic

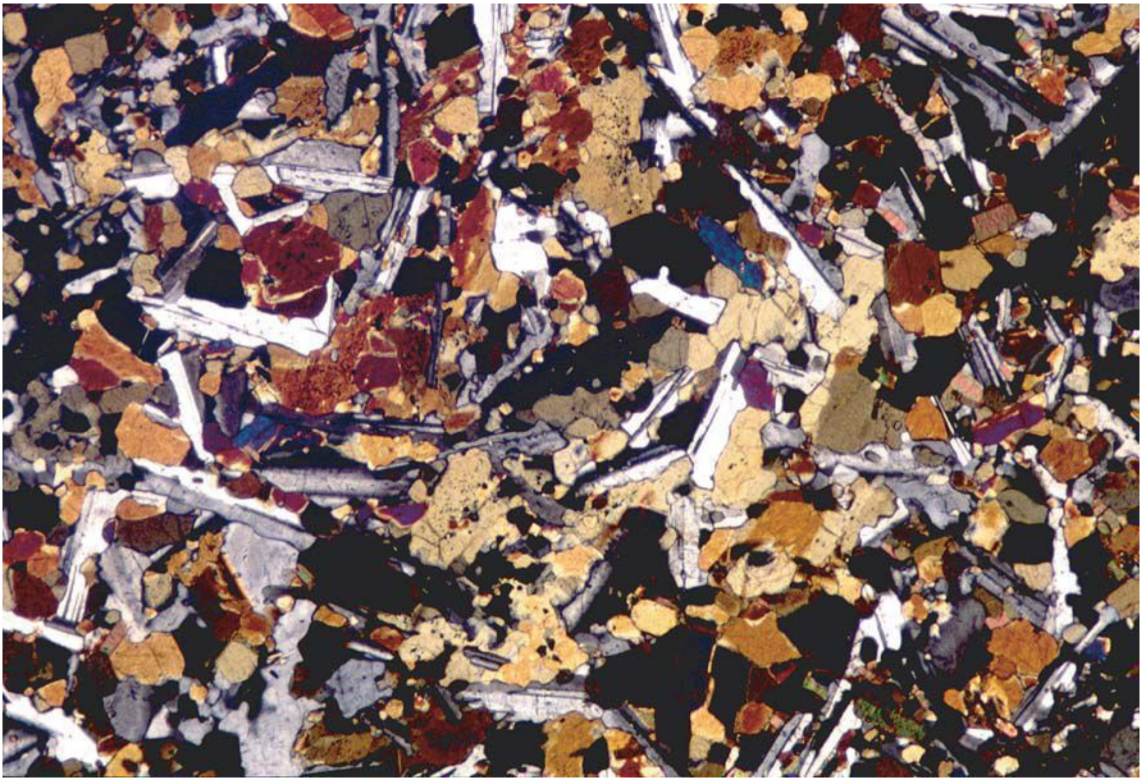

Fig. 4.78: Metadolerite, consisting mainly of calcic plagioclase and brown hornblende, from Baja California, Mexico, showing residual shapes of elongate igneous plagioclase crystals, despite extensive recrystallization and/or neocrystallization of brown hornblende. Crossed polars; base of photo 1.7 mm.

magma; (3) meteorite impacts and fault zones, producing pseudotachylites; and (4) xenoliths, producing local melt patches. The microstructures of pseudotachylites have been mentioned in Section 3.5.8. In this section, the discussion is restricted to examples of partial melting in crustal rocks.

4.16.1 Partial melting of crustal rocks to form granitic magma

At temperatures above approximately 650 °C, many rocks begin to melt, forming *migmatites*, which cross the traditional division of 'igneous' and 'metamorphic' rocks. Traditionally, the melted part of a migmatite has been referred to as *neosome*, and the apparently unmelted part has been referred to as *palaeosome*, implying residual unaltered rock (Mehnert, 1968). However, the unmelted rock is commonly chemically modified during the melting process (Johannes, 1985,

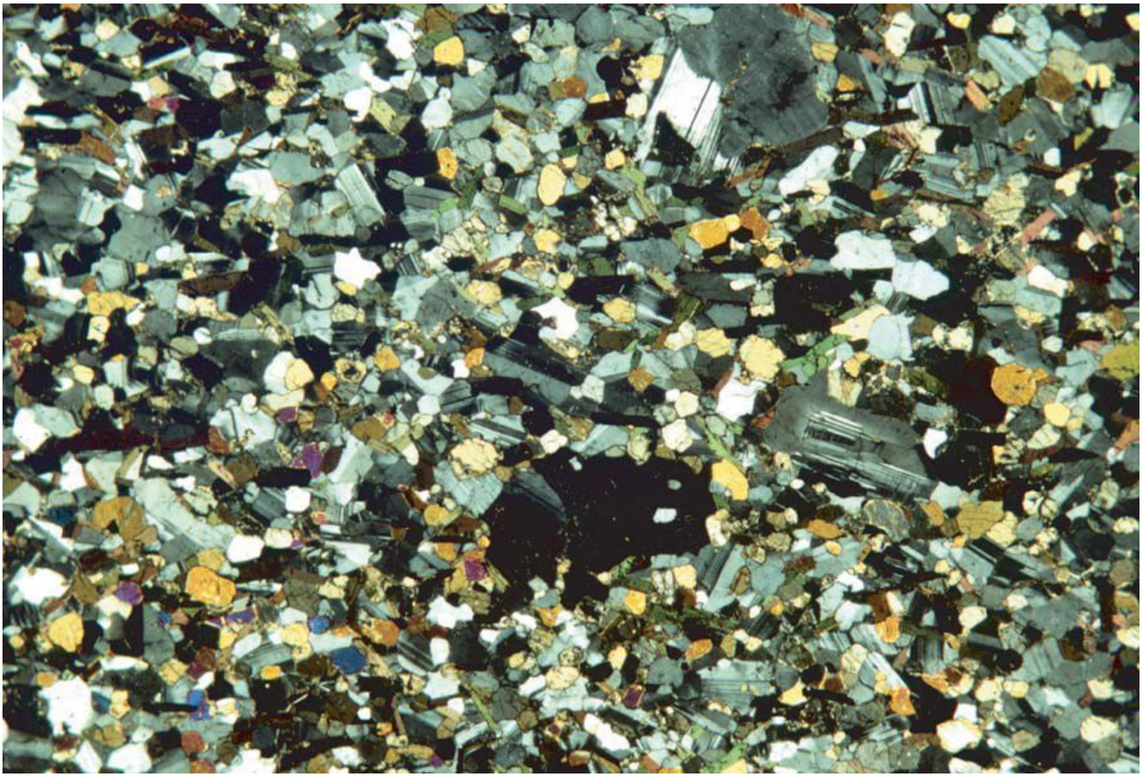

Fig. 4.79: Two-pyroxene granofels (granulite facies), Anmatjira Range, central Australia, showing extensive recrystallization and neocrystallization, but preserving a few plagioclase grains with elongate igneous crystal shapes and even a concentrically zoned plagioclase crystal (right of centre). Crossed polars; base of photo 10 mm.

1988), and so generally cannot be assumed to have the original unaffected rock composition. Nowadays it is generally referred to as *mesosome*, and consists of unreacted minerals, solid products of the melting reaction left behind by the mobile neosome, and in some instances, small dispersed pockets of melt. The neosome, which is inferred to represent the mobile products of the partial melting reaction, consists of light-coloured (leucocratic), predominantly felsic layers or pods (*leucosome*), generally inferred to represent the former liquid products of the melting reaction, together with borders of darker, more mafic rock (*melanosome*) inferred to represent solid products of the melting reaction that have segregated from the leucosome. However, leucosomes may move independently of solid products, so that melanosomes are not always in contact with them. For example, solid reaction products may nucleate on existing minerals in the unmelted rock, and so be left behind when the leucosome moves (see, for example, Vernon *et al.*, 2003a).

Leucosomes and neosomes may occur as patches or discontinuous veinlets, especially in relatively undeformed rocks that still show sedimentary bedding (*bedded migmatites*), the leucosome being retained in the source beds, typically metapelites (see, for example, Vernon *et al.*, 1990, 2003a; Greenfield *et al.*, 1996; Vernon & Johnson, 2000). However, in most migmatites, deformation assists the segregation of magma into lower-pressure sites parallel to the rock's foliation (see, for example, Robin, 1979; McLellan, 1988; Sawyer, 1994, 1996, 2001; Brown & Rushmer, 1997; Guernina & Sawyer, 2003). Layers (stroma) of leucosome commonly develop, forming *stromatic migmatites* (also commonly called *metatexites*). In many stromatic migmatites, dark selvedges border the leucosomes, these melanosomes generally being inferred to be the result of local (*in situ*) segregation of melt from crystals. Some stromatic migmatites result, at least in part, from the solid-state deformation of bedded migmatites (Vernon *et al.*, 2000, 2003a).

Neosomes consist largely of melt or melt products, such as crystals precipitated from the melt or from residual melt separated from precipitated crystals (Sawyer, 1987; Barbey *et al.*, 1996; Sawyer *et al.*, 1999). Unmelted crystals and crystals formed as solid products of the melting reaction (*peritectic minerals*), which commonly include cordierite and/or garnet in partly melted metapelites, may also be incorporated in leucosomes, but are more common in melanosomes and mesosomes. As a result of the commonly postulated low-pressure melting reaction: biotite + quartz + sillimanite = cordierite + K-feldspar + melt, some of the K-feldspar in the resulting leucosome is solid, the rest having precipitated from the melt.

Together the unmelted and peritectic minerals constitute *restite*, or the solid minerals remaining after a magma-producing reaction, as defined by Chappell & White (1991). Technically, 'restite' refers to the solid material resulting from the formation of a specific magma. Restite surviving from other melting reactions that did not produce the magma under discussion is not the restite for that batch of magma. Residual solid material of this type, together with any other unmelted material from the same immediate source terrane for that particular magma, is known as *resistate*. However, some people include resistate in the term 'restite'.

If the melt portion of a leucosome magma moves from the melting or initial accumulation site before crystallizing, it leaves behind restite and resistate. If only part of the leucosome melt leaves the melting or initial accumulation site, it leaves behind a modified leucosome that consists of peritectic and unmelted crystals, together with minerals that crystallize from the residual melt. Therefore, the composition of a leucosome or neosome is not necessarily a reliable indication of the original magma composition.

Some leucosomes have been inferred to result from hydrothermal mass-transfer or solid-state diffusion, rather than partial melting (*anatexis*), though most are inferred to be anatectic, provided the inferred metamorphic temperatures are high enough for melting to occur. Because of this mineralogical and chemical ambiguity, microstructural evidence (point 4 below) is helpful for identifying anatectic magma.

Evidence that a leucosome or neosome is due to anatexis includes: (1) temperatures appropriate for partial melting; (2) cotectic compositions, though the melt or part of the melt may be removed during deformation, leaving leucosome of non-magmatic composition, as explained above; (3) angular boudinage of mesosome in leucosome or neosome, reflecting the greater strength of the mesosome (consistent with a magmatic condition of the leucosome or neosome); and (4) igneous microstructures, such as those that follow.

(a) Crystal faces of plagioclase, K-feldspar and cordierite against quartz may occur (Kenah & Hollister, 1983; Vernon & Collins, 1988; Vernon, 1999a; Vernon *et al.*, 1990; Vernon & Johnson, 2000; Brown, 2001; Marchildon & Brown, 2003), as shown in Fig. 4.80. These minerals either crystallize from the melt or are solid products of the melting reaction. They are devoid of inclusion trails, which are typically abundant in grains of the same mineral in the host rock (Brown, 1998, fig. 6b; Vernon, 1999a; Vernon & Johnson, 2000). Commonly the inclusion-free euhedral crystals nucleate and grow on inclusion-rich grains of the same minerals in the original rock (Vernon, 1999a; Vernon & Johnson, 2000), as shown in Fig. 4.81.

(b) Simple twinning in K-feldspar is an indicator of igneous origin (Vernon, 1986a), as K-feldspar typically grows with simple twinning in magmas (Section 3.12), although it doesn't necessarily do so in anatectic magmas, because it can nucleate on existing K-feldspar (Fig. 4.81) instead of forming new nuclei (Vernon, 1999a).

(c) Aligned euhedral crystals in leucosomes/neosomes or in partly melted mesosomes are consistent with magmatic flow (see, for example, Collins *et al.*, 1989; Sawyer, 2001).

(d) In contrast to bell-shaped crystal size distributions of porphyroblasts in metamorphic rocks, CSD patterns of cordierite, plagioclase and K-feldspar in migmatite leucosomes, measured by Berger & Roselle (2001), are similar to those typical of igneous rocks, and are characteristic of nucleation and growth in a melt, rather than grain coarsening after crystallization.

These magmatic microstructures are best preserved in leucosomes or neosomes that have undergone minimal deformation or reheating after melting, and are commonly destroyed by the intense deformation that characterizes many migmatites, especially as deformation may be necessary to segregate melt into layers and vein networks (Collins & Sawyer, 1996; Sawyer, 2001, p. 291; Vernon *et al.*, 2003). However, euhedral shapes of K-feldspar phenocrysts are commonly preserved in intensely deformed granitic mylonites (Section 5.7.6), and so a similar degree of preservation could be expected in some stromatic migmatites. For example, in the Cooma Complex (south-eastern Australia), euhedral shapes of K-feldspar crystals are preserved in some deformed leucosomes, even where the

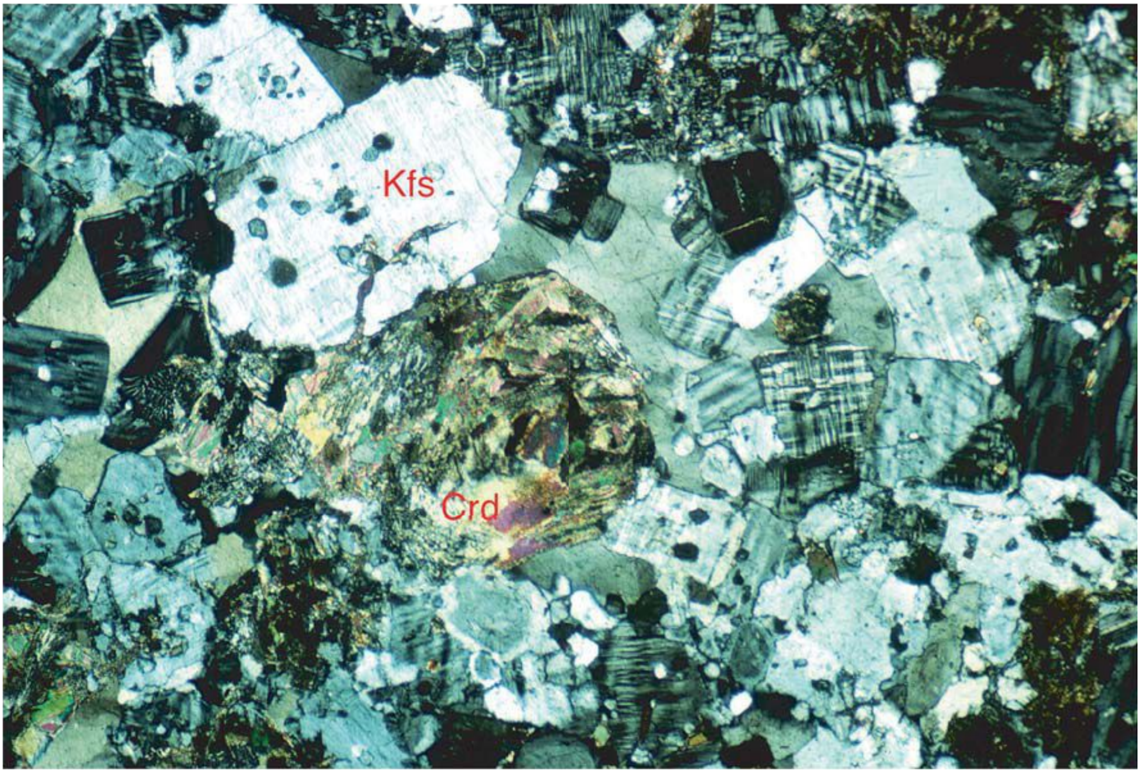

Fig. 4.80: Neosome in a migmatite, Mount Stafford, central Australia, showing crystal faces of microcline (Kfs, with tartan twinning) and cordierite (Crd; pseudomorphed by an aggregate of retrograde minerals, but preserving crystal faces) against quartz. The crystal faces reflect crystallization in a melt. Though the microcline twinning indicates some solid-state deformation, the neosome has not been sufficiently deformed to obliterate the igneous crystal shapes. Crossed polars; base of photo 10 mm.

quartz has been strongly recrystallized in deformation zones (Vernon & Johnson, 2000).

Mesosomes that are not deformed after solidification of melt that has not escaped may show good microstructural evidence of the former melt (Figs. 4.80–4.82) in the form of relatively small values of θ feldspar vs. quartz/quartz (Sawyer, 1999, 2000; Clemens & Holness, 2000; Rosenberg & Riller, 2000; Marchildon & Brown, 2003): distinctly smaller than equivalent angles in unmelted high-grade metamorphic rocks, measured by Vernon (1968). This implies that former melt solidified as feldspar (e.g. plagioclase or K-feldspar), depending on local nucleation conditions, the components of the quartz and the other feldspar having migrated and crystallized elsewhere, for example, on existing quartz and feldspar grains (Sawyer, 2000a,b, 2001), as shown in Fig. 4.82. The former melt occurs

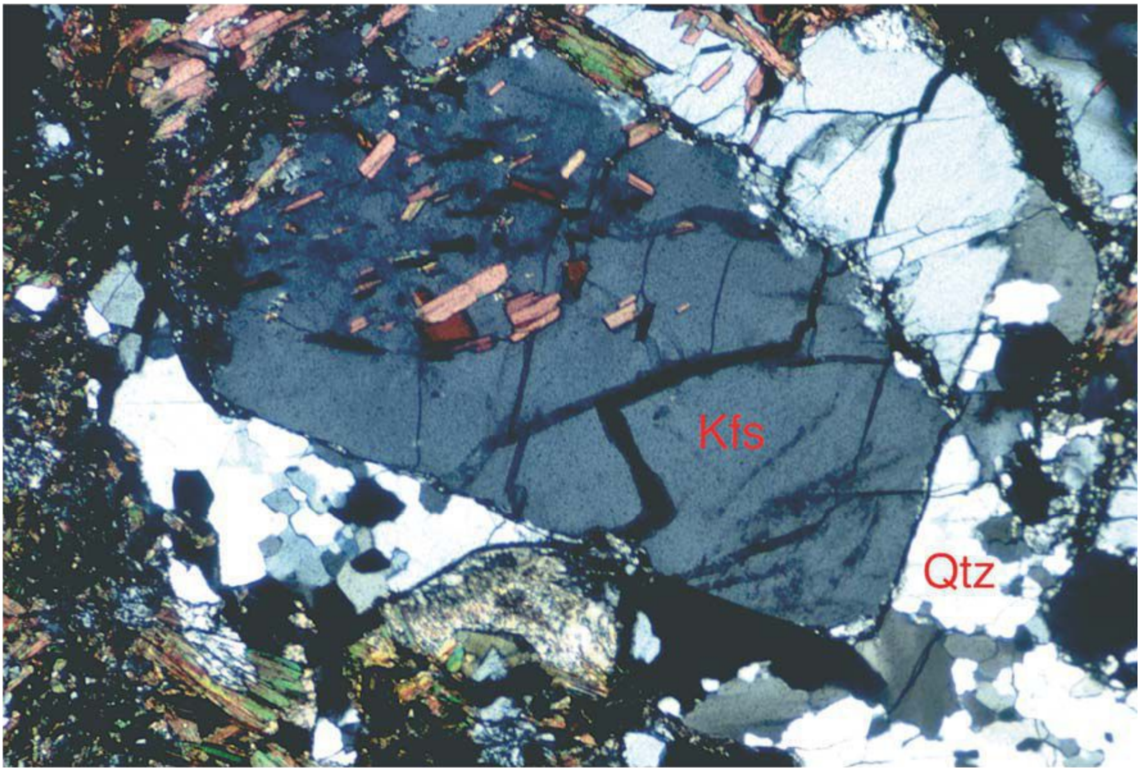

Fig. 4.81: K-feldspar (Kfs) and recrystallized quartz (Qtz) in a small patch of neosome in a migmatite, Cooma Complex, south-eastern New South Wales, Australia. The inclusion-free K-feldspar crystal in the centre has grown on a grain of inclusion-rich metamorphic K-feldspar in the adjacent mesosome. Crossed polars; base of photo 4 mm.

at grain corners and along grain edges between minerals involved in the melting reaction (Fig. 4.82), which is where melting begins in experiments (Mehnert *et al.*, 1973). The reacting minerals develop corroded or rounded shapes, and melt films grow in the grain boundaries, becoming wider and spreading to more grain boundaries as melting progresses (Büsch *et al.*, 1974), eventually to enter local shear zones. Natural examples have been described by Sawyer (2000a,b, 2001). Small dihedral angles and crystal faces have a better chance of survival in non-deformed rocks, because their microstructures are relatively unaffected by deformation-induced recrystallization (Section 5.4.2). Small melt patches (Fig. 4.82) may form (1) during melting, the process being quenched before segregation was complete, or (2) by draining back of melt into the mesosome from leucosome stroma after deformation ceased (Sawyer, 2001, p. 292).

The observed small dihedral angles may or may not be the same as the angles that occurred when the melt was actually present, and may represent some compromise in an attempt to reach an 'equilibrium angle' during cooling.

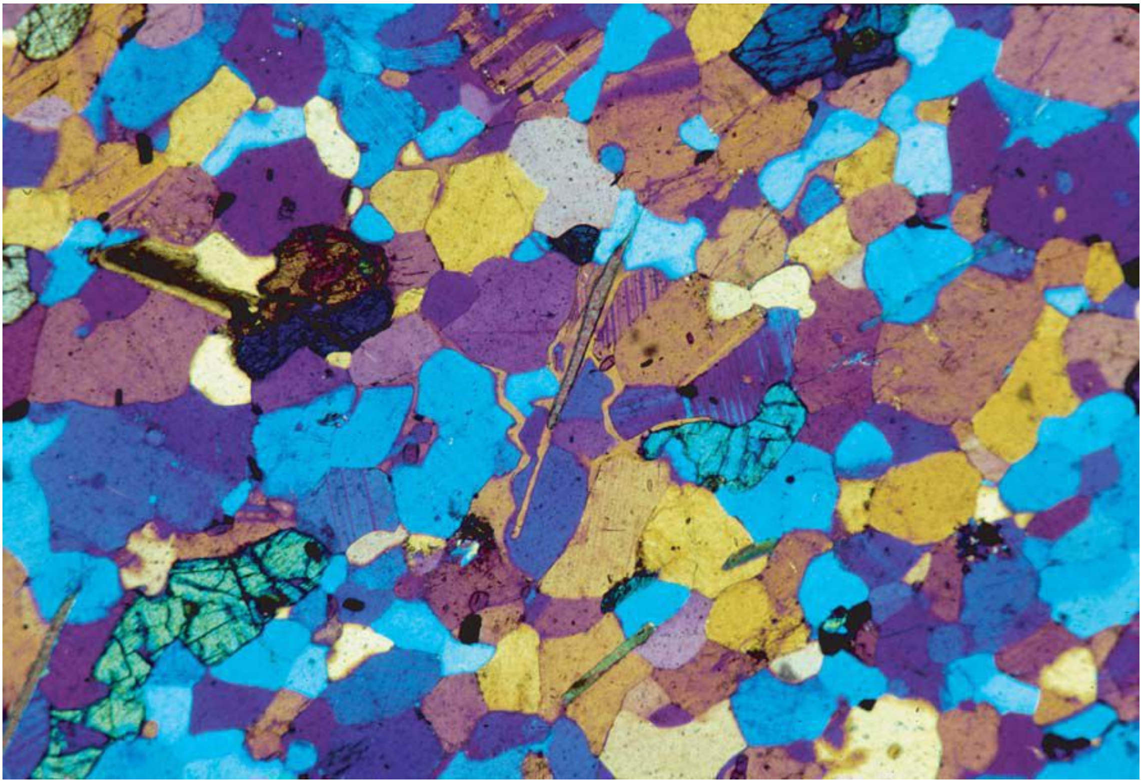

Fig. 4.82: Predominantly polygonal grains of quartz and feldspar, with scattered grains of orthopyroxene (high relief) and biotite (elongate crystals) in a granulite-facies migmatite from the Ashuanipi Subprovince, Canada. Veinlets and elongate pockets of former melt occur along some of the grain boundaries (especially centre and top-left of centre), and spectacular evidence of partial melting of biotite (preserving the elongate grain shape) is also evident (centre). Photo by Ed Sawyer. Crossed polars, with one-wave quartz plate; base of photo 3 mm.

Direct observation of melt ‘wetting’ grain boundaries has been made in some transmitted light experiments on organic analogue materials, as illustrated by Means (1989, fig. 7b). However, in all these studies, the observed angle is the true angle only if the grain boundaries are all perpendicular to the section. Otherwise, the observed angle may give a false impression of small dihedral angles in a photomicrograph. To obtain the true angles, a universal stage must be used to rotate the boundaries to the vertical position (Kretz, 1966a; Vernon, 1968, 1997), or statistical corrections can be made to flat-field measurements (Riegger & van Vlack, 1960; Holcombe, 1977; Jurewicz & Jurewicz, 1986; Rosenberg & Riller, 2000).

As explained by Smith (1953), if the dihedral angle (θ) of a melt against two solid grains is 60° or less, it spreads along all grain edges (though not covering all grain boundaries), forming a continuous flow-channel network, through which melt may move if sufficiently fluid, although the rock remains solid. Thus, melt can be efficiently removed, leaving behind an unmelted solid residue (see, for example, Sawyer, 2001). If θ is zero, the melt covers all grain boundaries (Fig. 4.22) and separates the grains, which would make the rock extremely weak, as discussed for other fluids in Section 4.4. If enough melt is present under these circumstances, the whole mass would tend to move as a magma containing melt, solid reaction products and restite (unmelted grains and aggregates). If frozen, the resulting rock is commonly called a *diatexite* (sometimes referred to as a *schlieren migmatite*), which is a migmatite characterized by obliteration of former structural features. Biotite may concentrate into layers (schlieren) during flow of diatexite magma (Milord & Sawyer, 2003), as discussed in Section 3.7.2.

Working on rocks in the Ballachulish contact metamorphic aureole, Scotland, Clemens & Holness (2000) found that θ feldspar vs. quartz/quartz in a partly melted feldspathic metaquartzite is bimodal, with peaks around 110° and 40–60°. The large angles were inferred to represent normal solid-state grain-boundary adjustment (Section 4.1.2) and the smaller angles solidified melt. Dihedral angles of this size are typical of experimentally produced felsic melts in quartz aggregates (Jurewicz & Watson, 1984, 1985; Laporte, 1994). In the Ballachulish aureole rocks, these small angles also occur in small cuspate extensions of original clastic feldspar grains, which were inferred to represent initiation of melting (Clemens & Holness, 2000). These projections become more elongate along quartz/quartz grain boundaries as the amount of melting increases, and small feldspar grains occur at quartz triple junctions (presumably representing cross-sections through the projections). The projections probably represent the feldspar component of a former felsic melt, the quartz component having crystallized on clastic quartz grains. After the feldspar crystallized, solid-state grain-boundary adjustment was inferred to have caused breakup of the feldspar projections into isolated, but crystallographically continuous, grains. More advanced melting was inferred to have produced 'microgranitic' patches and veinlets containing 40 volume percent quartz and 60 volume percent feldspar (Clemens & Holness, 2000).

If leucosomes or neosomes crystallize in their source rocks, they release the water used to form the melt (e.g. from the dehydration of muscovite, biotite or hornblende). This water can induce retrograde alteration (hydration) of the peritectic minerals in the neosome (e.g. cordierite or garnet), as well as high-grade minerals in the adjacent mesosome. This is often referred to as 'back-reaction' (see, for example, Waters, 2001). Theoretically, all the peritectic minerals should begin to hydrate as soon as crystallization of the melt begins, but many leucosomes show little or no retrograde alteration, and many granulite facies terranes show preservation of abundant high-grade minerals. The most common interpretation is that the hydrous melt escaped, leaving behind the solid reaction products (see, for example, Powell & Downes, 1990; Ellis & Obata, 1992; White & Powell, 2002; Brown, 2002). However, although this may explain many occurrences, it does not apply everywhere. For example, in the

Cooma Complex, south-east Australia, anatexis of metapelites involved biotite breakdown, forming immobile leucosomes with cordierite, K-feldspar and quartz in 'bedded migmatites' (Vernon & Johnson, 2000; Vernon *et al.*, 2001, 2003). Much of the cordierite and K-feldspar in the mesosomes has been extensively replaced by biotite–andalusite–quartz symplectite (Vernon, 1978b), probably in response to release of water from crystallizing leucosomes; yet some of the cordierite and K-feldspar in the leucosomes is less altered or even unaltered (Ellis & Obata, 1992). However, the suggestion of Ellis & Obata (1992) that loss of hydrous melt preserved the cordierite from alteration is unlikely to be correct, because of the absence of evidence for leucosome mobility in the Cooma metapelites (Vernon *et al.*, 2001, 2003a).

The problem is long-standing and difficult to solve (see, for example, Brown, 2002), although Grant (1985) and Waters (1988) have discussed alternative interpretations. Apart from physical separation of the melt from solid minerals (discussed above), (1) shielding of the anhydrous minerals by crystallization and (2) nucleation problems and/or sluggish reaction rates during falling temperature are possibilities. If crystallization of the melt initiates by heterogeneous nucleation on the solid anhydrous minerals, these minerals could be armoured by quartz or feldspar against reaction with water released from the crystallizing melt. If, as a result, the reaction rate was too slow for hydration to occur during this crystallization, the water released could either escape into the mesosome or perhaps be dissolved in the water-undersaturated melt. When crystallization is advanced enough to release water, the peritectic minerals in the leucosome are effectively protected from hydration, according to this interpretation.

4.16.2 Partial melting of crustal sulphide rocks

Lawrence (1967), Mavrogenes (2001), Frost *et al.* (2002) and Tomkins *et al.* (2004) have presented evidence that some sulphide orebodies have partly melted during regional metamorphism, for example at Broken Hill, Australia. The following are the main points of evidence for this hypothesis.

(1) Rounded sulphide inclusions in high-grade metamorphic silicate minerals are consistent with crystallization of melt droplets included in growing silicate minerals, although they are also known from unmelted metamorphic rocks, where they are due to solid-state grain-boundary adjustment (Section 4.2.7). Rounded multi-mineral inclusions are better indicators of sulphide melts, especially where dihedral angles do not occur at the intersections of sulphide grain-boundaries with the external sulphide–silicate boundary of the inclusion. Where these angles are present, the inclusions could be due to solid-state grain-boundary adjustment (as with multiple quartz inclusions in feldspar in metamorphic rocks) (Fig. 4.30) after incorporation of either melt or solid sulphide inclusions, and so are not diagnostic of sulphide melt.

(2) Very small interfacial angles between grains of sulphide minerals are consistent with crystallization from a melt, provided care is taken to correct for the section cut in polished sections (Section 4.16.1). In contrast, sulphides from equilibrium assemblages formed in the solid state have dihedral angles with other sulphide minerals of 102–134° (Stanton, 1964), as discussed in Section 4.2.4. For example, Frost *et al.* (2002) reported galena–sphalerite–sphalerite dihedral angles as low as 10° in the Broken Hill orebody.

(3) Low-melting-point metals (Ag, As, Au, Sn, Sb, Te, and Tl) with localized and irregularly distributed concentrations are consistent with mobile partial melt. Melting begins in the systems Pb–Sb–S, Fe–Sb–S, Cu–Sb–S, Sb–As–S, PbS–$AgSbS_2$ and Fe–As–S at temperatures of 525 °C or less, which are well within the medium- to high-grade metamorphic range. This has been confirmed recently by Mavrogenes *et al.* (2001), who showed that eutectic melting of galena–pyrrhotite–sphalerite, over a range of pressures, occurs at granulite facies conditions, additional components, such as Ag and Cu, further lowering the melting temperature.

(4) Many orebodies metamorphosed to amphibolite facies temperatures show concentrations of these low-melting-point metals in 'remobilized' ore, which may have been a sulphide melt. For example, in the Hemlo orebody, Ontario, Canada, Tomkins *et al.* (2004) observed that refractory metallic sulphide minerals (pyrite, molybdenite, pyrrhotite and sphalerite) occur in high-strain compressional sites, whereas minerals inferred to have crystallized from a mobile polymetallic sulphide melt (sulphosalts, native metals and tellurides) occur in dilational sites, such as extension fractures and boudin necks. Ore minerals occurring in tabular dyke-like bodies and fracture-fillings, some of them pegmatitic (Lawrence, 1967), also suggest mobility during deformation.

Chapter 5
Microstructures of deformed rocks

5.1 Introduction

Rocks are commonly subjected to tectonic deformation, with the result that they undergo a change of shape (*strain*), producing deformed rocks known as *tectonites*. Knopf (1931, p. 7) translated the original definition of tectonites (Sander, 1911, 1930) as 'metamorphic rocks deformed by differential movements that integrate into the tectonic movement as a whole'. In this definition, the word 'metamorphic' should be extended to include deformed rocks that undergo only small degrees of alteration. This involves rocks that many people would call 'diagenetic' (Section 2.2.7), there being a gradation between 'burial metamorphism' and diagenesis (see, for example, Vernon, 1976). The type and amount of strain depend on both the local directed pressure (*non-hydrostatic stress; deviatoric stress*) and the mechanical properties of the rock. The detailed, quantitative study of strain is a complex topic that is outside the scope of this book.

The aims of structural geology are to infer the deformation conditions from the structures in the rocks, observed both in the field and with the microscope, and to relate the deformation to the timing and nature of metamorphism. These can be difficult and complicated problems, and much has been written on them. Therefore, I will not try to be comprehensive, but will emphasize the more petrologically related aspects of deformation-related microstructures and the processes by which they are formed. I will not deal with the more geometrical aspects of structural geology, such as description and classification of folds and faults, stress/strain analysis, structural analysis of deformed areas, or regional tectonics, as these topics are treated effectively in structural geology textbooks (see, for example, Ramsay, 1967; Hobbs *et al.*, 1976; Ramsay & Huber, 1987; Passchier & Trouw, 1996). The nature and origin of crystallographic preferred orientations in deformed and recrystallized aggregates are also outside the scope of this book; they have been well reviewed by Turner & Weiss (1963), Law (1990), Shelley (1993) and Passchier & Trouw (1996).

Some relevant general textbooks and memoirs, especially those that concentrate more on microstructural aspects of mineral and rock deformation, are those by Knopf & Ingerson (1938), Fairbairn (1942), Turner & Weiss (1963), Spry

(1969), Hobbs *et al.* (1976), Vernon (1976), Barker (1990), Shelley (1993), Passchier & Trouw (1996) and Blenkinsop (2000). Spectacular pictures of deformed rocks at various scales are shown in Weiss (1972), Borradaile *et al.* (1982), Ramsay & Huber (1987), Passchier & Trouw (1996), Snoke *et al.* (1999), Vernon (2000b) and Blenkinsop (2000).

The chapter begins with a review of the main deformation mechanisms, and continues with discussions of recovery and recrystallization processes, the role of metamorphic reactions in deformation, deformation partitioning, foliation development, and the effects of fluids and mass transfer. Porphyroblast–matrix relationships are then discussed, especially with regard to the relative timing of deformation and metamorphic reactions. The chapter concludes with a discussion of the microstructures of partly melted rocks and the microstructural results of deformation in Earth's mantle.

5.2 Experimental evidence

Because deformation in Earth's crust and mantle cannot be observed in progress, it is necessary to rely heavily on experimental deformation of rocks and minerals at various temperatures and pressures. Some of the earliest experiments relating to microstructural development were carried out on minerals (Mügge, 1898). These experimental results on minerals guided the initial interpretation of the microstructures of metals, although subsequently experimental work on metals and ceramics guided the interpretation of deformed rocks (Sander, 1911, 1930, 1970; Schmidt, 1932; Knopf & Ingerson, 1938; Voll, 1960). In fact, many basic interpretations of the microstructures of deformed minerals and metamorphic rocks are based on microstructural interpretations of metals and ceramics, unifying basic concepts for both natural and synthetic materials.

However, systematic experiments on the microstructures and deformation properties of minerals have been possible since the development of various types of high-pressure, high-temperature deformation apparatus in the 1960s, and now a great deal of experimental information relevant to grain shapes, deformation mechanisms, recovery–recrystallization processes and preferred orientation of grains in rocks is available (see, for example, Turner *et al.*, 1954; von Steinemann, 1958; Griggs *et al.*, 1960; Carter *et al.*, 1964; Raleigh & Paterson, 1965; Hobbs, 1968; Raleigh, 1968; Carter & Ave'Lallemant, 1970; Paterson & Turner, 1970; Green *et al.*, 1970; Ave'Lallemant & Carter, 1970; Heard, 1960, 1972; Hobbs *et al.*, 1972; Weiss & Turner, 1972; Blacic, 1972; Green & Radcliffe, 1972; Tullis *et al.*, 1973; Nicolas *et al.*, 1973; Etheridge *et al.*, 1973; Etheridge & Hobbs, 1974; Etheridge, 1975; Marshall *et al.*, 1976; McClay & Atkinson, 1977; Rutter, 1974, 1983, 1995; Ave'Lallemant, 1978; Wilson & Bell, 1979; Guillopé & Poirier, 1979; Zeuch & Green, 1979; Schmid *et al.*, 1980; McQueen *et al.*, 1980; Chopra & Paterson, 1981; Toriumi, 1982; Karato *et al.*, 1982, 1986; Tullis, 1983; Carter & Hansen, 1983; Zeuch, 1983; Doukhan & Trepied, 1985; Wilson, 1986; Wilson *et al.*, 1986; Burg *et al.*, 1986; Hennig-Michaeli & Siemes, 1987; Rutter & Brodie, 1988a,b; Dell'Angelo & Tullis, 1988, 1989; Drury & Urai, 1990; Hacker & Christie, 1990; Kronenberg *et al.*, 1990; Hirth & Tullis, 1992; Green, 1992; Mares & Kronenberg, 1993; Rushmer, 1995; Rutter & Neumann, 1995; Daines & Kohlstedt, 1997).

Most deformation experiments have involved aggregates of single minerals, such as quartz, calcite, olivine, ice, halite, gypsum, feldspar, mica, pyroxene, hornblende, oxide minerals and sulphide minerals. Some of these results can be applied directly to the interpretation of microstructures of mineralogically simple rocks, such as quartzite, marble, dunite, pyroxenite, anorthosite and glacier ice, with due precautions about rate differences between experimental and natural processes. Some experiments (e.g. those of Bons & Urai, 1994) have involved the deformation of two-phase materials, such as salt–mica (Means & Williams, 1974) and ice–mica (Wilson, 1984), which also help when making interpretations of deformation in natural rocks.

However, because most common rocks are chemically complex systems involving several minerals deforming at different rates (Section 5.5), deformation of natural rocks is generally more complicated than in most experiments. Moreover, natural strain rates are much slower than those in typical experiments, which suggests that caution should be exercised when applying experimental results to rocks directly. Nevertheless, the relatively few experiments on actual rocks (see, for example, Shea & Kronenberg, 1993) have provided valuable evidence on deformation contrasts between different minerals (Section 5.5.1), as well as mechanisms of strain localization (deformation partitioning; Section 5.7).

In addition, during metamorphism, chemical reactions can affect deformation processes and *vice versa*, as discussed in Section 5.6. For example, prograde metamorphic reactions typically liberate fluid, which can have a major effect on the strength of minerals (Sections 5.6, 5.9). Moreover, chemical reactions produce new minerals, which may be stronger than the old minerals ('*reaction hardening*') or weaker than the old minerals ('*reaction softening*'), as discussed in Sections 5.6.2 and 5.6.3, respectively. Experiments on complex systems, especially with active chemical reactions and fluids, are more difficult to carry out, but some are being undertaken, especially in systems involving melting (see, for example, Arzi, 1978; van der Molen & Paterson, 1979; Rushmer, 1995; Dell'Angelo *et al.*, 1987; Wolf & Wyllie, 1991; Rutter & Neumann, 1995; Brown & Rushmer, 1997; Daines & Kohlstedt, 1997).

Deformation of low-melting-temperature minerals can be observed directly in experiments conducted in an apparatus mounted in a microscope. These have been carried out for ice, using transmitted light (Wilson, 1986; Burg *et al.*, 1986; Wilson *et al.*, 1986) and stibnite, using reflected light (McQueen *et al.*, 1980). Another approach, which has produced stimulating ideas for the interpretation of rock microstructure, is the use of low-temperature organic compounds as analogues of natural minerals. Because these compounds can be deformed, recrystallized and melted at room temperature, and because they are transparent (some helpfully coloured), changes in grain shape and distribution can be observed, photographed and videotaped in transmitted light in a microscope during the actual deformation of a thin section (Means, 1977, 1983, 1989; Means & Xia, 1981; Urai *et al.*, 1980a,b; Urai & Humphreys, 1981; Urai, 1983a,b, 1987; Tungatt & Humphreys, 1984; Jessell, 1986; Means & Jessell, 1986; Means & Ree, 1988; Bons *et al.*, 1993; Means & Park, 1994; Park & Means, 1996; Bons & Jessell, 1999; Nam *et al.*, 1999; Rosenberg & Handy, 2000). Means (1989, p. 168) has referred to the availability of videotapes of this *synkinematic microscopy* technique.

The main advantage of this 'see-through' experimental technique is that the entire microstructural history can be recorded, from the original to the deformed states, whereas in conventional experiments, only the starting material and finished product can be examined. This is because experiments on most common minerals must be conducted at high temperatures and pressures in strong experimental apparatus, in order to achieve ductile flow; direct observation has not been possible so far. The main disadvantage of the synkinematic microscopy technique is that very few real minerals are involved. Nevertheless, many of the microstructures produced resemble those in deformed natural rocks. Moreover, several unexpected grain-scale processes have been observed, which further emphasizes that caution should be exercised in the interpretation of natural rock microstructures.

Observations on naturally and experimentally deformed minerals are also being complemented by computer simulations of fabric development (see, for example, Jessell, 1988a,b; Jessell & Lister, 1990; Jessell *et al.*, 2001; Jessell & Bons, 2002; Piazolo *et al.*, 2001; Zhang *et al.*, 1994, 1996).

5.3 Deformation mechanisms

This section briefly reviews the various mechanisms by which minerals and rocks undergo deformation (change of shape, strain) at the scale of grains or small aggregates, with particular reference to the optical microstructures produced by each deformation mechanism. The topic has been reviewed extensively by, among others, Hobbs *et al.* (1976), Nicolas & Poirier (1976), Vernon (1976), Schmid (1982), Poirier (1985), Nicolas (1987), Knipe (1989), Knipe & Rutter (1990) and Blenkinsop (2000).

To relate microstructures to deformation mechanisms, (1) the microstructures produced by different deformation mechanisms must be known from natural and especially experimental observations, and (2) the microstructures must be stable enough to survive subsequent deformation and/or heating events.

Deformation mechanisms can be classified in various ways, but broadly we can distinguish between *brittle* and *ductile* deformation at the microscope scale. In brittle deformation, fractures occur across and/or between grains, and the resulting fragments move relative to each other. In ductile deformation, the grains change their shapes or move relative to each other without fracturing (loss of cohesion) at the grain scale (see, for example, Passchier & Trouw, 1996, p. 21). In both situations, but especially during brittle deformation, a change of shape of an aggregate may be accomplished or assisted by dissolution of minerals at some sites, transfer of dissolved chemical components in solution, and deposition at other sites in the deforming aggregate (*stress-induced solution transfer*), as discussed in Section 5.9.

5.3.1 Brittle deformation

Deformation by fracture and frictional processes is called *cataclastic flow* (*cataclasis*), and involves the formation of new surfaces, loss of cohesion by fracturing, and frictional sliding along the fracture surfaces. As summarized by Knipe (1989), this mode of deformation may be divided into two broad groups: (1) frictional grain-boundary sliding without thoroughgoing fracture, and (2) fracture processes.

Microstructures indicative of cataclastic flow include microfractures and displacements on cleavages (see, for example, Evans, 1988; Goodwin & Wenk, 1990), as well as rotations or displacements of rigid particles without internal crystal-plastic deformation (Figs. 5.1, 5.2). However, if microcracking is fine and pervasive, the deformation may appear to be ductile at the scale of the light microscope, although transmission electron microscopy (TEM) reveals the microfractures (Tullis & Yund, 1987; Green, 1992). For example, feldspar deforms by cataclastic flow over a wide range of conditions in Earth's crust, because it cracks easily on the two good cleavages and because dislocation motion (Section 5.3.3) is difficult in feldspar (Tullis & Yund, 1987). Although the microstructures of deformed feldspar aggregates may suggest ductile deformation on the scale of the light microscope, TEM observations commonly reveal few or no dislocations (Section 5.3.3), abundant microcracks, and microcrush zones containing grains smaller than 0.1 μm across (Tullis & Yund, 1987).

Therefore, much depends on the scale of observation. As pointed out by Paterson (1978), deformation that is cataclastic on a local (e.g. a grain or small aggregate) scale may appear to be cohesive and hence 'ductile' when viewed on the scale of a hand specimen or outcrop. In fact, grain-scale, transient fracturing may occur in many metamorphic rocks undergoing prograde metamorphism, and may well be the main mechanism for removing fluid produced in devolatilization reactions (Section 5.9). However, typically it leaves no microstructural evidence in the resulting rock.

Similarly, in mylonitic deformation (Section 5.7.6), some minerals may deform by cohesive flow and others by fracture processes in the same rock at the same time (Section 5.5.1). Although the overall process is one of ductile deformation (Vernon, 1974), because cohesive processes dominate over fracture processes, some of the deformation involves fracturing. Examples of predominant fracturing

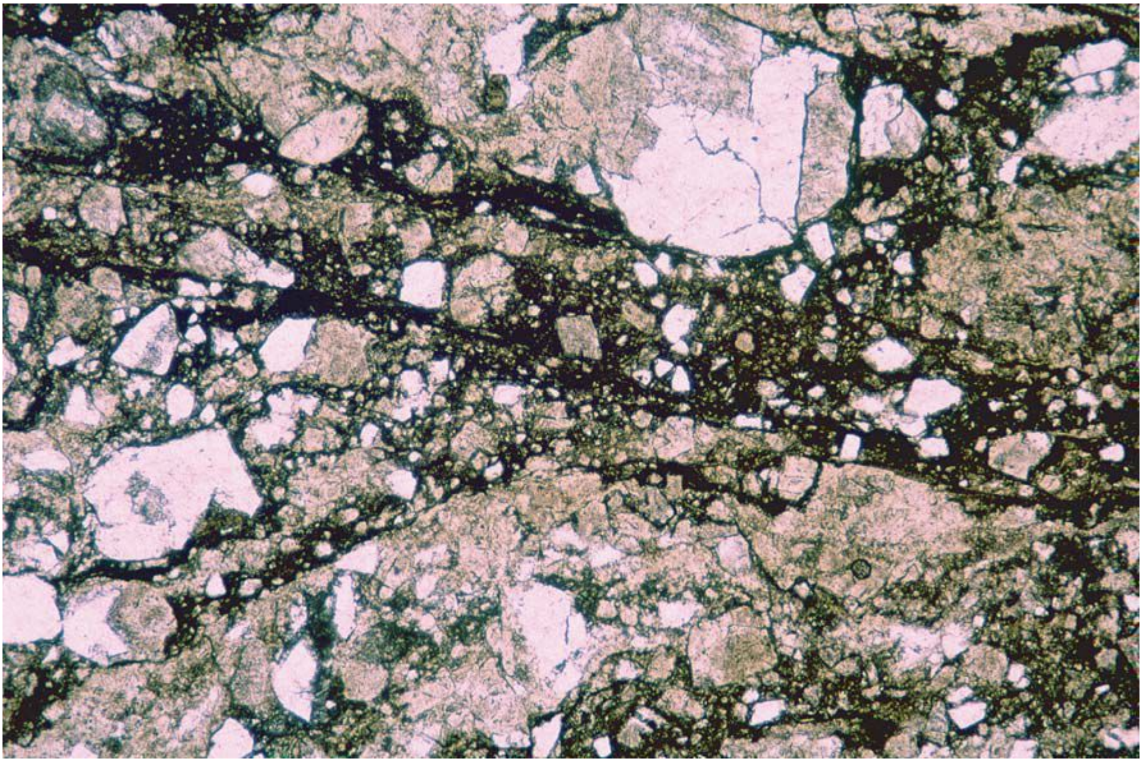

Fig. 5.1: Deformed granite (cataclasite; Section 5.7.5) from the Hunter Thrust, Mitchell's Flat, north-east of Singleton, New South Wales, Australia, showing microstructural evidence of brittle deformation, in the form of angular fragments of various sizes and dark, very fine-grained zones of intense microfracturing (fault gouge; Section 5.7.5). The quartz is clear and the feldspar is cloudy, owing to fine-grained alteration products (mainly clay minerals). Sample by courtesy of Tania Wilson. Plane-polarized light; base of photo 4 mm.

are provided by amphibolites deformed in a shear zone in the Ryoke metamorphic belt in Japan, the deformation initiating by cataclasis and proceeding by stress-induced solution–precipitation involving metamorphic reactions (Imon *et al.*, 2002). Furthermore, brittle and ductile processes may alternate, even during the deformation of the same mineral (McLaren & Pryer, 2001).

Shimamoto *et al.* (1991) used cathodoluminescence (CL) to more clearly reveal microstructural evidence of cataclastic deformation accompanied by solution–precipitation processes in the quartz and feldspar of low-temperature mylonites, and TEM observations have also revealed optically invisible microcracks and microcrush zones (Tullis & Yund, 1987), as mentioned previously.

(1) Frictional grain-boundary sliding

This involves the sliding of grains past each other, without the development of thoroughgoing fractures. This type of deformation is also called 'independent

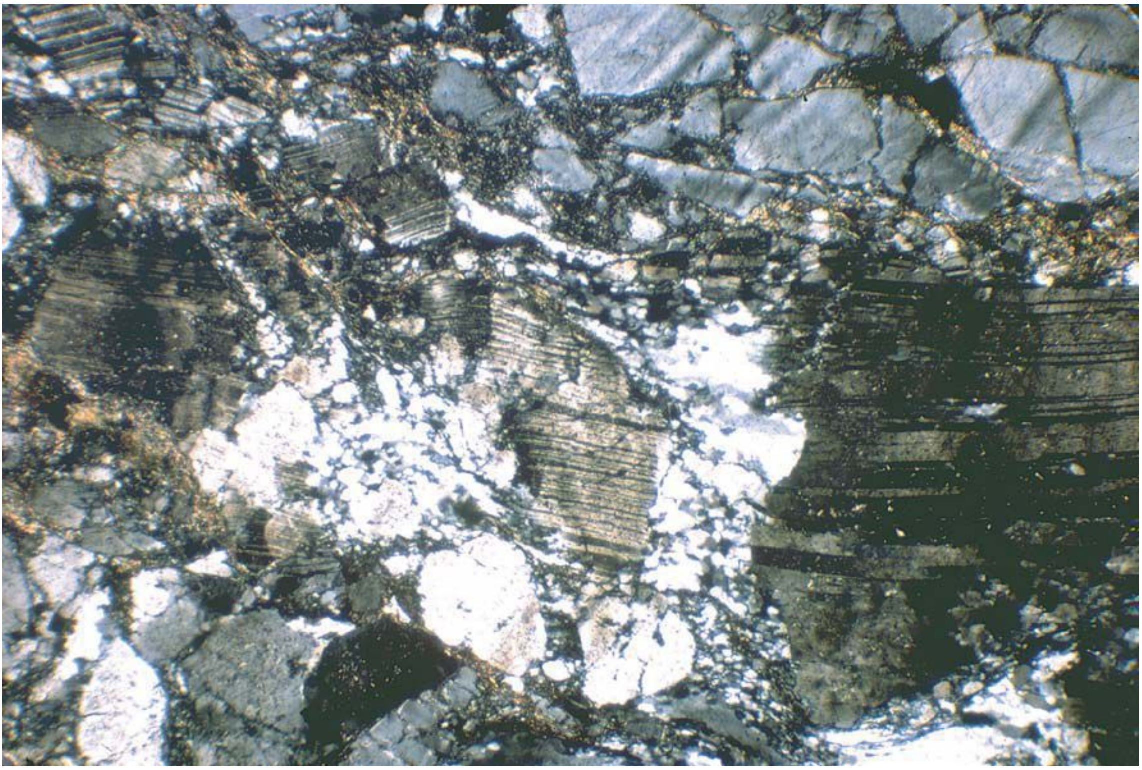

Fig. 5.2: Brittle deformation in feldspar, contrasted with ductile flow and fine-grained recrystallization in quartz, Swiss Alps. A large grain of twinned plagioclase (centre) has been broken into fragments that have been separated during the deformation (microboudinage). Crossed polars; base of photo 4.8 mm.

particulate flow' (Borradaile, 1981). The sliding depends on loss of cohesion and the overcoming of friction between grains, and so is distinguished from ductile grain-boundary sliding (Section 5.3.5), in which cohesion between grains is maintained (i.e. no fractures are formed), and movement of point defects (e.g. vacant atom sites in the mineral structure) or of dislocations (Section 5.3.3) controls the deformation.

Frictional grain-boundary sliding is favoured by low confining pressure, as well as high fluid pressure, which reduces the 'effective pressure'; i.e. the fluid pressure reduces grain-to-grain contacts. It is most common in slumping and faulting in unconsolidated sediments (Paterson & Tobisch, 1983; Maltman, 1981) and in fault gouges and cataclasites (Section 5.7.5). Compaction can produce shape (dimensional) alignment of clasts, such as quartz slivers and clay or mica flakes, by this mechanism, leading to bedding-parallel preferred orientations (Morritt *et al*., 1982; Paterson & Tobisch, 1983; Baker *et al*., 1993). The alignment is achieved by bodily rotation of elongate clasts, which may be assisted by flow of fluids in highly porous material. Metamorphic reactions (Chapter 4), resulting in the growth of new minerals, may obliterate the clastic grain shapes, although bedding-parallel foliations may be preserved by the aligned growth of new minerals in the bedding planes (*mimetic crystallization*) and so may be recognizable, at least in some low-grade slates and phyllites (Moore & Geigle, 1974; Morritt *et al.*, 1982).

(2) Fracture processes

Deformation controlled by fracture processes involves the formation of thoroughgoing fractures and movement along the fractures. Details of fracture processes in deformation and the various mechanisms of fracturing have been discussed by Knipe (1989, pp. 135–7) and Blenkinsop (2000).

5.3.2 Ductile deformation

As summarized by Paterson (2001), ductile flow of rocks can occur by the following three main mechanisms: (1) change of grain shape by *crystal plasticity*, which is referred to as *dislocation creep* (Section 5.3.3); (2) change of grain shape by diffusion through or around grains, called *diffusion creep* (Section 5.3.4); and (3) relative movement of grains, referred to as *granular flow* or *grain-boundary sliding* (Section 5.3.5).

In (3), in order to minimize the formation of fractures and voids (dilation or dilatancy), the grains must locally change their shapes by mechanisms (1) or (2), which distinguishes this deformation mechanism from frictional grain-boundary sliding (Section 5.3.1). Except for these local accommodations, very large strains may be achieved without change of overall grain shape, as in 'superplastic flow' of very fine-grained aggregates (Section 5.3.5).

In experiments on the ductile flow of minerals, an initial elastic (recoverable) deformation is followed (at the 'yield point') by permanent (plastic) deformation (Fig. 5.3). For plastic flow, the strain rate depends on several factors, including the differential stress (the difference between the maximum and minimum compressive stress acting on the mineral or rock sample), the amount of accumulated strain, the temperature, the fluid pressure, the grainsize, the activity of chemical components, and the distribution of small grains of other minerals.

5.3.3 Crystal plasticity (dislocation creep)

Crystal plasticity (*crystal plastic flow*) is permanent deformation by non-cataclastic flow (*ductile flow*), without loss of cohesion on the grain scale. The flow involves slip (*translation gliding*) and/or *deformation twinning* (Fig. 5.4). These processes enable a grain to change its shape by allowing one part of the crystal to undergo shear with respect to a neighbouring part (Hobbs *et al.*, 1976).

Microstructural evidence of crystal plastic deformation includes *kink bands* (Figs. 5.5–5.9), *deformation lamellae* (Fig. 5.10) and *deformation twins*

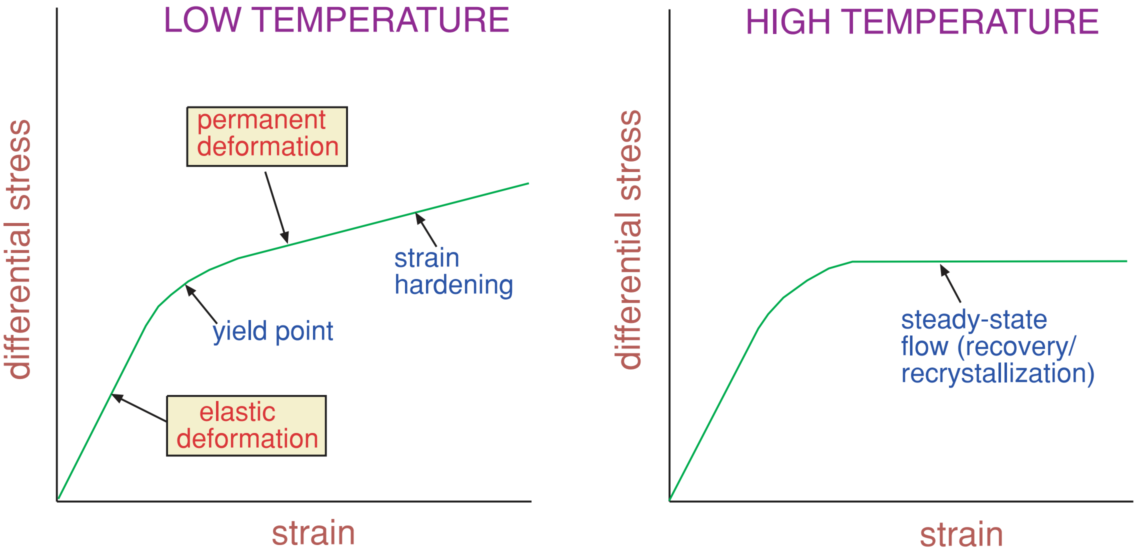

Fig. 5.3: General forms of typical stress–strain curves for experiments at constant strain rate and temperature. The differential stress (stress difference) is the difference between the maximum and minimum compressive stresses exerted on the mineral sample. An initial elastic (recoverable) deformation is followed (at the yield point) by permanent (plastic) deformation. At lower temperatures, the mineral becomes progressively harder to deform (strain hardening), owing to tangling of dislocations. In contrast, at higher temperatures, deformation can proceed at relatively low and approximately constant stress difference, owing to recovery and/or recrystallization accompanying the deformation.

(Figs. 3.89–3.91), described below. These microstructures have been duplicated experimentally (see references in Section 5.2). Individual grains may become very elongated, or may become converted to stretched-out aggregates of much smaller new grains formed by *recrystallization* (Section 5.4.2) during the deformation.

The mechanisms of crystal plastic flow are summarized in many textbooks and review articles on physical metallurgy, ceramics and mineral deformation (see, for example, Chalmers, 1959; Brophy *et al.*, 1964; Hobbs *et al.*, 1976; Nicolas & Poirier, 1976; Vernon, 1976; Barber, 1985; Poirier, 1985; Langdon, 1985; Gottstein & Mecking, 1985; Knipe, 1989; Barber & Meredith, 1990; Green, 1992).

Slip (translation gliding)

Slip is the main primary mechanism of deformation. It causes layers of a grain to slide past each other without fracturing and without changing the orientation of the slipped portion of the grain. Therefore, it cannot be detected in thin section, in contrast to deformation twinning (see below), in which a change of orientation is produced, as shown in Fig. 5.4. The shape of the grain is changed in the slip

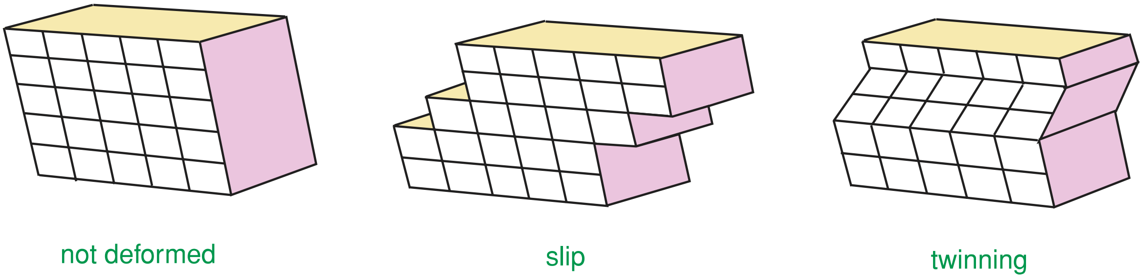

Fig. 5.4: Diagrams showing the general processes of slip and deformation twinning. Note that twinning produces a change in orientation, which shows up as a change in colour and/or birefringence in the microscope, but slip does not.

Fig. 5.5: Diagram showing the geometry of a kink band.

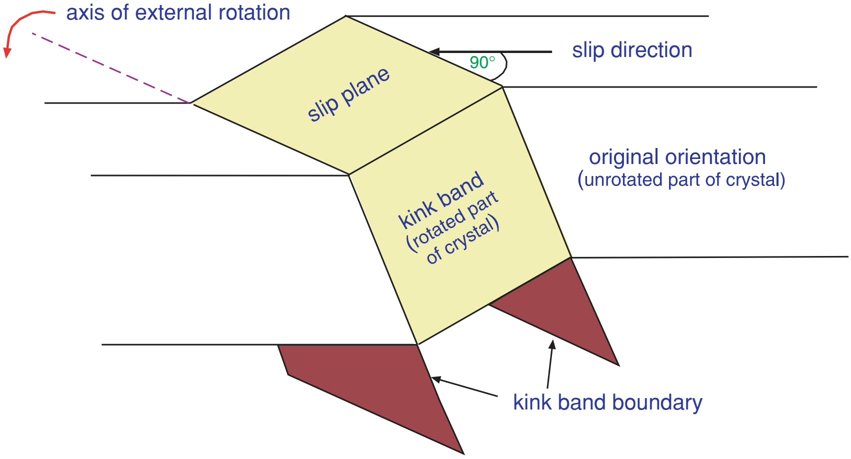

process. Slip occurs on specific planes (commonly planes of dense atomic packing) and in specific directions in the crystal. A *slip system* is the combination of a *slip plane* and a *slip direction* in this plane. Slip systems have been determined for many minerals at various temperatures (see, for example, Nicolas & Poirier, 1976; Hobbs *et al*., 1976, table 2.1; Bard, 1986; Barber & Meredith, 1990; Cox, 1987a). Because of the crystallographic control of slip planes, ductile deformation of grain aggregates typically results in a strong crystallographic preferred orientation.

The ease with which a slip system operates depends on the strain rate and temperature. For example, in some experiments conducted below about 700 °C, dry quartz deforms by slip on (0001) in the direction of one or more of the *a*-axes ('*a*-slip'), whereas above 700 °C, quartz deforms by slip on $\{10\bar{1}0\}$ planes in the direction of the *c*-axis ('*c*-slip'), as discussed by Christie *et al*. (1964), McLaren *et al*. (1967), Baëta & Ashbee (1969), Ave'Lallemant & Carter (1971),

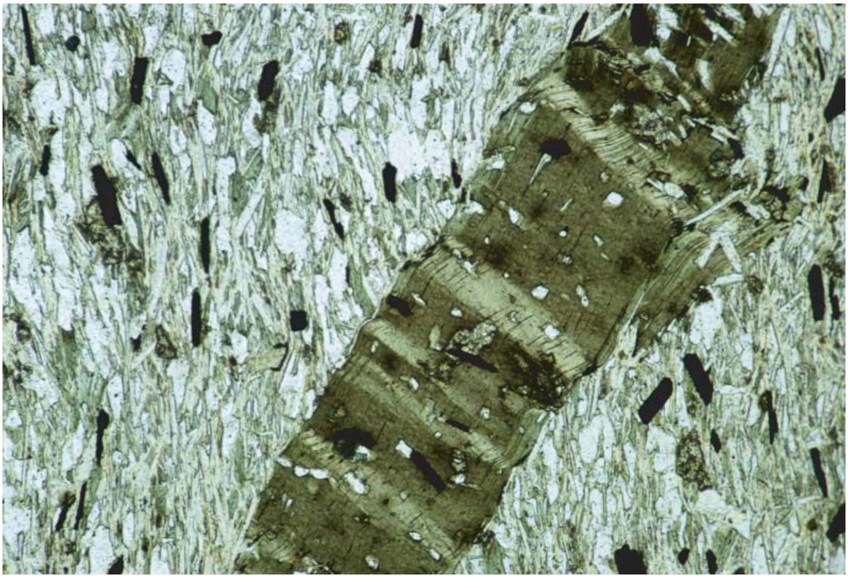

Fig. 5.6: Kinked crystal of biotite in a schist. The kink bands are revealed by differences in absorption colour, owing to their orientation differences. The widths and degrees of misorientation of the kink bands are variable, which distinguishes them from deformation twins, between which the misorientation is constant. Plane-polarized light; base of photo 1.5 mm.

Tullis *et al*. (1973), Blacic (1975), Lister & Dornsiepen (1982), Blumenfeld *et al*. (1986), Gapais & Barbarin (1986) and Mainprice *et al*. (1986). However, *c*-slip occurs at lower temperatures (400–600 °C) and at lower strain rates in water-bearing quartz (Griggs & Blacic, 1965; Blacic, 1975; Mainprice *et al*., 1986).

Some minerals with relatively high crystallographic symmetry, such as quartz, olivine and calcite, have several slip systems, and so can deform relatively easily over a range of conditions. In contrast, many other minerals (such as mica, plagioclase, hornblende, pyroxene and kyanite) are of lower symmetry and may have only one dominant slip system. For example, glacial ice (Wilson & Zhang, 1994) slips predominantly on (0001), and kyanite, hornblende and pyroxene slip only on (100) in the direction [001], as reported by Nicolas & Poirier (1976). Mica slips only on the basal plane (001), but in several directions (the *a*-axes) in that plane (Etheridge *et al*., 1973).

The more slip systems a mineral has, the more readily a grain of that mineral can change its shape in response to local differential stress. Minerals with at least five active independent slip systems can deform homogeneously by slip (von Mises, 1928; Kelly & Groves, 1970). Quartz and calcite are common examples, as are some cubic minerals, such as halite, galena, fluorite, sphalerite and magnetite (Siemes *et al*., 1994). However, the slip systems must be activated

Fig. 5.7: Very strongly kinked crystal of biotite (brown), the kink bands being parallel to subgrains and kink bands in adjacent quartz, in a heterogeneously deformed granite, Hillgrove Adamellite, New England area, New South Wales, Australia. Despite the strong deformation, residual igneous microstructures (characterized by elongate plagioclase laths in quartz) are also present. Crossed polars; base of photo 1.75 mm. From Vernon (2000a, fig. 8), with permission of Springer-Verlag.

at the temperature of the deformation event. For example, the high-symmetry mineral garnet is mostly rigid and brittle at many conditions in Earth's crust, but can undergo ductile flow at high temperatures and slow strain rates (Wang & Ji, 1999).

In grains of minerals with few slip systems, slip is commonly assisted by deformation twinning and kinking (see below). In effect, a set of kink bands or of deformation twins acts as an additional independent slip system, if repeated on a fine enough scale.

Grains that are unfavourably oriented for slip may deform by fracturing and displacement along cleavages. Moreover, because of the common contrast between the deformability of different minerals (Section 5.5.1), local transient voids at grain boundaries may be relatively common, especially during deformation at lower temperatures. These spaces could assist movement of fluid through otherwise coherent rocks (Section 5.9).

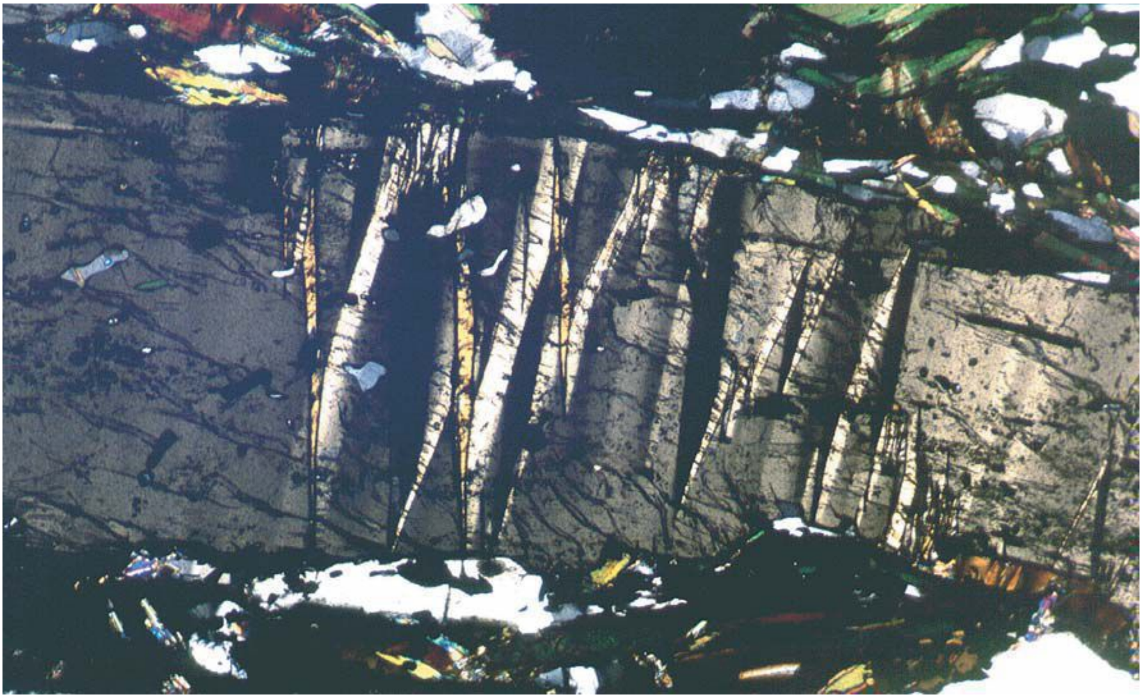

Fig. 5.8: Kinked crystal of kyanite, Chiwaukum Schist, Cascades, Washington, USA. The kink bands are lenticular and wedge-shaped. Crossed polars; base of photo 4 mm.

Slip takes place by movement of *dislocations*, as explained by Hobbs *et al.* (1976) and Vernon (1976, 2000b). The concept of dislocations and their relationship to crystal growth are discussed in Section 3.5.2. The movement of dislocations through crystals enables solid crystalline materials to change their shapes without breaking (Figs. 3.27–3.29, 5.11). Displacement can be achieved if all the atoms in a lattice row break at the same time, but this is fracture, and the stress required for flow has been found experimentally to be many orders of magnitude less than that required for fracture. Dislocations are *line defects*, in which one row of atoms is decoupled from the rest of the lattice (Figs. 3.28, 5.11A). Although in this sense a dislocation involves very local breaking of atomic bonds (hence the name), it isn't a fracture.

A good analogy is a large carpet on a floor. If you want to move the carpet, you can try pulling it from one end. However, this requires a lot of effort, owing to the weight of the carpet and the frictional forces that tend to stick it to the floor. A much easier way is to form a hump or bulge parallel to the edge of the carpet and simply move the hump along (Fig. 5.11B), which only requires overcoming the friction underneath the hump, not the whole carpet. As the hump is moved along, the carpet settles back onto the floor behind you and pulls away from the

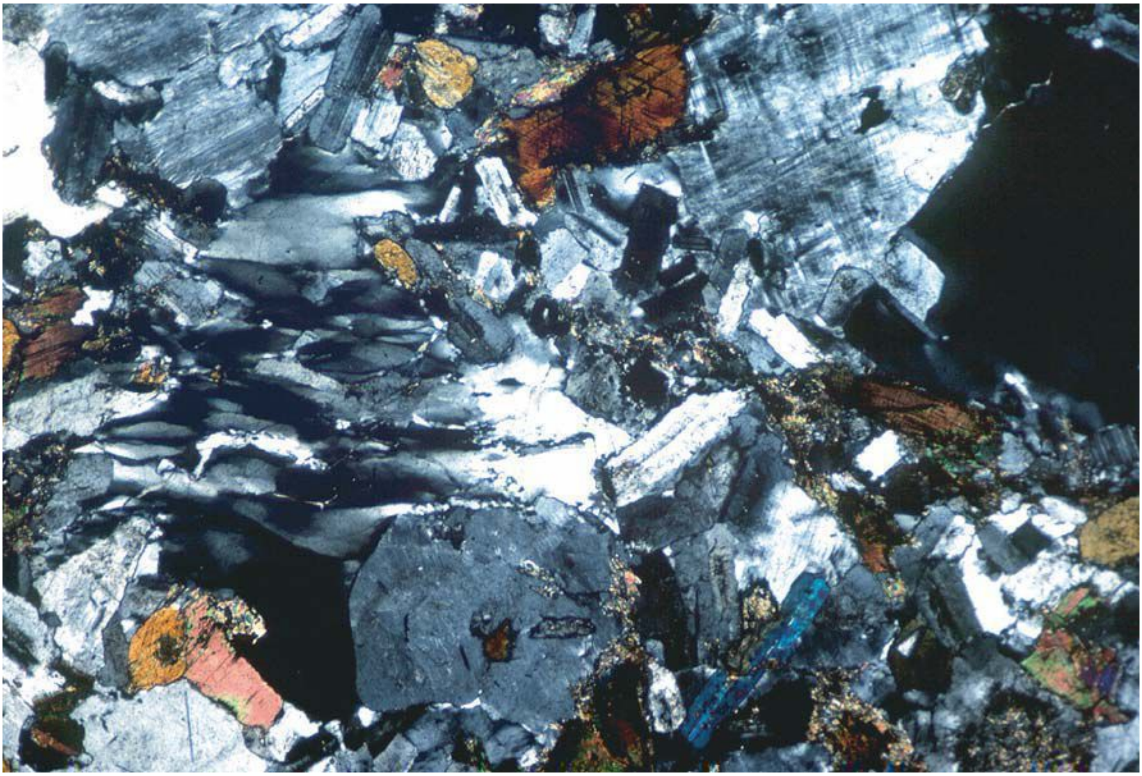

Fig. 5.9: Strongly deformed grain of quartz in a deformed granite from Hillgrove, New England area, New South Wales, Australia. The quartz shows both subgrains (with small misorientations) and sharp kink bands and/or deformation bands (with marked misorientations). Incipient recrystallization (Section 5.4.2) has occurred along some of the kink-band boundaries, this process representing the earliest stage of the formation of 'ribbon structure' (Section 5.5.1). Also shown are biotite (brown), a few small grains of hornblende, plagioclase (relatively small, elongate crystals), and microcline with tartan twinning formed during the deformation (Sections 4.8, 5.7.6, 5.7.9). This photo also illustrates a marked deformation contrast between quartz and feldspar at the prevailing conditions; the feldspar is so strong that igneous microstructures have been preserved in feldspar-rich parts of the rock. Crossed polars; base of photo 4.4 mm.

floor under the new position of the hump. Eventually the hump comes to the end of the carpet, which has then moved a small distance, equivalent to the size of the hump. If many of these humps are moved parallel to each other, carpet can be moved to where you want it.

A flowing mineral does something broadly similar to the hump in the carpet. The force acting on the mineral grain causes one row of atoms at a time to break. Then the next row breaks and the one behind it joins together again. So, successive rows break, one at a time, until the 'break' (dislocation) moves right through

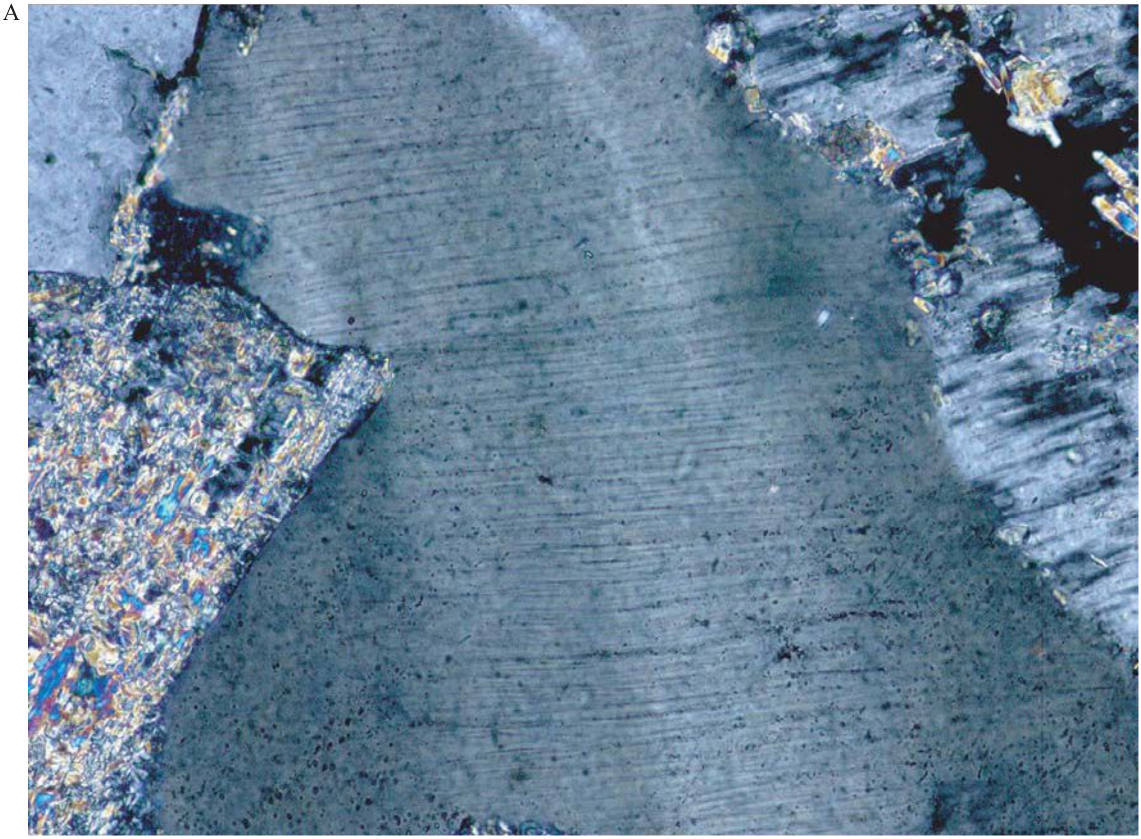

Fig. 5.10: (A) Deformation lamellae in quartz, Big Jim Pond, Maine, USA. Specimen by courtesy of Chris Gerbi. Crossed polars; base of photo 0.6 mm. (B) Planar deformation features (PDFs) in several directions in shocked quartz from an impact site, Gosse's Bluff, central Australia. Specimen by courtesy of Tom Bradley. Crossed polars; base of photo 0.5 mm.

the mineral, causing a displacement of one row of atoms (Fig. 5.11). If many thousands of these minute displacements occur, they can cause the mineral grain to change its shape. Each dislocation needs only a very small amount of energy, and the process does not require the mineral to change the overall arrangement of its atoms, so that it retains its identity during the deformation. The movement of dislocations is completely different from deformation by fracture, which involves the breaking of many rows of atoms at the same time.

Some dislocations are formed by growth mistakes as minerals crystallize. However, many more are generated by stress concentrations during deformation, especially near crystal defects, cracks and mineral inclusions. Images of dislocations (Fig. 5.12) are observable only in the transmission electron microscope (McLaren *et al.*, 1967; McLaren, 1991; McLaren & Retchford, 1969; Phakey

Fig. 5.10: (*cont.*)

et al., 1972; Green & Radcliffe, 1972; McLaren & Hobbs, 1972; Champness & Lorimer, 1976; Champness, 1977; McLaren & Etheridge, 1976; Murr & Lerner, 1977; Zeuch & Green, 1984; Allen *et al*., 1987; Cox, 1987a; Ando *et al*., 1993; Christoffersen & Kronenberg, 1993; Doukhan *et al*., 1994; Vogelé *et al*., 1998), as their strain effects are too small to affect light. However, their traces can be observed in the light microscope if the points of emergence of the dislocations are revealed by chemical etching (Carstens, 1969, 1971; Wegner & Christie, 1983; Ball & White, 1977; Frater, 1985) or 'decoration' by precipitation of other compounds on them (Kohlstedt *et al*., 1976; Karato, 1987; Jin *et al*., 1989; Yoshinobu & Hirth, 2002). This can indicate the positions of slip planes and subgrain boundaries (Section 5.4.1).

Kinking

This occurs when slip on a single slip plane is inadequate to maintain homogeneous deformation. The grain sharply bends (kinks) and the deformation localizes into *kink bands*, which enable shortening of the grain to continue (Figs. 5.6–5.8). The whole grain may divide into kink bands (Fig. 5.7) or the kink bands may be

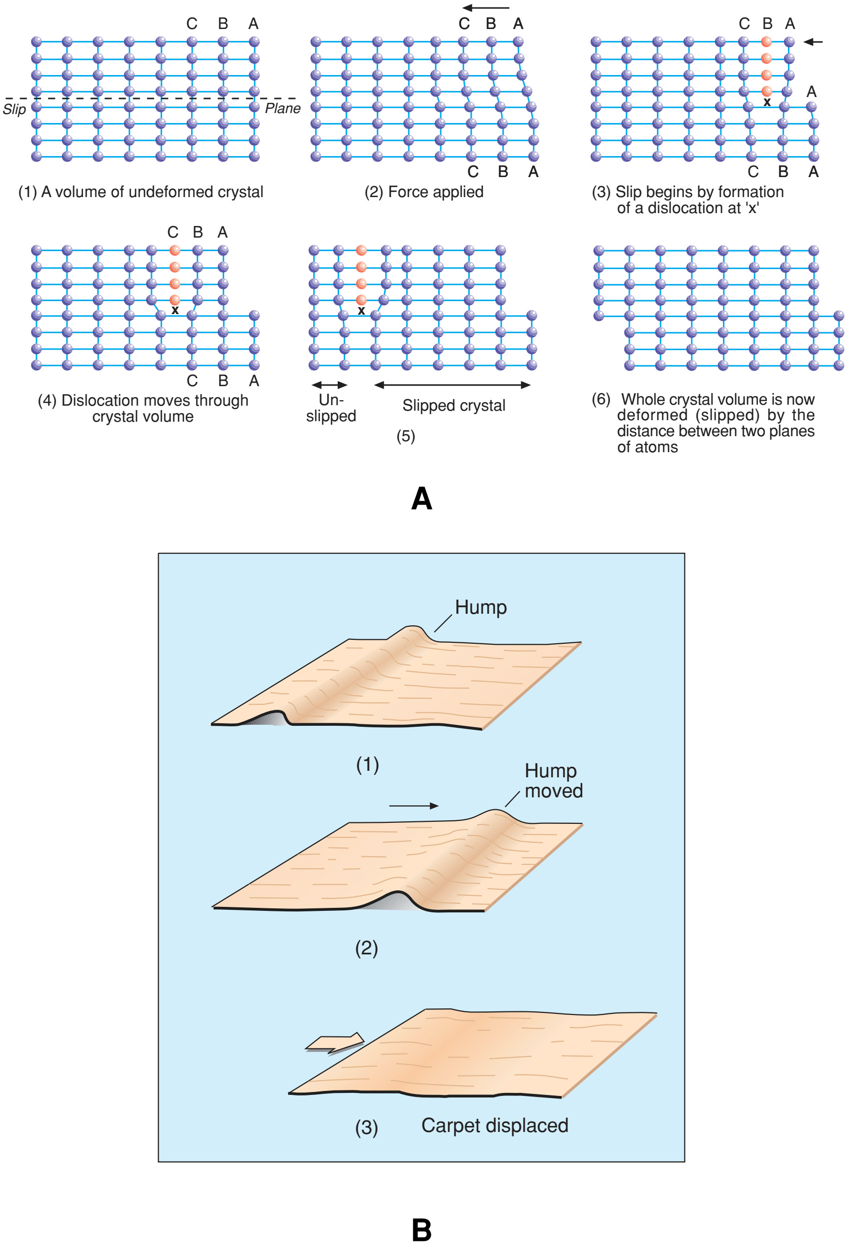

(1) A volume of undeformed crystal

(2) Force applied

(3) Slip begins by formation of a dislocation at 'x'

(4) Dislocation moves through crystal volume

(5)

(6) Whole crystal volume is now deformed (slipped) by the distance between two planes of atoms

(1)

(2)

(3) Carpet displaced

Fig. 5.11: (A) Sketch illustrating how a dislocation moves through part of a mineral, which is represented by a simplified grid of atoms, with bonds between them represented by lines. In real minerals, the atoms would touch each other, but they are separated in the sketch to show each atom clearly. In stage (1) the crystal is undeformed, but has a potential plane of atoms (a slip plane) along which deformation can occur if a force is applied. The force begins to be applied in stage (2). By stage (3), the atoms in plane A–A above the slip plane have linked up

separate and commonly lenticular or wedge-shaped (Fig. 5.8). A kink band may be defined as part of a grain that undergoes rotation with respect to the unkinked part of the grain, the axis of rotation coinciding with the line of intersection of the kink band and the slip plane, perpendicular to the slip direction (Spry, 1969; Nicolas & Poirier, 1976), as shown in Fig. 5.5. Broadly similar microstructures reflecting heterogeneous deformation from one layer to another in a deforming grain, but which cannot be described as kink bands according to this definition, are best referred to as ‘deformation bands’ (Spry, 1969; Hobbs *et al.*, 1976). However, their kink-like nature in quartz is indicated by abrupt deflection of deformation lamellae across their boundaries.

The misorientation across kink-band boundaries is typically greater than the misorientation across subgrain boundaries, across which the misorientation is generally no more than about 10° (Section 5.4.1), and is more variable than the misorientation across deformation twin boundaries, which is fixed by the twin law, as discussed below.

Elongate subgrains (extinction bands) formed by recovery (Section 5.4.1) in quartz and olivine are often referred to as ‘kink bands’, but should not be confused with kink bands formed by slip alone (Poirier & Nicolas, 1975). Elongate subgrains and kink bands may be present in the same grain of deformed olivine (Nicolas & Poirier, 1976), and an example of this in quartz is shown in Fig. 5.9.

Kinking is common in minerals with strongly anisotropic crystal structures and consequently only one slip plane, such as biotite (Figs. 5.6, 5.7), kyanite (Fig. 5.8), enstatite and molybdenite, but also occurs in minerals with several slip systems, such as quartz (Christie *et al.*, 1964), olivine (Nicolas & Poirier,

Fig. 5.11: (*cont.*) with the row of atoms B–B below the slip plane, forcing half of the B–B plane of atoms to break away along the line X (coming straight at you from the page), which is called a *dislocation*. This extra half-plane of atoms then links to the C–C row of atoms below the slip plane, forcing half of the C–C plane of atoms to break away along the line X (stage 4). In this way, the dislocation X (with its extra half-plane of atoms) can move right through the volume of crystal, producing a very small permanent deformation (stage 6). The dislocation marks the boundary between deformed (‘slipped’) and undeformed crystal, as shown for stage (5). Note that this process is not the same as going directly from stage (1) to stage (6), which would involve forming a fracture, which would require breaking *all* the bonds along the slip plane at the same time. Modified from Hobbs *et al.*, (1976, fig. 2.2) and Vernon (1976, fig. 33). (B) Sketch illustrating how a carpet can be moved along a floor by forming and moving a hump. This is much easier than trying to move the whole carpet at once by tugging at one end because only the frictional forces under the hump need to be overcome at any one time. Comparing this with (A), the floor is analogous to the slip plane in a crystal and the hump is analogous to the dislocation. From Vernon (2000b, fig. 32).

Fig. 5.12: Image of individual and tangled dislocations (curved dark lines) in quartz deformed experimentally, photographed in the transmission electron microscope (TEM) by John Fitz Gerald. Base of photo 3.5 μm.

1976), galena (Grigor'yev, 1961; Lyall, 1966; Lyall & Paterson, 1966; Ramdohr, 1969; Stanton & Gorman Wiley, 1970; Siemes, 1970, 1977a; Clark *et al.*, 1977; McClay, 1977, 1980, 1983; McClay & Atkinson, 1977; Siemes & Spangenberg, 1980; Richards, 1966; Cox, 1986, 1987a) and pyrite (Cox *et al.*, 1981). Kink bands have also been observed in pyrrhotite (Clark & Kelly, 1973; Atkinson, 1974; Craig & Vaughan, 1994) and stibnite (Craig & Vaughan, 1994).

Deformation lamellae

These are narrow (0.5–10 μm), planar, crystallographically oriented zones with a refractive index slightly different from that of the adjacent grain (Sander, 1930;

Turner, 1948; Carter *et al.*, 1964; Christie *et al.*, 1964; Carter, 1971; Green, 1972; White, 1973; Hobbs *et al.*, 1976; Drury, 1993; Blenkinsop & Drury, 1988), as shown in Fig. 5.10A. Deformation lamellae parallel to slip planes have been produced experimentally, but some natural deformation lamellae have complicated and variable structures, and may not reflect slip alone. Typically they are defined by dislocation walls or bands of variable dislocation and fluid inclusion concentration (Drury, 1993) and appear to involve recovery processes (Section 5.4.1), as discussed by Blenkinsop & Drury (1988). Deformation lamellae are typically aligned perpendicular to extinction bands (elongate subgrains). They are most common in quartz, but have also been observed in olivine (Boland *et al.*, 1971), plagioclase (Borg & Heard, 1970), calcite (Turner, 1948) and glacial ice (Wilson, 1986). They tend to be most common during lower-temperature deformation. Common deformation lamellae subparallel to the plane of the *a*-axes in quartz may indicate high-stress deformation (Drury, 1993).

Deformation lamellae typically occur in one plane in quartz, and may be slightly curved. Superficially similar features in several planes are characteristic of quartz subjected to shock deformation in meteorite impacts (Fig. 5.10B). These are known as *planar deformation features* (PDFs). They are very narrow (1 μm wide or less) and are 1–10 μm apart, as shown in the TEM. They vary from twins, through dislocation and bubble concentrations, to glass bands (Blenkinsop, 2000).

Deformation twinning (twin gliding)

Some minerals, such as calcite and plagioclase, undergo *deformation twinning* (mechanical twinning, secondary twinning, 'twin gliding') in response to deformation (Figs. 3.89–3.91, 5.4, 5.13). The distribution of twins within grains is typically heterogeneous (Figs. 3.89, 3.90). Deformation twinning operates by a limited amount of simple shear (on the microscopic scale, though it may be more complicated on the atomic scale) parallel to a unique glide plane (the *twin plane*) and in a particular direction (the *glide direction*), both of which depend on the crystal structure of the mineral, and which together constitute a *twinning system*. Thus, deformation twinning occurs in some minerals, but not others. The geometrical requirements of a twin are known as the 'twin law'. In contrast to slip, the amount of deformation that can be achieved by twinning is limited by these requirements, especially because twins have only one sense of shear. Each atomic layer is sheared (not translated) by an amount sufficient to produce a mirror image of the original crystal (Fig. 5.4). This restores the original structure, each half of the twin being misoriented symmetrically with respect to the other.

Twinning tends to be favoured over slip at lower temperatures and faster strain rates. Deformation (secondary) twins are distinguished from growth (primary) twins on the basis of their typically lenticular shapes, as discussed and illustrated in Section 3.12. Deformation twins are always multiple, never simple. They

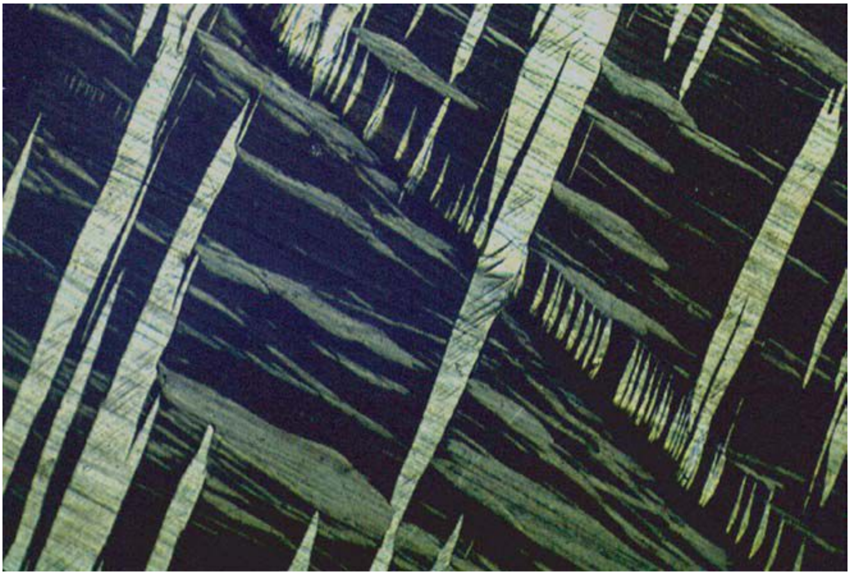

Fig. 5.13: Lenticular deformation twins in stibnite. Polished section in reflected light. Photo by Alec Whittle, kindly provided by Ross Both.

have been produced experimentally in metals, calcite, plagioclase and sulphide minerals.

Deformation twinning is common in plagioclase (Figs. 3.87, 3.98, 3.91). It occurs on two 'laws', namely *albite-law twinning*, for which the twin plane is (010) and the glide direction is the *c*-axis, and *pericline-law twinning*, for which the twin plane is an irrational plane and the glide direction is the *b*-axis. Both these twin laws are favoured by the same local stress system, and so both tend to operate simultaneously (Vernon, 1965).

Another example is calcite, for which the most common twin plane is $\{01\bar{1}2\}$ (Paterson & Turner, 1970). Ferrill (1991) found that, below 100–200 °C, deformation of calcite is accommodated by adding new narrow twins, whereas above this temperature, deformation is accommodated by widening existing twins. Burkhard (1993) reviewed deformation twinning in calcite, inferring that microtwins and straight, narrow twins (<1 μm thick) are characteristic of very low-temperature deformation, whereas above about 100 °C wider (>1–5 μm), fewer twins occur. Above *c*. 200 °C, curved twins, twins that are themselves twinned, and completely twinned grains occur, and above *c*. 250 °C, older twins commonly show evidence of boundary migration (Sections 4.11.1, 5.4.2).

Deformation twinning also occurs in dolomite and barite, as well as sulphide minerals, such as stibnite (Fig. 5.13), chalcopyrite, pyrrhotite and sphalerite (Clark & Kelly, 1973; Atkinson, 1974; Roscoe, 1975; Murr & Lerner, 1977; Siemes & Borges, 1979; McClay, 1982c; Cox, 1987a; Couderc & Hennig-Michaeli, 1989; Hennig-Michaeli & Couderc, 1989), galena (Lyall, 1966; Lyall & Paterson, 1966; Stanton & Gorman Wiley, 1970; Deer *et al*., 1992), native bismuth (Craig & Vaughan, 1994), and oxide minerals, such as rutile and hematite (Hennig-Michaeli, 1977).

Hardening and softening during deformation

Broadly speaking, crystal plasticity may be divided into low- and high-temperature types. *Low-temperature plasticity* occurs at less than roughly half the melting temperature at laboratory strain rates, and is dominated by glide of dislocations in slip planes. This leads to interference, tangling and hence immobilization of dislocations (Fig. 5.12), causing the mineral to increasingly resist strain (Fig. 5.3). The process is called 'strain hardening (strengthening)'. *High-temperature plasticity* is dominated by thermally activated *recovery* and *recrystallization* processes (Section 5.4), which cause 'softening (weakening)'. The process involves untangling of dislocations (Section 5.4.1) and consequently the mineral is able to continue to deform ('creep') at relatively small differential stresses (Fig. 5.3). The amount of strain accumulation depends on the competition between strain hardening and recovery/dynamic recrystallization.

Plastic deformation at high temperature (*dislocation creep*) is probably the main deformation process in the deeper parts of Earth's crust (see, for example, Yund & Tullis, 1991). The resulting grains may show undulose (undulatory) extinction and subgrains, sutured grain boundaries, 'core-and-mantle microstructure' (Section 5.4.7), and a pronounced shape and/or crystallographic preferred orientation. Some of these features are discussed in Section 5.4.2. At very high temperatures, ductile grain-boundary sliding may occur (Section 5.3.5). However, it should be kept in mind that water-assisted cataclastic deformation may be responsible for some subgrains and recrystallized grains in quartz that are optically identical to those commonly inferred to be due to dislocation creep (den Brok *et al.*, 1998, p. 84) as discussed in Section 5.4.8.

5.3.4 Diffusion creep

Diffusion creep (*diffusive mass transfer*) involves change of grain shape by diffusion of chemical components, either in aqueous solution ('*stress-induced solution transfer*' or '*dissolution–precipitation creep*') or by solid-state diffusion along grain boundaries ('Coble creep') or through crystals ('Nabarro–Herring creep', which requires high temperatures and so is most appropriate for very hot rocks, such as peridotites in Earth's mantle). Stress-induced solution transfer (also called 'pressure solution') is equivalent to Coble creep in dry rocks (Wheeler, 1992). Typically, material is removed from sites of high normal compressive stress and deposited at low-stress sites, with the result that a volume of rock changes its shape (see, for example, Rutter, 1976).

The term 'pressure solution' (Sorby, 1908) strictly refers to the actual dissolving of minerals, and so the term 'solution-transfer' (Durney, 1972) has been proposed for the overall process of solution, transfer and redeposition of chemical components. A preferable term is 'stress-induced solution transfer'

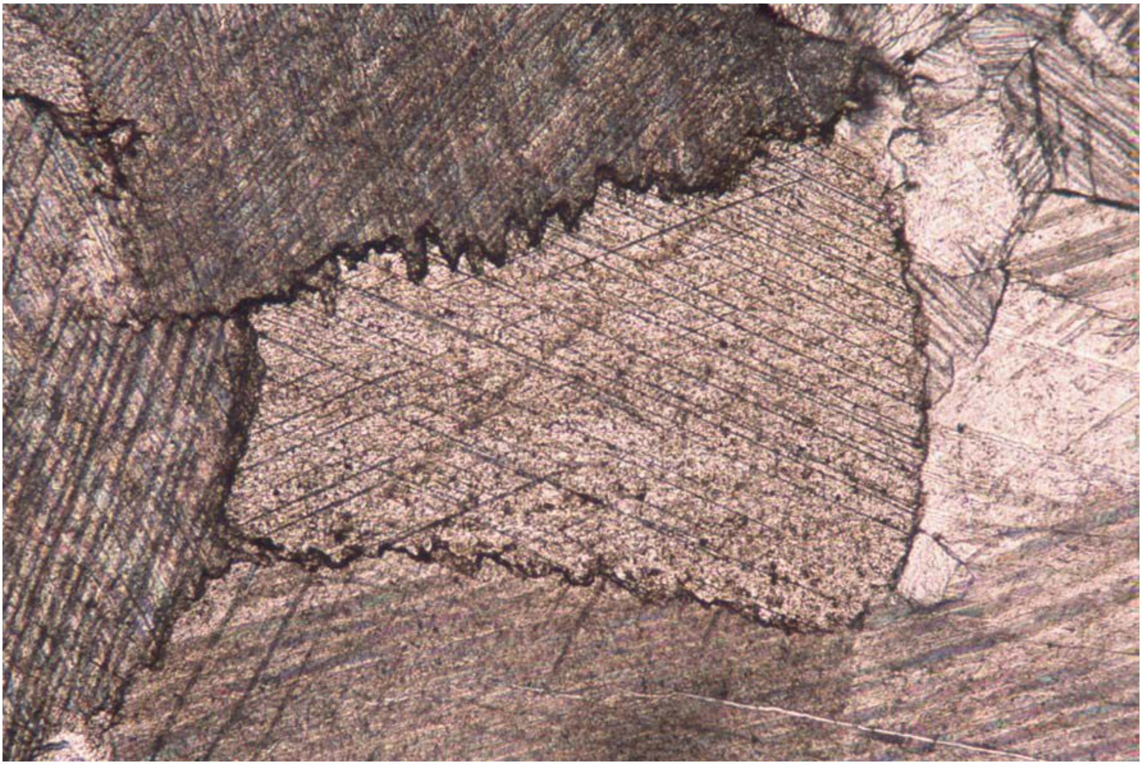

Fig. 5.14: Stylolites (irregular solution surfaces outlined by dark fine-grained residual material) formed along boundaries between calcite grains in a marble. Plane-polarized light; base of photo 1.5 mm.

(Passchier & Trouw, 1996, p. 26), which emphasizes the necessity for deformation in the process. The term 'dissolution–precipitation creep' or simply 'solution–precipitation creep' (den Brok & Spiers, 1991) also implies a deformation-controlled process.

Stress-induced solution transfer (dissolution–precipitation creep) is especially effective at low metamorphic grades, and produces microstructures such as truncated detrital grains (Figs. 2.1, 2.25), truncated ooids (Fig. 2.25), truncated fossils (Fig. 2.23), truncated pebbles (Mosher, 1980), stylolitic surfaces (Figs. 2.1, 2.25, 5.14), tectonic overgrowths, and 'beard' structures (McClay, 1977; Powell, 1982a; Cox & Etheridge, 1982), as shown in Fig. 5.15A. These features are discussed in Section 5.9.2. However, the process may also occur in the deformation of high- and medium-grade metamorphic rocks, producing veins and 'beard' structures (Lafrance & Vernon, 1993, 1999; Wintsch & Yi, 2002), as shown in Fig. 5.15B and discussed in Sections 5.3.6 and 5.8.2, as well as during fluid-assisted 'superplastic' deformation (Section 5.3.5), and especially in ductile shear zones (Section 5.7.6). McClay (1977) estimated that stress-induced solution transfer in fine-grained quartz and calcite rocks may produce geologically

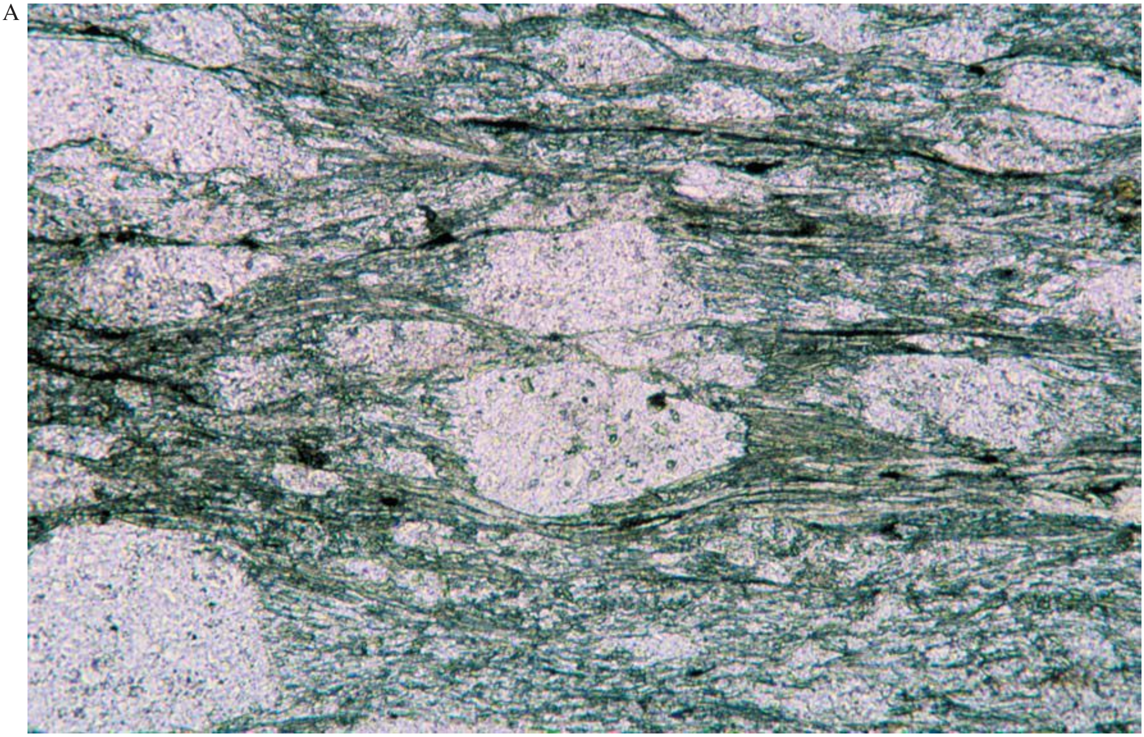

Fig. 5.15: (A) 'Beards' (aligned intergrowths of fibrous white mica and quartz) adjacent to a plagioclase clast and extending parallel to the slaty cleavage in a phyllite from the Hill End area, New South Wales, Australia. Plane-polarized light; base of photo 1.5 mm. (B) 'Beards' of hornblende on a relic of igneous clinopyroxene with plagioclase inclusions, in a gabbro deformed at upper amphibolite facies conditions, Guadalupe igneous complex, central Sierra Nevada, California, USA (Lafrance & Vernon, 1993, 1999). From Vernon (2000a, fig. 11), with permission of Springer-Verlag. Plane-polarized light; base of photo 4.4 mm.

reasonable strain rates at 200–300 °C, and that Coble creep in calcite rocks may produce geologically reasonable strain rates at around 300 °C.

Microstructures generally taken to indicate diffusion creep in deformed rocks include equant grain shapes, indented grains, overgrowths and a lack of crystallographic preferred orientation (Bons & den Brok, 2000). However, crystallographic preferred orientations due to crystallographic orientation-dependent dissolution and growth have been described by Becker (1995) for naturally deformed quartz-rich rocks, den Brok (1996) for experimentally deformed quartz rocks, and Heidelbach *et al.* (2000) for experimentally deformed albite aggregates. In addition, modelling by Bons & den Brok (2000) has indicated that dissolution–precipitation creep may be important in the development of crystallographic preferred orientations in rocks. Therefore, the presence of a crystallographic preferred orientation alone cannot be used as evidence for dislocation creep.

Fig. 5.15: (*cont.*)

Diffusion creep may grade into ductile grain-boundary sliding (Section 5.3.5) and frictional grain-boundary sliding (Section 5.3.1). For example, in low-grade metamorphic environments, pyrite commonly undergoes cataclastic deformation, but it may also be very ductile, probably involving stress-induced solution transfer and ductile grain-boundary sliding (McClay & Ellis, 1983). Another example is provided by deformation experiments on fine-grained (2–10 μm) albite with a small amount (<1%) of water, in which the deformation changes directly from cataclastic flow to grain-boundary diffusion creep with increasing temperature and decreasing strain rate, without any intermediate dislocation creep (Tullis & Yund, 1987, 1991). The resulting microstructures include rectangular grain shapes, overgrowths of different composition from the original grains, and low concentrations of dislocations, as seen in the transmission electron microscope (Tullis & Yund, 1991).

Den Brok (1998) has shown that rates of stress-induced solution transfer depend on microcracking, which may increase greatly with sudden increase in stress or fluid pressure; this can enhance grain-boundary diffusion rates and cause rock weakening.

Stress-induced solution transfer tends to predominate at lower temperatures, at which diffusion occurs more readily than dislocation creep, but dislocation creep tends to swamp stress-induced solution transfer at higher temperatures (Wheeler, 1992). However, because diffusion occurs along grain boundaries, stress-induced solution transfer is accentuated by finer grainsizes, and so may dominate dislocation creep, even at the high temperatures of the lower crust and upper mantle, at which dislocation creep would otherwise predominate (Rutter & Brodie, 1988a; Wheeler, 1992). Calculations made by Wheeler (1992) also suggest that stress-induced solution transfer is more effective in polymineralic rocks than in single-mineral aggregates, owing to chemical interactions during the deformation.

5.3.5 Ductile grain-boundary sliding

Some very fine-grained polyphase metal alloys, at certain conditions of temperature (at least half the melting temperature) and strain rate, can be deformed experimentally in tension up to strains of more than 1000%, without fracturing. This is referred to as *superplastic deformation* ('grainsize-sensitive flow'). The mechanism involved is *grain-boundary sliding*, which involves relative grain movement without loss of cohesion, and normally in the absence of fluid. Resulting potential gaps between grains are filled by diffusive mass transfer (Ashby & Verall, 1973a,b; Edington *et al.*, 1976; Nicolas & Poirier, 1976; Schmid *et al.*, 1977; Poirier, 1985), dislocation motion (Tullis, 1983) or both these processes (Kenkmann & Dresen, 2002), and so the aggregate remains coherent.

Superplasticity has been proposed for quartz (Boullier & Guegen, 1975; Vauchez, 1980; Behrmann, 1985; Behrmann & Mainprice, 1987), calcite (Behrmann, 1983), feldspar (Allison *et al.*, 1979), olivine (Kleinschrodt, 1994), and orthopyroxene and hornblende (Boullier & Guegen, 1975). Some have suggested that normal crystal plasticity may change rapidly to superplasticity below a critical grainsize (see, for example, Schmid *et al.*, 1977; Behrmann, 1983), possibly in millimetre-scale domains (Behrmann & Mainprice, 1987).

The problem is to determine the extent to which superplasticity occurs in natural rock deformation (see, for example, Gilotti & Hull, 1990). The following microstructural features have been suggested as indicators of superplastic behaviour in rocks (Boullier & Guegen, 1975; Schmid, 1982): (1) grains remaining equant, even after large accumulated strains; (2) very small grainsize, of around 1–10 μm; and (3) moderate concentrations of dislocations, without dislocation cells (i.e. no subgrains). However, small grainsizes and equant grains are also compatible with dynamic recrystallization during dislocation-induced flow (White, 1977; Schmid, 1982), so that superplasticity generally cannot be inferred with confidence from the microstructure alone. Another characteristic feature of superplasticity may be the absence of a strong preferred orientation, since diffusion-accommodated grain-boundary sliding tends to weaken existing preferred orientations, in contrast to aggregates recrystallized dynamically

(Sections 5.4.3, 5.4.4), which typically have crystallographic preferred orientations. However, before using a lack of strong preferred orientation to indicate superplasticity, care must be taken to exclude the possibility of static recrystallization, which may or may not reduce the strength of preferred orientations produced during dynamic recrystallization (Law, 1990). Perhaps more general terms such as 'non-cataclastic grainsize-sensitive flow' or 'non-cataclastic granular flow' (see, for example, Fitz Gerald & Stünitz, 1993b) are better for natural deformation.

In some rocks, non-cataclastic grainsize-sensitive flow may be promoted by the formation of transient, fine-grained reaction products in metamorphic reactions, or by fluid, which assists diffusion and results in a kind of high-temperature pressure-solution (Tullis & Yund, 1991; Tullis *et al.*, 1996). This can be called *fluid-assisted diffusion creep*. Experiments on deforming fine-grained feldspar aggregates have shown that fluid occurring in pores at hydrostatic conditions spreads along grain boundaries during deformation, causing a change from dislocation creep to diffusion creep, with consequent reduction in strength (Tullis *et al.*, 1996). The fluid reverts to isolated pores if the aggregate is heated after the deformation. This observed weakening by fluid activity could contribute to the formation of local high-strain zones (shear zones) in otherwise dry, high-grade metamorphic rocks (Tullis *et al.*, 1996).

Because minerals continuously dissolve in and precipitate from the fluid as deformation proceeds, microstructural evidence of this process may be difficult or impossible to distinguish from other forms of grainsize-sensitive flow. However, rectangular grain shapes and compositionally different grain overgrowths have been observed in high-temperature diffusion creep experiments on fine-grained sodic plagioclase (Tullis & Yund, 1991), and Drury & Humphreys (1988) observed diamond-shaped and tabular grain shapes, as well as asymmetrical grain-boundary bulges, in experiments on rock analogue materials.

Fluid-assisted ductile grain-boundary sliding should be conceptually distinguished from frictional grain-boundary sliding (Section 5.3.1), which not only involves an intergranular fluid, but also involves rotation of discrete fragments, rather than maintaining a coherent aggregate during deformation.

Grain-boundary sliding may also occur during the experimental deformation of partly molten rocks and analogue compounds (see, for example, Jin *et al.*, 1994; Hirth & Kohlstedt, 1995; Park & Means, 1996, 1997). The grains slide along melt-coated boundaries, as revealed in 'see-through' deformation experiments, although evidence of the process is generally not seen in the resulting microstructure (Rosenberg, 2001).

5.3.6 Conditions favouring various deformation mechanisms

Different deformation mechanisms dominate at different conditions of temperature, pressure, strain rate, differential stress, grainsize, fluid content and fluid composition, although several deformation mechanisms may operate simultaneously, even if one dominates. For example, higher confining pressure and lower fluid pressure tend to promote dislocation creep over cataclastic behaviour, and larger grainsizes tend to favour dislocation creep and deformation twinning, owing to greater ease of accommodation of strain produced by these processes at grain boundaries, compared with the situation in fine-grained aggregates.

Experiments have shown that the main factors favouring ductile flow of solid dry rocks are: (1) high confining pressure (which makes it difficult for the rock to expand and hence break during deformation), (2) high temperature (which assists dislocations to move freely through minerals), and (3) slow strain rate (which gives the dislocations enough time to move). Therefore, in dry rocks, flow tends to dominate in the deeper parts of Earth's crust and in the mantle, where the rocks are hot and under high confining pressures. In general, fracture dominates at depths of less than about 15 km and flow dominates at greater depths, though many exceptions occur, and the conditions vary with the mineral concerned. For example, quartz tends to be ductile at lower temperatures than feldspars (Section 5.5.1).

Microstructural evidence of dynamic recrystallization (Sections 5.4.3, 5.4.4) is generally taken to indicate relatively high temperature, but again the temperature varies greatly with the mineral. For example, although calcite typically undergoes ductile deformation and dynamic recrystallization (Sections 5.4.3, 5.4.4) at greenschist facies or higher temperatures (Rutter, 1976; Vernon, 1981; Busch & van der Pluijm, 1995), these processes may also occur in calcite at temperatures as low as 150–250 °C (Kennedy & White, 2001).

Fluids are also important in this context. For example, small amounts of water in the crystal structure increase the ductility of quartz, although the exact mechanism is not well understood (Section 5.6.3). However, water films on grain boundaries may block atomic bonding between grains and so reduce the 'effective pressure', leading to fracturing and brittle deformation. Thus, cataclastic deformation can persist to higher temperatures if fluid is present (Brodie & Rutter, 1985; Tullis & Yund, 1987; Lafrance & Vernon, 1993, 1999; Wintsch & Yi, 2002). On the other hand, water may assist diffusive flow in fine-grained calcite aggregates deformed at low differential stress (Rutter, 1974) and also greatly assists grain-boundary migration recrystallization (Mancktelow & Pennacchioni, 2004).

The overall situation, summarized by Wintsch & Yi (2002), is that at geological strain rates in quartz-rich rocks, brittle deformation dominated by fracture mechanisms changes to deformation by dislocation creep at about 200 °C. In plagioclase and pyroxene, this brittle-to-ductile transition occurs at about 450 °C and above 500 °C, respectively. If water is present, a field of stress-induced solution transfer displaces dislocation creep by 200–300 °C. Thus, creep by dissolution and replacement may occur at high temperatures during deformation in the presence of water, as noted by Lafrance & Vernon (1993, 1999) for gabbro deformed at high-temperature, amphibolite facies conditions and by Wintsch & Yi (2002) for granite deformed at 500–600 °C. Lafrance & Vernon (1993, 1999) inferred that plagioclase flowed by dislocation creep and recrystallized, but that pyroxene and hornblende mainly fractured and developed fringes of aligned grains ('beard' structures; Section 5.8.2) between boudins. Wintsch & Yi (2002) inferred that, although biotite and quartz deformed by dislocation creep, most of the deformation was accommodated by deformation-enhanced dissolution of minerals at grain boundaries perpendicular to the shortening direction (evidenced by truncated zoning patterns in plagioclase, orthoclase, epidote and titanite) and precipitation in the form of 'beards' on the ends of grains that face the extension direction (Fig. 5.15). Both these examples show that solution–precipitation creep can accompany and even dominate over dislocation creep at high temperatures in the presence of water.

5.4 Recovery and recrystallization

During deformation, dislocations in different slip planes may interfere with each other and form 'tangles' (Fig. 5.12), which inhibit their movement and hence further deformation of the mineral (strain strengthening or strain hardening). *Recovery* and *recrystallization* are processes that tend to reduce the concentration and/or tangling of dislocations, and so produce volumes of material capable of continued deformation. Thus, ductile deformation can be viewed as a competition between strain strengthening (hardening) and recovery processes.

5.4.1 Recovery

Recovery includes all processes that attempt to return a crystal to the undeformed state without the formation of high-angle (high-energy) boundaries (Hobbs *et al.*, 1976). In other words, no new grains are formed. Recovery may be *dynamic* or *static*, depending on whether or not it occurs during or after deformation, respectively.

During recovery, dislocations (Section 3.5.2) are able to free themselves from tangles by dislocation 'climb' (the movement of edge dislocations out of their slip planes by the addition or loss of points defects, which is a heat-activated process) and dislocation 'cross-slip' (the movement of screw dislocations from one slip plane to another). Both these processes untangle dislocations and so reduce the amount of strain strengthening. The freed dislocations migrate to form *subgrain boundaries* (Figs. 5.16–5.21), which are walls of organized dislocations (Chalmers, 1959; Kingery, 1960; Spry, 1969; Hobbs *et al.*, 1976), as shown in Fig. 5.16. This leaves relatively strain-free volumes (*subgrains*) between the subgrain boundaries, so that further deformation can proceed. Individual dislocations in subgrain boundaries are revealed by transmission electron microscopy (TEM), as shown in Fig. 5.16C.

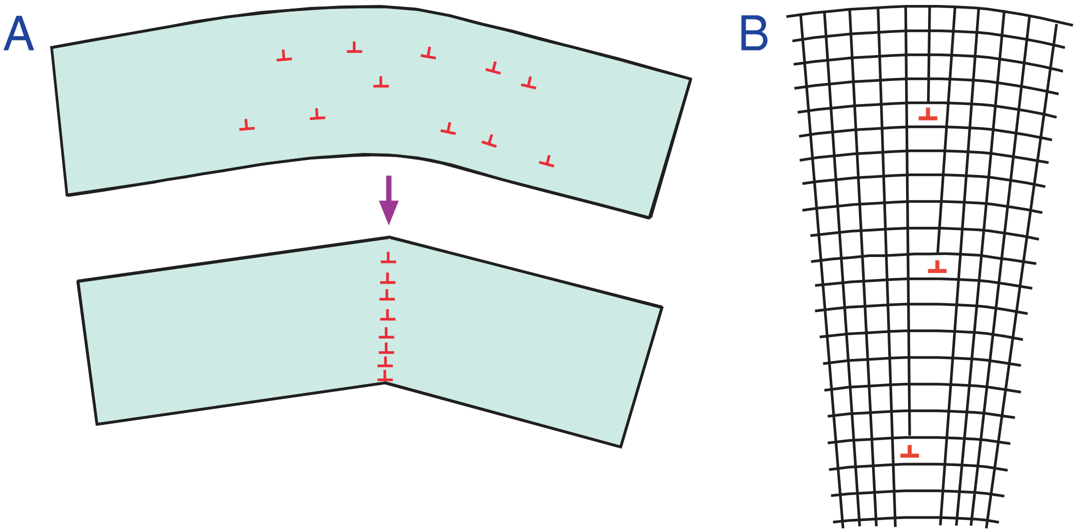

Fig. 5.16: (A) Sketch showing the change from a bent grain with random edge dislocations (top) to a grain with a subgrain (low-angle, low-energy) boundary (bottom) by the glide and climb of the dislocations. (B) Diagrammatic representation of a simple subgrain boundary formed by an evenly spaced array of edge dislocations. (C) TEM photo of subgrain boundaries in experimentally deformed water-bearing quartz, showing that the boundaries are composed of regular arrays of dislocations. Many minute (< 0.1 μm diameter) bubbles lie in the dislocations. Photo by John Fitz Gerald, from Boland & Fitz Gerald (1993, Section A, frontispiece, p. 2), with permission from Elsevier Science. Base of photo 3 μm.

Optically, subgrain boundaries tend to be relatively evenly spaced, and show small misorientation angles. Bending of grains (presumably involving dispersed dislocations) produces 'undulose (undulatory) extinction', which grades into slightly misoriented subgrain boundaries. However, TEM observations have revealed that some 'undulose extinction' seen in the optical microscope is actually due to subgrains (with simple tilt boundaries composed of dislocation arrays like those shown in Fig. 5.16B) with misorientations of a few degrees.

A maximum misorientation of 10° is often taken as a rough guide for subgrains in quartz (White, 1977) and 12° for olivine (Poirier & Nicolas, 1975). Fitz Gerald *et al.* (1983) found by TEM that 3–5° misorientation is appropriate for subgrains in albite, and Prior *et al.* (2002) observed subgrain misorientations of 3° in garnet. Larger misorientations produce grain boundaries, which have much higher free energies (Fig. 4.2). Precise distinction between subgrain and grain boundaries, on the basis of dislocation arrangements, requires transmission or scanning electron microscopy.

Moreover, slightly misaligned fragments that optically resemble subgrains can be formed by microfracturing (Urai *et al.*, 1986; Lloyd & Freeman, 1994; den Brok *et al.*, 1998), further complicating the optical identification of subgrains as being due to dislocation-dominated versus fracture-dominated processes. However, normally such microfractures are formed in the presence of fluid, and so subgrains of this type potentially may be recognized by the presence of healed lines of fluid inclusions along the subgrain boundaries, provided we can be sure that the inclusions were not formed along microfractures that developed along existing subgrain boundaries.

The optical relief of subgrain (low-angle) boundaries generally is not as marked as with grain (high-angle) boundaries, and this, together with the small misorientations, makes it clear that the subgrains occur within grains (hence the name). Subgrains may be equant (Figs. 5.17, 5.19–5.21) or elongate (Figs. 5.17, 5.18, 5.20). Elongate subgrains appear optically as 'extinction bands' at high angles to slip planes (Figs. 5.17, 5.18).

In the metallurgical literature, the process of forming subgrains is commonly referred to as 'polygonization', owing to the polygonal shapes of subgrains in some metals. However, this is not an ideal term, in view of the potential confusion with the polygonal grains produced by recrystallization in many minerals (Section 5.4.2). Note that the production of new polygonal grains by recrystallization (Section 5.4.2) is not 'polygonization', which refers only to recovery. Unfortunately, referring to recrystallization or neocrystallization as 'polygonization' is a common petrological error. The term is best replaced by 'recovery' or 'subgrain formation' to avoid ambiguity.

Subgrains have been observed in a variety of minerals, including quartz (see, for example, Hobbs *et al.*, 1976), calcite (Vernon, 1981), plagioclase (Vernon, 1975; Fitz Gerald *et al.*, 1983), olivine (Poirier & Nicolas, 1975), garnet (Prior

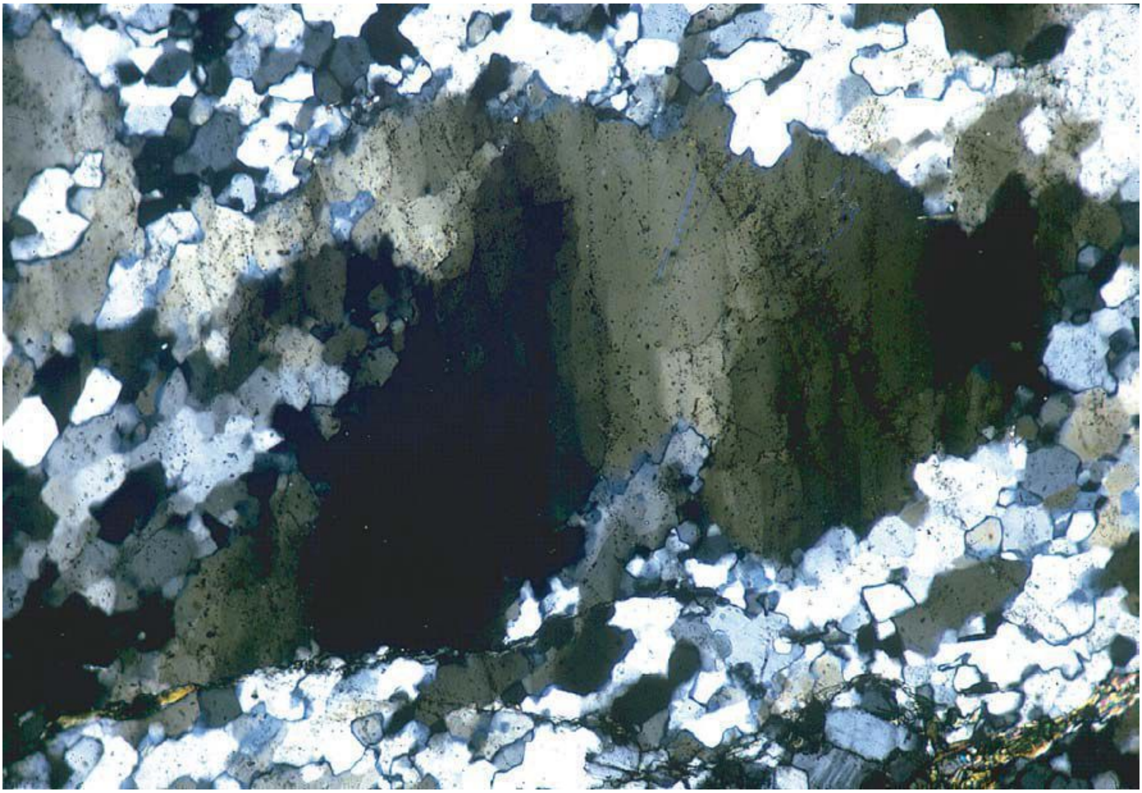

Fig. 5.17: Elongate and equant subgrains in a relic of deformed quartz surrounded by new (recrystallized) grains. Note the very small orientation differences between the subgrains, compared with the much larger orientation differences between most of the new grains. Crossed polars; base of photo 1.75 mm.

et al., 2000), cordierite (Fig. 5.21), galena (Richards, 1966; McClay, 1980) and pyrite (Boyle *et al*., 1998).

Elongate subgrain boundaries form perpendicular to slip planes (Fig. 5.16A). For example, below 400–700 °C (depending on water content and strain rate), quartz deforms by slip on (0001) in the direction of one or more of the *a*-axes ('*a*-slip') and subgrains develop parallel to the *c*-axis, whereas above 400–700 °C, quartz deforms by slip on $\{10\bar{1}0\}$ planes in the direction of the *c*-axis ('*c*-slip') and subgrains develop parallel to (0001), the plane of the *a*-axes. Therefore, whether *a*-slip or *c*-slip has operated can be detected by checking the orientation of the subgrain boundaries with a gypsum plate in grains with their *c*-axes subparallel to the thin-section plane; this determines the orientation of the fast (parallel to *a*) and slow (parallel to *c*) light-vibration directions. In addition, if *c*-slip operates, *a*-slip is also likely to operate, so that both sets of subgrain boundaries are visible. The resulting microstructure (Fig. 5.20) is called 'blocky subgrain

Next Page

Fig. 5.18: Elongate subgrains in deformed olivine surrounded by new (recrystallized) grains ('core-and-mantle' microstructure; Section 5.4.7). Note the very small orientation differences between the subgrains, compared with the much larger orientation differences and more sharply marked boundaries between the new grains. Crossed polars; base of photo 12 mm.

structure' or 'chessboard subgrain pattern'. It is most common in granulite-facies rocks, migmatites and high-temperature contact metamorphic rocks (Kruhl & Huntemann, 1991; Masberg *et al*., 1992; Kruhl, 1996), as well as granites deformed near their solidus temperatures (see, for example, Blumenfeld *et al*., 1986; Gapais & Barbarin, 1986; Mainprice *et al*., 1986; S. R. Paterson *et al*., 1989; Vernon, 2000a). Therefore, it is a potentially useful indicator of high-temperature deformation (Kruhl, 1996, 1998), although some have doubted its applicability (Okudaira *et al*., 1998).

5.4.2 Recrystallization

Recrystallization involves the formation of strain-free volumes in deformed grains by the creation and/or movement of grain boundaries, in response to

Previous Page

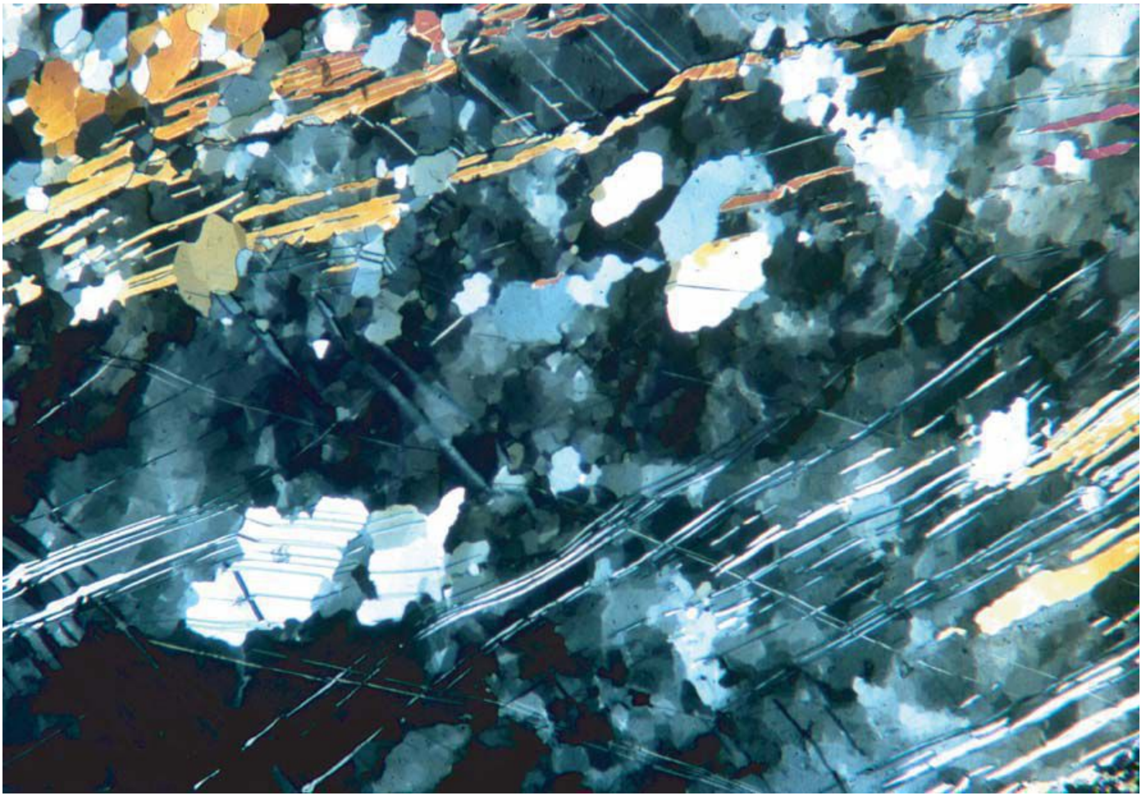

Fig. 5.19: Equant subgrains and new (recrystallized) grains in deformed calcite, Mount Lofty Ranges, South Australia. The subgrains occur in the darker areas, and show very small misorientations, whereas the new grains have sharp boundaries and marked misorientations between themselves and the areas of subgrains. The new grains are larger than most of the subgrains, as is common in recrystallization by subgrain rotation. Also shown are bulged twin lamellae, owing to strain-induced grain-boundary migration. Ultrathin section (0.005 mm). Crossed polars; base of photo 1.3 mm.

deformation (Figs. 5.17–5.26). During recrystallization, strain energy is reduced by: (1) migration of existing high-angle (high-energy, random, irrational) grain boundaries, kink-band boundaries or twin boundaries; (2) development and migration of new high-angle grain boundaries; and (3) development of new low-energy crystal faces, *all in the same mineral*. A generally applicable definition of recrystallization is 'the development and/or migration of high-angle (random) grain boundaries and/or crystal faces in the solid state, in response to deformation, and in the same mineral'.

Recrystallization typically produces aggregates of new (recrystallized) grains that are strain-free and therefore capable of continued deformation. The new grains may be: (1) polygonal, in minerals with relatively uniform

Fig. 5.20: 'Blocky' sub-grains in deformed quartz caused by intersecting sets of elongate subgrains, one parallel to the plane of the *a*-axes and the other parallel to the *c*-axis. Deformed granite, Bega Batholith, south-eastern New South Wales, Australia. Crossed polars; base of photo 4 mm.

three-dimensional lattice structures, such as quartz, feldspar, calcite or olivine (Figs. 5.17–5.24); (2) crystals with low-energy faces, in minerals with strongly anisotropic lattice structures, such as mica (Vernon, 1977b; Bell, 1978b, 1979; Etheridge & Hobbs, 1974), as shown in Fig. 5.26, or the elongate ('specularite') variety of hematite (Rosière *et al.*, 2001); or (3) irregularly shaped, where grain-boundary migration recrystallization is the dominant process (Fig. 5.27), as discussed below. An apparent anomaly is stibnite, which recrystallizes to polygonal aggregates (Edwards, 1947), despite having a strongly anisotropic crystal structure that is reflected in the development of very elongate crystals when grown freely in a liquid. The problem is discussed in terms of availability of fluid in Section 4.4.

Processes of recrystallization in metals, ceramics, other synthetic materials and minerals have been discussed by Chalmers (1959), Kingery (1960), Hobbs (1968), Hobbs *et al.* (1976), Nicolas & Poirier (1976), Poirier & Guillopé (1979), Vernon (1975, 1976, 1981), Cahn (1983), Fitz Gerald *et al.* (1983), Urai (1983b), Drury *et al.* (1985), Urai *et al.* (1986) and Nicolas (1987). A detailed account of processes operating during dynamic recrystallization (Sections 5.4.3, 5.4.4) has been given by Urai *et al.* (1986).

As noted above, recrystallization does not involve the production of new minerals. However, small compositional changes between new and old grains commonly occur in minerals with complex chemical compositions (see, for example, Etheridge & Hobbs, 1974; Vernon, 1975, 1977b) and can be accommodated in the definition of 'recrystallization'. Stünitz (1998) has shown that differences

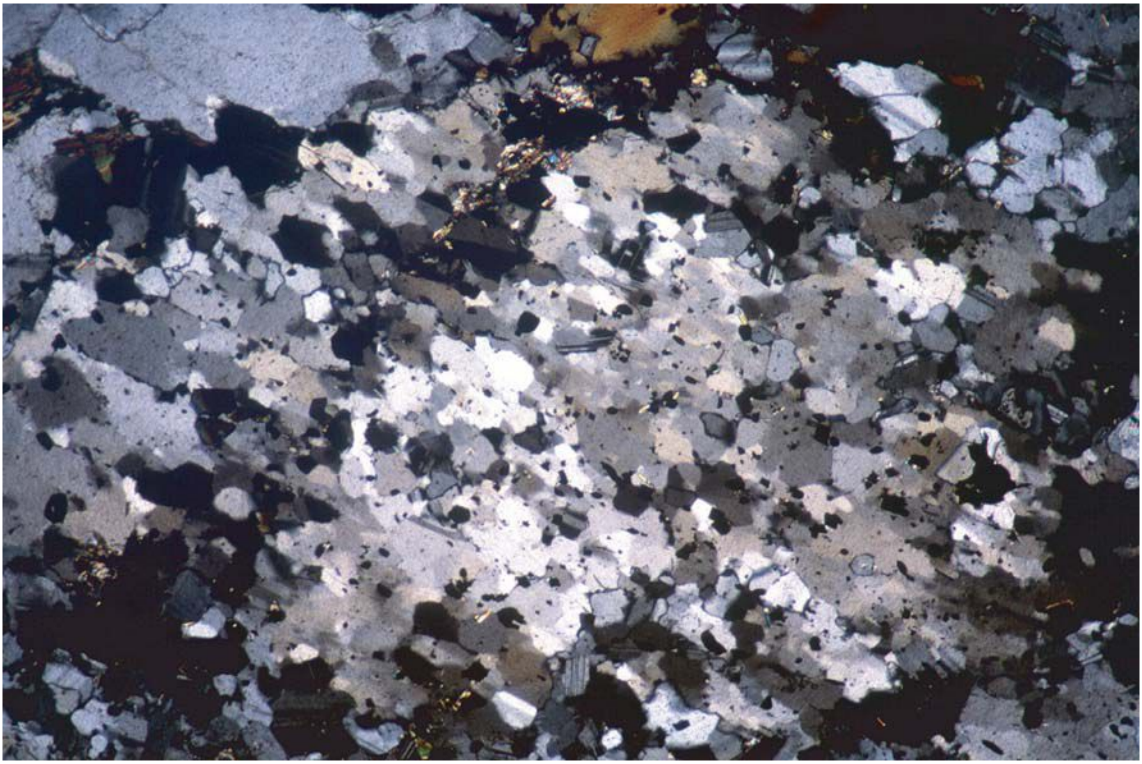

Fig. 5.21: Equant to irregular subgrains and new grains in deformed cordierite, Cambalong complex, south-eastern New South Wales, Australia. Crossed polars; base of photo 4 mm.

in composition between old and recrystallized plagioclase grains can contribute to the driving force for recrystallization. The formation of new minerals during deformation is better referred to as *neocrystallization*, which occurs where the migrating boundaries separate different minerals (Urai *et al*., 1986, p. 162), as shown in Fig. 5.26.

'Nucleation' of new grains during recrystallization (as opposed to neocrystallization) generally does not involve the formation of completely new grains from new nuclei developed randomly within old grains, but typically involves (1) *subgrain rotation*, (2) *strain-induced grain-boundary migration* ('bulge nucleation') or (3) *grain-boundary migration recrystallization*, as discussed below. Unfortunately, processes (1) and (2) can produce similar microstructures (Lloyd & Freeman, 1994), and, to complicate matters, microfracturing can produce slightly misaligned fragments that optically resemble subgrains (see, for example, Urai *et al*., 1986; Lloyd & Freeman, 1994; den Brok & Spiers, 1991; den Brok, 1992; den Brok *et al*., 1998), as discussed in Section 5.4.8. Therefore, care should be taken when attempting to interpret recrystallization microstructures.

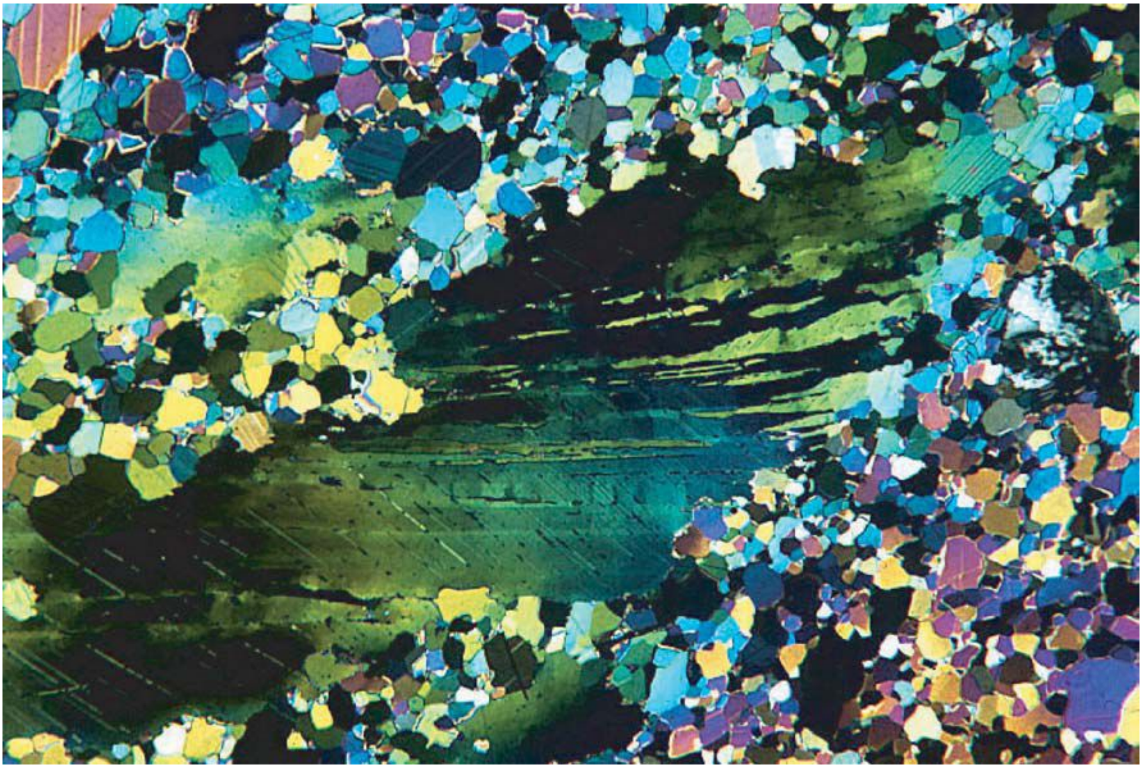

Fig. 5.22: Recrystallized aggregate of polygonal, undeformed grains of calcite surrounding a much larger deformed relic (porphyroclast) of calcite, with possible deformation bands (Section 5.3.3) and deformation twins with interfaces that have migrated in response to heat and/or strain (Sections 4.11.1, 5.4), in a marble from the Mount Lofty Ranges, South Australia. The section is only 0.007 mm thick, and therefore shows the grain boundaries and the subgrain features more clearly than in a section of normal thickness (Section 1.6). From Vernon (2000b, fig. 34). Crossed polars; base of photo 3.5 mm.

(1) *Subgrain rotation recrystallization* (Hobbs, 1968; Poirier & Guillopé, 1979; Guillopé & Poirier, 1979) occurs when dislocations accumulate in subgrain boundaries, causing the boundaries to progressively increase their complexity and misorientation. When a dislocation is added to a subgrain boundary, it changes the angular mismatch between the two subgrains. By this process, subgrain boundaries become grain (high-energy, high-angle) boundaries. The misorientation at which a subgrain boundary becomes a grain boundary probably depends on the mineral concerned, but 5–15° misorientation is commonly quoted, as mentioned previously. Thus, the process involves progressive crystallographic misorientation with limited grain-boundary migration, and orientation relationships between the old and the new (recrystallized) grains may be recognized (Hobbs, 1968; Poirier & Nicolas, 1975; Vernon, 1975; Urai, 1983a,b;

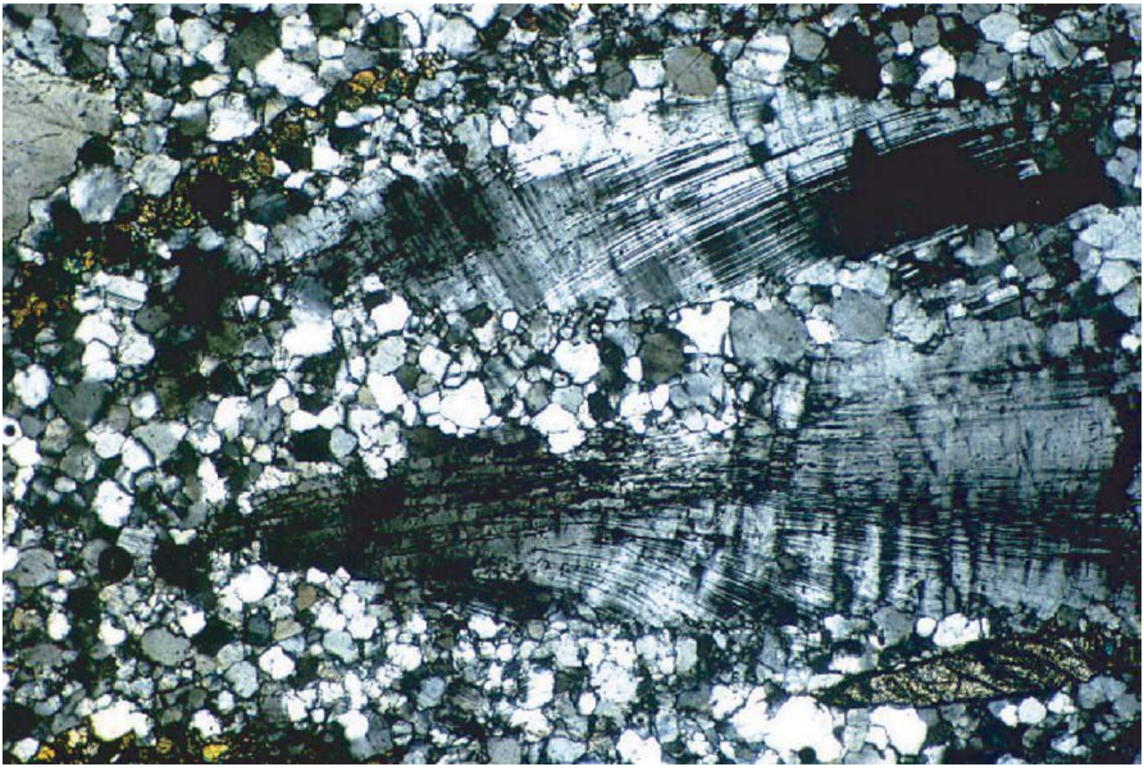

Fig. 5.23: Large, bent, strongly deformed grain of plagioclase with deformation twinning and local kink-like features (deformation bands) partly recrystallized to finer-grained polygonal aggregates of largely untwinned grains of plagioclase, during high-temperature deformation in an anorthosite from the Giles Complex, South Australia. From Vernon (2000b, fig. 35). Crossed polars; base of photo 4.4 mm.

McClay, 1983; White, 1990). For example, in rotational dynamic recrystallization of quartz, *c*-axes of the new grains tend to lie at 20–50° from the *c*-axis of the old grain (Hobbs, 1968). In this way, the shapes of domainal deformation features, such as deformation bands in quartz, may be preserved in extensively recrystallized aggregates; this is revealed most clearly when the aggregate is viewed with a gypsum accessory plate.

Subgrains leading to recrystallization have been observed in many minerals, including quartz (Fig. 5.17; Hobbs, 1968; Tullis *et al*., 1973), olivine (Fig. 5.18; Poirier & Nicolas, 1975), calcite (Fig. 5.19; Vernon, 1981), cordierite (Fig. 5.21), K-feldspar (Bell & Johnson, 1989b; Altenberger & Wilhelm, 2000) plagioclase (Vernon, 1975; Bell & Johnson, 1989b; Dornbusch *et al*., 1994, fig. 4a), glacial ice (Wilson, 1986), galena and chalcopyrite (Siemes, 1976; McClay, 1983; Cox, 1987a), and pyrite (Boyle *et al*., 1998).

'Core-and-mantle structure' (Figs. 5.17, 5.22–5.25; Section 5.4.7), typically involving progressive misorientation of subgrains from core to recrystallized

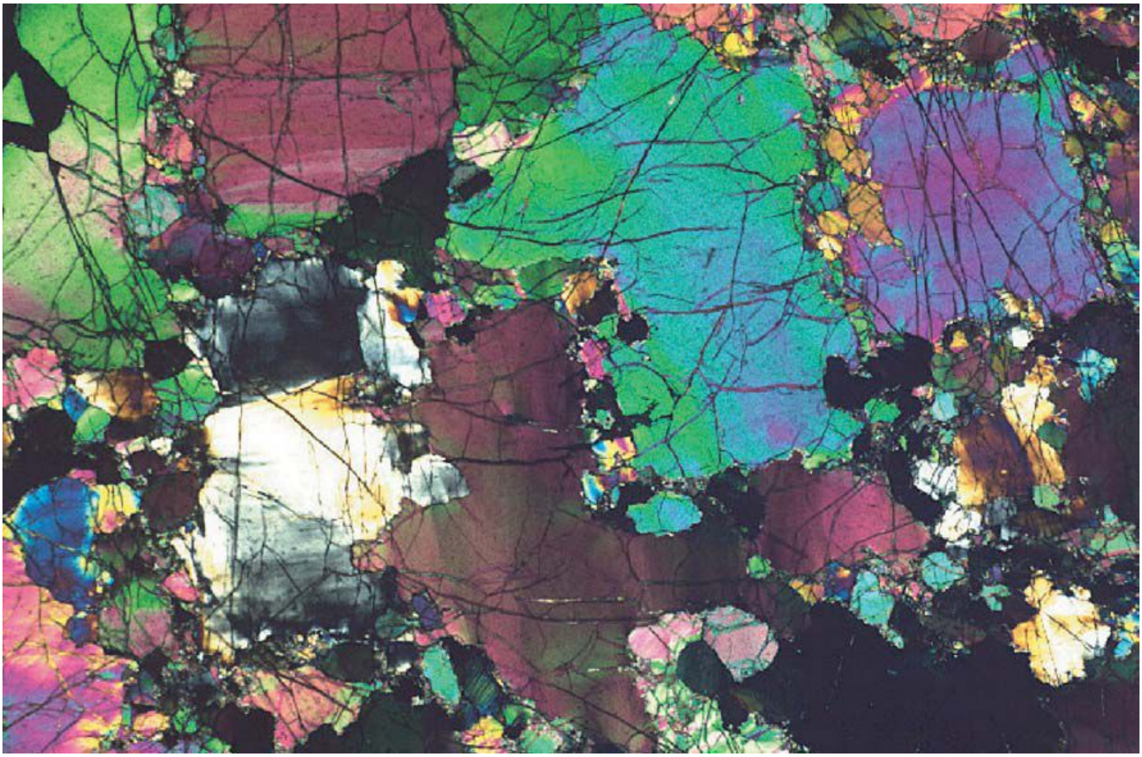

Fig. 5.24: Large deformed grains of olivine (with subgrains) partly recrystallized to finer-grained aggregates of olivine, some of which also have subgrains, consistent with recrystallization during the deformation (dynamic recrystallization), in a peridotite from Earth's mantle brought to the surface as a xenolith in basalt. From Vernon (2000b, fig. 36). Crossed polars; base of photo 2.5 cm.

mantle, is generally ascribed to progressive subgrain rotation (see, for example, S. H. White, 1976; J. C. White, 1990; Trimby *et al*., 1998), which typically causes recrystallization to concentrate in former grain-boundary regions of an aggregate.

Photographic evidence of progressive rotation of subgrains to produce new (recrystallized) grains during the deformation of transparent materials in the microscope has been presented by Means & Xia (1981, fig. 3) and Means (1989, fig. 4j–l).

(2) *Strain-induced grain-boundary migration* (grain-boundary bulging; bulging recrystallization; 'slow' grain-boundary migration) involves differential migration of parts of a high-angle boundary, such as a grain boundary (Figs. 5.20, 5.27), kink-band/deformation-band boundary (Fig. 5.28) or deformation-twin boundary (Figs. 4.63, 5.19, 5.22). It has been referred to as 'slow grain-boundary migration' (Poirier & Guillopé, 1979; Fitz Gerald & Stünitz, 1993b; Urai *et al*., 1986), to distinguish it from 'fast grain-boundary migration' or 'grain-boundary migration recrystallization' (see below).

A

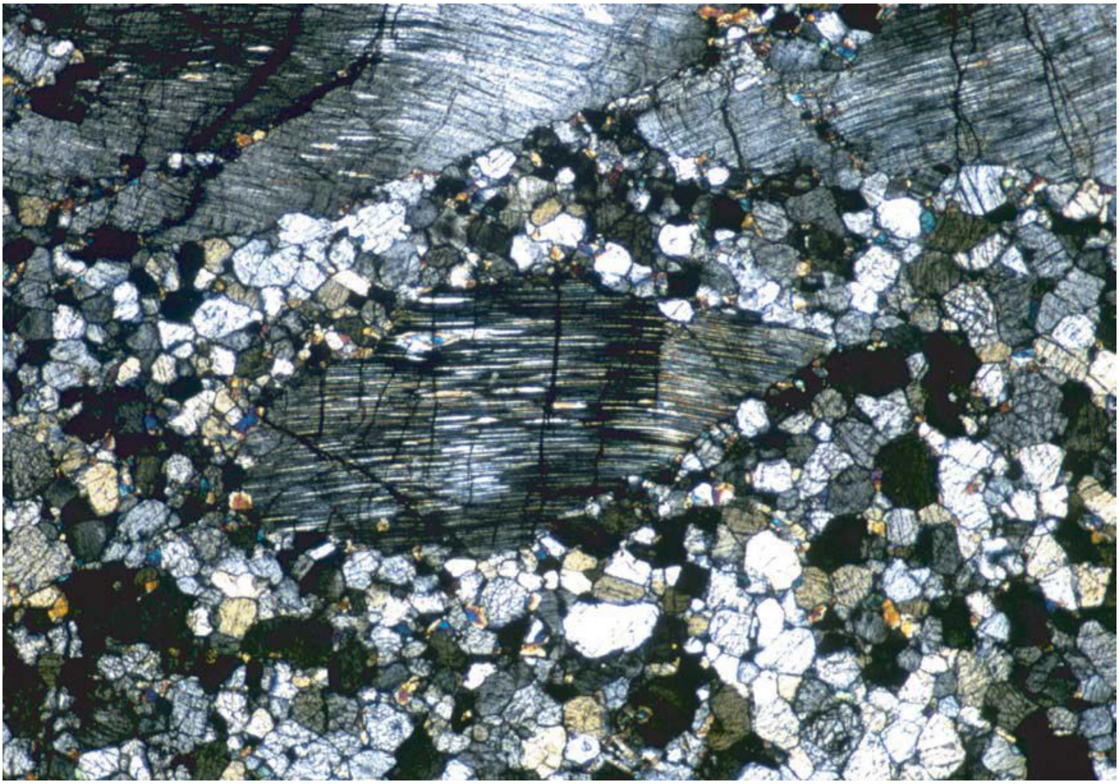

Fig. 5.25: (A) Relics (porphyroclasts) of deformed (bent and locally kinked) orthopyroxene (first-order grey maximum interference colours) with exsolution lamellae (Section 4.9) of clinopyroxene (second-order maximum interference colours), surrounded by recrystallized aggregates of polygonal grains of orthopyroxene and clinopyroxene, shown at higher magnification in C. (B) An intermediate stage between A and C, showing recrystallization along exsolution lamellae and kink-band boundaries, apparently involving strain-induced boundary migration. (C) Completely recrystallized aggregate, in which the two pyroxenes have segregated as separate grains. The rock is a deformed gabbro from the Giles Complex, South Australia. Crossed polars; base of A and B 4.4 mm; base of C 1.75 mm.

The migration occurs by diffusion of atoms across the boundary, which consequently moves in the opposite direction to the diffusion direction, and forms a 'bulge'. High-energy boundaries can move easily at high temperatures because they are very disordered (see, for example, Drury & Urai, 1990), and atoms can easily transfer from one crystal lattice to the adjacent one (see, for example, Smith, 1953, p. 559). Strain-induced grain-boundary migration is driven by strain energy differences (differences in the dislocation concentration) on either side of the grain, kink-band or twin boundary. The process tends to relax gradients in strain (recrystallization) or composition (neocrystallization) or both. So, as

B

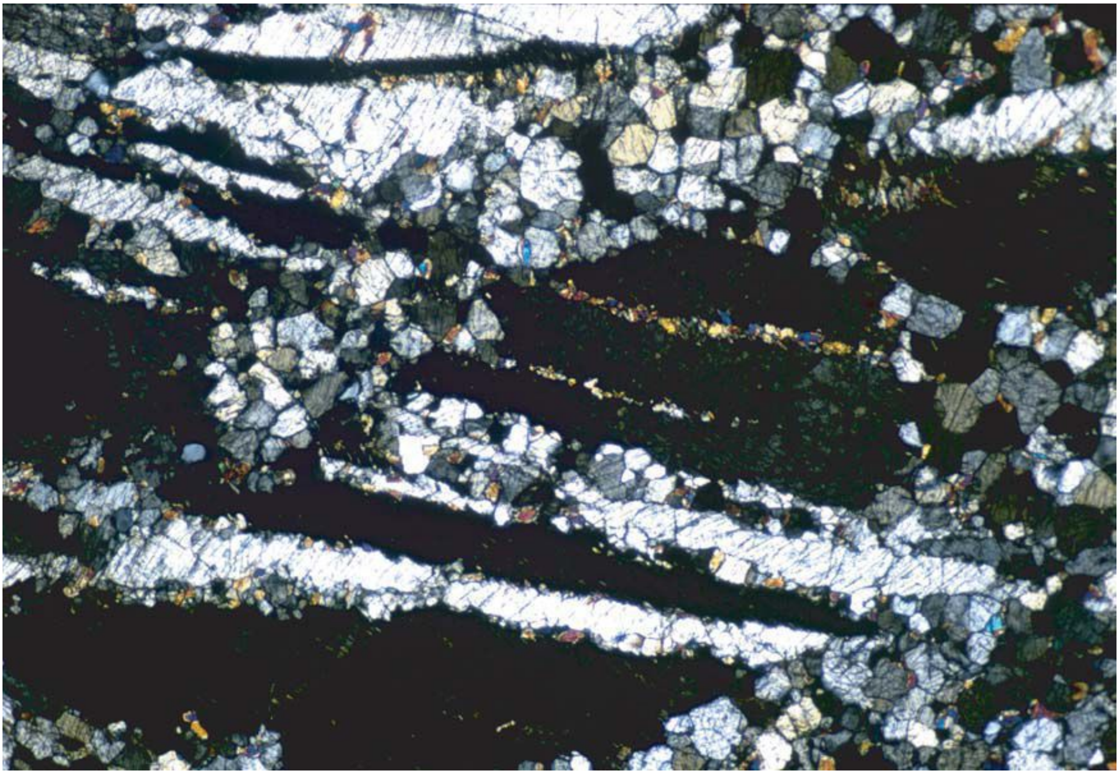

Fig. 5.25: (*cont.*)

the boundary moves into a deformed grain it leaves undeformed mineral behind it. The microstructural result is a *sutured* ('bulged') grain boundary (Figs. 5.20, 5.27), kink-band boundary (Fig. 5.28) or deformation twin boundary (Figs. 4.63, 5.19, 5.22), with markedly smaller new grains along the boundary. The process may occur at low temperatures in quartz and calcite (Schmid *et al*., 1980, 1987; Drury *et al*., 1985).

Mobile quartz grain boundaries may be 'pinned' by small dispersed grains of another mineral, such as mica, which also can cause bulges in the migrating boundary (Jessell, 1987). The grainsize of the recrystallized aggregate can be controlled by the spacing of the small grains if enough of them are present (Fig. 4.29B).

Sutured grain boundaries, kink-band boundaries and twin boundaries have been observed in a wide variety of minerals, including quartz, plagioclase, calcite (Vernon, 1981), K-feldspar (Altenberger & Wilhelm, 2000) glacial ice (Wilson, 1986), galena (Siemes, 1977b; McClay & Atkinson, 1977; McClay, 1980), stibnite, ilmenite, pyrite (Cox *et al*., 1981; McClay & Ellis, 1983, 1984) and chalcopyrite (Cox & Etheridge, 1984). In minerals with relatively 'isotropic' crystal structures (e.g. quartz, feldspar, calcite, olivine, ice, galena, pyrite), C

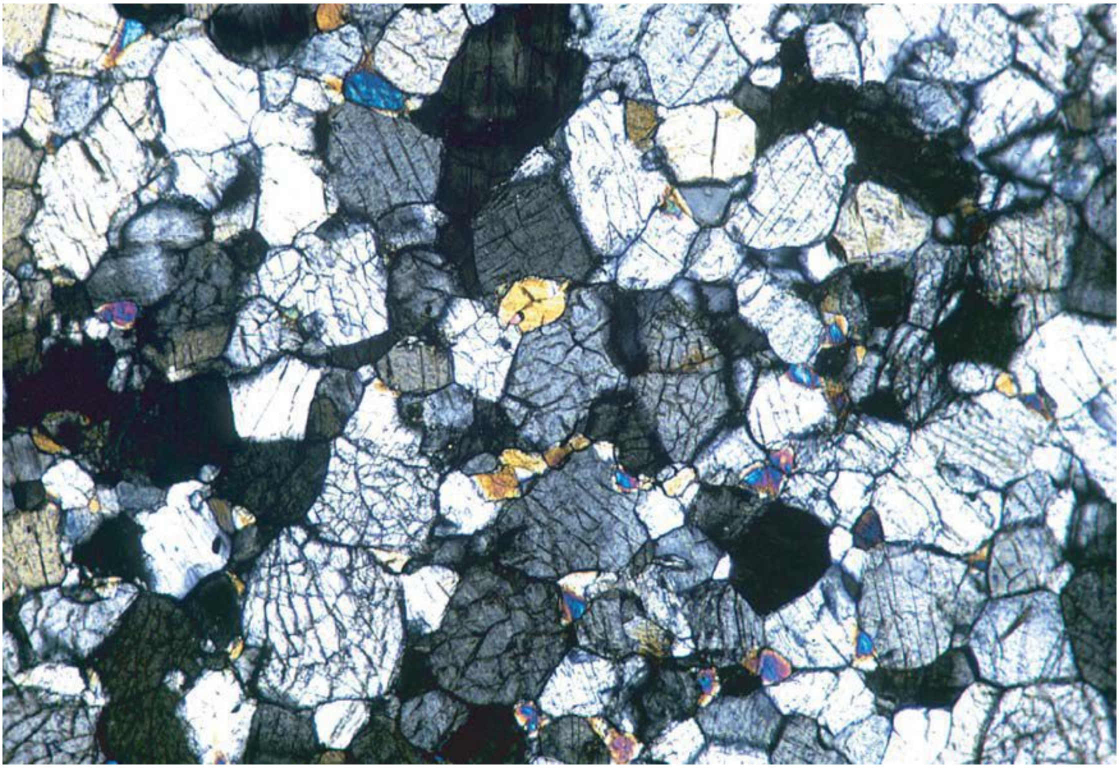

Fig. 5.25: (*cont.*)

strain-induced grain-boundary migration produces equant new grains (Figs. 5.27 and 5.28), whereas in minerals with strongly anisotropic crystal structures (e.g. sheet silicates) it produces aggregates of elongate new grains. Bulging recrystallization of minerals with exsolution lamellae (Section 4.9) tends to produce separate grains of the two minerals concerned in the recrystallized aggregate (Fig. 5.25); although the process produces new grains of minerals previously present only as exsolution lamellae, it can nevertheless be referred to as recrystallization, not neocrystallization, because no new minerals are produced. Examples include recrystallization of microperthite, forming separate grains of albite and K-feldspar (White & Mawer, 1988) and recrystallization of orthopyroxene with clinopyroxene exsolution lamellae, forming separate polygonal grains of each pyroxene (Fig. 5.25).

The processes of strain-induced grain, kink-band and twin boundary migration have been observed in action in experiments on transparent crystalline compounds deformed at low temperatures in the microscope (Means, 1981, fig. 3, 1989; Tungatt & Humphreys, 1984, fig. 13; Urai *et al.*, 1986; Blumenfeld & Wilson, 1991).

Poirier & Guillopé (1979) have pointed out that trace amounts of water increase the rate of grain-boundary migration, even in anhydrous minerals, such as quartz

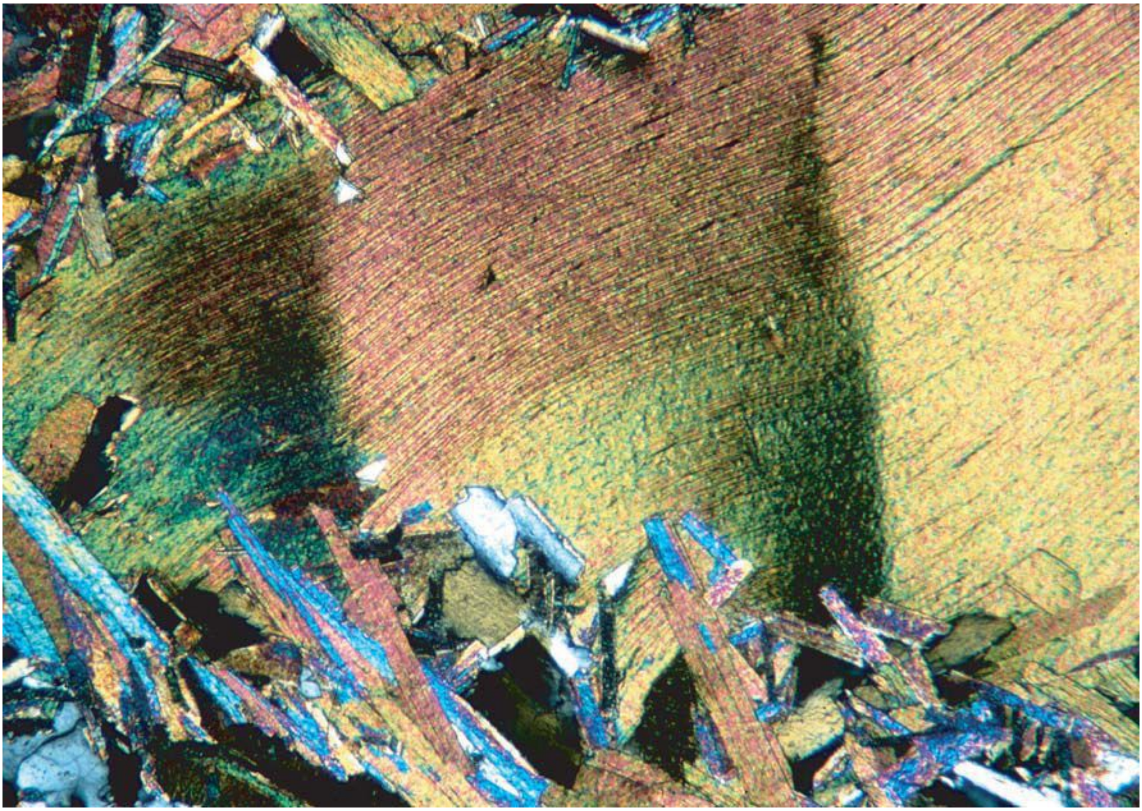

Fig. 5.26: Kinked grain of biotite that has been partly neocrystallized to much smaller new grains of biotite and muscovite with crystal faces, which are typical of mica aggregates (Sections 4.2.3, 5.4.2), Swiss Alps. Crossed polars; base of photo 3.5 mm.

(Green *et al*., 1970) and olivine (Zeuch & Green, 1979). They suggested that water may enhance grain-boundary mobility by increasing the glide and/or climb mobility of grain-boundary dislocations, in the same way as it appears to induce easier glide or climb of lattice dislocations (Griggs, 1974; McLaren & Retchford, 1969).

Although bulges in grain boundaries commonly appear rounded (except for minerals such as sheet silicates), long-lasting strain-induced grain-boundary migration at relatively high temperature can lead to a stepped (Fig. 5.30), rather than a smoothly sutured interface (Kruhl, 2001; Kruhl & Peternell, 2002). The steps or sharp deflections appear to be due to crystallographic control, such as the formation of rhombohedral planes in quartz (Voll, 1960, p. 521; Masberg *et al*., 1992, fig. 3). This effect is particularly evident in some examples of ‘fast’ grain-boundary migration, discussed below.

Kruhl & Nega (1996) suggested that the fractal dimension of sutured grain boundaries in quartz is larger for higher grades of metamorphism, and that

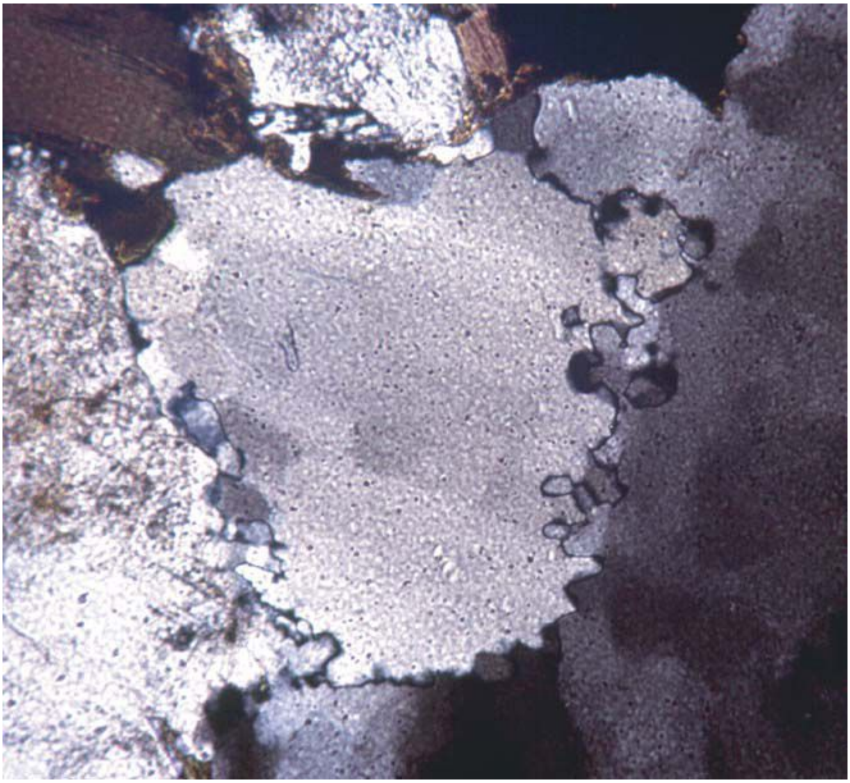

Fig. 5.27: Strain-induced grain boundary migration (bulging) in quartz, resulting in the formation of small new (recrystallized) grains behind the bulges on both sides of the migrating boundary, in a deformed granite from the Bega Batholith, south-eastern New South Wales, Australia. Blocky subgrains (Section 5.4.1) are present in the original grains. Crossed polars; base of photo 1.7 mm.

statistically the fractal dimension can be used as a deformation-related geothermometer. However, the effects of other factors, such as stress, strain-rate and fluids remain to be ascertained.

(3) *Grain-boundary migration recrystallization* (‘fast’ grain-boundary migration) is a more pronounced form of grain-boundary bulging that occurs during recrystallization. It has been observed in materials (e.g. octachloropropane) progressively deformed in the microscope (Urai, 1983b; Means, 1983, 1989; Jessell, 1986). The process produces bulges with long wavelengths (Figs. 5.29, 5.30A), of the order of the grainsize, which migrate through the aggregate, continuously converting parts of it from one lattice orientation to another. These changing ‘orientation domains’ move through the aggregate in a complex way, leading to irregular grain shapes (Fig. 5.29), although locally interfaces may have marked steps, suggesting crystallographic control, especially if fluid occurs along the grain boundaries (Fig. 5.30B). Although no new grains are produced, some may

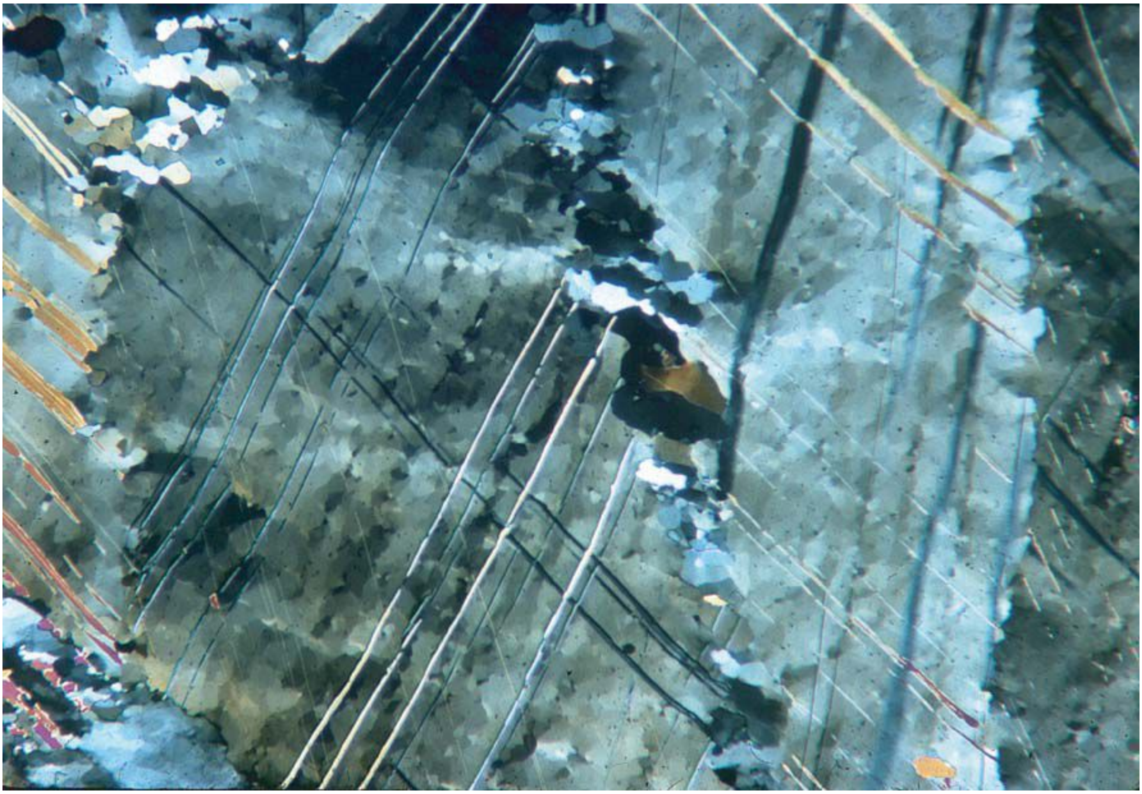

Fig. 5.28: Strain-induced grain-boundary migration (bulging) of deformation bands (left and right edges of photo) in calcite in a deformed marble from the Mount Lofty Ranges, South Australia. Also shown are abundant equant subgrains. The zone of recrystallization across the centre of the photo probably represents a completely recrystallized deformation twin or narrow deformation band. The section is only 0.005 mm thick, and therefore shows the grain boundaries and the subgrain features more clearly than in a section of normal thickness (Section 1.6). Crossed polars; base of photo 1.3 mm.

be removed or dissected, and others may coalesce or amalgamate by progressive reduction of misorientation. The process affects relatively large areas, so that original grains may be completely consumed (Urai *et al.*, 1986). 'Fast' grain-boundary migration may change catastrophically to 'slow' grain-boundary migration and *vice versa*, owing to sudden changes in the grain boundary structure or the absorption of impurities (Urai, 1983b, p. 147).

Grain-boundary migration recrystallization occurs at relatively high temperatures (amphibolite facies) in quartz and calcite (Schmid *et al.*, 1980, 1987; Schmid & Casey, 1986; Fitz Gerald & Stünitz, 1993a).

However, the process is also promoted by water on the migrating boundaries. For example, Mancktelow & Pennacchioni (2004) found that, in mylonite

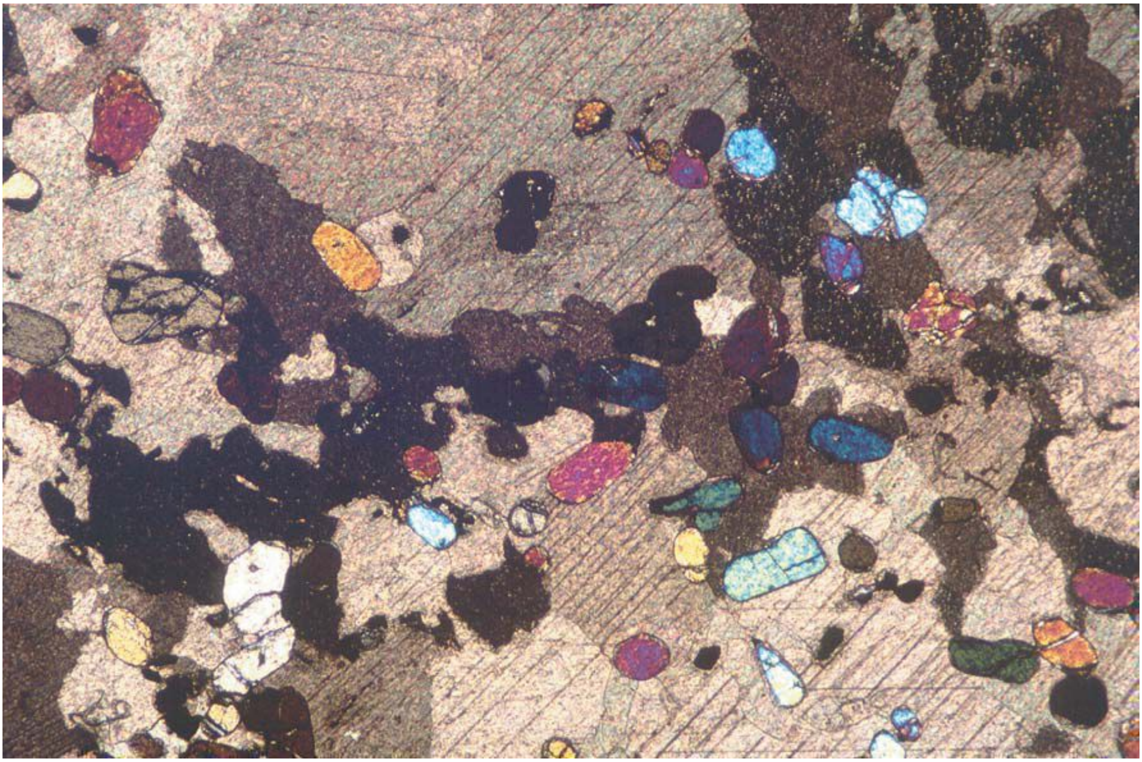

Fig. 5.29: Deeply scalloped grain boundaries in coarse-grained calcite, suggesting grain-boundary migration recrystallization ('fast' grain-boundary migration; Section 5.4.2) in a marble formed at high temperature. The areas at or near extinction are probably parts of the same grain, indicating the complex shapes of the large calcite grains. Also present are inclusions of olivine with crystal faces and rounded corners, indicating solid-state grain-boundary adjustment during metamorphism (Section 4.2.7). Crossed polars; base of photo 4 mm.

zones in the western Alps, dynamic recrystallization in dry quartz was dominated by subgrain rotation and 'slow' (bulging) grain-boundary migration (producing fine-grained granoblastic aggregates), whereas dynamic recrystallization in wet quartz was dominated by 'fast' grain-boundary migration, producing much larger grains with strongly indented boundaries, at least some of which appear to be crystallographically controlled (Fig. 5.30B).

This is supported by experiments on salt rocks, in which fluid-assisted grain-boundary migration recrystallization may produce new grains with crystal faces (Urai, 1983a, b; Urai *et al.*, 1986).

In wet samples, a continuous fluid film occurs along the migrating boundary, incorporating fluid inclusions (Section 4.4.5) as it moves. The film breaks up into arrays of isolated fluid bubbles when the migration stops, which is probably why fluid observed in grain boundaries in natural rocks invariably occurs as isolated bubbles. The boundary migration occurs by dissolution of the grain

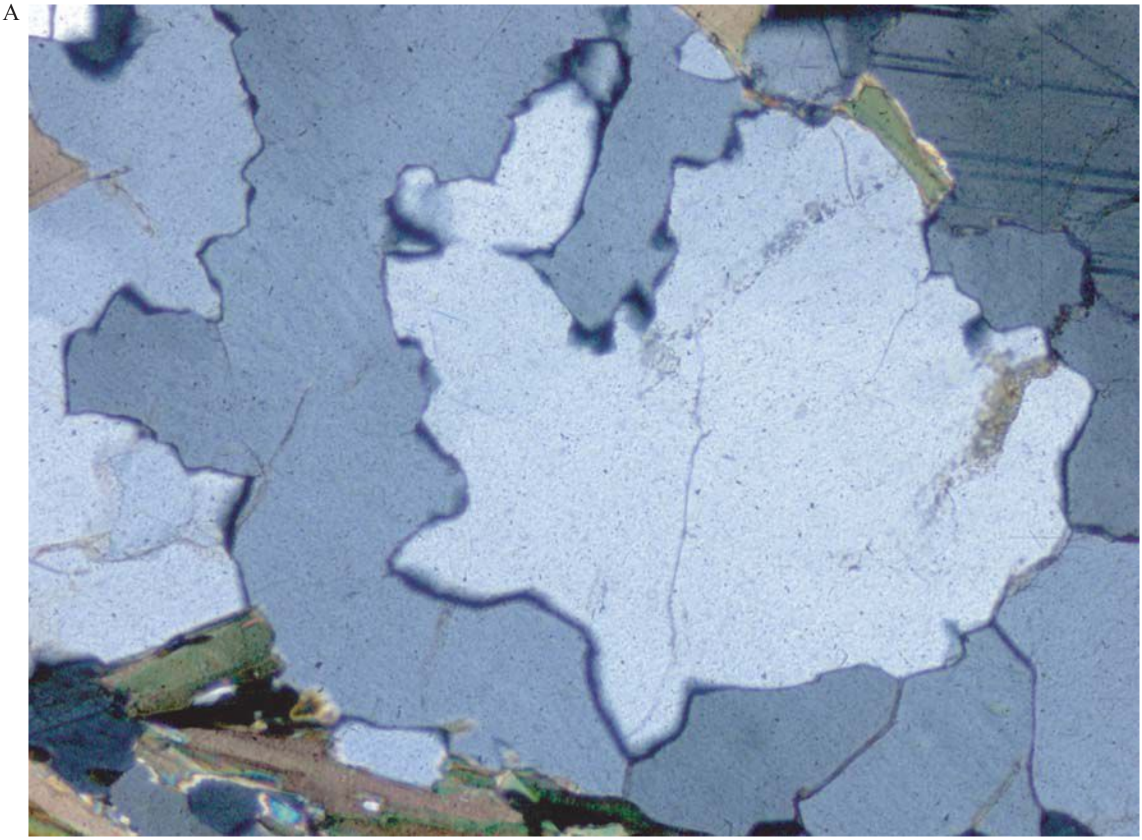

Fig. 5.30: (A) Deeply sutured boundaries in quartz formed by grain-boundary bulging in a deformed tonalite, San José pluton, Baja California, México. Crossed polars; base of photo 3 mm. (B) Planar indentations, probably crystallographically controlled, in quartz that has undergone 'fast' grain-boundary migration, Simplon area, western Alps. Photo by Neil Mancktelow. Crossed polars, base of photo 2.4 mm.

with the higher dislocation concentration, diffusion through the fluid film, and precipitation on the other grain (Bosworth, 1981; Urai, 1983a). In contrast, in dry aggregates the migrating boundary does not contain fluid and moves away from fluid inclusions (Urai, 1983a, p. 151).

The temperatures required for this process to operate in feldspars appear to be so high that no natural examples had been reported until Lafrance *et al.* (1995, 1998) inferred that irregular grain boundaries and dissected plagioclase grains in deformed anorthosite are the result of 'fast grain-boundary migration', possibly with some subgrain rotation, occurring at about 1050 °C during emplacement of the anorthosite intrusion. As noted above, evidence of fluid-assisted 'fast' grain-boundary migration occurs in granite deformed at amphibolite facies conditions in the Simplon area, western Alps (Mancktelow & Pennacchioni, 2004).

B

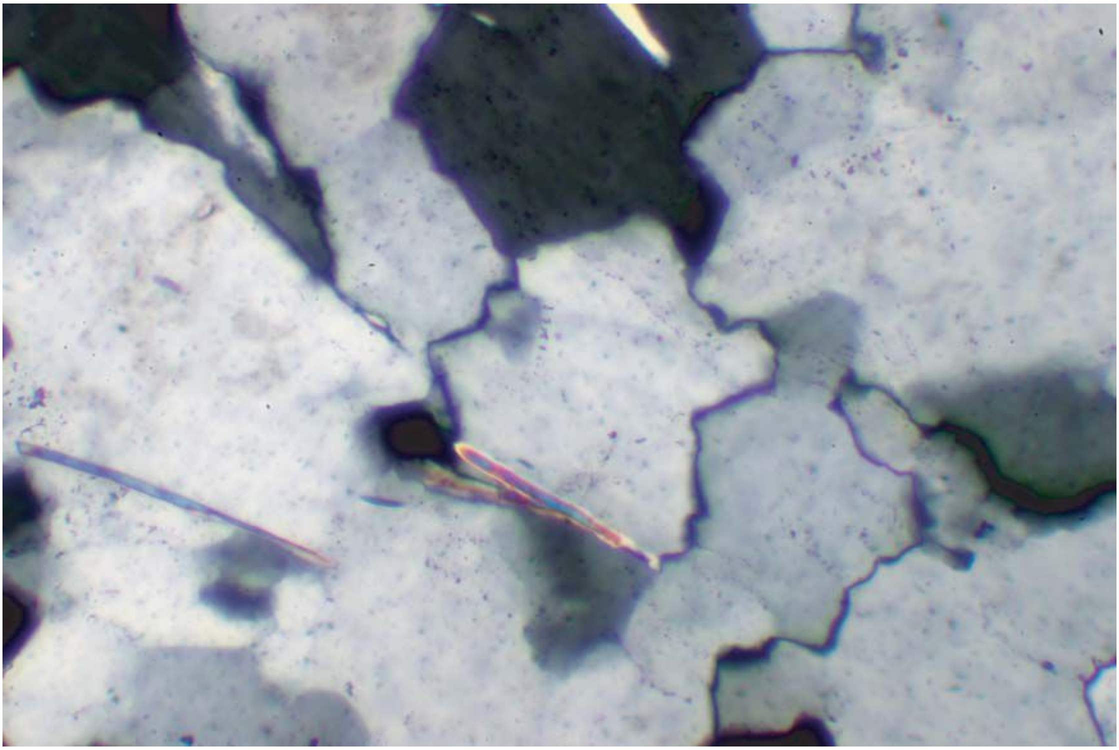

Fig. 5.30: (*cont.*)

5.4.3 Dynamic versus static recrystallization

In principle, recrystallization may occur either during deformation (*dynamic recrystallization* or *syndeformational recrystallization*) or after deformation (*static recrystallization*), which is equivalent to static grain growth (Section 4.2.1). Static recrystallization has been inferred to occur (1) if temperatures remain high enough for grain-boundary migration after strain rates decrease (by which process it could modify microstructures formed by dynamic recrystallization), and (2) in some contact metamorphic situations, involving heating of rocks deformed previously. However, the possibility of at least some deformation in these situations generally cannot be eliminated (see, for example, Vernon & Powell, 1976).

Dynamic recrystallization of low-melting-temperature minerals has been observed directly in *in situ* experiments in the microscope; for example in ice, using transmitted light (Wilson, 1986; Burg *et al.*, 1986; Wilson *et al.*, 1986), and stibnite, using reflected light (McQueen *et al.*, 1980). In addition, much experimental work has been carried out recently on transparent, low-melting-temperature, natural and synthetic materials that can be observed while being deformed and recrystallized in the microscope, such as halite, carnallite, bischofite, sodium nitrate, camphor, naphthalene, paradichlorobenzene and octachloropropane (Means, 1977, 1983, 1989; Tungatt & Humphreys, 1984; Means & Xia 1981; Jessell, 1986; Means & Jessell, 1986; Means & Ree, 1988; Urai, 1983a,b, 1987; Urai *et al.*, 1980a; Urai & Humphreys, 1981; Drury & Humphreys, 1988; Knipe, 1989; Blumenfeld & Wilson, 1991; Bons *et al.*, 1993; Bons & Jessell, 1999; Bauer *et al.*, 2000). This kind of study enables detailed observation of grain-boundary movements and changes in grain shapes with progressive deformation and recrystallization. For example, Urai (1983b) found that: (1) dynamically recrystallized grains do not necessarily have undulose extinction; (2) recrystallization may occur by grain- and twin-boundary migration (bulge nucleation) and progressive misorientation of subgrains; (3) recrystallization may occur along fractures; (4) grain boundaries may progress and regress cyclically; (5) one grain may be cut into two grains by grain-boundary movement; (6) two grains may coalesce into one; (7) incomplete elimination of serrations (bulges) may lead to the preservation of 'left-over grains'; (8) bimodal grainsize distributions may form; and (9) 'orientation families' of grains with similar orientations may develop, owing to different rates of boundary migration in different directions.

5.4.4 Microstructural criteria of dynamic versus static recrystallization

White (1977) suggested that dynamically recrystallized grains can be recognized by the presence of subgrains, deformation bands and deformation lamellae, in contrast to optically strain-free new grains expected from static recrystallization. This is especially clear where these strain features increase further away from the most recently recrystallized grains (White, 1977, p. 145). However, Urai (1983b) and Urai *et al.* (1986, p. 181) found that dynamically recrystallized grains do not necessarily have undulose extinction, which unfortunately removes a major optical criterion for recognizing the process. Nevertheless, new (recrystallized) grains with undulose extinction are at least consistent with dynamic recrystallization. In fact, as pointed out by Urai *et al.* (1986, p. 181), any evidence of deformation in new (recrystallized) grains is diagnostic of dynamic recrystallization, provided that the effects of a later phase of deformation can be eliminated (which may be impossible for many rocks). This evidence may be optical (e.g. subgrains) or observable in the transmission electron microscope, such as dislocation arrays, as discussed by White (1977).

'Orientation families' (Urai *et al.*, 1986) may also be reliable indicators of dynamic recrystallization. These are groups of several apparently independent grains with identical crystallographic orientations, which represent either (1) sections through projections or 'arms' from a grain of complex amoeboid shape or (2) remnants of such a grain that have been dissected by grain-boundary movement during dynamic recrystallization ('dissection microstructure'), as observed in *in situ* experiments in transmitted light (see, for example, Urai, 1983b).

Aggregates of relatively coarse-grained, optically strain-free polygonal grains such as those described in Section 4.2.1 have been interpreted as indicating static recrystallization (Voll, 1960, pp. 516–17). However, although these aggregates are consistent with static recrystallization, the fact that strain-free grains may be produced by dynamic recrystallization in experiments (see, for example, Urai *et al.*, 1986) casts some doubt on this interpretation. Some petrologists refer to static recrystallization as 'annealing recrystallization', but 'annealing' refers to a specific technological process involving heating without deformation, which is difficult to infer with confidence for natural rocks.

One potentially useful microstructural feature is the observation that boundaries of grains developing during strain-induced grain-boundary migration (dynamic recrystallization involving bulge nucleation) grow away from their centres of curvature, whereas the reverse applies to static grain growth (Section 4.2.1). However, strain-induced grain-boundary migration conceivably may occur long after deformation has ceased, in response to later heating (Section 4.11) under static conditions.

One of the difficulties in relating microstructures of prograde metamorphic rocks to deformation mechanisms is that increasing temperature promotes grain growth, which tends to remove intragranular evidence of deformation mechanisms, independently of deformation. Grain growth is especially active at the thermal peak, and may continue after the deformation has ceased, so that the result may be a coarse-, even-grained rock with no evidence of deformation processes (see, for example, Rutter & Brodie, 1990). This adds to the uncertainty surrounding the interpretation of strain-free polygonal aggregates.

5.4.5 Recrystallization and grainsize

In both subgrain rotation and strain-induced grain-boundary migration, the new grains are smaller than the original deformed grains, so that *grainsize reduction* is typical of dynamic recrystallization. However, the new grains tend to be much smaller at lower temperatures (250–300 °C for quartz and 400–450 °C for feldspar) and/or fast strain rates than at high temperatures (400–450 °C for quartz and >550 °C for feldspar) and/or slow strain rates. At the higher temperatures and slower strain rates, recrystallized grains tend to be larger than subgrains (though smaller than the original grains) and relatively equant (Tullis & Yund, 1991; Hirth & Tullis, 1992; Passchier & Trouw, 1996).

Experiments have suggested that the size of dynamically recrystallized grains varies inversely with the flow stress in single-mineral aggregates (see, for example, Post & Tullis, 1999; Tullis *et al.*, 2000). However, some caution is needed in making this inference for natural aggregates, because post-deformation grain growth may affect the grainsize.

5.4.6 Variation of recrystallization microstructure with temperature and strain rate

At relatively low temperatures (200–300 °C for quartz and 400–500 °C for feldspar) and/or fast strain rates, recrystallization mainly involves grain-boundary migration, which involves bulging of grain boundaries in response to variable dislocation concentrations, forming small strain-free grains. As the temperature rises and/or strain rate decreases, dislocation climb is facilitated and grains are more homogeneously flattened, resulting in elongate grains partly replaced by recrystallized aggregates. At temperatures lower than 400–500 °C, feldspar may recrystallize from fragmental aggregates (see, for example, Fitz Gerald & Stünitz, 1993a).

At high temperatures (>400 °C for quartz and >550 °C for feldspar) and/or slow strain rates, recrystallization occurs by subgrain rotation, as well as strain-induced grain-boundary migration (see, for example, Rosenberg & Stünitz, 2003). Original grains may be completely replaced by new (recrystallized) grains that are larger than the subgrains (Fig. 5.19). The resulting deformed grains may appear to be unstrained, but a strong crystallographic preferred orientation is common.

As noted previously (Section 5.4.3), grain-boundary migration recrystallization is restricted to relatively high temperatures, namely amphibolite facies conditions for quartz and calcite (Schmid *et al.*, 1980, 1987; Schmid & Casey, 1986; Fitz Gerald & Stünitz, 1993a) and granulite facies conditions for feldspar (Lafrance *et al.*, 1995).

Experimental studies on quartz aggregates have revealed three regimes of dislocation creep, defined by different mechanisms of dynamic recrystallization (Hirth & Tullis, 1992; Tullis *et al.*, 2000). These regimes operate at different temperatures and strain rates, and produce different microstructures. These microstructures have also been recognized in naturally deformed quartzites, but they form at much lower temperatures, owing to the slower natural strain rates.

Regime 1 occurs at the lowest temperatures of deformation, and is characterized by difficult dislocation climb, low grain-boundary mobility and high dislocation concentration contrasts between different grains. Dislocation glide is accommodated by recovery and strain-induced grain-boundary migration (bulging recrystallization) at slow rates, producing very small bulges. The bulging occurs mainly at triple junctions and along fractures, if present. *Regime 2* is characterized by recrystallization involving progressive subgrain rotation, and occurs at intermediate temperatures. *Regime 3* is characterized by grain-boundary migration recrystallization at fast rates, and occurs at high temperatures; during this recrystallization, whole grains may be swept clear of dislocations, and subgrain rotation is only important for the initial formation of new grains. Stipp *et al.* (2002) observed microstructural evidence of all three regimes in a mylonite zone in the Italian Alps, in which dynamic recrystallization occurred over a temperature range from 280 °C to 700 °C (inferred from syndeformational mineral assemblages).

Regime 1 has also been identified in experimentally deformed feldspar, and regimes 2 and 3 have been inferred from the microstructures of high-grade naturally deformed anorthosites (Lafrance *et al.*, 1995, 1998; Tullis *et al.*, 2000). Thus, inference of the temperature or strain rate of natural deformation events in feldspathic and quartzofeldspathic rocks could conceivably be made by comparing dislocation-creep microstructures with microstructures of experimentally deformed samples. Dislocation creep in natural feldspar (inducing, and so evidenced by, recrystallization) is usually found above temperatures of approximately 500 °C (Tullis *et al.*, 2000), whereas below these temperatures, deformation typically takes place by fracturing. However, neocrystallization (driven by compositional change as well as by strain energy) may occur at temperatures much lower than 500 °C in deformed rocks (see, for example, Fitz Gerald & Stünitz, 1993a). If the chemical compositions of new and old (host) grains are identical, dynamic recrystallization is indicated, but if they are markedly different, neocrystallization is suggested.

In quartz–feldspar rocks, quartz may deform in one regime and feldspar in another. For example, experimental deformation of a natural aplite has shown that at lower temperatures the feldspar is semi-brittle and the quartz deforms by regime 1 dislocation creep, whereas at higher temperatures the feldspar deforms by regime 1 dislocation creep and the quartz deforms by regime 2 dislocation creep (Dell'Angelo & Tullis, 1996; Tullis *et al.*, 2000).

Some (e.g. Kruhl, 1996, 1998) have suggested that microstructural evidence of deformation temperature regimes may be used to complement mineralogical and/or chemical methods of P–T determination (see, for example, Spear, 1993). Efforts are now being made to relate deformation effects to calculated P–T conditions, in order to develop reliable microstructural criteria.

5.4.7 'Core-and-mantle' microstructure

Microstructural evidence of recrystallization commonly takes the form of relatively small strain-free grains surrounding relics of large, strained grains (with kink bands, subgrains or undulose extinction), as produced experimentally (Figs. 5.17, 5.18, 5.22–5.26). This used to be called 'mortar texture', on the assumption that the small grains represent original fragments, but is now known as *core–mantle* or *core-and-mantle* microstructure. It is generally inferred to be due to dislocation creep and recovery (see, for example, S. H. White, 1977; Drury & Humphreys, 1986; Urai *et al.*, 1986; J. C. White, 1990), but see Section 5.4.8. It typically involves progressive misorientation of subgrains from core to mantle (recrystallization by subgrain rotation), and has been produced experimentally (see, for example, Hobbs, 1968). The microstructure is well shown in deformed gneissic rocks of granitic composition (Vernon *et al.*, 1983), deformed marbles (Vernon, 1981), deformed peridotites (Poirier & Nicolas, 1975), deformed anorthosites (Kehlenbeck, 1972; Lafrance *et al.*, 1995, 1998) and some deformed sulphide rocks involving galena and chalcopyrite (McClay, 1983).

5.4.8 Brittle versus ductile precursors of recrystallized grains

Although core-and-mantle microstructure is generally inferred to be due to dislocation creep and recovery, optically it may be difficult to distinguish the products of this process from those formed by fracturing (cataclasis) along fault-like zones to produce small fragments, followed by heating, which can cause the fragments to grow together ('sinter') to form recrystallized-looking aggregates (Sections 4.2, 4.6, 5.4.2). This problem for plagioclase has been pointed out by Vernon (1975), Fitz Gerald & Stünitz (1993a) and Tullis *et al.* (1990), and for various minerals by Vernon *et al.* (2004). For example, Brodie & Rutter (1985) pointed out that aggregates of polygonal amphibole grains, which are usually taken to indicate recrystallization in response to plastic deformation, may result from the growing together of fragments formed by cataclasis.

A fracture mechanism for the development of core-and-mantle structures in amphibole has been proposed by Nyman *et al.* (1992) and Ross & Wilkes (1996). Moreover, Bell (1978b, 1979) suggested that small, misoriented, partly detached, kink-like volumes inside biotite grains may rotate and grow into new grains during deformation. The possibility that some 'decussate' aggregates of biotite may result from recrystallization of fragments has been suggested by Vernon *et al.* (2004). Furthermore, Means (1989, fig. 7g, p. 173) observed thymol deforming by brittle processes in the microscope to produce a 'cataclasite', after which the aggregate transformed (by plastic deformation of the fragments, dynamic recrystallization and void-healing) into an aggregate closely resembling a typical quartz mylonite (Section 5.7.6). This is a reminder that 'some microstructures in rocks may have short memories of complex histories' (Means, 1989, p. 1973).

As a result of their experiments on octachloropropane, Bons & Jessell (1999) suggested that, in some instances, heterogeneous or even brittle deformation may be involved in the formation of apparently recrystallized aggregates. They suggested that mobile microshear zones dissect the outer parts of grains, the shear causing rotation of lenses ('subgrains' or fragments) between the shear zones (Bons & Jessell, 1999, fig. 5). The amount of rotation varies from lens to lens, resulting in progressive misorientation. Because the microshear zones are localized at the edges of the deforming grains, repeated dissection produces more 'subgrains' with a progressive misorientation from core to rim, and forms a typical core-and-mantle structure (Bons & Jessell, 1999). Microshear zones in granite deforming in the margin of the San José tonalite pluton, México, have been described by Vernon *et al.* (2004) and Johnson *et al.* (2004).

The TEM observations (mentioned in Section 5.3.1) of Tullis & Yund (1987) of microcrush zones inside feldspar that optically appear to have deformed in a ductile manner suggest that some zones of apparent recrystallization inside feldspar grains (as observed in the light microscope) could represent brittle crush zones that have been heated, inducing grain growth and the formation of polygonal aggregates resembling those produced by recrystallization of minerals deformed by plastic deformation (Vernon, 1975; Stünitz, 1998).

Den Brok *et al.* (1998) pointed out that about forty years ago subgrains and recrystallized grains in quartz were typically interpreted as being due to water-assisted brittle processes, whereas this interpretation has been almost completely supplanted by dislocation creep, owing to comparison with metal microstructures and TEM observations of experimentally and naturally deformed minerals. However, some recent experiments on quartz have revealed evidence of fracturing and water-assisted healing of fractures, producing features optically identical to natural subgrains and recrystallized grains (den Brok & Spiers, 1991; den Brok, 1992). This interpretation may apply especially to subgrain boundaries marked by lines of fluid inclusions, implying access of water along fractures that later healed. Alternatively, it may be argued that fractures follow existing subgrain boundaries. Moreover, many subgrains do not show fluid inclusions. Den Brok *et al.* (1998) performed long-term deformation experiments on crystals of the soluble, brittle compound sodium chlorate ($NaClO_3$), which they used as an analogue of quartz. The material deformed slowly by cataclastic creep, resulting in dissolution structures at highly stressed sites, which developed into very fine, aligned channel-like features, which in turn developed into fractures. The fractures migrated by solution transfer, producing polygonal aggregates of fragments that resembled grains characteristic of dynamic recrystallization.

All these observations suggest that we should have some reservations about inferring dislocation creep on the basis of optical observations alone. As noted by Tullis & Yund (1987), cataclastic flow is probably an important deformation mechanism in rocks, but may be overlooked because of misinterpretation of the resulting optical microstructures and because the resulting fine grainsize facilitates introduction of fluid, which can promote (1) formation of hydrous minerals (see, for example, O'Hara, 1988) or (2) a change to diffusion creep (Tullis *et al.*, 1996). The problem has been emphasized by Vernon *et al.* (2004) and Johnson *et al.* (2004), in relation to the deformation of partly crystallized granite intrusions. On the other hand, some mylonitic augen-type microstructures (Section 5.7.6) produced experimentally by ductile deformation (dislocation creep accompanied by grainsize reduction by recrystallization, discussed below) have been misinterpreted as being due to cataclastic flow, as pointed out by Tullis & Yund (1987).

5.5 Deformation of polymineral aggregates

5.5.1 Deformation contrasts between minerals in rocks

As mentioned previously, ductile behaviour of minerals and rocks is generally defined as the capacity to deform without fracturing on the grain scale (see, for example, Passchier & Trouw, 1996, p. 21). However, ductility has also been defined as ‘the capacity for substantial change of shape without gross fracturing’ (Paterson, 1978). This definition refers to megascopic or macroscopic flow, and is independent of the microscopic mechanisms of deformation, which can include not only crystal plasticity and diffusional flow (which maintain cohesion at the microscopic scale), but also cataclastic (microscopically brittle) mechanisms. In other words, on the basis of this definition, a rock can be ductile on the scale of a hand specimen or outcrop, but partly brittle on the microscope scale. However, in this book, the microscopic definition of ductility is used, to avoid confusion.

A major factor governing ductility is the number of slip systems available for deformation to occur without producing holes or cracks (Murrell, 1990). Five independent slip systems are necessary for plastic deformation without fracturing at grain boundaries (Groves & Kelly, 1963). However, as mentioned in Section 5.3.3, many minerals have strongly anisotropic structures (e.g. mica, kyanite) and so have fewer slip systems than those with more less-isotropic structures (e.g. quartz, olivine). The result is that some minerals are able to change their shapes in response to general local stress fields more readily than others. This can lead to localization of deformation into high-strain zones (Section 5.7.1) or to the opening of pores or local cracks, which are important in localizing fluids (Section 5.9) and melts (Section 5.11).

This situation produces deformation contrasts between different minerals, which occur when stronger and weaker minerals coexist. Natural rocks typically have several minerals with different deformation properties that can vary with external conditions (e.g. temperature, pressure, water activity). For example, strong feldspar and weak quartz typically coexist in granite deforming at relatively low temperatures (<500 °C). The feldspar deforms plastically a little before it fractures (brittle deformation), whereas the quartz flows and recrystallizes in a ductile manner (Figs. 5.2, 5.9, 5.31), commonly forming ‘ribbons’ of fine-grained recrystallized aggregates (Figs. 5.9, 5.31). The ribbons originate as kink bands or deformation bands that recrystallize with progressive deformation (Fig. 5.9). At temperatures greater than about 500 °C, dislocations can glide and climb more easily, so that feldspar weakens, but generally remains stronger than quartz (Tullis, 1983), though the reverse situation may apply if the feldspar is sufficiently fine-grained (Fitz Gerald & Stünitz, 1993b).

Another example is gabbro deforming at high temperatures (around 1100 °C) and differential stresses of less than 10 MPa, at which olivine is ductile, showing subgrains and evidence of dislocation creep, whereas plagioclase and pyroxene are strong, showing no evidence of dislocation creep (Yoshinobu & Hirth, 2002). Other examples of minerals deforming in different ways in the same rock are: (1) partly serpentinized peridotite, in which olivine deforms by dislocation creep involving recrystallization, but serpentine deforms by bending and kinking, owing to its much more strongly anisotropic atomic structure (Fig. 5.32); and (2) experiments in which plagioclase deforms by dislocation creep and

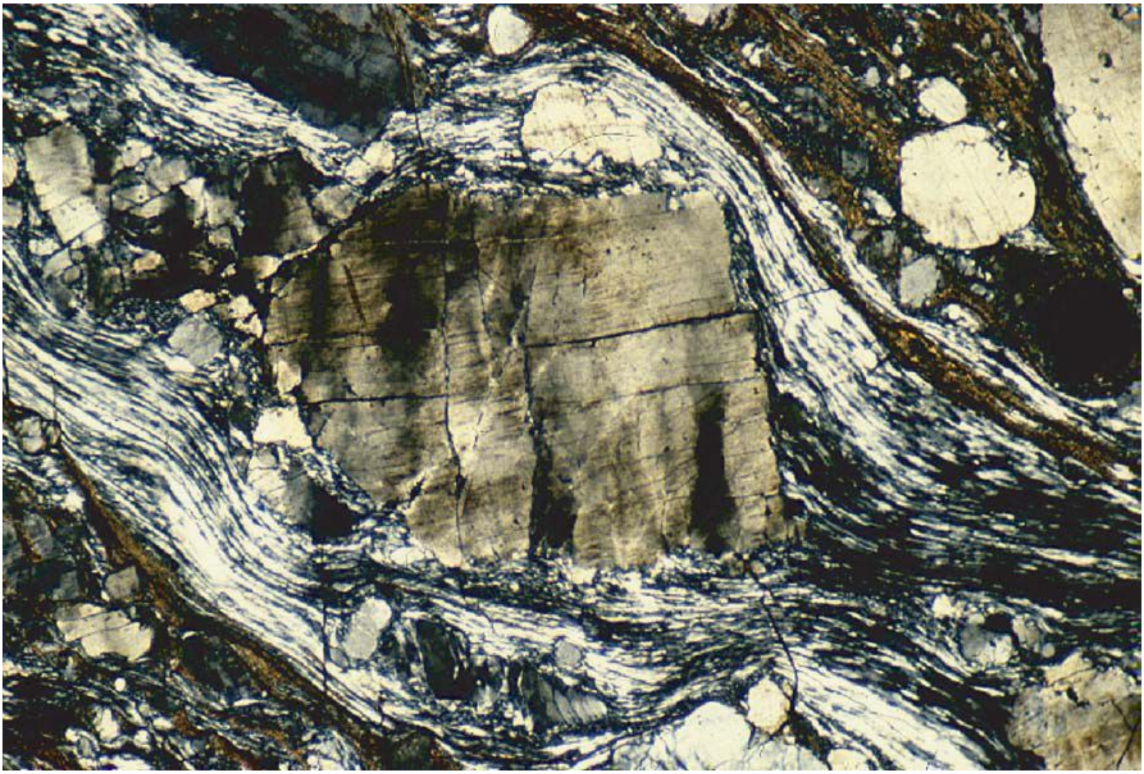

Fig. 5.31: Mylonite from east of Armidale, New England, New South Wales, Australia, showing marked contrast between quartz, which has flowed plastically and recrystallized to fine-grained aggregates with 'ribbon microstructure' (Section 5.5.1), and plagioclase, which shows evidence of much less plastic deformation and extensive fracturing and fragmentation. Also shown are thin folia of very fine-grained biotite (brown), which, like the quartz, has flowed and recrystallized readily. An early stage of the formation of quartz 'ribbons' is shown in Fig. 5.9. From Vernon (2000b, fig. 163). Crossed polars; base of photo 1.4 cm.

hornblende deforms by fracturing and mechanical rotation of fragments (Ross & Wilks, 1996).

Evidence of both ductile and brittle behaviour is seen in many felsic mylonites (Section 5.7.6), in which feldspar deforms cataclastically, whereas quartz and mica deform mainly by dislocation creep, commonly assisted by neocrystallization (Vernon *et al.*, 1983; O'Hara, 1988). On the other hand, in some deformed granites and granitic mylonites, biotite deforms by fracturing along the cleavage, forming 'shreds' or cleavage platelets that become stretched out along a developing foliation (Mancktelow, 1985; Vernon *et al.*, 2004; Johnson *et al.*, 2004), as indicated by some experimental results (Shea & Kronenberg, 1993).

Though fluid-enhanced microcracking is commonly an important deformation mechanism in these rocks, both brittle and ductile processes alternate, and

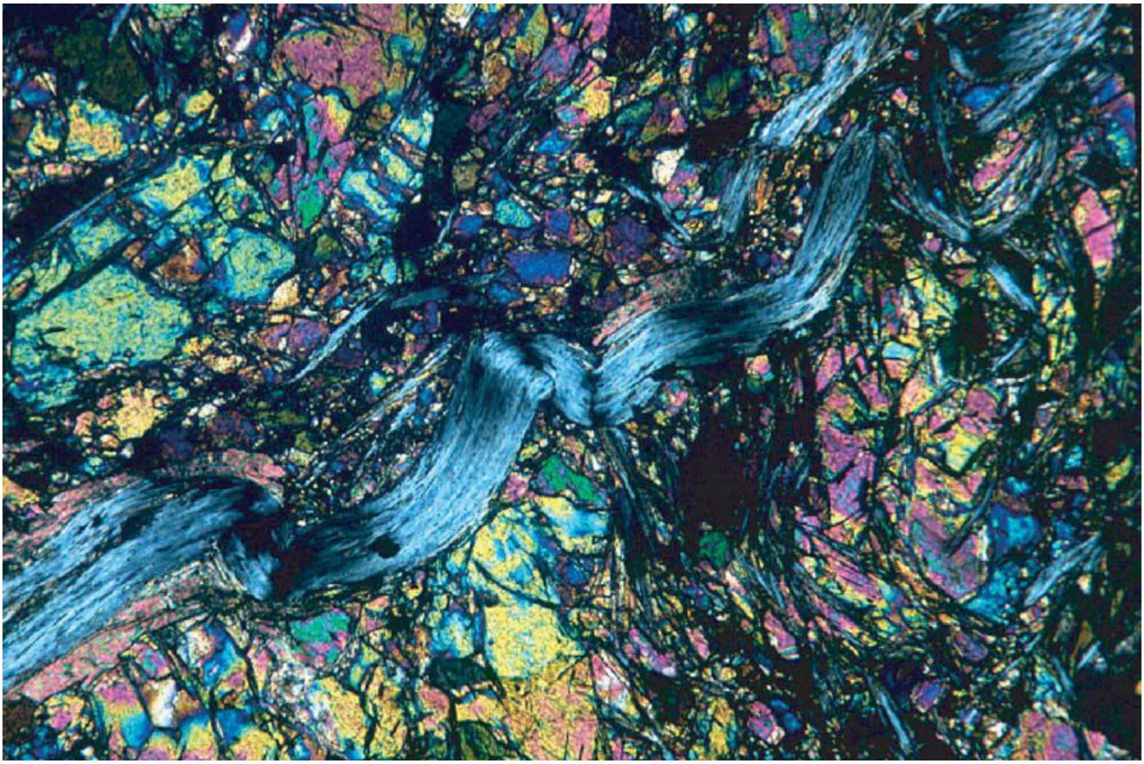

Fig. 5.32: Microfolds and kink bands in folia of serpentine (with anomalous grey-blue interference colours), in contrast to recrystallized olivine, in a deformed peridotite from Sweden. From Vernon (2000b, fig. 45). Crossed polars; base of photo 1.9 mm.

cohesion is maintained during the deformation (see, for example, White & White, 1983; Stel, 1986; Gapais, 1989). This has been referred to as 'semi-brittle' behaviour. Simultaneous fracture and flow have been observed in a hydrous mixture of potassium alum and mica deformed in the microscope (Means, 1977). In some rocks, hydrous minerals growing from fluids that enter the rock during brittle deformation undergo ductile deformation (Simpson, 1986; Stel, 1986), which may be followed by more fracturing and mineral growth, in a cyclic process (Stel, 1986).

In many rocks, deformation is so heterogeneous that it is strongly partitioned into zones rich in weak minerals, such as mica (Shea & Kronenberg, 1993; Goodwin & Tikoff, 2002; Johnson *et al.*, 2004) and/or fine-grained aggregates (Fitz Gerald & Stünitz, 1993b), promoting the formation of local zones of high-strain (shear zones), as discussed in Sections 5.7.1 and 5.7.6. In their experimental deformation of schists and gneisses, Shea & Kronenberg (1993) found that strain was localized in mica-rich folia (microshear zones) linked by fractured bridges of the stronger minerals quartz and feldspar; the mica deformed by both dislocation glide and grain-scale microcracking. Goodwin & Wenk (1990, 1995) found that biotite in a granitic mylonite at greenschist facies conditions deformed by fracturing and slip along cleavage (cataclastic flow), after which deformation continued by dynamic recrystallization, intracrystalline slip and mechanical rotation of grains, to produce a strong preferred orientation; the cataclasis localized the subsequent ductile flow. Vernon *et al.* (2004) and Johnson *et al.* (2004) observed microstructural evidence of partitioning of deformation into mica-rich zones in the marginal deformation of a tonalite pluton.

5.5.2 Effect of grainsize

Large grains generally deform more readily by dislocation flow than do smaller individual grains of the same mineral, probably because intracrystalline slip can occur with less interference from adjacent grains (see, for example, Rutter, 1976). However, in many rocks, large grains (phenocrysts and porphyroblasts) are stronger than surrounding finer-grained aggregates of different minerals, especially where the groundmass or matrix consists of finer-grained aggregates of weaker minerals (e.g. quartz and mica). The reason is that intergranular deformation is important in fine-grained aggregates (e.g. grain-boundary sliding, reaction-assisted diffusion), leading to increased strain rates (Etheridge & Vernon, 1981; Fitz Gerald & Stünitz, 1993b). This is especially the situation where a fine-grained matrix (metamorphic rock) or groundmass (igneous rock) is present originally, but also applies where a fine-grained matrix is produced by deformation and/or recrystallization during the deformation, as in mylonitic rocks (Section 5.7.6). However, as pointed out by de Bresser *et al.* (2001), dynamic recrystallization can lead to major zones of weakening and strain localization only if grain growth is inhibited, as in typical mylonite zones.

Examples of large strong grains are: (1) K-feldspar megacrysts in deforming granites (Vernon, 1986a); (2) quartz phenocrysts in deforming felsic volcanic rocks (Etheridge & Vernon, 1981; Vernon, 1986a; Williams & Burr, 1994); and (3) porphyroblasts in mica schists.

Deformation and accompanying recrystallization/neocrystallization of coarse-grained rocks (such as granites) involves grainsize reduction and foliation/lineation development (see, for example, Vernon *et al.*, 1983), both of which assist further deformation by (a) providing fine-grained, weaker aggregates and (b) partitioning deformation into more actively deforming zones (e.g. 'C-surfaces' in shear zones, as discussed in Section 5.7.6). For example, during the deformation of granites, K-feldspar megacrysts are commonly replaced at their margins by fine-grained myrmekite aggregates. These aggregates become progressively recrystallized to form fine-grained polygonal aggregates that develop into folia (Vernon *et al.*, 1983; Tsurumi *et al.*, 2003).

Another example is provided by some peridotite massifs, in which local shear zones are produced by grainsize reduction due to dynamic recrystallization at relatively high stress and moderate temperature (Jin *et al.*, 1998).

5.6 Metamorphic reactions during deformation

5.6.1 General aspects and effects of water

Chemical reactions typically accompany and affect deformation. They (1) provide new strain-free grains and so assist deformation, (2) may release or consume fluid, which affects mineral deformation, and (3) may produce stronger minerals ('reaction strengthening') or weaker minerals ('reaction weakening'), as discussed in the following sections. Rocks weakened or strengthened by metamorphic reactions in turn affect the future strain of those rocks (Wintsch & Dunning, 1985).

Conversely, deformation can assist metamorphic reactions. For example, Koons *et al.*, (1987) presented evidence that disequilibrium mineral assemblages in local microstructural domains grew in the earlier stages of deformation of a quartz diorite at eclogite facies conditions. The mineral compositions were controlled by proximity to reactant minerals and not by the bulk chemical composition of the rock. With increasing deformation, the equilibrium domains progressively enlarged, as the mineral compositions partly equilibrated to the bulk composition.

In addition, non-hydrostatic stress can assist processes such as exsolution (Kirby & Etheridge, 1981; Kirby & Stern, 1993), polymorphic transformations (Hacker & Kirby, 1993; Kirby & Stern, 1993) and local transfer of chemical components (Selverstone & Hyatt, 2003).

Studies that emphasize relationships between deformation and metamorphic reactions include: Max (1970), Wintsch (1978, 1985), White & Knipe (1978b), White *et al.* (1980), Brodie (1981), Kirby & Etheridge (1981); Rubie (1983); Wintsch & Knipe (1983), Vernon *et al.* (1983), Brodie & Rutter (1985), Knipe & Wintsch (1985), Murrell (1985), Stel (1986), Simpson (1986), Koons *et al.* (1987), Wheeler (1987), Rutter & Brodie (1988a,b), Cumbest *et al.* (1989), Dipple *et al.* (1990), Selverstone *et al.* (1991), Yund & Tullis (1991), Kirby & Stern (1993), Hacker & Kirby (1993), Fitz Gerald & Stünitz (1993a,b), Altenberger (1995b), Connolly (1997) and Stünitz (1998).

For example, Yund & Tullis (1991) found experimentally that deformation enhances exchange of chemical components between plagioclase grains of different composition. They concluded that the rate of chemical and isotopic exchange between minerals may be enhanced by deformation. Processes involved may be: (1) grainsize reduction, which provides shorter distances for diffusion of components; (2) dissolution and growth of grains by diffusion creep; and (3) movement of high-angle grain boundaries through deformed grains during recrystallization involved in dislocation creep, which provides paths of rapid diffusion.

Fluids can be very important in the deformation of rocks, for both physical and chemical reasons (see, for example, Rubie, 1986; Carter *et al.*, 1990; Kronenberg *et al.*, 1990; Rutter & Brodie, 1985; Tullis *et al.*, 1996). The following are examples of the effects of fluid. (1) Water increases the diffusivity of grain boundaries, assisting grain-boundary sliding (Rutter, 1972; White & Knipe, 1978b; Etheridge & Wilkie, 1979) and increasing the rates of chemical reactions. (2) Water promotes 'water weakening' inside grains (see, for example, Griggs, 1967, 1974; Griggs & Blacic, 1965; Blacic, 1972, 1975; Linker & Kirby, 1981; Blacic & Christie, 1984), although the mechanism for this process is unclear (Ord & Hobbs, 1986; Fitz Gerald *et al.*, 1991). (3) Water opens transient fractures as the local fluid pressure exceeds the local minimum compressive stress plus the local tensile strength of the rock in the direction of fracture opening (hydraulic fracturing or 'hydrofracturing'), reducing the effective mean stress, especially along grain boundaries. Fluid produced by prograde reactions must escape from the reaction sites for the reactions to proceed (Vernon, 1976), and process (3) could allow this to happen.

In addition, minute spaces between grains open during deformation, owing to (1) deformation contrasts between different minerals and (2) volume changes between reactant and product minerals in metamorphic reactions. These pockets of lower pressure 'suck in' fluid, so that zones of strong deformation may act as fluid channels. Such channels are potentially important for (a) fluid removal from rocks undergoing prograde metamorphism, (b) fluid introduction to rocks undergoing retrograde metamorphism, (c) melt transfer in rocks undergoing partial melting during high-grade metamorphism (Section 5.11.4), and (d) transfer of metal-bearing hydrothermal fluids in the formation of many metallic ore deposits.

Addition of water may also increase plasticity in rocks undergoing both brittle and ductile deformation processes at low temperatures, by mobilizing tangled dislocations, and so enhancing recovery and dynamic recrystallization in minerals that previously had undergone strain hardening (Liu *et al.*, 2002).

The scale of the effects of water in deforming metamorphic rocks is very variable. In prograde regional metamorphism, water is available pervasively on the regional scale, whereas in retrograde metamorphism it is available more locally, mainly in shear zones.

5.6.2 Reaction strengthening

A good example of reaction strengthening ('hardening') is the formation of porphyroblasts of strong minerals, such as cordierite, K-feldspar, andalusite and garnet, at high temperatures in the prograde metamorphism of shales. This makes metashales stronger than interbedded metasandstones (Vernon & Johnson, 2000; Vernon *et al.*, 2000, 2003) at high metamorphic grades, whereas the reverse is typically true at low and medium grades, where the more abundant, fine-grained quartz–mica matrix causes metashales to be weaker.

Dehydration reactions generally produce stronger minerals. However, they may produce transient fine-grained reaction products that can deform readily by grain-boundary sliding (see, for example, Schmid, 1976; White, 1976) and localize deformation in narrow zones. This process may occur also in reactions that do not involve fluids, such as the replacement of plagioclase by fine-grained jadeite and quartz at eclogite facies conditions (see, for example, Rubie, 1983).

However, the process can continue only until grain coarsening removes the weakening effect (White & Knipe, 1978b), which may be relatively short-lived, as in serpentine reacting to form olivine in experiments by Rutter & Brodie (1988b).

This concept of transitory reaction-enhanced ductility during prograde metamorphism led White & Knipe (1978b) to suggest that rocks are weakest during metamorphic reactions, and that deformation may be most intense when new minerals are being produced, before grain coarsening occurs. This inference is discussed in relation to porphyroblast growth in Section 5.10.2. Rubie (1986) extended the idea by suggesting that development of equilibrium mineral assemblages and microstructures in metamorphic rocks generally occurs in short time periods under transitory fluid-present conditions, caused by devolatilization reactions and/or infiltration of external fluid. Movement of fluid and consequent reaction enhancement would be assisted by deformation and *vice versa*.

5.6.3 Reaction weakening

Reaction weakening ('softening') can operate by (1) forming weaker minerals from strong minerals (e.g. chlorite from garnet; muscovite from feldspar), (2) grainsize reduction (e.g. the formation of fine-grained reaction products in deforming plagioclase and biotite undergoing alteration during the deformation of granites), and (3) pervasive release of water in prograde dehydration reactions.

A good example of reaction weakening is the replacement of feldspar by fine-grained aggregates rich in muscovite during hydration (e.g. in retrograde metamorphism). These aggregates deform much more easily than the original feldspar. Therefore, in volcanic rocks, feldspar phenocrysts may alter to these aggregates, which deform and so become part of the flowing former groundmass, leaving unaltered quartz phenocrysts as relics (Vernon, 1986b; Williams & Burr, 1994). Such 'quartz-eye rocks' (Fig. 4.75) are common in altered volcanic sequences associated with some orebodies, and the residual quartz phenocrysts have often been misinterpreted as porphyroblasts; this obscures the volcanic origin of the rocks and so can lead to incorrect ore-search models. The residual volcanic nature of the 'quartz-eyes' is shown by the common occurrence of embayments, which may persist even in rocks deformed at amphibolite facies conditions (Fig. 4.75), owing to the relative strength of the large quartz crystals compared with the fine-grained mica-bearing matrix (Vernon, 1986b; Williams & Burr, 1994).

A second example of reaction weakening is provided by schists in the Foothills terrane, central Sierra Nevada, California, where a prograde reaction converted porphyroblasts of cordierite to much finer-grained aggregates of biotite and white mica (Vernon *et al.*, 1993b). The new aggregates were weaker than the original cordierite under the prevailing conditions, and were drawn out into thin lenses, although adjacent porphyroblasts of andalusite, which are unaltered, remained strong and so preserved their original shapes (Fig. 4.17).

A third example of reaction weakening is provided by deformed granitic gneisses deformed at shallow crustal levels, in which the feldspar undergoing brittle deformation alters to weaker kaolinite as a result of water access (Evans, 1988).

A fourth example of reaction weakening is provided by stress concentrations produced on the high-stress sides of quartz clasts, causing stress-induced solution of some chemical components, which changed the local chemical composition sufficiently to promote the crystallization of porphyroblasts of the aluminous minerals staurolite, kyanite and chlorite (Selverstone & Hyatt, 2003). The stress gradients are caused by the differences in deformability of the quartz pebbles and the finer-grained quartz–mica matrix.

Not only are some new minerals inherently weaker than the original mineral, but if the new grainsize is much smaller, this may also assist deformation, for example by inducing diffusion-accommodated grain-boundary sliding (Stünitz, 1993; Stünitz & Tullis, 2001). Moreover, this need not be a transitory effect, as discussed previously for prograde reactions (Section 5.6.2), but may persist throughout subsequent deformation (see, for example, Etheridge & Vernon, 1981; Vernon *et al.*, 1983), provided grain growth is restricted, as is commonly the situation in retrograde metamorphism. Excellent examples are provided by the mylonitic deformation of some granites described by Fitz Gerald & Stünitz (1993b) and the experimentally observed weakening effect of fine-grained aggregates formed by chemical reactions in plagioclase (Stünitz & Tullis, 2001). Other examples are deformed metagabbros, in which pyroxene and hornblende neocrystallize to fine-grained actinolite, and plagioclase neocrystallizes to fine-grained albite and zoisite (Stünitz, 1993).

5.6.4 Deformation during prograde metamorphic reactions

Effects of deformation (with consequent enhanced access of water) on retrograde metamorphic reactions (Section 5.6.5) and *vice versa* have long been appreciated, but effects of deformation on prograde metamorphic reactions and *vice versa* are equally important. As water is pervasively released at the grain scale by dehydration reactions, it has a potential weakening effect, as discussed previously (Section 5.6.2), and this is likely to occur through relatively large rock volumes, compared with the relatively local effect of water in retrograde metamorphism.

In low-P/high-T regional metamorphism, granite intrusions may cause metamorphism to commence prior to foliation-forming deformation (Vernon *et al.*, 1993a). The heating and pervasive release of water in the resulting dehydration prograde reactions, together with initial small grainsizes of product minerals, may promote deformation, which in turn may assist reactions. As mentioned previously (Section 5.6.2), White & Knipe (1978b) suggested that rocks are weakest during metamorphic reactions, and that deformation may be most intense when new minerals are being produced, before grain coarsening occurs. However, this coarsening effect may not apply to porphyroblasts; these grow very rapidly compared with matrix minerals, which remain fine-grained and so potentially susceptible to fluid-induced grain-boundary sliding.

The following examples illustrate various ways in which prograde metamorphic reactions can contribute to deformation (see, for example, Rutter & Brodie, 1985, 1990; Murrell, 1985).

(1) As discussed previously (Section 5.6.2), transient, fine-grained reaction products may permit grainsize-sensitive flow processes (e.g. grain-boundary sliding and possibly even superplasticity), until sufficient grain growth eliminates this possibility (White & Knipe, 1978b; Rutter & Brodie, 1990).

(2) Transient pore fluid pressures are increased by devolatilization (especially dehydration) reactions, which reduce the effective lithostatic pressure, and so may promote local cataclastic deformation. An experimental example is the dehydration of serpentinite (Raleigh & Paterson, 1965). Grain-scale hydrofracturing is probably a component of deformation in nearly all metamorphic rocks undergoing prograde metamorphism, because most prograde reactions liberate fluid (water or carbon dioxide mainly, depending on the reacting minerals), which must escape from the reaction site for the reaction to proceed. If the fluid pressure locally exceeds the minimum normal compressive stress (σ_3) plus the tensile strength of the rock, a fracture must form, even if only small and transient (Etheridge *et al.*, 1983, 1984). Opening, propagation and closing of these transient fractures appears to be an effective way of removing fluids from reaction sites at realistically rapid rates, and may also contribute to deformation. Thus, deformation during prograde metamorphism may be a combination of grain-scale ductile and cataclastic processes, although the overall process can be viewed mesoscopically as 'non-cataclastic ductile flow', because ductile processes probably dominate over fracture processes, and because evidence of the transient fractures is generally not visible.

(3) At higher metamorphic grades, partial melting may liberate melt pervasively and so cause weakening, especially by hydraulic fracturing (Carney *et al.*, 1991, p. 468).

(4) Mineral volume changes may relate to deformation. For example, Brodie (1995) described symplectites of plagioclase + orthopyroxene + spinel oriented parallel to the foliation and the regional stretching direction. She inferred that the symplectite grew in dilatant (expanded) sites, being inhibited in high-stress sites, owing to the volume increase of the symplectite-forming reaction.

(5) Fine-grained aggregates of jadeite and quartz produced by replacement of plagioclase at eclogite facies conditions may be highly ductile, leading to the formation of mylonitic rocks (Rubie, 1983).

(6) Some reactions may depend as much on deformation as on temperature at low grades of metamorphism. For example, Dempster & Tanner (1997) found that the biotite-forming reaction in metapelites in the Garonne dome, Central Pyrenees, strongly depended on deformation. The biotite formed from breakdown of

chlorite and white mica over a temperature interval (i.e. in a continuous prograde reaction). Because of slow diffusion rates in the white mica, the biotite-forming reaction occurred only in zones of active deformation. Dempster & Tanner (1997) concluded that such continuous reactions and the isograds inferred from them should not be regarded as being controlled only by temperature.

(7) Rocks that are dry and unreactive during prograde metamorphism may resist deformation, and so may preserve sedimentary and igneous structures into the highest metamorphic grades (see, for example, Tobisch, 1955; Vernon *et al.*, 1990; Vernon & Johnson, 2000). This assists in the determination of parent rock-types (Section 4.15). On the other hand, water introduced from nearby dehydrating rocks can cause local weakening in otherwise dry rocks (see, for example, White & Knipe, 1978b; Rubie, 1983, 1986).

5.6.5 Deformation during retrograde metamorphic reactions

Fluids are particularly important in retrograde metamorphism, and are closely related to deformation. The importance of grain-scale hydrofracturing in prograde metamorphism may also apply in retrograde metamorphism, in which the devolatilization reactions of prograde metamorphism are reversed (see, for example, Vernon & Ransom, 1971; Vernon, 1976). In retrograde metamorphism, reaction rates depend on the supply of fluid (mainly water or carbon dioxide, depending on the reactions concerned) from an external source (see, for example, Yardley *et al.*, 2000). The fluid must reach local reaction sites, and the most effective way for it to do this at realistic rates is to penetrate along transient microfractures that open during deformation.

Because retrograde metamorphic reactions require addition of volatile components (e.g. water), the development of reaction products is commonly patchy and incomplete, except in high-strain zones, through which water can pass. For example, Max (1970) described schistose amphibolite zones anastomosing around pods of unmetamorphosed dolerite. Also, at Broken Hill, Australia, granulite facies metamorphism uniformly dehydrated the rocks, after which they fractured during cooling, allowing water back into the rocks to form shear zones with lower amphibolite facies mineral assemblages. The shear-zone rocks are fine-grained, neocrystallized schists and mylonites, with few or no high-grade relics, but elsewhere the retrograde reactions were patchy, incomplete and pseudomorphous, owing to restricted deformation and access of water (Vernon & Ransom, 1971; Corbett & Phillips, 1981).

5.6.6 Cyclic reactions in deforming granites

Deformed granites provide good examples of the interaction of metamorphic reactions and deformation (see, for example, Kerrich *et al.*, 1980). As mentioned previously, deformation of coarse-grained rocks, such as granites, involves grainsize reduction and foliation development (Vernon *et al*., 1983). Both these processes involve recrystallization (e.g. of quartz and feldspar) and neocrystallization (e.g. of biotite and feldspar), as well as local fragmentation in some examples.

For example, deformation of granite in the Wologorong Batholith (south-east Australia) involved the replacement of igneous plagioclase by white mica, epidote and albite, the replacement of igneous biotite by new biotite, muscovite and titanite, with or without epidote, and the replacement of igneous K-feldspar by myrmekite and muscovite (Vernon *et al*., 1983). The reactions are *cyclic*, in that chemical components released in one local reaction are used in another local reaction. For example, K released in the replacement of K-feldspar was used in the replacement of plagioclase by white mica, which released Ca used in the replacement of biotite by epidote and the growth of myrmekite in K-feldspar (Section 4.10.4). Similarly, Simpson & Wintsch (1989) suggested that Ca and Na from reacting plagioclase are transported to sites of myrmekite growth in K-feldspar, which liberates K to form mica in plagioclase and recrystallized K-feldspar in strain-shadows at the ends of K-feldspar augen.

Flame perthite (Fig. 4.54) has been ascribed to similar cyclic reactions in deformed granites at greenschist facies conditions (Pryer & Robin, 1995). It also occurs in high-grade metapelites at Cooma, south-east Australia, where it appears to have formed at amphibolite facies conditions by different reactions (Vernon, 1999b).

5.7 Deformation partitioning

5.7.1 General aspects

Deformation is typically variable on all scales, because of the mechanical heterogeneity of rocks (Max, 1970; Bridgwater *et al*., 1973a, plate 7, fig. 3; Bridgwater *et al*., 1973b, fig. 2; Cobbold, 1977; Bell, 1981; Williams, 1991). The deformation is 'partitioned' into higher-strain zones that typically anastomose around lower-strain zones (Max, 1970; Cobbold, 1977; Bell, 1981; Bell & Rubenach, 1983; Choukroune & Gapais, 1983; Simpson, 1983; Gapais, 1989). Because deformation involves minerals with different deformability ('competence') at any one set of temperature–pressure conditions (Section 5.5.1), strain incompatibilities along boundaries between domains of different competences can produce mechanical instabilities, resulting in the formation of shear bands (Goodwin & Tikoff, 2002), as discussed in Section 5.7.6. For example, mica-rich domains may localize strain in this way, because mica readily deforms by slip along (001) planes (see, for example, Johnson *et al*., 2004).

Strain localization in microshear zones has been investigated by Platt & Vissers (1980), Gapais & White (1982) and Platt (1984). However, shear localization in a deforming rock can be transient, and therefore evidence of deformation partitioning on the grain and intragrain scales may be reset or obliterated, owing to progressive deformation, recrystallization and metamorphism (see, for example, Means, 1981; Urai *et al.*, 1986; Ree, 1991; Ree & Park, 1997). For example, Bons & Jessell (1999) found that anastomosing microshear zones on the grain and subgrain scales formed during the experimental deformation of octachloropropane (a commonly used rock analogue material). The shear zones continually moved through the aggregate (partly with migrating grain boundaries), homogenizing accumulated strain, and leaving no clear microstructural evidence of the fact that they accommodated up to 75% of the total deformation. Thus, rocks may not reveal all the critical evidence needed to evaluate their history of partitioned deformation.

A common example of deformation partitioning is provided by slates, phyllites and many schists with a lenticular domainal structure ('slaty cleavage' and 'crenulation cleavage') that reflects the tendency of deformation to be partitioned into high- and low-strain domains, called 'P' (or 'M') and 'Q' domains (for 'phyllosilicate-rich' (or 'mica-rich') and 'quartz-rich'), respectively, as described in Sections 5.8.2 and 5.8.3. The P domains are commonly rich in aligned white mica, chlorite, and/or fine-grained, dark, carbonaceous and/or iron–titanium oxide aggregates, and anastomose around Q domains that consist mainly of detrital quartz grains, with feldspar in some rocks, and less aligned phyllosilicate grains. This separation into compositionally distinct domains is generally called 'metamorphic differentiation' (Stillwell, 1918).

Minerals in the low-strain pods and minerals in the anastomosing folia commonly form at the same time, and so generally belong to the same metamorphic assemblage (Vernon, 1987b, 1996a). For example, in the Anmatjira Range, central Australia, garnet and cordierite porphyroblasts in low-strain pods were formed at the same time as adjacent, fine-grained, strongly foliated, anastomosing aggregates of biotite and sillimanite (Vernon, 1996a). This example emphasizes the following important features, also mentioned in Chapter 4. (1) Grainsize is a function of $N : G$. (2) Some minerals grow as porphyroblasts (low $N : G$ and others as fine-grained aggregates (high $N : G$). (3) Some minerals (e.g. mica and sillimanite) can exist in high-strain M domains (probably because they can undergo intergranular slip), whereas others (e.g. garnet) dissolve in high-strain zones, and so are confined to low-strain zones (Bell & Rubenach, 1983; Bell *et al.*, 1986). Similarly, fibrous sillimanite aligned in high-strain P domains may grow at the same time as radiating and random arrays of fibrous sillimanite crystals in low-strain Q domains (Vernon, 1987b).

Of course, minerals in the folia (P domains) may be younger and of lower temperature than minerals in low-strain pods (porphyroclasts), especially in retrograde schists and mylonites (Section 5.7.6). Care is required in identifying compatible and incompatible mineral assemblages.

P domains may be intensified adjacent to larger clasts in slates (see, for example, Woodland, 1985, figs. 8a, 8b), presumably owing to greater stress and/or strain concentration at these sites. Similarly, porphyroblasts in schists cause

Next Page

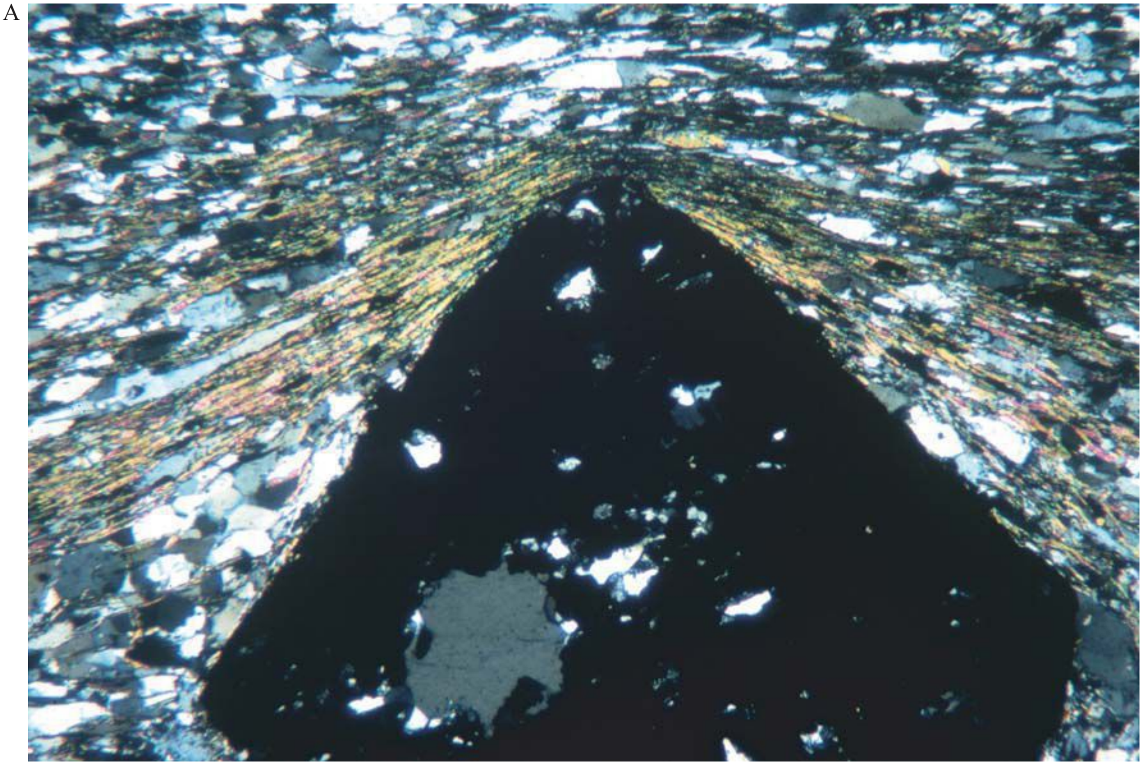

Fig. 5.33: (A) Concentration of mica (forming a local P domain) against a strong porphyroblast of garnet in a schist from the Karakoram, Himalayas. Crossed polars; base of photo 3.5 mm. (B) Initiation of mica folia (local P domains) on a porphyroblast of altered cordierite in a schist from Cooma, south-eastern Australia. Also shown are incipient strain shadows (zones protected from the deformation, and richer in quartz) parallel to the foliation on each side of the porphyroblast. Plane-polarized light; base of photo 4.8 mm.

deformation partitioning, P domains initiating or intensifying against them (Hanmer, 1979; Olesen, 1982; Vernon, 1989; Paterson & Vernon, 2001; Goodwin & Tikoff, 2002), as shown in Fig. 5.33. P domains anastomose around porphyroblasts and their ‘strain shadows’ (Bell, 1981; Vernon, 1989), as shown in Figs. 4.31, 5.34 and 5.35. However, all foliations tend to anastomose, even in the absence of porphyroblasts (Bell, 1981), owing to mechanical heterogeneities along and between layers during deformation (Fig. 5.35).

5.7.2 Preservation of older structures during deformation

Many metamorphic rocks show local preservation of earlier structures, even in strongly deformed regions (Section 4.15). Sedimentary and igneous outcrop-scale structures are commonly preserved in stronger rock-types, especially in low-strain zones. Thus, deformation partitioning can assist in the identification of parent

Previous Page

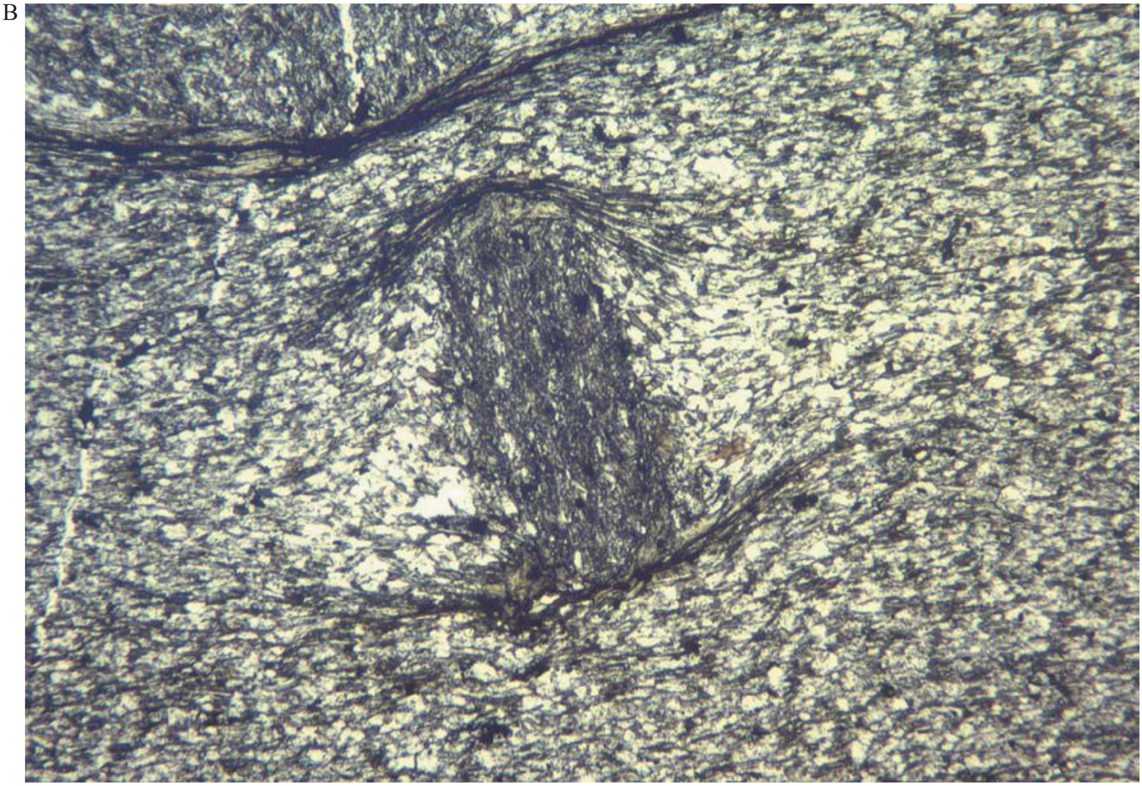

Fig. 5.33: (*cont.*)

rock-types. For example, sedimentary structures, such as cross-bedding and ripple marks, can occur in quartz-rich rocks adjacent to multiply deformed mica schists (Weiss & McIntyre, 1957; Vernon *et al*., 1990), and graded bedding may be preserved, even in granulite facies rocks, in low-pressure/high-temperature metamorphic terranes (see, for example, Vernon *et al*., 1990). In addition, microscopic relics, such as detrital grain shapes (Fig. 4.74), residual fossil shapes (Figs. 4.6, 4.38), embayed quartz phenocrysts (Fig. 4.75), simply twinned and oscillatory-zoned K-feldspar megacrysts (Section 5.7.9), and elongate plagioclase grains (Fig. 4.78) can help identify a parent rock-type, as summarized by Vernon (1999a).

5.7.3 Deformation partitioning in dry high-grade rocks

After regional metamorphism, high-grade rocks are relatively dry. If fluids do not enter them, they can deform only by high-temperature, isochemical, isomineralic plasticity (Rutter & Brodie, 1990, p. 151). Where high strains occur, they tend to be localized into mylonitic shear zones (Section 5.7.6), characterized

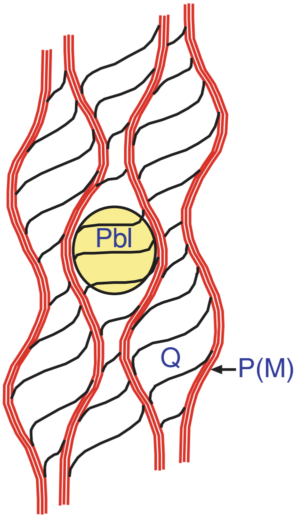

Fig. 5.34: Sketch showing deformation partitioning into anastomosing P (M) and Q domains, deflected around a porphyroblast (Pbl), in a crenulation cleavage (Sections 5.7.1 and 5.8.3). The porphyroblast is inferred to have remained in its original orientation while the matrix underwent further deformation (indicated by more rotated foliation), according to the model of Bell (1985).

by strong grainsize reduction (see, for example, White, 1976), so that grainsize-sensitive deformation mechanisms predominate, and 'fabric softening' (White *et al.*, 1980) – which should not be confused with the alleged attributes of certain laundry products – may occur. However, grainsize reduction associated with dynamic recrystallization alone is unlikely to produce much softening, as the grainsize is in equilibrium with the dislocation-creep stress (Etheridge & Wilkie, 1979). Some other process is needed to promote further grainsize reduction, such as the pinning of mobile grain boundaries by small grains of other minerals or the introduction of water. Thus, the development of local high-strain rocks (mylonite zones) generally involves increased permeability and associated fluid flow, reaction-enhanced ductility, strain-enhanced reaction, grainsize reduction and shear heating (Rubie, 1983; Brodie & Rutter, 1985; Rutter & Brodie, 1985; Wintsch, 1985; Jamieson, 1986; Tullis *et al.*, 1990; Fitz Gerald & Stünitz, 1993a). Very fast strain rates in earthquake zones in dry rocks may produce so much local frictional heat that melting occurs, forming pseudotachylite, as discussed in Section 5.7.10.

5.7.4 Fault rocks

Fracture processes, together with frictional grain-boundary sliding and fluid-assisted dilation, constitute the overall process called cataclasis (Section 5.3.1),

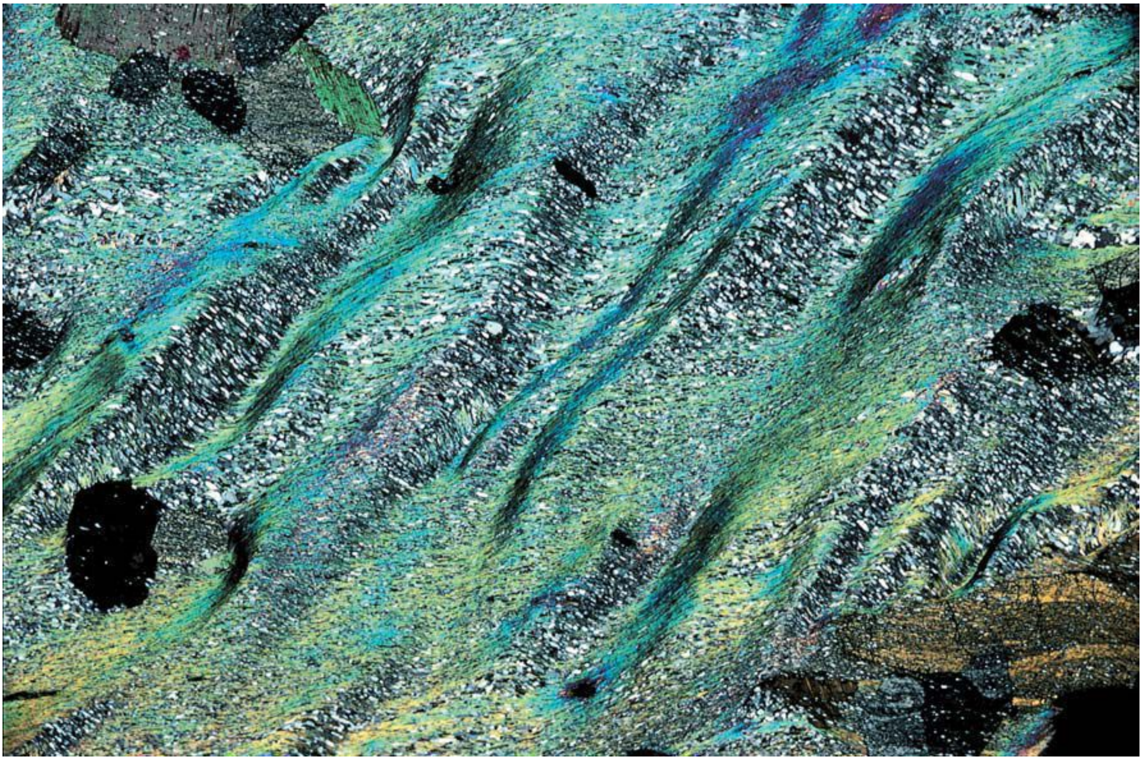

Fig. 5.35: Anastomosing P and Q domains forming a crenulation cleavage in a schist from the Picuris Range, New Mexico, USA. Also shown are porphyroblasts of garnet (optically isotropic) and staurolite (yellow first-order interference colours; bottom right). From Vernon (2000b, fig. 27). Crossed polars; base of photo 1.8 cm.

which dominates faulting ('seismic slip') at high levels in the crust. It produces fragmental rocks, such as fault gouges and fault breccias. The formation of gouges and breccias is favoured by the presence of fluid, which reduces the 'effective pressure' by keeping grains apart, and so promotes fracturing. However, as noted by Sibson (1975), if faulting occurs in dry rocks without introduced water, friction quickly builds up high temperatures, and the result is *frictional melting*. The melted rocks cool very fast, forming glassy rocks called *pseudotachylites*, as discussed in Section 5.7.10.

Sibson (1977, 1990) pointed out the distinction between (1) incohesive fault rocks, such as *fault gouge* and *fault breccia* (commonly rich in clay minerals, indicating low temperature), and (2) cohesive fault rocks, such as *cataclasite* (with mainly random microstructure) and *mylonite* (with penetrative aligned microstructure).

For a felsic crust, the typical sequence of rock-types with increasing depth in a shear zone is: gouge/breccia → cataclasite → mylonite → mylonitic gneiss (Fig. 5.36). The depth of transition from incohesive gouge/breccia to cohesive

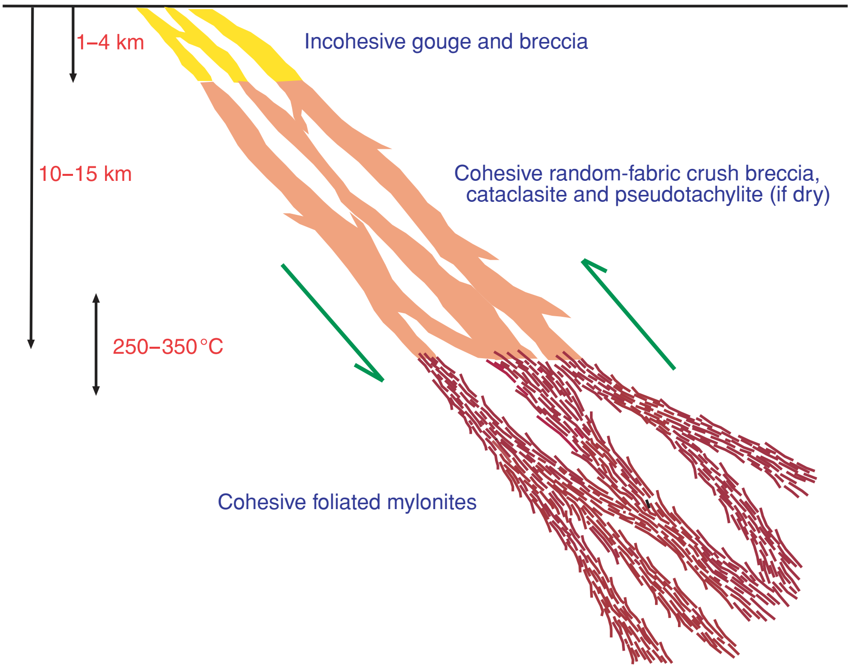

Fig. 5.36: Diagrammatic representation of the general change from incohesive to cohesive fault rocks with increasing depth, after Sibson (1990, fig. 4.9). With permission of the Mineralogical Association of Canada and the Geological Society of London.

cataclasite is in doubt, but because clay minerals are unstable at temperatures above about 100 °C, the depth is probably about 3–5 km. The change from cataclasite to mylonite represents a major change from fracture to plastic flow, which becomes dominant at > *c*. 300–350 °C in quartz and > *c*. 450 °C in feldspar (Sibson, 1977, 1990). Thus, the onset of dominant ductile deformation in fault zones coincides roughly with the onset of the greenschist metamorphic facies. Water-assisted diffusive mass transfer (stress-induced solution transfer; Section 5.9) may be important at 200–400 °C, thereby contributing to the ductile deformation, especially as the grainsize is reduced by cataclasis or dynamic recrystallization (McClay, 1977; Sibson, 1990).

5.7.5 Cataclasites, gouges and fault breccias

The main processes involved in cataclastic (brittle) deformation are frictional grain-boundary sliding and deformation by fracturing (Section 5.3.1), typically in the presence of fluid, which contributes to the deformation, as well as low-temperature mineral reactions (see, for example, Evans, 1990). Cataclasites are characterized by abundant angular fragments and heterogeneous deformation, including high-strain fracture zones (Figs. 5.1, 5.2). Foliations, if present, are defined by preferred orientation of fragments and clay minerals (formed mainly by the low-temperature action of water on feldspar), as well as aligned high-strain zones (see, for example, Chester & Logan, 1987). Some cataclasites contain zoned

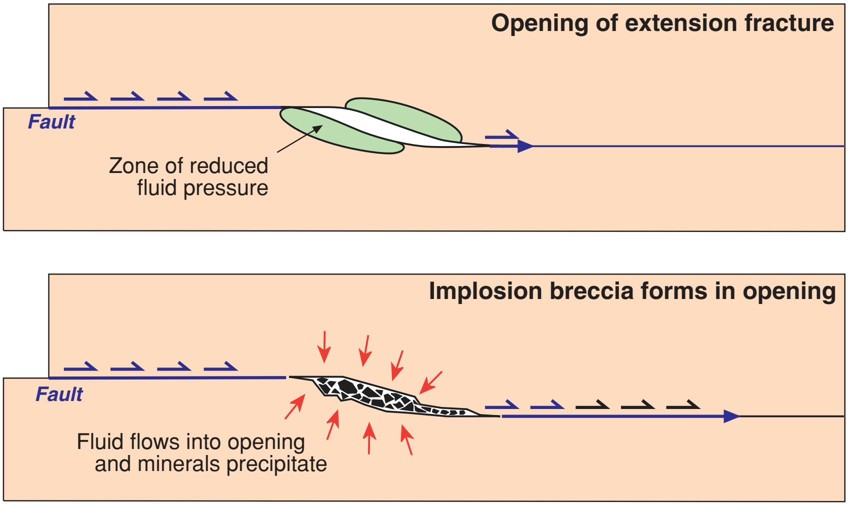

Fig. 5.37: Diagram showing the formation of an opening in a step ('jog') in a fault (or a join between two faults), resulting in implosion of the wall rocks into the opening to form a fault breccia. The arrows show the direction of flow of fluid along the fault. Redrawn from a diagram by Mike Etheridge. From Vernon (2000b, fig. 97).

quartz crystals with evidence of plastic deformation (undulose extinction, deformation lamellae and grain-boundary recrystallization), suggesting a repeated cyclic operation of brittle deformation, crystal growth and plastic deformation (Stel, 1981). Cataclasites and fault gouges have been discussed by Engelder (1974), Stel (1981), House & Gray (1982), Aydin & Johnson (1983), Wise *et al.* (1984, 1985a,b), Sibson (1977, 1981, 1986), Chester & Logan (1987) and Knipe (1989).

Water travelling along major faults may encounter openings formed by irregularities in the fault surface. Because these openings are sites of lower pressure than the surrounding rock pressure, the wall-rocks may expand ('implode') into the cavities and break into fragments (Fig. 5.37). This may fill the opening with loosely packed pieces of wall-rock. Aqueous solutions travelling along the fault may deposit minerals between the fragments, forming a fault breccia.

5.7.6 Mylonite zones (ductile shear zones)

Some of the best examples of deformation partitioning on regional, outcrop and microscope scales, are provided by *mylonites*, which are strongly foliated and lineated rocks that (1) occur in discrete zones (mylonite zones, ductile shear zones) and (2) show higher strain accumulation and finer grainsize than the adjacent rocks (see, for example, Johnson, 1960, 1967; Christie, 1960, 1963; Bell & Etheridge, 1973; Hobbs *et al.*, 1976; White *et al.*, 1980; Passchier, 1984, 1986; Hanmer & Passchier, 1991; Goodwin & Wenk, 1995; Passchier & Trouw, 1996; Snoke *et al.*, 1999). Mylonite zones may be less than a millimetre to several kilometres wide.

Although the original definition of 'mylonite' (Lapworth, 1885) implied brittle deformation processes, mylonites show microstructural evidence of dominant

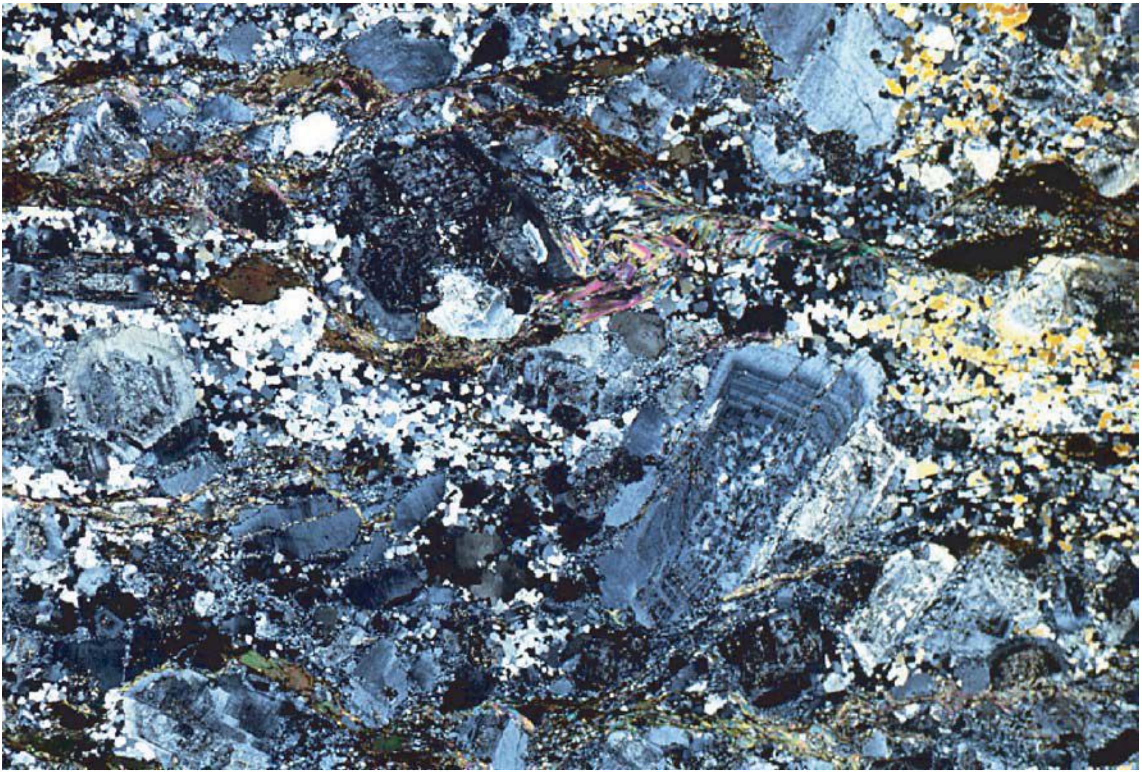

Fig. 5.38: Strongly deformed granite, Wologorong Batholith, southern New South Wales, Australia, showing fractured relics of K-feldspar and plagioclase (some with oscillatory zoning) interspersed with elongate aggregates of recrystallized quartz and foliated aggregates of neocrystallized mica (muscovite, new biotite and epidote formed by reactions involving the igneous biotite). The plagioclase has resisted the deformation, in marked contrast to the quartz and mica, which have recrystallized/neocrystallized to fine-grained aggregates and flowed readily, forming an anastomosing, mylonitic foliation. From Vernon (2000b, fig. 162). Crossed polars; base of photo 2.4 cm.

ductile flow, in contrast with cataclasites. Some minerals may flow plastically while others fracture during the same deformation (Section 5.5.1), but the overall deformation at the microscope scale is typically cohesive. Owing mainly to recrystallization and neocrystallization during deformation, mylonites are typically finer-grained than the adjacent rocks, into which they grade.

Most mylonites consist of relatively continuous, fine-grained, recrystallized/neocrystallized folia anastomosing around lenses of less deformed material (see, for example, Choukroune & Gapais, 1983; Vernon *et al.*, 1983; Simpson, 1983; Gapais, 1989). At the microscope scale, these lenses are commonly relics of originally larger grains that show evidence of internal deformation and marginal recrystallization (Figs. 5.31, 5.38–5.40). These are called *porphyroclasts*, and represent minerals that were much stronger than the matrix at the prevailing

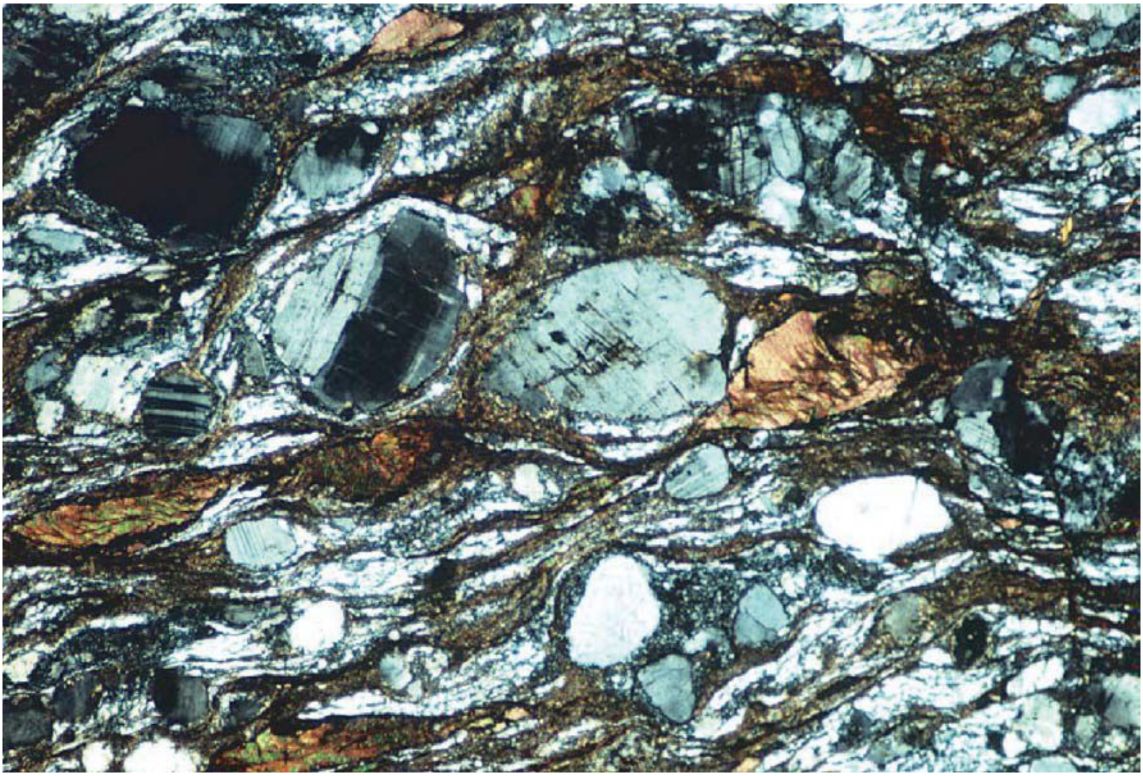

Fig. 5.39: Mylonite formed by the intense deformation of granite, Wongwibinda Fault, New England area, New South Wales, Australia. Residual rounded grains ('augen') of feldspar show some evidence of plastic deformation, but have mainly fractured and fragmented, whereas biotite (brown) has deformed plastically into elongate lenses and has recrystallized to very fine-grained aggregates drawn out into a foliation, and quartz has been drawn into very thin, finely recrystallized 'ribbons' (Section 5.5.1). From Vernon (2000b, fig. 30). Crossed polars; base of photo 4.4 mm.

conditions of temperature, fluid activity and strain rate. For example, in the mylonitic deformation of granite at a wide range of conditions, feldspar is stronger than quartz and recrystallizes/neocrystallizes less readily than mica, with the result that thin folia ('ribbons') of recrystallized quartz (Section 5.5.1) and neocrystallized aggregates rich in mica anastomose around porphyroclasts of feldspar (Figs. 5.31, 5.39).

The formation of most mylonites involves *grainsize reduction* of originally coarser-grained rocks (see, for example, Hobbs *et al*., 1976; Vernon, 1974, 1976; Vernon *et al*., 1983; Passchier & Trouw, 1996). Porphyroclasts deform, recrystallize and/or neocrystallize at their margins as they rotate during flow of the mylonite matrix, with the result that they become more rounded in shape and commonly develop 'tails' or 'wings' of fine-grained recrystallized and/or

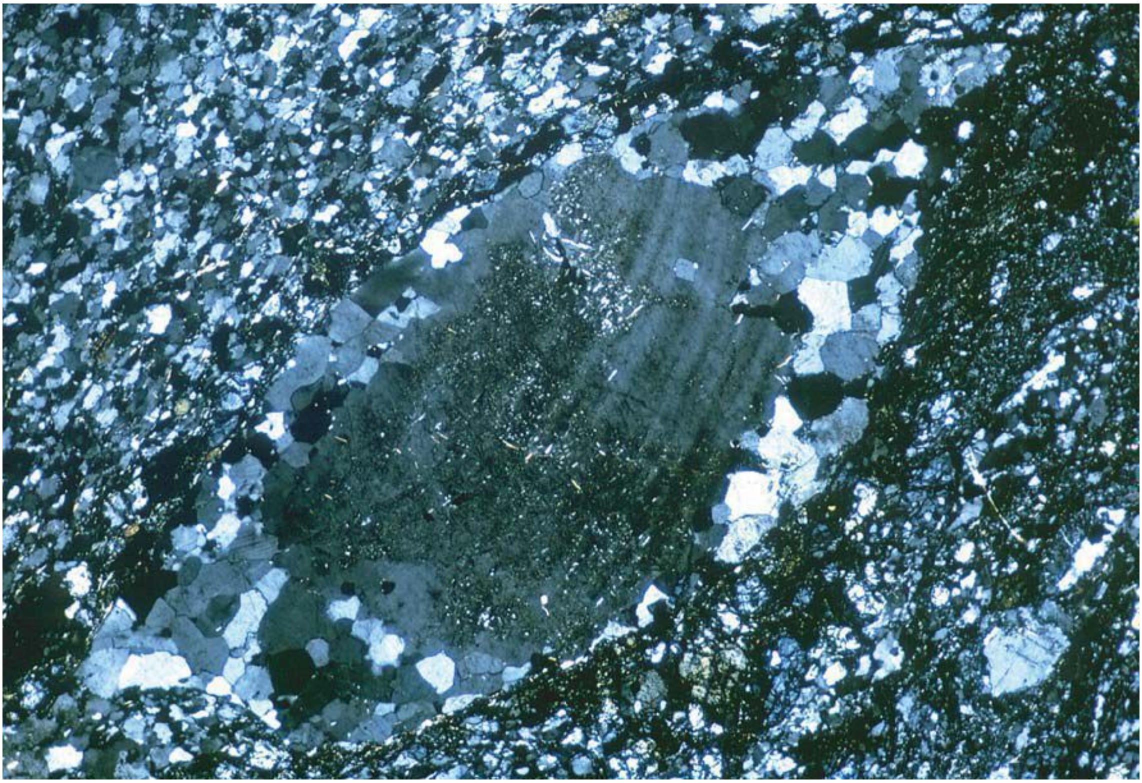

Fig. 5.40: Porphyroclast ('auge') of plagioclase with recrystallized 'tails' in a mylonite from Lochcarron, Scotland. Crossed polars; base of photo 4.4 mm.

neocrystallized aggregates (Figs. 5.39, 5.40). Such porphyroclasts are called 'mantled porphyroclasts'. Because porphyroclasts perturb the flow of the matrix, the shapes and arrangements of the 'tails' reflect the sense of shear involved in the deformation of the mylonite, when viewed in sections parallel to the mineral-stretching lineation (Fig. 5.41). Large porphyroclasts with relatively symmetrical tails (Figs. 5.39, 5.40, 5.51, 5.52) resemble eyes, and are commonly referred to as *augen* (the singular being 'auge'). In many places, transitions from coarse-grained igneous or high-grade metamorphic rocks, through *augen gneisses*, to mylonites can be observed.

Mylonitic rocks have been classified on the ratio of porphyroclasts to matrix (Spry, 1969; Sibson, 1977; Passchier & Trouw, 1996). Rocks with a high proportion of porphyroclasts (10–50% matrix) are called *protomylonites*, rocks with 50–90% matrix are called *mylonites*, and rocks with more than 90% matrix are called *ultramylonites*. However, although this classification can reflect increasing strain accumulation, not all parent rocks are coarse-grained, and so porphyroclasts are not always present in mylonites.

Fig. 5.41: Diagrams showing asymmetrical porphyroclasts and other microstructures indicating sense of shear in mylonites. They are seen only in sections parallel to the mineral stretching lineation, sections perpendicular to the lineation showing symmetrical microstructures.

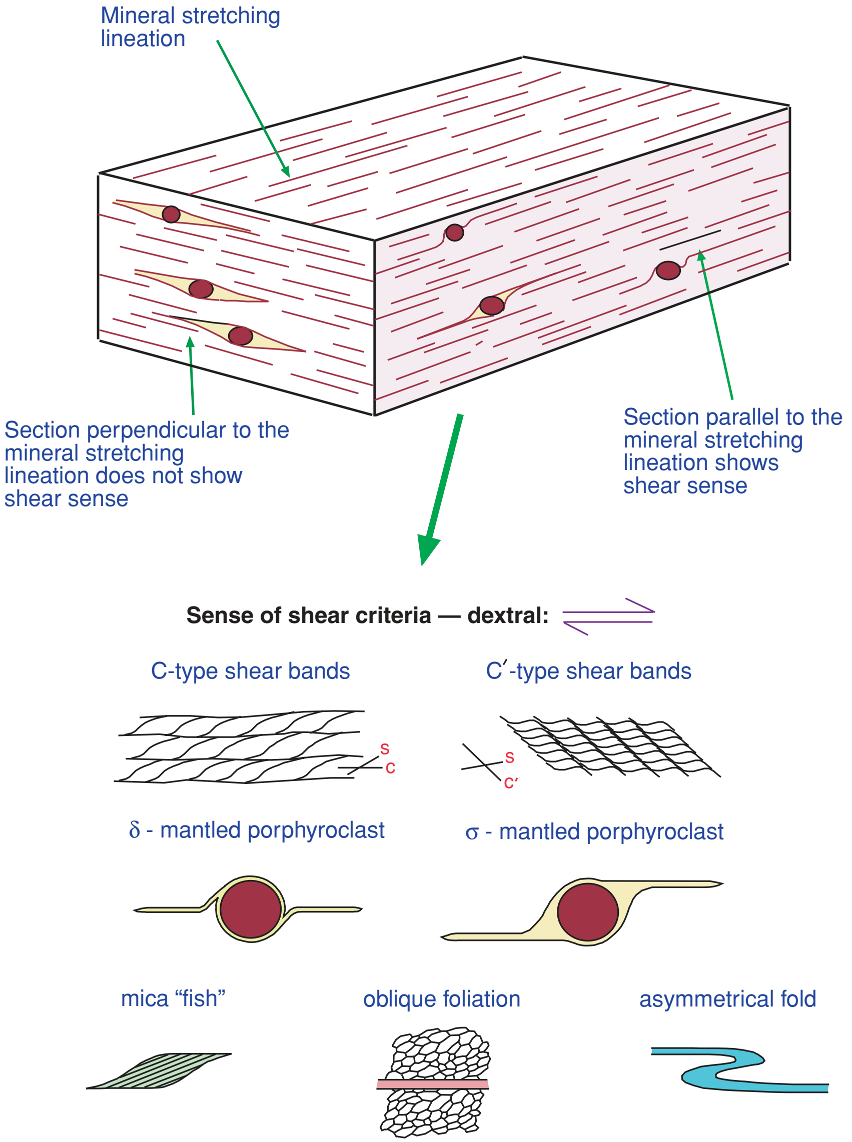

Commonly the foliation and lineation of mylonites are defined by variations in composition inherited from the original rock. Recrystallized/neocrystallized aggregates replacing different originally large grains may maintain some individuality as they are drawn out into lenses or rods during the intense deformation (see, for example, Katz, 1968; Ramsay & Graham, 1970; Moore, 1973; Ross, 1973; Vernon, 1974; Vernon *et al.*, 1983; Lafrance & Vernon, 1993).

Differences in the deformability of different minerals (Section 5.5.1) reveal themselves in mylonites most clearly at lower metamorphic grades, in the

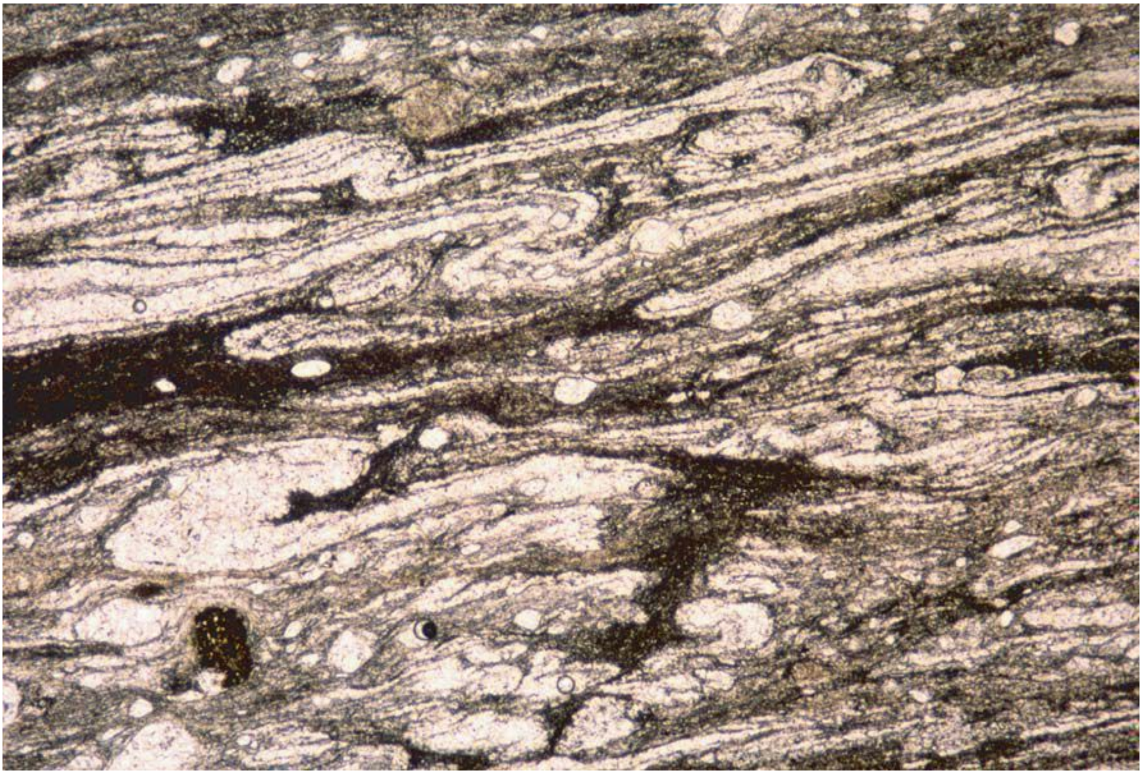

Fig. 5.42: Asymmetrical microfolds and isolated ('rootless') fold hinges in a mylonite from the Wyangala Batholith, New South Wales, Australia. Plane-polarized light; base of photo 4 mm.

form of 'ribbons' of finely recrystallized quartz and thin continuous folia of recrystallized/neocrystallized mica anastomosing around strong porphyroclasts of feldspar (Fig. 5.31). However, more intense deformation commonly results in reduction in the size of the porphyroclasts (Fig. 5.42). Grainsize differences are also reduced at higher metamorphic grades, so that mylonitic rocks at high grades are commonly relatively even-grained, granoblastic rocks with few or no porphyroclasts, although the intensity of deformation may be revealed by lenticular recrystallized/neocrystallized aggregates or isolated ('rootless') fold hinges (Fig. 5.42).

Kenkmann & Dresen (2002) described evidence of a strain-dependent change from grainsize-insensitive creep to grainsize-sensitive creep in the formation of mafic mylonite at amphibolite facies conditions. Although compositionally layered mylonite characterized by dynamically recrystallized plagioclase layers was formed at moderate strain, increasing strain and grainsize reduction involved nucleation of new grains of plagioclase and amphibole in each other and in

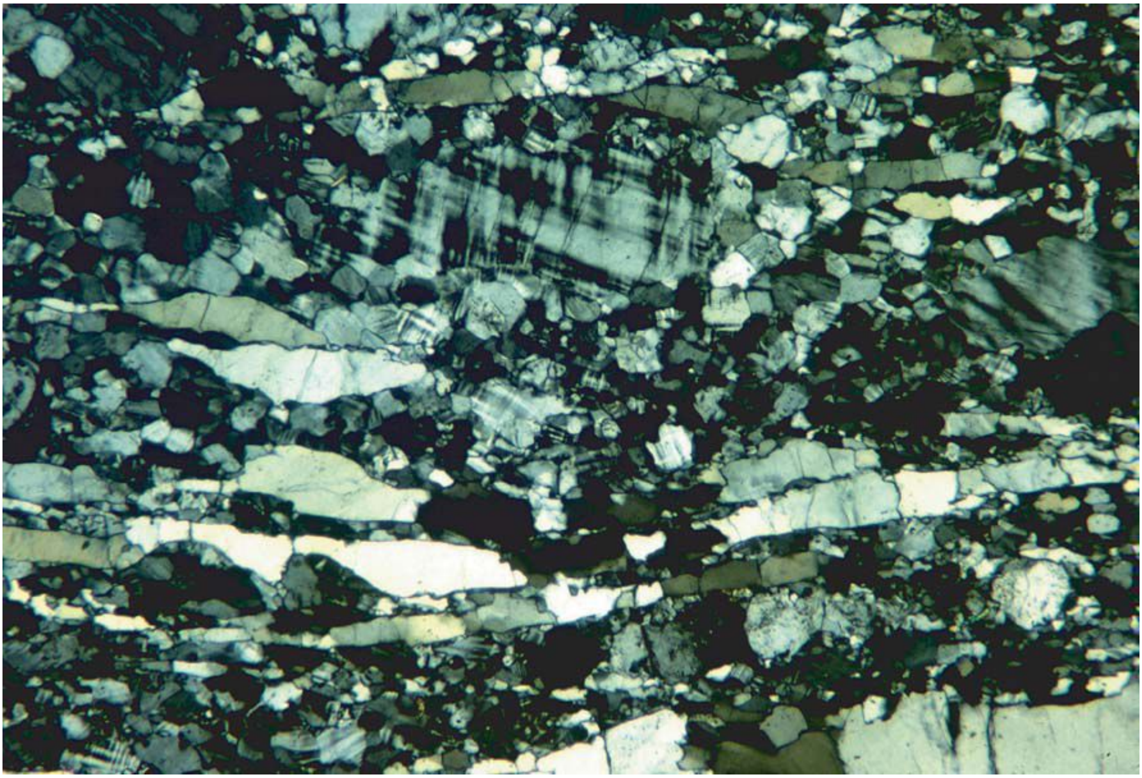

Fig. 5.43: Pegmatite from central Australia that has been strongly deformed at high temperature (granulite facies), showing aggregates of recrystallized feldspar (with a few elongate porphyroclasts) alternating with elongate aggregates of coarsely recrystallized quartz. These aggregates probably represent the distorted equivalents of coarse-grained quartz and feldspar in the original rock. Crossed polars; base of photo 4.8 mm.

dilatant sites, progressively replacing the layering by dispersed aggregates of the two minerals.

The formation of mylonites in single-mineral rocks (e.g. quartzite, marble and dunite) involves only recrystallization, but most mylonites involve neocrystallization as well. This is because metamorphic reactions accompany change of temperature and/or fluid activity during the deformation (see, for example, Vernon & Ransom, 1971; Vernon *et al.*, 1983; Tsurumi *et al.*, 2003). Mylonite zones developed in high-grade metamorphic rocks commonly show clear examples of the effect of deformation on metamorphic reactions. For example, at Broken Hill, Australia, granulite facies metapelites and metabasites have undergone patchy pseudomorphous retrograde metamorphism, except in high-strain zones (mylonite zones), in which the deformation and access of water has promoted much more complete neocrystallization to amphibolite-facies assemblages

(Vernon & Ransom, 1971; Corbett & Phillips, 1981). Similarly, in several terranes, gabbros or dolerites partly metamorphosed to eclogite or granulite facies mineral assemblages (with reaction coronas) are more completely neocrystallized in high-strain zones (see, for example, Austrheim & Griffin, 1985; Pognante, 1985; Rubie, 1990; White & Clarke, 1997).

Some mylonites have been attributed to the influx of water in the deformation zones (see, for example, Boundy *et al.*, 1992). This may be due to the opening of minute pores between grains deforming at different rates, owing to their contrasting response to the deformation (Section 5.6.1). The water helps the reactions to go to completion in the mylonite zones (see, for example, Austrheim, 1987; Austrheim & Griffin, 1985; Rubie, 1990; White & Clarke, 1997). Klaper (1990) described an example of hydrous eclogite facies assemblages developed in shear zones in dry granulite facies rocks, involving a feedback between deformation and reaction. Introduction of water promoted the formation of new minerals, which, coupled with grainsize reduction by dynamic recrystallization, changed the mechanical properties of the rocks. Other examples, in which the rocks remained dry, have been attributed to shear heating in deformation zones (Camacho *et al.*, 2001).

Reasons for the initiation and localization of mylonite zones are not clearly understood, but introduction of water along cracks (Segall & Simpson, 1986) is one way of initiating mylonites in relatively homogeneous rocks, such as granite. Rubie (1986) inferred that basement rocks typically remain dry for long periods, punctuated by short periods of localized infiltration of aqueous fluid, which promotes metamorphic reactions and weakening in ductile shear zones. In addition, Tullis *et al.* (1990) have shown experimentally that feldspar aggregates in cataclastic fault zones may recrystallize and develop into local ductile deformation zones.

Once the deformation has begun, localization could be maintained and intensified by ‘strain softening’ promoted by processes such as: (1) grainsize reduction caused by dynamic recrystallization/neocrystallization, which can produce a change from dislocation flow to ductile grain-boundary sliding (Section 5.3.5) as the main deformation mechanism (see, for example, Schmid *et al.*, 1977; White *et al.*, 1980), provided grain growth is inhibited (de Bresser *et al.*, 2001) and provided some other process (such as the pinning of grain boundaries by small dispersed grains of another mineral, such as mica, or by introduction of water) can reduce the grainsize from the equilibrium value for the dislocation-creep stress involved in the deformation (Etheridge & Wilkie, 1979); (2) grain-boundary migration recrystallization, which produces new, strain-free grains that can be relatively easily deformed; (3) reaction weakening (Section 5.6.2); (4) stress-induced solution transfer facilitated by opening of small transient voids caused by the different mechanical response of different minerals to the deformation, and (5) diffusion of water into mineral grains, causing potential ‘water weakening’ (Section 5.6).

For example, McCaig (1984) and O'Hara (1988) suggested that reaction-enhanced weakening was important in localizing mylonite formation in the Pyrenees and North Carolina, respectively. In addition, reactions involving replacement of K-feldspar by myrmekite during the mylonitic deformation of granitic rocks (Vernon *et al.*, 1983; Simpson & Wintsch, 1989; Vernon, 1991b; Tsurumi *et al.*, 2003) produce fine-grained aggregates that develop into folia, thereby contributing to the deformation.

Experiments by Tullis & Yund (1987, 1991) and Tullis *et al.* (1996) have shown that small amounts (<1%) of water in deforming fine-grained plagioclase aggregates cause a change from cataclastic deformation or dislocation creep to diffusion creep, with a resulting marked decrease in strength. Because feldspars are very liable to grainsize reduction by cataclasis (Tullis & Yund, 1987) or dynamic recrystallization (Tullis & Yund, 1985), this water-weakening effect in fine-grained feldspar aggregates could be a major factor in the localization of deformation to form shear zones in essentially dry feldspar-rich rocks in the mid-crust.

Ultramafic mylonites (Section 5.12), which are deformed and recrystallized peridotites from Earth's mantle, may occur as peridotite xenoliths in basalts (Green & Radcliffe, 1972, fig. 1c), in alpine peridotites (Green & Radcliffe, 1972, fig. 10; van der Wal *et al.*, 1992), and at the base of ophiolite sheets (Boudier & Nicolas, 1982a,b; Suhr, 1993).

5.7.7 Structures in mylonites

Mylonites commonly show a strong lineation formed by elongation ('stretching') of recrystallized and/or neocrystallized aggregates. This is commonly known as a 'mineral stretching' lineation, to distinguish it from lineations formed by intersection of foliations. Sections cut perpendicular to the mineral stretching lineation commonly appear to be less deformed and show symmetrical structures (e.g. symmetrically mantled porphyroclasts), whereas sections cut parallel to the lineation appear to be much more deformed and show asymmetrical structures that can be used as shear-sense indicators (Simpson & Schmid, 1983; Lister & Snoke, 1984; Mawer, 1987; Hanmer & Passchier, 1991; Passchier & Trouw, 1996), as shown in Fig. 5.41.

Microfolding is very common in mylonites, the folds typically being tight to isoclinal, with axes commonly parallel to the mineral lineation of the mylonite (Fig. 5.42). The asymmetry of the folds has been used to indicate the sense of shear during the deformation (Figs. 5.41, 5.42), and this has been confirmed by experiments (Bons & Cox, 1994). Generally the axial-surface foliations of these folds are identical to the main foliation, so that the folds represent local perturbations of the flow during a continuous deformation, and not separate deformation events. These flow perturbations can lead to the essentially contemporaneous formation of several foliations slightly oblique to each other in the one mylonite.

In fact, mylonitic foliations are typically *composite* (Section 5.8.5), owing to complex local deformation, and are characterized by truncations of folia and folds. Rootless fold hinges are common (Fig. 5.42), the limbs losing continuity owing to the intense deformation.

Foliations that develop simultaneously are good shear-sense indicators. For example, an alignment of elongate grains at an angle to the main foliation (*oblique foliation*) is a characteristic feature of mylonites, especially in single-mineral layers of quartz, carbonate or olivine (see, for example, Means, 1981; Lister & Snoke, 1984; Law *et al.*, 1984; van der Wal *et al.*, 1992; Passchier & Trouw, 1996). The relationship of the oblique foliation to the main foliation can be used as a shear-sense indicator (Figs. 5.41, 5.44). Other asymmetrical microstructures that can be used as shear-sense indicators (Fig. 5.41) include mica 'fish' (Figs. 5.41, 5.44) and asymmetrical mantled porphyroclasts (Figs. 5.41, 5.45, 5.46). Mantled porphyroclasts have been produced experimentally in limestone–halite aggregates (Jordan, 1987) and in analogue materials (ten Brink & Passchier, 1995). Imbricated feldspar porphyroclasts (Fig. 5.47) have also been used (Simpson & Schmid, 1983), though this criterion on its own may be unreliable (Passchier & Trouw, 1996, p. 126).

Also characteristic of mylonites are minor parallel shear zones that constitute a *shear band cleavage* (White, 1979; Gapais & White, 1982), as shown in Fig. 5.48. For example, continuous and finely laminated '*C* folia' are typically oblique to generally less regular '*S* folia' (Figs. 5.41, 5.48, 5.49), as described by Berthé *et al.* (1979), Vernon *et al.* (1983), Lister & Snoke (1984), Simpson (1984), Choukroune *et al.* (1987), Gapais (1989), Schulmann *et al.* (1996) and Passchier & Trouw (1996). The *S* folia form at high angles to the local shortening direction and the *C* folia form approximately parallel to the shear zone, reflecting a large component of shearing deformation. Coarse-grained minerals of the *S* folia curve into and become *C* folia, as they recrystallize and neocrystallize into finer-grained aggregates (Fig. 5.48B). This suggests that *S* folia form first, and that *C* folia develop as deformation increases, as suggested by Simpson (1984) and illustrated in Fig. 5.49. However, once both are formed, they appear to develop simultaneously. As deformation proceeds, the angle between the two folia decreases and they more closely resemble each other, virtually coinciding in the most strongly deformed mylonitic rocks (Fig. 5.49). The curvature of *S* folia into *C* folia reflects the sense of shear (Figs. 5.41, 5.49).

C shear band cleavage is best developed in mica-poor rocks, especially deformed granite (e.g., Berthé *et al.*, 1979; Vernon *et al.*, 1983; Simpson, 1984; Gapais, 1989). Magmatic flow folia (Section 3.9) or aligned elongate enclaves, if present, commonly form the initial *S* surfaces (Vernon *et al.*, 1983; Simpson, 1984). *S–C* foliation arrangements with the same orientation and sense of shear as an inferred magmatic imbrication (Section 3.9) of the same minerals in the same rock suggest that deformation can be continuous from the magmatic to the solid state (Blumenfeld, 1983; Gapais, 1989; Blumenfeld & Bouchez, 1988;

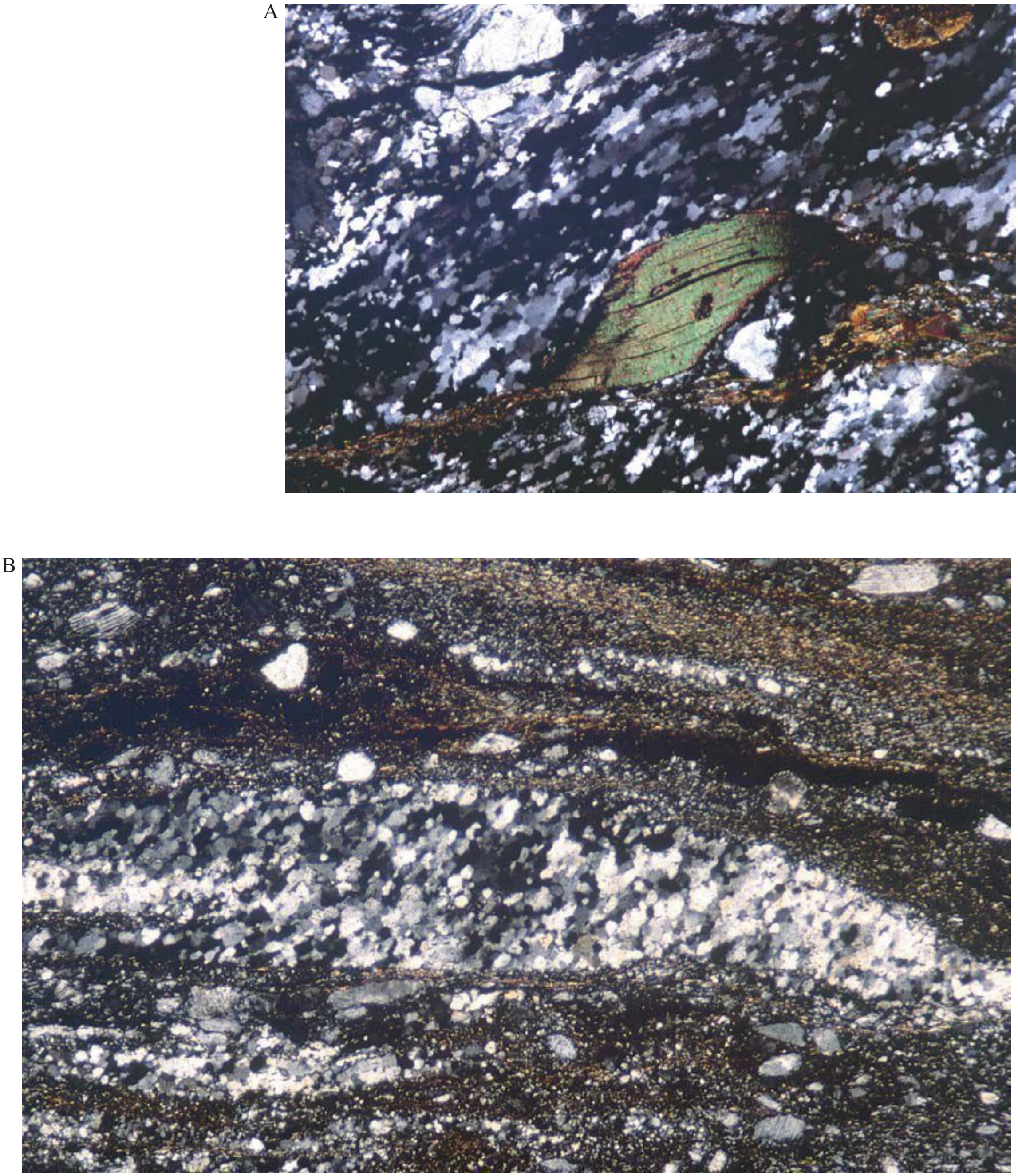

Fig. 5.44: (A) Mylonite from east of Armidale, New England area, New South Wales, Australia, showing a biotite 'fish' and a foliation formed by elongate grains of recrystallized quartz markedly oblique to the main mylonitic foliation, which is approximately parallel to the base of the photo. Both the oblique foliation and the 'fish' indicate a dextral sense of shear (Fig. 5.41). Crossed polars; base of photo 4 mm. (B) Oblique foliation, indicating a dextral sense of shear, in a quartz layer in a fine-grained mylonite (ultramylonite) from the Wyangala Batholith, central-western New South Wales, Australia. Crossed polars; base of photo 4 mm.

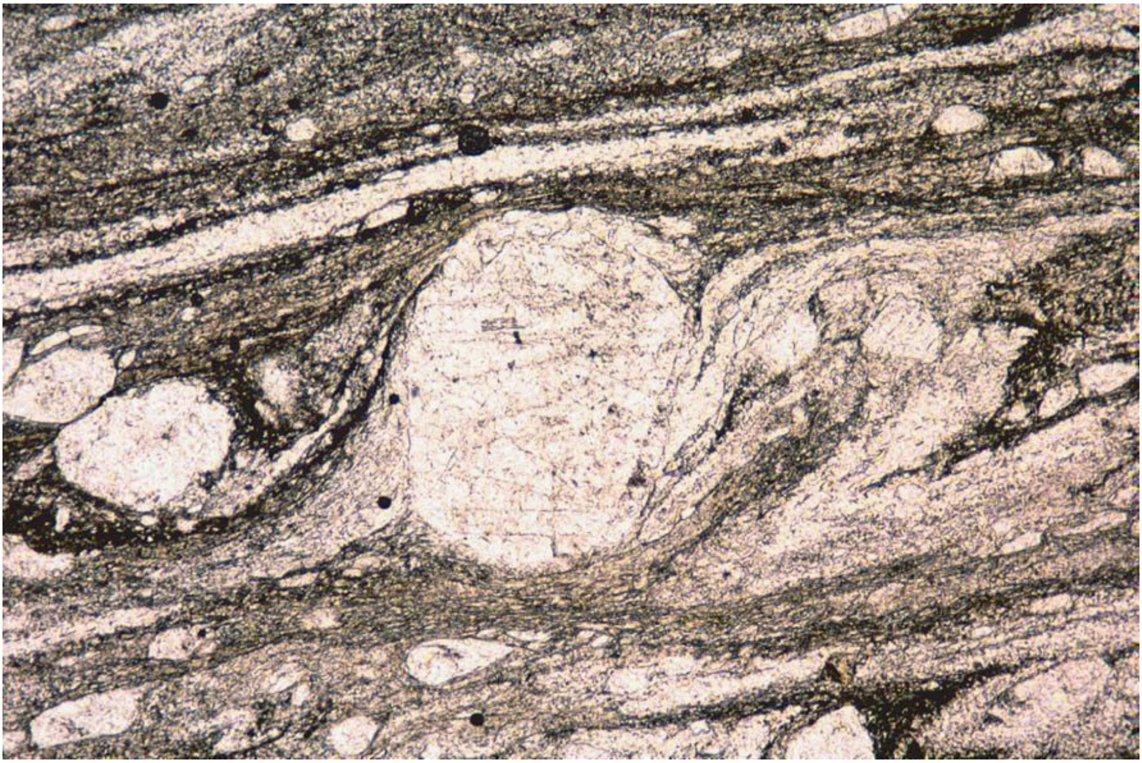

Fig. 5.45: Mantled porphyroclast (δ-type) of K-feldspar with folded 'wings' indicating a dextral sense of shear, in a fine-grained mylonite (ultramylonite) from the Wyangala Batholith, central-western New South Wales, Australia. Plane-polarized light; base of photo 4 mm.

Miller & Paterson, 1994). In deforming granites with K-feldspar megacrysts, the shear bands tend to be localized by the megacrysts, owing to strong competence contrasts between them and the finer-grained matrix (Goodwin & Tikoff, 2002).

Another type of shear band cleavage is provided by *C′* folia (Figs. 5.49, 5.50), which are not only oblique to the main mylonitic foliation, but also oblique (15–35°) to the shear zone boundaries (Berthé *et al.*, 1979; White, 1979; Platt & Vissers, 1980; Simpson, 1984; Passchier & Trouw, 1996). This cleavage has been referred to as 'extensional crenulation cleavage' by Platt & Vissers (1980). The *C′* folia are generally less continuous and regular than *C* folia, and may consist of retrograde minerals (McCaig, 1987; Norrell *et al.*, 1989). This suggests that, in contrast to *C* folia, the *C′* folia form relatively late in the deformation history, after a strong foliation has been developed, possibly as a result of increasing difficulty of flow involving a single foliation. Simpson (1984) has shown how *C′* surfaces may develop after intense mylonitic deformation at the stage when *S* and *C* planes are almost parallel. *C′* shear band cleavage may also be used as a

Fig. 5.46: Mantled porphyroclast (σ-type) of K-feldspar with 'wings' of a fine-grained opaque mineral, indicating a sinistral sense of shear, in a fine-grained mylonite (ultramylonite) from the Strangways Range, central Australia. Sample kindly provided by Tony Norman. Plane-polarized light; base of photo 4 mm.

shear sense indicator, its asymmetry in relation to *C* folia being opposite to that of *S* folia (Figs. 5.41, 5.49).

5.7.8 Bulk chemical changes in mylonites

Many mylonitic rocks show abundant evidence of high fluid permeability, material transport and metamorphic reactions (e.g., Beach & Fyfe, 1973; Beach, 1976, 1980; Sinha *et al.*, 1986; Kerrich, 1986; Simpson, 1986; Stel, 1986; McCaig, 1984, 1997; O'Hara, 1988; McCaig & Knipe, 1990; Altenberger, 1995a,b, 1996a,b). McCaig & Knipe (1990) emphasized that the process involves a complex local interplay between contrasting processes, such as diffusion versus infiltration, continuous versus episodic effects, and channelized versus pervasive reactions. Later deformation and metamorphism may destroy much of the microstructural evidence (see, for example, Beach, 1980; O'Hara, 1988), though Selverstone (1993) inferred that small, asymmetrically zoned, internally

Fig. 5.47: Imbricated K-feldspar porphyroclast, Wyangala Batholith, central-western New South Wales, Australia. Crossed polars; base of photo 11 mm.

undeformed grains of feldspar and large radiating porphyroblasts of hornblende in feldspathic ductile shear zones reflect rapid growth involving fluid along grain boundaries.

Although many rocks deformed in mylonitic shear zones show little evidence of bulk chemical change (see, for example, Kerrich *et al.*, 1980), others show major changes, indicating substantial movement of fluid through the zones during deformation (see, for example, Beach & Fyfe, 1973; Beach, 1973, 1976; Kerrich *et al.*, 1977; Sinha *et al.*, 1986; O'Hara, 1988; Jamtveit *et al.*, 1990; Dipple *et al.*, 1990; Selverstone *et al.*, 1991; Glazner & Barley, 1991; Früh-Green, 1994; Streit & Cox, 1998). However, it is necessary to determine whether or not the fluid infiltration, hydration and other metasomatic changes (where present) accompany deformation or occur later (see, for example, Rutter & Brodie, 1985, p. 563), especially as the extent of alteration is not necessarily related to strain accumulation (see, for example, Altenberger, 1996b). Kerrich *et al.* (1977) inferred that changes of bulk chemical composition and volume in mylonites are more likely to occur at lower temperatures, whereas higher-temperature deformation, which tends to be accommodated mainly by dislocation creep, is more commonly isochemical and isovolumetric.

Fluid flow in mylonite zones appears to occur mainly by microcracking (Brantley *et al.*, 1990; Tobisch *et al.*, 1991; Oliver, 2001). The microcracking is favoured by (1) grain-boundary sliding in aggregates of different minerals, which deform at different rates and so tend to open grain-boundary cracks, and (2) formation of new minerals during deformation, which could lead to the same

A

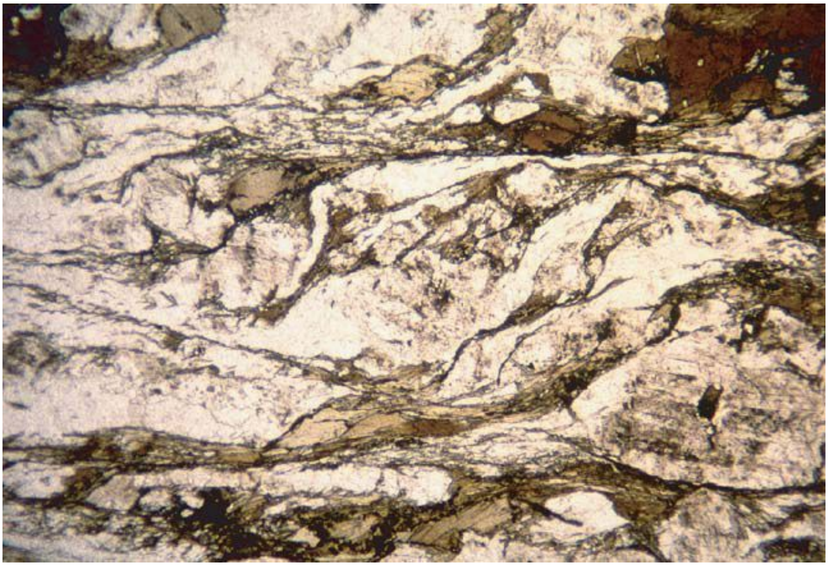

Fig. 5.48: (A) *S*–*C* relationships in a deformed granite, Abroi Gneiss, east of Armidale, New South Wales, Australia. The *S*-surfaces trend from the lower left to upper right, and the *C*-surfaces trend parallel to the length of the photo. Plane-polarized light; base of photo 11 mm. (B) Coarse-grained biotite that has been deformed and marginally neocrystallized to fine-grained aggregates of new biotite, muscovite, epidote and titanite in a deformed granite with *S*–*C* structure from the Wologorong Batholith, southern New South Wales, Australia. The biotite is elongate in an '*S*' folium (running from the bottom right towards the top left of the photo) and curves into a much finer-grained, continuous '*C*' folium (running parallel to the top of the photo) composed of these new minerals plus recrystallized quartz and feldspar. Plane-polarized light; base of photo 4.4 mm.

effect or which could produce new interfaces that are potentially permeable, such as mica–quartz or mica–feldspar (Section 4.4), especially when they are well aligned, as is common in shear zones. Although ductile processes in mylonites have been emphasized in recent years (see, for example, Bell & Etheridge, 1973), crystal-plastic processes are likely to give way to mass transfer and volume change at lower metamorphic grades (Kerrich *et al*., 1977). Recent experiments and studies of mylonites have concentrated more on the complex interaction between metamorphism, fluids, cataclasis and crystal-plastic deformation processes (see, for example, Dixon & Williams, 1983; Knipe & Wintsch, 1985; Murrell, 1985; Rutter & Brodie, 1985).

5.7.9 K-feldspar augen in felsic gneisses and mylonites

Large crystals ('augen') of K-feldspar are common in felsic gneisses and mylonites (Figs. 5.39, 5.40, 5.51, 5.52). Some petrologists have interpreted them

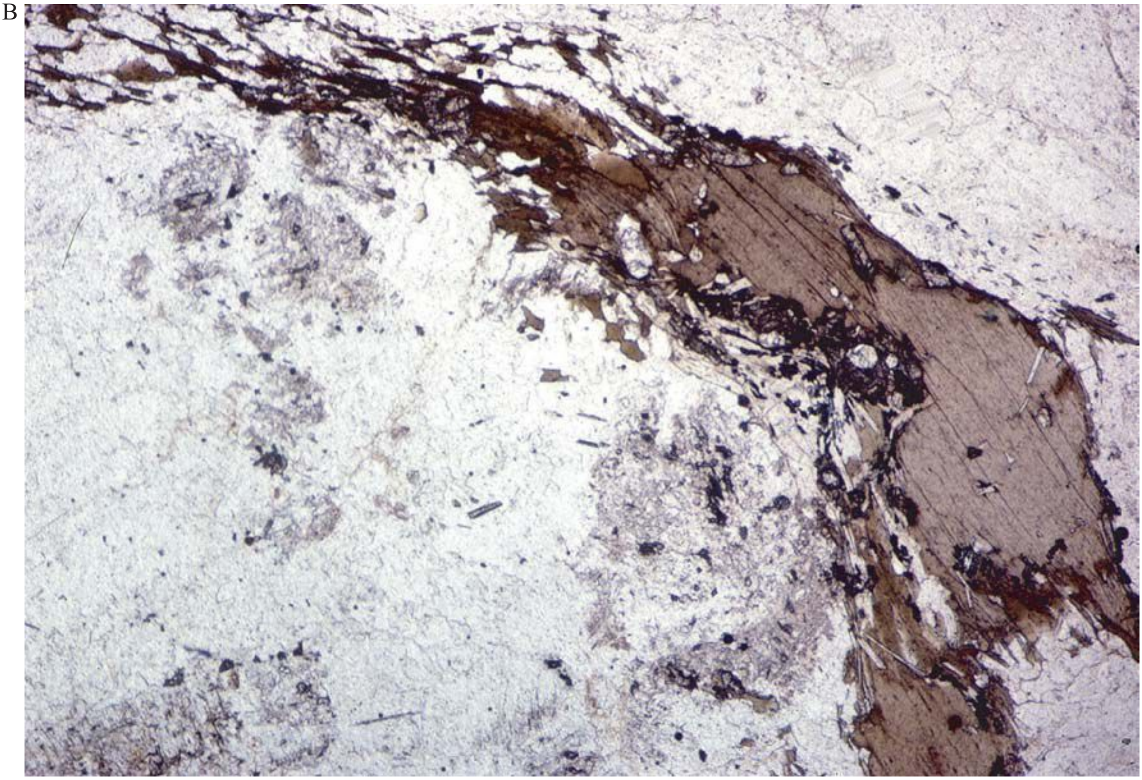

Fig. 5.48: (*cont.*)

as *porphyroblasts* that grow during or after the deformation responsible for the gneissic/mylonitic foliation and lineation (see, for example, Dickson, 1996). The alternative interpretation is that the augen are residual phenocrysts (*porphyroclasts*) in a deformed granite (see, for example, Vernon *et al.*, 1983; Mehnert & Büsch, 1985; Vernon, 1986a, 1990b; Debat *et al.*, 1978; Vernon & Williams, 1988; Schulmann *et al.*, 1996; Vernon & Paterson, 2002). The implication of this hypothesis is that the augen are at least partly preserved because they are large single crystals that are much stronger than the surrounding, finer-grained quartz and mica, which deform and recrystallize/neocrystallize much more readily, and so form the foliated matrix (see, for example, Vernon & Flood, 1988; Vernon *et al.*, 1983). If the augen are residual phenocrysts, they should show microstructural evidence of deformation and recrystallization, as is commonly the situation. The following criteria are useful for identifying K-feldspar augen that are former phenocrysts and distinguishing them from K-feldspar porphyroblasts (Vernon, 1990b, 1999a; Vernon & Paterson, 2002).

(1) Euhedral plagioclase inclusions are arranged concentrically, parallel to any concentric compositional zoning that may be present (Fig. 5.52), which

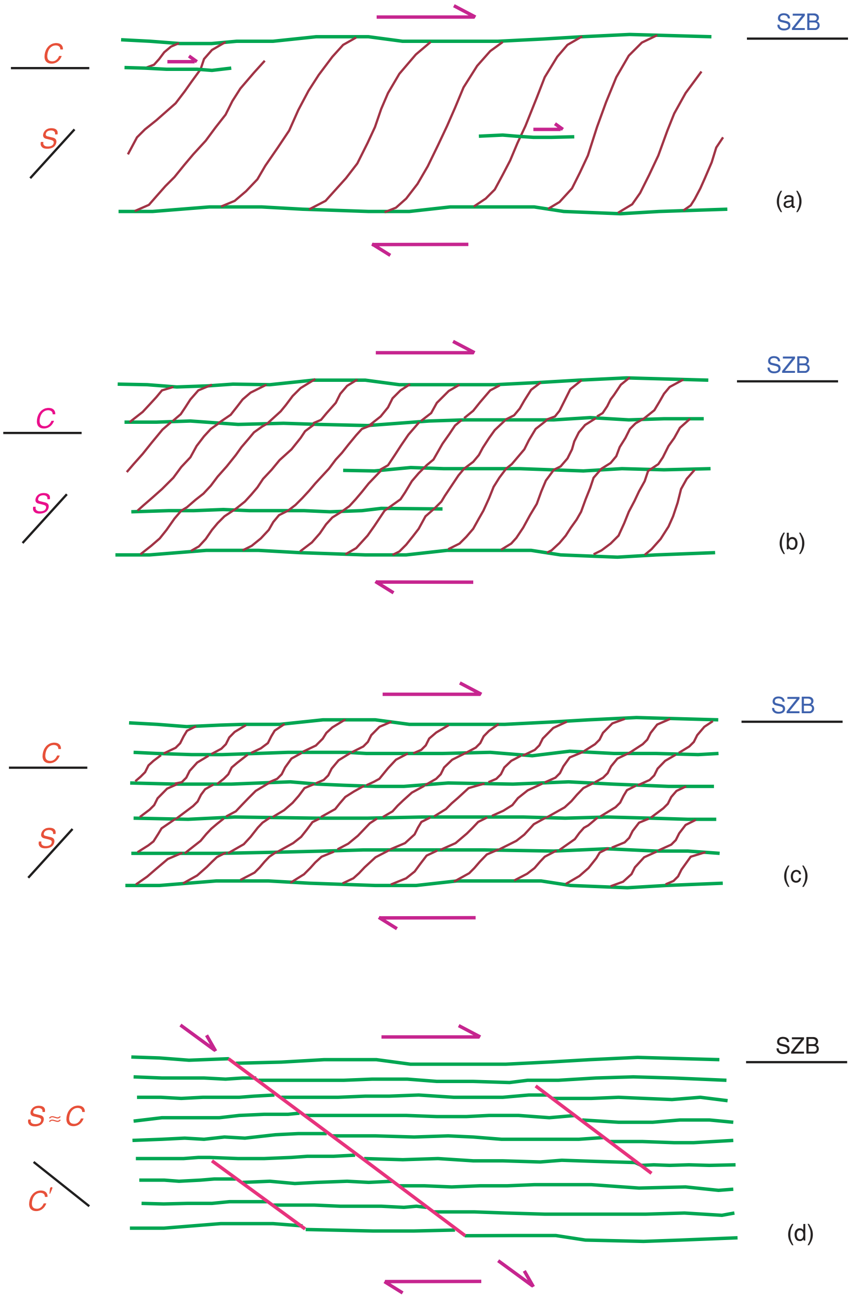

Fig. 5.49: Sketches showing the development of *S*–*C* folia and eventual *C′* folia in a mylonite zone (shear zone) in a relatively homogeneous rock, such as a granite, undergoing dextral shear, after Simpson (1984, fig. 2), with permission from Elsevier. At low bulk strain (a), the deformation is relatively homogeneous and is dominated by *S* folia, with a few incipient *C* folia. As strain increases (b and c), *C* folia develop and operate with the *S* folia. Finally (d) the deformation is so intense that the angle between the *S* and *C* folia decreases to such an extent that the folia are indistinguishable at the mesoscopic scale, and *C′* folia may develop as the deformation 'locks up' in the later stages of deformation. The sense of shear indicated by the *C′* folia is consistent with that indicated by the *S*–*C* folia.

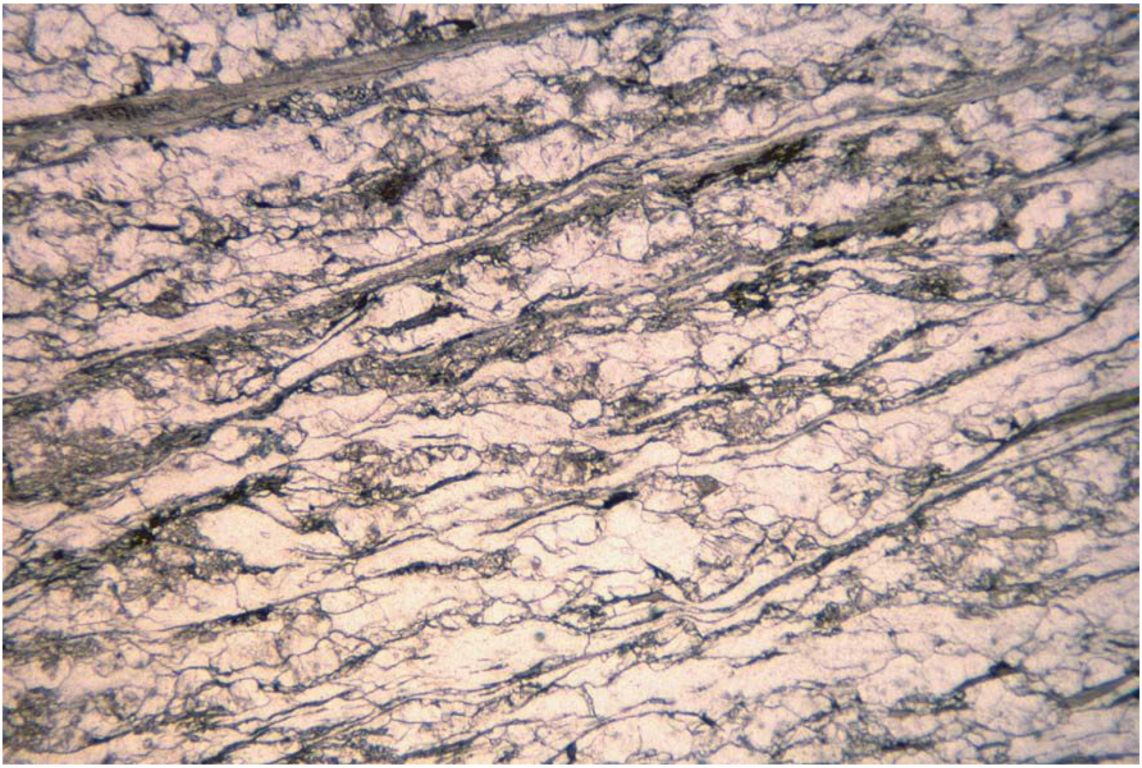

Fig. 5.50: *C′* folia (running from top right to bottom left), delineated by very fine-grained retrograde aggregates, in a felsic mylonite, Strangways Range, central Australia. Thin section kindly provided by Tony Norman. Plane-polarized light; base of photo 11 mm.

is a characteristic feature of K-feldspar megacrysts that crystallize in granites (Figs. 3.12, 3.75). In contrast, K-feldspar porphyroblasts are characterized by spherical quartz and plagioclase inclusions (Vernon, 1968), as shown in Fig. 4.30, or arranged in curved trails reflecting an overgrown matrix foliation. These inclusion trails are independent of the crystallographic orientation of the K-feldspar host. Curved inclusion trails occur in K-feldspar porphyroblasts in metapelitic rocks, but are so rare in felsic gneisses that this criterion alone probably eliminates the porphyroblast hypothesis for nearly all, if not all, examples.

(2) Quartz inclusions in the megacrysts may be much less deformed and recrystallized than quartz in the matrix (Booth, 1968).

(3) K-feldspar phenocrysts commonly have complex oscillatory barium zoning patterns (Section 3.11.5), some with steps (Mehnert & Büsch, 1985). These features appear to be strong indicators of magmatic crystallization of K-feldspar (Vernon, 1986a), and so reflect an igneous precursor if found in K-feldspar in metamorphic or mylonitic rocks (Fig. 5.52). Hour-glass zoning (Sections 3.11.11,

Previous Page

Fig. 5.51: Mylonite formed by the intense deformation of megacrystic granite, east of Armidale, New England area, New South Wales, Australia, showing large porphyroclasts (residual megacrysts) of K-feldspar. The porphyroclasts retain their euhedral shapes, and the mylonitic foliation is deflected around the porphyroclasts. Crossed polars; base of photo 4.9 cm.

4.12.2) may also be present (Brigham, 1984; Dickson & Sabine, 1967; Dickson, 1996).

(4) Simple twinning is common in igneous K-feldspar, but rare to absent in metamorphic K-feldspar. Many augen in felsic gneisses and mylonites show simple twinning (Vernon, 1986a, 1990b, 1999a).

(5) Some K-feldspar augen show planar crystal faces (Fig. 5.51), which are common in magmatic rocks. In contrast, metamorphic K-feldspar porphyroblasts are typically equant and xenoblastic.

(6) The megacrysts are variably deformed, as indicated by microcline twinning (Debat *et al.*, 1978; Eggleton, 1979; Eggleton & Buseck, 1980; Fitz Gerald & McLaren, 1982; Bell & Johnson, 1989b), subgrains, partial recrystallization and neocrystallization. The augen may vary considerably in shape, from rounded to euhedral, depending on the amount of strain they have undergone (see, for

Fig. 5.52: K-feldspar megacryst (auge, porphyroclast) in a mylonite at the western edge of the Papoose Flat granite pluton, Inyo Mountains, California, USA. The megacryst retains its igneous concentric oscillatory zoning and its concentrically arranged euhedral inclusions of plagioclase and biotite. The mylonitic foliation is deflected around the porphyroclast, and 'strain shadows' have been formed at the top left and bottom right ends of the porphyroclast. The zoning pattern indicates that the bottom right part of the porphyroclast is missing, owing to deformation and recrystallization/neocrystallization. The K-feldspar shows patchy tartan twinning (best shown in the K-feldspar grain at right), which is consistent with deformed microcline (Section 4.8). Though it has been deformed, especially at its edges, the megacryst was strong enough to resist the deformation, most of which occurred in the finer-grained matrix. From Vernon & Paterson (2002, *Journal of Electronic Geosciences*, volume 7, page 34, fig. 8, with permission of Springer-Verlag). Crossed polars; base of photo 1.3 cm.

example, Vernon, 1990b), as shown in Figs. 5.51 and 5.52. Crystal faces may be preserved, even in mylonites (Vernon, 1986a, 1990b), as shown in Fig. 5.51.

(7) Concentric compositional zoning and/or zonal arrangement of plagioclase inclusions may be truncated by the external boundaries of an auge, owing to removal of its outer parts by solution and/or recrystallization/neocrystallization during deformation (Vernon & Paterson, 2002), as shown in Fig. 5.52. In contrast, compositional zoning of metamorphic origin follows the metamorphic grain

boundaries, rather than being truncated by them, and so presumably this should also apply to inferred K-feldspar porphyroblasts.

(8) The augen may be replaced marginally and/or along internal fractures by myrmekite (Section 4.10.4), with or without muscovite, especially at sites of high local strain (Vernon *et al.*, 1983; Simpson & Wintsch, 1989; Vernon, 1990b, 1991b; Schulmann *et al.*, 1996; Vernon & Paterson, 2002; Tsurumi *et al.*, 2003). The myrmekite may recrystallize to polygonal aggregates that develop into folia with progressive deformation (see, for example, Vernon *et al.*, 1983; Tsurumi *et al.*, 2003). The formation of abundant myrmekite appears to be strongly correlated with solid-state deformation (Simpson & Wintsch, 1989; Vernon, 1991b; Tsurumi *et al.*, 2003).

(9) Flame perthite (Pryer & Robin, 1995, 1996) is typical of K-feldspar that has undergone solid-state deformation (Fig. 4.54), though typically sporadic in its development. In addition, Debat *et al.* (1978) described aligned sigmoidal lamellae of albite formed in tension gashes during the brittle deformation of K-feldspar megacrysts in augen gneisses.

(10) Fracture of megacrysts, as well as imbrication and boudinage of the resulting fragments (Fig. 5.47), may occur (see, for example, Simpson & Schmid, 1983; Passchier & Trouw, 1996).

(11) The matrix foliation is characteristically deflected around the augen, indicating deformation of the matrix around a strong, existing crystal. The alternative explanation, that megacrysts can push aside the foliation during syndeformational growth, is much less likely, as discussed in Section 5.10.11.

(12) Recrystallized or neocrystallized 'strain-shadows' or 'tails' on K-feldspar porphyroclasts are common in augen gneisses and mylonites (see, for example, Debat *et al.*, 1978; Simpson & Schmid, 1983; Vernon, 1990b; Passchier & Trouw, 1996), as shown in Fig. 5.52. The style of curvature of the tails may indicate the sense of shear of the deformation responsible for the mylonite (Section 5.7.6), and so constitutes good evidence of the existence of the megacryst prior to the mylonitic deformation.

(13) K-feldspar phenocrysts are commonly aligned in granites, in response to magmatic flow (Sections 3.9, 5.11.6). They also commonly show evidence of rotation during flow of the matrix in augen gneisses and mylonites (Simpson & Schmid, 1983). However, in many mylonites they remain random, despite strong flow of the matrix between them; thus, they can persist almost undeformed (apart from microcline twinning and slight marginal recrystallization), complete with igneous features, such as oscillatory compositional zoning and zonally arranged inclusions of igneous plagioclase (Fig. 5.52). This is because the deformation is partitioned preferentially into weaker matrix folia, which are typically rich in quartz and/or mica. Examples are provided by deformed granitoids of the Sandia granite, New Mexico (Vernon, 1986a), the Papoose Flat pluton, California (Paterson *et al.*, 1991), and the Abroi gneiss, New England area, Australia (Vernon, 1990b).

(14) K-feldspar megacrysts in deformed microgranitoid enclaves in an augen gneiss or mylonite are good indicators of an igneous origin (Vassallo & Vernon, 2000), as they are common in such enclaves in non-deformed megacrystic granites, as a result of magma mixing (Section 3.10.3).

5.7.10 Frictional melting (pseudotachylite)

Rapid brittle sliding between rock volumes in the absence of water can build up frictional heat at a fast enough rate to cause partial melting. The resulting rock is called *pseudotachylite* (*pseudotachylyte*), which occurs in veins with sharp contacts with the original rock. Pseudotachylite is formed in faults (Jeffreys, 1942; Philpotts, 1964; Sibson, 1975; Grocott, 1981; Passchier, 1984; Masch *et al.*, 1985; Maddock, 1983, 1986, 1992; Magloughlin, 1989; Passchier *et al.*, 1990; Spray, 1995; Camacho *et al.*, 1995), meteorite impacts (Shand, 1916; Spray & Thompson, 1994), and at the base of thrust blocks (Scott & Drever, 1953) and even large landslides (Masch *et al.*, 1985; Legros *et al.*, 2000). It has been produced by frictional sliding experiments (Spray, 1987, 1995). The generation of pseudotachylite is commonly related to seismic activity (see, for example, McKenzie & Brune, 1972; Sibson, 1975). Friction melts in faults reflect very rapid heat buildup and dissipation on slip surfaces during earthquakes (seismic shearing), whereas the non-melted foliated–lineated fabrics of mylonites are probably due to slow, aseismic shearing (Sibson, 1990).

Pseudotachylite forms by extremely rapid fragmentation, frictional heating, partial melting and rapid cooling (quenching of the melt). The minerals undergo ‘shock’ deformation and some partly melt. Chilling of the melt produces glass and dendritic crystal forms, similar to those described in Section 3.5.3 (Maddock, 1992; Camacho *et al.*, 1995). Vesicular, amygdaloidal and spherulitic microstructures may also be formed (see, for example, Maddock *et al.*, 1987; Camacho *et al.*, 1995). High-temperature metastable minerals (such as pigeonite) may occur, owing to the rapid cooling (Camacho *et al.*, 1995).

The term ‘pseudotachylite’ (Shand, 1916) implies that, although the rock looks like tachylite (basalt glass) in the hand sample, it is chemically different, many analyses indicating a felsic composition. However, careful microprobe analyses of the melted portion (free of unmelted fragments), or recalculation of bulk chemical analyses by removing clast compositions, commonly reveals a relatively mafic composition (see, for example, Sibson, 1975; Magloughlin, 1989; Maddock, 1992; Camacho *et al.*, 1995), as in the example discussed below.

A spectacular example of pseudotachylite occurs in the eastern Musgrave Ranges, central Australia (Camacho *et al.*, 1995), where felsic granulites (consisting mainly of quartz, plagioclase, K-feldspar and orthopyroxene) were involved in a thick mylonite zone and later faulted. The dry rocks built up heat, and melted to form huge amounts of pseudotachylite (4% of a zone 1 km thick), consisting of rock and mineral fragments enclosed in glass with stretched gas bubbles

(Fig. 3.42). Chilling formed spherulitic aggregates in altered glass (Fig. 3.44), spectacular dendritic overgrowths on fragments of plagioclase (Fig. 3.43), tendril-like branches of pigeonite on fragments of orthopyroxene, and feathery dendrites of pigeonite throughout the former melt (Fig. 3.43). The dendritic to fibrous habits of these crystals and aggregates are characteristic of high degrees of supersaturation (Sections 3.5.3, 3.5.5). The presence of pigeonite (a metastable high-temperature calcium-poor clinopyroxene) indicates rapid cooling from very high temperature (>1000 °C). Careful chemical analysis with the electron microprobe (excluding unmelted fragments) shows that the melt composition is mafic, not felsic, because only the mafic minerals melted. This may be because the internal structures of the pyroxene and plagioclase were more disturbed by the shock deformation than those of the quartz or K-feldspar.

5.8 Foliations and lineations

Tectonic foliations and *lineations* are planar structures (compositional layering and/or parallel alignment of minerals) and linear structures (compositional rods and/or linear alignment of minerals), respectively, produced by deformation. These structures are especially abundant on the outcrop scale, but are also commonly seen in the microscope. Examples of different types of foliations and lineations have been illustrated by Turner & Weiss (1963) and Passchier & Trouw (1996).

As well as superimposed tectonic foliations, sedimentary bedding may be preserved, especially in relatively weakly deformed and low-grade metamorphic rocks. In outcrop, its identification may be assisted by sedimentary structures, but in thin sections it appears as a layered compositional variation (Fig. 5.53), which may require correlation with outcrop structures for certain identification. Graded bedding may be observable in thin section, although metamorphic neocrystallization may produce coarse-grained minerals (e.g. porphyroblasts) in the more pelitic parts of the graded beds, thereby inverting the depositional grainsize variation. True bedding is oblique to the axial surfaces of microfolds in their hinge areas, but intense deformation may transpose the bedding into a new orientation parallel to newer foliations in the limbs of tight folds. In strongly deformed metamorphic rocks, bedding may be largely removed or even obliterated by transposition (strong modification and realignment of a foliation into a new orientation) and/or recrystallization/neocrystallization (Section 5.7.6).

5.8.1 Bedding-plane foliation

Bedding-parallel mineral alignments are common in pelitic sedimentary rocks that have not been strongly deformed tectonically (see, for example, Williams, 1972; Etheridge & Lee, 1975; Holeywell & Tullis, 1975; Knipe & White, 1977; Beutner, 1978; Maltman, 1981; Bennett *et al.*, 1981, 1991; Morritt *et al.*, 1982;

Fig. 5.53: Schist from the Picuris Range, New Mexico, USA, with (1) inferred bedding (shown by broad compositional variations: quartz-rich versus mica-rich) trending from the upper left towards the lower right of the photo, (2) an early, fine-grained, tectonic foliation (slaty cleavage) crenulated by later folds, but trending from the lower left to the upper right, and (3) a crenulation cleavage (more spaced, anastomosing, strongly compositionally differentiated foliation) trending steeply from upper left to lower right. Also shown are porphyroblasts of staurolite, biotite and garnet. Crossed polars; base of photo 1.8 cm.

Baker *et al.*, 1993). The alignment is called bedding-plane foliation (see, for example, Morritt *et al.*, 1982) or diagenetic foliation (Passchier & Trouw, 1996). The aligned minerals are typically detrital clay minerals or mica, and grains rotate in response to compaction (Baker *et al.*, 1993). TEM and SEM studies have revealed the detailed microstructure of clays and shales (Bennett *et al.*, 1981, 1991). Moore & Geigle (1974) described bedding-parallel foliation formed by alignment of platy and elongate minerals in Pleistocene mudstones from the Aleutian Trench and the Gulf of Mexico.

In slates, clastic mica is commonly kinked, especially where oblique to the bedding (Morritt *et al.*, 1982), as a result of compaction or incipient folding. The detrital nature of the mica is characterized by frayed ends and a very high length-to-width ratio, both features being caused by abrasion and splitting along the cleavage during transport. The fact that the mica is not due to metamorphism is confirmed by the typical detrital shapes of quartz grains in the rock (Morritt *et al.*, 1982). However, compaction generally does not produce a slaty cleavage (Section 5.8.2), unless it continues during the early stages of folding, when axial-surface cleavages begin to form. In some slates, the bedding-plane foliation is so strong that the first recognizable folds are crenulations, which typically develop in finely foliated rocks (Williams, 1972; Morritt *et al.*, 1982), as discussed in Section 5.8.3.

5.8.2 Slaty cleavage

Many areas of low-grade metamorphosed shale, siltstone and sandstone develop one dominant foliation, known generally as *slaty cleavage* (Figs. 5.54, 5.55). The foliation is typically developed parallel to the axial surfaces of folds. If the folds are isoclinal, the cleavage tends to be subparallel to bedding in the limbs and oblique to bedding in the hinges of the folds. The analogous cleavage in deformed sandy rocks is called *penetrative domainal cleavage* or 'rough cleavage' (Durney & Kisch, 1994), as shown in Fig. 5.56.

Slaty cleavage consists of narrow dark folia of fine-grained, well-aligned phyllosilicate minerals (especially white mica and chlorite) and/or graphite (P or M domains), anastomosing around stronger domains containing detrital fragments, mainly of quartz (Q domains), as shown in Figs. 5.54 and 5.55. Thus, slaty cleavage is typically compositionally differentiated. In some slates and schists, the Q domains appear to be largely unmodified, showing detrital microstructures (see, for example, Williams, 1972; Etheridge *et al.*, 1983, fig. 2), whereas in other slates and some metasandstones the quartz grains in the Q domains have overgrowths of quartz or of quartz–phyllosilicate fringes or 'beards' of fibrous grains extending parallel to the cleavage (see, for example, Powell, 1969, figs. 3, 5; Williams, 1972), as shown in Figs. 5.15 and 5.54. In many slates, the quartz clasts in Q domains are weakly deformed or non-deformed, with slight to no undulose extinction and little or no evidence of recrystallization, despite a strong tendency towards rectangular grain shapes and elongation parallel to the slaty cleavage (Fig. 5.56). This indicates that their change into elongate shapes is due largely to solution of parts of clasts adjacent to cleavage folia, rather than to crystal-plastic processes (Williams, 1972; Gray, 1978; Bell, 1978a; Gregg, 1985; Vernon, 1998, fig. 6). P domains rich in fine-grained dark material in some slates (Fig. 5.56) resemble stylolitic solution seams (see, for example, Williams, 1990).

Some slates show evidence of grain rotation, at least in the early stages of cleavage formation (Knipe & White, 1977; Roy, 1978; Bell, 1978a; Gray, 1979; Knipe, 1979, 1981; White & Johnston, 1981; van der Pluijm & Kaars-Sijpesteijn, 1984). This mechanism for forming slaty cleavage was suggested by Sorby (1853). Moreover, weak foliations have been observed in unconsolidated sediments (Paterson *et al.*, 1985), especially in slumps (Williams *et al.*, 1969; Maltman, 1981; Paterson

& Tobisch, 1983), the foliation being formed mainly by rotation of existing phyllosilicate grains. A range of structures related to incipient cleavage development in consolidated sediments has been described by Durney & Kisch (1994).

Moore & Geigle (1974) described folded mudstones from the Aleutian Trench and the Gulf of Mexico with an axial surface foliation (incipient slaty cleavage), the intensity of the foliation increasing with the tightness of the folds. The degree of carbonization of organic matter indicates that the temperature reached only 68 °C, and compaction tests indicate pressures of 120–859 bar, at an estimated strain rate of 10–13 s^{-1}. The folds may have been produced by slumping, which is common at continental margins. Moore & Geigle (1974) suggested that deformation of semi-lithified sediments may initiate folds and cleavages in many complexly deformed tectonites.

Several studies have shown that cleavages may initiate mechanically during diagenesis and continue to develop by chemical–mechanical processes during low-grade metamorphism (Williams *et al.*, 1969; Spang *et al.*, 1979; Mackenzie *et al.*, 1987; Tranter, 1992; Hammond, 1987; Boyer, 1984). However, many more recent investigations (Williams, 1972; Wood, 1974; Boulter, 1974; Etheridge & Lee, 1975; Holeywell & Tullis, 1975; Geiser, 1975; Groshong, 1976; White & Knipe, 1977, 1978a; Beutner, 1978; Gray, 1978; Bell, 1978a; Gregg, 1985; Knipe, 1981; Woodland, 1985; Williams, 1983; Lee *et al.*, 1986; Kanagawa, 1991) have inferred that most of the phyllosilicate alignment and cleavage development occurs by solution of old grains (phyllosilicate minerals, quartz and/or carbonate) and neocrystallization, as well as physical grain rotation, but after most or all of the dewatering and lithification of the sediment. Because chemical reactions are intimately involved with at least the later stages of the formation of slaty cleavage (Knipe, 1979, 1981), the process cannot be regarded as purely mechanical. In addition, the compositional domains of slaty cleavages require redistribution of chemical components.

Deformation of detrital, bedding-parallel phyllosilicate grains may produce kink bands parallel to the developing cleavage (Bell, 1978a; van der Pluijm & Kaars-Seijpesteijn, 1984). Growth of these segments and/or nucleation of new mica grains parallel to them could lead to oriented mica aggregates in developing P domains. These interpretations of observations of natural examples support models for mica preferred orientation suggested by Etheridge & Hobbs (1974) and Williams *et al.* (1977). Knipe & White (1977), Knipe (1981) and Weber (1981) suggested, from SEM studies on Welsh and German slates, respectively, that the earlier stages of cleavage formation (on the SEM scale) may involve crenulation of earlier (e.g. bedding-parallel) foliations, after which syndeformational neocrystallization of phyllosilicates in the new foliation becomes the main mechanism for producing aligned phyllosilicate aggregates.

Some slates have lenticular to ellipsoidal intergrowths (‘stacks’) of chlorite and white mica with their cleavages mainly oriented obliquely to the slaty

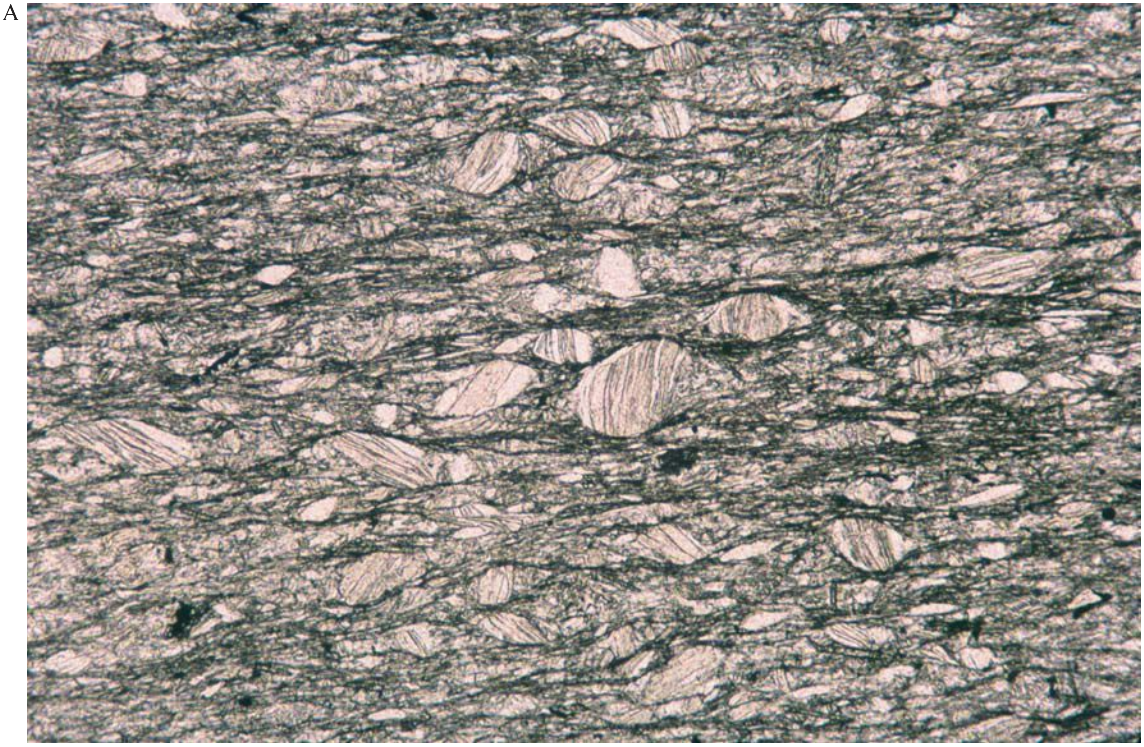

Fig. 5.54: (A) Slaty cleavage, composed of thin mica–chlorite–graphite folia anastomosing around clastic grains of quartz and lenticular aggregates ('stacks') of chlorite (pale green) interlayered with white mica. The slate is from the Hill End area, New South Wales, Australia. Many of the quartz clasts and mica–chlorite aggregates are elongate parallel to the foliation, and have shapes suggestive of solution processes (Fig. 5.56). The cleavage of the intergrown chlorite and white mica in the 'stacks' varies from perpendicular to only slightly oblique to the slaty cleavage. Plane-polarized light; base of photo 1.5 mm. (B) Same field of view, but in crossed polars, to show the lower birefringence of the chlorite (some with anomalous blue interference colours), compared with the white mica, in the 'stacks.'

cleavage though they vary from perpendicular to only slightly oblique to the slaty cleavage, and a few 'stacks' may even have the cleavage approximately parallel to the slaty cleavage (Fig. 5.54). Several workers have interpreted the 'stacks' as primary clasts (for example, of biotite) modified by fracturing and growth of secondary phyllosilicate (Beutner, 1978; Roy, 1978; van der Pluijm & Kaars-Sijpesteijn, 1984; Milodowski & Zalasiewicz, 1991; Clark & Fisher, 1995). This could account for the scarcity of 'stacks' with cleavage parallel to the slaty cleavage, because these would probably have deformed by slip on the phyllosilicate cleavage, thereby becoming part of the slaty cleavage itself. However, the 'stacks' do not resemble typical unmodified detrital mica clasts (Gregg, 1986), which tend to be very elongate, owing to splitting along the cleavage

Fig. 5.54: (*cont.*)

during transport. In contrast, many 'stacks' are much thicker perpendicular to their cleavage than parallel to it, which could be taken to imply growth in Q domains during development of the slaty cleavage. Alternatively, it could be due to solution and consequent truncation by the slaty cleavage of formerly much longer mica clasts.

Most observations are consistent with the general inferences that (1) slaty cleavage may begin to develop at submetamorphic temperatures, and continue to develop with prograde metamorphism, and (2) mechanical rotation and/or kinking of detrital grains may dominate in the earlier stages, whereas solution and neocrystallization dominate in the later, probably most important, stages of cleavage development.

5.8.3 Crenulation cleavage

The foliation in medium- to high-grade regional metamorphic rocks (schists) is generally called *schistosity* or *schistose foliation*. The minerals defining schistose foliations typically are coarser-grained than in slates and phyllites. Many of these foliations constitute a *crenulation cleavage* (Figs. 5.35, 5.53), which may also occur in slates and phyllites (Fig. 5.55). The origin of crenulation cleavage

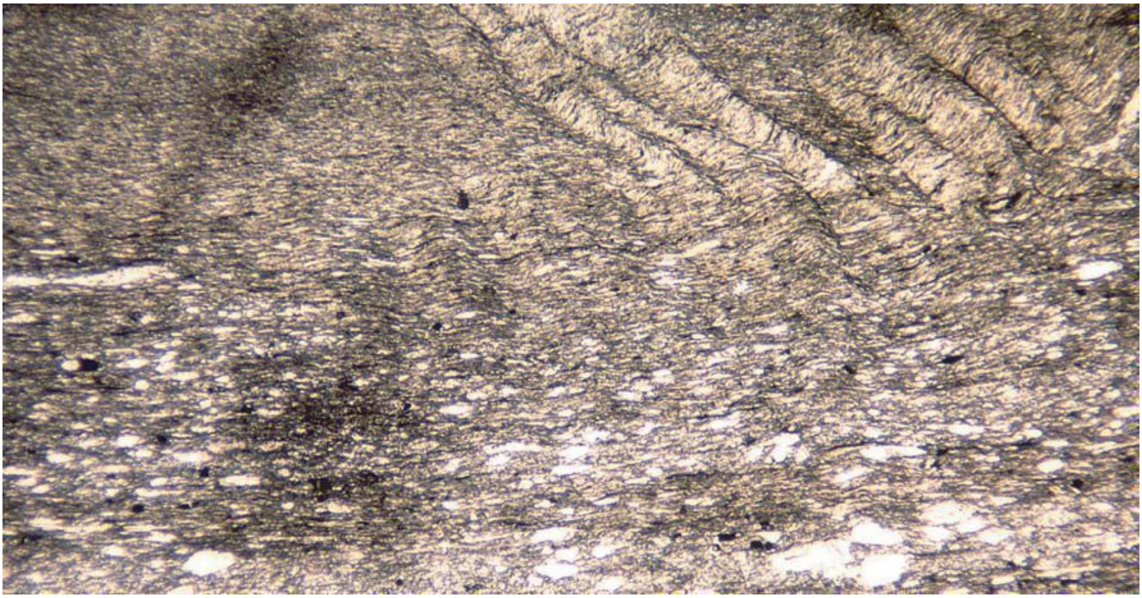

Fig. 5.55: Local development of crenulation cleavage in slate, Hill End area, New South Wales, Australia. The crenulation cleavage has been formed only in the most micaceous layer (bed), but even there its development is patchy. The slaty cleavage in the non-crenulated bed shows micaceous folia anastomosing around lenticular clasts, mainly of quartz. Plane-polarized light; base of photo 11 mm.

has been discussed by many workers (e.g. Williams, 1972, 1990; Cosgrove, 1976; Gray 1977a,b, 1978, 1979; Gray & Durney, 1979a,b; Marlow & Etheridge, 1977; Hanmer, 1979; Bell & Rubenach, 1983). Crenulated schistosity formed by elongate hematite ('specularite') grains has also been observed in deformed hematite rocks (Rosiére *et al*., 2001).

Generally, a previous tectonic foliation, such as a slaty cleavage or an earlier crenulation cleavage, is present, but crenulations may also form in rocks with a strong depositional bedding-parallel foliation or fissility ('shaly cleavage'), as discussed in Section 5.8.2. The new cleavage typically initiates at a high angle to the earlier slaty or crenulation cleavage (Fig. 5.55), as observed in experiments on the kinking and crenulation of layer silicate aggregates (see, for example, Etheridge *et al*., 1973; Williams *et al*., 1977).

Crenulation cleavages are also compositionally differentiated into domains that are known as P (or M) and Q (see Section 5.7.1). The term 'crenulation cleavage' covers a large variety of crenulation-type foliations, ranging from *zonal* (with gradational layering) to *discrete* (with abrupt layering) types (Gray 1977a,b), as shown in Figs. 5.35 and 5.53. Zonal crenulation foliations may pass into discrete crenulation foliations. Some schists show a gradation from open zonal

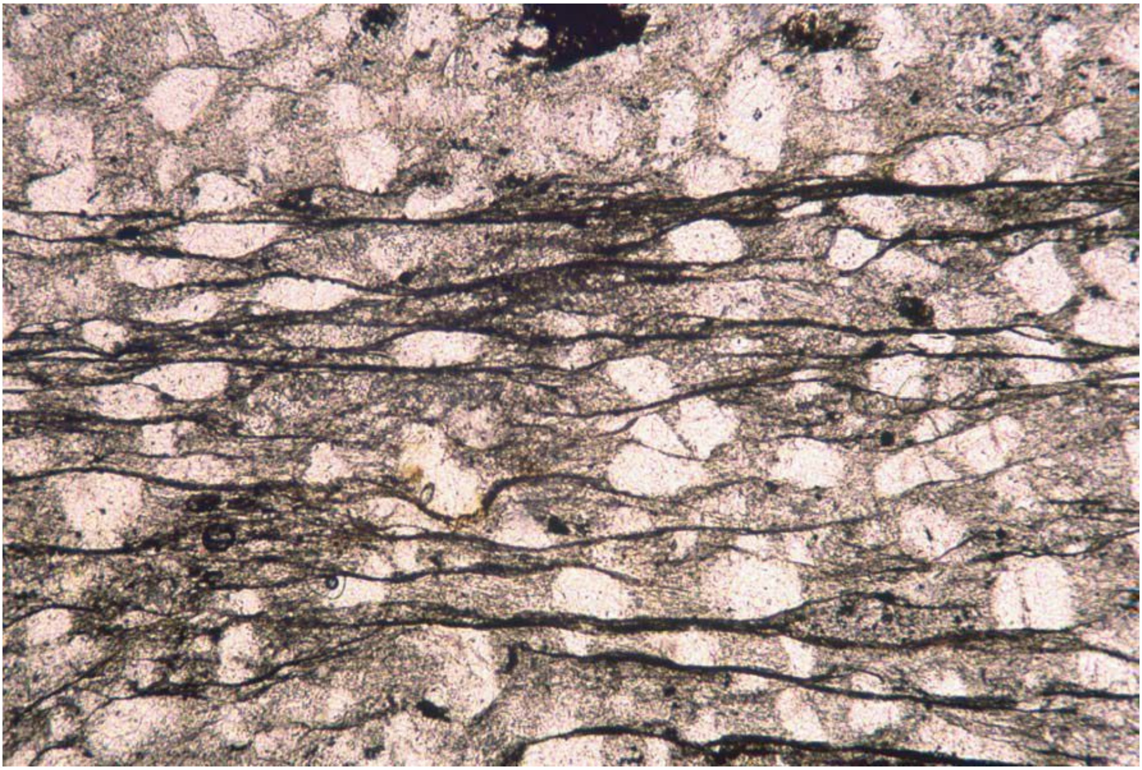

Fig. 5.56: Penetrative domainal cleavage in a muddy sandstone (analogous to slaty cleavage in a slate) from the root zone of the Wildhom nappe, Valais, Switzerland, showing dark folia (seams) formed by solution, anastomosing around clasts of quartz, the shapes of which suggest solution against the seams. This has resulted in somewhat rectangular grain shapes that are elongate parallel to the foliation, which can be compared with pre-cleavage grain shapes at the top of the photo. Fine-grained mica and chlorite between the seams occur mainly as aggregates aligned parallel to the foliation, forming 'beards' against the quartz clasts. Section cut perpendicular to the cleavage and parallel to the lineation. Sample by courtesy of David Dumey. Plane-polarized light; base of photo 1.5 mm.

crenulations, through progressively tighter differentiated crenulations, into thoroughly recrystallized rocks from which all vestiges of former microfolds have been removed (Bell & Rubenach, 1983), as shown in Fig. 5.57. The reason for this change from a differentiated to a non-differentiated aggregate has not been explained. It could involve a change from stress-induced solution transfer (at least partly responsible for forming the layering) to dominant dislocation creep and recrystallization.

P (M) domains commonly are interpreted as insoluble residues resulting from the solution and removal of quartz or carbonate, generally with evidence of

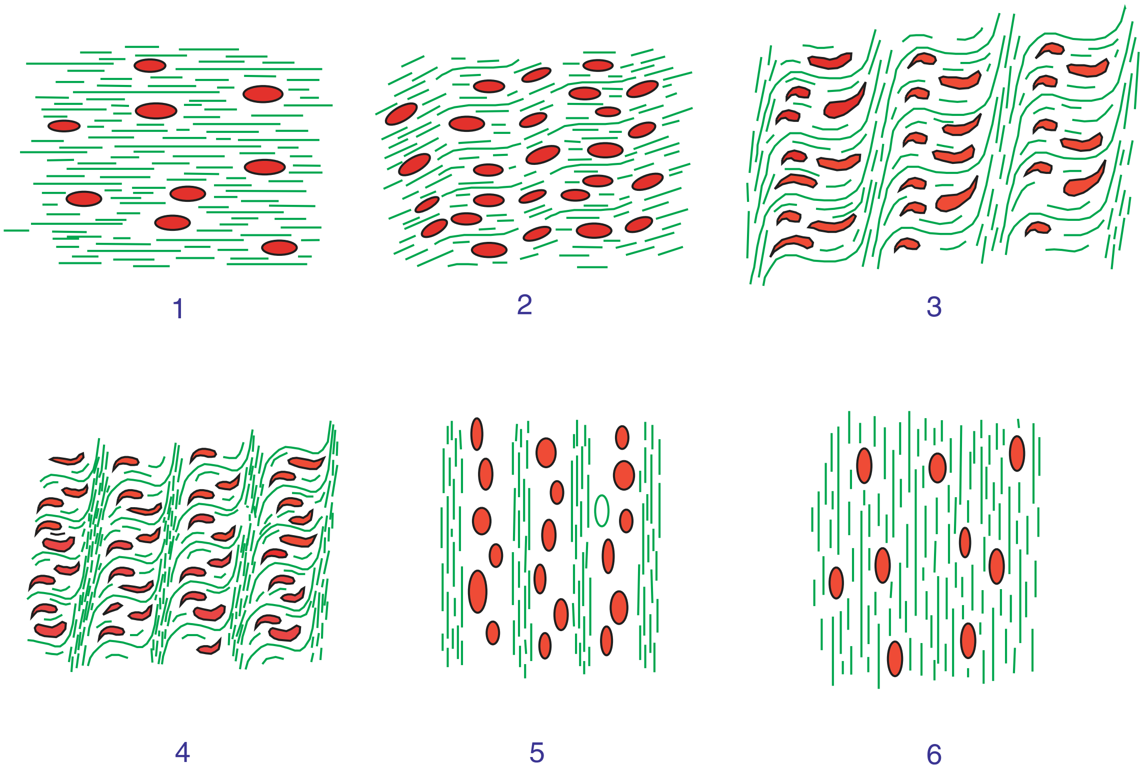

Fig. 5.57: Six stages of progressive development of a crenulation-foliation ('crenulation cleavage') suggested by Bell & Rubenach (1983). The sketches show (1) original foliation, (2) initiation of crenulations, (3) initiation of a compositional layering ('metamorphic differentiation') in the crenulation limbs ('septa'; P or M domains), (4) growth of new mica in P domains, (5) destruction of crenulations in fold hinges ('microlithons'; Q domains), and (6) homogeneous new foliation in a new orientation. Porphyroblasts and porphyroblasts with strain shadows are shown in red. Sketches after Johnson (1999b, fig. 2), with permission of the Mineralogical Society of America.

neocrystallization of phyllosilicates (or sillimanite at highest grades of metamorphism) parallel to the foliation. Though some curvature of phyllosilicate grains at the edges of Q domains into P domains is common, old phyllosilicate grains statistically parallel to an earlier foliation or bedding generally appear to have been dissolved against the developing P domains (see, for example, Lee *et al.*, 1986). Increased deformation in the high-strain limbs of crenulations causes solution and removal of minerals such as quartz, feldspar and calcite from these zones, leaving them enriched in minerals with a layered or strongly prismatic structure, such as biotite, white mica, chlorite or graphite at low to intermediate grades of metamorphism or sillimanite at high grades (see, for example, Vernon, 1987b), as shown in Fig. 5.58. These minerals survive presumably because they

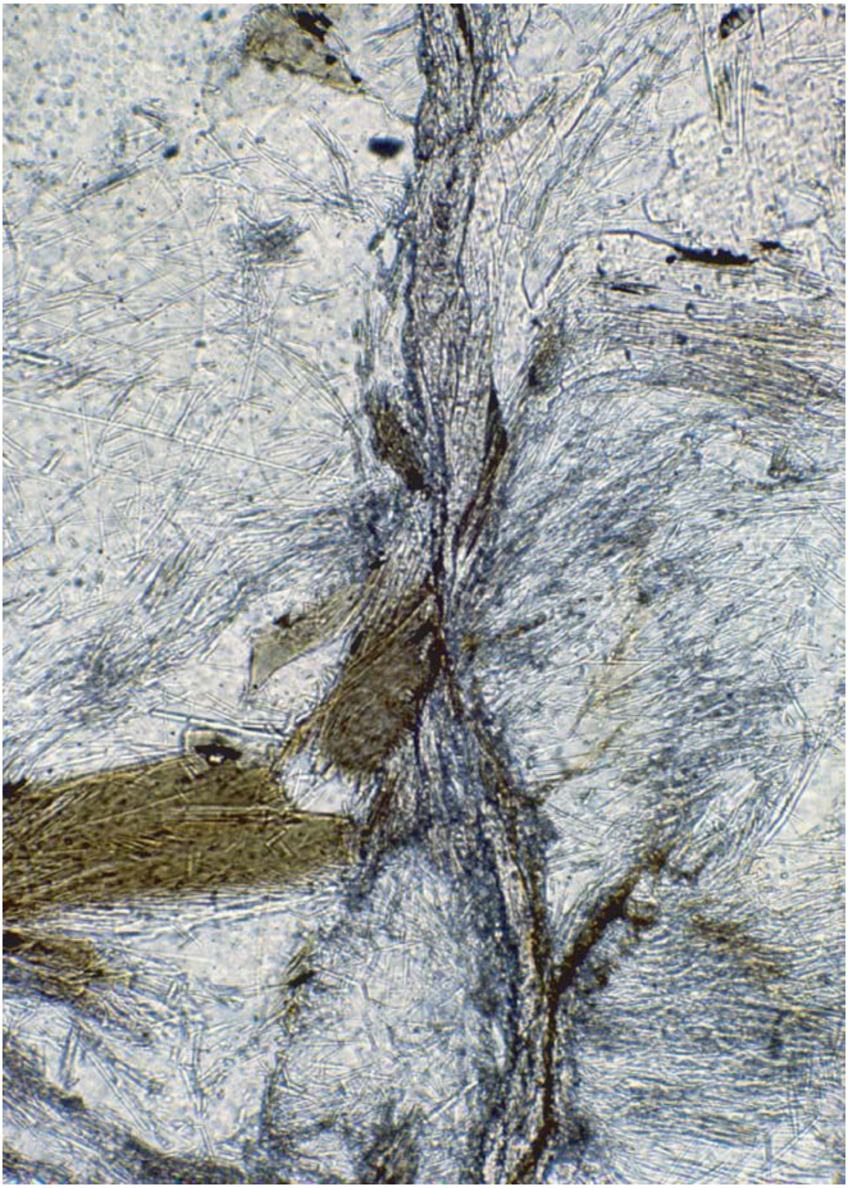

Fig. 5.58: Folium (P domain) of fibrous sillimanite in a crenulation cleavage in a high-grade schist from the Placitas–Juan Tabo area, New Mexico, USA. The adjacent Q domains show the earlier foliation, delineated by fibrous sillimanite and biotite, curving into the P domain. However, the sillimanite in both domains belongs to the same mineral assemblage. Plane-polarized light; base of photo 1.1 mm.

are relatively stable in an environment of strong, non-coaxial strain accumulation; this stability may be due to a relatively low solubility at high normal stress or a marked ability to slip on cleavages or grain boundaries, without much accumulation of lattice strain. This ability is probably related to the strongly anisotropic crystal structures of the minerals concerned, resulting in relatively weak bonding across rational crystal boundaries, such as $\{001\}$ planes in layer silicates, $\{0001\}$ planes in graphite and $\{110\}$ planes in sillimanite. Thus, they are able to undergo large amounts of non-coaxial strain without dissolving, as suggested by Bell & Rubenach (1983), Bell *et al.* (1986) and Vernon (1987b).

Stress-induced solution transfer (Section 5.9.2) could cause solution at high-stress sites, and internal strain in the form of concentrations and tangles of dislocations could cause increased solubility of the minerals concerned ('strain solution'). For example, Wintsch & Dunning (1985) showed that strain solution of quartz deformed at relatively low temperatures (with abundant dislocation tangles) may occur if the fluid : rock ratio is low. However, the relative contributions of stress and strain to the solution process in the formation of crenulation cleavage are uncertain.

Discrete crenulation cleavages (Fig. 5.53) consist of limb-zones (P or M domains) rich in sheet silicates and/or sillimanite alternating with or anastomosing around layers or elongate lenses, respectively, of lower-strain hinge-zones (Q domains, 'microlithons') rich in quartz, which preserve the approximate orientation of the pre-existing foliation. The P domains accommodate most of the non-coaxial strain, whereas the Q domains appear to deform mainly coaxially (Bell, 1981, 1985).

Compositional mapping with the electron microprobe has revealed untwinned plagioclase coexisting with quartz in the Q domains of some crenulated schists (Williams *et al.*, 2001). These maps have also shown that non-crenulated areas undergo compositional alteration and structural modification during the crenulation of adjacent areas, and so cannot be assumed to represent the original rock prior to the formation of the crenulations (Williams *et al.*, 2001).

The components of minerals dissolved from the P domains are inferred to be either (a) concentrated in hinge zones of the crenulations or (b) removed from the local observable system (e.g. on the scale of a large thin section, a hand specimen or even an outcrop), to be deposited in veins nearby or further afield. A controversy rages about which interpretation is correct, and possibly both are in different local circumstances, as discussed in Section 5.9.4.

P domains rich in very fine-grained opaque material in the limbs of microfolds crenulating earlier folia (slaty cleavage) that also have dark concentrations indicate that very similar or identical metamorphic differentiation processes can occur in the development of both slaty and crenulation cleavage (Williams, 1990; Vernon, 1998, fig. 7). In fact, transitions from domainal slaty cleavage to crenulation cleavage and vice versa are common (Hobbs *et al.*, 1976, p. 223; Williams, 1972, 1990; Bell & Rubenach, 1983). However, the P domains or films in slaty cleavages tend to have sharper boundaries and anastomose more than crenulation cleavages (Williams, 1990, p. 273), although crenulation cleavages generally also anastomose, especially around porphyroblasts (Fig. 5.35).

Worley *et al.* (1997) found that the mechanism of formation of crenulation cleavage varies with metamorphic grade. At chlorite–biotite zone conditions (around 520 °C), the formation of crenulation cleavage is dominated by local solution–deposition, resulting in distinct compositional differences between the

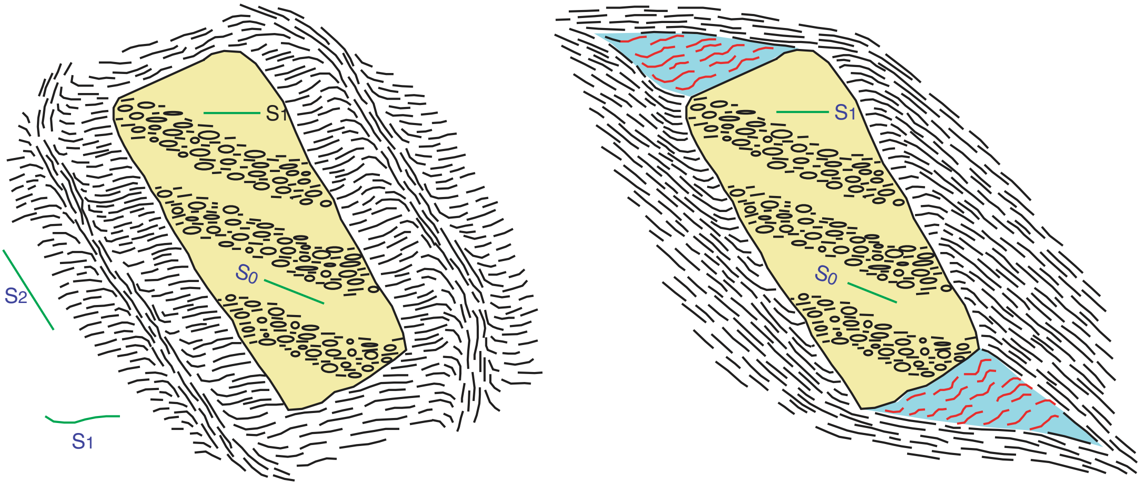

Fig. 5.59: The left sketch shows a porphyroblast with S_0 (bedding, indicated by compositional layering) and S_1 inclusion trails (e.g. slaty cleavage) in a schist developing a differentiated crenulation cleavage (S_2). S_1 is indicated by elongate inclusions oblique to S_0. The porphyroblast mostly grew before the crenulation folding began, but slight curvature of both S_0 and S_1 at the edges of the porphyroblast indicates that the crenulations began to form as the porphyroblast completed its growth. The right sketch shows a later stage of development of the matrix, the crenulations having been obliterated, either by intense deformation of the matrix to stage 6 of Bell & Rubenach (1983) (Fig. 5.57) or by reactivation of S_1 and consequent 'decrenulation' during a later deformation event (Bell, 1986). Despite the intense deformation, relics of crenulated S_1 are preserved in 'strain shadows' (shown in blue-green) at both ends of the porphyroblast, which were protected from the latest deformation.

mica of different structural domains. However, at garnet zone conditions, the mica compositions are homogeneous across domains, reflecting increasing importance of diffusion through mineral grains ('volume diffusion') and consequent equilibration of mineral compositions.

Multiple crenulation cleavages are typical of schists, owing either to repeated, separate deformation events or to continuous deformation being affected by mechanical heterogeneities, such as porphyroblasts. Even where the schistosity appears superficially to be a single foliation, detailed examination of protected, low-strain sites (e.g. adjacent to porphyroblasts) commonly reveals residual crenulation microfolds that have been obliterated from unprotected areas of the matrix (Fig. 5.59), as discussed below.

5.8.4 Gneissic foliation (gneissic layering)

With the exception of mylonitic rocks in high-strain zones (Sections 5.7.6, 5.8.5), foliations in high-grade metamorphic rocks are typically less continuous than in low- and medium-grade metamorphic rocks, owing to a coarser grainsize. Some high-grade rocks are so weakly foliated that they are called *granofelses*, which is a handy, non-genetic term for a granular metamorphic rock. In metapelitic gneisses, folia rich in biotite and/or sillimanite commonly anastomose strongly around large grains of garnet, K-feldspar or cordierite (Fig. 4.31), all these minerals belonging to the same compatible assemblage (Section 4.13). Gneisses of felsic igneous composition typically consist of xenoblastic aggregates of quartz and feldspar, with or without garnet or orthopyroxene, interspersed with discontinuous, anastomosing folia rich in biotite. Many gneisses of mafic igneous composition are commonly only weakly foliated, consisting of polygonal (*granoblastic*) aggregates of calcic plagioclase, pyroxene and hornblende (Figs. 4.23, 4.79).

High-grade metamorphic rocks may also show a compositional layering (see, for example, Myers, 1978). This may represent bedding in relatively weakly deformed metasedimentary gneisses, but is more likely to be transposed bedding and/or new compositional layering of tectonic origin in more strongly deformed rocks. Leucosome layering (Section 4.16.1), commonly folded and boudinaged, also occurs in migmatitic gneisses. Strong compositional layering is less common in felsic gneisses derived from the deformation and metamorphism of granites, although prominent quartz–feldspar layering occurs in rocks such as deformed pegmatites (Fig. 5.43). Compositional layering may occur in mafic gneisses, commonly formed by the deformation and transposition (strong modification and realignment) of an original igneous layering (Myers, 1978).

The development of compositional layering in the conversion of orthopyroxene granite to granulite facies gneiss has been studied in detail by M. L. Williams *et al.* (2000). They found that the layering was developed in three microdomains, namely: (1) former plagioclase phenocrysts, which recrystallized to finer-grained aggregates in a core-and-mantle microstructure (Section 5.4.7), followed by the development of recrystallized 'ribbons' or Platten (Section 5.5.1), augmented by the growth of garnet to form garnet-rich sublayers in the plagioclase domains; (2) former orthopyroxene phenocrysts, which neocrystallized to clinopyroxene and garnet (with or without hornblende, depending on local availability of water); and (3) former groundmass. They also found that quartz veins were emplaced and then deformed to form quartz-rich layers. The result is a strong mineral segregation inherited mainly from igneous precursor minerals.

Some high-grade mylonites and gneisses contain elongate layers or rods of quartz (commonly very coarse-grained) alternating with layers of granoblastic feldspar (Fig. 5.43). The quartz layers are generally attributed to strong deformation, coupled with recrystallization, of primary quartz grains, which probably is an appropriate explanation for the deformed pegmatite shown in Fig. 5.43. For example, Hippert *et al.* (2001) suggested that isolated quartz grains become elongated by crystal plastic flow, and then coalesce to form layers. However, Boullier

& Bouchez (1978) suggested that, although single-crystal quartz lenses formed at lower metamorphic grades are deformed formerly large quartz grains, elongate polycrystal aggregates are of more doubtful origin, some being deformed pre-existing quartz layers and others being formed by ductile deformation of formerly large quartz grains.

However, some have suggested that similar quartz layers may originate as veins during mylonitic deformation (Vollbrecht *et al.*, 1997; Williams *et al.*, 2000). Very elongate, vein-like grains and aggregates of quartz, ilmenite, titanite and scapolite may be formed by microfracturing and coupled mass transfer – deposition during mylonitic deformation of gabbro at high-temperature amphibolite facies conditions (Lafrance & Vernon, 1993, 1999).

5.8.5 Composite (transposed) foliations in mylonitic rocks

In zones of high strain, such as mylonite zones or thrusts, progressive deformation commonly produces complicated, very localized fold and foliation sequences that are closely related in time. Meneilly (1983), Williams (1985) and Tobisch & Paterson (1988) have shown that recognition of deformation sequences in such rocks is commonly difficult or even impossible. The structures involved have similar orientations, senses of movement and metamorphic grades, and are produced as a relatively continuous sequence in a geologically short time (Tobisch & Paterson, 1988). The resulting *composite foliations* are so complex and locally variable that conventional time-sequence terms, such as S_1, S_2, etc. and F_1, F_2, etc., which are useful in lower-strain terranes, are inappropriate.

For example, in mylonite zones in granitoid and similar rocks, complex refolding, truncation of foliations, isolated (truncated) fold hinges and divergent lineations are common (Fig. 5.42), and all may be formed by progressive deformation in the same general deformation event (see, for example, Hammond, 1987). Similarly, in high-strain zones in metasedimentary rocks, Tobisch & Paterson (1988) recognized sequences of foliation development on a very local scale (even that of a thin section), so that a morphological nomenclature for foliations is preferable to one with a temporal connotation. Though the usual temporal classification of folds and foliations may be applicable for a small area (e.g. part of a thin section) in such zones, temporal correlation cannot be made with similar sequences in other small areas. Therefore, Tobisch & Paterson (1988) emphasized that temporal notations should be used only if independent evidence indicates that structural elements can be related in time. They observed microstructural evidence of various kinds of 'transposition cycles' from continuous cleavage (similar or identical to slaty cleavage), through crenulation cleavage to transposed foliation, similar to the sequence proposed by Bell & Rubenach (1983), and suggested that plotting domains of similar transposition cycles on a map may reveal the location and extent of deformation partitioning on a scale broader than that of a single specimen or thin section. This would give a more realistic picture of deformation in high-strain zones than the assumption that sequences of foliations can be correlated in time. The general problem of correlating deformation sequences in time and space is discussed in Section 5.10.2.

5.8.6 Layering produced by partial melting

Neosomes and leucosomes in *stromatic migmatites* (Section 5.11) constitute layering that is generally attributed to partial melting (*anatexis*) during metamorphism at conditions of the upper amphibolite and granulite facies (Section 4.16.1). Neosomes represent former melted material plus crystals, and leucosomes mostly represent former melt that has segregated from crystals. The leucosomes/neosomes are segregated into layers ('stroma') parallel to a tectonic foliation, forming *stromatic migmatites* or *metatexites*. Some may be due to solid-state deformation of previously formed leucosomes (see, for example, Vernon *et al.*, 2000, 2003). The layers are best seen in outcrops, and in thin section generally appear as polygonal aggregates or recrystallized aggregates with irregular boundaries, mainly of quartz and feldspars, with less abundant mafic minerals. In general, the deformation and recrystallization have been so intense that no magmatic relics remain in the leucosome layers, but crystal faces in feldspar may remain in some examples (Vernon & Collins, 1988; Vernon & Johnson, 2000), as shown in Figs. 4.80 and 4.81. Where larger amounts of melt are formed, the foliated structure of metatexites is disrupted by flow *en masse*, producing *schlieren migmatites* or *diatexites*.

5.9 Fluid and mass transfer in deforming rocks

5.9.1 General aspects

Some of the relationships between fluids and deformation have already been mentioned. Other major effects of fluid in relation to deformation are discussed in this section.

In metamorphism, fluids are intimately involved with reactions and deformation. For example, during retrograde metamorphism (Sections 4.1.4, 4.13.2), fluids are introduced along fractures and shear zones, promoting hydration reactions (see, for example, Vernon & Ransom, 1971; Vernon, 1976; Yardley *et al.*, 2000). In prograde metamorphism, fluid may move through transient openings caused partly by local increase in the pressure of fluid produced by prograde metamorphic reactions and partly by the formation of local dilatant cracks caused by variations of the geometrical and mechanical properties of adjacent mineral grains (see, for example, Etheridge *et al.*, 1983, 1984).

The second process should be particularly important in situations such as metasomatism and retrograde metamorphism (Sections 4.1.4, 4.13.2), during which fluid is introduced (see, for example, Etheridge, *et al.*, 1983, 1984; Oliver *et al.*, 1990). It may also be important in the transfer of melts in deformation zones

(Section 5.11). Although it may occur at high metamorphic grades, microcracking through and between grains is likely to be most important at greenschist and sub-greenschist facies conditions (Barker & Zhang, 1998). Evidence of former microcracks may be preserved as planar arrays of fluid inclusions (Fig. 4.37), which are especially prominent in quartz veins (Section 5.9.3), deformed granites and deformed metasedimentary rocks (Kranz, 1983; Atkinson, 1984; Barker & Zhang, 1998).

TEM investigations have revealed small (nanometre to micrometre scale) voids (former fluid 'bubbles') along grain boundaries, with larger 'tubules' at grain triple junctions in metamorphic rocks (White & White, 1981). However, this may not give a reliable indication of the distribution of fluid during deformation. For example, in observable experiments by Urai (1983a,b) on transparent material (bischoffite) and in high-temperature (900 °C) experiments on feldspar by Tullis *et al.* (1996), the distribution of aqueous fluid changed from isolated pores at hydrostatic conditions to films along grain boundaries during deformation, and then back to isolated pores following the deformation.

Deformation may cause local solution of chemical components and their transfer in solution to other sites, where they may be deposited (*solution transfer*). In this way, a strain accumulation (shape change of an aggregate) may be achieved. Evidence of mass transfer in fluid during deformation is abundant (Section 5.9.2), especially in low-grade metamorphic rocks, in which extensive grain coarsening has not taken place to obliterate the microstructural evidence. However, it may also occur in the high-strain-rate deformation of high-grade metamorphic rocks (Lafrance & Vernon, 1993, 1999; Wintsch & Yi, 2002) and especially in ductile shear zones (Section 5.7.8). Chemical components may move in a static fluid (diffusive mass transfer) or be transported in a moving fluid (advective mass transfer). Solid-state diffusion is too slow to achieve much mass transfer in a reasonable time (Fyfe & Kerrich, 1985).

5.9.2 Stress-induced solution transfer and foliations

Mass transfer in fluid is a major mechanism for the development of foliations, especially slaty cleavage and discrete crenulation cleavage (Sections 5.8.2, 5.8.3) in low-grade metamorphic rocks (Durney, 1972; Siddans, 1972; Alvarez *et al.*, 1976; Beach, 1979; Rutter, 1983; Groshong, 1988; Wright & Henderson, 1992). It is generally referred to as 'pressure-solution' (Sorby, 1908) or 'solution-transfer' (Durney, 1972), although preferable terms are 'stress-induced solution transfer' or 'dissolution–precipitation creep', as discussed previously (Section 5.3.4). The idea is that material is dissolved from sites of high normal compressive stress and deposited at sites of low stress (see, for example, Durney, 1972). However, strain may also conceivably contribute to the solution.

Much mesoscopic and microscopic evidence exists for solution, transfer and redeposition of material during the formation of foliations in metamorphic rocks (see, for example, Plessman, 1964; Williams, 1972; McClay, 1977; Gray, 1977a, 1981; Beach, 1977; Mosher, 1980; Vernon, 1987b). For example, the following primary structures may be partly removed by solution, the remnants being transected by dark seams of residual material: fossils (see, for example, Durney, 1972, p. 316; Siddans, 1972, fig. 17) as shown in Fig. 2.23; ooids (Ramsay & Huber, 1987) as shown in Figs. 2.25 and 2.26; worm burrows (Wright & Henderson, 1992); pebbles (Mosher, 1980); sand volcanoes and dewatering pipes (Wright & Henderson, 1992); quartz and other detrital grains (Williams, 1972; Gray, 1978a; Bell, 1978a) as shown in Fig. 2.1; and early quartz veins (Wright & Henderson, 1992). Solution also occurs on discrete undulating surfaces (*stylolites*) in quartz, calcite and dolomite, leaving dark insoluble residues of clay minerals, mica, carbonaceous material or 'heavy minerals' (see, for example, Durney, 1972, p. 316; Blenkinsop, 2000), as shown in Figs. 2.23 and 2.25. Dark anastomosing seams in slates and mica folia in schists have also been attributed to solution processes. Another example of solution transfer is the formation of concentrations of mica and/or graphite at high-stress and/or high-strain sites adjacent to porphyroblasts of minerals such as garnet or staurolite, owing to solution and removal of other minerals (especially quartz and feldspar), as shown in Fig. 5.33.

Solution may also occur in high-grade metamorphic rocks, for example sillimanite seams and folia truncating zoned plagioclase (Vernon *et al.*, 1987) and mica folia truncating zoned garnet (Vernon, 1978a). Moreover, the sillimanite folia themselves (Figs. 4.31, 5.58) may result by concentration of Al and Si by base-cation leaching during deformation (Vernon, 1979, 1987b, 1998; Vernon *et al.*, 1987), as shown in Fig. 5.60.

Material dissolved by pressure- or strain-solution is redeposited at lower-pressure or low-strain sites, respectively, especially in veins (Section 5.9.3). Relatively clear features indicating deposition in Q domains include 'beard structures' (Fig. 5.15) and fibre growths (Gray & Willman, 1991; Gray & Wright, 1984; Waldron & Sandiford, 1988), quartz overgrowths on detrital quartz grains (Williams, 1972; Powell, 1969; Gregg, 1985; Sutton, 1991), as shown in Fig. 2.1, and quartz or carbonate fringes on pyrite crystals (Section 5.9.3). Evidence of precipitation in some P domains has also been observed (Waldron & Sandiford, 1988; Sutton, 1991), but overgrowths are more readily detected in the Q domains of slaty and penetrative domainal cleavages, which commonly partly preserve original detrital microstructures (see, for example, Williams, 1972). Evidence of precipitation is less clear in crenulation cleavages, owing to typically more extensive recrystallization/neocrystallization and consequent obliteration of original grain shapes.

Though many slates show abundant evidence of solution, especially of silica, resulting in the formation of P domains, and some show evidence of deposition in Q domains, a long-standing question is whether the chemical system is chemically closed (except for water) or whether volume and/or bulk chemical changes occur during cleavage development, on the mesoscopic (metre) scale, as discussed in Section 5.9.4.

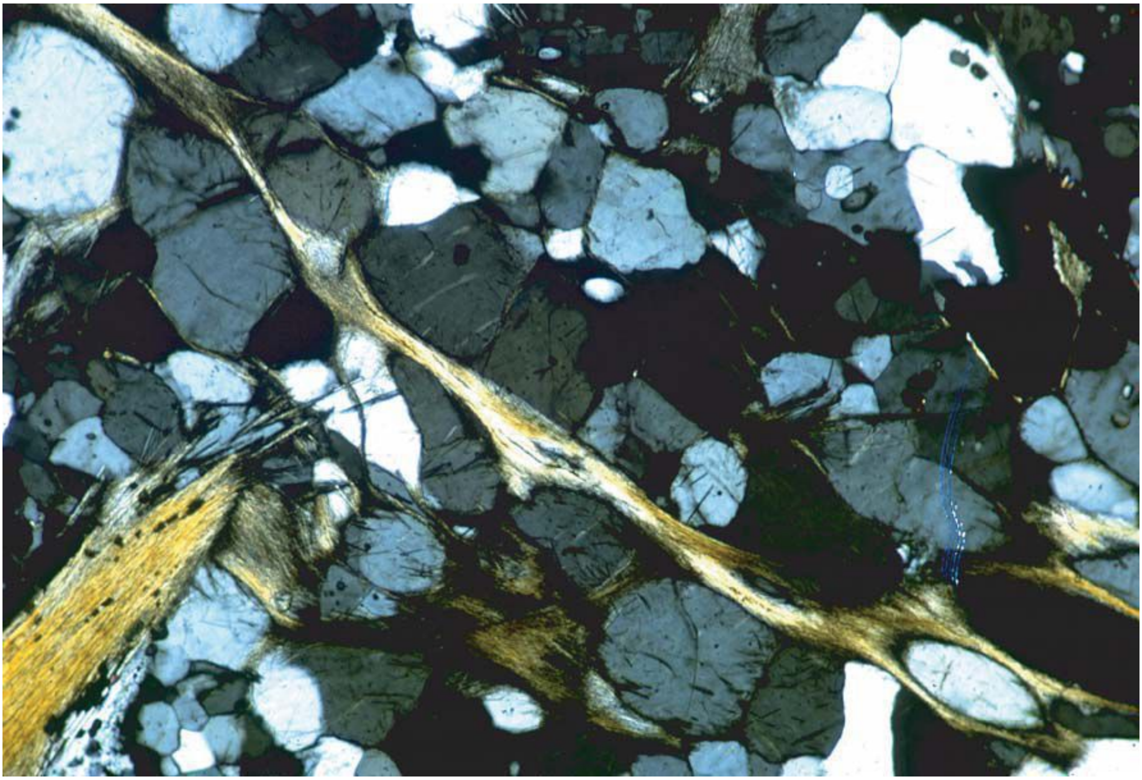

Fig. 5.60: Folium of fibrous sillimanite in a felsic hornfels (metamorphosed granite) from Kentucky, New England area, New South Wales, Australia. The quartz and feldspar have been partly dissolved along the folium, producing lenticular grain shapes that can be compared with the former grain shapes in the adjacent rock. The dissolved quartz and feldspar components not needed for sillimanite were removed. Thus, the sillimanite can be inferred to be a product of the leaching of base cations (Section 4.13.6), presumably in acid solution (Vernon, 1979), though whether some of the sillimanite components were also introduced to the precipitation site from local leaching nearby is unknown.

5.9.3 Veins in deformed rocks

Veins are common in deformed metamorphic rocks, especially at lower grades. Many represent fractures filled with minerals precipitated from fluid (see, for example, Fyfe *et al*., 1978; Ramsay, 1980b; Yardley, 1983, 1986; Rumble, 1989), whereas others ('accretionary veins') may result from growth of minerals by precipitation from infiltrating fluid at sites of relatively low stress. The fluid and its dissolved chemical components may come from a distant external source (see, for example, Ferry, 1991, 1994; Oliver, 1996) or may be of local origin (see, for example, Durney & Ramsay, 1973; Heinrich, 1986; Yardley & Bottrell, 1992; Cartwright *et al*., 1994; Widmer & Thompson, 2001).

The source of vein minerals is commonly obscure, but some veins are composed of components inferred to be dissolved during the development of foliations in deforming rocks, as discussed in Section 5.9.2. Fluid may be released from many sources, such as cooling magma bodies and metamorphic devolatilization (e.g. dehydration) reactions. Ague (1991, 1994, 1997) has described in detail veins formed during regional metamorphism, involving interaction of metamorphic minerals with fluids.

Fluid is transferred to fracture-filling veins through intragranular and intergranular fractures, as mentioned above. Local variations in the response of different minerals and rocks to deformation leads to the formation of fractures and local openings ('dilatant sites'). These low-pressure openings suck in percolating hydrous solutions, from which minerals precipitate. When solutions are sucked into such openings, they undergo a pressure decrease, which can cause saturation and consequent precipitation of chemical components dissolved in the solution. Deposition of minerals may seal the fractures, but the precipitated minerals may themselves be fractured, and repeated deposition and fracturing may occur in a process called 'crack–sealing' Figs. 5.61, 5.62). The *crack–seal mechanism* (Ramsay, 1980b; Cox & Etheridge, 1983) is an important process in the production of veins at relatively low-temperature (e.g. greenschist facies) conditions. It involves repeated opening of cracks, their sealing by deposition of minerals from solution, reopening as the fluid pressure builds up again, and resealing, leaving lines of small inclusions (*inclusion bands*) to indicate the former presence of the fractures (Figs. 5.61, 5.62). An alternative explanation involving 'crystallization pressure' has been suggested by Wiltschko & Moru (2001).

Fluid is inferred to be transferred to accretionary veins by diffusion, possibly from nearby sites at which pressure-solution is taking place (Durney & Ramsay, 1973). Deposition is inferred to occur on grain boundaries subjected to relatively low normal stress in a differentially stressed aggregate, producing a vein by dilation ('force of crystallization'; Sections 4.3.1, 5.10.11).

As shown diagrammatically in Fig. 5.63, veins and vein-like aggregates include (1) elongate, isolated veins, (2) more equant, isolated *vughs*, (3) 'pressure (strain) shadows' ('*pressure fringes*') adjacent to rigid objects, such as strong detrital clasts or porphyroblasts (Fig. 5.64A), and (4) aggregates in the 'necks' between separated fragments or boudins (Fig. 5.64B). The mineral aggregates may be fibrous (consisting of very elongate grains) or massive (consisting of relatively equant grains), as shown in Fig. 5.63.

Fibrous or columnar structures are characteristic of lower-temperature veins. Massive veins may also form at relatively low temperatures by growth from solution in open spaces. However, many massive veins have granoblastic (polygonal) microstructures that are due to deformation and recrystallization (Section 5.4), as shown in Fig. 5.65. Such veins occur at all metamorphic grades, but are especially common in high-grade metamorphic rocks.

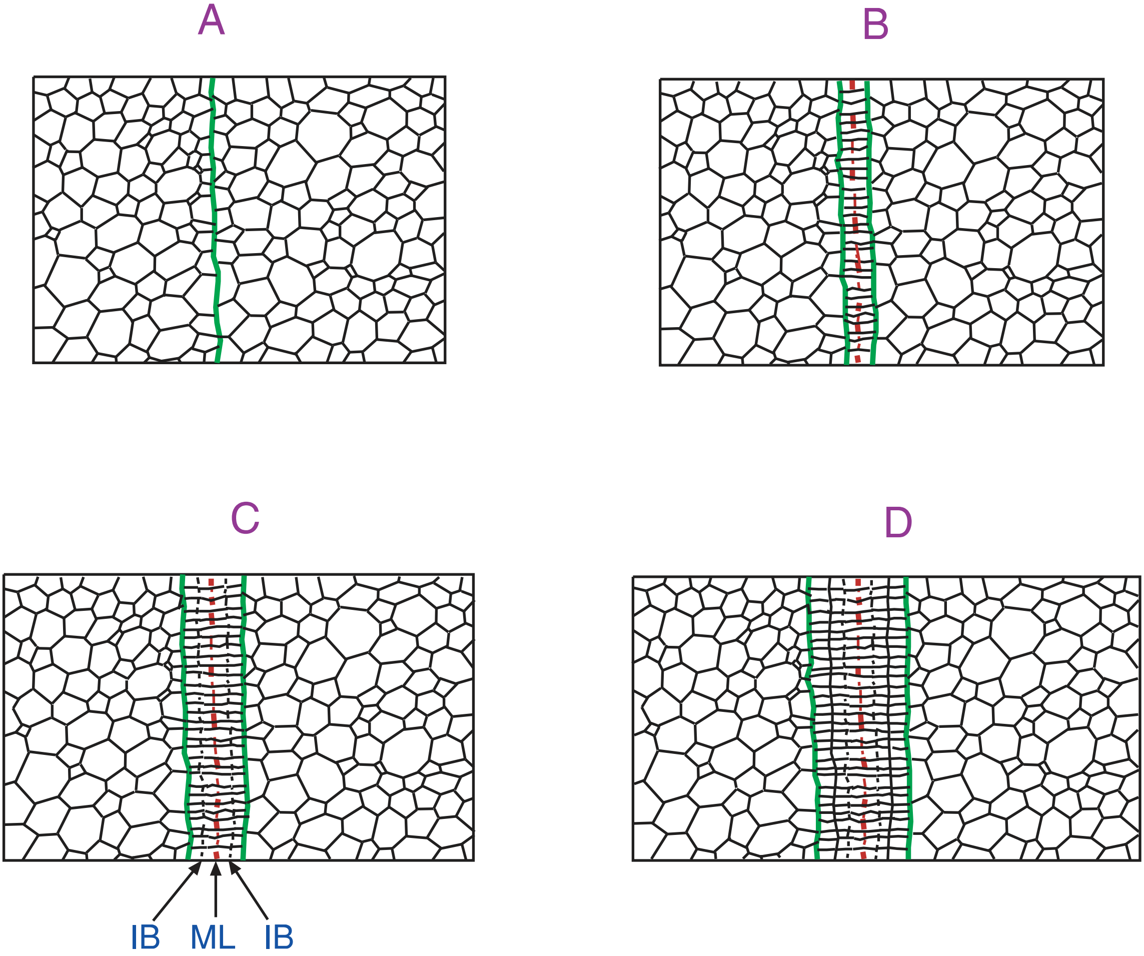

Fig. 5.61: Diagrams illustrating the crack–seal mechanism of vein formation. (A) A crack forms. (B,C) An opening along the crack is filled with fibrous quartz, growing outwards from the initial crack and leaving minute fragments of the solid rock (inclusion band, IB) along the line of the original crack (the median line, ML). (D) Repeated cracking and vein-filling occur, producing a crack–seal vein with inclusion bands (Fig. 5.62).

The most common vein minerals in metamorphic rocks are quartz, calcite and sulphide minerals, but mica and feldspar may also occur in veins, and rarely andalusite or sillimanite occur in veins at high metamorphic grades (Whitney & Dilek, 2000). Individual crystals may show concentric growth zoning (Fig. 5.66). Even quartz may show optically observable growth zoning (Fig. 5.67), which may be due to higher than usual concentrations of trace elements and/or concentrations of minute fluid inclusions (see, for example, Ridley, 2002).

A

Fig. 5.62: (A) Edge of a crack–seal vein of quartz and calcite (stained pink by an organic dye) cutting a dolomitic ironstone with chlorite oolites, Windgallen, Switzerland, which is the area from which crack–seal veins were first described (Ramsay, 1980b). The quartz, and locally also the calcite, show parallel bands of minute mineral inclusions (carbonate?) formed by repeated cracking and sealing by growth of the vein minerals. Specimen by courtesy of David Dumey. Plane-polarized light; base of photo 4 mm. (B) Same field of view, but in crossed polars, to show individual quartz grains. (C) Magnified view of the left side of A, showing the inclusion bands in the quartz and calcite (left) in more detail. Plane-polarized light; base of photo 1.5 mm.

The internal structure of veins and other cavity fillings may be complex. Cathodoluminescence (CL) is being increasingly used to reveal structures such as zoning and sealed microfractures, which may be difficult to detect in the normal microscope, especially in quartz or carbonate veins (Fig. 5.66). The SEM–CL technique has been used to reveal complexities in some quartz–sulphide veins (Rusk & Reed, 2002).

Some cavity fillings consist of regularly arranged, elongate crystals (Fig. 5.67), forming what is appropriately called '*comb structure*'. Others have bundles of

Fig. 5.62: (*cont.*)

fibres radiating into the cavity from a nucleation point (Figs. 3.98, 5.68). Radial growth from several nucleation sites produces sprays of needle-like ('acicular') or fibrous crystals in concentric layers. As growth proceeds, the separate radiating clusters merge to form a continuous layering (see, for example, Craig, 1990, fig. 6), as shown in Fig. 5.68. Veins and vughs commonly show layers of different minerals (*crustification*) formed by change in the composition of solutions passing through the cavity (see, for example, Edwards, 1947), as shown in Figs. 3.98 and 5.68.

Minerals in many veins form elongate (columnar or fibrous) crystals projecting from the walls of the vein and growing towards the centre (*syntaxial veins*). Typically these crystals nucleate heterogeneously on minerals of the wall-rocks, so that generally the fibres are closely related to minerals in the wall-rocks, for example, quartz veins in sandstones and calcite veins in limestones or marbles. Fibres that grow approximately perpendicular to the walls grow fastest. They eliminate crystals in less suitable growth orientations and meet at the centre of the vein (*median line*), as shown in Fig. 5.67. As they meet, they interfere and so lose

Fig. 5.62: (*cont.*)

their crystal faces, although evidence of their former presence may be revealed as patterns of concentric zoning (Fig. 5.67). If deformation accompanies the vein growth, producing curved fibres, the fibres at the contact remain perpendicular to the walls (Fig. 5.69).

In contrast to syntaxial veins, in which the youngest growth is in the centre, minerals that are different from those of the wall-rocks (e.g., calcite fibres in quartzite) commonly grow from the contacts of fibres and wall-rock (i.e., on two growth surfaces) towards the walls and away from the centre of the vein (*antitaxial veins*), as shown in Figs. 5.64, 5.69 and 5.70. The fibres show crystallographic continuity from one wall to the other. The centre-line (median line) is commonly marked by a line of small wall-rock fragments. If deformation accompanies the vein growth, producing curved fibres, the fibres at the contact remain perpendicular to the walls at the median line (Figs. 5.69, 5.70), because this represents the initial fracture opening.

Less common *composite veins* show evidence of both syntaxial and antitaxial growth histories (Fig. 5.69). *Stretched-crystal veins* (Durney & Ramsay, 1973) may also develop where minerals in the vein are the same as or similar to those in the wall-rocks; crystals that nucleate on each wall continue to grow right across the vein (Figs. 5.69, 5.71).

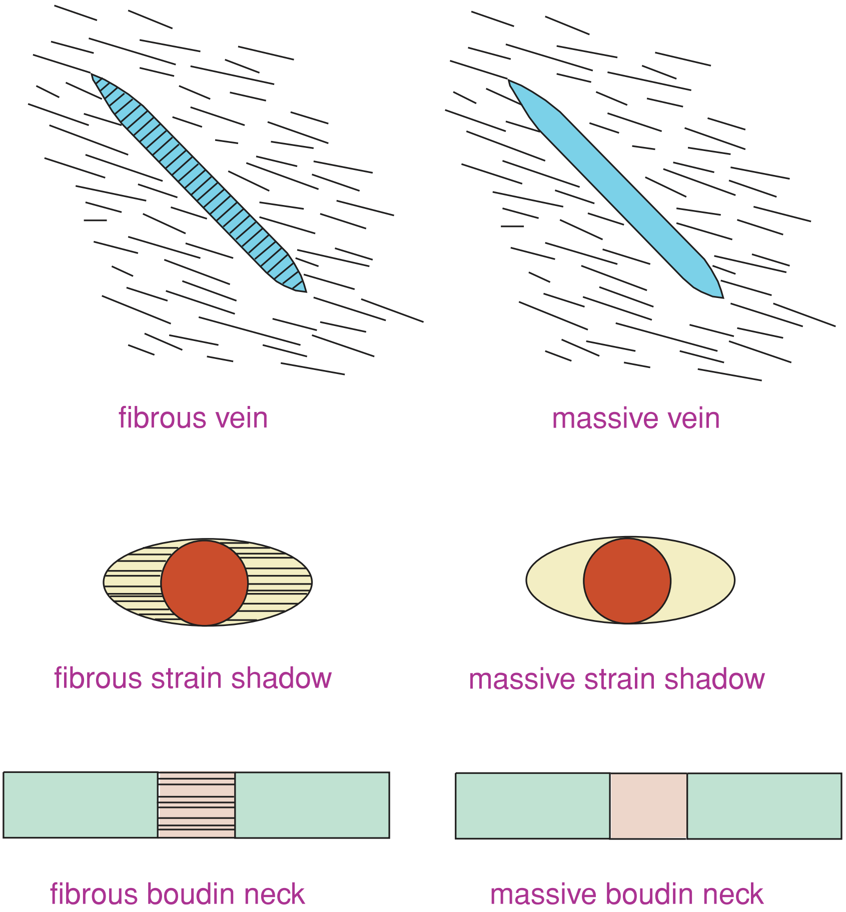

Fig. 5.63: Sketches showing various types of veins and vein-like structures, some fibrous, others massive (granoblastic).

Fibrous veins and pressure shadows may be very complex, because opening and filling are commonly repeated processes during deformation. Discontinuities and curvatures of fibres (Figs. 5.64, 5.69, 5.70) can provide evidence of progressive incremental strain and an indication of shear sense, as explained in detail by Ramsay & Huber (1983) and Passchier & Trouw (1996), and modelled by Echtecopar & Malavielle (1987).

Many studies have attempted to use fibrous growths to track the deformation history of rocks (see, for example, Mügge, 1931; Pabst, 1931; Zwart & Oele, 1966; Elliot, 1972; Durney & Ramsay, 1973; Wickham, 1973; Wickham & Anthony, 1977; White & Wilson, 1978; Ramsay & Huber, 1983; Cox & Etheridge, 1983; Ellis, 1986; Cox, 1987b; Echtecopar & Malavielle, 1987; Urai *et al.*, 1980a,b; Spencer, 1991). The underlying interpretation is that the fibre growth follows the movement of the vein walls (Taber, 1916; Durney & Ramsay, 1973), the crystals remaining non-deformed. However, the growth processes are not yet clear and appear to be very complex, depending on interactions between crystal growth mechanisms, strain and fluid distribution (see, for example,

Next Page

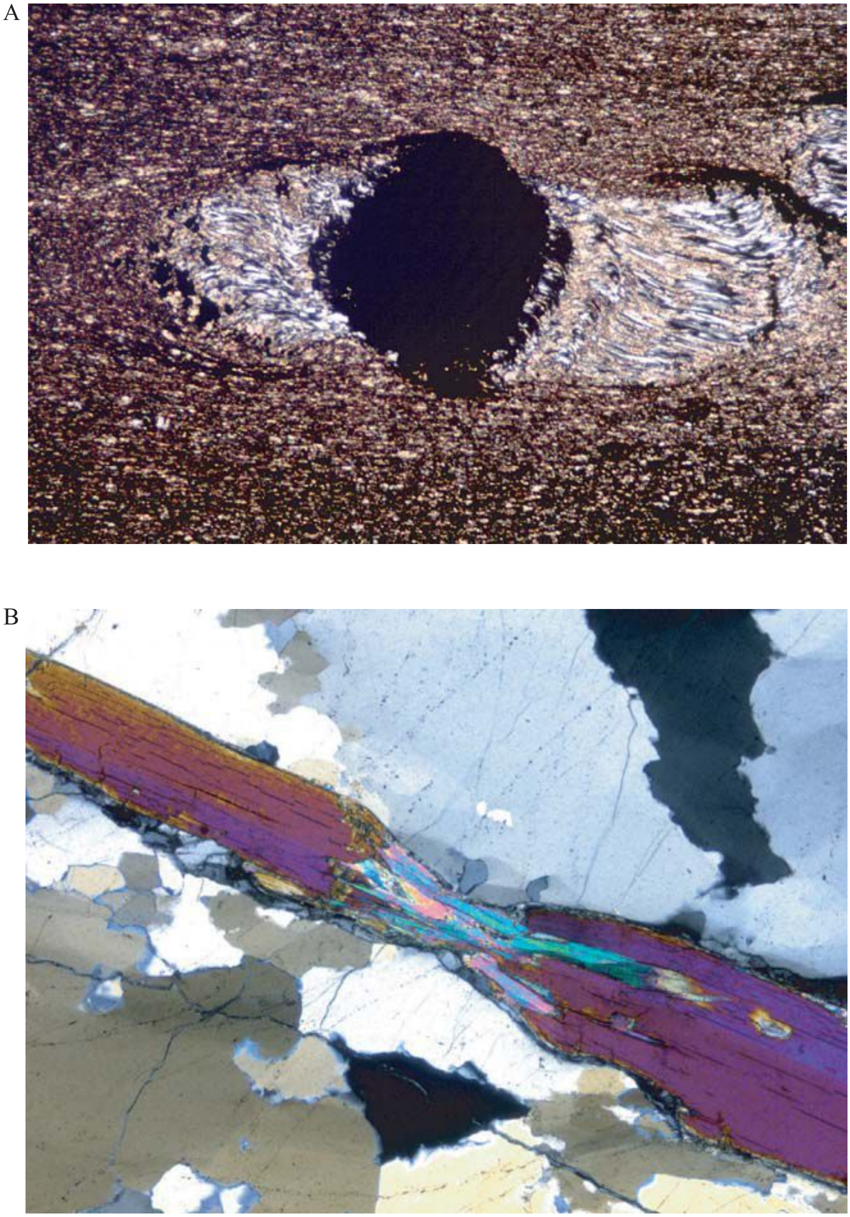

Fig. 5.64: (A) Strain shadows (pressure fringes) of fibrous quartz and calcite on a concretionary aggregate of very fine-grained pyrite (opaque, and so appearing to be a single grain in thin section) in a calcareous slate from Mesozoic cover rocks of the Aiguilles Rouges massif, l'Au d'Arbignon, Valais, Switzerland. The fringes are antitaxial (i.e. they grew towards the pyrite), are essentially non-deformed, and are curved, owing to deformation of the adjacent rock during their growth. Sample by courtesy of David Dumey. Crossed polars; base of photo 11 mm. (B) Fibrous aggregate of muscovite forming a beard-like vein between two separated fragments (boudins) of kyanite in a schist from the Himalayas. Specimen by courtesy of Scott Johnson. Crossed polars; base of photo 3 mm.

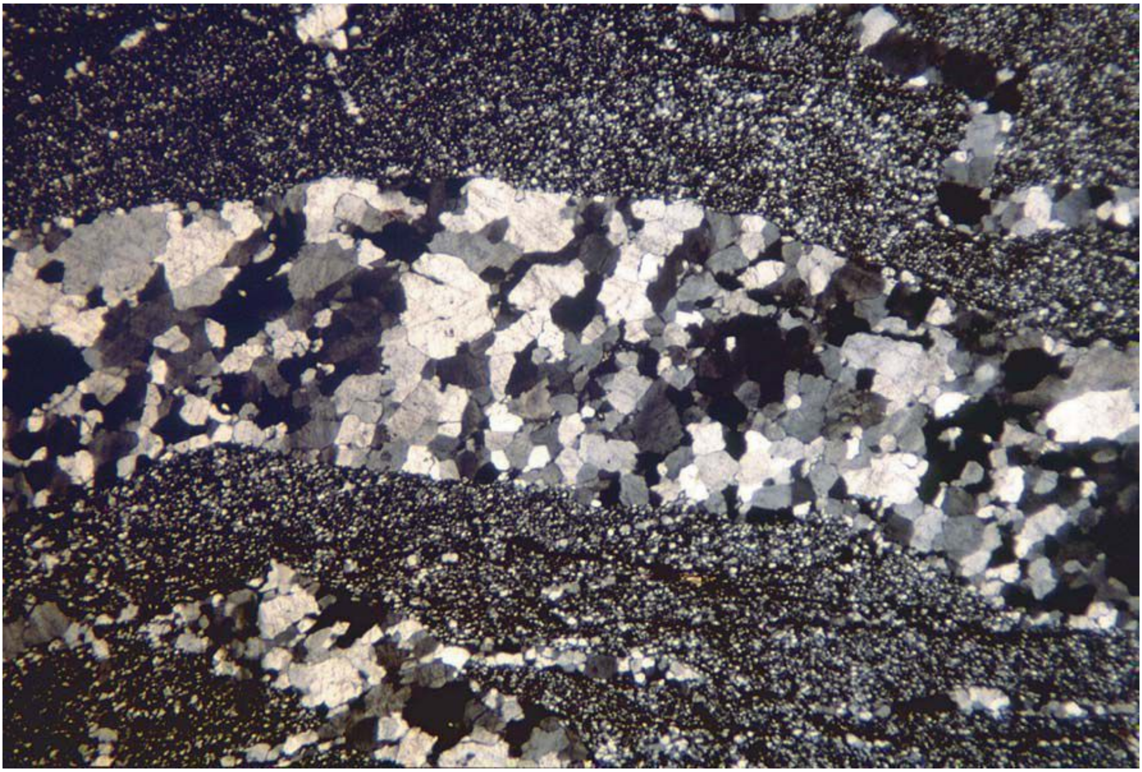

Fig. 5.65: Veins consisting of granoblastic (massive) quartz in a Cambrian chert, Murunna Point, south coast of New South Wales, Australia. The veins have been strongly deformed and recrystallized (Section 5.4), producing polygonal quartz aggregates. Sample by courtesy of David Durney. Crossed polars; base of photo 11 mm.

Hilgers & Urai, 1999; Koehn *et al.*, 2003). An alternative explanation for at least some curved-fibre veins is that the curvature is due to later deformation, rather than growth during deformation, the lack of obvious internal distortion of the fibres being ascribed to slip on fibre boundaries and/or recovery and recrystallization (Williams & Urai, 1989). However, recrystallization of quartz and calcite typically produces aggregates of equant grains, rather than single elongate grains. Experimental and computer modelling approaches are also being applied to the interpretation of complex fibrous growths (see, for example, Echtecopar & Malavielle, 1987; Urai *et al.*, 1980a,b; Kanagawa, 1996; Hilgers *et al.*, 1997; Hilgers & Urai, 1999; Koehn *et al.*, 1999, 2000, 2001, 2003).

Fracture-filling veins are very common in rocks through which solutions circulate at relatively low temperatures. This is partly because such rocks, being relatively cool and under relatively small confining pressure, tend to fracture more readily during deformation, providing openings for solutions. However,

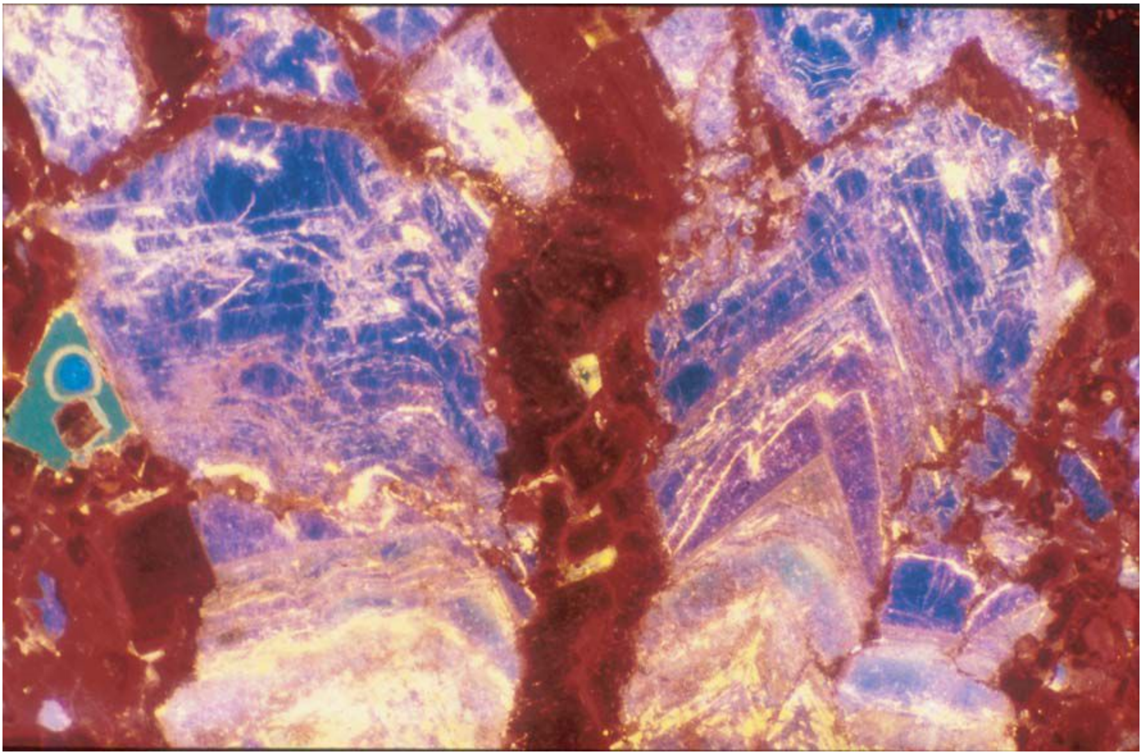

Fig. 5.66: Optical CL image showing concentric zoning in vein dolomite, and probable pathways for later fluid activity and deposition (dark red), southwestern margin of the Damara Orogen, Namibia. Photo by Bernd Leiss. Base of photo 10 mm.

veins can form at any depth if the fluid pressure is locally high enough. For example, local increase in the production of fluid (e.g. from prograde metamorphic reactions), aided by deformation, can cause the fluid pressure to exceed the minimum compressive stress (σ_3) plus the local tensile strength of the rocks, allowing fluid-filled fractures to form. This applies also to the formation of leucosome veins in migmatites (Section 5.11). Moreover, veins that are accretionary in origin do not require initial fractures (Durney & Ramsay, 1973).

Hot water may dissolve metals and sulphur from rocks through which it circulates, and may also transport these components as late-stage hydrothermal solutions released from magmas. The metals may be deposited later as metal sulphides in rock cavities. An open space may be produced as a fault moves. Water travelling along the fault may deposit minerals in the open space. In addition, water in cracks in the adjacent rocks is sucked into the opening, because of the lower pressure (Fig. 5.37). This water may deposit minerals from its dissolved chemical components. It may also mix with water travelling along the fault, and the resulting chemical reactions may cause metal sulphide minerals to be deposited in the cavity, including the spaces between any rock fragments

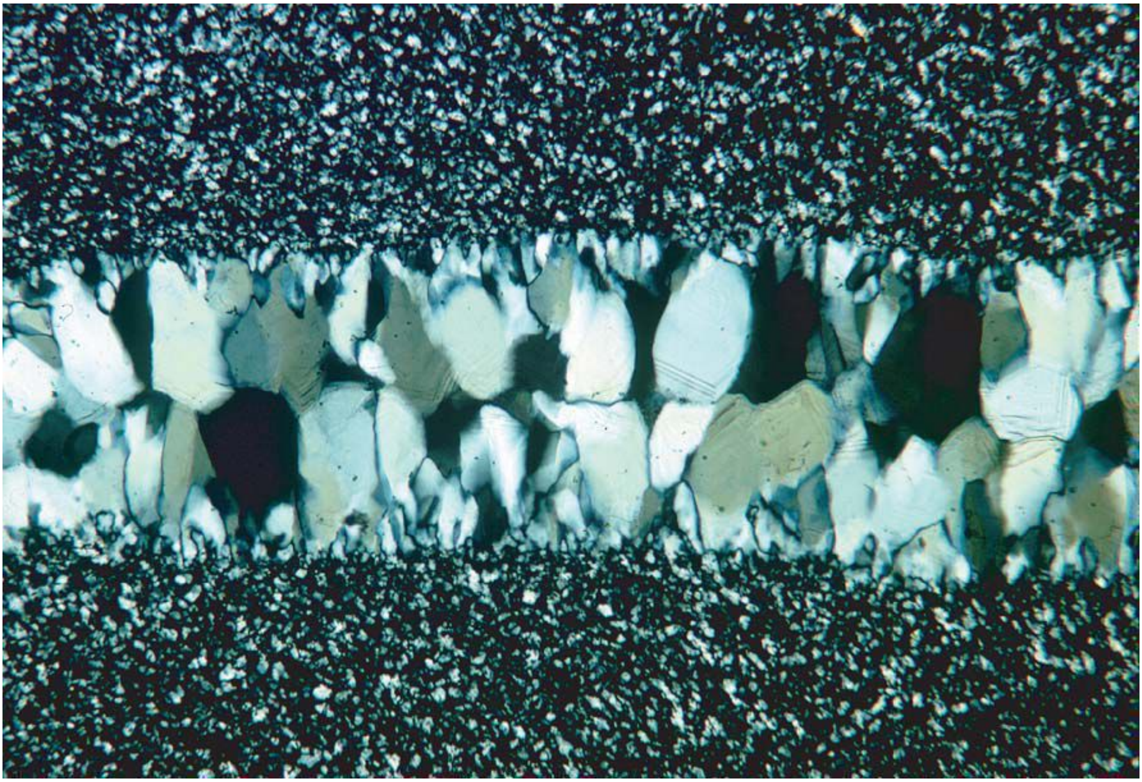

Fig. 5.67: Vein of quartz showing 'comb structure' caused by growth from the walls towards the centre as the vein opened (syntaxial growth; Fig. 5.69). The grains at the edges of the vein are the smallest because they nucleated on small quartz grains in the wall rock. Many of them were eliminated by faster-growing (more advantageously oriented) grains, which met at the centre of the vein in an irregular median line. Although the quartz grains do not show crystal faces, owing to mutual impingement during growth, the history of development of crystal faces before impingement is revealed by concentric growth zoning. The zoning may be due to higher than usual concentrations of trace elements (Section 3.14.5), possibly connected with concentrations of minute fluid inclusions. Crossed polars; base of photo 1.3 mm.

present (resulting from implosion, as discussed in Section 5.7.5). This cements the fragments together, forming a fault breccia. Fault breccias are major potential receptors of metallic ore minerals.

5.9.4 Fluids and volume loss

Much controversy exists about the extent of volume loss caused by solution during the formation of foliations (Vernon, 1998), especially slaty cleavage, but also differentiated crenulation cleavages at higher metamorphic grades. Most

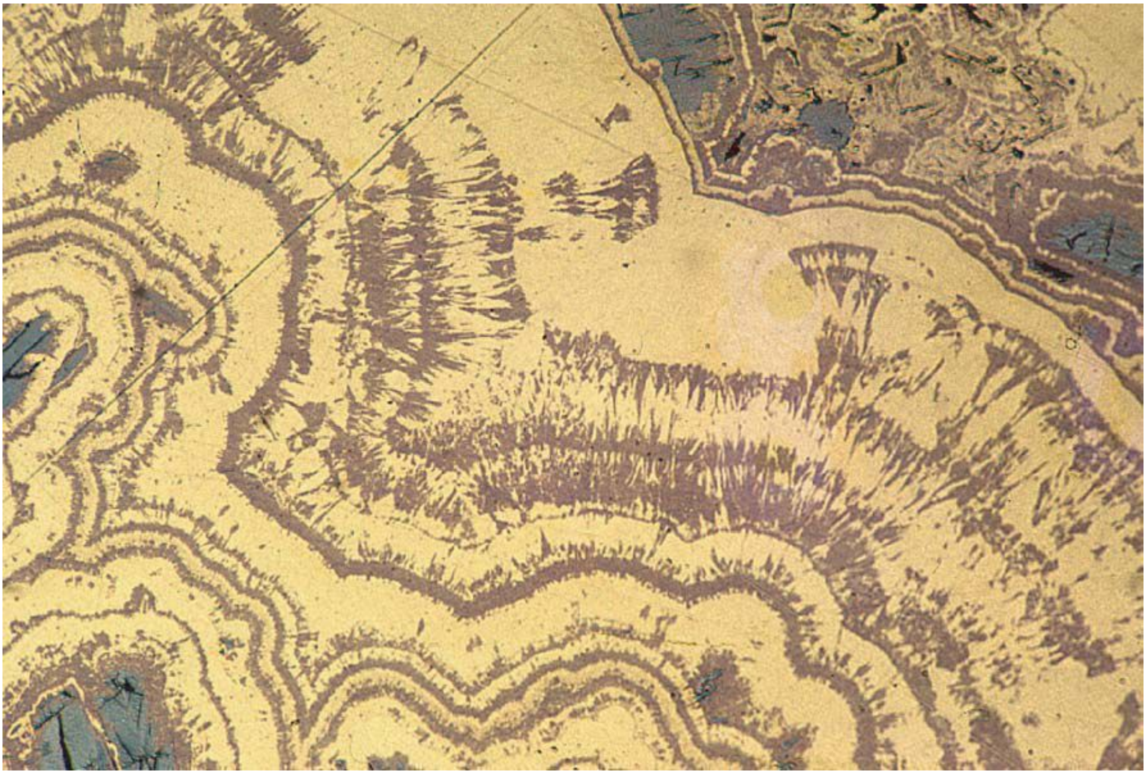

Fig. 5.68: Crustification in a vugh, formed by rhythmically deposited layers of fibrous, radiating chalcopyrite (yellow) and sphalerite (purplish grey), with minor covellite (blue). The sulphide minerals were precipitated from hydrothermal solutions, and grew from the edges of the cavity inwards. Sample kindly provided by John Lusk. From Vernon (2000b, fig. 139). Polished section, plane-polarized light; base of photo 2.7 mm.

work has concentrated on slates, because (1) solution processes dominate at low metamorphic grades, and (2) detrital grains and/or fossils commonly serve as markers of strain and the degree of solution (Section 5.9.3). However, crenulations at intermediate and high grades of metamorphism are commonly strongly compositionally differentiated (Section 5.8.3), and so the possibility of solution transfer and selective volume loss must be considered at all metamorphic grades.

From reduction spots in Welsh slates, Sorby (1853) estimated a volume loss of 50%, although he later reduced this to 11% (Sorby, 1908). Modern estimates of volume loss range from little or none (see, for example, Erslev & Mann, 1984; Waldron & Sandiford, 1988; Wintsch *et al.*, 1991; Gray *et al.*, 1991; Erslev, 1998) to 20% (Ramsay and Wood, 1973), 50% (Wright & Platt, 1982; Beutner

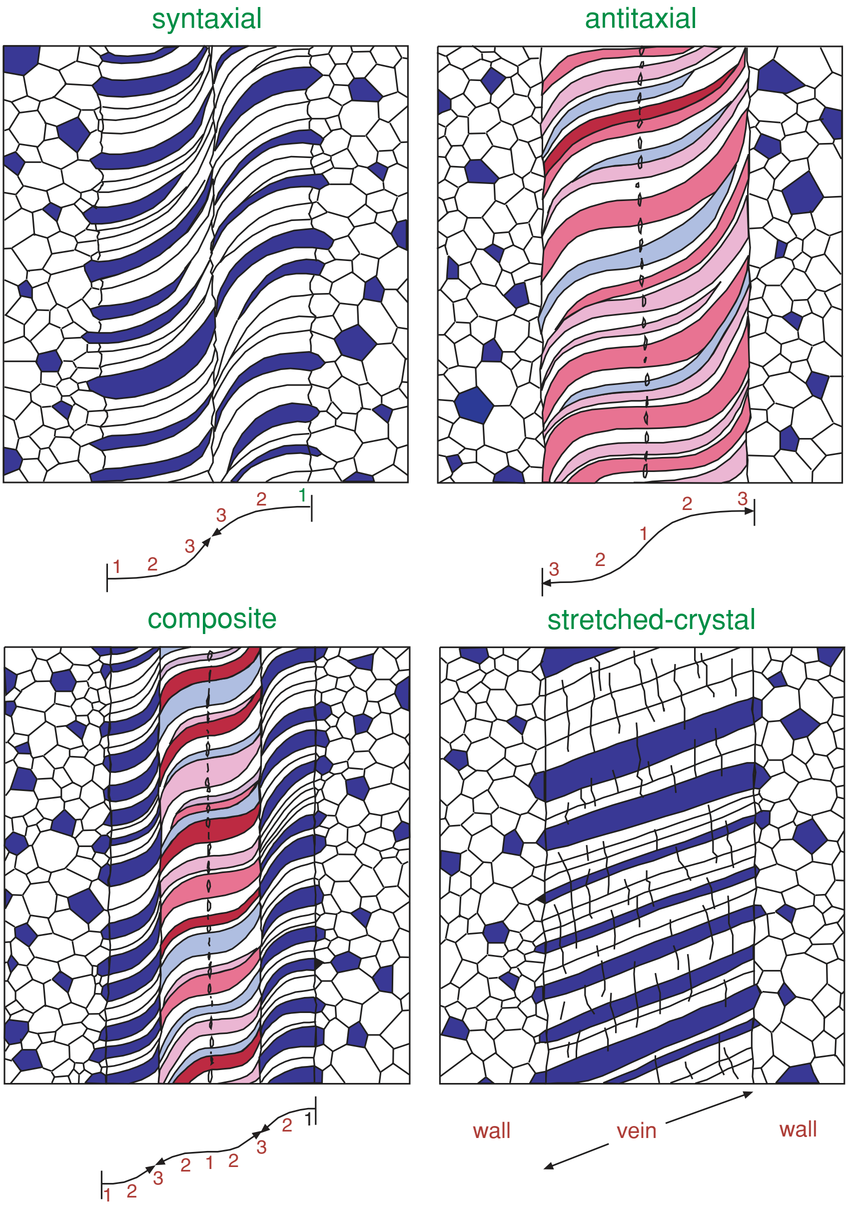

Fig. 5.69: Diagrams illustrating the main types of vein. For syntaxial, antitaxial and composite veins, the histories are represented below the diagrams as numbered stages in the growth history of the fibres. The minerals in syntaxial veins and the syntaxial parts of composite veins consist of the same minerals as in the wall-rocks, whereas the minerals in antitaxial veins and the antitaxial parts of composite veins are different from those in the wall-rocks. After Ramsay & Huber (1983) with permission from Elsevier.

& Charles, 1985), 55% (Goldstein *et al.*, 1995) and 60% (Wright & Henderson, 1992). Mosher (1980) showed that 51–58% volume loss occurred by pressure-solution in the deformation of conglomerates in shear zones on Rhode Island, USA, and O'Hara (1988) estimated a volume loss of 60% for mica-rich mylonites (phyllonites) in North Carolina, USA.

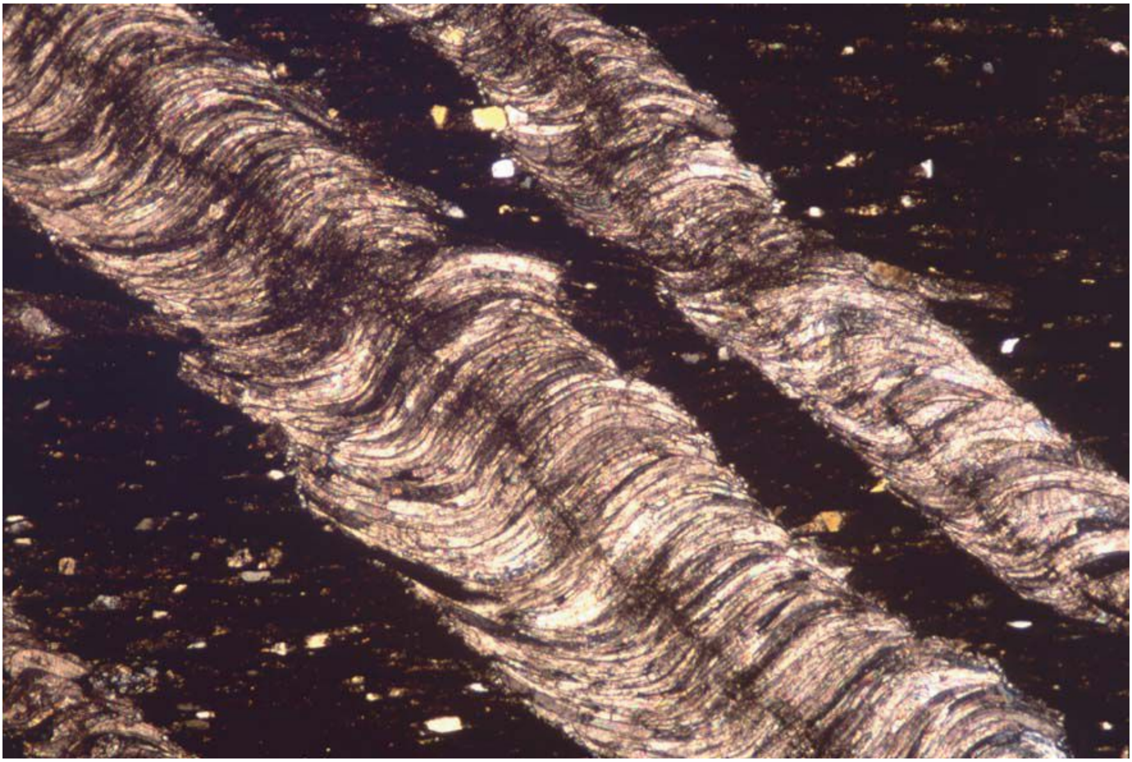

Fig. 5.70: Two antitaxial veins of calcite (extremely high interference colours) in slate (Upper Jurassic) in the sedimentary cover rocks of the Aiguilles Rouges massif, Bella Creta, Switzerland. Although the fibres are curved, they are perpendicular to the original direction of opening of the vein at the median line. Sample by courtesy of David Durney. Crossed polars; base of photo 4 mm.

Estimates based on microstructures and mesoscopic features involving strain markers generally indicate large volume losses, whereas estimates based on chemical ratios and isotopes generally indicate negligible losses (Vernon, 1998). The problem is to determine with confidence whether material dissolved from high-strain domains rich in layer silicates (P or M domains) has been deposited in adjacent low-strain domains rich in quartz (Q domains), or whether it has been removed from the local Q–P system, at least on the mesoscopic (metre) scale. The difficulty has not yet been resolved (Vernon, 1998), but a recent review by Gray (1997) indicates that volume losses in slates from the Martinsburg Formation, eastern USA, and the Lachlan Fold Belt, SE Australia, vary from zero to more than 50%, depending on the different processes operating in the development of the slaty cleavage. Gray (1997) found that the largest volume losses occur in slates with relatively widely spaced, distinct cleavages, and the smallest losses occur in slates with cleavages characterized by more penetrative grain alignments. Most

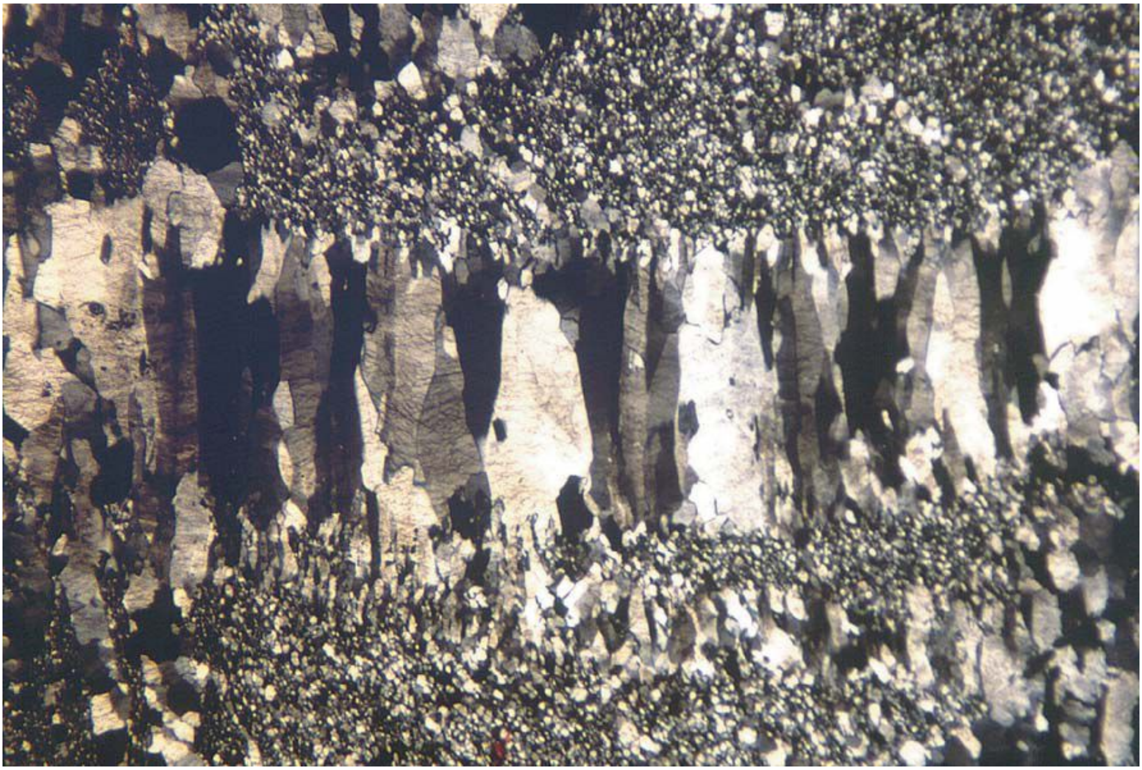

Fig. 5.71: Stretched-crystal vein of quartz in Cambrian chert, Murunna Point, south coast of New South Wales, Australia. The vein is finer-grained at its margins, owing to nucleation on small quartz grains of the wall-rock, but most of the fibres grew right across the vein. The quartz contains abundant fluid inclusions, many of which are in lines approximately parallel to the vein walls (compare with the sketch of a stretched-crystal vein in Fig. 5.69). Fluid inclusions from this vein are shown in more detail in Fig. 4.37. Crossed polars; base of photo 11 mm.

slates fall in between, with less than 10% volume loss, according to Gray (1997). Volume losses tend to be balanced by the proportion of veins in the deformed rocks (Beach, 1974).

5.10 Porphyroblast–matrix microstructural relationships during deformation

Microstructural relationships between inclusions in porphyroblasts (Section 4.3) and foliations in the surrounding matrix are potentially useful for inferring metamorphic and/or deformation histories, and many papers have been written on the subject. In this section, I discuss the approach and its uses, as well as precautions that should be taken.

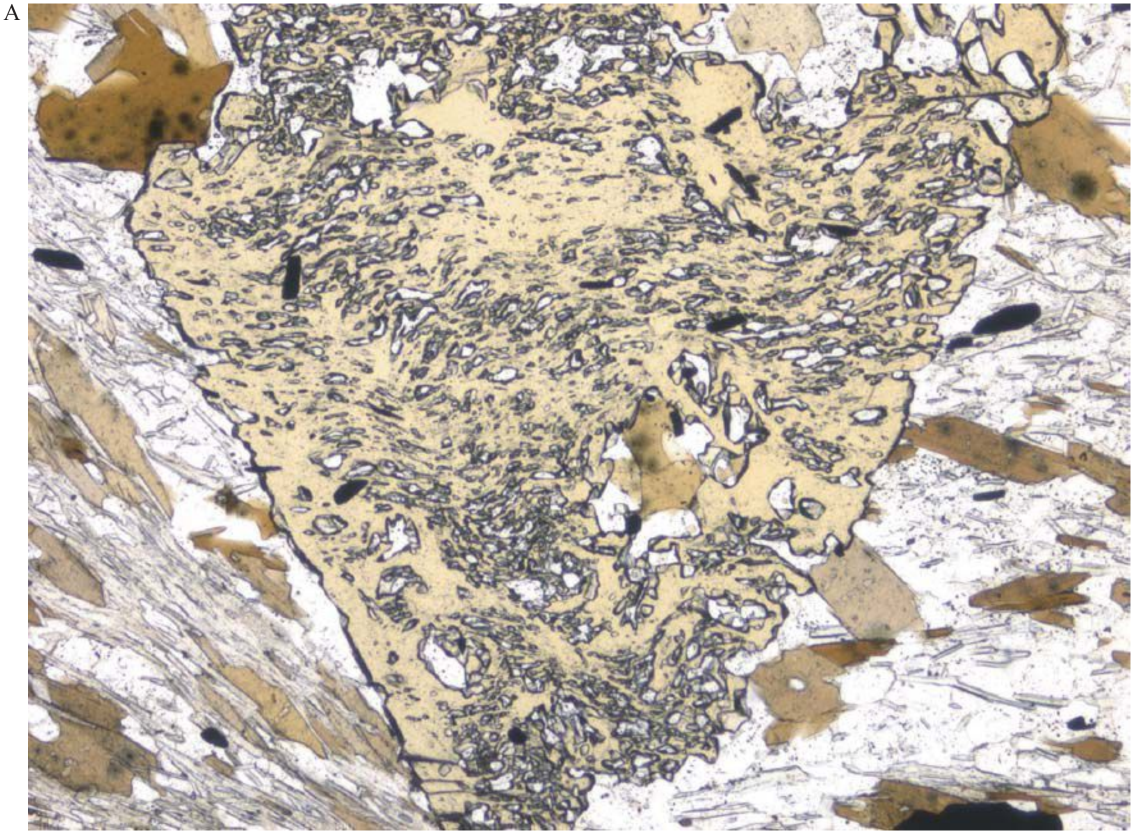

Fig. 5.72: (A) Staurolite with quartz inclusion trails preserving crenulations that are now absent from the adjacent matrix, Rangeley area, Maine, USA. Sample by courtesy of Charles Guidotti and Scott Johnson. Plane-polarized light; base of photo 3 mm. (B) Porphyroblast of staurolite (pale yellow) with folded trails of graphite (opaque) in a metapelite from the Chiwaukum Schist, Cascade Range, Washington, USA. After the porphyroblast grew, the matrix was intensely deformed, removing evidence of the microfolds. Thus, the porphyroblast preserves the only evidence of the earlier folding event. This porphyroblast can be inferred to have grown either during or after the microfolding, and before the late deformation of the matrix. From Vernon (2000b, fig. 149). Plane-polarized light; base of photo 4.4 mm.

5.10.1 Inclusion trails in porphyroblasts

As explained in Section 4.2, growing porphyroblasts overtake and incorporate growing grains of other minerals and/or grains of pre-existing stable or metastable minerals. Although many inclusions tend to develop rounded corners (Section 4.2.7), their initial elongation, if present, is commonly preserved. A shape (dimensional) preferred orientation of elongate inclusions forms *inclusion trails* (Figs. 4.30B, 5.59, 5.72). An inherited foliation, including sedimentary bedding, can

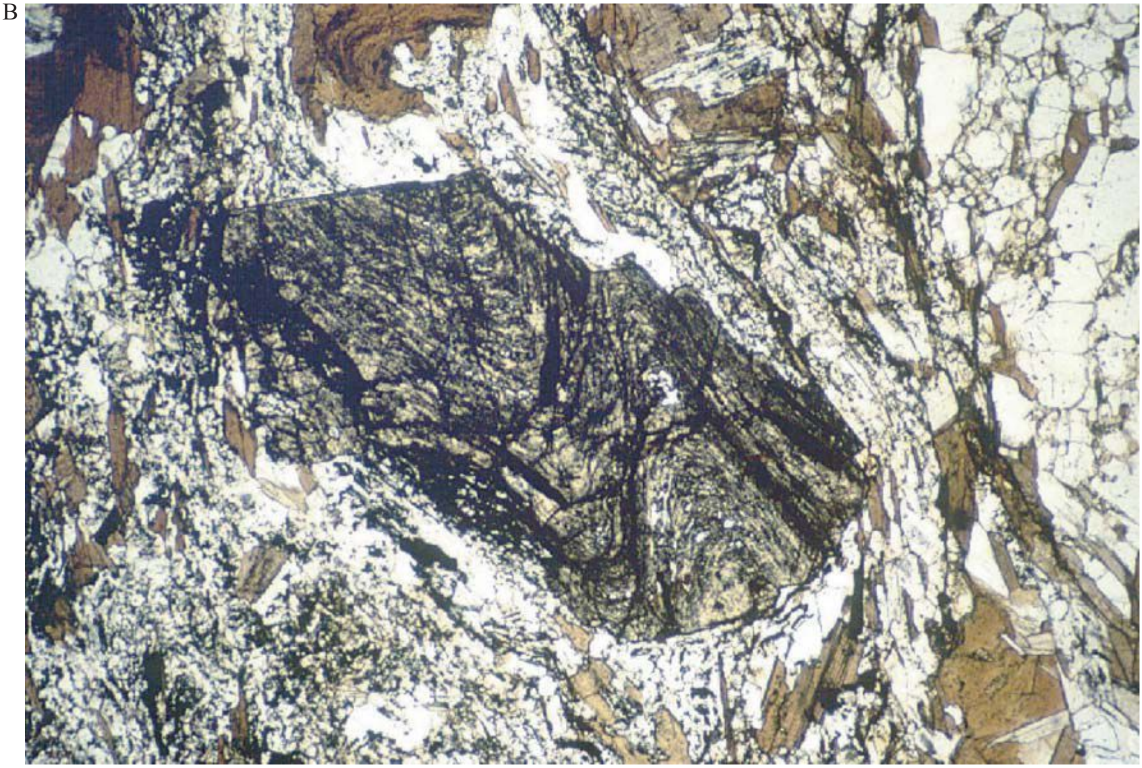

Fig. 5.72: (*cont.*)

also be revealed by different concentrations of inclusions, for example, relics of quartz-rich versus quartz-poor layers (Fig. 5.59). Because alignment of elongate minerals typically results from growth in a tectonic foliation, inclusion trails potentially allow the timing of growth of porphyroblastic minerals relative to the formation or deformation of a specific foliation. Patterns of foliations and microfolds outlined by the inclusion trails preserve evidence of the earlier stages of development or deformation of a foliation, or even generations of structures that have been obliterated from the adjacent matrix by subsequent deformation, recrystallization and neocrystallization (Figs. 5.59, 5.72). In some rocks, porphyroblasts preserve the only evidence of previous deformation events. Thus, porphyroblasts can preserve evidence of structural history (Section 5.10.2), even if only of local parts of a metamorphic terrane (Section 5.10.9).

5.10.2 Using porphyroblasts to determine the relative timing of metamorphic reactions and foliations

Provided suitable inclusion trails are present, porphyroblast–matrix microstructural relationships may be used to infer the timing of metamorphic reactions relative to foliation-forming deformation events. For example, Vernon (1988a) used porphyroblast–matrix microstructural relationships to infer a prograde metamorphic reaction in schists of the Cooma Complex, south-east Australia. Porphyroblasts of andalusite grew during the development of S_3, in response to a prograde reaction that consumed cordierite formed during the development of S_2.

It should be emphasized that considering the growth of porphyroblasts alone, without considering the growth of matrix minerals, is inadvisable. For example, if porphyroblasts of albite are inferred to have grown independently of neocrystallization of matrix minerals, the implication is that sodium metasomatism has occurred, and chemical evidence must be brought forward to substantiate this. Generally, all or nearly all minerals in a rock are involved in prograde metamorphic reactions, including those that produce porphyroblastic minerals, and so this should always be kept in mind when inferring the timing of the growth of porphyroblasts relative to deformation.

Metamorphic minerals can grow before, during or after a particular foliation-forming or foliation-folding deformation event, as discussed in detail in Section 5.10.6. Thus, a porphyroblast may be classified as being *prekinematic* (*predeformational*), *synkinematic* (*syndeformational*) or *postkinematic* (*postdeformational*) with respect to that event. However, as emphasized by Vernon (1977a, 1978a), these terms should not be applied without specifying a particular S-surface or fold set in the matrix. Furthermore, it is necessary to specify which of the following matrix features is being considered: (1) initiation of an S-surface; (2) flattening or folding of an existing S-surface; or (3) growth of the minerals defining an S-surface.

A basic set of microstructural criteria (Fig. 5.73) was suggested by Zwart (1960a,b, 1962), using geometrical relationships between S_i (the 'internal' foliation outlined by inclusion trails in the porphyroblast) and S_e (the 'external' foliation in the matrix). Subsequent work has shown that though these criteria are broadly applicable to the determination of relative time relationships between growth of porphyroblasts and deformation in regional metamorphic rocks, complications may occur, so that great care must be taken in their application (Vernon, 1978a). Many porphyroblast–matrix microstructural relationships are ambiguous, and so only clear, critical relationships should be used. Some relatively clear examples are shown in Figs. 5.72 and 5.74–5.80, but even some of these are subject to ambiguities in interpretation.

Jamieson (1988) has provided a summary of the approach. The best rocks for determining time relationships between deformation and prograde metamorphism are medium-grade metapelitic schists, which contain porphyroblasts and deform relatively easily. Most low-grade rocks lack porphyroblasts, which makes timing difficult. Some high-grade metamorphic rocks with porphyroblasts are suitable (see, for example, Vernon, 1989), as discussed in Section 5.10.10, but coarsening of the matrix commonly removes earlier microfolds and foliations. On the other hand, high-grade rocks are good for inferring retrograde metamorphic

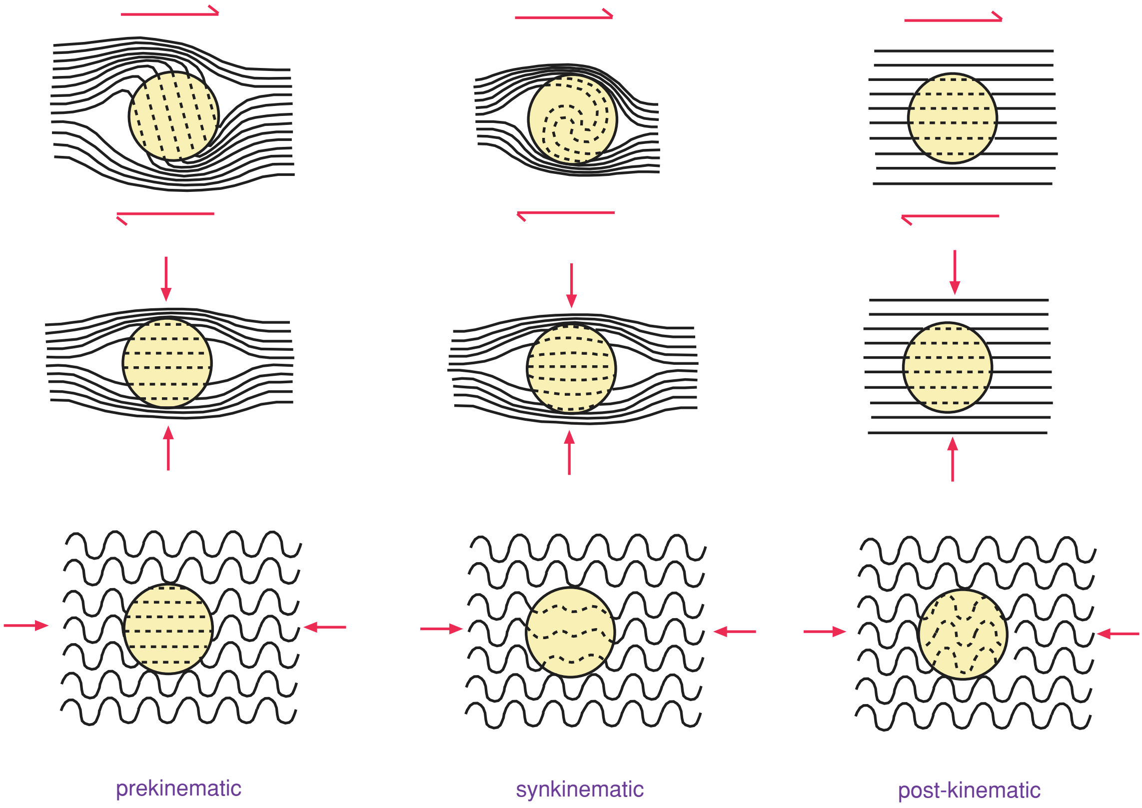

Fig. 5.73: Idealized porphyroblast–matrix relationships suggested by Zwart (1962) as indicators of growth of porphyroblasts pre-, syn- and post the development of a matrix foliation, depending on the type of strain (indicated by arrows).

histories, because the reactions are commonly incomplete and the grade contrast is obvious. Some medium-grade rocks may also be suitable for this purpose, but low-grade rocks have insufficient grade contrast.

A number of regional studies illustrating the modern use of porphyroblast–matrix microstructural relationships to help infer metamorphic and deformational histories in regional metamorphic terranes have been published. I will refer to a few of them, especially those relating to metamorphic problems. The general approach is illustrated in Fig. 5.81.

By using porphyroblast–matrix relationships, Bell & Rubenach (1983) worked out a sequence of crystallization of porphyroblastic minerals, and made inferences about the metamorphic history of the Robertson River Formation, north Queensland, Australia. They inferred a constant sequence of porphyroblast development, regardless of the local stage of development of crenulations that were forming during the metamorphism. For example, crenulations preserved as inclusion trails in andalusite porphyroblasts are always at an earlier stage of development than

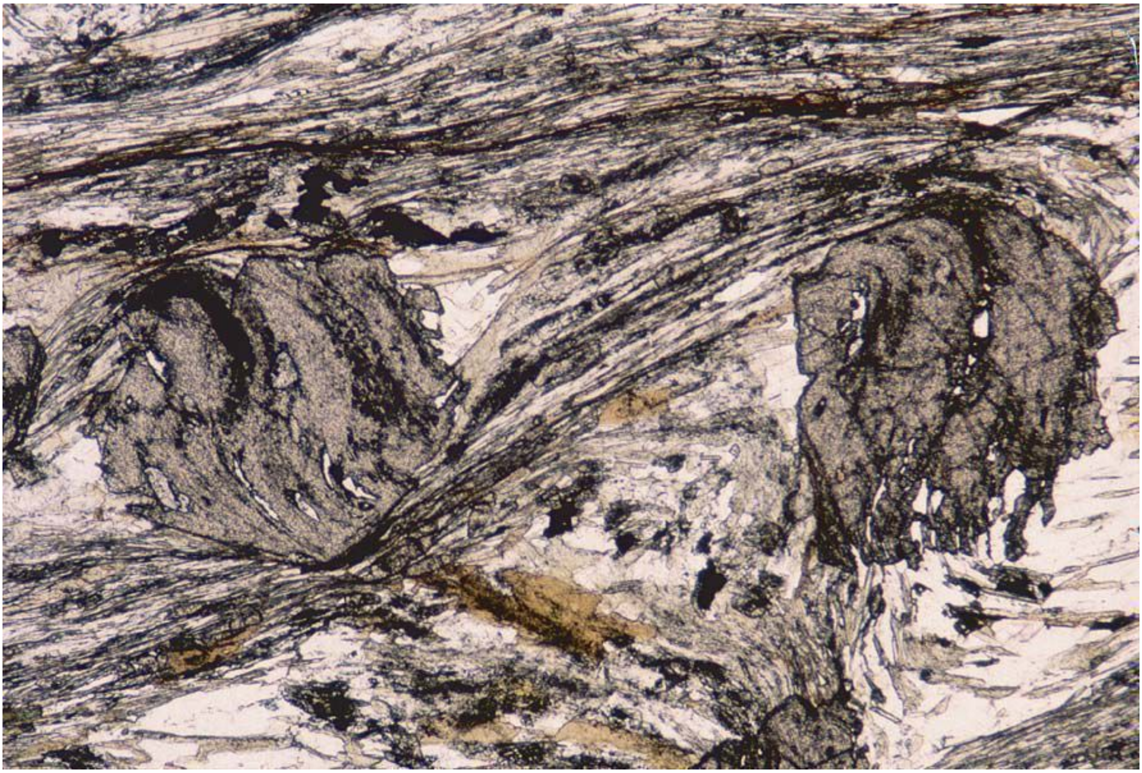

Fig. 5.74: Two garnet porphyroblasts with curved inclusion trails ('spirals') that are mainly continuous with the matrix foliation, suggesting growth during microfolding (crenulation) of the foliation; Chiwaukum Schist, Cascade Range, Washington, USA. Plane-polarized light; base of photo 4 mm.

those preserved in garnet porphyroblasts in the same rock, even though the stage of development of crenulations preserved in andalusite varies greatly from place to place, depending on the time of nucleation of andalusite relative to the local stage of development of the crenulations.

A good example of the relationship between growth of porphyroblastic minerals and progressive deformation, temperature and time is the study of prograde metamorphic mineral sequences in the Robertson River Formation and the Corella Formation, north Queensland, Australia, by Reinhardt & Rubenach (1989). They compared inclusion trails in porphyroblasts of each mineral with matrix foliations, from the first appearance of the mineral through its occurrences in higher-grade zones. They found that most of the foliations preserved as inclusion trails in the porphyroblasts represent a more advanced stage of crenulation development in lower-grade zones than for the same minerals in higher-grade zones. This result is to be expected from the tendency of higher-grade parts of a metamorphic terrane to begin to heat up earlier than lower-grade parts (den

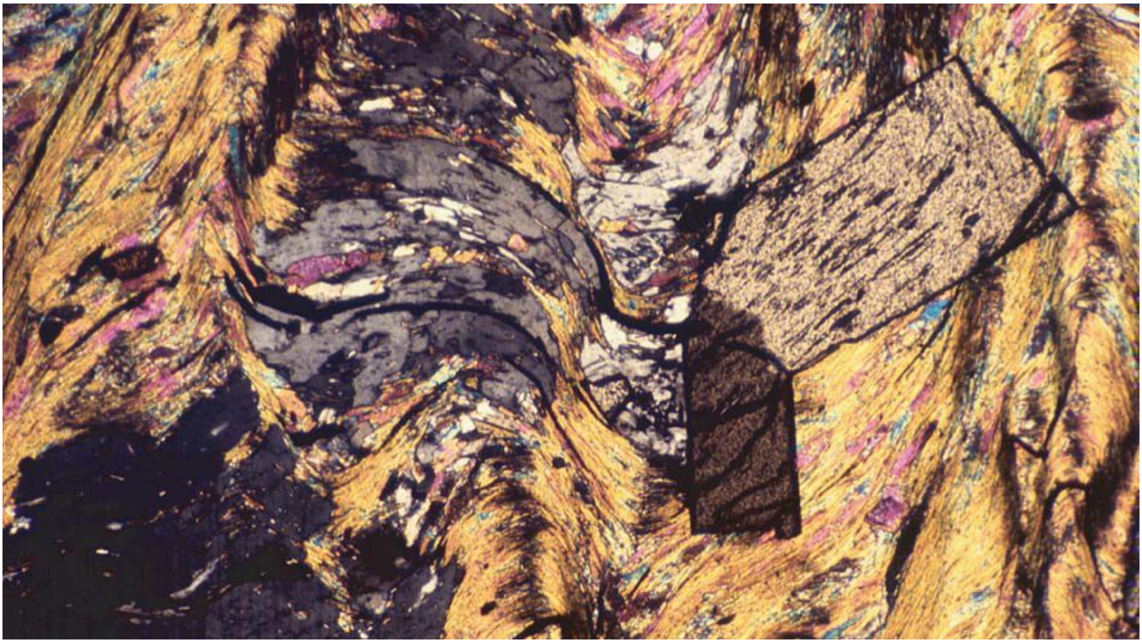

Fig. 5.75: Crenulated schist from the Lukmanier area, Swiss Alps, showing a porphyroblast of staurolite (right) with straight inclusion trails and a porphyroblast of plagioclase (left; grey first-order interference colours) with curved inclusion trails that are continuous with the matrix foliation; for example, individual elongate graphite inclusions (opaque) curve continuously from the plagioclase into the matrix. A reasonable interpretation is that the staurolite grew either before the crenulations or at least during the very early stage of their development (before the microfolds had tightened at the scale of the porphyroblast), and that the plagioclase grew during the development of the crenulations. The much smaller size of the inclusions in the staurolite is also consistent with its growth earlier than the plagioclase, i.e. when the matrix grainsize was smaller. Although a relative time difference between the growth of the two minerals at this particular place may be inferred, this could be due to local nucleation and growth conditions, and so need not apply everywhere, even in close proximity; therefore, both minerals could belong to the same mineral assemblage. Crossed polars; base of photo 4 mm.

Tex, 1963). Thus, porphyroblasts of a particular mineral should grow during the earlier stages of a particular crenulation-forming event at higher grades than at lower grades, assuming approximate contemporaneity of the crenulation event across the terrane. Of course, this assumption may or may not be justified, and conceivably both deformation and metamorphism could progress through a volume of rock at different and even spasmodic rates (see, for example, Johnson, 1999b, pp. 1713–14). Problems of correlating structures in multiply deformed areas have been discussed by Means (1963), Park (1969) and P. F. Williams (1985). M. L. Williams (1991) has shown that, in terranes that have been deformed

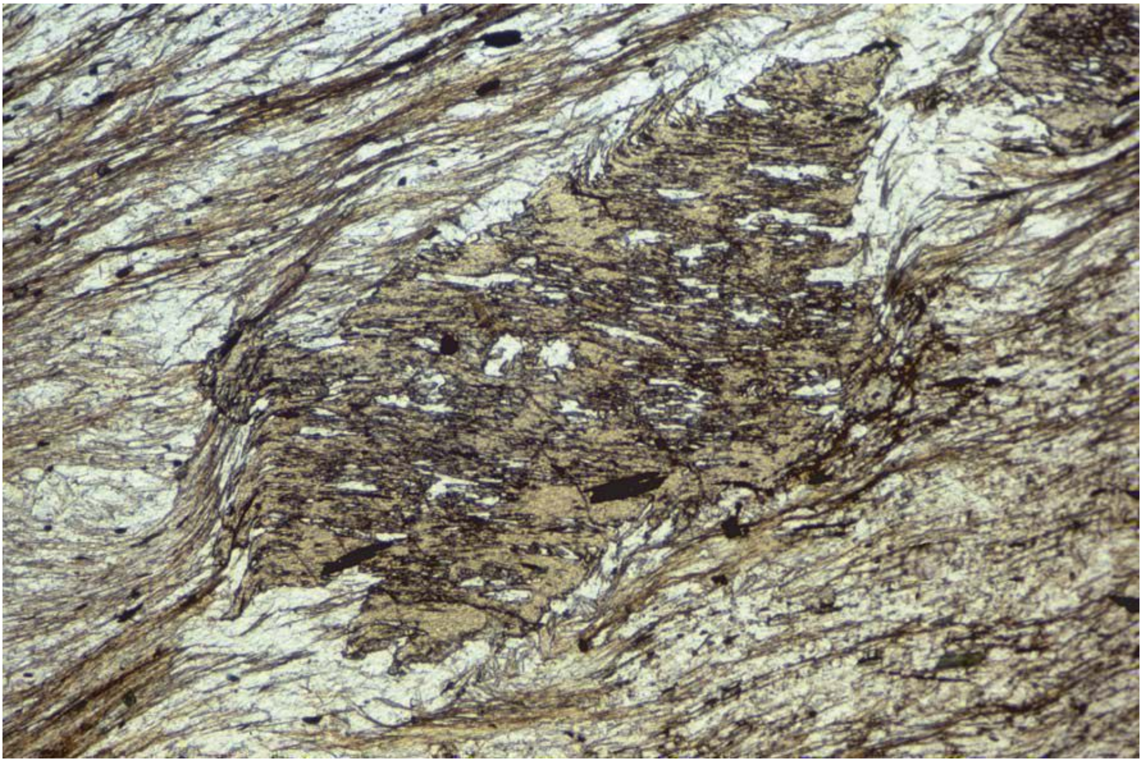

Fig. 5.76: Metapelitic schist from the Lukmanier area, Swiss Alps, showing a porphyroblast of staurolite (pale yellow) with straight inclusion trails that curve near the edge of the porphyroblast into the matrix foliation without truncation, indicating growth of the staurolite during the folding of the matrix foliation. The sense of curvature of the foliation at one end of the porphyroblast is opposite to that at the other end ('millipede structure'). Plane-polarized light; base of photo 4.4 mm.

heterogeneously, the structural histories of refolded and repeatedly sheared regions are only of local importance and are misleading on a regional scale. In addition, Alias *et al.* (2002) suggested that the development of foliation S_2 may be diachronous across the Adelaide Fold Belt, South Australia, reflecting variations in the thermal state of the lithosphere caused by heterogeneous production and ascent of magmas.

Regional metamorphic rocks typically show sequences of foliations (labelled S_0 for sedimentary bedding, and S_1, S_2, etc. for tectonic foliations) as discussed in structural geology textbooks (see, for example, Ramsay, 1967; Hobbs *et al.*, 1976; Ramsay & Huber, 1987; Passchier & Trouw, 1996). In the absence of detailed geochronological data to date the growth of porphyroblasts and/or development of foliations, it cannot be safely assumed that each foliation results from a tectonic event well separated in time or, alternatively, that all the foliations in an individual rock or area are formed in the same tectonic event.

Fig. 5.77: Graphite inclusion trails passing continuously from the matrix into and across three porphyroblasts of biotite in a schist from the Karakoram, Himalayas. This indicates that the biotite grew after the development of the matrix foliation. However, no reasonable inference can be made about the timing of biotite growth relative to the development of the crenulation at the left of the photo. The curvature of the inclusion trails in the left-hand biotite porphyroblast appears to rule out growth of the biotite before the crenulation; it could suggest growth either after the crenulation or during the early stages of its development. Plane-polarized light; base of photo 1.3 mm.

Many studies of pressure–metamorphic pressure–temperature–time (*P*–*T*–*t*) paths (tectonometamorphic history) assume a single heating–cooling event, implying that all foliations present formed more or less synchronously. This interpretation is supported by geochronological measurements on multiply foliated schists of the classical Barrovian sequence of Scotland (Baxter *et al*., 2002), which indicate no age difference (within the error of measurement) between the development of garnet zone rocks (500–550 °C) during deformation D_2 and the development of sillimanite zone rocks (*c*. 660 °C) during deformation D_3. On the other hand, geochronological evidence for repeated heating events in some areas has been obtained, as reviewed by Vernon (1996a) and discussed also in Section 5.10.3.

For example, Crowley *et al*. (2000) used U–(Th)–Pb dating to infer multiple periods of metamorphism and deformation in a Barrovian sequence in the

A

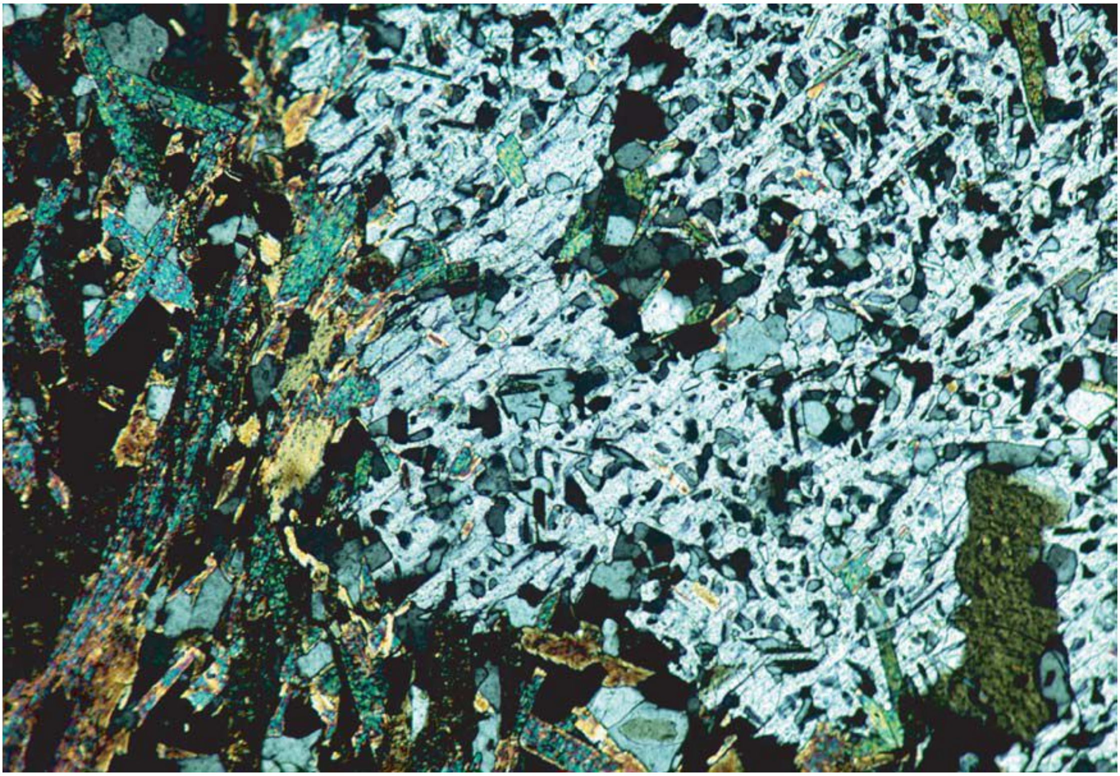

Fig. 5.78: Porphyroblasts showing evidence of overgrowth of pre-existing mica grains. This suggests constant-volume replacement of the matrix during growth of the porphyroblasts. (A) Schist from the Snowy Mountains, south-eastern New South Wales, Australia, showing a porphyroblast of andalusite (with grey first-order interference colours) with inclusions of quartz and biotite. The shapes of the intervening patches of andalusite between the inclusions suggest the former presence of random mica flakes, the components of which were preferentially used by the andalusite. They also suggest that the andalusite grew before a foliation had been developed. Since the growth of the andalusite, a foliation has developed in the matrix, the grainsize of which has coarsened appreciably. Crossed polars; base of photo 1.75 mm. (B) This schist also shows residual mica grain shapes preserved in a porphyroblast of staurolite (first-order yellow interference colours). However, the porphyroblast shows evidence of a more complicated history than that shown in A. The staurolite has overgrown an earlier foliation that itself shows evidence of later growth of mica, several grains of which transgress the foliation. Therefore, it is reasonable to infer the formation of a foliation, followed by static growth of mica, and then growth of staurolite. Staurolite–mica schist, Appleton Ridge, Maine, USA. Specimen by courtesy of Charles Guidotti and Scott Johnson. Crossed polars; base of photo 3 mm.

B

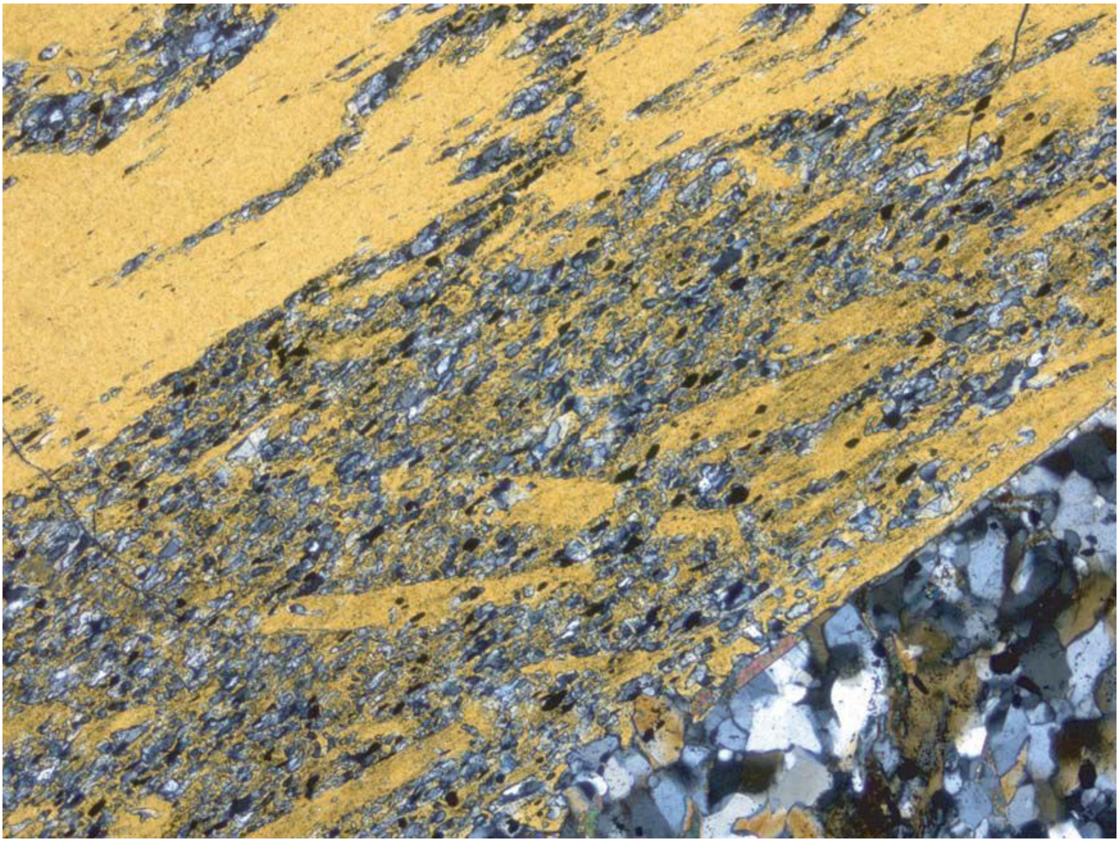

Fig. 5.78: (*cont.*)

Canadian Cordillera. They found that the thermal peak of metamorphism occurred at different times (roughly 10–50 Ma apart) in three kilometre-scale domains, the peak events coinciding with secondary events in the other domains. S_{1+2} developed before 72 Ma in domain 1, and at least partly at 61–58 Ma and 122–63 Ma in domains 2 and 3, respectively. Either the domains were tectonically assembled along unrecognized shear zones, or the events must have been relatively local (Crowley *et al.*, 2000), indicating potential problems in making correlations based on structural correlations alone.

This situation applies especially in low-pressure/high-temperature (LPHT) metamorphism (both contact and regional), for which local magmatic thermal pulses may control metamorphic reactions (see, for example, Vernon *et al.*, 1993a; Collins & Vernon, 1991; Collins *et al.*, 1991; Stüwe *et al.*, 1993; Williams, 1994), with the result that the same sequence of mineral growth and foliation development may occur in different areas at different times. This has been well illustrated by Williams (1994), who investigated three metamorphic terranes in Arizona

Next Page

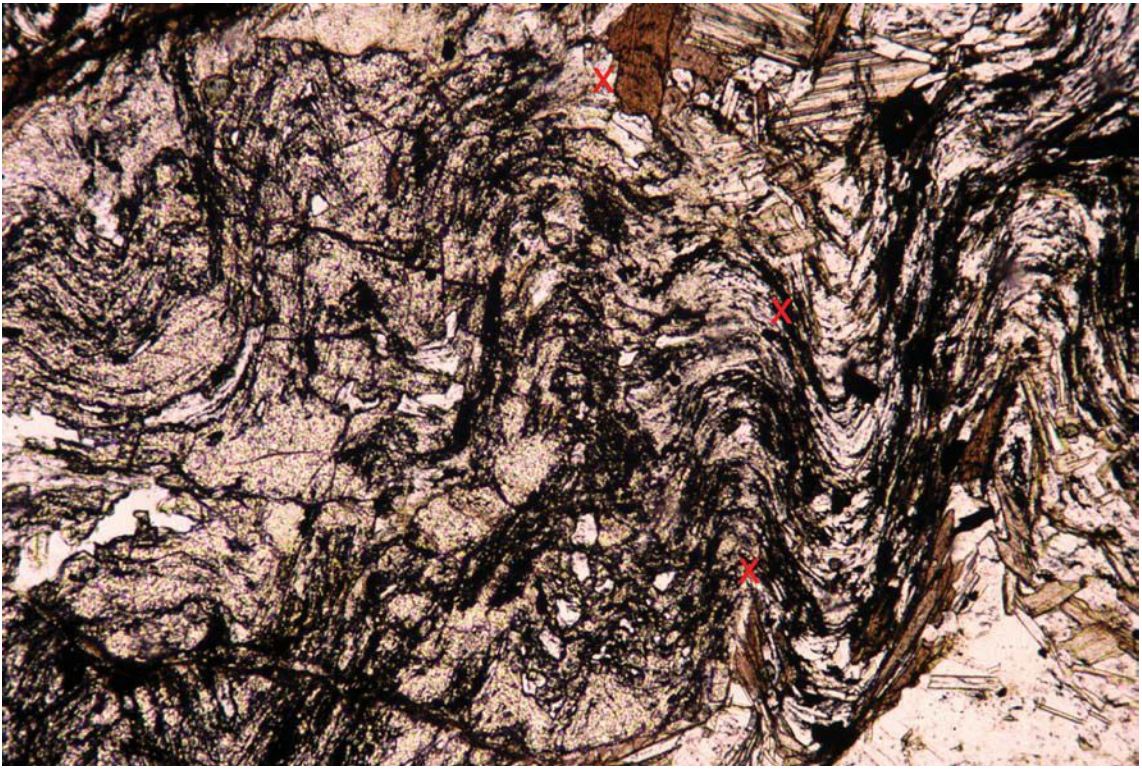

Fig. 5.79: Porphyroblast of staurolite (pale yellow) with folded trails of graphite (opaque) in a metapelite from the Chiwaukum Schist, Cascade Range, Washington, USA. The boundary between the porphyroblast (left) and the matrix (right) is marked X–X. The graphite microfolds extend continuously into the matrix, and have the same amplitude and wavelength inside and outside the porphyroblast. This indicates that the staurolite grew after the development of the microfolds, at least on the scale of observation. However, it does not necessarily indicate post-folding growth on a broader scale. Plane-polarized light; base of photo 1.7 mm.

and New Mexico (two contact metamorphic, one regional) that show the same sequence of porphyroblast–foliation development, despite being of different ages. Garnet, biotite, staurolite and andalusite porphyroblasts have inclusion trails indicating overgrowth of progressive stages in the transformation of a slaty cleavage (S_1) into a crenulation cleavage (S_2). Garnet and biotite have trails indicating stage 2 or 3 of Bell & Rubenach (1983), and staurolite and andalusite trails indicate stages 3–6. The transition from greenschist to amphibolite facies conditions coincides with the change from S_1 to S_2, and the transition from chlorite-dominated to biotite-dominated mineral assemblages occurs over a small temperature interval (400–450 °C). The rapid production of abundant water as the chlorite dehydrated may have weakened the rocks and so contributed to the evolving crenulation cleavage, during which time the porphyroblasts grew rapidly.

Previous Page

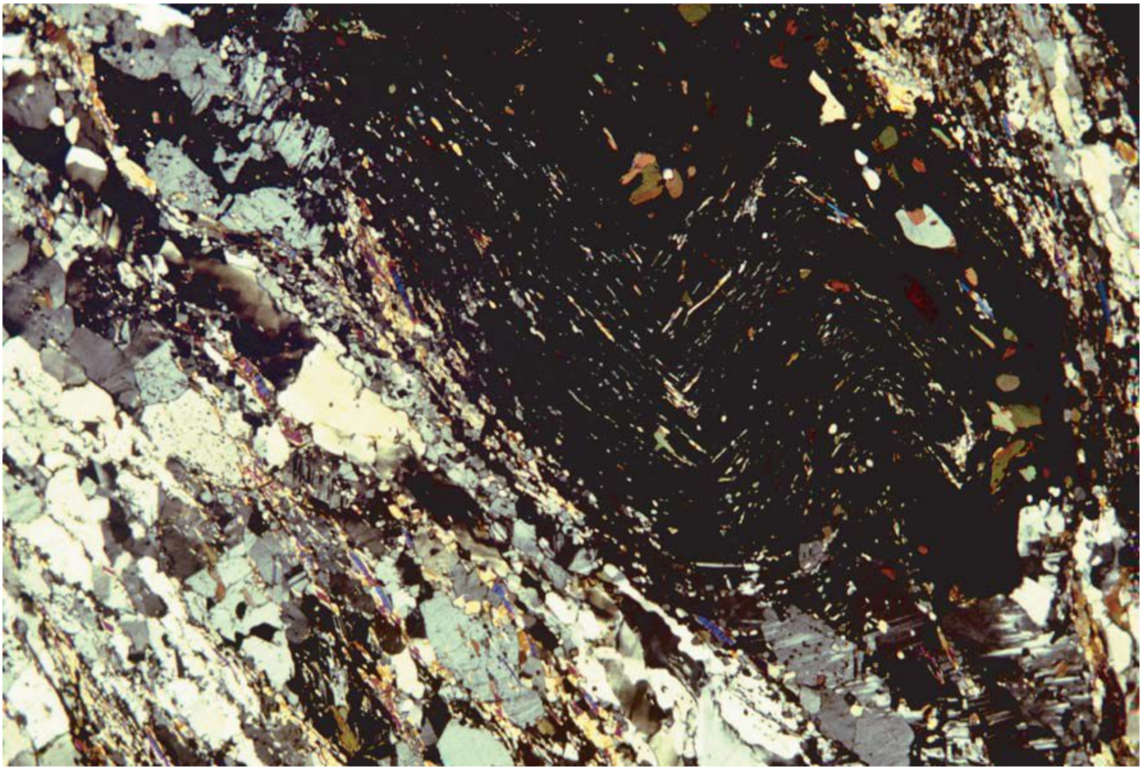

Fig. 5.80: High-grade (granulite facies) metapelitic rock from the Anmatjira Range, central Australia, showing a porphyroblast of garnet (optically isotropic) with folded inclusion trails of sillimanite. Such folds are absent from the matrix, which also contains sillimanite. This suggests that the garnet grew after the deformation that obliterated the microfolds in the matrix, but that the metamorphic conditions remained constant enough during this process, so that the garnet and sillimanite belong to the same mineral assemblage (paragenesis). Crossed polars; base of photo 12 mm.

Thus, metamorphism and deformation were intimately linked, producing growth–foliation sequences that are similar to those observed in many areas (Williams, 1994, p. 19). The links between deformation and metamorphism are of the following three types, each of which typically contributes (Williams, 1994).

(1) *Environment-controlled* links result from changes in *P*–*T*–fluid conditions that simultaneously affect both the growth of porphyroblasts and the foliation development.

(2) *Deformation-controlled* links involve selected microstructural sites, such as crenulation fold hinges, being favourable sites for porphyroblast nucleation and growth of porphyroblasts.

(3) *Reaction-controlled* links involve the production of water in dehydration reactions, which can affect the deformation and hence control the microstructures of developing foliations; this is a form of reaction weakening, as discussed in Section 5.6.3.

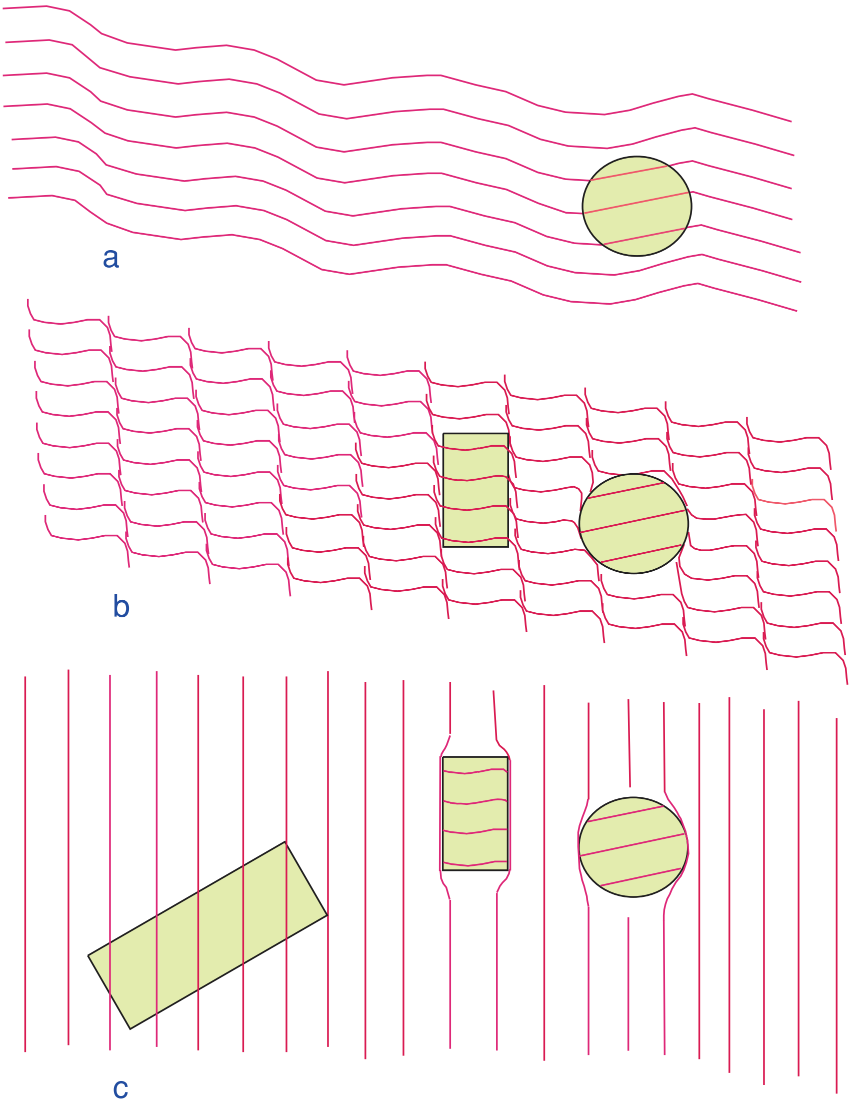

Fig. 5.81: Sketch showing how different porphyroblastic minerals can preserve evidence of different stages of foliation development. The round porphyroblast grew during the early stages of S_2 development, the vertical rectangular porphyroblast grew next, and the oblique rectangular porphyroblast grew last, during or after the development of S_2. After Johnson (1999b, fig. 4), with permission of the Mineralogical Society of America. Before major inferences about the relative timing of metamorphism and deformation can be made, care must be taken to ensure that such a sequence is applicable everywhere in the rocks being studied, and that it can be reconciled with inferred changes in other minerals in the rock.

These investigations show that careful interpretation of porphyroblast–matrix microstructural relationships can provide relatively clear evidence of sequential porphyroblast growth and prograde metamorphic reactions, especially with regard to the development of foliations in a single rock. However, correlations between rocks of different areas are based on the assumption of contemporaneity of foliation-forming deformation across the region concerned, which may not be justified.

Another outcome of the investigations of Williams (1994) is that porphyroblasts may grow relatively rapidly, especially in LPHT metamorphic terranes, in which relatively short magmatic heat pulses may control the metamorphism (see, for example, Collins & Vernon, 1991; Collins *et al*., 1991; Vernon *et al*., 1993a). He suggested that the growth durations of porphyroblasts may be no more than a few hundred thousand years, which supports an earlier estimate of 300–300 000 years by Paterson & Tobisch (1992). Microstructural evidence consistent with this inference includes (1) porphyroblasts with many small inclusions, implying rapid growth (Vernon, 1976), (2) porphyroblasts with small inclusions and no inclusion trails, implying growth before foliations had time to develop (Fleming & Offler, 1968; Vernon *et al*., 1993a), and (3) porphyroblasts either with straight inclusion trails curving slightly into the matrix foliation at their edges or with weakly crenulated inclusion trails, implying growth before crenulation of an existing foliation had time to develop.

Moreover, inferred rapid growth of porphyroblasts relative to foliation development implies growth in the early stages of deformation events (see, for example, Bell *et al*., 1986). This implies that deformation may be triggered or accentuated by metamorphic reactions, as discussed in Section 5.6.

5.10.3 Relationships between microstructures, deformation and *P–T–t* paths (*P–T–D–t* paths)

Much current effort in metamorphic geology goes into the determination of pressure (*P*)–temperature (*T*) conditions from mineral assemblages and compositions. Attempts are also made to determine how *P* and *T* vary with time (*t*) in a metamorphic terrane (i.e. the *P–T–t* path). This is done by using structural data, either (1) microstructural (e.g. by noting the replacement of one mineral or assemblage by another mineral or assemblage, or by using porphyroblast–matrix relationships) or (2) mesostructural (e.g. by observing assemblages in shear zones that cut earlier assemblages). Precautions that need to be taken have been discussed by Vernon (1996a).

It is also desirable to integrate inferred *P–T–t* paths with an inferred sequence of foliation-forming deformation events (the *D* path) — provided time differences between these 'events' can be successfully determined (Section 5.10.2) — producing *P–T–D–t* paths (Johnson & Vernon, 1995a,b). This is a complex problem, not only because of difficulties of microstructural interpretation (Johnson & Vernon, 1995a,b; Alias *et al*., 2002), but also because patterns of cyclic deformation and flow instabilities may fluctuate with changes in temperature and cooling rate, as emphasized by Knipe (1989). For example, the duration, temperature and stress experienced by a rock between deformation events affect the frequency of events and the instabilities developed. Also, the stress and temperature paths at the end of a deformation event influence the preservation of microstructures, so much so that some microstructures produced during prograde metamorphism may be obliterated.

A good example of a *P–T–D–t* path is provided by the investigation of porphyroblastic schists at Petrel Cove, South Australia, by Alias *et al*. (2002). They showed that the sequential syn-D2 and syn-D3 growth of cordierite, andalusite, staurolite and fibrous sillimanite, as well as the post-D3 growth of chlorite and muscovite occurred by a series of metamorphic reactions recording evidence of a pressure increase of about 1 kbar during cooling from about 580 °C.

Even where reliable evidence for *P–T–D–t* paths is available, detailed geochronological evidence on the microscopic scale is needed before the foliation-forming events can be separated in time. High-resolution compositional mapping and dating of monazite with the electron microprobe is a very promising technique for absolutely timing metamorphic assemblages and foliations (Williams & Jercinovic, 2002), and so providing firmer evidence for *P–T–D–t* paths. Because monazite contains Th and U, without much common Pb, it can be used for U–Pb dating. Moreover, because diffusion of major and minor elements is extremely slow in monazite, the mineral can retain chemical and geochronological information during younger metamorphic events. For example, Williams & Jercinovic (2002) were able to distinguish several stages of metamorphism in both the 1650–1700 Ma and 1400 Ma metamorphic/deformation events in southwestern USA, and four separate pulses of monazite growth in the 1900–1800 Ma event in northern Saskatchewan, Canada.

5.10.4 Precautions with porphyroblasts

The preceding two sections indicate problems with correlation based on porphyroblasts. Successful correlation depends on reliable timing of porphyroblast growth relative to the development of a foliation. Reliable inferences from porphyroblast–matrix microstructural relationships depend not only on careful and detailed observation, but also on the use of critically oriented sections. Fagan (1979) emphasized the importance of observing the right section for the correct identification and interpretation of porphyroblast–matrix relationships in folded, crenulated rocks. For example, a section cut parallel to the axes of crenulations shows only straight inclusion trails that pass into parallel folia in the matrix (Fig. 5.82). This may suggest that the porphyroblasts grew after the development of the present orientation of the matrix foliation, i.e. they could be misinterpreted as postdeformational porphyroblasts. On the other hand, a section cut perpendicular to the axes of the crenulations reveals not only microfolds in the matrix, but also curvature of inclusion trails in porphyroblasts (Figs. 5.82). Thus, evidence of syndeformational growth may be obtained. In addition, Cihan (2002) has suggested that sections cut parallel to the lineation and foliation may not reveal as much detailed information about inclusion trails as oblique sections.

General precautions that should be taken when using porphyroblast–matrix microstructural relationships (see, for example, Bell & Rubenach, 1983; Vernon, 1988a) include: (1) labelling S surfaces in the field and being careful to refer matrix foliations and inclusion trails to these labels; (2) making thin sections in several orientations; (3) observing as many sections (in the right orientation)

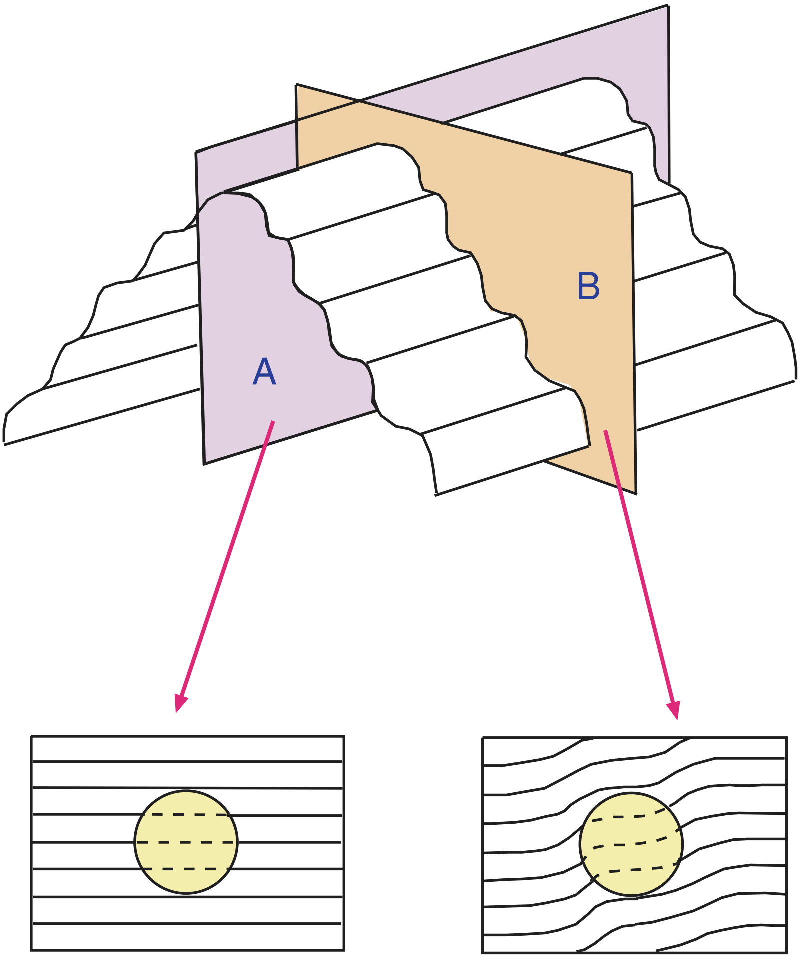

Fig. 5.82: Diagram showing how a section (A) cut parallel to microfold axes can falsely indicate postfoliation growth of porphyroblasts, whereas a section (B) cut perpendicular to the microfold axes indicates syn-crenulation growth.

as are necessary to reveal the critical evidence; (4) examining sections showing sedimentary bedding (S_0) wherever possible, so that you can be more confident about inferring the sequence of S surfaces in the rock; and (5) sectioning the hinge areas of the earliest folds, so that a clear obliquity between S_0 and S_1 can be seen. Other complications have been pointed out by Johnson & Vernon (1995a,b) and Cihan (2002).

Only porphyroblasts with clear inclusion trails should be used, and care should be taken to ensure that inclusion trails are not crystallographically controlled, for example, by exsolution or coaxial growth (Ingerson, 1938; Vernon, 1978a). Otherwise, spurious interpretations may result, as emphasized by Vernon (1978a). The following criteria (Ferguson & Harte, 1975, p. 474) can be used to argue against an exsolution or replacement origin of inclusions; (1) S_i is continuous from one edge of the porphyroblast to the other; (2) most S_i trails are not related to the crystallographic orientation of the host porphyroblast and

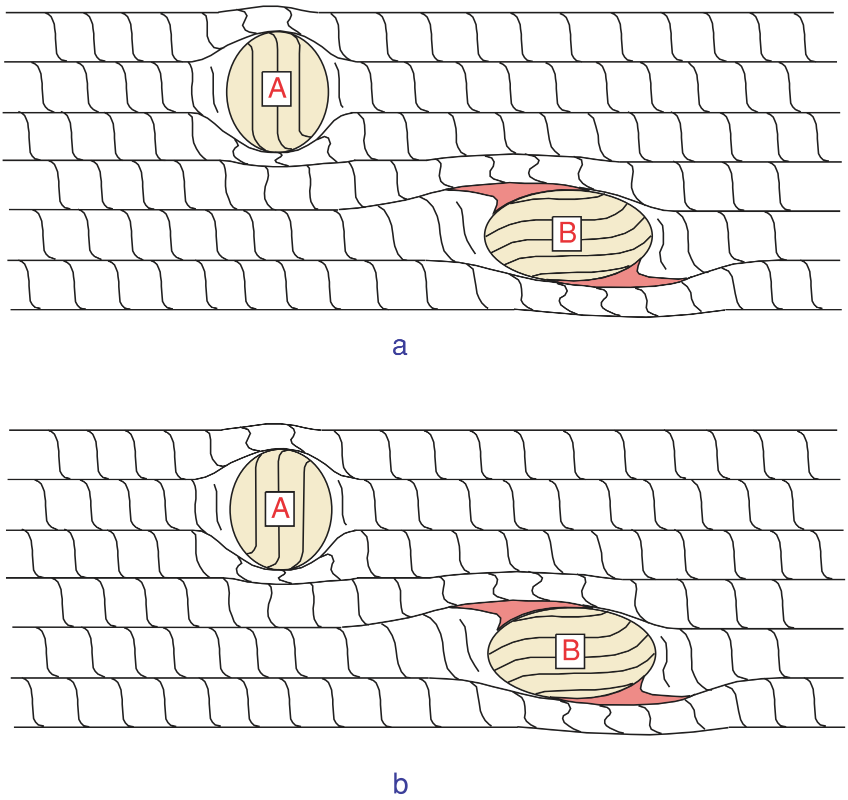

Fig. 5.83: Diagrams showing the importance of deformed strain-shadows and asymmetry of inclusion trail curvatures in determining relative time sequences of porphyroblast growth. (a) Porphyroblast A has inclusion trails with the same asymmetry as crenulations in the matrix, and the inclusion trails are continuous with folia in the matrix. These features are reliable evidence for inferring growth during development of the crenulation-foliation. Strain shadows around porphyroblast B are folded into the crenulation-foliation, and so B pre-dates both A and the matrix foliation. If the inclusion trails in A were not continuous with the matrix foliation, this correlation would be less certain. (b) The inclusion trails in A have the opposite asymmetry to the matrix crenulations, and lack continuity with the matrix folia. Therefore, A did not grow during the development of the crenulation-foliation, and the rock shows no reliable evidence of its timing with respect to B. After Johnson & Vernon (1995b) and Johnson (1999b), with permission of Elsevier and the Mineralogical Society of America.

are not deflected where they cross twin interfaces in the host; and (3) S_i passes continuously from the host mineral through relatively large inclusions of other minerals, where present.

Another important complication is that only porphyroblasts for which the inclusion trails are continuous with the matrix foliation (Figs. 5.74–5.77, 5.80) can be used to reliably time porphyroblast growth relative to the development of a matrix foliation (Johnson & Vernon, 1995b), as shown in Fig. 5.83. Porphyroblasts

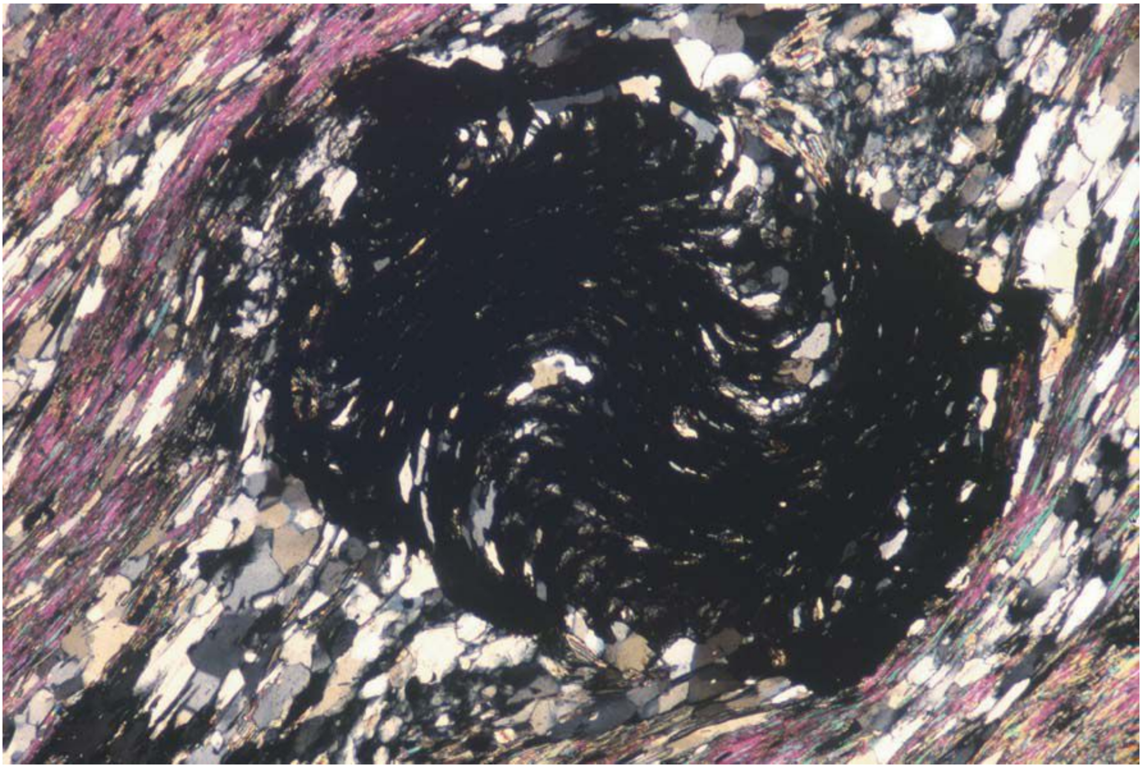

Fig. 5.84: Garnet porphyroblast (isotropic) with curved inclusion trails in a relatively homogeneous matrix, from the Himalayas. Crossed polars; base of photo 4 mm.

with curved inclusion trails truncated by the matrix foliation (Fig. 5.84) are unreliable in this respect, although they can be used to indicate growth before a particular matrix foliation.

Finally, the importance of local strain heterogeneity should not be underestimated when using porphyroblasts. As shown in Fig. 5.55, crenulations may be very patchy, especially in the earlier stage of their development, which means that porphyroblasts can grow simultaneously in crenulated and non-crenulated areas of the same rock (on the thin section scale), giving the false impression of different timing of growth relative to the crenulations.

5.10.5 Recent hypotheses about porphyroblasts

Earlier ideas on the interpretation of porphyroblast–matrix microstructural relationships in regional metamorphic rocks were summarized by Zwart (1962) and Vernon (1978a), and subsequent ideas were reviewed by Vernon (1989). In recent years, the investigation of porphyroblast–matrix microstructures has been intensified, and a model for the growth of porphyroblasts during the development of a crenulation-foliation has been developed, mainly by Bell & Rubenach (1983) and Bell *et al.* (1986). In effect, the following four hypotheses have been proposed, each of which is evaluated in the following sections.

Hypothesis 1:
Porphyroblasts nucleate only in low-strain, largely coaxially deformed, quartz-rich (Q) domains of a crenulation-foliation (Section 5.8.3), and are dissolved in active high-strain, non-coaxially deformed, mica-rich (P or M) domains. The spacing between Q and P domains limits the size of the porphyroblasts (Bell *et al.*, 1986).

Hypothesis 2:
Porphyroblasts are always syndeformational (Bell & Rubenach, 1983; Bell *et al.*, 1986).

Hypothesis 3:
Porphyroblasts generally do not rotate, with respect to geographical co-ordinates, during deformation, provided they do not deform internally (Bell, 1985).

Hypothesis 4:
Because they do not rotate, porphyroblasts may be used as reliable indicators of the orientation of former structural surfaces (Fyson, 1975, 1980; Fyson & Frith, 1979; Bell, 1985, 1986), allowing regional structural correlations, even on the scale of orogenic belts (Bell & Johnson, 1989a).

5.10.6 Evaluation of hypothesis 1: do porphyroblasts necessarily grow in a differentiated foliation?

Porphyroblasts commonly occur in rocks with a crenulation-foliation (Section 5.8.3). Bell *et al.* (1986) suggested that porphyroblasts grow only in lenticular zones of low, coaxial strain (quartz-rich or Q domains), around which anastomose active zones of strong, non-coaxial strain (P domains), in which only minerals such as mica, graphite or sillimanite (Vernon, 1987b) can grow. As explained in Section 5.8.3, the inference is that these minerals can slip on grain boundaries without accumulating much internal strain, whereas other minerals are inferred to build up high concentrations of dislocations around their margins and consequently tend to dissolve in the P domains (Bell *et al.*, 1986). According to this model, porphyroblasts cannot grow beyond the confines of the Q domains, as they tend to dissolve in active P domains. Thus, they commonly preserve a single crenulation as inclusion trails. However, according to this growth model, porphyroblasts may overgrow P domains that become inactive as progressive deformation partitions on different scales, thereby accounting for porphyroblasts with inclusion trails outlining several crenulations. Previously such porphyroblasts had been considered to be postdeformational. However, it is difficult to exclude the possibility that deformation was taking place while the porphyroblasts grew, but in P domains spaced more widely than the area being observed.

Although the model is stimulating current investigations, it has some problems (Vernon, 1989). For example, because porphyroblasts themselves cause partitioning of the deformation, by forcing P domains to anastomose around them or causing the nucleation of P domains on them (Hanmer, 1979; Olesen, 1982; Vernon, 1989; Paterson & Vernon, 2001; Goodwin & Tikoff, 2002), we must ask whether porphyroblasts grow in existing Q domains or whether P domains form around existing porphyroblasts. Both processes conceivably could occur in the same rock, of course. A problem with the first alternative is that typically only one porphyroblast occurs in each Q domain, whereas several nuclei might be expected to form, at least in the earlier stages of crenulation microfolding, when Q domains would be relatively wide, according to Bell *et al.* (1986). Therefore, the best evidence for the hypothesis that porphyroblasts nucleate and grow in Q domains would be a common observation of porphyroblasts smaller than the width between nearest P domains. A few observations of this type have been reported (see, for example, Vernon, 1989), but the situation appears to be uncommon. This could be taken to indicate that a differentiated foliation and associated strain partitioning are not necessary for the nucleation and growth of porphyroblasts, and that crenulations may nucleate on existing porphyroblasts, producing only one porphyroblast per Q domain (Vernon, 1989). The problem is readily solved by the second alternative, but can also be explained by tightening of crenulation-folia around porphyroblasts that grew according to the first alternative. Conclusive evidence is hard to find, but careful observation may resolve the difficulty.

Another problem with the model is that not everyone may accept that dislocations can concentrate sufficiently in grains in P domains to cause solution. However, strong evidence is accumulating that relatively large amounts of minerals such as quartz, feldspar and carbonate are commonly removed from P domains during the development of crenulation-foliations (Section 5.8.3). Therefore, some connection between solution and deformation is implied.

The most speculative part of the model of Bell *et al.* (1986) is the postulated transfer of components from P domains to fractures between deforming folia in Q domains, thereby promoting growth of porphyroblasts. This is difficult, if not impossible, to test by observational evidence. However, the components usually inferred to be removed from P domains (i.e. quartz, feldspar or calcite) are inappropriate for making most porphyroblasts.

5.10.7 Evaluation of hypothesis 2: are all porphyroblasts syndeformational?

Bell *et al.* (1986) suggested that all porphyroblasts nucleate and grow during deformation, even in contact metamorphism, where at least local deformation is probably typical (Vernon & Powell, 1976). The commonly straight, slightly curved or folded inclusion trails in porphyroblasts that are wrapped by mica-rich folia aligned at a high angle to the inclusion trails (Fig. 5.74) were interpreted as being formed by overgrowth of crenulation microfolds, initially at a relatively early stage of their development. The folds progressively tighten as the porphyroblast grows, thus enabling it to incorporate curving trails (Bell & Rubenach, 1983; Bell *et al.*, 1986). The microfolds may continue to tighten in the matrix after the porphyroblast has finished growing, during either the same deformation (see, for example, Hutton, 1979; Bell & Rubenach, 1983) or a later one (see, for example, Pitcher & Berger, 1972; Meneilly, 1983). Alternatively, the crenulations may be removed from the matrix (Bell, 1986) by intense flow and recrystallization/neocrystallization (producing a foliation more resembling a slaty cleavage, as shown in Fig. 5.57), during either the same deformation (Bell & Rubenach, 1983) or a later deformation (Bell, 1986). Evidence for the timing of porphyroblast growth relative to deformation is reviewed in the following sections.

Syndeformational porphyroblasts

Some of the better indicators of syndeformational porphyroblastic growth are: (1) progressive increase towards the edges of porphyroblasts in the curvature of inclusion trails formed from matrix folia deflected around the growing porphyroblasts (Zwart, 1962; Zwart & Calon, 1977); (2) progressive increase in the intensity of microfolding of inclusion trails towards the edges of porphyroblasts (see, for example, Vernon, 1989), as shown in Fig. 5.85; (3) 'millipede' microstructure (Bell & Rubenach, 1980; Johnson, 1993a,b; Johnson & Bell, 1996; Johnson & Moore, 1996), shown in Fig. 5.76; (4) 'paracrystalline microboudinage' (Misch, 1969, 1970; Vernon, 1976; Vernon & Flood, 1979; Benn *et al.*, 1999), shown in Fig. 5.86; and (5) inclusion spirals, which occur especially in garnet porphyroblasts (Rosenfeld, 1968, 1970; Schoneveld, 1977, 1979; Powell & Vernon, 1979; Johnson, 1993a,b), but which have also been observed in pyrite porphyroblasts (Craig, 1990b; Craig *et al.*, 1991). These 'snowball' porphyroblasts (Figs. 5.74, 5.87, 5.88) are generally considered to have rotated while they grew, although this interpretation has been challenged by Bell & Johnson (1989a), as discussed in Section 5.10.8. Fortunately, this difference in interpretation does not alter the inference that the 'snowball' porphyroblasts are syndeformational, provided their inclusion trails are continuous with the matrix foliation; trails discontinuous with the matrix foliation could indicate that the porphyroblast overgrew an earlier microfold or grew during an earlier deformation event. Unfortunately, all the foregoing features indicative of syndeformational porphyroblasts are relatively uncommon.

The most common microstructural evidence of syndeformational porphyroblasts is the presence of curved inclusion trails that are continuous with the matrix foliation (Fig. 5.74), as discussed by many people (e.g. Bell & Rubenach, 1983; Bell *et al.*, 1986; Jamieson & Vernon, 1987; Prior, 1987; Vernon, 1987a,

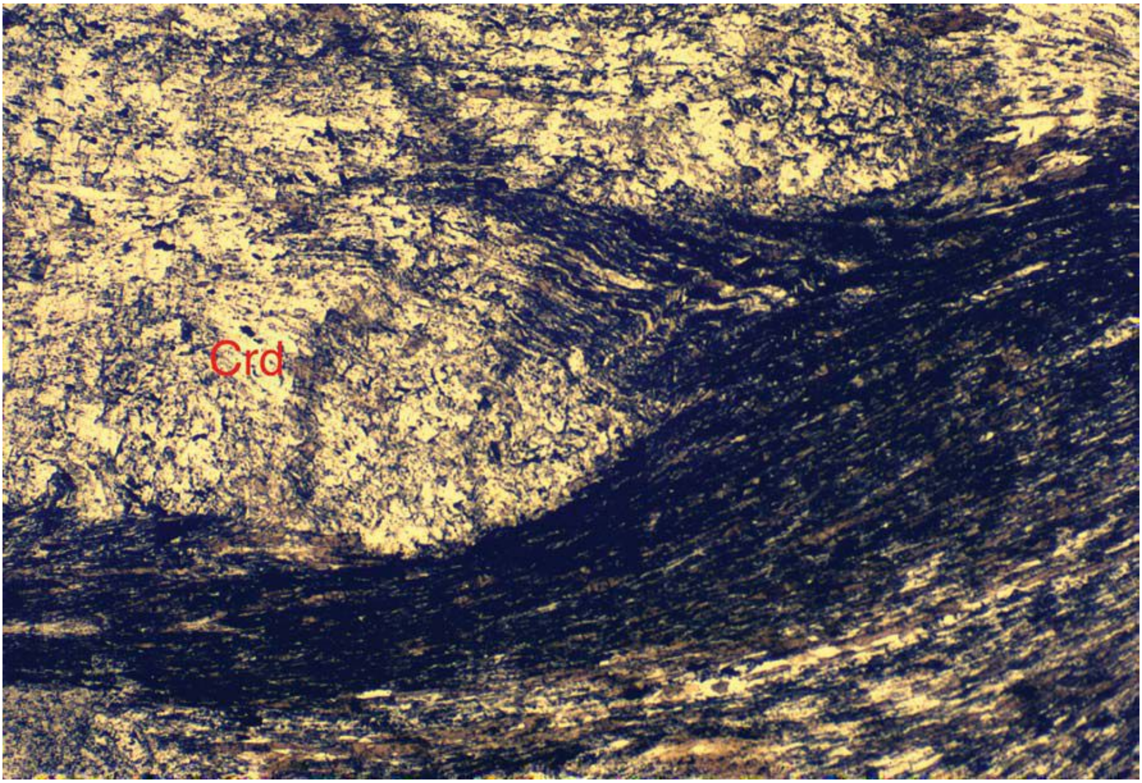

Fig. 5.85: Porphyroblast of cordierite (Crd; top left half of photo) in a schist from Cascade Bay, western Gulf of Alaska, with inclusion trails that are straight in the interior of the porphyroblast and show progressively tighter folding towards the edge of the porphyroblast. This indicates that the cordierite grew while the crenulations were developing. The microfolds preserved in the porphyroblast have been almost completely removed from the matrix, owing to intense deformation continuing after growth of the cordierite. Plane-polarized light; base of photo 2.7 mm.

1988a,b,c, 1989; Vernon *et al.*, 1993b; Johnson & Vernon, 1995a,b). Porphyroblasts with dominantly straight inclusion trails that curve into the matrix foliation at the edges of the porphyroblasts are generally interpreted as having grown in the early stages of development of a crenulation-foliation (see, for example, Bell *et al.*, 1986; Bell & Hayward, 1991).

The inclusion trails should curve inside the porphyroblast, as well as in the matrix. Straight inclusion trails continuous with curved matrix folia indicate post-porphyroblast deformation of the matrix. Curved inclusion trails that are discontinuous with matrix folia may indicate either syndeformational growth or postdeformational overgrowth of microfolds, and cannot be timed relative to the matrix foliation (Johnson & Vernon, 1995b).

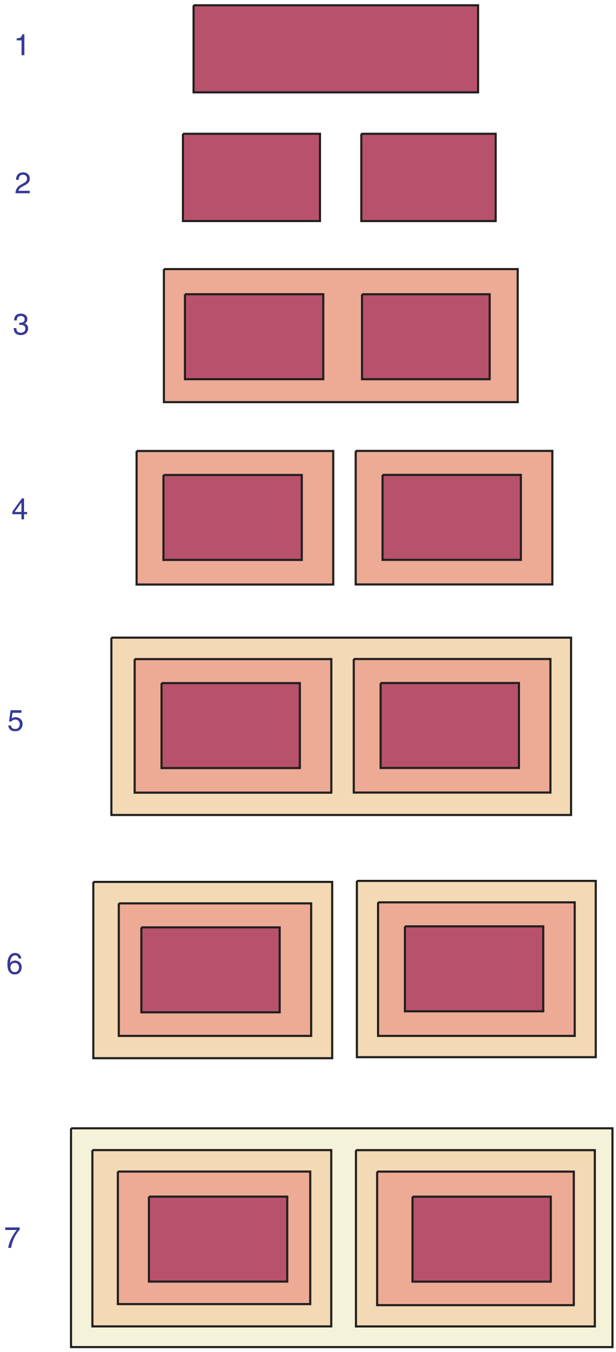

Fig. 5.86: Diagrammatic deformation–growth sequence involved in 'paracrystalline microboudinage' of chemically zoned grains with a single site of rupture. Although represented as finite steps, both stretching and accretion may occur simultaneously, the steps being infinitesimal. Based on Misch (1969, p. 48).

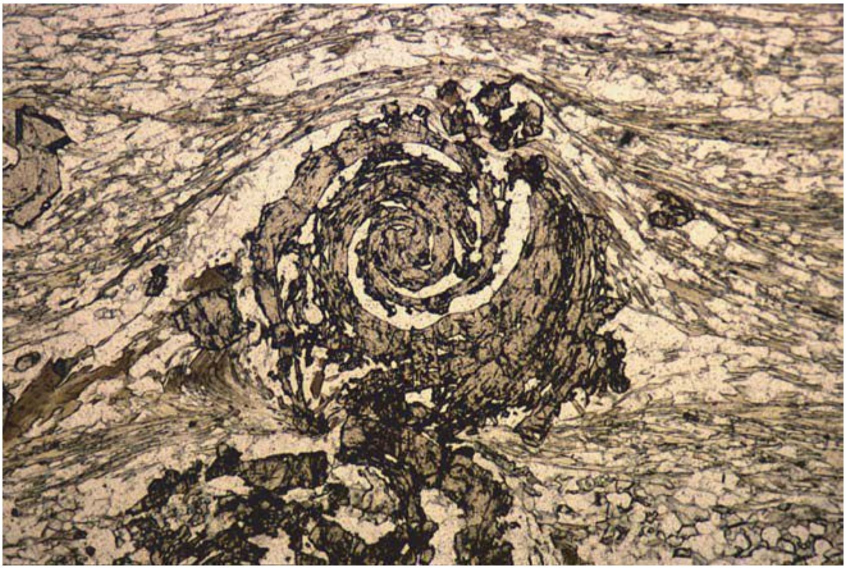

Fig. 5.87: Garnet porphyroblast (high relief) with spirals of graphite (opaque) and quartz (colourless) inclusions in a schist from the Himalayas. From Vernon (2000b, fig. 150). Plane-polarized light; base of photo 4.4 mm.

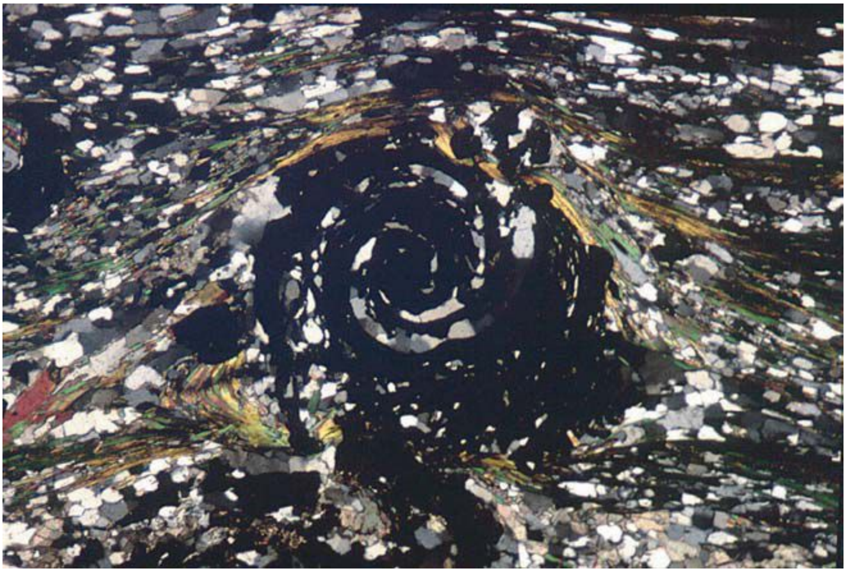

Fig. 5.88: Same field of view as shown in Fig. 5.87, but with crossed polars, to show isotropic garnet. From Vernon (2000b, fig. 151).

An important point is that 'decrenulation' may occur in the matrix by either (1) intense strain and neocrystallization at the culmination of the crenulation-forming event (Bell & Rubenach, 1983) or (2) reactivation of matrix foliations during a later deformation event (Bell, 1986; Vernon, 1989). This may leave porphyroblasts with curved or crenulated inclusion trails in a matrix from which all evidence of former crenulations has been obliterated, at least at first sight. However, close inspection of strain shadows adjacent to porphyroblasts or of low-strain areas elsewhere in the matrix commonly reveals residual crenulations (Fig. 5.59; Bell & Rubenach, 1983; Meneilly, 1983; Bell, 1985; Vernon, 1989), the orientation of which can be related to those preserved as inclusion trails in the porphyroblasts (see, for example, Bell, 1985; Vernon, 1989).

Porphyroblasts commonly show evidence of deformation and metamorphism continuing after their growth, confirming, at least in a general sense, that they grew during a deformational episode or series of episodes. For example, porphyroblasts commonly have matrix folia deflected around and crowded against them (Figs. 5.33, 5.74, 5.87, 5.88), as discussed in Section 5.10.11. In addition, relatively large strain accumulations adjacent to some porphyroblasts result in concentrations of mica and/or opaque material, probably due to solution of quartz (Fig. 5.33). The presence of metamorphic minerals consistent with the grade of metamorphism of the rest of the rock in the 'necks' between microboudins (see, for example, Vernon & Flood, 1979; Vernon *et al.*, 1993b) indicates that the microboudinage occurred during the same metamorphic event, so that the porphyroblasts were formed and deformed as part of the general prograde metamorphic history. Alternatively, the presence of retrograde aggregates in the 'necks' indicates that the microboudinage occurred during cooling or a later, lower-grade, metamorphic event.

Although all the preceding observations are consistent with a syndeformational origin for many or most porphyroblasts during prograde metamorphism, observations discussed in the following paragraphs suggest that some porphyroblasts may grow before or after deformation at the scale of observation.

Predeformational porphyroblasts

The best indicators of predeformational porphyroblasts are: (1) random inclusions that are very small, compared with the average grainsize of the matrix minerals (Zwart, 1960b; Johnson, 1962; Fleming & Offler, 1968; Vernon *et al.*, 1993a,b), the porphyroblasts apparently having grown before foliation development or matrix coarsening (Figs. 5.78A, 5.89); (2) porphyroblasts that have overgrown and preserve the shapes of former random mica grains (Fig. 5.78A); and (3) concentric 'arcs' rich in fine-grained chlorite, mica or opaque material in the matrix against the porphyroblast, similar to those discussed by Ferguson & Harvey (1972) and Ferguson *et al.* (1980) and mentioned in Sections 4.3.1 and 5.10.11. The occurrence of these 'arcs' all around porphyroblasts in a non-foliated matrix suggests that the porphyroblasts grew in the absence of foliation-forming deformation.

Postdeformational porphyroblasts

Some rocks (see, for example, Vernon *et al.*, 1993b) contain porphyroblasts that have overgrown and preserved the shapes of P and Q domains (Fig. 5.79) of a crenulation-foliation, without evidence of the development of a new foliation. If nutrient components are to be supplied to the growing porphyroblasts from

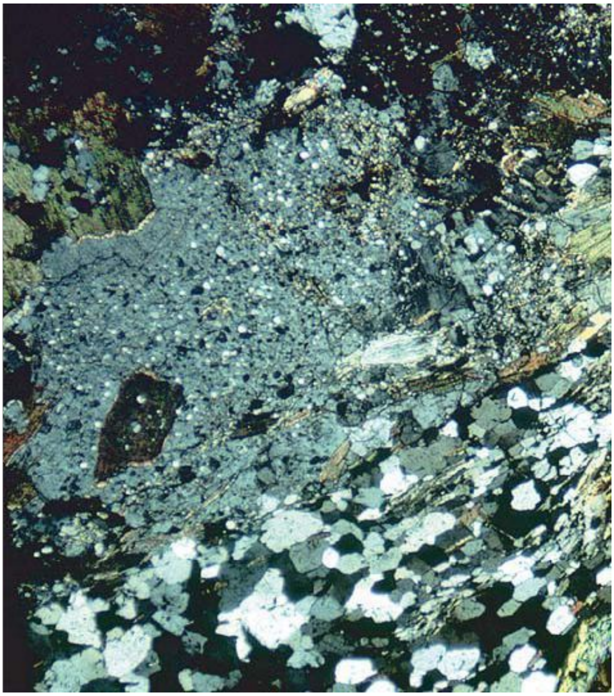

Fig. 5.89: Porphyroblast of K-feldspar with random inclusions of quartz and biotite that are much smaller than grains of the same minerals in the foliated matrix, suggesting that the K-feldspar grew before any foliation-forming deformation event, and before matrix coarsening occurred. Umberumberka area, north-west of Broken Hill, Australia. Crossed polars; base of photo 4.4 mm.

active P domains outside the porphyroblast, as required by the model of Bell *et al*. (1986), the P domains must be close enough to the growing porphyroblast for the diffusion to be effective. Therefore, if no such P domains are visible in the outcrops concerned, the most logical conclusion is that these porphyroblasts are effectively postdeformational, at least on the scale of the thin section.

Other examples of postdeformational porphyroblasts are random crystals and aggregates of white mica and chlorite that have overgrown and preserved matrix folia as inclusion trails (see, for example, Vernon *et al*., 1993b). The crystals typically are not deformed and some occur in radiating aggregates. Presumably they grew during retrograde cooling after deformation had ceased, on the scale of observation.

Of course, these observations do not preclude simultaneous deformation of other rocks in the same area; i.e. the observed rock could have been in a mesoscopic or macroscopic low-strain zone surrounded by actively deforming rocks. This may be suggested by the occurrence in the same general area of rocks showing microstructural evidence of syndeformational growth of porphyroblasts and post-porphyroblast deformation (see, for example, Vernon *et al.*, 1993b). Nevertheless, if active deformation zones spaced closer than the length of a large thin section or hand specimen are not observed in the field, the deformations could not have directly affected the development of the porphyroblast concerned, because they probably would be too far away from the growing porphyroblasts to contribute nutrient components to them.

However, care must be applied to the interpretation of radiating aggregates of fibrous sillimanite in Q domains between P domains that consist of abundant, aligned sillimanite in high-grade metapelitic schists (Vernon, 1987a,b). A superficial interpretation could be that the aligned sillimanite is syndeformational and that the radiating sillimanite is postdeformational, whereas both may grow simultaneously in zones of contrasting strain accumulation, i.e. both are syndeformational (Vernon, 1987a,b).

Rocks that undergo metamorphic peak heating late in their deformation history (possibly continuing after deformation effectively ceases) show (1) generally undeformed grains, (2) evidence of grain coarsening without reorientation of previously aligned minerals, and (3) occurrence of only the latest crenulation cleavage as inclusion trails in the grain margins (Williams, 1991).

5.10.8 Evaluation of hypothesis 3: do porphyroblasts rotate during deformation?

A relatively common microstructure shown by porphyroblasts is the presence of curved inclusion trails with similar senses of curvature and with parallel or oblique axial surfaces from one porphyroblast to another (see, for example, Olesen, 1982; Bell, 1985), as shown in Fig. 5.90. Alternative interpretations are: (1) the porphyroblasts rotated, with respect to geographical co-ordinates, by the same amount during homogeneous deformation of the matrix (Williams & Schoneveld, 1981; Olesen, 1982; Meneilly, 1983; Jiang, 2001); and (2) the porphyroblasts did not rotate, with respect to geographical co-ordinates, during matrix deformation, and overgrew matrix crenulations (*helicitic* microstructure).

According to the theoretical analysis of Jiang (2001), multilayer folding in response to layer-parallel shortening can produce the situation involved in the first interpretation. This interpretation treats the matrix as a mechanical continuum, analogous to a fluid, and is probably most appropriate for deformation of homogeneous rock materials, especially melt or glass. For example, phenocrysts in some volcanic rocks have folded trails of microlites in the adjacent groundmass glass, indicating rotation of the phenocrysts during magmatic flow (Vernon, 1987c), as shown in Figs. 3.60 and 3.61. The continuum approach may also be applicable to relatively homogeneous matrix deformation in some mylonitic rocks. For example, porphyroclasts of K-feldspar in mylonites commonly have rotated 'tails' in the adjacent matrix (see, for example, Simpson & Schmid, 1983), which are similar to those around rotated phenocrysts in volcanic rocks (Vernon,

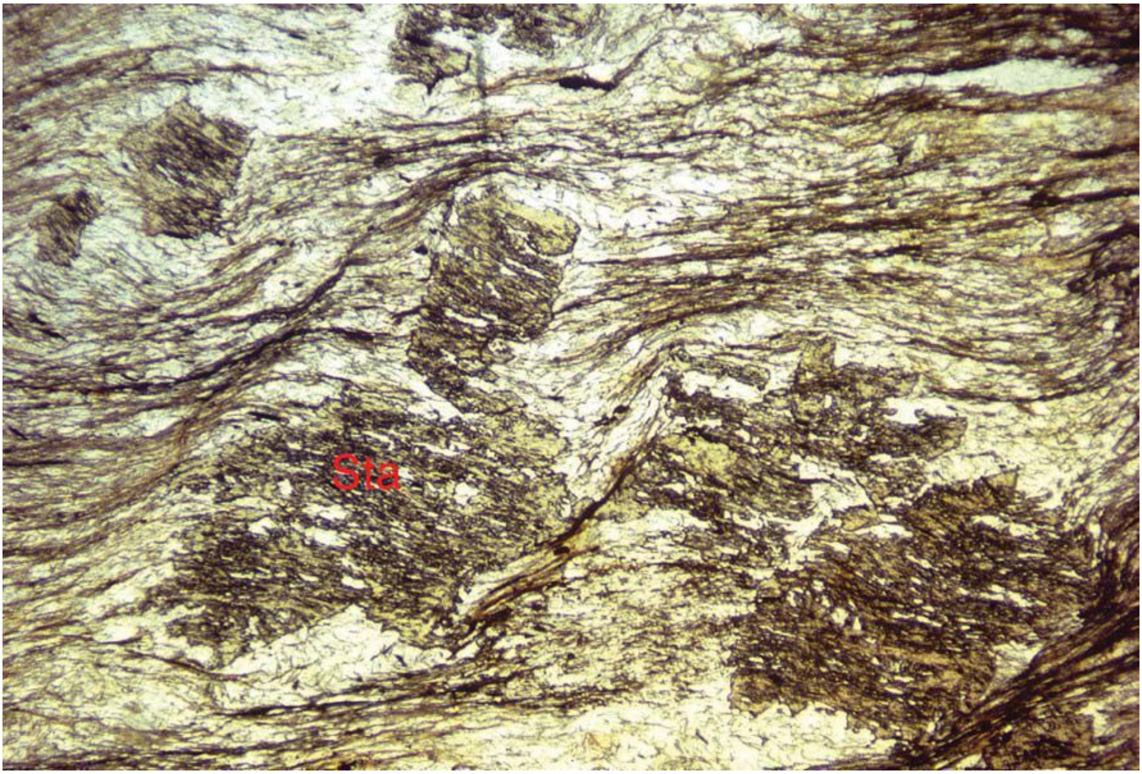

Fig. 5.90: Inclusion trails that are approximately parallel between several staurolite porphyroblasts in a crenulated schist from the Lukmanier area, Swiss Alps, suggesting that the porphyroblasts have not rotated, with respect to external co-ordinates, during the later crenulation. Plane-polarized light; base of photo 12 mm.

1987c). Possibly the continuum approach may also be extended to schists in which strong deformation has removed vestiges of former differentiated crenulations and produced a homogeneous matrix, as in 'stage 6' of the scheme of crenulation development (Fig. 5.57) suggested by Bell & Rubenach (1983), or during the reactivation and 'decrenulation' described by Meneilly (1983) and Bell (1986). However, folded 'tails' in the matrix around porphyroblasts are uncommon in schists (Vernon, 1988b; Johnson & Vernon, 1995b), providing at least some general support for the non-rotation hypothesis.

The second interpretation requires that the matrix deformation is heterogeneous and partitioned into high-strain, non-coaxial and low-strain, coaxial zones (Bell *et al*., 1986; Bell, 1985, 1986). In other words, strain is concentrated in zones of strong non-coaxial strain (P domains) in the matrix, which are not effectively coupled to the porphyroblasts (occurring in low-strain Q domains) during flow (Fig. 5.34).

Many people have suggested that, provided they do not deform internally, many porphyroblasts may not have rotated, with respect to geographical coordinates, during later deformation, even where microfolding or reactivation of the matrix foliation is intense (see, for example, Ramsay, 1962; Kennan, 1971; Fyson, 1975, 1980; Beutner, 1978; Bell, 1985; Vernon, 1987a, 1988b, 1989; Bell & Johnson, 1989a; Steinhardt, 1989; Hayward, 1990, 1992; Williams, 1994; Bell *et al.*, 1992a,b; Aerden, 1995; Hickey & Bell, 1999). Supporting evidence of non-rotation is provided by crenulations preserved in their original orientations (i.e. with the folded S-surface parallel to that preserved in the porphyroblast) in strain-shadows that are protected from matrix deformation by the porphyroblast (Figs. 5.34, 5.59).

A rotational interpretation appears to be most applicable to 'snowball' garnet porphyroblasts in a relatively homogeneous mica-rich matrix in high-strain deformation zones (Fig. 5.84, 5.87). In fact, 'snowball' garnet porphyroblasts generally have been interpreted as implying rotation during their growth (Spry, 1963; Rosenfeld, 1968, 1970; Powell & Treagus, 1969, 1970; Powell & MacQueen, 1976; Schoneveld, 1977, 1979; Powell & Vernon, 1979; Williams & Schoneveld, 1981; Masuda & Mochizuki, 1989; Busa & Gray, 1991; Gray & Busa, 1994; Williams & Jiang, 1999; Passchier *et al.*, 1992; Visser & Mancktelow, 1992; Biermeier & Stüwe, 2003). However, although the matrix in such zones generally shows no microstructural evidence of strain partitioning, in the sense of Bell (1981, 1986), this does not necessarily mean that strain partitioning did not occur. This is because strong recrystallization and neocrystallization during matrix deformation can convert a differentiated foliation into a homogeneous foliation, namely at 'stage 6' of the sequence of development of crenulations suggested by Bell & Rubenach (1983). So can reactivation of pre-existing surfaces, with accompanying 'decrenulation', according to Bell (1986).

Relatively clear examples of rotation of porphyroblasts are present in some schists (Vernon, 1988b; Chan & Crespi, 1999), as shown by albite porphyroblasts with strongly discordant inclusion trails in Fig. 5.92. Some of these rotated porphyroblasts show internal deformation, whereas others do not. Some porphyroblasts rotate in response to impingement against other porphyroblasts, as discussed by Bell (1985) and Vernon (1989). However, others are relatively widely separated, non-deformed porphyroblasts with inclusion trails that are oblique to one another in a homogeneous matrix (Figs. 5.93, 5.94), which implies that either (1) the porphyroblasts grew in former crenulation hinges with oblique foliations, evidence of which is preserved only in the porphyroblasts (Bell, 1985) or (2) the porphyroblasts have rotated during deformation of the homogeneous matrix. Evidence in support of the first interpretation would be rows of porphyroblasts, one above the other, with parallel inclusion trails, reflecting porphyroblasts that grew in the same crenulation hinge (Bell, 1985; Vernon *et al.*, 1993b), as shown in Fig. 5.93. Absence of such a relationship (Fig. 5.94) could suggest that the second interpretation is correct. Alternatively, it could be argued that the former

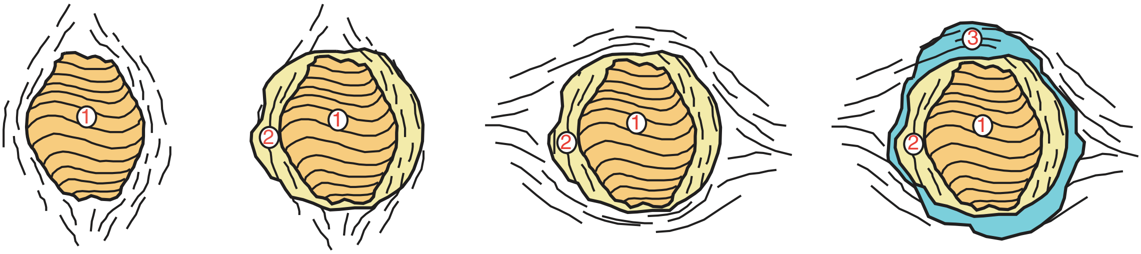

Fig. 5.91: Sketches showing progressive growth stages of a hypothetical porphyroblast during progressive, foliation-forming deformation of the matrix, according to the model of Bell & Johnson (1989a). Each matrix foliation is roughly perpendicular to the previous one, and each growth stage truncates the internal foliation in the previous one. The development of a matrix foliation was inferred to represent a separate tectonic event by Bell & Johnson (1989a).

crenulation hinges were so tight and lenticular that only one porphyroblast could grow in each hinge.

Chan & Crespi (1999) described albite porphyroblasts with syn-S_3 sigmoidal inclusion trail in their cores, which are truncated along straight boundaries by inclusion-free rims. Because the truncation planes have orientation ranges and means widely different from those of S_3, Chan & Crespi (1999) inferred that the porphyroblasts rotated, both with respect to S_3 and the geographic reference frame.

If the non-rotation hypothesis interpretation is correct, inclusion trails in porphyroblasts may reflect not only the nature of a foliation formed during growth of a porphyroblast, but also the orientation of that foliation (Fyson, 1975, 1980), even on the scale of a fold belt (Bell & Johnson, 1989a). The most adventurous application of this approach is that of Bell & Johnson (1989a), who re-examined garnet porphyroblasts with double-spiral inclusion trails ('snowball' porphyroblasts), many of which commonly curve continuously (Figs. 5.87, 5.88), although others show truncations of one set of trails by another (Fig. 5.91). Truncations are ascribed to interrupted growth by proponents of the rotation hypothesis. On the contrary, Bell & Johnson (1989a) regarded the spirals as preserving approximately orthogonal crenulation-foliations and microfolds that are truncated (Fig. 5.91) in response to repeated, orthogonal, regional deformations in a metasedimentary pile undergoing compressional thickening interspersed with gravitational sliding. This hypothesis has been applied in several areas (e.g., Johnson, 1990, 1992, 1999a,b; Hayward, 1992; Bell *et al.*, 1995, 1998; Bell & Hickey, 1999; Bell & Mares, 1999).

The hypothesis may remain controversial for some time, especially as Johnson (1993b, 1999b), after a detailed review of the problem, concluded that neither the rotation nor the non-rotation interpretation can be eliminated on the basis of geometrical relationships. Numerical simulations by Stallard *et al.* (2002) have

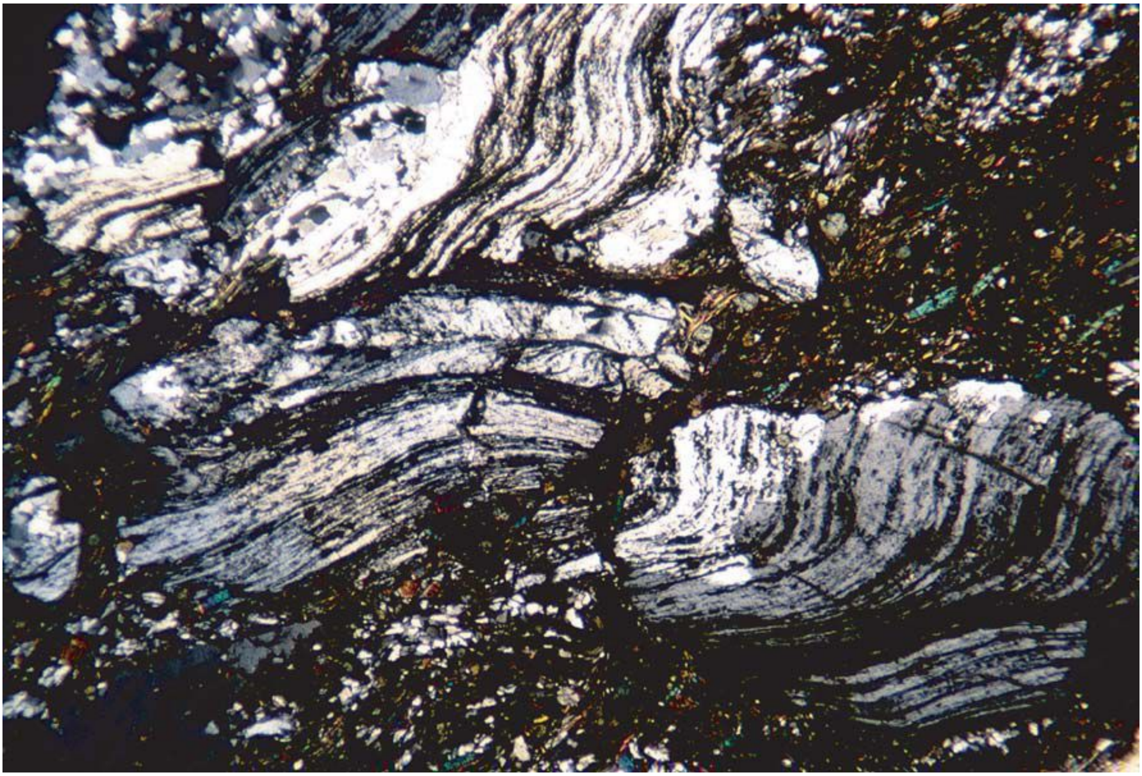

Fig. 5.92: Adjacent porphyroblasts of albite with markedly discordant graphite inclusion trails, suggesting that the porphyroblasts have rotated, relative to external co-ordinates, during deformation after growth of the porphyroblasts, Cascade Range, Washington, USA. Crossed polars; base of photo 11 mm.

confirmed this conclusion, indicating that complementary evidence is necessary, including three-dimensional revelation of spiral geometry and detailed microscopic and kinematic information from the matrix. Detailed crystallographic and chemical studies on some specific examples by T. Ikeda *et al*. (2002, 2003) were used to support rotation, but even these were shown to be ambiguous by Stallard (2003). Opposing sides of the controversy have been presented by Bell *et al*. (1992b) and Passchier *et al*. (1992).

Regardless of the more controversial aspects of their interpretation, porphyroblasts with inclusion trails are potentially useful for preserving a foliation indicating a former episode of deformation, which may not be preserved in the matrix. They may also preserve the orientation of that foliation, provided that (1) the trails are approximately parallel in separate porphyroblasts or the axial surfaces of microfolded inclusion trails are approximately parallel in separate porphyroblasts, and (2) uniform rotation can be eliminated as an alternative. However,

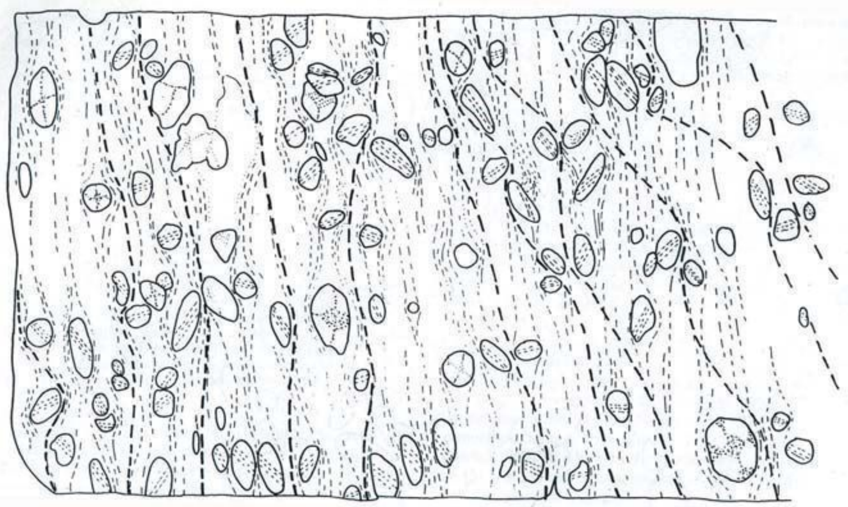

Fig. 5.93: Porphyroblasts with parallel inclusion trails in elongate domains that may reflect former crenulations, in a schist from the Foothills terrane, central Sierra Nevada, California, USA (from Vernon *et al.*, 1993a). With permission of Blackwell Publishing.

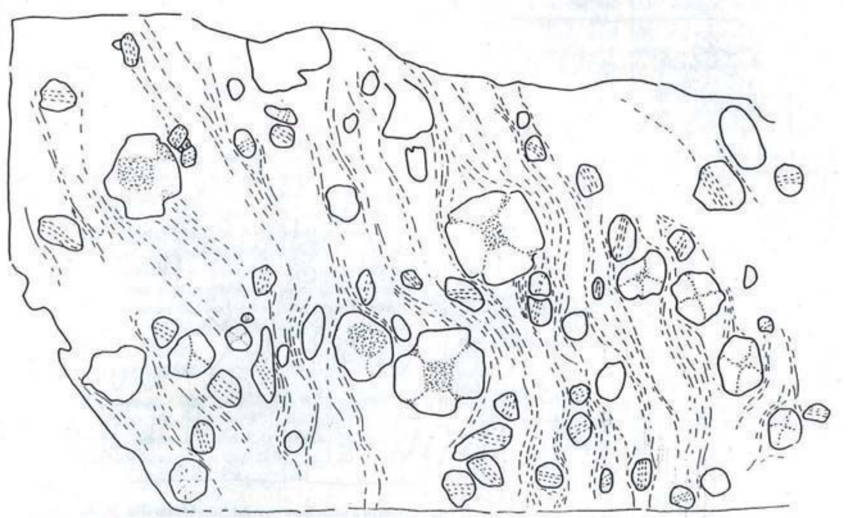

Fig. 5.94: Random porphyroblasts with oblique inclusion trails, in a schist from the Foothills terrane, central Sierra Nevada, California, USA (from Vernon *et al.*, 1993a). With permission of Blackwell Publishing.

work in progress on models involving synrotational growth and postgrowth rotation of porphyroblasts may indicate that uniform degrees of rotation are possible, and that microstructures supposedly indicative of static porphyroblasts are also consistent with rotational porphyroblasts.

5.10.9 Evaluation of hypothesis 4: can porphyroblasts be used for tectonic interpretations?

As mentioned previously, Bell & Johnson (1989a) suggested that inclusion trails in porphyroblasts could be used to trace the history of orogenic belts, and subsequent papers have developed this theme (Johnson, 1990, 1992, 1999a,b; Bell *et al.*, 1995, 1998; Bell & Hickey, 1999; Bell & Mares, 1999). Bell & Johnson (1989a) suggested that successive inclusion trail patterns (crenulation cleavages) develop statistically orthogonal to each other (Fig. 5.91). Their inference was that vertical and horizontal foliations represent alternating stages of compression and collapse of a mountain belt (Bell & Johnson, 1989b). An alternative model could be alternating periods of orogenic extension and contraction (Collins, 2002). However, as emphasized by Johnson (1999, p. 1186), many of the published examples of inferred orthogonal foliations are based entirely on microstructural evidence, and so 'it may be a big jump to infer orogen-scale processes from such small-scale observations'.

Moreover, not all statistical distributions indicate orthogonal foliations (Paterson & Vernon, 2001), and some sets of folia may be very oblique (Barker, 1994; Johnson, 1999b, p. 1721; Paterson & Vernon, 2001). Another important point is that strongly foliated materials, such as schists, invariably tend to crenulate or kink at high angles to the foliation, in response to a wide range of local stress distributions.

Even if it is accepted that orthogonal foliations really do represent regional deformation events driven by successive horizontal and vertical compression, and moreover are in their original positions, a major difficulty remains with accepting the current use of porphyroblast–matrix microstructural relationships to infer orogenic histories, such as multiple orthogonal, orogenic events and changing plate motions. The problem is that evidence for these inferred events outside porphyroblasts is generally lacking. For example, orthogonal crenulation-foliations are commonly missing from the matrix between the porphyroblasts. Bell and co-workers have explained this by inferring obliteration of the foliations during subsequent deformation, except in strain shadows adjacent to porphyroblasts; if so, the obliteration process is remarkably efficient throughout a metamorphic terrane. However, to avoid this problem, Bell & Hickey (1999) have suggested the alternative idea that the orthogonal foliations (crenulations) produced in response to orogenic movements form only right against the porphyroblasts, so that there is no need to postulate obliteration of foliations elsewhere. Paterson & Vernon (2001) have found excellent examples of such local crenulations against porphyroblasts in the Foothills terrane, California, although the axial surfaces of the crenulations are not necessarily orthogonal to the previous foliation (Fig. 5.95). However, why would major orogenic movements only affect the matrix immediately adjacent to porphyroblasts when orogenic movements typically produce widespread foliations? Some evidence of their existence outside

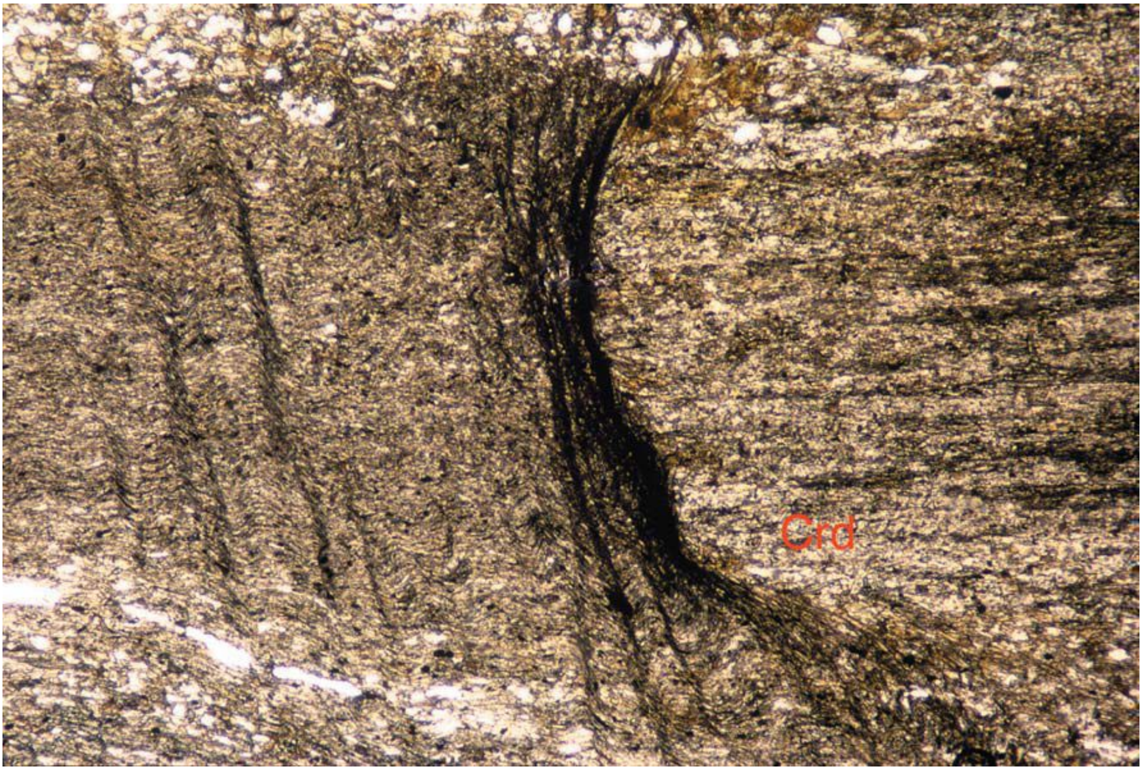

Fig. 5.95: Local crenulations developed against an altered cordierite (Crd) porphyroblast in a schist from the Foothills terrane, central Sierra Nevada, California, USA. The intensity of the crenulations decreases markedly away from the porphyroblast (Paterson & Vernon, 2001). The very localized occurrence of these crenulations suggests that they cannot be used as reliable indicators of a major tectonic event, but instead probably represent local increased strain accumulation around mechanical heterogeneities, namely porphyroblasts. Plane-polarized light; base of photo 4 mm.

porphyroblasts would be expected. Therefore, the observations may be better explained by local strain heterogeneities, rather than by inferring regional events (Paterson & Vernon, 2001). Similarly, the observation of Stallard & Hickey (2002) that different porphyroblasts in the same outcrop may show different growth histories, with reference to successive foliations, suggests that porphyroblast relationships may tend to reflect local strain heterogeneities, rather than regional deformation. In addition, the local nature of crenulations in their earlier stages of development (Fig. 5.55) could lead to growth of porphyroblasts with straight inclusion trails in non-crenulated areas and curved trails in crenulated areas of the same thin section, thereby causing misleading timing relationships.

Inferences about tectonic events have also been made from measurements of the orientation of the axis of rotation of curved inclusion trails, called the 'inflection/intersection axis' (FIA), as described by Hayward (1990, 1992), and Bell *et al.* (1995, 1998). However, Stallard *et al.* (2003) have shown that temporally related FIAs may have a large range of orientations (up to 147° in their measurements of the Canton Schist, Georgia, USA), making them unreliable for correlation purposes.

5.10.10 Porphyroblast–matrix relationships in high-grade metamorphic rocks

Most reported porphyroblast–matrix relationships are in medium-grade schists, where the matrix commonly is relatively fine-grained, so that S-surfaces, microfolds and inclusion trails are relatively clearly defined. However, if the inclusions are incorporated when the matrix of the rocks is relatively fine-grained, inclusion trails in porphyroblasts in high-grade metamorphic rocks may also be useful for elucidating relative timing of metamorphism and deformation, despite later coarsening of the matrix (Vernon, 1989). For example, inclusion trails of sillimanite in garnet porphyroblasts in high-grade gneisses and schists with K-feldspar and sillimanite in the SE Anmatjira Range, central Australia (Fig. 5.80) show that the high-grade metamorphism occurred during three fold generations (Vernon, 1989; Clarke *et al.*, 1989).

5.10.11 Can porphyroblasts push aside matrix folia during their growth?

A common microstructure is the deflection or draping of matrix folia around porphyroblasts (Figs. 5.33, 5.74, 5.80, 5.87, 5.88, 5.90), which some have interpreted as implying that the porphyroblasts mechanically pushed aside the matrix folia during growth (Misch, 1971, 1972a,b; Saggerson, 1974). If so, this microstructure could be taken to indicate postdeformational growth of porphyroblasts. Ferry (2001) has summarized the early experimental work on 'force of crystallization', and Buczynski & Chafetz (1987) and Dewers & Ortoleva (1990) described fracturing or displacement of quartz attributed to growth of calcite grains, in sedimentary rocks. The phenomenon is ascribed to non-hydrostatic stresses resulting from growth of a new crystal producing local dissolution of the replaced mineral at the interface between the new and replaced minerals (Maliva & Siever, 1988). However, many have expressed objection to the idea of crystals being able to push against lithostatic pressure in deep crustal rocks, although the possible assistance from pore fluid in reducing the effective overburden pressure (by reducing the normal compressive stress between grains in a rock) is generally neglected (Ferguson *et al.*, 1980).

Much of the evidence for an effective 'force of crystallization' in metamorphic rocks is not compelling (Rast, 1965; Spry, 1969, 1972; Shelley, 1972; Ferguson & Harvey, 1972). For example, growing crystals typically show no evidence of having pushed aside sedimentary bedding in contact metamorphic rocks (Spry, 1969, p. 150). Moreover, the common preservation in porphyroblasts of (1) pre-existing folded structures as inclusion trails continuous with the matrix foliation and (2) overgrown compositional layering or bedding indicates that porphyroblasts typically grow by replacement of the matrix and not by physical displacement (see, for example, Barker, 2002). Thus, evidence accumulated so far tends to favour the interpretation that deflection of matrix folia results from local deformation around pre-existing porphyroblasts (see, for example, Zwart, 1962; Vernon & Powell, 1976; Zwart & Calon, 1977; Vernon, 1978a), owing to the greater strength and consequent resistance to deformation of the porphyroblasts, relative to the fine-grained matrix. Thus, the microstructure mostly indicates deformation of the matrix after growth of the porphyroblasts, which is important in the relative timing of metamorphism and deformation.

As discussed in Section 4.3.1, the commonly observed opaque concentrations around the margins of andalusite and staurolite porphyroblasts (Fig. 4.19) result from accumulations of unreactive graphite ahead of the advancing porphyroblast boundary (Yardley, 1974; Ward, 1984a,c; Rice & Mitchell, 1991; Rice, 1993). However, the porphyroblasts grow by replacement of the matrix, and not by physical displacement, as generally no evidence of matrix displacement is observed. Instead, it appears that space for graphite rejected during the porphyroblast-forming reaction is made by dissolution of matrix minerals ahead of the porphyroblast–matrix interface.

A similar mechanism has been discussed in detail by Ferguson *et al.* (1980) to explain domes (arcs) rich in muscovite and graphite symmetrically arranged around garnet porphyroblasts. The muscovite in the domes is identical in shape and composition to muscovite in the adjacent matrix, and the volume of muscovite in the domes around a single garnet porphyroblast equals the amount that could be derived from the volume of normal matrix now occupied by the garnet. These observations suggest that the matrix mica and graphite grains, which were not involved in the garnet-forming reaction, were swept aside mechanically ahead of the advancing porphyroblast boundaries, producing domes with aligned mica and graphite crystals, space for which was made by dissolution of the other minerals formerly in that volume of matrix. So, rather than a physical forcing apart of the matrix by the growing porphyroblast against the lithostatic pressure, the process is more like dissolution, particle movement, rotation and alignment, involving reactions in the matrix at and ahead of the advancing interface.

Rubenach & Bell (1988) described porphyroblasts in mylonitic carbonaceous metapelites that were contact metamorphosed during a regional crenulation folding event by the Tinaroo Batholith, north Queensland, Australia. A pre-existing mylonitic foliation is not deflected around the porphyroblasts, whereas the crenulation-foliation is. Therefore, the porphyroblasts grew by replacement of the matrix, rather than by displacement, the anastomosing crenulation-foliation resulting from deformation around the porphyroblasts during and after their growth, as is typical of porphyroblastic crenulated schists (see, for example, Bell & Rubenach, 1983; Bell *et al.*, 1986; Vernon, 1988b). This supports arguments against the inference that deflection of matrix folia around porphyroblasts implies pushing aside of the matrix during growth of the porphyroblasts.

However, Durney & Ramsay (1973) suggested that many veins form by forcing apart of grain boundaries by precipitation of minerals from fluid at relatively low-stress sites, and Wiltschko & Moru (2001) have even suggested that microstructures similar to 'crack–seal' microstructures in veins (Section 5.9.3) may be produced by 'crystallization pressure'. This resurrects the possibility of the local pushing aside of weak matrix by a growing porphyroblast, which perhaps should not be dismissed at this stage, especially in view of the relatively small differential stresses that appear to be involved in deformation of rocks undergoing high- and even medium-grade metamorphism (see, for example, Etheridge, 1983). Such dismissals in geology can be dangerous!

Furthermore, evidence for very local volume changes involved in metamorphic reactions has been reported. For example, Wheeler (1987, p. 402) inferred that growth of prehnite in biotite caused bending of the biotite cleavage planes, and Hatch *et al.* (1949, fig. 117) illustrated fractures in adjacent grains evidently caused by reaction of olivine to serpentine. Wheeler (1987) suggested that the question is not whether local stresses are induced by metamorphism, but how large their effects may be. On the basis of available evidence, it appears that although the effects are probably local, they may nevertheless contribute to movement of metamorphic fluids and melts (Wheeler, 1987).

5.11 Deformation of partly melted rocks

5.11.1 General aspects

This section is relevant to the deformation of almost crystallized granite intrusions, as well as movement of neosomes and leucosomes and deformation of migmatites, the microstructures of which are discussed in Section 4.16. It is concerned with the deformation of rocks with high ratios of solid material to melt, so that flow involves both solid-state deformation and movement of melt. This is in contrast to the situation in Section 3.9, which discusses magmatic rocks with relatively small amounts of crystalline material, so that flow can occur by rotation and alignment of undeformed crystals in a very weak medium (melt).

5.11.2 Distinction between magmatic and solid-state flow

Microstructural evidence of magmatic flow has been discussed in Section 3.9. In contrast, microstructural evidence of solid-state deformation in originally igneous rocks includes the following microstructural features (Hobbs *et al.*, 1976; Vernon, 1976, 2000a; S. R. Paterson *et al.*, 1989), most of which are well known and easily recognized. Several are commonly found in the one rock.

(1) Internal deformation and recrystallization of grains, including 'core-and-mantle' microstructure, are typical of solid-state deformation (Section 3.4.7).

(2) Recrystallized 'tails' on deformed grains (porphyroclasts), are especially common in augen gneisses and mylonites (Section 5.7.6). Examples include feldspar or quartz–feldspar tails on feldspar porphyroclasts in deformed granites (Fig. 5.40) and pyroxene and/or amphibole tails on pyroxene or amphibole porphyroclasts in deformed gabbros (Fig. 5.15B).

(3) Elongation of recrystallized and neocrystallized aggregates (e.g. of quartz and mica) is very common in deformed granitic rocks (Section 5.7.6), as shown in Figs. 5.38, 5.39 and 5.44B.

(4) Grainsize reduction, owing mainly to recrystallization and neocrystallization, is typical of deformed coarse-grained rocks, such as granites (see, for example, Vernon *et al.*, 1983; Goodwin & Wenk, 1995) and gabbros (Lafrance & Vernon, 1993, 1999).

(5) Fine-grained folia anastomosing around less deformed relics reflect the heterogeneous strain that is characteristic of solid-state flow (see, for example, Bell & Rubenach, 1983; Vernon, 1987b), as discussed in Sections 5.7 and 5.10. This criterion needs to be distinguished from deflection of magmatic flow folia around phenocrysts in volcanic rocks, which typically is accompanied by alignment of elongate crystals without internal deformation.

(6) Microcline twinning (Section 4.8) is typical of K-feldspar in rocks deformed in the solid state (Section 5.7.6), and is intensified by deformation (Eggleton, 1979; Eggleton & Buseck, 1980; Fitz Gerald & McLaren, 1982; Bell & Johnson, 1989b).

(7) Myrmekite (Section 4.10.4) commonly replaces the margins of K-feldspar grains in deformed felsic rocks (Vernon *et al.*, 1983; Simpson & Wintsch, 1989; Vernon, 1991b; Tsurumi *et al.*, 2003), and subsolidus deformation may be a prerequisite for its formation (Vernon, 1991b). The reactions involved are complex, and require transport of chemical components in fluids from one part of the rock to another (Simpson & Wintsch, 1989). Myrmekite also grows with muscovite (Ashworth, 1972; Phillips *et al.*, 1972), especially along cracks in, and at the edges of, K-feldspar grains (Section 4.10.4).

(8) Flame perthite (Pryer & Robin, 1995, 1996) is typical of alkali feldspar that has undergone solid-state deformation (Fig. 4.54). However, it appears to require relatively specific stress conditions and magnitudes, as discussed by Pryer & Robin (1995, 1996), and so may be very local, even sporadic, in occurrence (Vernon, 1999b).

(9) Boudinage of strong minerals (e.g. hornblende and feldspar) is a good microstructural indicator of solid-state deformation, especially if recrystallized aggregates of weaker minerals (e.g. quartz and mica) occur between the boudins.

(10) An anastomosing foliation passing through, rather than around, microgranitoid enclaves (Section 3.10.3) is consistent with both host and enclaves having similar viscosities. This can also occur where both host and enclaves

are in a magmatic state (Pabst, 1928; Vernon, 1983). However, in that instance, the foliation does not have the grain-scale anastomosing character typical of a solid-state foliation, in either the host or the enclaves. Instead it has the characteristics described in Section 3.9, such as alignment of crystals without internal deformation.

(11) Very heterogeneous strain and local mylonitic zones (Section 5.7.6), at a range of scales, are characteristic of solid-state deformation (see, for example, Vernon *et al.*, 1983; Passchier & Trouw, 1996, pp. 102–4). Gapais (1989) suggested that heterogeneous deformation, with relatively widely spaced mylonitic zones, is characteristic of solid-state deformation in wet granitic rocks at temperatures below about 500 °C, whereas more homogeneous strain patterns, involving markedly more ductile behaviour of feldspar, is more characteristic of higher-temperature deformation.

(12) Evidence of combined brittle–ductile deformation is common in rocks deformed in the solid state, and brittle and ductile processes may alternate during deformation of the same mineral (McLaren & Pryer, 2001). Examples include feldspar clasts in ductile folia or 'ribbons' of quartz and/or mica (Section 5.7.6). Even during deformation at high-temperatures (upper amphibolite facies conditions), brittle processes may accompany plastic deformation by recrystallization-accommodated dislocation creep (see, for example, Lafrance & Vernon, 1993, 1999).

(13) Recrystallized biotite with a geochronological age younger than the intrusion age implies solid-state recrystallization after, and unrelated to, the cooling of a granite pluton.

5.11.3 Transitions from magmatic to solid-state flow

Transitions from magmatic to solid-state flow are likely to occur during cooling of bodies of magma undergoing regional deformation, for example the San Josétonalite pluton, Baja California, México (Vernon *et al.*, 2004; Johnson *et al.*, 2004). This is because, as magma crystallizes, the crystal : melt ratio increases, so that the magma changes from a crystal suspension to a crystal framework with an interconnected network of melt-filled pores, to an aggregate with restricted pore networks, and eventually to isolated pores just above the solidus. Flow at the late stage of crystallization ('submagmatic flow') involves 'grain-supported flow', as opposed to magmatic flow, which involves 'grain suspension flow' (grains effectively suspended in a weak fluid). In other words, submagmatic flow involves the deformation of the solid minerals, as well as flow of the small amount of melt present.

Recent experimental studies, reviewed by Paterson *et al.* (1998), indicate that a change from grain-supported flow to suspension flow in deforming granitic magmas typically occurs at between 20% and 40% melt, and that large amounts of strain may accumulate in magmas without being recorded by the final microstructure. At lower melt percentages, perhaps as low as a few percent, depending on the minerals and their shapes, strain may be accommodated by (a) melt-enhanced embrittlement, (b) melt-assisted grain-boundary sliding, (c) grain boundary migration assisted by contact-melting, (d) strain partitioning into melt-rich zones, (e) intracrystalline plastic deformation, and (f) transfer of melt to sites of low mean stress (Paterson *et al.*, 1998). Unfortunately, evidence of some of these processes may not show in the rock microstructure (Park & Means, 1996), and the only indication may be a 'magmatic-looking' rock (see, for example, Nicolas, 1992). Moreover, Park & Means (1996) have emphasized that some of the deformation mechanisms they were able to infer from direct observation of synkinematic experiments on low-temperature analogue compounds would be difficult to infer from the resulting microstructures.

Although very small amounts of melt permit magmatic (suspension) flow in gabbroic anorthosite, producing igneous microstructures (Nicolas, 1992), this may not apply to granitic magmas (see, for example, Vernon & Paterson, 1993, p. 21). The more irregular, variable and commonly equant grain and crystal shapes in granites may promote local stress concentrations large enough to cause some plastic deformation/recrystallization, even where local melt pockets remain. If so, magmatic flow microstructures conceivably may be destroyed by fracturing, crystal plasticity and recrystallization, even before the magma reaches its solidus (see, for example, Paterson *et al.*, 1998). Thus, many complications and limitations apply to the inference of 'submagmatic flow' from microstructural evidence.

Reliable microstructural criteria for submagmatic flow (S. R. Paterson *et al.*, 1989) are needed. Because a grain-supported microstructure, with small amounts of melt, is characteristic of this stage of cooling of the magma, evidence of high-temperature solid-state deformation, combined with evidence of melt movement, would be an ideal criterion of 'submagmatic flow'. The following criteria appear to be potentially useful indicators of submagmatic flow (Vernon, 2000a), although many are not sufficiently strong to use on their own.

(1) Recrystallized feldspar suggests temperatures above 450 °C at natural strain rates (Voll, 1976; Tullis, 1983). For example, recrystallized oligoclase is consistent with other evidence of relatively high-temperature deformation in the Wologorong Batholith, SE Australia (Vernon *et al.*, 1983). However, this criterion is especially applicable to recrystallized plagioclase with a composition identical to, or only slightly more sodic than, the primary (magmatic) plagioclase (Miller & Paterson, 1994, p. 856).

(2) Recrystallized K-feldspar with exsolution lamellae (Section 4.9.1) indicates crystallization at hypersolvus temperatures (see, for example, Vernon *et al.*, 1983, p. 140; S. R. Paterson *et al.*, 1989). However, this applies to normal exsolution lamellae (Section 4.9.1), not flame perthite (Sections 5.6.6, 5.7.9). Although flame perthite may be formed at high (amphibolite facies) temperatures (Vernon, 1999b), it may also develop at greenschist facies conditions (Pryer & Robin, 1995).

(3) Temperatures above the water-saturated solidus, obtained from the compositions of coexisting recrystallized plagioclase and K-feldspar, give at least a general indication of high recrystallization temperatures (see, for example, Vernon *et al.*, 1983).

(4) Relatively calcic plagioclase (e.g. oligoclase) in myrmekite replacing K-feldspar (Sections 4.10.4, 5.7.6) probably implies growth at relatively high temperatures (see, for example, Vernon *et al.*, 1983). Myrmekite grows at around 450–500 °C, according to Tribe & D'Lemos (1996), and between 500 and 670 °C, according to Wirth & Voll (1987).

(5) Evidence of *c*-slip (producing 'basal' subgrains parallel to the plane of the *a*-axes) in quartz indicates deformation at temperatures near the solidus, based on experimental work (Blumenfeld *et al.*, 1986; Gapais & Barbarin, 1986; Mainprice *et al.*, 1986; S. R. Paterson *et al.*, 1989). This contrasts with the lower-temperature *a*-slip, which produces subgrains parallel to the *c*-axis ('prismatic subgrains'). 'Blocky' subgrains in quartz (Fig. 5.20) reflect superimposition of *c*-slip on *a*-slip or *vice versa*.

(6) Evidence of a change from homogeneous to heterogeneous deformation (S. R. Paterson *et al.*, 1989) is consistent with experimental results, which show that deformation may become localized into high-strain or melt-rich zones when small amounts of melt are present. An example is the change during cooling from relatively homogeneous deformation involving rapid grain-boundary migration and the formation of relatively large, equant grains ('migration recrystallization') to heterogeneous deformation involving *a*-slip in quartz and grainsize reduction by rotation of subgrains to form smaller new grains ('rotation recrystallization'), as discussed by Gapais & Barbarin (1986).

(7) '*S–C*' foliation arrangements (Section 5.7.6) with the same orientation and sense of shear as inferred magmatic imbrication of the same minerals in the same rock suggest that deformation was continuous from the magmatic to the solid state (Blumenfeld, 1983; Blumenfeld & Bouchez, 1988; Miller & Paterson, 1994).

(8) Evidence of ductile deformation and recrystallization in hornblende (see, for example, Miller & Paterson, 1994, p. 856, fig. 5c) indicates deformation at relatively high temperatures. For example, evidence of ductile deformation in amphibole was observed in fault zones produced experimentally at 650–950 °C by Hacker & Christie (1990), whereas brittle deformation of hornblende is common at greenschist facies conditions (see, for example, Stünitz, 1993). However, cataclasis involving slip on fractures and boudinage of hornblende has been described for deformation at amphibolite facies conditions (Allison & La Tour, 1977; Lafrance & Vernon, 1993, 1999), and may be especially important where melt is present (Hacker and Christie, 1990).

(9) A strong point maximum of quartz *c*-axis orientations in strongly deformed rocks has been inferred to indicate crystal plastic deformation at temperatures at least as high as those of the amphibolite facies (Schmid & Casey, 1986; Law

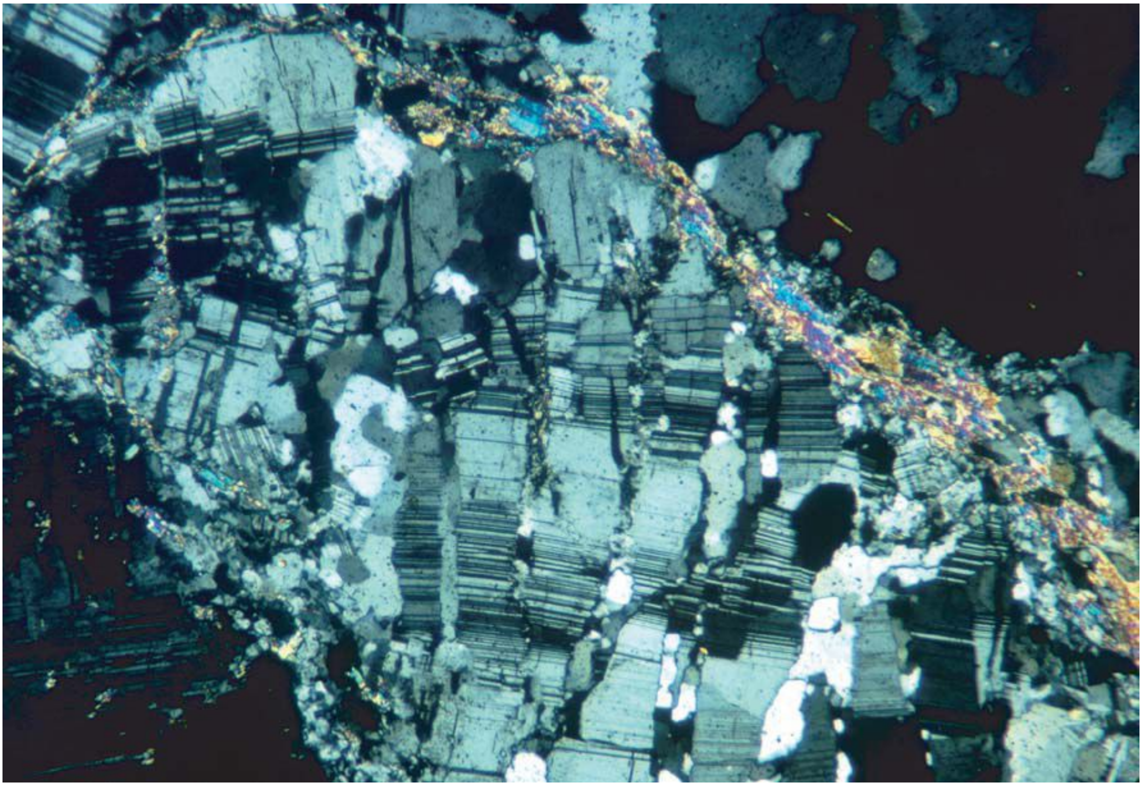

Fig. 5.96: Fragmented plagioclase grain, with quartz and K-feldspar between the fragments, which is consistent with the crystallization of late-stage melt that migrated into the opening space, in deforming granite, Wologorong Batholith, southern New South Wales, Australia. Compare with Fig. 5.97. Crossed polars; base of photo 3.5 mm.

et al., 1992). Mainprice *et al*. (1986) and Gapais & Barbarin (1986) suggested that a strong quartz *c*-axis maximum parallel to the inferred shear direction results from *c*-slip, and that the *c*-axes tend to be oriented more towards the normal to the shear direction, in response to *a*-slip, as the temperature of deformation is lowered.

(10) Late magmatic minerals in 'pressure shadows' or in zones between fragmented primary grains (see, for example, van der Molen & Paterson, 1979; S. R. Paterson *et al*., 1989) indicate solid-state deformation in the presence of migrating melt. For instance, Paquet *et al*. (1981), Bouchez *et al*. (1992), Davidson *et al*. (1996), de Saint Blanquat & Tikoff (1997), Büttner (1999) and Vernon *et al*. (2004) have suggested that quartz- and/or feldspar-filled fractures in plagioclase indicate submagmatic flow (Fig. 5.96). Bouchez *et al*. (1992) described and illustrated fragmented plagioclase crystals with the intervening spaces filled

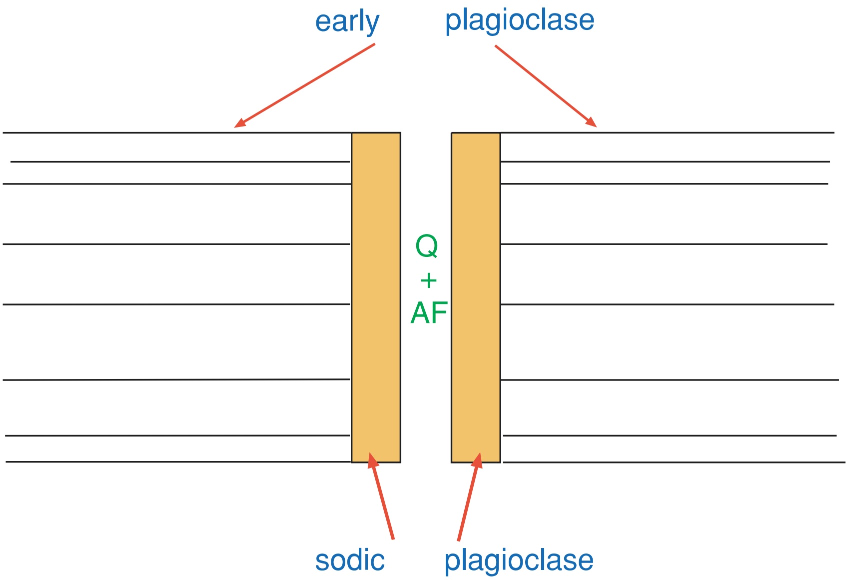

Fig. 5.97: Diagram showing evidence of late-stage melt that migrated to a zone between boudinaged plagioclase fragments during deformation of a granite magma with a small proportion of interstitial melt (Bouchez *et al.*, 1992). Quartz (Q) and alkali feldspar (AF) have grown from new nuclei in the melt pocket, and sodic plagioclase has grown on pre-existing plagioclase. Compare with Fig. 5.96.

by quartz and lower temperature feldspar (e.g. more sodic plagioclase, which may occur as optically continuous fringes on the fragments with twinning continuous from primary crystal to secondary overgrowth), as shown in Fig. 5.97. The fracture is confined to a single plagioclase crystal, and does not extend into the adjacent rocks (Davidson *et al.*, 1996). Some spaces are filled with quartz and two feldspars and, in some examples, the quartz is optically continuous with the immediately adjacent primary quartz. This is good evidence of melt migration during deformation. Vernon *et al.* (2004) described similar evidence of melt-present deformation of a granitic intrusion, and John & Stünitz (1997) presented evidence of intragranular and transgranular melt segregation on a wide range of scales, from the millimetre to hundreds of metres, during the cooling of a diorite–granodiorite intrusion.

(11) Microstructures clearly indicating ‘contact melting’ would constitute good evidence of melt-present deformation. This term was introduced by Park and Means (1996) to describe a solution process in deforming melt-present systems, similar to pressure solution or strain solution in melt-absent systems. They observed in experiments that contact melting generally occurs at boundaries oriented at high angles to the direction of shortening, suggesting that the melting could be related to high normal stress at these boundaries. Possible evidence for

contact melting in rocks includes truncation of mineral zoning, for example in plagioclase (Nicolas and Ildefonse, 1996; Rosenberg, 2001). However, sections through concentrically zoned, simply twinned, single crystals can resemble truncated zoning (Dowty, 1980a, fig. 1). So can sections through concentrically zoned crystals, one of which nucleates epitaxially on the other (Dowty, 1980a, fig. 2). The same can apply to crystals that nucleate obliquely on other crystals, which is common in plagioclase aggregates in basalts (see, for example, Kirkpatrick, 1977), as shown in Fig. 3.4. The problem is discussed in relation to a deformed tonalite by Vernon *et al.* (2004).

In view of these problems, care should be taken when evaluating these microstructures. Nevertheless, if the two impinging crystals, both with truncated zoning, have well-separated cores, and if each core is completely surrounded by some zones, separate nucleation and growth of the crystals followed by impingement can be inferred (Vernon *et al.*, 2004). The two main alternative explanations for the truncated zoning are: (1) fortuitous impingement and consequent cessation of growth at the contact; and (2) contact melting. A third possible interpretation is that large fragments of plagioclase, with zoning truncated by fracture surfaces, impinge and grow together in a kind of sintering process (Vernon *et al.*, 2004).

As pointed out by S. R. Paterson *et al.* (1989, p. 357), though the foregoing criteria suggest deformation at temperatures close to the solidus, most of them do not necessarily indicate a continuous transition from magmatic to solid-state deformation (unless high-temperature regional deformation can be excluded). However, parallelism of *S–C* structures with the same sense of shear as magmatic imbrication strongly suggests such a transition.

5.11.4 Movement of neosome and leucosome in migmatites

Movement of neosome and leucosome is common in deformed migmatites, forming foliation-parallel veins (*stroma*) in *stromatic migmatites* (*metatexites*) and transgressive bodies of non-foliated crystal–melt aggregates (*diatexites*). Migmatites may grade into local 'microplutons' 10–50 m across (Allibone & Norris, 1992), but connections between migmatites and large high-level granite intrusions are difficult to establish.

Evidence is accumulating that deformation assists the extraction of felsic magmas from their partly melted source-rocks (Hollister & Crawford, 1986; Davidson *et al.*, 1994; Brown *et al.*, 1995; Brown & Rushmer, 1997; Rutter, 1997; Sawyer *et al.*, 1999; Sawyer, 2000b, 2001; Marchildon & Brown, 2002). For example, Brown & Rushmer (1997) suggested that shear zones develop in zones of high strain and at fast strain rates in partly melted rocks, and that these shear zones are the main channels for magma extraction. They further suggested that increasing amounts of melt promote growth of the shear zone and that deformation assists accumulation of melt in the shear zone. This could occur by the opening of minute spaces between grains undergoing different types and degrees of deformation, melt being sucked into these lower-pressure sites. Activation of mylonitic zones existing prior to the melting could also help to transfer magma. Daines & Kohlstedt (1997) showed that elongate melt pockets form in response to stress in the experimental deformation of peridotite, and suggested that this process may assist extraction of basaltic melt from Earth's mantle.

Other deformation processes suggested for the extraction of magma from partly melted rocks (Wickham, 1987) are: (1) compaction and filter-pressing, which calculations have shown to be unlikely to produce granite plutons in a geologically reasonable time, though it may be capable of producing outcrop-scale segregations (Richter & McKenzie, 1984); and (2) extensional fracturing promoted by high magma pressure (see, for example, Collins & Sawyer, 1996). Escape of melt may be facilitated by positive volume changes in the melting reactions, especially in the dehydration melting of muscovite (Davidson *et al.*, 1994; Connolly *et al.*, 1997; Rushmer, 2001; Holyoke & Rushmer, 2002).

Microstructural evidence of melt migration in migmatites may be observable in the relatively less deformed parts of otherwise strongly deformed rocks (see, for example, Sawyer, 1996, 1999, 2000b; Clemens & Holness, 2000). For example, Sawyer (2000b) observed branching arrays of melt-filled grain boundaries in relatively low-strain parts of migmatites. Former melt segregated into grain boundaries and frozen there appears as narrow, vein-like grains showing dihedral angles that are not typical of solid-state aggregates of quartz or feldspar (Fig. 4.82).

Clemens & Holness (2000) have emphasized that permeability is not controlled only by the dihedral angle of melt versus crystals, because fluctuations in the volume of melt can open transient pores along grain boundaries by magma overpressure ('magma fracturing'). Deformation can also open transient pores along grain boundaries (especially between minerals of different deformation properties), providing low-pressure sites into which magma is sucked.

Rosenberg & Handy (2000) found that strain localizes where melt is present. Consequently, melt-bearing shear bands may develop parallel to a shear zone boundary and become high-strain zones, grainsize reduction occurring by intergranular fracturing. The result is an aggregate of polygonal quartz grains, with no internal deformation. Alternatively, rather than the melt localizing strain, the reverse could also happen. The deformation could open up transient spaces, owing to differential strengths of adjacent grains in relation to the locally imposed stresses. The low-pressure sites would suck in available melt, and so concentrate melt in the high-strain rocks, which would cause further weakening (Rosenberg & Handy, 2000).

An important consequence of melt migration in migmatites (see, for example, Sawyer, 1996) is that, although the entire neosome (melt plus crystals) may move (see, for example, Brown *et al.*, 1999), a common situation is for the

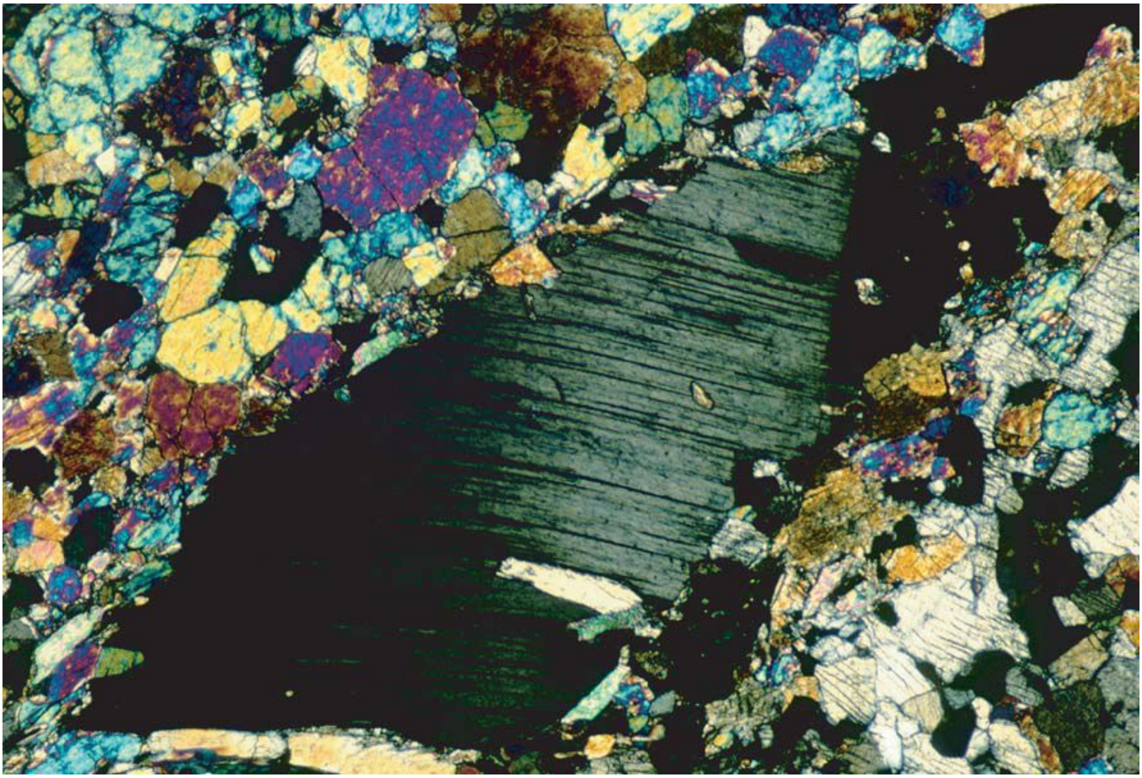

Fig. 5.98: Peridotite consisting of granoblastic olivine and warped orthopyroxene (first-order grey interference colours). The olivine has been extensively recrystallized to relatively fine-grained aggregates, but the orthopyroxene shows a much smaller degree of recrystallization (e.g. bottom right). Crossed polars; base of photo 4.8 mm.

melt to move, leaving behind all or some of the crystals. The composition of such a 'residual' leucosome could consist of restite, with or without crystals ('cumulate') precipitated from the magma before the melt left. Therefore, care should be exercised when inferring the composition of neosome magmas from the mineral and chemical composition of observed leucosomes (Section 4.16.1).

Although most leucosomes are parallel to the foliation in stromatic migmatites, they may also occur oblique to the foliation, especially parallel to the axial surfaces of folds. This is not intuitively expected, because the local σ_1 should be approximately perpendicular to the leucosome veins, but various processes can produce this situation (Vernon & Paterson, 2001).

5.11.5 Deformation of stromatic migmatites (metatexites)

As mentioned previously (Section 5.8.4), stromatic migmatites (metatexites) are commonly inferred to result from segregation of magma (neosome or

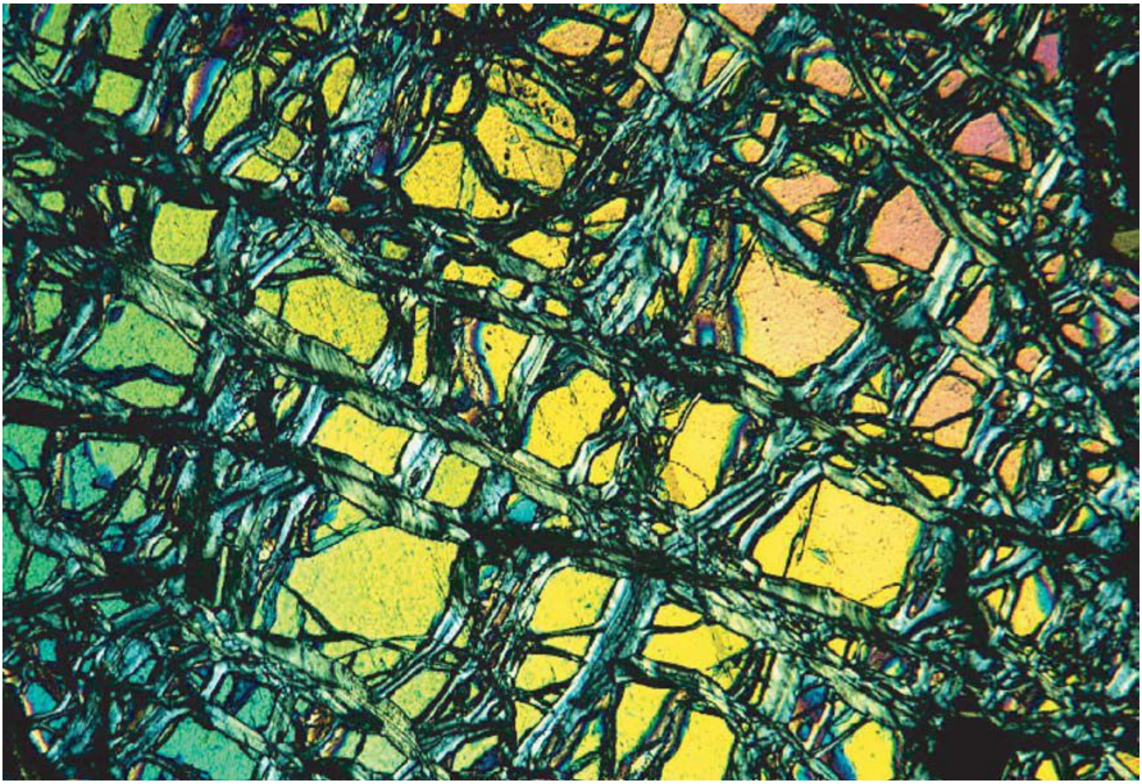

Fig. 5.99: Peridotite from New Caledonia, showing a large grain of olivine (higher-order interference colours) partly replaced along fractures by veins of serpentine (first-order anomalous grey-blue interference colours). From Vernon (2000b, fig. 44). Crossed polars; base of photo 3.5 mm.

leucosome) during deformation. Criteria for this interpretation include (1) magmatic microstructures in leucosomes (though these can be obliterated by later solid-state deformation), (2) mesosomes/leucosomes transgressing all kinds of beds or layers, owing to disruption of the layers during deformation and/or as a result of locally increased magma pressure, and (3) boudinage of the mesosome, with concentration of neosome/leucosome in interboudin necks (low-pressure sites), which implies that the leucosome is weaker than the mesosome and so probably magmatic.

An alternative explanation is that at least some stromatic migmatites are formed by solid-state deformation of migmatites in which the leucosomes or neosomes have crystallized (Vernon *et al*., 2003a). Criteria include: (1) boudinage of the mesosome/leucosome, indicating that the neosome/leucosome is stronger than the mesosome and so probably solid; (2) restriction of neosome/leucosome to selected beds or layers (i.e. not transecting adjacent beds or layers); (3) solid-state deformation features in the neosome/leucosome (a necessary, though not

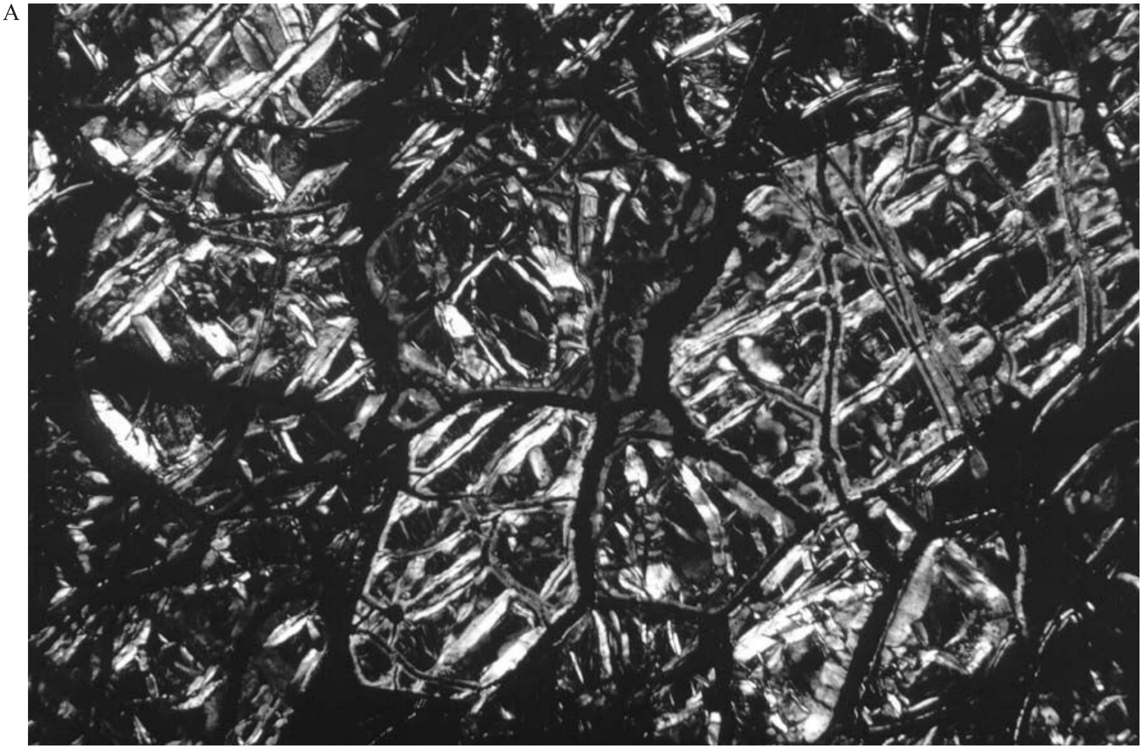

Fig. 5.100: (A) Serpentinite from the Great Serpentine Belt of New South Wales, Australia, showing pseudomorphs of serpentine after olivine, preserving original coarsely polygonal grain shapes and fracture patterns. This microstructure is sometimes known as 'mesh structure'. Crossed polars; base of photo 4 mm. (B) Same field of view in plane-polarized light, showing trails of minute opaque granules (magnetite and/or awaruite) outlining the former grain boundaries and fracture patterns.

sufficient, criterion); and (4) possible presence of high-strain zones with typical mylonitic microstructures, owing to heterogeneous strain.

5.11.6 Deformation of diatexites

Diatexites are migmatites with enough melt to flow *en masse*, thereby disrupting and destroying former structures. In view of their mobility, they can be regarded as crystal-rich magmas. The flow is mainly magmatic, and so criteria discussed in Section 3.9 apply. Microstructural criteria of magmatic flow in diatexites include: (1) igneous microstructures, such as alignment of rectangular feldspar crystals without much internal (plastic) deformation or recrystallization; (2) 'tiling' of euhedral crystals without internal deformation; (3) flow-sorting of crystals precipitated from the magma, as well as any restite that may be present, to form schlieren layering (without the minerals in the schlieren being internally deformed);

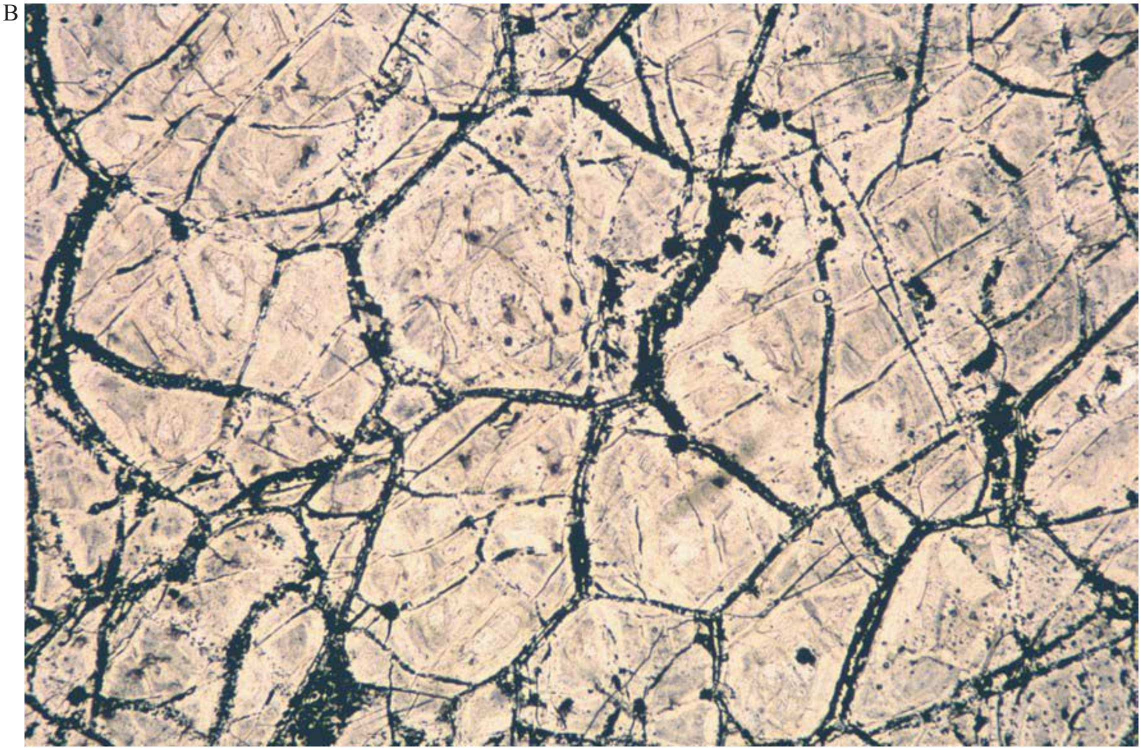

Fig. 5.100: (*cont.*)

(4) possible high-strain zones showing features described by Rosenberg & Handy (2000); and (5) possible movement of late magmatic liquids into low-pressure sites during solidification of the flowing diatexite, forming leucocratic segregations.

Diatexites may consist of melt, precipitated crystals, restite and resistate (solid material unaffected by the melting process). For example, diatexites at Cooma in south-eastern Australia were formed by partial melting of feldspathic metapsammites (Vernon *et al.*, 2000, 2003a) and consist of melt (now represented by quartz, K-feldspar, plagioclase and some biotite), together with restite (mainly quartz, with minor cordierite, biotite, andalusite and sillimanite) and resistate. The resistate consists of fragments of metapelite-derived stromatic migmatites (the leucosomes of which had previously crystallized) dismembered by the mobile, metapsammite-derived diatexites. This shows how complex diatexites may be originally, although reactions of restite and resistate with the melt commonly convert the original mafic minerals (e.g. cordierite, garnet or orthopyroxene) to biotite. Furthermore, field evidence of progressive clearing of crystals from diatexites indicates that separation of crystals from melt in flowing diatexites is an efficient process, and generally occurs close to the source rocks (Sawyer, 1996).

Next Page

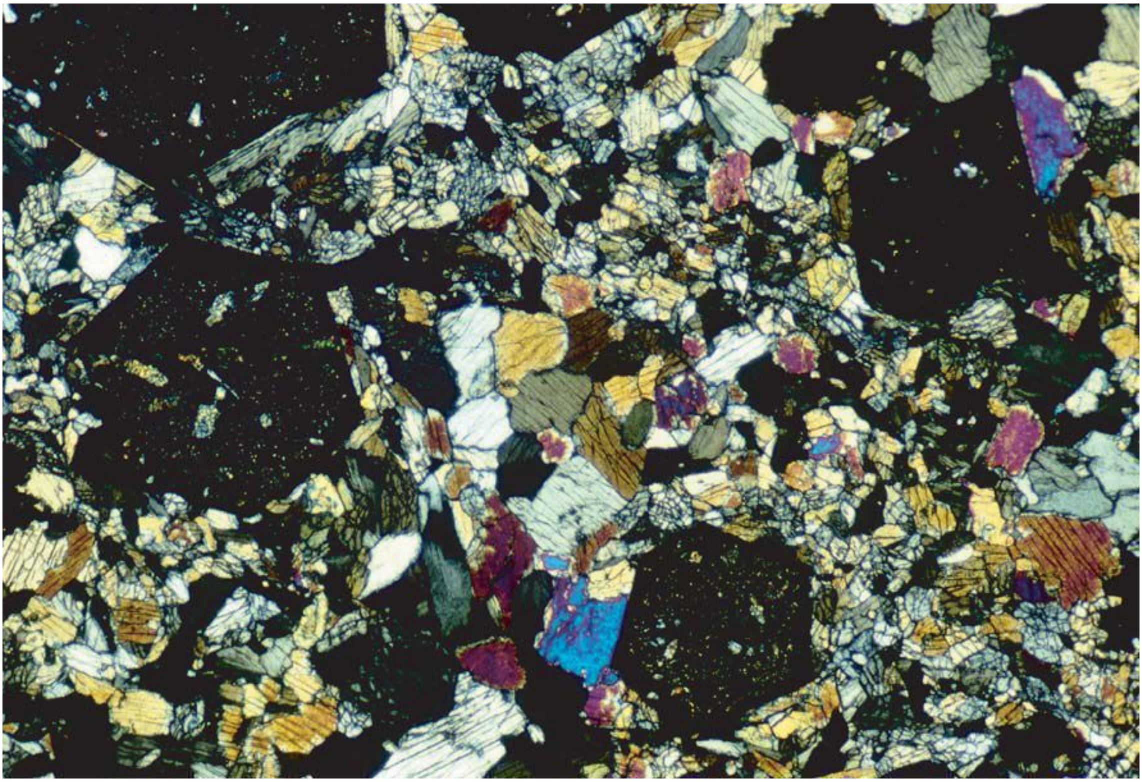

Fig. 5.101: Eclogite from San Francisco, California, USA, consisting of idioblastic garnet porphyroblasts (isotropic) interspersed with polygonal clinopyroxene. Crossed polars; base of photo 12 mm.

5.12 Deformation in Earth's mantle

Rocks in Earth's mantle are metamorphic rocks, in the sense that they owe their fabrics to solid-state processes, except for local partial melting, which blurs the boundary between igneous and metamorphic rocks, as with migmatites (Section 5.11). Mantle rocks are so hot that they are relatively weak and so flow easily. Because diffusion rates are high at these conditions, these rocks also recover and recrystallize readily. Microstructures of deformed mantle rocks are shown in Figs. 4.9, 5.18, 5.24, 5.98–5.100.

5.12.1 Peridotite

A good example of hot flowing rock is peridotite in Earth's outer mantle. Peridotites are olivine-rich rocks, with varying amounts of orthopyroxene and/or clinopyroxene. They have been observed in ultramafic sequences in ophiolites (oceanic complexes rich in mafic and ultramafic rocks) and in xenoliths in basalts

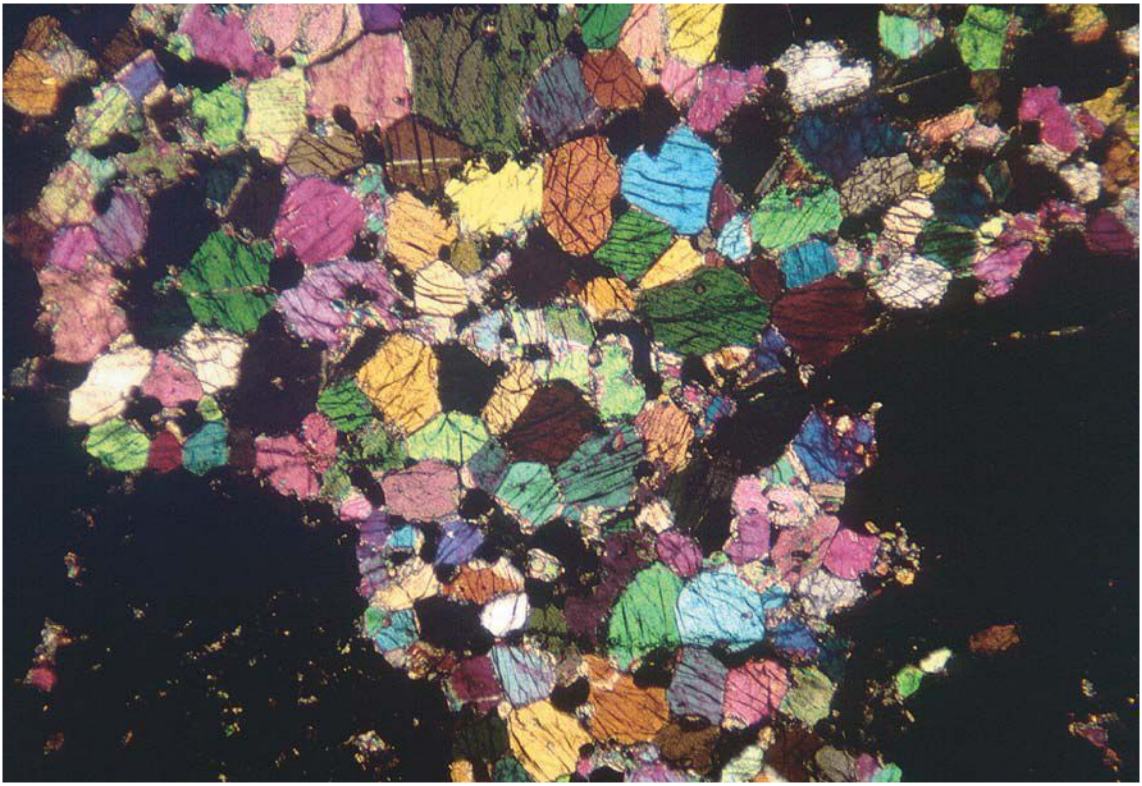

Fig. 5.102: Eclogite consisting of polygonal clinopyroxene interspersed with small grains of garnet (isotropic), the shapes of which indicate solid-state grain-boundary adjustment with the clinopyroxene (Section 4.2), and with scattered garnet porphyroblasts (bottom left; bottom right). Crossed polars; base of photo 11 mm.

(Fig. 4.9). In general, they show some evidence of high-temperature flow (Section 5.3.3). The less deformed parts of ophiolites show coarsely granular peridotites, with polygonal olivine grain shapes (indicating solid-state grain-boundary adjustment), widely spaced subgrains in olivine, a weak alignment of tabular olivine grains, a moderate to strong olivine crystallographic preferred orientation, and polygonal aggregates of orthopyroxene pseudomorphing former larger grains, these features being consistent with flow of hot rock in a mid-oceanic ridge environment (Boudier & Nicolas, 1982b). Other peridotites in ophiolites show evidence of stronger deformation, in the form of more pronounced shape and crystallographic preferred orientations, more closely spaced subgrains, and partial recrystallization of the deformed grains (Boudier & Nicolas, 1982a). The grain shapes are essentially polygonal, in response to minimization of interfacial energy (Section 4.2.2), as shown in Fig. 4.9.

Mercier & Nicolas (1975) described and classified the microstructures of peridotites from Earth's outer mantle, carried to the surface as xenoliths in basalts.

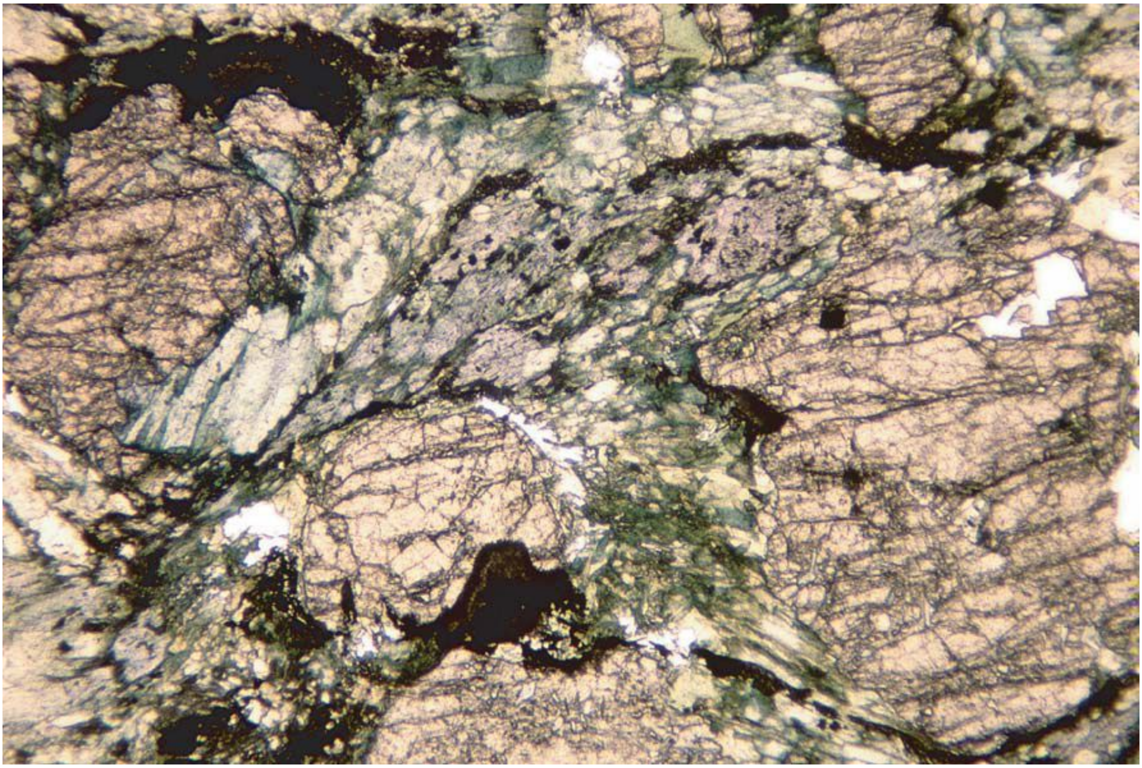

Fig. 5.103: Eclogite from the Swiss Alps, showing residual garnet (pink) and clinopyroxene (pale green) that has been partly replaced by blue-green amphibole and glaucophane (pale violet). Rutile (almost opaque) has been replaced around its edges by titanite. Plane-polarized light; base of photo 11 mm.

They noted that similar microstructures are shown by peridotites emplaced as solid bodies into Earth's crust ('alpine-type' peridotites). The microstructure they inferred to be the oldest (which they called *protogranular*) consists of large, almost undeformed, equant olivine grains with curvilinear boundaries and a weak shape preferred alignment (Fig. 4.9). Spinel and clinopyroxene occur as rounded inclusions in orthopyroxene. Mercier & Nicolas (1975) inferred that this microstructure is formed by recrystallization in the upper mantle, during the partial melting that depletes the peridotite of basaltic melt components. Evidently, it results from recrystallization of an unknown earlier microstructure. The recrystallization appears to be syn- to post-tectonic, as suggested by TEM studies (Green & Radcliffe, 1972). The olivine grains have few dislocation walls (subgrain boundaries), as observed by Poirier & Nicolas (1975), owing to the rearrangement of dislocations by recovery (Green & Radcliffe, 1972).

The next youngest microstructure, which Mercier & Nicolas (1975) called *porphyroclastic*, consists of large, heavily deformed xenoblastic residuals

A

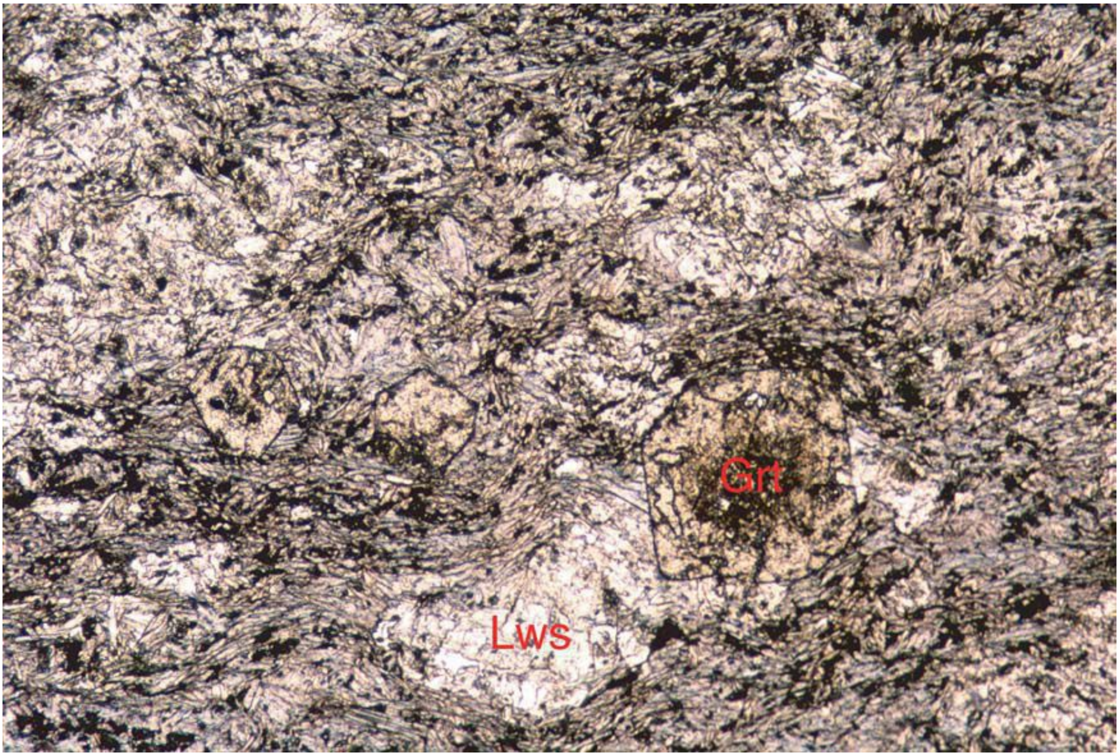

Fig. 5.104: (A) Blueschist from the Franciscan Formation, San Francisco, California, USA, consisting of idioblastic garnet (Grt) porphyroblasts in a foliated aggregate of glaucophane (pale violet) with idioblastic, rectangular colourless porphyroblasts of lawsonite (Lws) enclosing abundant glaucophane inclusions. The rock originally was an eclogite (Fig. 5.101), the clinopyroxene having been replaced by glaucophane and lawsonite, the garnet remaining largely unaltered. Plane-polarized light; base of photo 4 mm. (B) Same field of view, but in crossed polars.

(porphyroclasts) separated by aggregates of small, optically strain-free, equant, recrystallized grains (Figs. 5.18, 5.24). The porphyroclasts show a relatively strong alignment oblique to the strong alignment of the new grains, which forms a distinct foliation. Spinel commonly occurs between the olivine grains, owing to the recrystallization, though some may still be in contact with the pyroxene grains. The porphyroclasts contain prominent subgrain boundaries (Figs. 5.18, 5.24) composed of edge dislocations with a maximum misorientation of 12°, the angle increasing with increasing strain (Poirier & Nicolas, 1975).

The youngest microstructure, referred to as equigranular, has the finest grain-size, and consists of polygonal aggregates, with or without rare remnants of porphyroclasts. The ‘mosaic’ variety consists of equant, polygonal olivine grains, whereas the ‘tablet’ variety has numerous elongate olivine grains. These rocks were inferred to be formed by the complete to almost complete recrystallization

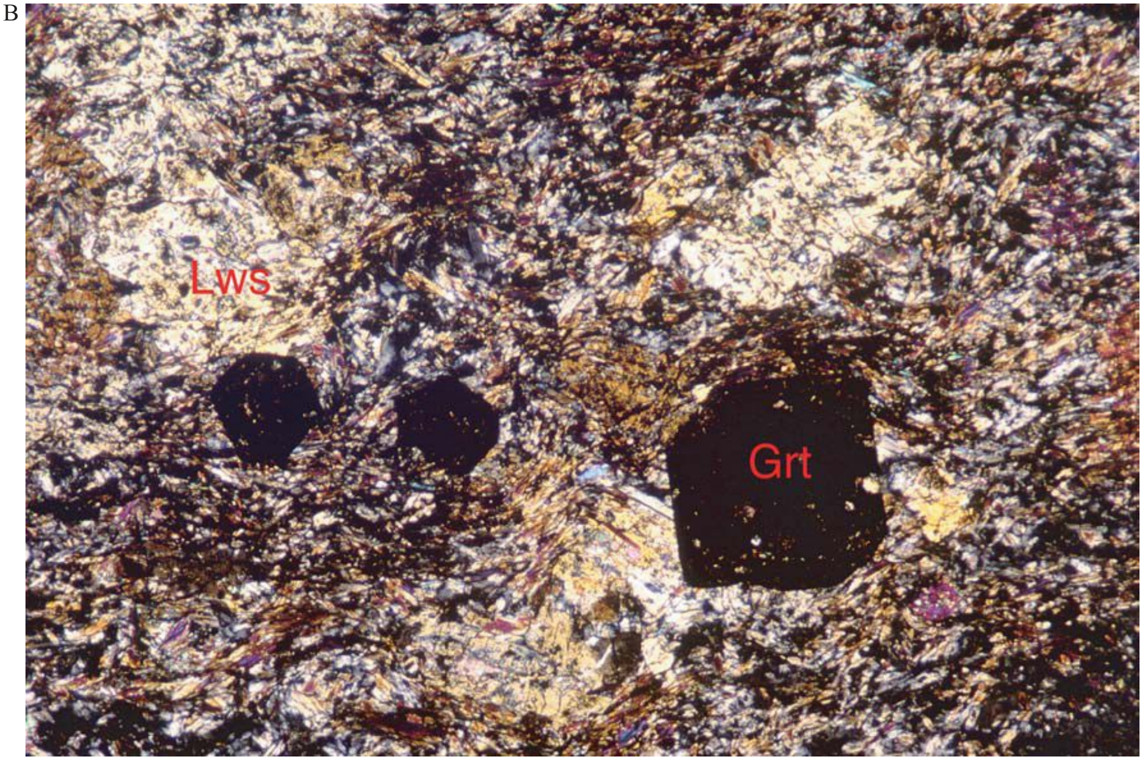

Fig. 5.104: (*cont.*)

of the porphyroclastic variety, in response to intense flow. Whether the recrystallization is syntectonic or post-tectonic is not clear, but the 'tablet' variety may result from static heating after syntectonic recrystallization (Mercier & Nicolas, 1975). Poirier & Nicolas (1975) found that the size of the new (recrystallized) grains is similar to that of equant subgrains in the porphyroclastic remnants, and observed evidence of a transition from subgrains to new grains, implying that subgrain rotation is the recrystallization mechanism.

Harte (1977) divided peridotite xenoliths into the following main microstructural categories: (1) *coarse* (without porphyroclasts); (2) *porphyroclastic* (with more than 10% of the olivine occurring as porphyroclasts); (3) *mosaic-porphyroclastic* (less than 10% of the olivine occurring as porphyroclasts); and (4) *granuloblastic* (porphyroclasts rare or absent).

Peridotites occurring both in ophiolites and as xenoliths in basalts were recognized as complex tectonites by den Tex (1969), who also distinguished between igneous flow microstructures (Section 3.9) and tectonic deformation microstructures in peridotites. Mylonitic microstructures in peridotite xenoliths have been observed and illustrated by Green & Radcliffe (1972, fig. 1c) and O'Reilly & Griffin (1987). Ultramafic mylonites may also occur in alpine peridotites (Green

& Radcliffe, 1972, fig. 10; van der Wal *et al.*, 1992), and at the base of ophiolite sheets (Boudier & Nicolas, 1982a,b; Suhr, 1993).

The types and arrangements of dislocations and the crystallographic preferred orientations shown by peridotites in xenoliths in basalts and at the base of ophiolites are identical to those produced by dislocation creep in high-temperature, high-pressure deformation experiments (Green & Radcliffe, 1972; Nicolas & Poirier, 1976; Zeuch & Green, 1984; Jin *et al.*, 1989). This implies that olivine and orthopyroxene in Earth's mantle, from 10 to 200 km depth, also flow by dislocation creep (Green, 1992). Marginal recrystallization occurs in both minerals, but is typically more advanced in olivine (Green & Radcliffe, 1972), as shown in Fig. 5.98. The common presence of CO_2 bubbles suggests that fluid may possibly assist minor grain-boundary sliding, though evidence of this process is generally not observed. The abundance of dislocations in mantle peridotites precludes a major amount of deformation by diffusion mass-transfer (Green & Radcliffe, 1972).

Reaction with water may occur as peridotites from the mantle are deformed in Earth's crust, producing *serpentinites*, dominated by the water-rich magnesium silicate serpentine, which pseudomorphs both olivine (Figs. 5.99, 5.100) and orthopyroxene. The serpentine aggregates commonly preserve the original coarsely polygonal grain shapes, as well as fracture patterns inside the original grains, both being outlined by opaque granules, which represent iron (formerly in the olivine and orthopyroxene, now magnetite or awaruite) rejected by the serpentine. Wicks & Whittaker (1977) have presented a detailed description of serpentine microstructures.

5.12.2 Eclogite

Eclogites are clinopyroxene–garnet rocks, commonly with rutile. They are typically formed by high-pressure/high-temperature metamorphism of oceanic basalts or gabbros subducted in Earth's mantle. The grain shapes in many eclogites are essentially polygonal, in response to minimization of interfacial energy (Section 4.2.2), as shown in Figs. 5.101 and 5.102. However, the microstructures of eclogites are variable, ranging from granoblastic to 'orthocumulate'-like (Hatton & Gurney, 1987). Some eclogites show evidence of solid-state deformation, involving elongation and recrystallization of the pyroxene.

Reaction with water may occur when eclogites are emplaced into and deformed in Earth's crust, producing *blueschists* containing hydrous minerals such as glaucophane and lawsonite (Figs. 5.103, 5.104), with or without other sodic amphiboles and epidote; rutile is commonly altered to titanite. Commonly the original clinopyroxene is replaced and the garnet partly or completely preserved.

Glossary of microstructural and related terms

Unnecessary jargon is best avoided in microstructure work. However, many specific structural names are in common use, and so students should be aware of them and have a place to look them up. This is the reason for this glossary, which defines many essential terms, as well as some less essential ones, with emphasis on igneous, metamorphic and deformation microstructures. Some terms are not restricted to the microscopic scale. The aim has been to use definitions that conform to those in glossaries in standard texts, modified to take into account my own experience. More detailed analysis of the terms may be found in the text sections indicated, and relevant figures are also indicated. Glossaries of igneous terms are in Johannsen (1939), Joplin (1964), Shelley (1993) and Best (2003); glossaries of metamorphic terms are in Joplin (1968), Shelley (1993) and Best (2003); and glossaries of some deformation terms are in Shelley (1993) and Best (2003).

Acicular (Fig. 3.24): With needle-like habit.

Adcumulate microstructure (Sections 3.7.2, 4.6.1; Figs. 4.40–4.42): Aggregate of grains, commonly (but not necessarily) of one mineral, precipitated and accumulated (either physically by crystal settling or floating, or by *in situ* crystallization of early minerals and removal of the interstitial liquid) in a mafic magma. The grains are typically polygonal, reflecting grain-boundary adjustment.

Allogenic mineral (Chapter 2): Mineral formed outside, and transported to the place of deposition of, a sedimentary rock; the opposite of *authigenic mineral*.

Allotriomorphic: Describes irregular grains showing no crystal-face boundaries in an igneous rock. Synonym of *anhedral* and *xenomorphic*. The equivalent term for metamorphic rocks is *xenoblastic* (q.v.).

Amygdaloidal: Containing amygdules (q.v.).

Amygdule (amygdale) (Section 3.14.2; Figs. 3.97, 3.98): Vesicle (q.v.) filled with secondary minerals, either deuteric (precipitated from hydrothermal solutions derived from the magma) or metamorphic.

Anatexis (Section 4.16.1): Partial melting of a solid rock at high-temperature metamorphic conditions.

Anhedral: Describes irregular grains showing no crystal-face boundaries in an igneous rock. Synonym of *allotriomorphic* and *xenomorphic*. The equivalent term for metamorphic rocks is *xenoblastic* (q.v.).

Annealing (Section 5.4.4): A technological process involving removal of strain by heating after deformation. An unsatisfactory term for rocks, because absence of deformation during the heating commonly cannot be determined, even in contact metamorphic environments.

Antitaxial veins (Section 5.9.3; Figs. 5.64A, 5.69, 5.70): Veins with minerals that are different from those of the wall-rock (e.g. calcite fibres in quartzite) and that grow from the contacts of fibres and wall-rock (i.e. on two growth surfaces) towards the walls and away from the centre of the vein, in contrast to syntaxial veins (q.v.), in which the youngest growth is in the centre.

Aphanitic: Describes fine-grained crystalline aggregates not distinguishable with the unaided eye; may be *microcrystalline* (q.v.) or *cryptocrystalline* (q.v.).

Aphyric: Describes the microstructure of volcanic rocks without phenocrysts.

Aplitic (Section 3.4.7; Fig. 3.14): Describes the structure of fine-grained, felsic rocks (aplites) with predominantly anhedral grain shapes.

Ash, volcanic (Section 2.3; Figs. 2.14–2.19): Clasts of volcanic origin, <2 mm in diameter.

Ash-fall tuff (Section 2.3; Figs. 2.14, 2.16): Sedimentary rock formed by the accumulation of volcanic ash.

Ash-flow tuff (ignimbrite) (Section 2.3; Figs. 2.17, 2.19): Sedimentary rock formed by the accumulation of volcanic ash, pumice and crystals from a pyroclastic flow resulting from an explosive eruption.

Aspect ratio: Ratio of length to width of crystals and grains.

Augen (Sections 5.7.6, 5.7.9; Figs. 5.39, 5.40, 5.51, 5.52): Residual large crystals (*porphyroclasts*) (q.v.) in strongly deformed (generally gneissic or mylonitic) rocks. The augen typically tend to be lenticular or eye-shaped, and the finer-grained mylonitic foliation is deflected around them The augen are commonly of K-feldspar in deformed granites. The singular is *auge* (German for ‘eye’).

Augen gneiss (Sections 5.7.6, 5.7.9; Figs. 5.39, 5.40, 5.51, 5.52): Gneissic rock containing augen (q.v.), commonly, but not necessarily, of K-feldspar.

Augen mylonite: Mylonite (q.v.) with augen (q.v.), commonly but not necessarily of K-feldspar; see augen gneiss.

Authigenic mineral (Sections 2.2.5, 2.2.7): Mineral formed in place in a sedimentary rock; the opposite of *allogenic mineral*.

Automorphic (Section 3.5.2): Describes a mineral with crystal faces in an igneous rock. Synonym of *euhedral* and *idiomorphic*. The equivalent term for metamorphic rocks is *idioblastic* (q.v.).

Axiolitic microstructure (Section 2.3; Fig. 2.18): Microstructure consisting of elongate spherulitic aggregates (q.v.) with fibres normal to and either side of a central axis (axiolites, axioliths). The fibres may grow inwards from the edges of a glass shard (Ross & Smith, 1961) or outwards from a fracture.

Beard structure (Section 5.8.2; Figs. 5.15, 5.64): Fibrous intergrowths ('beards') projecting out from clasts or porphyroblasts parallel to the foliation in deformed rocks.

Bedded migmatite (Section 4.16.1): Migmatite (q.v.) in which the neosome (q.v.) remains in the parent rock and bedding is preserved.

Blasto-, -blastic: Prefix and suffix, respectively, referring to growth in the solid state (i.e. in metamorphic rocks); for example, *blastophitic* (q.v.), *blastoporphyritic* (q.v.), *blastopsammitic* (q.v.), and *porphyroblastic* (q.v.).

Blastomylonite: Mylonite (q.v.) in which grain growth has occurred, either during or after the deformation.

Blastophitic: Describes metamorphosed igneous rock with residual ophitic (q.v.) microstructure.

Blastoporphyritic (Section 4.15.2; Figs. 4.75–4.77): Describes metamorphosed igneous rock with residual porphyritic (q.v.) microstructure.

Blastopsammitic (Section 4.15.1; Fig. 4.74): Describes metamorphosed sandstone with residual clastic (q.v.) microstructure.

Boudinage (Section 5.10.7; Figs. 5.64B, 5.86): The formation of boudins (q.v.) by deformation.

Boudins (Section 5.10.7; Figs. 5.47, 5.86): Lines of tablet- or sausage-shaped mineral grains or rock fragments enclosed in more ductile, deformed material; formed by the stretching and breaking of a stronger layer in weaker material that is extending in a ductile manner.

Breccia (Sections 5.7.4, 5.7.5; Fig. 5.37): Rock composed of mineral and/or rock fragments, generally formed by explosive volcanic activity (volcanic breccia) or deformation in fault zones (fault breccia).

Burial metamorphism (Section 2.2.8): Low-temperature regional metamorphism without obvious deformation, owing to deep burial; grades into diagenesis (q.v.). Residual igneous and sedimentary microstructures are typically preserved; similar minerals and microstructures can be produced by metamorphism in geothermal areas.

Cataclastic microstructure (Sections 5.3.1, 5.4.8, 5.7.5; Figs. 5.1, 5.2, 5.36): Microstructure of rocks (cataclasites) formed by brittle deformation, involving fracturing of grains and relative movement of fragments.

Chain structure (Section 3.7.2; Fig. 3.50): Open aggregates of chromite, pyroxene or plagioclase in igneous rocks. They could be formed by (i) self-nucleation or (ii) adhesion of fortuitous impinging crystals of the same mineral, essentially involving 'pressure-solution' at the points of contact.

Chondrite (Section 3.5.7; Figs. 3.22, 3.23): Stony meteorite with spherical globules ('chondrules') containing dendritic crystals, the shapes of which suggest that the globules were once droplets of melted rock; inferred to have accreted to form the inner planets of the solar system.

Clastic (detrital, fragmental) microstructure (Chapter 2): Microstructure dominated by detrital fragments (clasts) in sedimentary rocks.

Coincidence boundary (Section 4.2; Fig. 4.1): Grain boundary with a relatively high degree of atomic registry, and hence with a lower energy than a random grain boundary.

Comb layering (Section 3.5.4; Fig. 3.33): Arrangement of elongate crystals or grains in an igneous rock aligned normal to a boundary, which may be the wall of a magma chamber, an internal boundary, or an enclave boundary. The crystals are commonly in rhythmically repeated compositional layers. See also *orbicular structure*, to which comb layering is closely related.

Comb structure (Section 5.9.3; Fig. 5.67): Elongate crystals projecting approximately perpendicular to the walls of a vein in towards the centre, with the appearance of a comb.

Composite vein (Section 5.9.3; Fig. 5.69): Vein showing evidence of both syntaxial (q.v.) and antitaxial (q.v.) growth histories.

Core-and-mantle microstructure, core–mantle microstructure (Section 5.4.7; Figs. 5.17, 5.18, 5.22–5.25): Relatively small strain-free grains surrounding relics of large, strained grains; used to be called 'mortar texture' or 'mortar structure', on the assumption that the small grains represent original fragments. This microstructure is generally inferred to be due to dislocation creep, recovery and recrystallization, although recrystallization of fragments may be appropriate for some examples.

Corona (reaction rim) (Sections 4.1.2, 4.10.2, 4.13.3; Fig. 4.60): Rim or mantle resulting from incomplete reactions between two minerals or between a mineral and components in a fluid in a metamorphic rock. Coronas are commonly (though not necessarily) composed of symplectic intergrowths (q.v.). Reaction rims may also occur in igneous rocks as a result of incomplete magmatic reactions between crystals and melt.

Crack–seal veins (Section 5.9.3; Figs. 5.61, 5.62): Veins generally inferred to be formed by repeated cracking interspersed with sealing of the cracks by crystallization of vein mineral.

Crenulation cleavage (Section 5.8.3; Figs. 5.35, 5.53, 5.55): Foliation formed by alignment of the strongly deformed limbs of microfolds of a pre-existing foliation, commonly slaty cleavage (q.v.).

Cryptocrystalline: Describes very fine-grained, crystalline material that is incompletely resolved by the microscope.

Cryptoperthite (Section 4.9.1): Perthite (q.v.) with lamellae too narrow to be resolved in the optical microscope.

Crystallites (Sections 3.4.2, 3.5.3; Fig. 3.24): Minute, embryonic crystals in some glassy volcanic rocks, typically with acicular, dendritic, and intricately curved or hair-like shapes. Crystallites are too small to show birefringence.

Crystalloblastic: Adjective implying growth of minerals in solid metamorphic rocks.

Cumulate microstructures (Sections 3.6.1, 3.7, 4.6.1; Figs. 3.46, 4.40–4.42): Microstructures of cumulates, which are mafic–ultramafic rocks with more crystals than could be precipitated from the inferred parent magma. The accumulation of the crystals can be physical (e.g. by crystal settling or floating) or by crystallization processes (e.g. crystallization of early minerals and removal of the interstitial liquid).

Cumulus (Sections 3.6.1, 3.7): Early-formed crystals inferred to have accumulated in a magma (see *cumulate*). Minerals occurring between the cumulus minerals are often called 'intercumulus' minerals, but no inference about relative timing of the two sets of minerals can generally be made.

Decussate (Section 4.2.3; Fig. 4.13): Describes a microstructure characterized by criss-cross (random) arrangement of elongate mineral grains dominated by crystal faces (rational-impingement boundaries); common in sheet silicate minerals (e.g. biotite, muscovite) and wollastonite, especially in contact metamorphic aureoles.

Deformation bands (Section 5.3.3): Planar, kink-like microstructures reflecting heterogeneous deformation in a deforming grain, but which do not conform to the strict definition of kink bands (q.v.), according to Spry (1969) and Hobbs *et al*. (1976); Passchier & Trouw (1996, p. 34) regarded deformation bands as being transitional between undulose extinction (q.v.) and subgrain boundaries (q.v.).

Deformation lamellae (Section 5.3.3; Fig. 5.10A): Narrow (0.5–10 μm), planar, crystallographically oriented zones with refractive index slightly different from that of the adjacent grain; typically formed during relatively low-temperature deformation, and commonly aligned perpendicular to elongate subgrains.

Deformation twins (Figs. 3.87, 3.89–3.91, 5.4, 5.13): Lamellar (not simple) twins formed by deformation; commonly lenticular with pointed terminations.

Dendritic (Section 3.5.3; Figs. 3.15–3.17, 3.20, 3.21): Describes the shape of single crystals with spiky or branched habit precipitated from fluid at conditions of strong supersaturation.

Detrital microstructure: See *clastic microstructure*.

Deuteric minerals: Secondary minerals precipitated from aqueous fluids concentrated at the late magmatic stage, typically replacing primary (magmatic) minerals, the process being known as *deuteric alteration*.

Devitrification (Sections 3.5.5, 3.8): Replacement of volcanic glass by crystalline aggregates, as in the formation of *spherulites* (q.v.) or *axiolites* (q.v.).

Diagenesis (Section 2.2.8): Processes involving alteration (reactions between clastic minerals and aqueous fluid) and lithification of sediment, grading into *burial metamorphism* (q.v.). The adjective is *diagenetic*.

Diatexite (Section 4.16.1): Magma containing melt, solid reaction products and restite (q.v.); a migmatite characterized by obliteration of former structural features.

Differentiated layering (Sections 5.8.2, 5.8.3): Compositional metamorphic layering formed from an originally more compositionally homogeneous rock by segregation of chemical components (and consequently minerals), typically during deformation; see also *metamorphic differentiation*.

Dihedral angle (Section 4.2): Term used in two ways: (1) angle between two meeting grain boundaries (see, for example, Reed-Hill, 1973, p. 220; Cottrell, 1975, p. 343; Hobbs *et al.*, 1976, p. 111; Shelley, 1993, p. 416; Best, 2003), typically used for solid aggregates (e.g. metals, metamorphic rocks) and also the angle between meeting crystal–liquid interfaces; (2) interfacial angle of one mineral against two grains of another mineral or the angle formed where liquid meets two mineral grains, reserving 'interfacial angle' for boundaries between grains of the same mineral (see, for example, Smith, 1948; Voll, 1960, p. 528; Stanton, 1972, p. 237; Vernon, 1976, pp. 138–9; Passchier & Trouw, 1996, p. 44).

Dislocations (Sections 3.5.2, 5.3.3, 5.3.5, 5.4.1; Figs. 3.27–3.29, 5.11, 5.12, 5.16): Line defects in crystalline materials that assist crystal growth and deformation.

Doleritic: See *ophitic*.

Ductile grain-boundary sliding, granular flow (Sections 5.3.2, 5.3.5): Movement of adjacent grains without loss of cohesion during deformation. The process should be distinguished from *frictional grain-boundary sliding*, which involves a loss of cohesion at the boundaries.

Ejecta: Volcanic fragments ejected in an explosive eruption; also called *tephra* and *pyroclasts*.

Embayed phenocryst (Section 3.13; Figs. 3.37, 3.69, 3.92, 3.93, 4.75): Phenocryst (typically in a volcanic or shallow intrusive igneous rock) with smoothly curved embayments formed either by magmatic corrosion (re-solution in the magma, owing to changes in external conditions) or, in some instances, dendritic growth.

Enclave (Section 3.10; Figs. 3.66–3.74): Body of external origin in an igneous rock. The main varieties are *xenoliths* (fragments of solid rocks) and *microgranitoid enclaves* (former magma globules derived by mingling of magmas).

Epiclastic: Describes sediments formed by accumulations of fragments produced by the erosion of existing rocks.

Epitactic (often refered to as 'epitaxial'): Adjective of *epitaxis* (q.v.).

Epitaxis (epitaxy) (Section 4.2.1; Figs. 4.2, 4.3): Nucleation and growth of a mineral in another with a systematic relationship between the two crystal structures.

Equigranular, equant (Fig. 3.14): Even-grained.

Equilibrium form (**equilibrium shape**) (Section 3.5.2): The shape of a crystal bound by planes (faces) of lowest interfacial free energy.

Euhedral (Section 3.5.2): Mineral with crystal faces in an igneous rock. Synonym of *idiomorphic* and *automorphic*. The equivalent term for metamorphic rocks is *idioblastic* (q.v.).

Eutaxitic structure, eutaxitic foliation, ignimbritic structure (Section 2.3; Figs. 2.17, 2.19): Streaky microstructure caused by parallelism of flattened, welded glass shards and flattened, lenticular pumice fragments (*fiamme*) (q.v.) in ash-flow tuff (q.v.), usually welded.

Eutectic intergrowth: Intergrowth of two minerals crystallizing simultaneously from a magma at the minimum liquidus temperature in a two-component system.

Eutectoid intergrowths (Section 4.10.6): Symplectic intergrowths (q.v.) formed in the solid state in sulphide minerals. The term is used to distinguish these intergrowths from eutectic intergrowths (q.v.) formed by solidification of molten sulphides; the formation of some of these intergrowths involves closed-system segregation within a parent grain, whereas other intergrowths require components from an external source.

Exsolution, unmixing (Section 4.9; Figs. 4.30, 4.50, 4.51, 4.53, 4.54): Occurs when a homogeneous solid solution (i.e. a single mineral) becomes unstable and breaks down into two minerals, typically forming lamellar intergrowths.

Extinction bands (Section 5.4.1): Elongate subgrains.

Fault rock (Section 5.7.4): Rock formed by deformation in a fault zone; includes cataclasite (see *cataclastic*) and *mylonite* (q.v.).

Felted (Fig. 3.5): Describes tightly compressed microlites (q.v.) interwoven in a felt-like aggregate, owing to magmatic flow.

Fiamme, pumice lenses (Section 2.3): Flattened lenses of pumice (q.v.) in an ash-fall tuff (q.v.) or ash-flow tuff (q.v.). The singular is ‘fiamma’ (Italian for ‘flame’).

Fissility: Tendency of rocks to split into thin sheets along bedding or cleavage planes, owing mainly to strong alignment of sheet silicate minerals.

Flame perthite (Sections 5.6.6, 5.7.9, 5.11.3; Fig. 4.54): Oriented flame-like lamellae of albite in K-feldspar, formed as a result of reactions accompanying deformation; commonly very heterogeneously developed.

Fluidal (Section 3.9): With parallel alignment of crystals, microlites (q.v.) or crystallites (q.v.), reflecting flow of magma.

Foliation (Section 5.8): Penetrative planar structure of metamorphic-deformation origin.

Fragmental microstructure: See *clastic microstructure*.

Framboids (pyrite) (Section 2.2.8): Rounded, porous, raspberry-shaped (hence the name) structures in organic-rich sedimentary rocks.

Frictional grain-boundary sliding, independent particulate flow (Section 3.5.1): The sliding of grains past each other, without the development of thoroughgoing fractures.

Glass: See *volcanic glass.*

Glomeroporphyritic aggregate (Section 3.7): Aggregate of phenocrysts, formed by either heterogeneous nucleation or synneusis (q.v.).

Gneissic foliation, gneissosity (Section 5.8.4): Crudely layered foliation typical of coarse-grained metamorphic rocks and deformed coarse-grained rocks, characterized by folia (rich in minerals such as biotite, sillimanite or hornblende) anastomosing around lenticular pods of granoblastic aggregates (rich in minerals such as quartz, feldspar, cordierite or garnet).

Grain growth (Section 4.2.1): Solid-state changes in the sizes and shapes of grains and crystals (but not the minerals), to minimize the total interfacial free energy of the system.

Granitoid: Loose term for any coarse-grained intrusive rock of felsic to intermediate composition.

Granoblastic (Section 4.2.2): Describes an aggregate of xenoblastic, equant, predominantly polygonal grains in metamorphic rocks; common in aggregates of quartz (in quartzite), calcite (in marble) and olivine (in peridotite).

Granofels: Useful, non-genetic term to describe a granular metamorphic rock. It can often be used to replace 'granulite', which has metamorphic grade connotations.

Granophyric (Section 3.8; Fig. 3.54): Micrographic (q.v.) intergrowth of quartz and alkali feldspar. The term 'granophyre' was applied by Rosenbusch to a rhyolitic rock with micrographic groundmass (Johannsen, 1939, p. 255), and Tyrrell (1929, p. 114) described it as a microgranite with graphic intergrowths of quartz and feldspars. According to Barker (1970), the term 'granophyric' implies a graphic intergrowth of quartz and either K-feldspar or Na-rich feldspar, rather than a quartz and alkali feldspar solid solution, although Lentz & Fowler (1992) regarded it as the 'irregular, finer-grained counterpart' of the graphic intergrowth, and Best (2003, p. 699) equated it with 'micrographic'. However, 'micrographic' can also refer to microscopic intergrowths of minerals other than quartz and alkali feldspar, for example plagioclase and clinopyroxene.

Graphic intergrowth (Section 3.8; Figs. 3.54–3.56): Intergrowth of two minerals, each in optical continuity, resembling some forms of ancient writing; most commonly intergrowths of quartz and alkali feldspar.

Groundmass: Aggregate that is distinctly finer-grained than the phenocrysts (q.v.) in an igneous rock. The usage is similar to that of 'matrix' (q.v.) in a metamorphic rock.

Helicitic (Section 5.10.8): Describes microstructure characterized by curved trails of inclusions in porphyroblasts (commonly of garnet, but also albite, staurolite and chloritoid) formed by overgrowth of pre-existing microfolded structures; may be difficult to distinguish from rotational (snowball) microstructure (q.v.).

Holocrystalline: Completely crystallized.

Holohyaline: Completely glassy.

Hornfelsic: Not very useful term to describe the structure of a hornfels (contact metamorphic rock), which tends to be relatively even and fine-grained.

Hour-glass zoning: See *sector zoning*.

Hyaline: Glassy.

Hybridism, hybridization, magma mixing (Section 3.10.3): Mixing of two different magmas. The liquid components of both magmas mix, even though the solid crystals may only partly react in an attempt to equilibrate with the mixed melt; contrast with *magma mingling* (q.v.).

Hydrogen metasomatism, base-cation leaching (Sections 4.13.6, 5.9.2; Fig. 5.60): Leaching of cations by acid solutions. May produce unexpected Al-rich minerals, such as cordierite, andalusite and sillimanite, in metamorphosed felsic igneous rocks.

Hypidiomorphic-granular: An old-fashioned, not very useful term for granitic microstructure.

Idioblastic (Figs. 4.20, 4.35): Term describing crystals with well-formed (low-energy) crystal faces in metamorphic rocks; the equivalent term for igneous rocks is idiomorphic (q.v.).

Idiomorphic (Section 3.5.2): Describes a mineral with crystal faces in an igneous rock. Synonym of *euhedral* and *automorphic*. The equivalent term for metamorphic rocks is *idioblastic* (q.v.).

Ignimbrite (Section 2.3; Figs. 2.17, 2.19): See *ash-flow tuff*.

Ignimbritic (Section 2.3): See *eutaxitic structure*.

Imbrication: See *tiling*.

Inclusion: Mineral enclosed in a larger grain of another mineral; the term is sometimes used for enclaves (q.v.), but the former meaning is very widely accepted, and so should be reserved for it.

Inclusion trails (Section 5.10.1; Figs. 4.30B, 5.59, 5.72): Lines of included mineral grains (inclusions) in porphyroblasts, resulting from overgrowth of pre-existing foliations.

Inset: Phenocryst (q.v.).

Intercumulus (Sections 3.6.1, 3.7): Minerals between cumulate minerals (cumulus) (q.v.); no inference about relative timing of the cumulus and intercumulus minerals can generally be made.

Intergranular: Describes the microstructure of mafic igneous rocks (typically volcanic) in which interstices (q.v.) between feldspar laths are occupied by small, relatively equant grains of pyroxene, olivine or opaque oxide minerals.

Intergrowth: Aggregate of two or more minerals, generally arranged in a regular manner, formed by simultaneous growth or exsolution (q.v.).

Intersertal: Microstructure of mafic igneous rocks in which interstices between feldspar laths are occupied by a 'mesostasis' (q.v.) of quartz, *granophyric* intergrowths (q.v.), glass or *deuteric minerals* (q.v.).

Interstices: Angular cavities or interspace fillings between feldspar laths in igneous rocks. The singular is *interstice*.

Kelyphitic rim: Corona (q.v.) composed of a very fine-grained, fibrous, radiating mineral intergrowth.

Kink band (Section 5.3.3; Figs. 5.5–5.9): Part of a grain that responds to deformation by undergoing rotation with respect to the unkinked part of the grain, the axis of rotation coinciding with the line of intersection of the kink band and the slip plane, perpendicular to the slip direction. Broadly similar microstructures reflecting heterogeneous deformation from one layer to another in a deforming grain, but which cannot be described as kink bands according to this definition, are best referred to as 'deformation bands' (q.v.).

Leucosome (Sections 4.16.1, 5.11.4; Figs. 4.80, 4.81): Mobile, light-coloured (leucocratic), felsic material produced in migmatization (commonly involving partial melting or anatexis) when separated from solid mafic products of the melting reaction. Leucosome consists of melt or melt products, such as crystals precipitated from the melt or from residual melt separated from precipitated crystals; igneous microstructures are common in non-deformed or weakly deformed leucosomes.

Lineation: Linear structure (compositional rods and/or linear alignment of minerals) produced by deformation.

Liquid immiscibility (Section 3.15): Failure of two liquids, such as magmatic melts, to mix, producing globules of one liquid in the other.

M domain: See *P domain*.

Magma mingling (Section 3.10.3): Intimate interpenetration of two or more different magmas, without hybridization (q.v.), forming relatively fine-grained globules (magmatic enclaves, microgranitoid enclaves) of the magma with the higher liquidus temperature in the other. Although the magmas may be potentially miscible, relatively rapid cooling (and consequent increase in viscosity) of one of the magmas inhibits mixing. The magmatic enclaves may show chilled rims, which contrasts with *liquid immiscibility* (q.v.), for which both liquids are in equilibrium and so do not quench against each other.

Magma mixing, hybridism, hybridization: See *hybridism*.

Matrix (Section 4.3.1; Figs. 4.17–4.21): Aggregate that is distinctly finer-grained than the porphyroblasts in a metamorphic rock. The usage is similar to that of *groundmass* (q.v.) in an igneous rock.

Megacryst (Sections 3.4.5, 5.7.9; Figs. 3.12, 3.13, 3.53, 3.75, 5.51, 5.52): Very large phenocryst, usually referring to K-feldspar phenocrysts in a granitic rock. The adjective is *megacrystic*.

Melanosome (Section 4.16.1): Dark selvedge (mainly of mafic minerals, especially biotite) adjacent to the leucosome (q.v.) in some migmatites (q.v.); consists of solid products of the melting reaction that segregate from the leucosome.

Mesh structure, reticulated structure (Section 5.12.1; Figs. 5.99, 5.100): Microstructure formed by the replacement of olivine by serpentine, which initially replaces the olivine along cracks and then replaces the olivine between them, giving a meshed appearance.

Mesosome (Section 4.16.1): Darker volumes between light-coloured neosome or leucosome (q.v.) in a migmatite (q.v.); not necessarily representing the original rock, as it may be chemically modified during the migmatization process, e.g. during anatexis (q.v.), and may contain small amounts of former melt and/ or crystals produced in the melting reaction.

Mesostasis: Material filling interstices (q.v.) in relatively rapidly cooled igneous (especially mafic) rocks; the minerals are of late magmatic (e.g. quartz or alkali feldspar) or deuteric (q.v.) origin (e.g. calcite, chlorite, zeolites).

Meta-: Prefix denoting a metamorphic rock; e.g. metapelite (= metamorphosed pelite), metapsammite, metabasalt, metagabbro.

Metamorphic differentiation (Sections 5.7.1, 5.8.3): The formation of compositional layering during metamorphism in an originally uniform rock; see *differentiated layering*.

Metasomatism, allochemical metamorphism (Sections 4.13.6, 4.14): Change of bulk chemical composition of a rock during metamorphism; see also *hydrogen metasomatism*.

Miarole: See *miarolitic cavity*.

Miarolitic cavity, miarole (Section 3.14.6; Figs. 3.101, 3.102): Small, commonly approximately spherical to angular or elongate cavity in an igneous rock, into which small crystals of various minerals project.

Mica 'fish' (Section 5.7.7; Fig. 5.44A): Porphyroclasts of mica with asymmetry reflecting the shear sense in a mylonite (q.v.).

Microboudinage (Section 5.10.7; Figs. 5.64B, 5.86): Boudinage on the microscope scale.

Microcrystalline: Term describing the microstructure of a rock with crystal and grain shapes detectable at the microscope scale.

Micrngranitoid enclave, igneous enclave, 'mafic enclave' (Section 3.10.3; Figs. 3.66–3.74): Enclave with igneous microstructure in granitoid rocks, typically finer-grained and more mafic than the host rock. Some people use 'microgranular enclave', but this conveys little meaning, as it just implies multiple grains on the microscope scale, and many very different rocks can be described in this way. 'Microgranitoid' signifies a microstructure like that of typical granitoids, but finer-grained.

Micrographic (Section 3.8; Figs. 3.54–3.56, 4.65): Microscope-scale graphic (q.v.) intergrowth. Granophyric intergrowths are common examples.

Microlites (Sections 3.4.2, 3.5.3; Figs. 3.5, 3.7, 3.62): Very small, elongate crystals, large enough to show birefringence, in volcanic rocks.

Microperthite (Section 4.9.1; Figs. 4.30, 4.50, 4.51, 4.54): Perthitic intergrowth on the microscope scale.

Migmatite (Section 4.16): Metamorphic rock characterized by commonly mobile, light-coloured, relatively felsic aggregates or layers (*neosome*; q.v.) and darker rock (called *mesosome*; q.v.). Most neosomes are inferred to have been formed by partial melting (*anatexis*), though not all, and the distinction can be difficult. Igneous microstructures occur in the neosomes of some migmatites, indicating crystallization of magma. Neosomes are commonly separated into felsic (*leucosome*; q.v.) and mafic (*melanosome*; q.v.) portions.

'Millipede' structure (Section 5.10.7; Fig. 5.76): Microstructure of porphyroblasts with inclusion trails that curve into the matrix foliation by making opposite concave-outwards patterns at each end of the porphyroblast.

Mimetic crystallization: Growth of new minerals in bedding planes or foliations, thereby preserving or intensifying existing microstructures.

Monzonitic: Describes a microstructure in which euhedral crystals of plagioclase are enclosed or partly enclosed by much large crystals of K-feldspar; common in the intrusive igneous rock monzonite.

Mortar structure: Older term for fine-grained recrystallized aggregates surrounding porphyroblasts; equivalent to *core-and-mantle structure* (q.v.). The name implies a fragmental origin, which commonly is not appropriate.

Mylonite (Section 5.7.6; Figs. 5.31, 5.38–5.52): Thinly foliated and strongly lineated rock, commonly with porphyroclasts (q.v.), formed by intense deformation in elongate, relatively restricted zones.

Myrmekite (Sections 4.10.4, 5.6.6, 5.7.9; Figs. 4.56, 4.57, 4.61, 4.62, 4.65): Vermicular (worm-like, symplectic) intergrowth of quartz and sodic plagioclase (generally oligoclase), formed by replacement of K-feldspar, typically in deformed granitic rocks.

Neoblast: Term sometimes used for a grain or crystal of a new mineral that has grown in the solid state.

Neocrystallization (Chapter 4; Section 5.4.2; Fig. 5.26): Solid-state replacement of a mineral by grains of new minerals; contrast with *recrystallization* (q.v.).

Neosome (Section 4.16.1): Mobile material (commonly separated into leucosome and melanosome) (q.v.) formed in a migmatite, typically by anatexis (partial melting).

Ocelli (Section 3.10.3; Figs. 3.73, 3.74): Term used for (1) felsic segregations inferred to represent immiscible liquids, and (2) mantled xenocrysts (q.v.) in hybrid igneous rocks (i.e. rocks formed by hybridization or magma mixing). In view of the multiple use, the term is probably best avoided. The singular is *ocellus*.

Oikocryst: The host grain in poikilitic microstructure (q.v.).

Oolitic (Section 2.5; Figs. 2.24–2.26): Term describing the microstructure of a sedimentary rock composed largely or entirely of ooids (ooliths, ‘oolites’). Ooids are spherical or ellipsoidal accretions of chemically precipitated aggregates. Limestones rich in ooids are called oolitic limestones or calcareous oolites. Chlorite may also occur as ooids.

Ophitic (Section 3.6; Figs. 3.48, 3.49): Microstructure in which euhedral crystals of plagioclase are completely enclosed by much larger crystals of pyroxene; typical of the mafic intrusive igneous rock *dolerite*.

Orbicular structure (Section 3.5.4; Fig. 3.33): Spherical structure in granitoid rocks consisting of elongate to fibrous crystals projecting outwards from a nucleus (commonly a phenocryst or enclave) or arranged tangentially; typically the crystals are in rhythmically repeated compositional layers. See also *comb layering*, to which orbicular structure is closely related. The spherical objects making up orbicular structure are *orbs*, although they are often referred to as ‘orbicules’, which is an unnecessary word.

Order of crystallization (Section 3.6): Order of first crystallization of minerals, especially in igneous rocks; it is determined by melting experiments on the magma composition, and generally cannot be determined by inspection with the microscope.

Orthocumulate (Section 3.6.1; Fig. 3.46): Variety of poikilitic microstructure (q.v.) in a cumulate (q.v.) with cumulus crystals (q.v.) enclosed or partly enclosed by another mineral (intercumulus; q.v.), but without implication for an order of crystallization.

Ostwald ripening (Sections 3.3.2, 3.4.3, 3.4.5, 4.3): Solution of minute crystalline particles and corresponding growth of larger particles, reflecting the greater solubility of very small particles compared to larger ones, in response to the tendency to reduce the total surface free energy. It applies to particles crystallized from liquid or solid solution, and occurs at the nanometre to micrometre scales (e.g. at the scale of TEM observation). Crystals observable optically are probably too large to be controlled by this process, in view of their inherent stability and the prohibitively large diffusion distances (Jackson, 1967). Therefore, it appears to be most applicable to the nucleation and early growth stages, for which diffusion distances are very short, so that surface energy can drive diffusion. It occurs in synthetic materials, and evidence for the process has been observed in experiments on felsic and mafic magmatic systems. Consequently, it may be applicable to the very earliest stages of crystallization of magmas, though it is more doubtful for porphyroblasts in metamorphic rocks, owing to the low driving force of surface energy, which is many orders of magnitude smaller than the chemical potentials driving crystal growth controlled by normal nucleation and growth processes (Carlson, 1999, 2000). Normal solid-state grain growth (Section 4.2.1) is generally excluded from the definition (see, for example, Martin & Doherty, 1976, p. 234; Solomatov, 2002). This is justified on the grounds that solution and reprecipitation of grains of a mineral different from the main mineral are not involved in normal grain growth, just the modification and elimination of relatively large grains by local grain-boundary migration in the solid state. However, Shelley (1993) and Best (2003) have referred to normal grain growth as 'Ostwald ripening'.

Overgrowth: See *secondary enlargement*.

P domain, M domain (Sections 5.8.2, 5.8.3, 5.10.6; Figs. 5.35, 5.53–5.55): Elongate, relatively high-strain domains rich in mica or sillimanite, separated by lower-strain Q domains (rich in quartz or quartz + feldspar) in slates or crenulated schists.

Palaeosome (Section 4.16.1): Part of a migmatite that is unaffected by the migmatization process, thereby reflecting the original rock composition; however, commonly the unmelted or melt-poor parts of migmatites are chemically altered in the process, so that the term *mesosome* (q.v.) is generally used instead.

Paragenesis (mineral assemblage): Assemblage of minerals inferred to have grown simultaneously.

Penetrative domainal cleavage, 'rough cleavage' (Section 5.8.2; Fig. 5.56): Equivalent of slaty cleavage (q.v.) in a deformed sandy rock.

Peristerite (Section 4.9.1; Fig. 4.55): Exsolution intergrowth in sodic plagioclase, consisting of submicroscopic lamellae of An_0 and An_{25}; revealed by TEM.

Peritectic minerals (Section 4.16.1): Solid products of a melting reaction, such as cordierite and/or garnet in partly melted metapelites.

Perthite (Section 4.9.1; Figs. 4.30, 4.50, 4.51, 4.53, 4.54): Intergrowth of albite lamellae in K-feldspar, generally formed by solid-state exsolution of a homogeneous alkali feldspar solid solution during slow cooling in igneous and metamorphic rocks.

Phase (Section 3.1): A chemically and physically homogeneous part of a *system* (e.g. a body of magma) that is bound by an interface with other phases (e.g. the melt phase and other crystal phases in a magma).

Phenocryst (Section 3.4.4; Figs. 3.5, 3.7–3.9): Crystal (commonly euhedral) that is distinctly larger than the other minerals (which form the *groundmass;* q.v.) in igneous rocks.

Phyllonite: Mylonite (q.v.) rich in mica.

Pilotaxitic: Describes a microstructure characterized by subparallel arrangement of feldspar microlites, reflecting flow in relatively rapidly cooled magma; common in basalts.

Poikilitic: Term referring to large grains with many inclusions in igneous rocks.

Poikiloblast: Porphyroblast (q.v.) with many inclusions.

Poikiloblastic: Describes the structure of a porphyroblast with many inclusions (poikiloblast), and of a rock with pokiloblasts.

Polygonal aggregate (Section 4.2.2; Figs. 4.4–4.9): 'Foam-like' aggregate of grains with smoothly curved interfaces, formed by adjustment of grain boundaries in the solid state to minimize interfacial free energy; common in minerals with 'three-dimensional' atomic structures, such as quartz, calcite, olivine, feldspar, galena, pyrite and ice.

Porphyritic rock: Igneous rock with phenocrysts.

Porphyroblast (Sections 4.3, 5.10; Figs. 4.17–4.21): Large crystal, relative to the grainsize of the matrix (q.v.), in a metamorphic rock.

Porphyroblastic: Adjective that describes the structure of a rock with porphyroblasts.

Porphyroclast (Section 5.7.6, 5.7.9; Figs. 5.18, 5.24, 5.25, 5.40, 5.41, 5.45, 5.46, 5.52B): Large crystal, relative to the grainsize of the matrix, in a mylonite (q.v.), being a relic of a formerly large grain, such as a phenocryst (q.v.) or a porphyroblast (q.v.).

Porphyroclastic: Adjective that describes the structure of a deformed rock with porphyroclasts (q.v.).

Preferred orientation: Statistical alignment of mineral grains; may apply to shape (*dimensional preferred orientation*) and/ or crystal axes (*crystallographic preferred orientation*); synonym of *texture* in materials science.

Pressure-shadow, pressure fringe, 'beard' (Sections 5.3.4, 5.8.2, 5.9.3; Figs. 5.15, 5.64): Elongate aggregate of granoblastic or fibrous minerals (especially quartz and calcite) occupying dilated zones adjacent to a porphyroblast, extending parallel to the foliation.

Pressure-solution (Section 5.3.4; 5.9.2): See *stress-induced solution transfer*.

Protomylonite (Section 5.7.6): Mylonitic rock with a high proportion of porphyroclasts (10–50% matrix); however, not all parent rocks are coarse-grained, and so porphyroclasts are not always present in mylonites.

Pseudomorph (Sections 4.2.1, 4.3.2, 4.13.1, 4.13.3, 4.14; Figs. 4.2, 4.3, 4.17, 4.72, 4.73, 4.80): A mineral or aggregate of minerals replacing an older mineral grain or crystal, preserving the original size and shape.

Pseudomorphous: Adjective of *pseudomorph* (q.v.).

Pseudotachylite, pseudotachylyte (Sections 3.5.8, 5.7.10; Figs. 3.42–3.44): Glassy rock occurring in veins with sharp contacts with the original rock, formed by rapid brittle sliding between rock volumes in the absence of water, which can build up frictional heat at a fast enough rate to cause partial melting. Characterized by extremely rapid fragmentation, frictional heating, partial melting and rapid cooling (quenching of the melt).

Pumice (Section 3.14.3; Fig. 3.96): Felsic volcanic glass characterized by abundant gas bubbles (vesicles; q.v.) formed by rapid boiling, forming a 'glass froth' that is so light it can float on water.

Pumice lenses (fiamme) (Section 2.3; Figs. 2.14, 2.16): Flattened, lenticular pumice fragments ('lenticles') in a tuff.

Pumiceous (Section 3.14.3; Fig. 3.96): Describes the microstructure of pumice (q.v.).

Pyroclasts (Section 2.3; Figs. 2.14–2.20): Fragments of volcanic material ejected in an explosive eruption; also called *ejecta* and *tephra*.

Pyroclastic (Section 2.3; Figs. 2.14–2.20): Term describing a sediment dominated by pyroclastic fragments (volcanic glass and crystals from explosive eruptions).

Q domains (Sections 5.8.2, 5.8.3, 5.10.6; Figs. 5.35, 5.53–5.55): Elongate, relatively low-strain domains rich in quartz or quartz + feldspar, separated by higher-strain P (M) domains in slates or crenulated schists.

Rapakivi structure (Section 3.10.3; Fig. 3.75): The structure of phenocrysts of K-feldspar with rims (mantles) of smaller crystals of plagioclase (typically oligoclase) in some granitic rocks.

Reaction rim: Mineral layer formed by incomplete reaction between minerals, such as (1) an early-formed mafic mineral and a melt with which it is not in equilibrium (e.g. olivine mantled with orthopyroxene, pyroxene mantled with hornblende) in an igneous rock, and (2) a *corona* (q.v.) in metamorphic rocks.

Recovery (Section 5.4.1; Figs. 5.16–5.21): This term includes all processes that attempt to return a plastically deformed crystal to the undeformed state without the formation of high-angle (high-energy) boundaries; i.e. no new grains are formed. Recovery involves the organization of dislocations (line defects) into regular arrays (subgrain boundaries), forming *subgrains* in deformed crystals. Recovery may be either *dynamic* (during deformation) or *static* (after deformation), but most natural recovery is probably dynamic, as deformation typically accompanies metamorphism. In physical metallurgy, recovery is also known as 'polygonization'. Note that this refers to the formation of subgrains, NOT recrystallization. The fact that many recrystallized aggregates consist of polygonal grains has led some people to use 'polygonization' incorrectly as a term for recrystallization. 'Polygonization' is best avoided for rocks, to avoid ambiguity.

Recrystallization (Section 5.4.2; Figs. 5.17–5.26): Conversion of a mineral grain into an aggregate of smaller new grains of the same mineral, as a result of deformation. Recrystallization may be either *dynamic* (during deformation) or *static* (after deformation), but it can be difficult to distinguish between the two in the light microscope. Most natural recrystallization is probably dynamic, as deformation typically accompanies metamorphism. Some change in composition between old and new grains of the same mineral is common (e.g. in plagioclase), but the growth of new minerals is referred to as *neocrystallization*. The fact that many recrystallized aggregates consist of polygonal grains has led some people to use 'polygonization' incorrectly as a term for recrystallization. However, this term refers to recovery (q.v.), not recrystallization. 'Polygonization' is best avoided for rocks, to avoid ambiguity.

Relic (residual structure) (Section 4.15; Figs. 4.6, 4.38, 4.74–4.79, 5.53): Structure remaining after a deformation or metamorphic event, such as a porphyroclast in a mylonite, a phenocryst in a metamorphosed volcanic rock, or a partly replaced porphyroblast in a retrograde metamorphic rock. 'Relict' is sometimes used as an adjective for 'residual'.

Residual structure: See *relic*.

Resistate, resister (Section 4.16.1): Unmelted rock in a migmatite terrane.

Restite (Section 4.16.1): Solid material that is residual in a partial melting reaction, either (1) left behind in a migmatite, from which mobile melt has been removed, or (2) carried with the melt in a diatexite (q.v.).

Reticulated structure: See *mesh structure*.

Ribbon structure (Sections 5.5.1, 5.7.6; Figs. 5.9, 5.31): Elongate aggregates of minerals, typically quartz, in high-grade, granoblastic metamorphic rocks; formed either by intense ductile deformation or by crystallization in veins.

Rip-up clasts (Section 2.2.3; Fig. 2.10): Fragments of underlying mudstone beds incorporated as fragments in sand deposited by rapidly moving turbidity currents.

Schistose: Metamorphic rock with schistosity (q.v.).

Schistosity; schistose foliation (Section 5.8.3; Figs. 5.35, 5.53): Foliation consisting of elongate minerals (e.g. mica, sillimanite, amphibole), commonly anastomosing around porphyroblasts; characteristic of schists.

Schlieren (Section 3.9): Layers or streak-like concentrations, typically of relatively coarse-grained mafic minerals, with or without K-feldspar megacrysts (q.v.) and microgranitoid enclaves (q.v.) in intrusive rocks, especially granites; mostly formed by sorting during magmatic flow.

Scoriaceous (Section 3.14.3): Describes the structure of mafic volcanic rock (*scoria*) with abundant vesicles (q.v.).

Secondary enlargement (Section 2.2.6; Figs. 2.1, 2.13): Overgrowths on detrital grains, especially quartz in sedimentary rocks, forming part of the cement.

Sector zoning, hour-glass zoning (Sections 3.11.11, 4.12.2; Figs. 3.82–3.84, 4.18): Compositional differences between opposing sectors, commonly revealed by differences in colour or birefringence. Common in igneous pyroxene (especially titanaugite), less common in K-feldspar and plagioclase; common in metamorphic staurolite, less common in andalusite, chloritoid, epidote and kyanite; also occurs in sedimentary calcite and dolomite. 'Textural sector zoning' refers to differences in the concentration of inclusions between opposite sectors (Section 4.3.3).

Segregation vesicles (Section 3.14.5; Fig. 3.99): Vesicles partly filled with residual melt segregated from the surrounding magma, as distinct from amygdales (q.v.) and vughs (q.v.), which are filled with hydrothermal minerals.

Sheaf structure: Term (relatively uncommon these days) used for sheaf-shaped aggregates of fibrous minerals, such as anthophyllite, hornblende or wollastonite, in metamorphic rocks. Amphibole sheaves are characteristic of *garbenschiefer*, 'Garben' being the German for sheaves; the term is also used for some spherulitic aggregates (q.v.) in igneous rocks.

Skeletal crystal (Section 3.5.3; Figs. 3.15, 3.18, 3.22): Single crystal with a skeletal habit, formed at conditions of strong supersaturation; common in volcanic rocks and meteorites.

Slaty cleavage (Section 5.8.2; Figs. 5.54, 5.55): Foliation characterized by narrow dark folia of fine-grained, well-aligned phyllosilicate minerals (especially white mica and chlorite) and/or graphite (P or M domains), anastomosing around stronger domains containing detrital fragments, mainly of quartz (Q domains); typical of slates (metamorphosed shales). The analogous cleavage in deformed sandy rocks is called *penetrative domainal cleavage* (q.v.) or 'rough cleavage'.

Slip system (Section 5.3.3): Combination of a slip plane and a slip direction in this plane, referring to the plastic deformation of crystalline materials.

Snowball (rotational) structure (Section 5.10.7; Figs. 5.74, 5.88): Double-spiral inclusion trails in garnet porphyroblasts.

Snowflake structure (Sections 3.5.5, 3.8): Structure of micropoikilitic spherulites (q.v.), in which quartz grains enclose many feldspar fibres.

Spherulite (Sections 2.3, 3.5.5; Figs. 2.18, 2.19, 3.35–3.40): Spherical aggregate of radiating fibres (mainly K-feldspar, with or without silica minerals, especially quartz). Spherulites mainly grow in volcanic glass during devitrification (q.v.), although some may grow in strongly undercooled melt.

Spherulitic: Adjective describing the structure of a rock with spherulites; also refers to an aggregate of radiating fibres, not necessarily spherical.

Strain shadow: Region adjacent to a clast or porphyroblast that is protected from deformation, so that it may preserve earlier microstructures that have been obliterated from the rest of the matrix.

'Strain-slip' cleavage: An older term for crenulation cleavage (q.v.), not used much nowadays.

Stress-induced solution transfer, dissolution–precipitation creep, 'pressure-solution' (Sections 5.3.4, 5.7.4, 5.9.2): Change of grain shape by diffusion of chemical components in aqueous solution as material is dissolved from sites of high normal compressive stress and deposited at sites of low stress. Mass transfer in fluid is a major mechanism for the development of foliations, especially slaty cleavage and discrete crenulation cleavage (Sections 5.8.2, 5.8.3) in low-grade metamorphic rocks.

Stretched-crystal veins (Section 5.9.3; Figs. 5.69, 5.71): Veins in which minerals in the vein are the same as or similar to those in the wall-rocks; crystals that nucleate on each wall continue to grow right across the vein.

Stretched pebble: Pebble in a conglomerate that has been elongated by solid-state deformation.

Stromatic migmatite (Section 4.16.1): Migmatite in which the leucosome (q.v.) or neosome (q.v.) has segregated into layers (stroma).

Stylolite (adj.: **stylolitic**) (Sections 5.3.4, 5.9.2; Figs. 2.1, 2.25, 5.14): Curved, irregular or toothed surface, typically containing insoluble residues, formed by stress-induced solution transfer (q.v.).

Subgrains (Section 5.3.4; Figs. 5.16–5.21): Regions of small misorientation within an individual grain, formed by recovery in response to deformation; optically appear as extinction differences (undulose extinction). Elongate subgrains may be referred to as *extinction bands*.

Subhedral: Term describing a mineral with some crystal faces and some irregular boundaries in an igneous rock. Synonym of *subidiomorphic*. The equivalent term for a metamorphic rock is *subidioblastic* (q.v.).

Subidioblastic: Term denoting a mineral with some crystal faces and some irregular boundaries in a metamorphic rock. Equivalent terms for igneous rock are *subidiomorphic* and *subhedral* (q.v.)

Subidiomorphic: Term describing a mineral with some crystal faces and some irregular boundaries in an igneous rock. Synonym of *subhedral*. The equivalent term for a metamorphic rock is *subidioblastic* (q.v.).

Subophitic: Describes a microstructure in which euhedral crystals of plagioclase are partly enclosed in larger grains of pyroxene (compare with *ophitic*).

Superplastic flow, 'grainsize-sensitive flow' (Section 5.3.5): Deformation of very fine-grained aggregates to very large strains without fracturing and without change of overall grain shape. The mechanism involved is *grain-boundary sliding*, which involves relative grain movement without loss of cohesion, and normally in the absence of fluid.

Supersaturation (Section 3.5.1): The difference between the actual concentration of a chemical component in the liquid and the concentration at equilibrium (i.e. when the magma is just saturated in the component).

Sutured ('bulged') boundary (Section 5.4.2; Figs. 4.19, 4.63, 5.22, 5.28, 5.29): Curved, interlocking grain boundary, kink-band boundary or deformation twin boundary, typically resulting from strain-induced boundary migration.

'Swapped rims' (Section 4.10.4; Fig. 4.61): Rims of sodic plagioclase (which may or may not be myrmekitic) on each side of an original boundary between two perthite grains, with the same crystallographic orientation as the albite lamellae of the *opposite* parent grain; formed by the sodic plagioclase nucleating on albite lamellae in perthite, retaining the crystallographic orientation of the lamellae, and growing into the adjacent perthite grain.

Symplectite, symplectic intergrowth (Section 4.10; Figs. 4.56–4.62): Worm-like (vermicular) intergrowth of minerals. *Myrmekite* (q.v.) is the most common example.

Synneusis (Section 3.7.2; Fig. 3.51): The drifting together and mutual attachment of crystals suspended in a magma.

Syntaxial veins (Section 5.9.3; Fig. 5.67): Veins with elongate crystals (columnar or fibrous) crystals projecting from the walls of the vein and growing towards the centre. Typically these crystals nucleate heterogeneously on minerals of the wall-rocks, so that generally the fibres are closely related to minerals in the wall-rocks, for example, quartz veins in sandstones and calcite veins in limestones or marbles.

Tephra: Volcanic fragments ejected in an explosive eruption; also called *ejecta* and *pyroclasts*.

Texture: Used synonymously with 'microstructure' by some English-writing petrologists, but used for 'preferred orientation' by materials scientists and in some non-English languages. The IUGS Subcommission on the Systematics of Metamorphic Rocks has recommended that the term be replaced by 'microstructure' (Brodie *et al.*, 2002).

Tiling, imbrication (Sections 3.9, 5.11.2; Figs. 3.58, 3.64): Rotational alignment in magma of elongate euhedral crystals that are not internally deformed or of fragments of phenocrysts that have undergone boudinage.

Trachytic (Fig. 3.5): Describes a microstructure in which microlites (q.v.) of feldspar are strongly aligned and wrap around phenocrysts (q.v.), which may also be aligned, the alignment being due to flow of relatively viscous magma; typical of the volcanic rock *trachyte*.

Transposition: Strong modification and realignment of a foliation or bedding into a new orientation.

Tuff, ash-fall: See *ash-fall tuff*.

Tuff, ash-flow (ignimbrite): See *ash-flow tuff*.

Tuff, welded: See *welded tuff*.

Ultramylonite (Section 5.7.6; Figs. 5.44–5.46): Mylonitic rocks with fewer than 10% porphyroclasts (assuming the original rock was sufficiently coarse-grained to produce porphyroclasts).

Undulose (undulatory) extinction (Sections 5.3.3, 5.4.1, 5.4.4): Wavy, non-uniform extinction in a single grain, owing to slight bending of the crystal. Patchy, irregular undulose extinction can be due to submicroscopic fractures, kinks and dislocation tangles (Hirth & Tullis, 1992); common in quartz and olivine.

Variolitic (Section 3.5.5; Fig. 3.17): Refers to the microstructure of glassy basaltic rocks characterized by radiating (spherulitic, fan-like or sheaf-like) aggregates (varioles) of fibrous crystals, e.g. of plagioclase and clinopyroxene, or of plagioclase with interfibrillar clinopyroxene.

Vesicle (Section 3.14.2; Figs. 3.62, 3.95, 3.96): Spherical or ellipsoidal cavity caused by formation and expansion of gas, typically in a volcanic rock or shallow intrusion.

Vesicular: Adjective describing the structure of a rock with vesicles.

Vitrophyric rock: Rock with a glass groundmass.

Volcanic ash: See *ash, volcanic*.

Volcanic glass (Section 3.5.6; Figs. 3.7–3.9, 3.34, 3.36, 3.38, 3.39): Material formed by the rapid cooling (quenching) of melt (especially felsic melt, but also mafic melt, less commonly) on Earth's surface. Glass has the rigidity of a solid, but the atomic arrangement more akin to that of a silicate melt, characterized by short-range order, as opposed to the long-range order of atomic arrangements in crystalline materials, which makes glass optically isotropic. Because this less ordered arrangement of atoms represents a higher-energy situation than a compositionally equivalent crystalline material, glass is metastable and tends to crystallize ('devitrify') with time, especially in the presence of water, forming spherulitic or axiolitic aggregates.

Volcaniclastic: Term describing a sediment composed of fragments of volcanic origin.

Vugh (Section 4.12.2; Fig. 4.69): Cavity filled or partly filled with minerals that precipitate from hydrothermal solution.

Welded tuff (Section 2.3; Fig. 2.17): Pyroclastic rock formed when glass and pumice fragments become fused together by heat and pressure. The formerly sharp glass fragments become rounded and squashed in the welding process.

Widmanstätten structure (Section 4.9.2): Nickel-rich exsolution lamellae in an iron-rich host in iron meteorites.

Xenoblastic: Describes a structure of irregular grains showing no crystal-face boundaries in a metamorphic rock. The equivalent term for igneous rocks is *xenomorphic* (q.v.).

Xenocryst (Section 3.10.2): Solid fragment of a foreign mineral caught up in a magma. If they are out of equilibrium with the melt, xenocrysts commonly show partial alteration or resorption (solution), indicating reaction with the magma.

Xenolith (Section 3.10.2): Solid fragment of a foreign rock caught up in a magma, and which may show evidence of reaction with it; contrast with *microgranitoid enclave* (q.v.).

Xenomorphic: Irregular grains showing no crystal-face boundaries in an igneous rock. Synonym of *anhedral* and *allotriomorphic*. The equivalent term for metamorphic rocks is *xenoblastic* (q.v.).

References

Abbott, R. N. 1989: Internal structures in part of the South Mountain batholith, Nova Scotia, Canada. *Bulletin of the Geological Society of America*, **101**, 1493–506.

Adams, A. E., MacKenzie, W. S. & Guildford, C. 1984: *Atlas of Sedimentary Rocks under the Microscope.* Harlow, UK: Longman.

Aerden, D. G. A. M. 1995: Porphyroblast non-rotation during crustal extension in the Variscan Lys-Caillaouas Massif, Pyrenees. *Journal of Structural Geology*, **17**, 709–25.

Ague, J. J. 1991: Evidence of major mass transfer and volume strain during regional metamorphism of pelites. *Geology*, **19**, 855–8.

1994: Mass transfer during Barrovian metamorphism of pelites, south-central Connecticut. II: Channelized fluid flow and the growth of staurolite and kyanite. *American Journal of Science*, **294**, 1061–134.

1997: Crustal mass transfer and index mineral growth in Barrow's garnet zone, northeast Scotland. *Geology*, **25**, 73–6.

Ahn, J. & Cho, M. 2000: Application of cathodoluminescence to fine-grained pelitic schists of the Imjingang Belt, Korea. *European Journal of Mineralogy*, **12**, 1057–62.

Akouri, K., Conaghan, P. J., Walter, M. R., Bischoff, G. C. O. & Grey, K. 2000: Reconnaissance sedimentology and hydrocarbon biomarkers of Ediacarian microbial mats and arcitarchs, lower Ungoolya Group, Officer Basin. *Precambrian Research*, **100**, 235–80.

Alexandrov, P. 2001: Synneusis of zircon: why not? *Mineralogical Magazine*, **65**, 71–9.

Alias, G., Sandiford, M., Hand, M. & Worley, B. 2002: The *P-T* record of synchronous magmatism, metamorphism and deformation at Petrel Cove, southern Adelaide Fold Belt. *Journal of Metamorphic Geology*, **20**, 351–63.

Allègre, C. J., Provost, A. & Jaupart, C. 1981: Oscillatory zoning: a pathological case of crystal growth. *Nature*, **294**, 223–8.

Allen, F. M., Smith, B. K. & Buseck, P. R. 1987: Direct observations of dissociated dislocations in garnet. *Science*, **238**, 1695–7.

Allibone, A. H. & Norris, R. J. 1992: Segregation of leucogranite microplutons during syn-anatectic deformation: an example from the Taylor Valley, Antarctica. *Journal of Metamorphic Geology*, **10**, 589–600.

Allison, I., Barnett, R. L. & Kerrich, R. 1979: Superplastic flow and changes in crystal chemistry of feldspars. *Tectonophysics*, **54**, T41–6.

Allison, I. & La Tour, T. E. 1977: Brittle deformation of hornblende in a mylonite: a direct geometrical analogue of ductile deformation by translation gliding. *Canadian Journal of Earth Sciences*, **14**, 1953–8.

Allport, S. 1874: On the microscopic structure and composition of British Carboniferous dolerites. *Quarterly Journal of the Geological Society of London*, **30**, 529–67.

Altenberger, U. 1995a: Local disequilibrium of plagioclase in high-temperature shear zones of the Ivrea Zone, Italy. *Journal of Metamorphic Geology*, **13**, 553–8.

1995b: Long-term deformation and fluid-enhanced mass-transport in a Variscan peridotite shear zone in the Ivrea Zone, northern Italy: a microtextural, petrological and geochemical study of a reactivated shear zone. *Geologische Rundschau*, **84**, 591–606.

1996a: Material transport in channelized fluids – examples from high-temperature shear zones in the Central European Variscan belt. *Mineralogy and Petrology*, **57**, 51–72.

1996b: Fluid enhanced element redistribution, mass transport and volume changes in eclogite and amphibolite facies shear zones of different geological settings. *Chemie der Erde*, **56**, 1–24.

Altenberger, U. & Wilhelm, S. 2000: Ductile deformation of K-feldspar in eclogite facies shear zones in the Bergen Arcs, Norway. *Tectonophysics*, **320**, 107–21.

Alvarez, W., Engelder, J. T. & Lowrie, W. 1976: Formation of spaced cleavage and folds in brittle limestone by dissolution. *Geology*, **4**, 698–701.

Andersen, T., Griffin, W. L. & O'Reilly, S. Y. 1987: Primary sulphide melt inclusions in mantle-derived megacrysts and pyroxenites. *Lithos*, **20**, 279–94.

Andersen, T. B. 1984: Inclusion patterns in zoned garnets from Mageroy, north Norway. *Mineralogical Magazine*, **48**, 21–6.

Anderson, A. T. 1983: Oscillatory zoning of plagioclase: Nomarski interference contrast microscopy of etched polished sections. *American Mineralogist*, **68**, 125–9.

1984: Probable relations between plagioclase zoning and magma dynamics, Fuego Volcano, Guatemala. *American Mineralogist*, **69**, 660–76.

Anderson, A. T., Swihart, G. H., Artioli, G. & Geiger, C. A. 1984: Segregation vesicles, gas filter-pressing, and igneous differentiation. *Journal of Geology*, **92**, 55–72.

Anderson, J. E. 1969: Development of snowflake texture in a welded tuff, Davis Mountains, Texas. *Bulletin of the Geological Society of America*, **80**, 2075–80.

Ando, J., Fujino, K. & Takeshita, T. 1993: Dislocation microstructures in naturally deformed silicate garnets. *Physics of the Earth and Planetary Interiors*, **80**, 105–16.

Aramovich, C. J., Herd, C. D. K. & Papike, J. J. 2002: Symplectites derived from metastable phases in martian basaltic meteorites. *American Mineralogist*, **87**, 1351–9.

Arndt, N. T. 1986: Differentiation of komatiite flows. *Journal of Petrology*, **27**, 279–301.

Arndt, N. T., Naldrett, A. J. & Pyke, D. R. 1977: Komatiitic and iron-rich tholeiitic lavas of Munro Township, northeast Ontario. *Journal of Petrology*, **18**, 319–69.

Arndt, N. T. & Nisbet, E. G. (eds) 1982: *Komatiites*. Boston: Allen & Unwin.

Arzi, A. A. 1978: Critical phenomena in the rheology of partially-molten rocks. *Tectonophysics*, **44**, 173–84.

Ashby, M. F. & Verall, R. A. 1973a: Micromechanisms of flow and fracture and their relevance to the rheology of the upper mantle. *Philosophical Transactions of the Royal Society of London*, **A288**, 59–95.

1973b: Diffusion-accommodated flow and superplasticity. *Acta Metallurgica*, **21**, 149–63.

Ashworth, J. A. 1972: Myrmekites of exsolution and replacement origins. *Mineralogical Magazine*, **109**, 45–62.

Atkinson, B. K. 1974: Experimental deformation of polycrystalline galena, chalcopyrite and pyrrhotite. *Transactions of the Institution of Mining and Metallurgy*, **83**, B19–28.

1977: Experimentally induced kinking and annealing of single crystals of galena. *Tectonophysics*, **39**, 175–89.

1984: Sub-critical crack growth in geological materials. *Journal of Geophysical Research*, **89**, 4077–114.

Atherton, M. P. 1977: The metamorphism of the Dalradian rocks of Scotland. *Scottish Journal of Geology*, **13**, 331–70.

Austrheim, H. 1987: Eclogitization of the lower crustal granulites by fluid migration through shear zones. *Earth and Planetary Science Letters*, **81**, 221–32.

Austrheim, H. & Griffin, W. L. 1985: Shear deformation and eclogite formation within granulite facies anorthosites of the Bergen Arcs, western Norway. *Chemical Geology*, **50**, 267–81.

Ave'Lallemant, H. G. 1978: Experimental deformation of diopside and websterite. *Tectonophysics*, **48**, 1–27.

Ave'Lallemant, H. G. & Carter, N. L. 1970: Syntectonic recrystallization of olivine and modes of flow in the upper mantle. *Bulletin of the Geological Society of America*, **81**, 2203–20.

1971: Pressure dependence of quartz deformation lamellae orientations. *American Journal of Science*, **270**, 218–35.

Aydin, A. & Johnson, A. M. 1983: Analysis of faulting in porous sandstones. *Journal of Structural Geology*, **5**, 19–31.

Ayers, J. C., Miller, C., Gorisch, B. & Milleman, J. 1999: Textural development of monazite during high-grade metamorphism: Hydrothermal growth kinetics, with implications for U, Th-Pb geochronology. *American Mineralogist*, **84**, 1766–80.

Bacon, C. R. & Metz, J. 1984: Magmatic inclusions in rhyolites, contaminated basalts, and compositional zonation beneath the Coso volcanic fields, California. *Contributions to Mineralogy and Petrology*, **85**, 346–65.

Baëta, R. D. & Ashbee, K. H. G. 1969: Slip systems in quartz. II. Interpretation. *American Mineralogist*, **54**, 1574–82.

Baker, D. R. & Freda, C. 1999: Using models of undercooled binary system crystallization: Comparison with experimental and pegmatite textures. *American Mineralogist*, **84**, 725–32.

2001: Eutectic crystallization in the undercooled Orthoclase–Quartz–H_2O system: experiments and simulations. *European Journal of Mineralogy*, **13**, 453–66.

Baker, D. W., Chawla, K. S. & Krizek, R. J. 1993: Compaction fabrics of pelites: experimental consolidation of kaolinite and implications for analysis of strain in slate. *Journal of Structural Geology*, **15**, 1123–37.

Ball, A. & White, S. 1977: An etching technique for revealing dislocation structures in deformed quartz grains. *Tectonophysics*, **37**, T9–14.

Barbarand, J. & Pagel, M. 2001: Cathodoluminescence study of apatite crystals. *American Mineralogist*, **86**, 473–84.

Barber, D. J. 1985: Dislocations and microstructures. *In* Wenk, H.-R. (ed.): *Preferred Orientation in Deformed Metals and Rocks: an Introduction to Modern Texture Analysis*. London: Academic Press, pp. 149–82.

Barber, D. J. & Meredith, P. G. (eds) 1990: *Deformation Processes in Minerals, Ceramics and Rocks*. Boston: Unwin Hyman.

Barbey, P., Brouand, M., Le Fort, P. & Pecher, A. 1996: Granite-migmatite genetic link: example of the Manaslu granite and Tibetan Slab migmatites in central Nepal. *Lithos*, **38**, 63–79.

Bard, J.-P. 1986: *Microtextures of Igneous and Metamorphic Rocks*. Dordrecht: Reidel.

Barker, A. J. 1990: *Introduction to Metamorphic Textures and Microstructures*. Glasgow: Blackie.

1994: Interpretation of porphyroblast inclusion trails: limitations imposed by growth kinetics and strain rates. *Journal of Metamorphic Geology*, **12**, 681–4.

2002: Crack-fill porphyroblasts. *Journal of Metamorphic Geology*, **20**, 283–94.

Barker, A. J. & Zhang, X. 1998: The role of microcracking and grain-boundary dilation during retrograde reactions. *In* Treloar, P. J. & O'Brien, P. (eds): What drives metamorphism and metamorphic reactions? *Geological Society of London Special Publication*, **138**, 247–68.

Barker, C. E. & Kopp, O. C. 1991: *Luminescence Microscopy and Spectroscopy: Qualitative and Quantitative Applications. Society for Sedimentary Geology (SEPM) Short Course*, **25**, 195pp.

Barker, D. S. 1970: Compositions of granophyre, myrmekite, and graphic granite. *Bulletin of the Geological Society of America*, **81**, 3339–50.

Barnes, S. J. 1998: Chromite in komatiites, 1. Magmatic controls on crystallization and composition. *Journal of Petrology*, **39**, 1689–720.

Baronnet, A. 1972: Growth mechanisms and polytypism in synthetic hydroxyl-bearing phlogopite. *American Mineralogist*, **57**, 1272–93.

1975: Growth spirals and complex polytypism in micas – I. Polytypic structure generation. *Acta Crystallographica*, **A31**, 345–55.

1982: Ostwald ripening in solution. The case of calcite and mica. *Estudios geológicos*, **38**, 185–98.

1984: Growth kinetics of the silicates. A review of basic concepts. *Fortschritte Mineralogie*, **62**, 187–232.

Barrière, M. 1981: On curved laminae, graded layers, convection currents and dynamic crystal sorting in the Ploumanac'h (Brittany) subalkaline granite. *Contributions to Mineralogy and Petrology*, **77**, 217–24.

Barton, M. & van Gaans, C. 1988: Formation of orthopyroxene–Fe-Ti oxide symplectites in Precambrian intrusives, Rogaland, southwestern Norway. *American Mineralogist*, **73**, 1046–59.

Barton, P. B. 1970: Sulfide petrology. *Geological Society of America Special Paper*, **3**, 187–98.

Barton, P. B. & Bethke, P. M. 1987: Chalcopyrite disease in sphalerite: pathology and epidemiology. *American Mineralogist*, **72**, 451–67.

Bastin, E. S. 1950: Interpretation of ore textures. *Geological Society of America Memoir*, **45**, 101pp.

Bateman, P. C. & Chappell, B. W. 1979: Crystallization, fractionation, and solidification of the Tuolumne Intrusive Series, Yosemite National Park, California. *Bulletin of the Geological Society of America*, **90**, 465–82.

Bathurst, R. G. C. 1958: Diagenetic fabrics in some British Dinantian limestones. *Liverpool and Manchester Geological Journal*, **2**, 11–36.

1975: *Carbonate Sediments and their Diagenesis* (second edition). *Developments in Sedimentology*, **12**. Amsterdam: Elsevier.

Bauer, P., Rosenberg, C. & Handy, M. R. 2000: 'See-through' deformation experiments on brittle-viscous norcamphor at controlled temperature, strain rate and applied confining pressure. *Journal of Structural Geology*, **22**, 281–9.

Baxter, E. F., Ague, J. J. & DePaolo, D. J. 2002: Prograde temperature-time evolution in the Barrovian type-locality constrained by Sm/Nd garnet ages from Glen Clova, Scotland. *Journal of the Geological Society of London*, **159**, 71–82.

Beach, A. 1973: The mineralogy of high temperature shear zones at Scourie, N.W. Scotland. *Journal of Petrology*, **14**, 213–48.

1974: A geochemical investigation of pressure solution and the formation of veins in a deformed greywacke. *Contributions to Mineralogy and Petrology*, **46**, 61–8.

1976: The interrelations of fluid transport, deformation, geochemistry and heat flow in early Proterozoic shear zones in the Lewisian complex. *Philosophical Transactions of the Royal Society of London*, **A280**, 569–604.

1977: Vein arrays, hydraulic fractures and pressure-solution structures in a deformed flysch sequence, S.W. England. *Tectonophysics*, **40**, 201–25.

1979: Pressure solution as a metamorphic process in deformed terrigenous sedimentary rocks. *Lithos*, **12**, 51–8.

1980: Retrograde metamorphic processes in shear zones with special reference to the Lewisian complex. *Journal of Structural Geology*, **2**, 257–63.

Beach, A. & Fyfe, W. S. 1973: Fluid transport and shear zones at Scourie, Sutherland: evidence of overthrusting? *Contributions to Mineralogy and Petrology*, **36**, 175–80.

Becke, F. 1908: Über Myrmekit. *Mineralogisches und Petrographisches Mitteilungen*, **27**, 377–90.

Becker, A. 1995: Quartz pressure solution: influence of crystallographic orientation. *Journal of Structural Geology*, **17**, 1395–405.

Behrmann, J. H. 1983: Microstructure and fabric transitions in calcite tectonics from the Sierra Alhamilla (Spain). *Geologische Rundschau*, **72**, 605–18.

1985: Crystal plasticity and superplasticity in quartzite: a natural example. *Tectonophysics*, **115**, 101–29.

Behrmann, J. H. & Mainprice, D. 1987: Deformation mechanisms in a high-temperature quartz-feldspar mylonite: evidence for superplastic flow in the lower continental crust. *Tectonophysics*, **140**, 297–305.

Bell, T. H. 1978a: The development of slaty cleavage across the Nackara Arc of the Adelaide Geosyncline. *Tectonophysics*, **51**, 171–201.

1978b: Syntectonic nucleation of new grains in deformed mica. *Tectonophysics*, **51**, T31–7.

1979: The deformation and recrystallization of biotite in the Woodroffe Thrust mylonite zone. *Tectonophysics*, **58**, 139–58.

1981: Foliation development: the contribution, geometry and significance of progressive bulk inhomogeneous shortening. *Tectonophysics*, **75**, 273–96.

1985: Deformation partitioning and porphyroblast rotation in metamorphic rocks: a radical reinterpretation. *Journal of Metamorphic Geology*, **3**, 109–18.

1986: Foliation development and refraction in metamorphic rocks: reactivation of earlier foliations and decrenulation due to shifting patterns of deformation partitioning. *Journal of Metamorphic Geology*, **4**, 421–44.

Bell, T. H. & Etheridge, M. A. 1973: Microstructure of mylonites and their descriptive terminology. *Lithos*, **6**, 337–48.

Bell, T. H., Forde, A. & Hayward, N. 1992a: Can smoothly curving spiral-shaped inclusion trails form without rotation of the porphyroblast? *Geology*, **20**, 59–62.

Bell, T. H., Forde, A. & Wang, J. 1995: A new indicator of movement direction during orogenesis: measurement technique and application to the Alps. *Terra Nova*, **7**, 500–8.

Bell, T. H. & Hayward, N. 1991: Episodic metamorphic reactions during orogenesis: the control of deformation partitioning on reaction sites and reaction duration. *Journal of Metamorphic Geology*, **9**, 619–40.

Bell, T. H. & Hickey, K. A. 1999: Complex microstructures preserved in rocks with a simple matrix: significance for deformation and metamorphic processes. *Journal of Metamorphic Geology*, **17**, 521–35.

Bell, T. H., Hickey, K. A. & Upton, G. J. G. 1998: Distinguishing and correlating multiple phases of metamorphism across a multiply deformed region using the axes of spiral, staircase and sigmoidal inclusion trails in garnet. *Journal of Metamorphic Geology*, **16**, 767–94.

Bell, T. H. & Johnson, S. E. 1989a: Porphyroblast inclusion trails: the key to orogenesis. *Journal of Metamorphic Geology*, **7**, 279–310.

1989b: The role of deformation partitioning in the deformation and recrystallization of plagioclase and K-feldspar in the Woodroffe Thrust mylonite zone, central Australia. *Journal of Metamorphic Geology*, **7**, 151–68.

Bell, T. H., Johnson, S. E., Davis, B., Forde, A., Hayward, N. & Wilkins, C. 1992b: Porphyroblast inclusion-trail orientation data: eppure non son girate! *Journal of Metamorphic Geology*, **10**, 295–307.

Bell, T. H. & Mares, V. M. 1999: Correlating deformation and metamorphism around orogenic arcs. *American Mineralogist*, **84**, 1727–40.

Bell, T. H. & Rubenach, M. J. 1980: Crenulation cleavage development – evidence for progressive, bulk inhomogeneous shortening from millipede microstructures in the Robertson River Metamorphics. *Tectonophysics*, **68**, T9–15.

1983: Sequential porphyroblast growth and crenulation cleavage development during progressive deformation. *Tectonophysics*, **92**, 171–94.

Bell, T. H., Rubenach, M. J. & Fleming, P. D. 1986: Porphyroblast nucleation, growth and dissolution in regional metamorphic rocks as a function of deformation partitioning during foliation development. *Journal of Metamorphic Geology*, **4**, 37–67.

Benn, K. & Allard, B. 1989: Preferred mineral orientations related to magmatic flow in ophiolite layered gabbros. *Journal of Petrology*, **30**, 925–46.

Benn, K., Roest, W. R., Rochette, P., Evans, N. G. & Pignotta, G. S. 1999: Geophysical and structural signatures of syntectonic batholith construction: the South Mountain Batholith, Meguma Terrane, Nova Scotia. *International Geophysical Journal*, **136**, 144–58.

Bennett, R. H., Bryant, W. R. & Keller, G. H. 1981: Clay fabric of selected submarine sediments: Fundamental properties and models. *Journal of Sedimentary Petrology*, **51**, 217–32.

Bennett, R. H., O'Brien, N. R. & Hulbert, M. H. 1991: Determinants of clay and shale microfabric signatures: processes and mechanisms. *In* Bennett, R. H., Bryant, W. R. & Hulbert, M. H. (eds): *Microstructure of Fine-grained Sediments*. New York: Springer, pp. 5–32.

Berg, J. H. 1980: Snowflake troctolite in the Hettasch intrusion, Labrador: evidence for magma-mixing and supercooling in a plutonic environment. *Contributions to Mineralogy and Petrology*, **72**, 339–51.

Berger, A. & Roselle, G. 2001: Crystallization processes in migmatites. *American Mineralogist*, **86**, 215–24.

Berkebile, C. A. & Dowty, E. 1982: Nucleation in laboratory charges of basaltic composition. *American Mineralogist*, **67**, 886–99.

Berner, R. A. 1969: The synthesis of framboidal pyrite. *Economic Geology*, **64**, 383–4.

Berry, R. F. & Flint, R. B. 1988: Magmatic banding within Proterozoic granodiorite dykes near Streaky Bay, South Australia. *Transactions of the Royal Society of South Australia*, **112**, 63–73.

Berthé, D., Choukroune, P. & Jegouzo, P. 1979: Orthogneiss, mylonite and non-coaxial deformation of granites: the example from the South American shear zone. *Journal of Structural Geology*, **1**, 31–42.

2003: *Igneous and Metamorphic Petrology* (second edition). Malden, MA: Blackwell.

Bestmann, M. & Prior, D. J. 2003: Intragranular dynamic recrystallization in naturally deformed calcite marble: diffusion accommodated grain boundary sliding as a result of subgrain rotation recrystallization. *Journal of Structural Geology*, **25**, 1597–613.

Beutner, E. C. 1978: Slaty cleavage and related strain in Martinsburg Slate, Delaware Water Gap, New Jersey. *American Journal of Science*, **278**, 1–23.

Beutner, E. C. & Charles, E. G. 1985: Large volume loss during cleavage formation, Hamburg sequence, Pennsylvania. *Geology*, **13**, 803–5.

Bezzi, A. & Piccardo, G. B. 1971: Cumulus and skeletal olivine from ultramafic cumulates of the Ligurian ophiolites (Mattarana Quarry, Bracco Massif, Italy). *Estrato dagli Annali del Museo Civico di Storia Naturale di Genova*, **78**, 301–9.

Biermeier, C. & Stüwe, K. 2003: Strain rates from snowball garnet. *Journal of Metamorphic Geology*, **21**, 253–68.

Binns, R. A. 1966: Granitic intrusions and regional metamorphic rocks of Permian age from the Wongwibinda district, north-eastern New South Wales. *Journal and Proceedings of the Royal Society of New South Wales*, **99**, 5–36.

Bishop, G. H. & Chalmers, B. 1971: Dislocation structure and contrast in high angle grain boundaries. *Philosophical Magazine*, **24**, 515–26.

Blacic, J. D. 1972: Effect of water on the experimental deformation of olivine. *In* Heard, H. C., Borg, I. Y., Carter, N. L. & Raleigh, C. B. (eds): *Flow and Fracture of Rocks. Geophysical Monograph Series*, **16**, 109–15.

1975: Plastic deformation mechanisms in quartz: the effect of water. *Tectonophysics*, **27**, 271–94.

Blacic, J. D. & Christie, J. M. 1984: Plasticity and hydrolytic weakening of quartz single crystals. *Journal of Geophysical Research*, **89**, 4223–39.

Blackerby, B. A. 1968: Convolute zoning of plagioclase phenocrysts in Miocene volcanics from the western Santa Monica Mountains, California. *American Mineralogist*, **53**, 954–62.

Blake, D. H. 1981: Intrusive felsic-mafic net-veined complexes in north Queensland. *BMR Journal of Australian Geology and Geophysics*, **6**, 95–9.

Blake, D. H., Elwell, R. W. D., Gibson, I. L., Skelhorn, R. R. & Walker, G. P. L. 1965: Some relationships resulting from the intimate association of acid and basic magmas. *Quarterly Journal of the Geological Society of London*, **121**, 31–50.

Blatt, H., Middleton, G. & Murray, R. 1972: *Origin of Sedimentary Rocks*. Englewood Cliffs, NJ: Prentice-Hall.

Blenkinsop, T. G. 2000: *Deformation Microstructures and Mechanisms in Minerals and Rocks.* Dordrecht: Kluwer.

Blenkinsop, T. G. & Drury, M. R. 1988: Stress estimates and fault history from quartz microstructures. *Journal of Structural Geology*, **10**, 673–84.

Bloomer, S. H. & Hawkins, J. W. 1987: Petrology and geochemistry of boninite series volcanic rocks from the Mariana trench. *Contributions to Mineralogy and Petrology*, **97**, 361–77.

Blumenfeld, P. 1983: Le "tuilage des mégacristaux," un critère d'écoulement rotationnel pour les fluidités des roches magmatiques: application au granite de Barbey-Séroux (Vosges, France). *Bulletin de la Societé géologique de France*, **25**, 309–18.

Blumenfeld, P. & Bouchez, J.-L. 1988: Shear criteria in granite and migmatite deformed in the magmatic and solid states. *Journal of Structural Geology*, **10**, 361–72.

Blumenfeld, P., Mainprice, D. & Bouchez, J.-L. 1986: *C*-slip in quartz from subsolidus deformed granite. *Tectonophysics*, **127**, 97–115.

Blumenfeld, P. & Wilson, C. J. L. 1991: Boundary migration and kinking in stressed naphthalene. *Journal of Structural Geology*, **13**, 471–83.

Blundy, J. & Cahsman, K. 2001: Ascent-driven crystallisation of dacite magmas at Mount St Helens, 1980–1986. *Contributions to Mineralogy and Petrology*, **140**, 631–50.

Boggs, S. 1992: *Petrology of Sedimentary Rocks*. New York: Macmillan.

Boistelle, R. & Astier, J. P. 1988: Crystallization mechanisms in solution. *Journal of Crystal Growth*, **90**, 14–30.

Boland, J. N. & Fitz Gerald, J. D. (eds) 1993: *Defects and Processes in the Solid State: Geoscience Applications. The McLaren Volume.* Amsterdam: Elsevier.

Boland, J. N., McLaren, A. C. & Hobbs, B. E. 1971: Dislocations associated with optical features in naturally deformed olivine. *Contributions to Mineralogy and Petrology*, **30**, 53–63.

Boland, J. N. & van Roermund, H. L. M. 1983: Mechanisms of exsolution in omphacites from high temperature, type B, eclogites. *Physics and Chemistry of Minerals*, **9**, 30–7.

Bons, P. D. & Cox, S. J. D. 1994: Analogue experiments and numerical modelling on the relation between microgeometry and flow properties of polyphase materials. *Materials Science and Engineering*, **A175**, 237–45.

Bons, P. D. & den Brok, B. 2000: Crystallographic preferred orientation development by dissolution–precipitation creep. *Journal of Structural Geology*, **22**, 1713–22.

Bons, P. D. & Jessell, M. W. 1999: Micro-shear zones in experimentally deformed octachloropropane. *Journal of Structural Geology*, **21**, 323–34.

Bons, P. D., Jessell, M. W. & Passchier, C. W. 1993: The analysis of progressive deformation in rock analogues. *Journal of Structural Geology*, **15**, 403–12.

Bons, P. D. & Urai, J. L. 1992: Syndeformational grain growth: microstructures and kinetics. *Journal of Structural Geology*, **14**, 1101–9.

1994: Experimental deformation of two-phase rock analogues. *Materials Science and Engineering*, **A175**, 221–230.

Booth, B. 1968: Petrogenetic significance of alkali feldspar megacrysts and their inclusions in Cornubian granites. *Nature*, **217**, 1036–8.

Borchert, H. 1934: Über Entmischungen im System Cu-Fe-S und ihre Bedeutung als Geologische Thermometer. *Chemie der Erde*, **9**, 145–72.

Borg, I. Y. & Heard, H. C. 1970: Experimental deformation of plagioclases. *In* Paulitsch, P. (ed.) *Experimental and Natural Rock Deformation*. Berlin: Springer, pp. 375–403.

Borradaile, G. J. 1981: Particulate flow of rocks and the formation of cleavage. *Tectonophysics*, **72**, 305–21.

Borradaile, G. J., Bayly, M. B. & Powell, C. McA. (eds) 1982: *Atlas of Deformational and Metamorphic Rock Fabrics*. Berlin: Springer.

Bosworth, T. O. 1910: Metamorphism around the Ross of Mull Granite. *Quarterly Journal of the Geological Society of London*, **66**, 376–96.

Bosworth, W. 1981: Strain-induced preferential dissolution of halite. *Tectonophysics*, **78**, 509–25.

Bottinga, Y., Kudo, A. & Weill, D. 1966: Some observations on oscillatory zoning and crystallization of magmatic plagioclase. *American Mineralogist*, **51**, 792–806.

Bouchez, J.-L., Delas, C., Gleizes, G., Nedelec, A. & Cuney, M. 1992: Submagmatic microfractures in granites. *Geology*, **20**, 35–8.

Boudier, F. & Nicolas, A. 1982a: Peridotite microtextures (I): oceanic environments. *In* Borradaile, G. J., Bayly, M. B. & Powell, C. McA. (eds): *Atlas of Deformational and Metamorphic Rock Fabrics*. Berlin: Springer, pp. 384–5.

1982b: Peridotite microtextures (II): in tectonites from ultramafic sequences in ophiolites. *In* Borradaile, G. J., Bayly, M. B. & Powell, C. McA. (eds): *Atlas of Deformational and Metamorphic Rock Fabrics*. Berlin: Springer, pp. 386–8.

Boullier, A. M. & Bouchez, J.-L. 1978: Le quartz en rubans dans les mylonites. *Bulletin de la Société géologique de France*, **7**, 253–62.

Boullier, A. M. & Guegen, Y. 1975: SP mylonites: origin of some mylonites by superplastic flow. *Contributions to Mineralogy and Petrology*, **50**, 93–104.

Boullier, A. M. & Nicolas, A. 1975: Classification of textures and fabrics of peridotite xenoliths from South African kimberlites. *Physics and Chemistry of the Earth*, **9**, 467–76.

Boulter, C. A. 1974: Tectonic deformation of soft sedimentary clastic dikes from the Precambrian rocks of Tasmania, Australia, with particular reference to their relations with cleavages. *Bulletin of the Geological Society of America*, **85**, 1413–20.

Boundy, T. M., Donohue, C. L., Essene, E. J., Mezger, K. & Austrheim, H. 2002: Discovery of eclogite facies carbonate rocks from the Lindas Nappe, Caledonides, Western Norway. *Journal of Metamorphic Geology*, **20**, 649–67.

Boundy, T. M., Fountain, D. M. & Austrheim, H. 1992: Structural development and petrofabrics of eclogite facies shear zones, Bergen Arcs, Western Norway: implication for deep crustal deformational processes. *Journal of Metamorphic Geology*, **10**, 127–46.

Boyle, A. P., Prior, D. J., Banham, M. H. & Timms, N. E. 1998: Plastic deformation of metamorphic pyrite: new evidence from electron-backscatter diffraction and forescatter orientation-contrast imaging. *Mineralium Deposita*, **34**, 71–81.

Boyer, S. E. 1984: Origin and significance of compositional layering in Late Precambrian sediments, Blue Ridge Province, North Carolina, USA. *Journal of Structural Geolog*y, **6**, 121–33.

Bozhilov, K. N., Green, H. W. & Dobrzhinetskaya, L. F. 2003: Quantitative 3D measurement of ilmenite abundance in Alpe Arami olivine by confocal microscopy: Confirmation of high-pressure origin. *American Mineralogist*, **88**, 596–603.

Bragg, W. L. 1937: *Atomic Structure of Minerals.* Ithaca, NY: Cornell University Press.

Brantley, S. L., Evans, B., Hickman, S. H. & Crerar, D. A. 1990: Healing of microcracks in quartz: implications for fluid flow. *Geology*, **18**, 136–9.

Brearley, A. J. 1987: A natural example of the disequilibrium breakdown of biotite at high temperature – TEM observations and comparison with experimental kinetic data. *Mineralogical Magazine*, **51**, 93–101.

Brett, R. 1964: Experimental data from the system Cu-Fe-S and their bearing on exsolution textures in ores. *Economic Geology*, **59**, 1241–69.

Brett, R. & Kullerud, G. 1967: The Fe-Pb-S system. *Economic Geology*, **62**, 354–69.

Bridgwater, D., Escher, A. & Watterson, J. 1973a: Tectonic displacements and thermal activity in two contrasting Proterozoic mobile belts from Greenland. *Philosophical Transactions of the Royal Society of London*, **A273**, 493–512.

Bridgwater, D., Watson, J. & Windley, B. F. 1973b: The Archaean craton of the North Atlantic region. *Philosophical Transactions of the Royal Society of London*, **A273**, 513–33.

Brigham, R. H. 1984: *K-feldspar Genesis and Stable Isotope Relations of the Papoose Flat Pluton, Inyo Mountains, California.* Ph.D. thesis, Stanford University.

Brodie, K. H. 1981: Variation in amphibole and plagioclase composition with deformation. *Tectonophysics*, **78**, 385–402.

1995: The development of orientated symplectites during deformation. *Journal of Metamorphic Geology*, **13**, 499–508.

Brodie, K. H., Fettes, D., Harte, B. & Schmid, R. 2002: Towards a unified nomenclature in metamorphic petrology. Structural terms, including fault rocks. A proposal on behalf of the IUGS Subcommission on the Systematics of Metamorphic Rocks. Provisional recommendations; web version of 31 October, 2002. http://www.bgs.ac.uk/SCMR/scmr_products.html

Brodie, K. H. & Rutter, E. H. 1985: On the relationship between deformation and metamorphism with special reference to the behaviour of basic rocks. *In* Thompson, A. B. & Rubie, D. C. (eds): *Kinetics, Textures and Deformation. Advances in Physical Geochemistry*, **4**, 138–79. New York: Springer.

Brophy, J. H., Rose, M. & Wulff, J. 1964: *The Structure and Properties of Materials*. Volume II. *Thermodynamics of Structure*. New York: Wiley.

Brown, E. H. 1996: High-pressure metamorphism caused by magma loading in Fiordland, New Zealand. *Journal of Metamorphic Geology*, **14**, 441–52.

Brown, M. 1998: Unpairing metamorphic belts; *P-T* paths and a tectonic model for the Ryoke Belt, southwest Japan. *Journal of Metamorphic Geology*, **16**, 3–22.

2001: Orogeny, migmatites and leucogranites: A review. *Proceedings of the Indian Academy of Sciences (Earth and Planetary Science)*, **110**, 313–36.

2002: Retrograde processes in migmatites and granulites revisited. *Journal of Metamorphic Geology*, **20**, 25–40.

Brown, M., Averkin, Y. A., McLellan, E. L. & Sawyer, E. W. 1995: Melt segregation in migmatites. *Journal of Geophysical Research*, **100**, 15 655–79.

Brown, M. & Rushmer, T. 1997: The role of deformation in the movement of granitic melt: views from the laboratory and the field. *In* Holness, M. B. (ed.): *Deformation-enhanced Fluid Transport in the Earth's Crust and Mantle. Mineralogical Society Series*, **8**. London: Chapman and Hall, pp. 111–14.

Brown, M. A., Brown, M., Carlson, W. D. & Denison, C. 1999: Topology of syntectonic melt-flow networks in the deep crust: inferences from three-dimensional images of leucosome geometry in migmatites. *American Mineralogist*, **84**, 1793–818.

Brown, W. L. & Parsons, I. 1989: Alkali feldspars: ordering rates, phase transformations and behaviour diagrams for igneous rocks. *Mineralogical Magazine*, **53**, 25–42.

Brückner, R. 1983: Structure and properties of silicate melts. *Bulletin de Minéralogie*, **106**, 9–22.

Bryan, W. B. 1972: Morphology of crystals in submarine basalts. *Journal of Geophysical Research*, **77**, 5812–19.

Bucher, K. & Frey, M. 1994: *Petrogenesis of Metamorphic Rocks*. Berlin: Springer.

Buckley, H. E. 1961: *Crystal Growth.* New York: Wiley.

Buczynski, C. & Chafetz, H. S. 1987: Siliciclastic grain breakage and displacement due to carbonate crystal growth: An example from the Lueders Formation (Permian) of north-central Texas, U.S.A. *Sedimentology*, **34**, 837–43.

Budworth, D. W. 1970: The selection of grain-growth control additives for the sintering of ceramics. *Mineralogical Magazine*, **37**, 833–8.

Buerger, M. J. 1945: The genesis of twin crystals. *American Mineralogist*, **30**, 469–82.

1947: The relative importance of the several faces of a crystal. *American Mineralogist*, **32**, 593–606.

Buerger, M. J. & Washken, E. 1947: Metamorphism of minerals. *American Mineralogist*, **32**, 296–308.

Buntebarth, G. & Voll, G. 1991: Quartz grain coarsening by collective crystallization in contact quartzites. *In* Voll, G., Töpel, J., Pattison, D. R. M. & Seifert, F. (eds): *Equilibrium and Kinetics in Contact Metamorphism*. Berlin: Springer, pp. 251–65.

Burg, J.-P., Wilson, C. J. L. & Mitchell, J. C. 1986: Dynamic recrystallization and fabric development during simple shear deformation of ice. *Journal of Structural Geology*, **8**, 857–70.

Burkhard, M. 1993: Calcite twins, their geometry, appearance and significance as stress-strain markers and indicators of tectonic regime: a review. *Journal of Structural Geology*, **15**, 351–68.

Burton, K. W. 1986: Garnet-quartz intergrowths in graphitic pelites: the role of the fluid phase. *Mineralogical Magazine*, **50**, 611–20.

Busa, M. D. & Gray, N. H. 1991: Rotated staurolite porphyroblasts in the Littleton Schist at Bolton, Connecticut, USA. *Journal of Metamorphic Geology*, **10**, 627–36.

Büsch, W., Schneider, G. & Mehnert, K. R. 1974: Initial melting at grain boundaries. Part II: melting of rocks of granodioritic, quartzdioritic and tonalitic composition. *Neues Jahrbuch für Mineralogie Abhandlungen*, **133**, 345–70.

Busch, J. P. & van der Pluijm, B. A. 1995: Calcite textures, microstructures and rheological properties of marble mylonites in the Bancroft shear zone, Ontario, Canada. *Journal of Structural Geology*, **17**, 677–88.

Butler, B. C. M. 1965: A chemical study of some rocks of the Moine Series of Scotland. *Quarterly Journal of the Geological Society of London*, **121**, 163–208.

Büttner, S. H. 1999: The geometric evolution of structures during continuous deformation from magmatic to solid-state conditions: An example from the central European Variscan Belt. *American Mineralogist*, **84**, 1781–92.

Byron, D. N., Atherton, M. P., Cheadle, M. J. & Hunter, R. H. 1996: Melt movement and occlusion or porosity in crystallizing granitic systems. *Mineralogical Magazine*, **60**, 163–71.

Byron, D. N., Atherton, M. P. & Hunter, R. H. 1994: The description of the primary textures of Cordilleran granitic rocks. *Contributions to Mineralogy and Petrology*, **117**, 66–75.

1995: The interpretation of granitic textures from serial thin sectioning, image analysis and three-dimensional reconstruction. *Mineralogical Magazine*, **59**, 203–11.

Cabane, H., Laporte, D. & Provost, A. 2001: Experimental investigation of the kinetics of Ostwald ripening of quartz in silicic melts. *Contributions to Mineralogy and Petrology*, **142**, 361–73.

Cahn, R. W. 1970: *Physical Metallurgy.* Amsterdam: North-Holland.

1983: Recovery and recrystallization. *In* Cahn, R. W. & Haasen, P. (eds): *Physical Metallurgy*. Amsterdam: North-Holland, pp. 1595–676.

Camacho, A., McDougall, I., Armstrong, R. & Braun, J. 2001: Evidence for shear heating, Musgrave Block, central Australia. *Journal of Structural Geology*, **23**, 1007–13.

Camacho, A., Vernon, R. H. & FitzGerald, J. D. 1995: Large volumes of pseudotachylyte in the Woodroffe Thrust, eastern Musgrave Ranges, Australia. *Journal of Structural Geology*, **17**, 371–83.

Cameron, E. M. 1961: *Ore Microscopy*. New York: Wiley.

Campbell, I. H. 1978: Some problems with the cumulus theory. *Lithos*, **11**, 311–23.

1987: Distribution of orthocumulate textures in the Jimberlana intrusion. *Journal of Geology*, **95**, 35–54.

Candela, P. A. 1997: A review of shallow, ore-related granites: textures, volatiles, and ore metals. *Journal of Petrology*, **38**, 1619–33.

Candela, P. A. & Blevin, P. L. 1995: Do some miarolitic granites preserve evidence of magmatic volatile phase permeability? *Economic Geology*, **90**, 2310–16.

Cantagrel, J.-M., Didier, J. & Gourgaud, A. 1984: Magma mixing: origin of intermediate rocks and "enclaves" from volcanism to plutonism. *Physics of the Earth and Planetary Interiors*, **35**, 63–76.

Cardenas, A. A., Girty, G. H., Hanson, A. D., Lahren, M. M., Knaack, C. & Johnson, D. 1996: Assessing differences in composition between low metamorphic grade mudstones and high-grade schists using logratio techniques. *Journal of Geology*, **104**, 279–93.

Carlson, W. D. 1989: The significance of intergranular diffusion to the mechanisms and kinetics of porphyroblast crystallization. *Contributions to Mineralogy and Petrology*, **103**, 1–24.

1991: Competitive diffusion-controlled growth of porphyroblasts. *Mineralogical Magazine*, **55**, 317–30.

1999: The case against Ostwald ripening of porphyroblasts. *Canadian Mineralogist*, **37**, 403–13.

2000: The case against Ostwald ripening of porphyroblasts: reply. *Canadian Mineralogist*, **38**, 1029–31.

2002: Scales of disequilibrium and rates of equilibration during metamorphism. *American Mineralogist*, **87**, 185–204.

Carlson, W. D. & Denison, C. 1992: Mechanisms of porphyroblast crystallization – results from high-resolution computed x-ray tomography. *Science*, **257**, 1236–9.

Carlson, W. D., Denison, C. & Ketcham, R. A. 1995: Controls on the nucleation and growth of porphyroblasts: kinetics from natural textures and numerical models. *Geological Journal*, **30**, 207–25.

1999: High-resolution x-ray computed tomography as a tool for visualization and quantitative analysis of igneous textures in three dimensions. *Electronic Geosciences*, **4:3**.

Carmichael, D. M. 1969: On the mechanism of prograde metamorphic reactions in quartz-bearing pelitic rocks. *Contributions to Mineralogy and Petrology*, **20**, 244–67.

Carney, J. N., Treloar, P. J., Barton, C. M., Crow, M. J., Evans, J. A. & Simango, S. 1991: Deep-crustal granulites with migmatitic and mylonitic fabrics from the Zambezi Belt, northeastern Zimbabwe. *Journal of Metamorphic Geology*, **9**, 461–79.

Caroff, M., Maury, R. C., Cotten, J. & Clément, J.-P. 2000: Segregation structures and vapor-differentiated basaltic flows. *Bulletin of Volcanology*, **62**, 171–87.

Carozzi, A. V. 1960: *Microscopic Sedimentary Petrography*. New York: Wiley.

Carstens, H. 1969: Dislocation structures in pyropes from Norwegian and Czech garnet peridotites. *Contributions to Mineralogy and Petrology*, **24**, 348–53.

1971: Plastic stress relaxation around solid inclusions in pyrope. *Contributions to Mineralogy and Petrology*, **32**, 289–94.

1975: Thermal history of impact melt rocks in the Fennoscandian shield. *Contributions to Mineralogy and Petrology*, **50**, 145–55.

1983: Simultaneous crystallization of quartz-feldspar intergrowths from granitic magmas. *Geology*, **11**, 339–41.

Carswell, D. A., Möller, C. & O'Brien, P. J. 1989: Origin of sapphirine-plagioclase symplectites in metabasites from Mitterbachgraben, Dunkelsteinerwald granulite complex, Lower Austria. *European Journal of Mineralogy*, **1**, 455–66.

Carter, N. L. 1971: Static deformation of silica and silicates. *Journal of Geophysical Research*, **76**, 5514–40.

Carter, N. L. & Ave'Lallemant, H. G. 1970: High temperature flow of dunite and peridotite. *Bulletin of the Geological Society of America*, **81**, 2181–202.

Carter, N. L., Christie, J. M., & Griggs, D. T. 1964: Experimental deformation and recrystallization of quartz. *Journal of Geology*, **72**, 687–733.

Carter, N. L. & Hansen, F. D. 1983: Creep of rock-salt. *Tectonophysics*, **92**, 275–333.

Carter, N. L., Kronenberg, A. K., Ross, J. V. & Wiltschko, D. V. 1990: Control of fluids on deformation of rocks. *In* Knipe, R. J. & Rutter, E. H. (eds): *Deformation Mechanisms, Rheology and Tectonics. Geological Society of London Special Publication*, **54**, 1–13.

Cartwright, I., Power, W. L., Oliver, N. H. S., Valenta, R. K. & McLatchie, G. S. 1994: Fluid migration and vein formation during deformation and greenschist facies metamorphism at Ormiston Gorge, central Australia. *Journal of Metamorphic Geology*, **12**, 373–86.

Cashman, K. V. 1988: Crystallization of Mount St. Helens 1980–1986 dacite: a quantitative textural approach. *Bulletin Volcanologique*, **50**, 194–209.

1990: Textural constrains on the kinetics of crystallization of igneous rocks. *In* Nicholls, J. & Russell, J. K. (eds): *Modern Methods of Igneous Petrology: Understanding Magmatic Processes. Mineralogical Society of America, Reviews in Mineralogy*, **24**, 259–314.

Cashman, K. V. & Ferry, J. M. 1988: Crystal size distribution (CSD) in rocks and the kinetics and dynamics of crystallization III. Metamorphic crystallization. *Contributions to Mineralogy and Petrology*, **99**, 410–15.

Cashman, K. V. & Mangan, M. T. 1994: Physical aspects of magmatic degassing II. Constraints on vesiculation processes from textural studies of eruptive products. *In* Carroll, M. R. & Holloway, J. R. (eds): *Volatiles in Magmas. Mineralogical Society of America, Reviews in Mineralogy*, **30**, 447–78.

Cashman, K. V. & Marsh, B. D. 1988: Crystal size distribution (CSD) in rocks and the kinetics and dynamics of crystallization II. Makaopuhi lava lake. *Contributions to Mineralogy and Petrology*, **99**, 292–305.

Castro, J. M., Cashman, K. V. & Manga, M. 2003: A technique for measuring 3D crystal-size distributions of prismatic microlites in obsidian. *American Mineralogist*, **88**, 1230–40.

Cesare, B., Gómez-Pugnaire, M. T., Sánchez-Navas, A. & Grobety, B. 2002a: Andalusite-sillimanite replacement (Mazarrón, SE Spain): A microstructural and TEM study. *American Mineralogist*, **87**, 433–44.

Cesare, B. & Maineri, C. 1999: Fluid-present anatexis of metapelites at El Joyazo (SE Spain): constraints from Raman spectroscopy of graphite. *Contributions to Mineralogy and Petrology*, **135**, 41–52.

Cesare, B., Marchesi, C. & Connolly, J. A. D. 2002b: Growth of myrmekite coronas by contact metamorphism of granitic mylonites in the aureole of Cima di Vila, Eastern Alps, Italy. *Journal of Metamorphic Geology*, **20**, 203–13.

Cesare, B., Marchesi, C., Hermann, J. & Gómez-Pugnaire, M. T. 2003: Primary melt inclusions in andalusite from anatectic graphitic metapelites: Implications for the position of the Al_2SiO_5 triple point. *Geology*, **31**, 573–6.

Chalmers, A. F. 1999: *What Is this Thing called Science?* St Lucia, Queensland, Australia: University of Queensland Press.

Chalmers, B. 1959: *Physical Metallurgy*. New York: Wiley.

Chamberlain, T. C. 1890: The method of multiple working hypotheses. *Science*, **15**, 92–6.

Champness, P. E. 1977: Transmission electron microscopy in earth science. *Annual Reviews of Earth and Planetary Science*, **5**, 203–26.

Champness, P. E. & Lorimer, G. W. 1976: Exsolution in silicates. *In* Wenk, H.-R. *et al.* (eds): *Electron Microscopy in Mineralogy*. Berlin: Springer, pp. 257–65.

Chan, Y.-C. & Crespi, J. M. 1999: Albite porphyroblasts with sigmoidal inclusion trails and their kinematic implications: an example from the Taconic Allochthon, west-central Vermont. *Journal of Structural Geology*, **21**, 1407–17.

Chao, E. C. T. 1976: The application of quantitative interference microscopy to mineralogic and petrologic investigations. *American Mineralogist*, **61**, 212–28.

Chappell, B. W. & White, A. J. R. 1991: Restite enclaves and the restite model. *In* Barbarin, M. B. & Didier, J. (eds): *Enclaves and Granite Petrology*. Amsterdam: Elsevier, pp. 375–81.

Chen, T. T. 1978: Colloform and framboidal pyrite from the Caribou deposit, New Brunswick. *Canadian Mineralogist*, **16**, 9–15.

Chernoff, C. B. & Carlson, W. D. 1997: Disequilibrium for Ca during growth of pelitic garnet. *Journal of Metamorphic Geology*, **15**, 421–38.

1999: Trace element zoning as a record of chemical disequilibrium during garnet growth. *Geology*, **27**, 555–8.

Chester, F. M. & Logan, J. M. 1987: Composite planar fabric of gouge from the Punchbowl Fault, California. *Journal of Structural Geology*, **9**, 621–34.

Chinner, G. A. 1961: The origin of sillimanite in Glen Clova, Angus. *Journal of Petrology*, **2**, 312–23.

Chopra, P. N. & Paterson, M. S. 1981: The experimental deformation of dunite. *Tectonophysics*, **78**, 453–73.

Choukroune, P. & Gapais, D. 1983: Strain pattern in the Aar Granite (Central Alps): orthogneiss developed by bulk inhomogeneous flattening. *Journal of Structural Geology*, **5**, 411–18.

Choukroune, P., Gapais, D. & Merle, O. 1987: Shear criteria and structural symmetry. *Journal of Structural Geology*, **9**, 525–30.

Christie, J. M. 1960: Mylonitic rocks of the Moine thrust zone in the Assynt region, northwest Scotland. *Transactions of the Edinburgh Geological Society*, **18**, 79–93.

1963: The Moine thrust zone in the Assynt region, northwest Scotland. *University of California Publications in Geological Sciences*, **40**, 345–419.

Christie, J. M., Griggs, D. T. & Carter, N. L. 1964: Experimental evidence of basal slip in quartz. *Journal of Geology*, **72**, 734–56.

Christoffersen, R. & Kronenberg, A. K. 1993: Dislocation interactions in experimentally deformed biotite. *Journal of Structural Geology*, **15**, 1077–95.

Cihan, M. 2002: The pitfalls of sectioning rocks perpendicular to foliations and lineations in the matrix. *Geological Society of Australia Abstracts*, **67**, 162.

Clark, A. H., Pearce, T. H., Roeder, P. L. & Wolfson, I. 1986: Oscillatory zoning and other microstructures in magmatic olivine and augite: Nomarski interference contrast observations on etched polished surfaces. *American Mineralogist*, **71**, 734–41.

Clark, B. R. & Kelly, W. C. 1973: Sulfide deformation studies: I. Experimental deformation of pyrrhotite and sphalerite to 2000 bars and 500°C. *Economic Geology*, **68**, 332–52.

Clark, B. R., Price, F. R. & Kelly, W. C. 1977: Effects of annealing on deformation textures in galena. *Contributions to Mineralogy and Petrology*, **64**, 149–65.

Clark, M. B. & Fisher, D. M. 1995: Strain partitioning and crack-seal growth of chlorite-muscovite aggregates during progressive noncoaxial strain: an example from the slate belt of Taiwan. *Journal of Structural Geology*, **17**, 461–74.

Clarke, D. B. 1992: *Granitoid Rocks*. London: Chapman & Hall.

Clarke, D. B. & Clarke, G. K. C. 1998: Layered granodiorites at Chebutco Head, South Mountain batholith, Nova Scotia. *Journal of Structural Geology*, **20**, 1305–24.

Clarke, G. L., Daczko, N. R. & Nockolds, C. 2001: A method for applying matrix corrections to X-ray intensity maps using the Bence-Albee algorithm and Matlab. *Journal of Metamorphic Geology*, **19**, 635–44.

Clarke, G. L., Powell, R. & Vernon, R. H. 1995: Reaction relationships during retrograde metamorphism at Olary, South Australia. *Journal of Metamorphic Geology*, **13**, 715–26.

Clechenko, C. C. & Valley, J. W. 2003: Oscillatory zoning in garnet from the Willsboro wollastonite skarn, Adirondack Mts, New York: a record of shallow hydrothermal processes preserved in a granulite facies terrane. *Journal of Metamorphic Geology*, **21**, 771–84.

Clemens, J. D. & Holness, M. B. 2000: Textural evolution and partial melting of arkose in a contact aureole: a case study and implications. *Electronic Geosciences*, **5:4**.

Clemens, J. D. & Wall, V. J. 1981: Origin and crystallization of some peraluminous (S-type) granitic magmas. *Canadian Mineralogist*, **19**, 111–31.

Cloos, E. 1936: Der Sierra Nevada Pluton in Californien. *Neues Jahrbuch für Mineralogie, Geologie und Paläontologie Abhandlungen*, **76(B)**, 355–450.

Cobbold, P. R. 1977: Description and origin of banded deformation structures. I. Regional strain, local perturbations, and deformation bands. *Canadian Journal of Earth Sciences*, **14**, 1721–31.

Coble, R. L. & Burke, J. E. 1963: Sintering in ceramics. *Progress in Ceramic Science*, **4**, 197–251.

Collins, W. J. 2002: Hot orogens, tectonic switching, and creation of continental crust. *Geology*, **30**, 535–8.

Collins, W. J., Flood, R. H., Vernon, R. H. & Shaw, S. E. 1989: The Wuluma granite, Arunta block, central Australia: An example of in situ, near-isochemical granite formation in a granulite-facies terrane. *Lithos*, **23**, 63–83.

Collins, W. J. & Sawyer, E. 1996: Pervasive granitoid magma transfer through the lower-middle crust during non-coaxial compressional deformation. *Journal of Metamorphic Geology*, **14**, 565–79.

Collins, W. J. & Teyssier, C. 1989: Crustal scale ductile fault systems in the Arunta Inlier, central Australia. *Tectonophysics*, **158**, 49–66.

Collins, W. J. & Vernon, R. H. 1991: Orogeny associated with anticlockwise P-T-t paths: evidence from low-P, high-T metamorphic terranes in the Arunta Inlier, central Australia. *Geology*, **19**, 835–8.

Collins, W. J., Vernon, R. H. & Clarke, G. L. 1991: Discrete Proterozoic structural terranes associated with low-P, high-T metamorphism, Anmatjira Range, Arunta Inlier, central Australia: tectonic implications. *Journal of Structural Geology*, **13**, 1157–71.

Collins, W. J. & Wiebe, R. A. 1998: Depositional features and stratigraphic sections in granitic plutons: implications for the emplacement and crystallisation of granitic magmas. *Journal of Structural Geology*, **20**, 1273–89.

Connolly, J. A. D. 1997: Devolatilization-generated fluid pressure and deformation-propagated fluid flow during prograde regional metamorphism. *Journal of Geophysical Research*, **102**, 18149–73.

Connolly, J. A. D., Holness, M. B., Rubie, D. C. & Rushmer, T. 1997: Reaction-induced microcracking; an experimental investigation of a mechanism for enhancing anatectic melt extraction. *Geology*, **25**, 591–4.

Coombs, D. S. 1954: The nature and alteration of some Triassic sediments from Southland, New Zealand. *Transactions of the Geological Society of New Zealand*, **82**, 65–109.

Cooper, R. F. & Kohlstedt, D. L. 1984: Sintering of olivine and olivine-basalt aggregates. *Physics and Chemistry of Minerals*, **11**, 5–16.

Corbett, C. G. & Phillips, G. N. 1981: Regional retrograde metamorphism of a high grade terrain: the Willyama Complex, Broken Hill, Australia. *Lithos*, **14**, 59–73.

Corrigan, G. M. 1982: The crystal morphology of plagioclase feldspar produced during isothermal supercooling and constant rate cooling experiments. *Mineralogical Magazine*, **46**, 433–9.

Cosgrove, J. W. 1976: The formation of crenulation cleavage. *Journal of the Geological Society of London*, **132**, 155–78.

Cottrell, A. 1975: *An Introduction to Metallurgy* (second edition). London: Edward Arnold.

Couderc, J.-J. & Hennig-Michaeli, C. 1989: TEM study of mechanical twinning in experimentally deformed chalcopyrite ($CuFeS_2$) single crystals, Part I: (112) deformation twins. *European Journal of Mineralogy*, **1**, 275–93.

Covey-Crump, S. J. & Rutter, E. H. 1989: Thermally induced grain growth of calcite marbles on Naxos Island, Greece. *Contributions to Mineralogy and Petrology*, **101**, 69–86.

Cox, R. A., Dempster, T. J., Bell, B. R. & Rogers, G. 1996: Crystallization of the Shap Granite: evidence from zoned K-feldspar megacrysts. *Journal of the Geological Society of London*, **153**, 625–35.

Cox, S. F. 1986: High-temperature creep of single crystal galena (PbS). *In* Hobbs, B. E. & Heard, H. C. (eds): *Mineral and Rock Deformation: Laboratory Studies (The Paterson Volume). American Geophysical Union, Geophysical Monograph*, **36**, 73–98.

1987a: Flow mechanisms in sulphide minerals. *Ore Geology Reviews*, **2**, 133–71.

1987b: Antitaxial crack-seal vein microstructures and their relationship to displacement paths. *Journal of Structural Geology*, **9**, 779–87.

Cox, S. F. & Etheridge, M. A. 1982: Fiber development in deformed hydrothermally altered acid volcanic rock. *In* Borradaile, G. J., Bayly, M. B. & Powell, C. McA. (eds): *Atlas of Deformational and Metamorphic Rock Fabrics*. New York: Springer, pp. 304–5.

1983: Crack-seal fibre growth mechanisms and their significance in the development of oriented layer silicate microstructures. *Tectonophysics*, **92**, 147–70.

1984: Deformation microfabric development in chalcopyrite in fault zones. Mt. Lyell, Tasmania. *Journal of Structural Geology*, **6**, 167–82.

Cox, S. F., Etheridge, M. A. & Hobbs, B. E. 1981: The experimental deformation of polycrystalline and single crystal pyrite. *Economic Geology*, **76**, 2105–17.

Craig, J. R. 1990a: Textures of the ore minerals. *In* Jambor, J. L. & Vaughan, D. J. (eds): *Advanced Microscopic Studies of Ore Minerals. Mineralogical Association of Canada Short Course*, **17**, 213–61.

1990b: Ore textures and paragenetic studies – some modern case histories and sources of comparative data. *In* Jambor, J. L. & Vaughan, D. J. (eds): *Advanced Microscopic Studies of Ore Minerals. Mineralogical Association of Canada Short Course*, **17**, 263–317.

Craig, J. R. & Vaughan, D. J. 1994: *Ore Microscopy and Ore Petrography* (second edition). New York: Wiley.

Craig, J. R., Vokes, F. M. & Simpson, C. 1991: Rotational fabrics in pyrite from Ducktown, Tennessee. *Economic Geology*, **86**, 1737–46.

Cross, W. 1891: Constitution and origin of spherulites in acid eruptive rocks. *Bulletin of the Philosophical Society of Washington*, **11**, 411–44.

Crowley, J. L., Ghent, E. D., Carr, S. D., Simony, P. S. & Hamilton, M. A. 2000: Multiple thermotectonic events in a continuous metamorphic sequence, Mica Creek area, southeastern Canadian Cordillera. *Geological Materials Research*, **2**(6), 45pp.

Cumbest, R. J., Drury, M. R., van Roermund, H. L. M. & Simpson, C. 1989: Dynamic recrystallization and chemical evolution of clinoamphibole from Senja, Norway. *Contributions to Mineralogy and Petrology*, **101**, 339–49.

Czamanske, G. K. & Moore, J. G. 1977: Composition and phase chemistry of sulfide globules in basalt from the Mid-Atlantic Ridge rift valley near 37°N lat. *Bulletin of the Geological Society of America*, **88**, 587–99.

Daczko, N. R., Clarke, G. L. & Klepeis, K. A. 2002a: Kyanite-paragonite-bearing assemblages, northern Fiordland, New Zealand: rapid cooling of the lower crustal root to a Cretaceous magmatic arc. *Journal of Metamorphic Geology*, **20**, 887–902.

Daczko, N. R., Stevenson, J. A., Clarke, G. L. & Klepeis, K. A. 2002b: Successive hydration and dehydration of high-*P* mafic granofels involving clinopyroxene-kyanite symplectites, Mt Daniel, Fiordland, New Zealand. *Journal of Metamorphic Geology*, **20**, 669–82.

Daines, M. J. & Kohlstedt, D. L. 1997: Influence of deformation on melt topology in peridotites. *Journal of Geophysical Research*, **102**, 10257–71.

Daniel, C. G. & Spear, F. S. 1998: 3-dimensional patterns of garnet nucleation and growth. *Geology*, **26**, 503–6.

1999: The clustered nucleation and growth processes of garnet in regional metamorphic rocks from north-west Connecticut, USA. *Journal of Metamorphic Geology*, **17**, 503–20.

Davidson, C., Rosenberg, C. L. & Schmid, S. M. 1996: Synmagmatic folding of the base of the Bergell pluton: evidence from the western contact. *Tectonophysics*, **78**, 585–600.

Davidson, C., Schmid, S. M. & Hollister, L. S. 1994: Role of melt during deformation in the deep crust. *Terra Nova*, **6**, 133–42.

Dawson, J. B. & Reid, A. M. 1970: A pyroxene-ilmenite intergrowth from the Monastery mine, South Africa. *Contributions to Mineralogy and Petrology*, **26**, 296–301.

Dawson, J. W. 1859: On the microscopic structure of some Canadian limestones. *Canadian Naturalist and Geologist*, **4**, 161–9.

De, A. 1974: Silicate liquid immiscibility in the Deccan traps and its petrogenetic significance. *Bulletin of the Geological Society of America*, **85**, 471–4.

Debat, P., Soula, J.-C., Kubin, L. & Vidal, J.-L. 1978: Optical studies of natural deformation microstructures in feldspars (gneiss and pegmatites from Occitania, southern France). *Lithos*, **11**, 133–45.

de Bresser, J. H. P., ter Heege, J. H. & Spiers, C. J. 2001: Grain size reduction by dynamic recrystallization: can it result in major rheological weakening? *International Journal of Earth Sciences (Geologische Rundschau)*, **90**, 28–45.

Deer, W. A., Howie, R. A. & Zussman, J. 1992: *An Introduction to the Rock-Forming Minerals* (second edition). Edinburgh: Longman.

de Haas, G.-J. L. M., Nijland, T. G., Valbracht, P. J., Maijer, C., Verschure, R. & Andersen, T. 2002: Magmatic versus metamorphic origin of olivine-plagioclase coronas. *Contributions to Mineralogy and Petrology*, **143**, 537–50.

Dell'Angelo, L. N. & Tullis, J. 1988: Experimental deformation of partially melted granite aggregates. *Journal of Metamorphic Geology*, **6**, 495–515.

1989: Fabric development in experimentally sheared quartzites. *Tectonophysics*, **169**, 1–22.

1996: Textural and mechanical evolution with progressive strain in experimentally deformed aplite. *Tectonophysics*, **256**, 57–82.

Dell'Angelo, L. N., Tullis, J. & Yund, R. A. 1987: Transition from dislocation creep to melt-enhanced diffusion creep in fine-grained granitic aggregates. *Tectonophysics*, **139**, 325–32.

Dempster, T. J. & Tanner, P. W. G. 1997: The biotite isograd, Central Pyrenees: a deformation-controlled reaction. *Journal of Metamorphic Geology*, **15**, 531–48.

den Brok, B. 1996: The effect of crystallographic orientation on pressure solution in quartzite. *Journal of Structural Geology*, **18**, 859–60.

den Brok, B., Zahid, M. & Passchier, C. W. 1998: Cataclastic solution creep of very soluble brittle salt as a rock analogue. *Earth and Planetary Science Letters*, **163**, 83–95.

den Brok, S. W. J. 1992: An experimental investigation into the effect of water on the flow of quartzite. *Geologica Utraiectina*, **95**, 1–178. Ph.D. thesis, University of Utrecht, The Netherlands.

1998: Effect of microcracking on pressure-solution strain rate: The Gratz grain-boundary model. *Geology*, **26**, 915–18.

den Brok, S. W. J. & Spiers, C. J. 1991: Experimental evidence for water weakening of quartzite by microcracking plus solution–precipitation creep. *Journal of the Geological Society of London*, **147**, 541–8.

Denison, C. & Carlson, W. D. 1997: Three-dimensional quantitative textural analysis of metamorphic rocks using high-resolution computed X-ray tomography: Part II. Application to natural samples. *Journal of Metamorphic Geology*, **15**, 45–57.

Denison, C., Carlson, W. D. & Ketcham, R. A. 1997: Three-dimensional quantitative textural analysis of metamorphic rocks using high-resolution computed X-ray tomography: Part I. Methods and techniques. *Journal of Metamorphic Geology*, **15**, 29–44.

den Tex, E. 1963: A commentary on the correlation of metamorphism and deformation in space and time. *Geologie en Mijnbouw*, **42**, 170–6.

1969: Origin of ultramafic rocks, their tectonic setting and history: a contribution to the discussion of the paper "The Origin of Ultramafic Rocks" by P. J. Wyllie. *Tectonophysics*, **7**, 457–88.

de Saint Blanquat, M. & Tikoff, B. 1997: Development of magmatic to solid-state fabrics during syntectonic emplacement of the Mono Creek granite, Sierra Nevada Batholith, California. *In* Bouchez, J.-L., Stephens, W. E. & Hutton, D. E. (eds): *Granite: from Melt Segregation to Emplacement Fabrics*. Dordrecht: Kluwer, pp. 231–52.

Desborough, G. A., Anderson, A. T. & Wright, T. L. 1968: Mineralogy of sulfides from certain Hawaiian basalts. *Economic Geology*, **63**, 636–44.

Dewers, T. & Ortoleva, P. 1990: Force of crystallization during the growth of siliceous concretions. *Geology*, **18**, 204–7.

Dickey, J. S. 1973: A primary peridotite magma – revisited: olivine quench crystals in a peridotite lava. *In* Shagam, R., Hargraves, R. B., Morgan, W. J., van Houten, F. B., Burk, C. A., Holland, H. D. & Hollister, L. C. (eds): *Studies in Earth and Space Sciences (Hess Volume). Geological Society of America Memoir*, **132**, 289–97.

Dickson, F. W. 1996: Porphyroblasts of barium-zoned K-feldspar and quartz, Papoose Flat, Inyo Mountains, California, genesis and exploration implications. *In* Cooper, A. R. & Fahey, P. L. (eds): *Geology and Ore Deposits of the American Cordillera*. Reno: Geological Society of Nevada, pp. 909–24.

Dickson, F. W. & Sabine, C. 1967: Barium zoned large K-feldspars in quartz monzonites of eastern and southeastern California (abstract). *Geological Society of America Special Paper*, **115**, 323.

Didier, J. 1973: *Granites and Their Enclaves*. Amsterdam: Elsevier.

Didier, J. & Barbarin, B. (eds) 1991: *Enclaves and Granite Petrology*. Amsterdam: Elsevier.

Dipple, G. M., Wintsch, R. P. & Andrews, M. S. 1990: Identification of the scales of differential element mobility in a ductile fault zone. *Journal of Metamorphic Geology*, **8**, 645–61.

Dixon, J. & Williams, G. 1983: Reaction softening in mylonites from the Arnaboll thrust, Sutherland. *Scottish Journal of Geology*, **19**, 157–68.

D'Lemos, R. S., Kearsley, A. T., Pembroke, J. W., Watt, G. R. & Wright, P. 1997: Complex quartz growth histories in granite revealed by scanning cathodoluminescence techniques. *Geological Magazine*, **134**, 549–52.

Dobbs, H. T., Peruzzo, L., Seno, F., Spiess, R. & Prior, D. J. 2003: Unraveling the Schneeberg garnet puzzle: a numerical model of multiple nucleation and coalescence. *Contributions to Mineralogy and Petrology*, **146**, 1–9.

Doherty, R. 1975: Dendritic growth. *In* Pamplin, B. R. (ed.): *Crystal Growth*. Oxford: Pergamon, pp. 576–600.

Donaldson, C. H. 1974: Olivine crystal types in harrisitic rocks of the Rhum pluton and in Archean spinifex rocks. *Bulletin of the Geological Society of America*, **85**, 1721–6.

1976: An experimental investigation of olivine morphology. *Contributions to Mineralogy and Petrology*, **57**, 187–213.

1977: Laboratory duplication of comb layering in the Rhum pluton. *Mineralogical Magazine*, **41**, 323–36.

1979: An experimental investigation of the delay in nucleation of olivine in mafic magmas. *Contributions to Mineralogy and Petrology*, **69**, 21–32.

1985: A comment on crystal shapes resulting from dissolution in magmas. *Mineralogical Magazine*, **49**, 129–32.

Donaldson, C. H., Drever, H. I. & Johnston, R. 1976: Supercooling on the lunar surface: a review of analogue information. *Philosophical Transactions of the Royal Society of London*, **A285**, 207–17.

Donaldson, C. H. & Henderson, C. M. B. 1988: A new interpretation of round embayments in quartz crystals. *Mineralogical Magazine*, **52**, 27–33.

Dornbusch, H.-J., Weber, K. & Skrotzki, W. 1994: Development of microstructure and texture in high-temperature mylonites from the Ivrea Zone. *In* Bunge, H. J., Siegesmund, S., Skrotzki, W. & Weber, K. (eds): *Textures of Geological Materials*. Oberursel: DGM Informationsgesellschaft-Verlag, pp. 187–201.

Doukhan, J.-C., Doukhan, N., Koch, P. S. & Christie, J. M. 1985: Transmission electron microscopy of lattice defects in Al_2SiO_5 polymorphs and plasticity induced polymorphic transformations. *Bulletin de Minèralogie*, **108**, 91–6.

Doukhan, J.-C. & Trepied, L. 1985: Plastic deformation of quartz single crystals. *Bulletin de Minèralogie*, **108**, 97–123.

Doukhan, N., Sautter, V. & Doukhan, J.-C. 1994: Ultradeep, ultramafic mantle xenoliths – transmission electron microscopy preliminary results. *Physics of the Earth and Planetary Interiors*, **82**, 195–207.

Downes, M. J. 1974: Sector and oscillatory zoning in calcic augites from M. Etna, Sicily. *Contributions to Mineralogy and Petrology*, **47**, 187–96.

Dowty, E. 1976a: Crystal structure and crystal growth: I. The influence of internal structure on morphology. *American Mineralogist*, **61**, 448–59.

1976b: Crystal structure and crystal growth: II. Sector zoning in minerals. *American Mineralogist*, **61**, 460–9.

1980a: Synneusis reconsidered. *Contributions to Mineralogy and Petrology*, **74**, 75–84.

1980b: Crystal growth and nucleation theory and the numerical simulation of igneous crystallization. *In* Hargraves, R. B. (ed.): *Physics of Magmatic Processes*. Princeton: Princeton University Press, pp. 419–85.

Dowty, E., Keil, K. & Prinz, M. 1974: Lunar pyroxene-phyric basalts: crystallization under supercooled conditions. *Journal of Petrology*, **15**, 419–53.

Drever, H. I. & Johnston, R. 1957: Crystal growth of olivine in magmas and melts. *Transactions of the Royal Society of Edinburgh*, **63**, 289–317.

1972: Metastable growth patterns in some terrestrial and lunar rocks. *Meteoritics*, **7**, 327–40.

Droop, G. T. R. 1985: Alpine metamorphism in the south-east Tauern window. *Journal of Metamorphic Geology*, **3**, 371–402.

Droop, G. T. R. & Bucher-Nurminen, K. 1984: Reaction textures and metamorphic evolution of sapphirine-bearing granulites from the Gruf Complex, Italian Central Alps. *Journal of Petrology*, **25**, 766–803.

Drüppel, K., von Seckendorff, V. & Okrusch, M. 2001: Subsolidus reaction textures in the anorthositic rocks of the southern part of the Kunene Intrusive Complex, NW Namibia. *European Journal of Mineralogy*, **13**, 289–309.

Drury, M. R. 1993: Deformation lamellae in metals and minerals. *In* Boland, J. N. & Fitz Gerald, J. D. (eds): *Defects and Processes in the Solid State: Geoscience Applications. The McLaren Volume*. Amsterdam: Elsevier, pp. 195–212.

Drury, M. R. & Humphreys, F. J. 1986: The development of microstructure in Al-5% Mg during high temperature deformation. *Acta Metallurgica*, **34**, 2259–71.

1988: Microstructural shear criteria associated with grain-boundary sliding during ductile deformation. *Journal of Structural Geology*, **10**, 83–9.

Drury, M. R., Humphreys, F. J. & White, S. H. 1985: Large strain deformation studies using polycrystalline magnesium as a rock analogue. Part II: dynamic recrystallization mechanisms at high temperature. *Physics of the Earth and Planetary Interiors*, **40**, 208–22.

Drury, M. R. & Urai, J. L. 1990: Deformation-related recrystallization processes. *Tectonophysics*, **172**, 235–53.

Drury, M. R. & van Roermund, H. L. M. 1989: Fluid assisted recrystallization in upper mantle peridotite xenoliths from kimberlites. *Journal of Petrology*, **30**, 133–52.

Dunham, A. C. 1965: The nature and origin of the groundmass texture in felsites and granophyres from Rhum, Inverness-shire. *Geological Magazine*, **102**, 8–22.

Durazzo, A. & Taylor, L. A. 1982: Experimental exsolution textures in the system bornite-chalcopyrite: genetic implications concerning natural ores. *Mineralium Deposita*, **17**, 79–97.

Durney, D. W. 1972: Solution-transfer, an important geological deformation mechanism. *Nature*, **235**, 315–17.

Durney, D. W. & Kisch, H. J. 1994: A field classification and intensity scale for first-generation cleavages. *AGSO Journal of Australian Geology and Geophysics*, **15**, 257–95.

Durney, D. W. & Ramsay, J. G. 1973: Incremental strains measured by syntectonic crystal growths. *In* de Jong, K. A. & Scholten, R. (eds): *Gravity and Tectonics*. New York: Wiley, pp. 67–96.

Eberl, D. D., Kile, D. E. & Drits, V. A. 2002: On geological interpretations of crystal size distributions: Constant vs. proportionate growth. *American Mineralogist*, **87**, 1235–41.

Echeverría, L. M. 1980: Tertiary or Mesozoic komatiites from Gorgona Island, Colombia: field relations and geochemistry. *Contributions to Mineralogy and Petrology*, **73**, 253–66.

Edington, J. W., Melton, K. N. & Cutler, C. P. 1976: Superplasticity. *Progress in Materials Science*, **21**, 63–170.

Edwards, A. B. 1947: *Textures of the Ore Minerals and Their Significance.* (Revised 1954.) Melbourne: Australasian Institute of Mining and Metallurgy.

1949: Natural ex-solution intergrowths of magnetite and hematite. *American Mineralogist*, **34**, 759–61.

1952: The ore minerals and their textures. *Journal and Proceedings of the Royal Society of New South Wales*, **85**, 26–46.

Eggleton, R. A. 1979: The ordering path for igneous K-feldspar megacrysts. *American Mineralogist*, **64**, 906–11.

Eggleton, R. A. & Buseck, P. R. 1980: The orthoclase-microcline inversion: a high-resolution TEM study and strain analysis. *Contributions to Mineralogy and Petrology*, **74**, 123–33.

Eldridge, C. S., Bourcier, W. L., Ohmoto, H. & Barnes, H. L. 1988: Hydrothermal inoculation and incubation of the chalcopyrite disease in sphalerite. *Economic Geology*, **83**, 978–89.

Elliot, D. 1972: Deformation paths in structural geology. *Bulletin of the Geological Society of America*, **83**, 2621–38.

Elliott, M. T., Cheadle, M. J. & Jerram, D. A. 1997: On the identification of textural disequilibrium in rocks using dihedral angle measurements. *Geology*, **25**, 355–8.

Ellis, D. J. & Obata, M. 1992: Migmatite and melt segregation at Cooma, New South Wales. *Transactions of the Royal Society of Edinburgh: Earth Sciences*, **83**, 95–106.

Ellis, M. A. 1986: The determination of progressive deformation histories from antitaxial syntectonic growth fibres. *Journal of Structural Geology*, **8**, 701–9.

Engelder, J. T. 1974: Cataclasis and the generation of fault gouge. *Bulletin of the Geological Society of America*, **85**, 1515–22.

Erambert, M. & Austrheim, H. 1993: The effect of fluid and deformation on zoning and inclusion patterns in polymetamorphic garnets. *Contributions to Mineralogy and Petrology*, **115**, 204–14.

Eriksson, S. C. 1985: Oscillatory zoning in clinopyroxenes from the Guide Copper Mine, Phalaborwa, South Africa. *American Mineralogist*, **70**, 74–9.

Erslev, E. & Mann, C. 1984: Pressure solution shortening in the Martinsburg Formation, New Jersey. *Proceedings of the Pennsylvania Academy of Sciences*, **58**, 84–8.

Erslev, E. A. 1998: Limited, localized nonvolatile element flux and volume change in Appalachian slates. *Bulletin of the Geological Society of America*, **110**, 900–15.

Espenshade, G. H. & Potter, D. B. 1960: Kyanite, sillimanite and andalusite deposits of the southeastern States. *United States Geological Survey Professional Paper*, **336**, 121pp.

Etchecopar, A. & Malavielle, J. 1987: Computer models of pressure shadows: a method for strain measurement and shear-sense determination. *Journal of Structural Geology*, **9**, 667–77.

Etheridge, M. A. 1975: Deformation and recrystallization of orthopyroxene from the Giles Complex, central Australia. *Tectonophysics*, **25**, 87–114.

1983: Differential stress magnitudes during regional deformation and metamorphism: Upper bound imposed by tensile fracturing. *Geology*, **11**, 231–4.

Etheridge, M. A. & Hobbs, B. E. 1974: Chemical and deformational controls on recrystallization of mica. *Contributions to Mineralogy and Petrology*, **43**, 111–24.

Etheridge, M. A., Hobbs, B. E. & Paterson, M. S. 1973: Experimental deformation of single crystals of biotite. *Contributions to Mineralogy and Petrology*, **38**, 21–36.

Etheridge, M. A. & Lee, M. F. 1975: Microstructure of slate from Lady Loretta, Queensland, Australia. *Bulletin of the Geological Society of America*, **86**, 13–22.

Etheridge, M. A. & Vernon, R. H. 1981: A deformed polymictic conglomerate – the influence of grain size and composition on the mechanism and rate of deformation. *Tectonophysics*, **79**, 237–54.

Etheridge, M. A., Wall, V. J., Cox, S. F. & Vernon, R. H. 1984: High fluid pressures during regional metamorphism and deformation. *Journal of Geophysical Research*, **89**, 4344–58.

Etheridge, M. A., Wall, V. J. & Vernon, R. H. 1983: The role of the fluid phase during regional metamorphism and deformation. *Journal of Metamorphic Geology*, **1**, 205–26.

Etheridge, M. A. & Wilkie, J. C. 1979: Grain size reduction, grain boundary sliding and the flow strength of mylonites. *Tectonophysics*, **58**, 159–78.

Evans, B. W. & Berti, J. W. 1986: A revised metamorphic history for the Chiwaukum Schist, Washington Cascades. *Geology*, **14**, 695–8.

Evans, B. W. & Trommsdorf, V. 1974: On elongate olivine of metamorphic origin. *Geology*, **2**, 131–2.

Evans, J. P. 1988: Deformation mechanisms in granitic rocks at shallow crustal levels. *Journal of Structural Geology*, **10**, 437–44.

1990: Textures, deformation mechanisms, and the role of fluids in the cataclastic deformation of granitic rocks. *In* Knipe, R. J. & Rutter, E. H. (eds): *Deformation Mechanisms, Rheology and Tectonics. Geological Society of London Special Publication*, **54**, 29–39.

Evans, O. C. & Hanson, G. N. 1993: Accessory-mineral fractionation of rare-earth element (REE) abundances in granitic rocks. *Chemical Geology*, **110**, 69–93.

Ewart, A. 1971: Chemical changes accompanying spherulitic crystallization in rhyolitic lavas, Central Volcanic Region, New Zealand. *Mineralogical Magazine*, **38**, 424–34.

Fagan, R. A. 1979: *Deformation, Metamorphism and Anatexis of an Early Palaeozoic Flysch Sequence in Northeastern Victoria.* Ph.D. thesis, University of New England, Australia.

Fairbairn, H. W. 1942: *Structural Petrology of Deformed Rocks*. Cambridge, MA: Addison-Wesley.

Faure, F., Trolliard, G., Nicollet, C. & Montel, J.-M. 2003a: A developmental model of olivine morphology as a function of the cooling rate and degree of undercooling. *Contributions to Mineralogy and Petrology*, **145**, 251–63.

Faure, F., Trolliard, G. & Soulestin, B. 2003b: TEM investigation of forsterite dendrites. *American Mineralogist*, **88**, 1241–50.

Fenn, P. M. 1974: Nucleation and growth of alkali feldspars from a melt. *In* MacKenzie, W. S. & Zussman, J. (eds): *The Feldspars*. Manchester: Manchester University Press, pp. 360–1.

1977: The nucleation and growth of alkali feldspars from hydrous melts. *Canadian Mineralogist*, **15**, 135–61.

1986: On the origin of graphic granite. *American Mineralogist*, **71**, 325–30.

Fenner, C. N. 1938: Contact relations between rhyolite and basalt on Gardiner River, Yellowstone Park. *Bulletin of the Geological Society of America*, **49**, 1441–84.

1944: Rhyolite-basalt complex on Gardiner River, Yellowstone Park, Wyoming. *Bulletin of the Geological Society of America*, **55**, 1081–96.

Ferguson, C. C. & Harte, B. 1975: Textural patterns at porphyroblast margins and their use in determining the time relations of deformation and crystallization. *Geological Magazine*, **112**, 467–80.

Ferguson, C. C. & Harvey, P. K. 1972: Porphyroblasts and "crystallization force": Some textural criteria. Discussion. *Bulletin of the Geological Society of America*, **83**, 3839–40.

Ferguson, C. C., Harvey, P. K. & Lloyd, G. E. 1980: On the mechanical interaction between a growing porphyroblast and its surrounding matrix. *Contributions to Mineralogy and Petrology*, **75**, 339–52.

Ferguson, J. & Currie, K. L. 1971: Evidence of liquid immiscibility in alkaline ultrabasic dikes at Callander Bay, Ontario. *Journal of Petrology*, **12**, 561–85.

Ferrill, D. A. 1991: Calcite twin widths as metamorphic indicators in natural low-temperature deformation of limestone. *Journal of Structural Geology*, **13**, 667–75.

Ferry, J. M. 1991: Dehydration and decarbonation reactions as a record of fluid infiltration. *In* Kerrick, D. M. (ed.): *Contact Metamorphism. Mineralogical Society of America, Reviews in Mineralogy*, **26**, 351–93.

1994: Overview of the petrologic record of fluid flow during regional metamorphism in northern New England. *American Journal of Science*, **294**, 905–88.

2001: Patterns of mineral occurrence in metamorphic rocks. *American Mineralogist*, **85**, 1573–88.

Fershtater, G. B. & Borodina, N. S. 1977: Petrology of autoliths in granitic rocks. *International Geology Review*, **19**, 458–68.

Field, J. E. 1979: *The Properties of Diamond.* London: Academic Press.

Fitz Gerald, J. G., Boland, J. N., McLaren, A. C., Ord, A. & Hobbs, B. E. 1991: Microstructures in water-weakened single crystals of quartz. *Journal of Geophysical Research*, **96**, 2139–55.

Fitz Gerald, J. G., Etheridge, M. A. & Vernon, R. H. 1983: Dynamic recrystallization in a naturally deformed albite. *Textures and Microstructures*, **5**, 219–37.

Fitz Gerald, J. G. & McLaren, A. C. 1982: The microstructures of microcline from some granitic rocks and pegmatites. *Contributions to Mineralogy and Petrology*, **80**, 219–29.

Fitz Gerald, J. G. & Stünitz, H. 1993a: Deformation of granitoids at low metamorphic grade. I: Reactions and grain size reduction. *Tectonophysics*, **221**, 269–97.

1993b: Deformation of granitoids at low metamorphic grade. II: Granular flow in albite-rich mylonites. *Tectonophysics*, **221**, 299–324.

Fleet, M. E. 1975a: The growth habits of olivine – a structural interpretation. *Canadian Mineralogist*, **13**, 293–7.

1975b: Growth habits of clinopyroxene. *Canadian Mineralogist*, **13**, 336–41.

Fleet, M. E. & MacRae, N. D. 1975: A spinifex rock from Munro Township, Ontario. *Canadian Journal of Earth Sciences*, **12**, 928–39.

Fleischer, M., Wilcox, R. E. & Matzko, J. J. 1984: Microscopic determination of the nonopaque minerals. *United States Geological Survey Bulletin*, **1627**, 453pp.

Fleming, P. D. & Offler, R. 1968: Pre-tectonic metamorphic crystallization in the Mt. Lofty Ranges, South Australia. *Geological Magazine*, **105**, 356–9.

Fletcher, R. C. & Merino, E. 2001: Mineral growth in rocks: Kinetic-rheological models of replacement, vein formation and syntectonic crystallization. *Geochimica et cosmochimica Acta*, **65**, 3733–48.

Flinn, D. 1969: Grain contacts in crystalline rocks. *Lithos*, **3**, 361–70.

Flood, R. H. & Vernon, R. H. 1988: Microstructural evidence of orders of crystallization in granitoid rocks. *Lithos*, **21**, 237–45.

Folk, R. L. 1965: Henry Clifton Sorby (1826–1908), the founder of petrography. *Journal of Geological Education*, **13**, 43–7.

1968: *Petrology of Sedimentary Rocks*. Austin, TX: Hemphill's.

Foster, C. T. 1977: Mass transfer in sillimanite-bearing pelitic schists near Rangeley, Maine. *American Mineralogist*, **62**, 727–46.

1981: A thermodynamics model of mineral segregations in the lower sillimanite zone near Rangeley, Maine. *American Mineralogist*, **66**, 260–77.

1983: Thermodynamics models of biotite pseudomorphs after staurolite. *American Mineralogist*, **68**, 389–97.

1986: Thermodynamics models of reactions involving garnet in a sillimanite/staurolite schist. *Mineralogical Magazine*, **50**, 427–39.

1999: Forward modeling of metamorphic textures. *Canadian Mineralogist*, **37**, 415–29.

Foster, R. J. 1960: Origin of embayed quartz crystals in volcanic rocks. *American Mineralogist*, **45**, 892–4.

Fouqué, F. & Michel-Lévy, A. 1879: *Minéralogie micrographique. Roches éruptives françaises*. *Mémoirs de la Carte géologique de France*, Paris.

Franck, F. C. 1949: The influence of dislocations on crystal growth. *Discussions of the Faraday Society*, **5**, 48.

Frater, K. M. 1985: Mineralization at the Golden Grove Cu-Zn deposit, Western Australia. II: Deformation textures of the opaque minerals. *Canadian Journal of Earth Sciences*, **22**, 15–26.

Freda, C. & Baker, D. R. 2000: Crystal growth experiments in the undercooled orthoclase-quartz-H_2O system: Applications to pegmatite textures. *Geoscience Canada 2000 Abstracts*, pp. 763–4.

Friedman, G. M. & Sanders, J. E. 1978: *Principles of Sedimentology*. New York: Wiley.

Frondel, C. 1934: Selective incrustation of crystal forms. *American Mineralogist*, **19**, 316–29.

1935: The size of crystals. *American Mineralogist*, **20**, 469–73.

Frost, R., Mavrogenes, J. A. & Tomkins, A. G. 2002: Partial melting of sulfide ore deposits during medium- and high-grade metamorphism. *Canadian Mineralogist*, **40**, 1–18.

Frost, T. P. & Mahood, G. A. 1987: Field, chemical, & physical constraints on mafic-felsic magma interaction in the Lamarck granodiorite, Sierra Nevada, California. *Bulletin of the Geological Society of America*, **99**, 272–91.

Früh-Green, G. L. 1994: Interdependence of deformation, fluid infiltration and reaction progress recorded in eclogitic metagranitoids (Sesia Zone, Western Alps). *Journal of Metamorphic Geology*, **12**, 327–43.

Fullman, R. L. 1955: The growth of crystals. *Scientific American*, March issue, Freeman Reprint, **260**, 6pp.

1957: The equilibrium form of crystalline bodies. *Acta Metallurgica*, **5**, 638–48.

Fyfe, W. S. & Kerrich, R. 1985: Fluids and thrusting. *Chemical Geology*, **49**, 353–62.

Fyfe, W. S., Price, N. J. & Thompson, A. B. 1978: *Fluids in the Earth's Crust*. Amsterdam: Elsevier.

Fyson, W. K. 1975: Fabrics and deformation of Archean metasedimentary rocks, Ross Lake-Gordon Lake area, Slave Province, Northwest Territories. *Canadian Journal of Earth Sciences*, **12**, 765–76.

1980: Fold fabrics and emplacement of an Archean granitoid pluton, Cleft Lake, Northwest Territories. *Canadian Journal of Earth Sciences*, **17**, 325–32.

Fyson, W. K. & Frith, R. A. 1979: Regional deformations and emplacement of granitoid plutons in the Hackett River greenstone belt, Slave Province, Northwest Territories. *Canadian Journal of Earth Sciences*, **16**, 1187–95.

Gamble, J. A. 1979: Some relationships between coexisting granitic and basaltic magmas and the genesis of hybrid rocks in the Tertiary central complex of Slieve Gullion, northeast Ireland. *Journal of Volcanology and Geothermal Research*, **5**, 297–316.

Ganne, J., Bussy, F. & Vidal, O. 2003: Multi-stage garnet in the internal Briançonnais basement (Ambin Massif, Savoy): new petrological constraints on the blueschist-facies metamorphism in the Western Alps. *Journal of Petrology*, **44**, 1281–308.

Gapais, D. 1989: Shear structures within deformed granites: Mechanical and thermal indicators. *Geology*, **17**, 1144–7.

Gapais, D. & Barbarin, B. 1986: Quartz fabric transition in a cooling syntectonic granite (Hermitage Massif, France). *Tectonophysic*s, **125**, 357–70.

Gapais, D. & White, S. H. 1982: Ductile shear bands in naturally deformed quartzite. *Textures and Microstructures*, **5**, 1–17.

Garcia, D., Pascal, M.-L. & Roux, J. 1996: Hydrothermal replacement of feldspars in igneous enclaves of the Velay granite and the genesis of myrmekites. *European Journal of Mineralogy*, **8**, 703–17.

Geiser, A. 1975: Slaty cleavage and the dewatering hypothesis – an examination of some critical evidence. *Geology*, **3**, 717–20.

Gélinas, L. & Brooks, C. 1974: Archean quench-texture tholeiites. *Canadian Journal of Earth Sciences*, **11**, 324–40.

Gibb, F. G. F. 1974: Supercooling and the crystallization of plagioclase from a basaltic magma. *Mineralogical Magazine*, **39**, 641–53.

Gilbert, G. K. 1906: Gravitational assemblage in granite. *Bulletin of the Geological Society of America*, **17**, 321–8.

Gilotti, J. A. & Hull, J. M. 1990: Phenomenological superplasticity in rocks. *In* Knipe, R. J. & Rutter, E. H. (eds): *Deformation Mechanisms, Rheology and Tectonics. Geological Society of London Special Publication*, **54**, 229–40.

Ginibre, C., Kronz, A. & Wörner, G. 2002a: High-resolution quantitative imaging of plagioclase composition using accumulated backscattered electron images: new constraints on oscillatory zoning. *Contributions to Mineralogy and Petrology*, **142**, 436–48.

Ginibre, C., Wörner, G. & Kronz, A. 2002b: Minor- and trace-element zoning in plagioclase: implications for magma chamber processes at Parinacota volcano, northern Chile. *Contributions to Mineralogy and Petrology*, **143**, 300–15.

Gittins, J. 1973: The significance of some porphyritic textures in carbonatites. *Canadian Mineralogist*, **12**, 226–8.

Glassley, W. E. & Sørensen, K. 1980: Constant *P-T* amphibolite to granulite facies transition in Agto (West Greenland) metadolerites: implications and applications. *Journal of Petrology*, **21**, 69–105.

Glazner, A. F. & Barley, J. M. 1991: Volume loss, fluid flow and state of strain in extensional mylonites from the central Mojave Desert, California. *Journal of Structural Geology*, **13**, 587–94.

Goldstein, A., Pickens, J., Klepeis, K. & Linn, F. 1995: Finite strain heterogeneity and volume loss in slates of the Taconic Allochthon, Vermont, USA. *Journal of Structural Geology*, **17**, 1207–16.

Goodwin, L. B. & Tikoff, B. 2002: Competency contrast, kinematics, and the development of foliations and lineations in the crust. *Journal of Structural Geology*, **24**, 1065–85.

Goodwin, L. B. & Wenk, H.-R. 1990: Intracrystalline folding and cataclasis in biotite of the Santa Rosa mylonite zone: HVEM and TEM observations. *Tectonophysics*, **172**, 201–14.

1995: Development of phyllonite from granodiorite: mechanisms of grain-size reduction in the Santa Rosa mylonite zone, California. *Journal of Structural Geology*, **17**, 689–707.

Gottstein, G. & Mecking, H. 1985: Recrystallization. *In* Wenk, H.-R. (ed.): *Preferred Orientation in Deformed Metals and Rocks: an Introduction to Modern Texture Analysis*. London: Academic Press, pp. 183–218.

Götze, J. 2000: Cathodoluminescence microscopy and spectroscopy in applied mineralogy. *Freiberger Forschungshefte, Geowissenschaften*, **C485**.

Grant, J. A. 1985: Phase equilibria in partial melting of pelitic rocks. *In* Ashworth, J. A. (ed.): *Migmatites*. Glasgow: Blackie, pp. 86–144.

Grant, S. M. 1988: Diffusion models for corona formation in metagabbros from the Western Grenville Province, Canada. *Contributions to Mineralogy and Petrology*, **98**, 49–63.

Gray, D. R. 1977a: Differentiation associated with discrete crenulation cleavages. *Lithos*, **10**, 89–101.

1977b: Morphologic classification of crenulation cleavage. *Journal of Geology*, **85**, 229–35.

1978: Cleavages in deformed psammitic rocks from southeastern Australia: Their nature and origin. *Bulletin of the Geological Society of America*, **89**, 577–90.

1979: Microstructure of crenulation cleavages: an indicator of cleavage origin. *American Journal of Science*, **279**, 97–128.

1981: Compound tectonic fabrics in singly folded rocks from southwest Virginia, U.S.A. *Tectonophysics*, **78**, 229–48.

1997: Volume loss and slaty cleavage development. *In* Sengupta, S. (ed.): *Evolution of Geological Structures in Micro- to Macro-scales*. London: Chapman & Hall, pp. 273–91.

Gray, D. R. & Durney, D. W. 1979a: Investigations on the mechanical significance of crenulation cleavage. *Tectonophysics*, **58**, 35–79.

1979b: Crenulation cleavage differentiation: implications of the solution-redeposition process. *Journal of Structural Geology*, **1**, 73–80.

Gray, D. R., Gregory, R. T. & Durney, D. W. 1991: Rock-buffered fluid-rock interaction in deformed quartz-rich turbidite sequences, eastern Australia. *Journal of Geophysical Research*, **96**, 19681–704.

Gray, D. R. & Willman, C. E. 1991: Thrust-related strain gradients and thrusting mechanisms in a chevron-folded sequence, southeastern Australia. *Journal of Structural Geology*, **13**, 691–710.

Gray, D. R. & Wright, T. O. 1984. Problems of volume loss, fabric development, and strain determination in low-grade pelitic rocks, Martinsburg Formation, U.S.A. *Journal of Structural Geology*, **7**, 492.

Gray, N. H. & Busa, M. D. 1994: The three-dimensional geometry of simulated porphyroblast inclusion trails: inert marker, viscous flow models. *Journal of Metamorphic Geology*, **12**, 575–87.

Green, H. W. 1972: The nature of deformation lamellae in silicates. *Bulletin of the Geological Society of America*, **83**, 847–52.

1992: Analysis of deformation in geological materials. *In* Buseck, P. R. (ed.): *Minerals and Reactions at the Atomic Scale: Transmission Electron Microscopy. Mineralogical Society of America, Reviews in Mineralogy*, **27**, 425–54.

Green, H. W., Griggs, D. T. & Christie, J. M. 1970: Syntectonic recrystallization and annealing of quartz aggregates. *In* Paulitsch, P. (ed.): *Experimental and Natural Rock Deformation*. Berlin: Springer, pp. 272–335.

Green, H. W. & Radcliffe, S. V. 1972: Deformation processes in the upper mantle. *In* Heard, H. C., Borg, I. Y., Carter, N. L. & Raleigh, C. B. (eds): *Flow and Fracture of Rocks. Geophysical Monograph Series*, **16**, 139–56.

Greenfield, J. E., Clarke, G. L., Bland, M. & Clark, D. J. 1996: *In-situ* migmatite and hybrid diatexite at Mt Stafford, central Australia. *Journal of Metamorphic Geology*, **14**, 413–26.

Greensmith, J. T. 1989: *Petrology of the Sedimentary Rocks* (seventh edition). London: Unwin Hyman.

Gregg, W. J. 1985: Microscopic deformation mechanisms associated with mica film formation in cleaved psammitic rocks. *Journal of Structural Geology*, **7**, 45–56.

1986: Deformation of chlorite-white mica aggregates in cleaved psammitic and pelitic rocks from Islesboro, Maine, U.S.A. *Journal of Structural Geology*, **8**, 59–68.

Gresens, R. L. 1971: Application of hydrolysis equilibria to the genesis of pegmatite and kyanite deposits in northern New Mexico. *Mountain Geologist*, **8**, 3–16.

Gribble, C. D. & Hall, A. J. 1992: *Optical Mineralogy Principles and Practice.* London: UCL Press.

Griffin, W. L. 1971: Genesis of coronas in anorthosites of the upper Jotun Nappe, Indre Sogn, Norway. *Journal of Petrology*, **12**, 219–43.

1972: Formation of eclogites and the coronas in anorthosites, Bergen Arcs, Norway. *Geological Society of America Memoir*, **135**, 37–62.

Griggs, D. T. 1967: Hydrolytic weakening in quartz and other silicates. *Geophysical Journal*, **14**, 19–31.

1974: A model of hydrolytic weakening in quartz. *Journal of Geophysical Research*, **79**, 1653–61.

Griggs, D. T. & Blacic, J. D. 1965: Quartz: anomalous weakness of synthetic crystals. *Science*, **147**, 292–5.

Griggs, D. T., Paterson, M. S., Heard, H. C. & Turner, F. J. 1960: Annealing recrystallization in calcite crystals and aggregates. *Geological Society America Memoir*, **79**, 21–37.

Grigor'yev, D. P. 1961: Three types of plastic deformation in galena. *International Geological Review*, **3**, 586–97.

Grocott, J. 1981: Fracture geometry of pseudotachylyte generation zones: a study of shear fractures formed during seismic events. *Journal of Structural Geology*, **3**, 169–78.

Groshong, R. H. 1976: Strain and pressure solution in the Martinsburg Slate, Delaware Water Gap, New Jersey. *American Journal of Science*, **276**, 1131–46.

1988: Low-temperature deformation mechanisms and their interpretation. *Bulletin of the Geological Society of America*, **100**, 1329–60.

Grout, F. F. 1937: Criteria of origin of inclusions in plutonic rocks. *Bulletin of the Geological Society of America*, **48**, 1521–72.

Groves, G. W. & Kelly, A. 1963: Independent slip systems in crystals. *Philosophical Magazine*, **8**, 877–87.

Guernina, S. & Sawyer, E. W. 2003: Large-scale melt-depletion in granulite terranes: an example from the Archean Ashuanipi Subprovince of Quebec. *Journal of Metamorphic Geology*, **21**, 181–201.

Guidotti, C. V. & Johnson, S. E. 2002: Pseudomorphs and associated microstructures of western Maine, USA. *Journal of Structural Geology*, **24**, 1139–56.

Guillopé, M. & Poirier, J.-P. 1979: Dynamic recrystallisation during creep of single crystals of halite: an experimental study. *Journal of Geophysical Research*, **84**, 5557–67.

Gustafson, L. B. & Hunt, J. P. 1975: The porphyry copper deposits at El Salvador, Chile. *Economic Geology*, **70**, 857–912.

Guy, A. G. 1959: *Elements of Physical Metallurgy.* Reading, MA: Addison-Wesley.

Haack, U., Heinrichs, H., Boness, M. & Schneider, A. 1984: Loss of metals from pelites during regional metamorphism. *Contributions to Mineralogy and Petrology*, **85**, 116–32.

Haase, C. S., Chandam, J., Feinn, D. & Ortoleva, P. 1980: Oscillatory zoning in plagioclase feldspar. *Science*, **209**, 272–4.

Hacker, B. R. & Christie, J. M. 1990: Brittle/ductile and plastic/cataclastic transitions in experimentally deformed and metamorphosed amphibolite. *In* Duba, A. G., Durham, W. B., Handin, J. W. & Wang, H. F. (eds): *The Brittle-Ductile Transition in Rocks. American Geophysical Union, Geophysical Monograph*, **56**, 127–47.

Hacker, B. R. & Kirby, S. H. 1993: High-pressure deformation of calcite marble and its transformation to aragonite under non-hydrostatic conditions. *Journal of Structural Geology*, **15**, 1207–22.

Haggerty, S. E. 1976: Opaque mineral oxides in terrestrial silicate rocks. *In* Rumble, D. (ed.): *Oxide Minerals. Mineralogical Society of America Short Course*, **3**, Hg-101–300.

Hall, R. P., Hughes, D. J. & Friend, C. R. L. 1986: Complex sequential pyroxene growth in tholeiitic hypabyssal rocks from southern West Greenland. *Mineralogical Magazine*, **50**, 491–502.

Hammond, R. L. 1987: The influence of deformation partitioning on dissolution and solution transfer in low-grade tectonic mélange. *Journal of Metamorphic Geology*, **5**, 195–211.

Hanchar, J. M. & Miller, C. F. 1993: Zircon zonation patterns as revealed by cathodoluminescence and backscattered electron images: implications for interpretation of complex crustal histories. *Chemical Geology*, **110**, 1–13.

Hanmer, S. 1979: The role of discrete heterogeneities and linear fabrics in the formation of crenulations. *Journal of Structural Geology*, **1**, 81–90.

1982: Microstructure and geochemistry of plagioclase and microcline in naturally deformed granite. *Journal of Structural Geology*, **4**, 197–214.

Hanmer, S. & Passchier, C. W. 1991: Shear-sense indicators: a review. *Geological Survey of Canada Paper*, **90**, 1–71.

Harker, A. 1904: The Tertiary igneous rocks of Syke. *Geological Survey of Scotland Memoir*, 481pp.

1909: *The Natural History of Igneous Rocks.* London: Methuen.

1932: *Metamorphism*. London: Methuen.

Harker, A. & Marr, J. E. 1891: The Shap Granite, and the associated igneous and metamorphic rocks. *Quarterly Journal of the Geological Society of London*, **47**, 266–328.

Harker, D. & Parker, E. R. 1945: Grain shape and grain growth. *Transactions of the American Society for Metals*, **34**, 159–95.

Harley, S. L. & Fitzsimons, I. C. W. 1991: Pressure-temperature evolution of metapelitic granulites in a polymetamorphic terrane: the Rauer Group, East Antarctica. *Journal of Metamorphic Geology*, **9**, 231–43.

Harley, S. L., Hensen, B. J. & Sheraton, J. W. 1990: Two-stage decompression in orthopyroxene-sillimanite granulites from Forefinger Point, Enderby Land, Antarctica: implications for the evolution of the Archaean Napier Complex. *Journal of Metamorphic Geology*, **8**, 591–613.

Harloff, C. 1927: Zonal structures in plagioclase. *Leidse Geologische Mededelingen*, **2**, 99–114.

Harlov, D. E. & Wirth, R. 2000: K-feldspar–quartz and K-feldspar–plagioclase phase boundary interactions in garnet-orthopyroxene gneisses from the Val Strona di Omegna, Ivrea-Verbano Zone, northern Italy. *Contributions to Mineralogy and Petrology*, **140**, 148–62.

Harte, B. 1977: Rock nomenclature with particular reference to deformed and recrystallized textures in olivine-bearing xenoliths. *Journal of Geology*, **85**, 279–88.

Hartman, P. 1958: The equilibrium form of crystals. *Acta Crystallographica*, **11**, 459–64.

1973: Structure and morphology. *In* Hartman, P. (ed.): *Crystal Growth: an Introduction*. Amsterdam: North-Holland, pp. 367–402.

1978: Sur la morphologie des cristaux. *Bulletin de Minéralogie*, **101**, 195–201.

1982: Crystal faces: structure and growth. *Geologie en Mijnbouw*, **61**, 313–20.

Hartman, P. & Bennema, P. 1980: The attachment energy as a habit controlling factor. I. Theoretical considerations. *Journal of Crystal Growth*, **49**, 145–56.

Hartman, P. & Perdok, W. G. 1955: On the relations between crystal structure and morphology I, II, III. *Acta Crystallographica*, **8**, 49–52, 521–4, 525–9.

Hatch, F. H., Wells, A. K. & Wells, M. K. 1949: *The Petrology of the Igneous Rocks* (tenth edition). London: Murby.

Hatton, C. J. & Gurney, J. J. 1987: Roberts Victor eclogites and their relation to the mantle. *In* Nixon, P. H. (ed.): *Mantle Xenoliths*. Chichester, UK: Wiley, pp. 453–63.

Hawkes, D. D. 1967: Order of abundant crystal nucleation in a natural magma. *Geological Magazine*, **104**, 473–86.

Hayward, C. L. 1998: Cathodoluminescence of ore and gangue minerals and its application in the minerals industry. *In* Jambor, J. L. (ed.): *Modern Approaches to Ore and Environmental Mineralogy. Mineralogical Association of Canada Short Course*, **27**, 269–325.

Hayward, N. 1990: Determination of early fold axis orientations in multiply deformed rocks using porphyroblast inclusion trails. *Tectonophysics*, **179**, 353–69.

1992: Microstructural analysis of the classical spiral garnet porphyroblasts of south-east Vermont: evidence for non-rotation. *Journal of Metamorphic Geology*, **10**, 567–87.

Healy, B. C., Collins, W. J., Richards, S. W. & Wiebe, R. A. 2000: Chemical effects of squeezing a crystal mush during compressive deformation: the Kameruka pluton, Lachlan Fold Belt. *Geological Society of Australia Abstracts*, **59**, 216.

Heard, H. C. 1960: Transition from brittle to ductile flow in Solenhofen limestone as a function of temperature, confining pressure, and interstitial fluid pressure. *In* Griggs, D. T. & Handin, J. (eds): *Rock Deformation. Geological Society of America Memoir*, **79**, 193–226.

1972: Steady state flow in polycrystalline halite at a pressure of 2 kilobars. *In* Heard, H. C., Borg, I. Y., Carter, N. L. & Raleigh, C. B. (eds): *Flow and Fracture of Rocks. Geophysical Monograph Series*, **16**, 191–209.

Heidelbach, F., Post, A. D. & Tullis, J. 2000: Crystallographic preferred orientation in albite samples deformed experimentally by dislocation and solution precipitation creep. *Journal of Structural Geology*, **22**, 1649–61.

Heinrich, C. A. 1986: Eclogite facies regional metamorphism of hydrous rocks in the central Adula nappe. *Journal of Petrology*, **27**, 123–54.

Heinrich, W. & Gottschalk, M. 1995: Metamorphic reactions between fluid inclusions and mineral hosts. I. Progress of the reaction calcite + quartz = wollastonite + CO_2 in natural wollastonite-hosted fluid inclusions. *Contributions to Mineralogy and Petrology*, **122**, 51–61.

Hemley, J. J. & Jones, W. R. 1964: Chemical aspects of hydrothermal alteration with emphasis on hydrogen metasomatism. *Economic Geology*, **59**, 538–69.

Hennig-Michaeli, C. 1977: Microscopic structure studies of experimentally and naturally deformed hematite ores. *Tectonophysics*, **39**, 255–71.

Hennig-Michaeli, C. & Couderc, J.-J. 1989: TEM study of mechanical twinning in experimentally deformed chalcopyrite ($CuFeS_2$) single crystals, Part II: strain-induced (102) twins. *European Journal of Mineralogy*, **1**, 295–310.

Hennig-Michaeli, C. & Siemes, H. 1987: Experimental deformation of chalcopyrite single crystals at 200°C. *Tectonophysics*, **135**, 217–32.

Hermann, J., Rubatto, D., Korasakov, A. & Shatsky, V. S. 2001: Multiple zircon growth during fast exhumation of diamondiferous, deeply subducted continental crust (Kokchetav Massif, Kazakhstan). *Contributions to Mineralogy and Petrology*, **141**, 66–82.

Hess, P. C. 1980: Polymerization model for silicate melts. *In* Hargraves, R. B. (ed.): *Physics of Magmatic Processes*. Princeton: Princeton University Press, pp. 3–48.

1995: Thermodynamic mixing properties and the structure of silicate melts. *In* Stebbins, J. F., McMillan, P. F. & Dingwell, D. B. (eds): *Structure, Dynamics and Properties of Silicate Melts. Mineralogical Society of America and Geochemical Society, Reviews in Mineralogy and Geochemistry*, **32**, 145–89.

Hibbard, M. J. 1965: Origin of some alkali-feldspar phenocrysts and their bearing on petrogenesis. *American Journal of Science*, **263**, 245–61.

1979: Myrmekite as a marker between preaqueous and postaqueous phase saturation in granitic systems. *Bulletin of the Geological Society of America*, **90**, 1047–62.

1981: The magma-mixing origin of mantled feldspars. *Contributions to Mineralogy and Petrology*, **76**, 158–70.

1995: *Petrography to Petrogenesis*. Englewood Cliffs, NJ: Prentice-Hall.

Hickey, K. A. & Bell, T. H. 1999: Behaviour of rigid objects during deformation and metamorphism: a test using schists from the Bolton syncline, Connecticut, USA. *Journal of Metamorphic Geology*, **17**, 211–28.

Hicks, J. F. G. 1967: Structure of silica glass. *Science*, **155**, 459–61.

Higgins, M. D. 1994: Numerical modeling of crystal shapes in thin sections: Estimation of crystal habit and true size. *American Mineralogist*, **79**, 113–19.

1998: Origin of anorthosite by textural coarsening: Quantitative measurements of a natural sequence of textural development. *Journal of Petrology*, **39**, 1307–23.

1999: Origin of megacrysts in granitoids by textural coarsening: a crystal size distribution (CSD) study of microcline in the Cathedral Peak Granodiorite, Sierra Nevada, California. *In* Castro, A., Fernández, C. & Vigneresse, J.-L. (eds): *Understanding Granites: Integrating New and Classical Techniques. Geological Society of London Special Publication*, **168**, 207–19.

2000: Measurement of crystal size distributions. *American Mineralogist*, **85**, 1105–16.

2002: Reply to comment on “Closure in crystal size distributions (CSD), verification of CSD calculations, and the significance of CSD fans.” *American Mineralogist*, **87**, 1244.

Higgins, N. C. & Kawachi, Y. 1977: Microcline megacrysts from the Green Lake Granodiorite, eastern Fiordland, New Zealand. *New Zealand Journal of Geology and Geophysics*, **20**, 273–86.

Hilgers, C., Koehn, D., Post, A. D. & Bons, P. D. 1997: Fibrous vein microstructure: experimental and numerical simulation. *Aardkundige Mededelingen*, **8**, 107–9.

Hilgers, C. & Urai, J. L. 1999: Syntectonic antitaxial fibrous vein growth: inferences from the microstructure of natural samples. *In* Leiss, B., Ullemeyer, K. & Weber, K. (eds): *Textures and Physical Properties of Rocks. Göttinger Arbeiten zum Geologie und Paläontologie*, **Sb4**, 70–2.

Hippert, J., Rocha, A., Lana, C., Egydio-Silva, M. & Takeshita, T. 2001: Quartz plastic segregation and ribbon development in high-grade striped gneisses. *Journal of Structural Geology*, **23**, 67–80.

Hiraga, T., Nishikawa, O., Nagase, T., Akizuki, M. & Kohlstedt, D. L. 2002: Interfacial energies from quartz and albite in pelitic schist. *Contributions to Mineralogy and Petrology*, **143**, 664–72.

Hiroi, Y., Kishi, S., Nohara, T., Sato, K. & Goto, J. 1998: Cretaceous high-temperature rapid loading and unloading in the Abukuma metamorphic terrane, Japan. *Journal of Metamorphic Geology*, **16**, 67–81.

Hirsch, D. M., Ketcham, R. A. & Carlson, W. D. 2000: An evaluation of spatial correlation functions in textural analysis of metamorphic rocks. *Geological Materials Research*, **2/3**, 42pp.

Hirsch, D. M., Prior, D. J. & Carlson, W. D. 2003: An overgrowth model to explain multiple, dispersed high-Mn regions in the cores of garnet porphyroblasts. *American Mineralogist*, **88**, 131–41.

Hirth, G. & Kohlstedt, D. L. 1995: Experimental constraints on the dynamics of the partially molten upper mantle: deformation in the diffusion creep regime. *Journal of Geophysical Research*, **100**, 1981–2001.

Hirth, G. & Tullis, J. 1992: Dislocation creep regimes in quartz aggregates. *Journal of Structural Geology*, **14**, 145–60.

Hobbs, B. E. 1968: Recrystallization of single crystals of quartz. *Tectonophysics*, **6**, 353–402.

Hobbs, B. E., McLaren, A. C. & Paterson, M. S. 1972: Plasticity of single crystals of synthetic quartz. *In* Heard, H. C., Borg, I. Y., Carter, N. L. & Raleigh, C. B. (eds): *Flow and Fracture of Rocks. Geophysical Monograph Series*, **16**, 29–53.

Hobbs, B. E., Means, W. D. & Williams, P. F. 1976: *An Outline of Structural Geology*. New York: Wiley.

Hoffman, J. F. & Long, J. V. P. 1984: Unusual sector zoning in Lewisian zircons. *Mineralogical Magazine*, **48**, 513–17.

Hogan, J. P. 1993: Monomineralic glomercrysts: textural evidence for mineral resorption during crystallization of igneous rocks. *Journal of Geology*, **101**, 531–40.

Holcombe, R. J. 1977: The estimation of triple junction angles in opaque sections of annealed metals and metamorphic rocks. *Papers of the Department of Geology, University of Queensland*, **8**, 1–14.

Holeywell, R. C. & Tullis, T. E. 1975: Mineral reorientation and slaty cleavage in the Martinsburg Formation, Lehigh Gap, Pennsylvania. *Bulletin of the Geological Society of America*, **86**, 1296–304.

Hollister, L. S. 1969: Contact metamorphism in the Kwoiek area of British Columbia: an end-member of the metamorphic process. *Bulletin of the Geological Society of America*, **80**, 2465–94.

1970: Origin, mechanism, and consequences of compositional sector-zoning in staurolite. *American Mineralogist*, **55**, 742–66.

Hollister, L. S. & Crawford, M. L. 1981: *Short Course in Fluid Inclusions: Applications to Petrology. Mineralogical Association of Canada, Short Course*, **6**, 304pp.

1986: Melt-enhanced deformation: A major tectonic process. *Geology*, **14**, 558–61.

Hollister, L. S. & Gancarz, A. J. 1971: Compositional sector-zoning in clinopyroxene from the Narce area, Italy. *American Mineralogist*, **56**, 959–79.

Holness, M. B., Bickle, M. J. & Graham, C. M. 1991: On the kinetics of textural equilibration in forsterite marbles. *Contributions to Mineralogy and Petrology*, **108**, 356–67.

Holyoke, C. W. & Rushmer, T. 2002: An experimental study of grain scale melt segregation mechanisms in two common crustal rock types. *Journal of Metamorphic Geology*, **20**, 493–512.

Hopson, R. F. & Ramseyer, K. 1990: Cathodoluminescence microscopy of myrmekite. *Geology*, **18**, 336–9.

House, N. M. & Gray, D. R. 1982: Cataclasites along the Saltville thrust, U.S.A. and their implications for thrust-sheet emplacement. *Journal of Structural Geology*, **4**, 257–69.

Hubbard, F. H. 1966: Myrmekite in charnockite from south-west Nigeria. *American Mineralogist*, **51**, 762–73.

Hughes, C. J. 1971: Anatomy of a granophyre intrusion. *Lithos*, **4**, 403–15.

1972: Note on the variability of granophyric texture. *Bulletin of the Geological Society of America*, **83**, 2419–22.

Hulbert, L. J. & von Gruenewaldt, G. 1985: Textural and compositional features of chromite on the Lower and Critical Zones of the Bushveld Complex south of Potgietersus. *Economic Geology*, **80**, 872–95.

Hunter, R. H. 1987: Textural equilibrium in layered igneous rocks. *In* Parsons, I. (ed.): *Origins of Igneous Layering*. Dordrecht: Reidel, pp. 473–503.

1996: Texture development in cumulate rocks. *In* Cawthorn, R. G. (ed.): *Layered Intrusions* (*Developments in Petrology*, **15**). Amsterdam: Elsevier, pp. 77–101.

Hurlbut, C. S. 1935: Dark inclusions in a tonalite of southern California. *American Mineralogist*, **20**, 609–30.

Hurwitz, S. & Navon, O. 1994: Bubble nucleation in rhyolitic melts: Experiments at high pressure, temperature, and water content. *Earth and Planetary Science Letters*, **122**, 267–80.

Hutchison, M. N. & Scott, S. D. 1981: Sphalerite geobarometry in the system Cu-Fe-Zn-S. *Economic Geology*, **76**, 143–53.

Hutton, D. H. W. 1979: Dalradian structure in the Creeslough area, NW Donegal, Ireland. *In* Harris, A. L., Holland, C. H. & Leake, B. E. (eds): *The Caledonides of the British Isles – Reviewed. Geological Society of London Special Publication*, **8**, 239–41.

Iddings, W. 1891: Spherulitic crystallization. *Bulletin of the Philosophical Society of Washington*, **11**, 445–64.

Ikeda, S., Toriumi, M., Yosida, H. & Shimizu, I. 2002: Experimental study of the textural development of igneous rocks in the late stage of crystallization: the influence of interfacial energies under non-equilibrium conditions. *Contributions to Mineralogy and Petrology*, **142**, 397–415.

Ikeda, T., Shimobayashi, N., Wallis, S. & Tsuchiyama, A. 2002: Crystallographic orientation, chemical composition and three-dimensional geometry of sigmoidal garnet: evidence for rotation. *Journal of Structural Geology*, **24**, 1633–46.

2003: Reply to comment by A. Stallard on "Crystallographic orientation, chemical composition and three-dimensional geometry of sigmoidal garnet: evidence for rotation." *Journal of Structural Geology*, **25**, 1341–2.

Imon, R., Okudaira, T. & Fujimoto, A. 2002: Dissolution and precipitation processes in deformed amphibolites: an example from the ductile shear zone of the Ryoke metamorphic belt, Japan. *Journal of Metamorphic Geology*, **20**, 297–308.

Indares, A. 1993: Eclogitized gabbros from the eastern Grenville Province: textures, metamorphic context and implications. *Canadian Journal of Earth Sciences*, **30**, 59–73.

Ingerson, E. 1938: Albite trends in some rocks of the Piedmont. *American Journal of Science*, **A235**, 127–41.

Irvine, T. N. 1974: Petrology of the Duke Island ultramafic complex, Southeastern Alaska. *Geological Society of America Memoir*, **138**.

Jackson, K. A. 1958: Nature of solid–liquid interfaces. *In* Doremus, R. H., Roberts, B. W. & Turnbull, D. (eds): *Growth and Perfection of Crystals*. New York: Wiley, pp. 319–23.

1967: A review of the fundamental aspects of crystal growth. *In* Peiser, H. S. (ed.): *Crystal Growth*. Oxford: Pergamon, pp. 17–24.

Jackson, K. A., Uhlmann, D. R. & Hunt, J. D. 1967: On the nature of crystal growth from the melt. *Journal of Crystal Growth*, **1**, 1–36.

Jahns, R. H. 1953: The genesis of pegmatites. I. Occurrence and origin of giant crystals. *American Mineralogist*, **38**, 563–98.

1955: The study of pegmatites. *Economic Geology*, **50**, 1025–130.

1982: Internal evolution of pegmatite bodies. *In* Cerny, P. (ed.): *Granitic pegmatites in Science and Industry. Mineralogical Association of Canada Short Course*, **8**, 293–327.

Jahns, R. H. & Burnham, C. W. 1969: Experimental studies of pegmatite genesis: I. A model for the derivation and crystallization of granitic pegmatites. *Economic Geology*, **64**, 843–64.

Jahns, R. H. & Tuttle, O. F. 1962: Layered pegmatite-aplite intrusions. *American Mineralogist*, **47**, 94.

Jamieson, R. A. 1986: P-T paths from high temperature shear zones beneath ophiolites. *Journal of Metamorphic Geology*, **4**, 3–22.

1988: Textures, sequences of events, and assemblages in metamorphic rocks. *Mineralogical Association of Canada Short Course*, **14**, 189–212.

Jamieson, R. A. & Vernon, R. H. 1987: Timing of porphyroblast growth in the Fleur de Lys Supergroup, Newfoundland. *Journal of Metamorphic Geology*, **5**, 273–88.

Jamtveit, B. 1991: Oscillatory zonation patterns in hydrothermal grossular-andradite garnet: Nonlinear dynamics in regions of immiscibility. *American Mineralogist*, **76**, 1319–27.

Jamtveit, B. & Andersen, T. B. 1992: Morphological instabilities during rapid growth of metamorphic garnets. *Physics and Chemistry of Minerals*, **19**, 176–84.

Jamtveit, B., Bucher-Nurminen, K. & Austrheim, H. 1990: Fluid controlled eclogitization of granulites in deep crustal shear zones, Bergen Arcs, Western Norway. *Contributions to Mineralogy and Petrology*, **104**, 184–93.

Jamtveit, B., Wogelius, R. A. & Fraser, D. G. 1993: Zonation patterns of skarn garnets: records of hydrothermal system evolution. *Geology*, **21**, 113–16.

Janousek, V., Bowes, D. R., Braithwaite, J. R. & Rogers, G. 2000: Microstructural and mineralogical evidence for limited involvement of magma mixing in the petrogenesis of a Hercynian high-K calc-alkaline intrusion: the Kozárovice granodiorite, Central Bohemian Pluton, Czech Republic. *Transactions of the Royal Society of Edinburgh: Earth Sciences*, **91**, 15–26.

Jeffreys, H. H. 1942: On the mechanics of faulting. *Geological Magazine*, **79**, 291–5.

Jerram, D. A. & Cheadle, M. J. 2000: On the cluster analysis of grains and crystals in rocks. *American Mineralogist*, **85**, 47–67.

Jerram, D. A., Cheadle, M. J., Hunter, R. H. & Elliott, M. T. 1996: The spatial distribution of grains and crystals in rocks. *Contributions to Mineralogy and Petrology*, **125**, 60–74.

Jessell, M. W. 1986: Grain boundary migration and fabric development in experimentally deformed octachloropropane. *Journal of Structural Geology*, **8**, 527–42.

1987: Grain boundary migration microstructures in a naturally deformed quartzite. *Journal of Structural Geology*, **9**, 1007–14.

1988a: Simulation of fabric development in recrystallizing aggregates – I. Description of the model. *Journal of Structural Geology*, **10**, 771–8.

1988b: Simulation of fabric development in recrystallizing aggregates – II. Example model runs. *Journal of Structural Geology*, **10**, 779–93.

Jessell, M. W. & Bons, P. D. 2002: The numerical simulation of microstructure. *In* de Meer, S., Drury, M. R., de Bresser, J. H. & Pennock, G. M. (eds): *Deformation Mechanisms, Rheology and Tectonics: Current Status and Future Perspectives. Geological Society of London Special Publication*, **200**, 137–47.

Jessell, M. W., Bons, P. D., Evans, L., Barr, T. & Stüwe, K. 2001: Elle: the numerical simulation of metamorphic and deformation microstructures. *Computers and Geosciences*, **27**, 17–30.

Jessell, M. W., Kostenko, O. & Jamtveit, B. 2003: The preservation potential of microstructures during static grain growth. *Journal of Metamorphic Geology*, **21**, 481–91.

Jessell, M. W. & Lister, G. S. 1990: A simulation of the temperature dependence of quartz fabrics. *In* Knipe, R. J. & Rutter, E. H. (eds): *Deformation Mechanisms, Rheology and Tectonics. Geological Society of London Special Publication*, **54**, 353–62.

Jiang, D. 2001: Reading history of folding from porphyroblasts. *Journal of Structural Geology*, **23**, 1327–35.

Jin, D., Karato, S. & Obata, M. 1998: Mechanisms of shear localization in the continental lithosphere; information from the deformation microstructures of peridotites from the Ivrea Zone, northwestern Italy. *Journal of Structural Geology*, **20**, 195–209.

Jin, Z.-M., Green, H. W. & Borch, R. S. 1989: Microstructures of olivine and stresses in the upper mantle beneath Eastern China. *Tectonophysics*, **169**, 23–50.

Jin, Z.-M., Green, H. W. & Zhou, Y. 1994: Melt topology in partially molten mantle peridotite during ductile deformation. *Nature*, **372**, 164–7.

Johannes, W. 1985: The significance of experimental studies for the formation of migmatites. *In* Ashworth, J. R. (ed.): *Migmatites*. Glasgow: Blackie, pp. 36–85.

1988: What controls partial melting in migmatites? *Journal of Metamorphic Geology*, **6**, 451–66.

Johannsen, A. 1939: *A Descriptive Petrography of the Igneous Rocks.* Volume 1 (second edition). Chicago: University of Chicago Press.

John, B. E. & Stünitz, H. 1997: Magmatic fracturing and small-scale melt segregation during pluton emplacement: evidence from the Adamello Massif (Italy). *In* Bouchez, J.-L., Hutton, D. H. W. & Stephens, W. E. (eds): *Granite: From Segregation of Melt to Emplacement Fabrics*. Dordrecht: Kluwer, pp. 55–74.

Johnson, C. D. & Carlson, W. D. 1990: The origin of olivine-plagioclase coronas in metagabbros from the Adirondack Mountains, New York. *Journal of Metamorphic Geology*, **8**, 697–717.

Johnson, M. R. W. 1960: The structural history of the Moine thrust zone at Lochcarron, wester Ross. *Transactions of the Royal Society of Edinburgh*, **64**, 139–68.

1962: Relationships of movement and metamorphism in the Dalradian of Banffshire. *Transactions of the Edinburgh Geological Society*, **19**, 29–64.

1967: Mylonite zones and mylonite banding. *Nature*, **213**, 246–7.

Johnson, S. E. 1990: Deformation history of the Otago schists, New Zealand, from progressively developed porphyroblast-matrix microstructures: uplift-collapse orogenesis and its implications. *Journal of Structural Geology*, **12**, 727–46.

1992: Sequential porphyroblast growth during progressive deformation and low-P high-T (LPHT) metamorphism, Cooma Complex, Australia: The use of microstructural analysis in better understanding deformation and metamorphic histories. *Tectonophysics*, **214**, 311–39.

1993a: Unravelling the spirals: a serial thin section study and three-dimensional computer-aided reconstruction of spiral-shaped inclusion trails in garnet porphyroblasts. *Journal of Metamorphic Geology*, **11**, 621–34.

1993b: Testing models for the development of spiral-shaped inclusion trails in garnet porphyroblasts; to rotate or not to rotate, that is the question. *Journal of Metamorphic Geology*, **11**, 635–59.

1999a: Near-orthogonal foliation development in orogens: meaningless complexity, or reflection of fundamental dynamic processes? *Journal of Structural Geology*, **21**, 1183–7.

1999b: Porphyroblast microstructures: A review of current and future trends. *American Mineralogist*, **84**, 1711–26.

Johnson, S. E. & Bell, T. H. 1996: How useful are 'millipede' and other similar porphyroblast microstructures for determining synmetamorphic deformation histories? *Journal of Metamorphic Geology*, **14**, 15–28.

Johnson, S. E. & Moore, R. R. 1993: Reconstruction of three-dimensional surfaces from serially collected lines using the program Mathematica: example reconstruction and code. *Computers and Geosciences*, **19**, 1023–32.

1996: De-bugging the 'millipede' porphyroblast microstructure: a serial thin-section study and 3-D computer animation. *Journal of Metamorphic Geology*, **14**, 3–14.

Johnson, S. E. & Vernon, R. H. 1995a: Stepping stones and pitfalls in the determination of an anticlockwise P-T-t-deformation path in the low-P, high-T Cooma Complex, Australia. *Journal of Metamorphic Geology*, **13**, 165–83.

1995b: Inferring the timing of porphyroblast growth in the absence of continuity between inclusion trails and matrix foliations: can it be reliably done? *Journal of Structural Geology*, **17**, 1203–6.

Johnson, S. E., Vernon, R. H. & Upton, P. 2004: Initiation of microshear zones and progressive strain-rate partitioning in the crystallizing carapace of a tonalite pluton: microstructural evidence and numerical modeling. *Journal of Structural Geology* (in press).

Johnson, T. E., Brown, M. & Solar, G. S. 2003: Low-pressure subsolidus and suprasolidus phase equilibria in the MnNCKFMASH system: Constraints on conditions of regional metamorphism in western Maine, northern Appalachians. *American Mineralogist*, **88**, 624–38.

Jones, K. A. & Galwey, A. K. 1964: A study of possible factors concerning garnet formation in rocks from Ardara, Co. Donegal, Ireland. *Geological Magazine*, **101**, 76–92.

Joplin, G. A. 1964: *A Petrography of Australian Igneous Rocks*. Sydney: Angus & Robertson.

1968: *A Petrography of Australian Metamorphic Rocks*. Sydney: Angus & Robertson.

Jordan, P. G. 1987: The deformational behaviour of bimineralic limestone-halite aggregates. *Tectonophysics*, **135**, 185–97.

Judd, J. W. 1908: Henry Clifton Sorby, and the birth of microscopical petrology. *Geological Magazine* (New Series, Decade V), **5**, 193–204.

Jurewicz, S. R. & Jurewicz, A. J. G. 1986: Distribution of apparent angles on random sections with emphasis on dihedral angle measurements. *Journal of Geophysical Research*, **91**, 9277–82.

Jurewicz, S. R. & Watson, E. B. 1984: Distribution of partial melt in a felsic system: the importance of surface energy. *Contributions to Mineralogy and Petrology*, **85**, 25–9.

1985: The distribution of partial melt in a granite system: the application of liquid phase sintering theory. *Geochimica et Cosmochimica Acta*, **49**, 1109–21.

Kanagawa, K. 1991: Change in dominant mechanisms for phyllosilicate preferred orientation during cleavage development in the Kitakami Slates of NE Japan. *Journal of Structural Geology*, **13**, 927–43.

1996: Simulated pressure fringes, vorticity, and progressive deformation. *In* De Paor, D. G. (ed.): *Structural Geology and Personal Computers (Computer Methods in the Geosciences*, **15**). Oxford: Pergamon, Elsevier, pp. 259–83.

Kaneko, Y., Katayama, I., Yamamoto, H., Misawa, K., Ishikawa, M., Rehman, H. U., Kausar, A. B. & Shiraishi, K. 2003: Timing of Himalayan ultrahigh-pressure metamorphism: sinking rate and subduction angle of the Indian continental crust beneath Asia. *Journal of Metamorphic Geology*, **21**, 589–99.

Karabinos, P. 1984: Polymetamorphic garnet zoning from southeastern Vermont. *American Journal of Science*, **284**, 1008–25.

Karato, S. 1987: Scanning electron microscope observation of dislocations in olivine. *Physics and Chemistry of Minerals*, **14**, 245–8.

Karato, S., Paterson, M. S. & Fitz Gerald, J. D. 1986: Rheology of synthetic olivine aggregates: influence of grain-size and water. *Journal of Geophysical Research*, **91**, 8151–76.

Karato, S., Toriumi, M. & Fujii, T. 1982: Dynamic recrystallization of olivine single crystals during high temperature creep. *Geophysical Research Letters*, **7**, 649–52.

Katz, M. 1968: The fabric of the granulites of Mount Tremblant park, Quebec. *Canadian Journal of Earth Sciences*, **5**, 801–12.

Kehlenbeck, M. M. 1972: Deformation textures in the Lac Rouvray anorthosite mass. *Canadian Journal of Earth Sciences*, **9**, 1087–98.

Keith, H. D. & Padden, F. J. 1963: A phenomenological theory of spherulitic crystallization. *Journal of Applied Physics*, **34**, 2409–21.

Kelly, A. & Groves, G. W. 1970: *Crystallography and Crystal Defects*. London: Longman.

Kenah, P. & Hollister, L. S. 1983: Anatexis in the Central Gneiss Complex, British Columbia. *In* Atherton, M. P. & Gribble, C. D. (eds): *Migmatites, Melting and Metamorphism*. Cheshire, England: Shiva, pp. 142–62.

Kenkmann, T. & Dresen, G. 2002: Dislocation microstructure and phase distribution in a lower crustal shear zone – an example from the Ivrea-Zone, Italy. *International Journal of Earth Sciences (Geologische Rundschau)*, **91**, 445–58.

Kennan, P. 1971: Porphyroblast rotation and the kinematic analysis of a small fold. *Geological Magazine*, **108**, 221–8.

Kennedy, L. A. & White, J. C. 2001: Low-temperature recrystallization in calcite: Mechanisms and consequences. *Geology*, **29**, 1027–30.

Kerrich, R. 1978: An historical review and synthesis of research on pressure solution. *Zentralblatt für Mineralogie, Geologie und Paläontologie*, **5**, 512–50.

1986: Fluid infiltration into fault zones: chemical, isotopic, and mechanical effect. *Pure and Applied Geophysics*, **124**, 225–68.

Kerrich, R., Allison, I., Barnett, R. L., Moss, S. & Starkey, J. 1980: Microstructural and chemical transformations accompanying deformation of granite in a shear zone at Mieville, Switzerland: with implications for stress corrosion cracking and superplastic flow. *Contributions to Mineralogy and Petrology*, **73**, 221–42.

Kerrich, R., Fyfe, W. S., Gorman, B. E. & Allison, I. 1977: Local modification of rock chemistry by deformation. *Contributions to Mineralogy and Petrology*, **65**, 183–90.

Kerrick, D. M. 1969: K-feldspar megacrysts from a porphyritic quartz monzonite central Sierra Nevada, California. *American Mineralogist*, **54**, 839–48.

Kesler, S. E. & Wieblen, P. W. 1968: Distribution of elements in a spherulitic andesite. *American Mineralogist*, **53**, 2025–35.

Kile, D. E., Eberl, D. D., Hoch, A. R. & Reddy, M. M. 2000: An assessment of calcite crystal growth mechanisms based on crystal size distributions. *Geochimica et Cosmochimica Acta*, **64**, 2937–50.

King, B. C. 1964: The nature of basic igneous rocks and their relations with associated acid rocks. Part IV. *Science Progress*, **52**, 282–92.

Kingery, W. D. 1960: *Introduction to Ceramics*, New York: Wiley.

Kirby, S. H. & Etheridge, M. A. 1981: Exsolution of Ca-clinopyroxene from orthopyroxene aided by deformation. *Physics and Chemistry of Minerals*, **7**, 105–9.

Kirby, S. H. & Stern, L. A. 1993: Experimental dynamic metamorphism of mineral single crystals. *Journal of Structural Geology*, **15**, 1223–40.

Kirkpatrick, R. J. 1975: Crystal growth from the melt: a review. *American Mineralogist*, **60**, 798–814.

1977: Nucleation and growth of plagioclase, Makaoputi and Alae lava lakes, Kilauea Volcano, Hawaii. *Bulletin of the Geological Society of America*, **88**, 78–84.

1981: Kinetics of crystallization of igneous rocks. *In* Lasaga, A. C. & Kirkpatrick, R. J. (eds): *Kinetics of Geochemical Processes. Mineralogical Society of America, Reviews in Mineralogy*, **8**, 321–98.

1983: Theory of nucleation in silicate melts. *American Mineralogist*, **68**, 66–77.

Klaper, E. M. 1990: Reaction-enhanced formation of eclogite-facies shear zones in granulite-facies anorthosites. *In* Knipe, R. J. & Rutter, E. H. (eds): *Deformation*

Mechanisms, Rheology and Tectonics. Geological Society of London Special Publication, **54**, 167–73.

Kleinschrodt, R. 1994: Competing crystal-plastic and grain size sensitive deformation mechanisms in a peridotite mylonite from the Finero Complex (Ivrea Zone, NW-Italy). *In* Bunge, H. J., Siegesmund, S., Skrotzki, W. & Weber, K. (eds): *Textures of Geological Materials*. DGM Informationsgesellschaft-Verlag, pp. 201–19.

Knight, C. A. 1967: *The Freezing of Supercooled Liquids*. Princeton: Van Nostrand.

Knipe, R. J. 1979: Chemical changes during slaty cleavage development. *Bulletin de Minéralogie*, **102**, 206–9.

1981: The interaction of deformation and metamorphism in slates. *Tectonophysics*, **78**, 249–72.

1989: Deformation mechanisms – recognition from natural tectonites. *Journal of Structural Geology*, **11**, 127–46.

Knipe, R. J. & Rutter, E. H. (eds) 1990: *Deformation Mechanisms, Rheology and Tectonics. Geological Society of London Special Publication*, **54**, 535pp.

Knipe, R. J. & White, S. H. 1977: Microstructural variation of an axial plane cleavage around a fold – H.V.E.M. study. *Tectonophysics*, **39**, 355–80.

Knipe, R. J. & Wintsch, R. P. 1985: Heterogeneous deformation, foliation development and metamorphic processes in a polyphase mylonite. *In* Thompson, A. B. & Rubie, D. C. (eds): *Metamorphic Reactions. Kinetics, Texture and Deformation. Advances in Physical Chemistry*, **4**, 180–210.

Knopf, E. B. 1931: Retrogressive metamorphism and phyllonitization. *American Journal of Science*, **221**, 1–27.

Knopf, E. B. & Ingerson, E. 1938: *Structural Petrology. Geological Society of America Memoir*, **6**, 270pp.

Koehn, D., Aerden, D. G. A. M., Bons, P. D. & Passchier, C. W. 2001: Computer experiments to investigate complex fibre patterns in natural antitaxial strain fringes. *Journal of Metamorphic Geology*, **19**, 217–31.

Koehn, D., Bons, P. D. & Passchier, C. W. 2003: Development of antitaxial strain fringes during non-coaxial deformation: an experimental study. *Journal of Structural Geology*, **25**, 263–75.

Koehn, D., Hilgers, C., Bons, P. D. & Passchier, C. W. 2000: Numerical simulation of fibre growth in antitaxial strain fringes. *Journal of Structural Geology*, **22**, 1311–24.

Koehn, D., Passchier, C. W. & Bons, P. D. 1999: Kinematic analysis of strain fringes. *Journal of Conference Abstracts*, **4**, 830.

Kohlstedt, D. L., Goetze, C., Durham, W. D. & Vandersande, J. B. 1976: A new technique for decorating dislocations in olivine. *Science*, **19**, 1045–91.

Koons, P. O., Rubie, D. C. & Frueh-Green, G. 1987: The effects of disequilibrium and deformation on the mineralogical evolution of quartz diorite during metamorphism in the eclogite facies. *Journal of Petrology*, **28**, 679–700.

Korzhinskii, D. S. 1950: Phase rule and geochemical mobility of elements. *International Geological Congress Reports*, 18th Session, Part II, pp. 65–72.

1959: *Physicochemical Basis of the Analysis of the Paragenesis of Minerals.* New York: Consultants Bureau.

Koschek, G. 1993: Origin and significance of the SEM cathodoluminescence from zircon. *Journal of Microscopy*, **171**, 223–32.

Kouchi, A., Sugawara, Y., Kashima, K. & Sunagawa, I. 1983: Laboratory growth of sector zoned clinopyroxenes in the system $CaMgSi_2O_6$-$CaTiAl_2O_6$. *Contributions to Mineralogy and Petrology*, **83**, 177–84.

Krabbendam, M., Urai, J. L. & van Vliet, L. J. 2003: Grain size stabilization by dispersed graphite in a high-grade quartz mylonite: an example from Naxos (Greece). *Journal of Structural Geology*, **25**, 855–66.

Kranz, R. L. 1983: Microcracks in rocks: a review. *Tectonophysics*, **100**, 449–80.

Kretz, R. 1966a: Interpretation of the shape of mineral grains in metamorphic rocks. *Journal of Petrology*, **7**, 68–94.

1966b: Grain-size distribution for certain metamorphic minerals in relation to nucleation and growth. *Journal of Geology*, **74**, 147–73.

1969: On the spatial distribution of crystals in rocks. *Lithos*, **2**, 39–66.

1973: Kinetics of the crystallization of garnet at two localities near Yellowknife. *Canadian Mineralogist*, **12**, 1–20.

1974: Some models for the rate of crystallization of garnet in metamorphic rocks. *Lithos*, **7**, 123–31.

1983: Symbols for rock-forming minerals. *American Mineralogist*, **68**, 277–9.

1994: *Metamorphic Crystallization*. New York: Wiley.

Krogh, E. J. 1982: Metamorphic evolution of Norwegian country-rock eclogites, as deduced from mineral inclusions and compositional zoning in garnets. *Lithos*, **15**, 305–21.

Kronenberg, A. K., Kirby, S. H. & Pinkston, J. 1990: Basal slip and mechanical anisotropy of biotite. *Journal of Geophysical Research*, **95**, 19257–78.

Kruhl, J. H. 1996: Prism- and basal-plane parallel subgrain boundaries in quartz: a microstructural geothermobarometer. *Journal of Metamorphic Geology*, **14**, 581–9.

1998: Prism- and basal-plane parallel subgrain boundaries in quartz: a microstructural geothermobarometer: Reply. *Journal of Metamorphic Geology*, **16**, 142–6.

2001: Crystallographic control on the development of foam textures in quartz, plagioclase and analogue material. *International Journal of Earth Sciences (Geologische Rundschau)*, **90**, 104–17.

Kruhl, J. H. & Huntemann, T. 1991: The structural state of the former lower continental crust in Calabria (S. Italy). *Geologische Rundschau*, **80**, 209–302.

Kruhl, J. H. & Nega, M. 1996: The fractal shapes of sutured quartz grain boundaries: application as a geothermometer. *Geologische Rundschau*, **85**, 38–43.

Kruhl, J. H. & Peternell, M. 2001: Sutured grain boundaries of dynamically recrystallized quartz: Crystallographic orientation and temperature control. *Geological Society of Australia Abstracts*, **64**, 105.

2002: The equilibration of high-angle grain boundaries in dynamically recrystallized quartz: the effect of crystallography and temperature. *Journal of Structural Geology*, **24**, 1125–37.

Kruse, R. & Stünitz, H. 1999: Deformation mechanisms and phase distribution in mafic high-temperature mylonites from the Jotun Nappe, Southern Norway. *Tectonophysics*, **303**, 223–49.

Kuo, L.-C. & Kirkpatrick, R. J. 1982: Pre-eruption history of phyric basalts from DSDP Legs 45 and 46: Evidence from morphology and zoning patterns in plagioclase. *Contributions to Mineralogy and Petrology*, **79**, 13–27.

Kuo, L.-C., Lee, J. H., Essene, E. J. & Peacor, D. R. 1986: Occurrence, chemistry, and origin of immiscible silicate glasses in a tholeiitic basalt: A TEM/AEM study. *Contributions to Mineralogy and Petrology*, **94**, 90–8.

Kuritani, T. 2001: Replenishment of a mafic magma in a zoned felsic magma chamber beneath Rishiri Volcano, Japan. *Bulletin of Volcanology*, **62**, 533–48.

Kwak, T. A. P. 1981: Sector-zoned annite$_{85}$phlogopite$_{15}$ micas from the Mt. Lindsay Sn-W-F-(Be) deposit, Tasmania, Australia. *Canadian Mineralogist*, **19**, 643–50.

Laemmlein, G. 1930: Korrosion und Regeneration der Porphyr-Quarz. *Zeitschrift für Kristallographie*, **75**, 109–27.

Lafrance, B., John, B. E. & Frost, B. R. 1998: Ultra high-temperature and subsolidus shear zones: examples from the Poe Mountain anorthosite, Wyoming. *Journal of Structural Geology*, **20**, 945–55.

Lafrance, B., John, B. E. & Scoates, J. S. 1995: Syn-emplacement recrystallization and deformation microstructures in the Poe Mountain anorthosite, Wyoming. *Contributions to Mineralogy and Petrology*, **122**, 431–40.

Lafrance, B. & Vernon, R. H. 1993: Mass transfer and microfracturing in gabbroic mylonites of the Guadalupe Igneous Complex, California. *In* Boland, J. N. & Fitz Gerald, J. D. (eds): *Defects and Processes in the Solid State: Geoscience Applications. The McLaren Volume*. Amsterdam: Elsevier, pp. 151–67.

1999: Coupled mass transfer and microfracturing in gabbroic mylonites. *In* Snoke, A. W., Tullis, J. & Todd, V. R. (eds): *Fault-related Rocks: a Photographic Atlas*. Princeton: Princeton University Press, pp. 204–7.

Lang, H. M. & Gilotti, J. A. 2001: Plagioclase replacement textures in partially eclogitised gabbros from the Sanddal mafic-ultramafic complex, Greenland Caledonides. *Journal of Metamorphic Geology*, **19**, 495–515.

Langdon, T. G. 1985: Regimes of plastic deformation. *In* Wenk, H.-R. (ed.): *Preferred Orientation in Deformed Metals and Rocks: an Introduction to Modern Texture Analysis*. London: Academic Press, pp. 219–58.

Lanzirotti, A. 1995: Yttrium zoning in metamorphic garnets. *Geochimica et Cosmochimca Acta*, **59**, 4105–10.

Laporte, D. 1994: Wetting behaviour of partial melts during crustal anatexis: the distribution of hydrous silicic melts in polycrystalline aggregates of quartz. *Contributions to Mineralogy and Petrology*, **116**, 486–99.

Lapworth, C. 1885: The Highland controversy in British geology: its causes, course and consequences. *Nature*, **32**, 558–9.

Lasaga, A. C. 1998: *Kinetic Theory in the Earth Sciences*. Princeton: Princeton University Press.

Law, R. D. 1990: Crystallographic fabrics: a selective review of their applications to research in structural geology. *In* Knipe, R. J. & Rutter, E. H. (eds): *Deformation Mechanisms, Rheology and Tectonics. Geological Society of London Special Publication*, **54**, 335–52.

Law, R. D., Knipe, R. J. & Dayan, H. 1984: Strain path partitioning within thrust sheets: microstructural and petrographic evidence from the Moine Thrust zone at Loch Eriboll, northwest Scotland. *Journal of Structural Geology*, **6**, 477–97.

Law, R. D., Morgan, S. S., Casey, M., Sylvester, A. G. & Nyman, M. 1992: The Papoose Flat pluton, California: a reassessment of its emplacement history in the light of new microstructural and crystallographic observations. *Transactions of the Royal Society of Edinburgh: Earth Sciences*, **83**, 361–75.

Lawrence, L. J. 1967: Sulphide neomagmas and highly metamorphosed sulphide deposits. *Mineralium Deposita*, **2**, 5–10.

Lee, J. H., Peacor, D. R., Lewis, D. D. & Wintsch, R. P. 1986: Evidence for syntectonic crystallization for the mudstone to slate transition at Lehigh Gap, Pennsylvania, U.S.A. *Journal of Structural Geology*, **8**, 767–80.

Legros, F., Cantagrel, J.-M. & Devouard, B. 2000: Pseudotachylyte (frictionite) at the base of the Arequipa volcanic landslide deposit (Peru); implications for emplacement mechanisms. *Journal of Geology*, **108**, 601–11.

Lentz, D. R. 2002: Sphalerite and arsenopyrite at the Brunswick No. 12 massive-sulfide deposit, Bathurst camp, New Brunswick: constraints on P-T evolution. *Canadian Mineralogist*, **40**, 19–31.

Lentz, D. R. & Fowler, A. D. 1992: A dynamic model for graphic quartz-feldspar intergrowths in granitic pegmatites in the southwestern Grenville Province. *In* Martin, R. F. & Cerny, P. (eds): *Granitic Pegmatites. Canadian Mineralogist*, **30**, 571–85.

Lessing, P. & Standish, R. P. 1973: Zoned garnet from Crested Butte, Colorado. *Mineralogical Magazine*, **58**, 840–2.

Leung, I. S. 1974: Sector-zoned titanaugites: morphology, crystal chemistry, and growth. *American Mineralogist*, **59**, 127–38.

Lewis, B. 1974: The growth of crystals of low supersaturation. I. Theory. *Journal of Crystal Growth*, **21**, 29–39.

Likhanov, I. I. & Reverdatto, V. V. 2002: Mass transfer during replacement of andalusite by kyanite in ferroaluminous metapelites in Yenesei Ridge. *Petrologiya*, **10**, 543–60.

Lindgren, W. 1933: *Mineral Deposits* (fourth edition). New York: McGraw-Hill.

Linker, M. F. & Kirby, S. H. 1981: Anisotropy in the rheology of hydrolytically weakened synthetic quartz crystals. *In* Carter, N. L., Friedman, M., Logan, J. M. & Stearns, D. W. (eds): *Mechanical Behavior of Crustal Rocks: the Handin Volume*. Washington: American Geophysical Union, pp. 29–48.

Lister, G. S., Boland, J. N. & Zwart, H. J. 1986: Step-wise growth of biotite porphyroblasts in pelitic schists of the western Lys-Caillaouas massif (Pyrenees). *Journal of Structural Geology*, **8**, 543–62.

Lister, G. S. & Dornsiepen, U. F. 1982: Fabric transitions in the Saxony granulite terrane. *Journal of Structural Geology*, **4**, 81–92.

Lister, G. S. & Snoke, A. W. 1984: *S-C* mylonites. *Journal of Structural Geology*, **6**, 617–38.

Liu, J., Walter, J. M. & Webber, K. 2002: Fluid-enhanced low-temperature plasticity of calcite marble; microstructures and mechanisms. *Geology*, **30**, 787–90.

Lloyd, G. E. 1987: Atomic number and crystallographic contrast images with the SEM: a review of backscattered electron techniques. *Mineralogical Magazine*, **51**, 3–20.

Lloyd, G. E., Farmer, A. B. & Mainprice, D. 1997: Misorientation analysis and the formation and orientation of subgrain and grain boundaries. *Tectonophysics*, **279**, 55–78.

Lloyd, G. E. & Freeman, B. 1994: Dynamic recrystallization of quartz under greenschist conditions. *Journal of Structural Geology*, **16**, 867–81.

Lloyd, G. E. & Prior, D. J. 1999: EBSD technique and application in geosciences. *In* Leiss, B., Ullemeyer, K. & Weber, K. (eds): *Textures and Physical Properties of Rocks. Göttinger Arbeiten zum Geologie und Paläontologie*, **Sb4**, 112–13.

Loewinson-Lessing, F. Y. 1954: *A Historical Survey of Petrology*. Edinburgh: Oliver & Boyd.

Lofgren, G. E. 1971a: Spherulitic textures in glassy and crystalline rocks. *Journal of Geophysical Research*, **76**, 5635–48.

1971b: Experimentally produced devitrification textures in natural rhyolitic glass. *Bulletin of the Geological Society of America*, **82**, 111–24.

1973: Experimental crystallization of synthetic plagioclase at prescribed cooling rates (abstract). *EOS*, *Transactions of the American Geophysical Union*, **54**, 482.

1974: Temperature induced zoning in synthetic plagioclase feldspar. *In* MacKenzie, W. S. & Zussman, J. (eds): *The Feldspars*. Manchester: Manchester University Press, pp. 362–75.

1976: Nucleation and growth of alkali feldspar in dynamic crystallization experiments. *Geological Society of America Abstracts with Programs*, **7**, 982.

1980: Experimental studies on the dynamic crystallization of silicate melts. *In* Hargraves, R. B. (ed.): *Physics of Magmatic Processes*. Princeton: Princeton University Press, pp. 487–551.

1983: Effect of heterogeneous nucleation on basaltic textures. *Journal of Petrology*, **24**, 229–55.

Lofgren, G. E. & Donaldson, C. H. 1975: Curved branching crystals and differentiation in comb-layered rocks. *Contributions to Mineralogy and Petrology*, **49**, 309–19.

Lofgren, G. E., Donaldson, C. H., Williams, R. J., Mullins, O. & Usselman, T. M. 1974: Experimentally reproduced textures and mineral chemistry of Apollo 15 quartz normative basalts. *Proceedings of the Fifth Lunar Science Conference*. Houston, TX: NASA, pp. 549–67.

Lofgren, G. E. & Russell, W. J. 1986: Dynamic crystallization of chondrule melts of porphyritic and radial pyroxene composition. *Geochimica et Cosmoshimica Acta*, **50**, 1715–26.

London, D. 1992: The application of experimental petrology to the genesis and crystallization of granitic pegmatites. *In* Martin, R. F. & Cerny, P. (eds): *Granitic Pegmatites. Canadian Mineralogist*, **30**, 499–540.

1996: Granitic pegmatites. *Transactions of the Royal Society of Edinburgh: Earth Sciences*, **87**, 305–19.

1999: Melt boundary-layers and the growth of pegmatitic textures. *Canadian Mineralogist*, **37**, 826–7.

London, D., Morgan, G. B. & Hervig, R. L. 1989: Vapor-undersaturated experiments with Macusani glass + H_2O at 200 MPa, and the internal differentiation of granitic pegmatites. *Contributions to Mineralogy and Petrology*, **102**, 1–17.

Long, P. E. 1978: Experimental determination of partition coefficients for Rb, Sr, and Ba between alkali feldspar and silicate liquid. *Geochimica et Cosmochimica Acta*, **42**, 833–46.

Long, P. E. & Luth, W. C. 1986: Origin of K-feldspar megacrysts in granitic rocks: Implications of a partitioning model for barium. *American Mineralogist*, **71**, 367–75.

Long, P. E. & Wood, B. J. 1986: Structures, textures and cooling histories of Columbia River basalt flows. *Bulletin of the Geological Society of America*, **97**, 1144–55.

Lonker, S. W. 1988: An occurrence of grandidierite, kornerupine, and tourmaline in southeastern Ontario, Canada. *Contributions to Mineralogy and Petrology*, **98**, 49–63.

Loomis, T. P. 1976: A natural example of metastable reactions involving garnet and sillimanite. *Journal of Petrology*, **20**, 271–92.

1986: Metamorphism of metapelites: calculation of equilibrium assemblages and numerical simulations of the crystallization of garnet. *Journal of Metamorphic Geology*, **4**, 201–29.

Loomis, T. P. & Nimick, F. B. 1982: Equilibrium in Mn-Fe-Mg aluminous pelitic compositions and the equilibrium growth of garnet. *Canadian Mineralogist*, **20**, 393–410.

Love, L. G. & Amstutz, G. C. 1966: Review of microscopic pyrite from the Devonian Chattanooga Shale and Rammelsberg Banderz. *Fortschritte Mineralogie*, **43**, 273–309.

Lovett, R., Ortoleva, P. & Ross, J. 1978: Kinetic instabilities in first order phase transitions. *Journal of Chemical Physics*, **69**, 947–55.

Lowder, G. G. & Dow, J. A. S. 1978: Geology and exploration of porphyry copper deposits in North Sulawesi, Indonesia. *Economic Geology*, **73**, 628–44.

Lowenstern, J. B. 1995: Application of silicate-melt inclusions to the study of magmatic volatiles. *In* Thompson, J. F. H. (ed.): *Magmas, Fluids and Ore Deposits. Mineralogical Association of Canada Short Course*, **23**, 71–99.

Lowenstern, J. B. & Sinclair, W. D. 1996: Exsolved magmatic fluid and its role in the formation of comb-layered quartz at the Cretaceous Logtung W-Mo deposit, Yukon territory, Canada. *Transactions of the Royal Society of Edinburgh: Earth Sciences*, **87**, 291–303.

Lusk, J., Calder, B. O. E. & Freeman, T. E. 2002: Temperatures from triple-junction angles in sulfides. *American Mineralogist*, **87**, 1390–400.

Lusk, J. & Ostwald, J. 1983: Analysis of pyrrhotite properties accompanying recrystallization of some metamorphosed nickel sulfide ores from Kambalda, Western Australia. *Canadian Journal of Earth Sciences*, **20**, 113–19.

Lyall, K. D. 1966: The origin of mechanical twinning in galena. *American Mineralogist*, **51**, 243–7.

Lyall, K. D. & Paterson, M. S. 1966: Plastic deformation of galena (lead sulphide). *Acta Metallurgica*, **14**, 371–83.

MacGregor, A. J. 1950: Ice crystals in glaciers compared with quartz crystals in dynamically metamorphosed sandstone. *Journal of Glaciology*, **1**, 564–71.

MacKenzie, J. S., Needham, D. T. & Agar, S. M. 1987: Progressive deformation in an accretionary complex: An example from the Shimanto belt of eastern Kyushu, southwest Japan. *Geology*, **15**, 353–6.

MacLellan, H. E. & Trembath, L. T. 1991: The role of quartz crystallization in the development and preservation of igneous texture in granitic rocks: Experimental evidence at 1 kbar. *American Mineralogist*, **76**, 1291–305.

Maddock, R. H. 1983: Melt origin of fault-generated pseudotachylytes demonstrated by textures. *Geology*, **11**, 105–8.

1986: Partial melting of lithic porphyroclasts in fault-generated pseudotachylytes. *Neues Jahrbuch für Mineralogie Abhandlungen*, **155**, 1–14.

1992: Effect of lithology, cataclasis and melting on the composition of fault-generated pseudotachylytes in Lewisian Gneiss, Scotland. *Tectonophysics*, **204**, 261–8.

Maddock, R. H., Grocott, J. & van Nes, M. 1987: Vesicles, amygdales and similar structures in fault-generated pseudotachylites. *Lithos*, **20**, 419–32.

Magloughlin, J. F. 1989: The nature and significance of pseudotachylite from the Nason terrane North Cascade Mountains, Washington. *Journal of Structural Geology*, **11**, 907–17.

Magloughlin, J. F. & Spray, J. G. 1992: Frictional melt processes and products in geological materials: introduction and discussion. *Tectonophysics*, **204**, 197–204.

Mainprice, D., Bouchez, J.-L., Blumenfeld, P. & Tubià, J. M. 1986: Dominant *c* slip in naturally deformed quartz: implications for dramatic plastic softening at high temperature. *Geology*, **14**, 819–22.

Maliva, R. G. & Siever, R. 1988: Diagenetic replacement controlled by force of crystallization. *Geology*, **16**, 688–91.

Maltman, A. J. 1981: Primary bedding-parallel fabrics in structural geology. *Journal of the Geological Society of London*, **138**, 475–83.

Mancktelow, N. S. 1985: The Simplon Line: a major displacement zone in the western Lepontine Alps. *Eclogae Geologicae Helvetiae*, **78**, 73–96.

Mancktelow, N. S. & Pennacchioni, G. 2004: The influence of grain boundary fluids on the microstructure of quartz-feldspar mylonites. *Journal of Structural Geology*, **26**, 47–69.

Marchildon, N. & Brown, M. 2002: Grain-scale melt distribution in two contact aureole rocks: implications for controls on melt localization and deformation. *Journal of Metamorphic Geology*, **20**, 381–96.

2003: Spatial distribution of melt-bearing structures in anatectic rocks from Southern Brittany, France: implications for melt transfer at grain- to orogen-scale. *Tectonophysics*, **364**, 215–35.

Mares, V. M. & Kronenberg, A. K. 1993: Experimental deformation of muscovite. *Journal of Structural Geology*, **15**, 1061–75.

Marignac, C. 1989: Sphalerite stars in chalcopyrite: Are they always the result of an unmixing process? *Mineralium Deposita*, **24**, 176–82.

Marlow, P. C. & Etheridge, M. A. 1977: Development of layered crenulation cleavage in mica schists of the Kanmantoo Group near Macclesfield, South Australia. *Bulletin of the Geological Society of America*, **88**, 873–82.

Marmo, B. A., Clarke, G. L. & Powell, R. 2002: Fractionation of bulk rock composition due to porphyroblast growth: effects on eclogite facies mineral equilibria, Pam Peninsula, New Caledonia. *Journal of Metamorphic Geology*, **20**, 151–65.

Marsh, B. D. 1988a: Crystal size distribution (CSD) in rocks and the kinetics and dynamics of crystallization I. Theory. *Contributions to Mineralogy and Petrology*, **99**, 272–91.

1998b: On the interpretation of crystal size distributions in magmatic systems. *Journal of Petrology*, **39**, 553–600.

Marsh, B. D. & Higgins, M. D. 2002: Inherited correlation in crystal size distribution: Comment and reply. COMMENT. *Geology*, **30**, 284–5.

Marshall, D. B., Vernon, R. H. & Hobbs, B. E. 1976: Experimental deformation and recrystallization of a peristerite. *Contributions to Mineralogy and Petrology*, **57**, 49–54.

Marshall, D. J. 1988: *Cathodoluminescence of Geologic Materials*. London: Unwin Hyman.

Martin, J. W. & Doherty, R. D. 1976: *Stability of Microstructure in Metallic Systems*. Cambridge: Cambridge University Press.

Masberg, H. P., Hoffer, E. & Hoernes, S. 1992: Microfabrics indicating granulite-facies metamorphism in the low-pressure central Damara Orogen, Namibia. *Precambrian Research*, **55**, 243–57.

Masch, L., Wenk, H.-R. & Preuss, E. 1985: Electron microscopy study of hyalomylonites – evidence for frictional melting in landslides. *Tectonophysics*, **115**, 131–60.

Mason, R. 1967: Electron-probe microanalysis of coronas in a troctolite from Sulitjelma, Norway. *Mineralogical Magazine*, **36**, 504–14.

Masuda, T. & Mochizuki, S. 1989: Development of snowball structure: numerical simulation of inclusion trails during synkinematic porphyroblast growth in metamorphic rocks. *Tectonophysics*, **170**, 141–50.

Mathison, C. I. 1987: Pyroxene oikocrysts in troctolitic cumulates – evidence for supercooled crystallisation and postcumulus modification. *Contributions to Mineralogy and Petrology*, **97**, 228–36.

Matter, A. & Ramseyer, K. 1985: Cathodoluminescence microscopy as a tool for provenance studies of sandstones *In* Zuffa, G. C. (ed.): *Provenance of Arenites*. Dordrecht: Reidel, pp. 191–211.

Matthews, M., Harte, B. & Prior, D. J. 1992: Mantle garnets: a cracking yarn. *Geochimica et Cosmochimica Acta*, **56**, 2633–42.

Mavrogenes, J. A., MacIntosh, I. W. & Ellis, D. J. 2001: Partial melting of the Broken Hill galena-sphalerite ore: experimental studies in the system PbS-FeS-ZnS-(Ag_2S). *Economic Geology*, **96**, 205–10.

Mawer, C. K. 1987: Shear criteria in the Grenville Province, Ontario, Canada. *Journal of Structural Geology*, **9**, 531–8.

Max, M. D. 1970: Metamorphism of Caledonian metadolerites in north-west County Mayo, Ireland. *Geological Magazine*, **107**, 539–48.

McBirney, A. R. & Hunter, R. H. 1995: The cumulate paradigm reconsidered. *Journal of Geology*, **103**, 114–22.

McBirney, A. R. & Noyes, R. M. 1979: Crystallization and layering of the Skaergaard intrusion. *Journal of Petrology*, **20**, 487–554.

McCaig, A. M. 1984: Fluid-rock interaction in some shear zones from the Pyrenees. *Journal of Metamorphic Geology*, **2**, 129–41.

1987: Deformation and fluid-rock interaction in metasomatic dilatant shear bands. *Tectonophysics*, **135**, 121–32.

1997: The geochemistry of volatile fluid flow in shear zones. *In* Holness, M. B. (ed.): *Deformation-enhanced Fluid Transport in the Earth's Crust and Mantle*. London: Chapman and Hall, pp. 227–66.

McCaig, A. M. & Knipe, R. J. 1990: Mass-transport mechanisms in deforming rocks: recognition using microstructural and microchemical criteria. *Geology*, **18**, 824–7.

McClay, K. R. 1977: Pressure solution and Coble creep in rocks and minerals: a review. *Journal of the Geological Society of London*, **134**, 57–70.

1980: Sheared galena, textures and microstructures. *Journal of Structural Geology*, **2**, 227–34.

1982a: Schistosity in galena: recrystallization mechanisms. *In* Borradaile, G. J., Bayly, M. B. & Powell, C. McA. (eds): *Atlas of Deformational and Metamorphic Rock Fabrics*. Berlin: Springer, pp. 374–5.

1982b: Schistosity in galena: recrystallization fabrics. *In* Borradaile, G. J., Bayly, M. B. & Powell, C. McA. (eds): *Atlas of Deformational and Metamorphic Rock Fabrics*. Berlin: Springer, pp. 376–7.

1982c: Fabrics in ores: sphalerite, chalcopyrite, pyrite. *In* Borradaile, G. J., Bayly, M. B. & Powell, C. McA. (eds): *Atlas of Deformational and Metamorphic Rock Fabrics.* Berlin: Springer, pp. 382–3.

1983: Fabrics of deformed sulphides. *Geologische Rundschau*, **72**, 469–91.

McClay, K. R. & Atkinson, B. K. 1977: Experimentally induced kinking and annealing of single crystals of galena. *Tectonophysics*, **39**, 175–89.

McClay, K. R. & Ellis, P. G. 1983: Deformation and recrystallization of pyrite. *Mineralogical Magazine*, **47**, 527–38.

1984: Deformation of pyrite. *Economic Geology*, **79**, 400–3.

McKenzie, D. P. & Brune, J. P. 1972: Melting on fault planes during large earthquakes. *Geophysical Journal of the Royal Astronomical Society*, **29**, 65–78.

McLane, M. 1995: *Sedimentology*. Oxford: Oxford University Press.

McLaren, A. C. 1974: Transmission electron microscopy of the feldspars. *In* Mackenzie, W. S. & Zussman, J. (eds): *The Feldspars.* Manchester: Manchester University Press, pp. 378–423.

1986: Some speculations on the nature of high-angle grain boundaries in quartz rocks. *In* Hobbs, B. E. & Heard, H. C. (eds): *Mineral and Rock Deformation: Laboratory Studies (The Paterson Volume). American Geophysical Union, Geophysical Monograph*, **36**, 233–45.

1991: *Transmission Electron Microscopy of Minerals and Rocks*. Cambridge: Cambridge University Press.

McLaren, A. C. & Etheridge, M. A. 1976: A transmission electron microscope study of naturally deformed orthopyroxene. *Contributions to Mineralogy and Petrology*, **57**, 163–77.

McLaren, A. C., Fitz Gerald, J. D. & Williams, I. S. 1994: The microstructure of zircon and its influence on the age determination from Pb/U isotopic ratios measured by ion microprobe. *Geochimica et Cosmochimica Acta*, **58**, 993–1005.

McLaren, A. C. & Hobbs, B. E. 1972: Transmission electron microscope investigation of some naturally deformed quartzites. *In* Heard, H. C., Borg, I. Y., Carter, N. L. & Raleigh, C. B. (eds): *Flow and Fracture of Rocks. Geophysical Monograph Series*, **16**, 55–66.

McLaren, A. C. & Pryer, L. L. 2001: Microstructural investigation of the interaction and interdependence of cataclastic and plastic mechanisms in feldspar crystals deformed in the semi-brittle field. *In* Boland, J. & Ord, A. (eds): *Deformation Processes in the Earth's Crust. Tectonophysics*, **335**, 1–15.

McLaren, A. C. & Retchford, D. T. 1969: Transmission electron microscope study of the dislocations in plastically deformed synthetic quartz. *Physica Status Solidi*, **33**, 657–68.

McLaren, A. C., Retchford, D. T. & Griggs, D. T. 1967: Transmission electron microscope study of Brazil twins and dislocations experimentally produced in natural quartz. *Physica Status Solidi*, **19**, 631–44.

McLean, D. 1957: *Grain Boundaries in Metals*. Oxford: Oxford University Press.

McLean, W. H. 1969: Liquidus phase relations in the FeS-FeO-Fe_3O_4-SiO_2 system and their application in geology. *Economic Geology*, **64**, 865–84.

McLellan, E. L. 1988. Migmatite structures in the Central Gneiss Complex, Boca de Quadra, Alaska. *Journal of Metamorphic Geology*, **6**, 517–42.

McLelland, J., Morrison, J., Selleck, B., Cunningham, B., Olson, C. & Schmidt, K. 2002a: Hydrothermal alteration of late- to post-tectonic Lyon Mountain Granitic Gneiss, Adirondack Mountains, New York: Origin of quartz-sillimanite segregations, quartz-albite lithologies, and associated Kiruna-type low-Ti Fe-oxide deposits. *Journal of Metamorphic Geology*, **20**, 175–90.

McLelland, J., Goldstein, A., Cunningham, B., Olson, C. & Orrell, S. 2002b: Structural evolution of a quartz-sillimanite vein and nodule complex in a late- to post-tectonic leucogranite, Western Adirondack Highlands, New York. *Journal of Structural Geology*, **24**, 1157–70.

McMillan, K. 1986: Spatially varied marioles in the albite porphyry of Cuchillo Mountain, southwestern New Mexico. *American Mineralogist*, **71**, 625–31.

McMurry, J. 2001: Crystal accumulation and shearing in a megacrystic quartz monzonite: Bodocó pluton, northeastern Brazil. *Journal of Petrology*, **42**, 251–76.

McPhie, J., Doyle, M. & Allen, R. 1993: *Volcanic Textures*. Hobart: Centre for Ore Deposit and Exploration Studies, University of Tasmania.

McQueen, D. R., Kelly, W. C. & Clark, B. R. 1980: Kinematics of experimentally produced deformation bands in stibnite. *Tectonophysics*, **66**, 55–81.

McSween, H. Y., Coish, R. A. & Norman, M. D. 1979: Coexisting acidic and basic melts: geochemistry of a composite dike – discussion. *Journal of Geology*, **87**, 211–16.

Means, W. D. 1963: Mesoscopic structures and multiple deformation in the Otago schist, New Zealand. *New Zealand Journal of Geology and Geophysics*, **6**, 801–16.

1977: A deformation experiment in transmitted light. *Earth and Planetary Science Letters*, **35**, 169–79.

1981: The concept of steady-state foliation. *Tectonophysics*, **78**, 179–99.

1983: Microstructure and micromotion in recrystallization flow of octachloropropane: a first look. *Geologische Rundschau*, **72**, 511–28.

1989: Synkinematic microscopy of transparent polycrystals. *Journal of Structural Geology*, **11**, 163–74.

Means, W. D. & Jessell, M. W. 1986: Accommodation migration of grain boundaries. *Tectonophysics*, **127**, 67–86.

Means, W. D. & Park, Y. 1994: New experimental approach to understanding igneous texture. *Geology*, **22**, 323–6.

Means, W. D. & Ree, J.-H. 1988: Seven types of subgrain boundaries in octachloropropane. *Journal of Structural Geology*, **10**, 765–70.

Means, W. D. & Williams, P. F. 1974: Compositional differentiation in an experimentally deformed salt-mica specimen. *Geology*, **2**, 15–16.

Means, W. D. & Xia, Z. G. 1981: Deformation of crystalline materials in thin section. *Geology*, **9**, 538–43.

Mees, F., Sennen, R., van Geet, M. & Jacobs, P. 2003: *Applications of X-ray Computed Tomography in the Geosciences. Geological Society of London Special Publication*, **215**.

Mehnert, K. R. 1968: *Migmatites*. New York: Elsevier.

Mehnert, K. R. & Büsch, W. 1981: The Ba-content of K-feldspar megacrysts in granites: a criterion for their formation. *Neues Jahrbuch für Mineralogie Abhandlungen*, **140**, 221–52.

1985: The formation of k-feldspar megacrysts in granites, migmatites and augengneisses. *Neues Jahrbuch für Mineralogie Abhandlungen*, **151**, 229–59.

Mehnert, K. R., Büsch, W. & Schneider, G. 1973: Initial melting at grain boundaries of quartz and feldspar in gneisses and granulites. *Neues Jahrbuch für Mineralogie Monatshefte*, **1973**, 165–83.

Meneilly, A. W. 1983: Development of early composite cleavage in pelites from west Donegal. *Journal of Structural Geology*, **5**, 83–97.

Mercier, J.-C. C. & Nicolas, A. 1975: Textures and fabrics of upper-mantle peridotites as illustrated by xenoliths from basalts. *Journal of Petrology*, **16**, 454–87.

Miller, R. B. & Paterson, S. R. 1994: The transition from magmatic to high-temperature solid-state deformation: implications from the Mount Stuart batholith, Washington. *Journal of Structural Geology*, **16**, 853–65.

Milner, H. B. 1962: *Sedimentary Petrography* (fourth edition). London: Allen and Unwin.

Milodowski, A. E. & Zalasiewicz, J. A. 1991: The origin and sedimentary, diagenetic and metamorphic evolution of chlorite-mica stacks in Llandovery sediments of central Wales, U.K. *Geological Magazine*, **128**, 263–78.

Milord, I. & Sawyer, E. W. 2003: Schlieren formation in diatexite migmatite: examples from the St Malo migmatite terrane, France. *Journal of Metamorphic Geology*, **21**, 347–62.

Misch, P. 1969: Paracrystalline microboudinage of zoned grains and other criteria for synkinematic growth of metamorphic minerals. *American Journal of Science*, **267**, 43–63.

1970: Paracrystalline microboudinage in a metamorphic reaction sequence. *Bulletin of the Geological Society of America*, **81**, 2483–6.

1971: Porphyroblasts and “crystallization force”: Some textural criteria. *Bulletin of the Geological Society of America*, **82**, 245–51.

1972a: Porphyroblasts and “crystallization force”: Some textural criteria. Reply. *Bulletin of the Geological Society of America*, **83**, 921–2.

1972b: Porphyroblasts and “crystallization force”: Some textural criteria. Reply. *Bulletin of the Geological Society of America*, **83**, 1203–4.

Miyake, A. 1993: Rotation of biotite porphyroblasts in pelitic schist from the Nukata area, central Japan. *Journal of Structural Geology*, **15**, 1303–13.

1998: Monte Carlo simulation of normal grain growth in 2- and 3-dimensions: the lattice-model independent grain size distribution. *Contributions to Mineralogy and Petrology*, **130**, 121–33.

Miyazaki, K. 1991: Ostwald ripening of garnet in high P/T metamorphic rocks. *Contributions to Mineralogy and Petrology*, **108**, 118–28.

Mongkoltip, P. & Ashworth, J. R. 1983: Quantitative estimation of an open-system symplectite-forming reaction: restricted diffusion of Al and Si in coronas around olivine. *Journal of Petrology*, **24**, 635–61.

Moore, A. C. 1973: Studies of igneous and tectonic textures and layering in the rocks of the Gosse Pile intrusion, Central Australia. *Journal of Petrology*, **14**, 49–80.

Moore, J. C. & Geigle, J. E. 1974: Slaty cleavage: incipient occurrences in the deep sea. *Science*, **183**, 509–10.

Moore, J. G. & Lockwood, J. P. 1973: Origin of comb layering and orbicular structure, Sierra Nevada batholith, California. *Bulletin of the Geological Society of America*, **84**, 1–20.

Mora, C. I. & Ramseyer, K. 1992: Cathodoluminescence of coexisting plagioclases, Boehls Butte anorthosite: CL activators and fluid flow paths. *American Mineralogist*, **77**, 1258–65.

Mora, C. I. & Valley, J. W. 1991: Prograde and retrograde fluid-rock interaction in Wallace Formation calc-silicates northwest of the Idaho batholith: Stable isotopic evidence. *Contributions to Mineralogy and Petrology*, **108**, 162–74.

Morrison, J. & Valley, J. W. 1988: Post-granulite facies fluid infiltration in the Adirondack Mountains. *Geology*, **16**, 513–16.

Morritt, R. F. C., Powell, C. McA. & Vernon, R. H. 1982: Bedding-plane foliation. *In* Borradaile, G. J., Bayly, M. B. & Powell, C. McA. (eds): *Atlas of Deformational and Metamorphic Rock Fabrics*. Berlin: Springer, pp. 46–9.

Mosher, S. 1980: Pressure solution deformation of conglomerates in shear zones, Narragansett basin, Rhode island. *Journal of Structural Geology*, **2**, 219–25.

Moss, B. E., Haskin, L. A. & Dymek, R. F. 1995: Redetermination and reevaluation of compositional variations in metamorphosed sediments of the Littleton Formation, New Hampshire. *American Journal of Science*, **295**, 988–1019.

1996: Compositional variations in metamorphosed sediments of the Littleton Formation, New Hampshire, and the Carrabassett Formation, Maine, at sub-hand specimen, outcrop, and regional scales. *American Journal of Science*, **296**, 473–505.

Mügge, O. 1898: Über Translationen und verwandte Erscheinungen in Kristallen. *Neues Jahrbuch für Mineralogie, Geologie und Paläontologie Abhandlungen*, **1**, 71–159.

1931: Bewegungen von Porphyroblasten in Phylliten. *Neues Jahrbuch für Mineralogie, Geologie und Paläontologie Abhandlungen*, **61**, 469–520.

Müller, A., Kronz, A. & Breiter, K. 2002a: Trace elements and growth patterns in quartz: a fingerprint of the evolution of the subvolcanic Podlesí granite System (Krusné hory Mts., Czech Republic). *Bulletin of the Czech Geological Survey*, **77**, 135–45.

Müller, A., Lennox, P. & Trzebski, R. 2002b: Cathodoluminescence and micro-structural evidence for crystallisation and deformation processes of granites in the Eastern Lachlan Fold Belt (SE Australia). *Contributions to Mineralogy and Petrology*, **143**, 510–24.

Müller, A., Seltmann, R. & Behr, H.-J. 2000: Application of cathodoluminescence to magmatic quartz in a tin granite – a case study from the Schellerhau Granite Complex, Eastern Erzgebirge, Germany. *Mineralium Deposita*, **35**, 169–89.

Müller, G., Schuster, A. K. & Zippert, Y. 1988: Spinifex textures and texture zoning in fayalite-rich slags of medieval iron-works near Schieder Village, NW-Germany. *Neues Jahrbuch für Mineralogie Monatshefte*, **1988** (**3**), 111–20.

Murr, L. E. & Lerner, S. L. 1977: Transmission electron microscopic study of defect structure in natural chalcopyrite ($CuFeS_2$). *Journal of Materials Science*, **12**, 1349–54.

Murrell, S. A. F. 1985: Aspects of relationships between deformation and metamorphism that causes evolution of water. *In* Thompson, A. B. & Rubie, D. C. (eds): *Metamorphic Reactions. Kinetics, Textures, and Deformation. Advances in Physical Geochemistry*, **4**, 211–41.

1990: Brittle-to-ductile transitions in polycrystalline non-metallic materials. *In* Barber, D. J. & Meredith, P. G. (eds): *Deformation Processes in Minerals, Ceramics and Rocks*. Boston: Unwin Hyman, pp. 109–37.

Myers, J. S. 1978: Formation of banded gneisses by deformation of igneous rocks. *Precambrian Research*, **6**, 43–64.

Mysen, B. O. 1988: *Structure and Properties of Silicate Melts (Developments in Geochemistry*, **4**). New York: Elsevier.

1999: Structure and properties of magmatic liquids from haplobasalt to haploandesite. *Geochimica et Cosmochimica Acta*, **63**, 95–102.

Mysen, B. O., Virgo, D. & Scarfe, C. M. 1980a: Relations between the anionic structure and viscosity of silicate melts – a Raman spectroscopic study. *American Mineralogist*, **65**, 690–710.

Mysen, B. O., Ryerson, F. J. & Virgo, D. 1980b: The influence of TiO_2 on the structure and derivative properties of silicate melts. *American Mineralogist*, **65**, 1150–65.

1981a: The structural role of phosphorus in silicate melts. *American Mineralogist*, **66**, 106–17.

Mysen, B. O., Virgo, D. & Kushiro, I. 1981b: The structural role of aluminum in silicate melts. *American Mineralogist*, **66**, 678–701.

Nakamura, M. & Shimakita, S. 1998: Dissolution origin and syn-entrapment compositional change of melt inclusions in plagioclase. *Earth and Planetary Science Letters*, **161**, 119–33.

Nakamura, Y. 1973: Origin of sector-zoning of igneous clinopyroxenes. *American Mineralogist*, **58**, 986–90.

Nam, T. N., Otoh, S. & Masuda, T. 1999: In-situ annealing experiments of octachloropropane as a rock analogue: kinetics and energetics of grain growth. *Tectonophysics*, **304**, 57–70.

Nesbitt, R. W. 1971: Skeletal crystal forms in the ultramafic rocks of the Yilgarn Block, Western Australia: evidence for an Archaean ultramafic liquid. *Geological Society of Australia Special Publication*, **3**, 331–47.

Ng, J. D., Lorber, B., Witz, J., Théobald-Dietrich, A., Kern, D. & Giegé, R. 1996: The crystallization of biological molecules from precipitates: evidence for Ostwald ripening, *Journal of Crystal Growth*, **168**, 50–62.

Nicolas, A. 1987: *Principles of Rock Deformation*. Dordrecht: Reidel.

1992: Kinematics in magmatic rocks with special reference to gabbros. *Journal of Petrology*, **33**, 891–915.

Nicolas, A., Boudier, F. & Boullier, A. M. 1973: Mechanisms of flow in naturally and experimentally deformed peridotites. *American Journal of Science*, **273**, 853–76.

Nicolas, A. & Ildefonse, B. 1996: Flow mechanism and viscosity in basaltic magma chambers. *Geophysical Research Letters*, **23**, 2013–16.

Nicolas, A. & Poirier, J.-P. 1976: *Crystalline Plasticity and Solid State Flow in Metamorphic Rocks*. New York: Wiley-Interscience.

Nixon, G. T. & Pearce, T. H. 1987: Laser-interferometry study of oscillatory zoning in plagioclase: The record of magma mixing and phenocryst recycling in calc-alkaline magma chambers, Iztaccihuatl volcano, Mexico. *American Mineralogist*, **72**, 1144–62.

Nockolds, S. R. 1933: Some theoretical aspects of contamination in acid magmas. *Journal of Geology*, **41**, 561–89.

Nold, J. L. 1984: Myrmekite in Belt Supergroup metasedimentary rocks – northeast border zone of the Idaho batholith. *American Mineralogist*, **69**, 1050–2.

Norrell, G. T., Teixell, A. & Harper, G. D. 1989: Microstructure of serpentinite mylonites from the Josephine ophiolite and serpentinization in retrogressive shear zones, California. *Bulletin of the Geological Society of America*, **101**, 673–82.

Nyman, M. W., Law, R. D. & Smelik, E. A. 1992: Cataclastic deformation mechanism for the development of core-mantle structures in amphibole. *Geology*, **20**, 455–8.

O'Brien, A. H., Irving, A. J. & McCallum, S. 1988: Complex zoning and resorption of phenocrysts in mixed potassic mafic magmas of the Highwood Mountains, Montana. *American Mineralogist*, **73**, 1007–24.

O'Brien, P. J. 1999: Asymmetric zoning profiles in garnet from HP-HT granulite and implications for volume and grain boundary diffusion. *Mineralogical Magazine*, **63**, 227–38.

O'Hara, K. 1988: Fluid flow and volume loss during mylonitization: an origin for phyllonite in an overthrust setting, North Carolina, U.S.A. *Tectonophysics*, **156**, 21–36.

Okudaira, T., Takeshita, T. & Toriumi, M. 1998: Prism- and basal-plane parallel subgrain boundaries in quartz: a microstructural geothermobarometer. Reply. *Journal of Metamorphic Geology*, **16**, 141–2.

Olesen, N. Ø. 1982: Heterogeneous strain of a phyllite as revealed by porphyroblast-matrix relationships. *Journal of Structural Geology*, **4**, 481–90.

Oliver, N. H. S. 1996: Review and classification of structural controls on fluid flow during regional metamorphism. *Journal of Metamorphic Geology*, **14**, 477–92.

2001: Linking of regional and hydrothermal systems in the mid-crust by shearing and faulting. *In* Boland, J. & Ord, A. (eds): *Deformation Processes in the Earth's Crust. Tectonophysics*, **335**, 147–61.

Oliver, N. H. S., Valenta, R. K. & Wall, V. J. 1990: The effect of heterogeneous stress and strain on metaporphic fluid flow, Mary Kathleen, Australia, and a model for large-scale fluid circulation. *Journal of Metamorphic Geology*, **8**, 311–31.

Ord, A. & Hobbs, B. E. 1986: Experimental control of the water-weakening effect in quartz. *In* Hobbs, B. E. & Heard, H. C. (eds): *Mineral and Rock Deformation: Laboratory Studies (The Paterson Volume). American Geophysical Union Geophysical Monograph*, **36**, 51–71.

O'Reilly, S. Y. & Griffin, W. L. 1987: Eastern Australia – 4000 kilometres of mantle samples. *In* Nixon, P. H. (ed.): *Mantle Xenoliths*. Chichester, UK: Wiley, pp. 267–80.

Orlov, Y. L. 1973: *The Mineralogy of Diamond.* New York: Wiley.

Ostwald, J. & Lusk, J. 1978: Sulfide fabrics in some nickel sulfide ores from Kambalda, Western Australia. *Canadian Journal of Earth Sciences*, **15**, 501–15.

Ostwald, W. 1901: *Analytisch Chemie* (third edition). Leipzig: Engelmann.

Owen, M. R. & Carozzi, A. V. 1986: Southern provenance of the upper Jackfork Sandstone, southern Ouachita Mountains: Cathodoluminescence petrology. *Bulletin of the Geological Society of America*, **97**, 110–15.

Pabst, A. 1928: Observations on inclusions in the granitic rocks of the Sierra Nevada. *University of California Publications in Geological Sciences*, **17**, 325–86.

1931: "Pressure shadows" and the measurement of the orientation of minerals in rocks. *American Mineralogist*, **16**, 55–70.

Padovani, E. R., Shirey, S. B. & Simmons, G. 1982: Characteristics of microcracks in amphibolite and granulite facies rocks from southeastern Pennsylvania. *Journal of Geophysical Research*, **87**, 8605–30.

Pagel, M., Barbin, V., Blanc, P. & Ohnenstetter, D. 2000: *Cathodoluminescence in Geosciences.* Berlin: Springer.

Palache, C. 1923: The largest crystal. *American Mineralogist*, **17**, 362–3.

Pan, Y. 2001: Inherited correlation in crystal size distribution. *Geology*, **29**, 227–30.

2002a: Inherited correlation in crystal size distribution: Comment and reply. REPLY. *Geology*, **30**, 283–4.

2002b: Inherited correlation in crystal size distribution: Comment and reply. REPLY. *Geology*, **30**, 285–6.

2002c: Comments on Higgins: "Closure in crystal size distributions (CSD), verification of CSD calculations, and the significance of CSD fans." *American Mineralogist*, **87**, 1242–3.

Paquet, J., François, P. & Nédélec, A. 1981: Effect of partial melting on rock deformation: experimental and natural evidences on rocks of granitic compositions. *Tectonophysics*, **78**, 545–65.

Park, R. G. 1969: Structural correlation in metamorphic belts. *Tectonophysics*, **7**, 323–38.

Park, Y. & Hanson, B. 1999: Experimental investigation of Ostwald-ripening rates of forsterite in the haplobasaltic system. *Journal of Volcanology and Geothermal Research*, **90**, 103–13.

Park, Y. & Means, W. D. 1996: Direct observation of deformation processes in crystal mushes. *Journal of Structural Geology*, **18**, 847–58.

1997: Crystal rotation and growth during grain flow in a deforming crystal mush. *In* Sengupta, S. (ed.): *Evolution of Geological Structures in Micro- to Macro-scales*. London: Chapman and Hall, pp. 245–58.

Passchier, C. W. 1984: The generation of ductile and brittle shear bands in a low-angle mylonite zone. *Journal of Structural Geology*, **6**, 273–81.

1986: Mylonites in the continental crust and their role as seismic reflectors. *Geologie en Mijnbouw*, **65**, 167–76.

Passchier, C. W., Hoek, J. D., Bekendam, R. F. & de Boorder, H. 1990: Ductile reactivation of Proterozoic brittle fault rocks; an example from the Vestfold Hills, east Antarctica. *Precambrian Research*, **47**, 3–16.

Passchier, C. W. & Trouw, R. A. J. 1996: *Microtectonics*. Berlin: Springer.

Passchier, C. W., Trouw, R. A. J., Zwart, H. J. & Vissers, R. L. M. 1992: Porphyroblast rotation: eppur si muove? *Journal of Metamorphic Geology*, **10**, 283–94.

Paterson, B. A. & Stephens, W. E. 1992: Kinetically-induced compositional zoning in titanite: Implications for accessory phase/melt partitioning of trace elements. *Contributions to Mineralogy and Petrology*, **109**, 373–85.

Paterson, B. A., Stephens, W. E. & Herd, D. A. 1989: Zoning in granitoid accessory minerals as revealed by backscattered electron imagery. *Mineralogical Magazine*, **53**, 55–61.

Paterson, M. S. 1978: *Experimental Rock Deformation – the Brittle Field.* Berlin: Springer.

2001: A granular flow theory for the deformation of partially molten rock. *In* Boland, J. & Ord, A. (eds): *Deformation Processes in the Earth's Crust. Tectonophysics*, **335**, 51–61.

Paterson, M. S. & Turner, F. J. 1970: Experimental deformation of constrained crystals of calcite in extension. *In* Paulitsch, P. (ed.): *Experimental and Natural Rock Deformation*. Berlin: Springer, pp. 109–41.

Paterson, S. R., Brudos, T., Fowler, K., Carlson, C., Bishop, K. & Vernon, R. H. 1991: Papoose Flat pluton: forceful expansion or post-replacement deformation? *Geology*, **19**, 324–7.

Paterson, S. R., Fowler, T. K., Schmidt, K. L., Yoshinobu, A. S., Yuan, E. S. & Miller, R. B. 1998: Interpreting magmatic fabric patterns in plutons. *Lithos*, **44**, 53–82.

Paterson, S. R. & Tobisch, O. T. 1983: Pre-lithification structures, deformation mechanisms, and fabric ellipsoids in slumped turbidites from the Pigeon Point Formation, California. *Tectonophysics*, **222**, 135–49.

Paterson, S. R. & Vernon, R. H. 1992: Rates of processes in magmatic arcs: implications for the timing and nature of pluton emplacement and wall rock deformation. *Journal of Structural Geology*, **14**, 291–300.

2001: Inclusion trail patterns in porphyroblasts from the Foothills Terrane, California: a record of orogenesis or local strain heterogeneity? *Journal of Metamorphic Geology*, **19**, 351–72.

Paterson, S. R., Vernon, R. H. & Tobisch, O. T. 1989: A review of criteria for the identification of magmatic and tectonic foliations in granitoids. *Journal of Structural Geology*, **11**, 349–63.

Paterson, S. R., Vernon, R. H. & Zac, J. 2004: Mechanical instabilities and accumulations of K-feldspar megacrysts in granitic magma, Tuolumne Intrusive Suite, California, USA. *Virtual Geoscience* (in review).

Paterson, S. R., Yu, H. & Oertel, G. 1985: Primary and tectonic fabric intensities in mudrocks. *Tectonophysics*, **247**, 105–19.

Pattison, D. R. M. & Bégin, N. J. 1994: Zoning patterns in orthopyroxene and garnet in granulites: implications for geothermometry. *Journal of Metamorphic Geology*, **12**, 387–410.

Pearce, T. H. 1984a: Multiple frequency laser interference microscopy: a new technique. *The Microscope*, **32**, 69–81.

1984b: Optical dispersion and zoning in magmatic plagioclase: laser interference observations. *Canadian Mineralogist*, **22**, 383–90.

2001: Pristine surface growth features on 100 Ma garnet phenocrysts: Interference imaging results. *American Mineralogist*, **86**, 1302–6.

Pearce, T. H., Griffin, M. P. & Kolisnik, A. M. 1987a: Magmatic crystal stratigraphy and constraints on magma chamber dynamics; laser interference results on individual phenocrysts. *Journal of Geophysical Research*, **92**, 13745–52.

Pearce, T. H. & Kolisnik, A. M. 1990: Observations of zoning using interference imaging. *Earth-Science Reviews*, **29**, 9–26.

Pearce, T. H., Russell, J. K. & Wolfson, I. 1987b: Laser-interference and Nomarski interference imaging of zoning profiles in plagioclase phenocrysts from the May 18, 1980, eruption of Mount St. Helens, Washington. *American Mineralogist*, **72**, 1131–43.

Pedersen, A. K. 1979: Basaltic glass with high-temperature equilibrated immiscible sulphide bodies with native iron from Disko, Central West Greenland. *Contributions to Mineralogy and Petrology*, **69**, 397–407.

Penniston-Dorland, S. 2001: Illumination of vein quartz textures in a porphyry copper ore deposit using scanned cathodoluminescence: Grasberg Igneous Complex, Irian Jaya, Indonesia. *American Mineralogist*, **86**, 652–66.

Peppard, B. T., Steele, I. M., Davis, A. M., Wallace, P. J. & Anderson, A. T. 2001: Zoned quartz phenocrysts from the rhyolitic Bishop Tuff. *American Mineralogist*, **86**, 1034–52.

Petersen, J. S. 1985: Columnar-dendritic feldspars in the lardalite intrusion, Oslo region, Norway: 1. Implications for unilateral solidification of a stagnant boundary layer. *Journal of Petrology*, **26**, 223–52.

Peterson, J. D. 1996: A refined technique for measuring crystal size distributions in thin section. *Contributions to Mineralogy and Petrology*, **124**, 395–405.

Petford, N. & Miller, J. A. 1992: Three-dimensional imaging of fission tracks using confocal scanning laser microscopy. *American Mineralogist*, **77**, 529–33.

Petford, N., Miller, J. A. & Rankin, A. H. 1995: Preliminary confocal scanning laser microscopic study of fluid inclusions in quartz. *Journal of Microscopy*, **178**, 37–41.

Petreus, I. 1978: The divided structure of crystals. I. Lineage and sectoral structure in pyrite and beryl. *American Mineralogist*, **63**, 725–31.

Pettijohn, F. J. 1949: *Sedimentary Rocks*. New York: Harper.

Phakey, P., Dollinger, G. & Christie, J. 1972: Transmission electron microscopy of experimentally deformed olivine crystals. *In* Heard, H. C., Borg, I. Y., Carter, N. L. & Raleigh, C. B. (eds): *Flow and Fracture of Rocks. Geophysical Monograph Series*, **16**, 117–37.

Phillips, E. R. 1968: Some plutonic rocks from a northern part of the New England Batholith. *University of Queensland Papers, Department of Geology*, **6**, 159–206.

1974: Myrmekite – one hundred years later. *Lithos*, **7**, 181–94.

1980: On polygenetic myrmekite. *Geological Magazine*, **17**, 29–36.

Phillips, E. R. & Ransom, D. M. 1968: The proportionality of quartz in myrmekite. *American Mineralogist*, **53**, 1411–13.

Phillips, E. R., Ransom, D. M. & Vernon, R. H. 1972: Myrmekite and muscovite developed by retrograde metamorphism at Broken Hill, New South Wales. *Mineralogical Magazine*, **38**, 570–8.

Phillips, J. A. 1880: On concretionary patches and fragments of other rocks contained in granite. *Quarterly Journal of the Geological Society of London*, **36**, 1–21.

Philpotts, A. R. 1964: Origin of pseudotachylites. *American Journal of Science*, **262**, 1008–35.

1966: Origin of the anorthosite-mangerite rocks in southern Quebec. *Journal of Petrology*, **7**, 1–64.

1971: Immiscibility between feldspathic and gabbroic magmas. *Nature Physical Science*, **229**, 107–9.

1976: Silicate liquid immiscibility: its probable extent and petrogenetic significance. *American Journal of Science*, **276**, 1147–77.

1977: Archean variolites – quenched immiscible liquids: discussion. *Canadian Journal of Earth Sciences*, **14**, 139–44.

1979: Silicate liquid immiscibility in tholeiitic basalts. *Journal of Petrology*, **20**, 99–118.

1982: Compositions of immiscible liquids in volcanic rocks. *Contributions to Mineralogy and Petrology*, **80**, 201–18.

1990: *Principles of Igneous and Metamorphic Petrology*. Engelwood Cliffs, NJ: Prentice-Hall.

Philpotts, A. R. & Asher, P. M. 1994: Magmatic flow-direction indicators in a giant diabase feeder dike, Connecticut. *Geology*, **22**, 363–6.

Philpotts, A. R., Brustman, C. M., Shi, J., Carlson, W. D. & Denison, C. 1999: Plagioclase-chain networks in slowly cooled basaltic magma. *American Mineralogist*, **84**, 1819–29.

Philpotts, A. R. & Dickson, L. D. 2002: Millimeter-scale modal layering and the nature of the upper solidification zone in thick flood-basalt flows and other sheets of magma. *Journal of Structural Geology*, **24**, 1171–7.

Philpotts, A. R. & Doyle, C. D. 1980: Immiscibility in tholeiites: a discussion. *Mineralogical Magazine*, **43**, 939–40.

Philpotts, A. R., Shi, J. & Brustman, C. 1998: Role of plagioclase crystal chains in the differentiation of partly crystallized basaltic magma. *Nature*, **395**, 343–6.

Piazolo, S., Jessell, M. W., Bons, P. D. & Evans, L. 2001: Animations of dynamic recrystallization with the numerical modelling system Elle. *In* Rawling, T. & Ailleres, L. (eds): *Animations in Geology; Visualising the Earth. Journal of the Virtual Explorer* (online), **B**, 45–9.

Piccoli, P., Candela, P. & Rivers, M. 2000: Interpreting magmatic processes from accessory phases: titanite – a small-scale recorder of large-scale processes. *Transactions of the Royal Society of Edinburgh: Earth Sciences*, **91**, 257–67.

Pitcher, W. S. 1993: *The Nature and Origin of Granite.* London: Blackie.

Pitcher, W. S. & Berger, A. R. 1972: *The Geology of Donegal: A Study of Granite Emplacement and Unroofing.* New York: Wiley.

Platt, J. P. 1984: Secondary cleavages in ductile shear zones. *Journal of Structural Geology*, **6**, 439–42.

Platt, J. P. & Vissers, R. L. M. 1980: Extensional structures in anisotropic rocks. *Journal of Structural Geology*, **2**, 397–410.

Plessman, W. 1964: Gesteinslösung, ein Hauptfaktor beim Schieferungsprozess. *Geologische Mitteilungen*, **4**, 69–82.

Pognante, U. 1985: Coronitic reactions and ductile shear zones in eclogitized ophiolite metagabbro Western Alps, north Italy. *Chemical Geology*, **50**, 99–109.

Poirier, J.-P. 1985: *Creep of Crystals. High-temperature Deformation Processes in Metals, Ceramics and Minerals*. New York: Cambridge University Press.

Poirier, J.-P. & Guillopé, M. 1979: Deformation induced recrystallization of minerals. *Bulletin de Minéralogie*, **102**, 67–74.

Poirier, J.-P. & Nicolas, A. 1975: Deformation induced recrystallization due to progressive misorientation of subgrains, with special reference to mantle peridotites. *Journal of Geology*, **83**, 707–20.

Post, A. D. & Tullis, J. 1999: A recrystallized grain size piezometer for experimentally deformed feldspar aggregates. *Tectonophysics*, **303**, 159–73.

Poty, B., Stalder, H. A. & Weisbrod, A. M. 1974: Fluid inclusion studies in quartz from fissures of Western and central Alps. *Schweizerische Mineralogische und Petrographische Mitteilungen*, **50**, 109–30.

Powell, C. M. 1969: Intrusive sandstone dykes in the Siamo Slate near Negaunee, Michigan. *Bulletin of the Geological Society of America*, **80**, 2585–94.

1982a: Overgrowths and mica beards on rounded quartz grains enclosed by cleavage folia. *In* Borradaile, G. J., Bayly, M. B. & Powell, C. McA. (eds): *Atlas of Deformational and Metamorphic Rock Fabrics*. New York: Springer, pp. 300–1.

1982b: Reduction of clastic grain size within cleavage zones. *In* Borradaile, G. J., Bayly, M. B. & Powell, C. McA. (eds): *Atlas of Deformational and Metamorphic Rock Fabrics*. New York: Springer, pp. 302–3.

Powell, C. M. & Vernon, R. H. 1979: Growth and rotation history of garnet porphyroblasts with inclusion spirals in a Karakoram schist. *Tectonophysics*, **54**, 25–43.

Powell, D. & MacQueen, J. A. 1976: Relationships between garnet shape, rotational inclusion fabrics and strain in some Moine metamorphic rocks of Skye, Scotland. *Tectonophysics*, **35**, 391–402.

Powell, D. & Treagus, J. E. 1969: On the geometry of S-shaped inclusion trails in garnet porphyroblasts. *Mineralogical Magazine*, **36**, 453–6.

1970: Rotational fabrics in metamorphic minerals. *Mineralogical Magazine*, **37**, 801–14.

Powell, R. & Downes, J. 1990: Garnet porphyroblast-bearing leucosomes in metapelites: Mechanisms, phase diagrams, and an example from Broken Hill, Australia. *In* Ashworth, J. R. & Brown, M. (eds): *High-temperature Metamorphism and Crustal Anatexis*. London: Unwin Hyman, pp. 105–23.

Pringle, G. J., Trembath, L. T. & Pajari, G. J. 1974: Crystallization history of a zoned plagioclase. *Mineralogical Magazine*, **39**, 867–77.

Prior, D. J. 1987: Syntectonic porphyroblastic growth in phyllites: textures and processes. *Journal of Metamorphic Geology*, **5**, 27–39.

Prior, D. J., Boyle, A. P., Brenker, F., Cheadle, M. C., Day, A., Lopez, G., Peruzzo, L., Potts, G. J., Reddy, S., Spiess, R., Timms, N. E., Trimby, P., Wheeler, J. & Zetterström, L. 1999: The application of electron backscatter diffraction and orientation contrast imaging in the SEM to textural problems in rocks. *American Mineralogist*, **84**, 1741–59.

Prior, D. J., Trimby, P. W., Weber, U. D. & Dingley, D. J. 1996: Orientation contrast imaging of microstructures in rocks using forescatter detectors in the scanning electron microscope. *Mineralogical Magazine*, **60**, 859–69.

Prior, D. J., Wheeler, J., Brenker, F. E., Harte, B. & Matthews, M. 2000: Crystal plasticity of natural garnet: new microstructural evidence. *Geology*, **28**, 1003–6.

Prior, D. J., Wheeler, J., Peruzzo, L., Speiss, R. & Storey, C. 2002: Some garnet microstructures: an illustration of the potential of orientation maps and misorientation analysis in microstructural studies. *Journal of Structural Geology*, **24**, 999–1011.

Pryer, L. L. & Robin, P.-Y. F. 1995: Retrograde metamorphic reactions in deforming granites and the origin of flame perthite. *Journal of Metamorphic Geology*, **14**, 645–58.

1996: Differential stress control on the growth and orientation of flame perthite: a palaeostress-direction indicator. *Journal of Structural Geology*, **18**, 1151–66.

Puffer, J. H. & Horter, D. L. 1993: Origin of segregation veins within flood basalts. *Bulletin of the Geological Society of America*, **105**, 738–48.

Pugliese, S. & Petford, N. 2001: Reconstruction and visualization of melt topology in veined microdioritic enclaves. *Electronic Geosciences*, **6:2**.

Putnis, A. 1992: *Introduction to Mineral Sciences*. Cambridge: Cambridge University Press.

2002: Mineral replacement reactions: from macroscopic observations to microscopic mechanisms. *Mineralogical Magazine*, **66**, 689–708.

Putnis, A. & McConnell, J. D. C. 1980: *Principles of Mineral Behaviour*. Oxford: Blackwell.

Pyke, D. R., Naldrett, A. J. & Eckstrand, O. R. 1973: Archean ultramafic flows in Munro Township, Ontario. *Bulletin of the Geological Society of America*, **84**, 955–78.

Pyle, J. M. & Spear, F. S. 1999: Yttrium zoning in garnet: Coupling of major and accessory phases during metamorphism. *Geological Materials Research*, **1/6**, 49pp. [*American Mineralogist*, **88**, 708, 2003.]

Raam, A. 1968: Petrology and diagenesis of Broughton Sandstone (Permian). Kiama district, New South Wales. *Journal of Sedimentary Petrology*, **38**, 319–31.

Rakovan, J. & Jaszczak, J. A. 2002: Multiple length scale growth spirals on metamorphic graphite {001} surfaces studied by atomic force microscopy. *American Mineralogist*, **87**, 17–24.

Raleigh, C. B. 1968: Mechanisms of plastic deformation of olivine. *Journal of Geophysical Research*, **73**, 5391–406.

Raleigh, C. B. & Paterson, M. S. 1965: Experimental deformation of serpentinite and its tectonic implications. *Journal of Geophysical Research*, **70**, 3963–85.

Ramdohr, P. 1969 (second edition 1980): *The Ore Minerals and their Intergrowths.* Oxford: Pergamon.

Ramsay, J. G. 1962: The geometry and mechanics of formation of 'similar' type folds. *Journal of Geology*, **70**, 309–27.

1967: *Folding and Fracturing of Rocks*. New York: McGraw-Hill.

1980a: Shear zone geometry: a review. *Journal of Structural Geology*, **2**, 83–99.

1980b: The crack-seal mechanism of rock deformation. *Nature*, **284**, 135–9.

Ramsay, J. G. & Graham, R. H. 1970: Strain variation in shear belts. *Canadian Journal of Earth Sciences*, **7**, 786–813.

Ramsay, J. G. & Huber, M. I. 1983: *The Techniques of Modern Structural Geology*. Volume 1. *Strain Analysis*. London: Academic Press.

1987: *The Techniques of Modern Structural Geology*. Volume 2. *Folds and Fractures*. London: Academic Press.

Ramsay, J. G. & Wood, D. S. 1973: The geometric effects of volume change during deformation processes. *Tectonophysics*, **13**, 263–77.

Ramseyer, K., Baumann, J., Matter, A. & Mullis, J. 1988: Cathodoluminescence colours of $\alpha-$quartz. *Mineralogical Magazine*, **52**, 669–77.

Rast, N. 1965: Nucleation and growth of metamorphic minerals. *In* Pitcher, W. S. & Flinn, G. S. (eds): *Controls of Metamorphism*. Edinburgh: Oliver & Boyd, pp. 73–102.

Ree, J. H. 1991: An experimental steady-state foliation. *Journal of Structural Geology*, **13**, 1001–11.

Ree, J. H. & Park, Y. 1997: Static recovery and recrystallization microstructures in sheared octachloropropane. *Journal of Structural Geology*, **19**, 1521–6.

Reed-Hill, R. E. 1973: *Physical Metallurgy Principles* (second edition). New York: D. van Nostrand.

Reeder, R. J. & Paquette, J. 1989: Sector zoning in natural and synthetic calcites. *Sedimentary Geology*, **65**, 239–47.

Reeder, R. J. & Prosky, J. L. 1986: Compositional sector zoning in dolomite. *Journal of Sedimentary Petrology*, **56**, 237–47.

Reid, J. B., Evans, O. C. & Fates, D. G. 1983: Magma mixing in granitic rocks of the central Sierra Nevada, California. *Earth and Planetary Science Letters*, **66**, 243–61.

Reid, J. B., Murray, D. P., Hermes, O. D. & Steig, E. J. 1993: Fractional crystallization in granites of the Sierra Nevada: How important is it? *Geology*, **21**, 587–90.

Reinhardt, J. & Rubenach, M. J. 1989: Growth of porphyroblasts relative to progressive deformation, temperature increase and time during prograde metamorphism. *Tectonophysics*, **158**, 141–61.

Reynolds, I. M. 1985: The nature and origin of titaniferous magnetite-rich layers in the Upper Zone of the Bushveld complex. *Economic Geology*, **80**, 1089–108.

Rice, A. H. N. 1993: Textural and twin sector-zoning and displacement of graphite in chiastolite and pyralspite and grandite garnets in the Variscides of south-west England. *Proceedings of the Usher Society*, **8**, 124–31.

Rice, A. H. N. & Mitchell, J. I. 1991: Porphyroblast textural sector-zoning and matrix displacement. *Mineralogical Magazine*, **55**, 379–96.

Richards, S. M. 1966: Mineragraphy of fault-zone sulphides, Broken Hill, NSW. *CSIRO Mineragraphic Investigations Technical Paper*, **5**, 1–24.

Richter, F. M. & McKenzie, D. P. 1984: Dynamical models for melt segregation from a deformable matrix. *Journal of Geology*, **92**, 729–40.

Rickers, K., Raith, M. & Dasgupta, S. 2001: Multistage reaction textures in xenolithic high-MgAl granulites at Anakapalle, Eastern Ghats Belt, India: examples of contact polymetamorphism and infiltration-driven metasomatism. *Journal of Metamorphic Geology*, **19**, 561–80.

Rickwood, P. C. 1981: The largest crystals. *American Mineralogist*, **66**, 885–907.

Ridley, J. 1985: The effect of reaction enthalpy on the progress of a metamorphic reaction. *In* Thompson, A. B. & Rubie, D. C. (eds): *Metamorphic Reactions. Kinetics, Textures and Deformation. Advances in Physical Geochemistry*, **4**, 80–97.

2002: Pathways and modes of fluid release from granites in the cores of active orogenic belts. *Geological Society of Australia Abstracts*, **67**, 214.

Riegger, O. K. & van Vlack, L. H. 1960: Dihedral angle measurements. *Metallurgical Society Transactions* (AIME), **21**, 933–5.

Rigsby, G. P. 1968: The complexities of the three-dimensional shape of individual crystals in glacier ice. *Journal of Glaciology*, **7**, 233–51.

Robin, P.-Y. F. 1979: Theory of metamorphic segregation and related processes. *Geochimica et Cosmochimica Acta*, **43**, 1587–600.

Rockhold, J. R., Nabelek, P. I. & Glascock, M. D. 1987: Origin of rhythmic layering in the Calamity Peak satellite pluton of the Harney Peak Granite, South Dakota: The role of boron. *Geochimica et Cosmochimica Acta*, **51**, 487–96.

Roedder, E. 1965: Liquid CO_2 inclusions in olivine-bearing nodules and phenocrysts from basalts. *American Mineralogist*, **50**, 1746–82.

1972: The composition of fluid inclusions. *United States Geological Survey Professional Paper*, **440JJ**, 164pp.

1979a: Fluid inclusions as samples of ore fluids. *In* Barnes, H. L. (ed.): *Geochemistry of Hydrothermal Ore Deposits* (second edition). New York: Wiley, pp. 684–737.

1979b: Silicate liquid immiscibility in magmas. *In* Yoder, H. S. (ed.): *The Evolution of the Igneous Rocks*. Princeton: Princeton University Press, pp. 15–57.

1979c: Origin and significance of magmatic inclusions. *Bulletin de Minéralogie*, **109**, 487–510.

1984: *Fluid Inclusions. Mineralogical Society of America, Reviews in Mineralogy*, **12**, 646pp.

Roedder, E. & Coombs, D. S. 1967: Immiscibility in granitic melts, indicated by fluid inclusions in ejected granitic blocks from Ascension Island. *Journal of Petrology*, **8**, 417–51.

Roedder, E. & Weiblen, P. W. 1970: Silicate liquid immiscibility in lunar magmas, evidenced by melt inclusions in lunar rocks. *Science*, **167**, 641–4.

1971: Lunar petrology of lunar melt inclusions, Apollo 11 and 12, and terrestrial equivalents. *In* Second Lunar Science Conference Proceedings. *Geochimica et Cosmochimica Acta* (Supplement **2**), **1**, 507–28.

Rogers, J. J. W. & Bogy, D. B. 1958: A study of grain contacts in granitic rocks. *Science*, **17**, 470–1.

Roscoe, W. E. 1975: Experimental deformation of natural chalcopyrite at temperatures up to 300°C over the strain rate range 10^{-2} to 10^{-6} sec^{-1}. *Economic Geology*, **70**, 454–72.

Rosenberg, C. L. 2001: Deformation of partially molten granite: a review and comparison of experimental and natural case studies. *International Journal of Earth Sciences (Geologische Rundschau)*, **90**, 60–76.

Rosenberg, C. L. & Handy, M. R. 2000: Syntectonic melt pathways during simple shearing of a partially molten rock analogue (Norcamphor-Benzamide). *Journal of Geophysical Research*, **105**, 3135–49.

Rosenberg, C. L. & Riller, U. 2000: Partial melt topology in statically and dynamically recrystallized granite. *Geology*, **28**, 7–10.

Rosenberg, C. L. & Stünitz, H. 2003: Deformation and recrystallization of plagioclase along a temperature gradient: an example from the Bergell tonalite. *Journal of Structural Geology*, **25**, 389–408.

Rosenbusch, H. 1873 (second edition 1885, third edition 1892, fourth edition 1904): *Mikroskopische Physiographie der petrographisch wichtigen Mineralien*. First edition, Stuttgart.

1877 (second edition 1887, third edition 1887, fourth edition 1907–8): *Mikroskopische Physiographie der massigen Gesteine.* First edition, Stuttgart: Schweizerbart'sche Verlagshandlung (E. Koch).

Rosenfeld, J. L. 1968: Garnet rotations due to the major Paleozoic deformations in southeast Vermont. *In* Zen, E-an, White, W. S., Hadley, J. B. & Thompson, J. B. (eds): *Studies of Appalachian Geology: Northern and Maritime*. New York: Wiley, pp. 185–202.

1970: Rotated garnets in metamorphic rocks. *Geological Society of America Special Paper*, **129**, 1–102.

Roser, B. P. & Nathan, S. 1997: An evaluation of elemental mobility during metamorphism of a turbidite sequence (Greenland Group, New Zealand). *Geological Magazine*, **134**, 219–34.

Rosière, C. A., Siemes, H., Quade, H., Brokmeier, H.-G. & Jansen, E. M. 2001: Microstructures, textures and deformation mechanisms in hematite. *Journal of Structural Geology*, **23**, 1429–40.

Ross, C. S. 1962: Microlites in glassy volcanic rocks. *American Mineralogist*, **47**, 713–40.

Ross, C. S. & Smith, R. L. 1961: Ash-flow tuffs: their origin, geologic relations and identification. *United States Geological Survey Professional Paper* **366**, 81pp.

Ross, J. V. 1973: Mylonitic rocks and flattened garnets in the southern Okanagan of British Columbia. *Canadian Journal of Earth Sciences*, **10**, 1–17.

Ross, J. V. & Wilks, K. R. 1996: Microstructure development in an experimentally sheared orthopyroxene granulite. *Tectonophysics*, **256**, 83–100.

Rostoker, W. & Dvorak, J. R. 1965: *Interpretation of Metallographic Structures.* New York: Academic Press.

Rougvie, J. R. & Sorensen, S. S. 2002: Cathodoluminescence record of K-metasomatism in ash-flow tuffs: Grain-scale mechanisms and large-scale geochemical implications. *Geology*, **30**, 307–10.

Roy, A. B. 1978: Evolution of slaty cleavage in relation to diagenesis and metamorphism: a study from the Hunsrückschiefer. *Bulletin of the Geological Society of America*, **89**, 1775–85.

Roycroft, P. D. 1989: Zoned muscovite from the Leinster Granite, S. E. Ireland. *Mineralogical Magazine*, **53**, 633–5.

1991: Magmatically zoned muscovite from the peraluminous two-mica granites of the Leinster batholith, southeast Ireland. *Geology*, **19**, 437–40.

Rubatto, D. & Gebauer, D. 2000: Use of cathodoluminescence for U-Pb dating by ion microprobe; some examples from the Western Alps. *In* Pagel, M., Barbin, V., Blanc, P. & Ohnenstetter, D. (eds): *Cathodoluminescence in Geosciences*. Berlin: Springer, pp. 373–400.

Rubatto, D., Williams, I. S. & Buick, I. S. 2001: Zircon and monazite response to prograde metamorphism in the Reynolds Range, central Australia. *Contributions to Mineralogy and Petrology*, **140**, 458–68.

Rubenach, M. J. & Bell, T. H. 1988: Microstructural controls and the role of graphite in matrix-porphyroblast exchange during synkinematic andalusite growth in a granitoid aureole. *Journal of Metamorphic Geology*, **6**, 651–66.

Rubie, D. C. 1983: Reaction-enhanced ductility: the role of solid-solid univariant reactions in deformation of the crust and mantle. *Tectonophysics*, **96**, 331–52.

1986: The catalysis of mineral reactions by water and restrictions on the processes on the presence of aqueous fluid during metamorphism. *Mineralogical Magazine*, **50**, 399–415.

1988: Disequilibrium during metamorphism: the role of nucleation kinetics. *In* Treloar, P. J. & O'Brien, P. (eds): *What drives metamorphism and metamorphic reactions? Geological Society of London Special Publication*, **138**, 199–214.

1990: Role of kinetics in the formation and preservation of eclogites. *In* Carswell, D. A. (ed.): *Eclogite Facies Rocks*. Glasgow: Blackie, pp. 111–40.

Rumble, D. 1989: Evidence of fluid flow during regional metamorphism. *European Journal of Mineralogy*, **1**, 731–7.

Rumble, D. & Finnerty, T. A. 1974: Devonian grossularite-spessartine overgrowths on ordovician almandine from eastern Vermont. *American Mineralogist*, **59**, 558–62.

Rushmer, T. 1995: An experimental deformation study of partially molten amphibolite: Application to low-melt fraction segregation. *Journal of Geophysical Research*, **100**, 15681–95.

2001: Volume change during partial melting reactions: Implications for melt extraction, melt geochemistry and crustal rheology. *Tectonophysics*, **342**, 389–405.

Rusk, B. & Reed, M. 2002: Scanning electron microscope–cathodoluminescence analysis of quartz reveals complex histories in veins from the Butte porphyry copper deposit, Montana. *Geology*, **20**, 727–30.

Rutter, E. H. 1972: The influence of interstitial water on the rheological behaviour of calcite rocks. *Tectonophysics*, **14**, 13–33.

1974: The influence of temperature, strain rate and interstitial water on the experimental deformation of calcite rocks. *Tectonophysics*, **22**, 311–34.

1976: The kinetics of rock deformation by pressure solution. *Philosophical Transactions of the Royal Society of London*, **A283**, 203–19.

1983: Pressure solution in nature, theory and experiment. *Journal of the Geological Society of London*, **140**, 725–40.

1995: Experimental study of the influence of stress, temperature and strain on the dynamic recrystallization of Carrara marble. *Journal of Geophysical Research*, **100**, 24651–63.

1997: The influence of deformation on the extraction of crustal melts: a consideration of the role of melt-assisted granular flow. *In* Holness, M. B. (ed.): *Deformation-enhanced Fluid Transport in the Earth's Crust and Mantle. Mineralogical Society Series*, **8**. London: Chapman and Hall, pp. 82–110.

Rutter, E. H. & Brodie, K. H. 1985: The permeation of water into hydrated shear zones. *In* Thompson, A. B. & Rubie, D. C. (eds): *Kinetics, Textures and Deformation. Advances in Physical Geochemistry*, **4**, 242–50.

1988a: Experimental approaches to the study of deformation/metamorphism relationships. *Mineralogical Magazine*, **52**, 35–42.

1988b: Experimental syntectonic dehydration of serpentinite under controlled pore water pressure. *Journal of Geophysical Research*, **93**, 4907–4932.

1990: Some geophysical implications of the deformation and metamorphism of the Ivrea zone, northern Italy. *Tectonophysics*, **182**, 147–60.

Rutter, E. H. & Neumann, D. H. K. 1995: Experimental deformation of partially molten Westerly granite under fluid-absent conditions, with implications for the extraction of granitic magmas. *Journal of Geophysical Research*, **100**, 15697–715.

Sagan, C. 1996: *The Demon-Haunted World: Science as a Candle in the Dark*. New York: Random House.

Saggerson, E. P. 1974: Porphyroblastesis and displacement: some new textural criteria from pelitic hornfels. *Mineralogical Magazine*, **39**, 793–7.

Sampson, E. 1932: Magmatic chromite deposits in southern Africa. *Economic Geology*, **27**, 113–44.

Sander, B. 1911: Über Zusammenhänge zwischen Teilbewegung und Gefüge in Gesteinen. *Tschermaks mineralogische und petrographische Mitteilungen*, **30**, 281–314.

1930: *Gefügekunde der Gesteine*. Vienna: Springer.

1970: *An Introduction to the Study of Fabrics of Geological Bodies* (Phillips F. C. & Windsor, G., translators of a 1950 publication in German). New York: Pergamon.

Sanders, I. S. 1986: Gas filter-pressing origin for segregation vesicles in dykes. *Geological Magazine*, **123**, 67–72.

Sawyer, E. W. 1987: The role of partial melting and fractional crystallization in determining discordant migmatite leucosome compositions. *Journal of Petrology*, **28**, 445–73.

1994: Melt segregation in the continental crust. *Geology*, **22**, 1019–1022.

1996: Melt-segregation and magma flow in migmatites: implications for the generation of granite magmas. *Transactions of the Royal Society of Edinburgh: Earth Sciences*, **87**, 85–94.

1999: Criteria for the recognition of partial melting. *Physics and Chemistry of the Earth* (A), **24**, 269–79.

2000a: Grain-scale and outcrop-scale distribution and movement of melt in a crystallising granite. *Transactions of the Royal Society of Edinburgh: Earth Sciences*, **91**, 73–85.

2000b: Melt distribution and movement in anatectic rocks. *Geophysical Research Abstracts*, **2**.

2001: Melt segregation in the continental crust: distribution and movement of melt in anatectic rocks. *Journal of Metamorphic Geology*, **19**, 291–309.

Sawyer, E. W., Dombrowski, C. & Collins, W. J. 1999: Movement of melt during synchronous regional deformation and granulite facies anatexis, an example from the Wuluma Hills, central Australia. *In* Castro, A., Fernandez, C. & Vigneresse, J.-L. (eds): *Understanding Granites; Integrating New and Classical Techniques. Geological Society of London Special Publication*, **158**, 221–37.

Schaeben, H., van den Boogaart, K., Mock, A. & Breitkreuz, C. 2002: Inherited correlation in crystal size distribution: Comment and reply. COMMENT. *Geology*, **30**, 282–3.

Schieber, J. 2002: Sedimentary pyrite: A window into the microbial past. *Geology*, **30**, 531–4.

Schmid, S. M. 1976: Rheological evidence for changes in the deformation mechanism of Solenhofen limestone towards low stress. *Tectonophysics*, **31**, 21–8.

1982: Microfabric studies as indicators of deformation mechanisms and flow laws operative in mountain building. *In* Hsu, K. J. (ed.): *Mountain Building Processes*. London: Academic Press, pp. 95–110.

Schmid, S. M., Boland, J. N. & Paterson, M. S. 1977: Superplastic flow in fine-grained limestone. *Tectonophysics*, **43**, 257–92.

Schmid, S. M. & Casey, M. 1986: Complete fabric analysis of some commonly observed quartz *c*-axis patterns. *In* Heard, H. C. & Hobbs, B. E. (eds): *Mineral and Rock Deformation Studies* (*the Paterson Volume*). *American Geophysical Union Monograph*, **36**, 263–86.

Schmid, S. M., Panozzo, R. & Bauer, S. 1987: Simple shear experiments on calcite rocks: rheology and microfabric. *Journal of Structural Geology*, **9**, 747–78.

Schmid, S. M., Paterson, M. S. & Boland, J. N. 1980: High temperature flow and dynamic recrystallization in Carrara marble. *Tectonophysics*, **65**, 245–80.

Schmidt, W. 1932: *Tektonik und Verformungslehre.* Berlin: Bornträger.

Schneider, N. 1993: Das lumineszenzaktive Strukturinventar von Quarzphänokristen in Rhyolithen. *Göttinger Arbeiten zum Geologie und Paläontologie*, **60**, 1–81.

Schoneveld, C. 1977: A study of typical inclusion patterns in strongly paracrystalline-rotated garnets. *Tectonophysics*, **39**, 453–71.

1979: *The Geometry and the Significance of Inclusion Patterns in Syntectonic Porphyroblasts.* Ph.D. thesis, University of Leiden.

Schreyer, W. & Abraham, K. 1978: Symplectitic cordierite-orthopyroxene-garnet assemblages as products of contact metamorphism of pre-existing basement granulites in the Vredefort structure, South Africa and their relation to pseudotachylite. *Contributions to Mineralogy and Petrology*, **68**, 53–62.

Schulmann, K., Mlcoch, B. & Melka, R. 1996: High-temperature microstructures and rheology of deformed granite, Erzgebirge, Bohemian Massif. *Journal of Structural Geology*, **18**, 719–33.

Schumacher, R., Rötzler, K. & Maresch, W. V. 1999: Subtle oscillatory zoning in garnet from regional metamorphic phyllites and mica schists, western Erzgebirge, Germany. *Canadian Mineralogist*, **37**, 381–402.

Schutkenberg, A. G., Punin, Y. O., Frank-Kamenetskaya, O. V., Kovalev, O. G. & Sokolov, P. B. 2001: On the origin of anomalous birefringence in grandite garnets. *Mineralogical Magazine*, **65**, 445–59.

Schwartz, G. M. 1931: Textures due to unmixing of solid solutions. *Economic Geology*, **26**, 739–63.

Schwindinger, K. R. & Anderson, A. T. 1989: Synneusis of Kilauea Iki olivines. *Contributions to Mineralogy and Petrology*, **103**, 187–98.

Scott, J. S. & Drever, H. I. 1953: Frictional fusion along a Himalayan thrust. *Proceedings of the Royal Society of Edinburgh*, **65**, 121–42.

Seager, A. F. 1953: The surface structure of crystals. *Mineralogical Magazine*, **30**, 1–25.

Segall, P. & Simpson, C. 1986: Nucleation of ductile shear zones on dilatant fractures. *Geology*, **14**, 56–9.

Seifert, K. E. 1964: The genesis of plagioclase twinning in the Nonewaug granite. *American Mineralogist*, **49**, 297–320.

Selley, R. C. 1970: *Ancient Sedimentary Environments. A Brief Survey.* London: Chapman and Hall.

Selverstone, J. 1993: Micro- to macroscale interactions between deformational and metamorphic processes, Tauern Window, eastern Alps. *Schweizerische Mineralogische und Petrographische Mitteilungen*, **73**, 229–39.

Selverstone, J. & Hyatt, J. 2003: Chemical and physical responses to deformation in micaceous quartzites from the Tauern Window, Eastern Alps. *Journal of Metamorphic Geology*, **21**, 335–45.

Selverstone, J., Morteani, G. & Staude, J.-M. 1991: Fluid channeling during ductile shearing: transformation of granodiorite into aluminous schist in the Tauern Window, eastern Alps. *Journal of Metamorphic Geology*, **9**, 419–31.

Sempels, J.-M. 1978: Evidence for constant habit development of plagioclase crystals from igneous rocks. *Canadian Mineralogist*, **16**, 257–63.

Shand, S. J. 1916: The pseudotachylite of Parijs (Orange Free State), and its relation to "trop-shotten gneiss" and "flinty crush-rock." *Quarterly Journal of the Geological Society of London*, **72**, 198–221.

1950: *Eruptive Rocks* (revised third edition). London: Murby.

Shannon, J. R., Walker, B. M., Carten, R. B. & Geraghty, E. P. 1982: Unidirectional solidification textures and their significance in determining relative ages of intrusions at the Henderson mine, Colorado. *Geology*, **10**, 293–7.

Shaw, D. M. 1956: Geochemistry of pelitic rocks. Part III: Major elements and general geochemistry. *Bulletin of the Geological Society of America*, **67**, 919–34.

Shaw, H. R. 1965: Comments on viscosity, crystal settling, and convection in granitic magmas. *American Journal of Science*, **263**, 120–52.

Shea, W. T. & Kronenberg, A. K. 1993: Strength and anisotropy of foliated rocks with varied mica contents. *Journal of Structural Geology*, **15**, 1097–121.

Shelley, D. M. 1972: Porphyroblasts and "crystallization force": Some textural criteria. Discussion. *Bulletin of the Geological Society of America*, **83**, 919–20.

1985a: *Optical Mineralogy* (second edition). New York: Elsevier.

1985b: Determining paleo-flow directions from groundmass fabrics in the Lyttleton radial dykes, New Zealand. *Journal of Volcanology and Geothermal Research*, **25**, 69–79.

1993: *Igneous and Metamorphic Rocks under the Microscope.* London: Chapman and Hall.

Sheppard, C. J. R. & Shotton, D. M. 1997: *Confocal Laser Scanning Microscopy.* Oxford: BIOS Scientific. New York: Springer.

Shima, H. & Naldrett, A. J. 1975: Solubility of sulfur in an ultramafic melt and the relevance of the system Fe-S-O. *Economic Geology*, **70**, 960–7.

Shimamoto, T., Kanaori, Y. & Asai, K. 1991: Cathodoluminescence observations on low-temperature mylonites: potential for detection of solution and precipitation microstructures. *Journal of Structural Geology*, **13**, 967–73.

Shimizu, N. 1981: Trace element incorporation into a growing augite phenocryst. *Nature*, **289**, 575–7.

Shore, M. & Fowler, A. D. 1996: Oscillatory zoning in minerals: a common phenomenon. *Canadian Mineralogist*, **34**, 1111–26.

Shumskii, P. A. (Kraus, D., translator) 1964: *Principles of Structural Glaciology*. New York: Dover.

Sibley, D. F., Vogel, T. A., Walker, B. M. & Byerly, G. 1976: The origin of oscillatory zoning in plagioclase: a diffusion and growth controlled model. *American Journal of Science*, **276**, 275–84.

Sibson, R. H. 1975: Generation of pseudotachylite by ancient seismic faulting. *Geophysical Journal of the Royal Astronomical Society*, **43**, 775–94.

1977: Fault rocks and fault mechanisms. *Journal of the Geological Society of London*, **133**, 191–214.

1981: Control on low-stress hydrofracture dilatancy in thrust, wrench and normal fault terrains. *Nature*, **289**, 655–67.

1986: Brecciation processes in fault zones: inferences from earthquake rupturing. *Pure and Applied Geophysics*, **124**, 159–75.

1990: Faulting and fluid flow. *In* Nesbitt, B. E. (ed.): *Fluids in Tectonically Active Regimes of the Continental Crust. Mineralogical Association of Canada Short Course*, **18**, 93–132.

Siddans, A. W. 1972: Slaty cleavage – a review of research since 1815. *Earth-Science Reviews*, **8**, 205–32.

Siemes, H. 1970: Experimental deformation of galena ores. *In* Paulitsch, P. (ed.): *Experimental and Natural Rock Deformation*. Berlin: Springer, pp. 165–208.

1976: Recovery and recrystallization of experimentally deformed galena. *Economic Geology*, **71**, 763–71.

1977a: Fabric analysis and fabric development in ores. *Geologiska Föreningens i Stockholm Förhandlingar*, **99**, 172–85.

1977b: Recovery and recrystallization of deformed galena. *Tectonophysics*, **39**, 171–4.

Siemes, H. & Borges, B. 1979: Experimental deformation of sphalerite single crystals under confining pressures of 3,000 and 5,000 bars and temperatures between 25°C and 450°C. *Neues Jahrbuch für Mineralogie, Abhandlungen*, **134**, 288–304.

Siemes, H., Jansen, E. M. & Niederschlag, E. 1994: Crystallographic preferred orientations of experimentally deformed sulfide ores. *In* Bunge, H. J., Siegesmund, S., Skrotzki, W. & Weber, K. (eds): *Textures of Geological Materials.* Oberursel: DGM Informationsgesellschaft-Verlag, pp. 231–50.

Siemes, H. & Spangenberg, H. J. 1980: Shear fabrics in naturally deformed galena. *Journal of Structural Geology*, **2**, 235–41.

Simpson, C. 1983: Strain and shape-fabric variations associated with ductile shear zones. *Journal of Structural Geology*, **5**, 61–72.

1984: Borrego Springs–Santa Rosa mylonite zone: A Late Cretaceous west-directed thrust in southern California. *Geology*, **12**, 8–11.

1985: Deformation of granitic rocks across the brittle-ductile transition. *Journal of Structural Geology*, **7**, 503–11.

1986: Fabric development in brittle-to-ductile shear zones. *Pure and Applied Geophysics*, **124**, 269–88.

Simpson, C. & Schmid, S. M. 1983: An evaluation of criteria to deduce the sense of movement in sheared rocks. *Bulletin of the Geological Society of America*, **94**, 1281–8.

Simpson, C. & Wintsch, R. P. 1989: Evidence for deformation-induced K-feldspar replacement by myrmekite. *Journal of Metamorphic Geology*, **7**, 261–75.

Sinha, A. K., Hewitt, D. A. & Rimstidt, J. D. 1986: Fluid interaction and element mobility in the development of ultramylonites. *Geology*, **14**, 883–6.

Sippel, R. F. & Glover, E. D. 1965: Structures in carbonate rocks made visible by luminescence petrography. *Science*, **150**, 1283–7.

Skinner, B. J. & Peck, D. L. 1969: An immiscible sulfide melt from Hawaii. *In* Wilson, H. D. B. (ed.): *Magmatic Ore Deposits. Economic Geology Monograph*, **4**, 310–22.

Smith, C. S. 1948: Grains, phases and interfaces: an interpretation of microstructure. *Transactions of the American Institute of Mining and Metallurgical Engineers*, **175**, 15–51.

1953: Microstructure. *Transactions of the American Society for Metals*, **45**, 533–75.

1954: The shape of things. *Scientific American*, **190**, 58–64.

1960: *A History of Metallography*. Chicago: University of Chicago Press.

1964: Some elementary principles of polycrystalline microstructure. *Metallurgical Reviews*, **9**, 1–48.

Smith, J. V. 1974: *Feldspar Minerals*. Volume 2. *Chemical and Textural Properties*. New York: Springer.

1983: Phase equilibria of plagioclase. *In* Ribbe, P. H. (ed.): *Feldspar Mineralogy* (second edition). *Mineralogical Society of America, Reviews in Mineralogy*, **2**, 223–39.

Smith, J. V. & Stenstrom, R. C. 1965: Electron-excited luminescence as a petrologic tool. *Journal of Geology*, **73**, 627–35.

Smith, R. E. 1967: Segregation vesicles in basaltic lava. *American Journal of Science*, **265**, 696–713.

Smith, R. K. 1983: An analytical and experimental study of zoning in plagioclase. *Lithos*, **16**, 153–68.

Snoke, A. W., Tullis, J. A. & Todd, V. R. (eds) 1999: *Fault-related Rocks: a Photographic Atlas*. Princeton: Princeton University Press.

Solomatov, V. S. 2002: Constraints on the grain size in the mantles of terrestrial planets. *Lunar and Planetary Science*, **33**, abstract no. 1446.

Song, S. G., Yang, J. S., Xu, Z. Q., Liou, J. G. & Shi, R. D. 2003: Metamorphic evolution of the coesite-bearing ultrahigh-pressure terrane in the North Qaidam, Northern Tibet, NW China. *Journal of Metamorphic Geology*, **21**, 631–44.

Sorby, H. C. 1851: On the microscopical structure of the Calcareous Grit of the Yorkshire coast. *Quarterly Journal of the Geological Society of London*, **7**, 1–6.

1853: On the origin of slaty cleavage. *Edinburgh New Philosophical Journal*, **55**, 137–48.

1856: On slaty cleavage as exhibited in the Devonian limestones of Devonshire. *Philosophical Magazine* (Series 4), **11**, 20–37.

1858: On the microscopical structure of crystals, indicating the origin of minerals and rocks. *Quarterly Journal of the Geological Society of London*, **14**, 453–500.

1864: On the microscopical photographs of various kinds of iron and steel. *Report of the 34th Annual Meeting of the British Association for the Advancement of Science*, Part II, p. 189.

1870: On the application of the microscope to the study of rocks. *Monthly Microscopical Journal*, **4**, 148–9.

1877: The application of the microscope to geology. *Monthly Microscopical Journal*, **17**, 113–36.

1879: Structure and origin of limestones. *Quarterly Journal of the Geological Society of London*, **35**, 56–95.

1887: On the microscopical structure of iron and steel. *Journal of the Iron and Steel Institute*, Part 2, pp. 254–88.

1908: On the application of quantitative methods to the structure and history of rocks. *Quarterly Journal of the Geological Society of London*, **64**, 171–232.

Southin, R. T. & Chadwick, G. A. 1969: Crystallization from the melt. *Science Progress*, **57**, 353–70.

Spang, J. H., Oldershaw, A. E. & Stout, M. Z. 1979: Development of cleavage in the Banff Formation at Pigeon Mountain, Front Ranges, Canadian Rocky Mountains. *Canadian Journal of Earth Sciences*, **16**, 1108–15.

Spanner, B. G. & Kruhl, J. H. 2002: Syntectonic granites in thrust and strike-slip regimes: the history of the Carmo and Cindacta plutons (southeastern Brazil). *Journal of South American Earth Sciences*, **15**, 431–44.

Spear, F. S. 1993: *Metamorphic Phase Equilibria and Pressure-Temperature-Time Paths.* Washington, DC: Mineralogical Society of America.

Spear, F. S. & Daniel, C. G. 1998: Three-dimensional imaging of garnet porphyroblast sizes and chemical zoning: Nucleation and growth history in the garnet zone. *Geological Materials Research*, **1/1**, 44pp. [*American Mineralogist*, **88**, 245, 2003.]

2001: Diffusion control of garnet growth, Harpswell Neck, Maine, USA. *Journal of Metamorphic Geology*, **19**, 179–95.

Spear, F. S., Kohn, M. J., Florence, F. P. & Menard, T. 1991: A model for garnet growth in pelitic schists: implications for thermobarometry and *P-T* path determinations. *Journal of Metamorphic Geology*, **8**, 683–96.

Spencer, S. 1991: The use of syntectonic fibres to determine strain estimates and deformation paths: an appraisal. *Tectonophysics*, **194**, 13–34.

Spiess, R. & Bell, T. H. 1996: Microstructural controls on sites of metamorphic reaction: a case study of the inter-relationship between deformation and metamorphism. *European Journal of Mineralogy*, **8**, 165–86.

Spiess, R., Peruzzo, L., Prior, D. J. & Wheeler, J. 2001: Development of garnet porphyroblasts by multiple nucleation, coalescence and boundary misorientation-driven rotations. *Journal of Metamorphic Geology*, **19**, 269–90.

Spray, J. G. 1987: Artificial generation of pseudotachylite using friction welding apparatus: simulation of melting on a fault plane. *Journal of Structural Geology*, **9**, 49–60.

1995: Pseudotachylyte controversy: fact or friction? *Geology*, **23**, 1119–22.

Spray, J. G. & Thompson, L. M. 1994: Friction melt distribution in a multi-ring impact basin. *Nature*, **373**, 130–2.

Sprunt, E. S. 1978: Effects of impurities on quartz cathodoluminescence. *EOS*, *Transactions of the American Geophysical Union*, **59**, 1216.

1981: Causes of quartz cathodoluminescence colors. *Scanning Electron Microscopy*, **1**, 525–35.

Sprunt, E. S. & Nur, A. 1979: Microcracking and healing in granites. New evidence from cathodoluminescence. *Science*, **205**, 495–7.

Spry, A. 1963: The origin and significance of snowball structure in garnet. *Journal of Petrology*, **4**, 211–22.

1969: *Metamorphic Textures*. Oxford: Pergamon.

1972: Porphyroblasts and “crystallization force”: Some textural criteria. Discussion. *Bulletin of the Geological Society of America*, **83**, 1201–2.

Stallard, A. 2003: Comment on “Crystallographic orientation, chemical composition and three-dimensional geometry of sigmoidal garnet: evidence for rotation” by T. Ikeda, N. Shimobayashi, S. Wallis and A. Tsuchiyama. *Journal of Structural Geology*, **25**, 1337–9.

Stallard, A. & Hickey, K. 2002: A comparison of microstructural and chemical patterns in garnet from the Fleur de Lys Supergroup, Newfoundland. *Journal of Structural Geology*, **24**, 1109–23.

Stallard, A., Hickey, K. & Upton, G. J. 2003: Measurement and correlation of microstructures: the case of foliation intersection axes. *Journal of Metamorphic Geology*, **21**, 241–52.

Stallard, A., Ikei, H. & Masuda, T. 2002: Numerical simulations of spiral-shaped inclusion trails: can 3D geometry distinguish between end-member models of spiral formation? *Journal of Metamorphic Geology*, **20**, 801–12.

Stamatelopoulou-Seymour, K., Vlassopoulos, D., Pearce, T. H. & Rice, C. 1990: The record of magma chamber processes in plagioclase phenocrysts at Thera Volcano, Aegean Volcanic Arc, Greece. *Contributions to Mineralogy and Petrology*, **104**, 73–84.

Stanton, R. L. 1964: Mineral interfaces in stratiform ores. *Transactions of the Institution of Mining and Metallurgy*, **74**, 45–79.

1972: *Ore Petrology*. New York: McGraw-Hill.

Stanton, R. L. & Gorman, H. 1968: A phenomenological study of grain boundary migration in some common sulfides. *Economic Geology*, **63**, 907–23.

Stanton, R. L. & Gorman Wiley, H. 1970: Natural work-hardening in galena, and its experimental reduction. *Economic Geology*, **65**, 182–94.

1971: Recrystallization softening and hardening in sphalerite and galena. *Economic Geology*, **66**, 1232–8.

Stebbins, J. F., McMillan, P. F. & Dingwell, D. B. (eds) 1995: *Structure, Dynamics and Properties of Silicate Melts. Mineralogical Society of America and Geochemical Society, Reviews in Mineralogy and Geochemistry*, **32**, 616pp.

Steinhardt, C. 1989: Lack of porphyroblast rotation in non-coaxially deformed schists from Petrel Cove, South Australia, and its implications. *Tectonophysics*, **158**, 127–40.

Stel, H. 1981: Crystal growth in cataclasites: diagnostic microstructures and implications. *Tectonophysics*, **78**, 585–600.

1986: The effect of cyclic operation of brittle and ductile deformation on the metamorphic assemblage in catclasites and mylonites. *Pure and Applied Geophysics*, **124**, 289–307.

Stel, H. & Breedveld, M. 1989: Crystallographic orientation patterns of myrmekitic quartz: a fabric memory in annealed ribbon gneisses. *Journal of Structural Geology*, **12**, 19–28.

Stillwell, F. L. 1918: The metamorphic rocks of Adelie Land. *Australasian Antarctic Expedition 1911–14 Scientific Report, Series A*, **3**, 1–320.

Stimac, J. A., Pearce, T. H., Donnelly-Nolan, J. M. & Hearn, B. C. 1990: The origin and implications of undercooled andesitic inclusions in rhyolites, Clear Lake Volcanics, California. *Journal of Geophysical Research*, **95**, 17729–46.

Stipp, M., Stünitz, H., Heilbronner, R. & Schmid, S. M. 2002: Dynamic recrystallization of quartz: correlation between natural and experimental conditions. *In* de Meer, S., Drury, M. R., de Bresser, J. H. P. & Pennock, G. M. (eds): *Deformation Mechanisms, Rheology and Tectonics: Current Status and Future Perspectives*. *Geological Society of London Special Publication*, **200**, 171–90.

St Onge, M. R. 1987: Zoned poikiloblastic garnets: P-T paths and syn-metamorphic uplift through 30 km of structural depth, Wopmay orogen, Canada. *Journal of Petrology*, **28**, 1–21.

Streit, J. E. & Cox, S. F. 1998: Fluid infiltration and volume change during mid-crustal mylonitization of Proterozoic granite, King Island, Tasmania. *Journal of Metamorphic Geology*, **16**, 197–212.

Stünitz, H. 1993: Transition from fracturing to viscous flow in a naturally deformed metagabbro. *In* Boland, J. N. & Fitz Gerald, J. D. (eds): *Defects and Processes in the Solid State: Geoscience Applications. The McLaren Volume*. Amsterdam: Elsevier, pp. 121–50.

1998: Syndeformational recrystallization – dynamic or compositionally induced? *Contributions to Mineralogy and Petrology*, **131**, 219–36.

Stünitz, H. & Tullis, J. 2001: Weakening and strain localization produced by syn-deformational reaction of plagioclase. *International Journal of Earth Sciences (Geologische Rundschau)*, **90**, 136–48.

Stüwe, K. 1997: Effective bulk composition changes due to cooling: a model predicting complexities in retrograde reaction textures. *Contributions to Mineralogy and Petrology*, **129**, 43–52.

Stüwe, K., Sandiford, M. & Powell, R. 1993: Episodic metamorphism and deformation events in low pressure, high temperature terrains. *Geology*, **21**, 829–32.

Sugaki, A., Kitakatze, A. & Kojuma, S. 1987: Bulk compositions of intimate intergrowths of chalcopyrite and sphalerite and their genetic implications. *Mineralium Deposita*, **22**, 26–32.

Sugaki, A., Shima, H., Kitakatze, A. & Maroda, H. 1975: Isothermal phase relationships in the system Cu-Fe-S under hydrothermal conditions at 350°C and 300°C. *Economic Geology*, **70**, 806–23.

Suhr, G. 1993: Evaluation of upper mantle microstructures in the Table Mountain Massif (Bay of Islands ophiolite). *Journal of Structural Geology*, **15**, 1273–92.

Sunagawa, I. 1964: Growth spirals on phlogopite crystals. *American Mineralogist*, **49**, 1427–34.

1974: Growth of crystals in nature. *In*: *Mineral Genesis*. Sofia: Bulgarian Academy of Sciences Geological Institute, pp. 79–90.

1977: Natural crystallization. *Journal of Crystal Growth*, **42**, 214–23.

1981: Characteristics of crystal growth in nature as seen from the morphology of mineral crystals. *Bulletin de Minéralogie*, **104**, 81–7.

1984: Growth of crystals in nature. *In* Sunagawa, I. (ed.) *Material Science of the Earth's Interior*. Tokyo: Terra Scientific Publishing Company, pp. 63–105.

1987: Morphology of minerals. *In* Sunagawa, I. (ed.): *Morphology of Crystals*. Dordrecht: Reidel, pp. 509–81.

Sunagawa, I. & Koshino, Y. 1975: Growth spirals on kaolin group minerals. *American Mineralogist*, **60**, 407–12.

Sunagawa, I., Koshino, Y., Asakura, M. & Yamamoto, T. 1974: Growth mechanisms of some clay minerals. *Fortschritte Mineralogie*, **52**, 217–24.

Sutton, S. J. 1991: Development of domainal slaty cleavage at Ococee Gorge, Tennessee. *Journal of Geology*, **99**, 789–800.

Swanson, S. E. 1977: Relation of nucleation and crystal-growth rate to the development of granitic textures. *American Mineralogist*, **62**, 966–78.

Swanson, S. E. & Fenn, P. M. 1986: Quartz crystallization in igneous rocks. *American Mineralogist*, **71**, 331–42.

Swanson, S. E., Naney, M. T., Westrich, H. R. & Eichelberger, J. C. 1989: Crystallization history of Obsidian Dome, Inyo Domes, California. *Bulletin of Volcanology*, **51**, 966–78.

Taber, S. 1916: The origin of veins of the asbestiform minerals. *Proceedings of the National Academy of Sciences*, **2**, 659–64.

Taylor, T. R., Vogel, T. A. & Wilband, J. T. 1980: The composite dikes at Mount Desert Island, Maine: an example of coexisting acid and basic magmas. *Journal of Geology*, **88**, 433–44.

Teall, J. J. H. 1885: The metamorphosis of dolerite into hornblende schist. *Quarterly Journal of the Geological Society of London*, **41**, 133–45.

1886: *British Petrography*. Birmingham: Watson Brothers & Douglas.

ten Brink, C. E. & Passchier, C. W. 1995: Modelling of mantled porphyroclasts using non-Newtonian rock analogue materials. *Journal of Structural Geology*, **17**, 131–46.

'T Hart, J. 1978a: The structural morphology of olivine. I. A qualitative derivation. *Canadian Mineralogist*, **16**, 175–86.

1978b: The structural morphology of olivine. II. A quantitative derivation. *Canadian Mineralogist*, **16**, 547–60.

Thompson, A. B., Tracy, R. J., Lyttle, P. & Thompson, J. B. 1977: Prograde reaction histories deduced from compositional zonation and mineral inclusions in garnet from the Gassetts Schist, Vermont. *American Journal of Science*, **277**, 1152–67.

Thompson, R. N. 1969: Tertiary granites and associated rocks of the Marsco area, Isle of Skye. *Quarterly Journal of the Geological Society of London*, **124**, 349–85.

Thost, D. E., Hensen, B. J. & Motoyoshi, Y. 1991: Two-stage decompression in garnet-bearing mafic granulites from Sostrene Island, Prydz Bay, East Antarctica. *Journal of Metamorphic Geology*, **9**, 245–56.

Tikare, V. & Cawley, J. D. 1998: Application of the Potts model simulation of Ostwald ripening. *Journal of the American Ceramic Society*, **81**, 485–91.

Tiller, W. A. 1964: Dendrites. *Science*, **146**, 871–9.

Tobisch, O. T. 1955: Observations on primary deformed sedimentary structures in some metamorphic rocks from Scotland. *Journal of Sedimentary Petrology*, **35**, 415–9.

Tobisch, O. T., Barton, M. D., Vernon, R. H. & Paterson, S. R. 1991: Fluid-enhanced deformation: transformation of granitoids to banded mylonites, western Sierra Nevada, California, and southeastern Australia. *Journal of Structural Geology*, **13**, 1137–56.

Tobisch, O. T., McNulty, B. A. & Vernon, R. H. 1997: Microgranitoid enclave swarms in granitic plutons, central Sierra Nevada, California. *Lithos*, **40**, 321–39.

Tobisch, O. T. & Paterson, S. R. 1988: Analysis and interpretation of composite cleavages in areas of progressive deformation. *Journal of Structural Geology*, **10**, 745–54.

Tomkins, A. G., Pattison, D. R. M. & Zaleski, E. 2004: The Hemlo gold deposit, Ontario: a type example of melting and mobilization of a precious metal-sulfosalt assemblage during amphibolite facies metamorphism and deformation. *Economic Geology* (in Press).

Tomura, S., Kitamura, M. & Sunagawa, I. 1979: Surface microtopography of metamorphic white micas. *Physics and Chemistry of Minerals*, **5**, 65–81.

Toramaru, A. 1991: Model of nucleation and growth of crystals in cooling magmas. *Contributions to Mineralogy and Petrology*, **108**, 106–17.

Toriumi, M. 1982: Grain boundary migration in olivine at atmospheric pressure. *Physics of the Earth and Planetary Interiors*, **30**, 26–35.

Touret, J. 1977: The significance of fluid inclusions in metamorphic rocks. *In* Fraser, D. G. (ed.): *Thermodynamics in Geology*. Boston: Reidel, pp. 203–27.

Tracy, R. J. 1982: Compositional zoning and inclusions in metamorphic minerals. *In* Ferry, J. M. (ed.): *Characterization of Metamorphism through Mineral Equilibria. Mineralogical Society of America, Reviews in Mineralogy*, **10**, 355–97.

Tracy, R. J. & McLellan, E. L. 1985: A natural example of the kinetic controls of compositional and textural equilibration. *In* Thompson, A. B. & Rubie, D. C. (eds): *Metamorphic Reactions. Kinetics, Textures and Deformation. Advances in Physical Geochemistry*, **4**. New York: Springer, pp. 118–37.

Tranter, T. H. 1992: Underplating of an accretionary prism: An example from the LeMay Group of central Alexander Island, Antarctic Peninsula. *Journal of South American Earth Sciences*, **6**, 1–20.

Trepmann, C. A. & Stöckhert, B. 2003: Quartz microstructures developed during non-steady state plastic flow at rapidly decaying stress and strain rate. *Journal of Structural Geology*, **25**, 2035–51.

Tribe, I. R. & D'Lemos, R. S. 1996: Significance of a hiatus in down-temperature fabric development within syn-tectonic quartz diorite complexes, Channel Islands, UK. *Journal of the Geological Society of London*, **153**, 127–38.

Trimby, P. W., Prior, D. J. & Wheeler, J. 1998: Grain boundary hierarchy development in a quartz mylonite. *Journal of Structural Geology*, **20**, 917–35.

Tsurumi, J., Hosonuma, H. & Kanagawa, K. 2003: Strain localization due to a positive feedback of deformation and myrmekite-forming reaction in granite and aplite mylonites along the Hatagawa Shear Zone of NE Japan. *Journal of Structural Geology*, **25**, 557–74.

Tuffen, H., Dingwell, D. B. & Pinkerton, H. 2003: Repeated fracture and healing of silicic magma generates flow banding and earthquakes? *Geology*, **31**, 1089–92.

Tullis, J. 1983: Deformation of feldspars. *In* Ribbe, P. H. (ed.): *Feldspar Mineralogy* (second edition). *Mineralogical Society of America, Reviews in Mineralogy*, **2**, 297–323.

Tullis, J., Christie, J. M. & Griggs, D. T. 1973: Microstructures and preferred orientations of experimentally deformed quartzites. *Bulletin of the Geological Society of America*, **84**, 297–314.

Tullis, J., Dell'Angelo, L., & Yund, R. A. 1990: Ductile shear zones from brittle precursors in feldspathic rocks: the role of dynamic recrystallization. *In* Duba, A., Durham, W., Handin, W. & Wang, H. (eds): *The Brittle-ductile Transition. American Geophysical Union, Geophysical Monograph*, **56**, 67–82.

Tullis, J., Stünitz, H., Teyssier, C. & Heilbronner, R. 2000: Deformation microstructures in quartzo-feldspathic rocks. *In* Jessell, M. W. & Urai, J. L. (eds): *Stress, Strain and Structure. A Volume in Honour of W D Means*. *Journal of the Virtual Explorer*, **2** (print and CD).

Tullis, J. & Yund, R. A. 1985: Dynamic recrystallization of feldspar: A mechanism for ductile shear zone formation. *Geology*, **13**, 238–41.

1987: Transition from cataclastic flow to dislocation creep of feldspar: Mechanisms and microstructures. *Geology*, **15**, 606–9.

1991: Diffusion creep in feldspar aggregates: experimental evidence. *Journal of Structural Geology*, **13**, 987–1000.

Tullis, J., Yund, R. A. & Farver, J. 1996: Deformation-enhanced fluid distribution in feldspar aggregates and implications for ductile shear zones. *Geology*, **24**, 63–6.

Tungatt, P. D. & Humphreys, F. J. 1984: The plastic deformation and recrystallization of polycrystalline sodium nitrate. *Acta Metallurgica*, **32**, 1625–35.

Turner, F. J. 1948: Note on the significance of deformation lamellae in quartz and calcite. *Transactions of the American Geophysical Union*, **29**, 556–69.

1981: *Metamorphic Petrology. Mineralogical and Field Aspect*s (second edition). New York: McGraw-Hill.

Turner, F. J., Griggs, D. T. & Heard, H. C. 1954: Experimental deformation of calcite crystals. *Bulletin of the Geological Society of America*, **65**, 883–934.

Turner, F. J. & Weiss, L. E. 1963: *Structural Analysis of Metamorphic Tectonites*. New York: McGraw-Hill.

Tyrrell, G. W. 1929: *The Principles of Petrology* (second edition). London: Methuen.

Ulff-Möller, F. 1985: Solidification history of the Kitdlît lens: immiscible metal and sulphide liquids from a basaltic dyke on Disko, central west Greenland. *Journal of Petrology*, **26**, 64–91.

Urai, J. L. 1983a: *Deformation of Wet Salt Rocks*. Ph.D. thesis, State University of Utrecht, The Netherlands.

1983b: Water-assisted dynamic recrystallization and weakening in polycrystalline bischofite. *Tectonophysics*, **96**, 125–57.

1987: Development of microstructure during deformation of carnalite and bischofite in transmitted light. *Tectonophysics*, **135**, 251–63.

Urai, J. L. & Humphreys, F. J. 1981: The development of shear zones in polycrystalline camphor. *Tectonophysics*, **78**, 677–85.

Urai, J. L., Humphreys, F. J. & Burrows, S. E. 1980a: *In situ* studies of the deformation and dynamic recrystallization of rhombohedral camphor. *Journal of Materials Science*, **15**, 1231–40.

Urai, J. L., Means, W. D. & Lister, G. S. 1986: Dynamic recrystallisation of minerals. *In* Hobbs, B. E. & Heard, H. C. (eds): *Mineral and Rock Deformation: Laboratory Studies (The Paterson Volume)*. *American Geophysical Union Geophysical Monograph*, **36**, 161–99.

Urai, J. L., Williams, P. F. & van Roermund, H. L. M. 1980b: Kinematics of crystal growth in syntectonic fibrous veins. *Journal of Structural Geology*, **13**, 823–36.

Usselman, T. M. & Lofgren, G. E. 1975: Crystallization of mare basalts: pyroxene zoning (abstract). *EOS*, *Transactions of the American Geophysical Union*, **56**, 471.

1976: The phase relations, and mineral chemistries of high-titanium mare basalts as a function of oxygen fugacity and cooling rate. *Proceedings of the Seventh Lunar Science Conference*. Houston, TX: NASA, pp. 1345–63.

Valiant, R. I., Barnett, R. L. & Hodder, R. W. 1983: Aluminum silicate-bearing rock and its relation to gold mineralization, Bousquet Mine, Bousquet Township, Quebec. *CIM* (*Canadian Institute of Mining and Metallurgy*) *Bulletin*, **76**, 81–90.

van der Molen, I. & Paterson, M. S. 1979: Experimental deformation of partially melted granite. *Contributions to Mineralogy and Petrology*, **70**, 299–318.

van der Pluijm, B. A. & Kaars-sijpesteijn, C. H. 1984: Chlorite-mica aggregates: morphology, orientation, development and bearing on cleavage formation in very low-grade rocks. *Journal of Structural Geology*, **6**, 399–407.

van der Voo, R., Fang, W., Wang, Z., Suk, D., Peacor, D. R. & Liang, Q. 1993: Paleomagnetic and electron microscopy of the Emeishan Basalts, Yunnan, China. *Tectonophysics*, **221**, 367–79.

van der Wal, D., Vissers, R. M. D. & Drury, M. R. 1992: Oblique fabrics in porphyroclastic Alpine peridotites: a shear sense indicator for upper mantle flow. *Journal of Structural Geology*, **14**, 839–46.

van Lamoen, H. 1979: Coronas in olivine gabbros and iron ores from Susimaki and Riuttamaa, Finland. *Contributions to Mineralogy and Petrology*, **68**, 259–68.

van Vlack, L. H. 1964: *Elements of Materials Science* (second edition). Reading, MA: Addison-Wesley.

Vance, D. & Holland, T. B. J. 1993: A detailed isotopic and petrological study of a single garnet from the Gassetts Schist, Vermont. *Contributions to Mineralogy and Petrology*, **114**, 101–18.

Vance, J. A. 1961: Polysynthetic twinning in plagioclase. *American Mineralogist*, **46**, 1097–119.

1962: Zoning in igneous plagioclase: normal and oscillatory zoning. *American Journal of Science*, **260**, 746–60.

1965: Zoning in igneous plagioclase: patchy zoning. *Journal of Geology*, **73**, 636–51.

1969: On synneusis. *Contributions to Mineralogy and Petrology*, **24**, 7–29.

Vance, J. A. & Gilbreath, J. P. 1967: The effect of synneusis on phenocryst distribution patterns in some porphyritic igneous rocks. *American Mineralogist*, **52**, 529–36.

Vaniman, D. 1978: Crystallization history of sector-zoned microcline megacrysts from the Godani valley pluton, Nigeria. *Mineralogical Magazine*, **42**, 443–51.

Vassallo, J. J. & Vernon, R. H. 2000: Origin of megacrystic felsic gneisses at Broken Hill. *Australian Journal of Earth Sciences*, **47**, 733–48.

Vauchez, A. 1980: Ribbon texture and deformation mechanisms in quartz in a mylonitized granite of Great Kabylia (Algeria). *Tectonophysics*, **67**, 1–12.

Vavra, G. 1990: On the kinetics of zircon growth and its petrogenetic significance: a cathodoluminescence study. *Contributions to Mineralogy and Petrology*, **106**, 90–9.

Veksler, I. V., Thomas, R. & Schmidt, C. 2002: Experimental evidence of three coexisting immiscible fluids in synthetic granitic pegmatite. *American Mineralogist*, **87**, 775–9.

Vernon, R. H. 1965: Plagioclase twins in some mafic gneisses from Broken Hill, Australia. *Mineralogical Magazine*, **35**, 488–507.

1968: Microstructures of high-grade metamorphic rocks at Broken Hill, Australia. *Journal of Petrology*, **9**, 1–22.

1970: Comparative grain-boundary studies in some basic and ultrabasic granulites, nodules and cumulates. *Scottish Journal of Geology*, **6**, 337–51.

1974: Controls of mylonitic compositional layering during non-cataclastic ductile deformation. *Geological Magazine*, **111**, 121–31.

1975: Deformation and recrystallization of a plagioclase grain. *American Mineralogist*, **60**, 884–8.

1976: *Metamorphic Processes*. London: Murby. New York: Wiley.

1977a: Relationships between microstructures and metamorphic assemblages. *Tectonophysics*, **39**, 439–52.

1977b: Microfabric of mica aggregates in partly recrystallized biotite. *Contributions to Mineralogy and Petrology*, **61**, 175–85.

1978a: Porphyroblast-matrix microstructural relationships in deformed metamorphic rocks. *Geologische Rundschau*, **67**, 288–305.

1978b: Pseudomorphous replacement of cordierite by symplectic intergrowths of andalusite, biotite and quartz. *Lithos*, **11**, 283–9.

1979: Formation of late sillimanite by hydrogen metasomatism (base-leaching) in some high-grade gneisses. *Lithos*, **12**, 143–52.

1981: Optical microstructure of partly recrystallized calcite in some naturally deformed marbles. *Tectonophysics*, **78**, 601–12.

1983: Restite, xenoliths and microgranitoid enclaves in granites (Clarke Memorial Lecture). *Journal and Proceedings of the Royal Society of New South Wales*, **116**, 77–103.

1984: Microgranitoid enclaves in granites – globules of hybrid magma quenched in a plutonic environment. *Nature*, **309**, 438–9.

1985: Possible role of superheated magma in the formation of orbicular granitoids. *Geology*, **13**, 843–5.

1986a: K-feldspar megacrysts in granites – phenocrysts, not porphyroblasts. *Earth-Science Reviews*, **23**, 1–63.

1986b: Evaluation of the "quartz-eye" hypothesis. *Economic Geology*, **81**, 1520–7.

1987a: Oriented growth of sillimanite in andalusite, Placitas-Juan Tabo area, New Mexico, U.S.A. *Canadian Journal of Earth Sciences*, **24**, 580–90.

1987b: Growth and concentration of fibrous sillimanite related to heterogeneous deformation in K-feldspar–sillimanite metapelites. *Journal of Metamorphic Geology*, **5**, 51–68.

1987c: A microstructural indicator of shear sense in volcanic rocks and its relationship to porphyroblast rotation in metamorphic rocks. *Journal of Geology*, **95**, 127–33.

1988a: Sequential growth of cordierite and andalusite porphyroblasts, Cooma Complex, Australia: microstructural evidence of a prograde reaction. *Journal of Metamorphic Geology*, **6**, 255–69.

1988b: Microstructural evidence of rotation and non-rotation of mica porphyroblasts. *Journal of Metamorphic Geology*, **6**, 595–601.

1989: Porphyroblast-matrix microstructural relationships – recent approaches and problems. *In* Daly, S. J. & Brown, M. (eds): *The Evolution of Metamorphic Belts. Geological Society of London Special Publication*, **43**, 83–102.

1990a: Crystallization and hybridism in microgranitoid enclave magmas: microstructural evidence. *In* Sawka, W. N. & Hildebrand, R. S. (eds): *Mafic Inclusions in Granites. Journal of Geophysical Research*, **95**, 17849–59.

1990b: K-feldspar augen in felsic gneisses and mylonites – deformed phenocrysts or porphyroblasts? *Geologiska Föreningens i Stockholm Förhandlingar*, **112**, 157–67.

1991a: Interpretation of microstructures of microgranitoid enclaves. *In* Didier, J. & Barbarin, B. (eds): *Enclaves and Granite Petrology*. Amsterdam: Elsevier, pp. 277–91.

1991b: Questions about myrmekite in deformed rocks. *Journal of Structural Geology*, **13**, 979–85.

1996a: Problems with inferring *P-T-t* paths in low-*P* granulite facies rocks. *Journal of Metamorphic Geology*, **14**, 143–53.

1996b: Observation versus argument by authority – the origin of enclaves in granites. *Journal of Geoscience Education*, **44**, 57–64.

1997: On the identification of textural disequilibrium in rocks using dihedral angle measurements: Comment. *Geology*, **25**, 1055.

1998: Chemical changes and volume loss during foliation development. *In* Treloar, P. J. & O'Brien, P. (eds): *What Drives Metamorphism and Metamorphic Reactions*? *Geological Society of London Special Publication*, **138**, 215–46.

1999a: Quartz and feldspar microstructures in metamorphic rocks. *Canadian Mineralogist*, **37**, 513–24.

1999b: Flame perthite in metapelitic gneisses in the Cooma Complex, SE Australia. *American Mineralogist*, **84**, 1760–5.

2000a: Review of microstructural evidence of magmatic and solid-state flow. *Electronic Geosciences*, **5:2**.

2000b: *Beneath Our Feet. The Rocks of Planet Earth*. Cambridge: Cambridge University Press.

Vernon, R. H., Clarke, G. L. & Collins, W. J. 1990: Local mid-crustal granulite facies metamorphism and melting: an example in the Mount Stafford area, central Australia. *In* Ashworth, J. R. & Brown, M. (eds): *High-temperature Metamorphism and Crustal Anatexis*, London: Unwin Hyman, pp. 272–319.

Vernon, R. H. & Collins, W. J. 1988: Igneous microstructures in migmatites. *Geology*, **16**, 1126–9.

Vernon, R. H., Collins, W. J. & Paterson, S. R. 1993a: Pre-foliation metamorphism in low-pressure/high-temperature terrains. *Tectonophysics*, **219**, 241–56.

Vernon, R. H., Collins, W. J. & Richards, S. W. 2003: Contrasting behaviour of leucosome in metapelitic and metapsammitic migmatites in some LPHT terranes. *Electronic Geosciences*, **7**, 31–9.

Vernon, R. H., Etheridge, M. A. & Wall, V. J. 1988: Shape and microstructure of microgranitoid enclaves: indicators of magma mingling and flow. *Lithos*, **22**, 1–11.

Vernon, R. H. & Flood, R. H. 1977: Interpretation of some metamorphic assemblages containing fibrolitic sillimanite. *Contributions to Mineralogy and Petrology*, **59**, 227–35.

1979: Microstructural evidence of time-relationships between metamorphism and deformation in the metasedimentary sequence of the northern Hill End Trough, New South Wales, Australia. *Tectonophysics*, **58**, 127–37.

1988: Contrasting deformation of S- and I-type granitoids in the Lachlan Fold Belt, eastern Australia. *Tectonophysics*, **147**, 127–43.

Vernon, R. H., Flood, R. H. & D'Arcy, W. F. 1987: Sillimanite and andalusite produced by base-cation leaching and contact metamorphism of felsic igneous rocks. *Journal of Metamorphic Geology*, **5**, 439–50.

Vernon, R. H. & Johnson, S. E. 2000: Transition from gneiss to migmatite and the relationship of leucosome to peraluminous granite in the Cooma Complex, SE Australia. *In* Jessell, M. W. & Urai, J. L. (eds): *Stress, Strain and Structure. A Volume in Honour of WD Means*. *Journal of the Virtual Explorer*, **2** (print and CD).

Vernon, R. H., Johnson, S. E. & Melis, E. A. 2004: Emplacement-related microstructures in the margin of a deformed tonalite pluton: the San José pluton, Baja California, México. *Journal of Structural Geology* (in press).

Vernon, R. H. & Paterson, S. R. 1993: The Ardara pluton, Ireland: deflating an expanded intrusion. *Lithos*, **31**, 17–32.

2001: Axial-surface leucosomes in anatectic migmatites. *In* Boland, J. N. and Ord, A. (eds): *Deformation Processes in the Earth's Crust* (*Hobbs Volume*). *Tectonophysics*, **335**, 183–92.

2002: Igneous origin of K-feldspar megacrysts in deformed granites of the Papoose Flat pluton, California, USA. *Electronic Geosciences*, **7**, 31–9.

Vernon, R. H., Paterson, S. R. & Foster, D. 1993b: Growth and deformation of porphyroblasts in the Foothills terrane, central Sierra Nevada, California: negotiating a microstructural minefield. *Journal of Metamorphic Geology*, **11**, 203–22.

Vernon, R. H. & Pooley, G. D. 1981: SEM/microprobe study of some symplectic intergrowths replacing cordierite. *Lithos*, **14**, 75–82.

Vernon, R. H. & Powell, C. McA. 1976: Porphyroblastesis and displacement: some new textural criteria from pelitic hornfels – a comment. *Mineralogical Magazine*, **40**, 787–8.

Vernon, R. H. & Ransom, D. M. 1971: Retrograde schists of the amphibolite facies at Broken Hill, New South Wales. *Journal of the Geological Society of Australia*, **18**, 267–77.

Vernon, R. H., Richards, S. W. & Collins, W. J. 2000: Migmatite-granite relationships: origin of the Cooma Granodiorite magma, Lachlan Fold Belt, Australia. *Physics and Chemistry of the Earth* (A), **26**, 267–71.

Vernon, R. H. & Williams, P. F. 1988: Distinction between intrusive and extrusive or sedimentary parentage of felsic gneisses: Examples from the Broken Hill Block, NSW. *Australian Journal of Earth Sciences*, **35**, 379–88.

Vernon, R. H., Williams, V. A. & D'Arcy, W. F. 1983: Grainsize reduction and foliation development in a deformed granitoid batholith. *Tectonophysics*, **92**, 123–45.

Viljoen, K. S. 2002: An infrared investigation of inclusion-bearing diamonds from the Venetia kimberlite, Northern Province, South Africa: implications for diamonds from craton-margin settings. *Contributions to Mineralogy and Petrology*, **144**, 98–108.

Viljoen, M. J. & Viljoen, R. P. 1969: Evidence for the existence of a mobile extrusive peridotite magma from the Komati Formation of the Onverwacht Group. *Geological Society of South Africa Special Publication*, **2**, 87–112.

Visser, P. & Mancktelow, N. S. 1992: The rotation of garnet porphyroblasts around a single fold, Lukmanier Pass, Central Alps. *Journal of Structural Geology*, **14**, 1193–202.

Vogel, T. A., Younker, L. W. & Shuraytz, B. C. 1987: Constraints on magma ascent, emplacement and eruption: Geochemical and mineralogical data from drill-core samples at Obsidian Dome, Inyo chain, California. *Geology*, **15**, 405–8.

Vogelé, V., Cordier, P., Sautter, V., Sharp, T. G., Lardeaux, J.-M. & Marques, F. O. 1998: Plastic deformation of silicate garnets II. Deformation microstructures in natural samples. *Physics of the Earth and Planetary Interiors*, **108**, 319–38.

Vogelsang, H. 1867: *Philosophie der Geologie und mikroskopische Gesteinsstudien*. Bonn.

Vogt, J. H. L. 1921: The physical chemistry of the crystallization and magmatic differentiation of igneous rocks. *Journal of Geology*, **29**, 318–50.

Voll, G. 1960: New work on petrofabrics. *Liverpool and Manchester Geological Journal*, **2**, 503–67.

1961: Zur Frage des Stofftransports auf den Korngrenzen metamorpher Gesteine. *Geologische Rundschau*, **51**, 395–405.

1976: Recrystallization of quartz, biotite and feldspar from Erstfeld to the Leventina Nappe, Swiss Alps, and its geological significance. *Schweizerische Mineralogische und Petrographische Mitteilungen*, **56**, 641–7.

1980: Ein Querprofil durch die Schweizer Alpen vom Vierwaldstätter See zur Wurzelzone – Strukturen und ihre Entwicklung durch Deformationmechanismen wichtiger Minerale. *Neues Jahrbuch für Geologie und Paläontologie Abhandlungen*, **160**, 321–35.

Vollbrecht, A., Siegesmund, S. & Flaig, C. 1997: High-temperature deformation of a granitoid from the Zone of Erbendorf-Vohenstrauβ (ZEV). *Geologische Rundschau*, **86**, S141–54.

von Mises, R. 1928: Mechanik der plastischen Formänderung von Kristallen. *Zeitschrift für Angewandte Mathematik und Mechanik*, **8**, 161–85.

von Steinemann, S. 1958: Experimentelle Untersuchung zur Plastizität von Eis. *Beitrage zur Geologie der Schweiz, Hydrologie*, **10**, 4–72.

Voorhees, P. W. 1992: Ostwald ripening of two-phase mixtures. *Annual Review of Materials Science*, **22**, 197–215.

Wager, L. R. 1961: A note on the origin of ophitic texture in the chilled olivine gabbro of the Skaergaard intrusion. *Geological Magazine*, **98**, 353–66.

1963: The mechanism of adcumulus growth in the layered series of the Sakaergaard intrusions. *Mineralogical Society of America Special Paper*, **1**, 1–9.

Wager, L. R. & Brown, G. M. 1968: *Layered Igneous Rocks*. Edinburgh: Oliver & Boyd.

Wager, L. R., Brown, G. M. & Wadsworth, W. J. 1960: Types of igneous cumulates. *Journal of Petrology*, **1**, 73–85.

Wager, L. R., Vincent, E. A., Brown, G. M. & Bell, J. D. 1965: Marscoite and related rocks of the Western Red Hills Complex, Isle of Skye. *Philosophical Transactions of the Royal Society of London*, **A257**, 273–308.

Wagner, C., Velde, D. & Mokhtari, A. 1987: Sector-zoned phlogopites in igneous rocks. *Contributions to Mineralogy and Petrology*, **96**, 186–91.

Wahrhaftig, C. 1979: Significance of asymmetric schlieren for crystallization of granites in the Sierra Nevada batholith, California. *Geological Society of America Abstracts with Programs*, **11**, 133.

Waldron, H. M. & Sandiford, M. 1988: Deformation volume and cleavage development in metasedimentary rocks from the Ballarat slate belt. *Journal of Structural Geology*, **10**, 53–62.

Waldron, K. A., Parsons, I. & Brown, W. L. 1993: Solution-redeposition and the orthoclase-microcline transformation: evidence from granulites and relevance to ^{18}O exchange. *Mineralogical Magazine*, **57**, 687–95.

Walker, D., Jurewicz, S. & Watson, E. B. 1988: Adcumulus dunite growth in a laboratory thermal gradient. *Contributions to Mineralogy and Petrology*, **99**, 306–19.

Walker, G. P. L. & Skelhorn, R. R. 1966: Some associations of acid and basic igneous rocks. *Earth-Science Reviews*, **2**, 93–109.

Walker, J. A., Roggensack, K., Patino, L. C. & Matías, O. 2003: The water and trace element contents of melt inclusions across an active subduction zone. *Contributions to Mineralogy and Petrology*, **146**, 62–77.

Walker, K. R., Joplin, G. A., Lovering, J. F. & Green, R. 1960: Metamorphic and metasomatic convergence of basic igneous rocks and lime-magnesia sediments of the Precambrian of north-western Queensland. *Journal of the Geological Society of Australia*, **6**, 149–78.

Walton, A. G. 1965: Nucleation of crystals from solution. *Science*, **148**, 601–7.

Wang, Z. & Ji, S. 1999: Deformation of silicate garnets: brittle-ductile transition and its geological implications. *Canadian Mineralogist*, **37**, 525–41.

Ward, C. M. 1984a: Magnesium staurolite and green chromian staurolite from Fiordland, New Zealand. *American Mineralogist*, **69**, 531–40.

1984b: Titanium and the color of staurolite. *American Mineralogist*, **69**, 541–45.

1984c: *Geology of the Dusky Sound Area, Fiordland, with Emphasis on the Structural-metamorphic Development of Some Porphyroblastic Staurolite Pelites*. Unpublished Ph.D. thesis, University of Otago, Dunedin.

Warren, P. H., Taylor, G. J., Keil, K., Shirley, D. N. & Wasson, J. T. 1983: Petrology and chemistry of two "large" granite clasts from the Moon. *Earth and Planetary Science Letters*, **64**, 175–85.

Wass, S. Y. 1973: The origin and petrogenetic significance of hour-glass zoning in titaniferous clinopyroxenes. *Mineralogical Magazine*, **39**, 133–44.

Waters, D. J. 1988: Partial melting and the formation of granulite facies assemblages in Namaqualand, South Africa. *Journal of Metamorphic Geology*, **6**, 387–404.

2001: The significance of prograde and retrograde quartz-bearing intergrowth microstructures in partially melted granulite-facies rocks. *Lithos*, **56**, 97–110.

Waters, D. J. & Charnley, N. R. 2002: Local equilibrium in polymetamorphic gneiss and the titanium substitution in biotite. *American Mineralogist*, **87**, 383–96.

Waters, D. J. & Lovegrove, D. P. 2002: Assessing the extent of disequilibrium and overstepping of prograde metamorphic reactions in metapelites from the Bushveld Complex aureole, South Africa. *Journal of Metamorphic Geology*, **20**, 135–49.

Watson, E. B. & Capobianco, C. J. 1981: Phosphorus and the rare earth elements in felsic magmas: An assessment of the role of apatite. *Geochimica et Cosmochimica Acta*, **45**, 2349–58.

Watson, E. B. & Liang, Y. 1995: A simple model for sector zoning in slowly grown crystals: Implications for growth rate and lattice diffusion, with emphasis on accessory minerals in crustal rocks. *American Mineralogist*, **80**, 1179–87.

Watt, G. R., Oliver, N. H. S. & Griffin, B. J. 2002: Evidence for reaction-induced microfracturing in granulite facies migmatites. *Geology*, **28**, 327–30.

Watt, G. R., Wright, P., Galloway, S. & McLean, C. 1997: Cathodoluminescence and trace element zoning in quartz phenocrysts and xenocrysts. *Geochimica et Cosmochimica Acta*, **61**, 4337–48.

Webber, K. L., Simmons, W. B., Falster, A. U. & Foord, E. E. 1999: Cooling rates and crystallization dynamics of shallow level pegmatite-aplite dikes, San Diego County, California. *American Mineralogist*, **84**, 708–17.

Weber, K. 1981: Kinematic and metamorphic aspects of cleavage formation in very low-grade metamorphic slates. *Tectonophysics*, **78**, 291–306.

Weedon, D. S. 1965: The layered ultrabasic rocks of Sgurr Dubh, Isle of Skye. *Scottish Journal of Geology*, **1**, 41–68.

Wegner, M. & Christie, J. M. 1983: Chemical etching of deformation substructures in quartz. *Physics and Chemistry of Minerals*, **9**, 67–78.

Weinberg, R. F., Sial, A. N. & Pessoa, R. R. 2001: Magma flow within the Tavares pluton, northeastern Brazil: Compositional and thermal convection. *Bulletin of the Geological Society of America*, **113**, 508–20.

Weis, P. L. 1980: Graphite skeleton crystals – A newly recognized morphology of crystalline carbon in metasedimentary rocks. *Geology*, **8**, 296–7.

Weisbrod, A. M., Poty, B. & Touret, J. 1976: Les inclusions fluides en géochimie-pétrologie: tendances actuelles. *Bulletin de Minéralogie*, **99**, 140–52.

Weiss, L. E. 1972: *The Minor Structures of Deformed Rocks*. New York: Springer.

Weiss, L. E. & McIntyre, D. B. 1957: Structural geometry of Dalradian rocks at Loch Leven, Scottish Highlands. *Journal of Geology*, **65**, 575–602.

Weiss, L. E. & Turner, F. J. 1972: Some observations of translation gliding and kinking in experimentally deformed calcite and dolomite. *In* Heard, H. C., Borg, I. Y., Carter, N. L. & Raleigh, C. B. (eds): *Flow and Fracture of Rocks. Geophysical Monograph Series*, **16**, 95–107.

Wheeler, J. 1987: The significance of grain-scale stresses in the kinetics of metamorphism. *Contributions to Mineralogy and Petrology*, **97**, 397–404.

1992: Importance of pressure solution and Coble creep in the deformation of polymineralic rocks. *Journal of Geophysical Research*, **97**, 4579–86.

Wheeler, J., Prior, D. J., Jiang, Z., Speiss, R. & Trimby, P. W. 2001: The petrological significance of misorientations between grains. *Contributions to Mineralogy and Petrology*, **141**, 109–24.

White, J. C. 1990: Albite deformation within a basal ophiolite shear zone. *In* Knipe., R. J. & Rutter, E. H. (eds): *Deformation Mechanisms, Rheology and Tectonics. Geological Society of London Special Publication*, **54**, 327–33.

White, J. C. & White, S. H. 1981: On the structure of grain boundaries in tectonites. *Tectonophysics*, **78**, 613–28.

1983: Semi-brittle deformation within the Alpine fault zone, New Zealand. *Journal of Structural Geology*, **5**, 578–89.

White, R. W. & Clarke, G. L. 1997: The role of deformation in aiding recrystallization: an example from a high pressure shear zone. *Journal of Petrology*, **38**, 1307–29.

1999: SHRIMP U-Pb zircon dating of Grenville-age events in the western part of the Musgrave Block, central Australia. *Journal of Metamorphic Geology*, **17**, 465–81.

White, R. W. & Powell, R. 2002: Melt loss and the preservation of granulite facies mineral assemblages. *Journal of Metamorphic Geology*, **20**, 621–32.

White, R. W., Powell, R. & Clarke, G. L. 2002: The interpretation of reaction textures in Fe-rich metapelitic granulites of the Musgrave Block, central Australia: constraints from mineral equilibria calculations in the system K_2O-FeO-MgO-Al_2O_3-SiO_2-H_2O-TiO_2-Fe_2O_3. *Journal of Metamorphic Geology*, **20**, 41–55.

White, S. H. 1973: Deformation lamellae in naturally deformed quartz. *Nature, Physical Science*, **245**, 26–8.

1976: The effects of strain on the microstructures, fabrics and deformation mechanisms in quartzite. *Philosophical Transactions of the Royal Society of London*, **A283**, 69–85.

1977: Geological significance of recovery and recrystallisation processes in quartz. *Tectonophysics*, **39**, 143–70.

1979: Large strain deformation: report on a tectonic studies group discussion meeting held at Imperial College, London; introduction. *Journal of Structural Geology*, **4**, 333–9.

White, S. H., Burrows, S. E., Carreras, J., Shaw, N. D. & Humphreys, F. J. 1980: On mylonites in ductile shear zones. *Journal of Structural Geology*, **2**, 175–87.

White, S. H., & Johnston, D. C. 1981: A microstructural and microchemical study of cleavage lamellae in a slate. *Journal of Structural Geology*, **3**, 279–90.

White, S. H. & Knipe, R. J. 1977: Microstructural variation of an axial plane cleavage around a fold – a H.V.E.M. study. *Tectonophysics*, **39**, 355–80.

1978a: Microstructure and cleavage development in selected slates. *Contributions to Mineralogy and Petrology*, **66**, 165–74.

1978b: Transformation- and reaction-enhanced ductility in rocks. *Journal of the Geological Society of London*, **135**, 513–16.

White, S. H. & Wilson, C. J. L. 1978: Microstructure of some quartz pressure fringes. *Neues Jahrbuch für Mineralogie, Geologie und Paläontologie Abhandlungen*, **134**, 33–51.

Whitney, D. L. & Dilek, Y. 2000: Andalusite-sillimanite-quartz veins as indicators of low-pressure – high-temperature deformation during late-stage unroofing of a metamorphic core complex, Turkey. *Journal of Metamorphic Geology*, **18**, 59–66.

Wickham, J. S. 1973: An estimate of strain increments in a naturally deformed carbonate rock. *American Journal of Science*, **237**, 23–47.

Wickham, J. S. & Anthony, M. 1977: Strain paths and folding of carbonate rocks near Blue Ridge, central Appalachians. *Bulletin of the Geological Society of America*, **88**, 920–4.

Wickham, S. M. 1987: The segregation and emplacement of granitic magmas. *Journal of the Geological Society of London*, **144**, 281–97.

Wicks, F. J. & Whittaker, E. J. W. 1977: Serpentine textures and serpentinization. *Canadian Mineralogist*, **15**, 459–88.

Widmer, T. & Thompson, A. B. 2001: Local origin of high pressure vein material in eclogite facies rocks of the Zermatt-Saas Zone, Switzerland. *American Journal of Science*, **301**, 627–56.

Wiebe, R. A. 1968: Plagioclase stratigraphy: a record of magmatic conditions and events in a granite stock. *American Journal of Science*, **266**, 690–703.

1973: Relations between coexisting basaltic and granitic magmas in a composite dike. *American Journal of Science*, **273**, 130–51.

1974: Coexisting intermediate and basic magmas, Ingonish, Cape Breton Island. *Journal of Geology*, **82**, 74–87.

1994: Silicic magma chambers as traps for basaltic magmas: the Cadillac Mountain intrusive complex, Mount Desert Island, Maine. *Journal of Geology*, **102**, 423–37.

1996: Mafic-silicic layered intrusions: the role of basaltic injections on magmatic processes and the evolution of silicic magma chambers. *Transactions of the Royal Society of Edinburgh: Earth Sciences*, **87**, 233–42.

Wiebe, R. A., Blair, K. D., Hawkins, D. P. & Sabine, C. P. 2002: Mafic injections, in situ hybridization, and crystal accumulation in the Pyramid Peak granite, California. *Bulletin of the Geological Society of America*, **114**, 909–20.

Wiggins, L. B. & Craig, J. R. 1980: Reconnaissance of the Cu-Fe-Zn-S system: sphalerite phase relations. *Economic Geology*, **75**, 742–51.

Wilcox, R. E. 1944: Rhyolite-basalt complex on Gardiner River, Yellowstone Park, Wyoming. *Bulletin of the Geological Society of America*, **55**, 1047–80.

1999: The idea of magma mixing: history of a struggle for acceptance. *Journal of Geology*, **107**, 421–32.

Williams, H. & McBirney, A. R. 1979: *Volcanology*. San Francisco: Freeman.

Williams, H., Turner, F. J. & Gilbert, C. M. 1954: *Petrography. An Introduction to the Study of Rocks in Thin Sections*. San Francisco: Freeman.

Williams, I. S., Buick, I. S. & Cartwright, I. 1996: An extended episode of early Mesoproterozoic metamorphic fluid flow in the Reynolds Range, central Australia. *Journal of Metamorphic Geology*, **14**, 29–47.

Williams, M. L. 1991: Heterogeneous deformation in a ductile fold-thrust belt: The Proterozoic structural history of the Tusas Mountains, New Mexico. *Bulletin of the Geological Society of America*, **103**, 171–88.

1994: Sigmoidal inclusion trails, punctuated fabric development, and interactions between metamorphism and deformation. *Journal of Metamorphic Geology*, **12**, 1–21.

Williams, M. L. & Burr, J. L. 1994: Preservation and evolution of quartz phenocrysts in deformed rhyolites from the Proterozoic of southwestern North America. *Journal of Structural Geology*, **16**, 203–21.

Williams, M. L. & Jercinovic, M. J. 2002: Microprobe monazite geochronology: putting absolute time into microstructural analysis. *Journal of Structural Geology*, **24**, 1013–28.

Williams, M. L., Melis, E. A., Kopf, C. F. & Hanmer, S. 2000: Microstructural tectonometamorphic processes in the development of gneissic layering: a mechanism for metamorphic segregation. *Journal of Metamorphic Geology*, **18**, 41–57.

Williams, M. L., Scheltema, K. E. & Jercinovic, M. J. 1972: Development of metamorphic layering and cleavage in low grade metamorphic rocks at Bermagui, Australia. *American Journal of Science*, **272**, 1–47.

1983: Timing of deformation and the mechanism of cleavage development in a Newfoundland mélange. *Maritime Sediments and Atlantic Geology*, **19**, 31–48.

1985: Multiply deformed terrains – problems of correlation. *Journal of Structural Geology*, **7**, 269–80.

1990: Differentiated layering in metamorphic rocks. *Earth-Science Reviews*, **29**, 267–81.

2001: High-resolution compositional mapping of matrix phases: implications for mass transfer during crenulation cleavage development in the Moretown Formation, western Massachusetts. *Journal of Structural Geology*, **23**, 923–39.

Williams, P. F., Collins, A. R. & Wiltshire, R. G. 1969: Cleavage and penecontemporaneous deformation structures in sedimentary rocks. *Journal of Geology*, **77**, 415–25.

Williams, P. F. & Jiang, D. 1999: Rotating garnets. *Journal of Metamorphic Geology*, **17**, 367–78.

Williams, P. F., Means, W. D. & Hobbs, B. E. 1977: Development of axial-plane slaty cleavage and schistosity in experimental and natural materials. *Tectonophysics*, **42**, 139–58.

Williams, P. F. & Schoneveld, C. 1981: Garnet rotation and the development of axial plane crenulation cleavage. *Tectonophysics*, **78**, 307–34.

Williams, P. F. & Urai, J. L. 1989: Curved vein fibres: an alternative explanation. *Tectonophysics*, **158**, 311–33.

Williams, R. E. 1968: Space-filling polyhedrons in relation to aggregates of soap bubbles, plant cells and metal crystallites. *Science*, **161**, 276–7.

Wilshire, H. G. 1969: Mineral layering in the Twin Lakes Granodiorite, Colorado. *Geological Society of America Memoir*, **115**, 235–61.

Wilson, C. J. L. 1984: Shear bands, crenulation and differentiated layering in ice-mica models. *Journal of Structural Geology*, **6**, 303–19.

1986: Deformation-induced recrystallization of ice: the application of *in situ* experiments. *In* Heard, H. C. & Hobbs, B. E. (eds): *Mineral and Rock Deformation: Laboratory Studies (The Paterson Volume). American Geophysical Union Geophysical Monograph*, **36**, 213–32.

Wilson, C. J. L. & Bell, I. A. 1979: Deformation of biotite and muscovite: optical microstructure. *Tectonophysics*, **58**, 179–200.

Wilson, C. J. L., Burg, J.-P. & Mitchell, J. C. 1986: The origin of kinks in polycrystalline ice. *Tectonophysics*, **127**, 27–48.

Wilson, C. J. L. & Zhang, Y. 1994: Comparison between experiments and computer modelling of plane strain simple shear ice deformation. *Journal of Glaciology*, **40**, 46–55.

Wiltschko, D. V. & Moru, J. W. 2001: Crystallization pressure versus "crack seal" as the mechanism for banded veins. *Geology*, **29**, 79–82.

Winkler, H. G. F. & Schultes, H. 1982: On the problem of alkali feldspar phenocrysts in granitic rocks. *Neues Jahrbuch für Mineralogie Monatshefte*, **12**, 558–64.

Wintsch, R. P. 1978: A chemical approach to the preferred orientation of mica. *Bulletin of the Geological Society of America*, **89**, 1715–18.

1985: Possible effects of deformation on chemical processes in metamorphic fault zones. *In* Thompson, A. B. & Rubie, D. C. (eds): *Metamorphic Reactions. Kinetics, Textures, and*

Deformation. Advances in Physical Geochemistry, **4**. New York: Springer, pp. 251–68.

Wintsch, R. P. & Dunning, J. 1985: The effect of dislocation density on the aqueous solubility of quartz and some geological implications: a theoretical approach. *Journal of Geophysical Research*, **90**, 3649–57.

Wintsch, R. P. & Knipe, R. J. 1983: Growth of a zoned plagioclase porphyroblast in a mylonite. *Geology*, **11**, 360–3.

Wintsch, R. P., Kvale, C. M. & Kisch, H. D. 1991: Open-system, constant volume development of slaty cleavage, and strain-induced replacement reactions in the Martinsburg Formation, Lehigh Gap, Pennsylvania. *Bulletin of the Geological Society of America*, **103**, 916–27.

Wintsch, R. P. & Yi, K. 2002: Dissolution and replacement creep: a significant deformation mechanism in mid-crustal rocks. *Journal of Structural Geology*, **24**, 1179–93.

Wirth, R. & Voll, G. 1987: Cellular intergrowth between quartz and sodium-rich plagioclase (myrmekite) – an analogue of discontinuous precipitation in metal alloys. *Journal of Materials Science*, **22**, 1913–18.

Wise, D. U., Dunn, D. E., Engelder, J. T., Geiser, P. A., Hatcher, R. D., Kish, S. A., Odom, A. L. & Schamel, S. 1984: Fault-related rocks: suggestions for terminology. *Geology*, **12**, 391–4.

1985a: Reply to Mawer on "Fault-related rocks: suggestions for terminology." *Geology*, **13**, 379.

1985b: Reply to Raymond on "Fault-related rocks: suggestions for terminology." *Geology*, **13**, 218–19.

Wolf, D. & Merkle, K. L. 1992: Correlation between the structure and energy of grain boundaries in metals. *In* Wolf, D. & Yip, S. (eds): *Materials Interfaces*. London: Chapman and Hall, pp. 87–150.

Wolf, M. B. & Wyllie, P. J. 1991: Dehydration melting of solid amphibolite at 10 kbar: Textural development, liquid interconnectivity and applications to the segregation of magmas. *Contributions to Mineralogy and Petrology*, **44**, 151–79.

Wood, D. S. 1974: Current views of the development of slaty cleavage. *Annual Reviews of Earth and Planetary Sciences*, **2**, 369–401.

Woodland, B. G. 1985: Relationship of concretions and chlorite-muscovite porphyroblasts to the development of domainal cleavage in low-grade metamorphic deformed rocks from north-central Wales, Great Britain. *Journal of Structural Geology*, **7**, 205–15.

Worden, R. H., Droop, G. T. R. & Champness, P. E. 1991: The reaction antigorite → olivine + talc + H_2O in the Bergell aureole, N. Italy. *Mineralogical Magazine*, **55**, 367–77.

Worley, B., Powell, R. & Wilson, C. J. L. 1997: Crenulation cleavage formation: Evolving diffusion, deformation and equilibration mechanisms with increasing metamorphic grade. *Journal of Structural Geology*, **19**, 1121–35.

Wright, T. O. & Henderson, J. R. 1992: Volume loss during cleavage formation in the Meguma Group, Nova Scotia, Canada. *Journal of Structural Geology*, **14**, 281–90.

Wright, T. O. & Platt, L. B. 1982: Pressure dissolution and cleavage in the Martinsburg Shale. *American Journal of Science*, **282**, 122–35.

Yang, P. & Rivers, T. 2002: The origin of Mn and Y annuli in garnet and the thermal dependence of P in garnet and Y in apatite in calc-pelite and pelite, Gagnon terrane, western Labrador. *Geological Materials Research*, **4/1**, 35pp.

Yardley, B. W. D. 1974: Porphyroblasts and ‘crystallization force’: Discussion of some theoretical considerations. *Bulletin of the Geological Society of America*, **85**, 61–2.

1977a: Relationships between the chemical and modal compositions of metapelites from Connemara, Ireland. *Lithos*, **10**, 235–42.

1977b: The nature and significance of the mechanism of sillimanite growth in the Connemara Schist, Ireland. *Contributions to Mineralogy and Petrology*, **10**, 235–42.

1983: Quartz veins and devolatilization during metamorphism. *Journal of the Geological Society of London*, **140**, 657–63.

1986: Fluid migration and veining in the Connemara schists, Ireland. *In* Walther, J. V. & Wood, B. J. (eds): *Fluid-Rock Interaction During Metamorphism. Advances in Physical Geochemistry*, **5**, 109–31.

1989: *An Introduction to Metamorphic Petrology.* Edinburgh: Longman.

Yardley, B. W. D. & Bottrell, S. H. 1992: Silica mobility and fluid movement during metamorphism of the Connemara schists, Ireland. *Journal of Metamorphic Geology*, **10**, 453–64.

Yardley, B. W. D., Gleeson, S., Bruce, S. & Banks, D. 2000: Origin of retrograde fluids in metamorphic rocks. *Journal of Geochemical Exploration*, **69–70**, 281–5.

Yardley, B. W. D. & Lloyd, G. E. 1989: An application of cathodoluminescence to the study of textures and reactions in high grade marbles from Connemara, Ireland. *Geological Magazine*, **126**, 333–7.

Yardley, B. W. D., Rochelle, C. A., Barnicoat, A. C. & Lloyd, G. E. 1991: Oscillatory zoning in metamorphic minerals: an indicator of infiltration metasomatism. *Mineralogical Magazine*, **55**, 357–65.

Yoshinobu, A. S. & Hirth, G. 2002: Microstructural and experimental constraints on the rheology of partially molten gabbro beneath ocean spreading centers. *Journal of Structural Geology*, **24**, 1101–7.

Yund, R. A. 1983: Microstructure, kinetics and mechanisms of alkali feldspar exsolution. *In* Ribbe, P. H. (ed.): *Feldspar Mineralogy* (second edition). *Mineralogical Society of America, Reviews in Mineralogy*, **2**, 177–202.

Yund, R. A. & McCallister, R. H. 1970: Kinetics and mechanisms of exsolution. *Chemical Geology*, **6**, 5–30.

Yund, R. A. & Tullis, J. 1991: Compositional changes of minerals associated with dynamic crystallization. *Contributions to Mineralogy and Petrology*, **108**, 346–55.

Zeuch, D. H. 1983: On the inter-relationship between grain size sensitive creep and dynamic recrystallization of olivine. *Tectonophysics*, **93**, 151–68.

Zeuch, D. H. & Green, H. W. 1979: Experimental deformation of an “anhydrous” synthetic dunite. *Bulletin de Minèralogie*, **102**, 185–7.

1984: Experimental deformation of a synthetic dunite at high temperature and pressure. II. Transmission electron microscopy. *Tectonophysics*, **110**, 263–96.

Zhang, Y., Hobbs, B. E. & Jessell, M. W. 1994: The effect of grain-boundary sliding on fabric development in polycrystalline aggregates. *Journal of Structural Geology*, **16**, 1315–25.

Zhang, Y., Jessell, M. W. & Hobbs, B. E. 1996: Experimental and numerical studies of the accommodation of strain incompatibility on the grain scale. *Journal of Structural Geology*, **18**, 451–60.

Zieg, M. J. & Marsh, B. D. 2002: Crystal size distributions and scaling laws in the quantification of igneous textures. *Journal of Petrology*, **43**, 85–101.

Zinkerngel, U. 1978: Cathodoluminescence of quartz and its application to sandstone petrology. *Contributions to Sedimentology*, **8**, 69pp.

Zirkel, F. 1863: Mikroskopische Gesteinsstudien. *Sitzberichte der Akademie Wissenschaften Wien*, **47**, 226–70.

1866 (last edition 1893–4): *Lehrbuch der Petrographie*. Bonn: Leipzig.

1876: *Microscopical Petrography*. Washington: United States Geological Survey, Exploration of the Fortieth Parallel.

Zwart, H. J. 1960a: The chronological succession of folding and metamorphism in the central Pyrenees. *Geologische Rundschau*, **50**, 203–18.

1960b: Relations between folding and metamorphism in the central Pyrenees, and their chronological succession. *Geologie en Mijnbouw*, **39**, 163–80.

1962: On the determination of polymetamorphic mineral associations, and its application to the Bosost area (Central Pyrenees). *Geologische Rundschau*, **52**, 38–65.

Zwart, H. J. & Calon, T. J. 1977: Chloritoid crystals from Curaglia; growth during flattening or pushing aside? *Tectonophysics*, **39**, 477–86.

Zwart, H. J. & Oele, J. A. 1966: Rotated magnetite crystals from the Rocroi Massif (Ardennes). *Geologie en Mijnbouw*, **45**, 70–4.

INDEX

Index Terms **Links**

Page numbers of definitions in the glossary are in bold type.

Index Terms **Links**

Index Terms **Links**

Index Terms **Links**

Index Terms **Links**

Index Terms | Links